JP0250277

JAERI-Conf
2002-004

Proceedings of the International Symposium NUCEF 2001

— Scientific Bases for Criticality Safety, Separation Process and Waste Disposal —

October 31 - November 2, 2001,
Japan Atomic Energy Research Institute (JAERI),
Tokai, Ibaraki, Japan

March 2002

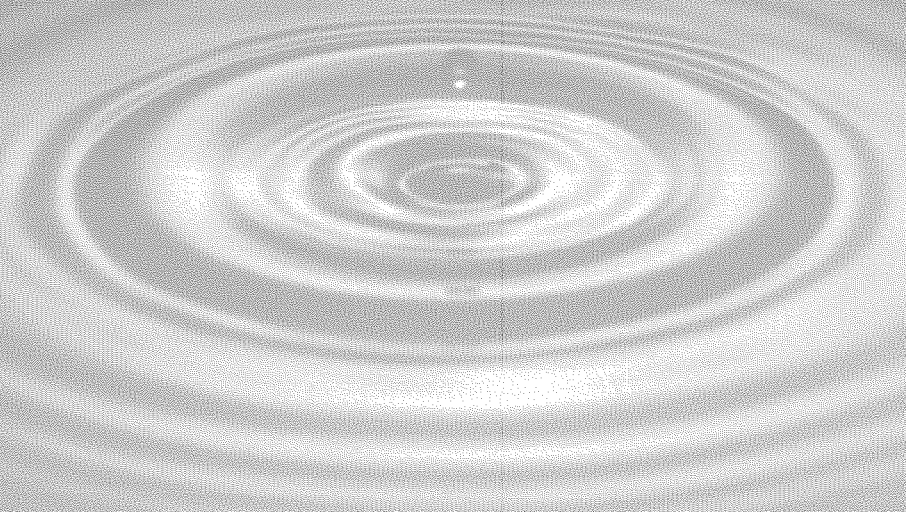

NUCEF 2001 Symposium Working Group

Organized and Sponsored by
Japan Atomic Energy Research Institute (JAERI)
In Cooperation with
Atomic Energy Society of Japan (AESJ)

日 本 原 子 力 研 究 所
Japan Atomic Energy Research Institute

本レポートは，日本原子力研究所が不定期に公刊している研究報告書です。
入手の問合わせは，日本原子力研究所研究情報部研究情報課（〒319-1195　茨城県那珂郡東海村）あて，お申し越しください。なお，このほかに財団法人原子力弘済会資料センター（〒319-1195　茨城県那珂郡東海村日本原子力研究所内）で複写による実費頒布をおこなっております。

This report is issued irregularly.
Inquiries about availability of the reports should be addressed to Research Information Division, Department of Intellectual Resources, Japan Atomic Energy Research Institute, Tokai-mura, Naka-gun, Ibaraki-ken, 319-1195, Japan.

© Japan Atomic Energy Research Institute, 2002

編集兼発行　　日本原子力研究所

JAERI-Conf 2002-004

Proceedings of the International Symposium
NUCEF 2001
- Scientific Bases for Criticality Safety, Separation Process and Waste Disposal -

October 31 - November 2, 2001
Japan Atomic Energy Research Institute (JAERI), Tokai, Ibaraki, Japan

NUCEF 2001 Symposium Working Group※

Tokai Research Establishment
Japan Atomic Energy Research Institute
Tokai-mura, Naka-gun, Ibaraki-ken

(Received February 8, 2002)

These proceedings contain 94 papers presented at NUCEF2001, that was held on October 31 - November 2, 2001, in Tokai-mura, Japan. NUCEF2001 is the 3rd international symposium of the series, following the 1st symposium NUCEF'95 (Proceedings: JAERI-Conf 96-003) and the 2nd symposium NUCEF'98 (Proceedings: JAERI-Conf 99-004). The subtitle of NUCEF2001 was " Scientific Bases for Criticality Safety, Separation Process and Waste Disposal". The papers were presented in oral and poster sessions on the research fields: Criticality Safety, Separation Process, Radioactive Waste Disposal and TRU Chemistry.

Keywords: NUCEF, Criticality Safety, Separation Process, Reprocessing, Partitioning, Radioactive Waste Disposal, TRU Chemistry, Nuclear Fuel Cycle.

※ S. Fujine, S. Dojiri, T. Banba, Y. Nomura, Y. Miyoshi, G. Uchiyama, Y. Morita, H. Ogawa, H. Kimura, S. Nakayama, K. Minato, H. Mineo, T. Tanaka, A. Yamada, T. Sato, T. Kaneko, K. Tonoike, Y. Tsubata, H. Yanagisawa, K. Kobayashi
Editor of these proceedings are T.Banba and Y.Tsubata.

JAERI-Conf 2002-004

国際シンポジウムＮＵＣＥＦ２００１報文集
- 臨界安全性、分離プロセスおよび放射性廃棄物処分に関する科学的基盤 -
2001年10月31日-11月2日　日本原子力研究所東海研究所、東海村

日本原子力研究所東海研究所
NUCEF 2001ワーキンググループ※

(2002年2月8日受理)

本報文集は、2001年10月31日-11月2日に日本原子力研究所東海研究所で開催された国際シンポジウムＮＵＣＥＦ２００１で報告された９４件の報告書をまとめたものである。ＮＵＣＥＦ２００１は、1995年の第1回（報文集JAERI-Conf 96-003）及び1998年の第2回（報文集JAERI-Conf 99-004）に引き続いて開催されたものであり、副題を「臨界安全性、分離プロセスおよび放射性廃棄物処分に関する科学的基盤」とした。本シンポジウムでは、基調講演及び口頭発表、ポスター発表による研究発表など、臨界安全性、分離プロセス、放射性廃棄物処分、TRU化学などの分野において報告が行われた。

東海研究所：〒319-1195 茨城県那珂郡東海村白方白根２－４
※ 藤根幸雄、土尻　滋、馬場恒孝、野村　靖、三好慶典、内山軍蔵、森田泰治、小川弘道、木村英雄、中山真一、湊　和生、峯尾英章、田中忠夫、山田昭男、佐藤　猛、金子貞夫、外池幸太郎、津幡靖宏、柳澤宏司、小林一成
この報告書は、馬場恒孝と津幡靖宏によって編集された。

Contents

Preface

1. Opening Session 1

Opening Address 3
M. Maeda (JAERI)

Progress of Safety Research in NUCEF on Nuclear Fuel Cycle 7
S. Fujine (JAERI)

2. Plenary Session 17

***The US Nuclear Criticality Safety Experience, Needs, and Future in a Global Economy** . . 19
C. M. Hopper (ORNL, USA)

***Overview of the Hydrometallurgical and Pyrometallurgical Processes Studied World-wide for the Partitioning of High Active Nuclear Wastes** 27
C. Madic (CEA, France)

***Decision-in-principle on Final Disposal of Spent Fuel in Finland** 39
J. Vira (Posiva Oy, Finland)

***Communication of Nuclear Power Concepts to Stakeholders -The Use of Nature's Own Laboratories-** 47
J.M. West, W.R. Alexander, K. Kaku, I.G. Mckinley (NAGRA, Switzerland) and
A. Shimmura (Obayashi Corp., Japan)

3. Oral Session 55
Criticality Safety
Session Coordinators: Y. Nomura and Y. Miyoshi

***Development and Application of Consensus Standards in Criticality Safety in the USA** . . 57
T. P. McLaughlin (LANL, USA)

***Regulations for the Transport of Nuclear Fuel Material in Japan** 65
S.Fukuda (CRIEPI, Japan)

***A UK Regulatory Perspective of Criticality Safety -Past, Present and Future-** 73
D.N. Simister (Health & Safety Executive , UK)

Development of Burnup Credit Evaluation Methods at JAERI 81
Y. Nomura, H. Okuno and K. Suyama (JAERI)

The REBUS Experimental Programme for Burn-up Credit 91
P.D'hondt, K. van der Meer, P. Baeten (SCK-CEN, Belgium), D. Marloye, B. Lance and
J. Basselier (Belgonucleaire , Belgium)

* Invited paper

Comparison of Nuclide Evolution Analyses between Japanese and French Codes · · · · · · 99
T. Iwasaki, H. Hiraizumi (Tohoku University, Japan), and G. Youinou (CEA, France)

High-precision Analog Type Neutron Monitoring System · · · · · · · · · · · · · · · · · · 105
N.Oda, Y. Kita, and K. Ishizawa (Toshiba Co., Japan)

***Improving Safety in a MOX Plant by Qualification of Neutron Measurements and Criticality Evaluation** · 111
A. Renard, P. Kockerols, H. Libon and D. Marloye (Belgonucleaire, Belgium)

Subcritical Limit Parameters of MOX Fuel · 125
S. Sakurai and S. Mitake (NUPEC, Japan)

Criticality Safety Control at the Plutonium Fuel Production Facility · · · · · · · · · · · · 133
J. Ninagawa, S. Takahashi, Y. Yamamoto, S. Fujiwara, K. Kuniyasu and T. Ohtani (JNC, Japan)

Application of Dedicated Safeguards Solution Monitoring Instrumentation towards Improved Process Control for Criticality Safety · 141
B. A. Hunt, D. Landat, L. Dechamp and M. Caviglia (EC-Joint Research Centre, Italy)

***Subcritical Measurements and Their Applications** · 147
T. E. Valentine (ORNL, USA)

Status of the FETCH Transient Criticality Code and Application to TRACY Data and Dosimetry Applications · 155
C.C. Pain[1], Y. Yamane[2], C.R.E.de Oliveira[1] and A.J.H. Goddard[1] ([1]ICST, UK, [2]JAERI)

Subcriticality Measurement by Source Multiplication Method with Higher Mode Flux · · · · 165
T. Misawa (Kyoto Univ., Japan)

Study on Neutronic and Thermal Characteristics of the Precipitation Vessel in JCO Criticality Accident · 173
Y. Miyoshi, T. Yamamoto, K. Nakajima, Y. Yamane and S. Watanabe (JAERI)

Separation Process · 181
Session Coordinators: G. Uchiyama and Y. Morita
***Present Status of R&D on Reprocessing Process in COGEMA** · · · · · · · · · · · · · · · 183
M.F. Debreuille, P. Pradel (COGEMA, France) and F. Drain (SGN, France)

***SUPERPUREX as a TBP - Compatible Process for Recovery and Partitioning of Long-lived Radionuclides from NPP Spent Fuel** · 189
B. Ya. Zilberman, Yu.S. Fedorov, E.N. Mishin, L.V. Sytnik, O.V. Shmidt, D.N. Kukharev, N.D. Goletsky, R.G. Glekov, Yu.V. Palenik and S.Yu. Sukhareva (KRI, Russia)

PARC Process as Advanced PUREX Process · 197
G. Uchiyama, H. Mineo, T. Asakura, S. Hotoku, M. Iizuka, S. Fujisaki, H. Isogai, Y. Itoh, M. Sato and N. Hosoya (JAERI)

* Invited paper

***Recent Studies of Heterogeneous and Homogeneous Reduction – Oxidation Reactions of U(IV) Ions in Nitric Acid and TBP Phases** · 205
R.J. Taylor (BNFL, UK), V.S. Koltunov, V.I. Marchenko (Bochvar All-Russia Research Institute of Inorganic Materials, Russia), C. Boxall and S. Xiao (University of Central Lancashire, UK)

***Study on U Crystallization for Advanced Reprocessing** · · · · · · · · · · · · · · · · · · · 213
K. Nomura A. Shibata and A. Aoshima (JNC, Japan)

Development of New Reprocessing Technology, FLUOREX, for LWR Fuel Cycle –Hybrid Process of Fluoride Volatility and Solvent Extraction– · · · · · · · · · · · · · · · · · · · 217
O. Amano (TEPCO, Japan), F. Kawamura, T. Fukasawa, and A. Sasahira (Hitachi, Ltd., Japan)

An Advanced Aqueous Process for Nuclear Fuel Reprocessing · · · · · · · · · · · · · · · · 225
Y.-Z. Wei, T. Arai, H. Hoshi, M. Kumagai (IRI, Japan), A. Bruggeman, M. Gysemans (SCK·CEN, Belgium) and T. Sawa (Hitachi, Ltd., Japan)

***R&D of the Partitioning of the Long-lived Radionuclides in France** · · · · · · · · · · · · · 237
M. Lecomte, P. Baron, and M. Masson (CEA, France)

***Overview of the Research Activity in Partitioning at Institute of Nuclear Energy Technology** · 239
C. Song (Tsinghua Univ., China)

UNEX Process Testing of the Removal of Cesium, Strontium, and Actinide Elements from Radioactive Acidic Waste · 247
V.N. Romanovskiy, V.A. Babain, V.M. Esimantovskiy, I.V. Smirnov, B.N. Zaitsev (KRI, Russia), R.S. Herbst, J.D. Law and T.A. Todd (Bechtel BWXT Idaho, USA)

Actinide Separation by TODGA Extraction · 255
Y. Morita, Y. Sasaki and S. Tachimori (JAERI)

***Systematic Characteristics of Lanthanides and Actinides in Pyrochemical and Aqueous Conditions** · 261
H. Yamana (Kyoto Univ., Japan)

TRU Recovery from HLLW by a Pyrometallurgical Process · · · · · · · · · · · · · · · · · · 263
M. Kurata, K. Kinoshita and T. Inoue (CRIEPI, Japan)

New Developments in Dicarbollide Extractions · 273
J. Rais, P. Selucky, N. Sistkova (NRI-Rez, Czech Republic), J. Plesek, B. Grüner and B. Casensky (Institute of Inorganic Chem. CAS, Czech Republic)

Aggregation of the Neodymium Complexes of HDEHP, Cyanex 272, Cyanex 302, and Cyanex 301 in Toluene · 281
M. P. Jensen, R. Chiarizia, V. Urban and K. L. Nash (ANL, USA)

* Invited paper

Radioactive Waste Disposal · 289
Session Coordinators: H. Ogawa and H. Kimura
***Overview of the Main Results Concerning Waste Management in France** · · · · · · · · · 291
Ph. Leconte (CEA, France)

R&D on Disposal Concept for High-level Radioactive Waste: Technical Subject on HLW Disposal at Coastal Area in Japan · 293
M. Kawanishi, T. Hasegawa (CRIEPI, Japan), T. Igarashi (Hokkaido Univ., Japan), H. Tsuchi (NUMO, Japan) and F. Ono (TEPCO, Japan)

Separated Disposal of HLW Wastes for Reducing the Total Occupational Area of the Repository · 301
T. Ohe, K. Nakamura, A. Tsukagoshi and T. Nishiyori (Tokai Univ., Japan)

Wastes Generated by Application of JAERI Partitioning-transmutation System to High Level Radioactive Waste · 309
S. Nakayama, Y. Morita, K. Nishihara, H. Hayashi, and O. Shirai (JAERI)

***Status and Future Needs in Actinide Chemistry for Performance Assessment of Nuclear Waste Disposal** · 315
D. Rai (PNNL, USA) and M. Yui (JNC, Japan)

***Is Thermodynamic of Actinides Applicable to Natural Dynamic Systems?** · · · · · · · · · 323
J. I. Kim (FZK, Germany)

Present Status of the Study on Radionuclide Diffusion in Barrier Materials · · · · · · · · · 325
T. Yamaguchi and S. Nakayama (JAERI)

Overview of Waste Form Degradation Process Models for Performance Assessment · · · · · 333
F. M. G. Wong (Stone & Webster, Inc., USA), C. Stockman, R. Rechard, and P. Brady (SNL, USA)

***Thermodynamic Models and Data for Assessing Radionuclide Migration in the Near Field : Uses and Limitations** · 341
M. Ochs (BMG Engineering Ltd., Switzerland)

The Role of Titanate Ceramics in Immobilisation of Wastes Arising from Partitioning and Weapons Disposition · 349
K.P. Hart, Y. Zhang, B.D. Begg, Z. Aly, A. Brownscombe, R. A. Day, M.W.A. Stewart, G.R. Lumpkin, E. R. Vance and A. Jostsons (ANSTO, Australia)

Field Test of Nuclide Migration in Bentonite-based Materials at Aerated Zone - Cooperative Research Program on Field Migration Test between CIRP and JAERI - · · · · · · · · · · · 355
Z. Fan, A. Cui, C. Gu, Y. Zhao, Q. Sun (CIRP, China), M. Mukai, T. Maeda, J. Matsumoto, T. Tanaka, and H. Ogawa (JAERI)

Recent Activities at Underground Research Laboratories in Japan · · · · · · · · · · · · 361
K. Aoki (JNC, Japan)

* Invited paper

TRU Chemistry · · · 363
Session Coordinators: S. Nakayama and K. Minato
***Molecular Interfacial Reactions between Plutonium and Manganese Oxide Hydroxide Surfaces** · · · 365
H. Nitsche (LBNL, USA)

Microbial Transformations of Radionuclides in Transuranic Wastes · · · 367
A. J. Francis (BNL, USA)

Electrochemical Investigation of Actinide Ions for Redox Flow Battery · · · 375
T. Yamamura, N. Watanabe and Y. Shiokawa (Tohoku Univ., Japan)

Supercritical Fluid Technology for Advanced Nuclear Fuel Cycle · · · 381
Z. Yoshida, Y. Meguro, S. Iso, T. Kimura (JAERI), O. Tomioka, Y. Enokida, I. Yamamoto (Nagoya Univ., Japan), J. Ougiyanagi, and K. Ohashi (Ibaraki Univ., Japan)

4. Poster Session · · · 389
Criticality Safety · · · 389

Reactivity Effect of Spent Fuel Due to Spatial Distributions of Coolant Temperature and Burnup · · · 391
T. Hayashi, Y. Yamane (Nagoya Univ., Japan), K. Suyama (OECD/NEA) and H. Mochizuki (The Japan Research Institute, Ltd., Japan)

Reactivity Effect of Axial Burnup Shapes for a Realistic PWR Spent Fuel Transport Cask · · · 399
H.A. Tuan, H. Okuno and Y. Nomura (JAERI)

Calculation of OECD/NEA Source Convergence Benchmark Problem No.1 by Using MCNP and Solving Fission Matrix Equation · · · 407
T. Kuroishi and Y. Nomura (JAERI)

The Calculation Results of OECD/NEA Source Convergence Benchmark Problem No.2 and No.4 by Using MCNP · · · 415
T. Kiyosumi and Y. Miyoshi (JAERI)

Critical and Subcritical Mass Calculations of Fissionable Nuclides Based on JENDL-3.2 · · · 423
H. Okuno (JAERI) and H. Kawasaki (CRC Solutions Institute, Inc., Japan)

Current Status of Criticality Safety Benchmarks for Single Core Composed of Low Enriched Uranyl Nitrate Solution Using STACY · · · 431
Y. Miyoshi and T. Yamamoto (JAERI)

Study on Release Behavior of Radioactive Noble Gases and Iodine Species from Fuel Solution under Simulated Nuclear Criticality Accident · · · 439
H. Abe, S. Tashiro, T. Koike, S. Okagawa and G. Uchiyama (JAERI)

* Invited paper

Development of Solution Behavior Observation System under Criticality Accident Conditions · 447
A. Ohno, H. Yanagisawa, K. Ogawa, E. Aizawa and K. Sakuraba (JAERI)

Measurement of Power Profiles for Long-sustained Criticality Accident Using TRACY · · · 453
K. Nakajima, S. Watanabe, Y. Miyoshi, K. Ogawa and A. Ohno (JAERI)

Power Profile Evaluation of the JCO Precipitation Vessel Based on Record of the Gamma-ray Monitor · · · 459
K. Tonoike, T. Nakamura, Y. Yamane and Y. Miyoshi (JAERI)

Basic Test on Cooling Characteristics of JCO Precipitation Vessel Using a Mock-up Device · · 467
S. Watanabe, Y. Miyoshi, Y. Yamane and H. Shimizu (JAERI)

Separation Process · · · 473

Evaluation of Safety Limit for Handling of Hydroxylamine Nitrate/Nitric Acid Solution as a Plutonium Reductant · · · 475
S. Sugikawa, M. Umeda, J. Sekino (JAERI), T. Matsuda and T. Kodama (JNFL, Japan)

Evaluation Models of Inorganic Solids as Separation and Containment Media · · · 481
M.Tsuji (TIT, Japan)

Spent Fuel Test on Extraction in Advanced Reprocessing Process · · · 489
S. Hotoku, G. Uchiyama, T. Asakura, M. Sato, Y. Itoh and H. Mineo (JAERI)

Fundamental Study on the Control of Minor Nuclides (Np, Tc) Behavior by Electrolytic Reduction · · · 497
T. Asakura (JAERI), H. Hoshi, Y.-Z. Wei, M. Kumagai (IRI, Japan) and G. Uchiyama (JAERI)

Study on the Adsorbent with Amidoxime Functional Group Utilized to Recover Useful Metals from Sea-water · · · 503
T. Asakura, D. T. Hong, A. Zhang and G. Uchiyama (JAERI)

Spent Fuel Dissolution Test Including Dissolver Off-gas Treatment in the NUCEF Alpha-gamma Cell: Spent Fuels with Burnups up to 44 $GWDT^{-1}$ · · · 511
H. Mineo, M. Iizuka, S. Fujisaki, H. Isogai, S. Hotoku, T. Asakura, and G. Uchiyama (JAERI)

On the Rate of Reaction between Plutonium Dioxide and Silver (II) · · · 519
P.J.W. Rance (BNFL, UK) and G.P. Nikitina (KRI, Russia)

Examination of Reaction Conditions for Oxidation of Salt Waste · · · 527
F. Sato, M. Myochin (JNC, Japan), H. Terunuma and O. Arai (KAKEN Co., Japan)

Extraction of Radionuclides from Nitric Acid Solutions by a TRUEX Solvent · · · 533
T. Fujii, H. Yamana, and H. Moriyama (Kyoto Univ. , Japan)

Evaluation of Confinement Capability of Radioactive Materials under the Fire Accident in Nuclear Fuel Facility with CELVA-1D · · · 541
K. Watanabe, H. Abe, J. Takada, S. Tashiro and G. Uchiyama (JAERI)

Clogging Characteristics of Ventilation Filter under the Fire Accident · · · · · · · · · · 549
S. Tashiro, K. Watanabe, H. Abe, J. Takada and G. Uchiyama (JAERI)

Study on Supercritical Fluid Extraction of Uranium and Transuranium Complexes with β-diketones and Other Complexones as Applied to Decontamination · · · · · · · · · · · 557
A.Yu. Shadrin, A.A. Murzin, V.N. Romanovsky and V.A. Starchenko (KRI, Russia)

Thermodynamic Study of Am (III) and Eu(III) Extraction by Iso-butyl-bis-triazinyl-pyridine · 567
C. Hill and C. Roube (CEA, France)

SANEX-BTP Process Development Studies · 573
C. Hill, D. Guillaneux, L. Berthon and C. Madic (CEA, France)

Development of Fractionation Process of ^{129}I in Preparation for Transmutation of LLFP · · · 579
K. Takeshita and Y. Nakano (TIT, Japan)

Research on Pyrochemical Process for Nitride Fuel at JAERI · · · · · · · · · · · · · · · 589
Y. Arai, T. Iwai, O. Shirai, H. Hayashi and K. Minato (JAERI)

TRU-HITEC - A New Facility for TRU High Temperature Chemistry · · · · · · · · · · · 597
K. Minato, M. Akabori, A. Maeda (JAERI), S. Miyamoto (JAPC, Japan), O. Amano (TEPCO, Japan) and T. Arai (Tohoku Electric Power Co., Japan)

Development of Solvent Washing Process Using Butylamine Compounds · · · · · · · · · · 603
Y. Itoh, K. Kamei, S. Hotoku, T. Asakura, H. Mineo and G. Uchiyama (JAERI)

Radioactive Waste Disposal · 609

Field Tracer Migration Test in Aquifer: Tracer Migration Test in Assembly - Cooperative Research Program on Safety Assessment Methodology between CIRP and JAERI - · · · · · 611
Yang Yuee, Wang Zhiming, Liu Chunli, Jing Ling, Jiang Hong (CIRP, China), M. Mukai, T. Maeda, J. Matsumoto, T. Tanaka and H. Ogawa (JAERI)

Diffusion Coefficient Test of ^{237}Np in Bentonite Backfill Materials · · · · · · · · · · · · · 621
Anxi Cui, Zhiwen Fan, Jinsheng Zhang, Cunli Gu (CIRP, China), M. Mukai, T. Maeda, J. Matsumoto, T. Tanaka and H. Ogawa (JAERI)

Study on the Distribution Coefficient for Evaluation of Neptunium Migration in Loess Media - Cooperative Research Program on Field Migration Test between CIRP and JAERI - · · · · 627
T. Tanaka, T. Maeda, M. Mukai, J. Matsumoto, H. Ogawa (JAERI), Zhentang Li, Hongqing Zhang, Xudong Wang, Anxi Cui and Liangtian Guo (CIRP, China)

Analysis of Field Test of Nuclide Migration in Aerated Loess Layer - Cooperative Research Program on Field Migration Test between CIRP and JAERI - · · · · · · · · · · · · · · · 635
M. Mukai, T. Tanaka, T. Maeda, J. Matsumoto, H. Ogawa (JAERI), Jinsheng Wang, Shushen Li, Yingjie Zhao, Qinghua Wu and Zhiming Wang (CIRP, China)

Development of Airless Core Sampling System (ALCS) for Safety Assessment of Geological Disposal of HLW · · · 643
K. Araki, A. Oushika, M. Ueda and G. Okano (Chuou-Kaihatsu Co., Japan)

Correlation between Molecular Size and Functional Groups of Humic Acid on the Complexation with ^{237}Np, ^{238}Pu and ^{241}Am · · · 651
T. Tanaka, S. Nagao and H. Ogawa (JAERI)

Sorption Behavior of Neptunium onto Smectite under Reducing Conditions in Carbonate Media · · · 659
A. Kitamura, T. Tomura and T. Shibutani (JNC, Japan)

Effect of Temperature on the Sorption of Neptunium on Magnetite · · · 667
K. Nakata, S. Nagasaki, S. Tanaka (Univ. of Tokyo, Japan), Y. Sakamoto, T. Tanaka and H. Ogawa (JAERI)

The Effects of Silica Sand Content and Temperature on Diffusion of Selenium in Compacted Bentonite under Reducing Conditions · · · 675
H. Sato and S. Miyamoto (JNC, Japan)

Colloids-associated Concentrations Model and Experimental Studies for a Waste Form Degradation Process Model · · · 683
F.M.G. Wong[1], C. Stockman[2], C. Mertz[3], S. Alcorn[4], and R. Aguilar[2] ([1]Stone & Webster, Inc., USA, [2]SNL, USA, [3]ANL, USA, [4]Management Solutions, USA)

Effects of Iron on Leaching Behavior of Slag Layer of Molten Solidified Products · · · 691
T. Maeda, T. Banba and H. Ogawa (JAERI)

Review of Immobilization Techniques of Radioactive Iodine for Geological Disposal · · · 697
H. Kato, O. Kato and H. Tanabe (RWMC, Japan)

TRU Chemistry · · · 705

Actinide Chemistry in Concentrated Alkali: Implications for Cleanup of Processing Plants · · · 707
K.L. Nash, A.V. Guelis, M.P. Jensen, J.C. Sullivan, A.H. Bond (ANL, USA), A. Yu. Garnov and L. Rao (LBNL, USA)

Electrochemistry Studies of $UO_2(acac)_2L$ (acac = acetylacetonate, L = dimethyl sulfoxide, N,N-dimethyl formamide, tetrahydrofuran) Complexes in Non-aqueous Solvents · · · 709
S. Kim, G. Uchiyama (JAERI), K. Mizuoka and Y. Ikeda (TIT, Japan)

目　次

序文

1. オープニングセッション · 1

開会の挨拶 · 3
前田　充（原研）

NUCEF における燃料サイクル安全性研究の進展 · 7
藤根幸雄（原研）

2. プレナリーセッション · 17

*米国の臨界安全性に関わる経験、ニーズ及び世界経済における未来 · · · · · · · · · · · · · 19
C. M. Hopper (ORNL, USA)

*高レベル廃棄物の群分離における湿式、乾式プロセスに関する研究の国際的動向 · · · · · · · · 27
C. Madic (CEA, France)

*フィンランドの使用済燃料地層処分に関する決定原則 · · · · · · · · · · · · · · · · · · · 39
J. Vira (Posiva Oy, Finland)

*原子力概念のコミュニケーション；天然ラボの利用 · 47
J.M. West, W.R. Alexander, K. Kaku, I.G. Mckinley (NAGRA, Switzerland) and A. Shimmura (Obayashi Corp., Japan)

3. 口頭発表セッション · 55
臨界安全性
セッションコーディネータ：野村　靖、三好慶典

*米国における臨界安全総意標準の開発と適用 · 57
T. McLaughlin (LANL, USA)

*日本における核燃料輸送規制について · 65
福田佐登志（電中研）

*英国の臨界安全に関わる過去、現在、未来にわたる展望 · · · · · · · · · · · · · · · · · · 73
D.N. Simister (Health & Safety Executive , UK)

*原研における燃焼度クレジット評価手法の開発 · 81
野村　靖、奥野　浩、須山賢也（原研）

燃焼度クレジット導入に関する実験計画 · 91
P.D'hondt, K. van der Meer, P. Baeten (SCK-CEN, Belgium), D. Marloye, B. Lance and J. Basselier (Belgonucleaire , Belgium)

臨界安全解析のための核種燃焼生成計算コードの日仏比較 · · · · · · · · · · · · · · · · · 99
岩崎智彦、平泉宏明（東北大）、G. Youinou (CEA, France)

高精度アナログ型中性子モニタシステム · 105
小田直敬、北　好夫、石澤和哉（東芝）

*招待講演

*中性子測定と臨界安全評価の高品質化による MOX 加工施設の安全性向上 · · · · · · · · · · · · 111
A. Renard, P.Kockerols, H. Libon and D. Marloye (Belgonucleaire, Belgium)

MOX 燃料の未臨界制限値 · 125
櫻井俊吾、三竹 晋 (NUPEC)

プルトニウム燃料第三開発室における臨界安全管理 · 133
蜷川純一、高橋三郎、山本 裕、藤原茂雄、国安和房、大谷哲雄（サイクル機構）

臨界安全のための工程管理改良に向けた保障措置用溶液燃料監視装置の応用 · · · · · · · · · · 141
B. A. Hunt, D. Landat, L. Dechamp and M. Caviglia (EC-Joint Research Centre, Italy)

*未臨界測定法とその応用 · 147
T.E. Valentine (ORNL, USA)

過渡臨界解析コード FETCH の TRACY のデータ及びドシメトリーへの適用 · · · · · · · · · · · 155
C.C. Pain[1], Y. Yamane[2], C.R.E.de Oliveira[1] and A.J.H. Goddard[1] ([1]ICST, UK, [2]JAERI)

高次モードを伴う中性子源増倍法による未臨界度測定 · 165
三澤 毅（京大）

JCO 臨界事故における沈殿槽の核熱特性に関する評価 · 173
三好慶典、山本俊弘、中島 健、山根祐一、渡辺庄一（原研）

分離プロセス · 181
セッションコーディネータ：内山軍蔵、森田泰治

*COGEMA における再処理プロセスについての研究開発の現状 · · · · · · · · · · · · · · · · 183
M.F. Debreuille, P. Pradel (COGEMA, France) and F. Drain (SGN, France)

*SUPERPUREX-原子力発電所使用済燃料から長寿命放射性核種を回収・分離するTBP溶媒と共存できるプロセス · 189
B. Ya. Zilberman, Yu.S. Fedorov, E.N. Mishin, L.V. Sytnik, O.V. Shmidt, D.N. Kukharev, N.D. Goletsky, R.G. Glekov, Yu.V. Palenik and S.Yu. Sukhareva (KRI, Russia)

高度化 PUREX プロセスとしての PARC プロセス · 197
内山軍蔵、峯尾英章、朝倉俊英、宝徳忍、飯塚勝、藤崎進、磯貝光、伊東芳紀、佐藤真人、細谷哲章（原研）

*アクチノイドイオンの硝酸／TBP の単相および二相系における酸化－還元反応の最近の研究 · · ·205
R.J. Taylor (BNFL, UK), V.S. Koltunov, V.I. Marchenko (Bochvar All-Russia Research Institute of Inorganic Materials, Russia), C. Boxall and S. Xiao (University of Central Lancashire, UK)

*先進再処理のためのウラン晶析技術の研究 · 213
野村和則、柴田淳広、青嶋 厚（サイクル機構）

軽水炉サイクル用の新しい再処理技術、FLUOREX 法、の開発―フッ化物揮発法と溶媒抽出法のハイブリッド再処理法― · 217
天野治（東京電力）、河村文雄、深澤哲生、笹平朗（日立製作所）

*招待講演

核燃料再処理のための先進湿式プロセス ・・・・・・・・・・・・・・・・・・・・・・・・・・・225
韋 悦周、新井 剛、星 陽崇、熊谷幹郎（産業創造研究所）、A. Bruggeman, M. Gysemans (SCK·CEN, Belgium)、澤 俊雄（日立製作所）

*フランスにおける長寿命放射性核種群分離の研究開発 ・・・・・・・・・・・・・・・・・・・・・237
M. Lecomte, P. Baron, M. Masson (CEA, France)

*清華大学原子力エネルギー技術研究所における群分離研究開発の概要 ・・・・・・・・・・・・・239
C. Song (Tsinghua Univ., China)

酸性廃液に含有されるセシウム、ストロンチウム及びアクチニド元素除去のための UNEX プロセス試験 ・・・247
V.N. Romanovskiy, V.A. Babain, V.M. Esimantovskiy, I.V. Smirnov, B.N. Zaitsev (KRI, Russia), R.S. Herbst, J.D. Law and T.A. Todd (Bechtel BWXT Idaho, USA)

TODGA 抽出によるアクチノイドの分離 ・・・・・・・・・・・・・・・・・・・・・・・・・・・255
森田泰治、佐々木祐二、館盛勝一（原研）

*乾式と湿式でのアクチニドとランタニドの化学系統性 ・・・・・・・・・・・・・・・・・・・・261
山名 元（京大）

乾式分離法による高レベル廃液からの TRU の回収 ・・・・・・・・・・・・・・・・・・・・・・263
倉田正輝、 木下賢介、井上 正（電中研）

ジカルボリド抽出法開発の進展 ・・・・・・・・・・・・・・・・・・・・・・・・・・・・・・・273
J. Rais, P. Selucky, N. Sistkova (NRI-Rez, Czech Republic), J. Plesek, B. Grűner and B. Casensky (Institute of Inorganic Chem. CAS, Czech Republic)

トルエン中の HDEHP, Cyanex 272, Cyanex 302 及び Cyanex 301 とのネオジム錯体の凝集 ・・・・281
M. P. Jensen, R. Chiarizia, V. Urban and K. L. Nash (ANL, USA)

放射性廃棄物処分 ・・・・・・・・・・・・・・・・・・・・・・・・・・・・・・・・・・・・・・・289
セッションコーディネータ：小川弘道、木村英雄

*フランスにおける放射性廃棄物管理 ・・・・・・・・・・・・・・・・・・・・・・・・・・・・・291
Ph. Leconte (CEA, France)

高レベル放射性廃棄物処分概念に関する技術開発 わが国における沿岸域処分に係わる技術課題 ・・・293
河西 基、長谷川琢磨 （電中研）、五十嵐敏文（北大）、土 宏之（原子力発電環境整備機構）、小野文彦（東電）

処分場面積削減のための高レベル放射性廃棄物分離型処分 ・・・・・・・・・・・・・・・・・・・301
大江俊昭、中村清懇、塚越淳史、西依毅弘（東海大）

原研型システムによる高レベル放射性廃棄物の分離変換から発生する廃棄物 ・・・・・・・・・309
中山真一、森田泰治、西原健司、林 博和、白井 理（原研）

*放射性廃棄物処分の性能評価のためのアクチニド化学の現状と今後の必要性 ・・・・・・・・・315
D. Rai (PNNL, USA) and M. Yui (JNC, Japan)

*招待講演

*非平衡系である天然にアクチニドの熱力学は適用可能か？ ・・・・・・・・・・・・・・・・・・・・・323
J. I. Kim (FZK, Germany)

バリア材中における放射性核種の拡散に関する研究の現状 ・・・・・・・・・・・・・・・・・・・・325
山口徹治、中山真一（原研）

性能評価のための廃棄体劣化モデル ・・・・・・・・・・・・・・・・・・・・・・・・・・・・・・・333
F.M.G. Wong (Stone & Webster, Inc., USA), C. Stockman, R. Rechard, and P. Brady (SNL, USA)

*ニアフィールドにおける放射性核種移行評価のための熱力学モデルとデータ：その利用と限界・・341
M. Ochs（BGM Engineering Ltd., Switzerland）

群分離および兵器解体から発生する廃棄物固化のためのチタンセラミックの役割 ・・・・・・・349
K.P. Hart, Y. Zhang, B.D. Begg, Z. Aly, A. Brownscombe, R. A. Day, M. W. A. Stewart, G. R. Lumpkin, E. R. Vance and A. Jostsons (ANSTO, Australia)

通気層におけるベントナイト材中の核種移行野外試験　野外移行試験に関する日中協力研究 ・・・355
Z. Fan, A. Cui, C. Gu, Y. Zhao, Q. Sun (CIRP, China)、向井雅之、前田敏克、松本潤子、田中忠夫、小川弘道（原研）

我が国の深地層の研究施設における最近の活動 ・・・・・・・・・・・・・・・・・・・・・・・・・361
青木和弘（サイクル機構）

TRU 化学 ・・・363
セッションコーディネータ：中山真一、湊　和生

*プルトニウムとマンガン酸化物・水酸化物表面との界面反応に関する分子レベルの研究 ・・・・365
H. Nitsche (LBNL, USA)

TRU 廃棄物中の放射性核種の微生物による変態 ・・・・・・・・・・・・・・・・・・・・・・・・367
A. J. Francis (BNL, USA)

アクチニドイオンの電気化学的検討とレドックスフロー電池 ・・・・・・・・・・・・・・・・・・375
山村朝雄、渡辺宣隆、塩川佳伸（東北大）

核燃料サイクルの高度化のための超臨界流体技術 ・・・・・・・・・・・・・・・・・・・・・・・381
吉田善行、目黒義弘、磯　修一、木村貴海（原研）、富岡　修、榎田洋一、山本一良（名古屋大）、扇柳仁、大橋弘三郎（茨城大）

4. ポスターセッション ・・・・・・・・・・・・・・・・・・・・・・・・・・・・・・・・・・・・・389
臨界安全性 ・・・389

冷却材温度分布と燃焼度分布が使用済燃料の反応度に及ぼす影響 ・・・・・・・・・・・・・・・391
林　高史、山根義宏（名古屋大）、須山賢也（OECD/NEA）、望月弘樹（日本総研）

軸方向燃焼度分布非対称性が現実的な PWR 使用済燃料輸送容器の反応度に及ぼす影響 ・・・・・399
H.A. Tuan, 奥野　浩、野村　靖（原研）

MCNP コードと核分裂源マトリクスの解による OECD/NEA 臨界収束性ベンチマーク問題
No. 1 の計算 ・・407
黒石　武、野村　靖（原研）

*招待講演

OECD/NEA ソース収束性ベンチマーク問題 No.2 と No.4 に対する解析 ・・・・・・・・・・・・・・・ 415
清住武秀、三好慶典（原研）

核分裂可能な核種の臨界及び未臨界質量に関する JENDL-3.2 に基づく計算 ・・・・・・・・・・・ 423
奥野　浩（原研）、川崎弘光（CRC ソリューションズ）

STACY における低濃縮硝酸ウラン溶液単一炉心の臨界安全ベンチマークの現状 ・・・・・・・・・・ 431
三好慶典、山本俊弘（原研）

臨界事故時の溶液燃料からの放射性希ガス及びヨウ素の放出挙動に関する研究 ・・・・・・・・・ 439
阿部　仁、田代信介、小池忠雄、岡川誠吾、内山軍蔵（原研）

臨界事故条件下の溶液挙動観察システムの開発 ・・・・・・・・・・・・・・・・・・・・・・・・ 447
大野秋男、柳澤宏司、小川和彦、会澤栄寿、桜庭耕一（原研）

TRACY を用いた長時間継続する臨界事故の出力変化の測定 ・・・・・・・・・・・・・・・・・・・ 453
中島　健、渡辺庄一、三好慶典、小川和彦、大野秋男（原研）

ガンマ線エリアモニターの観測値に基づく JCO 沈殿槽出力履歴の評価 ・・・・・・・・・・・・・ 459
外池幸太郎、中村剛実、山根祐一、三好慶典（原研）

モックアップ試験装置を用いた JCO 沈殿槽の冷却特性に関する基礎試験 ・・・・・・・・・・・・ 467
渡辺庄一、三好慶典、山根祐一、清水　宏（原研）

分離プロセス ・・ 473

プルトニウム還元剤硝酸ヒドロキシルアミン／硝酸溶液の取扱いにおける安全限度の評価 ・・・ 475
杉川　進、梅田　幹、関野純一（原研）、松田孝司、小玉貴司（日本原燃）

分離、閉じ込め媒体としての無機固体の評価モデル ・・・・・・・・・・・・・・・・・・・・・・ 481
辻　正道（東工大）

高度化再処理プロセスにおける使用済燃料抽出試験 ・・・・・・・・・・・・・・・・・・・・・・ 489
宝徳　忍、内山軍蔵、朝倉俊英、佐藤真人、伊東芳紀、峯尾英章（原研）

電解還元によるマイナー核種（Np、Tc）の挙動制御に関する基礎研究 ・・・・・・・・・・・・・ 497
朝倉俊英[1]、星　陽崇[2]、韋　悦周[2]、熊谷幹郎[2]、内山軍蔵[1]（[1]原研、[2]産業創造研究所）

アミドキシム官能基を有する吸着剤を用いた海水からの有用金属回収についての研究 ・・・・・・ 503
朝倉俊英、 D. T. Hong、A. Zhang、内山軍蔵（原研）

NUCEF $\alpha\gamma$ セルにおける使用済燃料溶解および溶解オフガス処理試験：燃焼度 44 $GWDT^{-1}$ ・・・・・ 511
峯尾英章、飯塚　勝、藤崎　進、磯貝　光、宝徳　忍、朝倉俊英、内山軍蔵（原研）

電解生成した銀（II）を用いた PuO_2 の溶解速度 ・・・・・・・・・・・・・・・・・・・・・・・ 519
P.J.W. Rance (BNFL, UK) and G.P. Nikitina (KRI, Russia)

塩廃棄物の酸化反応条件の研究 ・・・・・・・・・・・・・・・・・・・・・・・・・・・・・・・・ 527
佐藤史紀、明珍宗孝（サイクル機構）、照沼　仁、新井　修（化研）

TRUEX 溶媒による硝酸からの放射性核種の抽出 ・・・・・・・・・・・・・・・・・・・・・・・・ 533
藤井俊行、山名　元、森山裕丈（京大）

CELVA-1Dを用いた核燃料施設における火災事故時の放射性物質閉じ込め性能評価 ・・・・・・・・541
渡邊浩二、阿部 仁、高田準一、田代信介、内山軍蔵（原研）

火災事故時における換気フィルターの目詰まり特性評価 ・・・・・・・・・・・・・・・・・・・・・・549
田代信介、渡邊浩二、阿部 仁、高田準一、内山軍蔵（原研）

除染への応用としてのウランおよび超ウラン元素のβジケトンおよびその他の錯体の超臨界流体抽出の研究 ・・557
A.Yu. Shadrin, A.A. Murzin, V.N. Romanovsky and V.A. Starchenko (KRI, Russia)

BTPによるAm(III)およびEu(III)抽出についての熱力学的研究 ・・・・・・・・・・・・・・・・・・567
C. Hill and C. Roube (CEA, France)

SANEX-BTPを用いたプロセスの開発研究 ・・・・・・・・・・・・・・・・・・・・・・・・・・・・・573
C. Hill, D. Guillaneux, L. Berthon and C. Madic (CEA, France)

長半減期FPの核変換処理システム構築のための^{129}I分別回収プロセスの開発 ・・・・・・・・・・579
竹下健二、中野義夫（東工大）

原研における窒化物燃料の高温化学再処理の研究 ・・・・・・・・・・・・・・・・・・・・・・・・589
荒井康夫、岩井 孝、白井 理、林 博和、湊 和生（原研）

TRU-HITEC- TRU高温化学のための新しい実験設備 ・・・・・・・・・・・・・・・・・・・・・・・・597
湊 和生、赤堀光雄、前多 厚（原研）、宮本智司（日本原子力発電）、天野 治（東電）、新井智昭（東北電力）

ブチルアミン化合物による溶媒洗浄プロセスの開発 ・・・・・・・・・・・・・・・・・・・・・・・603
伊東芳紀、亀井一成、 宝徳 忍、朝倉俊英、峯尾英章、内山軍蔵（原研）

放射性廃棄物処分 ・・609

帯水層における野外トレーサ試験：アセンブリ中移行試験 野外移行試験に関する日中協力研究 ・・・・・・・・・・・・・・・・・・・・・・・・・・・・・・・・・・・・・・611
Yang Yuee, Wang Zhiming, Liu Chunli, Jing Ling, Jiang Hong (CIRP, China), 向井雅之、前田敏克、松本潤子、田中忠夫、小川弘道（原研）

ベントナイト材中における^{237}Npの拡散試験 ・・・・・・・・・・・・・・・・・・・・・・・・・・621
Anxi Cui, Zhiwen Fan, Jinsheng Zhang, Cunli Gu (CIRP, China), 向井雅之、前田敏克、松本潤子、田中忠夫、小川弘道（原研）

黄土層中におけるネプツニウムの移行評価のための分配係数に関する研究 野外移行試験に関する日中協力研究 ・・・・・・・・・・・・・・・・・・・・・・・・・・・・・・・・・・・・・・627
田中忠夫、前田敏克、向井雅之、松本潤子、小川弘道（原研）、Zhentang Li, Hongqing Zhang, Xudong Wang, Anxi Cui, Liangtian Guo (CIRP, China)

通気層黄土中における核種移行野外試験の解析 野外移行試験に関する日中協力研究 ・・・・・635
向井雅之、田中忠夫、前田敏克、松本潤子、小川弘道（原研）、Jinsheng Wang, Shushen Li, Yingjie Zhao, Qinghua Wu, Zhiming Wang (CIRP, China)

無酸素ボーリングコア採取システム(ALCS)の開発と高レベル放射性廃棄物地層処分安全評価への適用性 ・・643
荒木邦夫、大鹿明文、上田正人、岡野軍治（中央開発）

^{237}Np, ^{238}Pu および ^{241}Am との錯生成におけるフミン酸の分子サイズと官能基の関係 ・・・・・・・651
田中忠夫、長尾誠也、小川弘道（原研）

還元条件・炭酸共存下におけるネプツニウムのスメクタイトに対する収着挙動 ・・・・・・・・・659
北村 暁、戸村 努、渋谷朝紀（サイクル機構）

マグネタイトへのネプツニウムの吸着に対する温度の効果 ・・・・・・・・・・・・・・・・・・・667
中田弘太郎 、長崎晋也、田中 知（東大）、坂本義昭、田中忠夫、小川弘道（原研）

還元条件における圧密ベントナイト中でのセレンの拡散に及ぼすケイ砂混合率および温度の影響 ・・・675
佐藤治夫、宮本真哉（サイクル機構）

廃棄体劣化モデルのためのコロイド濃度モデルと実験的研究 ・・・・・・・・・・・・・・・・・・683
F.M.G. Wong[1], C. Stockman[2], C. Mertz[3], S. Alcorn[4], and R. Aguilar[2] ([1]Stone & Webster, Inc., USA, [2]SNL, USA, [3]ANL, USA, [4]Management Solutions, USA)

溶融固化体スラグ層の浸出挙動に及ぼす鉄成分の影響 ・・・・・・・・・・・・・・・・・・・・・691
前田敏克、馬場恒孝、小川弘道（原研）

地層処分における放射性ヨウ素の固定化技術に関するレビュー ・・・・・・・・・・・・・・・・・697
加藤博康、加藤 修、田辺博三（原子力環境整備促進・資金管理センター）

TRU化学 ・・・705

濃厚アルカリ溶液中におけるアクチニド化学：プラント除染への適用 ・・・・・・・・・・・・・・707
K. L. Nash, A.V. Guelis, M.P. Jensen, J.C. Sullivan, A.H. Bond (ANL, USA), A. Yu. Garnov, L. Rao (LBNL, USA)

非水溶媒中における $UO_2(acac)_2L$ (acac = acetylacetonate, L = dimethyl sulfoxide, N,N-dimethyl formamide, tetrahydrofuran) 錯体の電気化学的研究 ・・・・・・・・・・・・・・・・・・・・・・・709
金 聖潤、内山軍蔵（原研）、水岡康一朗、池田泰久（東工大）

Members of Steering Committee:

A. Suzuki (Chairman, University of Tokyo)
K. Higashi (Kyoto University)
M. Hirano (NUPEC)
T. Kawata (JNC)
H. Ojima (JNC)
S. Matsumoto (Saitama University)
S. Matsuoka (JNFL)
H. Moriyama (Kyoto University)
S. Muto (FEPC)
K. Nishina (Aichi Shukutoku University)
Y. Yamane (Nagoya University)
A. Yamato (AESJ)
S. Fujine (JAERI)
K. Noda (JAERI)
Y. Suzuki (JAERI)
I. Takeshita (JAERI)
M. Tanaka (JAERI)

Program Coordinators:

J. Bouchard (Director, Direction de l'Energie Nucleaire, CEA, FRANCE)
S. Ion (Director, Technology & Operations, BNFL, UK)
J.A. Lake (2000-01 President of American Nuclear Society, USA)
I. Takeshita (Deputy Director General, Tokai Research Establishment, JAERI)

Members of Symposium Working Group (JAERI's Staffs):

S. Fujine (Leader, Conference Secretary)
S. Dojiri
T. Banba (Editor of Proceedings)
Y. Nomura (Session Coordinator)
Y. Miyoshi (Session Coordinator)
G. Uchiyama (Session Coordinator)
Y. Morita (Session Coordinator)
H. Ogawa (Session Coordinator)
H. Kimura (Session Coordinator)
S. Nakayama (Session Coordinator)
K. Minato (Session Coordinator)
H. Mineo
T. Tanaka
A. Yamada
T. Sato
T. Kaneko
K. Tonoike
Y. Tsubata (Editor of Proceedings)
H. Yanagisawa
K. Kobayashi

Preface

The International Symposium NUCEF2001 was held in Tokai-mura, Japan from October 31 to November 2, 2001. The subtitle of the symposium was "Scientific Bases for Criticality Safety, Separation Process and Waste Disposal". The first NUCEF International Symposium was held in October 1995 at the opportunity of the start of hot operation in NUCEF facility, and the second symposium was held in November 1998. NUCEF2001 the third symposium opened with the Opening Address by Dr. Mitsuru Maeda, Director General of Tokai Research Establishment, Japan Atomic Energy Research Institute and with the Welcome Address by Professor Atsuyuki Suzuki of the University of Tokyo, Chairman of Steering Committee of this symposium.

This symposium was successful as the international forum for the exchange of scientific information on R&D for nuclear fuel cycle and radioactive waste management. There were over 250 participants from 14 countries at the NUCEF 2001 symposium. The principal topics addressed in this symposium included: (1)Criticality Safety; criticality characteristics of solution fuel, phenomena of super criticality; sub criticality monitor; burn-up credit; JCO accident assessment; (2)Separation Process; new concept of reprocessing; partitioning; nuclide behavior in chemical processes; (3)Radioactive Waste Disposal; concept and option of waste disposal; performance assessment; waste management R&D, and (4)TRU Chemistry.

The chairpersons of each sessions were:

Opening Session: I. Takeshita (JAERI)

Plenary Session: K. Nishina (Aichi Shukutoku Univ., Japan), K. Higashi (Kyoto Univ., Japan)

Oral Session:

Criticality Safety- C. M. Hopper (ORNL, USA), Y. Nomura (JAERI). T. McLaughlin (LANL, USA), Y. Miyoshi (JAERI), P. d'Hondt (SCK-CEN, Belgium), M. Kanamori (JNC, Japan), A.J. Goddard (ICST, UK), K. Nakajima (JAERI),

Separation Process- R. Taylor (BNFL, UK), H. Ojima (JNC, Japan), B. Ya. Zilberman (KRI, Russia), G. Uchiyama (JAERI) C. Madic (CEA, France), S. Tachimori (JAERI), V. Romanovski (KRI, Russia), K. Minato (JAERI),

Waste Disposal- J. Vira (Posiva, Finland), S. Muraoka (NMCC, Japan), H. Moriyama (Kyoto Univ., Japan), T. Ohe (Tokai Univ., Japan), J. West (British Geological Survey, UK), T. Banba (JAERI)

TRU Chemistry- J. I. Kim (FZK, Germany), O. Tochiyama (Tohoku Univ., Japan),

We appreciate all the participants who contributed for the success of NUCEF2001 International Symposium.

This is a blank page.

1. Opening Session

This is a blank page.

OPENING ADDRESS

Mitsuru MAEDA

Director General
Tokai Research Establishment
Japan Atomic Energy Research Institute (JAERI)

Thank you Mr. Chairman.
Good morning Ladies and Gentlemen. On behalf of JAERI, I welcome you all for your participation to NUCEF2001.

This symposium is organized and sponsored by JAERI in cooperation with Atomic Energy Society of Japan (AESJ) and Division of Nuclear Fuel Cycle and Environment of AESJ. I hear from secretary that we have about 250 attendees from domestic research organizations, universities, industries, and about 40 participants from 12 over sea countries. It is a great honor for us to have so big symposium, here, Tokai Research Establishment, JAERI.

In this symposium, we discuss "Scientific basis for criticality safety, separation process and waste disposal," in nuclear fuel cycle and waste management. I believe that this NUCEF symposium provides good opportunity for the experts to exchange the newest information in this field. I think you could remember that the first NUCEF symposium was held in October 1995, at the opportunity of the start of hot operation in NUCEF facility. And we had the second symposium in November 1998. Three years have passed after the second NUCEF symposium.

In the meantime, JCO criticality accident took place in September 1999 in Tokai-mura. We are very disappointed that such a disastrous accident could happen in the vicinity of our safety research activity and feel deep regret to two workers who passed away caused by their irradiation dose in the accident. Although the NUCEF made great contribution in counter-measuring activities and investigation of the JCO accident, our hope is such an accident never happens again.

Please take a look at this picture. NUCEF is the scientific research center for the research and development in the field of nuclear fuel cycle and radioactive waste disposal. We will carry out our research in cooperation with foreign organizations, Government, Private Industries, Government-affiliated research organization and Universities. There are important subjects ahead in this field; Plutonium recycle, MOX utilization, Reprocessing and Waste management, and Transmutation. It is not exaggeration to say that the future of nuclear industry actually depends on the success of the measures to these subjects. I promise you we, JAERI, will make maximum effort to ensure the safety of future nuclear facilities and figure out the future of nuclear technology in cooperation with those who are making effort in the world.

Here, I have to express my hearty thanks to all the members of Conference Steering Committee NUCEF2001, in particular, Prof. Suzuki, Prof.Higashi and Prof. Nishina. I

appreciate Prof. Suzuki who chairs the Committee and participating today under the heavy works at his important position as a member of the Nuclear Safety Commission.

And, I express my appreciation to the members of Program Coordinators; Dr. Jacques BOUCHARD, Director, Nuclear Energy Division, CEA, FRANCE. Dr. Sue ION, Director, Technology & Operation, BNFL, UK, and Dr. James LAKES, 2000-2001 President of American Nuclear Society, USA. and Dr. Isao Takeshita, Deputy director general, Tokai research establishment, JAERI. I appreciate Dr. Takeshita who presides over the Program Coordinators. Although the other foreign Program Coordinators are not participating here today, they contributed to arrange the program of this symposium in the global perspective. They have sent us their appeal of international cooperativeness and togetherness in the nuclear fuel cycle field for promoting the research and development for the future. I have learned that international symposium ATALANTE2000 has been successfully held in south France, last year. The symposium is named after their research facility ATALANTE at Marcoule, France, just like NUCEF2001 is named after research facility NUCEF at Tokai, Japan.

I sincerely hope that NUCEF2001 will be very fruitful and successful, and lively exchange of information through three days symposium will contribute to the future research in the field of nuclear fuel cycle and waste disposal. I also hope that your stay in Japan will be very pleasant. I am afraid you would have some inconveniences because of our countermeasures against terror attack. We strongly condemn the barbarous terror attack in New York. However, here, in this symposium, let us discuss the safety of nuclear facility and secure of the future energy in the civilized manner.

Thank you very much for your kind attention.

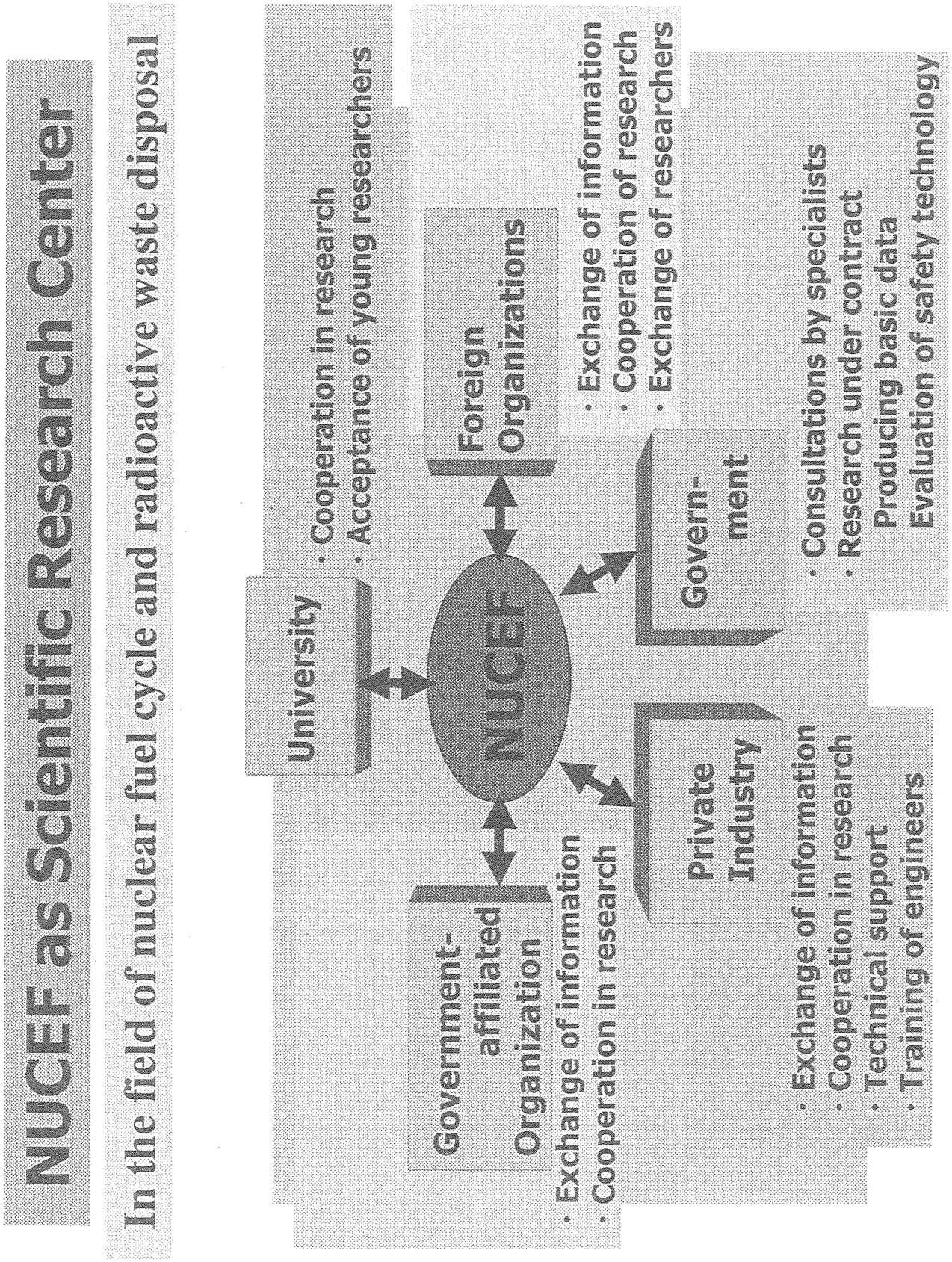
NUCEF as Scientific Research Center
In the field of nuclear fuel cycle and radioactive waste disposal
University
· Cooperation in research
· Acceptance of young researchers
Foreign Organizations
· Exchange of information
· Cooperation of research
· Exchange of researchers
NUCEF
Govern-ment
· Consultations by specialists
· Research under contract
Producing basic data
Evaluation of safety technology
Government-affiliated Organization
· Exchange of information
· Cooperation in research
Private Industry
· Exchange of information
· Cooperation in research
· Technical support
· Training of engineers

This is a blank page.

JP0250278

PROGRESS OF SAFETY RESEARCH IN NUCEF ON NUCLEAR FUEL CYCLE

Sachio FUJINE
Japan Atomic Energy Research Institute
Tokai-mura, Naka-gun, Ibaraki-ken, 319-1195 Japan
E-mail: fujine@popsvr.tokai.jaeri.go.jp

ABSTRACT

Research activities of JAERI related to nuclear fuel cycle and waste management are overviewed as the opening presentation of NUCEF2001. The third conference NUCEF2001 in this series is subtitled "Scientific basis of criticality safety, separation process and waste disposal" The scope of this symposium is not limited in the activity of NUCEF and not limited in safety research, but includes more general view of the issue as far as fuel cycle and waste management are concerned.

Key words: criticality, separation, disposal, plutonium, long-lived nuclide, waste

1. NATIONAL POLICY AND RESPONSIBILITIES

1.1 Governmental Structure

In Japan, Atomic Energy Commission AEC has the responsibility on the matters concerning national policy for research, development and utilization of atomic energy. And Nuclear Safety Commission NSC has the responsibility on the matters concerning regulation for ensuring safety of atomic energy.

As the reflection of JCO criticality accident that took place at the end of September 1999, Nuclear Safety Commission (NSC) is reinforced at April 2000. The Office of NSC, which supports NSC activities as the secretariat, has been established by increased the staff number from 20 to 92 and transferred to Prime Minister's Office from STA; Science and Technology Agency. On the occasion of the Governmental restructuring program, January 2001, further reinforcement was made by transferring NSC and the Office for NSC to the newly-born Cabinet Office. The NSC in Cabinet Office has strong function of government-wide planning and inter-ministry coordination.

In the governmental restructuring program, Safety Regulatory Responsibilities are re-allocated. Re-allocation is shown in Fig.1. The responsibilities on the nuclear fuel cycle facilities related to fuel fabrication business, reprocessing business and waste management business, which responsibility used to be in STA, has been transferred to METI; Ministry of Economy, Trade and Industry, more exactly newly-born NISA; Nuclear and Industrial Safety Agency, in METI. NISA has now the safety regulatory responsibilities both on the fuel cycle facilities and on commercial nuclear power plant, and spent fuel interim storage facility as well. STA, used to be the supervising Agency of JAERI, has merged with Ministry of Education into new MEXT, Ministry of Education, Culture, Sports, Science and Technology.

The supervising Ministry of JAERI has been changed from STA to MEXT. Regarding nuclear energy, MEXT deals with scientific and technological aspect. METI deals with its energy use aspect. Accordingly, JAERI's research activities are directed to scientific and technological aspect of nuclear energy.

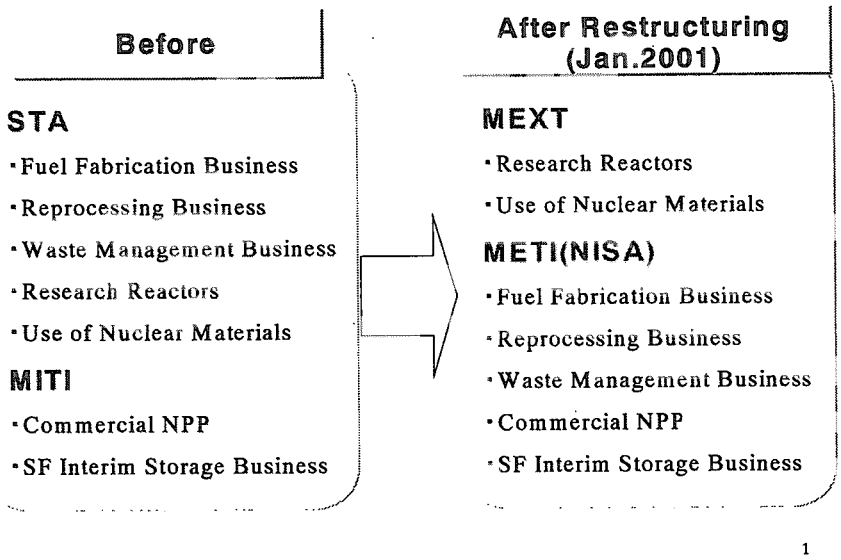

Fig. 1 Re-allocation of Safety Regulatory Responsibilities

1.2 New Movement in Japan

The Atomic Energy Commission (AEC) has defined the new "Long-term Program of Research, Development and Utilization of Nuclear Energy" in November 2000. Japan's policy is not essentially changed in the program. Japan's policy of nuclear fuel cycle is to reprocess spent fuels and recycle the recovered plutonium into LWR as thermal MOX fuel, under the principle of no surplus plutonium. High-level vitrified radioactive waste from reprocessing will be disposed in a deep geological formation after the storage for several tens years. The spent fuel exceeding the available reprocessing capacity will be stored in the interim Away-From-Reactor storage facility as the potential energy resources, until being reprocessed. Research and development of FBR fuel cycle technology have been supported as one of the greatest potential among the options of resource-saving energy technologies for the long-term future.

New movements are emerging in Japan. In fuel cycle, at JNFL-Rokkasho Reprocessing Plant, cold test has been started this year. The commencement of operation of main part of the plant is scheduled at July 2005. JNFL-MOX fabrication plant is formally proposed to local authorities of Rokkasho site, requesting cooperation for the facility construction there. The commencement of operation is expected at Spring 2009. As for Interim AFR Storage Facility, operation is expected at 2010.

Regarding waste disposal, report on clearance level of solidified materials arising from nuclear power plant was issued from special committee of NSC at March 1999. Final

Disposal Act for Vitrified HLW is legislated in June 2000. The legal framework of HLW disposal (Fig.2) has been established based on this legislation. Radioactive waste must be safely treated, conditioned and disposed of by the generators. Power companies, the generator of HLW, have the responsibilities to share the cost for final disposal. The Government, METI, has the responsibility for settling on the basic policy and final disposal plan. NUMO; Nuclear Waste Management Organization of Japan, and RWMC; Radioactive Waste Management Funding and Research Center have the responsibilities of the implementation and funding management, respectively. The Nuclear Safety Commission is now discussing on the safety regulation. The Government; NSC and METI, should provide guidance to or regulate the generators to ensure that the treatment, conditioning and disposal are conducted properly and safely.

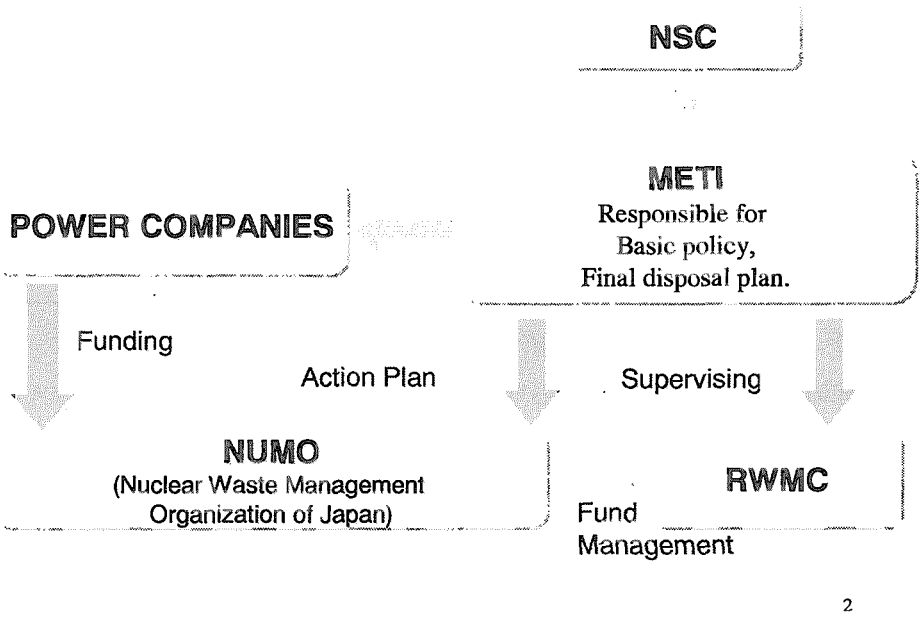

Fig.2 Roles and Responsibilities of Organizations in Vitrified HLW Disposal

In our country, radioactive wastes are categorized according to the generation step in the fuel cycle, which is illustrated in Fig.3. High-level waste arises from reprocessing. TRU waste arises from reprocessing and MOX fabrication. Uranium waste arises from uranium fuel fabrication. Power plant waste arises from power plants. Research and development work in research institute, like JAERI, and radioisotope utilization, too, generate wastes. The category of the waste arising from research institute and radioisotope, RI, utilization is named RI and Research Institute Waste. The generators have the responsibility for its safely treatment, conditioning, and disposal. In order to secure the research capability of using radioactive materials in atomic energy research organizations and to secure the safety of waste management in those institutes, New organization RANDEC; Radioactive Waste Management and Nuclear Facility Decommissioning Technology Center, has been established to implement

the related investigation, in cooperation with JAERI, JNC and JRA (Japan Radioisotope Association). The NSC is discussing the guidelines of regulations on these wastes disposal.

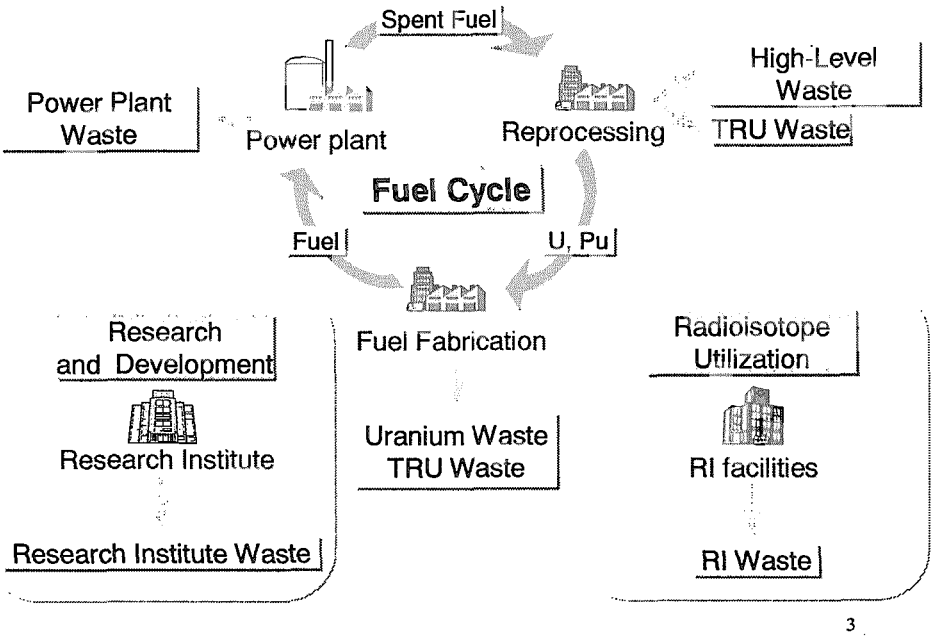

Fig.3 Radioactive Waste Category in Japan

2. THE ROLE OF JAERI

2.1 Research Activities

JAERI is conducting the safety research for current or near future technology and fundamental research for long-term future technology options.

Safety is the highest priority for the use of nuclear energy. The safety is essentially important for the people to accept the policy of nuclear power utilization. As for JAERI, it is important to study the scientific basis for securing nuclear safety and the phenomena of accidents to work out how to cope with for prevention and mitigation. Major objectives of safety researches are to develop safety criteria and establish scientific basis for licensing, to improve the safety of current or near future technology and to clarify the safety margin of licensed technology. Our research works are focused mainly on criticality safety, radio-nuclide confinement safety, and waste disposal safety. Current key words in prioritizing these safety researches are plutonium or MOX and long-lived nuclides.

Objectives of fundamental research for long-term future technological options are to show or clarify the chemical or scientific feasibility of advanced system such as for recycling minor actinides or for incinerating long-lived nuclides. Various researches are underway such as on partitioning of HLLW, new-type chemical processes, transmutation of trans-uranium with accelerator, and so on.

2.2 Introduction of NUCEF

NUCEF; Nuclear Fuel Cycle Safety Engineering Research Facility, is the scientific research center that provides the support of experiment for these researches, especially for hot experiments using uranium, plutonium, minor actinides and spent fuels. The operation started in 1995. There are two criticality facilities, STACY and TRACY, and research laboratory-BECKY composed of $\alpha\ \gamma$ concrete cells, many glove boxes and hoods for handling radioactive materials.

In STACY; Static Critical Experiment Facility, using 10% enriched uranyl nitrate solution, criticality mass are measured. Figure.4 shows the STACY cylindrical core tank placed in a water tank that keeps the temperature constant. Measuring devices are inserted in the core. Cylindrical core can be replaced to slab tank. Now, the experiment of two slab-tank system is underway to study the neutron interaction effect between two tanks.

TRACY; Transient Critical Experiment Facility is to study supercritical phenomena of fuel solution. Figure.5 shows the core tank. The size of 50 cm diameter is similar size to that of precipitation tank in which JCO criticality accident took place. Figure 5 shows the observed power emission under supercritical condition. First, a power burst is observed just after supercritical condition is achieved. Then, the power is decreased because of bubble evolution in solution and power swing continues. In the pictures of this figure, the radiolytic gas bubbles emerged to the surface of the solution is observed with the remote sensing device in the tank. Researches done in STACY and TRACY were very useful to countermeasure and investigate what really happened in JCO. The result of study on JCO accident is presented in the Session of Criticality Safety of this conference.

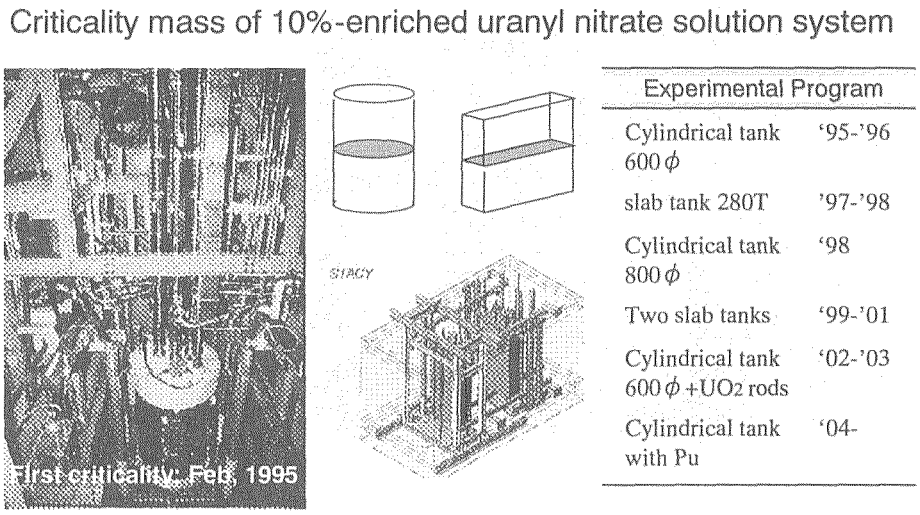

Fig. 4 STACY: Static Critical Experiment Facility

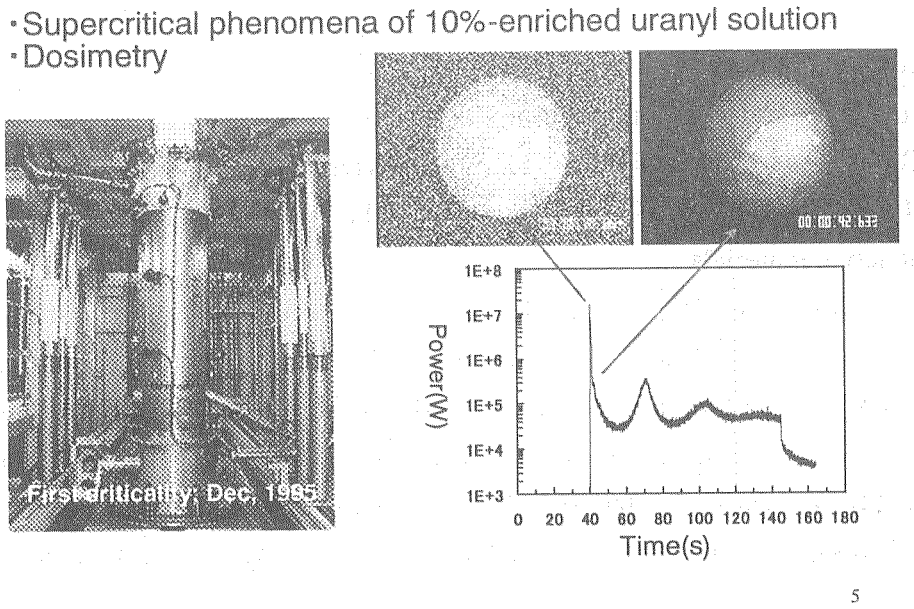

Fig. 5 TRACY: Transient Critical Experiment Facility

STACY and TRACY are placed in the building A of NUCEF. In the building B of NUCEF, research laboratory-BECKY is facilitated. $\alpha\ \gamma$ concrete cells for reprocessing and partitioning process equipment and many glove boxes and fume hoods have been installed for radioactive materials handling.

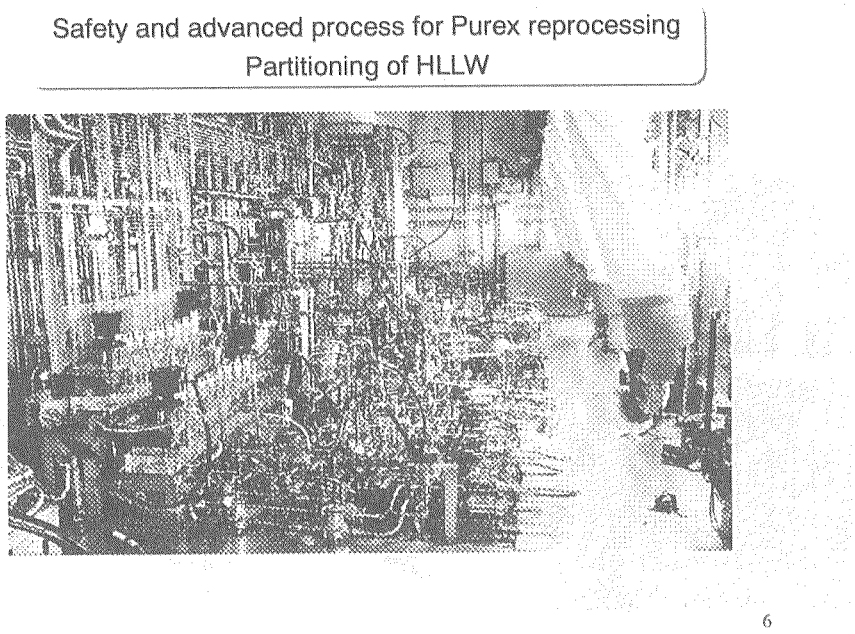

Fig. 6 BECKY $\alpha\ \gamma$ cell for Research on Reprocessing and Partitioning

Figure 6 shows the inside of BECKY $\alpha\ \gamma$ cell. The study of safety and advanced process for Purex reprocessing and process for partitioning of HLLW are conducted here using spent fuels of power plant. Research on radioactive waste disposal is conducted in glove boxes shown in Fig.7. Glove boxes of anaerobic condition is facilitated to simulate underground condition. Thermodynamic data of TRU elements are obtained to study the behavior in deep underground. Field test is also carried out to study the actual behavior of radioactive nuclides in underground facility in cooperation with CIRP; China Institute for Radiation Protection. The result will be presented in the Session of Waste Disposal and Poster Session, today.

Most of these studies related to criticality, process, waste disposal are conducted according to the new Five-Year Program of Safety Research which is defined by Nuclear Safety Commission NSC, last year.

2.3 Endeavor to Develop Resource-saving and Innovative Energy Technology

The "Long-term Program of Research, Development and Utilization of Nuclear Energy" of Atomic Energy Commission is promoting research and development of FBR fuel cycle technology as one of the greatest potential among the options to develop resource-saving energy technologies for the long-term future. According to this direction, JNC is conducting "Feasibility Study on a Commercialized FBR Cycle System." Meanwhile, JAERI is conducting the study on "Reduced-Moderation Water Reactor System (RMWR)" and "Transmutation in Accelerator-Driven System". Studies on the fuel cycle system applicable to these systems is important from the viewpoint of resource-saving energy technologies.

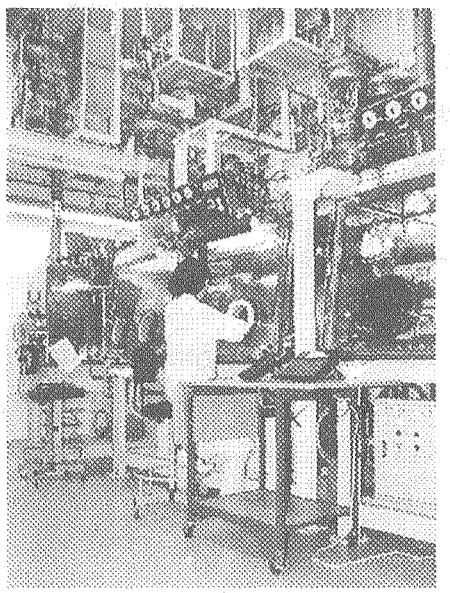

Data acquisition for the estimation of the behavior of radio-nuclides in deep underground.

Anaerobic grove box
(Ar, O_2<1ppm)
Simulate underground condition

7

Fig.7 Anaerobic Grove Box for Research on Radioactive Waste Disposal

The role of Reduced Moderation Water Reactor (RMWR, Fig.8) is in between the current LWR system and the future FBR system. The technology of RMWR is based on the current LWR technology but much advanced in the aspect of Pu control in the reactor core. The reactor of RMWR concept is available as burner or breeder of Pu by control. The fuel cycle technology applicable to RMWR system is also based on LWR fuel cycle technology but much advanced in the aspect of simplification of the process. Realization of RMWR system is envisaged to be much easier than FBR system. The intention of RMWR development is to resolve the subjects; saving uranium resources by Pu utilization, control of surplus separated Pu, reduction of spent fuel in storage and eventually establishment the alternative for fossil fuels. Simplification of reprocessing process is the important subject in the fuel cycle technology development for RMWR. It will be carried out in BECKY facility.

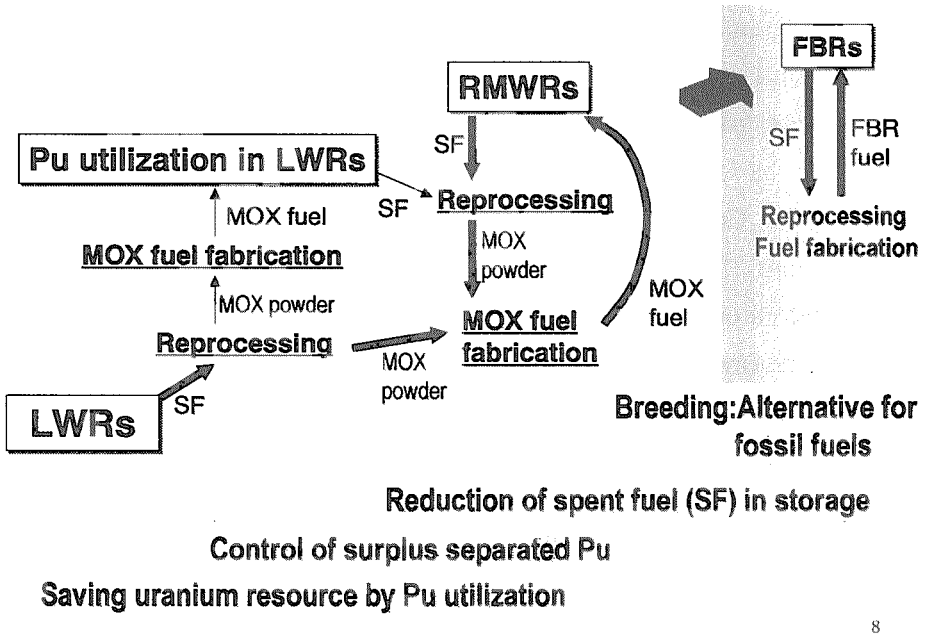

Fig. 8 The role of Reduced Moderation Water Reactor (RMWR) Recycle System

In building B of NUCEF, installation of a new equipment, Module for TRU High-Temperature Chemistry (TRU-HITEC, Fig.9), is underway. This equipment is composed of three hot cells shielded by steel and polyethylene. Fundamental researches on pyro-chemical process with TRU-containing molten chlorides are planned. Some new-type chemical processes are studied for future application. The extractant TODGA is a replacement of DIDPA for present JAERI's partitioning process for actinides separation from HLLW. Result of this study will be presented in the Session of Separation Process. Supercritical carbon dioxide is another new medium to extract actinides. Result of this study is presented in the Session of TRU chemistry.

3. MAINTAINING TECHNICAL COMPETENCE

The roles of atomic energy research organizations are to provide expertise and technical capabilities to assist government regulatory activities, to promote R&D for the future utilization of atomic energy, and to educate students, train professionals and inform general public for better understanding nuclear science and technology. However, recent trends are reduction of research fund and personnel because of re-orientation of science and technology. We observe this trend worldwide.

Nuclear energy is a technology that must essentially be addressed from an international point of view, because of the wide range of activities involved and the magnitude of its importance to the people everywhere in the world. In order to ensure the safety of future nuclear facilities and promote development, research facilities and personnel must be maintained at the necessary level. We think maintaining technical competence is very important for the world nuclear community. From that point of view, international collaboration by sharing financial burden and expertise is the efficient mechanism among concerned countries and regions.

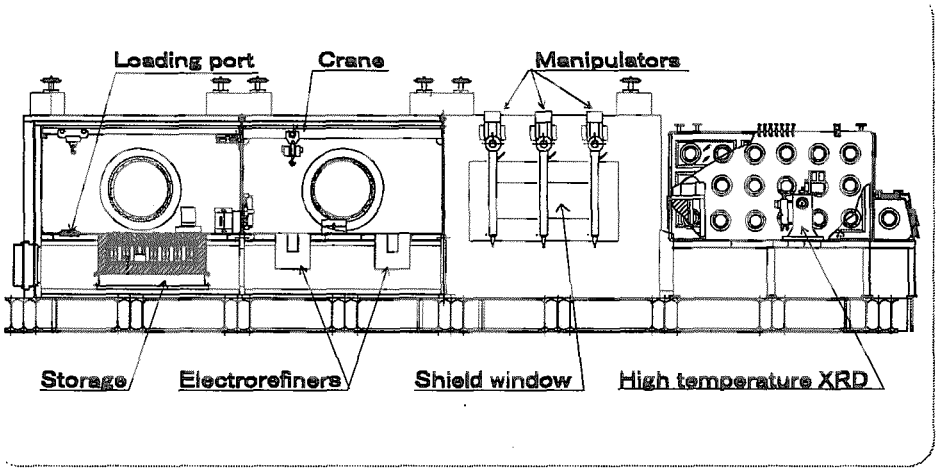

9

Fig. 9 Module for TRU High-Temperature Chemistry (TRU-HITEC, to be available in 2003)

It is important for Japan to make maximum efforts in establishing international nuclear safety standards. As the effort of such direction, we are planning to conduct critical experiments of plutonium solution in STACY, which is one of the very few critical experiment facilities that can handle Plutonium solution in large scale in the world. As shown in Fig.10, critical experiment will be conducted using commercial-use plutonium solution to develop advanced criticality control techniques such as sub-critical monitoring and to validate criticality safety analysis methods. Experiment is planned to start at 2006 with

low-concentration condition at first.

4. SUMMARY

Japan has launched a new research program based on a new long-term nuclear policy with reorganized government structure. NUCEF is the scientific research center on the safety research and fundamental research for the world nuclear community. Maintaining technical competence is important to ensure safety of the use of nuclear energy and promote development of future technology. Efficient international collaboration is encouraged to this purpose. We think that providing the idea and data useful for ensuring the safety and securing future energy is required to recover the people's confidence in the utilization of future nuclear technology.

Critical Experiments of Plutonium Solution

STACY

- Criticality Data of Commercial-Use Pu Solution
- Development of Advanced Criticality Control Techniques
- Validations of Criticality Safety Analysis Methods

PHASE I (2006-2007)
- Low-concentration Pu Experiments
- Temperature Coefficient of Low-Concentration Pu

PHASE II (2007-2009)
- Higher Enrichment U/Pu Experiments
- Lower Enrichment U/Pu Experiments

PHASE III (2010-)
- Criticality Data of Wide Range Pu Concentration

Fig. 10 Critical Experiments of Plutonium Solution

2. Plenary Session

This is a blank page.

JP0250279

JAERI-Conf 2002-004

THE U.S. NUCLEAR CRITICALITY SAFETY EXPERIENCE, NEEDS, AND FUTURE IN A GLOBAL ECONOMY

CALVIN M. HOPPER
Oak Ridge National Laboratory, P.O. Box 2008, Oak Ridge, Tennessee 37831-6370 USA
Ph: 1 - (865) 576-8617, Fax: 1 - (865) 576-3513, e-mail: hoppercm@ornl.gov

Nuclear criticality safety in the United States of America (U.S.) has experienced recent shifts in administrative, economic, regulatory, and technological demands. These demands are being imposed on the U.S. nuclear criticality safety (NCS) for existing and new production objectives. Most of these objectives are new and place NCS in new "technological space" with regard to the available databases for addressing these objectives. Additionally, there have been growing administrative demands for programmatically justifying research and development for experimental evidence/data to support the use or development of generalized and multipurpose theoretical models, computational techniques, and measurement methods. This growing administrative demand has shifted emphases from historically generalized national support to specific program/project funding. The isolated pursuit of specific information without infrastructure and general support is generally costly and usually not budgeted for by the original project designers. This shift has retarded the maintenance of reliable NCS capabilities in the U.S. to address the evolving technology. Growing global commercial competition provides an increasing economic demand for NCS to accommodate novel productivity improvements resulting in increased production with simultaneous cost-reduction. Such economic demands frequently place NCS in difficult positions.
Key words: criticality, safety, experience, administration, regulation, needs, economy

1. INTRODUCTION

Nuclear criticality safety (NCS) is being tasked with meeting existing and new production objectives to address recent economic, administrative, regulatory, and resulting technological demands. These production objectives include

- the maintenance of historic nuclear capabilities for national electric power and defense purposes;
- the fabrication of new plutonium-uranium mixed oxide (MOX) fuel-blend types;
- the characterization of fissionable-material-process nuclear criticality accidents for emergency preparedness, training, response, and safety documentation;
- storage, transport, and disposal of spent fuel;
- partitioning of major actinides for
  - radioactive thermal-electric generators (RTG)
  - selective actinide production
  - fissionable material waste disposal
  - transmutation;
- disposal and storage of containerized high-level waste in geological repositories;
- disposal and storage of containerized low-level waste and earth-blended waste in geological repositories.

Within the U.S., existing and, most recently, accelerating new economic administrative, regulatory, and technological demands have placed NCS in new technological and regulatory space. The future of nuclear energy in the U.S. is unquestionably influenced by the experiences and needs of our industry to satisfy these demands. Nuclear criticality safety, though seemingly a small expense in the overall scheme of national nuclear energy programs, is a long-term, and nearly always overlooked, expense that impacts nearly all phases of nuclear energy programs using fissionable materials. This is especially true within the U.S. economic, administrative, and regulatory experience, current needs and future participation in the global economy.

2. ECONOMIC DEMANDS

Many NCS economic issues are apparent from the operational, administrative, and technical research and development topics being presented at this NUCEF 2001 Symposium. The U.S. experience with the economic issues of NCS has been highly varied over the past 55 years. Almost no economic consideration was given to the use and potential for nuclear energy during its infancy in the U.S. Some national economic issues were considered during the 1950s "Atoms for Peace" initiative with the growing popularity and evolution of U.S. nuclear research and industry. In the late 1950s and 1960s our power utilities could see the potential of nuclear power and anticipated improved power production efficiencies and cost reduction. Our coordinated and operating research programs and experimental facilities were viewed as a desirable national asset to be maintained as a necessary governmental infrastructure for the new technology. Further, the facilities were judged to assist industry in "boot-strapping" itself into a waiting global opportunity. Existing facilities such as Los Alamos Scientific Laboratory, later renamed Los Alamos National Laboratory (LANL); Oak Ridge National Laboratory (ORNL); and Livermore Radiation Laboratory, later named Lawrence Livermore National Laboratory (LLNL), were joined in their research efforts by numerous follow-on laboratories such as Savannah River and Hanford and commercial facilities such as Pratt and Whitney, Babcock and Wilcox, General Electric, Westinghouse, and numerous others. The economic costs of these laboratories were accepted as prerequisites for obtaining the data, creating the technological and competitive advantages, and educating the personnel to carry forward the "natural" initiatives of a national economic resource, nuclear energy.

Other nations also moved forward into the nuclear energy economy, most out of a recognized need for cost-effective and efficient power generation. In the late 1960s the U.S. moved to develop a commercial breeder reactor which was ultimately thwarted by a national anti-proliferation initiative to ban spent-fuel reprocessing. Shortly thereafter, in 1978, the U.S. experienced its last nuclear criticality accident after 14 years of no accidents. That accident received little national notice and had little economic impact. However, the following year, on March 28, 1979, the U.S. experienced the accident at the Three Mile Island Unit 2 (TMI2) nuclear power plant near Middletown, Pennsylvania. The national reaction had significant repercussions for the nuclear energy industry. The public judged operational and safety risks to be unacceptable irrespective of the actual impact of the event (the best estimates are that the average dose to about 2 million people in the area was about 1 millirem and about 100 millirem to a person who might be and remain at the site boundary).

However, the accident permanently changed the U.S. nuclear industry and significantly broadened the U.S. Nuclear Regulatory Commission's (NRC's) regulations and oversight activities. Until the U.S. nuclear industry was able to accommodate these changes, there were significant cost impacts on power reactor facilities. Those impacts influenced the operations of nuclear fuel fabrication facilities and their nuclear criticality safety programs. While, these changes strengthened public perceptions of the safety of nuclear energy, the commercial power industry had already started to respond to the economic impacts of intervening litigates, increased licensing difficulties, and increased costs of operations. In the U.S., all reactor orders made over the past 20 years have subsequently been cancelled. Between 1972 and 1990, construction of 119 nuclear plants was cancelled by U.S. utilities. The decline in commercial interest in nuclear energy was accompanied by the closure of critical experimental facilities. By the late 1980s, all but one general purpose critical experiments facilitator — the Los Alamos Critical Experiments Facility (LACEF) — were closed within the U.S.

Today, U.S. nuclear fuel fabrication facilities have turned their attention to the global market, selling processes and reactor fuels and participating in joint ventures. Some previously U.S. — owned nuclear fuel processing and fabrication companies have either been sold to international entities or have formed joint ventures to continue the use of the facilities.

What might the future be for NCS as influenced by economics in the U.S.? California's energy crisis this past year and the public's recognition that there will likely be energy shortages as a result of not building power plants over the last decade has renewed interest in the possibilities of nuclear energy in the U.S. The Nuclear Energy Institute reported that a group of utility executives approached them last year to form a task force to determine what would be necessary to deploy a new nuclear plant. The group's idea is to form a consortium of companies that would order several plants, which would be standardized and would benefit from economies of scale of production.

There are mounting concerns which enhance the economic profile of nuclear energy in the U.S. These concerns include

- the CO_2 "greenhouse" effects on global warming;
- the questionable reliability of oil and coal supplies in a highly charged political, emotional, and spiritual world;
- the inability of alternative energy sources to provide reliable energy without environmental impacts;
- the recent unavailability of significant power-producing plants in the U.S.; and
- the problems associated with the U.S. open-ended fuel cycle spent fuel and waste disposition issues.

These concerns serve to accelerate the need for an U.S. national energy policy that is based upon sound economics as supported by sound technology.

International involvement in U.S. fuel fabrication has historically included Siemens Power Corporation and, more recently, British Nuclear Fuels Limited and Framatome Cogema Fuels. Recently, the U.S. nuclear industry has been posturing itself to weather the above mentioned concerns and uncertainties by participating in global exchanges. Currently, there is a joint venture of Duke-Cogema-Stone & Webster in the U.S. to receive excess weapons-grade plutonium, blend it with uranium, and fabricate mixed plutonium-uranium oxide (MOX) commercial fuel elements. General Electric Company (GE) of America; Hitachi, Ltd.; and Toshiba Corp. established Global Nuclear Fuel (GNF), an international nuclear-fuel joint venture, on January 1, 2000. The three companies have integrated their nuclear fuel marketing, design, development, and manufacturing functions into the new company, which established business bases in both Japan and the U.S. These and other joint international business ventures within the U.S. assure a global economic future that will require the continued participation by NCS.

3. ADMINISTRATIVE DEMANDS

For the past 25 years there have been evolving administrative or management mind-sets and perceptions that have created growing fiscal and regulatory demands on U.S. nuclear industries. These mind-sets have changed as the result of the same social and economic events reviewed in Sections 1 and 2 above. Administrative and management mind-sets have shifted from the willingness in the '50s, '60s, and early '70s to generally embrace a promising and lucrative technology with fiscal and intellectual support. From the late 1970s through the mid-1990s there was a desire to separate fiscal responsibilities and administrative accountability from a technology perceived as a liability. Recently, since the late 1990s, the

administrative and management perception is that nuclear energy may be a promising business venture requiring limited, if any, additional intellectual or fiscal support for research and development. It is this last perception that places a substantial technological burden on NCS to address seemingly simple but in actuality complex problems with limited fiscal resources, knowledge, computational tools, and data resources.

The fiscal demands on individual programs or projects are to justify specific needs of research for experimental evidence or data and the development of generalized and multi-purpose theoretical models, computational techniques, and measurement methods. This demand has shifted to the current requirement that individual programs or projects provide their own specific project-related information (e.g., critical experiments, improved cross-section data, improved computational tools) on a limited budget without infrastructure and general support. Therefore, limited fiscal resources are available to acquire needed information. This shift has retarded the development and maintenance of NCS capabilities in the U.S. for addressing the evolving "technological space" imposed by new programs and projects. Maintaining reliable NCS capabilities requires reliable experimental data from critical and/or subcritical systems. Additionally, neutron cross-section measurements and evaluations are needed for the production objectives of concern, which may involve fission products, unusual blends of fissionable materials, geologic materials, and often, unusual neutron energy spectra that may carry the fission chains.

4. REGULATORY DEMANDS

Regulatory demands on NCS parallel the temporal changes in the economic and administrative demands imposed by the social and economic changes in the U.S. The means of addressing regulatory demands on NCS have varied over the decades, ranging from

- relatively informal (by today's standards) memos by eminent scientists who were participating in the emerging studies of the 1940s; to
- structured analytical and safety analysis protocols used by scientific apprentices and technical engineering graduates and accepted by regulatory bodies during the 1950s, 1960s, and early 1970s; to
- increasingly complex and voluminous safety evaluation and safety analysis reports prepared by formally educated nuclear engineers and reviewed by facility management staff and regulatory personnel during the late 1970s to the late 1990s; to
- guidance that may develop from the U.S. Department of Energy (DOE) to include detailed safety analysis report criticality safety controls for DOE central review and approval.

Additionally, the U.S. American Nuclear Society (ANS) has proposed an initiative to develop standard guidance for the performance of probabilistic risk analysis for nuclear facility criticality safety analyses.

The International Organization for Standardization (ISO) has a relatively active working group on nuclear criticality safety within the ISO Technical Committee 85 (TC 85), *Nuclear energy*, Subcommittee 5 (SC 5), *Nuclear fuel technology*, Working Group 8 (WG 8), *Standardization of calculations, procedures and practices related to criticality safety.* Existing NCS ISO standards include; ISO 1709, *Principles of criticality safety in storing, handing and processing*, and ISO 7753, *Performance and testing requirements for criticality detection.* Those standards are being supplemented with developing standards on *Administrative criteria related to criticality safety* and *Nuclear criticality control and safety of plutonium-uranium oxide fuel mixtures outside of reactors.* A standard on *the Estimation of nuclear criticality accident yields* has been suggested but has not yet been initiated. These

existing and developing ISO standards on NCS are likely to play a prominent role in the future in collaborative international ventures involving fissionable materials.

5. TECHNOLOGICAL DEMANDS

The growing global commercial competition provides an increasing economic demand for NCS to accommodate novel process improvements that may result in increased production with simultaneous cost reduction. The changing administrative or management demands challenge NCS staffs to provide their administrators and managers with information and insights to recognize the trade-offs associated with the lack of technical resources for addressing the technical issues. The shifting regulatory expectations in the U.S., and seemingly throughout the world, demand greater levels of elementary justifications and demonstrations of subcriticality for safety with increasingly greater levels of statistical confidence and vanishingly small probabilities of failure.

Those demands, coupled with some existing and mostly new production objectives, place new, unusual, and sometimes conflicting demands on NCS to accommodate programmatic needs. Within the U.S. we are working on approaches and methods to address these demands.

The NRC has considered various evolving issues that are being generated from these typically new processes and technological demands. It has supported

- the acquisition of critical experimental data from intermediate enriched uranium experiments for consideration in the evaluation of fabrication processes for extended-life reactor fuels in combination with the development of a prototypic sensitivity and uncertainty method for examining ranges of the applicability of experimental data to safety evaluations;[1]
- studies to evaluate the influences of fissionable material waste matrixes[2] on subcriticality as it could be affected by reconcentrating hydrogeochemical mechanisms;[3 7] and
- examination of spent nuclear fuel issues.[8, 9, 10, 11]

Following the Recommendation 97-2 of U.S. Defense Nuclear Facility Safety Board,[12] DOE, with senior U.S. NCS personnel assistance, designed a comprehensive DOE Implementation Plan for a high-level national DOE Nuclear Criticality Safety Program (NCSP) to assist DOE NCS programs and engineers in meeting some of the above-mentioned demands. The NCSP provides support for the

- acquisition of data (e.g., subcritical and critical experiments measurements[13, 14] neutron cross-section measurements and evaluations[15, 16]);
- maintenance and expansion of computational methods (e.g., MCNP[17] and other codes[18, 19, 20]);
- training and guidance of NCS and facility personnel (e.g., issuance of training modules and assistance in the development of regulations/guides and the conduct of classes); and
- sharing and communicating of information (e.g., workshops, conferences, OECD Handbook of Criticality Safety benchmark evaluations[21] and the dissemination of handbook and logbook information[22]).

Much of the information and some of the computational tools that have evolved from the U.S. NRC research support and DOE NCSP have been used to address some of the demands on NCS.[23]

6. U.S. NCS IN A GLOBAL ECONOMY

The NUCEF 2001 Symposium has numerous presentations that address national and global production objectives and their associated demands on NCS programs and engineers to function in the new "technological space." Clearly, innovative applications of science and technology are needed to accommodate these demands in a competitive and growing global economic markets. Through joint international ventures and the sharing of innovative solutions and information at symposiums such as this, the U.S. is likely to remain a partner in the global economy for the success of nuclear energy. This participation is needed and is inevitable for the benefit of the environment that includes us humans.

REFERENCES

[1] NRC JCN W6479, "Development and Applicability of Criticality Safety Software for Licensing Review," Revision 0 dated 9/13/95, Revision 1 dated 4/26/96 and Revision 2 dated 05/27/97.

[2] C. M. Hopper, R. H. Odegaarden, C. V. Parks, and P. B. Fox, *Criticality Safety Criteria for License Review of Low-Level-Waste Facilities*, NUREG/CR-6284 (ORNL/TM-12845), U.S. Nuclear Regulatory Commission, Oak Ridge National Laboratory, March 1995.

[3] L. E. Toran, C. M. Hopper, M. T. Naney, C. V. Parks, J. F. McCarthy, B. L. Broadhead, and V. A. Colten-Bradley, *The Potential for Criticality Following Disposal of Uranium at Low-Level Waste Facilities. Volume 1: Uranium Blended with Soil*, NUREG/CR-6505, Vol. 1 (ORNL/TM-13323/V1), U.S. Nuclear Regulatory Commission, Oak Ridge National Laboratory, June 1997.

[4] L. E. Toran, C. M. Hopper, C. V. Parks, and V. A. Colten-Bradley, *The Potential for Criticality Following Disposal of Uranium at Low-Level Waste Facilities, Volume 2: Containerized Disposal*, NUREG/CR-6505, Vol. 2 (ORNL/TM-13323/V2), U.S. Nuclear Regulatory Commission, Oak Ridge National Laboratory, June 1999.

[5] C. M. Hopper, K. R. Elam, C. V. Parks, and J. J. Lichtenwalter, "Bounding Values for Low-Level-Waste Transport Exemptions and Disposal," Vol. I, pp. 438–446 in *Proc. ICNC'99, Sixth International Conference on Nuclear Criticality Safety*, September 20–24, 1999, Palais des Congrès, Versailles, FRANCE.

[6] K. E. Elam, C. M. Hopper, C. V. Parks, and T. E. Harris, *Emplacement Considerations for Criticality Safety in Low-Level-Waste Disposal*, ORNL/TM-13765, UT-Battelle, LLC, Oak Ridge National Laboratory, June 2001.

[7] C. W. Forsberg, "Long-Term Criticality Control in Radioactive Waste Disposal Facilities Using Depleted Uranium," pp. 99–106 in *Proc. Topical Meeting on Criticality Safety Challenges in the Next Decade, Session: Criticality Safety Challenges in Long-Term Disposal*, September 7–11, 1997, Chelan, Washington.

[8] S. M. Bowman and L. C. Leal, "ORIGEN-ARP: Automatic Rapid Process for Spent Fuel Depletion, Decay, and Source Term Analysis," NUREG/CR-0200, Rev. 6 (ORNL/NUREG/CSD-2R6), Vol. I, Part 2, Sect. D1, of *SCALE: A Modular Code System for Performing Standardized Computer Analyses for Licensing Evaluation*, May 2000. Available from Radiation Safety Information Computational Center at Oak Ridge National Laboratory as CCC-545.

[9] B. L. Broadhead and I. C. Gauld, "Rankings of Nuclide Importance in Spent Fuel for Shielding Applications," pp. 702–709 in *Proc. ANS2000 Radiation Protection and Shielding Division Topical Conference, Radiation Protection for Our National Priorities: Medicine, the Environment and the Legacy*, September 17–20, 2000, Spokane, Washington.

[10] J. C. Wagner and C. V. Parks, *A Critical Review of the Practice of Equating the Reactivity of Spent Fuel to Fresh Fuel in Burnup Credit Criticality Safety Analyses for PWR*

Spent Fuel Pool Storage, NUREG/CR-6683 (ORNL/TM-2000/230), U.S. Nuclear Regulatory Commission, Oak Ridge National Laboratory, September 2000.
[11] D. E. Carlson, C. J. Withee, and C. V. Parks, "Spent Fuel Burnup Credit in Casks: An NRC Perspective," in *Proc. Twenty-Seventh Water Reactor Safety Information Meeting*, October 25–27, 1999, Bethesda, Maryland. NUREG/CP-0169, pp. 419–436, March 2000.
[12] Defense Nuclear Facilities Safety Board Recommendation 97-2, *Continuation of Criticality Safety*, May 1997.
[13] R. W. Brewer and R. G. Sanchez, "SiO_2 — Polyethylene Reflected Critical Assembly," LA-R-1-50, Los Alamos National Laboratory, 2001.
[14] R. G. Sanchez, D. J. Loaiza, and J. Bennion, "Critical Masses of Highly Enriched Uranium Diluted with Gd and Polyethylene," Los Alamos National Laboratory, 2001.
[15] N. M. Larson, L. C. Leal, and H. Derrien 1999, "Merger of Nuclear Data with Criticality Safety Calculations," in *Proc. 6th Int. Conf. on Nuclear Criticality Safety*, September 20–24, 1999, Versailles, France.
[16] H. Derrien, J. A. Harvey, N. M. Larson, L. C. Leal, and R. Q. Wright, *Neutron Total Cross Sections of ^{235}U from Transmission Measurements in the Energy Range 2 keV to 300 keV and Statistical Model Analysis of the Data*, ORNL/TM-2000/129, UT-Battelle, LLC, Oak Ridge National Laboratory, April 2000.
[17] J. F. Briesmeister, "MCNP: A General Monte Carlo n-Particle Transport Code," Los Alamos, New Mexico: Los Alamos National Laboratory, 2000.
[18] E. Greenspan, Y. Karni, L. M. Petrie, and D. Regev, *SWANS: A Prototypic SCALE Criticality Sequence for Automated Optimization Using the SWAN Methodology*, ORNL/TM-1999/274 (UCBNE-4226), UT-Battelle, LLC, Oak Ridge National Laboratory, December 2000.
[19] B. L. Broadhead, R. L. Childs, and C. M. Hopper, "Illustrative Examples of Least-Squares Methods for Criticality Safety," in *Proc. ANS/ENS 2000 International Winter Meeting and Embedded Topical Meetings*, November 12–16, 2000, Washington, DC. *Trans. Am. Nucl. Soc.* **83**, 100–103, 2000.
[20] B. T. Rearden and R. L. Childs, "Prototypical Sensitivity and Uncertainty Analysis Codes for Criticality Safety with the SCALE Code System," in *Proc. ANS/ENS 2000 International Winter Meeting and Embedded Topical Meetings*, November 12–16, 2000, Washington, DC. *Trans. Am. Nucl. Soc.* **83**, 98–100, 2000.
[21] *NEA Nuclear Science Committee International Handbook of Evaluated Criticality Safety Benchmark Experiments*, NEA/NSC/DOC(95)03, September 2000. The International Criticality Safety Benchmark Evaluation Project is an official activity of the Organization for Economic Cooperation and Development — Nuclear Energy Agency (OECD-NEA), Paris, France.
[22] T. P. McLaughlin, S. P. Monahan, N. L. Pruvost, V. V. Frolov, B. G. Ryazanov, and V. I. Sviridov, "A Review of Criticality Accidents 2000 Revision," LA-13638, Los Alamos National Laboratory, Los Alamos, New Mexico, May 2000.
[23] M. E. Dunn and B. T. Rearden, "Application of Sensitivity and Uncertainty Analysis Methods to a Validation Study for Weapons-Grade Mixed-Oxide Fuel," in *Proc. of 2001 ANS Embedded Topical Meeting on Practical Implementation of Nuclear Criticality Safety*, November 11–15, 2001, Reno, Nevada.

This is a blank page.

JP0250280

JAERI-Conf 2002-004

Overview of the Hydrometallurgical and Pyrometallurgical Processes Studied World-wide for the Partitioning of High Active Nuclear Wastes

by

Charles MADIC

DEN
CEA/Saclay, 91191 Gif-s-Yvette, France
E-mail : madic@amandin.cea.fr

ABSTRACT

Since more than 10 years, a revival of the interest for the partitioning of high active nuclear wastes (HAWs) exists world-wide in connection with possible improvements of the management of the HAWs actually produced and with futuristic nuclear fuel cycles. The main aim of the partitioning processes is to separate, from the complex mixtures of HAWs, the long-lived radionuclides (LLRNs), belonging either to the minor actinides (MAs) or to the Fission Products (FPs) families of elements, in order to prepare fuels and/or targets suitable for their subsequent transmutation (P&T strategy). An other possible strategy consists in the special conditioning of the separated LLRNs into stable dedicated matrices (P&C strategy).
The LLRNs considered for Partitioning are the MAs, neptunium, americium and curium, but also the FPs, caesium, technetium and iodine.
Most of the partitioning processes studied so-far belongs to the domain of hydrometallurgy, but, recently, a new impetus was observed in the field of pyrometallurgical processes.
The main aim of this talk is to present a brief status of the development of both "hydro" and "pyro" processes for the partitioning of LLRNs developed world-wide, with a special emphasis on the benefits/drawbacks of each process.

I. INTRODUCTION

Since the end of the 80's, a renewal of interest is observed world-wide for LLRNs partitioning techniques from nuclear wastes (HAWs). This interest is connected with two main fields:
(i) the conventional LWR closed fuel cycle using the PUREX process.
New management methods for nuclear wastes are considered, the so-called Partitioning-Transmutation (P&T) and Partitioning-Conditioning (P&C) scenarios. For this domain, hydrometallurgy is the main route for LLRNs partitioning process development, while pyrometallurgy is a also subject of some research,
(ii) « New » fuel cycles associated with the development of Fast Reactors (FRs), Accelerator-Driven-Systems (ADSs) and Fused Salt Reactors (FSRs). For this field, pyrometallurgy is the main route considered for spent fuel reprocessing and wastes partitioning, while a small interest still remains for the hydrometallurgical route.
The aim of the present article is to give a brief overview of the progress realised world-wide in the recent years in the field of partitioning of LLRNs by hydrometallurgical and pyrometallurgical processes.

II. PARTITIONING PROCESSES: AN OVERVIEW

II.1. General considerations [1]

II. 1. 1. Target elements for the separations

Actinides:
For P&T and P&C scenarios, the elements considered for partitioning are the so-called minor actinides (MAs): neptunium (Np), americium (Am), and curium (Cm), while for « New » fuel cycles scenarios, uranium (U), plutonium (Pu) and the MAs are all concerned with partitioning/reprocessing process development.

Fission Products
For P&T and P&C scenarios, iodine (I), technetium (Tc) and caesium (Cs) are the three main elements considered for partitioning. Some P&C scenarios also consider the partitioning of caesium and strontium.
In Japan, the separation of the platinum group metals (PGMs) from nuclear wastes is also studied for industrial uses of the separated PGMs.

II.1. 2. Goals for the separations
The most important goals for the separations are:
- minimisation of the long-term radiotoxic inventory of the wastes conditioned in « conventional matrices, e.g. in glasses (removal of LLRNs of MAs and FPs families),
- minimisation of the heat load of the conditioned wastes (removal of ^{137}Cs and ^{90}Sr),
- more often, high purities of the separated LLRNs are required, for target or fuel fabrication for subsequent transmutations of these LLRNs.

II.1.3 Consequences
Owing to the fact that efficient separation methods are needed with low losses of LLRNs and high purities of the separated LLRNs, multi-stage processes are most often necessary.

II.2. Hydro processes for actinides and FPs partitioning

II.2.1 Examples of separation strategies
Examples of separation strategies are given for some countries and some research organisations.

- **Japan**
  - JNC

For FRs closed fuel cycle, JNC develops an integrated approach based on hydrometallurgical steps including the: (i) dissolution of MOx FR spent fuels with an aqueous nitric acid solution, (ii) iodine volatilisation, (iii) electrolytic extraction of technetium (Tc), palladium (Pd) and selenium (Se), (iv) crystallisation of most of the uranium contained within the spent fuel dissolution liquor in the form of hydrated uranyl nitrate, (v) single PUREX extraction step for recovery of remaining U + Pu + Np, (vi) SETFICS process for Am and Cm partitioning.

  - JAERI

JAERI proposed to separate Np and Tc during the implementation of the PUREX process. This organisation develops also, since many years, the so-called four-group partitioning process for the treatment of the wastes issuing the reprocessing by the PUREX process of UOx or MOx LWR spent fuels. This partitioning process includes the following steps: (i) MAs partitioning (Np, Am and Cm), (ii) Cs + Sr extraction, (iii) PGMs extraction. The remaining mixture of wastes constitutes the 4th category of elements of the initial mixture treated.

- **USA**

The situation in the USA is peculiar because partitioning processes developed concern the treatment of defence wastes, in particular those accumulated at DOE's Hanford site during the cold war. Several processes were developed for the partitioning of radionuclides from the wastes: (i) TRUEX process for transuranic extraction, (ii) SREX process for Sr removal and (iii) CSEX process for Cs extraction. It should be also noted that in 1999, a Report named *"A Roadmap for Developing Accelerator Transmutation of Wastes (ATW) Technology"* was published by the DOE [2], which considers the possible treatment of the LWR spent fuels accumulated in the USA in order to separate: (i) U for final disposition as low level waste and (ii) TRUs for burning in ATW systems. The processes considered for these separations are: (i) the UREX process, which consists in a modified PUREX process aiming to only extract U, (ii) pyrometallurgical partitioning process for TRU separation from the UREX wastes and for the ATW fuel cycle.

- **France (CEA)**

The strategy developed by the CEA for partitioning the nuclear wastes of LWR closed cycle concerns 6 LLRNs to separate from the wastes: 3 MAs (Np, Am and Cm) and 3 FPs (I, Tc and Cs). This strategy is based on the development of successive liquid-liquid extraction processes: (i) the improved PUREX process for U, Pu, Np, I and Tc separations, (ii) the DIAMEX process for trivalent Am+Cm extraction (FP lanthanides (III), Ln, are co-extracted), (iii) the SANEX process for Am+ Cm/Ln(III) separation, (iv) the SESAME process for Am/Cm separation, (v) the CALIX-CROWN process for Cs separation.

In some organisations (e.g. in USA, Japan, Czech Rep. or Russia), instead of developing a succession of separation processes for peculiar LLRNs, the integration of processes for MAs and FPs extraction are studied. For example, the use of a solvent containing a mixture of cobalt dicarbollide + dioxide of diphosphine allows the combined extraction of Cs + Sr + (Am+Cm) + Ln.

II.2.2 MAs partitioning

- **One cycle processes**

° **DIDPA process (JAERI, Japan)**

This process for MAs partitioning is based on the use of *di*-isodecylphosphoric acid (DIDPA). The extraction mechanism is the following:

$$M^{n+} + \overline{n\,(HA)_2} \Longleftrightarrow \overline{M(HA_2)_n} + n\,H^+ \qquad (1)$$

The separation of the TRU elements is done by successive stripping from the loaded solvent, including the use of diethylenetriaminopentaacetic acid (DTPA) complexing agent for actinides(III)/Ln(III) separation (TALSPEAK like process, *vide infra*).

The DIDPA process was recently tested successfully in the BECKY hot-cell at NUCEF (JAERI, Tokai-Mura).
Among the possible drawbacks of this process one can mention the: (i) required feed acid adjustment, (ii) solvent degradation and its delicate clean-up, (iii) limited solvent loading with metal ions.

° **SETFICS (JNC, Japan)**
The SETFICS process constitutes a modification of the TRUEX process (*vide infra*) based on the use of the extractant *di*-isobutyl-phenyl-octylcarbamoylmethylphosphine oxide ($\Phi C_8H_{17}P(O)CH_2C(O)(i\text{-}C_4H_9)_2$ = CMPO).
The extraction mechanism is as follows:

$$M^{n+} + n\,NO_3^- + m\,\overline{CMPO} \Longleftrightarrow \overline{M(NO_3)_n(CMPO)_m} \qquad (2)$$

The separation of TRUs is done by successive stripping from the loaded solvent, including also the use of DTPA for An(III)/Ln(III) separation. This process has not been tested yet with genuine HAWs. The possible drawbacks of this process are: (i) the limited stripping efficiency, (ii) the management of salts and DTPA containing effluents.

° **PALADIN (CEA, France)**
This process is based on the use of a mixture of extractants: a malonamide (DIAMEX process extractant) + *di*-ethylhexylphosphoric acid (HDEHP), the extractant of the TALSPEAK process.
The extraction and separation mechanisms are the following.
Extraction :

$$M^{3+} + 3\,NO_3^- + 2\,\overline{DIAM} \Longleftrightarrow \overline{M(NO_3)_3(DIAM)_2} \qquad (3)$$

An(III)/Ln(III) separation: done after contacting the loaded solvent with a pH adjusted aqueous solution containing DTPA selective trivalent actinide complexing agent. For pH range HDEHP is the extractant, while at the metal nitrate extraction step, carried out with acidic feeds 3 to 5 mol/L in nitric acid, trivalent An and Ln are extracted with the malonamide.
This process was recently successfully tested in the ATALANTE facility (CEA/Marcoule, Fr.).
The possible drawbacks of this process are the: (i) necessity to use 2 extractants, (ii) need of pH adjustment, (iii) co-extraction of numerous ions, (iv) solvent clean-up not yet defined.

- <u>**Multi cycle processes**</u>

- ***1st step: An + Ln co-extraction***

° **TRUEX (USA, Japan, Russia, Italy and India)**
This process is based on the use of the CMPO extractant. This process was developed by Horwitz (ANL) and Schulz (Hanford) in the USA in the 80s. The advantages of the TRUEX process are the following: (i) it can extract An (and Ln) salts from acidic feeds, (ii) its efficiency has been demonstrated with genuine HAWs, (iii) a large experience has been gained world-wide. The main drawbacks of the TRUEX process are the: (i) necessity to use large concentration of *tri*-n-butylphosphate (TBP) as solvent modifier added to the solvent to

prevent third phase formation, (ii) stripping of metal ions which are not so efficient, (iii) delicate solvent clean-up.

° **DIAMEX (France, Italy, Germany, Europe, Japan, USA and India)**
This process is based on the use of a malonamide extractant. The main interests of the process are: (i) An (and Ln) salts can be extracted from acidic feeds, (ii) its efficiency has been demonstrated on genuine HAWs, (France, Europe), (iii) no secondary solid wastes generated owing to the CHON character of the malonamide extractant. Its main drawback relies in the partial co-extraction of palladium (Pd) and ruthenium (Ru) with the MAs.

A process based on a new type of diamide, a diglycolamide (DGA), which is a terdendate ligand having better affinity for An(III) than the malonamide, is under development at JAERI (Tokai, Japan).

° **TRPO (INET, Tsinghua University, China)**
The TRPO process is based on the use of a mixture of *tri*-alkyl phosphine oxides ($R_3P(O)$, with R = alkyl groups) as extractant. This process has been tested successfully in China with genuine HAW. Its main drawbacks concern the necessity: (i) to adjust the feed acidity, (ii) to use a concentrated nitric acid solution for An(III)+Ln(III) stripping, which complicates the subsequent An(III)/Ln(III) partitioning step.

- ***2nd step: An(III)/Ln(III) separation***

° **TALSPEAK and CTH processes**
The TALSPEAK process, developed at ORNL (USA) in the sixties and then adapted (CTH process) at Chalmers University, Göteborg, Sweden, can be considered as the reference process for An(III)/Ln(III) group separation. It is based on the use of HDEHP as extractant and DTPA as the selective An(III) complexing agent. The An(III)/Ln(III) separation is performed by the selective stripping of An(III) from the HDEHP solvent loaded with the mixture of An(III)+Ln(III) under the action of an aqueous solution containing DTPA and an hydroxocarboxylic acid, like lactic, glycolic or citric acids. The advantages of this process are: (i) the large experience gained world-wide, (ii) its good efficiency. Among the main drawbacks one can cite: (i) the necessity to adjust the pH of the feed, (ii) the limited solvent loading of metal ions, (iii) the difficult solvent clean-up.

° **SANEX concept (acidic S-bearing extractants)**
- **CYANEX 301 process (China, USA, Germany)**

The CYANEX 301 extractant consists in a dialkyldithiophosphinic acid (R_2PSSH, with R= an alkyl group). Its use for An(III)/Ln(III) was first proposed by Zhu at Beijing (China) in 1995. The main interest of the process relies in: (i) the large efficiency for An(III)/Ln(III) separation, (ii) the fact that the process has been tested with genuine An(III)+Ln(III) mixtures. Nevertheless, for an efficient use of this process the feed solution should be adjusted to pH 3 to 5, which is not so easy to carried out industrially. Moreover, the solvent clean-up is also a weak point.

- **ALINA process (Germany)**

To cope with the main drawbacks of the CYANEX 301 process mentioned above, Odoj and Modolo at Jülich (Germany) proposed the use of a syngergistic mixture made of

bis(chlorophenyl)dithio-phosphinic acid ($(Cl\Phi)_2PSSH$) + tri-*n*-octylphosphine oxide (TOPO) to perform the An(III)/Ln(III) group separation. If the separation factors between An(III) and Ln(III) are less than those observed with CYANEX 301, the concentration of nitric acid in the feed can be as high as 1.5 mol/L, which makes the ALINA process more attractive than the CYANEX 301 one. The ALINA process was successfully tested with genuine wastes. The possible drawbacks of this process are: (i) the solvent clean-up process not yet defined, (ii) the generation of P- and S-bearing wastes (from the degraded extractants) which should be managed.

° SANEX concept (neutral N-bearing extractants)

- BTPs (Germany, France, Europe)

After the discovery by Kolarik at FZ Karlsruhe (Germany) of the astonishing properties of the bis-triazinyl-1,2,4-pyridines (BTPs) for An(III)/Ln(III) separation, a process was readily developed and tested in the frame of the European so-called NEWPART project [3]. Successful hot tests were achieved both at the CEA/Marcoule and at the ITU in Karlsruhe using the n-propyl-BTP. Large efficiency of the BTP process was obtained. One should mention also that the feed of the n-propyl-BTP process can be acidic ($[HNO_3]$ = 1 mol/L). Nevertheless, even if this system seems very promising, an instability of the n-propyl-BTP extractant was observed. As a consequence, efforts are underway at the CEA to modify the solvent formulation to suppress this major drawback.

- TMAHDPTZ + octanoïc acid (CEA, France)

A synergistic mixture made of the terdendate N-ligand, 2-(3,5,5-trimethylhexanoylamino)-4,6-di-(pyridin-2-yl)-1,3,5-triazine (TMAHDPTZ), and octanoïc acid was developed at CEA/Marcoule. A process flowsheet was defined and successfully tested with genuine effluent with good efficiency. The main drawbacks of this process are: (i) the required pH adjustment of the feed, (ii) the management of secondary wastes not yet defined.

- 3rd step: Am/Cm separation

For this step, processes based on the selective oxidation of Am at the + VI or + V oxidation states are developed, the curium remaining unchanged as Cm(III), allowing simple Am/Cm separation processes to be defined.

° SESAME process (CEA, France, Hitachi, Japan)

In strong oxidising conditions, Am can be oxidised from Am(III) to Am(VI). This can be done, for example, by electrolysis in the presence of heteropolyanions (HPA) acting as catalyst. The so-generated Am(VI) can be separated from Cm(III) by extraction, for example by TBP. This is the principle of the so-called SESAME process developed at CEA/Marcoule. At Hitachi (Hitachi city, Japan), oxidation of Am to Am(VI) is obtained by the use of ammonium persulphate. Then, Am(VI) is extracted by TBP. The SESAME process exhibits a great efficiency for Am/Cm separation. A large experience was obtained at the CEA at pilot scale during the last twenty years with a SESAME like process (kg amounts of ^{241}Am were purified). Nevertheless, the industrialisation of the process is faced with difficulties such as: (i) the instability of Am(VI), (ii) the non-easiness to develop a multi-stage process, (iii) the generation of secondary solid waste (made of HPA constituents).

° Am(V) precipitation (JNC, Japan)

The selective precipitation of double carbonate of Am(V) and potassium (K) is one of the oldest method for Am/Cm or Am/Ln separations, developed at the end of the 60's in the USA.

This method requires the use a 2 mol/L K_2CO_3 solution in which the mixture of Am(III) and Cm(III) is dissolved. After chemical or electrochemical oxidation of Am(III) to Am(V), Am(V) precipitates from the solution as the solid crystalline $K_5AmO_2(CO_3)_3 \cdot nH_2O$, while Cm(III) remains in solution. After filtration, Am is separated from Cm. This process: (i) is simple, (ii) is selective for Am, (iii) has been largely used world-wide. The process main drawbacks are: (i) the Am losses with Cm, which are not so low, (ii) the fact that it exists only one stage for the process, (iii) the large amounts of secondary wastes generated.

II.2.3 FPs Partitioning

- **Iodine (^{129}I)**

The separation of iodine is done just after the spent fuel dissolution step within the PUREX process. Oxidation of iodide ion, I^-, into elemental iodine (I_2) induces its transfer to the dissolver off-gases (DOGs) where iodine is recovered through DOGs basic washing. To recover most of the iodine spent fuel inventory at that step, slight improvement of the efficiency of the transfer of iodine from the dissolution liquor to the DOGs seems required.

- **Technetium (^{99}Tc)**

The soluble fraction of Tc contained in the spent fuels exists in the dissolution liquor as Tc(VII) (TcO_4^-). Its co-extraction with Zr(IV), then U(VI) and Pu(IV), by TBP is well known. So, for example, the separation of the Tc soluble fraction is achieved through a solvent special scrubbing step in the course of the implementation of the PUREX process at Cogéma La Hague reprocessing plants. If high Tc partitioning yield is required, the main problem concerns the recovery of the Tc fraction that is contained within the solid insoluble residues remaining after spent fuel dissolution. A special process is required for this Tc recovery, which actually does not exist.

- **Caesium and strontium or caesium alone**

Many processes were developed world-wide in this field, including the use of:

(i) inorganic sorbents, like for the JAERI's 4 group partitioning process,
(ii) crown-ether extractants, like for the SREX and CSEX processes developed in the USA (ANL),
(iii) cobalt dicarbollide extractants, as developed in Czeck Republic, Russia and Western Europe,
(iv) calix-crown extractants, as developed in France, Western Europe and in the USA.

Most of these processes were successfully tested with radioactive effluents.

II.3. Pyro processes for actinide partitioning [4]

II.3.1 Selected media and possible separation techniques

- **Selected media**

Most of the "pyro" processes developed so-far are based on the use of one or two of the following high temperature liquid phases:

° Fused salts. The most popular fused salts studied are:

(i) molten chloride eutectic, such as LiCl + KCl,
(ii) molten fluoride eutectic, such as LiF + CaF_2.

° Fused metal, such as Cd, Bi, Al, *etc...*

▪ **Separation techniques**

To partition the actinides contained within the fused salt baths, three main techniques are studied and developed:

° actinide electrodeposition on solid (pyrographite or metal) or liquid metal cathodes,

° liquid-liquid extraction of actinide between fused salt bath and a metal bath containing a reductive metal solute (Li for example),

° actinide oxide precipitation from the fused salt under the proper control of the oxygen thermodynamic activity within the salt bath.

II.3.2. Examples of strategies and "pyro" processes

▪ **USA (ANL, Chicago)**

A "pyro" process was developed at ANL in relation with the treatment of FR metallic fuels (EBR II's type) for stabilisation of these Na bonded fuels. The aims of the process is limited. It consists in the separation of the spent fuel into three major fluxes: (i) most of the uranium as a low level waste, (ii) cladding + noble metals + Zr as metallic waste, (iii) TRUs + FPs + Na + salt incorporation into a zeolithe matrix in order to obtain a ceramic waste after hot pressing. The key step consists, after the oxidative dissolution of the spent metallic fuel in LiCl + KCl eutectic bath at 500 °C, into the separation of most of the uranium by electrorefining on a solid cathode. A demonstration campaign involving the treatment of 100 core assemblies (0.4 ton of spent HEU) and 25 blanket assemblies (1.2 tons of spent depleted U) was successfully carried out at Argonne West in the recent years. License for pyroprocessing the whole EBR II spent fuel inventory was obtained recently.

▪ **Russia (RIAR, Dimitrovgrad)**

The pyro-process developed at RIAR concerns the treatment of spent oxide fuels (UOx and MOx) in order to recover U and Pu for MOx fuel re-fabrication by the vibro-compaction process.

The spent oxide fuel is dissolved by chloration in a Li, Na, K, Cs chloride fused salt bath at 650-700 °C. Separation of U, Pu or mixture of U + Pu from the salt bath can be obtained by electrodeposition or precipitation. For example:

° U can be separated as UO_2 (which is a good electric conductor) by electrodeposition on a cathode made of pyrographite, while chlorine gas is generated at the anode,

° as PuO_2 is a bad electric conductor, it cannot be electrodeposited on solid cathode. But PuO_2 can be selectively separated by precipitation after bubbling a mixture of Cl_2 + O_2 gases into the fused salt bath,

° under the addition of a mixture of Cl_2 + O_2 gases into the fused salt bath, which stabilises Pu as oxychlorides, electrolysis generates a deposit of $(U,Pu)O_2$ onto the pyrographite cathode while chlorine gas evolves at the anode.

An important experience with spent fuel pyroprocessing has been obtained at RIAR with the treatment of:

° 3.3 kg of UO_2 spent fuel (1 % burn-up) from the VK-50 reactor, done in 1968,

° 2.5 kg of UO_2 spent fuel (7.7 % burn-up) from the BOR-50 reactor, done in 1972-73,

° 4.1 kg of $(U,Pu)O_2$ spent fuel (4.7 % burn-up) from the BN-350 reactor, done in 1991,

° 3.5 kg of $(U,Pu)O_2$ spent fuel (21-24 % burn-up) from the BOR-60 reactor, done in 1995.

- **Japan**

° **CRIEPI**

The "pyro" process developed at CRIEPI concerns both the treatment of spent fuels from LWRs (oxide fuels) or FRs (metallic fuels) and the partitioning of TRU elements from the wastes issuing the reprocessing of spent LWR fuels by the PUREX process. The fused salt selected is the LiCl + KCl eutectic in which the spent fuels or the oxides of high active wastes are dissolved by a carbo-chloration technique. After dissolution, U can be electrodeposited as a metal on a solid cathode, then the TRUs can be recovered by electrolysis using a liquid cadmium or bismuth cathode. CRIEPI is also studying the partitioning of MAs by liquid-liquid extraction using a LiCl+ KCl salt bath and Cd or Bi metallic solvents containing Li as a reducing agent. In this case, liquid-liquid extraction corresponds to the reductive transfer of a metal from the salt bath, where it exists as M^{n+} cation, to the metal solvent, where M exists as a M^0 solute. The equation of the extraction reaction can be written as follows:

$$M^{n+}_{(salt)} + n\,Li^0_{(Cd\ or\ Bi\ metal\ phase)} \Longleftrightarrow M^0_{(Cd\ or\ Bi\ metal\ phase)} + n\,Li^+_{(salt)} \qquad (4)$$

Large expertise has been gained by CRIEPI in this field but only with surrogates of actinides. A joint CRIEPI-ITU program is under way to test the process with actinides.

° **JAERI**

JAERI is studying pyroprocessing for the possible treatment of nitride, oxide or metallic spent fuels in order to prepare nitride fuels enriched with ^{15}N for FRs. After dissolution of the spent fuels into a LiCl + KCl eutectic salt bath, the actinides will be electrodeposited on solid or liquid (Cd) cathodes. The recovered actinide metals will then be converted into actinides nitrides after their dissolution in liquid cadmium. The nitruration agent will be N_2 or Li_3N.

° **PNC**

PNC is also engaged in the development of pyro processes aiming to reprocess FR spent fuels. The method selected are similar to those studied by CRIEPI : (i) choice of LiCl + KCl eutectic bath, (ii) electrodeposition method, (iii) liquid-liquid extraction between salt bath and liquid Cd metal.

- **France**

Two years ago, the CEA has launched a programme dedicated to the partitioning of MAs by "pyro" processing. A research team was created at CEA/Marcoule and special hot facilities have been created. The programme selected is rather wide. It will consider both chloride and fluoride melts and the most important separation techniques known to be effective in "pyroprocessing", *i. e.*: (i) electrodeposition, (ii) oxide precipitation, (iii) liquid-liquid extraction between fused salt bath and a metallic solvent. The results obtained to-date concern mainly the basic understanding of the chemistry of actinides (U, Pu and Am) in solution in the fused melts. Process developments are also underway and active tests on irradiated objects are foreseen to be done before 2005.

- **Czech Republic**

At Rez Institute, Czech scientists are developing a process based on the dual use of actinide hexafluoride volatilisation and pyroprocessing of the wastes from a fluoride melt. This research programme is connected with the interest of Czech Republic for the development of

the molten salt reactor (MSR) technology. Facilities are under construction at Rez Institute for testing the pyro-processes.

III. CONCLUSIONS-PERSPECTIVES

Conclusions

Numerous concepts have been consolidated or newly developed during the last few years, both in "Hydro" and "Pyro" processing of HAWs or spent fuels and targets for "new" nuclear systems.

Tests on "real objects" were carried out successfully in several countries, including the EBR II demonstration test at Argonne-West (UA) on pyroprocessing of FRs spent fuels.

In the domain of "Hydro", blooming of concepts is observed. Multi-step processes look promising but most of the systems developed so-far appear complex. Efforts to simplify the processes seem required.

In the domain of "Pyro", strong consolidations of "old concepts" were obtained, including fluoride volatilisation.

Perspectives

- **Hydro**

It seems important to work in order to increase the "simplicity" and "compacity" of the MAs and LLFPs separation processes. Some routes for improvement can be proposed:

(i) one cycle process,
(ii) consideration of High Active Concentrates instead of High Active Raffinates for process development (large volume reduction factor),
(iii) integration of MAs and LLFPs separation processes,
(iv) consideration of possibly new LLFPs for partitioning,
(v) maintaining alive the "CHON principle" (minimisation of secondary solid wastes).

- **Pyro**

Directions for improving the processes appear to be :

(i) minimisation of TRU losses in wastes and increase of the purities of the separated actinides which can be obtained through the combined use of several separation techniques and multi-stage techniques,

(ii) the waste problem, which is mostly corrosion related owing to the aggressive character of the media and the high process temperatures, needs to be precisely estimated,

(iii) consideration of the possible separation of LLFPs.

- **Collaborations**

It seems a pressing necessity to maintain, or best to increase, the collaborations in this complex field at:

(i) National levels: maintain or create network(s) between academic and applied research bodies. As example in France it exist two Networks working under the auspices of the December 1991 Nuclear Waste Act: the so-called PRACTIS and NOMADE Groupes de Recherches,

(ii) Bi-national levels: numerous collaborations exist, e.g. CRIEPI-ANL, CEA-JNC, CEA-JAERI *etc...*

(iii) regional level. As example at the European level it exist common works partly financed by the EU, e.g. the PARTNEW, CALIXPART and PYROREP programs within the 5th FWP of EU (2000-2003). The role of ITU at Karlsruhe is also very important for European and wider collaborations,

(iv) at the International level, the roles of OECD/NEA for Workshops and Working Parties managements and also of IAEA appear essential.

So, within few years, one an predict that a large array of robust "hydro" and "pyro" processes will be available for the definition of new scenarios for the management of nuclear wastes generated through LWRs and FRs closed fuel cycles, but also for the fuel cycles of futuristic nuclear systems, such as the MSRs or the ADSs.

REFERENCES

Only very few references will be mentioned here.

[1] Proceedings of EURADWASTES Conference, Luxembourg, November 1999.

[2] Anonymous, DOE/RW-0519, (1999), "*A Roadmap for Developing Accelerator Transmutation of Waste (ATW) Technology. A Report to Congress*".

[3] C. Madic; M.J. Hudson; J. O. Liljenzin; J. P. Glatz; R. Nannicini,; A. Facchini; Z. Kolarik and R. Odoj, (2000), EUR 19149 EN, " *New Separation Techniques for Minor Actinides*".

[4] "*Pyrochemical Separations*", Workshop Proceedings, Avignon, France, 14-16 March 2000, OECD/NEA.

This is a blank page.

JP0250281

JAERI-Conf 2002-004

DECISION-IN-PRINCIPLE ON FINAL DISPOSAL OF SPENT FUEL IN FINLAND

Juhani Vira
Posiva Oy, Töölönkatu 4, FIN-00100 Helsinki
Fax: +358-9-2280 3719, e-mail: juhani.vira@posiva.fi

ABSTRACT
The main target of the Finnish programme for spent fuel disposal is the year 2020 when everything should be ready to start disposal. The most important milestone so far has been the selection of the Olkiluoto area in the municipality of Eurajoki as the site of the repository. The selection was formally accepted by the Finnish Parliament in the so-called Decision-in-Principle in May 2001.
The choice of Olkiluoto as the repository site was based on a long investigation process started in the early 1980's and including deep drillings and other geologic investigations on several candidate sites since 1987. The site selection was based on the outcome of the Environmental Assessment Process (EIA) conducted in 1997–1999. The EIA also included an assessment of the long-term safety of disposal ("TILA-99").
The Decision-in-Principle means that the further work on geologic disposal can be based on a KBS-3 type concept and the site investigations can be concentrated at Olkiluoto. In January 2001 Posiva published a programme for research, development, technical planning and design work for the period preceding the construction license. A substantial part of the programme focuses on the planned underground rock characterisation facility, ONKALO, at Olkiluoto.
Key words: spent fuel, geologic disposal, siting, environmental impact assessment

1. INTRODUCTION

According to the present legislation all spent fuel from the Finnish nuclear power plants must be handled, stored and permanently disposed of in Finland. For disposal the two nuclear power plant owners, Teollisuuden Voima Oy (TVO) and Fortum Power and Heat Oy have established a joint company, Posiva Oy, to take care of the research and development needed and later to construct and operate the disposal facility.
The guidelines and time schedules for the work towards final disposal were first set in a Government decision of 1983. The time table still continues to be valid (Fig. 1). The main target is the year 2020 when Posiva should be ready to start disposal. However, the most important milestone so far has been the selection of the site for the repository, which, according to the guidelines, was to be made by the end of the year 2000.
In May 1999 Posiva submitted an application for the so-called Decision-in-Principle (DiP) on the final disposal facility of spent fuel to the Finnish Government [1]. In this application Posiva proposed that the spent fuel from the Loviisa and Olkiluoto nuclear power plants should be disposed of in a KBS-3 type final repository which would be built at Olkiluoto near the Olkiluoto power plant site. The main purpose of the DiP is to judge whether the facility is in line "with the overall good of society", but an important part of the judgement is the decision on the suitability of the intended site of the facility. According to the Nuclear Energy Act the decision is made by the government but has also to be ratified by the Parliament.
The application was based on the outcome of some twenty years of research and investigations and on the environmental impact assessment (EIA) that was carried out in the years 1997–1999 for the final disposal facility [2]. The law requires a DiP before any significant commitment (e.g., investments) to a nuclear facility is made in Finland. In this case the decision was needed before making the decision on an underground rock characterisation facility.

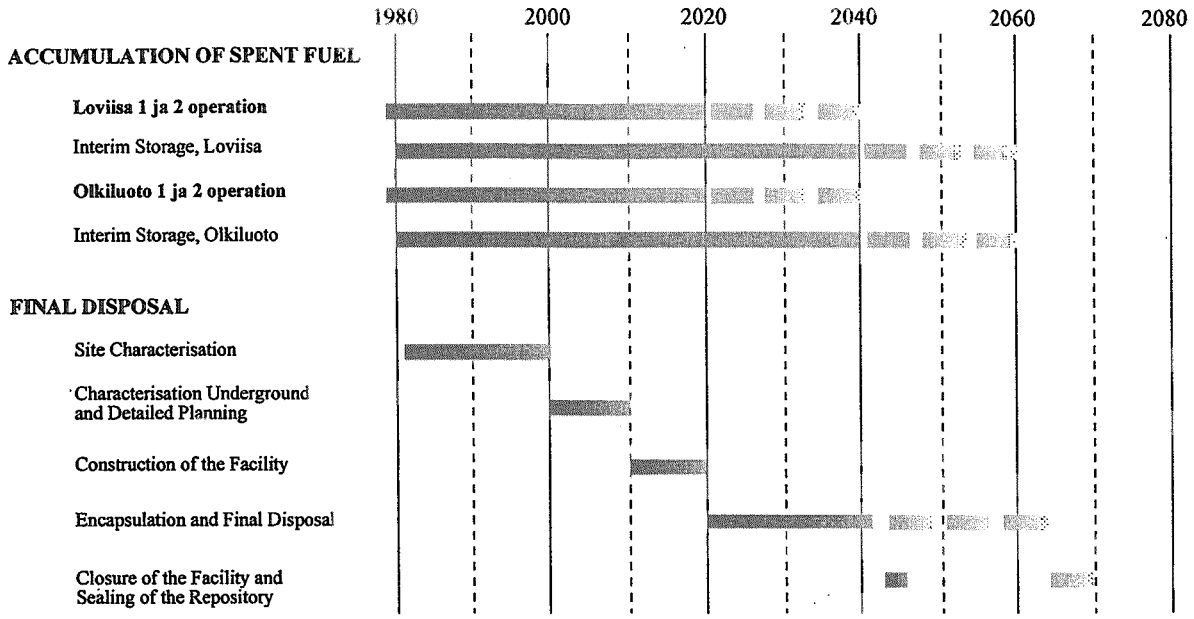

Figure 1. Time schedule for the spent fuel management in Finland.

The Government approved Posiva's application in December 2000 and the decision was ratified by the Parliament in May 2001. The next major milestone will now be the construction licence, the application for which is planned to be submitted in 2010.

2. THE DECISION-IN-PRINCIPLE

According to the Nuclear Energy Act the "construction of a nuclear facility... shall require the [Government's] decision in principle that the construction project is in line with the overall good of society." For this purpose the Government must judge that the following conditions are fulfilled:

- "the use of nuclear energy... shall be in line with the overall good of society."
- "the use of nuclear energy must be safe"

and this has to be done

"... paying particular attention to: ...the suitability of the intended site of the facility".

The first requirement basicly means a political judgement about the acceptability of the proposed nuclear facility. A prerequisite for the second judgement is that no factors are indicated which should make it suspect that a safe facility could be built. In practice it means that the "preliminary safety assessment" made by the regulatory agency, STUK, is positive – or at least "non-negative".

A prerequisite for the site suitability is the willingness of the intended host municipality to accept the siting proposal. In practice the decision is made by the municipality council. With this decision the municipality has an absolute veto to stop the DiP process: no nuclear facility can be sited in Finland against the municipality's will.

The process is schematically described in Figure 2. Accordingly, both STUK and the municipality can veto the decision. However, even with their acceptance the Government is, of course, free to make any decision. In this respect the DiP is more a political decision than a judgement of technical or scientific soundness of the proposal. This is further emphasised by the fact that the Government's decision has to be ratified by the Parliament.

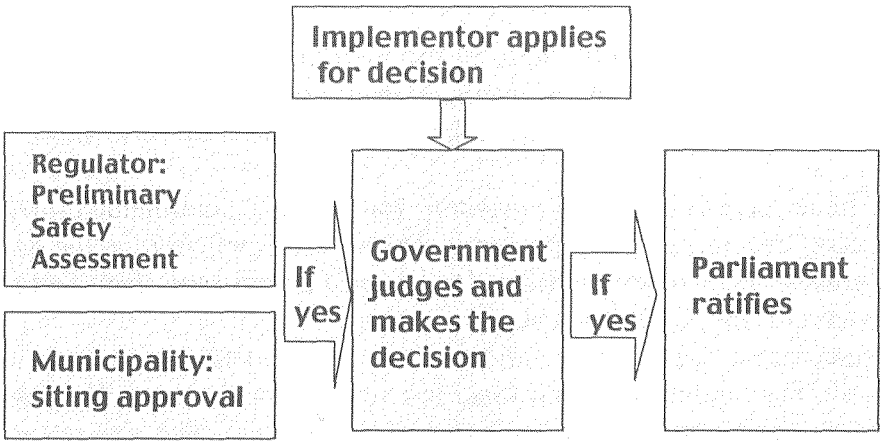

Figure 2. The Decision-in-Principle process according to the Nuclear Energy Act.

3. DISPOSAL CONCEPT

Posiva's plans for final disposal of spent fuel are based on the KBS-3 concept developed by the Swedish SKB. The spent fuel elements will be encapsulated in metal canisters and emplaced at the depth of several hundreds of meters in the bedrock (Fig. 3). Between rock and canisters, a buffer of bentonite clay would be installed; after completion of the disposal effort, all access routes from the surface to the disposal galleries would be closed and sealed, and the repository would need no further control or maintenance.

In the application for the DiP Posiva proposes that disposal should be based on a KBS-3 *type* concept. This means that the possibility for modifications of the technical concept is left open. One alternative option would be the horizontal placement of the canisters according to the so-called Medium Long Hole (MLH) concept.

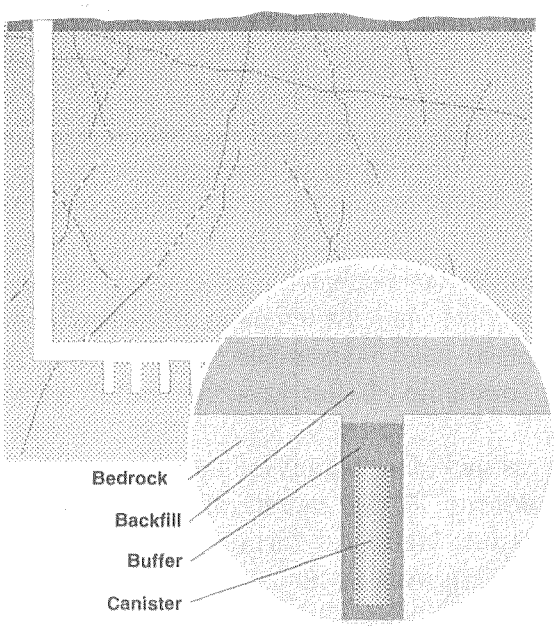

Figure 3. The KBS-3 concept for disposal of spent fuel.

4. SITE SELECTION PROCESS

The selected repository site is at Olkiluoto in the vicinity of the Olkiluoto nuclear power plant. Olkiluoto is an island belonging to the municipality of Eurajoki near the city of Rauma on the western coast of Finland. Eurajoki has a population of little more than 6,000 inhabitants.

Near the power plant there is already a repository for low- and intermediate-level operating waste from Olkiluoto reactors (VLJ Repository). This repository is built at the depth of 60 to 100 meters and consists of two vertical silos. The planned area for the spent fuel repository is a few kilometres east of the existing repository.

Olkiluoto was selected as one of the candidates for the spent fuel repository site in 1986 together with four other candidates: Romuvaara in Kuhmo, Veitsivaara in Hyrynsalmi, Syyry in Sievi and Kivetty in Konginkangas (later part of Äänekoski). The site selection process between 1983-2000 is outlined in Figure 4.

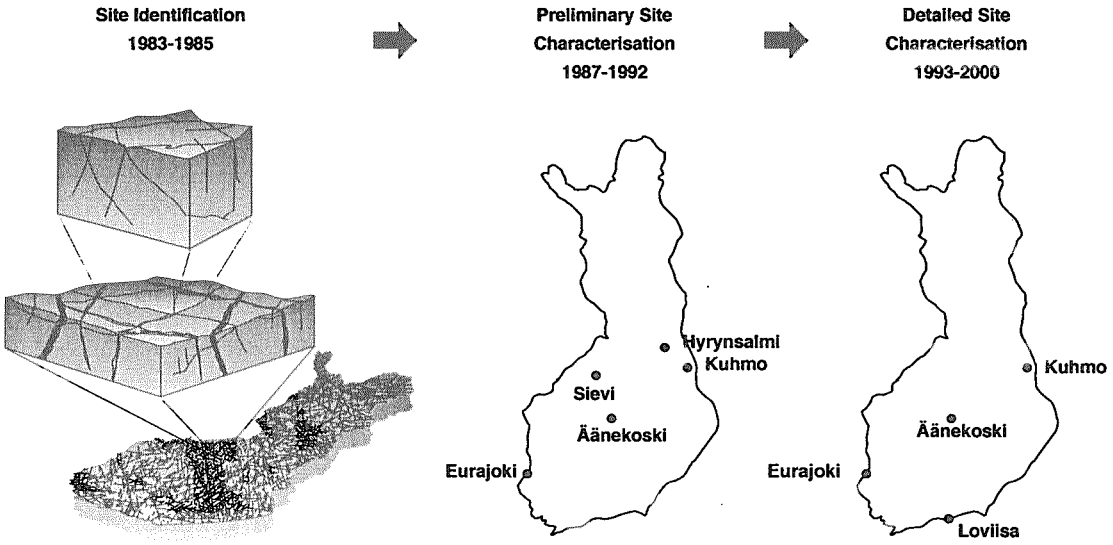

Figure 4. The stepwise site characterisation and evaluation process for siting the deep repository in Finland.

Each of the four candidate sites has been subject to an extensive programme of surface-based investigations and modelling studies. At least ten deep drillholes (of depths between 500 and 1000 metres) have been made at each site; at Olkiluoto already fourteen. The final site selection was based on the outcome of the Environmental Assessment Process (EIA) conducted in 1997–1999 [2].

The whole site selection process including the investigations carried out has been described in a summary report [3]. In addition to the investigations history the report makes some conclusions as regards the lessons learnt for further studies by Posiva and also for other programmes planning site characterisation work.

5. ENVIRONMENTAL IMPACT ASSESSMENT

The basis for the DiP application was laid in the report from the Environmental Impact Assessment published in May 1999 [2]. Research into the long-term safety of a KBS-3 type repository (reference concept) had already been carried out in Finland since the early 1980's.

For the purposes of the EIA the scope of the research programme was substantially extended to topics outside the technical and scientific safety issues.
A great deal of the new studies were devoted to the expected social impact. The areas addressed in the social impact assessment included

- effects brought about by changes in the physical environmental (related to every-day living conditions and general living standards, amenities, social well-being)
- effects on community and population structures and infrastructures
- effects on local and regional economics and well-being
- psychosocial effects (worries, anxiety, psychic effects)

The socio-economical assessment was based on traditional input-output analyses taking into account the direct and indirect effects on local and regional economic activity. The sociological and psychological aspects of the planned activity were on the one hand discussed in terms of the outcome of interviews and opinion surveys, on the other hand based on recent scientific studies and literature. Common to the whole assessment of the social impact was the issue of image. A considerable amount of effort was spent on attempts to elaborate the meaning of image and constituents thereof, as it was clearly affecting people's opinion both in the likely economic impact and the future social well-being.
Of course, safety was still a key issue in the assessment. A new long-term safety assessment, "TILA-99" was produced as a part of the EIA activity [4]. TILA-99 considers the long-term safety of the disposal concept against the general regulations issued in a March 1999 Government decision [5]. The discussion is specific of the four candidate sites taking into account all the results from the site investigations conducted since 1987.
In addition to the long-term safety assessment, new assessments were prepared on the operational safety [6] and the safety of transportation of spent fuel from the power plants to the encapsulation facility [7], which in the reference design is planned to be co-located with the repository. A review was also made on possible chemical hazards arising from the disposed materials [8].
The general conclusion of the EIA was that the likely impact on public health and natural conditions would always be small. The facility will have some impact on the local economic activity and employment, but this effect will most likely be positive. There may be some negative social effects also which mainly arise from the negative image and risk concerns that are sometimes associated with nuclear wastes.
The assessment of long-term safety concludes that most probably there will never be releases that would lead to meaningful radiation doses by any individual and even in the worst unlikely future scenarios the doses would not exceed the background level. All in all, the regulatory requirements can be met with considerable safety margins independent of which site is chosen. The conclusions of the studies into operational and transportation safety are similar: there should never be any significant health detriment from the planned operations and even the likelihood of a significant radioactive release from the plant or transport casks is minimal.
An important part of the EIA was the assessment of alternatives. This included several levels:

- assessment of alternative spent fuel management concepts
- assessment of different technical concepts of geologic disposal
- comparison of the proposed concept with the zero alternative (continued interim storage under surveillance)
- assessment of the site alternatives.

The outcome of the comparison between technical alternatives was that the reference KBS-3 type concept would promise the best potential for further development.
The conclusion from the comparison of the reference concept with the zero alternative was that both alternatives were technically feasible and both alternatives could provide sufficient

protection of man and environment – however, the zero alternative only assuming continuos maintenance of the storage. The active development of a permanent, passively safe method of disposal was considered necessary to provide against the risk of discontinuation of the maintenance.

The assessment of alternative sites for the disposal facility was based on a number of factors including

- long-term safety
- constructability
- possibility of expanding the repository
- operation of the disposal facility
- social impact
- land-use and environmental loading
- availability of infrastructure
- costs.

As regards long-term safety an important conclusion of the TILA-99 safety assessment was that there is no possibility of objective ranking of the alternative sites in terms of the long-term performance of the repository. There were differences between the sites, but none of the sites was clearly superior or inferior to other sites.

The most evident difference between the sites was concerned with social acceptance and the expected social impact. On the basis of the studies the expected social impact would clearly be smallest in Eurajoki.

6. DECISION PROCESS

In the application for the Decision-in-Principle Posiva proposed that the Olkiluoto site be selected as the site of the disposal facility. The proposal was largely based on the conclusions of the EIA. Among the factors supporting the choice of Olkiluoto were particularly the fact that most of the spent fuel accumulated is already at Olkiluoto and the judgement based on the EIA that at Eurajoki any major social controversies can probably be avoided.

According to the Nuclear Energy Act, the regulatory authority (STUK) has to make a preliminary assessment of the proposed facility vis-à-vis the legal requirement that the use of nuclear energy has to be safe. STUK's assessment was reported to the Government in January, 2000. In the statement STUK considers that, first, the DiP is justified on safety grounds and, secondly, the DiP not only can be made but it should be made.

Shortly after the statement of STUK was published the municipality council of Eurajoki made their decision. After a vote (20–7) the council approved the proposed siting of the disposal facility within its area. The council decision gave rise to two appeals to the regional court of administration and later to the supreme court of administration, but all these appeals were rejected. In December 2000, the Finnish Government approved the application.

The Parliament started discussing the decision in February 2001. The debate (in two Parliament committees and two plenary sessions) was very much focused on the availability and status of alternatives, retrievability of the spent fuel after disposal, knowledge about long-term safety, and the subsequent decision-making process. The final vote on 18 May, 2001, was 159–3 in favour of the ratification (37 absent).

It seems that among the factors contributing to the almost unanimous ratification were

- the fact that spent fuel exists and needs to be managed
- the lack of feasible alternatives to geologic disposal at the moment
- the possibility of stepping back (further licences still needed; retrieval possible even after repository closure)
- trust in the process.

One of the reasons for timing the DiP application had been the need to go underground for further studies of the Olkiluoto bedrock. The need for underground characterisation was emphasised by many Parliament members as well.

7. THE FUTURE

In January 2001 Posiva published a programme for research, development, technical planning and design work for the period preceding the construction license [9]. According to the guidelines Posiva is preparing to submit the application in 2010. The construction of the disposal facility could then be started later in the 2010's, which would enable the start of disposal operations in 2010.

A substantial part of the programme activities will be staged according to the progress of the planned underground rock characterisation facility, ONKALO, at Olkiluoto. At the moment different alternative designs and layouts are being considered for the facility. The main interest is in the rock properties at the actual repository depth for which one or several investigation tunnels would be excavated. Two access ways are planned to this level: either by a shaft and an access tunnel or by two horizontal shafts, as depicted in Figure 5. The plan is to start the construction of ONKALO in 2003–2004.

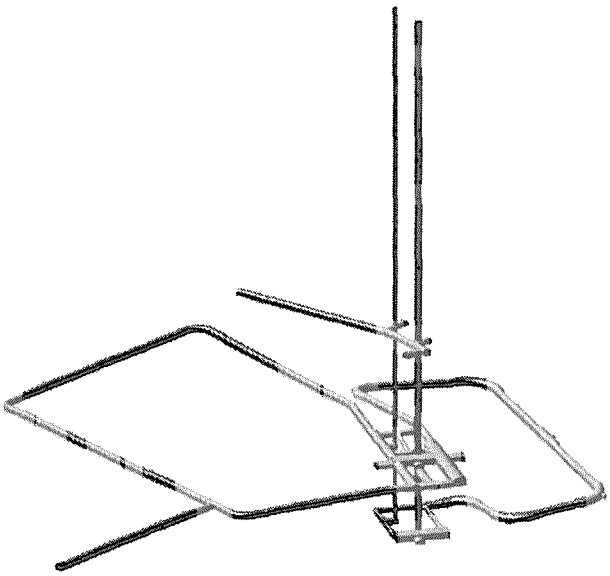

Figure 5. An example of the possible layout for the ONKALO rock characterisation facility.

LIST OF REFERENCES

[1] Posiva Oy 1999a. Application for a decision in principle on the final disposal facility of spent fuel. Posiva Oy, Helsinki (in Finnish).

[2] Posiva Oy 1999b. The final disposal facility for spent nuclear fuel – Environmental impact assessment report. Posiva Oy, Helsinki.

[3] McEwen, T. & Äikäs, T. 2000. The site selection process for a spent fuel repository in Finland – Summary report. Report POSIVA 2000-15, Posiva Oy, Helsinki.

[4] Vieno, T. & Nordman, H. 1999. Safety assessment of spent fuel disposal in Hästholmen, Kivetty, Olkiluoto and Romuvaara – TILA-99. Report POSIVA 99-07. Posiva Oy, Helsinki.

[5] STUK 1999. Government Decision on the safety of disposal of spent nuclear fuel (478/1999). Radiation and Nuclear Safety Authority, Report STUK-B-YTO195, Helsinki.

[6] Rossi, J., Raiko, H., Suolanen, V. & Ilvonen, M. 1999. Assessment of radiation doses due to normal operation, incidents and accidents of the final disposal facility. Report Posiva 99-16. Posiva Oy, Helsinki (in Finnish).
[7] Suolanen, V., Lautkaski, R. & Rossi, J. 1999. Assessment of health risks brought about by transportation of spent fuel. Report POSIVA 99-17, Posiva Oy, Helsinki (in Finnish).
[8] Raiko, E. & Nordman, H. 1999. Chemical toxicity in final disposal of spent nuclear fuel. Working Report 99-18. Posiva Oy, Helsinki (in Finnish).
[9] Posiva Oy 2000. Disposal of spent fuel in Olkiluoto bedrock – Programme for research, development and technical design for the pre-construction phase. Report POSIVA 2000-14. Posiva Oy, Helsinki.

JP0250282

JAERI-Conf 2002-004

COMMUNICATION OF NUCLEAR POWER CONCEPTS TO STAKEHOLDERS - THE USE OF NATURE'S OWN LABORATORIES

J M West[1], W R Alexander[1], K Kaku [1], I G McKinley[1] and A Shimmura[2]

[1] Nagra (National Co-operative for the Disposal of Radioactive Waste), Hardstrasse 73, 5430 Wettingen, Switzerland (email: isp@nagra.ch)
[2] Obayashi Corporation, Technology Department No. 6, Civil Engineering Technical Division, Shinagawa Intercity Tower B, 2-15-2 Konan, Minato-ku, Tokyo 108-8502, Japan

ABSTRACT

The history of nuclear technology development has generated a legacy of nuclear fear in many people, which becomes more acute when the problem of radioactive waste is highlighted. Thus a significant element of increasing confidence in nuclear power is to generate confidence in the industry's ability to safely dispose of its waste. The use of natural analogues as a key vehicle for such communication is now recognised as an influential approach. This paper will examine how analogues can be used to convey difficult concepts to stakeholders and develop an outline communication programme.
Keywords: natural analogues, nuclear power concepts, communication, stakeholders

INTRODUCTION

Nuclear power development has a historical legacy of irrational fear for many people (association with nuclear weapons, teratogenesis, carcinogenesis, and environmental pollution). Nevertheless the considerable benefits - such as plentiful electric power - have generated a half-hearted acceptance of the technology by some stakeholders. This fear, however, becomes more acute when the 'yet to be solved' problem of the geological disposal of radioactive waste is highlighted. Reluctant acceptance often becomes active opposition - effectively stopping geological waste disposal programmes in several countries. Thus a significant challenge in increasing confidence in nuclear power is to generate confidence in the industry's ability to safely dispose of its waste.

Considerable efforts have been made over the past 3 decades to develop rigorous methods for the geological disposal of radioactive waste (including siting, design and performance assessment). However, much of the work has been highly complex and difficult to communicate - even to technical audiences. Additionally, many scientists lack communication skills and are ill equipped to communicate their work to non specialists - particularly when attempting to provide clear and unambiguous answers to difficult questions [1]. As a result, stakeholder groups (defined here as everyone who benefits from nuclear electric power) often have little confidence in the ability of the nuclear power industry to safely dispose of radioactive waste. This lack of confidence in the industry can be demonstrated in Japan by the May 2001 plebiscite rejection of the use of recycled plutonium at the Kariwa nuclear plant. Following this Prime Minister Junichiro Koizumi said 'The government and utility companies should think about how we can gain public support for nuclear energy, and make further efforts' (Associated Press, 28th May 2001). As a result, a government liaison council (involving ministries and agencies) has been devising educational and publicity measures to try to improve confidence in Japan's nuclear energy policy. A similar lack of confidence in the industry can also be seen in Germany where large-scale demonstrations in 2001 also highlighted concerns about the movement of nuclear waste. Such high profile reactions can be compared to those generated by other industry

wastes (coal, oil, chemical etc) where responses, in general, have a lower profile - probably because these industries have longer histories and have built a degree of confidence (however limited) in their stakeholders. Without confidence in the nuclear industry, radioactive waste disposal programmes in many democratic countries are in grave danger of failing. This has been recognised at high levels within the industry. At a recent Nuclear Energy Agency workshop Mr Matsuura, Chairman of the Nuclear Safety Commission, Japan said 'In order to restore public confidence there is no other course but to be prepared for difficulty and work honestly to our fullest ability, with all steps made openly and honestly' [2]. Such confidence is possible to build as demonstrated by progress in disposal programmes in Scandinavia where stakeholders have been involved in specific waste management decisions. However, new ways have been sought to try to communicate radioactive waste concepts to stakeholders (particularly to the general public) and to improve their confidence in waste disposal. Natural analogues are now recognised as a key vehicle for such communication.

REQUIREMENTS FOR BUILDING CONFIDENCE IN STAKEHOLDER GROUPS

Building confidence in the industry's ability to safely dispose of waste (particularly of high-level waste, HLW) must be put in the context of an overall communication strategy which identifies the key concerns of different stakeholder groups. Such a strategy should demonstrate the honesty, openness and high level of technical competence of all involved organisations. It should also show consistent policy and the use of technical arguments which both recognise the concerns of stakeholders and acknowledge the importance of dialogue.

Many concepts require communication to stakeholder groups, including, in particular, the following:

- radioactivity occurs naturally and it is only the particularly high concentration of radionuclides in HLW which makes it so hazardous;
- radioactivity is easy to measure and easily shielded if the source is compact;
- radioactivity in waste decreases with time, with highest specific activity nuclides decaying fastest;
- the long period of waste isolation needed can be provided by deep geological repositories.

The stability of a deep geological repository is acknowledged to be particularly difficult to communicate in Japan where the tectonic activity of the country is evident from the many volcanoes and regular earthquakes.

THE USE OF ANALOGY AND THE ROLE OF NATURAL ANALOGUES

Visual and mental images play a key role in the advertising industry. For example, the use of a particular product is often linked in a picture to a particular lifestyle. The buyer is thus invited to emulate the lifestyle by buying that product. In a similar way, analogies are used in the broadcast media to present difficult concepts to non-specialists. For example, the term 'aquifer' has been explained as 'a giant bathroom sponge' in a recent radio programme and this mental image quickly and simply gives a useful visual impression of the concept that the non-specialist can understand. Analogies are also powerful in putting across emotional

issues. A useful example can be seen in presenting risk in a way that invites a reaction at the 'gut' rather than at the intellectual level. Rail, air and road travel is inherently risky with the possibility of catastrophic failure but there is widespread acceptance of its risks. In comparison, a deep geological repository, where no catastrophic failure is possible, generates widespread fear and poor acceptance. This fear is focused, in part, on the perception that the construction of a geological repository is novel, untested and hence risky and will result in waste leakage. Using geological analogies, such as the Oklo natural fission reactors in Gabon (a natural 'nuclear reactor') it is possible to show that radioactivity does not move and has been isolated for billions of years. Images are the key with this method of presentation, which acknowledges the fear of a repository but puts it into the context of an emotional reaction.

Analogies have been used in the radioactive waste industry for many years. Before a repository can be built and operated it's safety must be adequately evaluated through formal performance assessment (PA) which requires detailed mathematical analysis of all aspects of the repository system and its evolution with time. Natural analogue (geological and archaeological) studies have the objective of providing information which can be used directly to support a safety PA [e.g. 3, 4, 5]. There are many different definitions of 'natural analogue'. A very general example is '...an occurrence of materials or processes which resemble those expected in a proposed geological waste repository' [6]. In technical applications, where the emphasis is on testing or validation of models (conceptual, qualitative or quantitative), specific definitions have been proposed. An example is '...the essence of a natural analogue is the aspect of testing of models, whether conceptual or mathematical, and not a particular attribute of the system itself' [7]. For this paper, which focuses on communication and confidence building, natural analogues can be viewed as 'occurrences of materials or processes that provide visual or mental images of the fundamental concepts or expected behaviour of repositories for radioactive waste'. For both technical and communication definitions the key aspect is the **application** of natural analogues - for communication this means carefully clarifying the link between the analogue and the repository system.

Used in a careful and imaginative way, natural analogues can be presented to opinion formers, politicians, concerned academics and the public to explain safety, for example, by showing what happens to rocks through geological time. Another example would be to show the concept and stability of glass waste forms (often perceived by the non-specialist as being like a glass vessel containing liquid waste) using manufactured uranium glass products which contain uranium as a colouring agent. In addition, natural analogues provide evidence of the fundamental feasibility of long-term isolation of waste in an underground repository. Care must be taken, however, as there is a risk in using inappropriate analogues or of over-interpreting data, both of which will lead to loss of credibility.

EXAMPLES OF NATURAL ANALOGUES

Over the past 15 years, most natural analogue studies have had broad scientific objectives rather than objectives related directly to confidence building or communication. Scientifically based natural analogue studies have been performed on a wide range of natural phenomena, such as ore deposits, marine and lake sediments, hyperalkaline springs, and ancient preserved forests. These studies have provided the opportunity to investigate various

natural processes that have operated over geological time periods. In addition, numerous analogue studies have examined archaeological artefacts, similar to the materials used in building a repository, which have been subjected to natural alteration and corrosion processes over historical time periods (for details of many of these studies, see reference [8]).

The key to communicating successfully the concepts and messages given above, using a natural analogues based confidence building programme, is to match them to stakeholder concerns and questions thus changing any negative images. These concerns will need detailed assessment and clarification. However, the science behind the natural analogues must underpin this dialogue in order to maintain credibility. Information from natural analogues can thus form the bedrock to structured communication programmes. Some specific examples of how some existing analogue studies could address questions and negative images from members of the public and convey positive images are given in Table I. Most of these examples are from studies outside Japan and, as such, they will probably be less intrinsically interesting and relevant to some Japanese stakeholders. There is, therefore, a strong case to instigate more research on selected analogues (both geological and archaeological) which will attract interest in Japan. For example, it is of crucial importance to convey the message that the geologically active nature of the Japanese islands does not preclude building a geological repository. Images of the after-effects of the Kobe earthquake could be contrasted against those of ancient Japanese tombs and ore bodies to demonstrate stability in the long term. However, it must be realised that the use of analogues does have limitations. Clearly, there can be no perfect analogue site or artefact. Further, some published studies are not scientifically robust and/or mismatch the analogue to a particular repository concept. There is also a common tendency to oversimplify complex issues in the analogue literature.

THE USE OF NATURAL ANALOGUES FOR CONFIDENCE BUILDING - INTERNATIONAL EXPERIENCE

International experience has shown that the use of using natural analogues in confidence building must be built on a well established technical programme. For example, in Switzerland, Nagra was one of the first organisations to use analogues in confidence building and this was linked to a significant technical programme (reference [9] provides a review and bibliography). The programme was used to address a variety of audiences including opinion formers, technically literate groups, scientific peers and school children. Nagra was also the lead organisation for the production of the natural analogue video "Traces of the future" which was sponsored by eight national waste disposal organisations and has been translated into nine languages including Japanese. Other international initiatives include the Natural Analogue Working Group co-ordinated by the European Union (which Nagra currently chairs) and IAEA sponsorship of several technical projects, workshops and expert reviews on analogues. Other national organisations have also used natural analogues for confidence building notably including AECL, Canada; SKB, Sweden; Nirex, UK and the US NRC. However, it is of note that, to date, no programme has tried to assess the success of specific confidence building strategies in a detailed manner (although this is now changing) but it can be seen that strategies have evolved with time in some programmes. In Switzerland and Scandinavia, in particular, the use of natural analogues (and Public Relations overall) has matured with the national disposal programme, moving

Table I. Examples of how basic questions and negative images from members of the public can be answered using positive natural analogue images

Questions and negative images		Answers and positive natural analogue images	
Questions	**Negative images**	**Answers**	**Positive images**
What is radiation? Is it not very dangerous? Is radioactive waste something completely new?	Atomic bombs. Cancer. Birth deformities. Environmental pollution.	Radiation is natural. Radiation can be handled safely.	Morro do Ferro, Brazil (very high natural radiation but no health effects). Other high background areas.
What is a repository?	Piles of glowing waste in large water-filled pits. Waste buried in dungeon-like crypts.	Repository designs mimic nature where U ore has been isolated for billions of years. Geological disposal can be a safe and appropriate method	Oklo, Gabon - a natural 'nuclear reactor' where radioactivity has not moved.
Are you sure that geological disposal is safe?	Exploding waste spraying radiation over homes, people etc. Leaking waste causing deformities. Monsters emerging from waste.	Long-term isolation, no surface indications of the radiation from the orebodies so surface environment remains safe.	Cigar Lake, Canada and Tono, Japan ore bodies.
How do you know that the barriers will last?	Cars rusting after only a few years use. Decaying 40 year old concrete apartment blocks. 'Rivers' flowing in rocks bringing waste to the surface	Natural and archaeological materials can last for thousands of years.	Archaeological analogues e.g. Roman nail cache - little corrosion despite 2000 years burial. Dunarobba forest, Italy - trees have not decayed despite 2 million years burial. Maqarin, Jordan - naturally occurring cements which are 1-2 million years old. Chinese tomb - thousand years' isolation by clay layer.

from generic issues to specifics as sites were identified and repository designs became more defined.

It is now recognised that any confidence building programme has to evolve and develop at the same time as the audience. As more information is provided to stakeholders their views will change and awareness levels will rise accordingly. Thus any programme will need to be iterative, constantly changing and adapting to changing perceptions and concerns. The *overall approach must be positive, proactive and dynamic in outlook.* It must also be aware of anti-nuclear information coming from other sources.

A COMMUNICATION STRATEGY FOR JAPAN

The use of natural analogues in communicating radioactive waste concepts must be placed in the context of a structured communication strategy. The strategy would need to integrate all existing Japanese waste disposal programmes with organisations involved in radioactive waste management so that a consistent communication approach can be taken. Audiences must be identified and key messages and communication methods and tools (including natural analogues) defined. The specific views and prejudices of audiences must also be characterised so that a 'baseline' of perceptions is established. Changes in this 'baseline' can then be monitored as the communication programme takes effect. It is also important that the programme is structured to evolve together with the national disposal programme. Consequent developments in the national programme must also be fully integrated into communication efforts. This is particularly important given the speed of development of electronic communication where inconsistencies in information will be immediately obvious.

USING NATURAL ANALOGUES FOR CONFIDENCE BUILDING IN JAPAN

The use of natural analogues as a communication tool requires an organisational framework which would draw together technical workers in the natural analogues field from all involved Japanese organisations (such as CRIEPI, JNC) with end users (predominantly from PA and Public Relations) and other key contributors (e.g. university professors). The group could also be complemented, as necessary, with appropriate foreign experts. An integrated programme of analogue projects could then be developed focusing on archaeological and geological analogues of particular relevance to the Japanese repository concepts. An overall concept publication will be necessary to convey the aims of the analogues project and should be made widely available together with regular updates on progress. In order to bring the group and its projects to the notice of technical audiences - both in Japan and internationally, it could organise workshops and major symposia. Such events, if handled correctly and in a stimulating way, using communication experts, could serve as a focus for communication to all Japanese stakeholders.

In order to reach as large an audience as possible, defined messages will need to be communicated at 3 overall levels:

- Level 1 - Educational
- Level 2 - Media
- Level 3 - Opinion formers and politicians (local, national and international)

Establishing two way dialogues with stakeholders is essential and should be mediated by Japanese communication professionals. Communication methods are diverse and should be tailored to each level. All of the information should be made available in as many media forms as possible (e.g. print, the internet, CDs, DVD etc) to enable it to reach as many people as possible. Development of the Internet is likely to increase over the next few years and this method of disseminating information will be critical and it could be the main point of access for all data. A web site should contain all information (including detailed technical details) which would be accessible to everyone. The site should also be structured in such a way that allows browsers to select information at a level of complexity of their choosing, thus promoting a culture of openness (Figure 1). As a result, children could find out basic facts, journalists would be able to find basic digests and briefings, politicians would find opinion polls and a forum for international debate and scientists could access technical information. Feedback and reaction should be encouraged through a contact point.

A variety of other communication methods will also be needed. For example, press releases are important sources of news for the media, as are press conferences. Video and television productions and advertisements are also powerful communication tools if material is presented in an interesting, dynamic manner. However, it is essential that all methods use the same information and communicate the same messages.

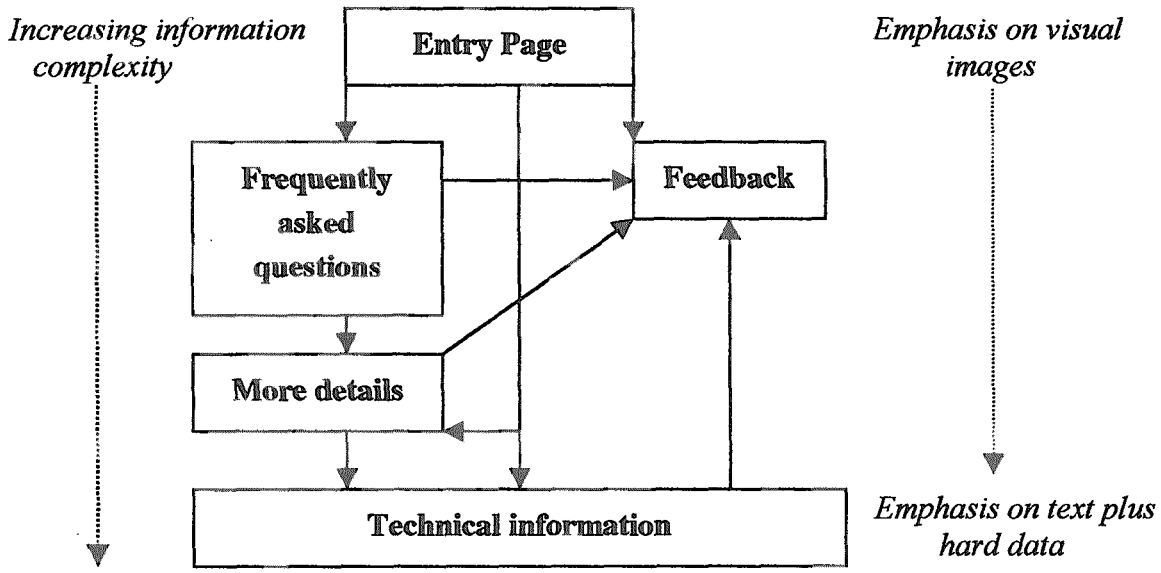

Figure 1. Diagram illustrating development of information complexity within a website. Note that direct access is possible to all levels and that the user can self select the level required to meet their information needs. Feedback is vital to establish dialogue.

CONCLUSIONS

There is an increasing requirement to build confidence in the ability of the nuclear industry to safely dispose of its radioactive waste. This has been recently demonstrated by the plebiscite result in Kariwa, which showed the strength of feeling generated by nuclear issues

in Japan. As a result, an integrated communication strategy is needed to tackle these concerns. Natural analogues provide an approach to address some of the most difficult questions posed by stakeholders.

ACKNOWLEDGEMENTS

Thanks to Hilary Heason (Political and Media Liaison, British Geological Survey), Drs Bill Miller and Caroline Taylor (Enviros QuantiSci) for their help in the development of the ideas presented in this paper. In addition, the invaluable support of David McKie and Aline Playfair (Nagra) and Peter Hogarth (British Trade International) is gratefully acknowledged. J M West is on sabbatical leave from the British Geological Survey until January 2002.

REFERENCES

[1] West, J. M. (2000) Life with Auntie (British Broadcasting Corporation - BBC). Biologist, 47 (3) 136-138.

[2] Matsuura, M. (2001) Challenge for reconstruction of public confidence. In: Investing in Trust: Nuclear Regulators and the Public, Nuclear Energy Agency Workshop Proceedings Paris, 29 November - 1 December 2000 pp 27 - 34, OECD, Paris, France.

[3] IAEA (1999) Use of natural analogues to support radionuclide transport models for deep geological repositories for long lived radioactive wastes. IAEA Technical Report 1109, International Atomic Energy Agency, Vienna, Austria.

[4] Smellie, J. A. T., Karlsson, F. and Alexander, W. R. (1997) Natural analogue studies: present status and performance assessment implications. J. Contaminant Hydrology, 26, 3-17.

[5] McKinley, I. G. and Alexander, W. R. (1996) The uses of natural analogue input in repository performance assessment - an overview. In: von Maravic, H. and Smellie, J. (editors) Natural analogue working group, sixth meeting, Santa Fe, September 1994. CEC Nuclear Science and Technology Report, EUR 16761.

[6] Come, B. and Chapman, N. A. (1986) Natural analogue working group, first meeting, Brussels, November 1985. CEC Nuclear Science and Technology Report EUR 10315, CEC, Luxembourg.

[7] McKinley, I. G. (1989) Applying natural analogues in predictive performance assessment. Unpublished Nagra Internal Report, Nagra, Wettingen, Switzerland.

[8] Miller, W. M., Alexander, W. A., Chapman, N. A., McKinley, I. G. and Smellie, J. A. T. (2000) Geological disposal of radioactive wastes and natural analogues. Pergamon Waste Management Series, Volume 2, Oxford, UK.

[9] Alexander, W. R., Gautschi, A. and McKinley, I.G. (2001) Overview of the Swiss natural analogue programme. In: von Maravic, H. and Alexander, W. R. (editors) Natural analogue working group, 8th meeting, Strasbourg, March 1998. CEC Nuclear Science and Technology Report, EUR (in press).

3. Oral Session

Criticality Safety

This is a blank page.

JP0250283

DEVELOPMENT AND APPLICATION OF CONSENSUS STANDARDS IN CRITICALITY SAFETY IN THE USA

Thomas P. McLaughlin
Los Alamos National Laboratory, Los Alamos, NM USA
Email: tpm@lanl.gov
Telephone: 505-667-7628

ABSTRACT

The development of national consensus standards in the USA had its beginnings in the document series titled "The Nuclear Safety Guide". This document was the product of collaboration among criticality safety and critical experiment specialists from the major fissile material processing sites nationwide. Starting in 1964 with the first standard, the number has grown to sixteen, with two currently under development. They provide guidance in essentially all aspects of criticality safety that are important to accident prevention. The two regulatory bodies in the USA, which oversee operations with significant quantities of fissile materials, the Nuclear Regulatory Commission and the Department of Energy, both adopt all of these sixteen nuclear criticality safety standards as the basis for regulation. The application of philosophies and technical guidance found in these standards is judged to be the underlying reason for the very low criticality accident rate that exists in the USA and, indeed, in the world today.

HISTORICAL DEVELOPMENT

The earliest appearance of guidance for criticality safety in process operations in a document authored by and with input from specialists at several installations across the USA was in 1956. This guidance was contained in the first edition of "The Nuclear Safety Guide" [1]. The authors represented Oak Ridge National Laboratory, the Hanford Works, the Rocky Flats Plant, and Los Alamos Scientific Laboratory, but additional contributors to the document represented the Savannah River Plant, the General Electric Company, Goodyear Atomic, Philips Petroleum, Union Carbide (Y-12 Plant and K-25 Plant) and Livermore National Laboratory.

This first edition of the Nuclear Safety Guide was followed by a series of revisions to accommodate the rapidly expanding knowledge base resulting from vigorous critical experiment programs at many sites within the USA as well as expanded discussions among the pioneers in the field concerning improved safety administration and philosophy. The second edition appeared in 1957, a third edition in 1961, a fourth edition in 1978, and after significant changes, a fourth edition with a revised title, "The Nuclear Criticality Safety Guide", in 1996 [2,3,4,5].

It was at the time that the third edition was being worked on, about 1960, that the first criticality safety standard was begun. The finished, approved standard was first printed in 1964 with the title "Safety Standard for Fissionable Materials Outside Reactors". Its contents are still found today, largely intact, in its descendant standard, ANS-8.1, "Nuclear Criticality Safety in Operations with Fissionable Materials Outside Reactors". Nuclear criticality safety standards in the USA are now developed and maintained by Subcommittee ANS-8, under the secretariat of the American Nuclear Society within the administrative oversight of the American National Standards Institute, ANSI.

Over the subsequent 37 years, 13 additional standards have been developed and issued by Subcommittee ANS-8 and 4 more are currently under development. However, it was the basic guidance that first appeared in the Nuclear Safety Guide and was subsequently incorporated into the first standard that formed the foundation for criticality safety practices worldwide that exists largely unchanged to this day. A list of the current and proposed standards is provided in Table I on the following page (3).

KEY REQUIREMENTS

Three points pertaining to the practice of criticality safety are discussed below. These are examples of important principles recognized and documented by the early practitioners in the 1956 Nuclear Safety Guide and the 1964 consensus standard. These requirements are only three of hundreds in the sixteen standards, but they are judged to be some of the most significant.

1) Responsibility for criticality safety lies with the line organization, not with the criticality safety staff. The criticality safety staff provides support to the line organization. In the 1956 edition of the Nuclear Safety Guide one finds the words:

> ***"The responsibility for nuclear safety in the plant considered is placed upon line organization. Individuals directing activities which are of such a nature as to involve nuclear hazards are responsible for control in these activities to the same extent that they are responsible for research, design, maintenance, and operation."***

In the current version of the ANS-8.1 and 8.19 standards, one finds:

> ***4.1.1Responsibilities.....Supervision should be made as responsible for nuclear criticality safety as for production, development, research, or other functions.***
>
> ***5.1 Each supervisor shall accept responsibility for the safety of operations under his control.***

2) Subcriticality is to be assured whenever practical through control of the dimensions of the vessels and piping - including the spacing between adjacent components. It is recognized that fixed neutron absorbers may prove very cost-effective in some large-scale operations and also that at some point waste solutions can usually only be practically handled in large, unfavorable geometry vessels. In the 1956 edition of the Nuclear Safety Guide one finds the words:

> ***"The nuclear safety of any process will be assured, whenever possible, by the dimensions of the components – such as pipe size and container capacities – including spacing between individual components of the same or adjacent systems."***

TABLE 1

ANSI STANDARDS SUBCOMMITTEE 8 PRODUCTS

ANS-8.1	Nuclear Criticality Safety in Operations with Fissionable Materials Outside Reactors (1998)
ANS-8.3	Criticality Accident Alarm Systems (1997)
ANS-8.5	Use of Borosilicate-Glass Raschig Rings as Neutron Absorber in Solutions of Fissile Material (1996)
ANS-8.6	Safety in Conducting Subcritical Neutron-Multiplication Measurements in Situ (1995)
ANS-8.7	Nuclear Criticality Safety in the Storage of Fissile Materials (1998)
ANS-8.10	Criteria for Nuclear Criticality Safety Controls in Operations with Shielding and Confinement (1999)
ANS-8.12	Nuclear Criticality Control and Safety of Plutonium-Uranium Fuel Mixtures Outside Reactors (1993)
ANS-8.14	Use of Soluble Neutron Absorbers for Criticality Control of Aqueous Homogeneous Solutions – Proposed
ANS-8.15	Nuclear Criticality Control of Special Actinide Elements (1995)
ANS-8.17	Criticality Safety Criteria for the Handling, Storage, and Transportation of LWR Fuel Outside Reactors (1997)
ANS-8.19	Administrative Practices for Nuclear Criticality Safety Training (1996)
ANS-8.20	Nuclear Criticality Safety Training (1999)
ANS-8.21	Use of Fixed Neutron Absorbers in Nuclear Facilities Outside Reactors (1995)
ANS-8.22	Nuclear Criticality Safety Based on Limiting and Controlling Moderators (1997)
ANS-8.23	Nuclear Criticality Accident Emergency Planning and Response (1997)
ANS-8.24	Validation of Computer Codes . . . Proposed
ANS-8.25	Postings, Signs, Labels . . . Proposed
ANS-8.26	Criticality Safety Engineer Training and Qualification Program . . . Proposed

In the current version of ANS-8.1 one finds:

> ***4.2.3 Geometry Control. Where practicable, reliance should be placed on equipment design in which dimensions are limited rather than on administrative controls.***
>
> ***4.2.4 Neutron Absorbers. Reliance may be placed on neutron-absorbing materials, such as cadmium and boron, which are incorporated in process materials or equipment or both.***
>
> It is important to note that statement on geometry control uses the verb "should" which means a "recommendation" while the statement on the use of neutron absorbers uses the verb "may" which is not a recommendation but only "permission". That is, the hierarchy of importance of the statements in the standards is first those that use the verb "shall" then those that use the verb "should" and lastly those that use the verb "may".

3) Where subcriticality based on geometry alone cannot be assured, then multiple barriers to prevent the accident should be present. This is now commonly called the Double Contingency Principle and in essence states that defense in depth must be present such that no single, credible process upset would lead to the accident happening. In the 1956 edition of the Nuclear Safety Guide one finds the words:

> ***"Where safety based on geometry alone is precluded, designs may be predicated on batch size and/or chemical concentrations, or combinations of them with geometry, and such designs will be considered satisfactory only if two or more simultaneous and independent contingencies must occur to promote a chain reaction."***
>
> In the original 1964 version of the current ANS-8.1 standard, there are the words:
>
> ***"(1) Process designs should, in general, incorporate sufficient factors of safety to require the occurrence of at least two unlikely, independent and concurrent changes in one or more of the conditions originally specified as essential to nuclear safety before a nuclear accident is possible."***
>
> In the current (1998) edition of ANS-8.1 one finds the words:
>
> ***4.2.2 Double Contingency Principle. Process designs should, in general, incorporate sufficient factors of safety to require at least two unlikely, independent and concurrent changes in process conditions before a criticality accident is possible.***

While the words describing the Double Contingency Principle (DCP) have changed slightly over the years, it is clear that the intent has remained the same. The goal is to have multiple barriers to the accident and not rely on a single barrier.

Note that the verb "should" is used in the DCP and not the verb "shall." Thus the DCP is a recommendation (and not a requirement) since not all process operations can be practically accomplished and still comply with the DCP. For this reason, perhaps the most important statement in all the standards is duplicated in both ANS-8.1 (Section 4.1.2) and 8.19 (section 8.1) and reads:

> ***"Before a new operation with fissionable materials is begun or before an existing operation is changed, it shall be determined that the entire process will be subcritical under both normal and credible abnormal conditions."***

Note that the verb is "shall" and thus this statement is a requirement.

Another way to appreciate the relative importance of these two statements in the standards, the "should" in the DCP, and the "shall" in determining subcriticality, is to recognize that the DCP is in reality a guide for the preferred way to provide assurance of subcriticality. Hugh Paxton, one of the original authors of both the Nuclear Safety Guide and the original, 1964 version of ANS-8.1, stated this about the DCP [7]:

Double Contingency Principle. The so-called double-contingency principle is generally accepted as a guide to the proper degree of protection against operational abnormalities that are improbably but still cannot be ignored. This rule calls for controls such that no single mishap can lead to a criticality accident regardless of its probability of occurrence. It is understood, further, that there should be protection against chains of related mishaps and against combinations of other abnormalities that cannot be considered improbable. Obviously, this rather subjective rule does little more than establish a point of view about criticality control – it cannot substitute for expert judgment. Experience and common sense usually provide the only basis for classifying a conceivable mishap as "likely" or "unlikely", or for ruling it out as an impractical concept. For example, leakage between a water jacket and the vessel that it surrounds may be in any one of these categories, depending upon such things as material, type of construction, and operating temperatures. Before leaving this subject, we should add that a mistake in a record of chemical analysis is hardly ever classed as a remote possibility, because of the frequency of slipped decimal points and transcription errors.

While one cannot prove that the recognition and application of important practices such as those stated above were the major reasons for the dramatic decline (see Figure 1 below) of criticality accidents worldwide in the late 1960's, it is strongly suggestive. Discussions in the late 1990's between the US and Russian authors of the third edition of the document, "A Review of Criticality Accidents", indicate that the Russians also had reached similar conclusions as to these three major points. Unfortunately criticality accident likelihood will never reach zero in spite of the best standards and guides. However more recent standards provide expanded guidance that, if followed, should reduce the likelihood even further. For example, particular aspects of two newer standards, ANS-8.19 on administrative practices and 8.20 on training, if implemented, might have prevented the recent criticality accident in Japan.

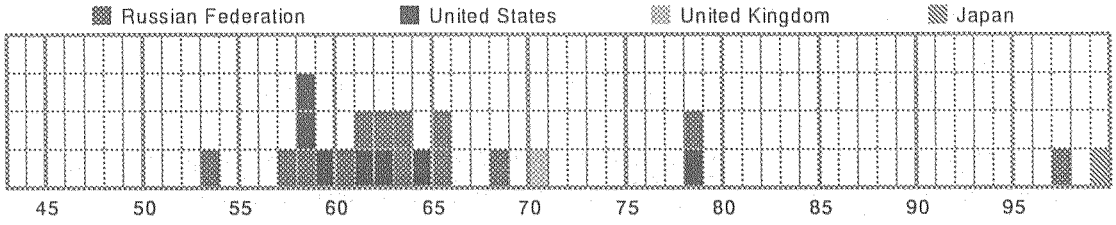

Figure 1: Reported Process Criticality Accident Worldwide (7)

CURRENT APPLICATION

Initially criticality safety in the USA was practiced under the oversight of policies and procedures at the individual installations, with documents such as the Nuclear Safety Guide and the early ANS-8 standards being the foundation for these policies and procedures. Beginning in the late 1960's in the USA, regulatory bodies began to issue directives that discussed criticality safety. These directives generally were consistent with the guidance found in the ANS-8 standards, but not identical. Eventually it was recognized by the government agencies with criticality safety concerns, the Nuclear Regulatory Commission and the Department Of Energy, that it would be best to simply endorse all the ANS-8 standards as the basis for criticality safety regulation. That is the status today, with only minor exceptions.

The ANS-8 standards have been used as the template for the few existing international standards, e.g., ISO 1709 which is analogous to ANS-8.1 There are also additional ISO standards under development which will parallel 8.19 and other ANS-8 standards.

SUMMARY

Essential guidance that was first documented in the 1950's, even before the first criticality accident in the USA, remains today as the foundation of criticality safety. This guidance is embodied in the ANS-8 standards in the USA and is accepted and endorsed by both regulatory bodies with oversight for operations with significant quantities of fissile materials, the Nuclear Regulatory Commission and the Department of Energy. Many other countries also use the ANS-8 standards as a basis for their internal criticality safety guidance and regulations.

The historical record of criticality accidents strongly suggests that actions such as maximizing the use of geometry control and defense in depth, which were heavily implemented in the 60's, were large influences in the dramatic drop in the accident frequency from about one a year during the 50's and 60's to about one per ten years thereafter, as shown in Figure 1 on the previous page.

This is a blank page.

JP0250284

REGULATIONS FOR THE TRANSPORT OF NUCLEAR FUEL MATERIAL IN JAPAN

S. FUKUDA
Central Research Institute of Electric Power Industry (CRIEPI) 2-11-1 Iwadokita, Komae-shi, Tokyo JAPAN
Fax: 81 3 3480 7950, e-mail: fukuda@criepi.denken.or.jp

As of the end of July 2001, nuclear power generating capacity totaled about 45,000 MW in Japan, with 51 commercial power reactors in operation. And nuclear power accounted for about 35% of total generated electricity in Japan. Fresh fuels and spent fuel are transported between nuclear power plants and nuclear fuel cycle facilities by land and sea. MOX fuel transportation from Europe to Japan was started in 1999. Vitrified high level waste (HLW) is transported from Europe periodically. Low level radioactive waste generated from nuclear power plants are transported to LLW burial site. Nuclear fuel materials and nuclear wastes of total amounts 2,050 tones were 180 times transported within Japan in 2000. In accordance with the reform of Japanese administrative authorities on January 6, 2001, competent authorities for transportation of radioactive materials have been changed. Competent authorities are Ministry of Economy, Trade and Industry(METI), Ministry of Education, Culture, Sports, Science and Technology(MEXT) and Ministry of Land, Infrastructure and Transport (MLIT). Japanese competent authorities revised domestic regulations based on laws for transport of radioactive materials by June 15 in accordance with 1996 edition of IAEA Regulations for the Safe Transport of Radioactive Material (ST-1), and those regulations have become effective since July 1, 2001.

Key words: nuclear fuel material, transportation, regulation system, IAEA ST-1

1. INTRODUCTION

While Japan has not blessed with rich energy resources, it is essential for Japan to ensure energy security in order to sustain economic growth and social activities. To secure stable energy supply, establishing nuclear fuel recycling has a vital role in using and developing nuclear power. Therefore, it is essential and increasing its importance in the field of nuclear fuel cycle on safe and smooth transport among various nuclear fuel recycling facilities, enrichment plants, re-conversion plants, fuel fabrication plants, reprocessing plants, etc. In the nuclear fuel recycle policy of Japan, using plutonium thermal, that burns plutonium in the form of mixed oxide fuel(MOX fuel) with uranium in a Light Water Reactor, has been positively considered with views to utilize plutonium generated by spent fuel reprocessing and to achieve more effective use of uranium. Japanese government has a principle not to maintain excess plutonium and from this point of view, plutonium thermal use is the best way of utilizing plutonium. Japanese government, based on the cabinet approval "Promotion Plan for Developing Nuclear Fuel Cycle, Feb.4 1997", requested governors of three prefectures, Fukui, Fukushima and Niigata , where nuclear power plants are located, to accept implementing plutonium thermal use at those power plants and to assist it. When local governments and local communities accept it, plutonium thermal use would be promoted and it would be lead to a large amount of MOX fuel transportation. But the implementation of plutonium thermal use has been postponed, as it was opposed at the resident referendum held in Kariha-mura village, Niigata prefecture on May 2001.

2. NUCLEAR POWER PLANTS AND NUCLEAR FUEL CYCLE FACILITIES IN JAPAN

2.1 Nuclear Power Plants

As of the end of July 2001, nuclear power generating capacity totaled about 45,000 megawatts (MW) in Japan, with 51 commercial power reactors in operation. And nuclear power accounted for about 35% of total generated electricity in Japan. There are 10 units of the commercial power reactors under construction or at the stage of preparation. If those reactors are included, there will be 61 units in all, total generating capacity of about 57,000 MW.

2.2 Nuclear Fuel Cycle Facilities

There are 2 units of enrichment plants, one unit of re-conversion plant and 4 units of fuel fabrication plants in Japan. Almost all of nuclear fuel materials such as uranium hexafluoride (UF_6) or uranium dioxide(UO_2) powder used in Japan are imported from abroad, and are processed in these nuclear fuel cycle facilities. The reprocessing plant is under construction with the aim of starting operation on and after July 2005, and spent fuel reception pools have been completed at present. Meanwhile, the low-level radioactive waste(LLW) burial facility and the high-level radioactive waste(HLW) management facility are both located in Rokkasho-mura village, Aomori prefecture. The LLW burial facility has been in operation since 1992, and the HLW facility, in which vitrified residue canisters returned from France are kept, has been in operation since 1995.

3. STATUS OF NUCLEAR FUEL CYCLE AND NUCLEAR FUEL MATERIAL TRANSPORTATION

3.1 Outline

Table shows the amount of nuclear fuel materials transported for nuclear power plants and nuclear fuel cycle facilities from 1996 to 2000. The amount of fresh fuel transported (tons of uranium) has been decreasing since 1996 due to reduction of initial core fuel for new power plants and promotion of high burn-up fuel.

Table Amount of Transportation of Nuclear Fuel

(Unit: tons of uranium)

		1996		1997		1998		1999		2000	
		T	Q	T	Q	T	Q	T	Q	T	Q
Fresh fuel	UF_6	50	720	52	704	34	418	32	534	32	387
	UO_2 etc	79	747	74	745	83	731	70	556	66	475
	Fuel Assemblies	77	1217	51	825	66	1101	65	902	64	1085
Fresh fuel Subtotal		206	2684	177	2274	183	2259	167	1992	162	1947
Spent fuel		22	199	9	127	6	69	10	107	8	102
HLW(Unit : tons)		1	20			1	30	1	20		
Others		27	1.6	23	2.7	10	0.3	12	0.2	9	

T: Number of transportation Q: Total quantity

NOTE

1.This table shows nuclear fuel materials transported subject to confirmation by code, which are type A

2.UF_6 refers to enriched uranium hexafuoride,

UO_2 refers to uranium dioxide, uranium trioxide and other uranium oxides,

Fuel Assemblies refers to bundles of UO_2 fuel and MOX fuel,

HLW refers to high-level radioactive waste,

Others refers to LLW (low-lever radioactive waste) etc.

Fig.1 shows the current situation of major transportation of nuclear fuel materials in Japan.

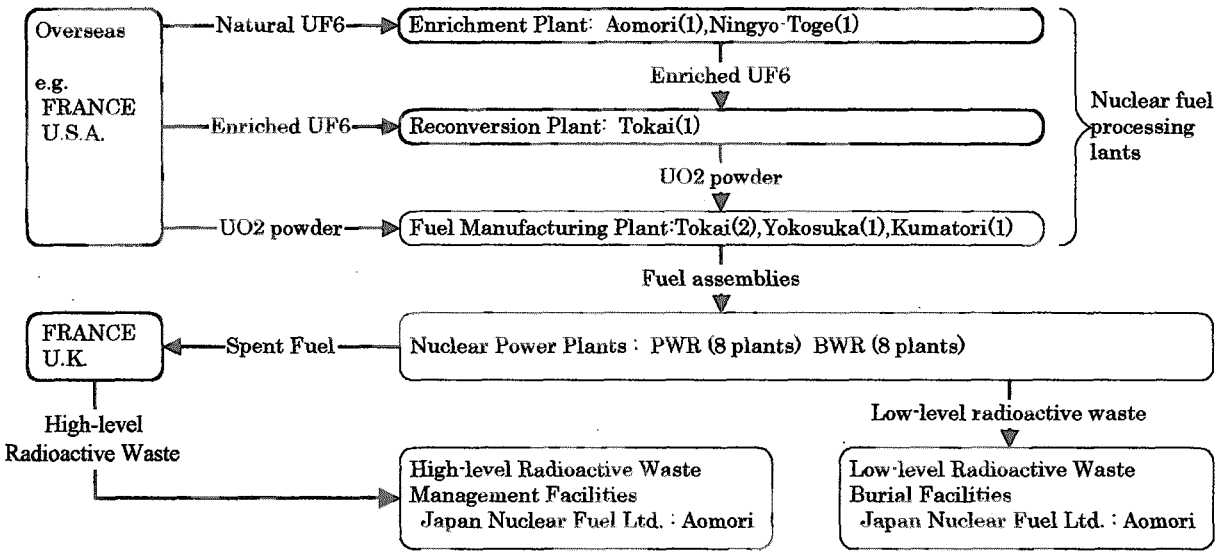

Fig.1 Current Situation of Major Transportation of Nuclear Fuel Materials

3.2 Transportation of Nuclear Fuel Materials and Fuel Assemblies

Uranium for nuclear fuel used at nuclear power plants is mainly imported in either form of uranium hexafluoride (UF_6) or uranium dioxide (UO_2) powder from abroad, and is transported overland from ports to respective nuclear fuel fabrication plants. Imported UF_6 is changed into enriched UO_2 through the enrichment process and the reconversion process, and finally becomes fuel assemblies at fuel fabrication plants. Such nuclear fuel materials and fuel assemblies are regularly transported among fuel cycle processing plants and nuclear power plants. Those materials and assemblies are mainly transported by land using trucks or trailers, but some fuel assemblies are carried by ship depending upon the location of the nuclear power plant.

3.3 Transportation of MOX Fuel

The first shipment of MOX fuel, mixture of uranium and plutonium oxides fuel, for commercial use in a light water reactor was carried out from July to October 1999, and the second shipment was accomplished by sea in 2001.

3.4 Transportation of Spent Fuel

In August 1999, transportation of spent fuel to the reprocessing plant of Japan Nuclear Fuel Ltd. located in Rokkasyo-mura Village, Aomori prefecture was carried out for the first time, and calibration test of burn-up monitors was conducted. After the agreement on safety assurance of the facility and preservation of environment around was concluded among local governments and Japan Nuclear Fuel Ltd. which operates the plant, several shipments of spent fuel have been conducted by the ship of exclusive use since December 2000.

3.5 Transportation of LLW

Low-level radioactive waste produced from operation and periodical inspection of nuclear power plants is packed in drums mixed with cement, asphalt or other materials after reducing its capacity by burning. After temporary storage in exclusive storage houses, these filled drums are contained in shock-resistant containers and sent to the LLW burial site of Japan Nuclear Fuel Ltd. (JNFL) located at Rokkasyomura Village, Aomori prefecture

3.6 Transportation of HLW

Liquid waste with high level radioactivity generated from reprocessing of spent fuel is melted and mixed together with glass which is extremely stable and they are poured into stainless steel canister for hardening. These canisters have been transported several times, as it is arranged that high-level radioactive waste generated from reprocessing plants in abroad is to be returned back to Japan. Throughout those shipments, canisters of HLW are contained in the transport packagings conforming to IAEA Regulations for the Safe Transport of Radioactive Materials (ST-1), and the packages are transported by ship which compiled with IMO's SOLAS Convention and INF code (international regulations concerning safe maritime transportation of Irradiated Nuclear Fuel).

4. JAPANESE COMPETENT AITHORITY AND REGULATION SYSTEM

4.1 Competent Authority

In accordance with the reform of Japanese administrative authorities on January 6, 2001, competent authorities for transportation of radioactive materials have been changed. Through the above development, control for transportation of nuclear fuel materials used in commercial nuclear power plants is executed currently for land transportation under "Law on the Regulation of Nuclear Source Material, Nuclear Fuel Material and Reactors (Reactor Regulation Law)" by Ministry of Economy, Trade and Industry (METI) , Ministry of Land, infrastructure and Transport (MLIT) and Public Safety Commission , for marine transportation under "Ship Safety Law" by MLIT and Japanese Coast Guard, and for air transportation under "Civil Aviation Law" by MLIT, respectively. **Fig.2** shows the radioactive material transport mode and regulation assignment. Meanwhile, the authorities concerned with transportation of nuclear materials, "Ministry of Economy, Trade and Industry", "Ministry of Land, Infrastructure and Transport", "Japanese Coast Guard", "Ministry of Education, Culture, Sports, Science and Technology", "National Police Agency" and "Fire Defense Agency" , hold coordinating meetings periodically to discuss about countermeasures for safe transport and established safety measures to be taken in case of an accident in February 1984.

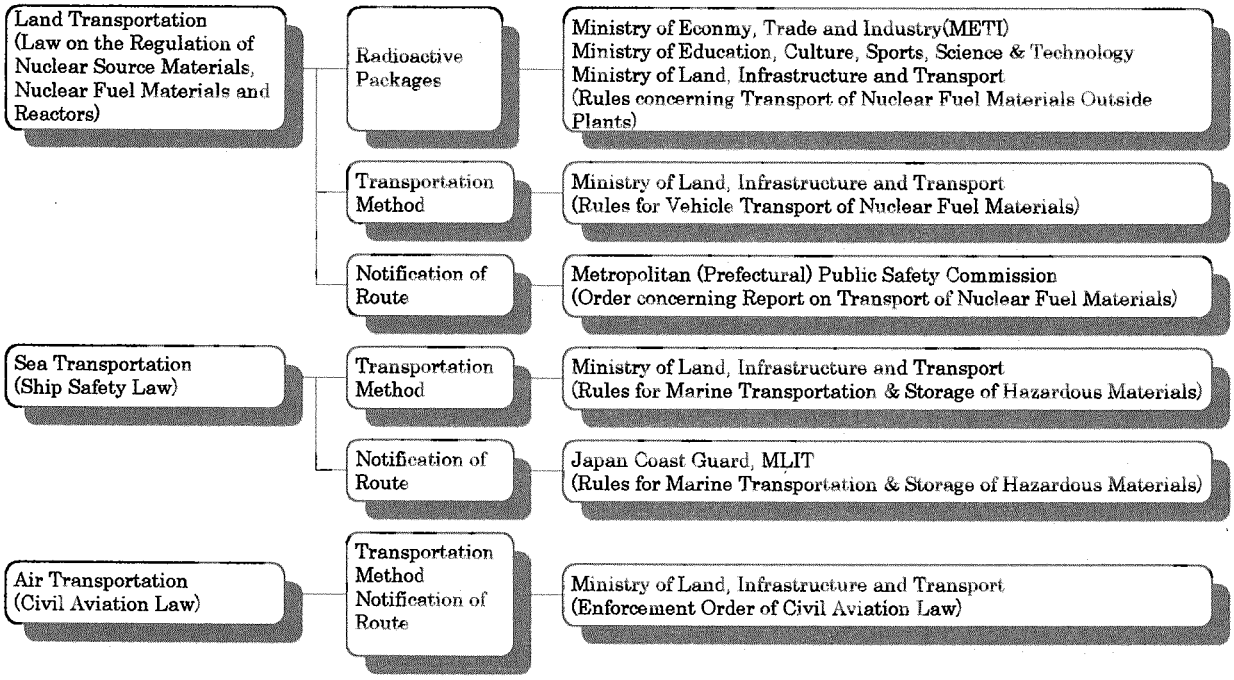

Fig.2 Radioactive Material Transport Mode and Regulation Assignment

4.2 Regulation System

4.2.1 Safety Regulation on Land Transportation

Ministry of Economy, Trade and Industry (METI) executes standards concerning safe transport of nuclear fuel packages including "Rules concerning Transport of Nuclear Fuel Materials Outside Plants" under Reactor Regulation Law, and verifies that nuclear fuel packages comply with the safety standards specified in the rules upon each occasion of such transport. These safety standards are established according to the regulations set up by the IAEA so that safety is ensured not only during normal transport but also incase of erroneous cargo handling or traffic accidents. Upon confirmation of nuclear fuel materials, strict review is executed by METI to verify that the design of packages complies with the safety standards, then design approval is given to those recognized as complying. Then, it is confirmed that the individual transport container are fabricated to the approved design and maintained accordingly, finally, approval for packages will be issued. After all these procedures, it is verified, upon each transportation, that the nuclear fuel materials housed comply with the approved design specifications and they are housed in the approved containers before any transport certificate is issued by respective authority. On the other hand, Ministry of Land, Infrastructure and Transport (MLIT) established safety standards concerning transportation methods including methods of loading nuclear fuel packages onto vehicles, signs to be put up on vehicles and the maximum package per vehicle in the order of MLIT, "Rules for Vehicle Transport of Nuclear Fuel Materials" under Reactor Regulation Law.

4.2.2 Safety Regulation on Marine Transportation

For marine transportation, basically the same safety control system is applied as for land transportation. Ministry of Land, Infrastructure and Transport (MLIT) has established safety standards concerning nuclear fuel packages and methods of transportation including methods of loading onto the ship in the order of MLIT, "Rules concerning Marine Transportation and Storage of Hazardous Materials" under Ship Safety Law . If it is recognized that the shipment is to be handled subject to Ship Safety Law, MLIT verifies, upon each occasion of loading, that the subject packages and the transportation method concerned comply with these safety standards. As these safety standards for nuclear fuel packages are basically the same as those for nuclear fuel packages to be handled by land transportation, those nuclear fuel packages to be seamlessly handled through land and marine transportation are regarded as those verified by MLIT as stipulated by Ship Safety Law if they have been verified by Ministry of Economy, Trade and Industry (METI) under Reactor Regulation Law.

4.2.3 Safety Regulation on Air Transportation

Safety standards for air transportation of nuclear fuel materials are set out in rules such as the order of Ministry of Land, Infrastructure and Transport, "Enforcement Order for the Civil Aviation Law" under Civil Aviation Law.

Fig.3 shows the code system concerning transportation of nuclear fuel materials.

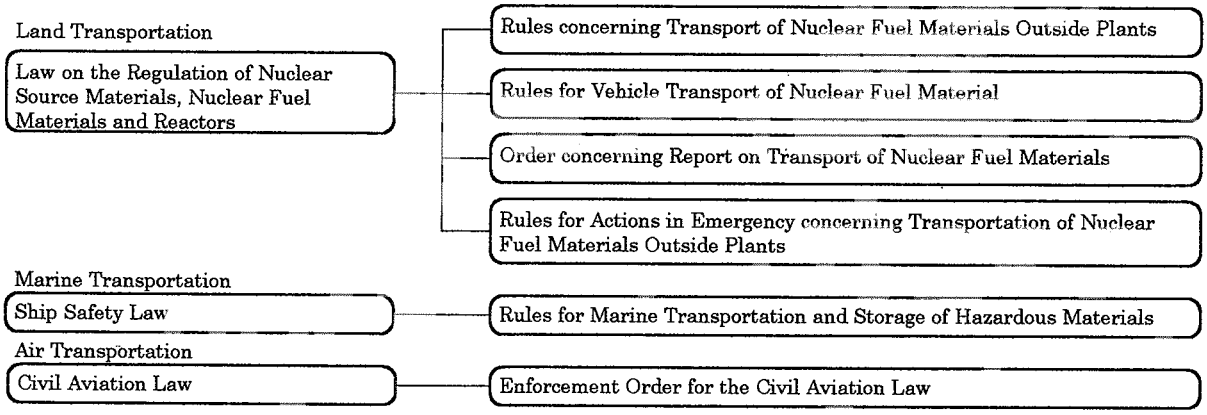

Fig.3 Code System concerning Transportation of Nuclear Fuel Materials

4.3 Approval System in Japan

Japanese regulation system has not only approval of package design, same as IAEA Regulation's approval of package design, but also "Package Approval". On each shipment competent authority examine that each package meet regulation code. Examining items are shown below.

- Package design shall meet regulation standards
- Each packaging shall fulfill approved package design
- Each Package shall meet regulation standards (contents, radiation level, contamination etc.)

Licensees could get approval of package design and approval of each packaging beforehand. With those approvals, licensees do not have to submit documents explaining package's conformity to regulation and could be approved by a approval organization designated by competent authority. "Approval of packaging" requires that each packaging is manufactured in accordance with approved package design and maintained in good condition. Fig.4 shows the flow chart of confirmation of packages.

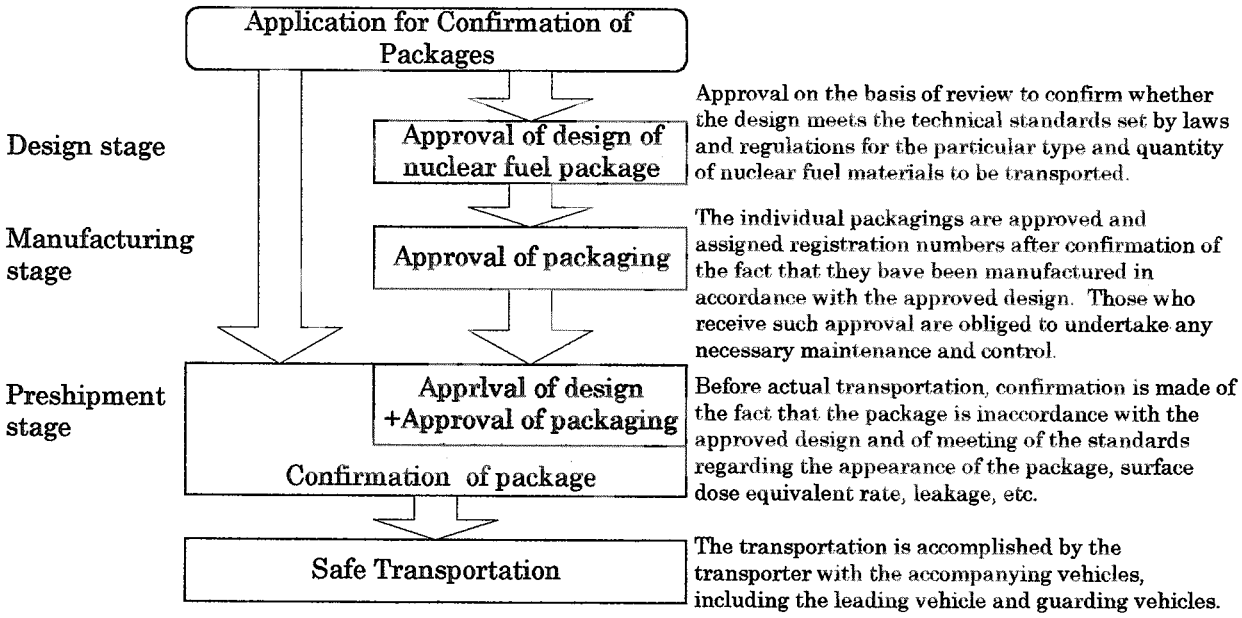

Fig.4 Flow Chart of Confirmation of Packages
(the case of Land Transportation)

5. ADOPTION OF 1996 EDITION OF IAEA SAFE TRANSPORT REGULATIONS TO JAPANESE REGULATIONS

In order to enhance safety regulation, laws concerning transportation of nuclear fuel materials through discussion by the Radiation Council, which were enforced after April 1, 1979, complying with "Guidelines for Safety Standards for Transport of Radioactive Materials" established in January, 1975 by the Atomic Energy Commission subject to the "Regulation for Safe Transport of Radioactive Materials (1973)" issued by the International Atomic Energy Agency (IAEA). This effort was followed by amendment of the laws subject to the IAEA's "Regulation for Safe Transport for Radioactive Materials (1985)", which amendment formed the former regulations. Japanese competent authorities revised domestic regulations based on laws for transport of radioactive materials by June 15 in accordance with 1996 edition of Regulations for the Safe Transport of Radioactive Material (ST-1), and those regulations have become effective since July 1, 2001. The revision was examined by both Nuclear Safety Committee and Radiation Council. Japanese competent authorities will continue to participate in the ongoing work of revising 1996 edition of IAEA transport regulation.

6. IMPLEMENTATION OF MANDATED REQUIREMENTS OF THE INF CODE UNDER THE SOLAS CONVENTION SINCE 2001

Up to the end of 2000, Japan had made an effort to ensure ship's safety by issuing order imposing necessary requirements equivalent to the INF Code as well as additional domestic regulations. Recognizing the situation of INF Code becoming mandatory from the beginning this year and the revision of safety regulation policy on maritime transport after critical accident occurred in Japan, INF Code and additional requirements were incorporated into Ship Safety Law and its regulation, which entered into force on January 1, 2001. Thus, Japanese competent authority has strengthened safety measure for maritime transport, in terms of hull constructions and onboard equipments of ships carrying irradiated nuclear fuel etc. as well as shipment approval system.

REFERENCES

[1] S. Hamada, S. Fukuda and I. Nakazaki: "Nuclear Fuel Material Transportation in Japan" Proc. of the 13 th International Symposium of the Packaging and Transportation of Radioactive Materials , Chicago (2001), (in preparation)

[2] IAEA Safety Standards Series," Regulations for the Safe Transport of Radioactive Material(ST-1)" (1996 Edition)

This is a blank page.

JP0250285

JAERI-Conf 2002-004

A UK REGULATORY PERSPECTIVE OF CRITICALITY SAFETY - PAST, PRESENT AND FUTURE

D N SIMISTER

HM PRINCIPAL INSPECTOR OF NUCLEAR INSTALLATIONS, HEALTH AND SAFETY EXECUTIVE, ST PETER'S HOUSE, BALLIOL ROAD, BOOTLE, MERSEYSIDE, UK, L20 3LZ

This paper reflects on past experiences in the development of the UK nuclear industry from a criticality safety perspective and identifies some key aspects which have helped to influence current UK industry practices and regulatory thinking. It will then identify a number of activities which contribute effectively to maintaining current high standards of criticality safety and awareness and then propose a number of areas which may be of importance to criticality practitioners and regulators in the future.

The Health and Safety Executive (HSE) is the lead UK regulatory agency responsible for the enforcement of health and safety legislation at nuclear sites in the UK. This includes inspection and assessment of safety arrangements and for controlling risks from criticality in nuclear plant.

Regulation of nuclear safety in the UK is largely based upon a permissioning licensing system combined with an overriding requirement to reduce risks to workers and the public to a level which is as low as reasonably practicable. The licensing system permits a flexible approach to criticality safety enabling the operator or licensee to develop safety cases suited to local plant conditions. The responsibility for safety rests firmly with the operator and as regulators HSE needs to be satisfied on the adequacy of arrangements which are in place to ensure safety. In order to assist nuclear inspectors in forming a view on adequacy HSE has developed and published it Safety Assessment Principles which describe goal setting standards for the design and operation of nuclear plant including aspects relating to criticality safety.

INTRODUCTION

UK regulatory arrangements

Risks to health and safety at nuclear sites in the UK are controlled mainly by the Health and Safety at Work etc Act 1974(1), the Nuclear Installations Act 1965 (2) and the Ionising Radiations Regulations 1999(3). This regulatory framework sets out requirements for licensees to produce arrangements for safety cases to demonstrate the safety of operations and to demonstrate that risks to workers and members of the public have been reduced so far as reasonably practicable. The Health and Safety Executive is responsible for enforcing this legislation in the UK and the Nuclear Installations Inspectorate is that part of HSE which undertakes licensing, inspection and enforcement activities on nuclear sites. A key point to note in NII's approach to regulation is that site licences and the conditions attached to them are non-prescriptive and goal setting. This provides licensees with the flexibility to develop safety cases suited to local applications allowing practitioners to make best use of the various methods for reducing the risks from plant criticality.

Assessment and standards

An important part of HSE's activities is the production of principles and standards by which it can judge the adequacy of a licensee's safety cases. A starting point in the development of such standards is a reflection of current UK best industry practice and a knowledge of what is considered acceptable internationally. HSE has already published two documents. The Tolerability of Risk from Nuclear Power (TOR) (4) and NII Safety Assessment Principles (5) (commonly referred to as SAPs). TOR considers the public perceptions and attitude towards risks and identifies those which are considered just tolerable and those which are broadly acceptable. The SAPs provide a framework for assessing the design, construction, commissioning, operation and decommissioning of nuclear installations and cover a range of technical disciplines including criticality. They are by their very nature, broad ranging and goal setting. They set out fundamental principles, dose and risk constraints for normal and fault conditions and engineering principles. The SAPs have been published but are intended mainly for internal guidance for NII assessors and are not considered to be prescriptive or mandatory in the regulatory sense.

A common theme which runs across both the SAPs and TOR documents is the principle that risks to workers and members of the pubic must be kept as low as reasonably practicable - ALARP. This concept has been interpreted by NII into a set of numerical design targets incorporating an upper level, the Basic Safety Limit (BSL) - a level of tolerability beyond which actions must be taken to reduce risks and a lower level the Basic Safety Objective (BSO) which defines a point beyond which regulatory assessors need not necessary seek further improvements in safety. Between these two levels is the so-called 'ALARP' region where a safety case must be made to demonstrate why further improvements are not reasonably practicable.

HSE's Safety Assessment Principles, which are intended to be broad and wide ranging, do not explicitly cover specific methods such as moderation control, a means of criticality control. Safety Assessment Principle SAP P284 is the starting point for criticality safety assessment within the UK regulatory framework. Assessors and practitioners need to take account of the need to minimise reliance upon operational control for adequate control of criticality safety but to rely preferentially on passive engineered features, this is reflected in SAPs P61 and P62. The recent criticality accident at Tokai Mura in Japan has highlighted the difficulties where arrangements rely upon operational control and has demonstrated the need to include engineered safety features where practicable. HSE supports the use of a range of appropriate methods for criticality control in plant design. As regulators we expect these aspects to be fully covered in the safety case.

HSE's starting point in assessing the adequacy of criticality safety cases is to identify the extent to which elements of robust engineering design has been used in preference to other measures such as operational control or probabilistic arguments. We have seen examples where it is not always possible to design vessels or structures used for holding fissile materials entirely within the constraints

of safe geometrical dimensions. Reasons for extending the design scope beyond this principle and for perhaps including neutron absorbers may include the need for compliance with chemical engineering flow sheet specifications, the desire to eliminate certain unlikely fault conditions and the need to provide additional diverse safety measures which result in defence in depth. The use of probabilistic assessments in criticality safety cases is encouraged to ensure that all likely faults are identified and equally weighted. As regulators we have seen examples where the use of PSA becomes important if passive features are not possible and in difficult cases we have accepted an approach based upon 'multi-legged arguments'.

Past criticality experiences

In 1957 one of the reactors at the Windscale site (now Sellafield) went on fire following a routine operation to relieve the build up of energy in the graphite core. The fire caused fuel melting and the release of radioactivity across the UK and northern Europe. The news programmes at the time showed milk being poured down the drains. By today's standards it would have been classified as an INES 5 event and it was and remains the worst nuclear accident in the UK's history.

As a result of this the Government of the day introduced the first Nuclear Installations Act in 1959 to provide regulation of the emerging commercial nuclear power programme, but the complex at Windscale and the other UKAEA sites were excluded from the provisions of this Act. This Act was a licensing and Insurance Act which gave considerable powers to the Minister to regulate the nuclear industry through a licensing regime. The Minister was given powers to appoint inspectors to assist him in this licensing process and the Inspectorate of Nuclear Installations INI was born. This lead to the Nuclear Installations Inspectorate (NII) as we know it today which was incorporated into the Health and Safety Executive in 1974 - an organisation which in the UK take the regulatory lead for most aspects of work related safety.

The early days of criticality safety in the UK were dominated by the UKAEA - a government organisation charged with developing nuclear power in the UK. Criticality safety was characterised during the 1950's and 1960's by a number of factors including the lack of firm experimental data (it was often necessary to extrapolate from a few data points), the need for secrecy (where applications were defence related) and a need to know basis, the absence of computation power and codes and the urgent need to design, build and operate nuclear facilities. This has left practitioners today with a number of legacies - particularly the desire to impose large safety margins in the application of prudence and caution.

Criticality expertise was centred on the UKAEA's Health Authority and Safety Branch (AHSB) at Risley, which encouraged amongst other things the development of Monte-Carlo computational techniques including the novel and unique use of 'hole' geometry, eventually leading to the development of the UK standard code MONK. This was augmented by experimental facilities centred upon the Dimple reactor at Winfrith which closed in the early 1990s. The AHSB also pioneered the

first programme of independent plant criticality inspections of nuclear facilities which is still encouraged today as an example of good industry practice.

Criticality safety in the UK during the 1970's and 1980's saw a period of rapid expansion in terms of criticality safety practitioner numbers and activities being boosted by an expansion of the nuclear industry, particularly the design and construction of the THORP Plant at Sellafield, new enrichment plants at Capenhurst, the New Oxide Fuels Complex at Springfields and the prospect of a family of PWR reactors led by Sizewell B - although planning permission was granted for a second PWR, economic conditions prevented further expansion of this programme. A number of design improvements were also introduced which minimised reliance upon operational control, for example, the introduction of pulsed columns based upon safe geometry in preference to mixer-settlers which relied upon concentration control. This period also witnessed the development of more sophisticated Safety Mechanisms - sometimes in the form of non-destructive assay, equipment, used to estimate the quantity of fissile materials present in the process. Examples of plant applications are the Thorp hulls monitor at Sellafield and monitors to assay plutonium contaminated materials (PCM).

The UK's record of criticality safety throughout this period was generally good with many plants, such as the B205 Magnox reprocessing plant at Sellafield operating successfully. The one and only criticality accident in the UK occurred at the UKAEA Windscale site in 1971. This facility is now part of the BNFL Sellafield site. It should be noted that this criticality had minimal consequences ie no fatalities because it was within a shielded facility but was partly caused by modifications to the plant design. There have been a number of instances of loss of management control (near-misses) where criticality was a possibility. An example, which happened at BNFL Sellafield in 1992 is fully reported in ref 6, in this case a large quantity of concentrated plutonium nitrate leaked out of an evaporator to form the so-called stalactites and stalagmites. One learning point from this incident was that despite the facility having a comprehensive safety case the fault/mal-operation had not been considered.

Present position

The field of criticality safety and other related areas such as reactor physics and shielding may be considered to be mature technical disciplines. This potentially has both advantages and disadvantages. The advantages for both practitioners and regulators include the fact that there is a good track record of operational experience and applications, an extensive set of good quality experimental benchmarks exist for most industrial applications and computer codes are generally well developed to meet most challenges. The criticality code MONK and reactor physics code WIMS enjoy a good international reputation and are widely used outside the UK. One possible disadvantages is the need to maintain and recruit suitable qualified and experience staff in order to support 'key teams within industry. Even with a narrow area such as criticality there are further specialist areas such as nuclear data evaluation, code development, experimental practices, safety case

applications. It is important that the necessary key skills and competencies are identified and maintained - this necessarily involves a number of non-technical areas such as education, career rewards, progression and remuneration. In the UK, a new initiative has begun in 2001 as a result of co-operation between a number of organisations which seeks to actively promote continuing nuclear education.

The UK has well developed arrangements to co-ordinate generic research into criticality safety and other related issues through the mechanism of HSE's Nuclear Research Index and the Industry Management Committee (IMC) (ref 7). This focusses on generic safety issues and complements research initiated by industry which may be more commercially focused.

The nuclear licensing regime in the UK has been in place for over 40 years and is based upon a non-prescriptive permissioning system and incorporates a number (36) of standard nuclear site licence conditions, some of which relate to criticality safety. Fundamental to criticality safety is the need for an adequate safety case (Licence Condition 14). Arrangements in the UK are working well and all relevant facilities have current safety cases which are subject to a system of peer review and updating. Recent advances in safety case methodology have seen a move away from standard 'criticality clearance certificates" and "nuclear safety assessments" towards a more holistic plant safety case which views criticality as one of many potential hazards which might affect workers and the public - this has the advantage of including criticality safety assessment into a broader analysis of possible plant faults. This aspect is regarded as important in balancing the overall risks from the plant, including hazards from criticality, so that the overall risk may be reduced to as low as reasonably practicable (ALARP). This also has the benefit of concentrating scare resources on the hazards which matter most - we have seen examples as regulators where too many safety rules can have disadvantages as well too few. The application of balancing risks allows other methodologies, such as burn-up credit, to be successfully introduced. Whilst the fundamentals of criticality are still based upon the double contingency principle and the need to provide diversity, redundancy and defence in depth, some operators in the UK have recently found advantages in developing approaches based upon design basis analysis - focusing on engineering rather than PSA aspects and basket methodology which identifies the need for an adequate number of protection systems.

The UK criticality community continues to co-ordinate national and international activities through the Working Party on Criticality which has successfully operated on a voluntarily basis for over 20 years. The existence of such a group provides an opportunity for information to be exchanged between organisations for the benefit of all, subject to normal commercial considerations. Effective use of scarce resources can be made when co-ordinating UK participation in international meetings, and benefits can be gained by both industry and regulators in the development of consensus best practice guidance. Current topics of interest include emergency arrangements to respond to radiation (criticality) accidents, the introduction of burn-up credit and the archiving of safety dose records.

Future

This section looks forward and identifies possible threats and opportunities for criticality practitioners in the UK. Decision makers both in Government and industry need to have an awareness of emerging issues which may need to be addressed in order to maintain and improve standards of criticality safety.

I Operational vs Engineered Control

An important challenge to criticality practitioners in the future may take the form of increasing the extent to which deterministic engineered controls are employed to control criticality safety rather than placing reliance upon operational or administrative systems, this is known in the UK as the SAP P61/P62 hierarchy and is a particularly important feature for new plants at the design definition stage. As regulators we would expect to see a justification for each stage of the hierarchy ie removal of hazard, passive design features, engineered controls, operational and administrative arrangements. HSE's Safety Assessment Principles discusses this hierarchy of control and in the UK as regulators we see further opportunities to reduce risks from criticality to a point which is ALARP (as low as reasonably practicable) - a concept which is built into UK legislation. Engineered improvements could take several forms for example; re-designing or replacing existing process technology with improved methods, undertaking further safety case assessment work to further understand criticality scenarios thereby eliminates unnecessary contingencies, replacing operator requirements by engineered controls or re-evaluating safety case requirements to reduce them from 'safety' status to 'good-housekeeping'. Such an approach may have a number of direct commercial and process benefits. As regulators we see advantages in focusing operators limited time to a few key safety principles which are important rather than being diverted by a multiplicity of low-level, sometimes unnecessary, procedures. A further socio-political challenge is to enhance confidence in the operation of the industry / regulators by reducing the number of low-level infractions which result from an operator reliant culture which may ultimately lead to reduced public and stakeholder confidence.

II Waste disposal

Regulators and industry in the UK are becoming increasingly aware of the future needs to address the issue of the long term surface storage and eventual underground disposal of intermediate level waste (ILW) which may contain fissile materials. UK Nirex Ltd is the organisation which takes the lead for developing plan for disposal of the UK's radioactive waste inventory. Current estimates suggest that the fissile inventory of a future repository may include 20 te Pu (total) and 50 te U-235 arising from various waste streams much of which is in the form of contaminated waste materials. We have identified a number of regulatory issues which will need to be considered in the future including; stakeholder involvement - the need for

safety arguments to be understood by non-technical decision makers, passive safety based upon engineered packaged designs, safety margins which reflect the purpose and mission of the facility. There is increasing acceptance amongst practitioners that it will be very difficult, if not impossible, to completely eliminate a criticality event in such a facility by deterministic engineered means, but the aim should be to reduce the frequency of an accident to as low as reasonably achievable and to minimise the risk of damage to the engineered barriers put in place in such a disposal facility. An important aspect in this technical area is gaining an understanding of the likely consequences arising from a transient criticality accident. The experiment facilities at Tokai Mura and other facilities in France and USA provide an important means to understand this phenomena and are assisted in this mode by theoretical advances in computational modelling by groups such as that at Imperial College in the UK. The results of this work will provide the public, regulators, practitioners and other stakeholders with the confidence which is needed.

III Suitably qualified and experienced staff

Staff mature with the industry and retire, often taking a lifetime of experience and skills with them. In the future, criticality safety faces a number of possible challenges - two of current concern are the recruitment and retention of suitable staff and the implementation of a strategy for practitioners to gain skills. In many countries, the nuclear industry may no longer seen as an attractive opportunity for a lifetime of employment (evidence may actually contradict this widely held view), the result being that high calibre professionals are difficult to recruit and retain. This may lead to a 'generation gap' where younger professionals may perceive limited career opportunities and progression potential. We have found that remuneration is one factor, but not the only feature needed to capture the imagination of potential recruits. Other issues which may need to be explored are a sound programme of nuclear education offered at degree level, followed by suitable development and training leading to recognised professional qualifications which are both recognised and transparent by both the individual and employers alike. A further possible challenge may be the provision of suitable training and experience for staff wishing to undertake criticality safety assessments. Experience has shown that it can take several years for suitable practical skills to be gained either through on-the-job training or through structured causes although the availability of training opportunities is becoming more limited. Opportunities may exist to address these questions on either a national or international basis. In the UK, a recent initiative has been suggested to more formally structure and record continuing professional development.

CONCLUSIONS

The UK has a good criticality safety record. This has been achieved through the development of soundly based industry practices and through engagement of competent operational criticality safety practitioners operating within the context of a

strong but flexible regulatory regime based upon a non-prescriptive licensing system. Examples have been given which highlight possible areas of future interest to criticality practitioners - but if there must be one message then this is the need for continuing vigilance in order to maintain high safety standards.

The views expressed in this paper are those of the author and not necessarily those of the Health and Safety Executive.

References

1. Health and Safety at Work etc Act 1974.

2. Nuclear Installations Act as amended 1965.

3. Ionising Radiations Regulations 1999.

4. The Tolerability of Risk from Nuclear Power

5. NII Safety Assessment Principles.

6. Leakage into the B205 plutonium evaporator cell at Sellafield. ISBN 0-7176-0721-6, HSE.

JP0250286

DEVELOPMENT OF BURNUP CREDIT EVALUATION METHODS AT JAERI

YASUSHI NOMURA, HIROSHI OKUNO AND KENYA SUYAMA
Fuel Cycle Safety Evaluation Laboratory
Japan Atomic Energy Research Institute,
Tokaimura, Nakagun, Ibarakiken, PC 311-1195, Japan
Fax: 81-29-282-6479, e-mail:nomura@popsvr.tokai.jaeri.go.jp

A guide material to introduce the burnup credit in Japan has been prepared and published by the name of *a Guide Introducing Burnup Credit, Preliminary Version*. In this *Guide*, correction factors expressed by C/E (ratio of calculated isotopic composition to measured one) are prepared to apply to the results calculated by the ORIGEN 2.1 depletion code. A total of 38 sets of PIE data from PWR such as Obrigheim, Genkai-1, Mihama-3 and Takaham-3 have been used for this preparation. In addition, two simplified evaluation methods, "Equivalent Uniform Burnup" and "Equivalent Initial Enrichment", have been developed and prepared to perform criticality safety analysis by the ORIGEN2.1 depletion code and the KENO-Va criticality code without any detailed modelling.
Keywords: burnup credit, ORIGEN2.1, KENO-Va, isotopic composition, correction factors, equivalent uniform burnup, equivalent initial enrichment

1. INTRODUCTION

Recently, it becomes evident that light water rectors (PWR and BWR) are continually operated to generate electric power in the long run in Japan, and spent fuel is more and more exhausted to be accumulated. Most spent fuel is now stored in on-site wet storage pools, and partly at on-site dry storage facilities. In anticipation of lack of storage capacity in the next few decades, an off-site intermediate spent fuel storage facility has been decided for operation from around 2010. In addition, the first domestic commercial reprocessing plant is now under construction and is expected to begin operation from 2005.

In Japan, it is traditional to assume fresh fuel in criticality safety assessments for spent fuel transport and storage, resulting in an excessive safety margin taken in the facility design.

In consideration of the above situation, new challenges have emerged to introduce burnup credit into criticality safety assessments among utilities and related industries for pursuit of efficient facility design and management of spent fuel storage and transportation.

In order to implement burnup credit in the design and management of spent fuel storage and transportation systems, *A Guide Introducing Burnup Credit, Preliminary Version* [1], has been successfully prepared and published by the Working Group on Nuclear Criticality Safety Data (Leader: Professor Dr. Yoshihiro Yamane of Nagoya University) under the Special Committee on Nuclear Criticality Safety with JAERI.

2. AN EXAMPLIFIED ANALYSIS FOR SPENT FUEL AMOUNT IN STORAGE POOL

Capacity of spent fuel transportation/storage can be increased by introducing burnup credit when the available space is limited, thus improving economic feature of the facilities. To make sure of this statement, an analysis has been made to illustrate how much spent fuel can be

increased per unit area by introducing burnup credit. As a result, it is shown that about twice amount of PWR spent fuel could be stored in a water pool in assumption of 50 GWd/t burnup after 10 year cooling with fission products taken into consideration [1].

3. *A GUIDE FOR INTRODUCING BURNUP CREDIT, PRELIMINARY VERSION*

This Guide states that it is published as a supplement to the *Nuclear Criticality Safety Handbook Version 2* [2] in chapter 1. Basic principles and procedures for criticality safety assessment introducing burnup credit are depicted in chapter 2 as shown in Fig.1. In chapters 3 and 4 are described methods for evaluation of spent fuel composition and criticality safety, such as methods to derive correction factors applied to nuclide composition data calculated by ORIGEN2.1 and simplified methods called "Equivalent Uniform Burnup" and "Equivalent Initial Enrichment," together with relevant data and information. The last chapter 5 contains important remarks for implementing burnup credit, together with methods to ensure burnup of spent fuel during handling operation.

4. CORRECTION FACTORS FOR CALCULATED NUCLIDE COMPOSITION

Correction factors have been derived to apply to the results obtained by ORIGEN2.1, which is used world wide to calculate nuclide composition in spent fuel [3]. In this attempt, 38 experimental sample data of spent fuel from PWRs, such as Obrigheim, Genkai-1, Mihama-3 and Takahama-3, are analyzed in combination with various nuclear data libraries to give (C/E), namely the ratio of calculated result divided by the experimental one. The correction factor can be chosen as the minimum value among (C/E)s given for fissile actinides, and as the maximum value among (C/E)s given for absorptive nuclides in respect of reaction with neutrons. In addition, the value of 1.0 is given to the correction factor whenever the minimum value goes below 1.0 and the maximum value goes above 1.0 in order to assure further conservatism. Table 1 shows a list of the correction factors derived by the method described above. These factors are listed in *A Guide Introducing Burnup Credit, Preliminary Version.*

4. *EQUIVALENT UNIFORM BURNUP* AND *EQUIVALENT INITIAL ENRICHMENT*

Based on the PWR spent fuel composition chemical analysis data measured at JAERI, two kinds of simplified methods, "Equivalent Uniform Burnup" and "Equivalent Initial Enrichment", have been introduced for simplified criticality safety evaluation of spent fuel storage pool and transport casks taking burnup of spent fuel into consideration [4].

These simplified methods can be used to obtain an effective neutron multiplication factor for a spent fuel storage/transportation system by using ORIGEN2.1 burnup code and KENO-Va criticality code without considering axial burnup profile in spent fuel and other various factors producing calculated errors. "Equivalent Uniform Burnup" is set up so that its criticality analysis will be reactivity equivalent with detailed analysis, in which the experimentally obtained isotopic composition together with a typical axial burnup profile and various factors such as irradiation history are considered on the conservative side. On the other hand, "Equivalent Initial Enrichment" is set up so that its criticality analysis will be reactivity equivalent with detailed analysis such as above when used in the so called fresh fuel assumption. The methods to derive "Equivalent Uniform Burnup" and "Equivalent Initial Enrichment" are shown in Fig.2 and Fig.3. Examples of "Equivalent Uniform Burnup" and "Equivalent Initial Enrichment", applied to a spent fuel infinite array submerged in water simulating a storage pool and a spent fuel transport cask, are illustrated in Fig.4 through Fig.7.

5. REACTIVITY EFFECT OF SPENT FUEL DEPENDING ON BURNUP HISTORY

Composition of spent fuel depends on various parameter changes throughout a burnup period. These parameters are the boron concentration and its change pattern, the coolant temperature and its spatial distribution, the specific power, the operation mode, and the inspection duration. The composition variation due to these parameter changes has been analyzed by the integrated burnup calculation code system SWAT [5] which was developed at JAERI. In addition, to estimate the reactivity effect caused by these composition variation, criticality analyses have been performed for an infinite array of spent fuel with the continuous energy Monte Carlo code MVP. As a result, the parameters giving the maximum reactivity effect on the spent fuel management system have been identified to be used for their criticality safety assessment taking burnuo credit into consideration [6].

6. CONCLUDING REMARKS

A Guide for Introducing Burnup Credit, Preliminary Version has been successfully prepared and published. Materials containing relevant data and detailed consideration will be published soon to give theoretical and practical background to this Guide. Presently, actinide only burnup credit (Level 1) has been introduced and advancement will be made with fission products data available in the near future. Correction factors have been prepared to apply to ORIGEN2.1 calculated results for PWR spent fuel nuclide composition. It is anticipated that those for BWR spent fuel should be obtained hereafter. Criticality experiments with fresh MOX fuel have been conducted so far and the obtained data have been utilized to validate criticality codes for Level 1 burnup credit application. To promote to Level 2 burnup credit application, criticality experiments with spent fuel will be needed. Finally, burnup monitor is mainly used at present to determine burnup of spent fuel prior to loading to storage pool and transport casks. In consideration of its complexity and tedious maintenance work, monitoring device should be replaced by the methods referring only to reactor management data.

REFERENCES

[1] Working Group on Nuclear Criticality Safety Data, Nuclear Fuel Cycle Facility Safety Research Committee, "A Guide Introducing Burnup Credit, Preliminary Version", Japan Atomic Energy Research Institute, July 2001.

[2] Working Group on Nuclear Criticality Safety Data, Nuclear Fuel Facility Safety Research Committee, "Nuclear Criticality Safety Handbook Version 2", Japan Atomic Energy Research Institute, March 1999.

[3] K.Suyama, M.Murazaki*, H.Mochizuki* and Y.Nomura, "Derivation of Correction Factor to be applied for Calculated Results of PWR Fuel Isotopic Composition by ORIGEN2 Code", JAERI-Tech 2001-074 (2001).

[4] Y.Nomura, M.Murazaki* and H.Okuno, "Introduction of "Equivalent Uniform Burnup" and "Equivalent Initial Enrichment" for Burnup Credit Evaluation", JAERI-Data/Code 2001-029 (2001).

[5] K.Suyama, T.Kiyosumi* and H.Mochizuki*, "Revised SWAT – The Integrated Burnup Calculation Code System – ", JAERI-Data/Code 2000-027.

[6] T.Hayashi*, K.Suyama, H.Mochizuki* and Y.Nomura, "Reactivity Effect of Spent Fuel Depending on Burnup History", JAERI-Tech 2001-041.

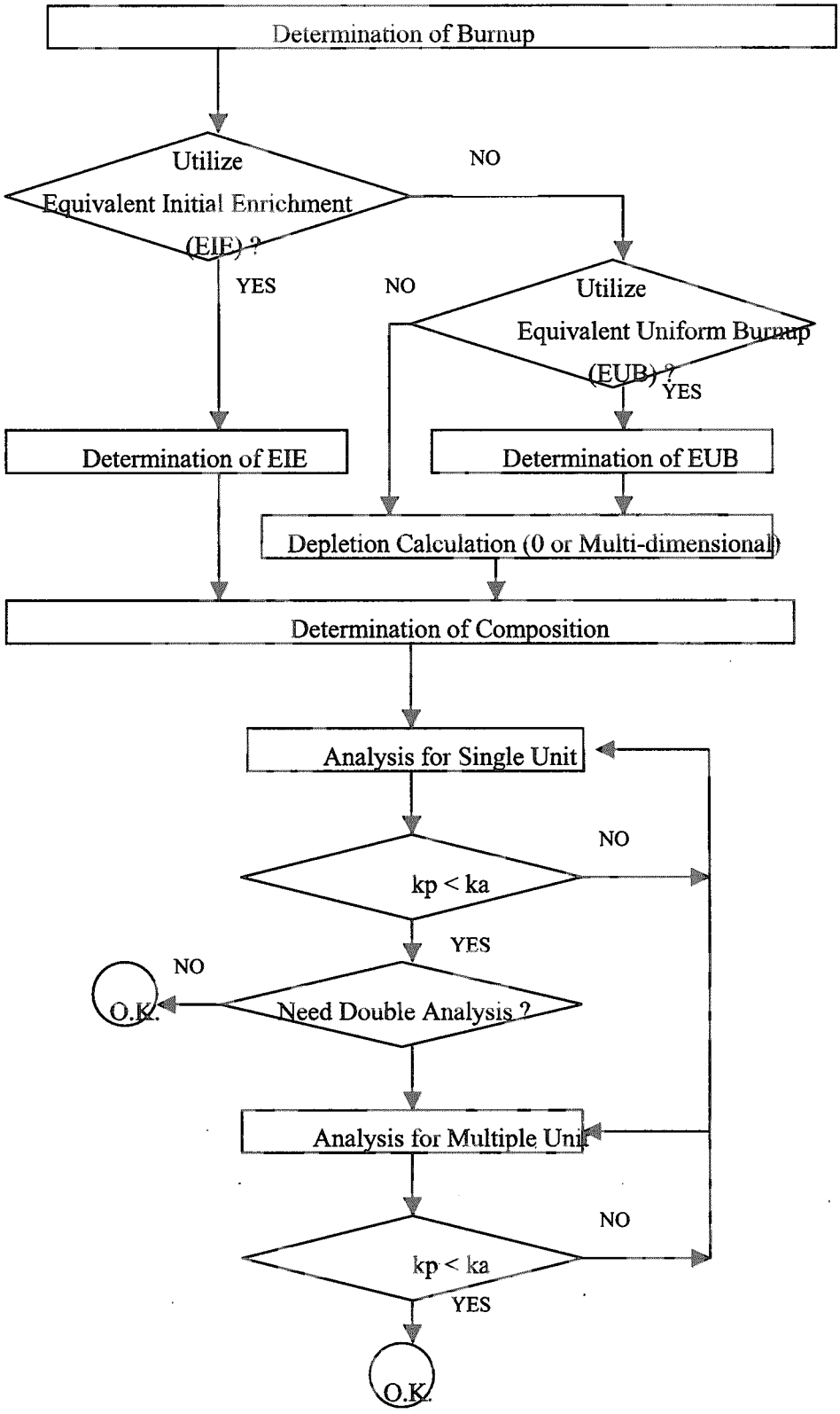

Fig.1 Procedure for criticality safety evaluation of spent fuel transport and storage system taking burnup credit into consideration.

Table 1 Correction Factors to apply to ORIGEN2.1 calculated results

Isotope	Obrigheim		Mihama-3		Genkai-1		Takahama-3	
	PWR-U	PWR-US	PWR-U	PWR-US	PWR-U	PWR-US	PWR-UE	PWR41J32
U-234	-	-	1.15	1.15	1.00	1.00	1.30	1.29
U-235	0.73	0.69	0.91	0.87	0.88	0.82	0.89	0.99
U-236	1.09	1.10	1.06	1.07	1.00	1.00	1.00	1.00
U-238	1.01	1.01	1.01	1.01	1.01	1.01	1.01	1.01
Pu-238	1.49	1.59	1.00	1.01	1.00	1.00	1.10	1.00
Pu-239	0.94	0.95	0.85	0.83	0.86	0.94	0.91	0.97
Pu-240	1.36	1.23	1.08	1.01	1.00	1.00	1.16	1.07
Pu-241	0.94	0.99	0.78	0.84	0.86	0.81	0.86	0.92
Pu-242	1.85	1.96	0.94	1.08	0.87	0.86	0.93	0.99
Am-241	2.41	2.62	1.06	1.18	0.82	0.78	1.51	1.62

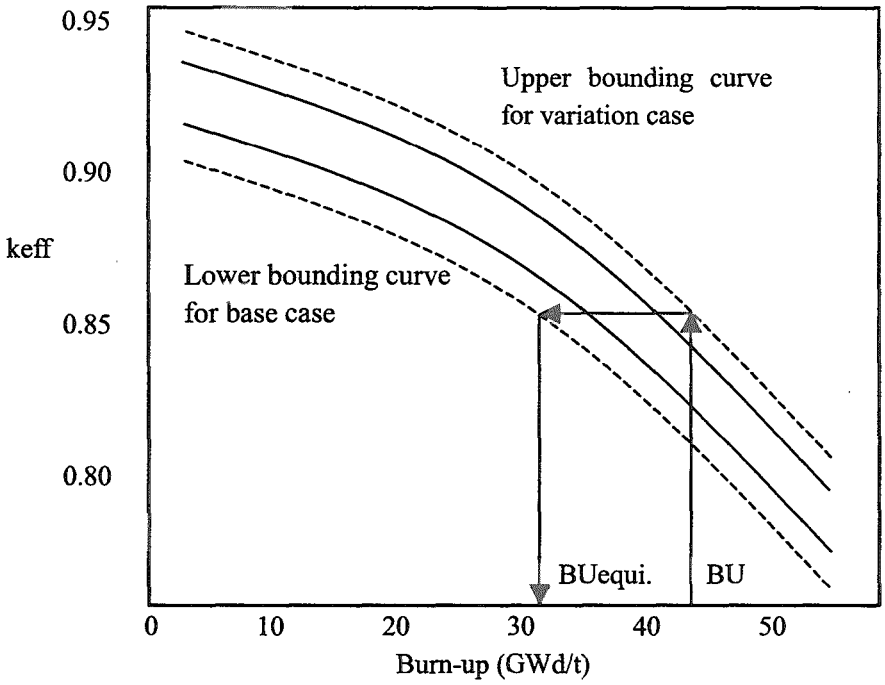

Fig.2 Diagram to obtain "Equivalent Uniform Burnup", where variation case means criticality calculation considering burnup distribution with nuclide composition measured by chemical analyses, and base case means criticality calculation considering uniform burnup distribution with nuclide composition calculated by ORIGEN2.1 code.

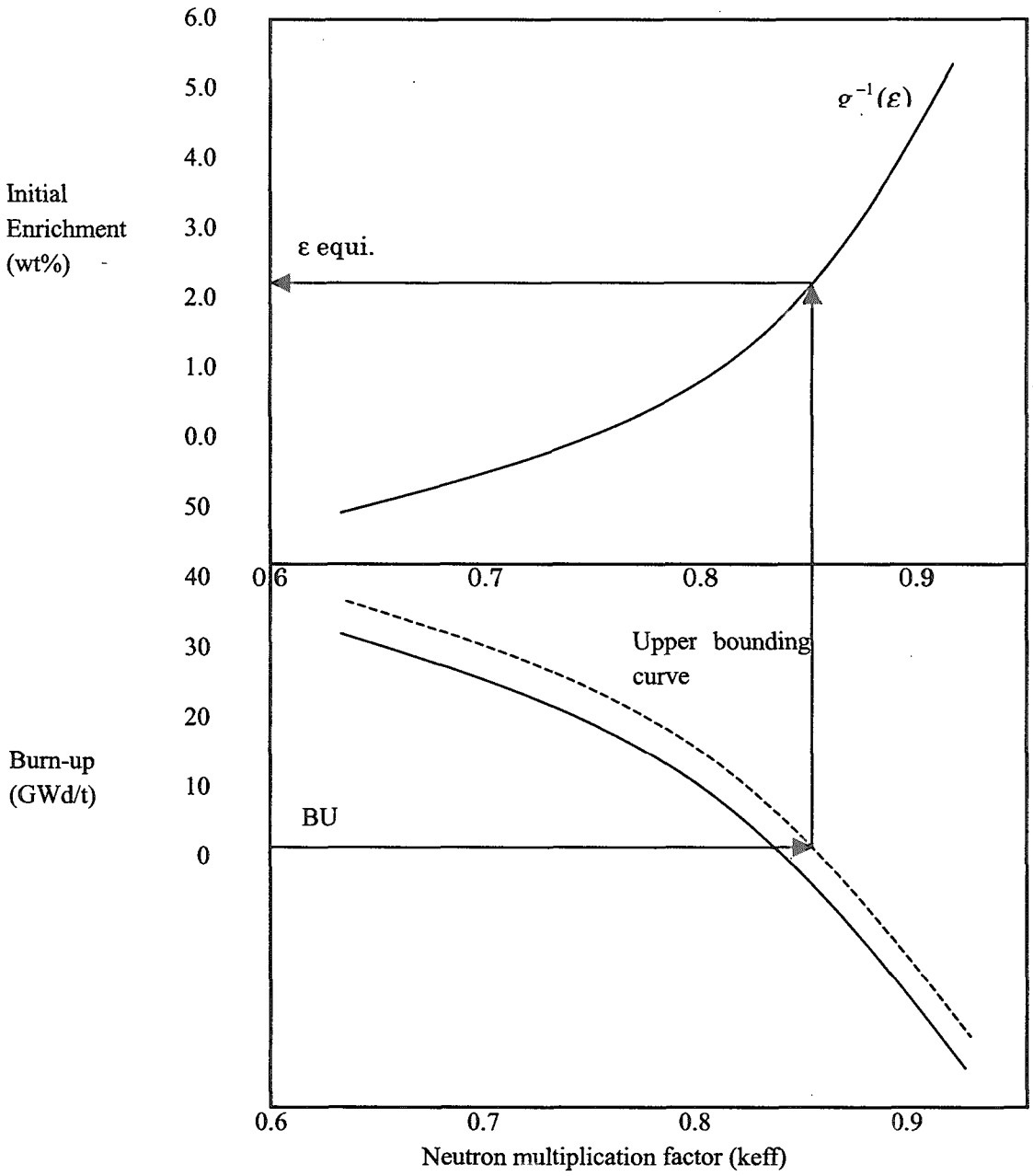

Fig.3 Diagram to obtain "Equivalent Uniform Burnup", where variation case means criticality calculation considering burnup distribution with nuclide composition measured by chemical analyses.

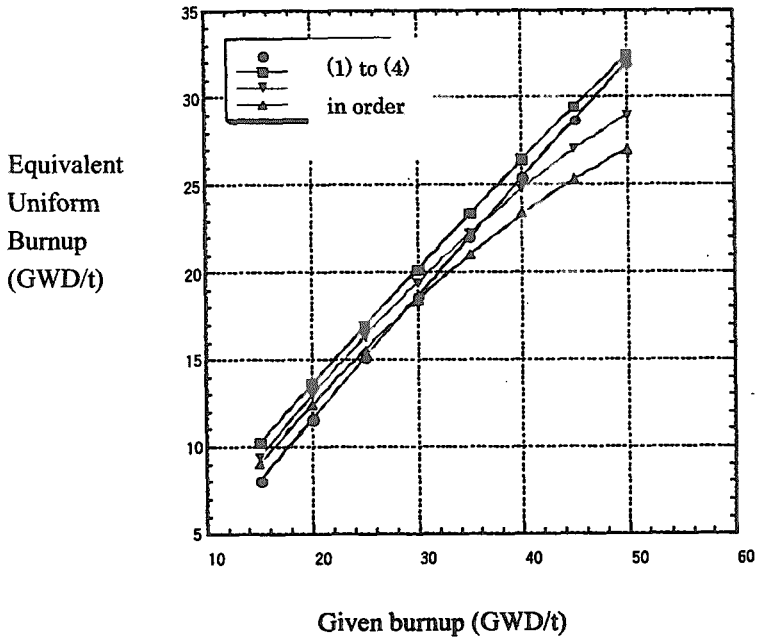

Fig.4 Correlation diagram of "Equivalent Uniform Burnup" for an unit cell infinite array system simulating spent fuel storage pool, showing the cases (1) for actinides only with 0 cooling, (2) for actinides only with 30 years cooling, (3) for actinides plus fission products with 0 cooling and (4) for actinides plus fission products with 0 cooling.

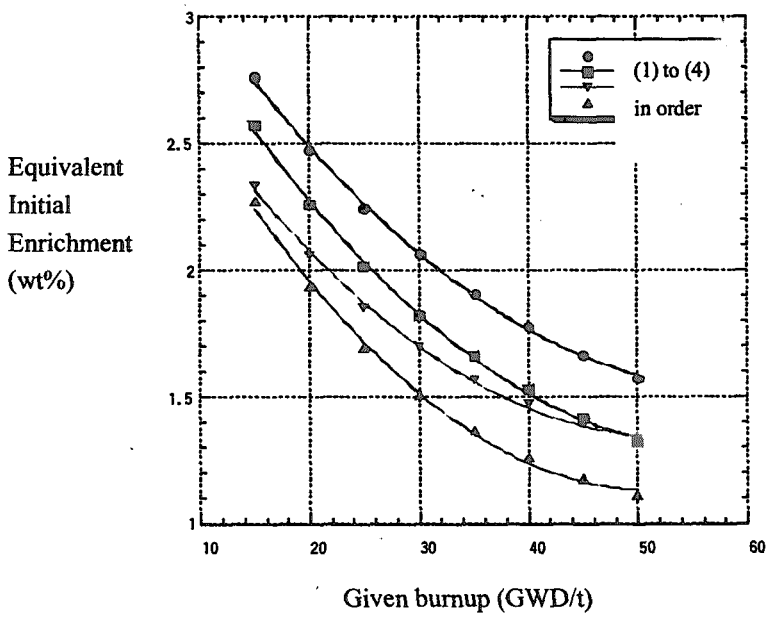

Fig.5 Correlation diagram of "Equivalent Initial Enrichment" for an unit cell infinite array system simulating spent fuel storage pool, showing the same cases as in Fig.4.

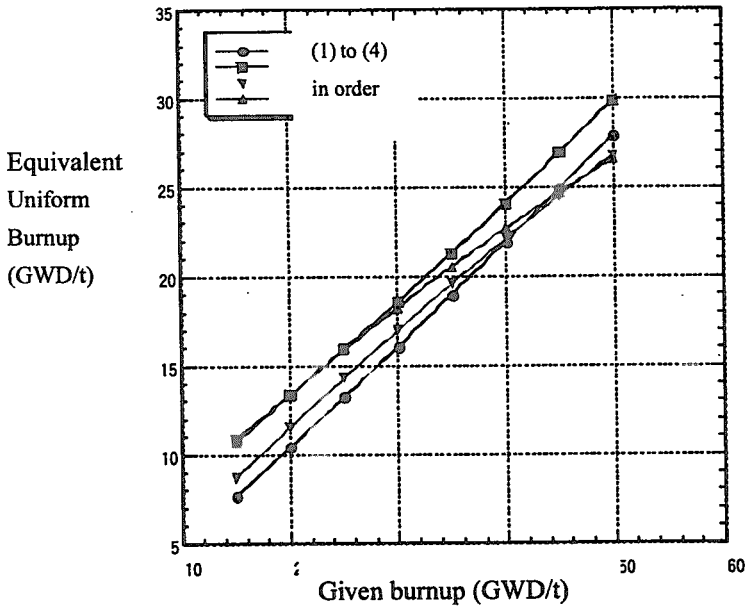

Fig.6 Correlation diagram of "Equivalent Uniform Burnup" for a spent fuel transport cask system simulating spent fuel storage pool, showing the same cases as in Fig.4 and Fig.5.

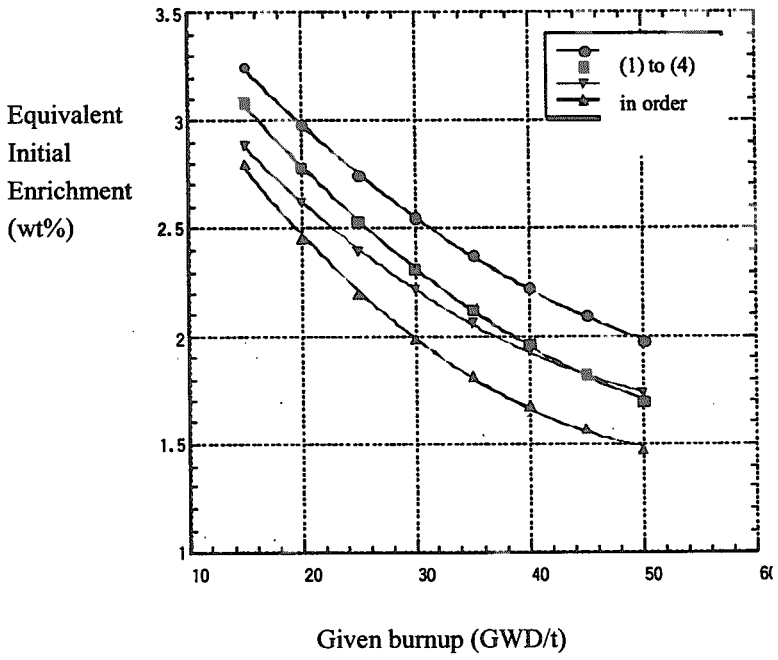

Fig.7 Correlation diagram of "Equivalent Initial Enrichment" for a spent fuel transport cask system simulating spent fuel storage pool, showing the same cases as in Fig.4, Fig.5 and Fig.6.

Among the eleven samples, in this study, three samples (Sample No.1, 3, 8) with different exposures were selected for the present analysis. The irradiation power of each sample and the irradiation time are described in the ref [1].

3. Analysis Method

Two code systems of Japan and France were used for analyzing the PIE data. The Japanese code was SWAT [3] that has been developed in JAERI. SWAT is the code system to analyze nuclide evolution problems by using SRAC [4] (a Japanese standard reactor analysis code) and ORIGEN2 [5] (a nuclide evolution calculation code). The nuclide evolution analysis code system DARWIN [6] in France was employed. The DARWIN is the code system combined APOLLO2 with PEPIN2. SRAC and APOLLO2 calculate one-group effective cross section for nuclide evolution calculation using collision probability method. The 107-group library based on JENDL-3.2 and the 172-group library based on JEF-2.2 were used in the calculation by SRAC and APOLLO2, respectively. ORIGEN2 (Japan) and PEPIN2 (France) calculate nuclide evolution. In the nuclide evolution calculation by SWAT, it should be noted that the fission yield data was also improved by using JNDCFPV2 [7] (JNDC Nuclear Data Library of Fission Products, Second Version) from the original ORIGEN2 library.

4. Analysis Result

Table 4-1 shows the calculation results for the nuclides of which the C/E values exceeded over 10%. The calculation results of the other nuclides were agreed with the experimental values within a few %. It has to be emphasized, however, that in order to facilitate the comparison between the codes, only a simple cell model was used, whereas for the qualification of DARWIN, more elaborate models are used. Therefore the French C/E values in Table 4.1 are not exactly representative of the DARWIN actual qualification [8].

4.1 Actinide

For ^{238}Pu, ^{243}Am and ^{244}Cm, the calculations underestimated in both analyses. Discrepancies were also shown between the Japanese and French results.

To clarify the reason of the discrepancies, at first, the results of two countries are investigated. The generation amount of an actinide depends on (n,γ) reaction, (n,fission) reaction, (n,2n) reaction and (n,3n) reaction of not only the actinide but also the parent actinides on the generation chain. Among those reactions, the (n,γ) reaction will be the most important reaction. To examine the (n,γ) reaction, we introduce the probability of the (n,γ) reaction, P_c. The P_c value was calculated by the following equation.

$$p_c = \frac{\sigma_c \phi}{\sigma_c \phi + \sigma_f \phi + \lambda} \approx \frac{\sigma_c}{\sigma_c + \sigma_f} = \frac{\sigma_c}{\sigma_a}$$

p_c : (n,γ) reaction Probability, σ_c : Capture Cross Section

σ_f : Fission Cross Section, σ_a : Total Absorption Cross Section

This is a blank page.

JP0250287

THE REBUS EXPERIMENTAL PROGRAMME FOR BURN-UP CREDIT

Pierre D'hondt, Klaas van der Meer, Peter Baeten
SCK•CEN, Mol, Belgium

Daniel Marloye, Benoit Lance, Jacques Basselier
BELGONUCLEAIRE, Brussels, Belgium

ABSTRACT

An international programme called REBUS (REactivity tests for a direct evaluation of the Burn-Up credit on Selected irradiated LWR fuel bundles) for the investigation of the burn-up credit has been initiated by the Belgian Nuclear Research Center SCK•CEN and Belgonucléaire with the support of USNRC, EdF from France, VGB, representing German nuclear utilities and NUPEC, representing the Japanese industry. The programme aims to establish a neutronic benchmark for reactor physics codes. This benchmark will qualify the codes to perform calculations of the burn-up credit.

The benchmark exercise investigates the following fuel types with associated burn-up:

- Reference 3.3% enriched UO_2 fuel
- Fresh commercial PWR UO_2 fuel
- Irradiated commercial PWR UO_2 fuel (51 GWd/tM)
- Fresh PWR MOX fuel
- Irradiated PWR MOX fuel (20 GWd/tM)

Reactivity effects are measured in the critical facility VENUS. Fission rate and flux distributions in the experimental bundles will be determined. The accumulated burn-up of all rods is measured non-destructively in a relative way by gross gamma-scanning, while some rods are examined by gamma-spectrometry for an absolute determination of the burn-up. Some rods will be analyzed destructively with respect to accumulated burn-up, actinides content and TOP-19 fission products (i.e. those non-gaseous fission products that have most implications on the reactivity). Additionally some irradiated rods have undergone a profilometry and length determination.

The experimental implementation of the programme has started in 2000 with major changes in the VENUS critical facility.
Gamma scans, profilometry, length determination and gamma-spectrometry measurements on the MOX fuel have been performed. In the course of October 2001 the first fresh fuel configuration will be investigated. In the same period the commercial irradiated fuel will arrive at the SCK•CEN hot cells and will be refabricated into fuel rodlets of 1 meter length.

Key words: Burn-up Credit, Critical Experiments.

1. INTRODUCTION

Present criticality safety calculations of irradiated fuel often have to model the fuel as fresh fuel, since no precise experimental confirmation exists of the decrease of reactivity due to accumulated burn-up. In other occasions only actinide depletion is allowed to be taken into account and the influence of fission products has to be disregarded. The fact that this so-called "burn-up credit" cannot (completely) be taken into account has serious economical implications for transport, storage and reprocessing of irradiated fuel. For long-term geological storage it is almost imperative to apply burn-up credit.

Therefor, an international programme called REBUS (REactivity tests for a direct evaluation of the Burn-Up credit on Selected irradiated LWR fuel bundles) has been initiated.
The aim of this programme is to establish an experimental benchmark for validation of reactorphysics codes for the calculation of the loss of reactivity due to burn-up, both for UO_2 and MOX fuel bundles.
The reactivity effect of PWR UO_2 spent fuel will be measured in the VENUS critical facility on a bundle of commercial spent fuel with a burn-up of 51 GWd/tM. The same will be done on a MOX bundle with a burn-up of 20 GWd/tM. Other fuel types can be investigated in future extensions of the programme, like BWR fuel.
At the same time we will measure fission rate and flux distributions in the different configurations.
Together with a precise measurement of the reactivity effect, it is also indispensable to have a good characterization of the fuel. The characterization of the spent fuel is performed in two steps:
The first step is non-destructive and is performed before the reactivity measurements. All spent fuel rods will be measured by gross gamma-scanning in order to determine the distribution of total gamma activity in the fuel rods. One specific rod will be investigated by gamma-spectrometry, together with a well-qualified calibration source, to determine the ^{137}Cs content and in this way the burn-up of the rod. Via the gross gamma-scans this will give a good picture of the burn-up of all rods. This first step is necessary to verify that the selected rods have a similar burn-up.
The second step is destructive and is consequently performed after the reactivity measurements. It aims at determining both the actinides content, some burn-up indicators (Cs, Nd) and the 19 most important fission products with respect to neutron absorption (representing >80% of the neutron absorption in the spent fuel). The sample for this destructive, radiochemical assay is taken from the same rod, on which gamma-spectrometry has been performed.
The fresh fuel content has been well-documented during fabrication.

2. SHORT DESCRIPTION OF THE VENUS REACTOR

The VENUS critical facility is a water-moderated zero-power reactor. It consists of an open (non- pressurized) stainless-steel cylindrical vessel including a set of grids which maintain fuel rods in a vertical position. After a fuel configuration has been loaded, criticality is reached by raising the water level in the vessel.
Parameters that are measured with the VENUS reactor are the critical water level h_c, the reactivity coefficient $\delta\rho/\delta h$, the axial fission rate distribution, the horizontal fission rate distribution, spectrum indices F5/F9, F8/F9, C8/F9, fission rate distribution inside fuel rod, detector response and the delayed neutron fraction β_{eff}.
For details of the measurements performed in the VENUS we refer to reference [1], except for the flux measurements that are described below.

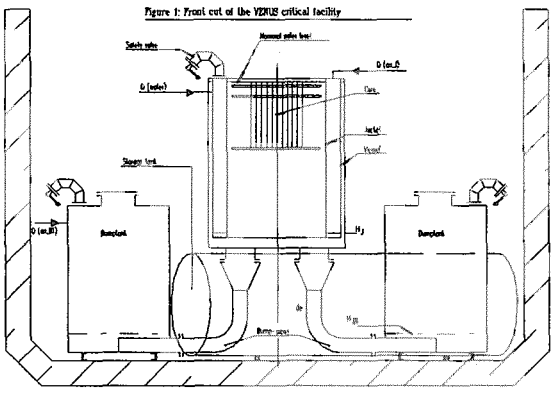

Figure 1. Vertical cross-section of the VENUS critical facility

Unlike the fission rate distribution, that is measured directly via the fission products created in the fuel rods, the flux distribution is determined by the insertion of activation wires (e.g. Co) at several positions in the reactor in between the fuel rods and measuring the activity of these wires after irradiation in the VENUS facility. The activation wires typically have a length of 1 cm and are placed diagonally between the fuel rods in perspex tubes. The aim of the perspex is to perturb the water environment as little as possible with respect to neutron behaviour.
The flux is derived from the measured activity of the wires. Since this activity is due to both the thermal and epithermal neutron flux, a certain amount of calculational interpretation is required. However, this is limited due to the fact that more than 90% of the activity is caused by thermal neutrons.
The flux distribution measurements will be performed simultaneously with fission rate distribution measurements in order to make a comparison between the results of both methods. In the irradiated fuel bundles only flux distribution measurements will be performed, since fission rate measurements are not possible on irradiated fuel.

3. REACTIVITY MEASUREMENTS PERFORMED AT VENUS IN THE FRAMEWORK OF REBUS

Five fuel bundles or assemblies will be investigated in the framework of the REBUS programme. These five bundles are:

- Reference 3.3% enriched UO_2 fuel
- Fresh commercial PWR UO_2 fuel, fabricated by Framatome ANP (formerly SIEMENS)
- Irradiated commercial PWR UO_2 fuel (51 GWd/tM), originating from Neckarwestheim NPP, Germany
- Fresh PWR MOX fuel, originating from the BR3, an experimental Belgian PWR
- Irradiated PWR MOX fuel (20 GWd/tM), also from the BR3 reactor

All test bundles will be loaded as a 7x7 fuel assembly in the center of a 3.3% enriched UO_2 fuel driver zone. The 7x7 assembly is chosen because calculations show that such an assembly will result in a reactivity effect that is large enough for benchmark purposes (~1500-2000 pcm) and for practical reasons because the VENUS reactor has removable grids where this assembly fits in.
The reference 3.3% enriched UO_2 fuel bundle consists of the same 3.3% enriched UO_2 fuel as there is in the driver zone. Its purpose is to validate a k_{eff} calculation.

The fresh commercial fuel bundle (figure 2a) consists of a 5x5 fuel assembly. The fuel is 3.8% enriched UO_2 fuel, fabricated at Framatome ANP (formerly SIEMENS), Germany. It is the original composition of the irradiated commercial fuel.
The irradiated commercial fuel bundle is the same as the fresh bundle, as is obvious for experimental reasons (clean comparison of the fresh and irradiated bundle). The fuel is provided by GKN, the operator of the Neckarwestheim NPP in Germany.

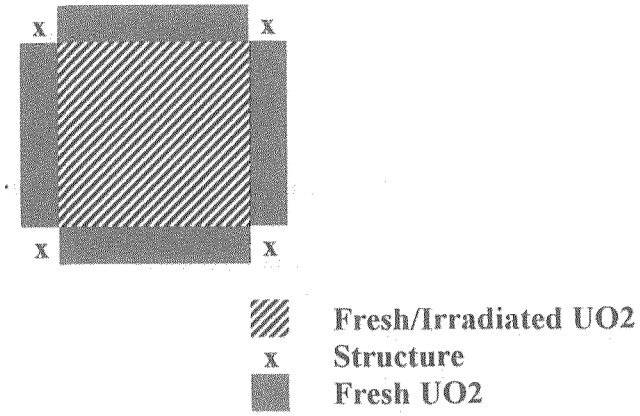

Figure 2a. Central 7x7 UO_2 bundle

The fresh BR3 MOX fuel bundle (figure 2b) consists of 24 fuel rods (a 7x7 overmoderated assembly). In this way the highest reactivity effect could be obtained with the available rods.
The fuel is 6.9% enriched fissile MOX fuel, fabricated at Belgonucléaire, Belgium. It is the original composition of the irradiated BR3 fuel.
The irradiated PWR MOX fuel of intermediate burn-up originates from the BR3 reactor, Belgium. The fuel is provided by SCK•CEN. The bundle design is the same as for the fresh bundle (figure 2b).

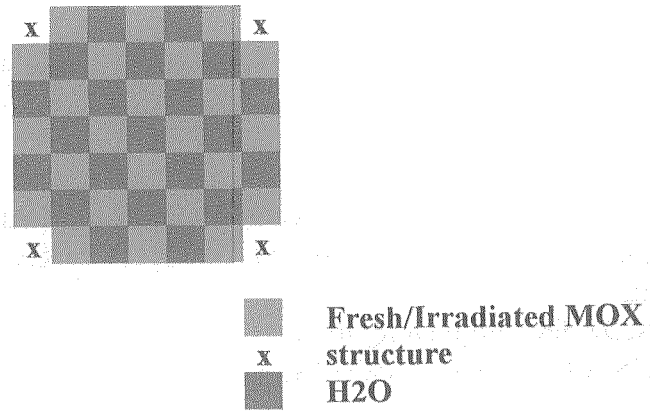

Figure 2b. Central 7x7 MOX bundle

The reactivity effect will be measured by loading the different bundles in the center of the driver zone and measuring each time the critical water level and the reactivity effect of a change of the water level. From these measurements the reactivity effect can be estimated. However, a more direct way of validating the reactor codes is simply calculating the k_{eff} for the different configurations at the measured critical water levels. In this case there is no need

in using the measured reactivity effect, which reduces the measurement uncertainty on the experimental data and increases the performance of the benchmark test.
In addition of the reactivity measurements the fission rate distribution and the flux distribution at the main axes will be measured. Due to the impossibility of measuring this parameter in the spent fuel assembly, wire activation measurements will be performed in this assembly to measure the thermal and epithermal neutron flux.

Table I gives an overview of the measurements in the different configurations.

Table I. Overview of measurements in the VENUS critical facility

configuration	critical level	reactivity effect	fission rate distribution	flux distribution	validation purpose
reference UO_2	x	x			k_{eff}
fresh UO_2	x	x	x	x	k_{eff} and fission rate
irradiated UO_2	x	x	in driver	x	k_{eff} and fission rate
fresh MOX	x	x	x	x	k_{eff} and fission rate
irradiated MOX	x	x	in driver	x	k_{eff} and fission rate

4. REFABRICTION AND MEASUREMENTS PEROFORMED AT HOT CELL LABORATORY, RADIOCHEMICAL MEASUERMENTS

The refabrication of the commercial spent fuel rods from 4 meter rods into 1 meter rodlets will be executed in the SCK•CEN hot cell laboratory. Afterwards the rodlets will be cleaned thoroughly, since the contamination level of the VENUS reactor has to remain very low. Also the BR3 spent fuel rods have to be cleaned, but no refabrication is needed.
After cleaning the rodlets will be assembled in the experimental 7x7 bundle. This is performed at the hot cell of the BR2, SCK•CEN's MTR.
Details of the measurement techniques used in the hot cell laboratory and of the radiochemical measurements are given in reference [1].

5. PRELIMINARY CALCULATIONS

Some preliminary calculations have been performed to support the design of the bundles. The main objective of the REBUS programme is validation of reactorphysics codes, therefore it is indispensable to create a reactivity effect that is significantly larger than the uncertainty of the calculations. Since the uncertainty of the calculations is estimated to be between 300 and 500 pcm (0.3 to 0.5 % on k_{eff}), it is considered necessary to create an experimental reactivity difference of about 1500 pcm.
Preliminary calculations showed a reactivity difference of 2135 pcm for the high burn-up commercial fuel with respect to fresh fuel. For the MOX case the calculated difference is about 1500 pcm.

6. RESULTS

The first results of the REBUS programme deal mainly with the characterization of the fuel. The fresh fuel rods originating from the VENUS and BR3 (driver zone, reference bundle and MOX fuel) have already been used in previous benchmark programmes and their characteristics are well-documented. Additionally, the VENUS rods have been elongated from 50 cm to 1 m and during this elongation we took the opportunity to perform some extra

measurements with respect to the cladding inner and outer diameter and the position of the lower end plug.
The irradiated MOX fuel from the BR3 has been examined in the hot cell laboratory with respect to gross-gamma scanning, burn-up by gamma-spectrometry, profilometry and fuel column length. Typical results are shown in the following figures.

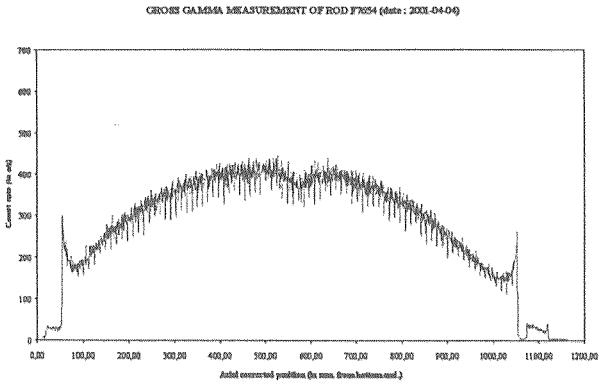

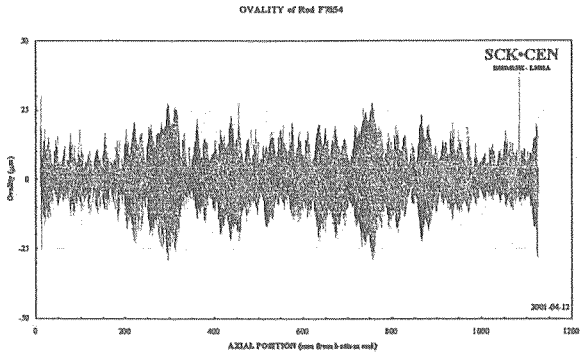

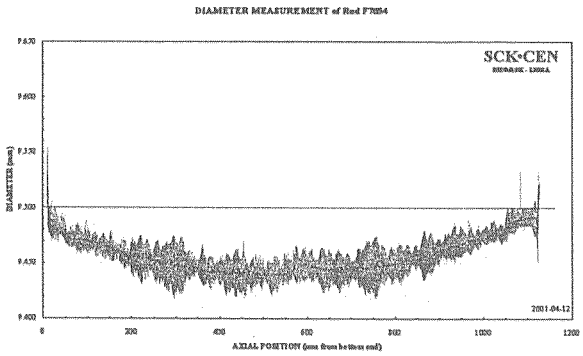

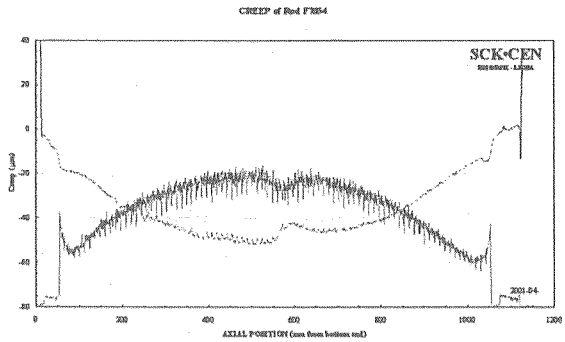

The gross-gamma scan results show for certain MOX rods a rather high degree of Cs migration, indicating a high linear power during irradiation. Since this Cs migration behaviour is not similar for all rods, we have to make some adjustments with respect to the gamma self-absorption for the 660 keV gamma peak of ^{137}Cs in order to compensate the differences.

7. VALUE OF THE REBUS BENCHMARK

The critical water level of configurations in the VENUS reactor is measured with a random uncertainty of 0.02 cm and a systematic uncertainty of 0.05 to 0.07 cm, the latter being mainly due to the uncertainty of the fuel bottom. So the total uncertainty is between 0.05 to 0.07 cm, which results in an uncertainty expressed in pcm of about 25 pcm (the reactivity effect of the present core is about 350 pcm/cm for a critical level of 45 cm). The random uncertainty is smaller, about 7 pcm.
For the REBUS configurations the critical level will be in the range of 60 to 80 cm with a corresponding lower reactivity effect of the water level, resulting in a smaller uncertainty. However, due to the large reactivity effect between the fresh and spent fuel bundle the difference in critical height will be large, resulting in a change of water level reactivity effect. A simple approximation to determine the total reactivity effect $\Delta\rho$ is shown in the following equation:

$$\Delta\rho = \Delta h_c \times \frac{\partial\rho}{\partial h}$$

where Δh_c is the measured difference in critical height for the two compared configurations and $\partial\rho/\partial h$ the averaged value of the reactivity effect of the water level.
When due to the large difference in critical height the values of $\partial\rho/\partial h$ will be too different for the two configurations, in principle an integration should be used for the determination of the total reactivity effect $\Delta\rho$:

$$\Delta\rho = \int_{h_{c1}}^{h_{c2}} \frac{\partial\rho}{\partial h} dh_c$$

The uncertainty related to the measurement of the reactivity effect $\Delta\rho$ in this way is estimated to be 20 pcm, based on the present value for a lower critical value (10 pcm), where the higher critical level will decrease the uncertainty, but where the high value of the reactivity effect will increase the uncertainty due to the change of $\partial\rho/\partial h$ in function of the critical height.

The uncertainty of the non-destructive ^{137}Cs burn-up measurement is estimated to be 4 to 5%.

The uncertainties of the determination of the actinides, the burn-up indicators and the fission products by radiochemical analysis are shown in the next tables:

Uncertainties by radiochemical analysis for the different actinides							
^{234}U	5-10%	^{238}Pu	3-10%	^{241}Am	2-5%	^{242}Cm	3-7%
^{235}U	0.5-2%	^{239}Pu	0.2-0.5%	^{242}Am	2-10%	^{243}Cm	30-50%
^{236}U	0.5-5%	^{240}Pu	0.2-0.5%	^{243}Am	2-5%	^{244}Cm	3-6%
^{238}U	0.3-0.5%	^{241}Pu	0.2-0.5%			^{245}Cm	3-10%
		^{242}Pu	0.2-0.5%			^{246}Cm	5-15%
^{237}Np	3-10%	^{244}Pu	50%				

Uncertainties by radiochemical analysis for the different burn-up indicators							
^{137}Cs	2-4%			^{143}Nd	0.5-1%	^{146}Nd	0.5-1%
^{144}Ce	5-10%			^{144}Nd	0.5-1%	^{148}Nd	0.5-1%
				^{145}Nd	0.5-1%	^{150}Nd	0.5-1%

Uncertainties by radiochemical analysis for the different fission products (TOP-19), representing 80-90% of the anti-reactivity of all long-living fission products							
^{147}Sm	0.5-2%	^{153}Eu	0.5-2%	^{103}Rh	10-20%	^{143}Nd	0.5-1%
^{149}Sm	2-4%	^{154}Eu	2-5%	^{109}Ag	15-30%	^{145}Nd	0.5-1%
^{150}Sm	0.5-2%	^{99}Tc	10-20%	^{155}Gd	5-10%	^{133}Cs	2-5%
^{151}Sm	0.5-2%	^{95}Mo	10-20%	^{105}Pd	10-20%	^{135}Cs	2-5%
^{152}Sm	0.5-2%	^{101}Ru	10-20%	^{108}Pd	10-20%		

8. CONCLUSIONS

The REBUS programme will provide an experimental benchmark for burn-up credit, taking into account both fissile isotopes depletion and the production of neutron absorbing fission products. However, no distinction between both contribuants is possible within the framework of the programme.

With the results of the REBUS programme a validation of reactorphysics codes with respect to burn-up credit of PWR UO_2 fuel with intermediate and high burn-up will be possible. Based on the results of this validation, and the quoted uncertainties of the experiment, safety margins can be determined that have to be implemented for burn-up credit calculations.

The REBUS programme will be executed completely at SCK•CEN in its hot cell laboratory, radiochemistry lab and the VENUS reactor. All these facilities have already proven their capability to execute large-scale international benchmark exercises, like DOMO, HBC, CALLISTO (hot cells, radiochemistry), ARIANE (radiochemistry) and VIP, VIPO, VIPEX (VENUS reactor).

Future extensions of the REBUS programme can deal with BWR and high burn-up MOX fuel.

9. REFERENCES

[1] K. van der Meer et al., "REBUS: A Burn-Up Credit Experimental Programme", IAEA TCM on the Evaluation and Review of the Implementation of Burnup Credit in Spent Fuel Management Systems, Vienna, July 10-14, 2000.

[2]H. Adachi, J. Basselier, L. Leenders, " "Burnothèque", A Valuable Standard for Accurate Burn-up Determination by Non-destructive Examination", ESARDA 10, proceedings, p. 162, 1st ESARDA symposium, Brussels, April 1979.

[3]D.F.G. Reher, B. Denecke, E. De Roost, K. van der Meer, "Standardization of a 50 GBq ^{152,154}Eu extended volume source", ICRM Conference and International Symposium on Radionuclide Metrology and its Applications, Teddington, UK, 7-11 June, 1993, Nuclear Instruments and Methods in Physics Research A 339 (1994) 334-338 North-Holland.

JP0250288

Comparison of nuclide evolution analyses between Japanese and French codes

T. Iwasaki*, H. Hiraizumi*, G. Youinou**
*Department of Quantum Science and Energy Engineering, Tohoku University
Aoba 01, Aramaki, Sendai, 980-8579, JAPAN
Fax. +81-22-217-7908, E-mail. tomohiko.iwasaki@qse.tohoku.ac.jp
**Commissariat à l'Energie Atomique (CEA)
Reactor Physics and Fuel Cycle Service, 13108 St-Paul-Lez-Durance, France

Benchmark problem based on Japanese Post Irradiation Experiment (PIE) data was analyzed by Japanese nuclide evolution analysis code and French one under the cooperative research program between the Japanese University Association (JUA) in Japan and Commissariat a l'Enegie Atomique (CEA) in France. Significant discrepancies over 10% were found between the Japanese and French results for ^{238}Pu, ^{243}Am, ^{244}Cm, ^{125}Sb, ^{154}Eu, ^{134}Cs and ^{144}Ce. It was found that those differences were almost caused by the differences of the cross sections and the fission yields. Furthermore, as for the effect to critical safety, multiplication factors were analyzed based on the isotopic compositions calculated by the codes. However, no significant effect to the multiplication factors was observed between Japan and French results.

Key Words: PIE, NUCLIDE EVOLUTION, SWAT, DARWIN

1. Introduction

Various analysis codes are being employed for nuclide evolution analysis in the world. To improve accuracy of the analysis, it is useful to compare those codes. In this study, we have compared the Japanese code (SWAT) and the French one (DARWIN) under the cooperative research program between the Japanese University Association (JUA) in Japan and Commissariat à l'Energie Atomique (CEA) in France. The data analyzed here is Post Irradiation Experiment (PIE) data for the irradiated fuels in the Mihama atomic power plant unit-3 (PWR) of the Kansai Electric Power Co., Inc.

This paper describes the PIE, the benchmark specifications for the PIE, the calculation methods of both codes and their results, and the multiplication factor calculations. However, it should be remarked that the results of the nuclide evolution calculations have been presented in the ref [1] in details. Therefore, only the summary for the nuclide evolution calculations is presented in this paper.

2. Post Irradiation Experiment (PIE) data

The PIE was carried out in the chemical department of the Japan Atomic Energy Research Institute (JAERI) for the research of the dissolution of high exposure fuels [2]. Eleven samples discharged from the Mihama unit-3 and Genkai unit-1 were measured in the experiment. The feature of the PIE is summarized in **Table 2-1**. **Table2-2** shows the exposures of the samples.

(1) ^{238}Pu

The generation chain of ^{238}Pu is in **Fig.4-1**. **Table 4-2** shows the C/E(J/F) value which is the ratio of the Japanese C/E value and the French one, and the P_c(J/F) value which is the ratio between the Japanese and French values of the P_c on the chain. There was no difference for P_c between Japan and France in the chain of ^{238}Pu generation. Although the fission probability (P_f), which was similarly defined as P_c, was also examined, there were no significant differences in the P_f(J/F) values. For ^{238}Pu, two other generation paths exist. One is the (n,2n) reaction of ^{239}Pu and the other is the decay from ^{242}Cm. The examination were performed for the two paths. As the results, both paths have little contribution to the differences of the ^{238}Pu amount. More study should be done for understanding the discrepancy of ^{238}Pu.

(2) ^{243}Am

The generation chain of ^{243}Am is in **Fig.4-2.** The comparison of P_c for ^{243}Am is shown in **Table 4-4**. Except for ^{242m}Am, there was no difference between Japan and France. The P_c(J/F) value of ^{242m}Am (0.93) was considerably small than 1. The Japanese P_c value was low than the French value. It is supposed that this difference of ^{242m}Am resulted in the C/E discrepancy of ^{243}Am (C/E(J/F)=0.93).

(3) ^{244}Cm

The generation chain of ^{244}Cm from ^{243}Am is in **Fig.4-3**. The P_c(J/F) for ^{244}Cm is shown in **Table 4-5**. There was no difference between Japan and France, in the P_c value of the isotopes on the generation chain from ^{243}Am to ^{244}Cm. It is supposed that the difference between Japan and France for ^{244}Cm is caused by the same reason as ^{243}Am, i.e. the difference of the capture cross section of ^{242m}Am.

4.2 FP

To investigate the reason of the discrepancy of ^{125}Sb, ^{154}Eu, ^{134}Cs and ^{144}Ce, we examined the cross section and the fission yield. **Table 4-6** shows the C/E value when the cross section library of FP was changed to JENDL-3.2 from the ORIGEN2 original library, and the fission yield data was varied from the ORIGEN2 original library to JNDCFPV2 in the ORIGEN2 analysis.

(1) ^{125}Sb

It is found from Table 4-6 that the C/E value was changed to 1.18 from 2.19 by using JNDCFPV2 as the fission yield data. The Japanese C/E values were nearly 1 by using JNDCFPV2 as the fission yield library, although the French values were from 1.34 to 1.97. Newer fission yield library is useful for improving the accuracy of the nuclide evolution calculation of ^{125}Sb.

(2) ^{154}Eu

It is observed from Table 4-6 that the C/E value was changed to 1.14 from 2.01 by using JENDL-3.2 as the cross section library of FP. The Japanese C/E value were nearly 1 by using JENDL-3.2 for the cross section library of FP, although the French values were from 1.23 to 1.80. For FP nuclides, it is important to use new cross section library.

(3) ^{134}Cs & ^{144}Ce

The Japanese and French C/E value is lower than (0.75~0.91) for higher exposure samples (Sample 3 and 8), although the value for sample1 was almost 1. The C/E value did not change largely by the change of the cross section library of FP and the fission yield library as shown in Table 4-6. The difference was almost 10% and was not larger than those of ^{125}Sb and ^{154}Eu, however, another study should be performed in both countries.

5. Analysis Related to Critical Safety

The difference of the isotopic compositions between Japan and France may influence on multiplication factor. Therefore, we performed the calculation of multiplication factor at the end-of-irradiation by using SRAC. In the SRAC calculation, the isotopic composition was considered in a pin cell geometry and the two multiplication factors based on the two compositions calculated by Japan and French codes. The results were shown in **Table 5-1**. As shown in the table, the differences are very small. Although the code difference between Japan and France produce significant difference for several nuclides, it is confirmed that the difference of isotopic composition owing to the code difference does not cause the difference of multiplication factor. As for critical safety, no significant difference exists in the nuclide evolution analysis of both.

6. Conclusion

We compared the nuclide evolution calculation codes that have employed for the analysis in Japan and France widely, in order to improve the accuracy of those codes. The large discrepancies of C/E over 10% were found for ^{238}Pu, ^{243}Am, ^{244}Cm, ^{125}Sb, ^{154}Eu, ^{134}Cs and ^{144}Ce. It is supposed that the difference of C/E for ^{243}Am and ^{244}Cm between Japanese results and French ones is due to the (n,γ) reaction of ^{242m}Am. The C/E values for ^{125}Sb and ^{154}Eu are improved by changing the cross section and fission yield libraries. For ^{238}Pu, ^{134}Cs and ^{144}Ce, extensive studies should be performed. Furthermore, as for the effect to critical safety, multiplication factors based on isotopic compositions calculated by each code were analyzed. But, no significant effect to multiplication factor was observed.

Acknowledgement

The authors would like to express the grateful thanks to Dr. K.Suyama of JAERI, for his helpful comments and suggestions.

References

[1] T. Iwasaki, H. Hiraizumi, G. Youinou "Analysis of Recent Post Irradiation Tests by Japanese and French Burnup Analysis Code Systems" Nuclear Data for Science and Technology, October 7-12,2001, Tsukuba, Japan, (2001)

[2] T. Adachi, *et al*, "Dissolution Studies of Spent Nuclear Fuels," JAERI-M 91-010, Japan

Atomic Energy Research Institute (JAERI), (1991).

[3] K. Suyama, T. Kiyosumi, H. Mochizuki, "Revised SWAT –The Integrated Burnup Calculation Code System," JAERI-Data/Code 2000-027, Japan Atomic Energy Research Institute (JAERI), (2000)

[4] K. Okumura, K. Kaneko, K. Tsuchihashi, "SRAC95; General Purpose Neutronics Code System," JAERI Data/Code 96-015 Japan Atomic Energy Research Institute, (1996)

[5] A. G. Croff. "ORIGEN2 –A Revised and Updated Version of the Oak Ridge Isotope Generation and Depletion Code," ORNL-5621, (1980).

[6] A. Tsilanizara et al, "DARWIN, an evolution code system for a large range of application", ICRS-9, Oct. 1999, Tsukuba, Japan, (1999)

[7] K. Tasaka, J. Katakura, H. Ihara, *et al.*, "JNDC Nuclear Data Library of Fission Products -Second Version-" JAERI-1320, (1990)

[8] P. Marimbeau et al, "The DARWIN fuel cycle package – Procedure for material balance calculation and qualification", ENC'98, Oct. 1998, Nice, France, (1998)

Table 2-1 Feature of PIE (Mihama unit-3)

Reactor	Westing-House type PWR
Electric Power	826 Mwe
Thermal Power	2432 MWt
Fuel	15x15 PWR fuel (no Gd)
Core Diameter	3.04 m
Core Active Height	3.66 m
Fuel	UO2 (3.2%)
Clad	Zr-4
Pellet Diameter	0.4645 cm
Clad Diameter	0.5360 cm
Irradiation Time	1978-1982
Measurement Time	1986-
Sample	9 samples (6900-34000 MWd/tU)
Measured Nuclides	25 nuclides ^{235}U, ^{236}U, ^{238}U, ^{237}Np, ^{238}Pu, ^{239}Pu ^{240}Pu, ^{241}Pu, ^{242}Pu, ^{241}Am, ^{243}Am ^{242}Cm, ^{244}Cm, ^{106}Ru, ^{125}Sb, ^{134}Cs ^{137}Cs, ^{143}Nd, ^{144}Ce, ^{144}Nd, ^{145}Nd ^{146}Nd, ^{148}Nd, ^{150}Nd, ^{154}Eu

Table 2-2 Exposure of Each Sample (MWd/t)

Reactor	Sample No.	MWd/MtU
Mihama-3	1	6900
	2	15300
	3	21200
	4	14600
	5	29440
	6	32300
	7	33700
	8	34100

Table 4-1 C/E

Isotope		Sample1		Sample3		Sample8	
		Japan	France	Japan	France	Japan	France
MA	^{238}Pu	0.84	0.94	0.69	0.75	0.81	0.87
	^{243}Am	0.56	0.62	0.75	0.80	0.88	0.91
	^{244}Cm	0.74	0.87	0.55	0.61	0.65	0.69
FP	^{125}Sb	0.99	1.34	0.98	1.59	1.09	1.97
	^{134}Cs	0.93	1.01	0.81	0.86	0.88	0.91
	^{144}Ce	1.03	1.03	0.86	0.86	0.75	0.76
	^{154}Eu	0.97	1.23	0.74	1.32	0:87	1.80

Table 4-2 Ratio of P_c on the chain of ^{238}Pu

	C/E(J/F)	P_c(J/F)
^{235}U	1.00	0.98
^{236}U	0.99	1.00
^{237}U	-	-
^{237}Np	0.97	1.00
^{238}Np	-	-
^{238}Pu	0.92	1.00

Table 4-3 Amount at the end of burnup

	Sample1	Sample3	Sample8
^{242}Cm	5.85E-02	4.14E+00	1.58E+01
^{238}Pu	2.82E+00	3.62E+01	1.40E+02

Table 4-4 Ratio of P_c on the chain of ^{243}Am

	C/E(J/F)	P_c(J/F)
^{238}U	1.00	1.01
^{239}U	-	-
^{239}Np	-	-
^{239}Pu	0.98	1.01
^{240}Pu	0.99	1.00
^{241}Pu	0.98	1.02
^{242}Pu	0.98	1.00
^{243}Pu	-	-
^{241}Am	0.98	1.00
^{242m}Am	-	0.87
^{243}Am	0.93	1.00

Table 4-5 Ratio of P_c on the chain of ^{244}Cm

	C/E(J/F)	P_c(J/F)
^{243}Am	0.93	1.00
^{244}Am	-	-
^{244}Cm	0.90	1.01

Table 4-6 C/E at Changing Library in SWAT

Cross Section	ORIGEN2	JENDL-3.2	ORIGEN2	JENDL-3.2
Fission Yield	ORIGEN2	ORIGEN2	JNDCFPV2	JNDCFPV2
^{125}Sb	2.19	2.16	1.18	1.16
^{154}Eu	2.01	1.14	1.96	1.12
^{134}Cs	0.99	0.97	0.99	0.96
^{144}Ce	0.83	0.83	0.84	0.84

Table 5-1 Difference of multiplication factors by French and Japanese codes

	Sample1	Sample3	Sample8
k (Japan)	1.2684	1.1445	1.0642
k (France)	1.2692	1.1471	1.0625
k (Japan) - k (France)	-0.0008	-0.0026	0.0017

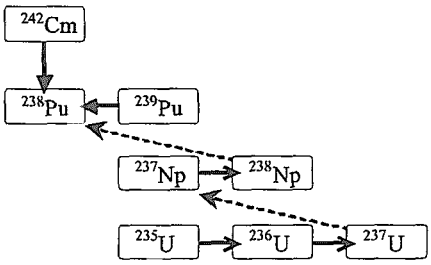

Fig.4-1 ^{238}Pu generation chain

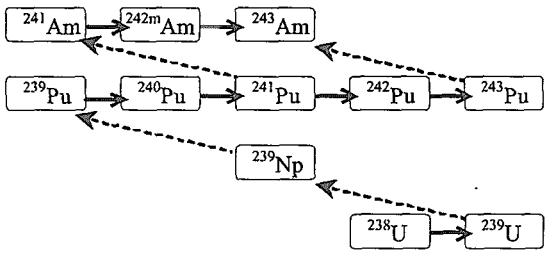

Fig.4-2 ^{243}Am generation chain

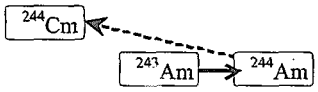

Fig.4-3 ^{244}Cm generation chain

This is a blank page.

JP0250289

JAERI-Conf 2002-004

High-precision Analog Type Neutron Monitoring System

NAOTAKA ODA, YOSHIO KITA*) AND KAZUYA ISHIZAWA**)
Toshiba Corporation Power System & Services Company,
8, Shinsugita-cho, Isogo-ku, Yokohama 235-8523
Fax: 81-45-770-2054, e-mail: naotaka.oda@toshiba.co.jp
* Toshiba Corporation, Fuchu Operations-Power Systems,
1, Toshiba-cho, Fuchu-shi, Tokyo 183-8511
Fax: 81-42-333-0144, e-mail: yoshio.kita@toshiba.co.jp
** Toshiba Corporation Display Devices & Components Company
Shimoishigami, Otawara-shi, Tochigi 324-8550
Fax: 81-287-26-6061, e-mail: kazuya.ishizawa@toshiba.co.jp

An analog type neutron monitoring system has been developed, that is applicable to criticality safety management. The measurement range can be set to 5 decades (10^{-1}~10^{4} [s^{-1}]). The system consists of detector and measurement equipment. Absolute accuracy of set point comparison is achieved as within ±3 [%] by preparing two parts of circuit for exclusive use in this system. One part is for an indication and display and another is for setpoint comparison, respectively. Moreover, ^{10}B coated type neutron proportional counter has been developed, that is applied high radio frequency (RF) sputtering process for boron coating. With the detector and simplified measurement equipment, the system has seismic-proof performance and is applicable to a safety system.

Key words: neutron monitoring, neutron detector, boron coating, re-processing facility

1. Introduction

For criticality safety management, monitoring the inventory of nuclear-fissile material on real time is desired. For instance, an effective example is reported that applied the neutron monitoring system to confirm the criticality safety in re-processing facilities. This system measures the neutron induced by plutonium (Pu), and monitors the Pu inventory. Generally, no special functions are required for this neutron monitoring system except for neutron measurement and set point comparison. That means, it does not need the high-class measurement equipment that is added the superior intelligent function. According to such a situation, the analog type neutron monitoring system has been developed, that is strengthened with the required function rationally.

This paper shows the required specification, contents of development, and verification results about the system.

2. System Requirements and Target Specifications

The following is just required to satisfy as necessary and enough conditions, when measuring the neutron from Pu by a neutron monitoring system.

1) To have sufficient sensitivity for measuring the inventory of Pu
2) To take a wide measurement range.
3) To have general functions as an instrumentation system (such as comparison measured value with set point and interface with the other system)

Thus, the system requirements have been limited to the function of necessary minimum. Thereby, the system equipment can be simplified. This will make the system:

4) To have seismic-proof performance and to be applicable as a safety system.

As mentioned above, four requirements (requirements from 1) to 3) and item 4) added) were determined as a development target of the neutron monitoring system.

In order to attain these requirements, high-class measurement equipment with the intelligent function does not need to be applied. For this reason, the measurement equipment was planned to be constituted of the analog circuit specialized in the above-mentioned requirements.

Detail target specification is shown below.

2.1 Sensitivity

In order to measure neutron by high sensitivity, we examined applying neutron proportional counter (called as "NPC"). Two (2) types are examined: helium-3 enclosed type (^{3}He type) and boron-10 coated type (^{10}B type). We call the ^{3}He type neutron proportional counter "NPC-H" and ^{10}B type "NPC-B." The target of sensitivity was specified into NPC-H: 14 [$s^{-1}/(cm^{-2}\cdot s^{-1})$] and NPC-B: 3.9 [$s^{-1}/(cm^{-2}\cdot s^{-1})$] in the case that the active length is 500 [mm] for the detectors.

2.2 Measurement range

The measurement range has been decided as 5 decades from 10^{-1} to 10^{4} [s^{-1}] so that the pulse from NPC can be measured in a large range. The lower limit of a range is determined as the value that can constitute an integration circuit with an analog system, in consideration of statistics fluctuation. The range of 5 decades has been set up as can curry out measurement of the large range.

2.3 General Function

The system compares measured value (count rate) with set point value. In the case that the measured value exceed the set point value, output (alarm) signal will be transmitted to external. The target of set point comparison accuracy is set to ±3[%]. Moreover, it could be made to transmit the measured value (count rate) as the external output. The system sends out the external output signals via fiber optics. This can avoid forming a large electric ground loop between the system and the external so as to have noise-proof performance.

2.4 Seismic-proof Performance (application as a safety system)

The development target was to achieve the above objectives without using any complicated apparatus. This can add the additional function to the target so that the system is possible to be an application as a safe system. The additional function is seismic-proof performance.

3. Development and Verification Results

The development targets are arranged in Fig. 1.

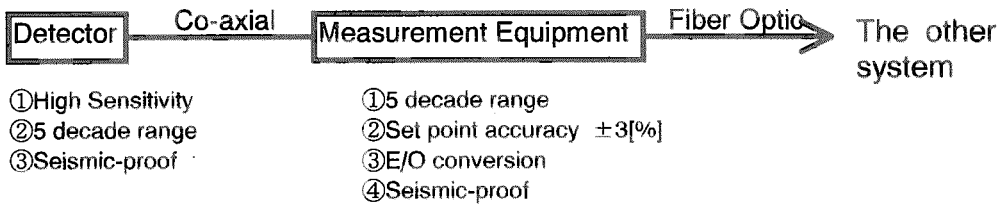

Fig.1 Development Target of the Neutron Monitoring System

The contents of development of detectors (NPC) and measurement equipment are shown henceforth.

3.1 Detector

3.1.1 Sensitivity

To achieve high sensitivity measurement, we have developed two kinds of neutron proportional counter (NPC), one is helium-3 enclosure type (NPC-H) and another is boron-10 coated type (NPC-B). A current amplifier is applied for the detector signal input portion of the measurement equipment to decrease an influence of gamma ray. (See 3.2.3). Hence, neutron measurement under high gamma dose rate can be achieved. The specification of the developed detectors is shown in Table- Ⅰ. This shows that the sensitivity has exceeded the target.

Table- Ⅰ Neutron Proportional Counter Specification

Items	Detector Type	
	NPC-H (He-3)	NPC-B (B-10)
Active Material	He-3 (Enclosed)	B-10 (Coated inside case)
Enclosed Gas	He-3	Ar
Case Material	SUS 304	
Outer Diameter	25.4 [mm]	
Core Wire Material	Pt	
Acceptable Gamma Dose Rate	2.58×10^{-3} [C·kg-1·h^{-1}] (10 [R/h])	1.29×10^{-1} [C·kg-1·h^{-1}] (500 [R/h])
Sensitivity	39 [s^{-1}/(cm^{-2}·s^{-1})] (Active length : 500mm)	5.5 [s^{-1}/(cm^{-2}·s^{-1})] (Active length : 500mm)

3.1.2 Seismic-proof function

The detectors have the same structure except active material and enclosure gas shown as Table- Ⅰ. They are designed to have the spiral part in the part of the core wire and the mechanism is considered to absorb vibration. The structure is designed as seismic-proof. Moreover, mechanical strength was raised, having used the detector outer case as stainless steel. In order to carry out coating of ^{10}B to inner stainless steel pipe, the high radio frequency (RF) sputtering process has been developed [1]. Thereby, uniform and strong ^{10}B coating has been attained.

Table- Ⅱ Seismic-proof Test Condition

Tests	Frequency	Acceleration
Vibration Test	~25[Hz]	Horizontal: ~7.8[m/s^2] (0.8[G]) Vertical: ~3.9[m/s^2] (0.4[G])
Shock Test	———	490[m/s^2] (50G)

Furthermore, it has been verified that the developed detectors have seismic-proof function by carrying out a vibration examination. The conditions of the vibration examination are shown in Table- Ⅱ.

3.2 Measurement Equipment

3.2.1 Wide Measurement Range and High Accuracy

The measurement equipment requires conflicting functions as measuring a wide range with sufficient accuracy. Generally, accuracy is decided as the relative value that depends on the full scale in an analog circuit. For this reason, if the range is requested to be wider, the absolute accuracy will become severe. Therefore the range must be narrowed, to improve the absolute accuracy.

In order to solve this inconsistency, the developed system has the composition that prepares

two circuit parts of exclusive use; one is the indication and display part and another is the set point comparison part, respectively. The indication and display part measures a large range by processing logarithmic data. The set point comparison part can measure precisely by narrowing a range and linear data processing.

For example, it is possible to have relative accuracy of ±1 [%] full scale in the case of a range 0-300 [s^{-1}]. This relative accuracy can realize absolute accuracy as ±3 [%] at 100 [s^{-1}] set point. By this circuit composition, the measurement range has been able to be set to 5 decades of $10^{-1} \sim 10^{4}$ [s^{-1}], and absolute accuracy of set point comparison to ±3 [%].

3.2.2 Statistics Fluctuation and Response

Moreover, a response of set point comparison is desired to be fast generally. Here, a response and a statistics fluctuation of radioactive measurement have the following correlation.

$$\sigma = \frac{1}{\sqrt{2 \cdot n \cdot \tau}} \tag{1}$$

where σ : the standard deviation of statistics fluctuation, n: count rate [s^{-1}], and τ : time constant of the counting circuit [s].

For monitoring the value and operating a plant, it is desired that the statistics fluctuation width is small and the response is fast (the time constant is short). However, these conflict from the equation (1). Hence both σ and τ that relate with monitoring and plant operation shall be set up pertinently. Considering the response of a re-processing plant process value, we made the time constant into 100 [s] in the development. In this case, 3σ becomes under 30 [%] at count rate 1 [s-1]. This value is acceptable for the plant operation.

3.2.3 General Function

The system composition of the developed measurement equipment is shown in Fig. 2.

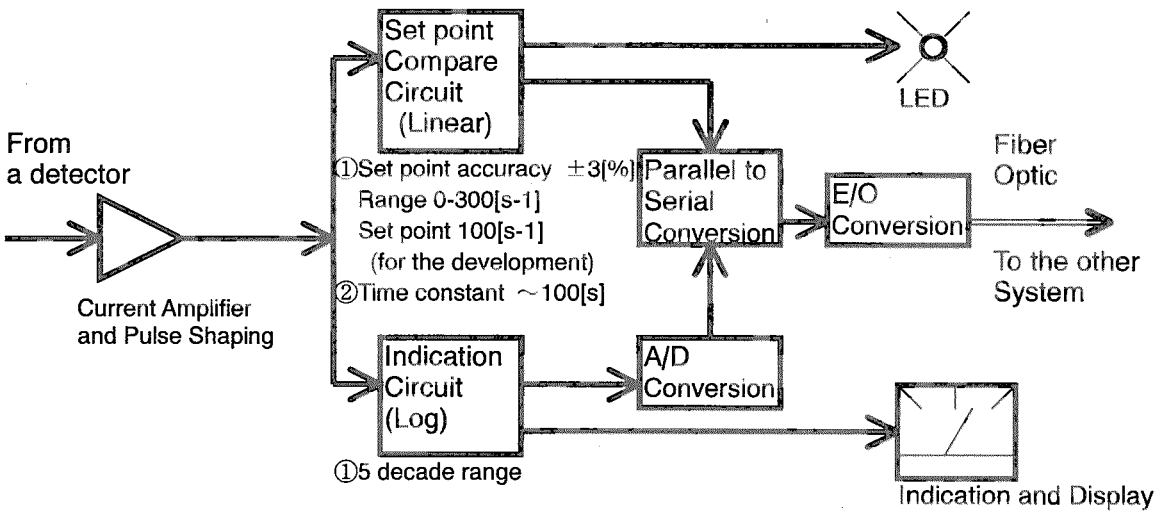

Fig.2 Circuit Configuration of Developed Neutron Monitoring System

In order that neutron monitoring system may process a minute signal, consideration of the

measure against noise is needed. We consider the following items as the measure:

a) To apply current amplifier for the detector signal amplitude

b) To transmit the signal to external system via fiber optics

a) Current Amplifier

Input impedance is decreased as 75[Ω] by applying a current amplifier. This has higher noise-proof performance than a capacitor amplifier.

Here, bias voltage for NPC-B is different from one for NPC-H. The developed system is for NPC-B. In applying NPC-H, what is necessary is just to change the power supply and related circuit that can supply higher voltage.

b) Interface with the Other System

It is anxious about the influence of the noise from the exterior. Therefore, concerning about the interface signal (measurement value and bit signal), the method is applied, that carries out electrical to optical conversion of this as a serial signal (digital signal). Serial conversion is curried out without using software, only using hardware. By carrying out optical-electrical conversion in a reception side, the signal will be able to be transmitted to any specified interface. This could prevent the neutron monitoring system from constituting the large electric ground loop with the other equipments.

3.2.4 Seismic-proof Function

The same vibration test as examined to the NPC's shows that the equipment has seismic-proof.

4. Consideration

When applying the system developed into a plant, such as evaluation of neutron-flux level and check of noise will be examination subjects.

4.1 Evaluation of Neutron Flux Level

By Pu isotope composition and the amount of actinides, even if it is the same amount (concentration) of Pu, the amount of neutron generating will change. Moreover, if a geometric system differs, even if it is the same amount of neutron generating, detection efficiency will differ. For this reason, in the case that neutron-flux level is evaluated, these plant conditions shall be considered.

4.2 Noise Confirmation

Noise conditions will change with the installation conditions in the plant and the conditions of other apparatus. In case a system is installed, it must be checked that a noise level is low enough to carry out pulse height discrimination. The integrated pulse height distribution characteristic of the developed system is shown in Fig.3. In this example, a pulse height discrimination level is adequately set as -120 [mV].

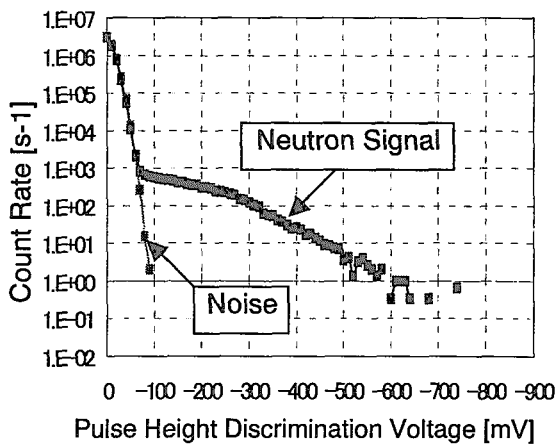

Fig.3 Integrated Pulse Height Distribution

5. Conclusion

The analog type neutron monitoring system applicable to criticality safety management has been developed.

Generally, a special function is not required of this neutron monitoring system that there should just be functions of detector pulse counting and set point comparison with measured value. From this, the function required for neutron monitoring has been analyzed and the system has been planned that is strengthened with the required function rationally. It is specifically as following:

1) To prepare the circuit of exclusive use about the indication and display part and the set point comparison part respectively, the measurement range is 5 decades of 10^{-1}-10^{4} [s^{-1}], and absolute accuracy of set point comparison to ± 3 [%].
2) NPC (Neutron Proportional Counter) which applied RF (radio frequency) sputtering for boron coating has been developed.

Thereby, it has seismic-proof and is applicable to a safety system.

6. Reference

[1] N. Oda et al., "Development of the neutron detector by sputtering coating," 2001 Ann. Mtg. of JAES, E40 (2001).

JP0250290

JAERI-Conf 2002-004

IMPROVING SAFETY IN A MOX PLANT BY QUALIFICATION OF NEUTRON MEASUREMENTS AND CRITICALITY EVALUATION

A.Renard, P.Kockerols*, H. Libon*, D.Marloye**
BELGONUCLEAIRE, Avenue Ariane 4, 1200 Brussels, Belgium
Fax. : (00) 32 2 774 06 14, e-mail : a.renard@belgonucleaire.be
*BELGONUCLEAIRE, Europalaan 20, 2480 Dessel, Belgium
Fax. : (00) 32 14 31 70 46, e-mail : h.libon@belgonucleaire.be
**BELGONUCLEAIRE; Avenue Ariane 4, 1200 Brussels, Belgium
Fax. : (00) 32 2 774 06 14, e-mail : d.marloye@belgonucleaire.be

ABSTRACT

Two of the major aspects of safety in a MOX fuel fabrication plant are radiation doses and criticality prevention. This paper presents two qualification processes which lead to improvements of the safety when handling and storing fissile materials.

1. Radiation protection of workers depends very much on the reliability of personal dosimeters. As a result of the introduction of the ICRP 60 recommendations and the increasing contribution of the neutron dose to the total dose of the Belgonucleaire personnel of the MOX fuel plant, the bubble detector became in use as a reliable personal neutron dosimeter.

To evaluate the impact of the neutron energy on the detector response, real neutron spectra in the plant were determined by a two-sided approach.

Measurements were carried out in rooms where representative neutron spectra were present, by means of a reference calibrated neutron spectrometer, in parallel with some types of personal bubble detectors. On the other hand, detailed calculations of the measured configurations were performed by means of the Monte Carlo MCNP 4 computer code with a 3D model.

Comparison between measurements and calculations reveals good agreement. Additional calculations clarify the influence of some parameters as the presence of structure materials. The calibrated calculations allow also to separate the contribution of the low energy neutrons in the total dose rate in order to qualify the method of correcting the calibration factors of the bubble detectors on the basis of the typical spectra, in relation with the last ICRP fluence-to-dose conversion coefficients.

2. Criticality safety is a permanent issue for a MOX fuel fabrication plant .

In order to reduce calculations uncertainties and improve consequently the safety while trying to reduce margins, BELGONUCLEAIRE is promoting the new KEOPS international R&D Program to be performed in collaboration with the Belgian Nuclear Research Centre (SCK•CEN), located close to the MOX fuel fabrication plant of BELGONUCLEAIRE.

The Safeguard department of SCK•CEN has developed for many years an original neutron-counting device, based on double and triple neutron coincidence counting. The K-effective of the measured configuration (which can be as large as a 200 l waste drum) can be derived from neutron multiplication measurements with high accuracy.

The KEOPS programme will consist on subcritical measurement of effective multiplication factors (K_{eff}) of several materials available in a MOX fuel fabrication facility : pure PuO2 powders, primary blends containing 30% PuO_2 and final product (fuel pellets). Simple and clean geometrical configurations, such as box or cylinder will be considered.

The following measurements are now planned : measurements on MOX pellets (case 1), measurements on PuO2 powder (case 2) whereas measurements on standard PuO2 canisters is under preparation (case 3).

The Pu isotopic composition, powder density, mass, moderation and geometry will be investigated in detail as criticality parameters. The expected accuracy on the k_{eff} is expected to be below 5% in absolute value.

The paper will present with more details the objectives, the experimental facility, the proposed tests and the method to be qualified.

Key words : neutron, exposure, bubble, criticality, calibration

INTRODUCTION

BELGONUCLEAIRE has a mixed Uranium/Plutonium oxide (MOX) fuel producing plant located in Dessel, Belgium. BELGONUCLEAIRE began producing MOX fuel for fast breeders and light water reactors in 1973. Fabrication was initially realized within the framework of demonstration programs. In 1986, when the Mixing and Master blend (MIMAS) fabrication process developed by BELGONUCLEAIRE had been fully demonstrated, commercial-scale production was begun. Since then, the plant has operated at a nominal annual capacity of around 35 tons of MOX.

RADIATION PROTECTION

Due to the increasing contribution of the neutron dose to the total dose of the BELGONUCLEAIRE personnel and the introduction of the ICRP 60 recommendations (ICRP Publication 60), the use of a good reliable personal neutron dosemeter has become even more important.

The BD-PND bubble detector (Ing 1997) manufactured by Bubble Technology Industries (BTI, Canada) seemed to be a very interesting alternative to the albedo dosemeter used in the past. An extensive investigation program was carried out at BELGONUCLEAIRE to determine its effectiveness in the fuel fabrication plant environment. A series of tests were conducted to get a better understanding of this type of dosemeter (calibration, temperature sensitivity, ageing , read-out accuracy).

To evaluate the impact of the neutron energy on the bubble detectors' response, it was important to have an idea of the real neutron spectra present in the fuel fabrication plant. To obtain these spectra, a two-sided approach was applied. Measurements were carried out at specific locations in the installations where representative neutron spectra are present. Also, detailed calculations of the same configurations as the measurements were performed in order to have a point of comparison with the measurements and to estimate the thermal part of the spectrum. After the initial comparisons between the measurements and the calculations, a number of supplementary calculations were performed to evaluate the effect of the spectra in other working areas.

This paper gives an overview of the performed calculations and measurements of the neutron spectra, and the method of correcting the calibration factor of the BTI bubble detectors on the basis of these spectra and the new ICRP 74 fluence-to-dose conversion coefficients (ICRP Publication 74).

MATERIALS AND METHODS

Measurements were carried out in a room used solely for the intermediate storage of fresh MOX fuel rods before their introduction into nuclear fuel assemblies. The fuel rods are placed in steel boxes which are stored in racks behind shielded doors. Three configurations were considered for the measurements and calculations.

1. a single steel box containing approximately 150 fresh MOX fuel rods
2. 16 steel boxes containing fresh MOX fuel rods placed in a concrete storage vault behind shielded doors, and

3. the same configuration as 2, but with an open door in front of four boxes

The neutron spectra measurements were carried out with the ROSPEC (Rosenstock 1997) neutron spectrometer of the Fraunhofer Institute (INT). The ROSPEC detector consists of four spherical gas proportional counters. Three of the gas proportional counters are filled with pure hydrogen at pressures of 0.75×10^5, 4×10^5 and 10^6 Pa respectively. The fourth is filled with a mixture of argon and methane at a pressure of 5×10^5 Pa. The neutrons are detected by the measurement of the recoil protons in the gas proportional counters. Each detector covers a well-defined energy range, overlapping with the energy range of the next detector, so that the neutron energy spectrum is measured from 50 keV to 4.5 MeV. The four detectors are mounted on a circular platform rotating about a vertical axis in order to average out local variations in the neutron field around the centre of the rotation circle. The unfolding of the measured pulse height spectra is performed by a modified version of the SPEC-4 code (Benjamin 1968).

Detailed calculations of the three configurations were performed by means of the Monte Carlo transport code MCNP 4A (Briesmeister 1991) using the standard neutron and photon libraries of this code system and three-dimensional geometrical models. The neutron source intensities were calculated by means of the ORIGEN2 code (Croff 1980) for the typical isotopic composition of the fuel. Standard energy spectra were associated with the neutrons from spontaneous fissions on one side, and with those produced from (alpha,n)-reactions on the other side.

The MCNP 4A code provides the neutron flux averaged over the volume of cells, defined in the model around the position of the spectrometer. The neutron flux spectrum was calculated for 40 energy groups including the groups of the measured spectrum between 50 keV and 4.5 MeV, plus 6 groups between 0.03 eV and 50 keV representing roughly the thermalized contribution. The relative error in MCNP was between 1 and 7% for the cases under study.

At the three positions under study, measurements were carried out with two types of bubble detectors available from BTI : the BD-PND detector and the BDT detector. The BD-PND type detector has a good dose equivalent response for neutron energies above 100 keV. However, the BD-PND has zero response for thermal neutrons, so the BD-PND type was used together with the BDT type detector. The BDT detectors' response is high for thermal neutrons and drops off with 1/v for epithermal neutrons. The dose response of the BDT for fast neutrons is about one twentieth of its thermal sensitivity. The combined use of both types of detector can give a dose-equivalent response over the entire neutron spectrum. Measurements with mono-energetic neutrons showed that the optimal combination to yield the ambient dose equivalent H*(10) according to ICRP 74 is obtained by using a multiplication factor of 1.04 for the BD-PND and 1.61 for the BDT (Vanhavere 1998). The uncertainty (one sigma level) on the bubble detector results is about 10%.

RESULTS AND DISCUSSION

Single box

The first case consisted of a single box containing 150 fresh MOX fuel rods placed on a support in the storage room. The box was oriented with its axes parallel to the ground and parallel to the closed door of one storage vault. The distance from the ground was about one

meter and the distance from the door was also one meter. Walls, ceiling and other storage vaults were at a distance of more than 5 meters and were not taken into account in the calculations. The point of measurement was located near the mid-length of the box, at 0.5 meter distance from the box.

Both the calculated and measured spectra are shown in Fig. 1 for this geometry. The comparison is based on the absolute values of the product [Energy x Flux (E)] in MeV/cm^2.s for each energy group of the spectrum. The energy range from 50 keV to 4.5 MeV is divided into 34 energy groups, both for the measured and the calculated flux.

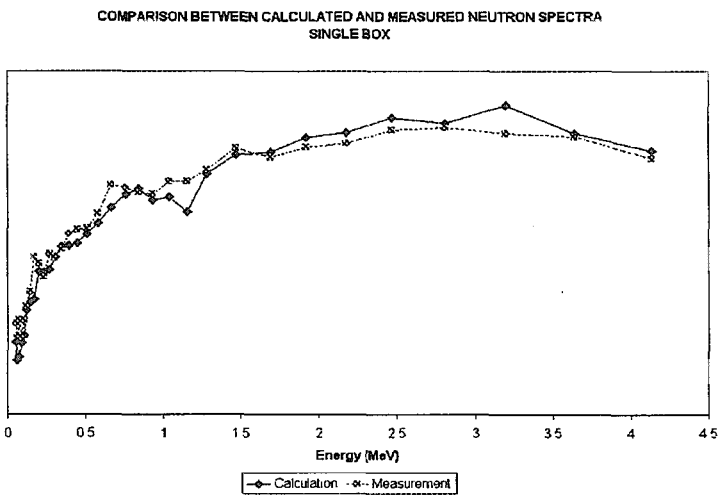

Fig. 1 : Comparison between measured and calculated neutron spectrum, single box

The Monte Carlo method evaluates the order of magnitude of the uncertainty on the total neutron flux which, for this case, is of the order of 1%. Of course, the uncertainty can be more for the flux in a specific energy group where the number of incident neutrons is not very large. The accuracy of the measured values can be estimated from the overlapping energy regions, and was about 5%.

The calculations reproduce the general shape of the measured spectrum well, especially between 0.2 and 2 MeV. For the highest energy groups, part of the disagreement may be due to the reference spectrum associated with the neutrons produced by the (alpha,n)-reactions in the source. For the lowest energy groups, the detector response is somewhat higher than the calculated figures, probably due to the influence of the background radiation in the room.

In Table 1 the resulting dose equivalent rates are presented. Fluence-to-dose conversion factors from the ICRP 74 report (ICRP Publication 74) were used to convert the ROSPEC and the calculated spectrum into dose equivalent rates. The results of the ROSPEC measurement and the bubble detectors show very good agreement with the calculations, taking into consideration the uncertainty level.

Table 1: Measured and calculated dose equivalent rates

	Single Box (μSv/h)	Open Storage Door (μSv/h)	Closed Storage Door (μSv/h)
ROSPEC Measurements	169	111	17.6
MCNP Calculations	174	132	10.5
BD-PND bubble detectors	172	131	14.7
BDT bubble detectors	10.7	10.5	1.6
Combination of both types of bubble detectors	196	153	17.9

Storage with shielding door open

The second case refers to the measurement in front of a storage vault containing 16 boxes. The door was open only in front of four boxes filled with fresh fuel rods. The other 12 boxes were located inside the vault behind the closed part of the door. The distance from the centre of the ROSPEC spectrometer to the front edge level of the boxes was one meter. The base of the detector was located at about one meter above the concrete floor. Again walls, ceiling and other storage vaults were not taken into account in the calculations.

Each of the four unshielded boxes was individually represented in the calculation model with the associated structures. The other boxes behind the door were also taken into account, but in a homogenized way together with the claddings, the steel boxes and the structures of the cells.

The comparison between the measured and the calculated values is presented in Fig. 2. The statistical uncertainty is higher than for the single box case due to the lower neutron flux at the detector position. The calculations reproduce the general shape of the measured flux well, especially above 0.15 MeV. The small peak in the measurement near 1.3 MeV is also reproduced by the calculations. As a result of parametric studies, this peak seems to be associated with neutron interactions with the steel structures. An even smaller peak near 0.66 MeV also appears in the calculated spectrum, but with a rather high uncertainty.

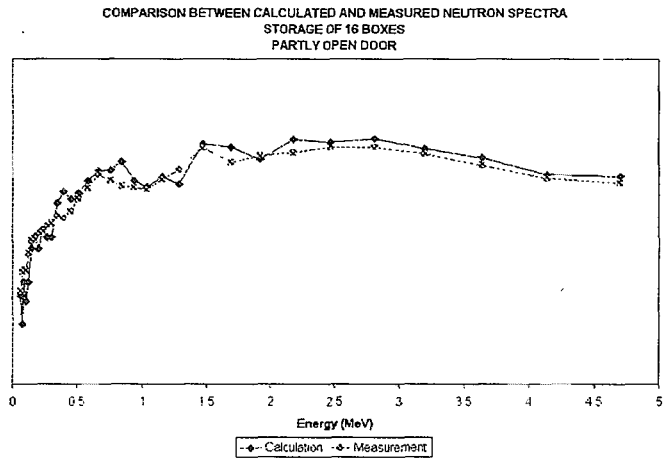

Fig. 2 : Comparison between measured and calculated neutron spectrum, storage with shielding door open

Storage with shielding door closed

The configuration for the final case was the same as in case two but the shielding door was entirely closed in front of the 16 boxes. Thermalized neutrons are more important for this case because of the closed doors. Therefore outer concrete walls and a ceiling were used in the calculational model to take into account the thermalization of the fraction of neutrons backscattered from the walls and the ceiling of the room. Also, the neutron flux at the detector position is very weak so that it was important to improve the statistics of the calculation. This was done by increasing the detector volume around its central position. This was an acceptable assumption since the flux and the spectrum do not change much near the detector. A homogenized source term representing all the 16 boxes with their content plus the structures of the cells was used.

Fig. 3 gives the measured and calculated spectra. The calculation reproduces the general shape of the measurement, but with an important underestimation of about 50% on average below 1.5 MeV. Especially the measured peak around 1.3 MeV does not appear in the calculation results. Above 1.5 MeV the agreement can be considered good with an average difference of 5%. As can be seen in Table 1, the calculated total neutron dose equivalent rate is lower than measured. This is due to the background radiation in the room coming from the other storage vaults. The background neutron dose rate in the middle of the storage room is about 10 μSv/h. Again the agreement of the experimental measured dose equivalent rates is good for both measurement techniques.

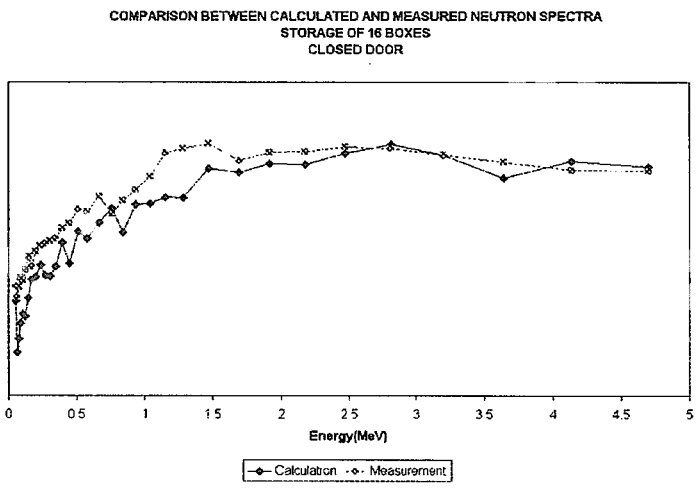

Fig. 3 : Comparison between measured and calculated neutron spectrum, storage with shielding door closed

Parametric study

In order to clarify the influence of the presence of some materials on the neutron flux, the model of the single box was slightly modified by adding screens or removing materials in the calculational model.

A pseudo-screen of 5 cm thickness was put between the box and the ROSPEC detector, the screen is made either of steel or concrete. The flux behind the steel screen was attenuated in

the high energy area, but a significant peak is introduced at 0.66 MeV. This peak also appears in the measured flux and the calculation of the open storage door. The flux behind the concrete screen has a reduced peak near 0.66 MeV and is, compared to a steel layer of the same thickness, attenuated over the entire energy spectrum. This agrees with the closed door results.

The contribution of the low energy neutrons to the dose equivalent rate can be separated from the total dose rate on the basis of the MCNP measurements. In Table 2 the resulting contribution from the low energy neutrons is shown considering everything under 100 keV to be low energy. Since the BD-PND bubble detectors have approximately 100 keV as a threshold energy, the combined result from both the BD-PND and BDT detector types could be used to calculate the low energy percentage of the dose equivalent. This is also given in Table 2. The agreement is reasonably good and seems to confirm the calculations. It is important to notice that at most the contribution due to thermalization is only about 3 to 5%.

Table 2: Percentage of dose equivalent from neutrons with energy less than 100 keV

	Single Box	Open Storage Door	Closed Storage Door
MCNP Calculations	0.7%	2.3%	3.2%
Combination of two types of bubble detectors	0.9%	2.4%	4.9%

Calibration factor

Another important issue during the investigation of the neutron bubble detector was the evaluation of the impact of the fluence-to-dose conversion coefficients, based on the ICRP 60 recommendations (ICRP Publication 60) and published in ICRP 74 (ICRP Publication 74), on the calibration factor of the bubble detector. From the beginning of the evaluation program at BELGONUCLEAIRE, it was the intention to follow these recommendations in assessing the neutron doses by means of the bubble detector and to use a calibration factor in accordance with the neutron spectra measured in the fabrication plant. An individual calibration factor for each bubble detector is provided by the producer. This calibration factor is based on the former radiation quality factors recommended by ICRP 21 (ICRP Publication 21). It is determined with an Am-Be neutron source. Because the spectrum of an Am-Be neutron source differs significantly from the spectra present in the fabrication plant it was necessary to correct for this difference. Therefore a correction factor F was determined, to be used in connection with the calibration factor provided by the producer BTI, in order to obtain a calibration factor representative of the situation at BELGONUCLEAIRE. This factor corrects on the one hand for the new ICRP 74 fluence-to-dose conversion coefficients and on the other hand for the real spectra in the working places of the controlled area :

$$G_{ICRP74,BN} = F \times G_{ICRP21,AmBe} \qquad (1)$$

$G_{ICRP21,AmBe}$ is the calibration factor (in bubbles per μSv) provided by the producer of the bubble detector, BTI, based on the fluence-to-dose conversion coefficients from ICRP Publication 21 and determined with an Am-Be neutron source.
$G_{ICRP74,BN}$ is the calibration factor (in bubbles per μSv) used at BELGONUCLEAIRE, based on the new ICRP 74 fluence-to-dose conversion coefficients and representative of the neutron

spectra present in the fuel fabrication plant.
In formula (1) :

$$F = \frac{d_{ICRP21,AmBe}}{r_{ICRP21,AmBe}} \times \frac{r_{ICRP74,BN}}{d_{ICRP74,BN}} \qquad (2)$$

with the factors $d_{ICRP21,AmBe}$, $r_{ICRP21,AmBe}$, $d_{ICRP74,BN}$ and $r_{ICRP74,BN}$:

$d_{ICRP21,AmBe}$:

$$d_{ICRP21,AmBe} = \frac{\int_0 h_{p,ICRP21}(E) \times \Phi_{AmBe}(E) \times dE}{\int_0 \Phi_{AmBe}(E) \times dE} \qquad (3)$$

$h_{p,ICRP21}(E)$: fluence-to-dose conversion coefficients according to ICRP 21 (Sv.cm²)
$\Phi_{AmBe}(E)$: Am-Be neutron spectrum (neutrons/cm²)

$d_{ICRP21,AmBe}$ is the dose per unit fluence corresponding with an Am-Be neutron spectrum and using fluence-to-dose conversion coefficients from ICRP Publication 21. This factor is used by BTI at their calibration facility and equals 3.7×10^{-12} Sv.cm².

$r_{ICRP21,AmBe}$:

$$r_{ICRP21,AmBe} = \frac{\int_0 R(E) \times \ddot{O}_{AmBe}(E) \times dE}{\int_0 \ddot{O}_{AmBe}(E) \times dE} \approx \frac{R \times \int_{100} \ddot{O}_{AmBe}(E) \times dE}{\int_{100} \ddot{O}_{AmBe}(E) \times dE} \approx R \qquad (4)$$

R(E) : energy response of a neutron bubble detector.

$r_{ICRP21,AmBe}$ is the normalized response (bubbles per unit fluence) of a bubble detector in an Am-Be neutron field. The energy response of the bubble detector is practically zero below a threshold energy of 100 keV and more or less constant above. If we assume that the bubble detectors' response is zero below 100 keV and constant above 100 keV, we can use a step function. Moreover the Am-Be neutron spectrum shows practically no neutrons with energies below 100 keV. Taking into account these assumptions the formula can be simplified as stated in Equation 4.

$d_{ICRP74,BN}$:

$$d_{ICRP74,BN} = \frac{\int_0 h_{p,ICRP74}(E) \times \Phi_{BN}(E) \times dE}{\int_0 \Phi_{BN}(E) \times dE} \qquad (5)$$

$h_{p,ICRP74}(E)$: fluence-to-dose conversion coefficients according to ICRP 74 (Sv.cm²)
$\Phi_{BN}(E)$: neutron spectrum in MOX fuel fabrication plant (neutrons/cm²)

$d_{ICRP74,BN}$ is the dose per unit fluence corresponding with the neutron spectrum present in the fuel fabrication plant and using fluence-to-dose conversion coefficients from ICRP Publication 74.

$r_{ICRP74,BN}$:

$$r_{ICRP74,BN} = \frac{\int_0 R(E) \times \Phi_{BN}(E) \times dE}{\int_0 \Phi_{BN}(E) \times dE} \approx \frac{R \times \int_{100} \Phi_{BN}(E) \times dE}{\int_0 \Phi_{BN}(E) \times dE} \qquad (6)$$

R(E) : energy response of a neutron bubble detector

$r_{ICRP74,BN}$ is the normalized response (bubbles per unit fluence) of a bubble detector in the neutron field present in the installations of BELGONUCLEAIRE. If we assume that the bubble detectors' response is zero below 100 keV and constant above 100 keV, the formula can be simplified as stated in Equation 6.

Combining these different formulas, the correction factor F can be written as :

$$F = 3.7\text{x}10^{-12} \times \frac{\int_{100} \Phi_{BN}(E) \times dE}{\int_0 h_{p,ICRP74}(E) \times \Phi_{BN}(E) \times dE} \qquad (7)$$

Thus the factor F converts the number of bubbles per μSv (i.e. the calibration factor) according to ICRP 21 and measured in an Am-Be neutron field into a number of bubbles per μSv according to ICRP 74 and measured in the neutron field at BELGONUCLEAIRE.

The factor F was determined for the 3 cases under study (single box, open storage door and closed storage door) using both the measured and calculated spectra. Table 3 gives the results of this comparison. Because the lower limit of the neutron energy in the measurements was 50 keV, this value was used as lower limit in the bottom integral of Equation 7. The agreement between the factor F based on the measurements and the factor F based on the calculations is very good and, as a result, four more calculations for other typical configurations in the MOX plant were performed.

An average factor F was determined based on the results of the seven calculated spectra. The lower limit of the bottom integral in Equation 7 was taken as 0 keV this time because the calculations provided the thermal part of the spectrum. In this way, the thermal neutrons were taken into account. The influence of the new fluence-to-dose conversion coefficients was estimated by replacing $h_{p,ICRP74}(E)$ with $h_{p,ICRP21}(E)$ in Equation 3. Table 4 summarizes the results of the comparison. The value of 1.07 was obtained when using the coefficients from ICRP 21 (ICRP Publication 21). The difference between the calibration spectrum and measured spectrum can be identified since the calibration coefficient determined by BTI is also based on ICRP 21. The measured spectra result in a reduction of approximately 7% compared to the calibration spectrum. One can see from Table 4 that the impact of ICRP 74 is more important than the influence of the neutron spectra. When using the fluence-to-dose conversion factors of ICRP 74 instead of ICRP 21, the correction factor is reduced by 17% (0.89/1.07).

These relatively small correction factors show the good dose equivalent characteristics of the BD-PND in this case.

Thus the correction factor of 0.89 was applied to the individual calibration factors provided by BTI. It is important to recognize that the main and individual calibration factors (in bubbles/μSv) are provided by the producer. The correction made at BELGONUCLEAIRE on the basis of the correction factor F is about 10%, resulting in higher recorded neutron doses.

Table 3: Comparison between the correction factor F based on the measurements and calculations of neutron spectra

Configuration	F_{BN}(measurement, > 50 keV)[a]	F_{BN}(calculation, > 50 keV)[b]
Single box, filled with fuel rods	0.91	0.91
Storage rack for fuel rods, neutron shielding open	0.94	0.95
Storage rack for fuel rods, neutron shielding closed	0.91	0.91

a : correction factor based on the ROSPEC measurements taking only neutrons above 50 keV into account
b : correction factor based on the MCNP calculations taking only neutrons above 50 keV into account

Table 4 : Comparison averaged correction factor with ICRP 74 and ICRP 21dose-fluence conversion coefficients

Configuration	F_{BN}(calculation, ICRP 74)[a]	F_{BN}(calculation, ICRP 21)[b]
Averaged correction factor (7 calculations)	0.89	1.07

a : correction factor based on the MCNP calculations, taking into account all neutron energies and using fluence-to-dose conversion factors from ICRP 74
b : correction factor based on the MCNP calculations, taking into account all neutron energies and using fluence-to-dose conversion factors from ICRP 21

CRITICALITY PREVENTION

The second aspect of safety in a MOX plant is the prevention of criticality. In order to reduce calculation uncertainties for subcritical systems and improve consequently the safety, BELGONUCLEAIRE is promoting the new KEOPS (Experimental Determination of Keffective on Various PuO_2 and MOX Pellets Configurations in Subcritical Conditions) international R&D programme. This should be performed in collaboration with the Belgian Nuclear Research Centre (SCK•CEN), located close to the MOX fuel fabrication plant of BELGONUCLEAIRE.
The experimental set-up consists in a Hexagon Neutron Counter (see Figure 4) developed at the SCK•CEN. It is formed by six polythene walls shielded by Cadmium absorber blades. Inside each of the CH2 blocks, three He-3 detectors are installed. The top and bottom of the set-up is designed on the same way. The combination of CH_2 and Cd-absorbers allows the capture of themalized neutrons coming from the measured system and also prevents the back-

scattering of the thermalized neutrons (in the CH_2 material). The set-up is presently used by the safeguard department of SCK•CEN for characterization of 200 L waste drums.

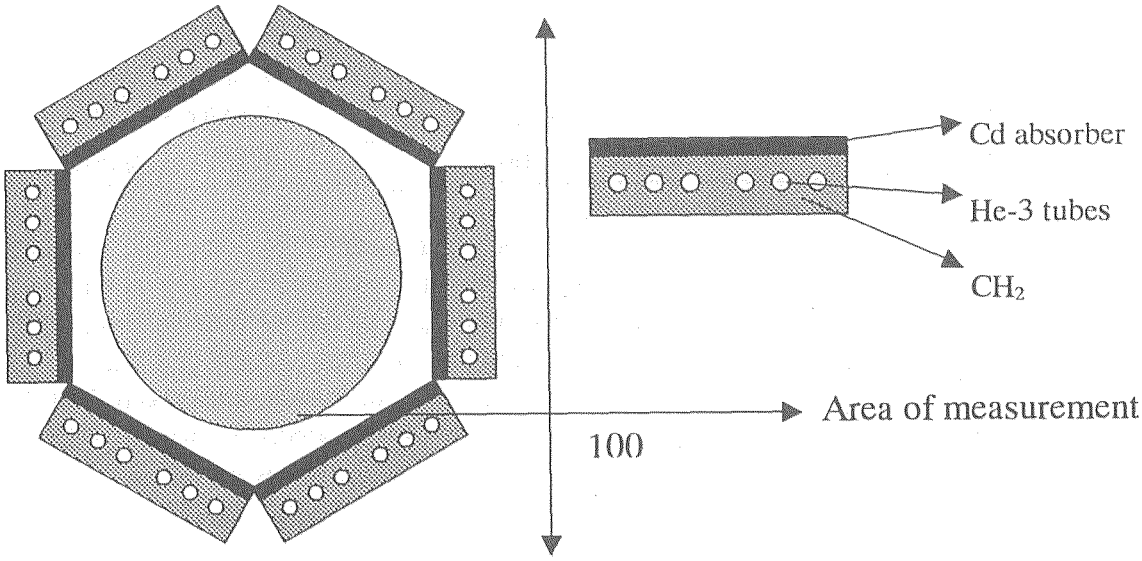

Fig. 4 : Hexagon Neutron Counter

The idea is now to use the same device for determination of subcritical levels of configurations containing spontaneous emitters (e.g. Pu 240), using the so-called "Coincidence Neutrons Measurement Method". Dead time corrected total count rates and double count rates will be measured and reported with their statistical uncertainty. The measured total count rates can be compared with the count rates calculated with a Monte Carlo code, such as MCNP. Moreover, by using the Neutron Multiplicity Equations for fast multiplication (point model), an experimental k-effective value may be derived and compared with the calculated one. To recall, the k-effective value k_{eff} is linked to the multiplicity through

$$k_{eff} = \frac{m-1}{m}$$

with the multiplicity m function of the single and double count rates, S and D and other parameters, as the detector efficiency, the spontaneous fission rate of the system, etc.

The present frame of the programme consists at measuring configurations made of compounds used in a MOX fuel fabrication facility : pure PuO_2 powders, primary blends containing 30% PuO_2 and the final product : the pellets. Several parameters may be varied : geometrical configuration, number of units, presence of structural material (e.g. stainless steel of the boxes), isotopic composition, etc. For the powders, the density aspect will also be investigated. The planning presently considers two cases :

Case 1 : measurements on MOX pellets ;

Case 2 : measurements on PuO_2 powder.

Previsional calculations have been performed for configurations of PuO_2 powder cans. These have been carried out with KENOVa fed by the 16 groups cross sections Hansen & Roach. The cans, made of stainless steel 1 mm thick, contain 3 kg PuO_2 (Pu 70/18/10/2) at density ~ 2.2 g/cm^3, with a certain amount of humidity. They are placed against each other, in the same radial plane, at the center of the experimental set-up, which is also modelized in the calculation. Table 5 shows typical k-effective values expected for such measurements, up to 4 cans, considering also an important compaction of the powder, up to 3.5 g/cm^3.

Table 5 : Calculated k-effective

	Density 2.2 g/cm^3	Density 3.5 g/cm^3
Number of cans	$k_{eff} \pm \sigma$	$k_{eff} \pm \sigma$
1	0.1527 ± 0.0007	0.2200 ± 0.0010
2	0.1869 ± 0.0008	0.2584 ± 0.0011
3	0.2228 ± 0.0009	0.3040 ± 0.0011
4	0.2417 ± 0.0009	0.3232 ± 0.0012

Increasing the number of cans inside the hexagon neutron counter increases the k-effective level so that a quantitative effect is measurable. Moreover, compaction of the powder is an important point to assess as it may lead to great fluctuations in the k-effective level. The k-effective could be still increased by increasing the number of cans radially and axially, but a compromise between the k-effective value and the tightness of the configuration is to be found. Numerical simulations of such a configuration with very low k-effective value (~ 0.2) have shown that an accuracy of 0.5% k_{eff} is achievable as soon as the statistics of the single and double count rates is sufficient ($\sigma < 0.3\%$ on S and D).
Further calculations must be performed in order to optimize the framework (tightness of the configuration, parameters to vary, etc.) and the amount of humidity in the powder. Moreover one has to investigate the experiment with the pellets.

CONCLUSIONS

Upon review of the neutron spectra of the three cases, the specific features of each spectrum appear clearly. In the single box case the spectrum is dominated by the high energy part. The open door case provides the highest neutron flux, except for the highest energy groups, while the closed door case flux spectrum includes a relatively more dominant low energy contribution. A parametric study made clear the influence of some structural materials on the spectrum.
In general, the results of the calculations agree with the measurements. Only for the closed door case is the result low, due to the background radiation coming from the other storage racks present in the room.
Both the calculations and the measurements indicate that the influence of the low energy neutrons in the spectrum on the dose equivalent rate is very small in comparison with the fast neutrons. There is no need to complement the BD-PND detectors with BDT detectors for personal neutron dosimetry.
On the basis of the calculations a correction factor was determined to be used in connection with the calibration factor provided by BTI to correct for the specific neutron spectra in the fuel fabrication plant and to determine a neutron dose in accordance with the ICRP 74 fluence-to-dose conversion coefficients. This factor appeared to be very stable with respect to the different neutron spectra in the installation.

Regarding the KEOPS international programme, it will lead to increased physical insight in subcriticality, on the basis of coincidence neutron measurements and Monte Carlo calculations.

REFERENCES

- R. Olaerts, P. Kockerols, A. Renard, W. Rosentock, T. Köble and F. Vanhaevere,

Determination of Neutron Spectra in a MOX Plant for the Qualification of the BD-PND Bubble Detector, Health Physics, 1999.

- Benjamin P.W., Kemshall C.D., Brickstock A., The analysis of Proton Recoil Spectra, AWRE Report (1968).
- Briesmeister J.F., MCNP-4A General Monte Carlo Code for Neutron and Photon Transport - Version 4, LA-7396-M, Rev 2, Los Alamos National Lab (1991).
- International Commission on Radiological Protection, Data for Protection against External Radiation. Oxford:Pergamon Press; ICRP Publication 21 (1973).
- International Commission on Radiological Protection, 1990 Recommendations of the International Commission on Radiological Protection. Oxford:Pergamon Press; ICRP Publication 60 (1996).
- International Commission on Radiological Protection, Conversion Coefficients for Use in Radiological Protection against External Radiation. Oxford:Pergamon Press; ICRP Publication 74 (1996).
- Ing H., Noulty R.A., McLean T.D., Bubble Detectors-A Maturing Technology, Rad. Meas. 27(1), 1-11 (1997).
- Rosenstock W., Köble T., Kruzinski G., Jaunich G., Calibration of a Neutron Spectrometer in the Energy Range 144 keV to 14.8 MeV with ISO Energies, Rad. Prot. Dos. 70, 299-303 (1997).
- Croff A.G., A User's Manual for the ORIGEN2 Computer Code, ORNL/TM-7175 (1980).
- Vanhavere F., Loos M., Plompen A.J.M., Wattecamps E., Thierens H., A Combined Use of the BD-PND and BDT Bubble Detectors in Neutron Dosimetry, Rad. Meas. 5, 573-577 (1998).
- P. BAETEN, M. BRUGGEMAN and R. CARCHON, "A physical model for the description of fast and thermal neutron multiplication effects in neutron coincidence and multiplicity counting", 21st Annual ESARDA Symposium on Safeguards and Nuclear Material Management, Proceedings EUR 18963 EN, 493-502 (1999).
- HANSEN, G. E. and ROACH W. H., Six And Sixteen Group Cross Sections For Fast And Intermediate Critical Assemblies", LAMS-2543 (1961).
- PETRIE, L. M. and LANDER, N. F., KENO-Va : An Improved Monte Carlo Criticality Program With Supergrouping Computing Telecommunication Division At ORNL (1990).

This is a blank page.

JP0250291

JAERI-Conf 2002-004

SUBCRITICAL LIMIT PARAMETERS OF MOX FUEL

SAKURAI Shungo and MITAKE Susumu

Institute of Nuclear Safety, NUPEC.

Fujita Kanko Toranomon Bldg., 7F, 17-1, 3-chome Toranomon, Minato-ku, TOKYO 105-001, JAPAN

FAX:+81(3)3435-3423, E-mail: s-sakurai@nupec.or.jp, mitake@nupec.or.jp

Abstract

Joining in an international corroborative work to reexamine the American Nuclear Society's standard ANS-8.12-1987 for 'Nuclear Criticality Control and Safety of Plutonium-Uranium Fuel Mixtures Outside Reactors,' extensive studies on the subcritical limits of MOX fuels were conducted at INS/NUPEC in the last couple of years.

Analyses were made both for the MOX fuel of homogeneous aqueous mixtures and for the MOX fuel of heterogeneous systems. The survey calculations were made using the XSDRNPM code with the SCALE44G library based on the ENDF/B-V nuclear data files. And for the heterogeneous systems, the effective cross-sections of the fuel were evaluated for a unit cell of dodecahedron containing a spherical MOX fuel pellet with surrounding water moderator.

The subcritical limit parameters, such as mass, thickness, volume or concentration of the MOX fuels, were obtained. Differences between these values with latest numerical analysis methods and those with rather simplified methods of over ten years ago are not so large, and the standard was unanimously reaffirmed.

1. Introduction

Now, practical utilization of plutonium in LWRs being close at hand in Japan, and the critical characteristics of the mixed oxide fuel is one of the great interests for Japanese criticality safety colleagues. And, it is becoming more important to confirm the applicability of our criticality safety evaluation systems, i.e. analytical codes and cross-section libraries, to MOX fuel system.

Under the prescribed five years review of the American National Standard ANSI/ANS-8.12-1978 for 'Nuclear Criticality Control and Safety of Plutonium-Uranium Fuel Mixtures Outside Reactors,' the standard was revised to include subcritical limits for heterogeneous lattices of mixed oxide fuel pins in water and published in 1987, and then reaffirmed in 1993. But, the last real effort of in this development was in the 1980s, and the subcritical limits rely significantly on computer calculations. So that, in 1997, considering recent substantial improvement of computational capability and cross-section data, revision of the standard was proposed and international participation by criticality personnel was called.

The standard gives the subcritical limit parameters for the MOX fuel of homogeneous aqueous mixtures and for the MOX fuel of heterogeneous systems: ten different physical

values are numerically given for the aqueous mixtures, and four values in graphically for the heterogeneous systems. The limit parameters are defined for four different plutonium contents of the mixed oxide [3, 8, 15 and 30 % in $PuO_2/(UO_2+PuO_2)$ weight ratio], and three different plutonium isotropic compositions;

- Composition I: Pu-239 100 %,
- Composition II: Pu-239 79 %, Pu-240 15 %, Pu-241 6% (in weight), and
- Composition III: Pu-239 60 %, Pu-240 25 %, Pu-241 15% (in weight).

Natural uranium is assumed for the uranium dioxide.

The study on the subcritical limits of MOX fuels at the INS was started in 1997, and has been continued as follows;

- In 1997 and 1998: Preliminary study on the aqueous mixtures with the MGCL-JINS library,
- In 1999: Study on the aqueous mixtures with the SCALE 44-group library, and
- In 2000: Study on the heterogeneous systems with the SCALE 44-group library.

2. Study on Homogeneous Mixtures

Each subcritical limit parameter was calculated using simple physical geometry of MOX fuels as showing below:

- Mass of plutonium in oxide mixture,
- Mass of (PuO2 + UO2), and
- Volume of oxide mixture: by sphere,
- Diameter of infinite cylinder: by cylinder, and
- Thickness of infinite slab,
- Areal density of plutonium, and
- Areal density of oxides: by slab.

All of these MOX fuels are reflected with H_2O layer of 30 cm-thickness.

Also calculated were:

- Concentration of plutonium,
- Concentration of oxides, and
- H:Pu atomic ratio: by slab of infinite thickness.

The survey calculations were made with SCALE 44 group library and XSDRNPM code. A k-effective or k-infinity value of 0.98 was applied to determine the parameter values that gave the subcritical limits.

Subcritical limits for the uniform aqueous mixtures of the oxides of plutonium and natural uranium obtained in this study are summarized in Table 1, in comparison with those in the standard.

3. Study on Heterogeneous Systems

Each subcritical limit parameter was obtained using simple physical geometry of the MOX fuel of heterogeneous systems as showing below.

- Mass of plutonium in oxide mixture and mass of (PuO_2 + UO_2): by sphere, and
- Volume of oxide mixture: by sphere,
- Cylinder diameter: by infinite cylinder, and
- Slab thickness: by infinite slab.

All of these MOX fuels are reflected with H_2O layer of 30 cm-thickness.

As shown in Fig. 1, effective nuclear cross-sections of the heterogeneous MOX fuel were evaluated for a unit cell of dodecahedron containing a spherical MOX fuel pellet with surrounding water moderator. And, the evaluations were made for a number of different sizes of the cell (or lattice pitch) and the pellet diameter, and the infinite neutron multiplication factors were also calculated for these cells.

The survey calculations, both for the effective cross-sections and for the subcritical limit parameters, were made using the XSDRNPM code and the SCALE 44G library based on the ENDF/B-V nuclear data files. The S_8 angular quadrature set was used, and for the convergence check of the eigenvalue and the fluxes, the criteria of 0.01% was applied. The minimal parameter values that gave the subcritical limits were determined by the k-effectives of 0.95.

Subcritical limits of the oxide mixtures for heterogeneous systems are summarized in Table 2, with the ratio to the homogeneous systems. And the limiting masses of the heterogeneous systems are plotted in the figure presented in the standard.

4. International Comparisons

Table 3 shows an example of international comparison of the results: the subcritical volumes of aqueous mixtures of the three different plutonium compositions. Relatively good agreement is resulted among the different calculation methods of the international participants for this rather simple configuration.

5. Concluding Remarks

This extensive study on the criticality characteristics of the MOX fuel is a very good experience for us to check the applicability of our criticality safety analysis systems to the MOX fuel systems. Differences between these values with the latest numerical analysis methods and those with rather simplified methods of over ten years ago are not so large. And, the standard was unanimously reaffirmed in the spring of 2001.

Table 1 Subcritical Limits for Uniform Aqueous Mixtures of the Oxides of Plutonium and Natural Uranium: Comparison of Limits Calculated by XSDRNPM Code and SCALE 44 Group Library with Those Tabulated in ANSI/ANS 8.12-1987

Pu Isotopic Composition[a)]	I				II				III			
$PuO_2/(UO_2+PuO_2)$, wt%	3%	8%	15%	30%	3%	8%	15%	30%	3%	15%	15%	30%
Mass of Plutonium in Oxide Mixture, kg[b)]	0.80 (0.73)	0.61 (0.61)	0.55 (0.54)	0.50 (0.50)	1.49 (1.35)	1.08 (1.06)	0.95 (0.94)	0.85 (0.87)	2.25 (2.00)	1.55 (1.53)	1.33 (1.28)	1.17 (1.16)
Mass of ($PuO_2 + UO_2$), kg[b)]	30.1 (27.5)	8.7 (8.6)	4.1 (4.1)	1.9 (1.9)	56.5 (51.3)	15.3 (15.1)	7.2 (7.1)	3.2 (3.3)	84.9 (75.9)	21.9 (21.7)	10.1 (9.7)	4.4 (4.4)
Diameter of Infinite Cylinder, cm[b)]	24.1 (24.3)	19.6 (19.8)	17.8 (17.8)	16.4 (16.2)	30.8 (30.8)	24.9 (24.9)	22.7 (22.5)	21.1 (21.0)	35.2 (34.8)	27.9 (27.5)	25.4 (24.8)	23.5 (23.4)
Thickness of Infinite Slab, cm[b)]	11.2 (11.0)	8.2 (8.2)	7.1 (6.9)	6.1 (5.9)	15.4 (14.9)	11.6 (11.2)	10.2 (9.6)	9.2 (8.7)	18.3 (17.4)	13.5 (12.9)	11.8 (11.0)	10.6 (9.9)
Volume of Oxide Mixture, liter[b)]	23.6 (23.5)	13.6 (14.0)	10.6 (11.0)	8.6 (8.5)	45.3 (44.8)	25.6 (25.9)	20.2 (20.4)	16.7 (16.8)	65.7 (63.4)	35.0 (34.4)	27.1 (26.6)	22.1 (21.6)

Notes:

a) Plutonium Isotopic Compositions: I - ^{239}Pu 100%, II - ^{239}Pu 79% ^{240}Pu 15% ^{241}Pu 6%, and III - ^{239}Pu 60%, ^{240}Pu 25%, ^{241}Pu 15% (wt%).

b) Upper row: Calculated values with SCALE 44 group library and XSDRNPM code. Lower row with parentheses: ANSI/ANS 8.12-1987.

Table 2 Subcritical Limits of Oxide Mixtures for Heterogeneous Systems

Pu Isotopic Composition		I (^{239}Pu 100%)				II (^{239}Pu 79%, ^{240}Pu 15%, ^{241}Pu 6%)				III (^{239}Pu 60%, ^{240}Pu 25%, ^{241}Pu 15%)			
$PuO_2/(UO_2+PuO_2)$, wt%		3%	8%	15%	30%	3%	8%	15%	30%	3%	8%	15%	30%
Mass of Plutonium In Oxide Mixtures, kg	Hetero (Calc)	0.58	0.50	0.50	0.55	0.94	0.76	0.73	0.78	1.24	0.96	0.91	0.94
	Hetero/ Homo	0.73	0.82	0.91	1.10	0.63	0.70	0.77	0.92	0.55	0.62	0.68	0.80
Mass of Oxide Mixtures, kg	Hetero (Calc)	22.0	7.1	3.8	2.1	35.7	10.8	5.6	2.9	47.0	13.6	6.9	3.6
	Hetero/ Homo	0.73	0.81	0.92	1.09	0.63	0.71	0.77	0.92	0.55	0.62	0.68	0.81
Volume of Oxide Mixtures, liter	Hetero (Calc)	17.1	10.5	8.4	6.9	26.5	16.4	13.3	10.9	32.1	19.6	15.7	12.9
	Hetero/ Homo	0.72	0.77	0.79	0.80	0.58	0.64	0.66	0.65	0.49	0.56	0.58	0.58
Diameter of Infinite Cylinder, cm	Hetero (Calc)	21.5	17.9	16.3	15.1	25.4	21.2	19.5	18.0	27.2	22.6	20.8	19.3
	Hetero/ Homo	0.89	0.91	0.92	0.92	0.82	0.85	0.86	0.85	0.77	0.81	0.82	0.82
Thickness of Infinite Slab, cm	Hetero (Calc)	9.7	7.2	6.2	5.4	12.1	9.4	8.2	7.3	13.4	10.3	9.2	8.0
	Hetero/ Homo	0.87	0.88	0.88	0.89	0.79	0.81	0.81	0.80	0.73	0.76	0.78	0.75

Notes:

Hetero (Calc): Limits of heterogeneous systems calculated with SCALE 44 group library (ENDF/B-V) and XSDRNPM.

Hetero/Homo: Ratio of Hetero(Calc)/[Limits of homogeneous systems shown in Table 1].

Table 3 Comparison of Results for Subcritical Volumes*

Subcritical (k=0.98) Volume (L), Pu-239 100%

Basis	3%	Delta	8%	Delta	15%	Delta	30%	Delta
ANS 8.12	23.5	-	14.0	-	11.0	-	8.5	-
J-Team (MGCL)	23.2	-1.3%	13.3	-5.0%	10.4	-5.5%	8.5	0.0%
J-Team (SCALE44)	23.6	0.4%	13.6	-2.9%	10.6	-3.6%	8.6	1.2%
Lester	24.1	2.6%	13.7	-2.1%	10.8	-2.3%	8.7	2.4%
Larry	-		-		-		-	
Debdas	24.0	2.1%	13.7	-2.1%	10.9	-0.9%	8.8	3.5%
UK Team (k=0.95)	23.5	0.0%	14.5	3.6%	10.3	-6.6%		
UK Team (k+3□=0.95)	22.1	-6.0%	13.7	-2.1%	10.1	-8.2%		
UK Team (k+3□=1)	25.0		15.5		11.1			

Subcritical (k=0.98) Volume (L), Pu-239 79%, Pu-240 15%, Pu-241 6%

Basis	3%	Delta	8%	Delta	15%	Delta	30%	Delta
ANS 8.12	44.8	-	25.9	-	20.4	-	16.8	-
J-Team (MGCL)	44.9	0.2%	25.3	-2.3%	20.0	-2.0%	16.5	-1.8%
J-Team (SCALE44)	45.3	1.1%	25.6	-1.2%	20.2	-1.0%	16.7	-0.6%
Lester	46.2	3.1%	25.8	-0.4%	20.3	-0.5%	16.8	0.0%
Larry	-		-		-		-	
Debdas	48.5	8.3%	26.7	3.1%	20.4	0.0%	17.5	4.2%
UK Team								

Subcritical (k=0.98) Volume (L), Pu-239 60%, Pu-240 25%, Pu-241 15%

Basis	3%	Delta	8%	Delta	15%	Delta	30%	Delta
ANS 8.12	63.4	-	34.4	-	26.6	-	21.6	-
J-Team (MGCL)	64.3	1.4%	34.4	0.0%	26.7	0.4%	21.7	0.5%
J-Team (SCALE44)	65.7	3.6%	35.0	1.7%	27.1	1.9%	22.1	2.3%
Lester	67.0	5.7%	35.5	3.2%	27.3	2.6%	22.1	2.3%
Larry	-		-		-		-	
Debdas	69.5	9.6%	36.1	4.9%	27.2	2.3%	22.1	2.3%
UK Team								

Notes:

Lester: With SCALE-5 and the 238-group library based on ENDF/B-V.
Larry: With SCALE-4.3 and the 238-group library based on ENDF/B-V.
Debdas: MCNPB and the ENDF/B-VI(.60c) continuous energy cross-section library.
UK Team: MONK7B and the UKNDL cross-section library.

* Prepared by S. C. Keeton and M. Sheaffer of LLNL, coordinator of the working group.

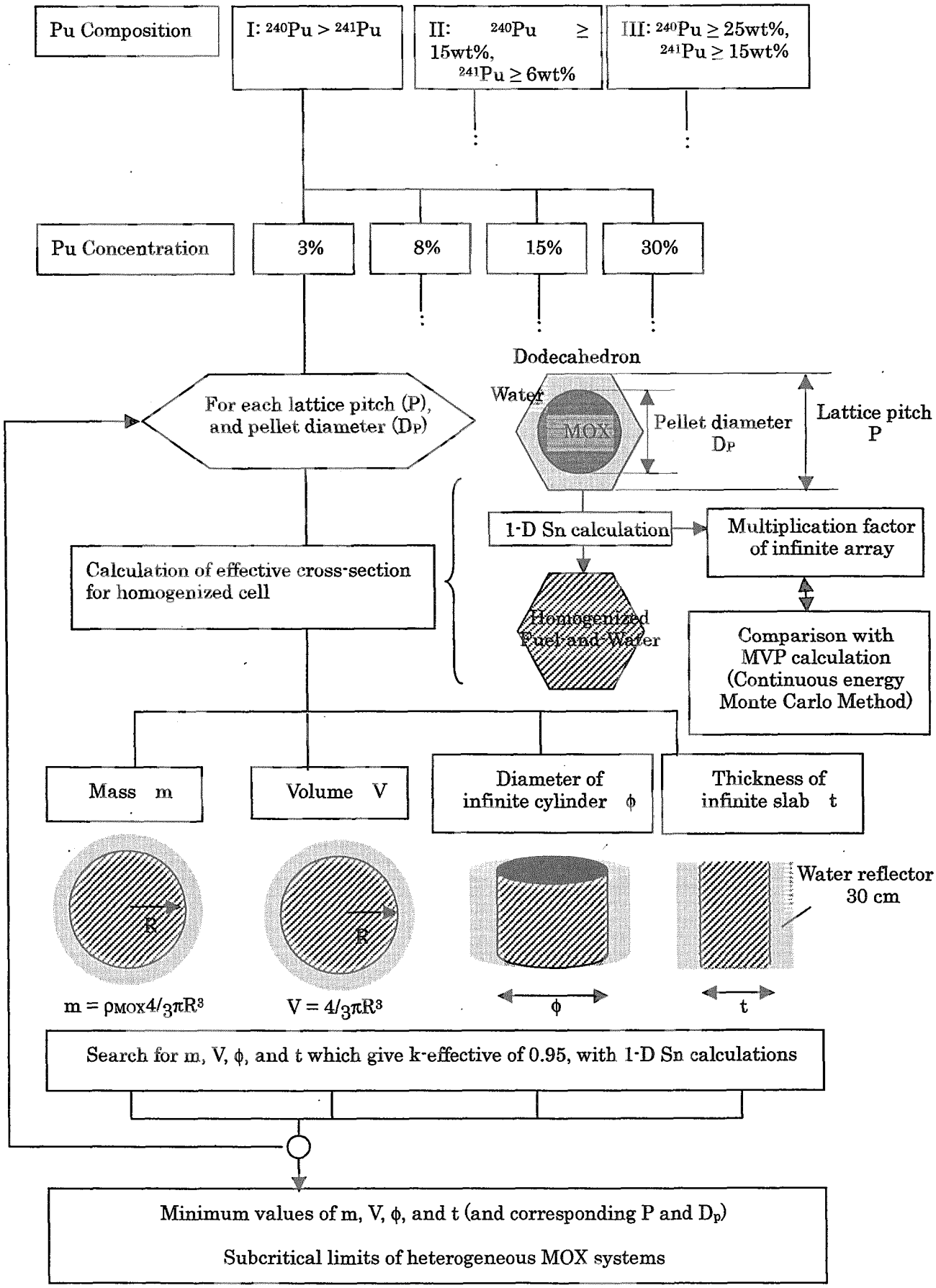

Fig. 1 Analytical procedures for subcriticality safety parameters of heterogeneous MOX fuel systems.

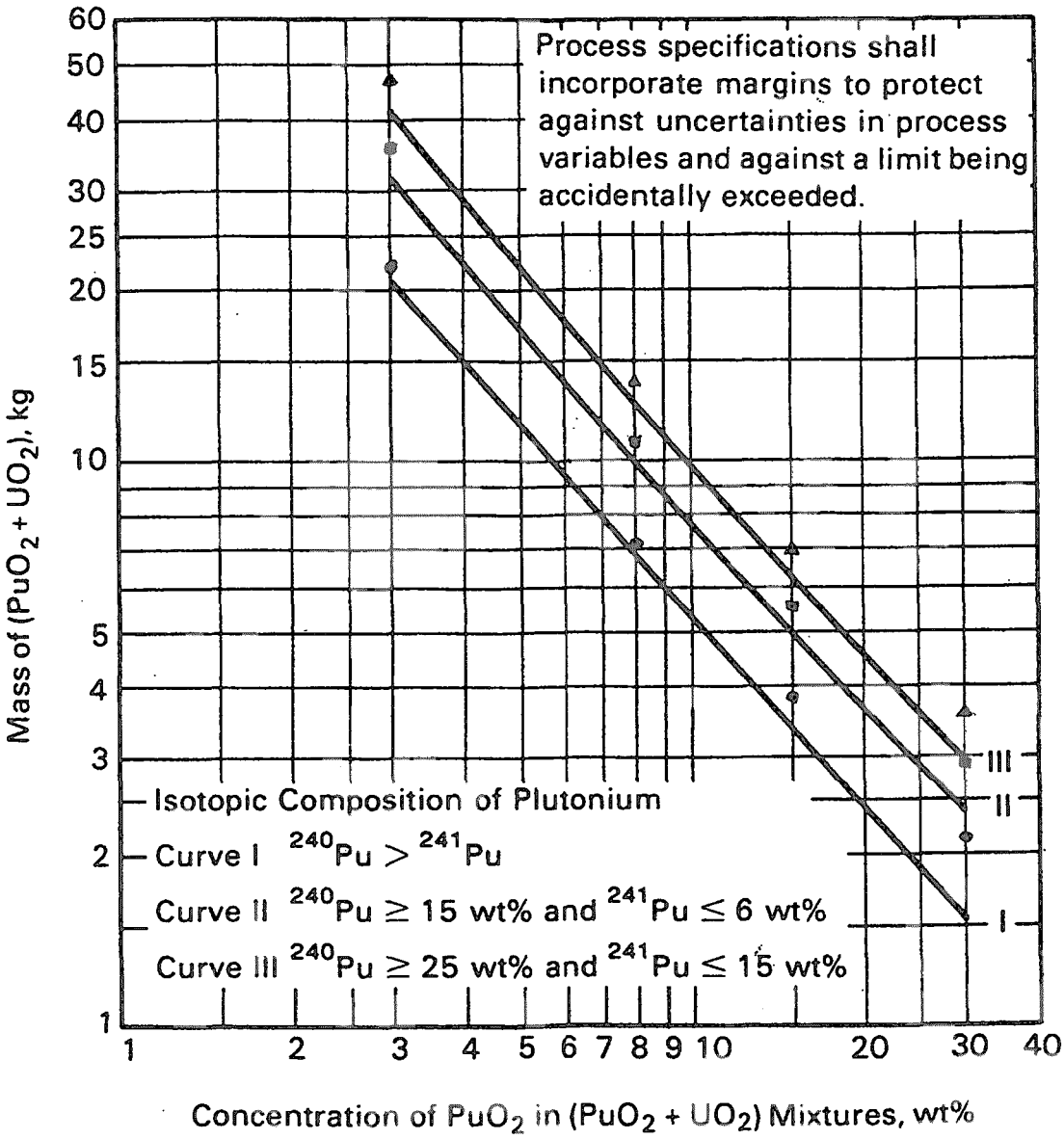

Fig. 2 Limiting mass of heterogeneous mixtures of the oxides of plutonium and natural uranium in water as a function of the plutonium oxide content (excerpt from the standard). The results of present study are plotted with marks corresponding to the three different plutonium compositions.

JP0250292

CRITICALITY SAFETY CONTROL AT THE PLUTONIUM FUEL PRODUCTION FACILITY

J.NINAGAWA, S.TAKAHASHI, Y.YAMAMOTO,
S.FUJIWARA, K.KUNIYASU and T.OHTANI

Plutonium Fuel Center, Tokai Works,
Japan Nuclear Cycle Development Institute,
4-33, Muramatsu, Tokai-mura, Nakagun, Ibaraki

ABSTRACT

Criticality safety in the Plutonium Fuel Production Facility (PFPF) is based on mass control. The nuclear material handling area is divided into some Criticality Control Units for criticality safety. One Criticality Control Unit (CCU) corresponds to one or more glove boxes or storage unit. For criticality safety, the amount of nuclear material handled in each CCU is limited with defined criticality limits. Nuclear material transfers between CCUs perform only after the confirming that the total of existing nuclear material at the destination CCU and the nuclear material to be transferred is less than the criticality limits. A computer system controls nuclear material transfers at PFPF. The computer system uses a 3-level hierarchy design.

Key words: criticality safety control, PFPF, MOX, mass control, computer system.

1. INTRODUCTION

The Plutonium Fuel Production Facility (PFPF) supplies mixed plutonium and uranium oxide (MOX) fuel assemblies for the JOYO experimental fast reactor and the MONJU prototype fast breeder reactor. PFPF was constructed based on MOX fuel fabrication technologies, plant operation and radiation control technologies developed by the Japan Nuclear Cycle Development Institute (JNC) and, PFPF demonstrates the possibility a large scale of MOX fuel fabrication.

The main objectives of the PFPF project are to improve productivity and reduce personnel radiation exposure compared to JNC's other two fuel fabrication facilities. To achieve these objectives, remote-controlled and automated fuel fabrication systems were adopted in PFPF. Furthermore, a dry process was adopted since it increases the production batch size over wet process. PFPF applies strict controls over nuclear material to avoid criticality. The criticality safety control at PFPF is based on mass control and moderation control (moisture content, etc.) are classified for each nuclear material. The criticality safety control system at PFPF was designed to avoid double loading with nuclear material.

The concept and design of criticality safety control system for pellet fabrication process in PFPF are mainly described in the following sections.

2. FUEL FABRICATION PROCESS

Fig. 1 shows the MONJU fuel fabrication process flow. The fuel fabrication process consists of three processes: pellet fabrication, fuel pin fabrication and assembling, and analytical laboratory. The fuel fabrication system is divided into a group of automated equipment and their control system.

The intermediate storages, which are connected to glove boxes for the pellet fabrication process by a transfer tunnel, are located in the center of the pellet fabrication process area. The glove boxes are arranged on both sides of the intermediate storage, like teeth of a comb. The arrangement enables to replace and to add the process glove box efficiently. Fig.2 shows the interconnection between a process glove box and an intermediate storage. The nuclear material is automatically transferred between each glove box by the computer control system.

3. CRITICALITY SAFETY CONTROL CONCEPT

3.1 CRITICALITY SAFETY CONTROL

The PFPF criticality safety is based on mass control. The nuclear material handling area is divided into Criticality Control Units for criticality safety. One Criticality Control Unit (CCU) used for the minimum unit for criticality control at PFPF. One CCU corresponds to one or more glove boxes or storage unit. For criticality safety, the amount of nuclear material handled in each CCU is limited with defined criticality limits.

Nuclear material transfers between CCUs perform only after the confirming that the total of existing nuclear material at the destination CCU and the nuclear material to be transferred is less than the criticality limits.

3.2 SAFETY FACTOR

The critical safety control system at PFPF avoids double loading of the nuclear material as follows.

The criticality safety for a nuclear material transfer is checked by both the Process Control Computer (PCC) and the Central Control Computer (CCC).

Nuclear material transfers occur only through the designated CCU entrances/exits. The transfer route of container is automatically determined. Therefore, the nuclear material can't be transferred over incorrect routes and using a wrong container.

Criticality shutters are installed on CCU entrance/exits. The shutters have an interlock function controlled by CCC with process-independent. Therefore, without the permission of CCC, the nuclear material transfer is physically impossible.

As mentioned above, we adopted safety factor (0.7[1]) in the mass control in consideration of the calculation error and the heterogeneous of the nuclear fuel under the condition of avoiding double loading of the nuclear material.

3.3 CRITICALITY LIMITS

Criticality limits for all nuclear materials are determined based on isotopic composition, density, shape, moderation, and other factors. The criticality limit is determined by multiplying the minimum critical mass by the safety factor. The minimum critical mass is calculated based on conservative parameters (plutonium fissile concentration, moisture concentration, etc.) and ideal conditions for becoming criticality. (spherical shape, full reflection by water, etc.)

The evaluation model of a multiple unit reduces the distance between single units more than the design value, and decreases the thickness of the material. The thickness of the material influences the effect of the neutron absorption and the effect of the reflection in the material. These allow for the possibility of a manufacturing error and an installation error.

The neutron multiplication factor is calculated by using verified code system to confirm of securing subcriticality.

Assessment conditions for PuO_2 feed powder minimum critical mass are as follows: Powder density is 4.5 g/cm^3, and the isotopic concentrations are 80% ^{239}Pu, 10% ^{240}Pu and 10 % ^{241}Pu. The moisture contents in the powder are (1) less than 1wt%, and (2) between 1 and 5wt%.

The minimum critical mass of PuO_2 (feed powder) and criticality limits are shown in Table I.

Table I: The minimum critical mass of PuO_2 (feed powder) and criticality limits

Parameter	mass (kg Pu*[a])	
	minimum critical mass	criticality limits
moisture content ≦ 1 wt%	37.5	26.2
1 wt%< moisture content ≦ 5 wt%	24.8	17.3
safety factor	0.7	

a. Pu*= ^{239}Pu+^{241}Pu+^{235}U

4.CRITICALITY CONTROL SYSTEM

The transfer control of the nuclear material at PFPF is performed by a computer system with 3-level hierarchy. The computer system has the layered structure composed of CCC, PCC and the Equipment Control System (ECS) as shown in Fig.3.

CCC located in the top layer, performs the criticality safety control and the material accounting in PFPF.

PCC is installed for each process including pellet fabrication, fuel pin fabrication and assembling and the analytical laboratory. The transfer schedules for the nuclear material are made by PCC, which performs remote operation of the process equipment and the process control.

ECS is installed with each process and directly controlled by PCC. ECS controls the local

process equipments. The ECS also controls the safety for the equipments.

The failure or breakdown of one of computers in PCC or ECS and the associated equipment controllers does not influence the other PCCs and ECSs. If the computer broke, following transfer of the nuclear material would be interrupted by ECS and PCC. The transfer of nuclear material would be stopped except transfer permitted, therefore, there is no influence in criticality safety.

5. COMPUTER SYSTEM FOR NUCLEAR MATERIAL TRANSFER CONTROL

The PFPF computer system must always manage the inventory of nuclear material in the facilities to perform the criticality safety control. The control of nuclear material transfers between CCUs is very important from the viewpoint of the criticality safety control.

The information exchange between computers to execute nuclear material transfers is shown in Fig.4. The nuclear material transfer control by the computer system is performed as follows.

PCC that performs operation and the management of the transfer equipment automatically decides the nuclear material's destination and the transfer route. After the PCC performs the criticality check for the transfer request, the nuclear material transfer request is transmitted from PCC to CCC.

CCC confirms that the sum of existing nuclear material and the material to be transferred is less than the criticality limits. Furthermore, after CCC confirms the transfer request, the operator in charge of the nuclear material management checks it again. CCC transmits transfer permission and signal that releases from the interlock of the criticality shutters to PCC. The nuclear material is transferred into the destination CCU.

The transfer information (container No., weight, position) about the nuclear material is transmitted to PCC from the transfer machine controller. Then the operator of process control section confirms the transfer information by ITV monitor. The transfer information is directly transmitted to CCC. This transfer is indicated on the graphic panel (watch board) and always watched by the operator in charge of the nuclear material management.

6. CONCLUSION

Criticality safety control is performed to maintain the mass of nuclear material lower than criticality limit by using the computer system with strict criticality condition and limits at PFPF.

Criticality safety control of facility with large-scale of bulk nuclear material was demonstrated at PFPF. The technologies developed and demonstrated at PFPF can be thought to make use of the design of the future commercial MOX fuel production plant.

REFERENCE

[1] "GUIDE DE CRITICITE" CEA-R-3314 (1967)

[2] K.Asakura, T.Ohtani, T.Ishibashi, "On-line computerized material accounting system for criticality safety", International seminar on nuclear criticality safety, pp.272-277, (1987).

[3] T.Ohtani, H.Nakano, M.Seya, S.Takahashi, "An introduction of automated MOX facility, PFPF", INMM 30th ANNUAL MEETING, (1998)

[4] M.Seya, T.Ohtani, S.Takahashi, Y.Yamamoto, S.Inose, "Fully computerized material accountancy system", INMM 30th ANNUAL MEETING, (1998)

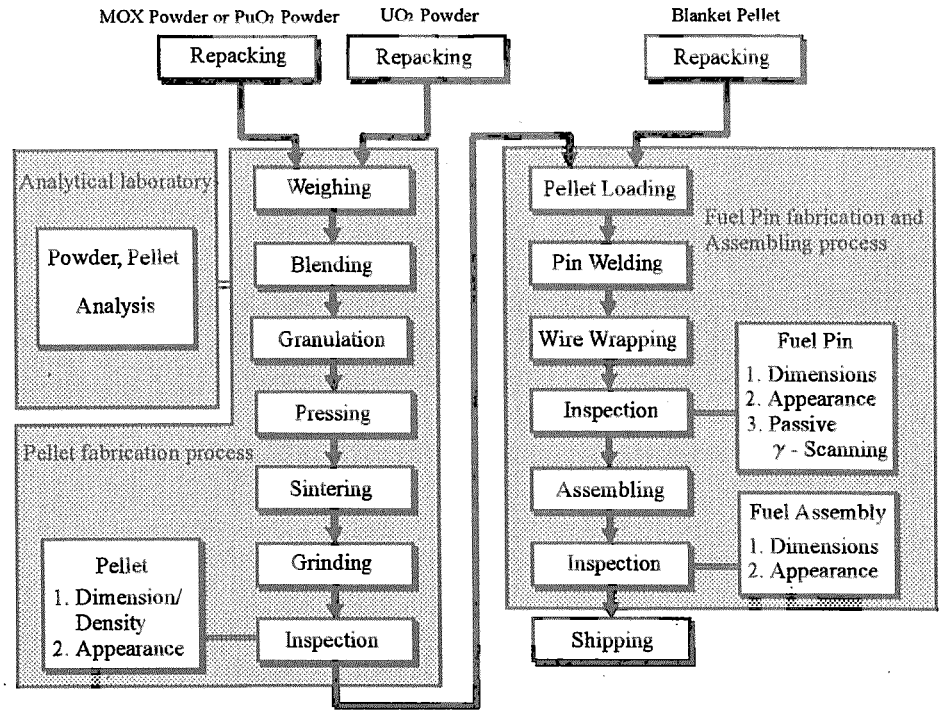

Fig.1 MONJU Fuel Fabrication Process Flow

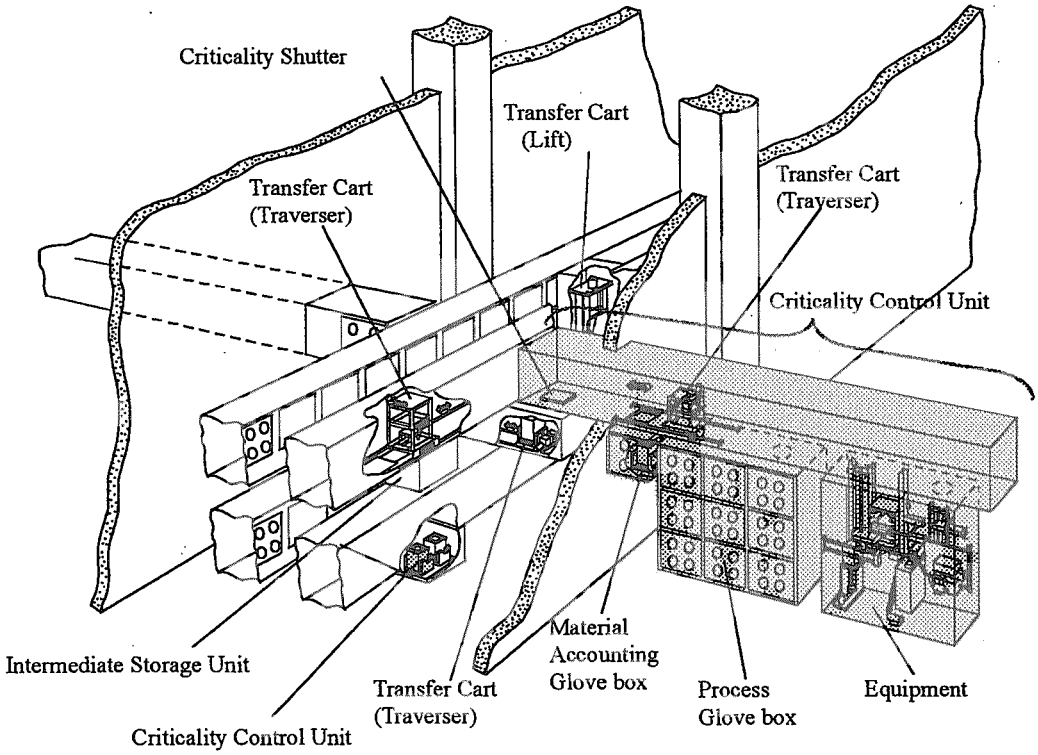

Fig.2 Typical arrangement of process glove box and intermediate storage

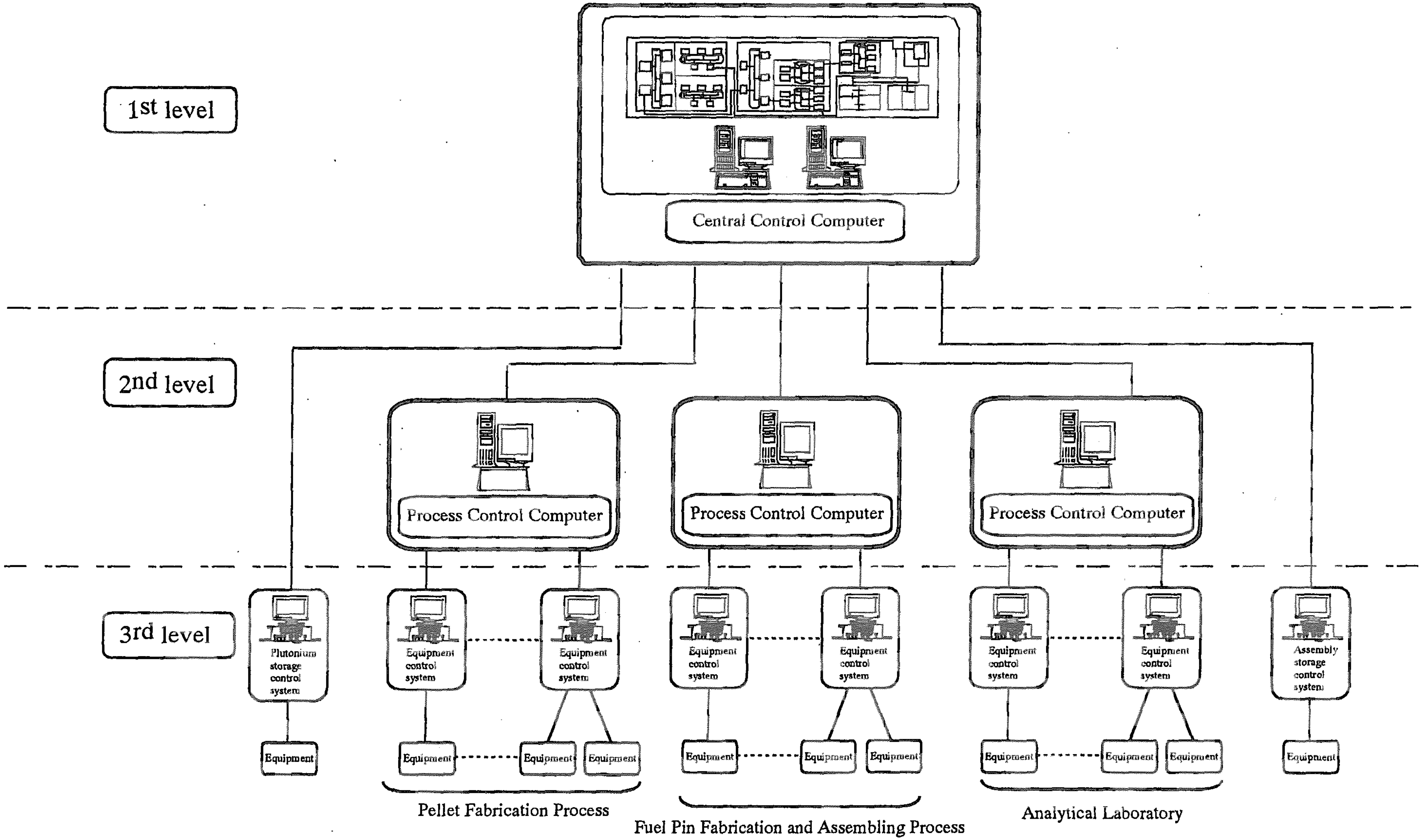

Fig.3 System structure of computer control system in PFPF

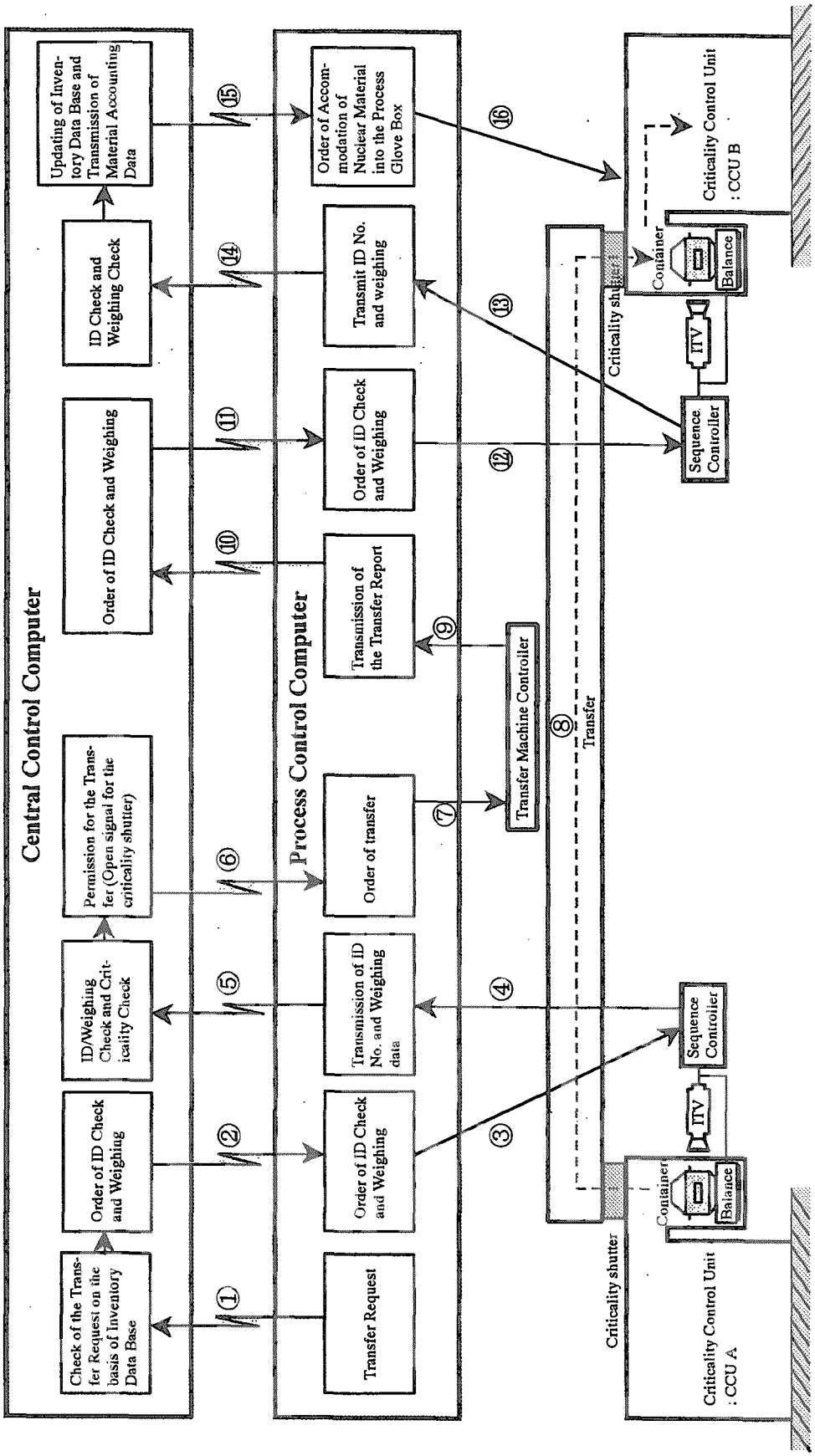

Fig.4 Nuclear Material Transfer Procedure (Example)

JP0250293

JAERI-Conf 2002-004

APPLICATION OF DEDICATED SAFEGUARDS SOLUTION MONITORING INSTRUMENTATION TOWARDS IMPROVED PROCESS CONTROL FOR CRITICALITY SAFETY

B. A. Hunt, D. Landat, L. Dechamp and M. Caviglia

European Commission, Joint Research Centre,
21020 Ispra (Va), Italy.

Fax: +39-0332-789683, email: brian.hunt@jrc.it

ABSTRACT

Solution monitoring can augment the safety of a plant by giving a timely response to changes in a tanks configuration, or density and solution levels. Assuming that a precise tank profile has been obtained through calibration activity, the profile can be constantly checked during the plant operations to ascertain whether any changes have occurred. These changes in tank profile could be from precipitation in the tank for example (or a diversion) with an accumulation of fissile material. Portable unattended instruments developed at the JRC for specific application in solution monitoring, house high precision digital pressure transducers of better than 0.01% accuracy supported by application software for rapid data interpretation. These instruments can detect tank profile changes. Several tanks can even be connected together for monitoring purposes. A quality control program needs to be elaborated and associated with the instrumentation to maintain continuity of knowledge on the vessel calibration results.

Key words: Solution Monitoring, portable, unattended, instruments.

1. INTRODUCTION

This paper describes some nuclear safeguards application work carried out in the mass/volume laboratory at the JRC Ispra site of the European Commission and its potential for improved process safety. Our laboratory was established some years ago principally to provide technical support to the nuclear inspectors in the field of measurement of radioactive liquids in both reprocessing and fabrication facilities. The technical support ranges from dedicated training courses in mass/volume methodology to the development, implementation and supply of specific solution monitoring instrumentation of high precision for inspector's usage in facilities. Although the objective has always been to provide the nuclear inspector with the capabilities for independent tank volume measurements for nuclear material accountancy purposes and data interpretation, indirectly the instrumentation provides accurate process parameter data particularly on the level and density measurements which is at the worst equal to the operator's control system but generally is far superior due to the high accuracy digital pressure transducers utilised and application software. The nuclear industry keeps accountancy records of the nuclear materials it processes for economic, legal and safety reasons. In the plants where nuclear fuels are processed measurements for accountancy purposes are made when the material is still in the process line mostly in the form of a nitric acid solution. The management procedure generally adopted includes among other things, tank volume measurements, the taking of one or more samples of the solution for subsequent chemical analysis and the computation to determine the quantity of nuclear material in the tank. For criticality safety management of fissile material solutions, quality control procedures are set in place and can be a variety of measures from ever safe tank design, concentration limitations, additions of neutron poisons or indeed the permanent presence of neutron absorbers.

2. MATERIAL ACCUMULATION

It is because of the very nature of nuclear fissile solutions that within the nuclear industry there are a variety of tanks of varying shapes and dimensions. Criticality calculations and analysis play important roles in providing the designer of tanks the necessary criteria who in turn matches this with the process requirements for conceptual design and eventual construction. All these tanks prior to commissioning need to be accurately calibrated for both process control and nuclear safeguards. For the latter some tanks are of more importance than others due to the nuclear content form and concentration. However from a criticality point of view considerations have to be taken into account of possible accumulations of fissile material over long time periods in tanks in the form of deposits via precipitation, crystallisation phenomena etc., due to favourable chemical conditions encouraging these effects. Solution monitoring instrumentation as proposed offers the potential to give advanced warning on possible solid accumulation in tanks.

3. SOLUTION MONITORING

It is worthwhile examining the needs of solution monitoring (SM) and consideration of its potential for safety improvement [1]. Our safeguards programme at the JRC Ispra involves support programme activities towards the inspectorate agencies, one such topic being solution monitoring. This activity has arisen from the mass/volume methodological training courses carried out at Ispra over a number of years in the calibrations of tanks of both small and large volumes. As a consequence of close collaboration with the inspectorate agency a safeguards approach for solution monitoring systems in the key processing areas, namely head-end, main process, waste handling, conversion and fabrication areas has been developed. The approach is based on our past and current experience in the application of developed unattended solution monitoring equipment [2].

Solution monitoring (SM) in tanks has the principle aim of collecting and determining the volume, mass and concentration information of the liquid inside the tank. The resulting data and information needs to be analysed in order to arrive at satisfactory accountancy data conclusions. To generate these data, tanks need some kind of measurement device for level and density measurement and also need to be accurately calibrated. Normally tanks in the nuclear processing facilities are usually equipped with a pneumatic measurement system which measures the pressures induced by the airflow through three dip-tubes (level, density and reference probes) as a result of the liquid level and density of the solution in a tank and sensors measuring the temperature of the solution. The capability and effectiveness of SM for safeguards purposes is heavily dependent on the prior work carried out both by the operator and the inspector and the monitoring instrumentation installed. Thus to arrive at a truly efficient and secure system for SM a series of essential activities need to be performed namely:

- Pre-calibration
- Familiarisation with tank operation
- Design Information Verification
- Calibration activities
- Instrumentation specifications
- Verification
- Data analyses

This is all part of an inspector's work but the importance cannot be over emphasised as the results provide valuable information in subsequent data analysis not only for safeguards but on early identification of tank profile changes during the lifetime operation of the tanks.

3.1 Pre - Calibration Activities

In order to study the mode of operation and sequence for measurements in a tank the following items are needed:

- An up-to-date Engineering Flow Sheet that indicates the adjacent tanks, all pipes and valves
- A detailed construction drawing of the tank, including details of all the internals. This is extremely important as it indicates where there are possible linear, non-linear zones
- A description on the mode of operation of the tank. This includes the way and sequence of operation of the mixing, sampling method, the volume measurement operation and the mechanism for liquid transfers both in and out.
- The operator's detailed proposal for calibration procedure.

3.2 Familiarisation with tank operation

Any tank to be calibrated is composed of several zones of interest. For each of these zones another calibration equation has to be used. In order to determine this equation in an adequate manner, a certain number of increments in that zone must be foreseen.

Possible zones of interest are:

The heel below the major (level) dip-tube. This value can be deduced from the detailed construction drawing or could be retrieved from an earlier (test) calibration. Once the vessel is operational, this portion of the vessel is not anymore directly verifiable. This is due to the fact that the vessel can never be emptied totally or even below the level of the lowest dip-tube.

The non-linear and linear part(s) of the tank.

During operations, any filling or emptying of the vessel will have been monitored. Although the solution flow rate is not absolutely constant, enough measurement points will be provided to clearly distinguish the salient points within these zones of the vessel. The number of points as measured at a fixed time interval in this area, will in itself be a measure of the solution flow rate. This information can be used to align the points within that area.

Analyses of the data would therefore concentrate on the decrease in one vessel and the increase in the receiving vessel and for each vessel the profile determined and compared to the original profile data for that particular region. This is particular important for points in the vessels where sudden slope changes occur. This data as mentioned previously will have been well determined. This is extremely important since during process operations and data acquisition, information can be obtained on possible changes in the tank profile and hence consideration on whether or not the changes are related to material accumulation

The overflow point.

This point is of vital interest to reconcile later calibration verifications or re-calibrations as it might be the only fixed physical point in the tank that permits a re-verification of the length of the dip-tubes.

3.3 Familiarisation with tank operation

Design information verification on site is an extremely important and arduous task to be performed. This usually involves a number of varying tasks, to name but a few, including

- Filling/Emptying
- Adjusting physical and chemical conditions

- Mixing and sampling
- Operator's measurement system versus Inspector's

3.4 Calibration activities
These activities are adequately described in reference 3, particularly on corrections to be implemented during data analyses, buoyancy, temperature, scale calibrations.

3.5 Instrumentation specifications

- Solution monitoring equipment is usually installed in a position close to the operator's pressure transducers and manifold. The equipment developed for inspector's usage is a a complete unit with data acquisition hardware, pressure transducers, associated electronics, programmable logic controller (PLC) including a local data storage capability (EPROM) and an uninterruptible power supply, all located in a sealed box.

At the core of these dedicated measurement systems is a digital pressure module with a manufacturer's precision of 0.01%. They have fully tested in our Tank Measurement laboratory and also engaged in nuclear facilities by inspectors and operators. Dedicated application software under fast data acquisitions (up to 8 acquisitions per second) helps to monitor events in a tank, interpreting tank profiles and matching with archived data, This allows conclusions to be drawn on tank profile changes during normal plant operations.

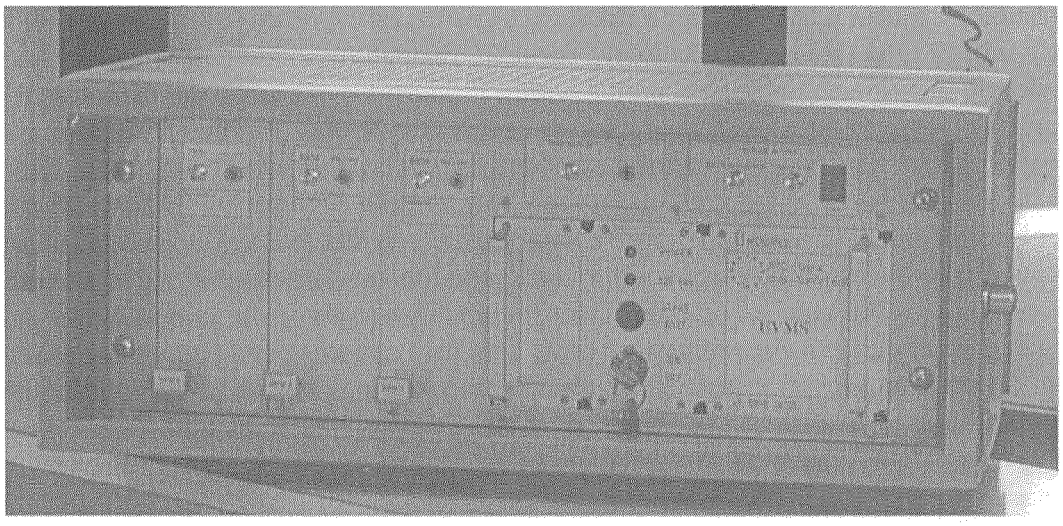

Figure 1. Photograph of an Unattended Volume Measurement Station utilised for Solution Monitoring

4. CONCLUSIONS
SM coupled with fast data acquisition, a precise tank calibration are the essential ingredients

in checking a tanks profile. The requirements for detecting anomalies or changes in tanks can only be detected by first obtaining all the relevant information as described in section 3 on SM. Further detection of possible material accumulation can only be established by elaborating a quality control program to maintain a continuity of knowledge and indeed to establish in a timely fashion whether or not material is accumulating in the tank.

Figure 2. Portable Pressure Measurement Device which can also be connected to the UVMS to extend the range of tanks to be monitored

5. REFERENCES

[1] F. Frassen, C.Foggi and B.A. Hunt, "Tank Data Acquisition & Evaluation in a Large Scale Reprocessing Plant", 17th ESARDA Annual Symposium pp 383-388, Aachen May 1995.

[2] D. Landat, B.A. Hunt, M.Caviglia, "Portable Solution Monitoring Instrumentation and Data Evaluation for Unattended Application in Nuclear Facilities", 42nd INMM Annual meeting Indian Wells, July 2001.

[3] ISO D382/4 Tank Calibration and Volume Determination for Nuclear materials Accountancy Vessels and Data Standardization.

This is a blank page.

JP0250294

JAERI-Conf 2002-004

SUBCRITICAL MEASUREMENTS AND THEIR APPLICATIONS

Timothy E. Valentine
Oak Ridge National Laboratory
P. O. Box 2008, Oak Ridge, TN 37831-6354
Fax: 1-865-574-6182, e-mail: valentinete@ornl.gov

Subcritical measurements have typically been used at critical experiment facilities as a means to monitor the approach to the critical condition. However, subcritical measurement methods have many more applications than simply to serve as indicators for the approach to critical. One of the more fundamental uses involves using them as benchmark measurements. Monte Carlo codes have been developed that can directly simulate a variety of subcritical measurements in the same manner in which the measurements are performed. Therefore, subcritical measurements can be used to validate Monte Carlo codes and nuclear data through direct calculation of subcritical quantities. Subcritical measurement methods can also be used to determine the subcriticality of fissile materials in-situ. This requires measurements to be performed and subsequent analyses of the measurements to determine the subcritical k_{eff} value. Subcritical measurement methods can also be used to monitor the reactivity of a fissile operation. The purpose of reactivity monitoring would not be to provide a highly precise k_{eff} value for the fissile operation but to provide an indication of a change in reactivity and when this change exceeds a specified threshold. This paper addresses the areas of subcritical benchmarking, in-situ subcritical measurements, and subcritical monitoring. Descriptions of the various applications are provided along with the issues and challenges in applying subcritical measurement methods. Finally, recommendations for resolving the issues and challenges for implementation of subcritical measurements are discussed.

Keywords: subcritical, benchmarking, in-situ, monitoring, noise analysis

1. INTRODUCTION

Subcritical measurements methods have many more applications than simply serving as indicators of the approach to critical. Subcritical measurements can serve multiple functions that include using them as benchmark measurements, as a means to determine the subcriticality of fissile materials in-situ, and as a method to monitor the reactivity for fissile material operations. These applications are related to each other but require slightly different approaches to implement the measurements and different levels of knowledge about the system being measured are needed.

The source-driven noise analysis measurement[1] is one subcritical measurement method that has several advantages as compared to other subcritical measurement techniques and has been applied to benchmark measurements and for the determination of the subcriticality of fissile configurations. Measurements have also been performed to investigate the use of this method as a reactivity indicating measurement.

This paper provides a brief description of the subcritical source-driven noise analysis measurement in Section 2. A description of how this method is used to benchmark Monte Carlo codes and nuclear data is provided in Section 3. Application of this measurement for in-situ reactivity measurements is provided in Section 4, while the use of this method as a reactivity monitor is provided in Section 5. Some concluding remarks are provided in Section 6 that include recommendations for extensions of subcritical measurement methods.

2. SOURCE-DRIVEN NOISE ANALYSIS MEASUREMENTS

The subcritical source-driven noise measurement[1] (known as the ^{252}Cf-source-driven noise analysis method) evolved from a simultaneous randomly pulsed neutron measurement and the Rossi-α measurement as an attempt to overcome some of the limitations of other subcritical measurement methods. Other subcritical measurement methods require a calibration measurement at delayed critical or knowledge of the effective delayed neutron

fraction to determine the neutron multiplication factor, k_{eff}. Additionally, many of these methods required some knowledge of the detection efficiency or source intensity to determine k_{eff}. A certain spectral ratio from the source-driven noise measurement can be directly related to the subcritical reactivity without need for a calibration measurement at delayed critical.

The source-driven noise measurement is based on simultaneous performance of the randomly pulsed neutron and Rossi-α measurements. The source-driven noise measurement differs from other subcritical measurements in that the data acquisition is actually performed using Fourier processors. The measurement involves the use of two or more detectors and a timed neutron source. The correlation of the various time dependent signatures is performed in the frequency domain over a time period specified by the data acquisition software. The frequency dependent signatures that are acquired include auto spectra and cross spectra. The simplistic point reactor kinetics models can be used to describe the time-evolution of neutrons in a fissile system and to determine the dependence of the various auto and cross spectra on the properties of the fissile system. The source-detector cross spectra $(S_{SX}(\omega))^2$ can be defined as

$$S_{SX}(s) = \frac{\varepsilon_s \varepsilon_1 \overline{\nu}_0 F_s}{\overline{\nu}\Lambda} \frac{1}{(j\omega + \alpha)}. \tag{1}$$

In this expression, s is the frequency variable, α is the prompt neutron decay constant, F_s is the average fission rate of the source, ε_s is the efficiency for detecting the source event, ε_1 is the detector efficiency in counts per fission, $\overline{\nu_0}$ is the average number of neutrons from the source, $\overline{\nu}$ is the average number of neutrons from fission, and Λ is the neutron generation time. The detector-detector cross spectrum $(S_{xy}(\omega))^2$ is

$$S_{xy}(\omega) = \frac{\varepsilon_1 \varepsilon_2}{(\overline{\nu}\Lambda)^2} \left[\overline{\nu(\nu-1)} \frac{\overline{\nu_0} F_s}{\alpha\Lambda} + \overline{\nu_0(\nu_0 - 1)} F_s + \overline{\nu(\nu-1)} \frac{\overline{\nu_I} F_I}{\alpha\Lambda} + \overline{\nu_I(\nu_I - 1)} F_I \right] \bullet \frac{1}{(\alpha^2 + \omega^2)}. \tag{2}$$

In this expression, ε_1 is the detector efficiency in counts per fission for the first detector, ε_2 is the detector efficiency in counts per fission for the second detector, $\overline{\nu_0}$ is the average number of neutrons from the source, $\overline{\nu}$ is the average number of neutron from fission, $\overline{\nu_I}$ is the average number of neutrons from an inherent source, $\overline{\nu(\nu-1)}$ is the reduced second moment of the neutron emission distribution for fission, $\overline{\nu_0(\nu_0 - 1)}$ is the reduced second moment of the neutron emission distribution for ^{252}Cf spontaneous fission, $\overline{\nu_I(\nu_I - 1)}$ is the reduced second moment of the neutron emission distribution for the inherent source, and F_I is the spontaneous fission rate of the inherent source. The detector-detector cross spectrum defined by Eq. 2 is the frequency domain equivalent of the two-detector Rossi-α measurement. The detector auto spectrum $(S_{xx}(\omega))^2$ is given by

$$S_{xx}(\omega)=\frac{\varepsilon_1\varepsilon_1}{(\bar{\nu}\Lambda)^2}\left[\overline{\nu(\nu-1)}\frac{\overline{\nu_0}F_s}{\alpha\Lambda}+\overline{\nu_0(\nu_0-1)}F_s+\overline{\nu(\nu-1)}\frac{\overline{\nu_I}F_I}{\alpha\Lambda}+\overline{\nu_I(\nu_I-1)}F_I\right]$$
$$\bullet\frac{1}{(\alpha^2+\omega^2)}+\varepsilon_1\left[\frac{\overline{\nu_0}F_s}{\alpha\Lambda}+\frac{\overline{\nu_I}F_I}{\alpha\Lambda}\right]. \tag{3}$$

The most significant advantage of the source-driven noise measurement is that a certain ratio of frequency spectra can be obtained that does not depend on detection efficiency. The detection efficiency is stated in terms of counts per fission and is not directly measurable. The spectral ratio of interest is defined as[2]

$$R(\omega)=\frac{S^*_{sx}(\omega)S_{sy}(\omega)}{S_{ss}(\omega)S_{xy}(\omega)}. \tag{4}$$

The term S_{sx} is the source-detector cross spectrum between the source s and the detector x. The asterisk denotes taking the complex conjugate of the source-detector cross spectrum, S_{sx}. The term S_{sy} is the source-detector cross spectrum between the source s and the detector y. The term S_{xy} is the detector-detector cross spectrum between detectors x and y. The term S_{ss} is the source auto spectrum and is simply equal to the source efficiency times the source fission rate ($S_{ss}=\varepsilon_s F_s$). The spectral ratio that includes an inherent source is of particular interest for interpreting measurements for spent nuclear fuel applications or for systems with significant amounts of plutonium. The spectral ratio including an inherent spontaneous fission source is expressed as

$$R(\omega)=\frac{\varepsilon_s\overline{\nu_0}}{\left[\frac{\overline{\nu(\nu-1)}}{|\rho|}+\frac{\overline{\nu_0(\nu_0-1)}}{\overline{\nu_0}}+\frac{\overline{\nu(\nu-1)}}{|\rho|}\frac{F_I}{F_s}+\frac{\overline{\nu_I(\nu_I-1)}}{\overline{\nu_I}}\frac{F_I}{F_s}\right]}. \tag{5}$$

As can be seen from Eq. 5, the spectral ratio that includes the effects of an inherent spontaneous fission source depends on the ratio of the inherent spontaneous fission rate to the ^{252}Cf source fission rate. These expressions are similar to those derived by others except that spatial correction factors and importance functions have been omitted in these equations. This dependence can be included in the appropriately weighted cross sections and neutron emission probabilities. The actual use of such expressions to interpret the measurements is quite limited and a more general approach using the Monte Carlo method has been developed that does not have the limitations of the point reactor kinetics models.[2] The expressions are only provided to provide an indication of how the various frequency spectra relate to the reactivity of a fissile system.

3. BENCHMARKING MONTE CARLO CODES

The use of subcritical measurements as a means to validate Monte Carlo codes and nuclear data substantially increases the reactivity and neutron spectrum regimes over which the codes and data are validated. In fact, subcritical benchmark measurements are the key to determining whether the code bias; i.e. the difference between measured and calculated reactivity indices, is a function of the degree of subcriticality. Subcritical measurements can be used to validate Monte Carlo codes and nuclear data through direct calculation of the measured quantities. Alternatively, the Monte Carlo codes and nuclear data can be validated from the k_{eff} value determined from the measurements. Interpretation of measurements

requires a model to relate what is measured to the neutron multiplication factor. In the past, the subcritical measurements were interpreted using equations developed from point kinetics models for the time-dependent behavior of neutrons in the subcritical configuration. This limited the application of the measurement to situations in which point kinetics was applicable. The most general model to relate the measured quantities to k_{eff} would involve the use of the generalized stochastic model developed by Munoz-Cobos et al.[3] Although an analytical solution of subcritical measurements in terms of the stochastic model is not practical, the Monte Carlo method provides a means to simulate the subcritical measurements and to also calculate the neutron multiplication factor. In fact, the same Monte Carlo code and nuclear data can be used for both calculations.

The Monte Carlo code MCNP-DSP[4] was developed to simulate a variety of subcritical measurements. MCNP-DSP can be used to directly calculate the frequency dependent spectra from the source-driven noise analysis measurement. Furthermore, MCNP-DSP can be used to determine k_{eff} using a perturbation method. The Monte Carlo codes are used to interpret the measurement by performing a calculation of the measured parameters and a separate eigenvalue calculation. For example, a comparison of measured and calculated values of the spectral ratio can be used to obtain the "experimental" k_{eff}. If the measured and calculated values of the spectral ratio are in agreement, then the bias in the spectral ratio is zero. The bias in the spectral ratio is defined as the difference between measured and calculated values of the spectral ratio (R_m-R_c) where R_m is the measured value and R_c is the calculated value. First order perturbation theory can be used to obtain an expression that can be used to determine the "experimental" k_{eff} and the bias in the k_{eff}. The low-frequency value of the spectral ratio has been shown in numerous experiments to be linear with k_{eff} over a wide range of values of k_{eff} with the values of k_{eff} being interpreted using point kinetics models. Given the linear dependence of the spectral ratio with k_{eff}, the bias in the spectral ratio varies linearly as the bias in k_{eff} (k_m-k_c). To determine the "experimental" k_{eff} value and its bias, the Monte Carlo models are slightly perturbed and new values of the spectral ratio (R_p) and k_{eff} (k_p) are obtained. If the linear dependence is valid, then the perturbation calculations can be used to obtain the "experimental" k_{eff} and its bias using the following linear relationship:

$$\frac{R_m - R_c}{k_m - k_c} = \frac{R_p - R_c}{k_p - k_c}. \tag{6}$$

This methodology simply uses a linear interpolation or extrapolation between the standard and perturbed values of the spectral ratio and k_{eff} to determine the "experimental" k_{eff}. Using this relationship, the value of k_m can be determined along with its bias k_m-k_c. Propagation of error is used to obtain the uncertainty in k_m and its bias. Even if the measured spectral ratio value and the calculated value agree, the perturbation analysis is performed. This is required to equate the uncertainty in the measured spectral ratio to the uncertainty in the inferred k_{eff} value.

This methodology has been successfully applied to benchmark source-driven noise measurements with uranyl nitrate solutions. The analysis of these measurements have been documented in the Handbook of the International Criticality Safety Benchmark Evaluation Project.[5] In the analysis of the uranyl nitrate solution experiments, a variety of perturbations were used to interpret k_{eff} and a variety of nuclear data sets used in the interpretations. The results demonstrated that the interpreted k_{eff} was independent of the perturbation method and had a very slight dependence on the nuclear data set. The interpreted (experimental) k_{eff} values for each different cross section data set are presented in Table I. As can be seen in this table, the interpreted k_{eff} values differ slightly depending on which cross section data set was used.

A general trend is observed that the interpreted k_{eff} values obtained using the ENDF/B-V cross section data are consistently higher than the interpreted values obtained from the ENDF/B-VI and JENDL-3.2 cross section data sets. The largest difference between the interpreted k_{eff} values among the results produced using the three different cross section data sets is approximately 0.003 Δk.

Table I. Interpreted experimental k_{eff} values for ENDF/B-V, ENDF/B-VI, and JENDL-3.2 cross section data sets for the high-enriched uranyl nitrate solution experiments.

Solution Height (cm)	ENDF/B-V "Experimental" k_{eff}	ENDF/B-VI "Experimental" k_{eff}	JENDL-3.2 "Experimental" k_{eff}
30.48	0.9631 ± 0.0052	0.9602 ± 0.0052	0.9610 ± 0.0050
27.94	0.9448 ± 0.0045	0.9430 ± 0.0045	0.9432 ± 0.0041
25.40	0.9229 ± 0.0052	0.9215 ± 0.0050	0.9204 ± 0.0056
22.86	0.8889 ± 0.0051	0.8888 ± 0.0048	0.8883 ± 0.0055
20.32	0.8582 ± 0.0055	0.8580 ± 0.0061	0.8571 ± 0.0052
15.24	0.7464 ± 0.0167	0.7511 ± 0.0200	0.7507 ± 0.0234

4. IN-SITU SUBCRITICAL MEASUREMENTS

The second area of applicability of subcritical noise measurements is for in-situ determinations of the subcritical neutron multiplication factor. The two ways that this can be achieved is by post analysis of the measurements using the Monte Carlo method previously described or by using the limited point reactor kinetics models to relate the measured quantity to the subcritical neutron multiplication factor. The latter method should only be considered if an on-line determination of k_{eff} is desired. In such applications, care must be taken to properly select the location of the source and detectors such that the point kinetics models are applicable. Furthermore, calculations of spatial correction factors and importance ratios are also required and must be supplied to the point reactor formulas to determine k_{eff}. The use of point reactor kinetics is discouraged because uncertainties in correction factors contribute directly to the uncertainty in the reactivity estimates. The Monte Carlo method is the preferred way to interpret the measurements because of the limitations of the point reactor models and because correction factors do not have to be computed.

In-situ subcriticality measurements performed at the Oak Ridge Y-12 Plant in Vault 16 demonstrated that these types of measurements are practical[6]. In these measurements, the subcriticality of an array of high-enriched uranium metal castings inside a concrete storage vault was determined using the Monte Carlo method. Measurements were performed with the source and detectors placed inside the array. The source was located in the center of the central casting and the detectors were placed on the periphery of the array. Prior to performing the noise measurements, flux profile measurements were performed to determine an array size that would approximate the results expected if the array was infinite. The detectors were placed on the outside of the essentially infinite array. The noise measurements were performed over many weeks to obtain statistically converged spectra because of the low coherence values. The measurements were interpreted using MCNP-DSP simulations. These simulations were also performed over several weeks. The Monte Carlo models contained as much detail as possible about the storage vault configuration; however, the composition of the concrete storage vault was not known. The analyses were performed assuming that the concrete was dry or wet. The resulting k_{eff} value obtained from the analyses did not depend on the exact knowledge of the concrete composition. Although the concrete composition was not exactly known, the concrete vault was 25 years old and should have been comprised of dry

concrete. Coincidentally, the calculated spectral ratio value for the dry vault agreed within one standard deviation of the measured value. The Monte Carlo models included as much detail as possible concerning the storage vault geometry and composition. The storage trays were modeled in great detail, as were the uranium metal castings. The composition of the storage trays, detectors, and the castings were well known and included in the models. Although the interpreted k_{eff} value for the HEU storage vault does not depend on the composition of the concrete, all other details about the measurement are known. The success of the interpretation of the HEU storage vault measurements occurs because the spectral ratio depends only on the induced fission events from the ^{252}Cf source. A significant inherent neutron source does not exist in this configuration.

The MCNP-DSP computed k_{eff} values and spectral ratio values for these measurements are provided in Table II along with the interpreted k_{eff} values from the perturbation analysis. Perturbations were made to various components of the vault and the subsequent interpreted k_{eff} values did not depend significantly on the perturbation. In fact, the assumption that the concrete was wet is a rather large perturbation as compared to the assumption that the concrete is dry. Even though large perturbations are necessary for the wet concrete model, the interpreted k_{eff} values are statistically equivalent. This application of the perturbation methodology demonstrates the robustness of the model. The success in the interpretation is due in great part to the fact that detailed information is known about the major components of this system with only the concrete composition being the major unknown in the measurements. If the vault system had a significant inherent source, the interpretation would have been further complicated because the inherent source may not permit a unique one-to-one relationship between the spectral ratio and k_{eff}.

Table II. MCNP-DSP calculated spectral ratio and k_{eff} values and interpreted k_{eff} values for HEU storage vault in-situ measurements.

Concrete Condition	Calculated Ratio (R_c)	Calculated k_{eff} (k_c)	Perturbation	Interpreted k_{eff}
Dry	0.3894 ± 0.0027	0.7920 ± 0.0005	Hydrogen content	0.7888 ± 0.0068
			^{235}U enrichment	0.7902 ± 0.0041
			Casting length	0.7901 ± 0.0045
Wet	0.5004 ± 0.0151	0.7354 ± 0.0005	Casting inner radius	0.7798 ± 0.0054
			Reduced concrete density	0.7945 ± 0.0068

[a]Measured spectral ratio (R_m) is 0.395 ± 0.012.

5. SUBCRITICAL MONITORING

Another useful application of subcritical noise measurements is to provide a way to monitor fissile material processing operations. This application would not focus on determining the subcritical neutron multiplication but would use the measured quantities as a way to ascertain normal operation. The enhanced sensitivity of the subcritical noise measurement would allow fissile processing operations to be monitored and controlled using the changes in spectral signatures as indicators to changes in the system. The spectral ratio is an ideal candidate for process monitoring because it is independent of detection efficiency and would not change due to drifts in the electronic system. Measurements and Monte Carlo simulations of a process condition could be performed to provide bounding values for the spectral ratio. The measured spectral ratio values could be equated to k_{eff} values for various operating conditions. Changes in the spectral ratio value could be monitored and used to ensure that the reactivity of the system remains below some desired value. This would enhance safety in operations with fissile material by providing some means estimate the

subcriticality of the fissile process. If the system is simple enough and the geometry is appropriate, then the point reactor kinetics models could possibly be used to provide an on-line estimation of k_{eff}; however, great care would need to be taken to properly estimate the uncertainty on the k_{eff} value from the point reactor kinetics model to ensure that the limits on the fissile operation can be properly constrained.

The greatest challenge in applying subcritical measurements for process monitoring is to measure a quantity that does not depend on changes in the detection system such as detector efficiency or dead time, on changes in any inherent neutrons sources that are capable of inducing fission, and on source intensity. The spectral ratio from the source-driven noise analysis measurement satisfies two of these criteria. However, the spectral ratio as shown in the simplistic models in Eq. 5 is dependent on the inherent sources. If the contribution of the inherent source to the spectral ratio is significant, then care must be taken to provide an indication of the change in the inherent neutron sources in the process. To circumvent this limitation, a modified spectral ratio termed the bi-spectral ratio could be acquired. The bi-spectral ratio depends only on induced fission events caused by the ^{252}Cf source and is independent of the source detection efficiency has been developed that requires the measurement of higher-order correlation functions[7]. These higher-order correlation measurements have yet to be applied to subcriticality measurements, but they have been theoretically shown to possess higher sensitivity to reactivity and are independent of all inherent sources. The bi-spectral ratio is closely related to the standard spectral ratio; however, the bi-spectral ratio involves only events correlated with the timed neutron source. The summary provided in this section follows directly from the developments of Mattingly[7]. The bi-spectral ratio is defined as

$$\Psi_{XY|S} = \frac{S_{SX}(0)S_{SY}(0)}{\bar{s}S_{SXY}(0,0)} = \frac{\overline{\nu_0}}{\dfrac{\overline{\nu_0(\nu_0-1)}}{\overline{\nu_0}} + \dfrac{\overline{\nu(\nu-1)}}{\bar{\nu}|\rho|}}. \tag{7}$$

In this expression $\bar{s}$ is the average source fission rate. The bi-spectral ratio is essentially equivalent to the standard spectral ratio for systems but is independent of the source detection efficiency, the detector efficiency, or an inherent source. This measurement requires pulse neutron measurements to be performed with two detectors. In addition, the bi-spectral ratio requires the correlation of the response of two detectors with the neutron source. This measurement can be thought of as a dual pulse neutron measurement. This measurement is only dependent on fission chains initiated by the neutron source and hence would be more generally applicable to in-situ measurements with plutonium and irradiated nuclear fuels. For systems close to delayed critical, the standard spectral ratio will be dependent on the delayed neutrons that will behave as an inherent neutron source. However, the bi-spectral ratio will not be affected by delayed neutrons and hence would be more useful for systems close to delayed critical. In theory, the bi-spectral ratio can be measured up to prompt critical. An equivalent signature can be acquired in the time domain by performing a three-way coincidence measurement between a timed neutron source and two detectors while at the same time performing two two-way coincidence measurements between the source and each detector. A time dependent signature could be acquired by varying the gate of the coincidence period. A ratio of the two source-detector coincidence measurements to the three-way coincidence measurement times the source detection efficiency would produce a quantity similar to the bi-spectral ratio that should also be independent of inherent neutron sources.

6. SUMMARY

Subcritical measurements can serve multiple functions. The measurements are ideal for use as benchmark measurements because many subcritical measurements such as the Rossi-α, noise analysis, and Feynman variance can be simulated using Monte Carlo codes. Quantities from the source-driven noise analysis measurements have been shown to be more sensitive to nuclear data than direct calculation of k_{eff} thereby making the simulation of the source-driven noise analysis measurements more applicable for testing Monte Carlo methods and nuclear data. Subcritical measurements can also be used to interpret in-situ applications. In this regard, the measurements are applied to determine k_{eff}. A model that relates the measured quantity to k_{eff} is used to interpret the measurements and should be fairly robust. Source-driven noise measurements have been performed to determine the subcritical reactivity of high-enriched uranium metal in storage configurations. These measurements demonstrated that the k_{eff} value could be determined without exact knowledge of all constituents of the storage vault. However, the success of the use of measurements for in-situ verifications is highly dependent on whether or not an inherent neutron source is present. The presence of an inherent source complicates the interpretation of the measurements and may limit the application of the measurements. The use of subcritical measurements as reactivity monitors is also feasible. For process monitoring applications, the subcritical measurement quantities should be evaluated for the limits of the standard operating conditions to equate the expected value of the subcritical measurement quantity to k_{eff}. The spectral ratio from the source-driven noise analysis measurement is an ideal candidate for process monitoring because this quantity does not depend on the source strength or changes in the detection system. However, the spectral ratio is dependent on inherent neutron sources that may change the spectral ratio value although the reactivity state may not have changed. For systems with an inherent neutron source, a signature that is independent of the inherent source such as the bi-spectral ratio or a multi-way coincidence measurement must be performed if the addition of the inherent neutron source is outside of the standard operating conditions. A detailed model such as the Monte Carlo method must also be used to equate the subcritical measured quantity to k_{eff} if k_{eff} is to be the monitoring parameter.

References

1. V. K. Paré and J. T Mihalczo, "Reactivity from Power Spectral Density Measurements with Californium-252," *Nucl. Sci. Eng.* **56**, 213 (1975).
2. T. E. Valentine, *Review of Subcritical Source-Driven Noise Analysis Measurements,* ORNL/TM-1999/288, Lockheed Martin Energy Research Corp., Oak Ridge National Laboratory, November 1999.
3. J. L. Muñoz-Cobo and G. Verdu, "*Neutron Stochastic Transport Theory with Delayed Neutrons,*" Annals Nuclear Energy **14**, 7,327 (1987).
4. T. E. Valentine, "MCNP-DSP Users Manual", ORNL/TM-13334-R2, Oak Ridge Nat. Lab, October 2000.
5. "International Handbook of Evaluated Criticality Safety Benchmark Experiments," NEA/NSC/DOC (95) 03, Nuclear Energy Agency, Organization for Economic Cooperation and Development (Sep. 2000).
6. J. T. Mihalczo, T. E. Valentine, L. D. Phillips, "Subcritical Measurements for a HEU Storage Vault at the Y-12 Plant Using the ^{252}Cf-Source-Driven Frequency Analysis Method," *Nuclear Safety*, **38**, 1, January-March 1997.
7. J. K. Mattingly, "High Order Statistical Signatures from Source-Driven Measurements of Subcritical Fissile Systems," Ph.D. Dissertation, University of Tennessee, Knoxville, Tennessee, August 1998.

JP0250295

JAERI-Conf 2002-004

STATUS OF THE FETCH TRANSIENT CRITICALITY CODE AND APPLICATION TO TRACY DATA AND DOSIMETRY APPLICATIONS

C C Pain, Y Yamane*, C R E de Oliveira and A J H Goddard

Computational Physics and Geophysics Group,
Department of Earth Science and Engineering,
Imperial College of Science, Technology and Medicine,
Prince Consort Rd, London, SW7 2BP, U.K.
** JAERI Visiting Fellow*
email: c.pain@ic.ac.uk

1. INTRODUCTION

This paper describes the current status of the FETCH coupled, transient, criticality/multi-phase flow model and outlines recent applications. The FETCH model has been developed to model criticality transients in multi-phase media (see [3, 4, 5]) and is applied here to fissile solution transient criticality. We describe, primarily, research on the application of the FETCH code to modelling three TRACY transients with step reactivity insertions of 2$, 2.5$ and 2.8$.

Previous work (focussing mainly on SILENE data) has demonstrated the ability of FETCH to achieve satisfactory agreement with measured power and pressures for high powered transients initiated by a step reactivity change. For transients over 1$ and less than 3.5$, and for short times relative to heat losses, detailed features are determined by radiolytic gas evolution. These solutions are typically highly enriched and have relatively low uranium concentrations. The solutions used in TRACY, on the other hand, are of a lower uranium enrichment and higher concentrations. We have investigated if FETCH can be used to predict TRACY data using the fundamental parameters (determining rate and quantity of radiolytic gas production) that were obtained when matching FETCH with SILENE pressure data, see [3]. In addition, the sensitivity of the TRACY simulations to these parameters is examined.

To complement modelling the behaviour of TRACY over short times, we also investigate its behaviour over 10's of seconds after the initial pulse - still in a time range where heat transfer out of the system is of minor significance. It is shown that there can be a second fission peak some 10 to 30 seconds after the initial peak and that the time evolution of this peak is determined by the assumed radiolytic gas bubble size used in the gas-liquid drag laws.

We conclude the paper with a short discussion of the use of FETCH in modelling dosimetric quantities, based on results from a transient analysis. That is, predicting the dose to various organs for a worker

located at a particular position relative to the vessel in question.

2. SUMMARY OF MODELLING APPROACH

In this section the approach to solving the radiation transport and multi-phase fluid equations [5] is discussed. The three fluids conservation equation sets cover mass, momentum and thermal energy. The mass equation represents the void fraction, densities and velocities of liquids in given phases and also allows the position of a free surface to be tracked. In addition to momentum transfer terms between phases, the momentum equation has terms for interfacial pressure and drag forces, virtual mass and lift [5]. Buoyancy forces evolve naturally on the appearance of temperature differences and radiolytic gas bubbles in the system.

Scalar field equations include those for delayed neutron precursors and dissolved radiolytic gas concentration. Delayed neutron precursors are assumed to exist only in the liquid phase and are in six delayed neutron precursor group form. The continuity equation for the liquid depends on an equation of state embodying the response of liquid density to pressure and temperature (via the speed of sound and the expansion coefficient respectively). This, together with the use of the ideal gas equation, for each of the constituent gases, allows the pressure to be calculated for both compressible and incompressible flow. Boundary conditions are those associated with no normal flow at the walls of the container and perfect slip for both the liquid and gas phase. At the top-most boundary of the domain we specify the temperature, density and pressure (atmospheric) for the inflowing gas. The boundary conditions for gas outflow are specified normal and zero shear stress conditions. The finite element discretisation and solution of the multi-phase flow equations are described in [1].

The Boltzmann neutron transport equations are solved using the even-parity principle, see [6]. To discretise the equations we have used finite elements in space, PN approximations in angle, finite difference in energy and a two level discretisation in time. In the examples shown six energy groups are used. The associated material cross sections are obtained by interpolating group condensed (by WIMS [7]) cross section sets in voidage and temperature, see [5]. Also the P1 approximation in neutron angle direction is used here.

3. SIMULATION RESULTS

The fuel has the following properties: The enrichment is 10% U_{235}; nominal 400g U /litre; a nitric acid molarity of 0.7 and an initial temperature of 25.5 Deg. C. The vessel consists of a stainless steel lined annulus, and the central region contains a control rod which is ejected, in the experiment, to produce the required reactivity insertion. The geometry of TRACY is described in [2]. A summary of the comparison of TRACY experiments with FETCH simulations is shown in 1.

3.1 Physics of the initial fission pulse

As the power rises it has a doubling time which is dictated largely by β_{eff} and at this stage the dynamics have no non-linear feedback mechanism. However when the solution temperature rises the negative coefficient terminates the rise. Around this maximum, radiolytic gas bubbles start to be produced in the solution. On comparing the maximum fission rate curves with and without radiolytic gases from FETCH, see figure 1(a), it is seen that gas feedback reduces the fission rate maximum by about 15%. Shortly after the maximum, radiolytic gas evolution becomes more important and quickens the decrease in the fission rate, significantly effecting the total yield in the first fission peak.

We have performed simulations with various quantities of radiolytic gas produced per fission (G value) of G=0.6 and G=1.5 (number of hydrogen molecules per 100 eV). The latter simulation seems to match the experimentally observed fission rate after the initial fission pulse and is the default value used here. However, it should be noted that the decrease in FETCH fission rate is slightly more rapid than that shown in the experiment. This can only be partly due to the relatively large time delay (some 0.01 s) of the fission rate sensor in the experiment when the fission rate is decreasing, see [2]. Most of the discrepancy implies that, in the model, too much radiolytic gas is produced at the trailing edge of the fission pulse. However, decreasing this quantity, that is slowing down the rate of bubble production, decreases the maximum pressure and reduces the agreement of the modelled pressure pulse with the experiment. This seemingly contradictory behaviour requires further study.

From the modelled pressure trace, shown in figure 1(b), for the 2.0 $ step case, it is evident that, in this simulation, much of the gas deposited is trapped in the liquid and therefore undergoes pressure oscillations which are damped due to viscous damping and the rise and bursting of radiolytic gas bubbles out of the liquid. This oscillatory expansion contraction of a pocket of gas bubbles also manifests itself in the modelled fission rate curve, figure 1(b), just after the large fission spike. For the higher powered 2.5 $ and 2.8 $ step transients, much of the gas quickly escapes the system and thus there is not a high frequency pressure oscillation, see figures 2(a).

The pressure and fission rate for the 2$ and 2.8$ step reactivity simulations are shown in figure 1(b), 2(a). The time axis has been shifted to match the maximum fission rate of the experiment. The following correlation is used to calculate the rate of radiolytic (hydrogen) gas mass produced in the form of bubbles:

$$F_l^c = h(C_l - C_0)\alpha_l N(C_l - \hat{C}_0)^n (C_l - C_0). \tag{1}$$

C_l is the concentration of radiolytic gas dissolved in the solution, C_0 is the critical concentration at which radiolytic gas bubbles start to appear in the solution [3], $\hat{C}_0$ is the concentration at the bubble surface for a bubble 2×10^{-5} cm in diameter in thermodynamic equilibrium, α_l is the liquid volume fraction

and $h(C_l - C_0)$ is the heavy side function. The sensitivity of the parameters n and N to the resulting pressure are shown along with the experimentally observed pressures in figures 2(b) 3(a),(b). The default parameters here are $n = 3$ and $N = 4.71 \times 10^{16}$ which were obtained in [3].

3.2 Dynamics after the initial fission pulse

Various fields modelled at 30 seconds into the simulation, for 2$ and 2.8$ step reactivity insertions, are shown in figures 6 and 7 respectively. In the temperature and 'longest lived delayed precursor' fields we can see the mixing associated with the overturning of the fluid. In addition, the power at 30 seconds is shown in the shortest lived delayed neutron group and shows a slight displacement of the peak power away from the central region (on the left) in which there is a void surrounded by steel.

The fission rate versus time curves for the 2$ and 2.8$ step reactivity insertion simulations are shown in figure 8(a). It is seen that there is a second fission peak which occurs at about 10 seconds in figure 8(a) following an increase in criticality of the system. This is due to the the rise of the bubbles out of the system. All simulations conducted here were performed with a bubble diameter of 0.5 mm. The exceptions to this have results shown shown in figure 8(a) in which we have repeated the 2.8$ step insertion simulation with bubble sizes of 0.2mm and 0.3mm. As expected the smaller the bubble size the longer it takes for the bubbles to rise out of the system and produce a second fission peak. The gas volume fraction in the solution is relatively small, see 7(a) for example. Thus the bubbles are fairly isolated and thus rise out of the system at approximately terminal velocity, with only a small swarm correction for the surrounding bubbles. In addition, the convoluted path the bubbles take to the free surface further increases the time they take to reach the surface. Thus the time to reach the surface is approximately twice that one would expect if they were isolated and were to rise vertically in a liquid at rest.

The overturning of the fluid can also been seen in figure 8 (b),(c) which shows the temperature at 3 detectors place in the liquid at 21 cm away from the central axes and in a vertical line at heights of 5 cm, 25cm and 45cm above the bottom of the liquid filled vessel. The maximum temperature versus time is also shown in figures 8(b),(c). The temperature graphs show in general the gradual equalisation of the temperature distribution, which is also evident in the temperature fields shown in figures 6(b) and 7(b).

4. 3-D modelling

We expect that at some point during the transients studied here the flow will break its axi-symmetry and become fully three dimensional. This is expected to occur shortly after the the radiolytic gases are initally deposited in the solution and at the stage when the mass of radiolytic gas bubbles, which initially take up a toroidal shape, start to rise to the free surface. Thus although the dynamics of the first pulse will be largely axi-symmetic this will not be the case subsequently. The exploration of 3-D aspects of the flow and its effect on power and pressures is currently underway.

5. Application of FETCH to dosimetry.

We have applied FETCH in a simplified, exploratory, study of the neutron dosimetry of worker A - who received the largest dose during the JCO Company criticality incident. This dose was received mainly in the first few seconds of the ensuing nuclear criticality transient (the 'burst' period). In addition to the multi-organ dosimetry of worker A, this work provides a method of helping to evaluate the yield in the initial phase of the criticality incident. This can be used to calibrate kinetic simulations which aim to investigate the physics behind the incident.

FETCH simulations of the accident [10] have yielded transients representing the time variation of fission rate within the tank.

The radiation transport code EVENT [6] was then used to find information concerning the flux within the uranyl nitrate solution due to each of the energy groups. The aim was to relate the steady- state fission rate to the flux at a series of 'pixels' at points outside the water jacket representing the locations of body organs. Ray-tracing techniques in the void combined with various neutron angular approximations ranging from P1 to P5 yield a value for the mean flux, ϕ', in each of the pixels due to each energy group. This relationship was converged for the P5 angular flux approximation, and were used to calibrate the FETCH modelled power distribution during the burst period to yield the fluence at each pixel. Conversion factors take into account the neutron cross section properties and energy dependence of the damage to the various organs. These were taken, assuming antero posterior geometry (AP) from ICRU report 57 ([8]).

The doses calculated to the various organs compare well with whole body doses estimated (see [9]) at between 16 Gy Eq and 20 Gy Eq calculated from the worker A's symptoms, lymphocyte counting, chromosome analysis and 24-Na activation. In addition the Tokai-Mura tank was modelled in good geometrical detail which has enabled us to show the influence of the vessel and moderating water jacket on the spatial variation of the dose. For example, the dose to the head was found to be particularly large due to the energy spectrum of the impinging radiation - the faster neutrons resulting in more biological damage. The comparison between modelling and published dose estimates indicates that the number of fissions to which worker A was exposed was approximately 7×10^{16}.

Aknowledgments

This research has been supported in part by the UK Health and Safety Executive (Nuclear Installations Inspectorate). We would like to thank Toshihiro Yamamoto and Ken Nakajima for providing advice on the TRACY simulations. However, the opinions expressed are those of the authors alone.

Table 1: Summary of FETCH (FETCH) simulations of TRACY (TRACY) experiments - comparison of results.

Case	K_{eff} -1 $	max Power(MW)	Max. pressure bars
R54 TRACY	2.0	500	2.6
R54 FETCH	2.0	470	2.6
R55 TRACY	2.5	900	5.4
R55 FETCH	2.5	880	4.3
R56 TRACY	2.8	1200	7.3
R56 FETCH	2.8	1193	5.3

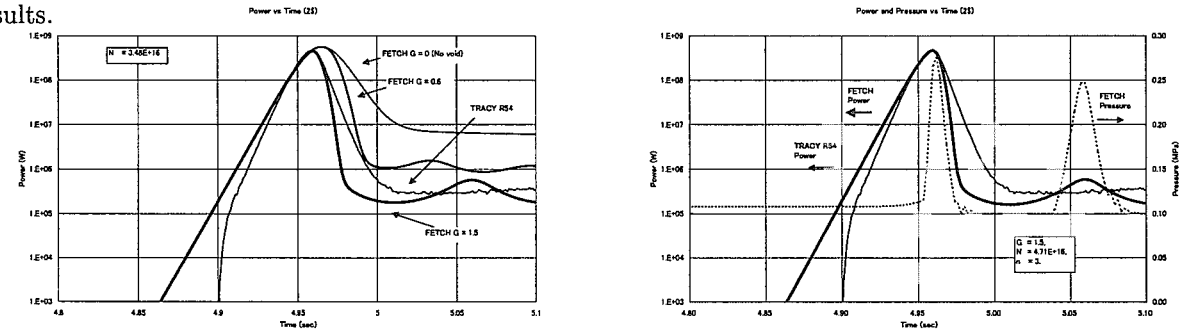

(a) $ 2.0 step variable G (b) $ 2.0 step

Figure 1: Simulated $ 2.0 step reactivity insertion. (a) fission rate for various quantities of gas production (G value). (b) pressure and fission rate.

References

[1] C C Pain, S Mansoorzadeh, C R E de Oliveira, A J H Goddard, 'Numerical Modelling of Gas-Solid fluidised beds using the two-fluid approach', International Journal of Numerical Methods in Fluids. 36, 91-124, (2000).

[2] H.Yanagisawa, A.Ohno, K.Ogawa, E.Aizawa, M.Yokoyama, 'Time Delay of Thermal Neutron Detection during Power Burst in TRACY', Nuclear Science and Engineering, 38, NO. 8, 591-599, (2001).

[3] C C Pain, C R E de Oliveira, A J H Goddard, A P Umpleby, 'Transient criticality in fissile solutions - compressibility effects', Nuclear Science and Engineering, 138, NO. 1, 78-95, 2001.

[4] C C Pain, C R E de Oliveira, A J H Goddard, A P Umpleby, 'Criticality behaviour of dilute plutonium solutions', Nuclear Technology, 135, NO. 3, 194-215, 2001.

[5] C C Pain, C R E de Oliveira, A J H Goddard, 'Non-Linear Space-Dependent Kinetics for Criticality Assessment of Fissile Solutions' , Progress in Nuclear Energy, 39, 53-114, (2001).

[6] C. R. E. de Oliveira, 'An Arbitrary Geometry Finite Element Method for Multigroup Neutron Transport with Anisotropic Scattering', Prog. in Nuclear Energy, 18, 227 (1986).

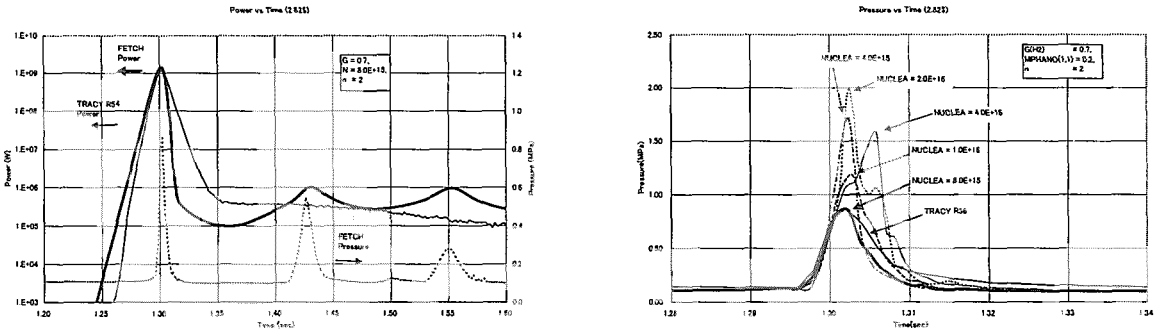

(a) pressure and power (fission rate) (b) assessment of nucleation

Figure 2: Simulated \$ 2.8 step reactivity insertion. (a) pressure and fission rate. (b) assessment of nucleation rate parameter N for $n = 2$, by comparison with pressure.

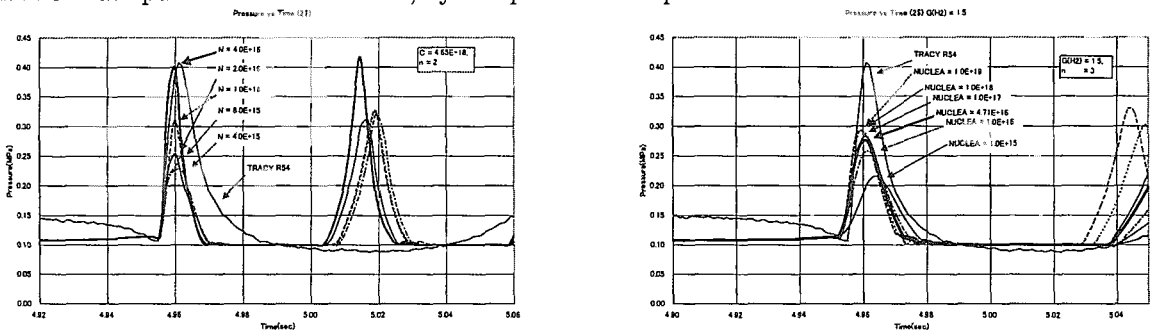

(a) \$ 2.0 step, $n = 2$, variable N (b) \$ 2.0 step, $n = 3$, variable N

Figure 3: Assessment of nucleation rate parameters n and N, by comparison with pressure.

[7] WIMS7 User Guide, AEA Technology Report ANSWERS/WIMS(95)4, June (1996).

[8] 'Conversion Coefficients for use in Radiological Protection Against External Radiation', ICRU Report 57.

[9] M. Akashi, 'Exposure to Neutron Irradiation in the Criticality Accident in Tokaimura', Division of Radiological Sciences Report, (2000).

[10] C. C. Pain, C R E de Oliveira, A J H Goddard, 'Transient analysis and dosimetry of the Tokaimura criticality incident' in prep.

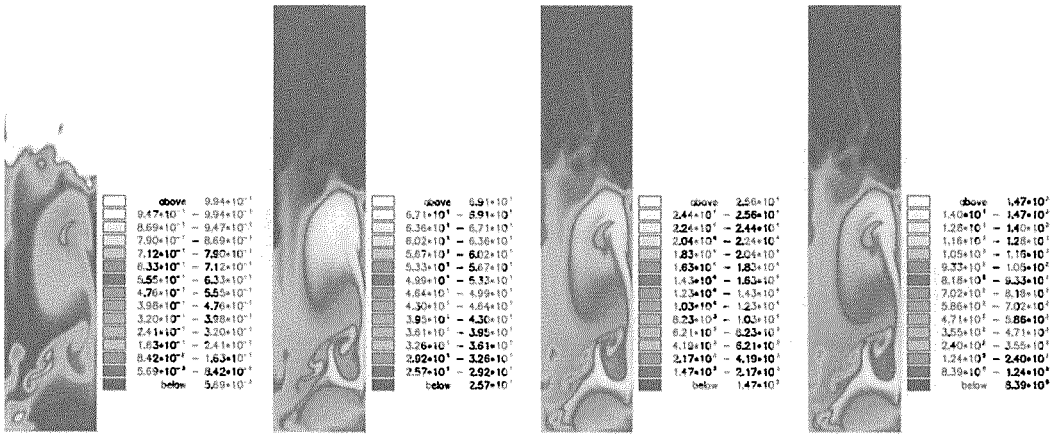

(a) volume frac. (b) liquid temp. (c) 1st delayed group. (d) 6th delayed group.

Figure 4: Various fields at 1 second into the simulation with a $ 2.0 step reactivity insertion. The diagrams show a cross section of an annular tank (TRACY geometry) modelled in rz-geometry.

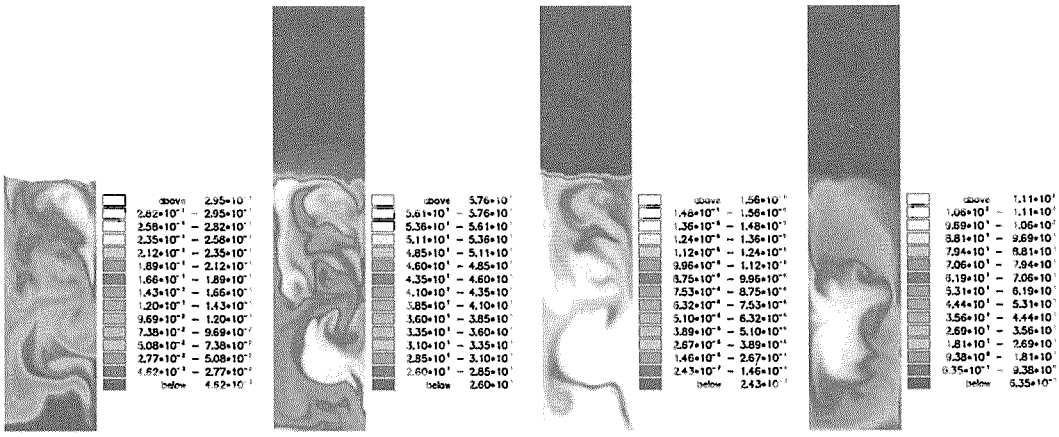

(a) volume frac. (b) liquid temp. (c) 1st delayed group. (d) 6th delayed group.

Figure 5: Various fields at 3.8 seconds into the simulation with a $ 2.0 step reactivity insertion. The diagrams show a cross section of an annular tank (TRACY geometry) modelled in rz-geometry.

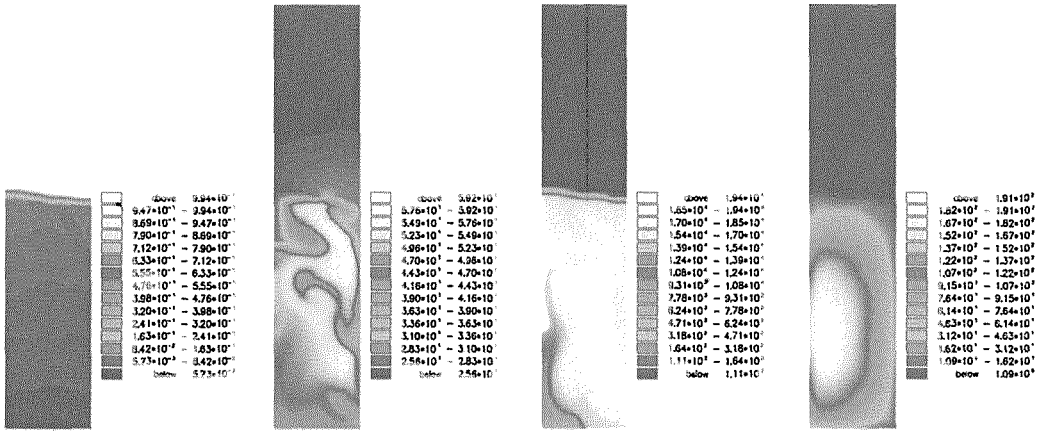

(a) volume frac. (b) liquid temp. (c) 1st delayed group. (d) 6th delayed group.

Figure 6: Various fields at 30 seconds into the simulation with a $ 2.0 step reactivity insertion.

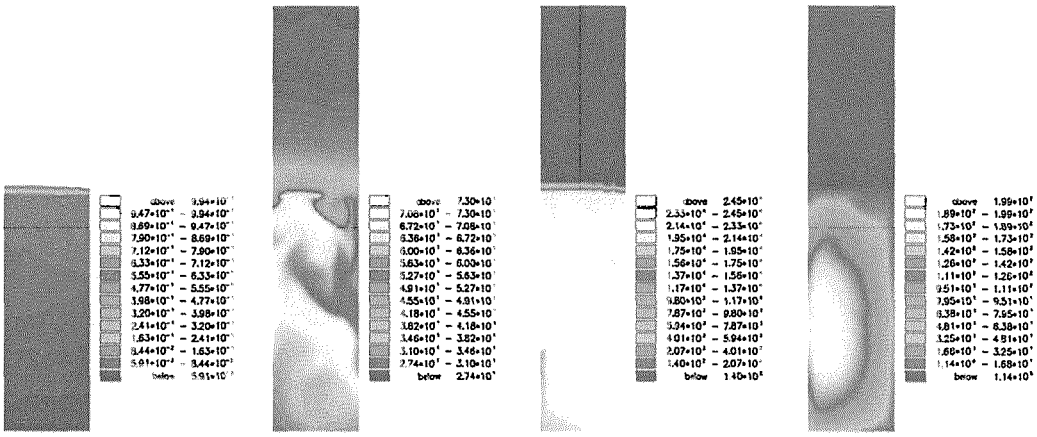

(a) volume frac. (b) liquid temp. (c) 1st delayed group. (d) 6th delayed group.

Figure 7: Various fields at 30 seconds into the simulation with a $ 2.8 step reactivity insertion.

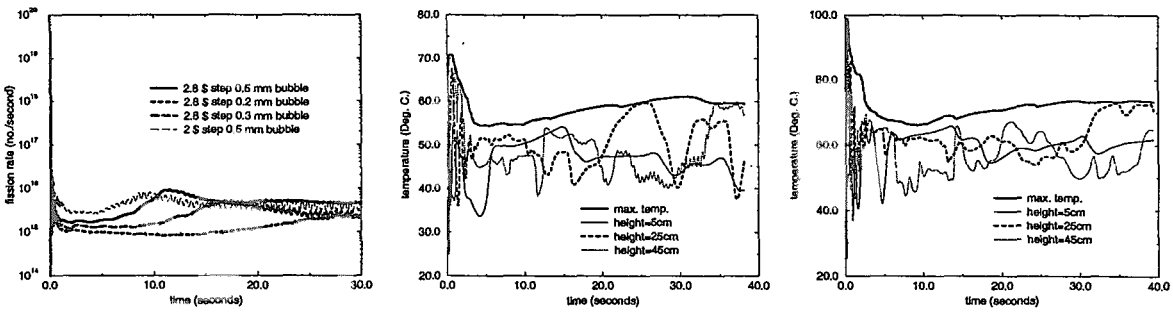

(a) fission rate (b) $ 2.0 step (c) $ 2.8 step

Figure 8: (a) Simulated fission rate also showing its sensitivity to bubbles size. (b) Simulated maximum temperature and temperature at 3 detectors placed in the liquid domain at 21cm from the central axis and heights 5cm, 25cm, 45cm above the bottom of the liquid filled vessel. The results are shown for the $ 2.0 and $ 2.8 step reactivity insertion.

This is a blank page.

JP0250296

Subcriticality Measurement by Source Multiplication Method with Higher Mode Flux

Tsuyoshi Misawa
Nuclear Energy Science Division
Research Reactor Institute, Kyoto University
Kumatori, Osaka 590-0494, Japan
Fax: 81-724-51-2603, e-mail: misa@kuca.rri.kyoto-u.ac.jp

New source multiplication method considering higher mode flux was developed to overcome the difficulty of the ordinary neutron source multiplication method, namely, position of both neutron detector and neutron source cannot be considered in analysis and it is possible to applied only to small subcriticality measurement. In the present method, neutron flux distribution with an external neutron source in subcritical state was expanded in a series of higher mode flux, and when neutron count of detector was measured at a known subcritical state, other un-known subcriticality can be obtained by measuring its neutron count. Numerical simulations were carried out to demonstrate the present theory by simulating a KUCA core experiment. It is found that in the present method subcriticality can be obtained accurately up to -20%dk/k, and detector position dependency of obtained subcriticality was also greatly decreased compared to the ordinary source multiplication method.

Key words: subcriticality measurement, source multiplication method, higher mode flux, NUMAC-3, KUCA

1. INTRODUCTION

Subcriticality measurement at nuclear fuel facility is one of the main issues in criticality safety study. For this purpose, several methods have been proposed and studied so far. For example, neutron source multiplication method, pulse neutron method with use of external pulse generator system, neutron noise analysis method such as Feynman-α method (variance to mean ratio method) and frequency analysis method and so on. Among these method, source multiplication method is a well-known method as its simplicity of measurement; use of an external neutron source and neutron detectors and method of data analysis is also simple way, and it has been often adopted in basic reactor experiments. Usually, its formulation of data analysis is based on the one point reactor theory with assumption of a bare homogeneous core, therefore, for accurate subcriticality measurement by this method, it is necessary to locate the neutron detectors carefully to eliminate the effect of higher mode components excited by an external neutron source, for example, the center of core is usually appropriate position for this measurement to obtain subcriticality accurately(1). However, when a detector is located at an arbitrary position of the core, such as in reflector region, the accuracy of measured result is assured only in a slightly subcritical state, roughly less than several dollars. One of the methods for taking into account the spatial dependence of neutron flux distribution in large subcritical state is to consider higher mode components of neutron flux excited by a neutron source. Recently, new reactor analysis code(2) was developed for calculation of higher mode flux accurately in multi-group and modified higher mode analysis

method was successfully applied to estimate the change of flux and reactivity caused by arbitrary perturbation[3]. The present study is preliminary application of higher mode analysis to the source multiplication method for accurate subcriticality measurement.

2. SOURCE MULTIPLICATION METHOD

In the ordinary source multiplication method, it is assumed that neutron count of detector (C_0), is proportional to external source intensity (S) and efficiency of detector (ε), and written as follows:

$$C_0 = \frac{\varepsilon S}{1-k_{eff}}, \tag{1}$$

where k_{eff} is multiplication factor. If neutron count C is measured at known subcriticality (ρ_0), it is possible to determine εS value through Eq. (1), then other unknown subcriticality (ρ) can be obtained using count C by the detector as follows:

$$\rho = \frac{1}{1-\frac{C}{\varepsilon S}} . \tag{2}$$

The derivation of above equation is based on simplified one-point reactor theory where both neutron detector position nor source position are not taken into account. Therefore ordinary source multiplication method has been applied to the measurement of small subcriticality.
To overcome this difficulty, new source multiplication method considering with higher mode flux, namely, higher harmonics of the system was developed. In this theory, neutron flux distribution with external neutron source is expanded by higher mode fluxes. Therefore, both detector and source position in each measurement can be considered in this theory.
Neutron balance equation of fundamental mode in static state can be written as follows:

$$L\phi = \frac{1}{\lambda_0} M\phi , \tag{3}$$

where L is a destruction operator such as absorption and leakage terms, M is a production operator such as fission term, ϕ is neutron flux, and λ_0 is eigenvalue of fundamental mode, which is unity in a critical state. If the system becomes subcritical because of change of destruction and production operators in Eq. (3), neutron balance equation with an external neutron source in subcritical state can be written as follows:

$$(L+\delta L)\phi' - (M+\delta M)\phi' = S\delta(x_0) , \tag{4}$$

where δL and δM are change of L and M operators, respectively, ϕ' is new neutron flux under subcritical state, S is source intensity, x_0 is source position, and $\delta(x)$ is the Dirac delta function.

Higher mode flux φ_i is defined by neutron balance equation of higher mode as follows:

$$L\varphi_i = \frac{1}{\lambda_i} M\varphi_i \ , \tag{5}$$

where λ_i is i-th higher mode eigenvalue. Then, ϕ' in Eq. (4) is expanded in a series of higher mode fluxes of Eq. (5) as follows:

$$\phi' = \sum_{i=0}^{N} c_i \varphi_i \ , \tag{6}$$

where N is maximum number of expansion modes and c_i is an expansion coefficient.

Multiplying adjoint flux of fundamental mode φ_0^+ in both sides of Eq. (4), and integrating over whole space and energy, the following equation can be obtained:

$$<\varphi_0^+ L \sum_{i=0}^{N} c_i\varphi_i> + <\varphi_0^+ \delta L\phi'> - <\varphi_0^+ M \sum_{i=0}^{N} c_i\varphi_i> - <\varphi_0^+ \delta M\phi'> = S\varphi_0^+(x_0) \ . \tag{7}$$

Using the following orthogonality equation for the higher mode flux,

$$<\varphi_i^+ M\varphi_j> = \delta_{ij} \ , \tag{8}$$

Eq. (7) is modified as follows:

$$\left(\frac{1}{\lambda_0} - 1\right) c_0 - <\varphi_0^+(-\delta L + \delta M)\phi'> = S\varphi_0^+(x_0) \ . \tag{9}$$

Here, using perturbation theory without assumption and Eq. (9), reactivity $\Delta\rho$ that is subcriticality can be obtained as follows:

$$\Delta\rho = \frac{<\varphi_0^+(-\delta L+\delta M)\phi'>}{<\varphi_0^+ M\phi'>} = -\frac{1}{c_0}\left\{S\varphi_0^+(x_0) - \left(\frac{1}{\lambda_0}-1\right)c_0\right\} \quad ; -\frac{1}{c_0}S\varphi_0^+(x_0) \tag{10}$$

In derivation of this equation (10), it is assumed that λ_0 is unity. Therefore, $\Delta\rho$ is in proportional to source intensity and adjoint flux of source position and inversely as an expansion coefficient of fundamental mode.

Same as fundamental mode, in order to derive coefficients of higher order term, multiplying higher mode adjoint flux in both sides of Eq. (7), the following equation can be obtained:

$$\left(\frac{1}{\lambda_i}-1\right)C_i - <\varphi_i^+(-\delta L+\delta M)\phi'> = S\varphi_i^+(x_0) \ . \tag{11}$$

Here, assuming that changes of both M and L operators are uniform in the system, second term of left hand side of above equation can be approximated as follows:

$$<\varphi_i^+(-\delta L+\delta M)\phi'> \ ; \ \frac{\delta M-\delta L}{M} <\varphi_i^+ M\phi'> \quad ; \quad \Delta\rho \quad <\varphi_i^+ M\phi'> = \Delta\rho \ c_i \ . \tag{12}$$

From these results of Eqs. (10) and (12), neutron flux of Eq. (6) in subcritical state can be written as follows:

$$\phi' = \sum_{i=0}^{N} C_i\varphi_i = \left\{-\frac{\varphi_0^+(x_0)}{\Delta\rho}\varphi_0 + \sum_{i=1}^{N}\frac{\varphi_i^+(x_0)}{\frac{1}{\lambda_i}-1-\Delta\rho}\varphi_i\right\}S \ . \tag{13}$$

Therefore, neutron count at position of x can be written as follows:

$$N_0 = \varepsilon\phi' = \left\{-\frac{\varphi_0^+(x_0)}{\Delta\rho}\varphi_0(x) + \sum_{i=1}^{N}\frac{\varphi_i^+(x_0)}{\frac{1}{\lambda_i}-1-\Delta\rho}\varphi_i(x)\right\}\varepsilon S \ . \tag{14}$$

When the neutron count is measured at an known subcritical state, and higher mode flux and higher eigenvalues are known beforehand through calculations, then εS can be determined by

the above equation (14). And when neutron count is measured at other unknown subcritical state, subcriticality is obtained by solving this equation numerically.

3. SIMULATION

To demonstrate the present formulation of new source multiplication method, numerical calculations were carried out to simulate a core of Kyoto University Critical Assembly (KUCA) at Kyoto University Research Reactor Institute[4]. The horizontal core configuration is shown in Fig. 1. Fuel element is composed of highly enriched uranium-aluminum alloy plates as fuel and polyethylene as moderator, and polyethylene reflectors surround the fuel elements. Control rods are located adjacent the core. An external neutron source in the reflector region is an ^{241}Am-Be and 16 neutron detectors are located at the reflector region as shown in Fig. 1.

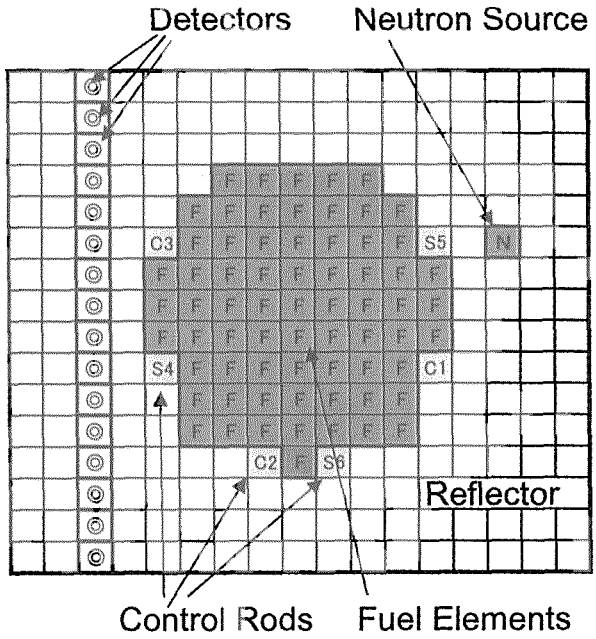

Figure 1 Horizontal cross section of core configuration

Before the source multiplication analysis, higher mode calculations were carried out to obtain higher mode fluxes and eigenvalues. For this purpose, NEUMAC-3 code that been developed by author and Nagoya University was used. NEUMAC-3 is based on two or three dimensional diffusion theory in multi energy groups, and has an ability to calculate higher mode flux and its eigenvalue by the deflation method with power iteration or the double QR method to solve operator matrix of diffusion equation directly. In the present study, 2-dimensional x-y geometry in 2-energy groups was adopted and higher mode fluxes up to 150-th order were solved. Figures 2 and 3 are examples of higher mode flux distribution of the present core calculated by NEUMAC-3 and Fig. 4 shows eigenvalues of each higher mode of the present core. It is found that higher mode eigenvalues decrease with an increase of mode number.

In the present analysis, neutron flux distribution with external neutron source was calculated by CITATION code, which is a multi-dimensional and multi-group diffusion code, and subcriticality of the core which was calculated by the eigenvalue calculation was changed from approximately -1 %dk/k to -20%dk/k by altering the vertical buckling to simulate the change of vertical length of the core. Figure 5 shows an example of neutron flux distribution with an external neutron source calculated by CITATION.

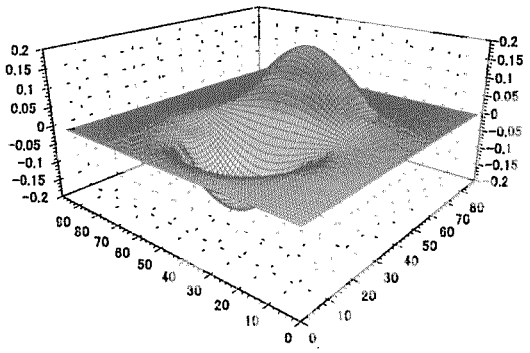

Figure 2 1-st higher mode flux of fast energy group

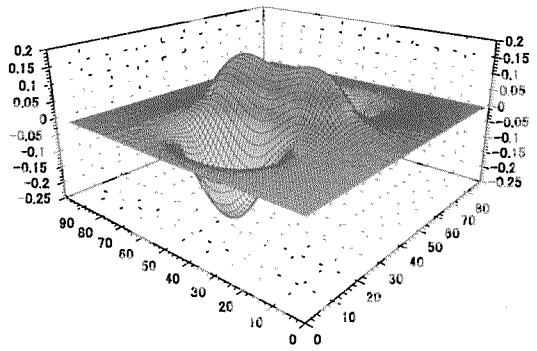

Figure 3 3-rd higher mode flux of fast energy group

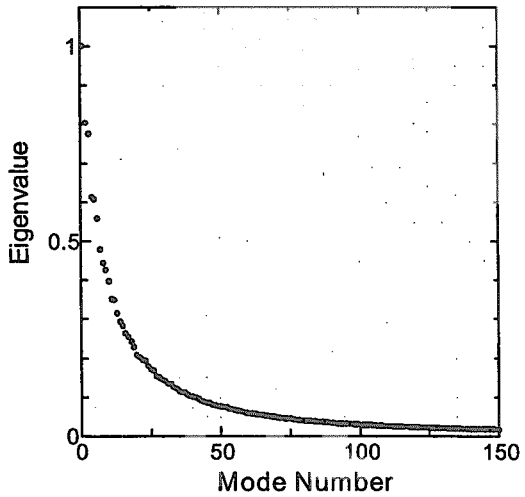

Figure 4 Eigenvalue of each higher mode

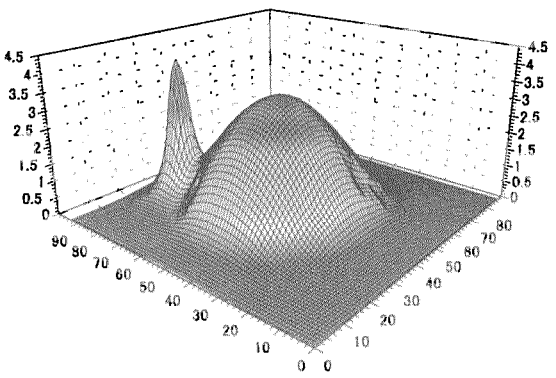

Figure 5 Neutron flux distribution of fast energy group with external neutron source

4. RESULTS

The results of present source multiplication method including higher mode flux to obtain subcriticality of each core are shown in Fig. 6 together with both the results of eigenvalue calculation by CITATION and ordinary source multiplication method. In this analysis, εS value in Eq. (14) was obtained at the smallest subcritical state by using its calculated subcriticality.

It is found that the results of ordinary source multiplication method are getting apart from calculated results when subcriticality is more than -7%dk/k and large discrepancy between

those results by different detector positions are observed especially when subcriticality is more than -10 %dk/k. On the other hand, the present results by new source multiplication method show fairly good agreement with calculated ones and dependency of detector position is also very small.

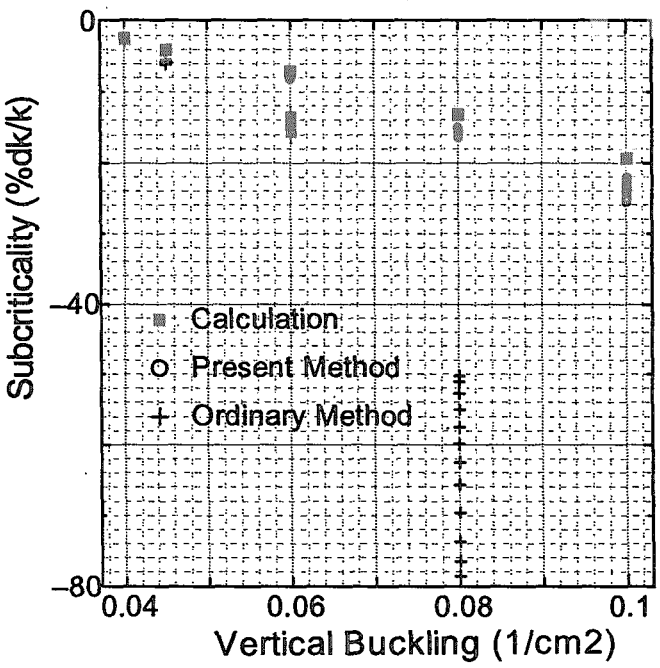

Figure 6 Results of subcriticality by the present source multiplication method together with both the results of eigenvalue calculation by CITATION and ordinary source multiplication method

5. CONCLUSION

Method of new subcriticality measurement by neutron source multiplication method with considering higher mode flux was developed. Through simulation, it is found that compared to the ordinary source multiplication method, the accuracy of the present neutron source multiplication method is much improved even in large subcritical state because the effect of higher mode flux on the neutron flux distribution becomes much remarkable with an increase of subcriticality, and detector position dependency of obtained subcriticality can be greatly decreased.

In the near future, experimental study to investigate applicability of the present source multiplication method will be carried out at KUCA.

References

[1] T. Misawa and S. Shiroya, Annu. Rep. Res. Reactor Inst. Kyoto Univ., 26, 125-128 (1993).

[2] T. Misawa, A. Yamamoto and Y. Yamane, J. Nucl. Sci. Technol., 33, 668-670 (1996).

[3] C. H. Pyeon, Y. Yamane, T. Misawa and S. Shiroya, Ann. Nucl. Energy, 27, 345-354 (2000).

[4] T. Misawa, S. Shiroya and K. Kanda, Nucl. Technol., 116, 11-20 (1996).

JP0250297

JAERI-Conf 2002-004

Study on Neutronic and Thermal Characteristics of the Precipitation Vessel in JCO Criticality Accident

Yoshinori MIYOSHI, ToshihiroYAMAMOTO, Ken NAKAJIMA,
Yuichi YAMANE and Shouichi WATANABE

Japan Atomic Energy Research Institute
Department of Fuel Cycle Safety Research
2-4 Shirakata Shirane, Tokai-mura, Naka-gun, Ibaraki-ken, 319-1195 Japan

In order to investigate the neutronic and thermal characteristics of the precipitation vessel in the JCO criticality accident, static and kinetic analyses were made to evaluate the initial reactivity and power profile in the initial burst part, respectively. In addition, a series of simulation tests using a thermal mock-up device were conducted to estimate the total amount of the evaporation and the temperature which reproduce the characteristics of power reduction of 19 hours in the plateau part.

Key words : JCO criticality accident, Static and kinetic analyses, MCNP-4B, AGNES2, Thermal mock-up device, Simulation test

1. INTRODUCTION

The first criticality accident in Japan occurred on September 30, 1999 in Tokai uranium fabrication plant of JCO. JAERI has evaluated the physical phenomena of this accident using calculation codes for static and kinetic analyses. For the evaluation of the inserted reactivity to the precipitation vessel, the condition of the 18.8% enriched uranyl nitrate solution fuel and the procedure of the two workers were investigated in detail. Based on the process sheet and the information from JCO staffs, the range of the excess reactivity which is dependent on the fuel concentration, acid molarity, and temperature, were evaluated with the validated calculation systems. The dimension of the precipitation vessel was measured on the JCO site, and detail of the structural material was confirmed. Reactivity effects of structural material surrounding the vessel, the side wall of the building and bodies of JCO workers were also evaluated by making a detail model of a continuous energy Monte Carlo code. For the evaluation of the power profile in the initial burst part (up to 25 minutes after accident initiation), a one-point kinetic code, AGNES 2 was used for evaluating the maximum peak power and fission number of the first pulse and the total fission number in the initial burst part. The accuracy of this code was confirmed by evaluating the transient data obtained by TRACY experiments.

The JCO criticality accident continued long time, which was mainly due to the cooling water surrounding the vessel. As the power profile in the plateau part is dependent on the thermal characteristics of the precipitation vessel, a series of thermal simulation tests were performed for determining the condition that reproduce the power profile. A main factor which affects the power decrease in the plateau region is considered to be water evaporation of the fuel solution. Main experimental parameters of the simulation test are the initial temperature of the plateau part corresponding the inserted reactivity and the flow rate of cooling water which has effect on the heat removal.

2. STATIC ANALYSES

2.1 Operating Condition

The precipitation vessel is designed essentially to be used to precipitate ammonium diuranate (ADU) by chemical reaction of uranyl nitrate solution with ammonium gas and is equipped with cooling system to control the temperature during the chemical reaction and stirrer to accelerate the reaction. Peeping hole is also equipped to it to see the inside. The chain reaction was initiated in the vessel when one worker almost finished to pour the seventh batch of uranyl nitrate solution in 5-liter stainless-steel beaker into the vessel though the peeping hole, while the another worker standing on the floor supported the funnel inserted in the hole. Initiating condition of the workers and precipitation vessel is shown in Figure 1. The supervisor of those operators was working at a desk in the next door, which was several meters far from the vessel. The stainless beaker was left on the floor near by the vessel, in which small amount of uranyl nitrate solution was remained not being poured. The cooling system of the vessel

was in operation, however, the stirrer was not working. Recording system of the temperature of the vessel was also switched off since two days before the accident. Ventilation system of the Conversion Test Building was being operated all through the accident period and the negative pressure in the buildings was maintained. Air from the building was being exhausted after filtering with HEPA filter. However, it is presumed that the vent gas line from the vessel was not in operation.

Gamma ray area monitoring system over the JCO facilities was in operation and workers in building of the JCO site started evacuation when the alarm sounded. Radiation level in the Conversion Test Building was too high to be recorded. On the other hand, gamma ray area monitor in the 1st Fabrication Building which is located about 100 m far from the precipitation vessel continuously recorded the dose which is proportional to the power of the precipitation vessel[1].

2.2 Criticality Characteristics

For evaluating the static criticality characteristics of the precipitation vessel, it is necessary to determine the solution height in the pouring procedure made by two workers. The uranium concentration was estimated 370gU/L as nominal value and the volume of each batch was estimated about 6.5 liter from the uranium mass of 2.4 kg-batch. The nitric acid of the uranyl nitrate solution was assumed 0.5 mol/L based on the specification of the fuel solution products.

The change of the effective neutron multiplication factor with the uranium solution height in the precipitation vessel was calculated. A system of the continuous energy Monte Carlo code MCNP-4B with Japanese Evaluated Nuclear Data Library JENDL3.1 was adopted for evaluating the neutron multiplication factor and excess reactivity. The calculation bias of above system had been confirmed to be small by the benchmark calculations using the critical data of uranyl nitrate solution at the Static Experiment Criticality Facility, STACY. The change in neutron multiplication factor is shown in Figure 2. It can be noted that the precipitation vessel was subcritical after the pouring of the fuel solution of the 6th batch and supercritical after that of the 7th batch.

The critical volume and critical solution height were estimated 41.0 liter and 28.5 cm, respectively. Figure 3 shows the dependence of the reactivity on the final uranium concentration. When the uranium concentration is smaller than this nominal value of 370 gU/L, reactivity of the precipitation vessel increases due to the increase in the solution height. Taking account of the uncertainty of the each parameter and calculation model, and reproductivity of the criticality safety code, the inserted reactivity to the precipitation vessel was evaluated in the range of 1.5 to 3.0 $, approximately. Sensitivity analyses of the reactivity for main criticality factors such as uranium concentration, free acid molarity and temperature were made to determine the possible range of the inserted reactivity. Figure 4 shows the contour of the inserted reactivity for uranium concentration and acid molarity of the fuel solution[2].

For the evaluation of the reactivity and the fundamental parameter used in analysis of the transient behavior, kinetics parameters such as prompt neutron generation time, effective delayed neutron fraction, temperature and void coefficients of reactivity were calculated with the calculation system, SRAC and TWODANT with the latest Japanese nuclear data file, JENDL3.2. Kinetic parameters are summarized in Table 1.

3. KINETICS ANALYSIS

3.1 Validation of AGNES2 Code

To investigate the power profiles of the criticality accident, we have conducted the kinetics analysis using a code AGNES2. AGNES2 is a one-point kinetics code developed at JAERI, to calculate the nuclear excursion in fissile solution systems. Since radiolytic gas voids are produced in the nuclear excursion, and they affect the power behavior significantly, the calculation model to treat the gas void effect has been developed and incorporated in the AGNES2 code.

The prediction accuracy of AGNES2 code was validated through the analysis of the TRACY experiments. Figure 5 shows the comparison between the calculations and the experiments for the peak power and the total fission yield of TRACY transient experiments. Those experiments were initiated by continuous feed of low-enriched uranium solution to the TRACY core tank, which is similar to the situation at the JCO accident. As seen in the figure, the calculation agrees well with the experiments, and the difference is smaller than 20%. Due to the similarity of JCO accident to the TRACY experiments, we conclude that the accuracy of the accident analysis using AGNES is assured.

3.2 Analysis of the First Pulse

In the JCO accident kinetics analysis, the inserted reactivity is one of key parameters. Figure 6 shows the results of AGNES2 calculation for the variety of inserted reacivities. The maximum reactivity, 3 dollars, was determined from the results of neutronic calculation as shown in the previous section. For all cases, the reactivity insertion time was assumed to be 12 seconds. Although the peak power varies slightly depending on the reactivity, the fission yield at the end of first pulse becomes almost same, about 6×10^{16}, independent of the reactivity. This is due to the fact that the inserted reactivity at the end of first pulse is almost same for all cases.

The comparison of calculated power profiles with the "measured power" is shown in Figure 7. The measured power in the figure was derived from the record of gamma-ray monitor which was installed at the JAERI-Naka site. Because of the slow response of the monitor, the record was proportional to the time-averaged profile of the nuclear power. By the fact that the measured power is between the calculations with the reactivities of 1.5 and 3 dollars, we estimate that the inserted reactivity in the accident is in that range.

3.3 Analysis of the Initial Burst Part

The power behavior for a prolonged period would be controlled by the cooling condition, because the temperature reactivity effect becomes dominated for that case. We have investigated the cooling effect in the JCO accident using AGNES2 by changing the heat transfer coefficient between the fissile solution and the cooling jacket as shown in Figure 8. In the calculation, the inserted reactivity is assumed to be 3 dollars. As seen in the figure, the power profile after about 200 seconds strongly depends on the heat transfer coefficient. In comparison with the record of gamma-ray area monitor, which has a peak around 1000 seconds, the result using the coefficient of about 180 [kcal·m-2·h-1·K-1] (≈210 [W·m-2·K-1]) reproduces the accident well. Since the power profile varies with inserted reactivity as well as the cooling condition, we have performed a series of calculations for different reactivity and cooling conditions. Finally, we have concluded that the fission yield in the "Burst part", which corresponds to the period up to 25 minutes, was about 2 to 5×10^{17}.

4. THERMAL CHARACTERISTICS USING A MOCK-UP

In the criticality accident of JCO precipitation vessel, a significant power level continued from the viewpoint of thermal feedback to reactivity, and the power was recorded as observed data of the JCO gamma-ray area monitor. A thermal mock-up device of the JCO precipitation vessel was manufactured[3], and a series of simulation tests of thermal characteristic were performed covering the plateau part by changing electric-heater power based on one point approximation of nuclear kinetics equation.

4.1 Mock-up Device

A mock-up of the JCO precipitation vessel is shown in Figure 9. The vessel to which a cooling-water jacket and an agitator are attached, mocks up dimensions and configurations of the major part of JCO precipitation vessel. The water in the vessel is heated by 3 electric heaters with 15kW(5kW×3) of maximum capacity. A funnel is inserted into a "hand hole". The inner diameter of the hole and the funnel are 83 mm and 46 mm, respectively. The solution volume is 43 L, and the solution dimensions are 45cm in diameter and 31 cm in height.

The measurement and control system of the mock-up device is shown in Figure 10. The heater power was controlled by a personal computer. Both the solution temperature which was determined by averaging values of 6 measure points in the solution, and the solution height which is reduced by the water evaporation flowing out through the hand hole are measured continuously. These measured values are considered as inputs for one point approximated nuclear kinetics equation. The solution was stirred slowly using the agitator considering volume-heating of the solution in the JCO precipitation vessel. The reactivity effect by the water evaporation was considered as follows:

The relation between the amount of water evaporation and the reactivity change was evaluated by using a Monte Carlo transport code, MCNP 4B with the continuous-energy cross sections based on the evaluated nuclear data library, JENDL-3.1. Reactivity change with evaporation in the simulation was given as a quadratic-function of the amount of the evaporation. Reactivity coefficient of evaporation was

estimated to be about -0.6 $/L.

4.2 Experimental Method

As parameters which affect the behavior of power level change, the initial solution temperature corresponding to the initial reactivity 1.5-2.7 dollars and the cooling-water flow rate were considered. The simulation tests were performed as follows: As an initial condition, power level was set to be 2kW, and the flow rate was determined so as to satisfy both the initial power and the equilibrium temperature of the solution. The simulation test in the plateau part was performed for 17 hours in order to confirm the evaporation effect and the consequent power level reduction. The reactivity feedback by the evaporation was considered after the start of the simulation, although the evaporation had been continued before the simulation. The test was continued for 3 hours after the cooling-water circulation stopped, in order to measure the transient of the power level.

4.3 Experimental Result

The relation between initial temperature and the water flow rate for the initial power was measured[3]. For the initial reactivity 1.5-2.7 dollars (reference temperature 25 ºC) which corresponds to initial temperature 66-91℃, the cooling-water flow rate which satisfied the initial condition of 2 kW of power was found to be 0.6-0.2 L/min. The simulation test was performed for the cases of 1.5-2.7 dollars with the cooling-water flow rate of 0.6-0.2 L/min. The result of the simulation test is shown in Figure 11. The power profile approached the observed power as the initial reactivity (temperature) increases. And the power level at the cooling-water circulation stop approached the observed power in the case of ~2.7 dollars.

The result of the test before and after the cooling-water circulation stop is shown in Figure 12. The solution temperature for each case approaches about 55-60 ℃, and shows higher value as the initial reactivity increases. On the other hand, the power level which corresponds to the solution temperature became about 0.3-0.4 kW, and also showed higher value as the reactivity increased. The power ratio before and after the cooling-water circulation stop, approached observed value of 0.34 in the case of ~2.5 dollars.

When considering the power profile after water circulation was stopped, and the possibility of the temperature increase of fuel solution in dissolution process which is mentioned previously, it is estimated that the initial reactivity of the precipitation vessel was～2.5 dollars and the total amount of the evaporation in the plateau part was about 2 L.

5. SUMMARY

It is not easy to determine the excess reactivity only by criticality analyses based on limited information concerning to fuel condition and working process. There is large uncertainties in initial temperature of the solution in the precipitation vessel and the uranium concentration of the 7th batch. Taking account the total uncertainty of the critical parameter that affect the neutron multiplication factor, the inserted reactivity was estimated from 1.5 to 3.0 dollars. The investigation on the kinetic behavior in the initial burst part is consistent with the result of the static characteristics taking account of the total fission number. In addition, the range of the expected inserted reactivity from the static and kinetic analyses covers the estimated value of 2.5 dollar obtained by the thermal mock-up simulation test with for a long plateau part.

REFERENCE

1) K. Tonoike et al., "Power Profile Evaluation of the JCO Precipitation Vessel based on Record of the Gamma-ray Monitor," Proceeding of NUCEF2001,PC-11 (2001)
2) Y. Miyoshi et al., "Study on Static and Kinetic Characteristics of JCO Criticality Accident," Proceeding of 2001, ANS Annual Meeting, Milwaukee, Wisconsin (2001)
3) S. Watanabe et al., "Basic Test on Cooling Characteristics of JCO Precipitation Vessel using a Mock-up Device," Proceeding of NUCEF2001, PC-12 (2001)

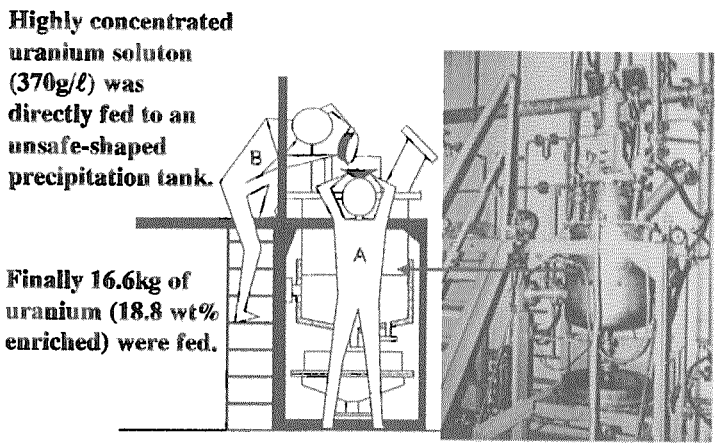

Fig. 1 Precipitation Vessel

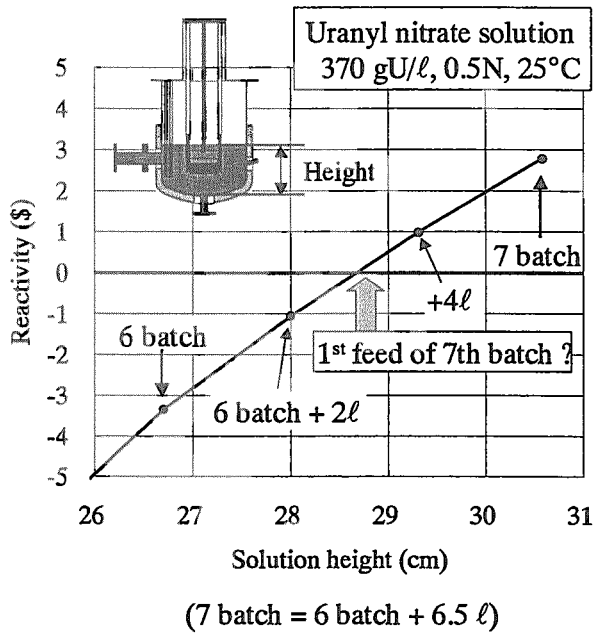

Fig. 2 Estimation of excess reactivity

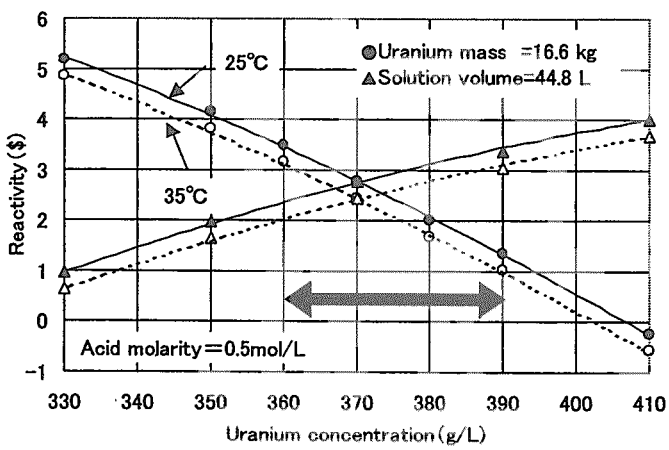

Fig. 3 Reactivity vs. Uranium Concentration

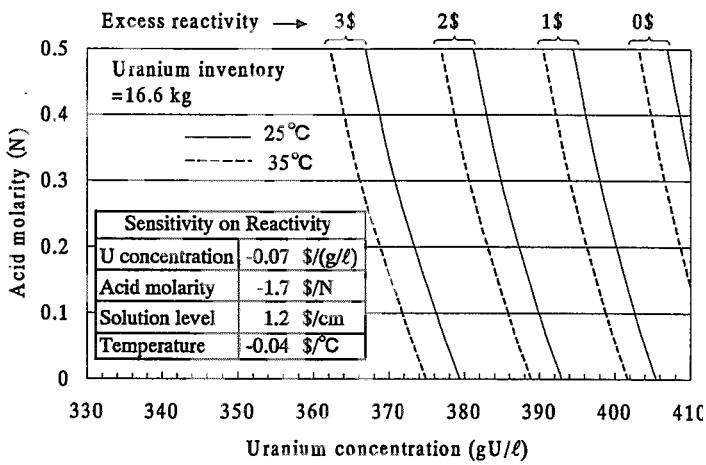

Fig. 4 Sensitivity of Reactivity on Fuel Condition

Table 1 Calculated kinetic parameters

β eff	0.00788
ℓ	3.0×10^{-5} (s)
Temp. cofficient	-0.0022%dk/k/°C
Void coefficent	-0.31%dk/k/*%void*
Fatman, room-return, and other effects < 20¢	

Calculated with TWODANT/JENDL-3.2

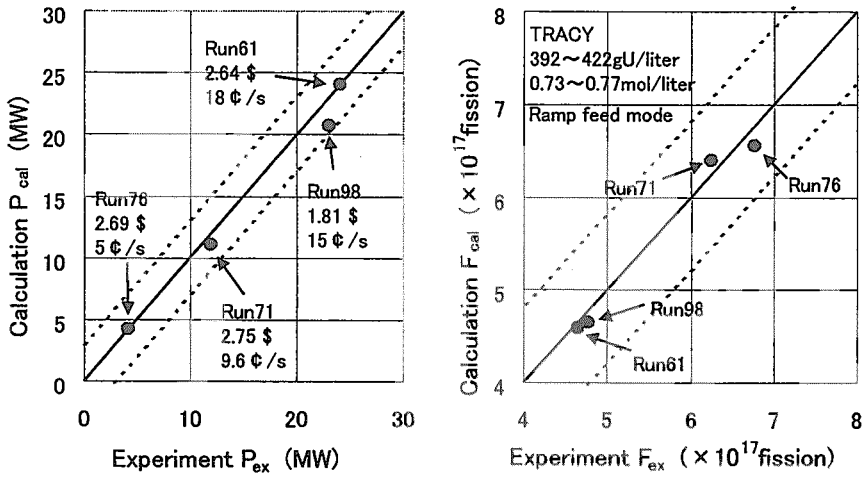

Fig. 5 Comparisons of Calculations (AGNES2 code) with TRACY Experiments. (P: Peak power, F: Total fission yield

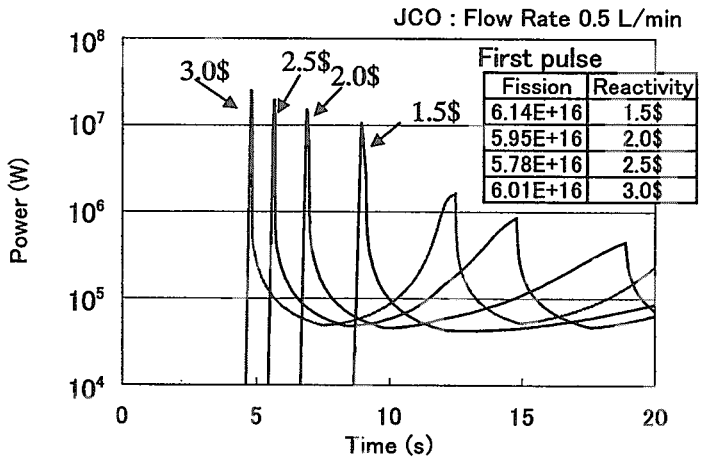

Fig.6 Calculated first pulse as a function of inserted reactivity.

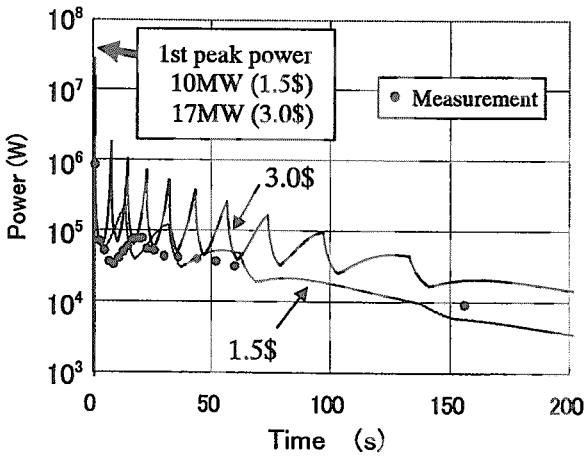

Fig.7 Calculated power profiles in comparison with measured data. (Inserted reactivity: 3$)

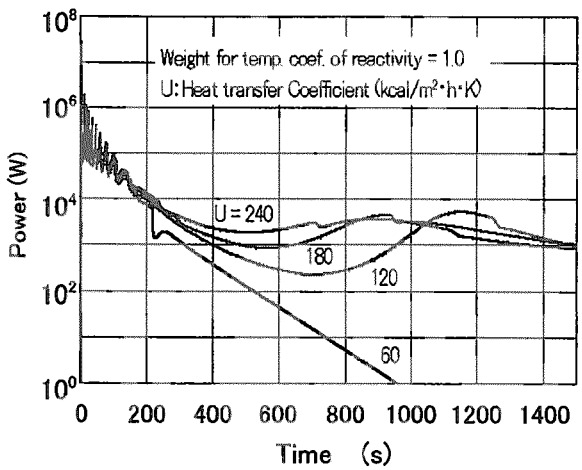

Fig.8 Effect of heat transfer coefficient on power profile.

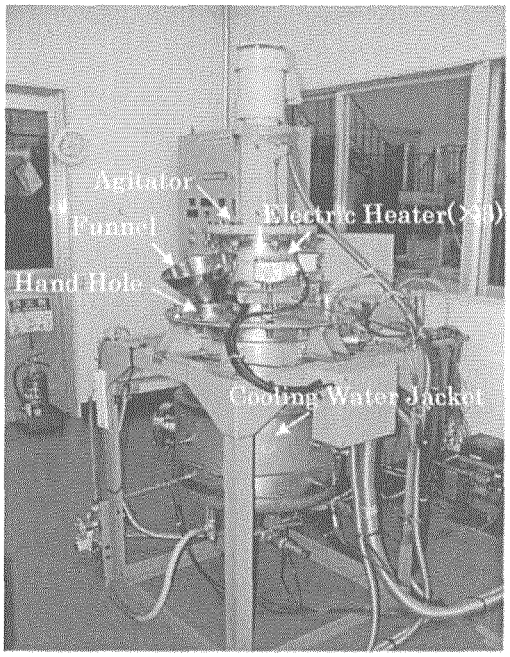

Fig. 9 Mock-up Device

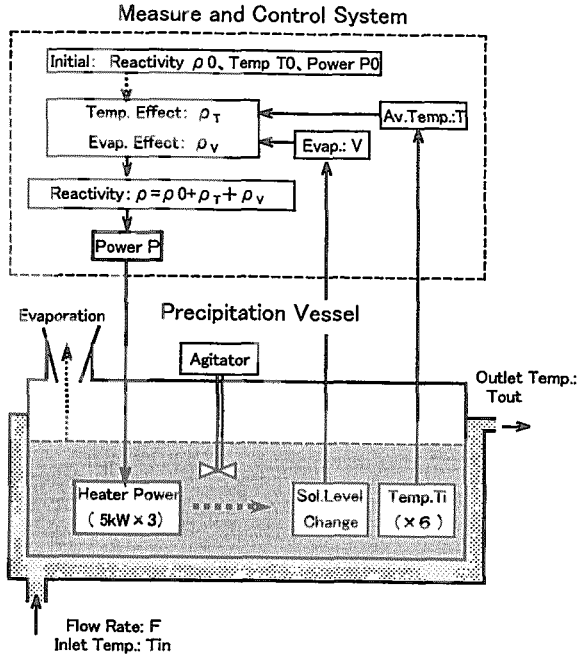

Fig. 10 Measurement and Control System

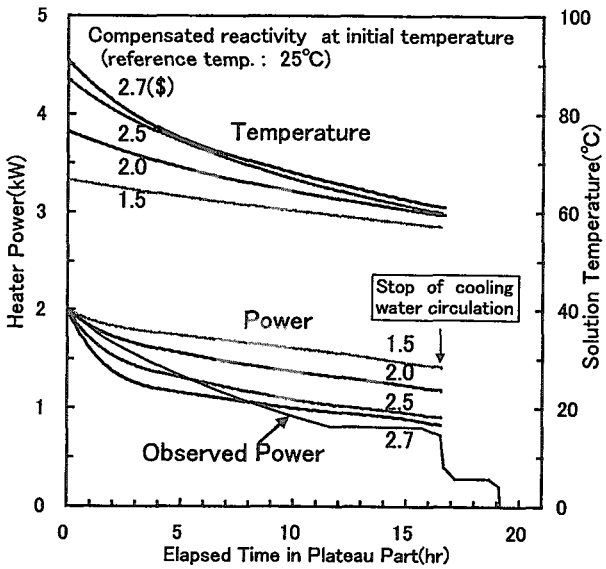

Fig. 11 Power and Solution Temperature
(Plateau Part)

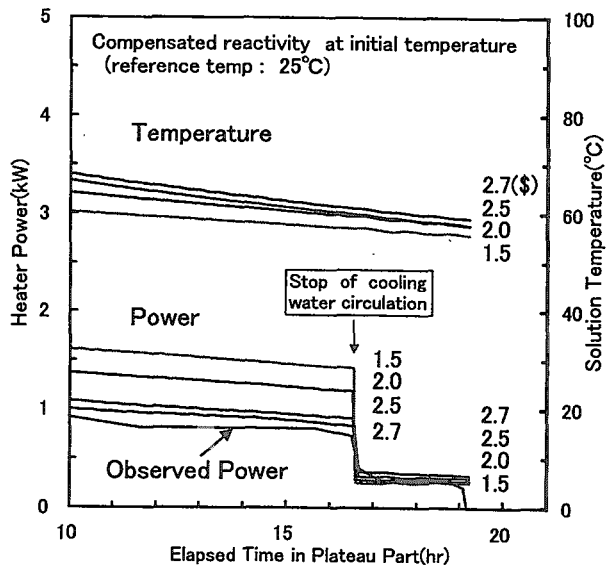

Figure 12 Power and Solution Temperature
(Before and After Flow Stop)

This is a blank page.

Separation Process

This is a blank page.

JP0250298

JAERI-Conf 2002-004

PRESENT STATUS OF R&D ON REPROCESSING PROCESS IN COGEMA

Marie-Françoise DEBREUILLE, Philippe PRADEL
COGEMA
2 rue Paul Dautier
B.P.4 78141 VELIZY CEDEX, FRANCE

François DRAIN
SGN
1 rue des Hérons
78182 SAINT QUENTIN YVELINES CEDEX, FRANCE

Introduction

Reprocessing is a complex industry.
The bases of PUREX process, universally adopted today, were established in the 50's, with plants designed for defence purposes. Later on, first generation of commercial plants dedicated to LWR oxide fuels appeared in Europe (France, Belgium and Britain) and in Japan. These plants have been designed and started up in the 60's and 70's and had limited capacity.
The requirement for process performances in commercial plants are stringent: very high purity of U and Pu end products and high recovery ratio, authorised limits for release becoming more and more severe, necessity to condition all waste.
The risks of criticality, contamination and irradiation have to be mitigated and the requirements are also more and more stringent, especially concerning dose to operators.
To cope with these difficulties and to become today the world leader for reprocessing, COGEMA has always maintained a high level of R&D and is continuing his effort today to prepare the future.

Second generation plant: the industrial maturity

At the end of the 70's, the bases of the second generation of commercial reprocessing plants were launched.
The main lessons from previous plants of COGEMA, i.e. UP2-400 in La Hague, started up in 1976, were as follows :

- Good safety records. No significant incident has been recorded, and release to the environment were significantly below authorised limits,
- Design capacity was reached slowly due to insufficient reliability during the very first years of operation. Indeed, UP2-400 reached nominal capacity roughly ten years after its start-up,
- Process performances were reached; however solvent quality was an item of concern and frequent renewal of solvent hold-up was necessary to maintain performances of extraction process,
- The process and technological waste were not conditioned.

Therefore the following objectives have been set up for the new plants:

- Increase plant availability through:
  - the use of corrosion free materials, especially for the equipment with boiling nitric acid solutions,
  - fully remote maintenance,

- duplication of most sensitive equipment,

- Improve process performances by adopting fully continuous process and through stable performances of extraction process,
- Improve safety records: reduction of dose rate to operators and of release to the environment,
- Conditioning all process and technological waste.

A huge R&D effort for more than 10 years and a strong co-operation between design team and operators from previous plant result in the construction of the two new reprocessing plants UP3 and UP2-800, entering commercial operation in 1990 and 1994.
The main features of both plants are:

- Continuous dissolution process using a rotary dissolver [1],
- New extraction equipment such as geometrically safe pulsed columns with efficient packing [2] [3],
- Improved solvent management including a distillation unit able to purify and recycle both solvent and diluent [4],
- Conditioning process for all waste: for instance vitrification for high active process waste and grouting for low and medium active technological waste[5].

The operational results demonstrate clearly that the objectives fixed at design stage have been fully reached, and in most of the cases far over the expectations [6]:

- very high plant availability demonstrated through the reprocessing of more than 12000 tons of oxide fuels since the start-up of UP3,
- very high and stable process performances,
- drastic reduction of dose to operators, of release to the environment and of volume of final waste.

La Hague plants: 10 years of improvement thanks to continuous R&D

After the successful start-up of new La Hague plants, R&D effort has been pursued and numerous advances have been made possible thanks to it. It is worth to notice that the strong co-operation between R&D, engineering and operators has played a key role in the success.
Some examples of the most significant improvements are given hereafter.

Core of the chemical process: decontamination of uranium

At design stage, two extraction cycles were foreseen to decontaminate uranium from neptunium, plutonium and fission products after its separation from plutonium in first extraction cycle. Immediately after active start-up of the plant it appeared that decontamination (for plutonium in uranium and for fission products) performances of first cycle was far over the expectations. The decontamination factor for neptunium in uranium cycle was also higher than expected, but still too low to reach neptunium specification with only one cycle. Operation was then optimised and additional R&D was launched. The resulting decontamination factor for Np is over 1000, and thus today only one cycle is used to purify uranium.

Vitrification facility [6]

There are two vitrification facility on La Hague site: R7 entered in active operation in June 1989 and began to treat the 1200m^3 stock of HLW solutions produced by UP2 plant since its start-up in 1966 and T7 facility is devoted to treat the HLW solutions produced by UP3 plant. It entered in active service in July 1992, 3 years after its "twin" facility R7.
Several significant improvements have been brought since active start-up:

- addition of an in-cell washable pre-filtering device on the ventilation of main hot cells (vitrification, pouring, dismantling) in order to protect HEPA filters from contamination;
- modification of the cranes to improve the reliability of some components and to reduce the need for their maintenance;
- improvement of the canister decontamination device (higher water pressure and throughput);
- optimisation of glass homogenisation;
- increase of service life of melting pot through optimisation of material and operating conditions.

Most of these improvements have been implemented while facilities were in active operation, demonstrating the flexibility of the design.

New liquid waste management [6]

Active operation of UP3 was started in 1989. The initial liquid waste management led to the production of two types of solid waste : glass canisters containing the bulk of activity and bitumen drums.

The very good decontamination performances of first extraction cycle gave the opportunity to modify liquid waste management in order to delete production of bituminised waste. Main features of this new management are:

- all salt free acidic waste and some of the salt bearing waste are concentrated by evaporation and concentrates are routed towards vitrification,
- most of the salt bearing waste have an activity low enough to be released to sea, after activity checking and filtration,
- three new evaporation units and a specific unit for treatment of laboratory waste, for which specific R&D has been conducted, [7]
- new piping and vessels to perform waste transfer to the new units.

The provisions taken into account in the original design have allowed to perform these modifications with extremely low dose rate to the personnel and within short duration, while the plant remained in active operation.

Light robotic equipment for in cell exceptional operations

R&D is pursued also in this domain. A recent example of application is the repair of the shear chute of R1 (head-end facilities of UP2-800 plant). A small hole, caused by wear was discovered in February 2001. A repair has been conducted as early as April, taking advantage of the ongoing R&D for light robotic.

Present R&D's main objectives

The R&D under way in COGEMA follows several objectives, the most significant being :

- reprocessing of high burn-up fuels, both uranium oxide and mixed oxide, and RTR fuels;
- increase of storage pools capacity and of flexibility of head-end process through use of burn-up credit;
- development of light robotics for in-cell inspection and repair after exceptional incident, such as in the case of shear chute mentioned here above;
- extraction process: further simplification with a single extraction cycle including neptunium barrier;
- evaluation of partitioning of actinides and other long life nuclides;
- simplification of vitrification facilities through development of cold crucible melter which could be used also for other incineration purposes. A large scale demonstration platform has been recently started-up;

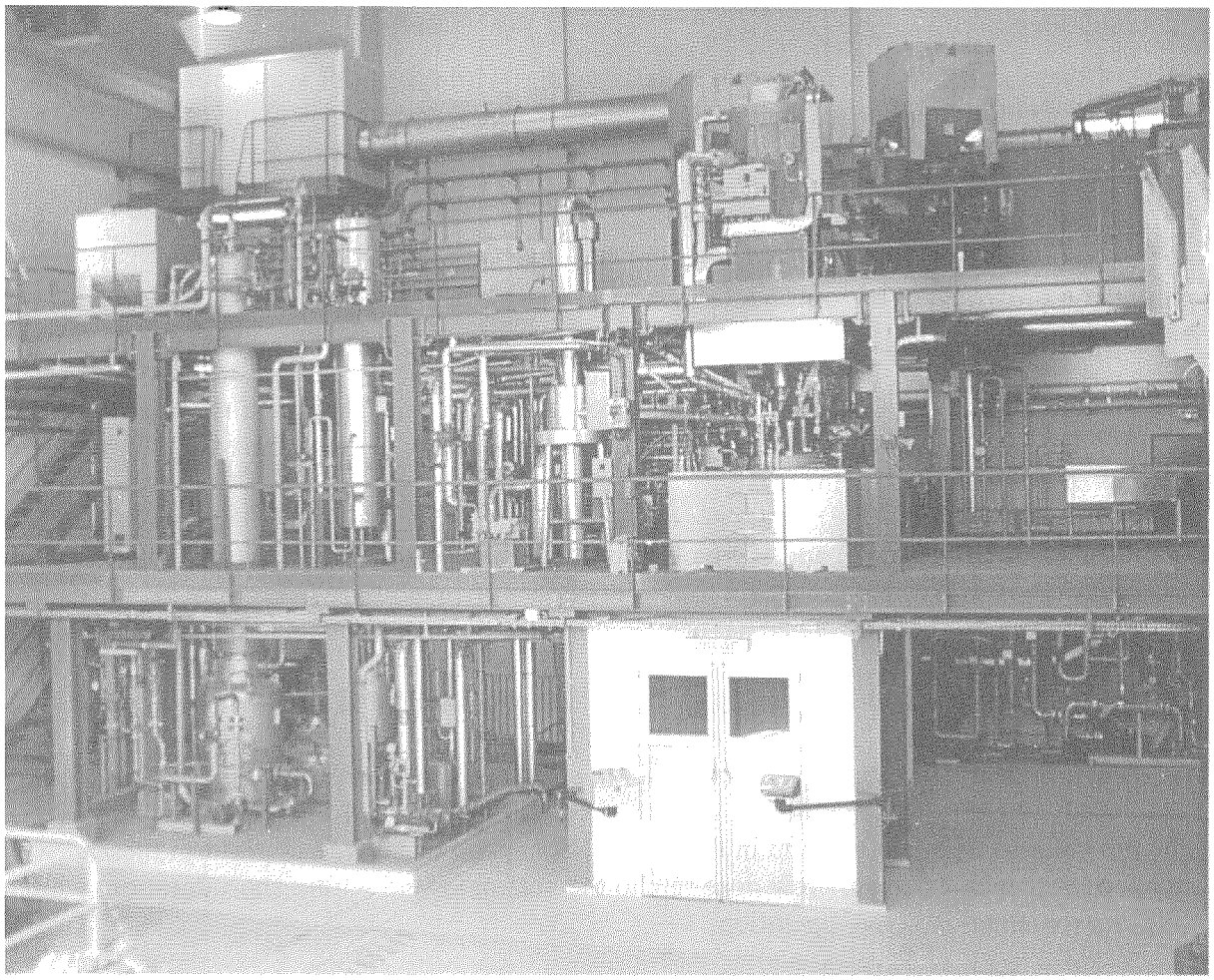

- liquid waste management: although a drastic decrease of release has already been achieved since second generation plants start-up, R&D is still performed to develop complementary technologies such as ultrafiltration;

- solid waste management: minimisation of generation of waste, recycling of equipment after repair, decontamination of waste prior to disposal, best appropriate conditioning process;
- decontamination and dismantling: the decontamination and dismantling of UP1 plant in Marcoule is going on. Large experience, sustained by extensive R&D, is gained on rinsing, new reagents, removal of hot spots. The main purpose is to downgrade waste and reduce their volume in order to minimise disposal costs.

Next generation facilities in COGEMA

Two new facilities on La Hague site are entering commercial service in 2002: plutonium finishing facility R4 [8] and hulls and end-pieces super-compacting facility ACC [9].
These two facilities are a first step towards a new generation of reprocessing plants.

R&D played key role in design of R4, which is characterised by:

- use of a single extraction cycle for plutonium purification and concentration, validated by specific R&D [10] and UP3 feed-back,
- technological innovations, such as centrifugal extractors, supported by extensive R&D program,
- extensive use of in-line measurement, allowing short response time and decreasing analytical workload and effluents,
- significant investment cost reduction.

The waste volume reduction is the main goal of ACC facilities. Compared to direct cementation, volume of final waste is divided by 4. The main other characteristics of ACC are:

- standardisation of package through use of universal canister,
- accommodation of technological waste,
- innovative nuclear measurement devices.

Conclusion

The steady efforts of COGEMA over the last 25 years led COGEMA to operate safely two modern reprocessing plants, highly reliable, with an outstanding record for throughput, low release rates and low occupational doses.
This was obtained thanks to an R&D effort which addressed the actual industrial challenges.
This effort is continued in order :

- First to give to COGEMA the capability to deal with new challenges: new fuel and new constraints.
- Second to be able to build new reprocessing plants as soon as there will be a need with significant lower capital costs than previous plants, thank to simplification of process and technologies based upon this R&D effort.

References

[1] Head-end process technology for the new reprocessing plants in France and Japan, F.J. PONCELET, D. HUGELMAN and al., RECOD 91
[2] Extraction process technology for the new reprocessing plants in France and Japan, F. DRAIN, B. BOULLIS and al., RECOD 91
[3] Uranium Plutonium Separation in Annular Pulsed Column, F. DRAIN, J.P. MOULIN, and al, GLOBAL '97, 250-254, Yokohama, Japan
[4] Advanced Solvent Management in Reprocessing: 5 years of industrial experience, F. DRAIN, J.P. MOULIN, and al., ISEC '96, p.789-794, Melbourne, Australia
[5] Management of waste from French nuclear fuel cycle: what are the key issues, V. LONDRES, R. DO QUANG, Ph. FOURNIER, International Youth Nuclear Congress 2000, Bratislava
[6] COGEMA Reprocessing Complex : Already 9 Years of Operation, Mature and Flexible, JL DESVAUX, F. DRAIN, RECOD 98
[7] Treatment of active laboratory liquid waste by ultrafiltration, R. LIBERGE and al., GLOBAL '97,Yokahama, Japan
[8] Innovative concept for the R4 plutonium finishing facility at La Hague, G.BERTOLOTTI, B. GILLET, I.V. de LAGUERIE and R. RICHTER RECOD'98
[9] A compaction facility for solid high level waste, F. CHOTIN, G. MAURIN, Safewaste 2000, Montpellier, France
[10] Plutonium purification cycle in centrifugal extractors : comparative study of flowsheets using uranous nitrate and hydroxylamine nitrate, P. BARON, B. DINH, F. DRAIN, B. GILLET and B. MAUBORGNE, RECOD'98

JP0250299

JAERI-Conf 2002-004

SUPERPUREX AS A TBP-COMPATIBLE PROCESS FOR RECOVERY AND PARTITIONING OF LONG-LIVED RADIONUCLIDES FROM NPP SPENT FUEL

B.Ya. Zilberman, Yu.S. Fedorov, E.N. Mishin, L.V. Sytnik, O.V. Shmidt, D.N. Kukharev, N.D. Goletsky, R.G. Glekov, Yu.V. Palenik, S.Yu. Sukhareva
V.G. Khlopin Radium Institute, 28, 2nd Murinsky av., St. Petersburg 194021, Russian Federation
Fax: 7 (812) 247-80-95; e-mail: zby@atom.nw.ru

Partitioning of long-lived radionuclides (minor actinides and fission products) is considered within the frameworks of Superpurex process, where Modified Purex-process using 30% tributyl phosphate (TBP) as a solvent is combined with TBP-compatible ZEALEX-process for extraction and separation of TPE and REE, as well as some other elements, which are not extracted by 30% TBP. Zirconium salt of dibutyl phosphoric acid (ZS HDBP) dissolved in 30% TBP is used in the ZEALEX unit as a solvent. The both extraction systems are compatible.

In the Modified Purex-process, U, Pu, Np, Tc and Zr are totally extracted and separated in three or four fractions. One or two of these fractions contain Np, Tc and Zr altogether or in a combination. Lanthanides, Y and TPE, as well as Mo and residual amounts of Np, Pu, U are extracted from high-level raffinate in 1st cycle of ZEALEX-process, TPE&REE being separated from the polyvalent elements by selective stripping. TPE/REE partitioning is achieved in the 2nd cycle of ZEALEX-process.

Salt-free reducing and complexing agents are used at all the stages of the process, to allow minimizing waste volume. Superpurex process flowsheet can be designed also as applied to peculiarities of FBR reprocessing.

Key words: extraction, partitioning, TBP, HDBP, zirconium salt, actinides, REE, Mo

INTRODUCTION

Current state and expected development of nuclear power industry are characterized by increasing fissile burn-up and raising content of fission products and minor actinides in the spent nuclear fuel (SNF). It should exert a significant influence on future fuel reprocessing, causing the necessity of further improvement of the processes used now at the plants. At the same time, the problem of radioactive waste minimization becomes more acute because of modern ecological requirements, which should be taken into aaccount when developing new reprocessing flowsheets.

Consideration is being given in this paper to development of an advanced technology intended for reprocessing of the fuels of higher burn-up. The technology, named Superpurex process, enables recovery and partitioning of practically all long-lived radionuclides, which are contained in NPP spent fuel, to ensure ecologically safe disposal of the nuclides. Principal process flowsheet of Superpurex is shown in Fig.1. It combines single-cycle Modified Purex-process and two-cycle ZEALEX-process.

U, Pu, Np, Tc and Zr are extracted in the Modified Purex-process, as completely as possible, and Zr, Tc and Np are localized in one or two fractions. U and Pu are stripped in two products, of which the first is U-Pu mixture, and the second contains the excess U. In the case of LWR SNF reprocessing and further production of mixed U-Pu oxides based on depleted uranium, the tasks of 1st extraction cycle should include U/Pu separation. So, the technology takes into consideration the possibility of utilization of the regenerated plutonium, in a mixture with uranium, for fabrication of MOX fuel.

ZEALEX-process is used for processing the high-level raffinate of the Purex-process, to separate TPE fraction and some other fractions.

Modified Purex-process implies usage of 30% TBP as a solvent, while ZEALEX-process uses a TBP-compatible solvent – Zr salt of dibutyl phosphoric acid (ZS HDBP) dissolved in

30% TBP. Accidental mixing of the two solvents can not cause a fatal violation of the process. The compatibility of the two extraction systems is based on the fact that HDBP is the degradation product of TBP and can be easily removed from the solvent by carbonate washing. When ZS HDBP admixing to the Purex-process solvent, no precipitates are formed, and ZS HDBP is removed from the solvent to waste during in-cycle carbonate washing of the solvent.

Salt-free reagents are used at all the stages of the Superpurex process.

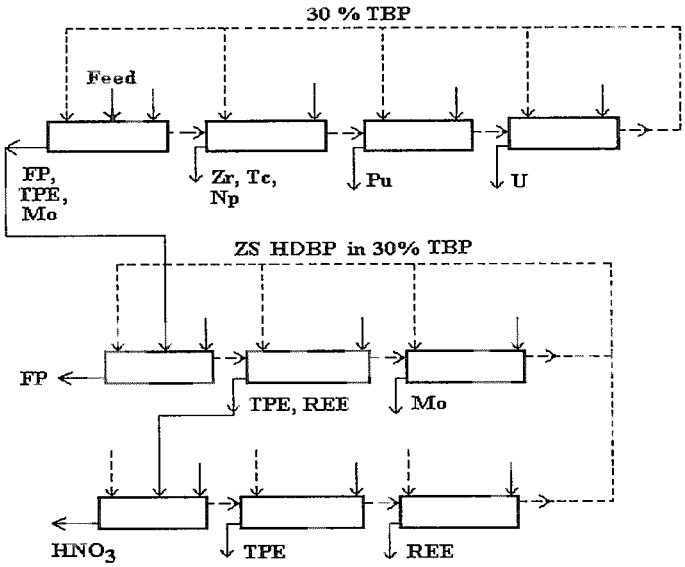

Fig.1. SUPERPUREX process principal flowsheet

MODIFIED PUREX-PROCESS

The main features of the Modified Purex-process are most comparable to those of UP-3 reprocessing plant in France [1] and, especially, of the Japanese PARC process [2].

Localization of Zr is one of the most hard task, as this element is moderately extracted by 30% TBP. Removal of Zr to high-level raffinate is complicated with the effect of higher Zr distribution coefficients in the U extraction zone of real unit (D_R), as compared to the values of the coefficients, predicted by laboratory-scale equilibrium database (D_B) [3]. The difference between DB and DR is increased with lowering acidity and rising U content, as Table I demonstrates.

Table I. Difference of Zr distribution coefficient in single-stage and multistage contactors

Uranium concentration, g/l	Zr distribution coefficient					
	In (4.5±0.5 M) HNO_3			In (3.5±0.5 M) HNO_3		
	D_B	D_R	D_B / D_R	D_B	D_R	D_B / D_R
0	0.6	0.6	1.0	0.1	0.1	1.0
42	0.25	0.45	1.8	0.05	0.13	2.6
76	0.09	0.27	3.0	0.02	0.10	5.0
106	0.02	0.09	4.5	0.004	0.048	12

Full extraction of Zr is attained by means of supporting the elevated acidity and by value of solvent-to-aqueous flow ratio not lesser than 2.7 in the head contactor [4]. These conditions also contribute to better recovery of Tc and Np. Recovery of Zr in 1st extraction cycle results in almost twofold reduction of the volume of the high-level raffinate and simplifies, therefore, further partitioning of long-lived radionuclides.

Practically full extraction of Zr, Tc and Np in 1st cycle is demonstrated already in the first version of the Modified Purex-process [5]. Extraction of these elements is realized then in the process flowsheet of projected Russian RT-2 reprocessing plant [6], which may be considered

as the next development stage of the Modified Purex-process. The two versions of the process flowsheet are distinguished with different combinations of Zr, Np and Tc during their localization within 1st extraction cycle. In the first version of the flowsheet, Zr is stripped together with Pu, while Np and Tc are directed to two individual streams. The second version of the flowsheet provides for separation of Zr as in an individual fraction, while Tc and Np are stripped jointly. However, combined stripping of Zr, Tc and Np, as it is described in joint patent of Khlopin Radium Institute (KRI) and BNFL [7] represents more effective variant of management of these elements (Fig.2). Later research allowed simplifying the process, as it is shown in Fig.1, combining barrier scrubbing and Pu stripping with the use of acetohydroxamic acid (AHA), which was proposed by us as an effective agent for complexing Pu, as well as Np [8] long ago.

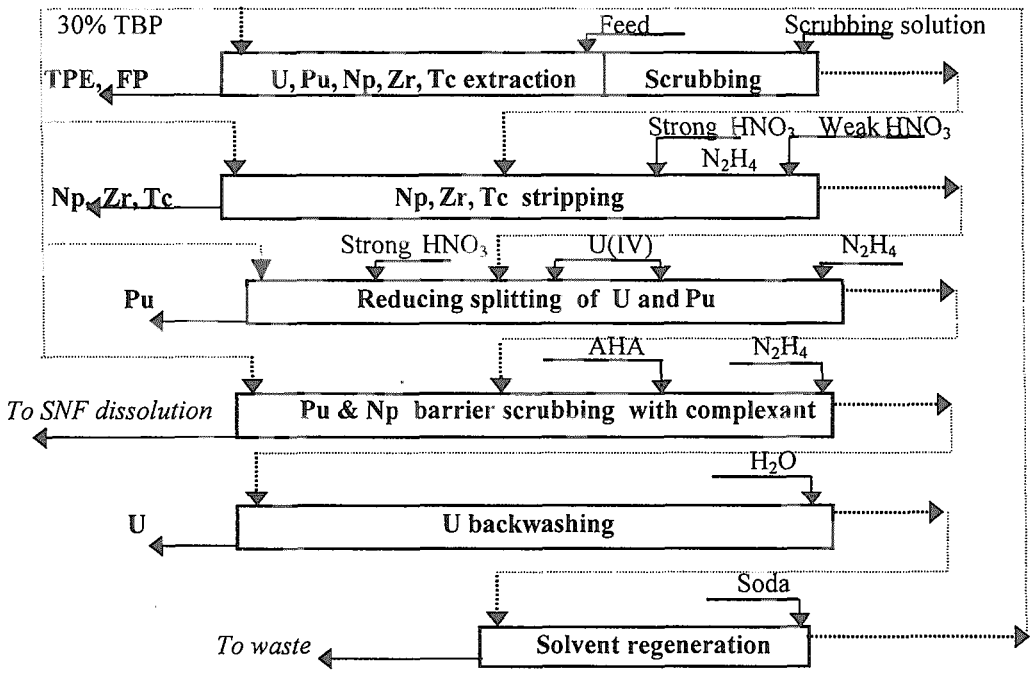

Fig. 2. 1st extraction cycle of Superpurex process for NPP SNF reprocessing

The process flowsheet was tested using simulate solutions in small-sized centrifugal-contactor facility. Flow diagram of the unit of joint Zr, Tc and Np stripping is shown in Fig.3, and the results of the test are present in Table II. The results point to possibility of gathering all Zr, Tc and Np in joint product, which is of relatively large volume and should be sent to evaporation facility for concentrating and nitric acid regeneration. About 2% Pu is stripped with the above elements; to suppress this effect, Pu(III) can be oxidized by hydrogen peroxide, as it has been proposed in the KRI& BNFL patent [7].

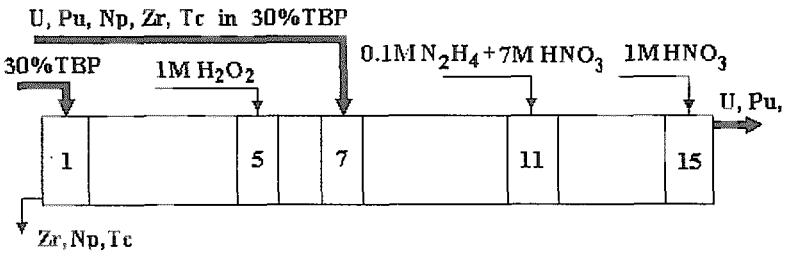

Fig. 3. Flow diagram of Zr, Tc and Np stripping unit

The last variant of the process flowsheet allows for two ways of Pu stripping: either formation of uranium-free strip solution (as in the project flowsheet of RT-2 reprocessing

plant) [7], or conjointly with a minor part of uranium, the main part of the last element being backwashed at the next stage of the process. The second way of Pu stripping looks promising, because joint Pu&U strip solution could be used for fabrication of MOX-fuel, while excess backwashed uranium should be sent to enrichment by U^{235}. The second way of Pu management is in better accordance with the requirements of fissile material non-proliferation as well. In both cases, Pu stripping is conducted with the use of AHA.

Table II. Test results on product composition in the unit of joint Zr, Tc and Np stripping

Stream	Concentration, g/l					
	HNO_3	Zr	Tc	Np	U	Pu
Feed	200	0.9	0.3	0.37	270	0.27
Raffinate	185	0.006	<0.01	<0.001	0.003	-
Solvent product	-	0.4	0.11	0.12	87	0.087
Zr, Np, Tc strip	280	0.41	0.29	0.11	0.03	0.006
U&Pu solvent product	-	-	-	0.008	72	0.075

PARTITIONING OF TPE AND REE USING ZEALEX-PROCESS

Within the Superpurex technology, the main task of Zealex-process consists in extraction of REE and TPE from the high-level raffinate and partitioning of these elements. Simultaneously with REE and TPE, some other elements (Mo, Fe) can be extracted and separated by fractions using the solution of ZS HDBP in 30% TBP diluted with paraffines as the solvent. In starting laboratory-scale experiments [9] it was found out that maximum extraction of REE&TPE by the solvent corresponds to Zr : HDBP ratio around 1 : 9 at HDBP concentration of 0.4 M.

In further investigation, concentration of ZS HDBP in the solvent was reduced twofold, in order to facilitate stripping of TPE and increase their concentrating. The real capacity of the solvent (0.2 M HDBP, Zr : HDBP = 1 : 9) happened to be 0.06–0.07 M for the sum of the extracted elements (REE + TPE + Mo), as follows from Fig.4. The dependence of distribution coefficients of some REE and TPE, as well as Mo, Y, Np, Pu and Fe on aqueous phase acidity is demonstrated in Fig.5. The dependence is most strong for Am and La (inverse proportion to about the cube of acidity), being a little weaker for Eu and much weaker in case of Y (inverse proportion to the square of acidity). It allows to separate Y not only from Am, but also from the cerium group of lanthanides, but it hinder in stripping Y by nitric acid solutions. Distribution coefficients of Fe and Mo first decrease to minimum values with the rise of acidity, but then slowly increase.

Maximum distribution coefficients of REE&TPE during extraction from low-acid solutions (1.5 M HNO_3) by the solvent containing 0.2 M HDBP also correspond to Zr-to-HDBP ratio around 1 : 9. At low solvent loading (not higher than 1% of the solvent capacity), Ce is extracted as well as Eu, while Am is weaker extracted (Fig.6A). In the area of 2.5 M HNO_3, maximum distribution coefficients of REE&TPE are attained at Zr-to-HDBP ratio 1 : 9 – 1 : 10 (Fig.6B), while the factor of separation of Ce&Eu from Am is near 3; however, the values of distribution coefficients of these elements can not ensure real separation of Am from Ce and Eu in a counter-current extraction cascade.

At the acidity of 5 M HNO_3, the distribution coefficients of REE&TPE do not change when Zr-to-HDBP ratio varies in the range from 1 : 8 to 1 : 25, though the values of the distribution coefficients are essentially lower than at the acidity of 2.5 M HNO_3, especially for TPE (Am) and cerium-group of REE [9]. It should allow partitioning of yttrium-group from cerium-group of REE (Fig.6C), ensuring separation factor from 5 to 50; in this case, TPE go with cerium-group, while Y is stripped much weaker, as well as Ho or Tm (the last two elements do not present in SNF). It can be used also for separation from Mo.

These date allows to elaborate the calculation code used for flowsheet designing and testing.

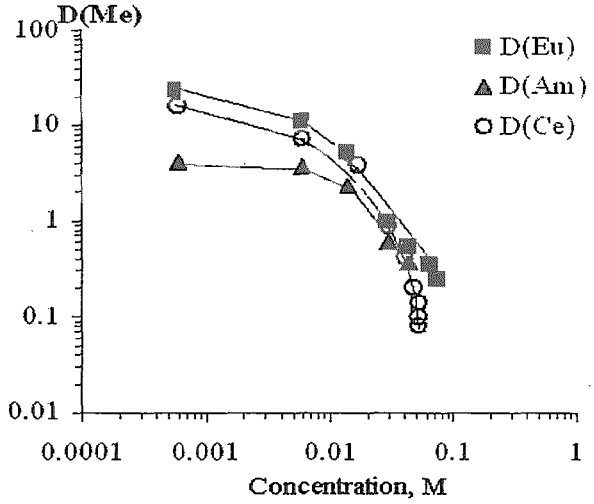

Fig.4. Dependence of some TPE and REE distribution coefficients D on the element concentration in solvent during extraction by ZS HDBP (0.2 M HDBP) in 30% TBP (decane as a diluent) from 1.5 M HNO_3.

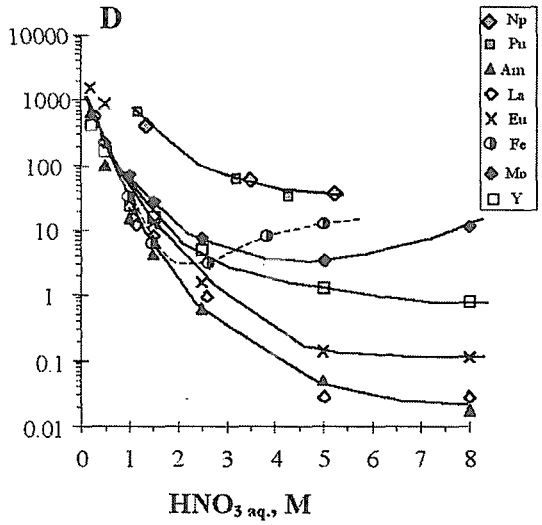

Fig.5. Dependence of TUE, REE, Y, Mo and Fe distribution coefficients (D) on nitric acid concentration at extraction by ZS HDBP (0.2 M HDBP) in 30% TBP (decane as a diluent).

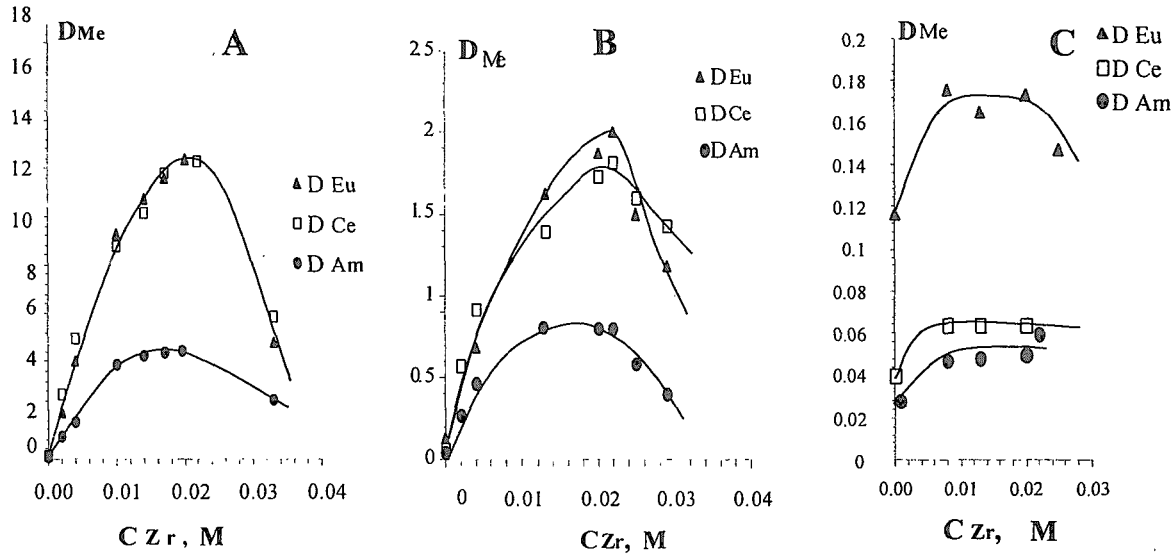

Fig.6. Influence of the Zr-to-HDBP ratio on distribution coefficients of Eu, Ce and Am at extraction by ZS HDBP solution (0.2 M HDBP) in 30% TBP (decane as a diluent). Aqueous concentrations: HNO_3 (equilibrium), M: **A**–1.5; **B**–2.5; **C**–5.0; REE (starting) 0.1 g/l.

Further investigation was developed in the direction of finding conditions for TPE/REE separation of with the use of a complexing agent. The mixture of diethylenetriaminopenta-acetate (DTPA) with an organic acid (see Table III) was used for complexing. The best results on Am/Eu separation were obtained when using DTPA mixed with one of the following organic acids: lactic, ascorbic and formic. However, the lactic acid destroys the solvent by stripping Zr from ZS HDBP, while ascorbic acid is relatively expensive. Therefore, the formic acid was selected for further research. Table IV presents the dependence of REE&Am distribution coefficients on DTPA concentration in 1.5 M formic acid. The data show that separation of the pair Eu/Am is critical, while the amount of the REE heavier than Eu is negligible in SNF. The separation coefficients for the pairs Ce/Am and Eu/Am equal, respectively 167,5 and 22,5

at the optimum concentration of 0.1 M DTPA. Increasing of the solvent loading leads to diminishing of the distribution coefficients, especially in case of Am, and, consequently, to the rise of REE/Am separation coefficient.

Table III. Eu&Am extraction by ZS HDBP (0.2 M HDBP) in 30% TBP (decane as a diluent) from solutions of DTPA (0.05 M) and organic acid (1.5 M). Starting Eu concentration – 2.0g/l.

Aqueous phase	pH	D_{Eu}	D_{Am}	D_{Eu}/D_{Am}	Zr in solvent, g/l
DTPA+ lactic acid	2.5	17.2	2.12	8.1	0.57
DTPA + aminoacetic acid	5.0	0.04	0.04	1.0	2.0
DTPA + formic acid	2.0	6.12	1.35	4.5	1.92
DTPA + ascorbic acid	2.5	5.54	1.08	5.1	1.92
DTPA + citric acid	1.5	21.3	16.6	1.3	1.33

Table IV. Distribution of REE and Am at extraction by ZS HDBP (0.2 M HDBP) in 30% TBP (saturated hydrocarbons as a diluent) from 1.5 M formic acid. Starting REE&Y content - 1 g/l.

DTPA content, M	Distribution coefficients						
	La	Ce	Nd	Eu	Dy	Y	Am
0.05		140		16			6.9
0.1	205	67	51	9	4.3	81	0.4
0.2		28.5		0.55			0.35
0.25		0.4		0.15			0.2

Possibility of partitioning of TPE and REE was also checked during stripping of these elements from ZS HDBP by the complexing mixture of 0.1 M DTPA with 1.5 M formic acid. HDBP concentration was chosen as low as 0.1 M. Optimum REE concentration in solvent product, as well as appropriate temperature and solvent-to-aqueous flow ratio were determined

Table V. Stripping of REE and Am during by 1.5 M formic acid containing DTPA. Solvent - ZS HDBP (0.1 M HDBP) dissolved in 30% TBP (Isopar L as a diluent). Summary REE&Y concentration 1-2 g/l.

Concentration of REE in solvent product, g/l	Tempera-ture, °C	Solvent-to-aqueous volume ratio	DTPA content, M	D(Me)		
				Ce	Eu	Am
1	20	1	0.2	3.9	0.38	0.08
	"		0.1	17	0.88	0.21
	40		0.1	13	0.43	0.15
1	20	2	0.1	12	1.3	0.69
	20		0.2	3.2	0.78	0.55
	40		0.1	9	0.51	0.09
1.4	20	1	0.1	3.1	0.6	0.08

Basing on the results of the above research, a two-cycle process flowsheet for REE and TPE partitioning (ZEALEX-process) was developed. The process provides for purification of TPE from Y and, partially, from Sm and Eu, as well as from Mo and Zr in 1st cycle, in solutions of considerable acidity. Final purification of TPE is carried out in 2nd cycle, using DTPA as a complexing agent. The process flowsheet is shown in Fig. 7.

The process was tested, using simulate solutions in a pilot facility containing 4 small-sized 12-stage centrifugal contactors. 1st partitioning cycle included the units as follows: the unit for REE, TPE and Mo extraction; the unit for stripping of TPE and cerium group of REE; the unit for stripping of Y, Mo and residual REE; the unit of removal of excess Zr. Concentration of HDBP in the solvent was of 0.2 M. The performance of the two-cycle process flowsheet can be seen in Table VI. Two strip solutions were obtained in 1st partitioning cycle, the first one

containing TPE and cerium group of REE, the other one containing Mo, Y, residual REE and less than 0.1% of TPE. If necessary, Mo can be preliminarily concentrated. Possibility of Zr stripping from a part of solvent product, to support Zr balance, was also successfully demonstrated. The extracted microamounts of U, Pu and Np are removed together with Zr.

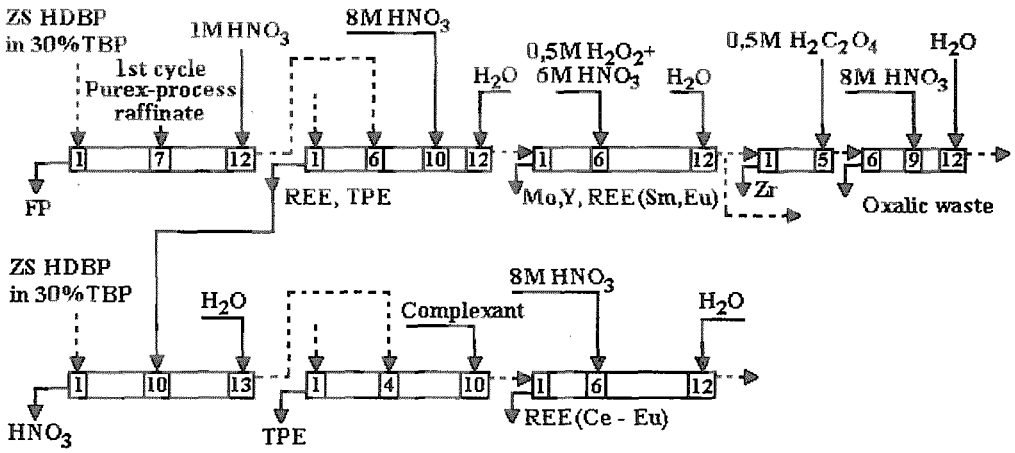

Fig 7. Two-cycle process flowsheet with the use of ZS HDBP for partitioning Mo, TPE, REE, Y from high level raffinate of Purex-process.

Table VI. Characteristics of two-cycle partitioning process products

Product	HNO_3, M	Element percentage (to starting amount), %				
		Am	REE	Y	Mo	Zr
Feed of 1st partitioning cycle	1.7	100	100	100	100	100
Raffinate of 1st partitioning cycle	1.8	< 0.5	<0.2		< 0.5	< 0.1
TPE&REE strip solution	4.3	99.3	38.5	< 0.1	< 0.1	< 0.1
Mo, Y and REE (Sm, Eu) strip solution	4.9	< 0.1	61	96	98.5	< 0.1
Zr strip solution	0.2	-	-	4	< 0.1	99
Feed of 2nd partitioning cycle	0.6	99.3	38.5	< 0.1	< 0.1	< 0.1
Raffinate of 2nd partitioning cycle	0.6	< 0.5	<0.2			
TPE strip solution	<0.1	99	~2			
REE strip solution	4.0	< 0.1	36.5			

Feeding solution for testing of 2nd partitioning cycle was simulated as diluted REE&TPE strip solution of 1st partitioning cycle. 0.1 M ZS HDBP in 30%TBP was used as a solvent. TPE (Am) was stripped with the use of complexant (DTPA with formic acid). It has been found out (Table VI), that Ce is completely separated from Am and passes to REE strip solution, while Nd distribution, because of high content of this element in SNF, is critical for Am purification. The resulted REE strip solution did not contain TPE (Am), while Am decontamination factors, according to composition of Am strip solution, were higher than 200 on La&Ce, 20-30 on Pr&Nd, and 3 on Sm& Eu. In both cycles, REE strip (including Y) contain less than 0.1% of TPE.

Interstage sampling through the both cycles and determination of distribution coefficients of the present elements allowed making computation of optimized product characteristics, using a simplified mathematical model of the process. The characteristics (Table VII) proved to be better than the experimental results.

CONCLUSION

The proposed version of the Modified Purex-process makes it possible to localize more than 99% of Tc and Np in 1st cycle of the process. It also provides for Zr localization as a separate

Table VII. TPE decontamination during partitioning in two-cycle process using ZS HDBP. Assumed burn-up of WWER-1000 spent fuel - 40GW*day/t

Element	Factor of Am purification from REE						Element content, gram per ton SNF				
	Experimental			Optimized process			Start	Experimental		Optim. process	
	Cycle1	Cycle2	Σ	Cycle1	Cycle2	Σ		1 cycle	2 cycles	1 cycle	2 cycles
Am	1	1	1	1	1	1	475	475	475	475	475
La	2.1	314	659	1.06	>1000	>1000	1637	779.5	2.5	1544	<1.5
Ce	2.2	234	515	1.5	>1000	>1000	3214	1461	6.2	2143	<2
Pr	2.3	31	71	1.9	193	367	1411	613	20	743	2
Nd	2.5	21	53	2.0	126	252	5590	2236	106	2795	11
Pm	-	-	-	*2.8*	75	210	310	-	-	110	1.5
Sm	3.4	3.4	12	3.5	23	81	1070.	315	93	306	4
Eu	3.3	3.7	12	6.1	29	177	52.4	16	4.3	8.6	0.05
Gd	-	-	-	8.0	20	160	223	-	-	28	1.4
Y	>10	-	-	36	14	504	728.5	<73	-	20	1.4
ΣREE	2.6	23	60	1.9	315	600	14236	5493	232	7588	23
ΣREE/Am							29.3	11.6	0.5	16	0.05

fraction and, due to it, for two-fold reduction of high-level raffinate flowrate, which is important for further TPE partitioning.

In two-cycle ZEALEX-process, TPE separation from REE процесса resulted in decontamination factor ~ 60; optimization of the process should allow obtaining TPE product containing only ~5% REE, mainly residual Nd.

As a whole, in combination with iodine-129 blowing-off at the stage of SNF dissolution, very effective partitioning of the main long-lived radionuclides can be attained, while no secondary organic waste is generated.

The work has been carried out with partial support of ISTC, Project #1608.

REFERENCES

[1] – Baron P., Boullis B., Germain M. et al. Proc. Int. Conf. Global'93. Vol.1, p.63-70.

[2] - Uchyama G., Asakura T., Hotoku S., Fujine S. The 5 th. Int. Nucl. Conf. Recycl. Cond. & Dispos. "RECOD'98" (1998, France). Vol.1. p.393-400.

[3] - Zilberman B.Ya., Mishin E.N., Fedorov Yu.S. et al. Chemical Technology (Rus). (2001), #7.

[4] - Zilberman B.Ya., Dzekun E.G., Nardova A.K. et al. "Method of spent fuel element processing". USSR Patent #1804652 (Bul. 11, 1993)

[5] - Zilberman B.Ya., Fedorov Yu.S., Mashkin A.N. Proc. Int. Topical Meet. on Nucl. and Hazardous Waste Management "Spectrum'94" (1994, Atlanta, USA). Vol.1, p.581-585.

[6] - Zilberman B.Ya., Russian Radiochemistry, (2000). Vol.42, #1, p.3 -15.

[7] - Zilberman B.Ya., Fedorov Yu.S., Denniss I.S. et al. "Process for NPP spent fuel reprocessing". Russian Patent # 2132578 (Bul. 18, 1999)

[8] - Zilberman B.Ya., Mashkin A.N., Nardova A.K. et al. "Method of spent nuclear fuel reprocessing". Russian Patent # 2012075 RU (Bul. 8, 1994).

[9] - Zilberman B.Ya., Fedorov Yu.S., Shmidt O.V. et al. Russian Radiochemistry,(2000). Vol. 42, #4, p.338-344, 345-348.

JP0250300

JAERI-Conf 2002-004

PARC PROCESS AS ADVANCED PUREX PROCESS

G. UCHIYAMA, H. MINEO, T. ASAKURA, S. HOTOKU, M. IIZUKA,
S. FUJISAKI, H.ISOGAI, Y.ITOH, M. SATO, N.HOSOYA

Process Safety Laboratory
Japan Atomic Energy Research Institute (JAERI)
Tokai-mura, Naka-gun, Ibaraki-ken, Japan, 319-1195
Fax:8129-282-6677, e-mail: uchiyama@procsafe.tokai.jaeri.go.jp

ABSTRACT

An advanced PUREX process, PARC process, has been developed for establishing the coming generation's fuel cycle technologies. Key technologies applied in the process are: 1) removal of carbone-14 and iodine-129 with adsorption techniques in dissolver off-gas, 2) separation of neptunium and technetium by selective reduction of Np(VI) by normal-butyraldehyde and the high acid scrubbing of technetium, 3) separation of americium from the raffinate of co-extraction step with adsorption technique, 4) solvent-washing with normal-butylamine compounds. The separation efficiency of long-lived nuclides in the process was studied in chemical flow sheet experiments using spent fuels burned up to 44,000 MWD/tU.

Keywords: Reprocessing, Long-lived nuclide, PUREX process, PARC process, Separation

INTRODUCTION

The utilization of nuclear energy as power generation is considered as a realistic countermeasure for the environmental problem relating to the CO_2 emission and for the energy security due to the increasing population. LWR fuel cycle age is extended further for the delay of establishment of FBR fuel cycle technologies and the use of MOX fuel in LWRs will be enlarged for saving energy resource. The reprocessing process technology in LWR fuel cycle applies a current PUREX process. Present commercial reprocessing plants have achieved a 99.88% recovery of the fissile material contained in spent fuel and have developed safe waste conditioning through vitrification for high-level waste [1]. The effort to applying new technologies to nuclear fuel reprocessing for long-term energy security is further continued for reduction of radioactive waste volume and minimization of toxicity based on the ALARA principle [2-6]. Also the improvement of the process safety on the capability of confining radioactive materials in the process and the cell ventilation systems are conducted under normal operation and accidental conditions such as fire, explosion and criticality in reprocessing plants [7-9].

In JAERI the process safety studies have been conducted mainly in NUCEF (Nuclear Fuel Cycle Safety Engineering Research Facility) according to the government five-year nuclear safety research plan [10]. Researches are radioactive nuclides confinement safety in reprocessing under normal conditions and accidental conditions such as criticality accident of uranium solution fuels, fire and explosion accident [11]. An advanced PUREX process, PARC (Partitioning Conundrum Key) process having a partitioning function of long-lived nuclides has been developed to improve the process safety in BECKY in NUCEF [12-18]. Also the distribution behaviors of radioactive nuclides in the process to evaluate the safety margin of radioactivity confinement capability have been studied. On the capability of confining radioactive materials in criticality accidents of fuel solutions, the release behavior of radiolysis gases and radioactive materials from the fuel solution to the gas phase in criticality accident of the fuel solution has been studied in TRACY [19-21]. On the capability of confining radioactive materials in fire and explosion accidents, data on the source terms, such as mass,

energy and smoke release rate from burning materials, and clogging properties of the HEPA and pre filters have been obtained in engineering scale equipment [22-23]. These researches lead to develop safety criteria and to establish technical base for licensing.
In this paper the outline of the development of PARC process is described in detail.

OUTLINE OF PARC PROCESS

PARC Process

The PARC process has been developed to enhance the confinement capability of long-lived nuclides in simplified reprocessing. Principal feature of the process is a simplification of PUREX process. In the development of the process, the following intentions are taken into consideration; 1) reduction of radioactive waste volume containing TRU elements, 2) reduction of environmental hazard risk due to long-lived nuclides such as technetium-99, carbon-14 and iodine-129, 3) enhancement of economical competitiveness, 4) enhancement of nuclear non-proliferation and 5)enhancement of process safety.
In an advanced fuel cycle in which the PARC process concept is applied, the power plant system consists of LWRs including reduced moderation water reactor (RMWR) and FBR with uranium, plutonium and some neptunium being recycled. Long-lived nuclides of technetium-99, carbon-14 and iodine-129 are separated and confined in a long-term storage facility. Transmutation devises are developed to reduce the waste volume in the long-term future[24].
The process consists of four systems. Iodine-129 and C-14 are removed from dissolver off-gas in the head-end treatment system. Tc and Np are extracted by TBP with U and Pu in improved co-extraction step. Extracted Np and Tc are separated effectively from U and Pu stream before U/Pu partitioning step. In this step selective reduction of Np(VI) to Np(V) in the presence of U(VI) and Pu(IV) is a significant technique. Figure 1 shows the comparison of the extraction step between current PUREX and PARC processes. In the Current PUREX process, there are three extraction cycles for recovery of purified U and Pu which are 1st cycle for extraction of U and Pu from spent fuel, U and Pu purification cycles as shown in Fig.1. On the other hand, the PARC process is only one cycle process for recovery of purified U and Pu without purification cycles. The decontamination of not only Np and Tc but also fission products from U and Pu are expected in the added separation steps of Np and Tc between co-decontamination and U/Pu partitioning steps.

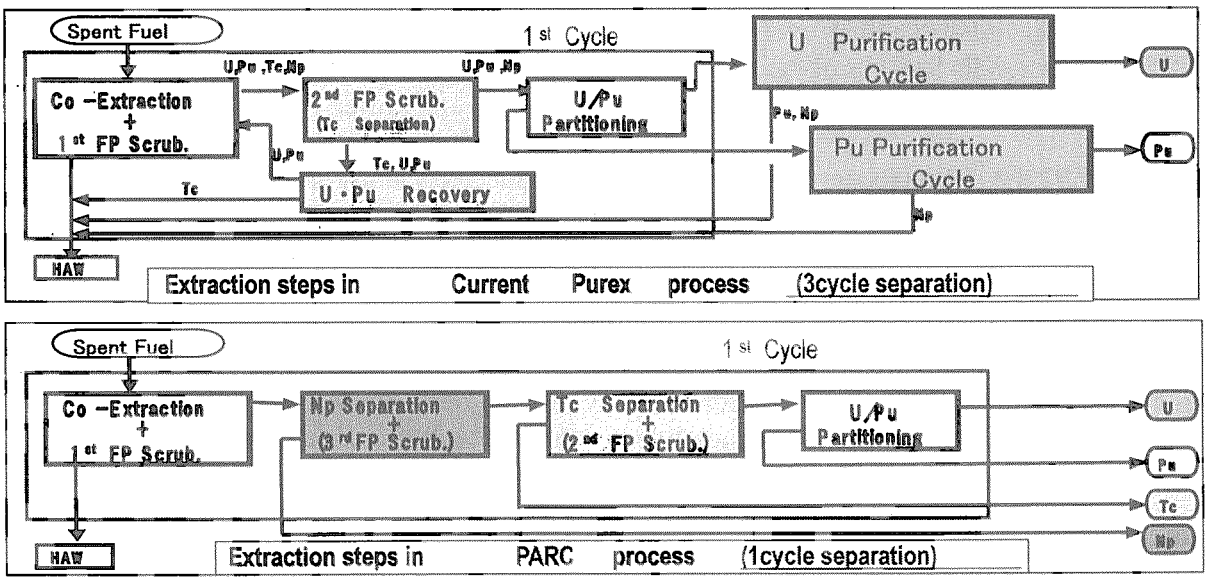

Fig.1 Comparison of extraction step between current PUREX process and PARC

Am and Cm are separated from the raffinate of the co-extraction step with adsorption technique. Reagents such as nitric acid and TBP solvent are treated and recycled in the process. Recovered U and Pu are recycled in the light water reactors as UO_2 fuel and MOX fuel. And others long-lived nuclides are transmuted with accelerator or fission reactors. In the PARC process U and Pu purification steps are not included, like one cycle process.

Target of decontamination factors

Targets of separation efficiency in the PARC process are shown in the Table I The targets of separation efficiency of iodine, Np-237, Tc-99 are determined based on the designed values of current reprocessing plant [25]. The target of separation efficiency of C-14 is almost the same as that of I-129. As for Am and Cm, the targets of separation efficiency are the same as those of Am and Cm from the high level liquid waste in the OMEGA project in Japan [26], where the targets of separation efficiency are determined to make the hazard index of a vitrified HLLW after storage for 1,000 years comparable to that for naturally occurring minerals containing 3% of uranium. In a current PUREX reprocessing plant, high decontamination factors were obtained, that is, the decontamination factor of fission products in 1st separation cycle is more than 2×10^5 for U and more than 8×10^4 for Pu [27]. In the extraction step of the PARC process, the decontamination factors for fission products will be beyond the designed values and required values for recycling and transmutation.

In order to find the feasibility of the PARC process, chemical flow sheet experiments have been conducted by using spent fuels burned up to 44,000 MWD/tU.

Table I. Target of separation efficiency of long-lived nuclides in PARC process

Step	Separation Efficiency	
Head-end	C-14	99 %
	I-129	99.6 %
Extraction	Np	99.4 %
	Tc	99.97 %
	U	99.96 %
	Pu	99.93 %
Aqueous waste treatment	Am	99.99 %
	Cm	99.9 %

CHEMICAL FLOW SHEET EXPERIMENT

Experimental

Chemical flow sheet experiments were conducted by using a small scale reprocessing process equipment (PARCY) installed in alpha-gamma cell in NUCEF as shown in Fig.2. The reprocessing process equipment consists of head-end, extraction, off-gas treatment and waste treatment steps. The head-end step consists of a batch-wise dissolver, an iodine-stripping tank, a clarification filter and a feed tank for extraction step.

Spent fuel of PWR 44,000 MWD/tU was dissolved in the dissolver under three different nitric acid conditions. Each experiment used about 400 g of the spent fuel. Iodine remained in the dissolver solution was stripped by the NO_X gas bubbling in the iodine stripping tank. The dissolver solution was clarified with the clarification filter. NO_X gas in the dissolver off-gas was

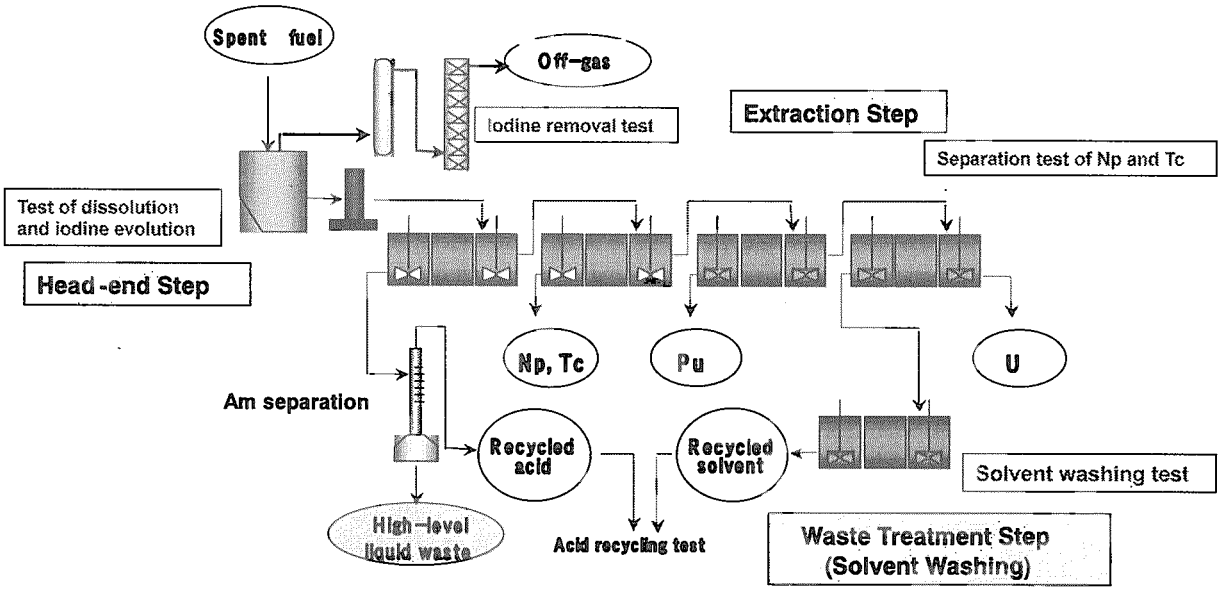

Fig. 2 Reprocessing process equipment installed in alpha-gamma cell in NUCEF

removed in the NO_X scrubber. Iodine in the dissolver off-gas was captured in the iodine adsorbent columns. Carbon-14 was treated in a trap mounted to the iodine adsorbent columns.
The extraction step with five mixer-settlers was used to investigate extraction behaviors of uranium, plutonium, neptunium, technetium, zirconium, ruthenium, cesium and iodine. The flow sheet consists of eight steps: co-decontamination, Np separation, Tc separation, U recovery and U/Pu partitioning, U stripping, diluent washing and solvent washing steps. Normal-butyraldehyde was used as a Np(VI) reductant. The scrubbing solutions for neptunium and technetium were 3 M and 6 M nitric acid, respectively. Uranium (IV) was used as a Pu(IV) reductant instead of iso-butyraldehyde in this experiment.
Purchased reagents such as TBP, n-butyraldehyde, n-butylamine compounds and n-dodecane were used without any special pretreatment. The dissolver solution of spent fuel as a feed contained 216 g/l uranium, 2.43 g/l plutonium and 3.1 M nitric acid. The valence states of plutonium and neptunium in the feed solution were mainly Pu(IV) and Np(V), respectively by a spectrophotometer analysis. The concentration of nitrous acid in the feed solution was about 6E-3 M. Tracers of technetium-95m, zirconium-95 and I-131 were added into the feed solution after diluted with nitric acid solution.

Results and discussion

In the study on the head-end step, the dissolution behavior of uranium, plutonium and fission products, the migration behavior of volatile elements such as iodine-129, carbon-14 and krypton and the characteristics of insoluble residues were focused. Iodine (I-129) was released into the dissolver off-gas and then collected in the absorbent columns loaded with silver impregnated silica-gel (AgS) as shown in Fig.3. It was confirmed that the adsorbent was effective for iodine removal in the actual spent fuel dissolution process. By the filtration of dissolver solution, the particle size diameter distribution of insoluble residue in the solution was obtained in the range of 0.4 μm to 10 μm.
In the extraction step, the concentrations of uranium and plutonium were almost constant in both the organic and the aqueous phases in the Np and the Tc separations steps. As for neptunium and technetium, the concentrations in both the organic and the aqueous phases in both the Np and the Tc separation steps are shown in Fig.4. About 75% of the neptunium that

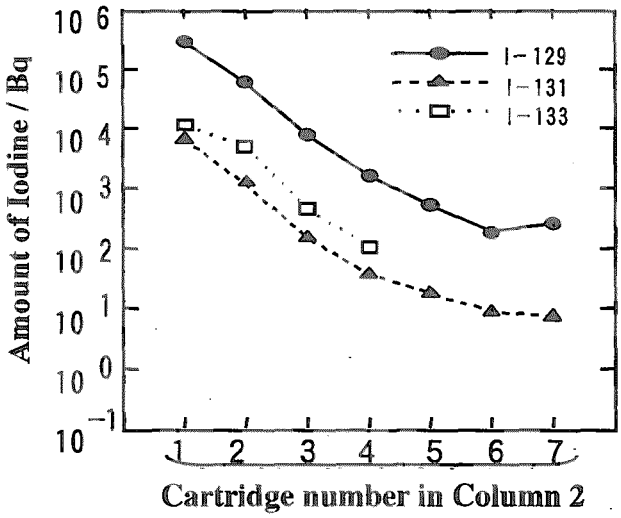

Fig. 3. Concentration profile of iodine in adsorbent column.

flowed to the Np separation step was back-extracted from the solvent stream loaded with uranium and plutonium and flowed to the neptunium product. This implies that Np(VI) was reduced to Np(V) by n-butyraldehyde.

As for technetium, about 90% of the technetium that flowed to the Tc separation step was back-extracted from the solvent stream and flowed to the technetium product. The separation efficiencies are not high enough due to the limit of conditions for experiments. The separation efficiencies will increase by optimizing the concentration of Np reductant, flow ratios (O/A) and separation stages in the steps. Simulation codes have been developed for designing and evaluating chemical flow sheet.

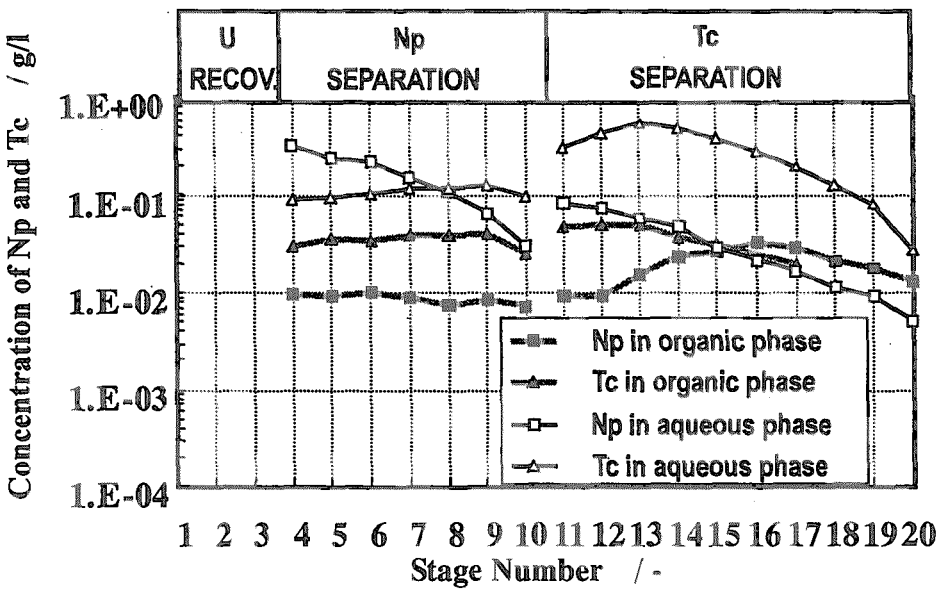

Fig. 4. Concentration profiles of Np and Tc in Np and Tc separation steps

In the U/Pu partitioning step, the plutonium concentration in both the organic and the aqueous phases decreased with approximately the same gradient as in the U/Pu partitioning step. More

than 99.8 % of the plutonium that flowed to the U/Pu partitioning step was back-extracted from the solvent stream and flowed to the plutonium product. The absorption spectrum of the plutonium product solution showed that the plutonium valency in the product solution was trivalent. It was found that Pu(IV) was reduced to Pu(III) by uranium (IV). As for the extraction behaviors of neptunium and technetium, only 5 % of the neptunium that flowed to the U/Pu partitioning step was back-extracted from the solvent stream loaded with uranium and flowed into the plutonium product solution. About 50 % the technetium that flowed to the step was back-extracted from the solvent stream loaded with uranium and flowed as plutonium product.

Am^{3+}-selective adsorption was studied by using an adsorbent to develop an actinides / lanthanide separation process. The adsorbent was made by porous silica-polymer composite material which supports nitrogen donor aromatic compound, 2,6-bis (5, 6-dialkyl-1,2, 4-triazin-3-yl) pyridine (Alkyl-BTP). In the case of Ethyl-BTP adsorbent, the distribution ratio of Am^{3+} was 60 $mL \cdot g^{-1}$. The valued of adsorption selectivity of Am^{3+} against Ce^{3+}, Eu^{3+} or Gd^{3+} was 390, 13, or 9.5, respectively. Therefore, it is possible to adsorb Am^{3+} ion selectively against lanthanides ions by that adsorbent [28].

In the solvent washing step, total alpha activity in the U stripped solvent decreased from 3,200 Bq/ml to 3.6 Bq/ml through the use of n-butylamine compounds (carbonate and oxalate). The decontamination factor for total alpha activity in the solvent washing step Ⅰ and Ⅱ were about 1,000. There was not a large difference in solvent washing effect between n-butylamine carbonate and oxalate in solvent washing step Ⅱ.

The destruction of butyraldehyde isomers and butylamine has been studied using a silver catalyzed electrochemical oxidation technique [29]. The destruction rates of the compounds were measured as a function of the concentrations of the compounds, silver and nitric acid in aqueous solution, anode potential and temperature. About 95 % of n-butyraldehyde in 3 M nitric acid was destroyed within 300 minutes by electrochemical oxidation at the anode potential of 1.6 versus a reference saturated calomel electrode (SCE). About 95 % of butylamine in 3 M nitric acid was destroyed within 270 minutes by electrochemical oxidation at the anode potential of 1.6 versus SCE. The process was found to be applicable to the destruction of butyraldehyde isomers in nitric acid solutions.

The effectiveness of the salt-free techniques of n-butyraldehyde as a Np reductant and n-butylamine compounds as washing reagents was found in the chemical flow sheet experiments. Further study is required to optimize the flow sheet conditions of the PARC process.

CONCLUSIONS

Demonstration experiments of an advanced PUREX process, PARC process, have been conducted by using spent fuel of 44,000 MWD/tU in NUCEF.

The dissolution behaviors of uranium, plutonium and fission products, the migration behaviors of volatile elements such as iodine-129 and carbon-14 and krypton and characteristics of insoluble residues were studied in head-end step. The distribution behaviors of minor nuclides such as neptunium and technetium in the PARC process were studied in extraction step.

It was found that Np(VI) was reduced to Np(V) by n-butyraldehyde selectively in the presence of U(VI), Pu(IV) and Tc(VII), high acid scrubbing was effective for technetium separation and that butylamine compounds (carbonate and oxalate) were effective solvent-washing reagents.

REFERENCES

[1]M.F.DEBREUILLE,P.PRADEL and F. DRAIN, "Present status of R&D on reprocessing process in COGEMA", JAERI-Conf, "The 3rd NUCEF International Symposium (NUCEF2001)", to be published.

[2] B.YA. ZILBERMAN, YU. S.FEDOROV, E. N. MISHIN, L.V.SYTNIK, O. V. SHMIDT and D. N. KUKHAREV, "SUPER PUREX-Process for partitioning of U, Pu, Np, TPE and some long-lived fission product at NPP spent fuel reprocessing ", Proc. SAFEWASTE 2000, Montepellier, France,736, 2000.

[3] SUE ION, "Current options for the back end of the fuel cycle", Proc, ATALANTE 2000, Avignon, France, I-03, 2000.

[4] V.S.KOLTUNOV, R.J.TAYLOR, S.M. BARANOV, E.A. MEZHAV, V.G. PASTUSHAK and G. V. KOLTUNOV, "Acetaldoxime-a promising reducing agent for Pu and Np ions in the PUREX process", Proc, ATALANTE 2000, Avignon, France, O1-06, 2000.

[5] C. CAU. D. COUMES, J. C. DUMAS and F. DEVISME, "PUREX dissolution off-gas treatment: Potentials of hydroxylammonium nitrate as a scrubbing reagent for iodine and nitrogen oxides", Proc, ATALANTE 2000, Avignon, France, O1-07, 2000.

[6] Y. WEI, M. KUMAGAI, Y. TAKASHIMA,H. YOKOI, T. HOSHIKAWA, "Development of silica-based chelating exchangers and their separation behavior for lanthanides and actinides by column chromatography", Proc. RECOD 98, Nice, France, 701, 1998.

[7] G. NISHIO, K. WATANABE, K. KOUNO, N. YAMAZAKI, S. MUKAIDA and I. YOSHIOKA, "Development of the CELVA-1D code to evaluate the safety of an air-ventilation system during postulated fire and explosion in the reprocessing plant", JAERI-DATA/Code 98-017, 1998 , in Japanese.

[8] S. TASHIRO, H. ABE, H. NAGAI, T. KIOKE, S. OKAGAWA and G. UCHIYAMA, "Release behavior of mist from fuel solution in transient critical experiment using TRACY", Proc. AAAR 2000, USA, 2000.

[9] H. ABE, S. TASHIRO, H. NAGAI, T. KIOKE, S. OKAGAWA and G.UCHIYAMA, "Studies on release behavior of radioactive noble gases from fuel solution under simulated nuclear criticality accident", J. Nucl. Sci. Technol, in press.

[10]Nuclear Safety Commission, "The five-year plan for nuclear safety research",2000.

[11] M. MAEDA, S. FUJINE, G. UCHIYAMA, T. KIHARA, T. SAKURAI and T. TSUJINO, "A process conception of an advanced reprocessing based on PUREX incorporating the partitioning", Proc. GLOBAL 1995, Versailles, France, 556, 1995.

[12] S. FUJINE, G. UCHIYAMA, T. KIHARA, T. ASAKURA and T. SAKURAI, "Radioactivity confinement capability of PARC concept for the future reprocessing", Progress in Nuclear Energy, 32, 1998.

[13]G. UCHIYAMA, T. ASAKURA, M. WATANABE, S. FUJINE and M. MAEDA, "The separation of neptunium and technetium in advanced PUREX process", Solvent Extr.. Ion Exch., 16, 1,191, 1998.

[14] G. UCHIYAMA, S. FUJINE and M. MAEDA, "Solvent-washing process using butylamine in reprocessing", Nucl. Technol., 120, 41, 1997.

[15] H. MINEO, T. YAGI, A. TAKAHASHI, G. UCHIYAMA, S. FUJINE, "Development of treatment technology for carbon-14 in dissolver off-gas of spent fuel", Proc. ICEM'99, 1999.

[16] T. ASAKURA, S.HOTOKU, M. IIZUKA, S. FUJISAKI, M. GOTOH, H. MINEO and G. UCHIYAMA, "Reprocessing experiment using spent fuel at NUCEF facility", Proc. ATALANTE 2000, Avignon, France, O1-03, 2000.

[17] K. KAMEI, S. HOTOKU, T. ASAKURA, M. WATANABE, G. UCHIYAMA and S. FUJINE, "A study on decomposition of butylamine solvent washing reagent",

JAERI-Research 2000-021, 2000, in Japanese.
[18] G. UCHIYAMA, T. ASAKURA, S. HOTOKU, H. MIMNEO, K. KAMEI, M. WATANABE, S. FUJINE, "Solvent Extraction Behaviors of Minor Nuclides in Nuclear Fuel Reprocessing Process", J. Radioanal. Nucl. Chem., **246**, 683, 2000.
[19] H.ABE, S.TASHIRO, H.NAGAI, T.KOIKE, S.OKAGAWA and M.MURATA, "Study on the release behavior of radioactive Iodine spices and noble gases from the fuel solution under simulated nuclear criticality accident", JAERI-Tech 99-067 (in Japanese), 1999.
[20] H.ABE, S.TASHIRO, H.NAGAI, T.KOIKE, S.OKAGAWA and M.MURATA, "Studies on Source Term Release Behavior from Fuel Solution under Simulated Nuclear Criticality Accident", ICNC'99 Proceeding Vol.3 p1293-1302, 1999.
[21] H.ABE, S.TASHIRO, T.KOIKE, S.OGAWA and G.UCHIYAMA, "Study on Release Behavior of Radioactive Noble Gases and Iodine Species from Fuel Solution under Simulated Nuclear Criticality Accident," JAERI-Conf, "The 3rd NUCEF International Symposium (NUCEF2001)", to be published.
[22] S.TASHIRO, K.WATANABE, H.ABE, J.TAKADA and G.UCHIYAMA "Clogging Characteristics of Ventilation Filter under the Fire Accident," JAERI-Conf, "The 3rd NUCEF International Symposium (NUCEF2001)", to be published.
[23] K.WATANABE, H.ABE, J.TAKADA, S.TASHIRO, and G.UCHIYAMA "Evaluation of Confinement Capability for Radioactive Materials of Nuclear Fuel Facility under the Fire Accident with Celva-1D," JAERI-Conf, "The 3rd NUCEF International Symposium (NUCEF2001)", to be published.
[24] K.NISHIHARA, H. TAKANO and K. MINATO, "Transmutation of minor actinide, iodeine129, technetium-99 using accelerator-driven system", Proc. GLOBAL2001,held in Paris, 2001.
[25] MHI, JNFS R-91-002, 1996.
[26] M. KUBOTA, S. DOJIRI, I. YAMAGUCHI, Y. MORITA, I. YAMAGISHI, and T. KOBAYASHI, "High Level Radioactive Waste and Spent Fuel Management, Vol. II, 537 , 1989.
[27] J.L. DESVAUX, F. DRAIN, F. DUTERTRE, P.H. HURON, J. N. PINEAU, R. VINOCHE, Proc. RECOD98, Nice, France, 1998.
[28] Y. WEI, N. SABHAWAL, M. KUMAGAI, T. ASAKURA, G.UCHIYAMA, S. FUJINE, "Preparation of novel silica-based nitrogen donor extraction resins and their adsorption performance for trivalent americium and lanthanides", J. Nucl. Sci. Technol., **37**, 1108, 2000.
[29] G. UCHIYAMA and S. FUJINE, "Destruction of butyraldehyde isomers using silver catalyzed electrochemical oxidation", J. Radioanal. Nucl. Chem., 230, 1998.

JP0250301

JAERI-Conf 2002-004

RECENT STUDIES OF HETEROGENEOUS AND HOMOGENEOUS REDUCTION – OXIDATION REACTIONS OF U(IV) IONS IN NITRIC ACID AND TBP PHASES

ROBIN J. TAYLOR, VALENTIN S. KOLTUNOV*, VALERY I. MARCHENKO*, COLIN BOXALL† AND SHAORONG XIAO†

BNFL Technology Centre, Research and Technology, BNFL Sellafield, Seascale, CA20 1PG, U.K.
Fax: 44 19467 79007, email: robin.j.taylor@bnfl.com

* A.A. Bochvar All-Russia Research Institute of Inorganic Materials, PO Box 369, Moscow, 123060, Russia.
Fax: 7095 196 4252, email: march@bochvar.ru

† Centre for Materials Science, University of Central Lancashire, Preston, Lancashire PR1 2HE, U.K.
Fax: 44 1772 892996 email: cboxall@uclan.ac.uk

The results from some of our recent investigations of actinide redox reactions in nitric acid and tributyl phosphate phases are reviewed, including the oxidation of U(IV) by HNO_3 and HNO_2 and by Np(VI) and Np(V) in 30 % TBP and by Np(VI) in HNO_3. The unusual interactions between U(IV), Tc(VII) and NH_3OH^+ in HNO_3 are also discussed. Finally, the photocatalytic heterogeneous reduction of U(VI) by a colloidal semiconductor is presented.

Key words: redox, kinetics, actinides, photocatalysis

1. INTRODUCTION

The behaviour of actinide ions in the Purex process is governed by the thermodynamics of their solvent extraction between HNO_3 and TBP and by the kinetics of their redox reactions and mass transfer [1]. Reaction kinetics are particularly important in contactors where redox reagents such as ferrous sulfamate or uranous nitrate are introduced and in contactors which have short residence times such as centrifugal contactors. It is well known that actinide ions undergo reactions in both aqueous and solvent phases and so, to properly understand and model the process, kinetic information on reaction rates in both phases are needed [1-2]. There is a large amount of historic data available in the literature but there are still surprising gaps in this database, where either the reaction has not been studied under relevant conditions or no conclusive understanding of the kinetics has been reached despite various investigations [1-3]. Also if we start to consider new redox-active reagents then kinetic data is needed in order to understand and model their behaviour in the process [3]. This paper summarises the results of some of our recent investigations in this field.

2. REDUCTION OF Np IONS BY U(IV)

The interaction between Np ions and U(IV) ions is important in the U/Pu separation stage of the Purex process, as it determines the routing of Np in the process [4]. The reduction of Np(VI) by U(IV) in the aqueous phase is a rapid reaction which has, surprisingly, only previously been studied in $HClO_4$ [5]. We investigated the reaction in HNO_3 and found it to be similar in many respects to the reaction in $HClO_4$ [6]. The reaction stoichiometry is the same as in $HClO_4$ (Eq. 1) and the rate of reaction was found to be independent of ionic strength and [U(VI)]. The rate equation is given in Eq. 2 where $k = (696 \pm 20)\ M^{-0.3}min^{-1}$ at 10 °C and $[NH_2SO_3H] = 0.0005$ M) and the activation energy is equal to $66.5 \pm 4.9\ kJmol^{-1}$.

$$2NpO_2^{2+} + U^{4+} + 2H_2O = 2NpO_2^{+} + UO_2^{2+} + 4H^{+} \qquad (1)$$

$$\frac{d[Np(V)]}{dt} = -\frac{d[Np(VI)]}{dt} = k\frac{[Np(VI)][U(IV)]}{[HNO_3]^{0.7}} \qquad (2)$$

The reaction in HNO_3 was found to be faster than that in $HClO_4$, which is quite common for Np redox reactions. The mechanism, via a slow stage of charge (H atom) transfer from the hydrolyzed reductant ion, UOH^{3+}, to the hydrated oxidant ion (Eq. 3), was thought to be retained in HNO_3. However, the variation in the order of reaction with respect to $[H^+]$ from –1 in $HClO_4$ to –0.7 in HNO_3 was attributed to a parallel reaction route in which Np(VI) reacts with non-hydrolysed U(IV) ions (Eq. 4-5, where stage (4) is a relatively slow stage and stage (5) is rapid).

$$NpO_2^{2+} + UOH^{3+} \rightarrow NpO_2H^{2+} + UO^{3+} \qquad (3)$$

$$NpO_2^{2+} + U^{4+} + 2H_2O \rightarrow NpO_2^{+} + UO_2^{+} + 4H^{+} \qquad (4)$$

$$NpO_2^{2+} + UO_2^{+} \rightarrow NpO_2^{+} + UO_2^{2+} \qquad (5)$$

So, the rate of reduction can be expressed as a combination of both slow stages (3) and (4). It was shown that these hypotheses were consistent with the experimental data and that the rate equation could actually be expressed in a form similar to that Sullivan [5] (Eq. 6, where the rate constants for stages (3) – (4) are k_3 = 404 min^{-1}, k_4 = 275 $M^{-1}min^{-1}$ and the 1st U(IV) hydrolysis constant β_1 = 0.009 M at 10 °C and μ = 2).

$$-\frac{d[Np(VI)]}{dt} = (k_3 + k_4[H^+])\frac{[Np(VI)][U(IV)]}{\beta_1 + [H^+]} \qquad (6)$$

The reduction of Np(VI) has been studied previously in the TBP phase but the results were not entirely conclusive [7]. Recent work has reinvestigated this reaction [8]. Complications were encountered due to the formation of complexes between Np(V) and U(VI) and U(IV). The Np(V)-U(VI) complex has been reported by several authors [e.g. see reference 9 and references therein] but the U(IV)-Np(V) complex is lesser known. This complex was identifiable by the growth of an absorption band at ~1000 nm which could not be related to Np(VI), U(IV) or the Np(V)-U(VI) complex (λ_{max} = 993 nm). Assuming an analogous 1:1 complex between U(IV) and Np(V) (probably of the form in Eq. 7), we obtained equilibrium constants (K) of 360 ± 40 M^{-1} at 15 °C[1] and 400 M^{-1} at 35 °C.

$$NpO_2NO_3.xTBP + U(NO_3)_4.2TBP \rightleftharpoons NpO_2.U(NO_3)_5.yTBP \qquad (7)$$

The rate equation for the Np(VI) – U(IV) reaction was ultimately found to be as in Eq. 8, where β_1 and β_2 are the 1st and 2nd U(IV) hydrolysis constants.

$$-\frac{d[Np(VI)]}{dt} = k\frac{[Np(VI)][U(IV)][H_2O]^2}{[HNO_3]^2 + \beta_1[HNO_3][H_2O] + \beta_2[H_2O]^2} \qquad (8)$$

The mean value of the rate constant was k = 59.3 ± 1.7 $M^{-1}min^{-1}$ at 20.0 °C and the activation energy was E = 66.6 ± 3.8 $kJmol^{-1}$. Interestingly, U(VI) was observed to increase the reaction rate in a linear manner.

Comparing the mechanisms of the Np(VI) – U(IV) reactions in TBP (Eq. 9-11) and aqueous (Eq. 3-5) solutions shows that, in both environments, hydrolyzed forms of U(IV) are active

[1] At $[H_2O]$ = 0.36 – 0.40M; $[HNO_3]$ = 0.26 – 0.31 M.

forms. However, in TBP, $U(OH)_2^{2+}$ ions seem to be more active as electron donors than UOH^{3+} ions. Also, although Np(VI) is reduced at a much higher rate in an aqueous solution than in 30% TBP, if the concentration of water in aqueous solution (~55 M) is substituted into equation (8), i.e. the reaction in TBP, the 2nd order rate constant in 1 M HNO_3 at 20.0 °C is only a factor of 3 less than that in aqueous solution under the same conditions. This clearly illustrates the important role of H_2O in TBP phase actinide redox reactions. It is also interesting to note the activation energies in aqueous and 30% TBP solutions are equivalent (66.5 and 66.6 $kJmol^{-1}$ respectively) but the activation entropies vary from +2 to –26 (±13) $JK^{-1}mol^{-1}$. It is, however, difficult to find a reasonable explanation of the acceleration of the TBP phase reaction in the presence of U(VI).

$$U^{4+} + 2H_2O \rightleftharpoons U(OH)_2^{2+} + 2H^+ \qquad (9)$$

$$NpO_2^{2+} + U(OH)_2^{2+} \rightarrow NpO_2^{+} + UO_2^{+} + 2H^+ \qquad (10)$$

$$UO_2^{+} + NpO_2^{2+} \rightarrow UO_2^{2+} + NpO_2^{+} \qquad (11)$$

The reduction of Np(V) has not previously been studied in TBP but only in the aqueous phase ($HClO_4$, HCl, HNO_3), where there is a further reduction (and then reoxidation) to Np(III) [10-12]. We [9] have determined the rate equation to be given by Eq. 12, where at 35 °C, k = 23.8 ± 2.7 $M^{-1}min^{-1}$. The activation energy (E_a) is equal to 89.0 ± 22.0 $kJmol^{-1}$. Within the concentration ranges studied[2], no dependence on $[HNO_3]$ or $[H_2O]$ were observed. The high error on the E_a value was due to the very approximate determination of the temperature dependence of the equilibrium constant K.

$$\frac{d[Np(IV)]}{dt} = k\frac{[Np(V)][U(IV)]}{1+\beta[U(IV)]} \qquad (12)$$

In this reaction, U(VI) retards the rate of reaction which is probably due to the incorporation of some Np(V) in to the unreactive Np(V)-U(VI) complex. It is interesting to compare the rates of the Np(V) – U(IV) reactions in TBP and HNO_3 [12]. The 2nd order rate constant in aqueous solution at 35 °C and $[HNO_3]$ = 1 M is approximately $k_1 \approx 0.006$ $M^{-1}min^{-1}$, but $k_1 \approx$ 50 $M^{-1}min^{-1}$ in TBP (at $[H_2O]$ = 0.3 – 0.5 M). The substantially accelerated rate of reduction of Np(V) with U(IV) in TBP indicates that the reaction is strongly inhibited by water as distinct from the Np(VI) – U(IV) reaction that was found to be catalyzed by water.

The mechanism of the Np(V) – U(IV) reaction in TBP is complicated by the formation of non-reactive complexes of pentavalent neptunium with U(IV) and U(VI), i.e., "$[NpO_2U(NO_3)_5]$" and "$[NpO_2UO_2(NO_3)_3]$". Charge transport thus occurs between non-complexed solvated nitrates of Np(V) and U(IV). Note that there was no evidence of further reduction to Np(III) unlike the aqueous phase reaction.

3. SOLVENT PHASE OXIDATION OF U(IV) IONS

The oxidations of U(IV) by HNO_3 and HNO_2 in TBP solutions have been well studied but there are many variations and inconsistencies between the published data [13]. We developed careful experimental methods to study these reactions under strictly controlled conditions [13].

[2] $[HNO_3]$ = 0.15 – 0.6 M and $[H_2O]$ = 0.33 – 0.64 M at 35 °C.

The oxidation by HNO_3 was shown to be autocatalytic, with an initial slow nitric acid oxidation followed by a faster nitrous acid oxidation (Eq. 13-14) once HNO_2 has accumulated within the reacting solution (the NO formed reacts to produce more HNO_2).

$$U^{4+} + HNO_3 + H_2O \rightarrow UO_2^{2+} + HNO_2 + 2H^+ \quad (13)$$

$$U^{4+} + 2HNO_2 \rightarrow UO_2^{2+} + 2NO + 2H^+ \quad (14)$$

If, however, HNO_2 is present as a reactant in the initial solution at t=0 then both reactions (13-14) occur from the outset. We found the rate equation for the oxidation of U(IV) by HNO_3 in 30% TBP/ n-dodecane to be given by Eq. 15, which is a combination of the rates of reactions 13 and 14 ("non-catalytic" and "autocatalytic" routes). Whereas the overall rate of the direct oxidation of U(IV) by HNO_2 in a HNO_3 solution of 30 % TBP is described by Eq. 16.

$$-\frac{d[U(IV)]}{dt} = k_1[U(IV)][HNO_3]^2 + k_3\frac{[U(IV)][HNO_2][H_2O]^2}{[HNO_3]^2 + \beta_1[HNO_3][H_2O] + \beta_2[H_2O]^2} \quad (15)$$

$$-\frac{d[U(IV)]}{dt} = k_1\frac{[U(IV)][HNO_2][HNO_3][H_2O]}{[HNO_3]^2 + \beta_1[HNO_3][H_2O] + \beta_2[H_2O]^2} \quad (16)$$

If we compare some of the features of the U(IV) – HNO_2 reaction obtained in the study of the direct reaction with those found in the study of the same reaction but as part of the autocatalytic route in the U(IV) – HNO_3 reaction [13], we see that they agree on the orders of reaction with respect to the reagents, U(IV) and HNO_2. There is also qualitative agreement on the effect of $[HNO_3]$ and $[H_2O]$ on the reaction rate but the actual values of the orders for these species differ substantially, at least under the conditions studied. Finally, the values of the rate constants estimated in the direct reaction are lower than those found in the autocatalytic reaction under comparable conditions. These differences suggest a change in part of the reaction mechanism, which we suggest is due to the reactive U(IV) species in the slow stage changing from the 1st hydrolysis product (17) to the 2nd hydrolysis product (18).

$$UOH^{3+} + HNO_2 \rightarrow UO_2^+ + NO + 2H^+ \quad (17)$$

$$U(OH)_2^{2+} + HNO_2 \rightarrow UO_2^+ + NO + H^+ + H_2O \quad (18)$$

It can be shown that the overall rate equations in each study can be derived assuming that the slow stage of the reaction proceeded via the 1st or 2nd hydrolysis products in the direct and autocatalytic reactions respectively. So, as the general case, it is suggested that the U(IV) – HNO_2 reaction in TBP can actually proceed via two parallel routes, which have the slow stages (17) or (18). The contribution each route makes to the observed reaction rate depends on the specific conditions under which the reaction occurs.

However, calculations suggest this only forms part of the explanation, so we have to consider the influence of the other reagent, HNO_2, on the rate of the reaction. It can be shown that the values of the 2nd order rate constants (k_2), which should be independent of $[HNO_2]_0$, actually decrease with increasing $[HNO_2]$. The values of k_2 at 0.1 M HNO_3 and ~0.4 M H_2O (T = 55 °C) were:

$[HNO_2]_0$	0	0.002	0.005	0.015	0.02
k_2 (min^{-1})	7.1	3.5	3.29	1.17	0.975

So, we have the strange conclusion that the rate (the rate constant, k_2) of the U(IV) – HNO_2 reaction in a HNO_3 solution of TBP must be a maximum when HNO_2 is *not* present in the original solution and minimal at a high initial concentration of HNO_2 (in our case at $[HNO_2]_0$ = 0.02 M). Further evidence is provided by the fact that the formal orders of reaction with respect to $[HNO_3]$ as $[HNO_2]_0 \rightarrow 0$ approach those observed in the autocatalytic reaction, where $[HNO_2]_0 = 0$.

These observations lead to a conclusion that HNO_2 in TBP solutions may exist in at least two forms which have different reactivities for U(IV). The more kinetically active form is produced in-situ in the reaction solution when HNO_3 is reduced by U(IV). The less kinetically active form predominates in the TBP stock solution of HNO_2, which was used to study the direct U(IV) – HNO_2 reaction. It may be that these forms are the cis- and trans- isomers of the TBP-HNO_2 complex [14]. Indirect evidence for this may be the fact that in both the cases (with and without adding HNO_2 to the initial solution) the activation energies have similar values. Hence, the observed difference between the reaction rates is due to the entropy factor ΔS^*, i.e., related to the steric features of the reacting forms (see Table I).

Table I. Activation Energies And Entropies For The U(IV) – HNO_2 Reaction In TBP

	E_A ($kJmol^{-1}$)	ΔS^* at 298K ($Jmol^{-1}K^{-1}$)
Direct reaction	112 ± 17	43
Autocatalytic reaction	93 ± 5	-6

4. U(IV) – Tc(VII) INTERACTIONS

The interactions of Tc with redox reagents such as U(IV) or N_2H_4 are well known to be both important and complex within the Purex process [1]. We have recently studied the reactions of Tc with NH_3OH^+ [3,15]. At moderate temperatures and $[HNO_3]$, solutions of TcO_4^- and NH_3OH^+ are essentially stable, as are NH_3OH^+ stabilised U(IV) solutions in HNO_3. However, when Tc(VII) is added to solutions containing U(IV)/ NH_3OH^+ in HNO_3, an unusual series of reactions are observed. Initially, there is a rapid oxidation of U(IV) followed by a slower zero order reaction which then speeds up towards the end of the oxidation. This situation is very different from the well known Tc(VII) catalysed oxidation of hydrazine. The addition of U(IV) to Tc – N_2H_4 solutions only eliminates the induction period by reducing Tc(VII) to a lower oxidation state more rapidly than N_2H_4. After this the reaction mechanism is essentially unchanged.

Clearly, this system is very complex but we have derived a kinetic equation for the slower zero order reaction under conditions in which NH_3OH^+ is a net scavenger of HNO_2 rather than a net generator. It is thought that HNO_2 is essentially unavailable at this point in the reaction cycles, because it is scavenged by NH_2OH, and also that the U(IV) + Tc(VII) reaction is rapid. The slow rate determining reactions are, therefore, considered to be the HNO_3 oxidations of U(IV) and Tc(IV) (Eq. 19-20). Kinetic analysis of the experimental data leads to the derivation of a rate equation (10) where the rate constants of reactions (19) and (20) are, respectively, $k_{19} = (2.8 \pm 0.10) \times 10^{-3}\ l^{1.05}mol^{-1.05}min^{-1}$; $k_{20} = 123 \pm 10\ l^{2.4}mol^{-2.4}min^{-1}$ at 35 °C. The activation energies are $E_{19} = 73 \pm 3$; $E_{20} = 86 \pm 2$ $kJmol^{-1}$. As the overall oxidation reaction proceeds, the initial U(IV) term in eqn. (21) decreases in importance, the Tc(IV)

oxidation reaction becomes solely rate determining and the reaction tends towards zero order relative to U(IV).

$$U^{4+} + HNO_3 + H_2O \rightarrow UO_2^{2+} + HNO_2 + 2H^+ \qquad \text{(Eq. 19)}$$

$$2TcO^{2+} + 3HNO_3 + 3H_2O \rightarrow 2TcO_4^- + 3HNO_2 + 6H^+ \qquad \text{(Eq. 20)}$$

$$-d[U(IV)]/dt = k_{19}[U(IV)][HNO_3]^{1.05} + k_{20}[Tc(IV)]^{1.8}[HNO_3]^{1.6} \qquad \text{(Eq. 21)}$$

Current work is in progress to try and understand the complex mechanisms of U(IV) – Tc – NH_3OH^+ reactions in the absence and presence of N_2H_4 [3], particularly the verification of intermediate Tc oxidation states.

5. PHOTOCATALYTIC GENERATION OF U(IV) IONS [16]

Using SnO_2 as a colloidal semiconductor we have investigated the feasibility of reducing various metal ions in HNO_3 using photocatalysis. In particular, we have studied the reduction of U(VI) ions in both H_2SO_4 (irradiation wavelength λ = 312 nm) and HNO_3 (λ = 350 nm) media using ethanol and hydrazine as hole scavengers. The reaction is followed potentiometrically on a Au electrode and the E vs. t graphs obtained experimentally can be converted to $[UO_2^{2+}]$ vs. t plots using equations based on a mixed potential approach. A steady state potential is reached after <180 s. It has been shown that the potential in H_2SO_4/CH_3CH_2OH is governed by the same species as in HNO_3/N_2H_4 – i.e. the process is the same, although the kinetics are different. The photopotentiometric responses can be theoretically modelled, showing that the photopotential is controlled by a transient concentration of U(V), which then disproportionates to U(IV) and U(VI), thus driving the reaction to complete U(IV) formation. UV/vis spectrophotometry, which can be used to follow the accumulation of the ultimate U(IV) product, indicates that 100 % 0.01 M U(VI) is photocatalytically reduced to U(IV) after ~30 minutes in H_2SO_4 using ethanol as a hole scavenger. In a HNO_3/N_2H_4 system, reduction is slower due to reduced light absorption at 350 nm compared with 312 nm. So, the combination of potentiometric and spectrophotometric results allows the modelling of the fast U(VI) → U(V) photocatalytic heterogeneous reduction and the subsequent U(V) disproportionation. Our mathematical treatment led to values of the photocatalytic valence control rate constants, k_{VC}, of 1.7×10^{-3} s^{-1} and 1.79×10^{-4} s^{-1} in H_2SO_4/CH_3CH_2OH and HNO_3/N_2H_4 respectively. The difference again being due to the greater light absorption at 312 nm in the H_2SO_4/CH_3CH_2OH system. We also estimated the homogeneous U(V) disproportionation rate constant to be 1300 $lmol^{-1}s^{-1}$ in HNO_3/N_2H_4, which compares approximately to literature values [e.g. see 17]. The rate of U(IV) generation is increased by the presence of O_2, probably due to oxygen facilitating the reaction of the appropriate hole scavenger. Photogenerated U(IV) in HNO_3/N_2H_4 is stable for >70 hours in air. It is also possible to reduce U(VI) photocatalytically in mixed HNO_3/TBP phases using the TBP as a hole scavenger, where it has been shown that the photoreduction occurs in the aqueous phase only and that this is slow compared to mass transfer between phases. Photogenerated U(IV) is stable in TBP for >70 hours in air. Early indications are that it is possible to photocatalytically reduce U(VI) in the presence of other metal ions.

6. CONCLUSIONS

The reactions of U(IV) in solutions of HNO_3 and TBP are important in the Purex process and are also of intrinsic interest. The rates of these reactions are needed for inclusion in to process models for the accurate computerised simulation of process flowsheets. We have recently investigated a series of U(IV) oxidation reactions in aqueous and solvent phases, including

those with Np(V,VI) ions (both phases), HNO_3 and HNO_2 (in TBP) and U(IV) oxidation in HNO_3 when Tc(VII) and NH_3OH^+ are simultaneously present. These reactions are generally rather complex but interesting features include the roles of water and hydrolysed U(IV) ions in the reaction mechanisms, particularly in TBP phases. We have also studied a novel method of efficiently generating U(IV) by the photoelectrochemical reduction of U(VI) in HNO_3 using a colloidal semiconductor. This process can be modelled theoretically. Further work is aimed at investigating the kinetics of Tc and Pu ion catalysed HNO_3 U(IV) oxidation in TBP and more detailed studies of reaction mechanisms. Further studies of controlling metal ion oxidation states photocatalytically are ongoing, including a continuous photoreactor design.

7. ACKNOWLEDGEMENTS

We would like to thank our colleagues at VNIINM (K.N. Dvoeglazov, O.A. Savilova, G.I. Zhuravleva, E.A. Mezhov, G.V. Koltunov), UCLAN (G. LeGurun) and BNFL (C.J. Broan, I.S. Denniss) for their contributions to the work presented here.

8. REFERENCES

[1] W. W. Schulz, L. L. Burger, J. D. Navratil and K. P. Bender, (ed.), "Science and technology of tributyl phosphate, Volume III. Applications of tributyl phosphate in nuclear fuel reprocessing", CRC Press Inc., Florida (1990).
[2] V. S. Koltunov, "The Kinetics of the actinide reactions", Atomizdat, Moscow (1974).
[3] R. J. Taylor and I. May, Sep. Sci. Tech., 36, 1225-1240 (2001).
[4] R. J. Taylor, I. S. Denniss and A. L. Wallwork, Nuclear Energy, 36, 39-46 (1997).
[5] J. C. Sullivan, A. J. Zielen and J. C. Hindman, J. Amer. Chem. Soc., 82, 5288 (1960).
[6] V. S. Koltunov, R. J. Taylor, V. I. Marchenko, G. I. Zhuravleva, E. A. Mezhov, G. V. Koltunov and K. N. Dvoeglazov, Radiochim. Acta, Under Review.
[7] L. M. Frolova, G. A. Timofeev and A. G. Rykov, Radiokhimiya, 15, 867-868 (1973).
[8] V. S. Koltunov, R. J. Taylor, V. I. Marchenko, E. A. Mezhov, G. I. Zhuravleva, K. N. Dvoeglazov and O. A. Savilova, Proc. Actinides 2001, forthcoming.
[9] N. J. Stoyer, D. C. Hoffmann and R. J. Silva, Radiochim. Acta, 88, 279 (2000).
[10] N. K. Shastri, A. E. Amis and J. O. Wear, J. Inorg. Nucl. Chem., 27, 2413 (1965).
[11] N. B. Blokhin, V. A. Ermakov and A. G. Rykov, Radiokhimiya, 355 (1974).
[12] I. V. Shilin and T. A. Rumyantseva, Radiokhimiya, 20, 536 (1978).
[13] V. S. Koltunov, R. J. Taylor, V. I. Marchenko, K. N. Dvoeglazov, O. A. Savilova and I. May, Radiochim. Acta, 86, 41-49 (1999).
[14] J. M. Fletcher, D. Scargill and J. Woodhead, J. Chem. Soc., 1705-1707 (1961).
[15] R. J. Taylor, I. S. Denniss, C. J. Broan, V. S. Koltunov, V. I. Marchenko, K. N. Dvoeglazov, O. A. Savilova and G. I. Zhuravleva, Proc. Actinides 2001, forthcoming.
[16] C. Boxall, X. Xhao and R. J. Taylor, In Preparation.
[17] H. Kaneki and H. Fukutomi, Bull. Res. Lab. for Nucl. Reactors, 5, 27-39 (1980).

This is a blank page.

JP0250302

JAERI-Conf 2002-004

STUDY ON U CRYSTALLIZATION FOR ADVANCED REPROCESSING

Kazunori NOMURA, Atsuhiro SHIBATA and Atsushi AOSHIMA
Tokai Works, Japan Nuclear Cycle Development Institute,
Tokai-Mura, Ibaraki, 319-1194, JAPAN
Fax: 81-29-287-2419, e-mail: kaz@tokai.jnc.go.jp

Key words: crystallization, advanced reprocessing, plutonium behavior

1. INTRODUCTION

JNC (Japan nuclear cycle development institute) has proposed the advanced fast reactor fuel cycle system as a part of the Feasibility Study (FS) [1]. The advanced cycle should have a basic concept constituting simple and compact processes under a nonproliferation accountability and minimum burden to environment.

In the PUREX process, uranium and plutonium are extracted into the organic phase, tri-n-butyl phosphate in dodecane, in the first extraction cycle. Then plutonium is stripped into the aqueous phase including reducing agent, while uranium remain in the organic phase. After the plutonium stripping, uranium is stripped into the dilute nitric acid.

Plutonium product is mixed with uranium in order to fabricate MOX fuel. If uranium/plutonium ratio in active feed solution to the first extraction cycle is adjusted as convenient to MOX fabrication, that is rather high plutonium ratio such as 50 % - Pu, suitable mixed product of uranium and plutonium is obtained by collective stripping of both uranium and plutonium. It causes uranium/plutonium partitioning process to be deleted and PUREX process to be shortened.

Generally, dissolver solution has higher ratio of uranium to plutonium than that of required product described above. Thus excess amount of uranium needs to be removed before simplified PUREX process. JNC has studied crystallization of uranium as the method for this partial uranium separation.

As uranium solubility in nitric acid solution decreases with decreasing of its temperature, a part of uranium is separated from the solution as uranyl nitrate hexahydrate (UNH) by lowering temperature of the solution. Quantity of UNH educed by crystallization can be controlled according to the solubility at cooled temperature. When crystallization method is applied to dissolver solution, uranium is precipitated with priority to other elements because concentration of uranium in dissolver solution is higher enough than that of other elements such as plutonium, fission products and so on. And only uranium concentration reaches own solubility at the temperature of initial cooling. It causes only uranium and not other

elements to be separated from the dissolver solution.
Partial separation of uranium from dissolver solution produces less liquid wastes, because the separation is done only by the control of temperature, that is to say, no additional chemical reagent is required for the crystallization. Furthermore the quantity of components to be processed by solvent extraction also decreases by applying the crystallization.
In this paper experimental results on uranium crystallization are described. Behavior of plutonium under crystallization condition is important in order to prevent plutonium from significantly accompanying uranium and that will be also discussed in this paper.

2. Crystallization of uranium

In dissolver solution of spent fuel from fast reactor (FR), a portion of insoluble residue is existed. Behavior of insoluble residue was confirmed by batch experiment with simulation powder in uranium-nitric acid solution under crystallization condition.

2.1 Experimental

Reaction vessel for crystallization shown in Figure 1 was made by glass and had a cooling jacket. 60 % - ethylene glycol that was controlled its temperature was used as coolant and flowed through the cooling jacket. Stirrer and thermocouple were installed into the vessel. Effective volume of the vessel was 500 mL.
Uranium solution of 500 g-U/L in 4.4 mol/L nitric acid was prepared and put into the reaction vessel. Uranium saturated temperature of this solution is 32 °C. Simulated insoluble residue was added into the uranium solution while stirring, then the solution was cooled from 40 °C to 10 °C at about 1 °C/min.
The mixture was filtered to recover UNH educed and simulated insoluble residue and liquid phase was taken as mother solution.

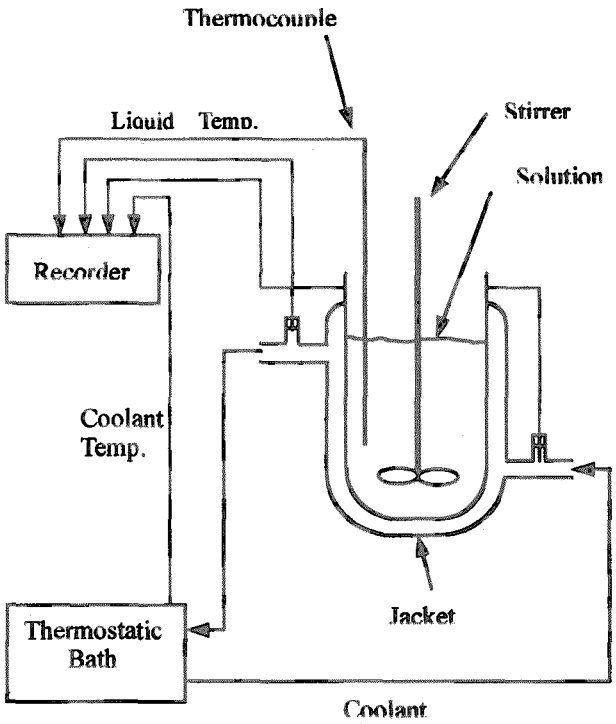

Figure 1 Outline of experimental apparatus

100 ml of 5 mol/L nitric acid solution was poured on the UNH and simulated insoluble residue on the filter in order to wash a part of mother solution stuck on their surface. This washing was performed 3 times.
Concentrations of uranium and nitric acid in mother solution and washing solution and weight of simulated insoluble residue in mother solution, washing solution and solid obtained on the filter were measured.

2.2 Result

Figure 2 shows record of temperature of the solution during uranium crystallization test. 10 minutes after of starting of the test, exothermic phenomenon was observed and it occurred at around 32 °C. Since the temperature that this uranium solution is saturated is 32 °C, this phenomenon is due to the reaction heat from UNH crystallization. That is to say, the presence of insoluble residue gave no influence in the UNH crystallizing temperature.

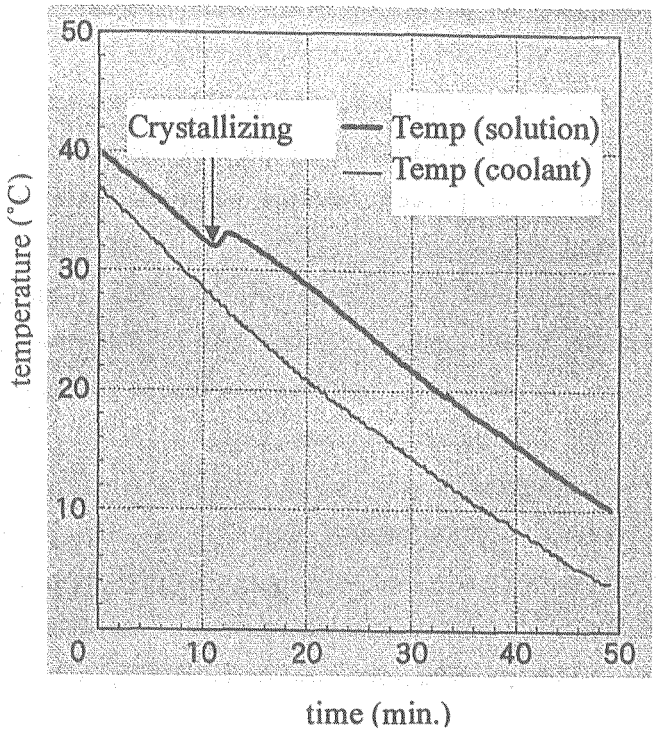

Figure 2 Temperature of the solution

Mass balance of insoluble residue in this experiment is tabled in Table I. Even after 3 times washing of the UNH crystal product by the nitric acid solution, about 20% of the insoluble residue still remained with the UNH crystal. Although the particle of the insoluble residue did not behave as the nucleus of the UNH crystal, it might stick on the UNH crystal even during the washing of the crystallization product.

Figure 3 shows the particle size distribution of UNH crystal obtained in this experiment. Left bar indicates particle size of crystal obtained from crystallization test without insoluble residue and right bar is from the test with insoluble residue.

Table I Mass balance of insoluble residue (%)

Initial	100
Mother solution	29
Washing (3 times)	53
Crystal (after washing)	18

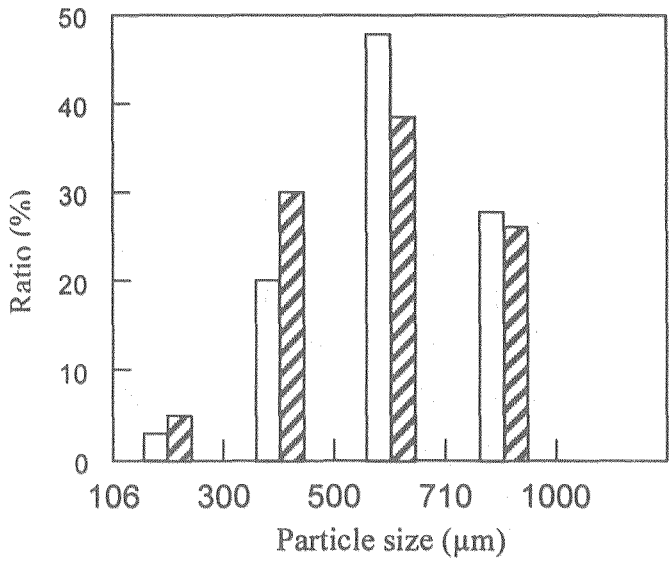

Figure 3 Particle size distribution

Both particle size distribution were similar, namely presence of insoluble residue was not influenced in particle size of UNH crystal.

As a result, the presence of insoluble residue in the initial solution did not influence the uranium crystallization behavior, but the clarification process is required to place before the crystallization process because of the difficulty of separating the residual particle from the UNH crystal particle.

3. Plutonium behavior under UNH crystallization condition

It is important to check the behavior of plutonium under the uranium crystallization operating condition because it can have different valence in the nitric acid solution and belong to actinide elements same as uranium.

3.1 Experimental

Two kinds of solutions of 200g/L – plutonium in 6 mol/L - nitric acid without uranium was prepared. In the first solution, plutonium was adjusted at tetravalent state, and in the other, plutonium was at hexavalent state. These valences were confirmed to adjust by the UV/VIS spectrometer. Each solution was cooled slowly until around –60 °C.

3.2 Result

No crystallization of plutonium was observed under any temperature until about -40 °C and finally the solution was solidified. This freezing temperature almost coincided with the freezing point of 6 mol/L - nitric acid solution, and H_2O and $HNO_3 \cdot 3H_2O$ are expected to crystallize. In both case, the freezing point of the solution was far lower than the operation temperature of uranium crystallization process. Valences of solutions both before cooling and after experiment were measured and there were no change of valence.

4. Conclusion

UNH crystallization batch experiment was performed with UNH solution with simulation insoluble residue. Although the presence of insoluble residue in the initial solution did not influence the uranium crystallization behavior, the clarification process was required to place before the crystallization process because of the difficulty of separating the residual particle from the uranium crystal particle.

Beaker scale plutonium tests were performed to confirm behavior of plutonium nitrate under temperature of UNH crystallization operation condition. Plutonium nitrate crystallization was not observed in both case of tetravalent and hexavalent. This result seems to mean that uranium is separated from the dissolver solution and no adjustment of valence of plutonium is needed to hold it in the mother solution. However, chemical similarity often brings different result from one obtained in the simple system such as described above and the behavior of hexavalent plutonium in the presence of uranium is expected to be important.

REFERENCE

[1] S. NOMURA, A. AOSHIMA, T. KOYAMA and M. MYOCHIN, GLOBAL 2001, 1, 042 (2001)

JP0250303

JAERI-Conf 2002-004

DEVELOPMENT OF NEW REPROCESSING TECHNOLOGY, FLUOREX, FOR LWR FUEL CYCLE
-Hybrid Process of Fluoride Volatility and Solvent Extraction-

O. Amano[1] , F. Kawamura[2], T. Fukasawa[2] and A. Sasahira[3]

[1]Nuclear Power R&D Center, Tokyo Electric Power Company
4-1 Egasaki, Tsurumi, Yokohama, 230-8510 Japan
[2]Nuclear Systems Division, Hitachi, Ltd.
3-1-1 Saiwai, Hitachi, Ibaraki, 317-8511 Japan
Fax:81-294-23-6626, e-mail:fumio_kawamura@pis.hitachi.co.jp
[3]Power and Industrial Systems R&D Laboratory, Hitachi, Ltd.
7-2-1 Omika, Hitachi, Ibaraki, 319-1221 Japan

A new reprocessing technology, FLUOREX was proposed for thermal reactors cycle and future thermal and fast reactors coexistence cycle. The proposed system is a hybrid system that combines fluoride volatility and solvent extraction methods where the major U in spent fuel is separated efficiently by fluoride volatility method and MOX is recovered by well-established conventional solvent extraction method. The system can recover pure U and MOX with the high decontamination factor and can drastically reduce the cost and waste generation compared with the conventional PUREX method. When FLUOREX reprocessing system is adopted in LWR fuel cycle, the conversion facility for re-enrichment can be deleted, which leads a large reduction in fuel cycle cost. One cycle scenario is that it will take long time to shift from present LWR to future FBR systems. In this shift period, interim storage of spent fuels is one option, which needs large storage space and interrupts the continuous Japanese recycle storategy. FLUOREX reprocessing system proposed here is suitable for this situation. Several features of the proposed system are discussed in the present paper.

Key words: spent fuel reprocessing, fluoride volatility, hybrid, storage, solvent extraction

1. INTRODUCTION

One of the most important factors to be considered for future nuclear fuel cycle technology is the flexibility of the technology to fit various cycle scenarios. Development of flexible nuclear fuel cycle system and transparent management of plutonium are quite important for the sustainability of nuclear power. In the present nuclear industry, it seems to take so long to replace all light water reactors (LWRs) with fast breeder reactors (FBRs) which can enhance much the utilization efficiency of uranium resource. Thus it is important to consider in the near future reasonable and transparent LWR fuel cycle system which can recycle MOX (mixture of plutonium and uranium), hold no excess plutonium, utilize much the existing technologies.

Requirements for the future nuclear fuel cycle system may become different depending on the phase from LWR era to FBR recycle age as shown in Table I . In the first phase nuclear power generation is dominantly made by LWRs and the second is the co-utilization period of both LWRs and FBRs, the third in which the independent FBR fuel cycle will be established. In the first phase, the role of fuel reprocessing is mainly in LWR fuel cycle in which Pu is

reprocessed to produce MOX fuel for Pu-thermal utilization and U is separated for re-enrichment or storage. In this phase high decontamination factor (DF) may be required for both U and Pu products. In the second phase, the fuel production for the initial fuel loading to FBRs will be added to the role of fuel reprocessing and high DF may not be need for MOX any more. However, the DF of U should be still high even in this period since excess U will be produced over the utilization in MOX fuel production due to the difference in the Pu contents of the fuels for LWRs and FBRs. From late second phase to third phase, fuel reprocessing will be performed to recycle FBR fuels. The low DF fuels may be adequately used in FBRs and thus simplified fuel reprocessing system will be adopted in this era.

Thus in the near future LWR fuel cycle system, U should be reprocessed with high DF and that of MOX should be flexible from low to high. As for the fuel production, it is desirable until the second phase to utilize the infrastructure of conventional fuel pellet production, although the more simplified vibratory packing method may be developed for less decontaminated fuel production in the third phase. Besides DF of the fuel products, the future nuclear fuel cycle system will need safety, reduction of the cycle cost, efficient utilization of resources, minimization of environmental burden, non-proliferation and technological maturity. In the present study, new reprocessing technology, FLUOREX was proposed to meet these future requirements laying emphasis on MOX recycling in LWRs.

Table I. Requirements for the future nuclear fuel cycle system

Item \ Phase	LWR Period (LWR to LWR)	Transition Period (LWR to FBR)	FBR Period (FBR to FBR)
Feature of Spent Fuel	Contents of U > 95% U enrichment > ~1%	Same as left	Driver: U: about 70% Pu: about 30% Blanket: U > about 95%
Usage of Recovered U and MOX	U: Re-enrichment or storage MOX: Fuel pellet	U: Same as left MOX: Fuel pellet or Vibro-packing	U: Fuel pellet or Vibro-packing MOX: Same as left
Required DF for Reprocessing	U: High DF MOX: High DF (DF > ~ 10^7)	U: Same as left MOX: Same as left	U: High/Low DF* MOX: Low DF (DF > ~ $10\text{-}10^2$)

* In the case that high DF U is used for blanket fuel (over aout 50% of FBR loaded fuels), blanket process can be neglected in the FBR fuel production.

2. SCHEME OF THE FLUOREX PROCESS

Spent fuel from LWRs contains about 94% uranium, 1% plutonium and 5% fission products. The key point of the cycle system is how to efficiently separate these elements into three parts: MOX for fuel fabrication, most of uranium for re-enrichment and fission products for wastes. The survey showed the high possibility of fluoride volatility process for the easy separation of spent fuel components into three parts and its difficulty to get pure MOX for conventional fuel fabrication facility. Thus, the authors proposed new fuel reprocessing technology, FLUOREX process, which is the combination of fluoride volatility

and solvent extraction methods, and started further technological investigation. Fluoride volatility process has been applied to remove most of uranium from spent nuclear fuels before purification of the mixture of plutonium and residual uranium from fission products by solvent extraction.

Several countries had stopped developing fluoride volatility reprocessing method in the 1970's due to difficulty in isolating pure plutonium with high recovery ratio[1-3]. This difficulty can be solved by the process improvement to recover dirty plutonium or to adopt PUREX method for plutonium purification. The proposed hybrid reprocessing process chose the latter to avoid the difficulty experienced in the past.

The FLUOREX reprocessing consists of seven main processes as shown in Fig. 1. Spent fuel from thermal reactors will be disassembled and fuel pins are sheared into short pieces. The fuel is pulverized and separated from cladding by dry oxidation and reduction method such as AIROX process. Fluorination of most uranium (about 90% in spent fuel) to volatile UF_6 can be easily achieved by fluoride volatility method with compact facility. Then the volatile UF_6 will be purified to high DF (10^7 to 10^9) by passing through adsorbents such as NaF and by rectification. Highly purified UF_6 can be transferred directly to re-enrichment facility without conversion (LWR recycle again), or to simple storage facility with or without conversion to store certain period for future FBRs. About 10% residues including plutonium, uranium and fission products (FP) will be de-fluorinated and then dissolved into nitric acid solution. This solution can be treated in well-established solvent extraction method (same as PUREX), and this process facility size will be reduced to about 1/10 of the conventional PUREX facility with same treatment capacity of spent fuel. Pure Pu and U mixture product (Pu 1%/U 4-19% in spent fuel) can be obtained by solvent extraction method without separating Pu and U, which is suitable for conventional MOX fuel fabrication. Another optional process for treating fluorination residues (Pu + FP) is to store them in a compact facility with adequate cooling system until the FBR era comes reality. This storage facility needs to store only Pu + FP, the volume of which is about 1/20 of spent fuel.

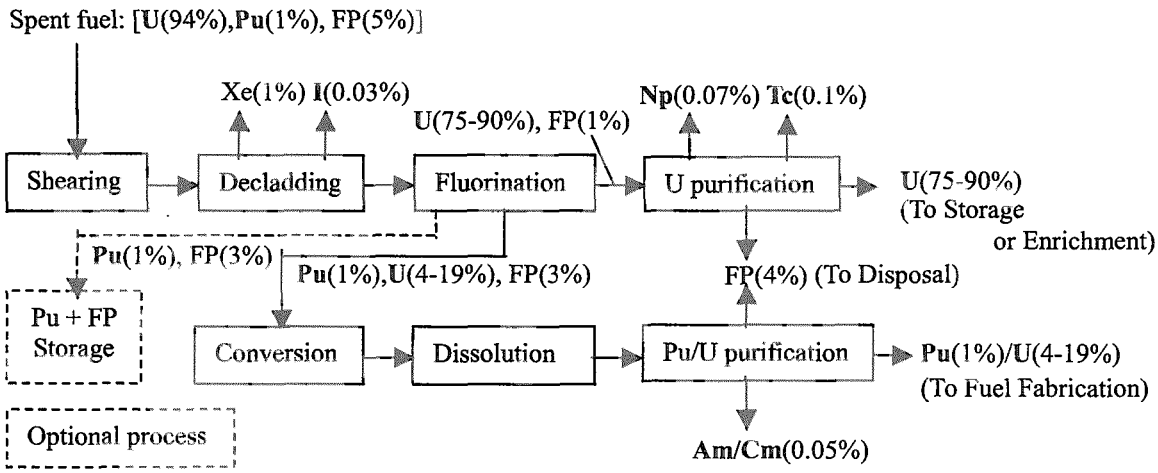

Fig. 1 Process flow of FLUOREX reprocessing for LWR cycle

The FLUOREX method has another feature in nuclear fuel cycle. Uranium enrichment industry produces large amount of depleted uranium (about 0.2% U-235) in a form of hexafluoride, which would need its transformation into more stable form such as oxide for its utilization and disposal, and produce plenty of fluorine. The FLUOREX process can effectively utilize and recycle fluorine in its nuclear fuel cycle.

Thus, the FLUOREX reprocessing has many merits compared with the present PUREX reprocessing and can meet the thermal reactor fuel cycle demands in near future and also has flexibility to be applied not only to thermal reactors cycle but also to future thermal and fast reactors coexistence cycle and FBR cycle.

3. FEATURES OF THE FLUOREX PROCESS

This system can drastically reduce the cost and waste generation (environmental burden), have high technical maturity, similar safety and energy sustainability (resource utilization efficiency), and higher proliferation resistance compared with conventional fuel cycle system. Preliminary estimation results are shown below on the features of the proposed FLUOREX system.

1) Technological Maturity and Collaboration

Technological investigation was conducted in this work and clarified that most techniques have already been developed industrially in the past and current nuclear fuel cycle worldwide, and only a few subjects remain to be solved for actual use. Solvent extraction has much experience in reprocessing industry of spent fuel including plutonium. Fluoride volatility has also much industrial experience in conversion between uranium oxide and fluoride and in uranium enrichment, and pilot scale experience in uranium purification. Remote handling technologies such as robotics developed in Japan and other countries could be applied to the FLUOREX system for its much safer and easier operation.

The technologies developed in the past in the world can accelerate the development of FLUOREX reprocessing system, which indicates the importance of worldwide collaboration for the industrialization of the system and for the sustainable utilization of nuclear energy. The worldwide information exchange and collaboration is also indispensable to emerge from the present global nuclear shrinkage situation.

2) Economics

The FLUOREX reprocessing has a compact fluorination and U purification equipments, and less than 10% materials in spent fuel (fluorination residues) are treated in solvent extraction process. This leads the large reduction in reprocessing plant volume. The second economical feature of the FLUORX system is the cost reduction in the low-level waste treatment. Since the amount of materials to be treated in solvent extraction is reduced to less than 10% of the conventional system, the amounts of reagents and solution to be used are reduced accordingly and thus the process scale and the treatment cost in the low-level waste treatment are reduced by one digit. Taking these features into account, the preliminary investigation revealed that the reprocessing plant volume can be reduced to about 60% that of the conventional system.

The third feature is the negligibility of conversion facility in the fuel cycle. Since the

chemical form of recovered U in FLUOREX system is UF_6 which is same as that in re-enrichment process, the conversion facility for re-enrichment can be deleted, while the conventional facilities of enrichment, re-conversion, fuel fabrication, thermal reactors and spent fuel storage can be utilized without any change.

3) Safety

Fluorination and U purification processes treat gaseous uranium, but its amount is only 2kg-U/d for 100t/yr capacity FLUOREX plant with reduced pressure equipments and cells. Volatile fission products are fixed in suitable adsorbents in U purification process and other fission products are treated in solid forms in the fluorination process. In the original fluoride volatility reprocessing, Pu is fluorinated to the volatile PuF_6 after U fluorination[1-3], but the FLUOREX system dose not include Pu fluorination process and thus no gaseous Pu exists in the whole system. This means FLUOREX system has much higher safety than the original fluoride volatility system.

In a solvent extraction processes, treated amount is less than 1/10 of the same capacity conventional aqueous plant (PUREX). Then the sufficient safety with ALARA can be predicted similar to the conventional reprocessing facilities.

4) Efficient Utilization of Resources

In FLUOREX system, high decontamination factor of recovered U from 10^7 to 10^9 is attainable by chemical sorption and rectification in U purification process. The same level of DF (10^7) is expected for MOX as the conventional solvent extraction (PUREX) system. These high DF for both U and MOX will enhance the nuclear energy utilization efficiency. Those fuels would also be utilized in advanced reactors such as reduced-moderation water reactors and fast breeder reactors, which can enhance more the sustainability of nuclear energy.

5) Minimization of Environmental Burden

The U purification processes generate small amount of adsorbents as radioactive waste because of a few volatile fission products accompanied with uranium. The solvent extraction processes generates less than 1/10 of waste compared with conventional facilities of same capacity. Then the total amount of the waste generated from FLUOREX reprocessing is about 1/10 of the conventional ones. In the FLUOREX cycle, conversion facility for recovered uranium can be deleted and waste from the facility is eliminated.

6) Proliferation Resistance

Plutonium always exists with uranium even in a purified form in FLUOREX solvent extraction processes, so the proliferation resistance is considered to be higher than a conventional PUREX system where plutonium alone exists in its purification process. If plutonium is stored with fission products for future, the resistance would be much higher.

4. KEY TECHNOLOGIES

The FLUOREX system is a hybrid system that combines fluoride volatility and solvent extraction methods. The adopted processes of each method themselves are well developed, but there are some subjects to be confirmed technologically in the interface processes of

adopted methods. Those subjects include:

(1) Selective volatilization of uranium from pulverized actual spent fuel.
Optimum fluorination conditions such as temperature and F_2 feed will be clarified based on the results of previous researches on the fluorination mechanism of Pu.

(2) Conversion of non-volatile fluoride residues to oxides soluble in nitric acid.
As for the uranium fluoride, oxide conversion has much experience in the conventional conversion facilities. Very little has been experienced on the conversion of plutonium fluorides, but it is expected from a thermodynamic evaluation that plutonium fluorides conversion will proceed more easily than uranium fluorides. Experiments will be performed using spent fuels to clarify this issue.

(3) Dissolution of the oxides.
Converted oxides are expected to have sufficient solubility and this will be confirmed with the experiments using spent fuels in conjunction with the those stated above.

Pulverization of actual spent fuel is another subject to be confirmed.

5. INTERIM STRAGE OPTION

One cycle scenario is that it will take long time to shift from present LWR to future FBR systems. In this shift period, interim storage of spent fuels is one option, which needs large storage space and interrupts the continuous Japanese recycle storategy. The FLUOREX process proposed here is suitable for this situation.

The above-mentioned, FLUOREX consists of two processes. First process removes the cladding materials of spent fuel, separates most (over 90%) uranium by its rapid fluorination (volatilization), and purifies the volatilized uranium to get pure UF6. On the other hand, solid fluorination residues, which contains small amount of uranium, plutonium and fission products (less than 10% of spent fuel), can be stored under closed noble gas condition with high proliferation resistance of plutonium. Volume of the residues is about 1/20 of the spent fuel assembly and the storage space, which is determined by heat removal, radiation shielding and criticality control (mainly heat removal), will be 1/5 compared with the direct storage of spent fuel as shown in Fig. 2.

During water can not enter the canister, solid fluoride residues maintains stable condition. However, when water invades in the canister, a part of residue (such as U, Pu and noble matal) reacts to water and generating HF, and is worried about the corrosion of the canister. When a large amount of water invades, a part of residue (such as alkali metal and noble matal) dissolves. Therefore, for the long term storage of the residues, fluorides might be converted to more stable oxides.

According to the preliminary evaluation including uranium fluorination separation, relative storage costs of spent fuel, fluorination residues, and fluorination residues after oxides conversion are estimated to be 1, 0.75, and 0.8, respectively. This evaluation considers only the storage costs and does not consider the value of pure UF6 which contains about 1% U-235.

In the era of FBR, stored residues, mixture of uranium, plutonium and fission products, should be treated in the second (solvent extraction) process of FLUOREX to get MOX fuels for FBR. The above two step concept has the following merits.

- It can maintain uranium resource security.
- It can reduce storage volume to about 1/5 with same proliferation resistance as spent fuel.
- It can respond rapidly in case of abrupt FBR realization.
- It is economical for the reprocessing of residues.

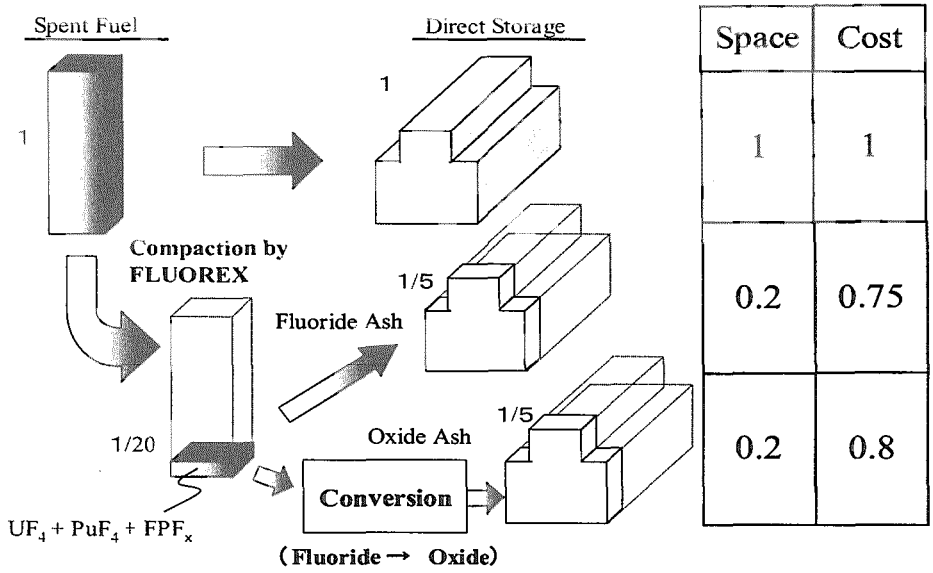

Space	Cost
1	1
0.2	0.75
0.2	0.8

Fig.2 Compared with the direct storage of spent fuel

6. CONCLUSION

New reprocessing technology, FLUOREX was proposed to meet the requirements for the near future LWR fuel cycle system. The FLUOREX system can recover pure U and MOX with the high decontamination factor and can drastically reduce the cost and waste generation.

The system also has high technical maturity, similar safety and energy sustainability and higher proliferation resistance compared with conventional fuel cycle system.

Most elemental technologies of FLUOREX method were already established worldwide and only a few subjects are remained for industrialization. Solvent extraction method is a part of industrialized PUREX process and fluoride volatility method is also industrialized as UF6 conversion and re-conversion processes.

Continuous development of FLUOREX can inherit the technologies and keep the scientists.

Acknowledgment

This work was financed by The Institute of Applied Energy (IAE). The authors gratefully acknowledge the IAE's permission to publish this work.

REFERENCES

[1] M. Kamoshida, F. Kawamura, A. Sasahira, T. Fukasawa, T. Sawa and J. Yamashita, "A New Concept for The Nuclear Fuel Recycle System: Application of The Fluoride Volatility Reprocessing", Proceedings of 3rd International Symposium on Global Environment and Nuclear Energy System, Tokyo Institute of Technology, December 14-17, Japan (1999).

[2] T. Fukasawa, T. Sawa, J. Yamashita, M. Kamoshida, A. Sasahira and F. Kawamura, "Hybrid Recycle System for The Recovery of Dirty Plutonium and Pure Uranium", Proceedings of 8th International Conference on Nuclear Engineering, ICONE-8627, April 2-6, Baltimore, MD USA (2000).

[3] M. Takahashi, T. Fukasawa, T. Sawa, J. Yamashita, M. Kamoshida, A. Sasahira and F. Kawamura, "Improved Fluoride Volatility Reprocessing for MOX Fuel Cycle", Proceedings of International Conference ATALANTE 2000, Scientific research on the back-end of the fuel cycle for the 21st century, p3.13, October 24-26, Avignon, France (2000).

JP0250304

JAERI-Conf 2002-004

AN ADVANCED AQUEOUS PROCESS FOR NUCLEAR FUEL REPROCESSING

Y.-Z. WEI[a], T. ARAI[a], H. HOSHI[a], M. KUMAGAI[a], A. BRUGGEMAN[b], M. GYSEMANS[b] and T. SAWA[c]

[a] Institute of Research and Innovation (IRI), 1201 Takada, Kashiwa, 277-0861 Japan, yzwei@iri.or.jp

[b]Belgian Nuclear Research Center (SCK・CEN) B-2400 Mol, Belgium

[c]Hitachi, Ltd., 7-2-1 Omika, Hitachi, 319-1221 Japan

Abstract

To develop an advanced aqueous reprocessing process using a minimal organic solvent and compact equipment to separate U, Pu and long-lived minor actinides from spent nuclear fuels, we have developed a new type of anion exchanger (AR-01) and several novel extraction resins containing a chelating ligand such as CMPO, Cyanex-301 and R-BTP. A hot separation experiment for a spent BWR-fuel solution was carried out by an ion exchange column packed with AR-01. To enhance the separation factor between U and FPs, electrolytic reduction of UO_2^{2+} to U^{4+} was studied using a flow type electrolysis cell with carbon-fiber electrode. Separation behavior of Am(III) from simulated HLW by CMPO and R-BTP impregnated resins were investigated. On the basis of the experimental results, an advanced aqueous process which consists of anion exchange as main separation method, electrolytic reduction for reducing U(VI) to U(IV) and extraction chromatography for MA partitioning has been designed and evaluated preliminarily.

Keywords: *reprocessing, anion exchange, electroreduction, extraction chromatography, minor actinides, process design*

1. IINTRODUCTION

Although the Purex process has been developed and applied to commercial reprocessing plants for about fifty years, there are also some significant unsolved disadvantages such as the generation of a great amount of waste and the utilization of large scale extraction equipment. In nitric acid solution, U and Pu exhibit distinct adsorption on an anion exchanger as they form anionic nitrato-complexes, while many fission product (FP) and minor actinide (MA) elements mostly exist as cations and show no or very weak adsorption[1)-3)]. This indicates that U and Pu could be separated principally from FP and MA (Am, Cm, etc.) in a nitric acid solution of spent nuclear fuels by anion exchange technology. Compared to the Purex process, an ion exchange process should have the following advantages: (1) a minimal organic solvent utilization, (2) compact equipment, and (3) simultaneous separation of multi-components.

In recent years, we have been studying an advanced aqueous reprocessing process which consists of anion exchange as main separation method, electrolytic reduction for reducing U(VI) to U(IV) and extraction chromatography for MA partitioning. We have developed a new type of anion exchanger, AR-01[2)3)] and several novel extraction-resins containing a chelating ligand such as CMPO, Cyanex 301 or R-BTP[4)5)]. These resins are immobilized in porous silica particles with a diameter of 50 μm. Compared to conventional polymeric matrix resins, these new type of resins have rapid adsorption-elution kinetics, excellent stability in nitric acid media and significantly low pressure drop in a packed column.

This article describes the configuration and preliminary evaluation of the advanced aqueous reprocessing process. Separation experiment results for a nitric acid solution of a spent LWR-fuel by AR-01 packed column are demonstrated. Furthermore, recent studies on electrolytic reduction

of U(VI) to U(IV), separation of U(IV) from FPs and partitioning of MA by novel extraction resins are also reported.

2. OUTLINE OF THE ADVANCED AQUEOUS PROCESS

Schematic flow sheet of the proposed aqueous reprocessing system is shown in Fig.1. This system consists of two anion exchange separation processes, one electrolytic reduction process and two extraction chromatography processes. In the main separation column packed with AR-01 anion exchanger, the elements contained in spent fuel solution are separated to the following five groups, i.e. (1) FP-Ln(lanthanides)-MA, (2) U-Np-FP, (3) Pu-Np, (4) Pd and (5) Tc, depending on their different adsorption-elution behavior. The purpose of the electrolytic reduction process is to reduce U(VI), Np(V,VI) and Ru(III) to U(IV), Np(IV) and Ru(II), respectively. Subsequently, the reduced solution is fed to the U-purification column packed with AR-01, where the U(IV) is isolated from the remained FP and Np(IV) due to the great difference in their adsorbability on AR-01. In order to isolate the trivalent MA, the effluent (1) from the main separation column is supplied to the first extraction chromatographic column packed with CMPO (or TOGGA) impregnated resin, where the elements can be separated to three groups, i.e. FP, Ln-MA and Zr-Mo. The effluent containing Ln-MA from CMPO impregnated resin column is then applied to the second extraction chromatographic column packed with R-BTP (or Cyanex-301) impregnated resin to isolate MA from Ln.

3. A HOT EXPERIMENT OF THE MAIN SEPARATION PROCESS

To demonstrate separation behavior of the elements in the main separation process, a hot experiment using a spent fuel solution was carried out by the anion exchange column packed with AR-01. The sample solution was prepared by dissolving a spent fuel discharged from a commercial BWR with burnup of 55,000 MWd/tHM in nitric acid solution. After filtration the resulting solution was adjusted to approximately 0.7 M (1 M=1 kmol/m^3) U and 6 M HNO_3. A small amount of $NaNO_2$ (to 0.05 M) was added to the solution to hold the Pu in tetravalent state (Pu(IV))[6]. The analysis results of main elements and nuclides in the sample solution are illustrated in Table I. The Pyrex-glass column (ϕ20mm$\times h$1,000mm) packed with the AR-01 was installed in a hot cell and the temperature in the cell was maintained at 296 K during the experiment. About 40 cm^3 of the sample solution was fed to the column by a metering pump at a constant line flow rate of 3.8 m/h. Then eluent and washing solutions were supplied to the column at the same flow rate, successively. The effluent from the column was collected by auto-fractional collector in 10 cm^3 aliquot. The concentrations of element or nuclide in each fraction were measured by ICP-mass spectrometry, α- or γ-spectrometry.

Figure 2 shows the results of the hot separation experiment. As can be seen, most FP elements such as Cs, Sr, Mo, Ru, Rh and the trivalent MA and Ln showed no or slight adsorption. These elements flowed out the column with the sample solution and the 6M HNO_3 washing solution. All the U was adsorbed on the anion exchanger and then eluted off by 6M HNO_3 and 1M HNO_3 solutions. Most of the above FP and MA elements were satisfactorily separated from U. However, a portion of the FP particularly Ru, Zr and Nb (weakly adsorptive FPs) were adsorbed and mixed with the U eluate fraction. A small portion of Ru finally appeared in the final eluate (0.1M and 9M HNO_3 solutions). Pu was completely adsorbed by the anion exchanger and it was

eluted out effectively by using 1 M HCOOH as the eluent, showing a sharp peak. Successful separation of Pu from U and FPs was achieved. Np showed a complicated elution behavior probably due to its different oxidation states. Np(V) and Np(VI) were mostly mixed with the U fraction, while Np(IV) was found in the Pu eluate fraction. Pd and Tc were not detected in all the effluents, although they were expected to be eluted by 0.1M $CS(HN_2)_2$ and 9M HNO_3 respectively as in cold experiments[2)3)7)]. The behavior and efficient elution method of Pd and Tc need to be investigated further.

4. ELECTROREDUCTION OF U(VI) TO U(IV) AND SEPARATION OF U(IV) FROM FPs

4.1 Electroreduction of U(VI) to U(IV)

The incomplete separation between U and the FP elements in the main separation column is considered to be due to the relatively low adsorbability of U(VI) in HNO_3 solution onto anion exchanger[3)]. To enhance the separation factor between U and FPs, we have investigated the electrolytic reduction of uranyl (UO_2^{2+}) to uranous ion (U^{4+}) which shows significantly higher adsorbability[8)9)]. Electroreduction experiments were carried out using a novel flow type electrolysis cell as shown in Fig. 3. The cathode of glassy carbon fibers filled in a cylindrical column of vycor glass (porous silica glass) works as the working electrode. The glass column works as both cathode compartment and separator. In the experiments, a sample solution containing U(VI) and/or some typical FPs in HNO_3 solution was introduced into the vycor glass column by metering pump. As a holding reducing agent of U(IV), hydrazine($N_2H_4 \cdot H_2O$) was added to the sample solution. The electroreduction was conducted at a constant potential. The concentration of U(IV) in the outlet solution of the cell was determined by UV spectrometry.

Figure 4 shows the experimental results of electroreduction for the sample solution containing 0.1M U(VI), 6.0M HNO_3 and 1M N_2H_4. The sample solution was passed trough the electrolysis cell at the flow rate of 2.0 cm/min once-through and the electrolytic potential was fixed at –300 mV (*vs.* Ag/AgCl). As can be seen in Fig. 4, despite of the high concentration of HNO_3 (6.0M), U(VI) was completely reduced to U(IV) with the conversion of 100%. The total current efficiency was higher than 90%, indicating the effect of side reactions such as HNO_3 decomposition is significantly slight. The observed constant current means that the reaction rate for U(VI) reduction was unchanged during the electrolysis. Although the standard redox potential of HNO_3 reduction (Table II) is much higher than that of U(VI) reduction, the very high U(IV) conversion and the current efficiency reveal that the reduction reaction of U(VI) to U(IV) took place predominantly.

On the other hand, from the hot experiment results shown in Fig. 2, the U eluate obtained from the main separation column contains U(VI), Np(V, VI) and a small portion of various FPs. In the electroreduction system for a practical process solution, the possible reactions taking place in the electrolysis cell are listed in Table II and the hot electrolysis experiment using spent fuel solution is in execution.

4.2 Separation of U(IV) from FPs by Anion Exchange

Separation experiments for simulated process solutions containing U and some typical FPs were carried out using AR-01 packed column before and after electrolytic reduction. Fig. 5 and Fig. 6 show the experimental results for the sample solution containing U, Sr, Fe, Ru, Zr and 6.0M HNO_3

before and after electroreduction, respectively. As seen in the case without electroreduction (Fig. 5), a part of Zr(IV) and most portion of Ru(III) were also adsorbed by the anion exchanger and mixed in the U(VI) eluate. The separation of U(VI) from the PFs, especially the adsorptive Ru(III) and Zr(IV) was not complete. On the other hand, after electroreduction as shown in Fig. 6 the U(IV) was strongly retained by the AR-01 and the adsorbed U(IV) was eluted off by using 0.1M HNO_3 as an eluent, showing a sharp peak. Perfect separation between U(IV) and the FPs was achieved. Note that the Ru in the reduced solution was not adsorbed by the AR-01 and showed the same behavior with the non-adsorptive Sr(II) and Fe(II). This indicates that the adsorptive Ru(III) was completely reduced to the non-adsorptive Ru(II) by the electrolysis[10].

5. SEPARATION OF MINOR ACTINIDES BY EXTRACTION CHROMATOGRAPHY

To separate the MA from the process solutions for the partitioning/transmutation option, several novel extraction resins were prepared by impregnating a chelating ligand such as CMPO, TODGA, R-BTP or Cyanex-301 into styrene-divinylbenzene copolymer which is immobilized in porous silica particles of 50 μm diameter (SiO_2-P). Fig. 7 shows the chemical structure of the ligands used in this work. CMPO and TODGA can efficiently extract trivalent MA and Ln from concentrated nitric acid solution, and have been extensively studied for the co-extraction of MA-Ln from HLW solution[11)12)]. R-BTP and Cyanex-301 are known as soft donor (N, S) ligands which have high extraction selectivity for MA over Ln(III)[4)5)13)14)].

Figure 8 presents a separation experiment result for a simulated HLW solution containing typical Ln(III) and FPs and 3M HNO_3 by the column packed with CMPO impregnated resin. As can be seen, the elements were essentially separated to three groups, i.e. (1) Sr-Rh-Ru; (2) Pd-Gd-Nd; and (3) Zr-Mo, although Ru and Pd showed complicate elution behavior. Sr(II) and Rh(III) were not adsorbed and leaked out firstly. The adsorbed Gd(III), Nd(III) and most Pd(II) were eluted off efficiently by using only water. On the other hand, we have found that Am(III) exhibits a very similar elution behavior with Nd(III)[15)] and would mixed in this effluent. Zr(IV) and Mo(V) showed strong adsorption and finally could be eluted and separated by using oxalic acid as an eluent.

In the MA partitioning process, the separation between trivalent MA and Ln is the most difficult step due to their similar chemical behavior. In recent years, Cyanex-301 and R-BTP were reported to be the promising ligands for MA/Ln separation[4)5)13)14)]. We have synthesized several R-BTP ligands with different alkyl groups (C=1-8) and impregnated them into the SiO_2-P support. Figure 9 shows the adsorption behavior of Am(III)(^{243}Am tracer), Ce(III), Eu(III) and Gd(III) from nitrate solution onto the Bu-BTP impregnated resin. Note that the adsorption of Am(III) increased dramatically with increasing NO_3^- concentration. Although the adsorption of Eu(III) and Gd(III) (heavier Ln) increased with NO_3^- concentration, the separation factor for Am/Eu-Gd is up to about 10^2. Moreover, Ce(III) (a light Ln) showed almost no adsorption and the separation factor for Am(III)/Ce(III) is as high as 10^4. From these results, it is expected that Am can be effectively separated from Ln by means of extraction chromatography using the R-BTP impregnated resins.

6. CONCEPTUAL DESIGN AND PRELIMINARY EVALUATION OF THE PROCESS

On the basis of the experimental results, conceptual design and preliminary evaluation of the proposed aqueous process as shown in Fig. 1 has been carried out by comparing with the

conventional Purex process. The process is designed for a reprocessing plant having capacity of 800 t-U/y with operation days of 200 d/y (1d = 24h). The structure, size, number and installation layout of main machines and equipments for separation processes were designed and estimated. Furthermore, chemical flow sheet, mass balances and the amounts of waste generation were calculated and evaluated.

Table III shows the preliminary evaluation results for the advanced aqueous process. Overall flow sheet of the process for reprocessing spent nuclear fuels is illustrated in Fig. 10. The required size for the columns was calculated from the adsorption capacity of the resins and the pressure drop in the packed column. As the results, the sizes of the AR-01 columns for the main separation and the U purification are 150 cm ϕ (diameter) x 160 cm h (height) and 100 cm ϕ x 160 cm h, respectively. In the MA separation process, since the Am and Cm are significantly less abundant than U and Pu in the spent fuel, so that the scale of the columns for their separation from concentrated HLW is considerably small. The column sizes of CMPO and R-BTP impregnated resins were estimated to be 15 cm ϕ x 50 cm h and 15 cm ϕ x 20 cm h, respectively. In the electroreduction process, a novel flow type of electrolysis vessel, which consists of parallel multi-cells, has been designed. The estimated size for the cubic electrolysis vessel is 280 cm (length) x 150 cm (width) x 180 cm (height). Besides the above main equipments, 5 pumps for solution supply and about 30 vessels for solution adjustment and storage are required. In a conventional Purex process with the same treatment capacity, some 35 units of extractors and contactors including the 12 units with 13 m in height as well as 32 vessels are needed[16]. Therefore, the number of the machinery and equipment can be reduced to approximately 1/2 and significantly compacter equipments are used in the advanced aqueous process. In addition, compared to the multi-stages separation procedures for extraction, striping and scrubbing in the Purex process, fewer and simpler operation procedures are realized.

In this process, the separations are based on the adsorption-desorption of nitrato-complexes, therefore the required amount of HNO_3 is large. However, about 95% of the HNO_3 is recovered for reuse. Since the high-level-waste is essentially determined by the amounts of FPs in spent fuel, its amount should be almost the same with the Purex process. Unlike the Purex process, the ion exchange process does not use the organic solvents such as TBP and dodecane, so a great amount of the alkaline waste solution resulted from the solvent cleanup will not be generated. Therefore, the low-level-waste generation was estimated to be less than 1/3 of the amount in the Purex process. Alternatively, the process utilizes the AR-01 ion exchange resin and the extraction resins containing CMPO and R-BTP, the AR-01 resin will be replaced after use for 2 years with approximately 20% degradation[17]. The depleted AR-01 resin for disposal was estimated to be 2-3 m^3/y. From the evaluation results described above, it is concluded that compared to the conventional Purex process, the size and number of required machinery and equipment as well as the amount of waste generation are expected to be reduced greatly in the advanced aqueous process. With these distinguished advantages, a considerable saving in the costs for plant construction and process operation can be expected.

7. COCLUSIONS

1) The separation experiments of a spent LWR-fuel solution using AR-01 anion-exchanger column demonstrated that most of the elements (Cs, Sr, Mo, Rh, Ln, Am, Cm) could be

separated from U(VI). Some FPs especially Ru, Zr, Nb showed weak adsorption and contaminated the U. The eluted U needs to be purified by the refining process.

2) Pu(IV) was eluted effectively by dilute HCOOH and successfully separated from U and FPs. Np showed a complicated elution behavior due to its different oxidation states. Pd and Tc presented significantly strong adsorption and their efficient elution needs to be investigated further.
3) The electroreduction of U(VI)→U(IV), Np(V,VI)→Np(IV), Ru(III)→Ru(II) was successfully performed by the novel flow type electrolysis cell. U(IV) presents significantly stronger adsorption onto AR-01 than U(VI) and perfect separation between U(IV) and the adsorptive FPs (Zr, Ru, etc) was obtained
4) CMPO impregnated resin showed effective group-separation of MA(Am,Cm)-Ln from high-level-waste. The soft-donor ligand, R-BTP impregnated resin exhibited high adsorption selectivity for MA over Ln with separation factor higher than 100. Effective separation of MA from Ln is expected by extraction chromatography using the novel extraction resin.
5) An advanced aqueous reprocessing process which consists of anion exchange, electrolytic reduction and extraction chromatography has been designed and evaluated preliminarily. Compared to the Purex process, the number and size of main equipment could be reduced to approximately 1/2-1/3. The amount of low-level-waste would be reduced to less than 1/3. A considerable cost-down in plant construction and process operation can be expected

Acknowledgement

This work was financed by the Ministry of Education, Culture, Sports, Science and Technology of Japan (MEXT). The authors gratefully acknowledge the ministry's permission to publish this work.

References

1) J.P. Faris and R.F. Buchanan, *Anal. Chem.*, **36**,1157–1158 (1964)
2) Y.-Z. Wei *et al.*, Ion Exchange Development and Application, J. A. Greig ed., SCI, London, 174-181 (1996)
3) Y.-Z. Wei, *et al.*, *J. Nucl. Sci. Technol.*, **35**, 357-364 (1998)
4) Y.-Z. Wei, *et al.*, *Nucl. Technol.*, **132**, 413-423 (2000)
5) Y.-Z. Wei, *et al.*, *J. Nucl. Sci. Technol.*, **37**, 1108-1110 (2000)
6) M. Benedict, T. H. Pigford and H. W. Levi, Nuclear Chemical Engineering, McGraw-Hill, New York, 478 (1981)
7) Y.-Z. Wei, *et al.*, *J. Alloys and Compounds*, **271-273**, 693-696 (1998)
8) E. L. Kazantsev and V. L. Korobeinikov, *Izv. Vysshikh Uchebn. Zavedenii Tsvetn. Met.*, **4**, 89-94 (1966)
9) Y. Z. Wei *et al.*, Ion Exchange at the Millennium, J. A. Greig ed., SCI, London, 116-123 (2000)
10) T. Arai, *et al.*, Proc. Global'2001, Paper-004, 9-13 Sep., 2001, Paris (France)
11) E. P. Horwitz, *et al.*, Proc. Solvent Extr. 1990, p. 357, T. SEKINE, Ed., Elsevier Sci. Pub. (1990)
12) Y. Morita, *et al.*, Proc. Global'2001, Paper-036, 9-13 Sep., 2001, Paris (France)
13) Y. Zhu, *et al.*, *Solvent Extr. Ion Exch.*, **14**, 61 (1996)
14) Z. Kolarik, *et al.*, *Solvent Extr. Ion Exch.*, **17**, 23 (1999)
15) Y.-Z. Wei, *et al.*, Proc. Actinides-2001, 4-9 Nov., 2001, Hayama (Japan) (in press)
16) Japan Atomic Information Center, "The Details of the Main Processes in Rokkasho Reprocessing Plant", Report No. 9408630 (in Japanese) (1994)
17) T. Hoshikawa, *et al.*, Proc. Global'97, 1454-1459, 5-10 Oct., 1997, Yokohama (Japan)

Table I Analytical results of elements and nuclides in the spent BWR-fuel solution

Element or nuclide	μg/g-soln	mM	Analysis method
U	122000	709	ICP-MS
U-235	768	4.52	ICP-MS
Pu-240	259	1.49	ICP-MS
Am-241	51.89	0.30	γ-spec
Np-237	68.3	0.40	ICP-MS
Eu-154	1.78	0.016	γ-spec
Eu-153	21.2	0.19	ICP-MS
Nd-145	123	1.17	ICP-MS
Ce-140	243	2.40	ICP-MS
Cs-137	193.92	1.96	γ-spec
Cs-133	214	2.23	ICP-MS
Ag-109	1.17	0.015	ICP-MS
Pd-105	23.7	0.31	ICP-MS
Rh-103	36.3	0.49	ICP-MS
Ru-101	63.9	0.88	ICP-MS
Tc-99	102	1.43	ICP-MS
Mo-95	27.6	0.40	ICP-MS
Nb-93	139	2.07	ICP-MS
Zr-91	99.3	1.51	ICP-MS
Y-89	100	1.56	ICP-MS
Sr-88	558	8.76	ICP-MS
HNO_3		6000	
$NaNO_2$		50	

Table II Possible reactions in the electrolysis cell

Reactions		Remark
In Cathodic Compartment:		
$UO_2^{2+} + e = UO_2^{+}$	(1)	$E^0 = 0.062$ V
$2UO_2^{+} + 4H^{+} = UO_2^{2+} + U^{4+} + 2H_2O$	(2)	$K_c = 9 \times 10^8$
$2UO_2^{2+} + 4H^{+} + 2e = U^{4+} + 2H_2O$	(3)	$E^0 = 0.327$ V
$NpO_2^{+} + 4H^{+} + e = Np^{4+} + 2H_2O$	(4)	$E^0 = 0.739$ V
$NpO_2^{2+} + 4H^{+} + 2e = Np^{4+} + 2H_2O$	(5)	$E^0 = 0.938$ V
$RuNO^{3+} + e = Ru^{2+} + NO$	(6)	$E^0 = 0.249$ V ?
$Fe^{3+} + e = Fe^{2+}$	(7)	$E^0 = 0.771$ V
$2H^{+} + 2e = H_2$	(8)	$E^0 = 0$ V
$HNO_3 + 2H^{+} + 2e = HNO_2 + H_2O$	(9)	$E^0 = 0.94$ V, slow
$HNO_2 + H^{+} + e = NO + H_2O$	(10)	$E^0 = 0.99$ V
$3HNO_2 = HNO_3 + 2NO + H_2O$	(11)	slow
$HNO_3 + NO + H^{+} + e = 2HNO_2$	(12)	fast
$HNO_3 + HNO_2 = 2NO_2 + H_2O$	(13)	autocatalytic, fast
$2Fe^{2+} + NO_3^{-} + 3H^{+} = 2Fe^{3+} + HNO_2 + H_2O$	(14)	
$U^{4+} + 2HNO_2 = UO_2^{2+} + 2H^{+} + 2NO$	(15)	
$HNO_2 + N_2H_5^{+} = HN_3 + 2H_2O + H^{+}$	(16)	
$HN_3 + HNO_2 = N_2O + N_2 + H_2O$	(17)	
In Anodic Compartment:		
$2H_2O - 4e = O_2 + 4H^{+}$		$E^0 = 1.229$V

Table III The results of preliminary evaluation for the advanced aqueous reprocessing process

Item	Estimated Amount	Remark
1. Machinery & Facility	Main equipment: 5 units Pumps for solution supply: 5 units Vessels for solution Adjustment & storage: ~30 units Construction area: ~1300 m^2	Two ion exchange columns (1.5mϕ x 1.6mh, 1.0mϕ x 1.6mh) One electrolysis vessel (2.8x1.8x1.5m) Two extraction chromatographic columns (15cmϕ x 50cm$h$, 15cmϕ x 20cm$h$)
2. Reagent*	Nitric acid: 306 kmol/day Formic acid: 11 kmol/day Thiourea: 1 kmol/day Hydrazine: 3 kmol/day	95% of nitric acid is recovered 70% of formic acid is recovered Thiourea is optional Hydrazine is the holding reductant of U(IV)
3. Waste Generation*	High level liquid waste: 93 m^3/day Low level liquid waste: 120 m^3/day Used nitric acid solution: 120 m^3/day Depleted resins: 2~3 m^3/year	 To nitric acid recovery process AR-01 resin is replaced every 2 years

* Those for MA separation process are not included.

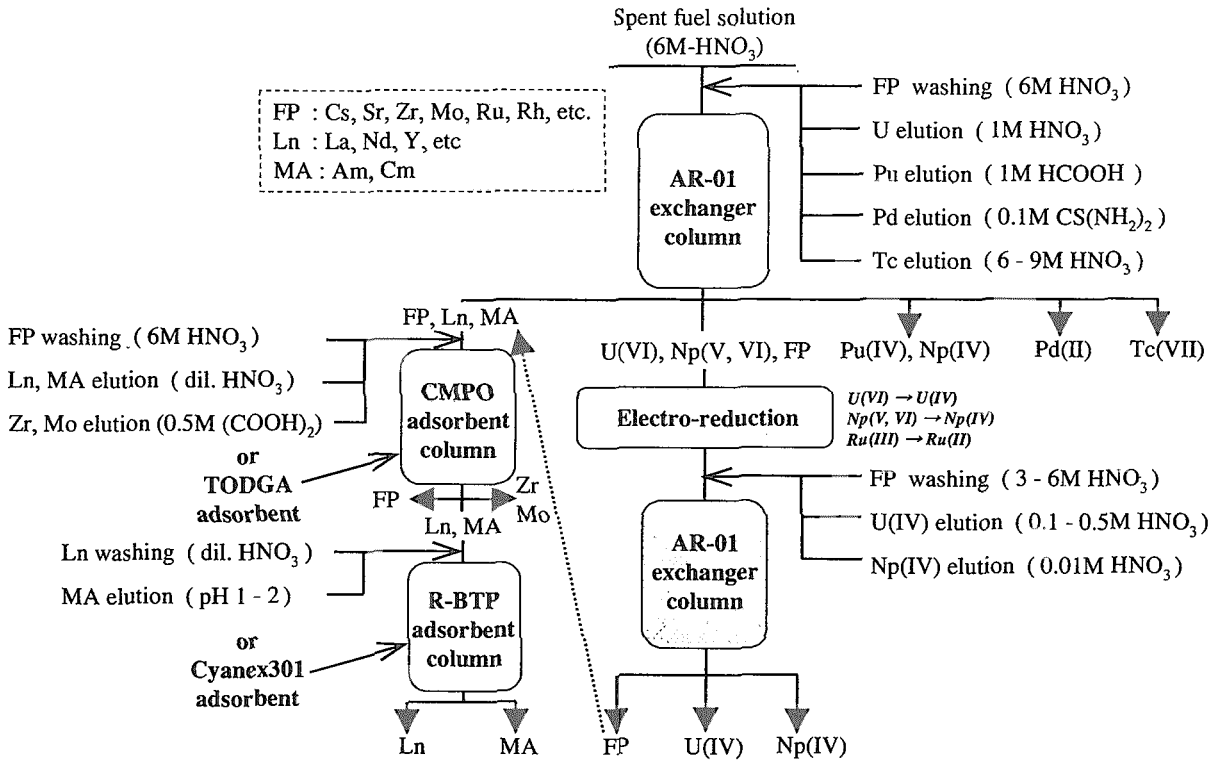

Fig. 1 Schematic flow sheet of the proposed aqueous process for reprocessing spent nuclear fuels

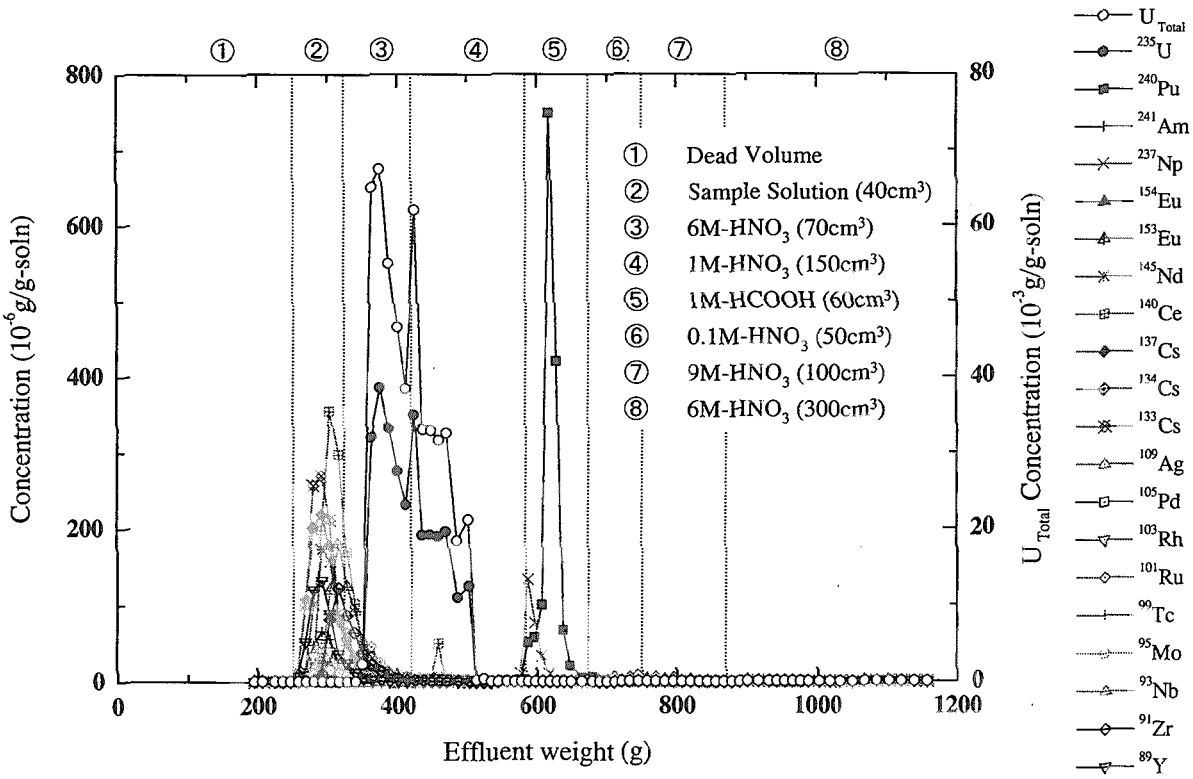

Fig. 2 Separation experiment results for a spent LWR-fuel solution by anion exchange
(Column 20 mm ϕ x1000 mm h, AR-01 BV 282cm^3, Flow rate 3.8 m/h, Temp. 296K)

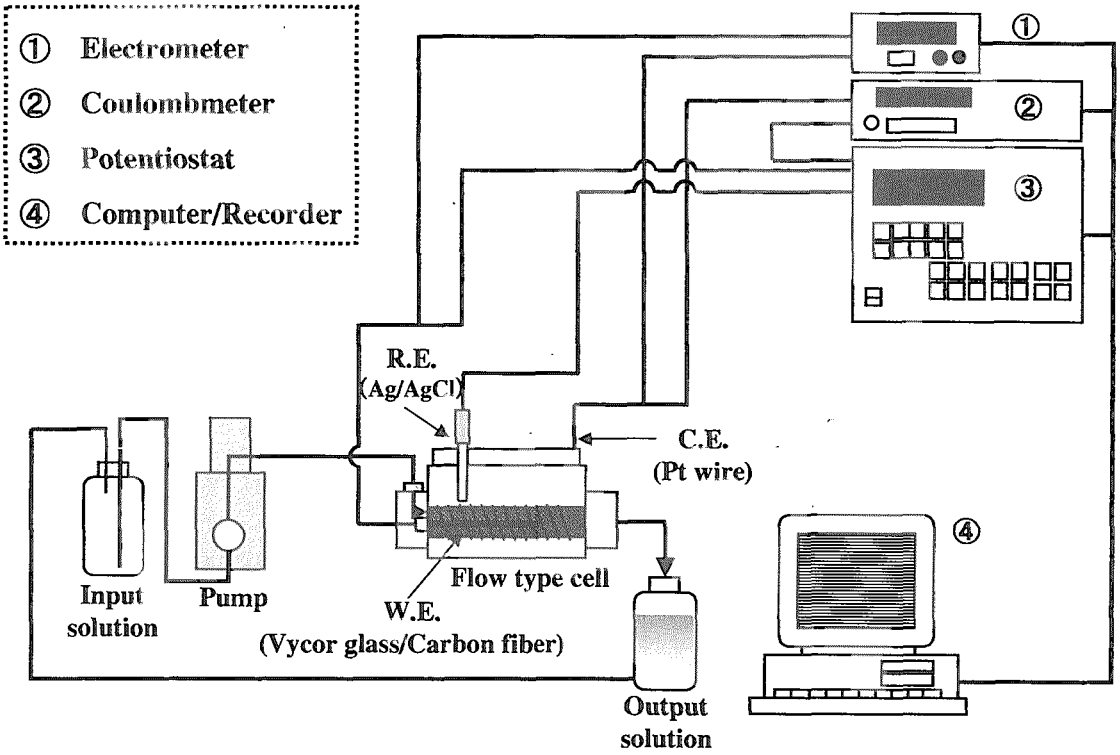

Fig. 3 Schematic diagram of the flow type electrolysis apparatus

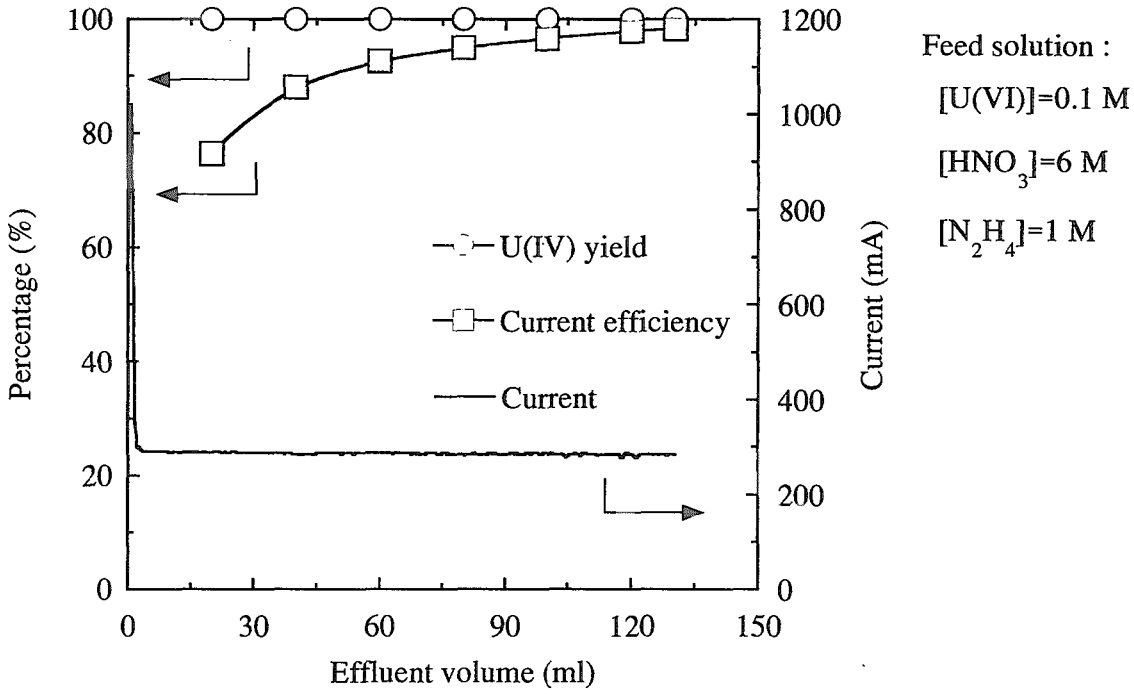

Flow rate : 1 ml/min, Potential : -300 mV(*vs.* Ag/AgCl), Temperature : 298 K

Fig. 4 Electroreducton behavior of U(VI) in nitric acid solution using the flow type electrolysis cell

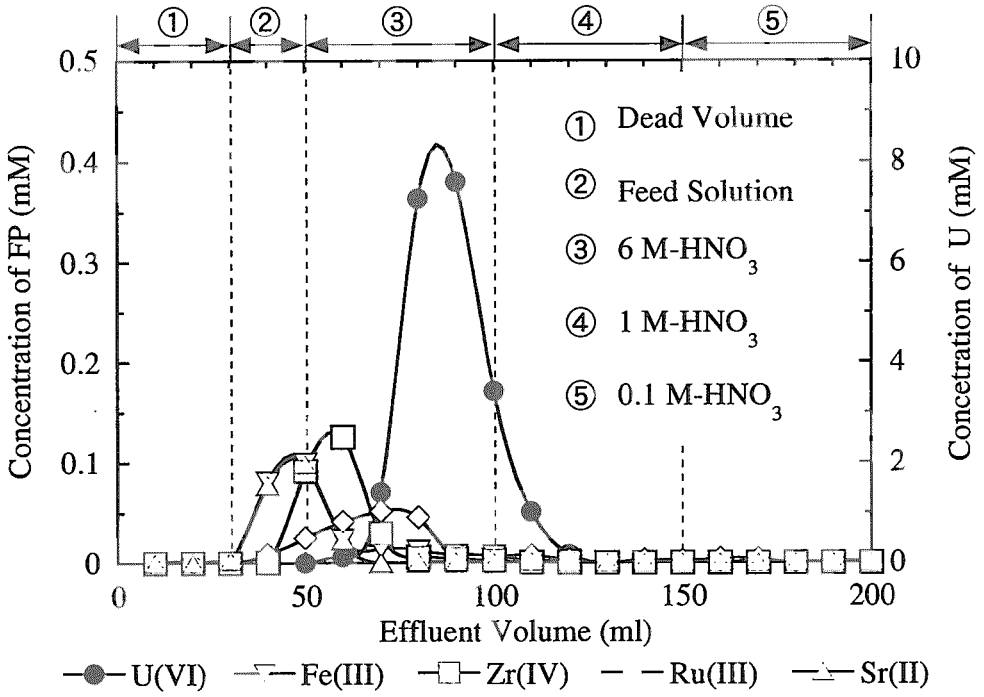

[U(VI)]=10 M, [Fe(III),Zr(IV),Ru(III),Sr(II)]=0.1 M, [HNO_3]=6 M , Temperature : 333 K

Fig. 5 Results of separation experiment for U-FPs solution by anion exchange before electrolytic reduction

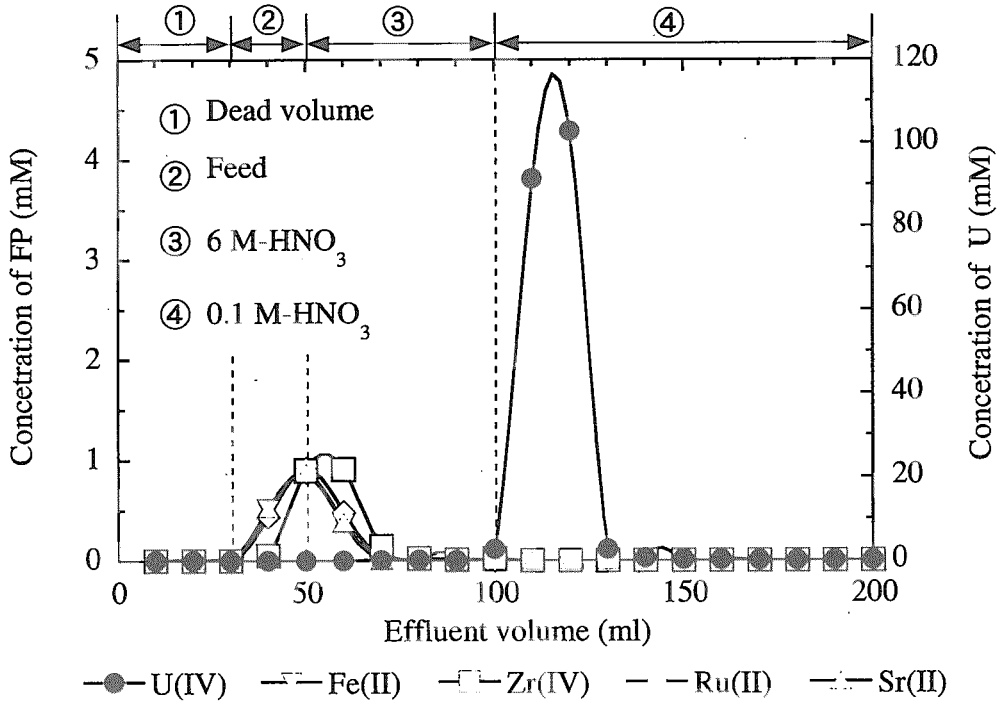

[U]=100 mM, [Fe, Zr, Ru, Sr]=1 mM, [HNO_3]=6 mM, Temperature : 300 K

Fig. 6 Results of separation experiment for U-FPs solution by anion exchange after electrolytic reduction

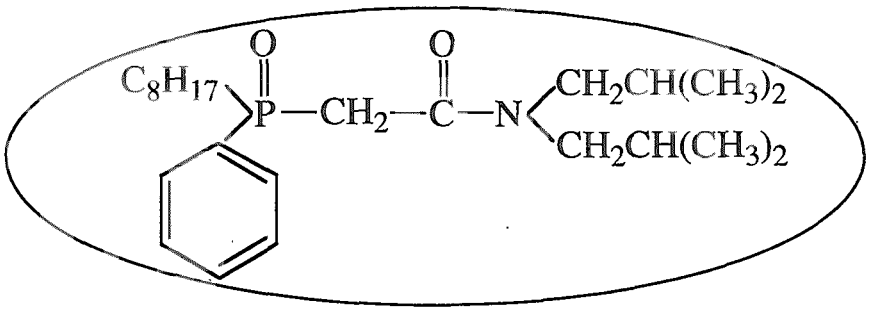

CMPO (Octyl(phenyl)-N, N-diisobutylcarbamoylmethylphosphine Oxide)

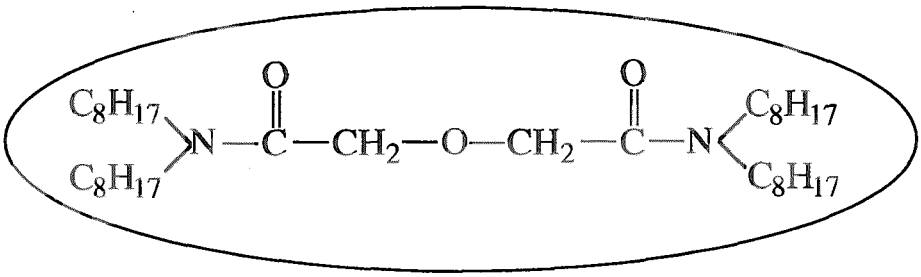

TODGA (N,N,N',N'-tetraoctyl-3-oxapentane-1,5-diamide)

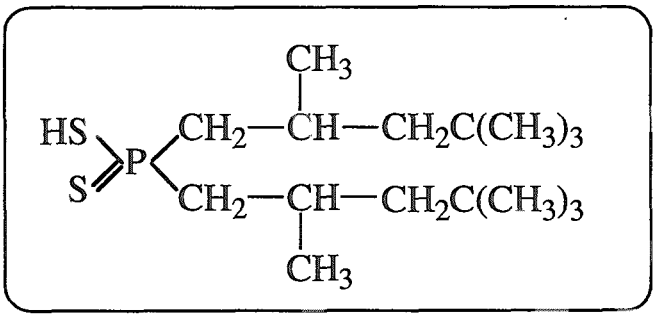

CYANEX-301 ((Bis(2,4,4-trimethylpentyl) Dithiophosphinic Acid)

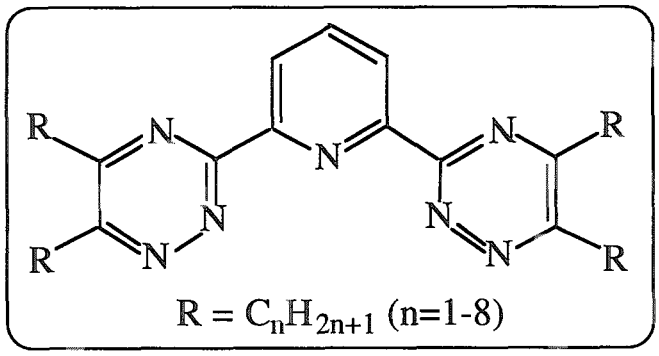

R-BTP (2,6-bis-(5,6-dialkyl-1,2,4-triazine-3-yl)-pyridine)

Fig.7 Chemical structure of the ligands impregnated in SiO_2-P support for MA separation

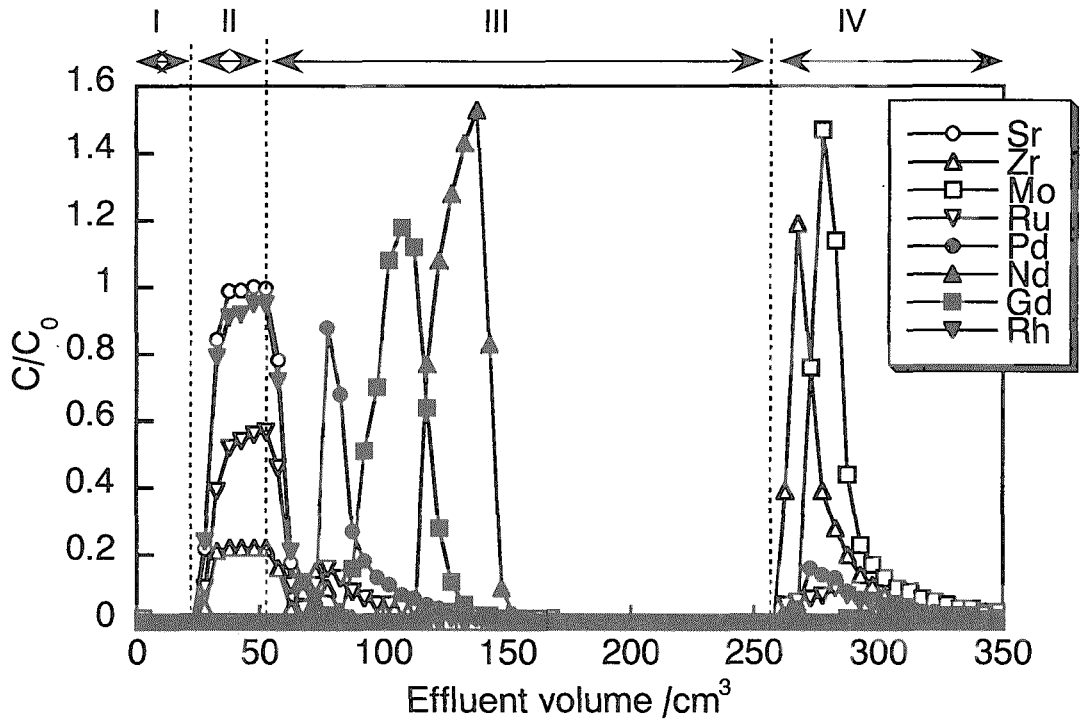

I Dead Volume; II Feed solution; III H_2O; IV 0.5M $(COOH)_2$

Fig. 8 Results of separation experiment for a simulated HLW solution using CMPO impregnated resin
(Column 10 mmϕx500 mm h, 0.5g CMPO/SiO_2-P, Flow rate 3.8 m/h, Temp. 333K)

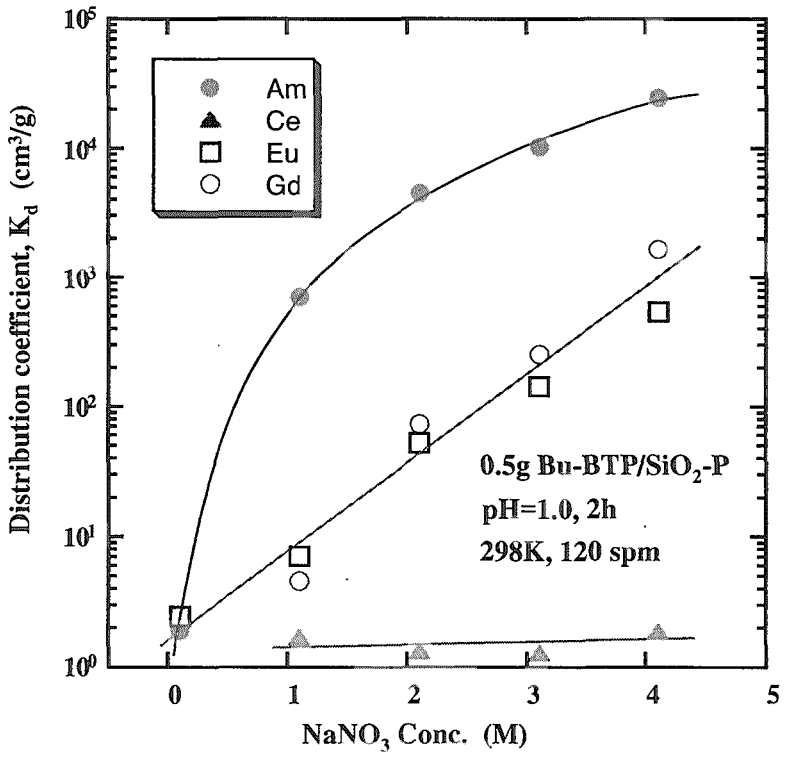

Fig. 9 Adsorption behavior of trivalent americium and lanthanides from nitrate solution onto Bu-BTP impregnated resin

JP0250305

R&D OF THE PARTITIONING OF THE LONG-LIVED RADIONUCLIDES IN FRANCE

M. Lecomte, P. Baron, M. Masson

Commissariat à l'Énergie Atomique (CEA), Valrhô–Marcoule, DEN/DRCP
BP 17171, 30207 Bagnols-sur-Cèze Cedex, France

In December 1991 the French parliament passed a law identifying three axes of research concerning long-lived and high-level radioactive waste management. The first axis is related to processes capable of separating long-lived radionuclides—notably the minor actinides (neptunium, americium and curium) but also the fission products (caesium, iodine and technetium) —for transmutation. The current reference strategy for separating the minor actinides from the high-level liquid waste stream (HLLW) produced by the reprocessing/recycling of the used fuel by the PUREX process is:
- firstly, to modify slightly the PUREX Process in order to separate neptunium,
- secondly, to develop liquid-liquid extraction processes involving two steps, considering the difficulty of separating the trivalent actinides (americium and curium) from the lanthanides and the strong acidity of the process solution:

- DIAMEX: coextraction of the actinides and lanthanides from HLLW
- SANEX: separation of the actinides from the lanthanides in the flow generated by the DIAMEX process (three variants are currently being investigated).

The CEA intends to select by the end of 2001 the best route for the demonstration of the minor actinides separation technological feasibility to be done before 2006.
This paper presents the recent advances of the development of long-lived radionuclides separation processes, focusing on the results obtained thanks to the hot tests conducted in ATALANTE Facility.

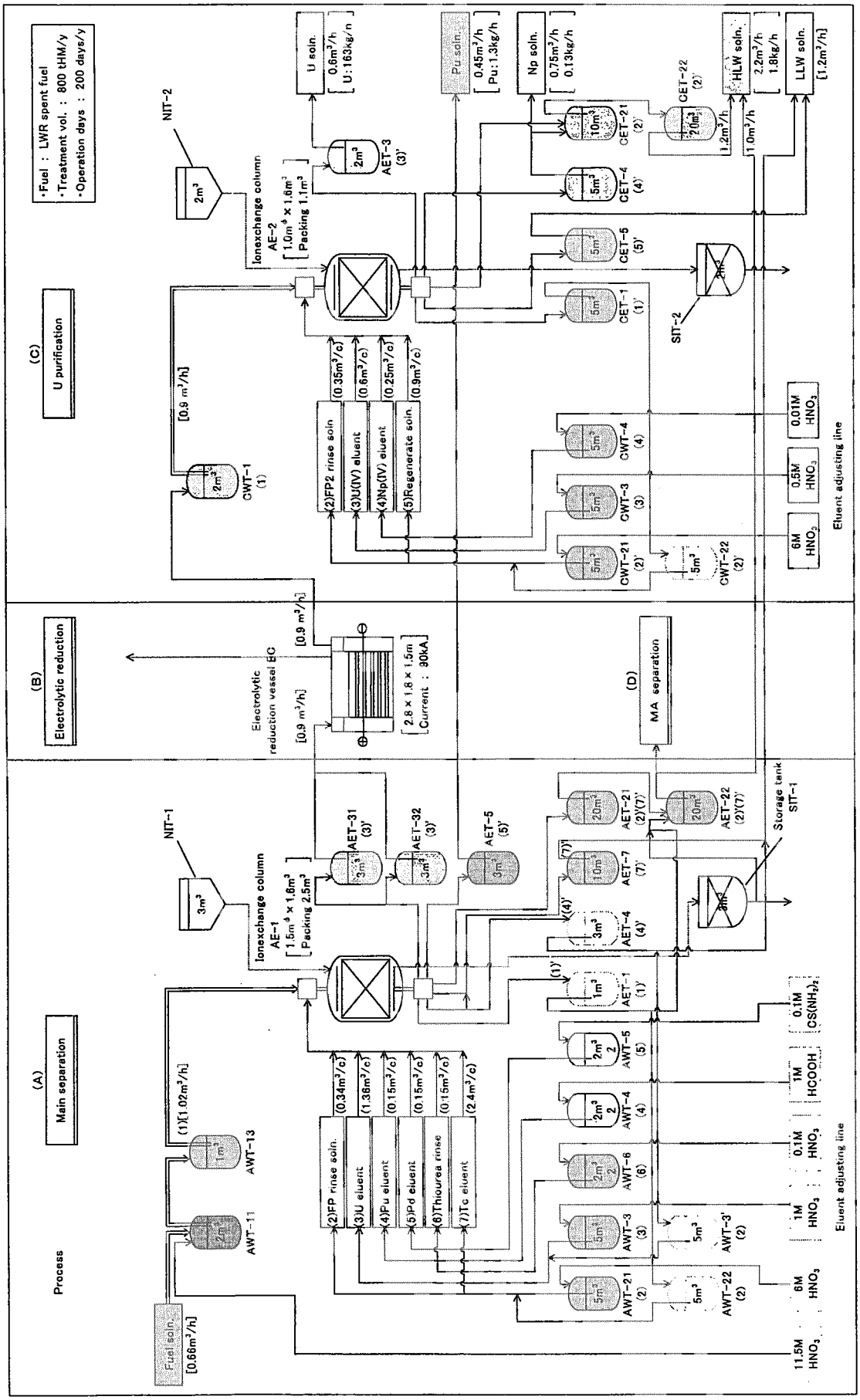

Fig. 10 Overall flow sheet of the advanced aqueous process for reprocessing spent nuclear fuels

JP0250306

JAERI-Conf 2002-004

OVERVIEW OF THE RESEARCH ACTIVITY IN PARTITIONING AT INSTITUTE OF NUCLEAR ENERGY TECHNOLOGY

CHONGLI SONG

Institute of Nuclear Energy Technology (INET), Tsinghua University
100084 Beijing, China
Fax: 86-10-6277 1150, e-mail: songchl@mail.tsinghua.edu.cn

The study on the partitioning of high lever radioactive liquid waste (HLLW) is undertaking in INET, Tsinghua University. The objective of the study is use the partitioning as a waste volume reduction method in near future and is use it in connected with transmutation (P&T) in the future to reduce long term risk of radioactive waste. A TRPO process was studied for the removal of actinide (An) from HLLW. A total partition process was developed to separate An as well as Sr and Cs from HLLW. A purified Cyanex 301 process was innovated for the separation of actinide and lanthanide. The Research activity in partitioning of HLLW at INET was reviewed.
Key words: Partitioning, HLLW, TRPO, Cyanex 301

1. INTRODUCTION

High level liquid waste (HLLW) contains more than 95% of radioactivity in spent nuclear fuel elements. The final disposal of high level radioactive waste (HAW) is a high public concerned subject. The transuranium (TRU) elements and long-lived nuclides such as ^{99}Tc and ^{129}I contained in HLLW have high toxicity and very long half-life. They dominate the long-term radiological risk of radioactive waste. Partitioning and Transmutation (P-T) of HLLW is an advanced nuclear fuel cycle[1]. The P-T concept involves chemical separation of transuranium (TRU) elements as well as long-lived nuclides (for example, ^{99}Tc, ^{129}I, etc.) from HLLW, and transmutation of them to either stable or short-lived nuclides. The P-T could decrease long-term risk of radioactive waste as well as the waste volume that should disposed in deep repository. It is a prospect technique for treatment and disposal of HLLW.

A clean use nuclear energy (CURE) concept[2] was proposed for the back-end of the nuclear fuel cycle. In CURE concept the partitioning requires not only to remove the TRU, ^{99}Tc and ^{129}I, but also to segregate ^{90}Sr and ^{137}Cs. After partitioning, the HLLW is downgraded to a non-α, low lever radioactive waste that will be eligible for near-surface disposal. The partitioning can used as a pretreatment method of HLLW to reduce α waste and HAW volume.

The study on the partitioning of HLLW is undertaking in INET, Tsinghua University. The objective of the study is use the partitioning as a waste volume reduction method in near future and use it in connected with transmutation (P&T) to reduce long term risk of radioactive waste in the future.

2. PARTITIONING OF TRU ELEMENTS BY TRPO PROCESS

The partitioning study in INET, Tsinghua University began in 1980. A trialkylphosphine oxide was found to have good extraction behavior for TRU elements[3].

2.1 TRPO extractant

The trialkylphosphine oxide is a commercial extractant. Its trademark is TRPO in China and Cyanex 923 in USA. It has different composition for various products but its main composition is a mixed phosphine Oxide with three alkyl groups of 6-8 carbon atoms. The TRPO has very good physical properties. It can mix with Kerosene or dodecane in any proportion and has very low solubility in water.

TRPO has quite good radiation stability no significant change in physical and extraction properties occurred until a radiation dose of 5×10^5Gy was absorbed[4]. Main gaseous radiolytic products and acidic radiolytic products of 30%TRPO-kerosene extractant were analyzed. Their radiation yield (G value) was determined[5]. When the radiation dose was above 2×10^6, some retention of heave elements were observed[6]. Research indicates that the polymeric products with high molecular weight cause the retention.

The chemical properties and extraction behavior of TRPO are similar to that of the tri-octyl phosphine oxide (TOPO). Tetra- and hexa- valent TRU ions are highly extractable in whole nitric acid concentration (0.05-10 M) by 30% TRPO. Trivalent TRU ions, such as Am(III), Cm(III), and Pu(III) are effectively extracted at low and medium nitric acid solution (from0.05 to 2 M). But the extraction of penta-valent NpO_2^+ is very poor. Among the fission product (FP) elements, Zr is highly extractable. The extraction ability of 30% TRPO for Tc(VII) is very high at low and medium nitric acid concentration, but it drops sharply with increases of nitric acid concentration. The extraction of Mo is sufficiently high[3].

2.2 TRPO process

A TRPO process had been developed for the partitioning of TRU elements from HLLW in 1980s[7-8]. In the TRPO process the HLLW is adjusted to 1-2 M nitric acid concentration. In the meantime the neptunium valence is adjust to the extractable Np(IV). The feed solution of HLLW is contacted with by 30% TRPO. The TRU elements are extracted into organic phase. The raffinate was downgrade to a non α HLLW raffinate. After washing with diluted nitric acid, the extracted TRU elements are stripped stepwise with 5.5 M nitric acid, 0.6 M oxalic acid and 5% sodium nitrate and divided into three groups: Am+Cm, Np+Pu and U respectively. The 30% TRPO organic phase is subsequently recycled into the process after washing with water. The non α HLLW raffinate can be sent to the further steps for separation of Sr- 90 and Cs-137.

A mathematical model was developed to calculate the extraction of Am, Nd and nitric acid in 30% TRPO/HNO_3 at different Na, Al, Fe, and RE concentrations[9]. The mathematical model was used to optimize the TRPO process parameters for removing Am from simulated Chinese HLLW. The experimental results fit very well with the calculated ones.

The counter current hot tests of the TRPO process were undertaken in the Institute for Transuranium Element (ITU) in Karlsruhe, Germany with genuine HLLW solutions of WAK reprocessing plant in 1993[10-11]. The hot test was completed with 24 stages of miniature centrifugal contactor in hot cell. The results of the hot tests showed that all TRU elements were completely extracted by TRPO and their concentration was decreased to the analytical detection limit. The extracted TRU elements are thoroughly stripped into three fractions by 5.5 M nitric acid (Am+Cm), 0.6 M oxalic acid (Pu+Np) and 5% sodium nitrate (U). The TRPO process can also extract ^{99}Tc from HLLW solution. The DFs of ^{99}Tc are as high as 1400. Among the fission product Zr, Mo and lanthanide elements are totally extracted. The hot tests

demonstrate that the TRPO process is an effective and prospective process for partitioning TRU elements as well as ^{99}Tc from HLLW.

2.3 Enhanced TRPO process

The enhancement of TRPO Process for commercial HLLW was studied to meet the required DF for CURE project. The optimal parameters of the TRPO process was calculated for a DF of 4.0×10^6 for Am[12]. A multistage counter current cascade experiment with simulated HLLW skipped with ^{241}Am was carried out with centrifugal extractor in glove box to verify the calculated results. The cascade included 12 stages for extraction, 2 stages for scrubbing and 6 stages for stripping. Very good results were obtained in the cascade experiments[13]. The obtained DF_{Am} was 1.25×10^6. The experiments show that the required DF for treating typical commercial HLLW to a waste, that is suitable for sallow land disposal, can be reached with the TRPO process.

3. TOTAL PARTITION PROCESS

In INET, the partitioning research is also focused on the waste volume reduction of Chinese HLLW. Chinese HLLW is a defense waste with high salt content. ^{90}Sr and ^{137}Cs are the two highly toxic nuclides and major heat generators in high level radioactive waste, so that they are quite important for the handling and disposal of HLLW. The removal of strontium and cesium from HLLW can degrade the HLLW to a low and intermediate level waste that eligible for near-surface disposal.

3.1 separation of strontium and cesium from HLLW

The extraction behavior of strontium and the ion exchange process for cesium have been studied. Dicyclohecano-18-crown-6 (DCH18C-6) in 1-octanol was used as an extractant. It has good extraction properties for strontium from nitric acid. The extraction properties of DCH18C-6 for strontium in simulated Chinese highly saline HLLW solution were studied in our laboratory[14]. A Crown Ether strontium Extraction (CESE) process and a strontium extraction calculation model (SECM) to separate ^{90}Sr from HLLW were developed. Finally, a hot test of the CESE process was carried out with genuine Chinese HLLW with centrifugal contactors[15]. The hot test results of the CESE process showed that after 10 extraction stages about 99.96 strontium were separated from genuine Chinese HLLW. More than 99.84% of strontium was back-extracted with 4 stripping stages. The hot test results showed that the CESE process could satisfy the partitioning requirement and SECM could be used to predict the strontium activity profiles and to optimize CESE process parameters.

Various inorganic ion exchangers were tested to remove Cs from HNO_3 waste solution. Spherical potassium titanium hexacyanoferrate(II) (KTiFC) ion exchanger was chosen. The KTiFC was prepared by sol-gel method and has excellent selectivity and high Cs absorption capacity from the highly saline nitric acid solution[16]. The static capacity of KTiFC for Cs is about 1 mmol/g in the simulated Chinese HLLW at 0.5M HNO3 and the dynamic exchange capacity of KTiFC was about 0.75 mmol/g at 90% breakthrough. It has good chemical resistance in 0.5-1.5 mol/L nitric acid solution as well as good radiation stability. Its static capacity and its appearance do not change until a dose of 1×10^6 Gy was adsorbed. The dynamic cold test was carried out with two columns connected in series and the results showed that 99 to 99.9% of Cs could be remove from simulated Chinese HLLW[17].

3.2 Total partition process for Chinese HLLW

A Total Partition process was developed in INET to partitioning TRU elements, Tc, Sr and Cs form Chinese HLLW and to degrade it to LLW or MAW[18]. The TP process includes the TRPO process for the removal of TRU elements, a crown ether extraction process (CESE) for the separation of Sr and a KTiFC ion exchange process to segregating ^{137}Cs. The hot test of the TP process was carried out in 1996 with genuine Chinese HLLW[19]. The hot test was completed with a compact centrifugal contactor set and a small ion exchange column. The compact contactor set contained 50 stages of φ 10 miniature centrifugal contactor including 12 extraction stages for the TRPO process and 10 extraction stages for the CESE process. Very encourage results have been obtained. The DFs for total α activity was 588, that for ^{99}Tc, ^{90}Sr and ^{137}Cs was 125, >2500, and >200 respectively. After partitioning the highly saline Chinese HLLW become a non α MAW that was suitable for cementation and shallow land disposal. High volume reduction factor for HAW waste was obtained. The TP process could be used to partitioning Chinese HLLW and to reduce HAW waste volumes.

3.3 Total partition process for commercial HLLW

In commercial HLLW, the salt content is much lower than that in Chinese HLLW but the radioactivity is much higher. The hot test of the TP process for Chinese HLLW had proved that the CESE and the KTiFC process could meet the required DFs of strontium and cesium in commercial HLLW. The enchanted TRPO described in paragraph 2.3 can meet the DF requirement for TRU elements to degrade the HLLW to a non α waste[13]. So the TP process for high saline HLLW can also be used for commercial HLLW after modification[20].

3.4 The auxiliary processes of the TP process

The auxiliary processes of the TP process are studied. The auxiliary processes make the TP process become a complete process. They include the microwave denitration and calcination for Am (RE) stripping solution, Np/Pu separation in $H_2C_2O_4$-HNO_3 solution, the conversion process for uranium stripping solution and immobilization process for Cs-loaded KTiFC ion exchanger.

4. ACTINIDE-LANTHANIDE SEPARATION

The separation of lanthanide and actinides is necessary not only for HLLW partitioning but also for degradation of HLLW to MAW. The separation chemistry and process is one of the research subjects in INET. The extractant with different donors such as P, N and S were studied for its extraction and separation ability of actinide/lanthanide. S-coordinated extractant has good behaviors for the separation of trivalent Am from Ln.

4.1 Actinide-Lanthanide separation process by HBTMPDTP extraction

In INET, Cyanex 301 has been proven to be an effective extractant for the separation of trivalent Am from Lns[21-22]. A purified Cyanex 301 has a composition of >99% bis (2,4,4,-trimethylpentyl) dithiophosphinic acid (HBTMPDTP). It prefers to extract Am rather than Ln and the separation factor is higher than thousands.

A conceptual Am/Lns separation flowsheet by HBTMPDTP extraction was proposed. The hot test with cross flow extraction was carried out and only ~3% Ln was extracted by HBTMPDTP. The average separation factor between Am and Ln was 3500 for first three stages[23]. The counter current hot test was carried out recently[24]. After denitration to 0.3 M HNO_3, the feed solution was first treated with Cyanex 301 to remove impurities. It was then fed into extraction section and contacted with saponified HBTMPDTP. More than 99.9% of

Am was extracted into the organic phase with 5 extraction stages. About 1% of Lns was co-extracted with Am. The hot test results proved that the separation process was effective.

4.2 The synergic extraction of Am and Ln by HBTMPDTP/TBP-Kerosene

The synergic extraction and separation of Am and Ln by HBTMPDTP/TBP-Kerosene was studied. At pH 2.8, quite high separation factor for Am/Ln could be obtained. A multistage counter current cascade experiment was performed included 7 stages for extraction, 3 stages for scrubbing and 2 stages for stripping. The separation factor of Am from Ln was 5×10^4 and the separation factor of Ln from Am was 2500[25].

4.3 The coordination structure of Am/Lns and HBTMPDTP

The coordination chemistry of Am/Lns and HBTMPDTP was studied. The structure of the extraction complexes in organic phase was characterized with EXAFS and other instruments. The EXAFS data[26-27] illustrates that the structures of the extraction complexes of Am(III) and Nd(III) with HBTMDTP are different. Together with the results from extraction experiment, the molecular formula of complex of Am(III) is deduced being $HAmL_4$ and that of Nd(III) being $HNdL_4 \cdot H_2O$. There are 8 S atoms from 4 extractants coordinated with Am in the complex of Am. But there are 7 S atoms from 4 extractants and one O atom from H_2O coordinated with Nd in the extraction complex of Nd. The excellent selectivity of HBTMDTP for Am(III) over Ln(III) in extraction behavior may derives from the deferent coordination structure of the complexes of Am(III) and Nd(III) with HBTMDTP.

5. INTEGRATED PROCESS

The integration process coupling with reprocessing and partitioning would simplify the back end of the nuclear fuel cycle and would make it more reasonable and economical. The integrated process based on the Purex process for nuclear fuel reprocessing and the TRPO partition process is studying in INET[28]. Different combination of the TBP and TRPO process is studying. The target is to make the integrated process more simple, more effect and more economic.

6. STUDY OF EXTRACTION EQUIPMENTS

The advanced extraction equipment such as pulsed column and centrifugal contactor for the TP process are also being studied. It has been proved that the pulsed column could be used in high viscous TRPO-kerosene-HNO_3 system. The study of the centrifugal contactor for nuclear industry is carried out. The module pattern of centrifugal contactor with rotor diameter φ 70 and φ 100 were produced and tested. They have good hydraulic and mass transfer properties. A prototype installation is planning to construct in order to test the flowsheet and equipment for the partition process.

7 REFERENCES

[1] A.C. Croff, J.O. Blomeke, Actinide Partitioning-Transmutation Program, Final Report, ORNL 5566(1980).

[2] S. E. BINNEY, CURE: Clean Use of Reactor Energy, WHC-EP-0206 Westinghouse Hanford Company, Richland, WA 99352 (1990).

[3] R. Jiao, S. Wang, S. Fan, B. Liu, Y. Zhu, H. Zheng, S. Zhou, S. Chen, Trialkyl (C_6-C_8) phosphine oxide for the extraction of actinides and lanthanides from high active waste,

Chinese J. Nucl. Radiochem. 7. 65 (1985). (In Chinese).

[4] R. Xin, P. Zhang, J. Liang, C. Song, Study on the radiation Stability of Trialkyl Phosphine Oxide, to be published.

[5] R. Xin, C. Song, J. Jiao, J. Liang, Investigation of Radiolytic Products of Trialkyl Phosphine Oxide by Gas Chromatography, Chinese J. Spectroscopy Laboratory, 16, 498-502 (1999).

[6] P. Zhang, C. Song, J. Liang, R. Xin, Solv. Extr. & Ion Exch., 19, 51 (2001).

[7] C. Song, Y. Zhu, D. Yang, L. He, J. Xu, The removal of actinide elements from HLLW by TRPO extraction –The cascade extraction experiment of the TRPO process with simulated feed solution, Chinese J. Nucl. Sci. Eng., 1992, 12 (3), 225 (in Chinese)

[8] Y. Zhu and C. Song, Recovery of Neptunium, Plutonium and Americium from Highly Active Waste, Tri-alkyl phosphine Oxide Extraction, in Transuranium Elements: A Half Century, Edited by L.R. Morss and J. Fuger, ACS, Washington D.C. USA, (1992) pp. 318-330

[9] C. Song, J-P. Glatz, Mathematical Model for the Extraction of Americium from HLLW by 30% TRPO and its Experimental Verification, in A Value Adding Through Solvent Extraction: International Conference on Solvent Extraction, The University of Melbourne, Australia, 1996, v2, pp

[10] C. Song, J-P. Glatz, X. He, H. Bokelund, L. Koch, Actinide Partitioning by means of the TRPO Process, RECORD'94, 24-28 April 1994, London UK

[11] J-P. Glatz, C. Song, L. Koch, H. Bokelund, H. He, Hot tests of the TRPO Process for the Removal of TRU Elements from HLLW, Proceedings of the Global'95 Conference, Versailles, France 10-14 Sept. (1995) vol. 1, pp548.

[12] J. Chen, J. Wang, C. Song, Tsinghua Science and Technology, 6, 180-4 (2001).

[13] J. Wang, Q. Wang, J. Chen, B. Liu, P. Zhang, C. Song, Cascade Test of Removing ND^{3+} and Am^{3+} from Simulated High Level Liquid Waste of Nuclear Power Station, J. Tsinghua University (Science and Technology) 40 (12), 21-4 (2000). (In Chinese).

[14] L. He, X. Weng, D. Yang, "Extraction of strontium from high-level active waste with crown-ether process study" Chinese J Nucl. Eng., 15, 76 (2001) (in Chinese).

[15] J. Wang and C. Song, Radiochim. Acta 89, 151-154 (2001)

[16] C. Jiang, S. Wang, C. Song, The removal of cesium from simulated HLLW with potassium titanium hexacyanoferrate, Chinese J. Nucl. Radiochem, 17, 99 (2001). (In Chinese)

[17] C. Song, S. Xu, Y. Sun, R. Jiao, Separation of Cesium from Highly Saline HLLW with Potassium Titanium Hexacyanoferrate, to be published in NRC4 4th International conference on Nuclear and Radiochemistry, 8-13 September 1996, St. Malo France.

[18] C. Song, The concept flow sheet of partitioning process for the Chinese high-level liquid waste, Atomic Energy Science and Technology, 1995, 29, 201-9 (in Chinese)

[19] C. Song, J. Wang, R. Jiao, Hot test of total partitioning process for the treatment of high saline HLLW, in Global'99: International Conference on Future nuclear systems, Proceedings (August 29-September 3, 1999, Jackson Hole, USA.)

[20] C. Song and J. Xu, Recent progress on partitioning study in Tsinghua university, Actinide and Fission Product Partitioning and Transmutation, OECD 6th Information Exchange Meeting, Madrid, Spain 11-13 December 2000

[21] Y. Zhu, J. Chen, R. Jiao, Solv. Extr. & ion Exch. 14, 61 (1996)
[22] J. Chen, Y. Zhu, R. Jiao, Nuclear Technology, 122, 64 (1998)
[23] J. Chen, R. Jiao, Y. Zhu, Radiochimica Acta, 76, 129 (1997)
[24] J. Chen, G.X. Tian, R.Z. Jiao, Y.J. Zhu, A hot test for separating Am from fission product lanthanides by purified cyanex 301 extraction, Actinides'2001, Japan
[25] X. Wang, Y. Zhu, R. Jiao, Separation of Am from Lanthanides by a Synergistic Mixture of Purified Cyanex 301 and TBP, to be published in J. Radioanal. Nucl. Chem.
[26] G. Tian, Y. Zhu, J. Xu, "Characterization of Extraction Complexes of Am(III) with Dialkyldithiophosphinic Acids by Extended X-ray Absorption Fine Structure Spectroscopy" Actinides'2001, Japan
[27] G. Tian, Y. Zhu, J. Xu, P. Zhang, Characterization of Extraction Complexes of Nd(III) with Dialkyldithiophosphinic Acids by EXAFS, to be publich in high energy and Nucl. Phy. (In Chinese)
[28] Zhu, Y.; Han, B.; Wu, Q. "Study on the integration of the Purex process and the TRPO process in nuclear fuel cycle backend" Global'99 Proceedings of the International Conference on Future nuclear systems, Aug.29-Sept.3, 1999.Jachson Hole, USA

This is a blank page.

JP0250307

JAERI-Conf 2002-004

UNEX PROCESS TESTING OF THE REMOVAL OF CESIUM, STRONTIUM, AND ACTINIDE ELEMENTS FROM RADIOACTIVE ACIDIC WASTE

V.N. ROMANOVSKIY[1], V.A. BABAIN[1], V.M. ESIMANTOVSKIY[1], I.V. SMIRNOV[1], and B.N. ZAITSEV[1]
R. S. HERBST[2], J. D. LAW[2], T. A. TODD[2]

[1]Khlopin Radium Institute, 28 2nd Murinsky Ave, St. Petersburg, Russia 194021
[2]Bechtel BWXT Idaho, LLC, P.O. Box 1625, Idaho Falls, ID 83415-5218

ABSTRACT

The presence of long-lived radionuclides presents a challenge to the management of radioactive wastes. Separation of the radionuclides from the waste solutions has the potential of significantly decreasing the costs associated with the immobilization and disposal of the radioactive waste by minimizing waste volumes. Typically, several separate processes are required for the separation of cesium, strontium and actinides from radioactive wastes. A novel solvent extraction process, the Universal Extraction (UNEX) process, has been developed for the simultaneous separation of cesium, strontium, and the actinides from radioactive acidic waste solutions. The UNEX process solvent consists of chlorinated cobalt dicarbollide for the extraction of ^{137}Cs, polyethylene glycol for the extraction of ^{90}Sr, and diphenyl-N,N-dibutylcarbamoyl phosphine oxide for the extraction of the actinides and lanthanides. A non-nitroaromatic polar diluent, phenyltrifluoromethyl sulfone, is used for this process. A UNEX flowsheet consisting of a single solvent extraction cycle has been developed as a part of a collaborative effort between the Khlopin Radium Institute (KRI) and the Idaho National Engineering and Environmental Laboratory (INEEL). This flowsheet has been demonstrated with actual dissolved radioactive calcine waste at the INEEL using 24 stages of 2-cm diameter centrifugal contactors installed in a shielded hot cell facility. For the major radionuclides, 99.99% of the ^{137}Cs, 99.73% of the ^{90}Sr, and >99.9% of the actinides in the initial dissolved calcine feed were extracted and recovered in the high activity fraction. For the stable matrix elements, 12% of the Mo, 0.7% of the Zr, and 2% of the Fe were extracted and recovered in the strip product. The minor components Ba and Pb were quantitatively extracted and recovered in the strip product; 23% of the Mn was also present in this fraction. Very little aluminium, Ca, Cr, Na, and Ni were extracted into the UNEX solvent.

INTRODUCTION

Waste treatment processes for the removal of radionuclides from acidic wastes are being developed worldwide in countries such as the United States, Britain, France, Japan, China, and Russia [1], Typically, the processes under development require several unit operations, each separating specific radionuclides from the waste solutions.

The use of a single process to remove the desired radionuclides, as opposed to a combination of different unit operations that remove these same radionuclides, evolved from previous collaborative efforts with scientists from the Khlopin Radium Institute and Bechtel BWXT Idaho [2]. A universal solvent containing chlorinated cobalt dicarbollide (CCD)

for the extraction of cesium, polyethylene glycol (PEG) for the extraction of strontium, and diphenyl-N.N-di-n-butylcarbamoyl phosphine oxide for the extraction of actinides and lanthanides from acidic waste solutions has subsequently been developed [3]. This Universal Solvent Extraction (UNEX) process provides a simplified and cost effective method for radionuclide separations as compared to using two or three separate unit operations.

The high and low-activity waste fractions resulting from the UNEX process would likely be disposed of as glass or grout waste forms, respectively. Separation of the radionuclides from the wastes must result in a reduced quantity of high-activity waste requiring disposal (e.g., a federal geological repository). This criterion requires minimization of the bulk matrix components (notably Zr and Ca) in the dissolved calcine feed that partition to the high-activity fraction.

The ultimate fate of the low-activity waste resulting from UNEX processing of the dissolved calcine is currently nebulous. A contact handled non-TRU grout waste for the low-activity raffinate from the UNEX process is currently the most probable final waste form that would meet near-surface disposal criteria. Thus, a conservative set of assumptions was used to anticipate the necessary radionuclide removal efficiencies required for the application of the UNEX process to calcine treatment. These assumptions include using the grout formulation developed for UNEX raffinate produced from treatment of the tank waste (45% waste loading resulting in 1.4 m^3 of grout formed per 1.0 m^3 of low-activity waste raffinate generated) [4]. The NRC Class A LLW limit for Cs (1.0 Ci/m^3 in the final waste form) and the non-TRU limit for the actinides (100 nCi/g in the grout) would conservatively suffice to insure the contact handled, non-TRU criteria are met. These assumptions would require >99.3% of the ^{137}Cs and >93% of the actinides be removed by the UNEX process.

The required ^{90}Sr removal requirements for calcine are even less clear. Previous results indicate extremely high Sr removal efficiencies can be obtained with the UNEX process applied to the liquid INEEL tank waste (>99.999%) [4]. However, this extremely high Sr removal efficiency slightly reduces ^{137}Cs and actinide removal. Consequently, the goals set for ^{90}Sr removal efficiency in this flowsheet testing were simply as "high as achievable" while maintaining the above described >99.3% and >93% removal of ^{137}Cs and actinides, respectively.

METHODOLOGY/EXPERIMENTAL PROCEDURE

Calcine Dissolution and Composition

A total calcine mass of 114.1 g was dissolved in 2.9 M HNO_3 at a ratio of 100 g calcine per 1.0 L of acid. The calcine/acid slurry was heated to boiling with constant reflux for 60 minutes. Under these conditions 95.8 wt. % of the calcine mass was dissolved. The dissolved calcine was diluted by 30% with 0.5 M HF to increase the *added* fluoride concentration to 0.1 M F^-. The additional fluoride ion was added in order to complex the Fe, Mo, Ca, and Zr thus minimizing their extraction by the actinide extractant (CMPO) in the UNEX solvent, ultimately reducing the volume of high activity waste. The composition of the solid calcine and the concentrations of select elements in the dissolved, diluted calcine solution are indicated in Table 1.

Table 1. Solid and dissolved calcine composition

	Solid Calcine	Dissolved Calcine (w/ HF Dilution)	
Stable Element:	(Wt. %)	(Hg/mL)	(M)
Al	9.8	7.87E+03	0.29
Ba	0.018	3.89	2.8E-05
Ca	26	2.09E+04	0.52
Fe	0.5	250	0.0045
K	0.67	483	0.012
Mn	0.09	68.1	1.24E-03
Mo	<0.01	14.3	1.5E-04
Na	2.8	2.30E+03	0.10
Pb	—	21.8	1.1E-04
Zr	7.32	5.80E+03	0.064
F^-	8.44	1.41E+04	0.74
H^+	—	—	0.86
Radionuclides:	(Bq/g)	(Bq/mL)	
Cs-137	8.4E+07	7.39E+06	
Sr-90	7.5E+07	6.17E+06	
Gross α	—	1.34E+05	
Am-241	3.4E+04	2.25E+03	
Pu-238	1.3E+06	5.19E+04	
Eu-154	6.7E+05	5.28E+04	

Analytical

Analysis of ^{137}Cs in the organic and aqueous samples was performed using High Purity Germanium Gamma Spectroscopy (HPGE). Alpha spectroscopy was used for gross α, ^{241}Am and ^{239}Pu analyses. Inductively Coupled Plasma Emission Spectroscopy (ICP-ES) was used for Al, Ba, Ca. Cr, Fe, Mn, Mo, Ni, Pb, and Zr analyses. Sodium and potassium analyses were performed using Atomic Absorption Spectroscopy (AAS).

Flowsheet Configuration and Centrifugal Contactors

The UNEX flowsheet demonstration was performed using 2-cm diameter centrifugal contactors installed in a shielded hot cell facility. The centrifugal contactors consist of 24 stages of 2-cm diameter centrifugal contactors, feed and receiving vessels, feed pumps, and an air purge system for the contactor bearings.

The centrifugal contactors were designed and fabricated by Argonne National Laboratory. The contactors were modified at the INEEL for remote installation and operation in the shielded hot cell facility.

RESULTS AND DISCUSSION

Countercurrent Flowsheet Test

Based on the above results, as well as those from previous batch contact and flowsheet tests with simulated and actual dissolved calcine [5,6], a flowsheet was proposed for integrated testing with actual, radioactive, dissolved calcine as indicated in Figure 1. The

UNEX flowsheet consisted of thirteen extraction stages an organic to aqueous phase ratio (O/A) of 1.5, one stage of scrub (0.2 M NH_4NO_3) at an O/A of 7.5, and 10 stages of strip (1 M guanidine carbonate, 20 g/L DTPA) at an O/A of 2.0.

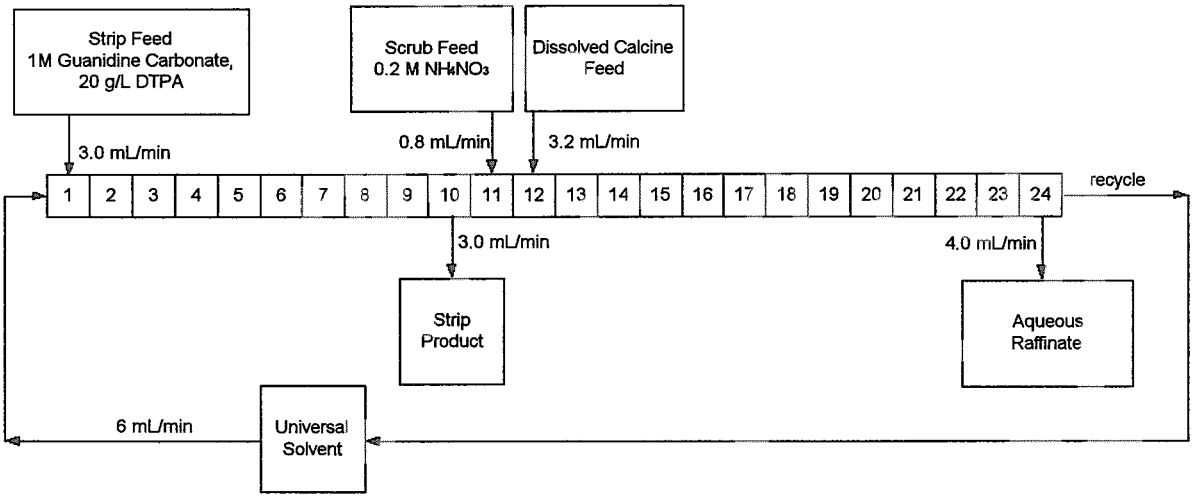

Fig 1. UNEX flowsheet configuration for testing with dissolved H-3 calcine

Flooding was not observed in the effluent streams. Precipitate formation was not observed in any of the samples taken during operation or in the contactors after shutdown.

The percentages of ^{137}Cs, ^{90}Sr, ^{154}Eu, total alpha, ^{241}Am, ^{238}Pu, in each of the effluent streams at shutdown are indicated in Table 2. Overall material balances (calculated as the percentage of out/in) are also indicated in Table 2. The activities of total alpha, ^{137}Cs and ^{90}Sr in the raffinate throughout the test are given in Figure 2. Distribution coefficients were measured for total alpha, ^{137}Cs, ^{90}Sr, ^{241}Am, and ^{238}Pu on select stages. The resulting distribution coefficients are given in Table 3.

Table 2. Percentage of radionuclides in the UNEX effluent streams

Stream	^{137}Cs	^{90}Sr	^{154}Eu	Gross α	^{241}Am	^{238}Pu
Raffinate	0.013%	0.27%	[a]ND	0.1%	<0.01%	0.071%
Strip	98.92%	103.0%	101.2%	97.94%	113.3%	179.2%
Organic	0.0002%	«0.1%	«0.1%	«0.1%	0.0006%	0.0001%
Material Balance	98.93%	103.3%	101.2%	98.04%	113.3%	179.3%

[a]ND = Not Detected

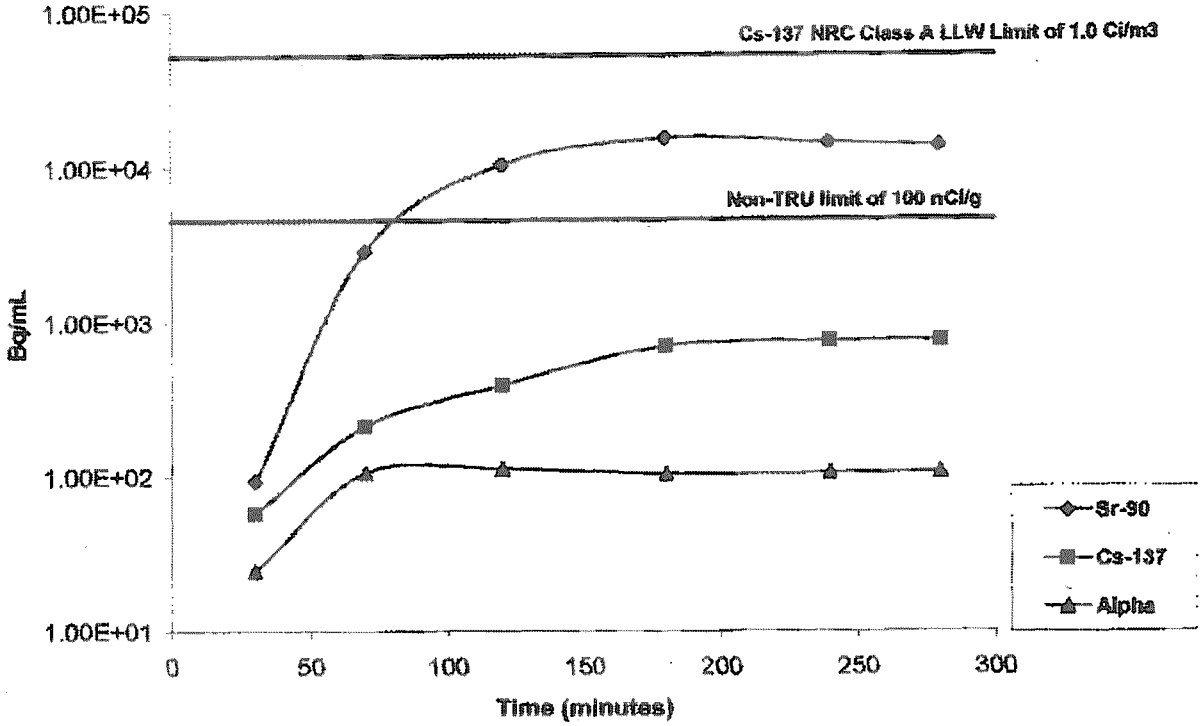

Fig. 2. Activity of ^{90}Sr, ^{137}Cs, and gross α in the raffinate as a function of time

Table 3. Distribution coefficients from the UNEX flowsheet demonstration

Stage		D_{Cs-137}	D_{Sr-90}	$D_{GROSS\ \alpha}$	D_{Am-241}	D_{Pu-238}
Extraction	24	0.611	0.75	0.23	—	—
	23	0.951	1.02	0.19	—	—
	20	1.87	1.38	0.42	—	—
	18	—	1.19	0.68	—	—
	16	1.88	1.25	0.29	—	—
	14	2.41	1.29	122	9.3	81
	13	3.44	1.29	108	10.2	203
	12	3.79	1.10	120	10.1	149
Scrub	11	4.64	61.6	106	177	846
Strip	10	0.05	0.001	0.006	0.015	0.006
	9	0.057	0.002	<0.001	0.001	0.001
	8	8.7E-05	0.15	0.006	0.006	0.009

The ^{137}Cs activity was reduced from 7.39E+06 Bq/mL in the feed to 7.53E+02 Bq/mL in the aqueous raffinate at shutdown of the system. This corresponds to a removal efficiency of 99.99%. In the strip section, the ^{137}Cs distribution coefficients ranged from 8.7E-05 to 0.057, resulting in >99.99% of the extracted ^{137}Cs exiting in the strip product. Assuming grout formulation similar to that developed for INEEL tank waste, 1.4 m^3 of grout would be generated from each 1.0 m^3 of low-activity waste. Under these assumptions, the ^{137}Cs activity in the final waste form of approximately 0.014 Ci/m^3, which is sufficiently low to insure a contact handled waste based on γ-activity.

The ^{90}Sr activity was reduced from 6.17E+06 Bq/mL in the feed to 1.37E+04 Bq/mL in the aqueous raffinate immediately prior to shutdown. This corresponds to a removal efficiency of 99.73%. Assuming, as before, that 1.4 m^3 of grout would be generated from each 1.0 m^3 of low-activity waste, the ^{90}Sr activity in the grout would be approximately 0.26 Ci/m^3 in the grout. In the strip section, distribution coefficients for ^{90}Sr ranged from 6.7E-04 to 0.15. As a result, the extracted ^{90}Sr quantitatively exited (>99.99%) in the strip product.

The alpha activity was reduced from 1.34E+05 Bq/mL in the feed to 107 Bq/mL in the aqueous raffinate immediately prior to shutdown. This corresponds to a removal efficiency of 99.9%. Under the previous assumptions for a final grout waste, the total alpha activity is approximately 1.1 nCi/g in the final waste form, well below the non-TRU limit of 100 nCi/g. Removal efficiencies of >99.99% and 99.93% were obtained for ^{241}Am and ^{238}Pu, respectively. In the strip section, the total alpha, ^{241}Am, and ^{238}Pu were quantitatively recovered (>99.9%) from the solvent.

The effluent streams were also analyzed for Al, Ba, Ca, Cr, Fe, Mn, Mo, Na, Ni, K, Pb, and Zr. The percentages of these elements and the overall material balances (calculated as the percentage of out/in) in the effluent streams are given in Table 4. The distribution coefficients of the more interesting matrix components, including Ca, Fe, Mo, and Zr, were measured on several select stages in the flowsheet. The measured distribution coefficients are listed in Table 5. Of the bulk matrix components, Ba and Pb were quantitatively extracted and exited in the strip product. Due to the minor amounts of these components in the calcine wastes (Table 1), efforts have not been directed at limiting the amount of these elements which extract and enter the strip product. Additionally, immobilization of Pb with the high-activity glass waste may be perceived as beneficial due the hazardous nature of Pb (from a RCRA perspective).

Table 4. Percentage of stable metals in the UNEX effluent streams

Stream	Al	Ba	Ca	Cr	Fe	Mn
Raffinate	107.6%	<0.17%	106.8%	102.6%	98.32%	77.15%
(Normalized)	*(99.88%)*	*(<0.19%)*	*(97.33%)*	*(98.74%)*	*(88.50%)*	*(77.27%)*
Strip	0.13%	93.96%	2.93%	1.31%	12.78%	22.68%
(Normalized)	*(0.12%)*	*(99.81%)*	*(2.67%)*	*(1.26%)*	*(11.50%)*	*(22.73%)*
Material Balance	107.8%	94.13%	109.7%	103.9%	111.1%	99.83%
Effluent	**Mo**	**Na**	**Ni**	**K**	**Pb**	**Zr**
Raffinate	88.82%	107.2%	103.5%	65.62%	<0.40%	99.30%
	(87.93%)	*(68.59%)*	*(98.71%)*	*(60.90%)*	*(<0.32%)*	*(93.03%)*
Strip	12.20%	49.12%	1.35%	42.14%	121.9%	7.44%
	(12.07%)	*(31.41%)*	*(1.29%)*	*(39.10%)*	*(99.68%)*	*(6.97%)*
Material Balance	101.0%	156.4%	104.9%	107.8%	122.3%	106.7%

Table 5. Measured distribution coefficients of select matrix metals

Stage		D_{Ca}	D_{Fe}	D_{Mo}	D_{Zr}
Extraction	14	0.034	0.42	0.11	0.05
	13	0.038	0.38	0.10	0.05
	12	0.034	0.53	0.09	0.05
Scrub	11	0.011	310	0.09	4.4
Strip	10	0.32	1.0	< 0.1	0.004
	9	–	1.7	< 1	0.05

Aluminum, Ca, Cr, Na, and Ni were not extracted into the UNEX solvent based on the percentages of these components in the raffinate relative to the feed. The limited extraction of the bulk matrix component Ca is an excellent indication that the fluoride addition was successful in limiting Ca extraction. The material balance for Na was particularly poor at ~156%, and is attributed to contamination of the strip product sample. Manganese (22.7%) and K (~40%) in the dissolved calcine solution were extracted into the UNEX solvent and exited with the strip product. Minor amounts of Mn and K are present in the calcine wastes (Table 1) and, as with Ba and Pb, efforts have not been directed at limiting the amount of these elements that extract and enter the strip product. Based on the raffinate samples, 12% of the Mo, 1.7% of the Fe, and 0.7% of the Zr in the waste feed were extracted by the UNEX solvent. Thus, the extraction of Zr, Fe, and Mo appear to be substantially suppressed, presumably due to the addition of fluoride ion to the dissolved calcine waste.

CONCLUSIONS

A novel solvent extraction process, the UNEX process, has been developed for the separation of cesium, strontium, and the actinides from acidic waste solutions. A counter-current UNEX flowsheet was successfully developed and demonstrated for the treatment of actual dissolved INEEL calcine waste. With the UNEX flowsheet, removal efficiencies of 99.99%, 99.73%, and 99.9% were obtained for ^{137}Cs, ^{90}Sr, and the actinides, respectively. These high removal efficiencies are currently believed to be sufficient to achieve a non-TRU, contact handled waste form for near surface disposal. Of the non-radioactive metals evaluated, Ba and Pb were quantitatively extracted and recovered in the strip product. Potassium, Mo, Zr, Mn, and Fe were also extracted (40%, 12%, 7%, 23%, and ~2 to 10%, respectively) and recovered in the strip product.

ACKNOWLEDGEMENTS

This work was supported by the U. S. Department of Energy Office of Science and Technology's Efficient Separations and Processing Crosscutting Program under the auspices of the Joint Coordinating Committee for Environmental Management (JCCEM), and the Tanks Focus Area.

REFERENCES

(1)E. P Horwitz and W. W. Schulz, Solvent Extraction in the Treatment of Acidic High-Level Liquid Waste: Where Do We Stand?, ANL/CHM/CP-93488, (1998).
(2)J. D. Law, R. S. Herbst, *et al.*, Proc. of SPECTRUM '96, August 18-23, 1996, Seattle, WA, 3, 2308,(1996).
(3)V. N. Romanovskiy, I. V. Smirnov, *et al.*, *Solvent Extr. Ion Exch.*, **19**(1): 1 (2001).
(4)J. D. Law, R. S. Herbst, *et al.*, *Solvent Extr. Ion Exch.*, **19**(1): 23 (2001).
(5)J. D. Law, R. S. Herbst, *et al.*, "Demonstration of a Universal Solvent Extraction Process for the Separation of Radionuclides from Actual INEEL Sodium-Bearing Waste and Dissolved Calcine," INEEL/EXT-98-01065, (1998).
(6)J. D. Law, R. S. Herbst, *et al.*, Proc. Of Waste Management, 2001, Tucson, AZ, Feb. 25-Mar. 1, (2001).

This is a blank page.

JP0250308

ACTINIDE SEPARATION BY TODGA EXTRACTION

YASUJI MORITA, YUJI SASAKI AND SHOICHI TACHIMORI

Japan Atomic Energy Research Institute, Tokai-mura, Ibaraki-ken, 319-1195 Japan
Fax: 81-29-282-5937, e-mail: morita@nucef.tokai.jaeri.go.jp

Extraction process for actinide separation from high-level liquid waste (HLLW) with N,N,N',N'-tetraoctyl-3-oxapentanediamide (TODGA) was preliminarily evaluated by simulation of Am and Sr behaviors. The solution volume required for the treatment of an unit amount of HLLW was also evaluated using data on extraction capacity of the solvent. Results of the calculation showed that it is possible to establish an extraction process with 0.2M TODGA in n-dodecane, where Am is extracted in a very high yield of more than 99.99% and more than 99.95% of Sr is kept in the aqueous phase. The present study also deals with the effects of the flow rate change of the scrub and the solvent on the Sr contamination in the Am fraction and the possibility of third phase formation in order to elucidate the characteristics of the extraction process by TODGA.

Key words: Actinide separation, N,N,N',N'-tetraoctyl-3-oxapentanediamide (TODGA), Process simulation, Sr separation, Process scale estimation

1. INTRODUCTION

The extraction with tridentate neutral ligands, diglycolamides (DGA), has been studied for the separation of actinides from high-level liquid waste (HLLW). From fundamental studies aiming at a high extractability toward actinides and a high solubility of the extractant in n-dodecane, N,N,N',N'-tetraoctyl-3-oxapentanediamide (tetraoctyldiglycolamide, called TODGA hereafter) was selected as the most proper DGA extractant[1]. Structure of TODGA is shown in Fig. 1. Distribution ratios of Am and Cm are high enough at the nitric acid concentration higher than 1M and are low enough for the back-extraction at 0.01M nitric acid. Lanthanides show the similar behavior as Am and Cm in the TODGA extraction.

In the present study, actinide separation from HLLW by TODGA extraction process was preliminary evaluated by calculation. Elements selected in the present evaluation are Am and Sr. Since two elements, Sr and Cs, are the main contributors for the radioactivity in HLLW, decontamination of them is one of the most important factors in the development of a separation process for actinides from HLLW. The distribution ratio of Cs is very low, but the distribution ratio of Sr (D_{Sr}) is a little high in the TODGA extraction[1]. For instance, D_{Sr} is 2.7 at 3M nitric acid in the extraction with 0.1M TODGA. It is, therefore, important to evaluate the Sr behavior and to find a condition which gives a good separation of Am from Sr.

In the present study, volume of the TODGA solvent required for the treatment of HLLW produced from an unit amount of spent fuel was also evaluated using experimental data on extraction capacity of the TODGA solvent. Volumes of various aqueous solutions were obtained from the flow rate ratio of the aqueous solutions to the solvent. The evaluation of the solution volume would contribute to the estimation of the process scale and applicability.

An additional evaluation was performed on the effects of the flow rate change of the scrub and the solvent on the Sr contamination in the Am fraction and the possibility of third phase formation in order to elucidate the characteristics of the extraction process by TODGA.

Although the present study lies in the preliminary stage of the process development, it reveals the important points of the DGA extraction process and also gives necessary information for experiments on continuous counter-current extraction.

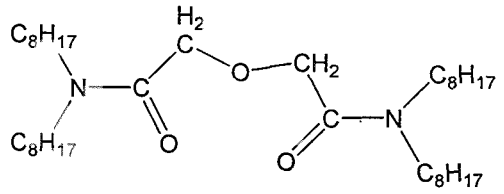

Fig. 1 Structure of TODGA

2. EVALUATION METHOD

2.1 Extraction System Evaluated

The system evaluated contains three sections: 5-stage extracting section, 3-stage scrubbing section and 4-stage stripping section, which is shown in Fig. 2. At the extracting section, Am, Cm and rare earth elements (RE) are extracted with TODGA – n-dodecane solvent from HLLW. In the present system, Cm and RE always show almost the same behaviors as Am. The nitric acid concentration of the HLLW feed was fixed to 3M. The solvent used in the evaluation was 0.2M TODGA in n-dodecane. Concentration of nitric acid in the scrub is one of the process parameters to be optimized. At the stripping section, the elements in the organic phase are back-extracted with 0.01M nitric acid. Flow rate ratios of the solvent, the scrub and the strip to the HLLW feed were adjusted to achieve the objective separation of Am and Sr. The objective value for the Am and Sr separation in the present study is more than 99.99% for Am recovery and less than 0.05% for Sr contamination in the Am fraction (more than 99.95% of Sr as an yield in the raffinate).

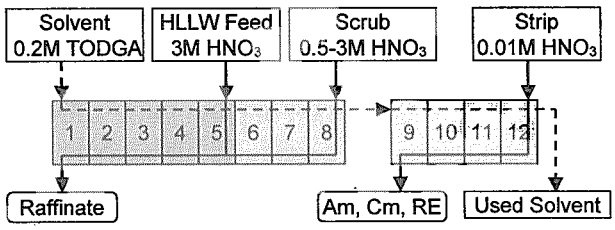

Fig. 2 Extraction process evaluated in the present study

2.2 Distribution Ratio

Data on the distribution ratio of nitric acid (D_{HNO3}) were obtained by batch extraction of nitric acid at various concentrations of TODGA (0.1-0.5M). A logarithmic plot of the equilibrium concentration of nitric acid between the organic and aqueous phases lay well on a straight line. The results showed that D_{HNO3} is proportional to the 0.7th power of the concentration of nitric acid in the aqueous phase and is proportional to the TODGA concentration. The values of D_{HNO3} obtained from these relationship were used in the calculation of nitric acid behavior in extraction processes[2].

The dependence of the distribution ratio of Am (D_{Am}) on the nitric acid concentration was obtained experimentally for 0.1M TODGA – n-dodecane. Using these data, an equation which gives D_{Am} as a function of the nitric acid concentration in the aqueous phase ($D_{Am}= F([HNO_3]_{Aq})$) was obtained by the method of try and error without any scientific basis[2]. Then, D_{Am} for 0.2M TODGA was calculated by the experimental data that D_{Am} is proportional to the 3.7th power of the TODGA concentration[1]. Dependence of distribution ratio on the element concentration was not considered in the present evaluation.

The distribution ratio of Sr (D_{Sr}) at 0.2M TODGA were obtained by the same method as in the case of Am described above, except that D_{Sr} is proportional to the second power of the TODGA concentration[1]. The distribution ratio of Ba is low enough and its extraction was not considered in the present study.

2.3 Calculation Method

Behaviors of nitric acid, Am and Sr in the system of extraction process employed in the present study were calculated by a spreadsheet software using mass balance equation and distribution ratio of each component at each stage. Stage efficiency was assumed to be 1.

A concentration profile of nitric acid was obtained first. Since D_{HNO3} depends on the nitric acid concentration, the profile cannot be obtained directly with analytical equations. Therefore, the repetition calculation method was employed.

Then, D_{Am} and D_{Sr} at each stage were calculated by the equation described above using the concentration of nitric acid at the stage. Concentration profiles and fractional distributions of Am and Sr can be obtained analytically.

2.4 Estimation of the Process Scale

Extraction capacity of the TODGA solvent was measured by performing the extraction of Nd at high concentration[2]. In the case of the TODGA solvent, the capacity is determined as the maximum element concentration where the third phase (the second organic phase) is not formed, and it depends on the nitric acid concentration in the aqueous phase. In the present study, it was assumed that the capacity against Am (and Cm, RE) and Sr is the same as the capacity against Nd.

The volume of the TODGA solvent required for the treatment of HLLW produced from an unit spent fuel was evaluated using the extraction capacity. The unit spent fuel used in the present study was 1ton of UO_2 spent fuel burned up to 45,000MWd/t in light water reactor. The HLLW produced from such unit spent fuel (the unit HLLW, hereafter) contains 103mol of Am+Cm+RE and 13mol of Sr. The total concentration of these elements in the organic phase was supposed to be able to increase up to 80% of the extraction capacity describe above. To determine the maximum total concentration, it is important to evaluate the element accumulation at the extracting and scrubbing sections. Volumes of aqueous solutions required for the treatment of the unit HLLW were obtained from the flow rate ratio of the aqueous solutions to the solvent in each process condition. The volume of the HLLW feed for the unit HLLW is one of the process parameters.

3. RESULTS AND DISCUSSION

3.1 Optimized Process

Various conditions of the extraction process were evaluated to achieve the objective separation of Am and Sr. Table I shows the conditions of selected processes from many evaluated processes and the calculated results on the behaviors of Am and Sr and the volumes of the solutions required for the treatment of the unit HLLW. Recovery (%) in Table I means the ratio of element amount in the stripped solution (the Am fraction) to the initial amount. Among these processes, the Process No.4 would be the most optimized process, where Am is recovered in a very high yield of more than 99.99% and the Sr contamination was less than 0.05%. Figure 3 shows the condition and the evaluated results on the Process No.4. The volume of the HLLW feed was 6.6 m^3, which means that the Purex raffinate can be used almost directly as the feed to this process. One of the drawbacks of this process is that the volume of the raffinate is increased 4 times as much as that of the HLLW feed.

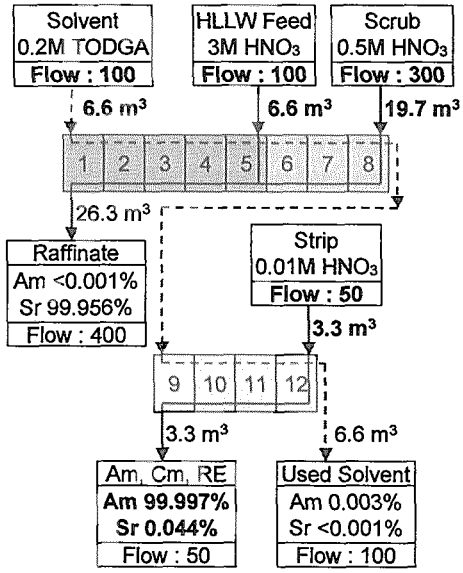

Fig. 3 The optimized process (Process No.4 in Table I)

Table I Results of the evaluation for the process with 0.2M TODGA

No.	[HNO_3] (M)			Flow rate ratio (-)				Recovery (%)		Volume (m^3) to treat the unit HLLW				
	Feed	Scrub	Strip	Solvent	Feed	Scrub	Strip	Am	Sr	Solvent	Feed	Scrub	Strip	Total
1	3	1	0.01	75	100	100	25	99.90	90.8	8.3	11.0	11.0	2.8	33.1
2	3	1	0.01	37.5	100	100	25	>99.99	16.0	7.6	20.3	20.3	5.1	53.4
3	3	0.5	0.01	100	100	200	50	>99.99	0.52	6.8	6.8	13.6	3.4	30.7
4	3	0.5	0.01	100	100	300	50	>99.99	0.044	6.6	6.6	19.7	3.3	36.2
5	3	0.5	0.01	150	100	450	75	>99.99	0.030	6.5	4.3	19.4	3.2	33.4
6	3	0.5	0.01	200	100	550	75	>99.99	0.037	6.3	3.1	17.3	2.4	29.1
7	3	3	0.01	75	100	100	75	>99.99	99.92	11.5	15.3	15.3	15.3	57.4

3.2 Effect of Flow Rate Change

Further evaluation was performed on the effects of the flow rate change of the scrub and the solvent on the Sr contamination in the Am fraction and the possibility of third phase formation in order to elucidate the characteristics of the optimized process which was shown in Fig. 3. Figure 4 shows the effect of the change in the scrub flow rate. As plotted in closed squares, the Sr contamination increased sharply with the decrease of the scrub flow rate. The change in the scrub flow rate was sensitive to the Sr contamination. On the other hand, maximum element concentration in the organic phase, which is plotted in open circles as the ratio to the extraction capacity, was less affected by the change in the scrub flow rate. Even by the 20% increase, the element concentration is kept lower than the extraction capacity. The value of 100% in this figure means that the element concentration in the organic phase reaches the extraction capacity. The third phase must be formed from this point.

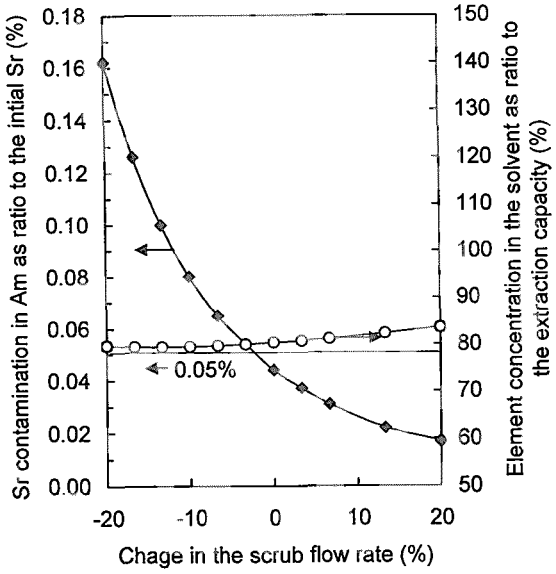

Fig. 4 Effect of the change in the scrub flow rate

The change in the solvent flow rate gives much effect both on the Sr contamination and on the maximum element concentration in the organic phase, as shown in Fig. 5. Only 10% decrease of the solvent flow rate would cause the third phase formation. Since the maximum element concentration is 80% of the extraction capacity in the normal condition, 20% decrease in the solvent flow rate should be acceptable, but the decrease of the solvent flow rate results in more accumulation of the elements in the extraction and scrub sections. This is the reason why only 10% decrease is acceptable. The flow rate of the solvent should be much more strictly controlled in order to avoid the third phase formation and to keep the Sr separation.

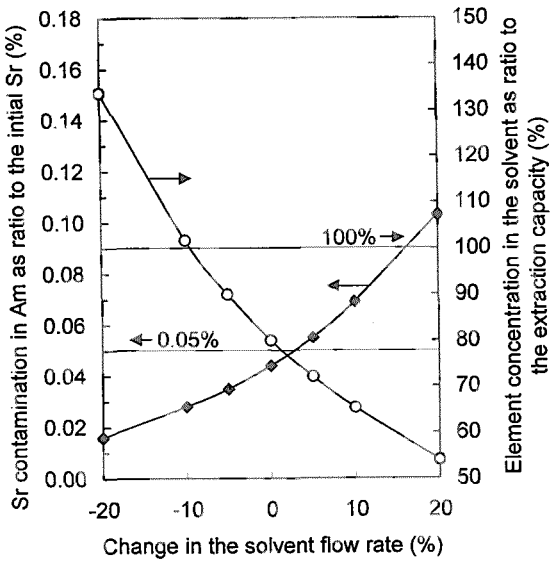

Fig. 5 Effect of the change in the solvent flow rate

3.3 Effect of decrease in distribution ratio

As described before, the drawback of the optimized process evaluated in the present study is the high scrub flow rate, which is due to the high distribution ratio of Sr. From the viewpoint of the volume reduction of the raffinate, hypothetical processes were evaluated when distribution ratios of both Am and Sr were decreased. The volume reduction of the raffinate would be very important because the raffinate should be treated for the separation of elements other than actinides, such as Cs, Sr and PGM, or for solidification.

The results of the evaluation showed that the volume of raffinate would be reduced from 26.3 m^3 to 19.9 m^3, which is 24% reduction, if distribution ratios of both Am and Sr were decreased to the half, as shown in Fig. 6. If distribution ratios of both Am and Sr were decreased to the 1/4, the volume of raffinate would be reduced to 15.0 m^3, which is 43% reduction.

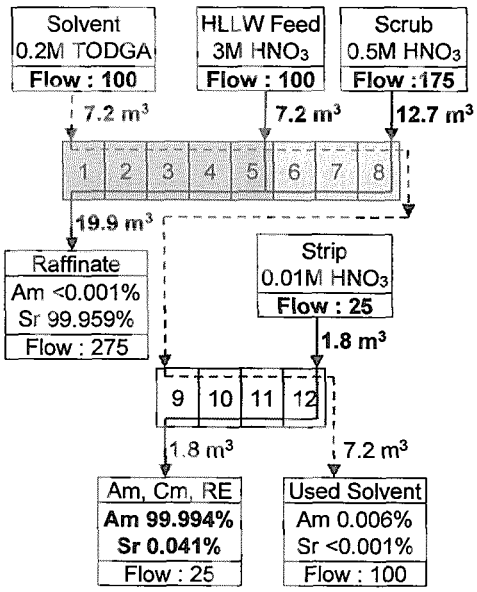

Fig. 6 The hypothetical process, when the distribution ratio is decreased to the half

3.4 Sr Separation at Strip Step

As was shown in the evaluated results for Process No.7 in Table I, it is also possible to extract Sr quantitatively with 0.2M TODGA. An additional evaluation was devoted to a process where both Am and Sr are extracted and they are separated from each other at the following two strip steps. At the first strip, Sr is back-extracted, and here an organic scrub is necessary to keep the Am in the organic phase. In the present evaluation, the first strip step composed of 8-stage stripping section for Sr back-extraction and 4-stage scrubbing section with the organic solvent for Am re-extraction. The nitric acid concentration of the first strip (strip 1) is one of the parameters to be optimized. The number of stage at the second strip step for Am back-extraction was increased to 6 stages in order to decrease the flow rate ratio of the second strip (strip 2). The most important point of this system is to recover Sr from the solvent in a high yield with low contamination of Am. The nitric acid concentration of the strip 1 and the flow rate ratios of the organic scrub and the strip 1 were adjusted in this point of view. The flow rate ratio of the scrub at the extraction step was decreased to extract Sr quantitatively.

Various process conditions were evaluated[2] and one of the process which gives the objective separation of Am and Sr is shown in Fig. 7. As shown in this figure, it is possible to establish a process where Sr is separated in a yield of more than 99.95% with the Am contamination less than 0.005% and Am is recovered in a yield of more than 99.99% with the Sr contamination less than 0.05%.

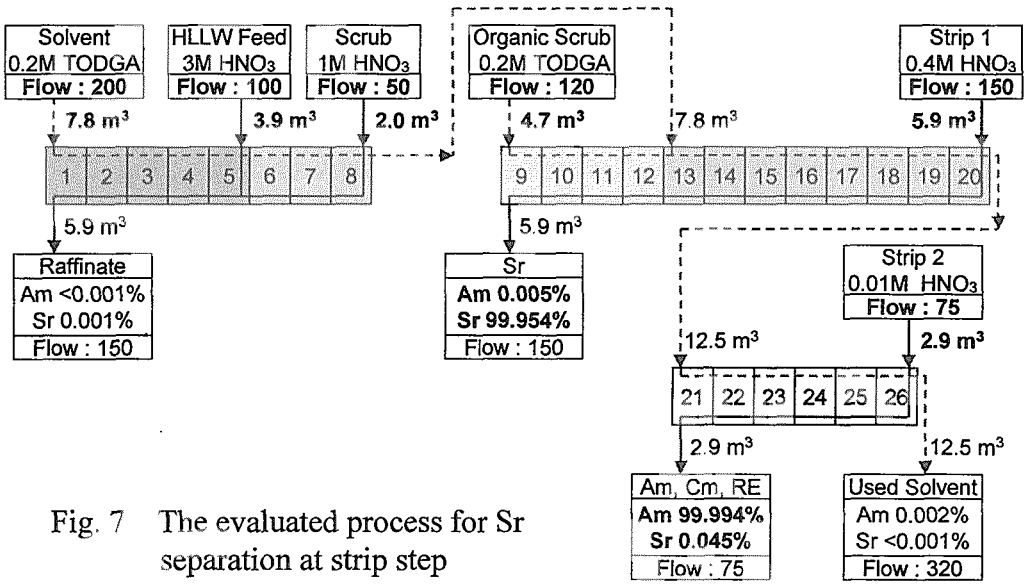

Fig. 7 The evaluated process for Sr separation at strip step

Compared to the Process No.4 where Sr is kept in the raffinate, the required volume of the solvent including the organic scrub had to be increased to about twice, but the total volume of the organic and aqueous solutions was reduced. The volume of the HLLW feed was 3.9 m^3.

Various factors such as the behaviors of other elements have to be examined in order to determine which extraction system would be better, the system as shown in Fig. 3 where Sr is kept in the raffinate or the system as shown in Fig. 7 where Sr is extracted together with Am and Cm and it is separated from them at strip step.

4. CONCLUSION

Extraction process for actinide separation from HLLW with N,N,N',N'-tetraoctyl-3-oxapentanediamide (TODGA) was preliminarily evaluated by simulation of Am and Sr behaviors. Results of the calculation showed that it is possible to establish an extraction process for the actinide separation from HLLW with 0.2M TODGA in n-dodecane, where Am is extracted in a very high yield of more than 99.99% and Sr is kept in the aqueous phase in a yield of more than 99.95%. The process is suitable to use the raffinate from the first cycle of the Purex process almost directly as the feed. It is, however, necessary to increase the scrub flow rate to 300% of the HLLW feed flow rate in order to achieve the above Sr separation.

Examinations on the effects of the flow rate change showed that the change in the solvent flow rate gives much effect both on the Sr contamination in the Am fraction and on the maximum element concentration in the organic phase. The flow rate of the solvent should be strictly controlled in order to avoid the third phase formation and to keep the Sr separation.

An additional evaluation was performed on a process where both Am and Sr are extracted and they are separated from each other at the following two strip steps. Results of the calculation showed that it is possible to establish a process where Sr is separated in a yield of more than 99.95% with the Am contamination less than 0.005% and Am is recovered in a yield of more than 99.99% with the Sr contamination less than 0.05%.

Although the present study still lies in the preliminary stage of the process development, it revealed the important points of the extraction process by diglycolamides (DGA). The results of the present study indicate that there is still some room for optimization of the actinide separation process by DGA extractants. The optimization would be achieved very effectively by using a solvent which has a higher extraction capacity and gives a lower distribution ratio of Sr.

For the process development, it is also necessary to examine and control the behaviors of other elements and to perform continuous counter-current extraction tests.

REFERENCES

[1] Y. Sasaki, Y. Sugo, S. Suzuki and S. Tachimori, Solvent Extr. Ion Exch., **19**, 91 (2001).

[2] Y. Morita, Y. Sasaki and S. Tachimori, Proceedings of International Conference on "Back-End of the Fuel Cycle: From Research to Solution" (GLOBAL2001), September 9-13, 2001, Paris, France, Paper No. 036 (published in CD-ROM) (2001).

JP0250309

SYSTEMATIC CHARACTERISTICS OF LANTHANIDES AND ACTINIDES IN PYROCHEMICAL AND AQUEOUS CONDITIONS

Hajimu Yamana

Research Reactor Institute, Kyoto University
Noda, Kumatori-cho, Sennan-gun, Osaka 590-0494, Japan

Pyrochemical processing techniques have received attentions for the future reprocessing and partitioning technique, and the assessments on their technological feasibility are now under way. Actinides and lanthanides are the major elements to be treated by this technique, and thus it is desired to establish a thorough interpretation of their complicated chemical characteristic. Among various scientific trials to investigate the chemical properties of actinide and lanthanide in pyrochemical systems, assessment of their systematic feature along the 4f(lanthanide)- and 5f(actinide)-series is a useful method for this purpose. In a pyrochemical system consisting of molten salt and liquid metal, the interaction of f-elements with the components of liquid phases significantly controls their chemical behaviors, and this creates a characteristic feature of the systematic variation of chemical properties along the series. In this presentation, the systematic variations of some chemical properties of lanthanides and actinides in pyrochemical and aqueous system are compared and discussed. Values of thermodynamic quantities of lanthanides and actinides in pyrochemical systems, which were experimentally determined or reported by literatures, are analyzed, and their systematic characteristics are compared with similar characteristics of aqueous system.

Experimentally determined formal potential between MCl_3 (M; lanthanide) and their metallic states in molten alkaline chloride corresponds to the standard Gibbs energy change of formation of MCl_3 that is dissolved in molten salt (ΔG_f^o[MCl_3 in S]), and relates to the excess Gibbs energy changes of MCl_3 dissolved in the molten salt (ΔG^{ex}[MCl_3 in S]). This is the result of the chemical interactions of M^{3+} with the components of the melt. ΔG^{ex}[MCl_3 in S] shows a rough tendency to decrease toward more negative side as the elements proceed along the 4f series. This rough decreasing trend of ΔG^{ex}[MCl_3 in S] in light lanthanides is similar to the solution enthalpy change of MCl_3 in aqueous solution (ΔH_{sol}[MCl_3 aq.]), suggesting that a rough similarity of the electrostatic mechanism of the formation of aquo-ions in aqueous solution and that of chloride complex in molten salt. However, the variation of ΔG^{ex}[MCl_3 in S] has less smoothness than the variation of ΔH_{sol}[MCl_3 aq.], which implies the possible presence of element-specific interaction of M^{3+} in the molten salt. This is different from the monotonic variation of the bonding in the aqueous system. The enthalpy changes arising when transferring gaseous M^{3+} into the liquid are estimated by Born-Harbor cycle procedures using reported ionization potentials and sublimation enthalpy changes. A slight difference can be seen in the comparison between aqueous system and molten chloride, and this is considered to show a difference of the chemical status in a solution and molten salt.

In the liquid metal phase, the thermodynamic stabilities of lanthanide show unique systematic variation along the series. It was found that ΔH^{ex}[M in B]'s of La, Gd, Tb, Dy, and Er approximately satisfy the semi-empirical rule for mixing two liquid metals with the use of a proper constant. But, Ce, Pr, and Nd were found to deviate from this rule, suggesting the irregularity of these three elements in the formation of intermetallic complex in the liquid bismuth[1][2]. The difference of the systematics of ΔH^{ex}[M in B]'s between lanthanide and actinide can be obviously seen in the behavior of light actinides[3].

UV-Visible spectrophotometric measurements of trivalent lanthanides and uranium in molten alkaline chloride were comprehensively carried out. For comparison, measurements of lanthanides in aqueous chloride solutions were carried out too. The hypersensitive absorption peaks observed in molten salt in a visible-region showed different magnitude of absorbance and slight shifts of wavelength compared with those observed in LiCl aqueous solutions. Hypersensitive absorbances of lanthanides are considered to indicate the status of coordination around the cation, and thus systematic variation of the hypersensitivities of lanthanides is expected to give informations of the difference of the surrounding conditions of lanthanide cations in the melt.

References

[1] H. Yamana, N. Wakayama, N. Souda, and H. Moriyama, *J. Nucl. Mater.*, 278(2000) 37
[2] H. Yamana, J. Sheng, N. Souda, and H. Moriyama, *J. Nucl. Mater.*, 294(2001) 232
[3] H. Yamana, J. sheng, K. Kawamoto, and H. Moriyama, *J. Nucl. Mater.*, 294(2001) 53

JP0250310

JAERI-Conf 2002-004

TRU recovery from HLLW by a pyrometallurgical process

MASAKI KURATA, KENSUKE KINOSHITA, AND TADASHI INOUE

Central Research Institute of Electric Power Industry,

Iwadokita 2-11-1, Komae-shi, Tokyo 201-8511, Japan

Fax: 81-33-480-7956, e-mail: kurata@criepi.denken.or.jp

A pyrometallurgical process to recover TRU from HLLW has been developed at Central Research Institute of Electric Power Industry since 1987. Based on the developed process flow sheet, two kinds of series test were performed to measure the material balance of various elements in the series of process operations and to clarify the major concerns that needed to be solved for industrial deployment. Reductive-extraction, electro-winning, and multistage-extraction of TRU were performed in the first series using molten salt containing TRU, and in the second one, denitration, chlorination, and reductive extraction were performed using simulated HLLW. In the first test, greater than 99% of TRU was recovered as metal with a condition of $DF_{RE} > 10$. In the second test, the material balance of various elements was measured and the molten salt prepared from simulated HLLW was confirmed to be suitable for reductive extraction. A demonstration test using genuine HLLW is planed to confirm the variation in the material balance, especially as this process applies to the recycling use of molten salt solvent.

Key words: HLLW, pyrometallurgical partitioning process, TRU

1. INTRODUCTION

A pyrometallurgical partitioning process (Pyro-partitioning) has been developed at Central Research Institute of Electric Power Industry (CRIEPI) to recover trans-uranium elements (TRU) from high-level liquid waste (HLLW) generated from reprocessing spent LWR fuels. Compared to conventional aqueous processes, Pyro-partitioning is expected to generate fewer process wastes and to favor more compact facilities, because inorganic solvents, reductants, and gases are used in Pyro-partitioning instead of the organic materials used in the aqueous processes. Nevertheless, many technical uncertainties must be resolved prior to the industrial deployment of Pyro-partitioning, especially in respect of maintaining the advantages shown above. One of the key issues is an accurate assessment of waste generation, including release of effluents and process wastes due to the volatilization of various materials or to the accumulation of FP or impurities. As the first step, two kinds of series tests were performed to measure the material balance of various elements in the series of process operations and to clarify the points to be resolved for industrial deployment. The first run performed reductive-extraction, electo-winning, and multistage-extraction of TRU using molten salt

containing TRU [1], and the second run performed denitration, chlorination, and reductive extraction using simulated HLLW [2].

2. PROCESS FLOW

Figure 1 indicates the process flow of Pyro-partitioning [3]. The various elements in HLLW are first dehydrated and denitrated to oxides by heating in the denitration step, then converted to chlorides via a reaction with chlorine gas in a LiCl-KCl eutectic salt bath in the chlorination step. These two steps produce chlorides suitable for the following pyrometallurgical processes. Since the alkali nitrates are stable and are not denitrated in the following denitration step with temperature maintained at 773K or lower, the alkali elements are separated from other oxides by rinsing with water after denitration. Rough separation of Fe, Zr, and Mo is performed in the chlorination step due to the high volatility of the chlorides. The chlorides recovered in the salt bath are supplied to the pyrometallurgical processes, which consists of (I) reductive extraction and (II) multistage extraction. (III) Electro-winning of U might be introduced between these two steps as an optional step, for the effective recovery of U. The reductive extraction is performed in a molten-salt/liquid-Cd system on the basis of the differences in the Gibbs energy of formation for chlorides in the molten-salt phase and the Gibbs energy of solution for solute metals in the liquid-Cd phase. The elements nobler than U are recovered in the liquid-Cd phase by adding Li reductants. The molten-salt phase is then supplied to the multistage extraction step, where the actinides are selectively reduced and extracted in the liquid-Bi phase by adding Li reductants in a molten-salt/liquid-Bi system, whereas alkaline-earth elements and RE remain in the molten-salt phase. In the spent salt treatment step, alkaline-earth elements and RE are recovered into a lead-electrode by electrolysis of the spent salt. Chlorine gas and LiCl-KCl generated in this step are recycled back to the chlorination step. The present process aims at recovering 99% or more of the actinides from HLLW with no accompanying FP other than RE. Concerning RE, accompanying RE weights comparable to TRU weights is, however,

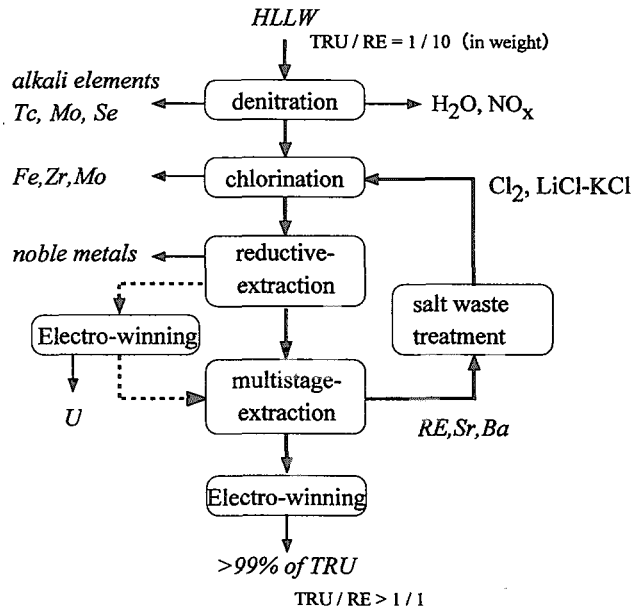

Fig.1 Process flow of Pyro-partitioning.

allowed for in the TRU transmutation, when the transmutation is carried out in metallic-fuel fast reactors [3].

3. FIRST SERIES TEST

3.1. Procedure

All operations for the first series test were performed in an Ar-atmosphere glove box. The starting composition and weight of various elements are listed in Table I, roughly corresponding to the products after chlorinating 50 ml of HLLW. Each chloride of these elements was dissolved in a molten salt bath. First, Fe was extracted and separated into liquid Cd by the addition of Cd-Li reductants. The applicability of the optional electro-winning process for U was investigated in the following manner. Various elements, with the exception of Sr and Eu, were reductively extracted into new liquid Cd by supplementary addition of Cd-Li reductants after replacing liquid Cd, and U was then recovered by electro-winning between the liquid Cd anode and a Ta cathode. Then, U and TRU remaining in the Cd anode were oxidized and extracted completely into the molten salt by the addition of $CdCl_2$. The molten salt was mechanically separated from Cd and then supplied to the 4 steps of multiple batch extraction, in which a Bi-Li alloy was used as a reductant. After each extraction, the Bi phase containing the extracted TRU was separated from the salt phase for submission to the succeeding stage. The loss of Am, which was the quantity of Am remaining in the salt phase after the fourth extraction, was estimated to be approximately 0.4%. As for Np and Pu, these losses were estimated to be smaller than those for Am, since Np and Pu are more easily reduced. Finally, the recovered Bi phase was used as an anode and TRU was collected on a Ta cathode by electro-winning. The temperature of these operations was around 773K.

Table I Initial condition of first series t

Element	Initial weight (mg)	Composition (wt%)
U	420.00	9.09
Np	119.21	2.58
Pu	14.50	0.31
Am	119.22	2.58
Fe	581.85	12.59
Zr	412.59	8.93
Y	102.76	2.22
LA	288.50	6.24
Ce	570.48	12.35
Pr	267.95	5.8
Nd	999.96	21.64
Eu	237.01	5.13
Gd	41.34	0.89
Sr	445.05	9.63

3.2. Results and discussion

Table II shows the material balance in the first series test. Observations on each step are summarized in 3.2.1. Concerns regarding industrial deployment arising from these observations are also summarized in 3.2.2.

Table II Material balance in first series test

element	(1) Reductive extraction of noble metal	(2) Reductive extraction of U, TRU, and	(3) Electro winning of U		(4) Multistage extraction				(5) Electro-winning of U and TRU	
	Ratio eliminated from salt w.r.t. initial amount (%)	Ratio remained in salt w.r.t. initial amount (%)	Ratio recovered on solid cathode w.r.t. input amount(%)	Composition in cathode deposit (wt%)	Recovering ratio after 1st stage w.r.t. input amount(%)	Recovering ratio after 2nd stage w.r.t. input amount(%)	Recovering ratio after 3rd stage w.r.t. input amount(%)	Recovering ratio after 4th stage w.r.t. input amount(%)	Ratio recovered on solid cathode w.r.t. input amount(%)	Composition in cathode deposit (wt%)
U	1.29	0.04	81.02	97.88	95.69	98.56	99.22	99.01	49.69	12.55
Np	0.01	0.01	1.59	0.89	95.34	99.20	99.82	99.84	93.59	54.54
Pu	0.097	0.00	0.78	0.08	94.46	98.96	99.79	99.90	96.67	10.74
Am	0.00	0.02	0.38	0.19	86.75	96.69	99.24	99.81	24.19	12.41
Fe	100.00	0.00	0.00	0.00	0.00	0.00	0.00	0.00	0.00	0.00
Zr	2.09	0.03	0.54	0.23	77.93	82.70	94.49	95.68	30.56	0.16
Y	0.22	0.30	0.00	0.00	0.15	0.15	0.17	0.33	8.62	0.04
LA	0.05	0.03	0.00	0.00	3.41	5.45	8.45	10.64	4.78	0.16
Ce	0.05	0.01	0.00	0.00	10.29	16.15	23.64	28.97	14.13	3.26
Pr	0.04	0.02	0.12	0.16	12.36	19.07	27.62	33.10	17.60	2.29
Nd	0.05	0.02	0.06	0.31	10.06	15.38	22.58	27.22	10.94	3.74
Eu	0.03	41.43	0.00	0.00	0.14	0.15	0.14	0.34	4.35	0.01
Gd	0.10	0.05	0.10	0.03	3.40	4.95	7.05	8.56	13.76	0.11
Sr	0.00	44.44	4.30	0.23	0.00	0.00	0.00	0.00	0.00	0.00

3.2.1. Observations

(1) Reductive extraction of noble metal

-Fe was completely eliminated from the salt and separated from other elements.

-The loss of each TRU extracted in liquid Cd was around 0.1% or less with respect to the initial input.

-Small amounts of U and Zr were extracted in liquid Cd.

(2) Reductive extraction of U, TRU, and RE

-Significant amounts of Eu and Sr still remained in the salt, separated from other elements.

-The loss of each TRU remaining in salt was less than 0.02% with respect to the initial input.

(3) Electro-winning of U

->80% of U was collected on a solid cathode.

-The end-product composition consisted of approximately 98% of U and 1% of TRU, plus 0.5% of RE and 0.5% of other impurities.

(4) Multi-stage extraction of U and TRU

->99% of U and >99.8% of TRU were extracted and recovered in liquid Bi.

-A significant amount of RE was separated from TRU, although some RE still accompanied the TRU.

(5) Electro-winning of U and TRU

->90% of Np and Pu were co-recovered on the solid cathode, as well as significant amounts of U and Am.

-RE concentration in the cathode deposit was less than 10 wt.%.

3.2.2. Concerns

-The Fe-solubility in Cd is too low to recover Fe as the liquid phase. Since some of noble metals have low solubility in Cd, the development of a recovery system for noble metal

sludge is necessary.

-The method of controlling reductant amount should be designed to be individually suitable for each step.

-Uranium acquires oxygen in this system. Since a small amount of UO_2 sludge is formed, it should be recovered, especially when recycling molten salt.

-The method of controlling the salt composition should be designed to maintain product composition.

-Since complete anode-dissolution of U and TRU is difficult, a method of recovery of U and TRU remaining in the anode should be designed.

-Since FP and other impurities are accumulated in liquid metal solvents, the effect on TRU-extraction should be estimated, especially in terms of recycling.

4. SECOND SERIES TEST

4.1. Procedure

Two samples were prepared. The starting concentrations and compositions are listed in Table III, which includes the contribution of concentrated raffinate, concentrated alkaline waste, insoluble residues, and corrosion product of claddings. These values are determined from a calculation using ORIGEN-II code, and assuming the following conditions: 48,000 MWD/t-U for PWR spent fuel, 4 years cooling, and 99.5% recovery of heavy metals using the PUREX process. To the alkali waste and corrosion products, Na and Fe, Ni, and Cr were added, respectively. To simplify the analysis, several elements are substituted with other elements. First, the simulated HLLW, 100 ml in volume, was heated at 373K to volatilize water and a surplus of nitric acid. Then, the sample was heated at 773K to decompose the various nitrates, except for the alkali elements. The denitrated sample was

Table III Initial composition and concentration of simulated HLLW in the second series test

element contained in	category	run-1 element used	run-1 comp. (at%)	run-1 conc. (g/l)	run-2 element used	run-2 comp. (at%)	run-2 conc. (g/l)
U, Np, Am, Cm	actinide	Actinide was not added in run-1.			U	2.50	12.01
Na	alkaline waste	Na	58.57	26.59	Na	56.48	26.21
Rb, Cs	alkali metal	Cs	3.45	9.05	Cs	3.28	8.79
Sr, Ba	alkaline-earth	Ba	2.61	7.09	Sr	3.02	5.34
Y, Gd	rare-earth	Y	0.93	1.63	Ce	5.60	15.83
La, Ce	rare-earth	Ce	3.83	10.59			
Pr, Nd	rare-earth	Nd	4.40	12.53	Nd	5.20	15.15
Sm, Eu	rare-earth	Sm	0.94	2.8			
Zr	Zr	Zr	5.63	10.13	Zr	5.55	10.22
Mo	Mo	Mo	5.23	9.90	Mo	5.05	9.79
Tc	Tc	Re	1.13	4.15	Re	1.03	3.85
Ru	noble metal	Ru	2.88	5.75	Ru	2.95	6.02
Rh	noble metal	Rh	0.61	1.24	Pd	2.89	6.21
Pd	noble metal	Pd	2.38	5.00			
Fe	corrosion product	Fe	4.38	4.83	Fe	5.60	6.31
Ni	corrosion product	Ni	1.48	1.72			
Cr	corrosion product	Cr	0.87	0.89	Cr	0.86	0.90
Se	calcogen	Se	0.10	0.16	Se and Te were not added in run-2.		
Te	calcogen	Te	0.59	1.49			

then rinsed with water to recover water-soluble alkali nitrate in an aqueous phase. The residue recovered with a centrifugal separator was calcinated again at 773K. The residue, approximately 10 g in weight, was then supplied to the subsequent chlorination test. The sample was heated at 973K in the molten LiCl-KCl salt, and then chlorinated by the introduction of chlorine gas. Since some chlorides were volatilized during chlorination, they were collected in a cold trap attached in an off-gas line. Three pieces of the chlorinated sample were supplied to the reductive extraction test. The first piece was made to react with Cd. The second and third pieces were made to react with a Cd-Li alloy, which contains Li sufficient to reduce approximately 80 and 120% of U and RE present in the salt, respectively.

4.2 Results and discussion

Table IV shows the material balance in the denitration and chlorination steps. Table V shows the material balance in the reductive extraction step. Observations on each step are summarized in 4.2.1. Concerns regarding industrial deployment arising from these observations are also summarized in 4.2.2.

Table IV Distribution of various elements in pre-treatment process (g)

run no.	element contained in HLLW	initial weight in 100ml	volatilized in denitration	recovered in aqueous phase	volatilized in chlorination	recovered in salt bath	sum of detected weight	detected ratio to initial value
1	Na	2.659	0.00569	2.529	0.00257	0.0327	2.570	96.6%
	Cs	0.905	0.00182	0.890	0.00232	0.00698	0.901	99.6%
	Ba	0.709	0.000376	0.000737	0.00762	0.765	0.773	109.1%
	Y	0.163	0.000103	ND	0.00099	0.156	0.157	96.4%
	Ce	1.059	0.000582	ND	0.00547	1.080	1.087	102.6%
	Nd	1.253	0.000789	ND	0.00871	1.207	1.216	97.1%
	Sm	0.280	0.000196	ND	0.00218	0.303	0.305	108.9%
	Zr	1.013	0.000294	ND	0.903	0.0286	0.932	92.0%
	Mo	0.990	0.000208	0.497	0.337	0.00171	0.836	84.4%
	Re	0.415	0.00252	0.421	0.00247	0.00404	0.430	103.5%
	Ru	0.575	0.138	ND	0.0104	0.429	0.577	100.3%
	Rh	0.124	ND	ND	ND	0.129	0.129	104.3%
	Pd	0.500	0.000865	ND	0.00952	0.462	0.473	94.5%
	Fe	0.483	0.000232	ND	0.452	0.0177	0.470	97.4%
	Cr	0.172	0.000421	0.0762	0.0181	0.0818	0.177	102.6%
	Ni	0.089	0.0000401	ND	0.00224	0.0851	0.087	98.2%
	Se	0.016	ND	0.0143	0.00236	ND	0.017	103.8%
	Te	0.149	ND	ND	0.150	0.0108	0.160	107.6%
2	U	1.201	ND	ND	0.0543	1.027	1.081	90.0%
	Na	2.621	0.00233	2.515	0.00307	0.0910	2.611	99.6%
	Cs	0.879	0.000721	0.890	0.00190	0.0197	0.912	103.7%
	Sr	0.534	0.000198	0.000395	0.00856	0.483	0.492	92.1%
	Ce	1.583	0.000190	ND	0.0211	1.522	1.543	97.5%
	Nd	1.515	0.000970	ND	0.0242	1.385	1.410	93.1%
	Zr	1.022	ND	0.0000818	0.831	0.0984	0.929	90.9%
	Mo	0.979	ND	0.372	0.456	0.00262	0.830	84.8%
	Re	0.385	0.000339	0.381	0.00684	0.000190	0.388	100.8%
	Ru	0.602	0.139	0.000223	0.00449	0.149	0.294	48.8%
	Pd	0.621	0.000484	ND	0.0124	0.654	0.667	107.4%
	Fe	0.631	0.000259	0.0000126	0.431	0.0447	0.476	75.5%
	Cr	0.090	ND	0.0774	0.00665	0.0100	0.094	104.5%

4.2.1. Observations

(1) Denitration and Rinsing

->98% of Na, Cs, and Re with respect to the initial 100% values were recovered in the aqueous phase, as well as significant amounts of Mo, Cr, and Se.

-Approximately 30% of Ru was volatilized in denitration.

-The morphology of recovered product was that of a very fine powder, suitable for the following chlorination step.

Table V Distribution of various elements in reductive-extraction process (g)

run no.	element contained in HLLW	initial weight in 100ml	remained in salt	recovered in liquid Cd	detected in third phase	sum of detected weight	detected ratio to initial value
1	Na	2.659	0.0310	0.000339	0.000209	0.032	1.2%
	Cs	0.905	0.00580	ND	ND	0.006	0.6%
	Ba	0.709	0.818	0.00283	0.000354	0.821	115.8%
	Y	0.163	0.00666	0.126	0.0239	0.157	96.3%
	Ce	1.059	0.00677	1.093	0.0426	1.142	107.9%
	Nd	1.253	0.00573	1.199	0.0603	1.265	101.0%
	Sm	0.280	0.119	0.0570	0.133	0.310	110.7%
	Zr	1.013	ND	0.0174	0.00923	0.027	2.6%
	Mo	0.990	ND	0.00112	0.000298	0.001	0.1%
	Re	0.415	ND	ND	ND	0.000	0.0%
	Ru	0.575	ND	0.426	0.00218	0.428	74.5%
	Rh	0.124	ND	0.132	0.000255	0.132	106.6%
	Pd	0.500	ND	0.468	0.000162	0.468	93.6%
	Fe	0.483	ND	0.0177	0.00242	0.020	4.2%
	Cr	0.172	ND	0.0715	0.0105	0.082	47.7%
	Ni	0.089	ND	0.0931	0.0000304	0.093	104.6%
	Se	0.016	ND	ND	ND	0.000	0.0%
	Te	0.149	ND	ND	ND	0.000	0.0%
2	U	1.201	ND	0.051	1.0895	1.141	95.0%
	Na	2.621	ND	ND	ND	ND	0.0%
	Cs	0.879	ND	ND	ND	ND	0.0%
	Sr	0.534	0.521	0.00268	0.000138	0.524	98.1%
	Ce	1.583	0.0401	1.525	0.0323	1.597	100.9%
	Nd	1.515	0.0384	1.459	0.0309	1.529	100.9%
	Zr	1.022	ND	0.1039	0.00426	0.108	10.6%
	Mo	0.979	ND	0.00346	ND	0.003	0.4%
	Re	0.385	ND	ND	0.000427	0.000	0.1%
	Ru	0.602	ND	0.00240	0.310	0.312	51.9%
	Pd	0.621	ND	0.601	0.00788	0.609	98.1%
	Fe	0.631	ND	0.0510	0.00828	0.059	9.4%
	Cr	0.090	ND	0.00912	0.000840	0.010	11.1%

(2) Chlorination

-Attained chlorination ratio greater than 99%.

->90% of Zr, Fe, Mo, and Te with respect to the amount of each supplied from denitration were volatilized and collected in the cold trap.

-A small amount of U was also volatilized and collected in the cold trap.

(3) Reductive extraction

-Noble metals and Ni were selectively recovered in the Cd phase without the addition of Li.

-A significant amount of Fe and Zr removed from the salt phase formed the intermetallic compounds.

->99% of Ce and Nd were removed from the chloride phase, along with the noble metals as well as a significant amount of Y and Sm, when Li-reductant was added to the system.

-The amount of intermetallic compound decreased when Li-reductant was added to the system.

-These facts suggest that the product supplied from the chlorination step is chemically suitable for the reductive extraction step.

4.2.2. Concerns

(1) Denitration and Rinsing

-A recovery system to collect volatile FP, mainly Ru, should be developed.

-A method to convert the volatile material and aqueous material to the proper waste forms should be developed.

-The development of a system for filtering and recovering powder is necessary.

(2) Chlorination

-A method of recovering volatile chlorides deposited on piping or on the wall of a chlorinator should be designed, although the amount of such chlorides is small.

-Crucible life should be increased.

(3) Reductive extraction

-In the context of transporting both the Cd and salt phase among steps, a method of treating the intermetallic compounds should be developed.

-Small amounts of RE formed oxides or oxychlorides by reacting with oxygen, and were deposited at the bottom of the salt phase. The recovery of this deposit is necessary.

5. SERIES TEST PLANNED USING GENUINE HLLW

A new series test using genuine HLLW is now planned in the context of a collaboration study between CRIRPI and the Institute for TransUranium elements (ITU). The collaboration study has been ongoing since 1997 and has as its aims (I) electro-refining of U, Pu, and minor actinides (MA) from U-Pu-Zr metal fuel, (II) multistage reductive extraction of MA, and (III) preparation of chloride from HLLW. Small amount of genuine HLLW (approximately 500 ml) will be prepared as the initial material for (III) in 2001.

6. SUMMARY

Two kinds of series test indicated that the proposed flow sheet for Pyro-partitioning is chemically feasible in laboratory-scale processes. The various elements contained in HLLW,

including alkaline waste, corrosion product, and nonsoluble residue, are efficiently chlorinated, although a small amount of chloride is volatilized. More than 99% of TRU is recovered in metal form suitable for transmutation using metallic fuel fast reactors. The issues to be solved for industrial deployment are thus clarified through the detailed observation of series test results.

REFERENCE

[1] K. Uozumi, K. Kinoshita, T. Inoue, S.P. Fusselman, D.L. Grimmett, J.J. Roy, T.S. Storvick, C.L. Krueger, and C.R. Nabelek, *J. Nucl. Sci. Technol.* **38** (2001) 36.

[2] M. Kurata, K. Kinoshita, and T. Inoue, *J. Nucl. Sci. Technol.* **37** (2000) 682-690.

[3] K. Kinoshita, T. Inoue, S.P. Fusselman, D.L. Grimmett, J.J. Roy, R.L. Gay, C.L. Krueger, and C.R. Nabelek, and T.S. Storvick, *J. Nucl. Sci. Technol.*, **36**, (1999) 189-197.

This is a blank page.

JP0250311

NEW DEVELOPMENTS IN DICARBOLLIDE EXTRACTIONS

J. RAIS, P. SELUCKÝ, N. ŠÍSTKOVÁ, J. PLEŠEK*, B. GRÜNER* and B. ČÁSENSKÝ*

Nuclear Research Institute plc Rez, 25068 Rez, Czech Republic
*Institute of Inorganic Chemistry CAS, 25068 Rez, Czech Republic

ABSTRACT

In this paper, the recent developments in the area of research on dicarbollide extractions performed at the title institutes are described. These consist in synthesis and testing of new specific dicarbollide derivatives, studies in the area of new potential synergists to be used with chlorinated dicarbollide and new non-toxic cheap solvents that might be used for dicarbollide.

KEY WORDS:
Extractions, dicarbollide extractants, synergists, solvents

INTRODUCTION

Dicarbollide anion [*closo-commo*-(1,2-$C_2B_9H_{11}$)$_2$-3Co)]$^{(-)}$ (COSAN) and especially its hexachlorinated derivative [(8,9,12-Cl_3-$C_2B_9H_8$)$_2$-3-Co]$^{(-)}$ (Cl-COSAN, BCl^-) (Figure 1) are used as extractants in nuclear technology of treatment of spent nuclear fuel for isolation of radioactive ^{137}Cs and ^{90}Sr. For an efficient isolation of the latter radionuclide, a synergist of the polyethylene glycol type, PEG, must be added to an extractant. The process was patented by the two title institutes and developed into industrial scale application during cooperation of the Radium Institute, St. Petersburg and NRI, Rez in early 80ties.

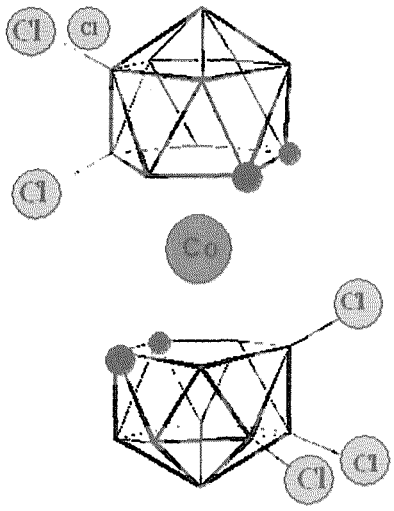

Fig 1 Cl-COSAN

The process is working until now as the only one process in the area of extraction processes in nuclear technology (besides PUREX process of course) operating on a full-scale level at Mayak, Russia.

The reasons for its success are extraordinary chemical and radiation stability of the used inorganic extractant in contrast to many proposed organic reagents. Hence, the extractant can be recycled many times without loss of its extraction efficacy.

Naturally, the success of this reagent has evoked many consecutive studies, the part of them performed recently at NRI, Rez and IICH, Rez is reported here.

Mainly technologically oriented studies are performed in Russia and in the frame of Russian – DOE, USA cooperation. From quite recent results, the UNEX process may be mentioned which is treated in another paper at this conference [1]. At the process, Cl-COSAN is used in a mixture with PEG 400 and diphenyl-N,N-dibutylcarbamoyl phosphine oxide. A new solvent phenyltrifluoromethyl sulfone (FS-13) is used. Other important achievement is a proposal to include dicarbollide extraction in a preceding part of PUREX process; this might remove the main portion of radioactivity prior to PUREX [2]. To a great satisfaction of the originators of the process, Cl-COSAN and PEG are again used in these newly proposed schemes.

In the frame of European cooperation, new boron derivatives are synthesized at the University of Barcelona, the University of Lyon and the Institute of Inorganic Chemistry, Czech Republic and their extraction behavior is tested at CEA, Cadarache and NRI, Czech Republic. The studies were performed in two consecutive EC COPERNICUS projects and are largely documented in the relevant articles and conferences.

Particular to own NRI studies are those of the use of various synergists added to Cl-COSAN and screening of new solvents applicable for dicarbollide extractions. Recent results covering both areas of research are presented here.

NEW DICARBOLLIDE DERIVATIVES

The following dicarbollide derivatives were all prepared at the Institute of Inorganic Chemistry, Czech Republic. One of the phosphorus substituted dicarbollide bridged derivative, COSBRIPHOS, is shown in Fig. 2. This derivative is soluble in nonpolar xylene and is effective for extraction of Eu^{3+} from acidic media. D_{Eu} = 4.8 for 1M HNO_3 and 0.247 for 5M HNO_3 if 0.01M reagent in xylene is used.

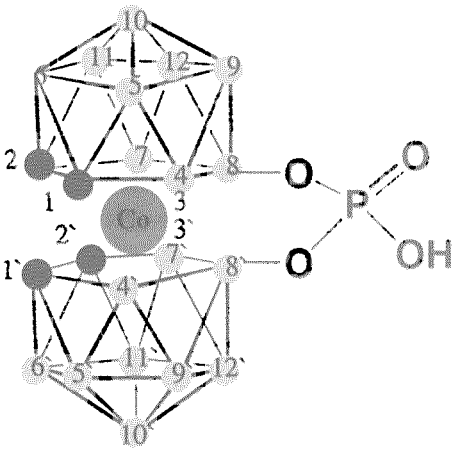

Fig. 2 COSBRIPHOS

Analogical to the above reagent is COSBRIPHEPHOS, see Fig. 3. This extractant is effective only at low acidities of aqueous phase, giving distribution ratios D_{Eu}, D_{Cs} and D_{Sr} equal to 32.2, 0.56 and 0.41, respectively for 0.01M reagent in xylene and 0.1M HNO_3.

Non-bridged dicarbollide derivatives with a substituted crown ether moiety were prepared recently. One of them with 21-crown-7 substituent, COS21CROWN7, is shown in Fig. 4. As expected, the derivative shows affinity for extraction of Cs and Sr, the distribution ratios of

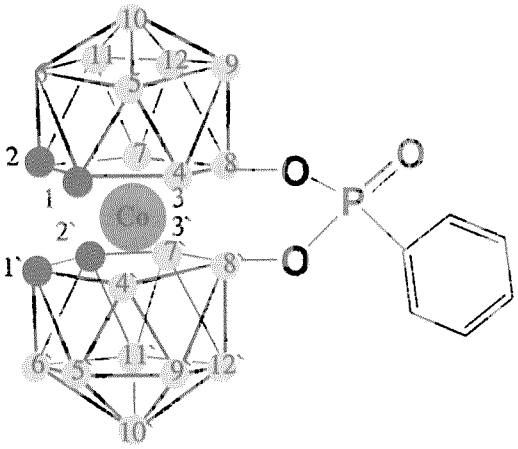

Fig. 3 COSBRIPHEPHOS

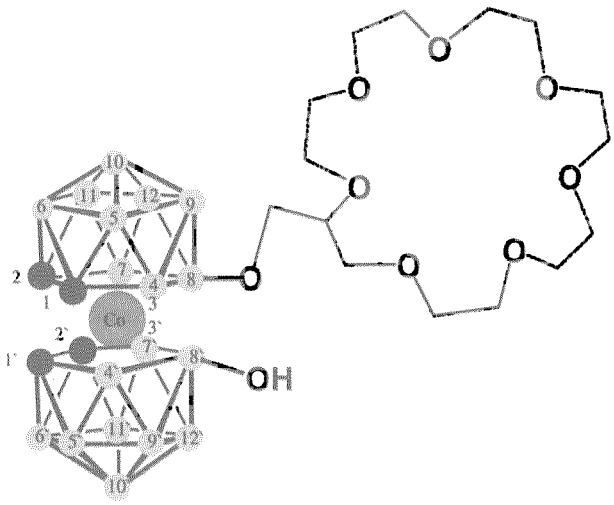

Fig. 4 COS21CROWN7

these two cations being 1.63 and 0.62, respectively, for extraction from 1M HNO_3 by 0.01M reagent in 1,2 – dichloroethane, whereas distribution of Eu at the same conditions is only D_{Eu} = 0.008.

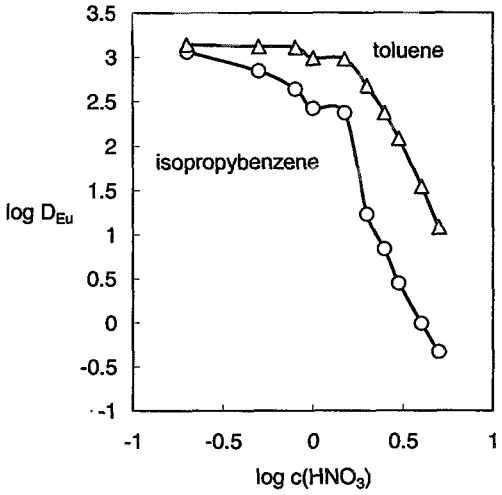

Fig. 5 Extraction of microamounts of Eu by 0.01M dodecylCMPO-like-COS in aromatic solvents

In analogy with CMPO substituted calixarenes [3], after a lot of study at the IICH, a CMPO dicarbollide derivatives **butylCMPO-like-COS** and **dodecylCMPO-like-COS** were synthesized. The exact structure of them, being object of possible patenting, is not given here, but the derivatives are typical dicarbollide anions containing bidentate CMPO group, thus presumably being able to selectively bind trivalent ions. This assumption is justified by results plotted in Fig. 5. In contrast to CMPO itself and CMPO substituted calixarenes, the extraction increases with decreasing acidity of the aqueous phase. This is true also for other solvents not shown in the Figure, like into 1,2 – dichloroethane.

In order to elucidate why the behavior of **butylCMPO-like-COS** is different from the classical CMPO extractants, the dependences of log D_{Eu} on the concentration of the reagent at various constant acidities of the aqueous phase were measured. These are shown in Figure 6. The log-log dependences are in a shown range of straight-line type with the slopes 0.5M HNO_3 2,14, 1M HNO_3 2,43, 2M HNO_3 2.66 and 3M HNO_3 2.29. From these results, it might be inferred that the most probable particle in the organic phase is rather EuB^+_2 than EuB_3. The effect seems to be connected with the fact that the ligand can play double role: (i) it is a selective ligand for Eu^{3+} and (ii) it is also a hydrophobic anion in the system. Perhaps due to the incomplete binding of the ligand to the cation, which might be caused by sterical reasons, only two ligands are bound to the cation. Hence, the originally assumed and expected scheme of binding, see Fig. 7a is less probable than a scheme shown in Fig. 7b, with a probable mechanism of extraction given by reaction $Eu^{3+}_a + 3B^-_a = EuB^+_{2,o} + B^-_o$. The synergetic effect of the ligand is very high, if comparing the distribution of Eu by non-substituted dicarbollide from about 0.5 M nitric acid, the enhancement of D_{Eu} is of the order of 10,000. The extraction - stripping cycle might be performed by extraction from some 3M HNO_3 and

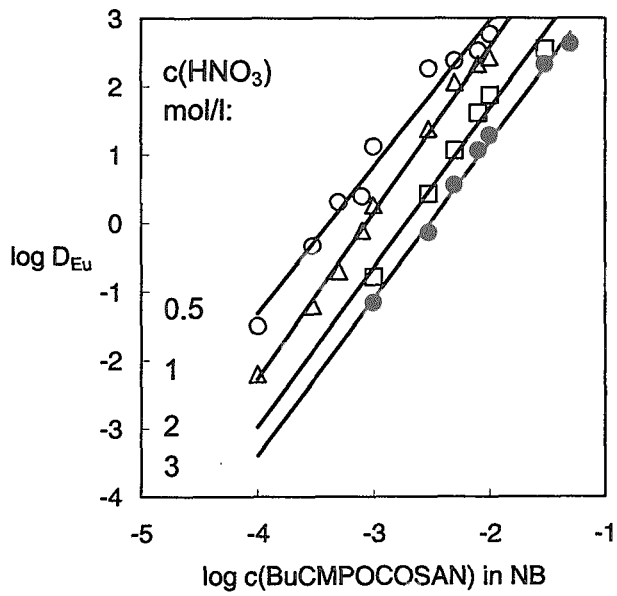

Fig. 6 Extraction of microamounts of Eu^{3+} by butylCMPO-like-COS into nitrobenzene at various aqueous acidities

stripping by 8M HNO_3 into suitable non-polar aromatic solvent or by using some complexing agent like DTPA for stripping.

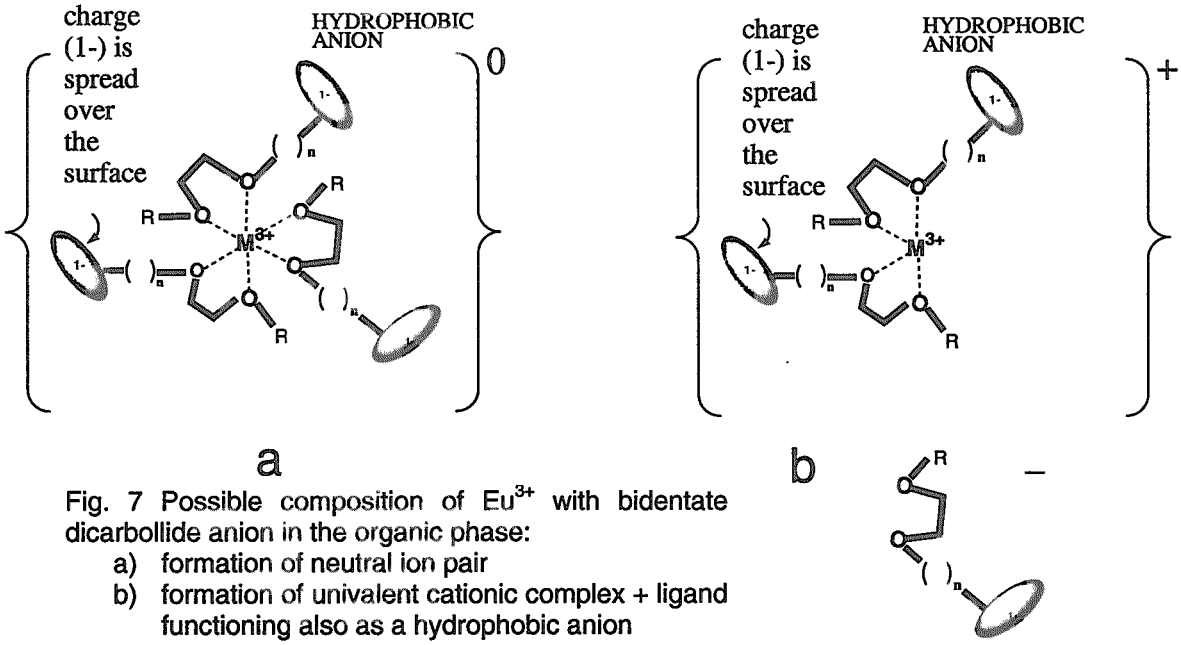

Fig. 7 Possible composition of Eu^{3+} with bidentate dicarbollide anion in the organic phase:
a) formation of neutral ion pair
b) formation of univalent cationic complex + ligand functioning also as a hydrophobic anion

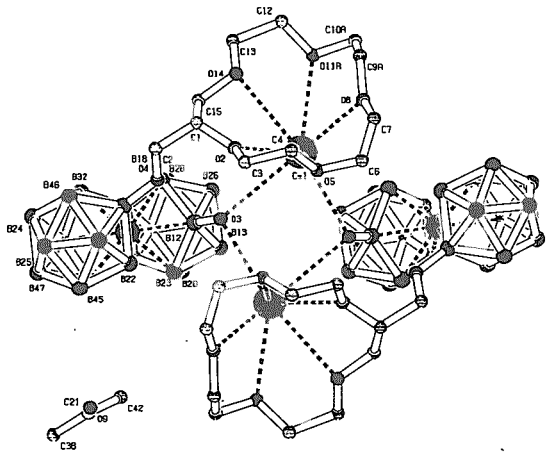

Besides the studies of liquid - liquid equilibria, the solid phase structures of some compounds were also evaluated. As an example a Platon presentation of the molecular structure of the Cs^+ complex of the [8-(15-crown-5-CH_2O)-8'-(OH)-COSAN]$^-$, congener with the smallest crown ether ring size is shown in Fig. 8 (two crown ether dicarbollide anions bound to two Cs^+ cations).

Fig. 8 Platon presentation of the molecular structure of the Cs^+ complex of the [8-(15-crown-5-CH_2O)-8'-(OH)-COSAN]$^-$

SYNERGETIC MIXTURES WITH Cl-COSAN

Continuing our studies on synergetic mixtures of Cl-COSAN with bidentate neutral extractants [4, 5], we have measured extraction efficacies for Eu^{3+} for a new malonamide **dimethyl dioctyl hexyl ethoxy malonamide**, DMDOHEMA (compound kindly supplied by Dr. Nicol, Marcoule, France) in mixtures with Cl-COSAN. Typical pattern for this compound

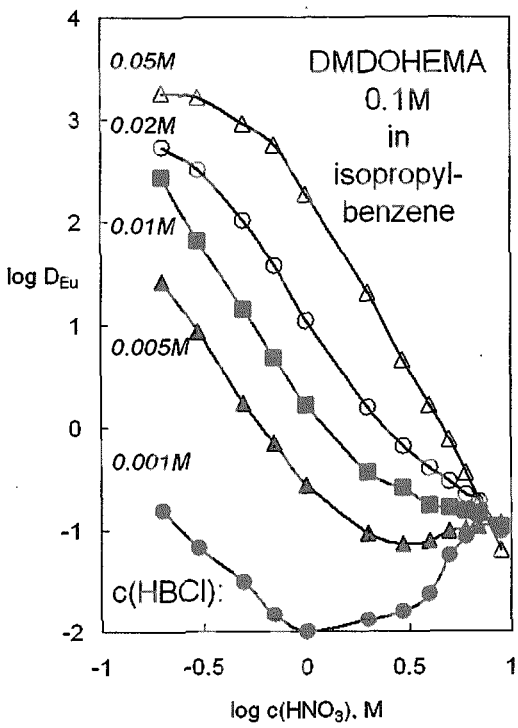

Fig. 9 Extraction of microamounts of Eu by 0.1M DMDOHEMA into isopropylbenzene with added HBCl, concentrations of HBCl given in Figure

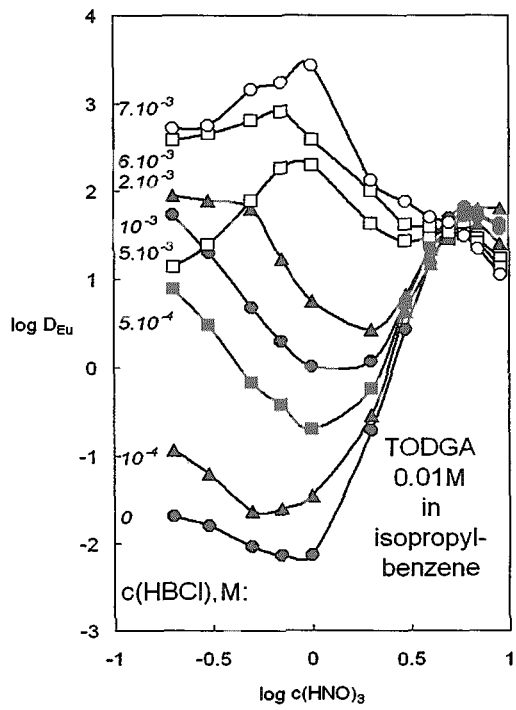

Fig. 10 Extraction of microamounts of Eu by 0.01M TODGA into isopropylbenzene with added HBCl, concentrations of HBCl given in Figure

is seen from Fig. 9. This does not differ much from the previously studied malonamides [4] and may be explained by applying the previous model [4, 5]. Namely, it is apparent that the particle Eu^{3+},xL.3NO^-_3 (where x = 2 or 3) existing in the organic phase in the absence of Cl-COSAN anion B^- is progressively substituted by Eu^{3+},xL.3B^-_3. The latter is much more hydrophobic than the former one; this explains large synergetic effect at low acidities.

More intriguing is the pattern with recently proposed tridentate ligand **tetraoctyl – 3 – oxapentane – 1,5 – diamide** (TODGA) from JAERI, Japan (compound kindly supplied by Dr. Tachimori), see Fig. 10. The behavior apparently can be divided into two separate regions, first, up to concentration of HBCl to $2x10^{-3}$M is characterized by gradual increase of D_{Eu} with increasing concentration of HBCl. In second region, the behavior is irregular and maximum appears at about 1M HNO_3. Interestingly enough for both reagents there exist an "isodistribution point" at which, disregarding the concentration of HBCl, the D_{Eu} is same, and this point lies nearly at the same concentration of nitric acid in the aqueous phase for both reagents. At present, the exact mechanism of extraction is yet to be elucidated. From practical point of view, the systems with malonamides can be used in extraction – strip cycles.

Certainly, it is not so for mixtures of TODGA with chlorinated dicarbollide. However, in the latter case conspicuously high D_{Eu} can be achieved from ca. 1M HNO_3 with very small concentrations of reagents (e.g. 0.01M TODGA + 0.005M HBCl, D_{Eu} = 200), so this variant might be well applicable for one-through process in which the organic extract is evaporated or destroyed.

NEW NONPOLAR SOLVENTS FOR Cl-COSAN

For a long time it was believed that a polar solvent is indispensable for the extractions with dicarbollides. In fact, the use of toxic nitrobenzene or other nitro – solvent was one of the main obstacles in implementing the dicarbollide process in several countries.

As seen above the choice of suitable solvents is broadened for several new substituted dicarbollides, enabling extractions into aromatic solvents like toluene, xylene etc. Also for mixtures of Cl-COSAN with particular synergists, as are bidentate phosphonates and malonamides or tridentate ligand TODGA, aromatic solvent like isopropylbenzene can be used.

In this work, we were mainly interested in finding out a nonpolar solvent for a basic process of ^{137}Cs and ^{90}Sr isolation. Moreover, the ultimate goal would be to have a solvent of the type of alkane used in PUREX process. Since dicarbollides are essentially insoluble in alkanes, a suitable modifier must be used and the question reduces to finding out such a modifier.

According to our detailed previous analysis of the data on Gibbs energies of transfer of univalent cations between two solvents [6], the main factor determining high selectivity is low basicity or donor number of the solvent. However, certain basicity is indispensable in the present case in order to form weak bonded H,S^+, BCl^- ion pair in nonpolar solvent. Other limiting factor at use of nonpolar solvents for HBCl is a formation of the third phase in the system; especially HBCl will tend to escape into a third phase of higher polarity formed from a mixture of two solvents - alkane and modifier. For extraction of Sr a suitable polyethylene glycol, PEG, must be added to the system and, as found by several preliminary experiments, the formation of the third phase is also strongly dependent on the type of the polyethylene glycol even if the PEG's are very similar. E.g., the results differed completely when using commercial PEG of m.w. 400 or similar $HO(CH_2CH_2O)_8(CH_2)_{11}CH_3$.

Thus, finding out appropriate recipe for a viable solvent combination is a question of fine-tuning of the kind and concentrations of used components. After number of experimental studies, we were successful at this task [7]. Only one working combination is shown here.

We have used TPH ("hydrogenated tetrapropene" used in France as a diluent in the PUREX process) as an alkane, dioctyl sebacate, DOS, as a modifier, and Slovafol 909 (p-nonylphenol nonaethylene glycol) as a synergist for Sr.

As is seen from Fig. 11, formation of the third phase takes place up to concentration of some 0.8 – 0.85M of DOS in TPH. The second organic phase was of lower volume and HBCl preferably concentrated in it what is also apparent from the distribution ratios of Cs and Sr between the aqueous phase and third organic phase shown in the Figure 11.

The system with no formation of third phase (1M DOS) can be used for extraction of both Cs and Sr from a medium of 1M HNO_3 with stripping of both radionuclides by some 4M HNO_3 as shown in Fig. 12.

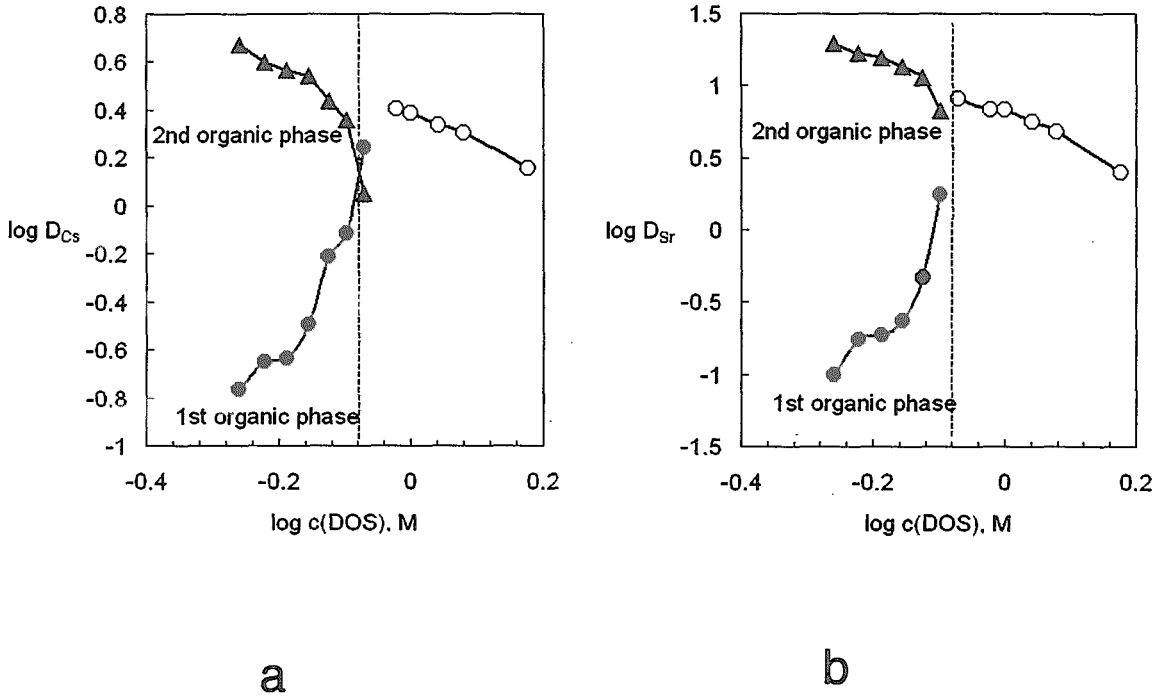

Fig. 11 Extraction of Cs and Sr from 1M HNO_3 by 0.12M HBCl and 0.4% Slovafol 909 into mixtures of dioctyl sebacate and TPH; a) extraction of Cs, b) extraction of Sr

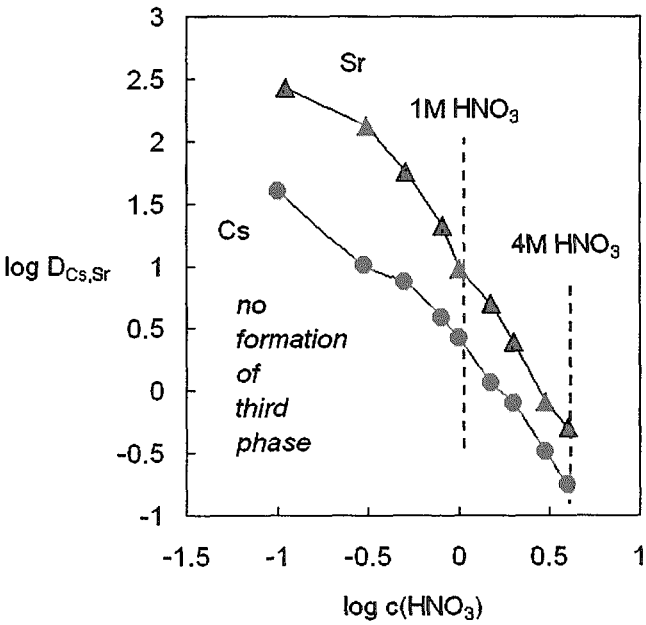

Fig. 12 Extraction of microamounts of Cs and Sr by 0.12M HBCl + 0.4% vol. Slovafol 909 into 1M DOS in TPH, dependence on acidity

CONCLUSIONS

The area of research in dicarbollide extractions is certainly not closed. Important achievements of the recent time are new dicarbollide derivatives with attached selective binding groups, new synergists for use with basic Cl-COSAN and newly proposed nonpolar nontoxic and cheap solvents based on the alkane solvent used in PUREX process.

ACKNOWLEDGEMENT

Authors are grateful to Dr. Nicol (CEA, Marcoule, France) and Dr. Tachimori (JAERI, Japan) for supply of new reagents. Our thanks are due to Dr. Císařová (Department of Inorganic Chemistry of the Faculty of Science of Charles university, Prague) for performing X – ray crystallographic studies. The works were financially supported by the Grant Agency of Czech Republic (Grants No.

104/01/0142 and 104/99/1096) and in the area of new boron compounds also by EEC Project IC15-CT98-0221.

REFERENCES

[1] V. Romanovski, UNEX process for Liquid Radioactive Waste Reprocessing, NUCEF 2001.
[2] B. Ya. Galkin, D. N. Shishkin, Extraction withdrawal of cesium and strontium radionuclides from the solution of spent nuclear fuel, Global 2001, September 9 – 13, 2001, Paris, France.
[3] L. H. Delmau, N. Simon, M. J. Schwing-Weill, F. Arnaud-Neu, J. F. Dozol, S. Eymard B. Tournois, C. Gruttner, C. Musigmann, A. Tunayar, V. Bohmer: Extraction of trivalent lanthanides and actinides by "CMPO-like" calixarenes, Separation Science and Technology 34, 863 (1999).
[4] J. Rais, P. Selucký, N. V. Šístková and J. Alexová, 2nd NUCEF Symposium, Hitachinaka, Japan, p. 215-225 (1998).
[5] J. Rais, P. Selucký, N. V. Šístková: Effect of anion and solvent in extractions of cations with neutral cation binding ligands, International Conference ATALANTE 2000, 24 – 26 October 2000, Avignon, France, p. 3-39.
[6] J. Rais, T. Okada: Linearities in Gibbs Energies of Transfer of Alkali Metal Cations between Two Solvents and a New Aspect of Resolvation Related to Gas Phase Data, J. Phys. Chem. A 2000, **104**, 7314.
[7] J. Rais, P. Selucký: Method of separation of radioactive cesium and strontium from acidic nuclear waste by extraction, Czech. Patent Appl., PV 2001 – 3468, (September 26, 2001).

JP0250312

JAERI-Conf 2002-004

AGGREGATION OF THE NEODYMIUM COMPLEXES OF HDEHP, CYANEX 272, CYANEX 302, AND CYANEX 301 IN TOLUENE

M. P. JENSEN,[1,*] R. CHIARIZIA,[1] V. URBAN,[2,3] and K. L. NASH[1]

[1]Chemistry Division, Argonne National Laboratory, Argonne, Illinois 60439 USA
[2]IPNS Division, Argonne National Laboratory, Argonne, Illinois 60439 USA
[3]Present address: European Synchrotron Radiation Facility, F-38043 Grenoble, France
[*] Fax: 1-630-252-7501, e-mail: mjensen@anl.gov

Visible absorption spectroscopy and small-angle neutron scattering have been used to study the morphology and aggregation of a series of purified acidic organophosphorus extractants with oxygen and sulfur donor atoms and the Nd(III) complexes of these extractants in toluene solutions. The extractants bis(2-ethylhexyl)phosphoric acid (HDEHP), bis(2,4,4-trimethylpentyl)phosphinic acid (HC272), bis(2,4,4-trimethylpentyl)monothiophosphinic acid (HC302), and bis(2,4,4-trimethylpentyl)dithiophosphinic acid (HC301) were studied. The phosphinic acid based extractants are the primary constituents of the commercial extractants Cyanex 272, Cyanex 302, and Cyanex 301 respectively. Small-angle neutron scattering experiments show that although 0.10 M solutions of the oxygen containing extractants HDEHP and HC302 are dimeric in toluene, HC301, which contains only sulfur donor atoms, is monomeric within the uncertainty of the experiment. When high concentrations of Nd (greater than 30% theoretical Nd capacity) are extracted into the organic phases, the oxygen containing extractants, HDEHP, HC272, and HC302 all form dinuclear complexes with a 2:6 metal:extractant ratio. The sulfur bearing extractant HC301, on the other hand, forms only 1:3 metal:extractant complexes when the Nd loading is less than 50% of the theoretical capacity of the solution. However, at higher Nd loading, 86% of the theoretical capacity, 2:6 Nd:C301 complexes are formed.

Key words: Solvent Extraction, Neodymium, Cyanex, Aggregation, Small-angle neutron scattering

1. INTRODUCTION

The chemistry of lanthanide and actinide cations with acidic organodioxophosphorus extractants like the dialkylphosphoric, -phosphonic, and -phosphinic acids has been well established by numerous studies of the tracer and macro scale extraction equilibria,[1] the coordination chemistry,[2-4] and even crystallization [5-7] of *f*-element-extractant complexes. The related acidic organophosphorus acid extractants that contain sulfur donors rather than oxygen donors are of interest for separating trivalent lanthanide and actinide cations. While the extraction equilibria of certain organo monothio- and dithiophosphorus extractants have been studied,[8-14] there is comparatively little information on the metal coordination or molecular structural of these sulfur containing complexes in organic solutions.

Fundamental studies of these extractants are important for developing useful separations processes, but the laboratory-scale studies are typically performed at low metal ion concentrations to discourage the formation of polynuclear aggregates in the organic phase. Industrial scale solvent extraction processes, on the other hand, usually are operated under conditions of high metal loading (i.e. high metal concentrations relative to the theoretical metal ion capacity of the extractant solution), which tends to promote the formation of polynuclear species. This work reports on the aggregation and morphology of a series of Nd^{3+} complexes at high metal loading in toluene with acidic organophosphorus extractants containing either two oxygen, one oxygen and one sulfur, or two sulfur donor atoms per extractant. The variation of the number of oxygen atoms attached to the phosphorus atom alters the acidity and hydrogen bonding characteristics of each extractant. In dilute metal ion solutions, this gives the *f*-ion complexes of dioxo, monothio, and dithio extractants different

structures and stoichiometries. Three of the ligands studied (Fig. 1) are the major components (75-90% [15]) of commercially available dialkylphosphinic acid based extractants intended for industrial scale processes: Cyanex 272 (bis(2,4,4-trimethylpentyl)phosphinic acid, HC272), Cyanex 302 (bis(2,2,4-trimethylpentyl)monothiophosphinic acid, HC302), and Cyanex 301 (bis(2,4,4-trimethylpentyl)-dithiophosphinic acid, HC301). The other extractant, bis(2-ethylhexyl)phosphoric acid or HDEHP, is the most extensively studied organophosphoric acid extractant. It is used for industrial scale intra-lanthanide separations.

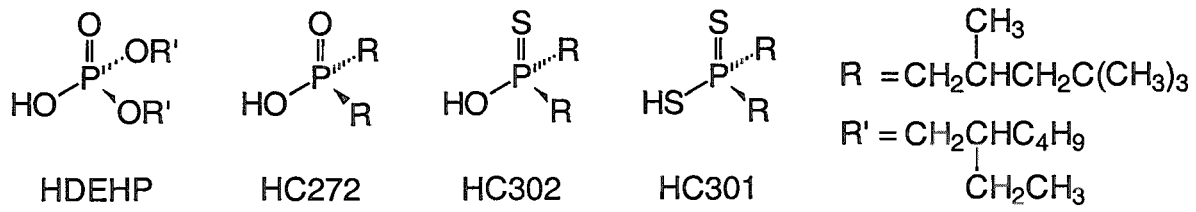

Fig. 1. Ligands used in this study

2. EXPERIMENTAL

Purification of the extractants, as described previously,[8, 16] resulted in purities of HDEHP: 99+%, HC272: 99%, HC302: 97%, and HC301: 99% as determined by ^{1}H and ^{31}P NMR. The extractants were dissolved in deuterotoluene (toluene-d_8 99 atom% D, Aldrich) to give 0.10 M solutions, except for HC272. The HC272 samples were not suitable for neutron scattering measurements because the maximum metal loading that could be achieved before the onset of precipitation was only 8% of the theoretical Nd loading capacity. (The theoretical Nd loading capacity is the maximum amount of Nd that would be present in the organic phase assuming that all of the extractant is present as Nd complexes with a 1:3 metal:extractant ratio). Therefore, HC272 was dissolved in normal, non-deuterated toluene (99.9%, Aldrich) for use in the spectrophotometric measurements. The organic phases were loaded with Nd by two phase titrations of aqueous 0.0337 M $Nd(ClO_4)_3$/0.10 M extractant in toluene with 1 M NaOH. Volume ratios of the organic to aqueous phases of 1.0 or 2.0 were used to vary the metal loading. Precipitates of the Nd-extractant complexes could be avoided if the NaOH titrant was added slowly in small increments. The concentration of Nd in the aqueous phases was determined by ICP-AES, and the organic phase Nd concentrations were calculated from the differences between the initial and final amount of Nd in the aqueous phases.

Small-angle neutron scattering (SANS) measurements on the HDEHP, HC302, and HC301 samples with and without Nd were made at the Argonne National Laboratory Intense Pulsed Neutron Source's time-of-flight Small-Angle Diffractometer, which was calibrated to give absolute scattering intensities. The instrument and data collection procedures have been described previously.[17-19] The SANS measurements were made at 22 ± 2 °C. The absorption spectra of the organic phases in 1.000 cm quartz cuvettes were measured from 350 to 850 nm using a modified Cary-14 spectrophotometer (OLIS, Inc.) at a fixed bandwidth of 0.06 nm and 25 °C. Fuller descriptions of the experimental conditions can be found in the literature.[20]

3. RESULTS

The results of a Guinier analysis [21] of the SANS data sets are summarized in Table I and Fig. 2. The neutrons are scattered most strongly by hydrogen atoms, which, in this case, are part of the extractant molecules. The presence of Nd, a comparatively poor neutron scatterer, is only observed indirectly, by its effect on the assembly of the small extractant molecules into

larger coordination complexes. Although Nd cations promote the assembly of extractant molecules into larger groups, none of the data sets show the telltale signs of large aggregates (aggregates composed of 20 or more monomers), increasing scattering intensity, *I(Q)*, for low values of *Q*, the momentum transfer.

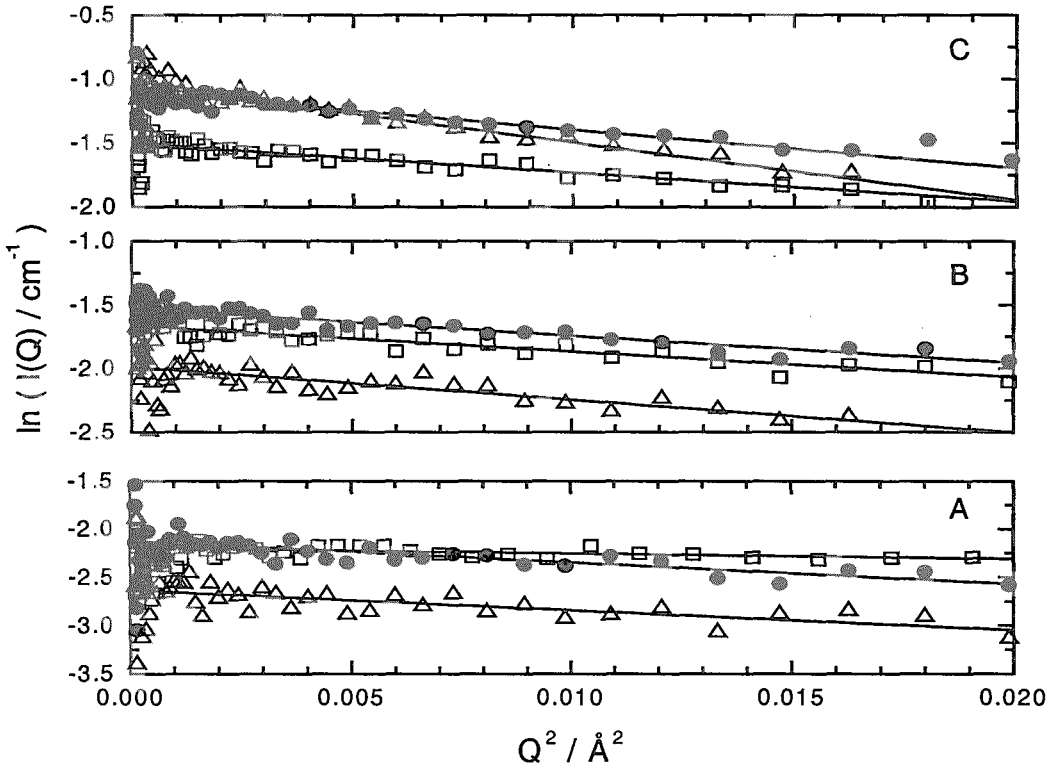

Fig. 2. Guinier plot of SANS data for (A) extractants only, (B) each extractant with lowest Nd loading, (C) each extractant with highest Nd loading, (□) HDEHP, (•)HC302, (Δ) HC301, and (—) linear least-squares fit.

The slope obtained from the Guinier analysis (when $QR_g \leq 1$) can be used to calculate the radius of gyration, R_g, which is a measure of the average spatial extension of the particles in the solution. The radius of gyration is the root-mean-squared distance of each atom in a particle from the center of gravity of the particle. This means that the geometric radius, diameter, or length of a given particle depends on the shape of the particle. For a spherical particle, for example, the actual geometric radius, *R*, is $(5/3)^{1/2}R_g$. The gyration radii increase when Nd is extracted into the solutions (Table I), demonstrating through simple geometry that the monomeric and dimeric molecules of extractant, which exist in the absence of the metal cations, are converted into larger, metal bound aggregates in the presence of Nd.

The magnitude and variation in the gyration radii suggest the presence of small aggregates in the solutions. The y-intercepts, *ln I(0)*, derived from the Guinier analysis can be used to calculate n_w, the weight average aggregation number of the extractant molecules in the scattering particles, using the equation

$$n_w = \frac{6.022\times10^{26} d_{HL} I(0)}{[L]_{total}\,\Delta\rho^2 MW_{HL}^2} = \frac{\sum_n n^2[(HL)_n]}{[L]_{total}},$$

where d_{HL} is the density of the undiluted extractant, $[L]_{total}$ is the total extractant concentration, $\Delta\rho$ is the difference of the scattering length densities of the extractant and solvent, and MW_{HL} is the molecular weight of the extractant.[18, 19]

Table I. Results of the Guinier analysis of the SANS data of the 0.10 M extractant solutions

HL	% Theoretical Nd Capacity	[HL]/[Nd]	R_g (Å)	n_w	Best n_w calc.	Modeled Nd Species
HDEHP	0		5.8 ± 1.7	2.0 ± 0.2		
	33	9.0	8.5 ± 0.6	3.3 ± 0.3	3.30	$Nd_2(DEHP)_6$
	36	8.2	8.0 ± 0.6	3.9 ± 0.3	3.43	$Nd_2(DEHP)_6$
HC302	0		9.2 ± 1.0	2.0 ± 0.2		
	48	6.3	8.2 ± 0.6	3.5 ± 0.3	3.89	$Nd_2(C302)_6$
	90	3.3	9.4 ± 0.4	5.3 ± 0.4	5.59	$Nd_2(C302)_6$
HC301	0		9.3 ± 0.6	1.07 ± 0.09		
	46	6.5	8.5 ± 1.0	2.0 ± 0.2	1.99	$Nd(C301)_3$
	86	3.5	11.9 ± 0.4	5.2 ± 0.4	5.33	$Nd_2(C301)_6$

All of the extractant species in the solution contribute to n_w and because each solution contains at least some uncomplexed extractant, the number of extractant monomers present in the Nd complexes cannot be directly derived from the aggregation numbers presented in Table I. However, the contribution of each species to n_w is directly proportional to its fraction of the total extractant concentration in the solution. Each n-mer of extractant, $(HL)_n$, which may or may not also contain Nd, contributes $n^2[(HL)_n]/[L]_{total}$ to n_w. This provides a mechanism to determine the predominant Nd species present even when there is a significant concentration of uncomplexed extractant. Assuming that $Nd(OH)_x^{3-x}$ or $Nd(ClO_4)_y^{3-y}$ complexes are not extracted under the conditions of the experiment, least-squares minimization of the n_w value calculated from a wide variety of integral Nd:extractant stoichiometries ($Nd_mL_£$ m = 1,2,3; £ = 3,4,5,6,9) should give the most probable formula of the predominant species. The best calculated n_w values and the corresponding Nd complexes are also summarized in Table I.

Only small concentrations of Nd could be dissolved in 0.10 M solutions of HC272 before a precipitate began to form. HDEHP, which could be loaded to ca. 35% of the theoretical Nd capacity under these conditions, was used for the SANS studies instead, assuming that the coordination and aggregation of the two dioxo extractants is similar. To support this assumption, the Nd coordination environment in the HC272 and HDEHP complexes was compared by visible absorption spectroscopy. The *f-f* transitions of Nd complexes are very sensitive to the coordination environment. The spectra of HDEHP and HC272 solutions between 500 and 625 nm are shown in Fig. 3 for solutions near each extractant's maximum Nd loading, and also for a HDEHP solution with low Nd loading. The spectra measured near the highest achievable Nd loading are indistinguishable, which indicates a similar coordination environment, i.e. Nd_2L_6, for both complexes. The intensity of the absorption bands are significantly lower for the Nd-HDEHP complex at high extractant concentration (1.5 M) and low Nd loading (3%), indicating the presence of a different complex.

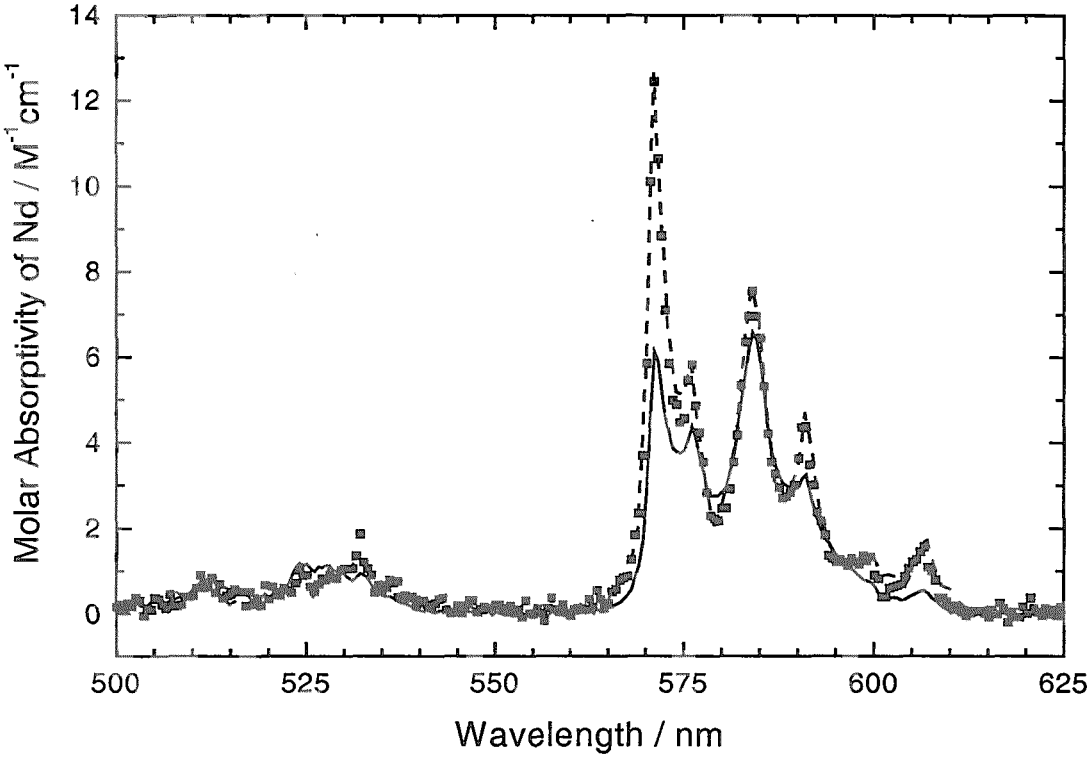

Fig. 3. Hypersensitive $^4I_{9/2} \rightarrow {}^4G_{5/2}$, $^2G_{7/2}$ transitions for the Nd^{3+} complexes of HDEHP and HC272, (—) low (3%) Nd loading of 1.5 M HDEHP in dodecane, (- -) high (8%) Nd loading of 0.10 M HC272 in toluene, and (■) high (33%) Nd loading of 0.10 M HDEHP in toluene.

4. DISCUSSION

The properties of the unpurified, commercial grade Cyanex extractants have been reported in the literature previously. Vapor phase osmometry has demonstrated that HC272 and HC302 exist primarily as dimeric species, $(HL)_2$, in non-polar organic solvents in the absence of metal ions, while the results of a variety of techniques have shown that dithiophosphinic and dithiophosphoric acids related to HC301 are primarily monomeric at concentrations below ca. 0.2 M.[22] These findings are completely corroborated by the SANS measurements presented here. At extractant concentrations of 0.10 M in deuterated toluene, the oxygen containing extractants exist as $(HDEHP)_2$ and $(HC302)_2$ ($n_w = 2.0 \pm 0.2$). In contrast, HC301, which does not contain any oxygen can be considered monomeric within the experimental uncertainty of the measurement ($n_w = 1.07 \pm 0.09$). The S-H···S hydrogen bonds required to form dimers of HC301 are much weaker than the O-H···O and S-H···O bonds found in $(HDEHP)_2$ and $(HC302)_2$.[23] They are too weak to promote dimerization of HC301 under these conditions.

The combination of the SANS data and the visible absorption spectra provide unequivocal evidence of the formation of dinuclear 2:6 (Nd:extractant) complexes for each of the extractants under certain conditions. The average aggregation number calculated for Nd_2L_6 (Table I) gives the best agreement with the measured aggregation numbers for all of the Nd containing solutions except for the HC301 solution at low loading (46% theoretical capacity). In this case, the 1:3 complex $Nd(C301)_3$ is superior at reproducing the measured value of n_w, which is 2.0_4 (calculated n_w = 1.99). As an example of the superiority of $Nd(C301)_3$ in

reproducing the measured aggregation number, the hypothetical complex $Nd(C301)_3(HC301)$ in the 46% Nd loaded HC301 solution gives a calculated n_w = 2.90, while the dinuclear complex $Nd_2(C301)_6$ gives a calculated n_w = 3.39. Other Nd:L stoichiometries were even worse at reproducing the measured aggregation number.

The presence of 1:3 and 2:6 Nd:L complexes in the organic phases agrees with the known structural chemistry of dithiophosphinate and monothiophosphinate complexes. Crystal structures of discrete 1:3 and 1:4 $R_2PS_2^-$ complexes of trivalent lanthanide cations have been reported in which steric constraints force the smaller trans-Nd lanthanide cations to form only the 1:3 complex with bis(cyclohexano)dithiophosphinic acid,[24] while Nd crystallized both as 1:3 and as 1:4 complexes. Both mononuclear 1:2 and dinuclear 2:4 M:L complexes of dithiophosphinic acid ligands with divalent *d*-transition metal cations have also been known for some time. The metal centers of the 2:4 complexes are bridged by two dithiophosphinate ligands, and each metal center is capped with an additional bidentate $R_2PS_2^-$ ligand.[25, 26] Similar structures for *d*-transition metal complexes of phosphinic and monothiophosphinic acid ligands are also known. The dinuclear lanthanide complexes of bis(methyl)-monothiophosphinic acid have also been studied by x-ray crystallography,[27, 28] and several different structures, with and without bridging sulfur atoms, were observed.

The Nd_2L_6 stoichiometry reproduces the values of n_w better than any other single species for the extractants that contain at least one oxygen atom, HDEHP and HC302. However, the calculated n_w values of the 2:6 Nd:C302 complexes are both modestly larger than the experimentally determined values, suggesting that smaller amounts of other species, possibly $Nd(C302)_3$,[22] could be present in the solution. An organic phase containing 99.5 mM HC302 and 15.8 mM Nd with an experimental $n_w = 3.52 \pm 0.26$ (the 48% theoretical capacity sample), could be composed of 4.3 ± 2.9 mM $Nd(C302)_3$ and 5.8 ± 1.4 mM $Nd_2(C302)_6$. An organic phase containing 99.5 mM HC302 and 29.8 mM Nd with an experimental $n_w = 5.34 \pm 0.40$ (the 90% theoretical capacity sample), could be composed of 2.8 ± 4.4 mM $Nd(C302)_3$ and 13.5 ± 2.2 mM $Nd_2(C302)_6$. By itself, the SANS data does not offer guidance in selecting between a $Nd_2(C302)_6$ only model or one that includes $Nd(C302)_3$ and $Nd_2(C302)_6$, but the absorption spectra are useful here. If the absorption spectra of $Nd(C302)_3$ and $Nd_2(C302)_6$ are different, which is likely since the absorption spectra of $Nd(C301)_3$ and $Nd_2(C301)_6$ are clearly different, the change in Nd speciation that would be caused by increasing the Nd loading when multiple Nd species are present would give the two solutions different absorption spectra. The visible absorption spectra of the Nd containing HC302 solutions are identical within the experimental uncertainty in the Nd concentration.[20] The equivalence of the Nd-HC302 spectra is a strong indication that the relative concentration of the Nd species is the same in both solutions, and, as a consequence, that $Nd_2(C302)_6$ is the only significant species in both solutions.

The absorption spectra of the Nd complexes with the dioxo ligands HDEHP and HC272 support and extend the findings of the SANS measurements. In the 0.10 M HDEHP solutions, a precipitate began to form when the Nd loading exceeded ca. 40% of the theoretical Nd capacity of the extractant with a 1:3 Nd:L ratio. Precipitation began at much lower Nd loadings (8% theoretical capacity) for the Nd containing solutions of the phosphinic acid extractant, HC272. Despite the difference in the loading capacities of the two extractants, the absorption spectra of the $Nd_2(DEHP)_6$ solution at 33% Nd loading and the Nd-HC272 solution at 8% Nd loading are indistinguishable (Fig. 3). This demonstrates that the Nd-HC272 complex has the same stoichiometry and coordination geometry as the HDEHP complex, $Nd_2(C272)_6$, even though the absolute Nd loading is significantly lower in the HC272 solution. The spectra in Fig. 3 also show that a different complex with different oscillator strengths, presumably the mononuclear $Nd[H(DEHP)_2]_3$ or $Nd(DEHP)_3$ complexes

observed at low metal loadings,[29, 30] predominates at high HDEHP concentrations and low (3%) Nd loading. The precise conditions of the formation of the 2:6 Nd:L complexes of dialkylphosphoric and dialkylphosphinic acid extractants is not a simple function of the metal loading. The mechanisms that affect the relative solubility of the complexes in the organic phase, like the nature of the alkyl groups and the extractant basicity, also appear to affect the formation of small oligomeric species, with the less soluble complexes forming oligomers at lower metal loadings. The Nd_2L_6 complexes that are observed for each of the ligands near Nd loadings that cause precipitate formation seem to be a discrete step from mononuclear complexes, like NdL_3, to neutral polymeric species with a metal:ligand ratio of n:3n that eventually become insoluble in the organic solvent.

5. ACKNOWLEDGEMENTS

The authors thank P. G. Rickert for purifying the extractants and D. Huff and S. Lopykinski of the Argonne Analytical Chemistry Laboratory for the ICP-AES determinations. This work was performed under the auspices of the Office of Basic Energy Sciences, Divisions of Material Science (for the SANS measurements made at the Intense Pulsed Neutron Source) and Chemical Sciences, U. S. Department of Energy under contract number W-31-109-ENG-38.

6. REFERENCES

[1] T. Sekine and Y. Hasegawa, "Solvent Extraction Chemistry", Marcel Dekker, New York (1977).
[2] T. Takahashi, Y. Suzuki and A. Yamasaki, "Solvent Extraction 1990: Proceedings of the International Conference on Solvent Extraction (ISEC'90)", Kyoto, Japan, Ed. By T. Sekine, Elsevier, New York, 189-193 (1992).
[3] Y. A. Barbanel and N. K. Mikhailova, Russ. J. Inorg. Chem., 18, 365-368 (1973).
[4] J. V. Beitz and J. C. Sullivan, J. Less-Common Met., 148, 159-166 (1989).
[5] V. G. Lebedev, K. K. Palkina, S. I. Maksimova, E. N. Lebedeva and O. V. Galaktionova, Russ. J. Inorg. Chem., 27, 1689-1690 (1982).
[6] D. N. Suglobov, Y. I. Trifonov, E. K. Legin and A. G. Tutov, J. Alloys Compd., 213-214, 523-527 (1994).
[7] A. Tomita, T. Kanki, T. Asano and N. Sano, J. Chem. Eng. Japan, 33, 661-664 (2000).
[8] Y. Zhu, J. Chen and R. Jiao, Solvent Extr. Ion Exch., 14, 61-68 (1996).
[9] Y. Zhu, J. Xu, J. Chen and Y. Chen, J. Alloys Compd., 271-273, 742-745 (1998).
[10] G. Modolo and R. Odoj, J. Alloys Compounds, 271-273, 248-281 (1998).
[11] C. Hill, C. Madic, P. Baron, M. Ozawa and Y. Tanaka, J. Alloys Compd., 271-273, 159-162 (1998).
[12] H. Hoshi, A. Tsuyoshi and K. Akiba, J. Radioanal. Nucl. Chem., 243, 621-624 (2000).
[13] Y. Zhu and R. Jiao, Radiochim. Acta, 69, 191-193 (1995).
[14] D. Li, A. Luo, C. Wang and M. Yuan, "Value Adding Through Solvent Extraction: Proceedings of the International Solvent Extraction Conference (ISEC'96)", Melbourne, Australia, Ed. by D. C. Shallcross, R. Paimin and L. M. Prvcic, University of Melbourne, Melbourne, 165-170 (1996).
[15] K. C. Sole and J. B. Hiskey, Hydrometallurgy, 30, 345-365 (1992).
[16] J. A. Partridge and R. C. Jensen, J. Inorg. Nucl. Chem., 31, 2587-2589 (1969).
[17] P. Thiyagarajan, H. Diamond, P. R. Danesi and E. P. Horwitz, Inorg. Chem., 26, 4209-4212 (1987).

[18] R. Chiarizia, V. Urban, P. Thiyagarajan and A. W. Herlinger, Solvent Extr. Ion Exch., 16, 1257-1278 (1998).
[19] R. Chiarizia, V. Urban, P. Thiyagarajan, A. H. Bond and M. L. Dietz, Solvent Extr. Ion Exch., 18, 451-478 (2000).
[20] M. P. Jensen, R. Chiarizia and V. Urban, Solvent Extr. Ion Exch., 19(5), in press (2001).
[21] A. Guinier and G. Fournet, "Small Angle Scattering of X-rays", John-Wiley and Sons, New York (1955).
[22] M. P. Jensen and A. H. Bond, Radiochim. Acta, submitted.
[23] G. Allen and R. O. Colclough, J. Chem. Soc., 3912-3915 (1957).
[24] A. A. Pinkerton, Y. Meseri and C. Rieder, J. Chem. Soc. Dalton Trans., 85-90 (1978).
[25] M. Calligaris, A. Ciana, S. Meriani, G. Nardin, L. Randaccio and A. Ripamonti, J. Chem. Soc. A, 3386-3392 (1970).
[26] G. Svensson and J. Albertsson, Acta Chem. Scand., 45, 820-827 (1991).
[27] K. M. Mühlsiepen and R. Mattes, Z. Anorg. Allg. Chem., 506, 115-124 (1983).
[28] K. M. Mühlsiepen and R. Mattes, Z. Anorg. Allg. Chem., 506, 125-132 (1983).
[29] J. M. Sánchez, M. Hidalgo, V. Salvadó and M. Valiente, Solv. Extr. Ion Exch., 17, 455-474 (1999).
[30] D. F. Peppard, G. W. Mason, J. L. Maier and W. J. Driscoll, J. Inorg. Nucl. Chem., 4, 334-343 (1957).

Radioactive Waste Disposal

This is a blank page.

JP0250313

JAERI-Conf 2002-004

OVERVIEW OF THE MAIN RESULTS CONCERNING WASTE MANAGEMENT IN FRANCE

PH. LECONTE

Nuclear Energy Division

CEA- Saclay, 91191 Gif sur Yvette, Cedex, France

France has launched a process of optimizing waste management by separating and recycling recoverable energy materials, reducing, conditioning and storing final waste. Once operations in the back-end of the cycle have been completed, long-lived highly radioactive waste (vitrified waste) represents the major portion of the waste's total radioactivity (99%), conditioned in a small volume (~ 150m^3/year of glass packages). Nevertheless, the radioactive content of the waste constitutes a potential risk for human beings and environment. The French Law of December 30,1991 set the major orientation for the public policy in the field of HLLW management, and constitutes the first global legislative instrument in that field. It prescribes the research areas to be explored in order to exploit the broadest range of scientific and technical expertise and to provide the elements needed to allow choices on how best to manage long-lived highly radioactive waste. The law set out three areas of R&D:

- minimization of the quantity and toxicity of waste, by studying their partitioning and transmutation;
- packaging and conditioning of long-lived radioactive materials in order to ensure safe and long-lasting containment, and also studying long-term storage;
- evaluation of the feasibility of a deep geological disposal whether reversible or irreversible; underground laboratories are essential tools for this research program.

Public authorities have designated a pilot for each area: the French Atomic Energy Commission (CEA) for partitioning-transmutation, and for conditioning and long term storage, and the National Radioactive Waste Management Agency (ANDRA) for disposal in geological formations.

The law defined a calendar which stipulates that a comprehensive report evaluating research will be submitted to the French Parliament in 2006, and decide whether it is appropriate to create a repository for HLLW.

Research is conducted in the framework of cooperation among CEA, Andra, partners in the nuclear industry – EDF, Cogema and Framatome – and in research – the French National Council for Scientific Research, CNRS, and universities. It benefits from significant cooperation at the European and international levels. It is constantly

evaluated by the National Evaluation Commission (CNE), which draws up and publishes an evaluation report annually.

The objective is to identify a set of complementary scientific and technical solutions, which serve to define open and flexible strategies for the back-end of the cycle and lay the groundwork for a decision in 2006.

The results already obtained and the future prospects will be presented in the paper. The most outstanding results lay in the domain of partitioning and in the domain of the assessment of the long term behavior of packages in storage or in deep geological disposal conditions.

JP0250314

JAERI-Conf 2002-004

R&D ON DISPOSAL CONCEPT FOR HIGH-LEVEL RADIOACTIVE WASTE: TECHNICAL SUBJECT ON HLW DISPOSAL AT COASTAL AREA IN JAPAN

M. KAWANISHI, T. HASEGAWA, T. IGARASHI*, H. TSUCHI ** and F. ONO ***

Central Research Institute of Electric Power Industry, 1646 Abiko, Abiko-shi, Chiba-ken., 270-1194 Japan, Fax: +81-471-82-2243, e-mail: kawanisi@criepi.denken.or.jp ,t-hase@criepi.denken.or.jp

* Graduate School of engineering, Hokkaido University, Kita 13, Nishi 8, Kita-ku, Sapporo, 060-8628 Japan Fax: +81-11-706-6308, e-mail: tosifumi@eng.hokudai.ac.jp

**Nuclear Waste Management Organization of Japan, (Mita NN Bldg.) 1-23, Shiba 4-Chome, Minato-ku, Tokyo, 108-0014 Japan, Fax: +81-3-4513-1599, e-mail: htsuch@numo.or.jp

*** Tokyo Electric Power Company, 1-3 Uchisaiwai-cho 1-Chome, Chiyoda-ku, Tokyo, 100-0011 Japan Fax: +81-3-3596-8562, e-mail: ono.fumihiko@tepco.co.jp

In Japan, the concept for high-level radioactive waste (HLW) disposal has been mainly studied in the based on the data of inland. However, Japan is an island country, so it is necessary to make clear the feasibility of coastal repository concept. In this paper, the present status of the research and development(R&D) for the repository concept, especially for coastal one in Japan is described. Based on the results of the R&D, we summarized the outline of feasibility and picked up the technical subject for future development on those repository concepts. From these results, it was shown that there is enough feasibility for the coastal concept as well as inland type of repository concept in Japan. Furthermore, for the coastal repository concept, there might be some technical subjects such as the influences of salinity, uplift/subsidence, sea-level change etc. on the performance of repository and it is necessary to proceed further R&D on these.

Key words: high-level radioactive, disposal concept, deep sub-seabed, coastal area, salinity influence, performance assessment

1. INTRODUCTION

In Japan, the law relating to final disposal of "specified" radioactive wastes was officially announced in June 2000[1]. Based on this law, the Nuclear Waste Management Organization of Japan (NUMO) was established in order to promote the implementation of disposal of HLW(vitrified waste) originating from nuclear power generation in October 2000. It is more important to proceed smoothly with the siting investigation for preliminary area and establish the rational concept of repository appropriate for several types of site condition in Japan. Until now, the HLW disposal concept has been mainly studied in the representative reports[2,3] based on the data of inland in Japan. However, Japan is an island country, so it is necessary to make clear the feasibility of coastal repository concept.

In this paper, the present status of the research and development(R&D) for the repository concept, especially for coastal one in Japan is described. Based on the results of R&D, we summarized the outline of feasibility and picked up the technical subject for future development on those repository concepts.

From these results, it was shown that there is enough feasibility for the coastal concept as well as inland type of repository concept in Japan. Furthermore, for the coastal repository concept, there might be some technical subjects such as the influences of salinity, uplift/subsidence, sea-level change etc. on the performance of repository and it is necessary to proceed further R&D on these[4,5].

2. AIMS OF THIS STUDY

Japan is an island country, so it might be more rational from the viewpoint of transportation etc. to site the repository of HLW in the deep geological formations or sub-seabed at the coastal area. Especially, for the deep sub-seabed repository concept, it is considered that there might be advantages to be able to reduce the performance of engineered barrier system (EBS) due to the very low groundwater flow velocity field. On the contrary, such a repository concept might have any disadvantages like salinity influences against the performance of the engineered or natural barrier system of repository. Fig.1 shows the illustrated concept of the groundwater and repository system at the coastal area.

In this paper, we show the outline of feasibility for HLW disposal at the coastal area, especially for the deep sub-seabed disposal concept considering the conditions of topographical, geo-hydrological, geo-chemical and geological environmental change of the Japan islands, so that we make clear the advantages or disadvantages of such a repository concept and the technical subject on the future R&D for establishing the more rational repository concept in Japan.

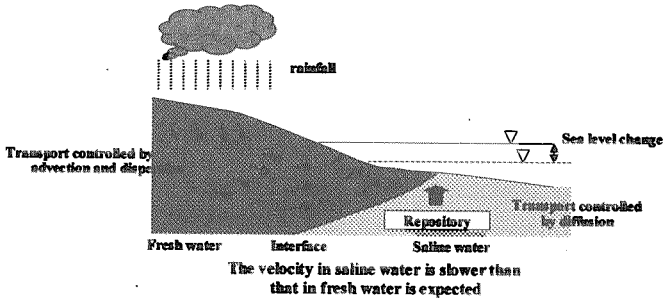

Fig.1 Conceptual model of groundwater flow at seashore

3. FEASIBILITY STUDY ON SUB-SEABED REPOSITORY CONCEPT

3.1 Topographical feature of Japanese Islands

The Japanese islands are located in the Pacific Ocean, surrounded by sea and with the continental shelf. In case of discussing the feasibility of HLW disposal at costal area in Japan, it is necessary to consider the long term stability for conditions of sea-level change, up-lift/ subsidence relating to the groundwater or intrusion scenario of the safety assessment. Fig.2 shows the representative contour lines of the elevation with a few hundred meters depth of seabed on the continental shelf around the Japan islands[4]. In this study, the feasibility of sub-seabed disposal concept is investigated considering the sea-level change and the topographic steep- or gentle- slope coastal site conditions.

3.2 Literature survey for observed data

Until now, the HLW disposal concept has been mainly studied for the deep repository of inland in Japan, so there is not so enough own data observed for the investigation of feasibility on the deep sub-seabed repository concept. Therefore, at the first step of feasibility study like this, it is necessary to survey the literatures including the existent observed data for

the undersea railroad tunnel and so on. For example, Fig.3 shows the data of chemical properties for the groundwater samples taken at a coal mine at the Hokkaido Area. It is shown that the saline groundwater under the coal-bearing formation is not the seawater based on this data and so on.

In this study, we investigate the feasibility of sub-seabed repository concept based on the literature survey data as follows.

3.3 Sea-level changes

Fig. 4 shows an example of sea-level changes during the past 350,000 years[3]. The sea level changed periodically by more than 100m during about 100,000 year cycles. In case of evaluating the effect of seawater intrusion into the groundwater, it is necessary to consider the sea-level changes, uplift/subsidence as well as topographical conditions et al. at coastal areas.

3.4 Groundwater flow modeling

As a preliminary performance assessment of deep sub-seabed disposal, we studied the feasibility of the disposal concept[4,5] as follows.

(1) Topographical site condition and discretization by finite element method

In this study, two different types of site condition were selected and the groundwater flow modeling relating to the sub-seabed geological disposal near coastal areas in Japan was conducted. The first site is a topographically gentle-slope site (Fig.5a) where is basically in continental shelf. The second one is a topographically steep-slope site (Fig.5b). The degree of effect for the sea-level changes and uplift/subsidence may be different between two sites. It shall be greater at the topographically gentle-site than the steep one.

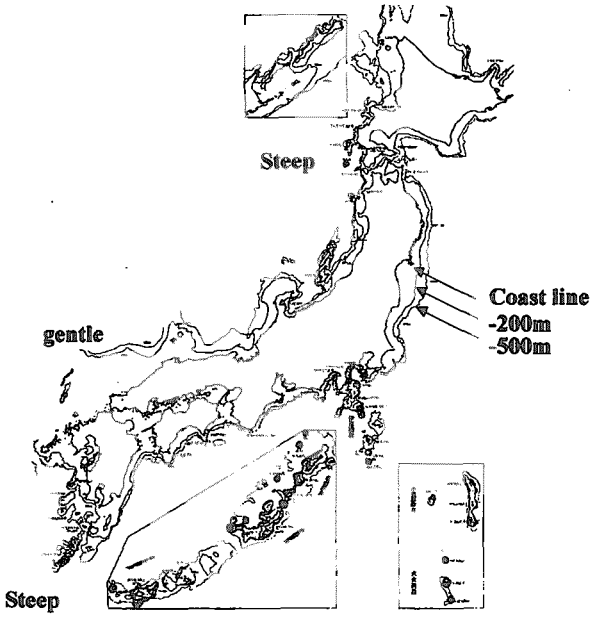

Fig.2 Seabed contour map around Japan

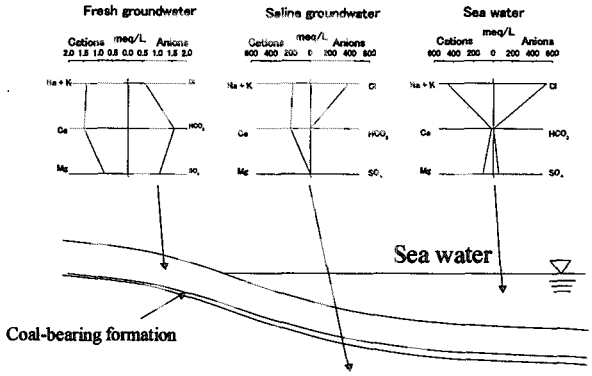

Fig.3 Example of observed data for distribution of fresh Groundwater and saline groundwater at seashore (T-coal mine, Hokkaido)

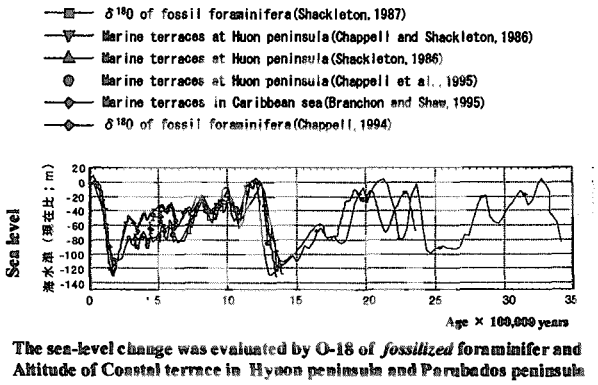

Fig.4 Sea-level changes during the past 350,000 years [3]

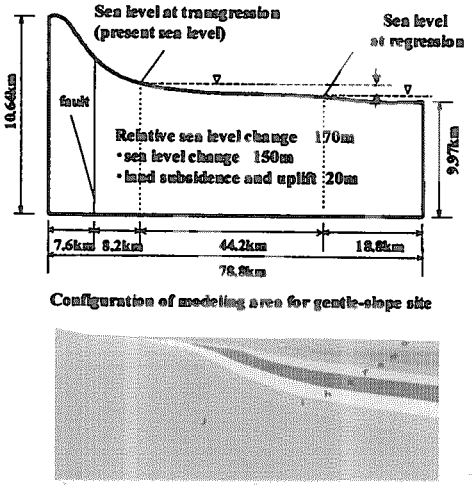

Fig.5a Geological formation and finite element discretization for gentle-slope site

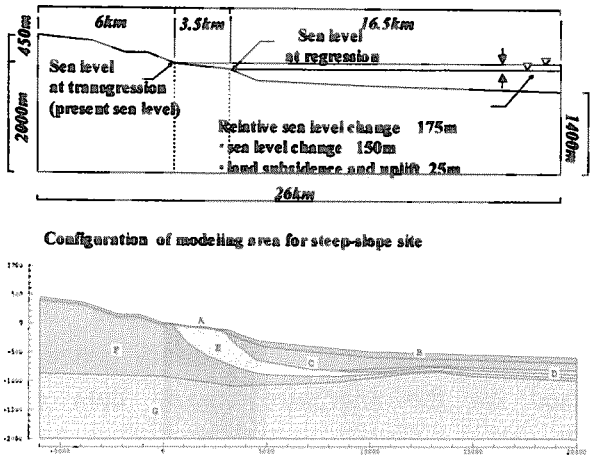

Fig.5b Geological formation and finite element discretization for steep-slope site

(2) Boundary conditions for groundwater flow analysis

Fig.6 shows the schematic view of boundary conditions for groundwater analysis. In this analysis, the sea-level changes due to the transgression and regression are considered as mentioned in Section 3.3.

(3) Results of groundwater flow analysis

Fig7a shows a normalized contour map of salinity and the velocity distribution calculated at transgression period for the gentle-slope site in this case study. Fig.7b is a result at regression period for the gentle-slope site.

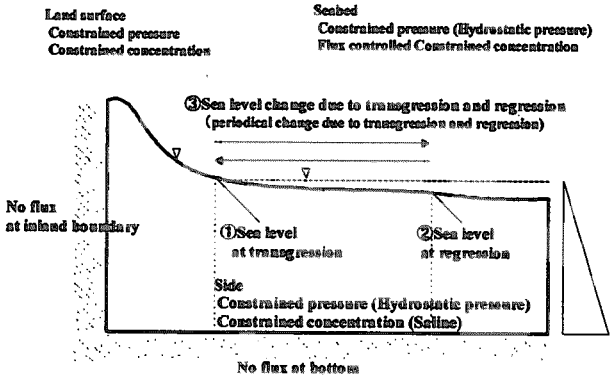

Fig6 Boundary conditions on groundwater flow

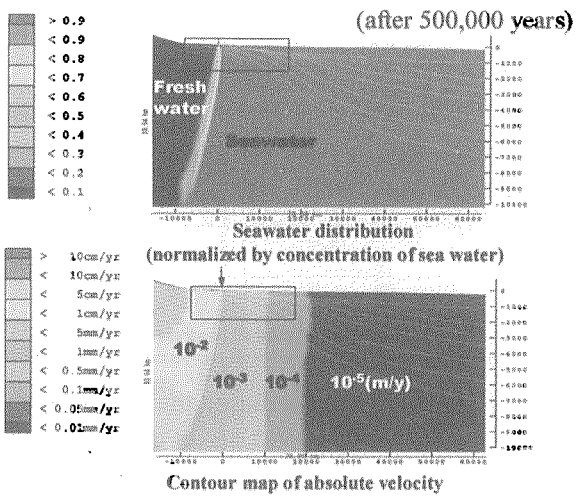

Fig7a Salinity and velocity distribution at transgression (gentle slope site)

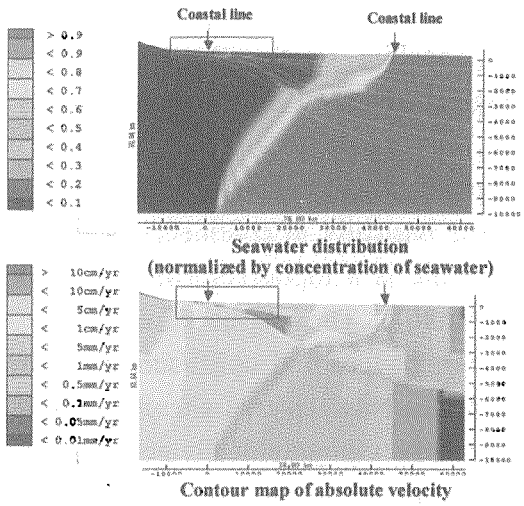

Fig7b Salinity and velocity distribution at regression (gentle slope site)

On the other hand, Fig.8a and 8b shows respectively the results with trajectory lines of flow pathway at transgression and regression period for the steep-slope site. The results show that the groundwater in seawater condition flows downward and that its velocity is one to two order slower than that in the fresh-water condition. However, for the gentle-slope site, the groundwater changes fresh to seawater at sub-seabed due to regression, even if the groundwater is saline at present condition. The difference in the velocity between minimum values and maximum values for the gentle-slope site was smaller than that the difference for the steep-slope site. These results depend on the topographical gradient and the movement of saltwater-freshwater interface due to the sea-level changes.

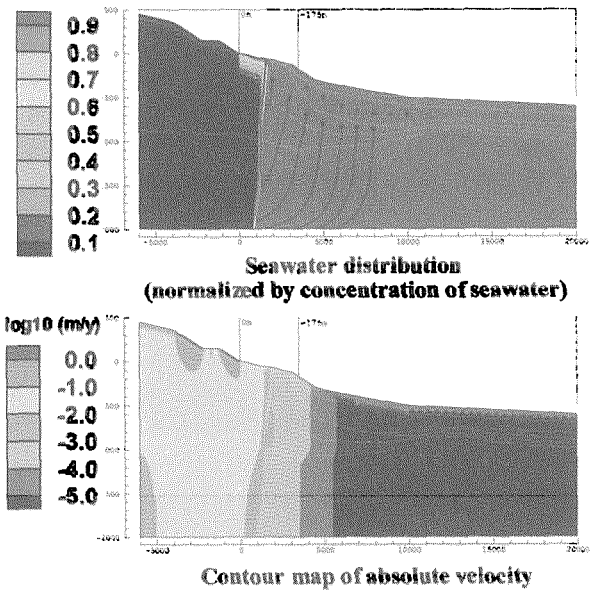

Fig.8a Salinity and velocity distribution with trajectories at transgression(steep-slope site)

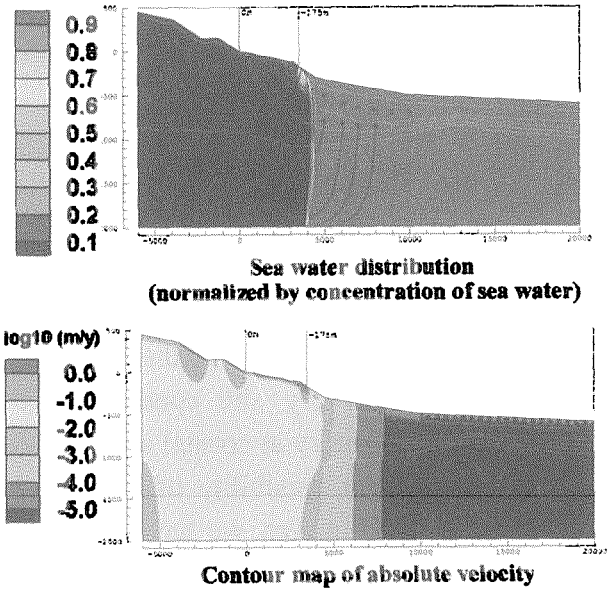

Fig.8b Salinity and velocity distribution with trajectories at regression(steep-slope site)

(4) Performance assessment

Radionuclide transport is evaluated by one-dimensional advection-dispersion analysis based on the trajectories calculated by groundwater flow analysis mentioned above. The results show that the main feature of transport is diffusion in saline condition and advection in fresh-water condition. This indicates that the groundwater flow near the boundary is very sensitive to the location. The seawater and fresh-water boundary caused by regression and transgression is shown to be important. Fig.9 shows the schematic flow of performance assessment of engineered barrier system and safety assessment for repository. Fig 10 shows an example of results of preliminary safety assessment for the sub-seabed repository sites with gentle-slope or steep-slope condition. The location of a repository might be changed from 1 to 6 km

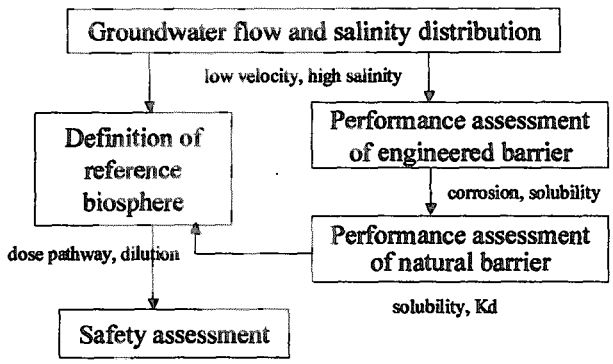

Fig.9 Schematic flow of performance assessment for engineered barrier system of repository

from coastal line, because the conditions of flow and salinity of groundwater might depend on the location. Discontinuity was found at t=120,000 years. In particular, that is remarkable for the steep-slope site because the groundwater of 4km offshore was suddenly changed from saline to fresh at that period. However, the difference between both sites was not remarkable, and the maximum dose rate was sufficiently low compared with that for the island disposal case[2,3].

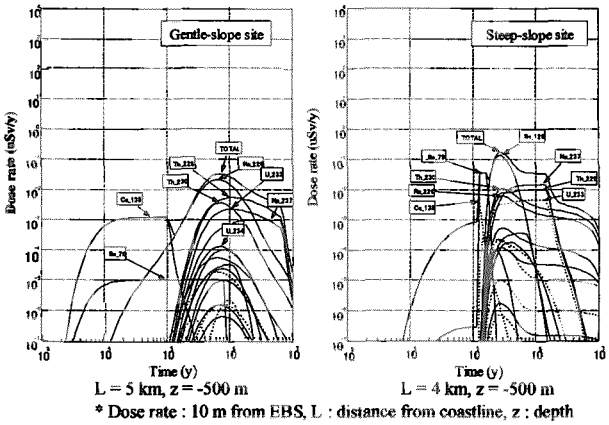

Fig.10 Results of preliminary safety assessment for sub-seabed disposal trajectories at gression(steep-slope site)

4. CONSIDERATION FOR FEASIBILITY OF REPOSITORY CONCEPT AT COASTAL AREAS

Fig.11 shows an example of options for the repository at coastal area. As shown in the preliminary case study for the feasibility of sub-seabed repository site conditions as an example of repository at coastal area, basically, there is sufficient feasibility of such type of repository. However, we have not enough data to establish the more detailed repository concept at coastal area, so it is necessary to consider the advantages or disadvantages and investigate the technical subjects for this type of repositories at near coastal areas.

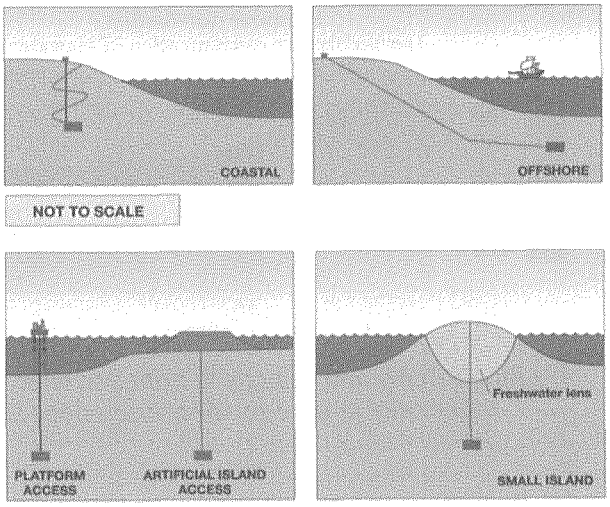

Fig.11 Option of HLW disposal concept at coastal area

The representative advantages and disadvantages might be as follows:

(advantage) ①Low groundwater flow velocity (diffusion > advection)
②Rational transportation and infrastructure
③Restriction of pathway in the biosphere

(disadvantage) ①High salinity (chemical influences to materials of bentonite, cement or over-pack, rocks, groundwater, radionuclide migration and so on)
②Uplift/Subsidence, Sea-level change (human intrusion scenario et al.)
③Site characterization techniques

For the disadvantages that are the future R&D subjects, furthermore, we need to investigate and integrate the technology for establishing the reasonable repository concepts based on each site conditions.

5. CONCLUSION REMARKS

In this paper, the feasibility study for the sub-seabed disposal at near coastal areas in

Japan was described. From these results, it was shown that there is enough feasibility for the coastal concept as well as inland type of repository concept in Japan.

From now on, the selection plan for the preliminary investigation areas will be started by NUMO. We expect that the results of this study will be reflected in proceeding such siting approach flexibly and steadily.

REFERENCES

[1] Specified Radioactive Waste Final Disposal Act, (2000).

[2] Central Research Institute of Electric Power Company and Federation of Electric Power Companies, Execution Techniques for High-Level Radioactive Waste Disposal, (1999).

[3] Japan Nuclear Cycle Development Institute, H12: Project to Establish the Scientific and Technical Basis for HLW Disposal in Japan, (2000).

[4] T. Igarashi, T. Hasegawa, CRIEPI's Research on Deep Sub-seabed Disposal of HLW Near Coastal Areas, Performance Assessment of Deep Sub-seabed Disposal of HLW Near Coastal Areas, Coastal Workshop for a Deep Repository for HLW: Topical Workshop, NAGRA, (2000).

[5] T. Hasegawa, et al., Study on Groundwater Flow Behavior for Sub-seabed Disposal at Coastal Areas, JSCE Annual Symposium, No.56, (2001).

This is a blank page.

JP0250315

JAERI-Conf 2002-004

Separated Disposal of HLW Wastes for Reducing the Total Occupational Area of the Repository

OHE Toshiaki, NAKAMURA Kiyone,
TSUKAGOSHI Atsushi, and NISHIYORI Takehiro

Energy Engineering Course, Applied Science Dept., Tokai University
1117, Kita-Kaname, Hiratsuka, 259-1292, JAPAN
FAX: +81-0463-50-2017, e-mail : ohe@keyaki.cc.u-tokai.ac.jp

This paper describes the efficiency of the segregated disposal to reduce the total load of the high-level waste into the repository. (1) The nuclides were classified into several groups having similar properties by using the cluster analysis. (2) The disposal depth required the maximum dose rate of each group was less than 10_ Sv/y was assigned by the simple migration analyses. (3) Disposal density were calculated by the thermal analysis to maintain the maximum temperature rise below 100°C. The grouping and configuration analyses imply some groups are not necessary to be disposed into deep underground and can be disposed more densely. The result emphasizes different repository design may be seen when the nuclide dependent characteristics are extracted and classified into certain groups.

Key words: high-level waste disposal, separated disposal, and partitioning, statistical analysis

1. INTRODUCTION

High-level radioactive waste (HLW) disposal becomes one of the key issues for the nuclear power to survive in the future. Although partitioning and transmutation (P&T) is considered to reduce the potential radio toxicity in HLW disposal [1], the goal of the P&T process such as the target of the separation elements, decontamination factors, and transmutation rates, are however not fully investigated from a viewpoint of the radiological impact so far. As for the partitioning, the selection of the element for grouping seems to be rather subjective because of the weak connection with the safety analysis in the selection process even though the potential hazard index is frequently used. It is claimed this index is not an optimum indicator of the radiological impact and does not show the safety of the disposal explicitly.

In this paper, a procedure to assign the goal of the element separation from HLW liquid in the reprocessing is presented. This procedure may show the advantage of the segregated disposal as used in a common treatment of ordinary non-radioactive waste.

2. METHOD

2.1 Consistency with the current management program

As for the discussion of the separation procedure of high-level radioactive waste, consistency among the different waste types was considered in the design criteria as shown in Table 1.

Table 1 Disposal concept consistent with the current management program

category	Criteria	Current program	Ref.
Minimum Isolation Period	300 years	LLW* by institutional control	[2]
Dose Objectives	10 μSv/y	LLW* for normal evolution	[2]
Integrated Engineered Barrier	Vitrified Glass	Non-separated HLW	[3]
	Overpack		
	Bentonite		
Maximum Temperature Rise	100°C		

* Low-level Waste disposal

2.2 Classification of elements

The authors employed two statistical methods for grouping of the nuclides into several groups: the cluster analysis and the principal component analysis.

1) Factors used in the statistical analyses

(1) Migration impact factor

The equation of the peak nuclide concentration in groundwater was simply derived [4] for instantaneous discharge of soluble nuclide by Eq.(1),

$$\frac{C_{max}(L)\cdot L}{MS} = \frac{10}{\sqrt{\pi\kappa}}\exp\left[-\frac{(10-\kappa)^2}{4\kappa} - \frac{\kappa}{10}\cdot\frac{\lambda R_f}{U_p}L\right] \qquad \text{Eq.(1)}$$

where, C : nuclide concentration [Bq/m^3] L : distance from the source [m]

M : nuclide inventory [Bq] S : cross-section [m^2] (set as 1)

λ : decay factor [y^{-1}] U_p : pore water velocity [m/y]

$$\kappa = \left[\sqrt{1+10^2\left(1+\frac{4}{10}\cdot\frac{\lambda R_f}{U_p}L\right)} - 1\right] \Big/ \left(1+\frac{4}{10}\cdot\frac{\lambda R_f}{U_p}L\right) \cong 10 \quad (\textit{for most cases}).$$

The above equations were characterized by a factor A(= $\lambda R_f L / U_p$) which was divided into the nuclide dependent term λR_f and the geologic term L/U_p and the latter was independent of nuclide property thus λR_f (or $T_{1/2}/R_f$) term was used for nuclide grouping.

(2) Thermal impact factor

For simplicity, the underground repository was treated as a spherical medium. The maximum temperature rise was calculated by the empirical expression Eq.(2) [4],

$$K\frac{\Delta T_{max}}{W_0} \cong \frac{3}{4\pi R}\left[\frac{1}{3} - 0.110\left(R^2\lambda\right)^{0.278}\right] \qquad \text{Eq.(2)}$$

where, ΔT_{max}: maximum temperature rise [°C]

K : thermal conductivity of surrounding medium [W/m K]

W_o : initial heat generation in a single waste [W]

R : waste radius [m].

The equation (2) indicates the general tendency of the temperature rise is a function of $R^2\lambda$ and the thermal impact of each nuclide having initial heat generation W_o can easily be speculated. The term of $K\Delta T_{max}/W_o$ was thus used as a representative factor of the thermal impact.

2) Cluster analysis for appropriate grouping

Grouping of nuclides was conducted by employing the cluster analysis [5]. In this analysis, the following factors were introduced to identify the properties of nuclide to be concerned: (1) $T_{1/2}/R_f$, (2) $K\Delta T_{max}$, (3) D_{con} (dose conversion factor in μSv/y / Bq/m^3), (4) M (inventory in Ci), (5) C_{sol}(solubility in mol/L), (6) LET (linear energy transfer in eV/mm), and (7) F_{chem} (chemical factor). The degree of the underground-water radiolysis by the nuclide was simply estimated by the LET value, which was linearly interpolated from the energy of the emitted α, β, γ – rays. The chemical factor F_{chem} was defined as the element property including (1)electronegativity, (2)Gibbs free energy of formation of the corresponding oxide in the waste form, (3)redox potential of the dominant valence species speculated in undergroundwater. The factor F_{chem} was determined as a single value for each element by using the principal component analysis [6]. This factor was introduced in the cluster analysis for simply taking into account (1) the degree of complex formation, (2) chemical stability in the waste form, and (3) redox sensitivity in the repository environment, respectively.

3) Repository deign for segregated disposal

According to the recent report [3] suggesting the key parameters to dominate the repository size are the dimensions of overpack, bentonite, and the disposal pitch, a very simple procedure to determine these factors was developed and applied to assign the

repository dimensions deigned for each waste types. Of course, the validity of the procedure had been checked prior to the analyses. A brief summary of the repository design criteria used here is shown in Table 2.

Table 2 Repository design criteria

	Method	Limit	Note
Nuclide Inventory	ORIGEN2	weight limit(15% as oxide) thermal limit(2.3kW)	use smaller limit Ref.7
Repository Depth	Eq.(1)	10μSv/y	Necessary migration length L
Overpack Dimension	ASME code	hydrostatic pressure + Bentonite swelling pressure	Ref.8
Bentonite Dimension	Eq.(3) (5)	relaxation of the volume expansion pressure due to overpack corrosion	after 300years overpack corrosion
Waste Configuration	Thermal analysis	Below 100 °C	

(1) Overpack corrosion

The corrosion during the 300 years was estimated using the empirical equation of the corrosion rate extracted from the natural analogue study of the embedded steel pipes of the drinking water supply system buried for 20 ~ 66 years [3]. The corrosion depth corresponds to the 300 years was estimated approximately 1 cm under oxidizing atmosphere from such an equation. This value was added on the estimated thickness to assure the mechanical stability after the 300 years corrosion.

(2) Simple mechanical interaction model

The stress arising from the volume expansion of the overpack was simply calculated by

$$\sigma = \frac{E_2 E_3 (2L_1 + L_2)}{E_2(2L_1 + L_2)L_3 + E_3(2L_1 + L_2 + L_3)L_2} \cdot (k_e + 1) \qquad \text{Eq.(3)}$$

where, σ : stress due to corrosion [MPa]

E_n : elasticity modulus of medium n [MPa]

L_n : thickness of medium n [m^2]

k_e : volume expansion rate (set as 2).

n : medium identifier (n=1:overapck, 2:corrosion layer, 3:buffer material).

The general expression for the radial displacement at radial position r is depicted as [9]

$$u(r) = \frac{p_1 r_1^2 \{(1-\nu)r^2 + (1+\nu)r_2^2\} - p_2 r_2^2 \{(1-\nu)r^2 + (1+\nu)r_2^2\}}{E(r_2^2 - r_1^2)} \qquad \text{Eq.(4)}$$

where, $u(r)$: radial displacement at radius r [m]

r_n : radius of a cylinder [m] (n =1:inner radius, 2:outer radius)

p_n : pressure on a cylinder [MPa] (n=1:internal pressure, 2:external pressure)

E : elasticity modulus [MP].

When one applies Eq.(4) on the corrosion layer and assumes $u(r_1)=0$ because of the hard overpack wall, the above equation may be simplified as below and this formula gives the loading pressure (p_1) on the overpack outer surface.

$$p_1 = \frac{p_2 r_2^2}{\left\{(1-\nu)r_1^2 + (1+\nu)r_2^2\right\}} \qquad \text{Eq.(5)}$$

where, p_1 : internal pressure of the corrosion layer [MPa]

υ : Poisson ratio of the corrosion layer (assumed 0.3)

p_2 : external pressure of the corrosion layer [MPa]
(= σ in Eq.(3) + swelling pressure)

r_n : radius of the corrosion layer [m] (n =1:inner radius, 2:outer radius)

The minimum thickness to relax the swelling pressure due to corrosion was calculated with changing the initial bentonite thickness to meet the Tresca's yield criterion [10].

(3) Waste configuration

The pitch between two wastes was mainly determined by the thermal analysis to maintain the temperature below 100°C. The temperature rise due to a single heat source with radioactive decay was derived [11] then the effect of 8 neighbor heat sources were accounted by the method of superposition. The underground repository was treated as a homogeneous and spherical medium and necessary correction of the thermal properties of composite media were carried out.

3. RESULTS & DISCUSSION

3.1 Appropriate grouping extracted by the statistical analyses

The data set for some typical nuclides used in the present analyses are shown in Table 3 below. Two nuclide groups were then extracted from the cluster analysis as seen in Fig.1 shown as a hierarchical tree. The result suggests there are two distinct groups of (α) fission products and (β) TRU & their daughters. The supplementary analysis using the principal component analysis also supports this findings and the results from both two statistical analyses suggest the independent disposal for (α) fission products and (β) TRU & their

daughters are plausible because of the different impact properties.

Table 3 Data set used in the statistical analyses

Nuclide	Log of Factors				
	$T_{1/2}$ / R_F [y]	K ΔT_{max} / W_0 [Ci^{-1}]	Inventory [Ci]	Dose Conversion Factor [Sv/y / Bq/m^3]	F_{chem}
Cs 135	1.397	-0.738	3.065	-0.326	-0.535
Am 243	-0.887	0.403	1.464	1.640	-1.560
Cm 247	0.924	0.405	-2.347	0.665	-0.744
I 129	3.691	-0.656	-1.282	-0.263	2.205
Np 237	0.835	0.393	0.640	0.500	-1.539
Pa 231	-0.155	0.388	-1.816	1.653	-0.093
Pd 107	1.642	-1.170	0.393	-2.704	0.842
Pu 244	1.700	0.381	-2.152	-0.183	-0.835
Ra 226	-0.704	0.073	-3.409	0.538	-0.432
Se 79	1.097	-0.812	0.672	-0.506	2.590
Sm 148	5.669	0.159	-3.992	-0.212	-1.698
Sn 126	0.111	-0.409	0.793	-0.146	1.280
Sr 90	-0.564	-0.002	3.142	-0.175	-0.349
Tc 99	1.914	-0.636	1.377	-2.057	1.235
U 238	2.643	0.347	0.587	-0.492	0.242
Zr 93	1.300	-1.002	0.979	-1.403	-0.254

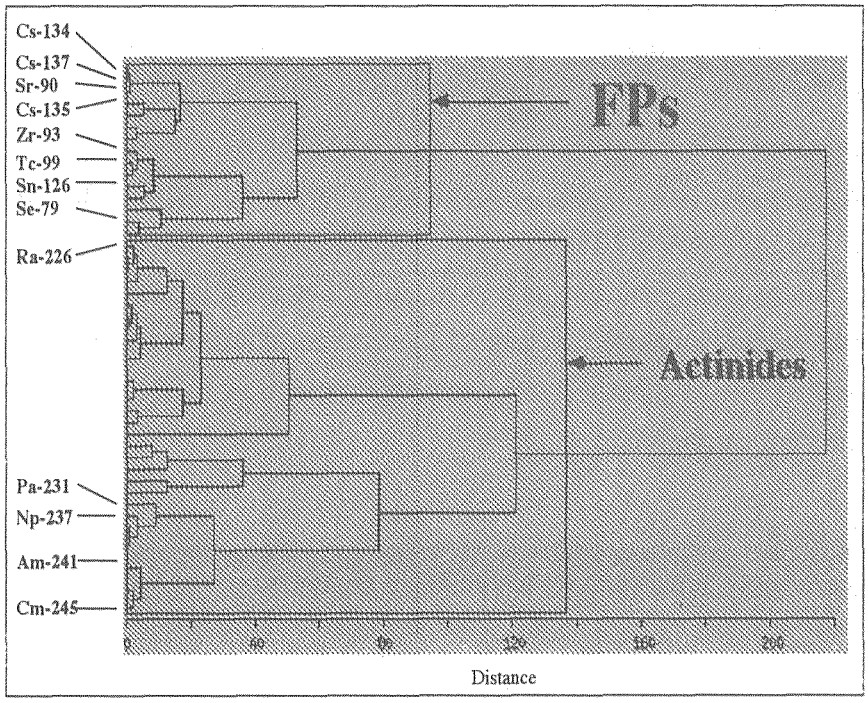

Fig.1 The hierarchical tree of the nuclides in the spent fuel

3.2 Repository depth

Minimum migration length to maintain the dose rate below 10μSv/y for some fission products were calculated by Eq.(1). The results indicate two distinct groups: one has short

distance below 100m and the other has long distance more than 10000m. In practical manner, the partitioning process can be developed by employing chemical separation technique. The grouping was thus revised by the element basis. The isotope with the maximum migration length was selected as the representative of each element and the grouping was conducted again. The appropriate element groups for partitioning from the viewpoint of underground disposal were extracted as follows. The group B (fission products with shorter half-lives) is not necessary to be disposed in deep geologic environment after appropriate decay period and another nuclides not shown here are to be included in this group B as well. On the contrary, groups A (fission products with extremely long half-lives) and C (TRU & their daughters) require the deep geologic disposal to attain the longer migration distance L and/or reducing environment. All decay chain member nuclides are included in the group C because the production and accumulation would occur and mix again sooner or later even if complete elemental separation is accomplished.

3.3 The variation of the engineered barrier system for the different waste types

The dimensions of the engineered barrier system for each type of waste are summarized in Table 4. When the proposed grouping is introduced, the total area of the repository corresponding 32000 MTU of spent fuel would be reduced about 50% if compare to the non-separated HLW disposal.

Table 4 Dimensions of the Engineered Barrier System for Different Waste Types

		A Long FP group	B Short FP group	C Actinides	HLW for comparison
No. of waste		1.75E+04	2.47E+04	3.22E+03	3.99E+04
Glass	diameter [cm]	43			
	height [cm]	135			
Overapck	isolation period [y]	1000	300	1000	1000
	corrosion depth [cm]	4	1	4	4
	wall [cm]	19	3.5	9	19
	rid [cm]	19	3.5	15	19
Bentonite	thickness [cm]	70	10	40	70
Repository	pitch [m]	6	1.6	4	6.5
	Repository [m^2]	6.30E+05	6.33E+04	1.71E+05	1.69E+06
	Area Reduced [%]	51.2			100

4. CONCLUSION

Separated disposal of the high level radioactive waste (HLW) is discussed by the following procedures; (1) the nuclides in the waste are classified into several groups having

similar properties by using the cluster analysis, (2) the disposal depth required that the maximum dose rate of each group is less than 10μSv/y is assigned by the simple migration analyses, (3) the dimensions of the engineered barrier system for segregated wastes are calculated by the simple procedures.

The grouping and configuration analyses imply that fission products with shorter half-lives is not necessary to be disposed in deep geologic environment after appropriate decay period and can be disposed more densely. On the contrary, fission products with extremely long half-lives and TRU & their daughters require the deep geologic disposal to attain the longer migration distance L and/or reducing environment. Even though, the total disposal area necessary for the three segregated wastes is about half of that for the non-separated HLW disposal. The result emphasizes the advantage of the segregated disposal for nuclear energy to survive in the future.

5. REFERENCES

[1] IAEA, "Safety and Environmental Aspects of Partitioning and Transmutation of Actinides and Fission Products", IAEA, (1995).

[2] Shimoda, S., Iimura, H., and Kuroda, T., J. Atomic Energy Society of Japan, 33(11), 1049, (1991). (in Japanese)

[3] Japan Nuclear Cycle Development Institute, Second Progress Report on Research and Development for the Geological Disposal of HLW in Japan, JNC TN1410 2000-001 ~ 2000-003, April, (2000).

[4] OHE, T., Proceedings of The Second Fujiwara International Seminar, S4-2, Susono, Japan, Nov.6-9, (2000). (will be published in J. Progress in Nuclear Energy, Elsevier)

[5] Anderberg,M.R., "*Cluster Analysis for applications*", Academic Press, (1973).

[6] Harris,R.J., "*A Primer of Multivariate Statistics*", Academic Press, New York, pp155, (1975).

[7] Croff, A.G., ORIGEN2 A Revised and Updated Version of the Oak Ridge Isotope Generation and Depletion Code, ORNL-5621, (1980).

[8] ASME, Pressure Vessel and Boiler Tube, Section III, Subsection NE, Division 1, pp55

[9] Blake,A., "*Practical Analysis in Engineering Design*", Marcel Dekker, New York, 1982).

[10] Derby,B., Hills,D.A., and Ruiz,C., "*Materials for Engineering: A fundamental Design Approach*", Logman Scientific & Technical, Harlow, pp71,(1992).

[11] Mufti,I.R., J.Geophys.Res., 8568, 76(35), (1971).

JP0250316

JAERI-Conf 2002-004

WASTES GENERATED BY APPLICATION OF JAERI PARTITIONING-TRANSMUTATION SYSTEM TO HIGH LEVEL RADIOACTIVE WASTE

SHINICHI NAKAYAMA*, YASUJI MORITA, KENJI NISHIHARA, HIROKAZU HAYASHI, AND OSAMU SHIRAI
Japan Atomic Energy Research Institute, Tokai, Ibaraki, 319-1195 Japan
*FAX: 81-29-282-5625, e-mail: nakayama@sparclt.tokai.jaeri.go.jp

Production of low-level radioactive wastes, as well as the reduction in radioactivity of HLW, are important in assessing the technological feasibility of a partitioning-transmutation system. We have begun to identify the chemical compositions and to quantify the amounts of radioactive wastes that may be generated by JAERI's processes. Long-lived radionuclides such as ^{14}C and ^{59}Ni and spallation products of Pb-Bi coolants are added to the existing inventory of the nuclides that are generated in the current fuel cycle. Spent salts of KCl-LiCl, which are not generated from the current fuel cycle, will be introduced as a waste.

Key words: partitioning-transmutation system, long-lived activation and spallation products, spent KCl-LiCl salt, Pb-Bi coolant and target

1. INTRODUCTION

Separation of short-lived fission products through partitioning reduces the initial radioactivity of high-level radioactive waste (HLW). Transmutation of long-lived minor actinides such as ^{237}Np reduces the radioactivity of HLW over tens of thousands of years. The partitioning-transmutation technology accordingly helps reduce the potential hazard of HLW[1].

The physical and chemical processes used during the application of partitioning-transmutation technology, however, generate other, low-level, radioactive wastes. Although the new LLW waste does not represent a significant increase in potential hazard after disposal, the waste may be produced in different chemical forms and may therefore require different waste immobilization forms from those in the current nuclear fuel cycle. The type of solidifying matrix material is chosen depending on the chemical compositions of the wastes. The volume of waste forms is determined by the matrix material employed, the quantity of loaded raw wastes, as well and level of radioactivity. The chemical compositions and the amount of the wastes influence the treatment method and the total waste volumes, and therefore the cost for final waste disposal.

Assessing the technological feasibility of the partitioning-transmutation system should include the feasibility of safe and reasonable treatment and disposal of radioactive and non-radioactive wastes that remain after the introduction of the system. The assessment is dependent on reliable information on the quantities and chemical compositions of the wastes, and of course their radioactivity.

We have begun to identify the chemical compositions and to quantify the amounts of radioactively contaminated wastes that may be generated by each of the partitioning-transmutation processes. There are two general waste sources – process losses, and wastes arising from the maintenance and decommissioning of the plants. The process losses can be estimated from the material balance calculations for each process, and so, in principle, the types and amounts of wastes generated can be assessed quantitatively. The types and amounts of plant maintenance and decommissioning wastes can be estimated, at least on a semi-quantitative basis, by using industrial experiences and expert judgment. This paper presents the results of estimates of process losses obtained so far by material flow analyses of the partitioning, transmutation, and nitride fuel reprocessing processes of the partitioning-transmutation system proposed by Japan Atomic Energy Research Institute, JAERI. The

analysis for the nitride fuel fabrication process has not been examined yet.

2. JAERI'S PARTITIONING AND TRANSMUTATION SYSTEM

JAERI has proposed a "double strata" nuclear fuel cycle, in which the current Japanese reprocessing fuel cycle would be the first stratum or layer of the cycle, and a partitioning-transmutation system would be the second layer. This cycle is shown schematically in Figure 1. The partitioning-transmutation cycle system is composed of four processes -- partitioning of elements into groups, fabrication of nitride fuel, accelerator-driven transmutation of the nitride fuel, and pyrochemical reprocessing of the nitride fuel after transmutation. This system is independent from the commercial power reactor fuel cycle.

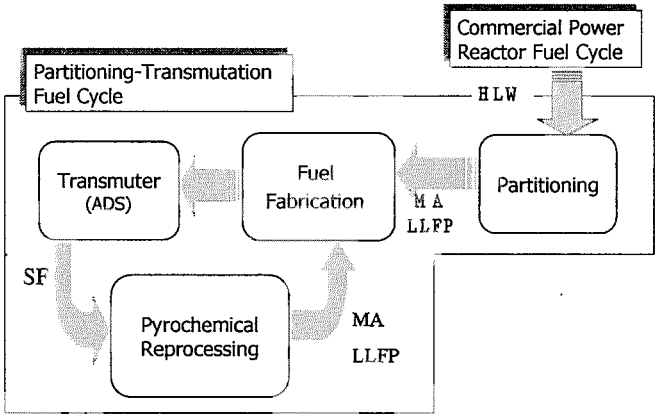

Figure 1: JAERI's "double strata" fuel cycle system. The commercial power reactor fuel cycle is the first stratum, and the partitioning-transmutation fuel cycle is the second. HLW: High Level Waste, MA: Minor Actinide, LLFP: Long-Lived Fission Product, SF: Spent Fuel. ADS: Accelerator-Driven subcritical System.

The partitioning-transmutation layer of the double strata cycle begins when high-level liquid waste, discharged from the fuel reprocessing plants of the first layer of the cycle, is received at the partitioning plant. Minor actinides and the long-lived fission product ^{99}Tc, are extracted in the partitioning process and converted into fuel for transmutation.

Material flow in the partitioning-transmutation system is summarized in Figure 2. The core inventory of minor actinides in the ADS, accelerator-driven subcritical system, is 2.25 tons. One and one-quarter tons of minor actinides (0.25 tons from the PUREX reprocessing plant - layer one, and 1.0 ton already in the system from pyrochemical reprocessing), are being fabricated into fuel, which is loaded into the core. In addition, one ton of the core inventory is returned for pyrochemical reprocessing, and is cooled for two years before being reprocessed. The system-wide inventory of minor actinides is then 5.5 tons at loading.

The 0.25 tons of minor actinides supplied from the PUREX reprocessing is the quantity of minor actinides produced by 195.7 tons of 45,000 MWd/t burnup spent nuclear fuel from light water reactors. Consequently, the following estimates are based on reprocessing and applying partitioning-transmutation technology to 195.7 tons of spent light water reactor fuel reprocessed each year.

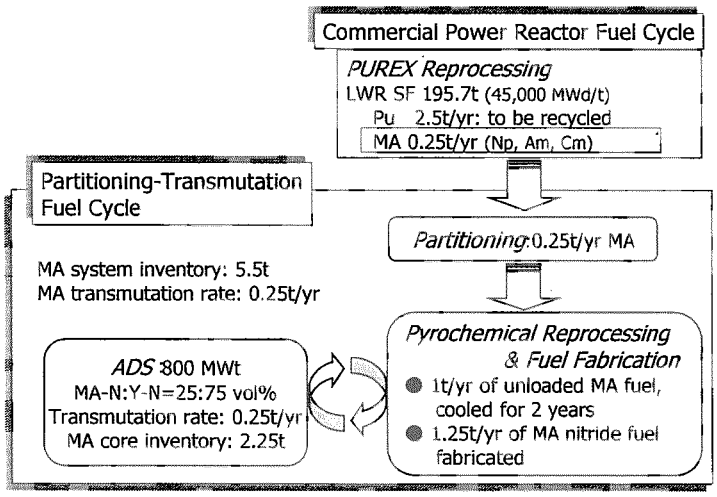

Figure 2: System-wide material flow in JAERI's partitioning-transmutation cycle system

The Accelerator-Driven subcritical System (ADS) is currently designed to be 800 MWt with a lead (Pb) - bismuth (Bi) eutectic coolant, and to transmute 0.25 tons of minor actinides per year[2]. The fuel composite is a homogeneous mixture of minor actinide nitrides and an yttrium

(Y) nitride in the volume ratio of 1 to 3. The yttrium nitride is an inert diluent to control the power density. Titanium and zirconium are alternative diluents to be considered in the future design optimization study. n. Zirconium(Zr) is used for vibropacked fuel element with Zr-N and minor actinide nitride microspheres. Our analysis in this study is on the yttrium option.

The irradiated nitride fuels are submitted to molten-salts electrorefining to remove fission products. This pyrochemical separation yields actinide metals, and the metals are converted into nitride fuel by nitridation.

3. EVALUATION OF GENERATED WASTES

3.1 Partitioning

Radionuclides in the high-level liquid waste are separated into four groups by the partitioning process: transuranium elements (TRU; Np, Pu, Am, Cm), Tc-platinum group metals (TC-PGM; ^{99}Tc, Ru, Rh, Pd), the elements Sr and Cs, and "other elements" (Zr, Mo, Fe and rare earth elements). Material flow for the partitioning process is fairly well established in the partitioning-transmutation system, with the assumption of 0.1 wt% of process loss[3]. Products and wastes generated by the partitioning process are estimated in Table 1.

Table 1 Products and Wastes generated from the Four-group Partitioning Process
(Calculated using software program [4], data in Ref.[5], and converted for 195.7 tons of LWR spent fuel producing 0.25 tons of minor actinides)

(a) Partitioned products

Group	Major nuclides or elements	Chemical form	Volume (m^3)	Treatment after partitioning
TRU	Np, Am, Cm	oxides	0.025	Converted into nitride fuel
Tc-platinum group metal (PGM)(*)	^{99}Tc, Ru, Rh, Pd	metal	0.088	Tc: Converted into nitride fuel PGMs: utilized *or* disposed
Sr-Cs	^{90}Sr, ^{137}Cs	calcined products	3.3	Storage followed by disposal
Others	Zr, Mo, Fe, rare earths	vitrified form (30 wt% of oxides loaded)	7.2	Storage, followed by disposal
Total			10.5	
Non-partitioned option		vitrified form (12 wt% of oxides loaded)	33	Storage followed by disposal

(*) Technetium, after separation from PGMs, is designated for conversion into nitride fuel for transmutation. However transmutation of Tc is not considered in the following burnup calculation due to an unsolved neutron balance problem. Technetium can be separated from PGMs without waste generation, and the separated PGMs utilized.

(b) Secondary wastes

Waste	Composition	Treatment/Waste form	α radioactivity
Spent solvent	DIDPA-TBP-dodecane	Thermal decomposition into 1.55 tons of $Ca_2P_2O_7$ yielding 9.2 m^3 in cemented form (10 wt% of $Ca_2P_2O_7$ loaded)	0.013 GBq/t
Washing liquid	$NaNO_3$, Na_2CO_3	56.6 tons of pelletized $NaNO_3$ are conditioned, yielding 56.6 m^3 in cemented form (50 wt% of pelletized $NaNO_3$ loaded)	0.2 GBq/t
Others	DTPA, oxalic acid	Decomposed in H_2O and CO_2	No data available

Partitioned transuranium elements and technetium will be converted into nitride fuel for transmutation. Platinum group metals separated from technetium may be retained for later use as noble metals and would not be included in the waste.

Strontium and cesium are solidified by calcinations of the loaded zeolites and titanic acid

into 3.3 m^3 of waste, and the remaining group of elements is solidified into 7.2 m^3 of vitrified waste. These last two groups are the primary wastes from partitioning, totaling 10.5 m^3. This is much less than the 33 m^3 of vitrified waste that would be produced by solidifying an equivalent quantity of non-partitioned high-level waste. This reduction in volume results from the removal of short-lived fission products ^{90}Sr and ^{137}Cs. The loading of high-level waste liquid into glass is limited by the temperature rise due to decay heat. Removal of ^{90}Sr and ^{137}Cs allows the increased loading into glass, and accordingly the number of glass waste forms is expected to decrease. The secondary wastes that would result from the partitioning process include spent solvent (DIDPA-TBP-dodecane) and sodium salt solutions (sodium carbonate and sodium nitrate). Calcium phosphate (9.2 m^3) from the spent solvent and 56.6 tons of pelletized sodium salts are solidified into cement waste forms. The calcined products with zeolites and titanic acid are wastes that are not generated from the current fuel cycle, but will be generated from the partitioning-transmutation system.

3.2 Accelerator-Driven subcritical System

Radionuclides produced by the ADS include short-lived fission products produced in nitride fuels, activation products and spallation products generated in fuel pins, and the Pb-Bi eutectic target and coolant.

Nitrogen-15, enriched from natural nitrogen, is used for the nitride fuel. Carbon-14 (5,730 yr) is produced through activation of the remaining ^{14}N during the transmutation process. The amount of ^{14}C produced is proportional to that of ^{14}N. A 90% enrichment of ^{15}N yields 20 TBq (110 g) of ^{14}C per year. Activation products of SUS316 fuel cladding include radionuclides of various lifetimes. Twenty thousand TBq of ^{58}Co (71 d) dominate the initial radioactivity of the discharged fuel, and 0.4 TBq of ^{59}Ni will dominate 10,000 years after fuel discharge from the ADS.

Some of the yttrium in the yttrium nitride in the fuel is activated during transmutation to produce 1×10^{18} Bq of ^{90}Y (64 hr). This isotope quickly decays to a stable isotope of ^{90}Zr. About 2.4 tons of Y and 5.6 kg of ^{90}Zr will remain, affecting the subsequent partitioning-transmutation processes, and finally will be disposed of as a waste.

About 7,000 tons of the Pb-Bi eutectic metal (target and coolant) of the ADS are a source of spallation and activation products. An example of calculation of radioactivities of the spallation and activation products for an 800 MWt ADS is shown in Figure 3. Polonium-210 (138 d; 8×10^{17} Bq) is one of the main radioactivity-dominating radionuclides that will be present at the end of 50-year operation of the ADS. This isotope is in radioactive equilibrium with the long-lived precursor, ^{210m}Bi (3×10^6 yr), after 10 years. A long-lived spallation product of ^{202}Pb(3×10^5 yr)-^{202}Tl(22 d) and an activation product of ^{210m}Bi-^{206}Tl(4.2 m) will contribute 50 TBq of total radioactivity at 10,000 years after the 50-year operation. This radioactively contaminated Pb-Bi metal is discharged in decommissioning the ADS facility. This waste will only be generated once in the lifetime of the facility, that is once in tens of years of operation. This radioactively contaminated Pb-Bi waste does not exist in the current fuel

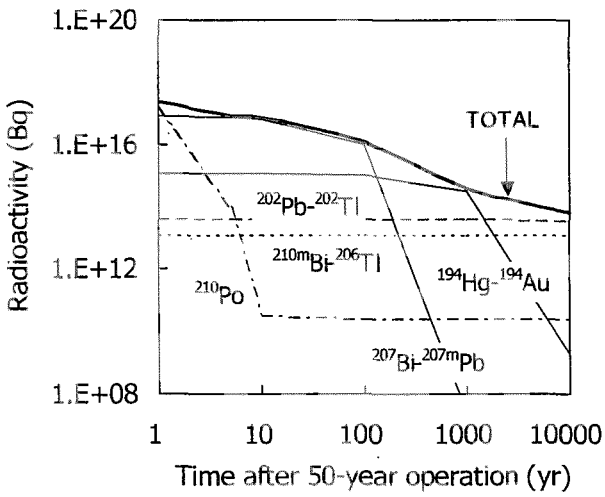

Figure 3: Radioactivity generated in the Pb-Bi target and coolant for 50 years of operation of the 800 MWt ADS. Partial results of the burn-up calculation[6] are plotted.

cycle, but will be generated from the partitioning-transmutation system. The radioactivity of the contaminated Pb-Bi waste is low. The chemical toxicity of these metals may dominate the risk of groundwater contamination when the waste is disposed of into the underground.

3.3 Fuel fabrication

JAERI's partitioning-transmutation system needs two different fuel fabrication processes as schematically shown in Figure 4. One is a wet process: Actinides extracted in the partitioning process are fed into sol-gel process followed by conversion into nitride fuel through carbo-thermic synthesis. The other fabrication is a dry reprocessing of spent fuel. Spent nitride fuel is first subject to pyrochemical treatment using molten KCl-LiCl salt to separate actinides. The obtained actinide metal/alloys are converted into nitride fuel though nitridation with ^{15}N.

Because the design of these fuel fabrication processes has not progressed as far as the designs of the partitioning and transmutation processes, engineering data are not yet available to quantify the material flow in the fuel fabrication processes. Data on the material losses therefore are much limited.

Typical wastes produced from the fuel reprocessing are hulls and fission product metals, and radioactively contaminated KCl-LiCl salt mixture. A semi-quantitative, preliminary evaluation with limited data indicates that the contaminated KCl-LiCl salt waste generated could range from 1 to 10 tons per year, depending mostly on the amount of Y remained in the waste.

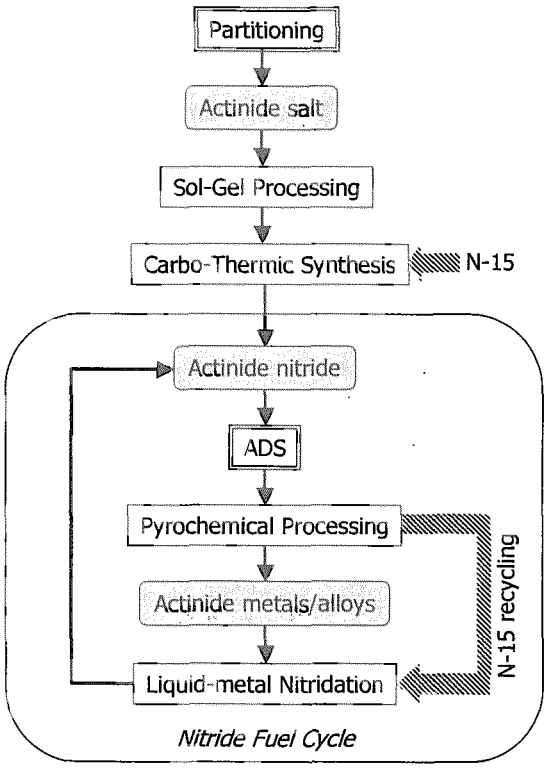

Figure 4: Fabrication process for the actinide nitride fuel in the JAERI partitioning-transmutation cycle (modified from Ref. [2].)

4. DISCUSSIONS AND CONCLUSION

Introduction of the partitioning-transmutation system into the current nuclear fuel cycle decreases both short- and long-term radioactivity of HLW, but it also produces various additional forms of low-level radioactive wastes. Long-lived radionuclides such as ^{14}C and ^{59}Ni and spallation products of Pb-Bi metal are added to the existing inventory of the wastes that are generated in the current fuel cycle. Wastes such as spent salts of KCl-LiCl, which are not generated from the current fuel cycle, will also be introduced by a partitioning-transmutation system.

Chlorine, Pb and N may be sources of groundwater contamination if disposed underground. The chemical toxicities may be of more concern than the radiological toxicity. These wastes should be treated and disposed of as safely as "radioactive wastes". In this sense, the production of the additional low-level radioactive wastes, as well as the reduction in radioactivity of HLW, are important performance indicators that should be quantitatively evaluated in assessing the viability of a partitioning-transmutation system.

Based on the current studies to quantifying the wastes, it is suggested that waste management utilizing JAERI's "double strata" fuel cycle may result in smaller sized "HLW" repositories designated for separated short-life, highly-active radionuclides, and may need de-

velopment of treatment and disposal technology to manage Pb-Bi metals and KCl-LiCl salt mixture. This is a concluding remark for for waste management considerations in introducing a new technology into the nuclear fuel cycle, the JAERI partitioning-transmutation system.

Acknowledgements

The authors wish to thank H. Yamana of Research Reactor Institute, Kyoto University, M. Kurata of Central Research Institute for Electric Power Industry, M. Shiotsuki of Japan Nuclear Cycle Development Institute, T. Ohe of Tokai University, and T. Omori and T. Kobayashi of Toshiba Corporation for their advice and discussion, and G. McCrank of Japan Nuclear Fuel Cycle Development Institute for his stylistic revisions. Part of this work was presented at the GLOBAL 2001 conference held at Paris on September 13 – 16.

References

[1] Japan Atomic Energy Commission's Advisory Committee on Nuclear Fuel Cycle Back-end Policy, "Research and Development of Technologies for Partitioning and Transmutation of Long-lived Nuclides - Status and Evaluation Report –", March 31, 2000 (In Japanese).

[2] T. Mukaiyama, T. Takizuka, M. Mizumoto, Y. Ikeda, T. Ogawa, A. Hasegawa, H. Takada, and H. Takano, "Review of Research and Development of Accelerator-driven System in Japan for Transmutation of Long-lived Nuclides", *Nucl. Energy*, 38, 107-134 (2001).

[3] Y. Morita et al., "The First Test of 4-group Partitioning Process with Real High-level Liquid Waste", *Proc. Fourth Int'l Conf. Future Nuclear Systems*, GLOBAL '99, August 29 – September 3, Jackson Hole (1999) (published in CD-ROM).

[4] Japan Atomic Energy Research Institute, "Mass Flow Computer Code for JAERIs' Partitioning Process: User's Manual" (2001) (In Japanese).

[5] M. Kubota and Y. Morita, "Preliminary Assessment on Four Group Partitioning Process Developed in JAERI", *Proc. Third Int'l. Conf. on Future Nuclear Systems*, GLOBAL'97, Vol.1, 458-462, October 5-10, 1997, Yokohama, Japan (1997).

[6] K. Nishihara and N. Sasa, "Estimation of Activity and Toxicity for Spallation Product from the Target for Accelerator-driven Transmutation System", JAERI-Research 2001-015, Japan Atomic Energy research Institute (2001).

JP0250317

JAERI-Conf 2002-004

STATUS AND FUTURE NEEDS IN ACTINIDE CHEMISTRY FOR PERFORMANCE ASSESSMENT OF NUCLEAR WASTE DISPOSAL

Dhanpat Rai[1] and Mikazu Yui[2]
[1]Pacific Northwest National Laboratory, Richland, WA, USA
[2]Japan Nuclear Cycle Development Institute, Tokai Works, Japan

ABSTRACT

Actinides are important components of nuclear wastes. Many actinide isotopes have such long half-lives that they are expected to persist in nuclear wastes over periods extending to hundreds of thousands to millions of years. Because the environmental behavior of actinides is highly dependent on many factors including chemical, physical, and mineralogical properties of waste-form/geologic media and these properties are not expected to stay constant over millions of years, fundamental approaches need to be developed to predict actinide behavior over long periods. Before these approaches can be developed, thermodynamic data pertaining to dominant aqueous species and solubility of environmentally important solid phases are required. These data are generally used to set upper limits on soluble actinide concentrations under specific environmental conditions. The reliability of the predicted concentrations will depend upon the quality and extensiveness of the thermodynamic data that is obtained.

This paper provides only a cursory discussion of the quality and extensiveness of currently available data for actinide reactions with environmentally important ligands. Areas where further fundamental actinide data are required include mixed and complex systems, elevated temperatures, solubility-controlling solid phases in waste forms, solid solutions, complexing/binding agents, and kinetic/equilibrium redox reactions. This paper provides examples that illustrate the importance of these various aspects and the challenges we face in acquiring the necessary data.

Key Words: Thermodynamic data, actinides, complexation, solubility

INTRODUCTION

Depending on the concentrations, radioactive materials are or will be disposed of in low-level or high-level waste geologic repositories. A common concern for both types of these repositories is that the disposal environments are expected to be quite diverse. The geologic environments may differ significantly in ionic strengths (e.g., salt repositories versus repositories in other geologic formations), pH, and redox conditions. In addition, the waste forms may themselves considerably modify the chemical environment in and around the repository. Because of the waste characteristics, low-level waste repositories, when compared with high-level waste repositories, are expected to have lower radioactive material concentrations and temperatures, and higher levels of organic matter, organic complexing ligands, and carbonate concentrations. The types of solid-phases/waste forms are expected to be quite different between low-level and high-level waste repositories. Chemical variations, along with the facts that the half-lives of most important actinides are hundreds of thousands of years, the chemical environment may change over time, and the long-term chemical behavior for site specific repositories cannot be determined experimentally, dictate that fundamental rather than empirical approaches are required to predict long-term actinide behavior under different repository environments. Thermodynamic data 1) provide a fundamental approach and long-term predictability, 2) help set reliable upper-limits of actinide concentrations, and 3) form the basis to predict the effects of different chemical environments and to develop fundamental data for adsorption and diffusion reactions. For

these reasons, this paper will emphasize the need for additional research and thermodynamic data for actinides important to radioactive waste disposal in geologic repositories as the primary objectives of this discussion.

DISCUSSION

Different actinides and their environmentally important oxidation states are shown in Fig. 1. Inorganic ligands, such as chloride, hydroxide, sulfate, carbonate, and phosphate, are present in most geologic environments. Based on the concentrations of these ligands, they can make strong complexes with actinide elements. Quite a large body of data on simple systems at room temperature for actinide complexes and solid phases with these ligands is either available or is being developed by several organizations. Among the data that are available are comprehensive reviews conducted by the Nuclear Energy Agency of the Organization for Economic Co-operation and Development for U[1], Am[2], and for Np and Pu[3]. In addition, recent reviews[4-6] conducted for the waste repositories in Japan provide a summary of available thermodynamic data for actinides. Since most of the available data have been adequately summarized, we will concentrate on discussing our views on where there is further need for additional data.

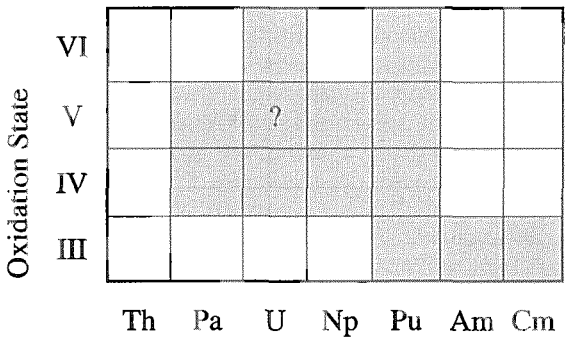

Fig. 1 Environmentally important idation states of actinides.

Although a large amount of room temperature data for most of the common ligands is available, validation of key data in some cases is still required. Extremely limited data are available in the areas of mixed systems, elevated temperatures (such as those expected to be present in high-level waste repositories), solubility-controlling solid phases in waste forms, solid solutions, complexing/binding agents (especially in low-level waste repositories), and kinetic/equilibrium redox reactions. The data needs in these areas are briefly discussed below.

Mixed Systems

Thermodynamic data are generally available for simple systems involving one ligand and a fixed concentration of ionic media. The challenge we face is to demonstrate, through further studies, that simple system data are applicable to mixed and complex systems (involving multiple ligands), and that the ionic media effects are predictable. We know that mixed systems can have a dramatic effect on the aqueous concentrations and activities of various ions. For example, a thermodynamic model based on ThO_2(am) solubility in Na_2CO_3 or $NaHCO_3$ solutions[7], when used to predict behavior in Na_2CO_3 solutions containing 4.7 m

NaCl (such as might be expected in low-level waste repositories in salt), showed that the predicted concentrations were up to 3 to 4 orders of magnitude higher than the concentrations actually observed in mixed carbonate-chloride systems, and they were up to 3 orders higher than those predicted assuming that mixed carbonate-perchlorate parameters are applicable to the mixed carbonate-chloride system (Fig. 2)[8]. These results show the impacts mixed and complex aqueous systems can have on the solubilities and the need to experimentally evaluate these aspects. These results also point out that without proper consideration of ionic media effects, thermodynamic values extrapolated from high and constant ionic strength systems involving mixed electrolytes will be of questionable quality. Reliable data for environmentally important mixed systems and actinides/oxidation states are currently lacking and represent an area for further study.

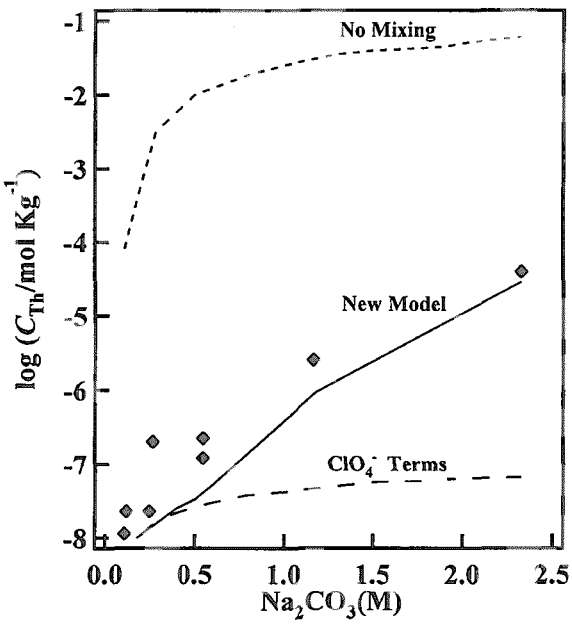

Fig. 2 Observed and predicted concentrations of Th in equilibrium with ThO_2(am) in the presence of 4.7 m NaCl and variable concentrations of Na_2CO_3 (after Felmy and Rai[8]).

Elevated Temperatures

Higher than ambient temperatures are expected in the high-level waste repositories. Elevated temperature can significantly affect aqueous concentrations through 1) changes in solubility products and complexation constants of actinide species, 2) changes in activities of ancillary species, and 3) changes in the crystallinity of actinide solid phases. For example, heating amorphous ThO_2 to 90°C converted it to crystalline ThO_2 resulting in about 10 orders of magnitude decrease in solubility (Fig. 3)[9]. Our unpublished data with the corresponding U(IV) system also shows similar dependencies on temperature. Extensive data on the effect of temperature on most of the aspects discussed above are lacking and are needed before we can make reliable predictions for the expected elevated temperatures in high-level waste repositories.

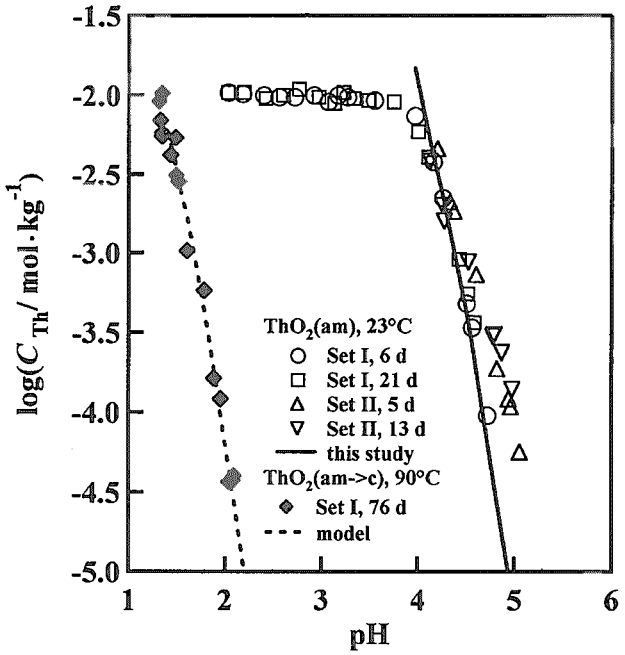

Fig. 3 The effect of heating equilibrated suspensions of ThO_2(am) in 0.1 M NaCl (after Rai et al.[9])

Characterization of Solubility-Controlling Solid Phases

In order to set reliable upper limits for actinide concentrations, data are needed on whether the concentrations in waste forms are solubility-limited, and if they are, then we need data for the exact nature of the solubility-controlling solid. The challenges we face in proper characterization of solubility-controlling solid phases in waste forms include 1) there may be multiple solid phases of a given actinide or oxidation state, 2) solids may be amorphous or crystalline, 3) the most soluble phase will initially control the solubility, 4) existing characterization techniques are inadequate, especially when solids are amorphous or when present in trace concentrations, and 5) thermodynamic data for all phases may not be available. Methodologies, therefore, must be developed to overcome these challenges. Comparing experimental solubilities of waste forms as a function of pH and other important variables to the solubilities of known solid phases can be used to predict the solubility-controlling phases that are otherwise difficult to characterize. For example, the close agreement between the solubility of Nd-doped glass in a CO_2 atmosphere as a function of pH and the predicted $NdOHCO_3$(c) showed that the solubility-controlling phase in this system must be $NdOHCO_3$(c) (Fig. 4)[10]. The solubility method is very sensitive and can, in some cases, also be used to characterize solid phases that are present in trace quantities. For example, the solubility of crystalline ThO_2 prepared at 750°C and as a function of pH successfully identified the presence of far less than 1% of a less crystalline phase (Fig. 5)[9].

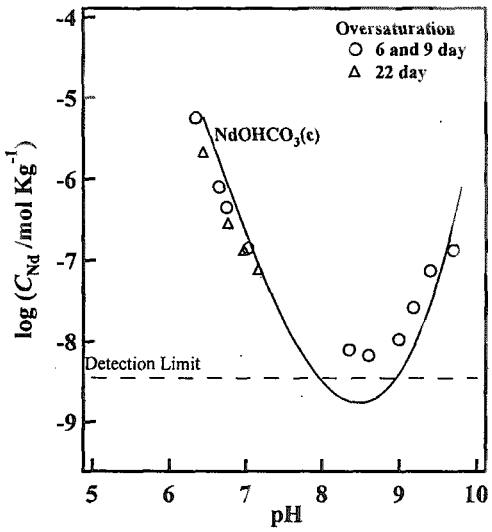

Fig. 4 Solubility-controlling solid of Nd in JNC glass equilibrated in 0.001539 atm. CO_2 (Rai et al.[10]).

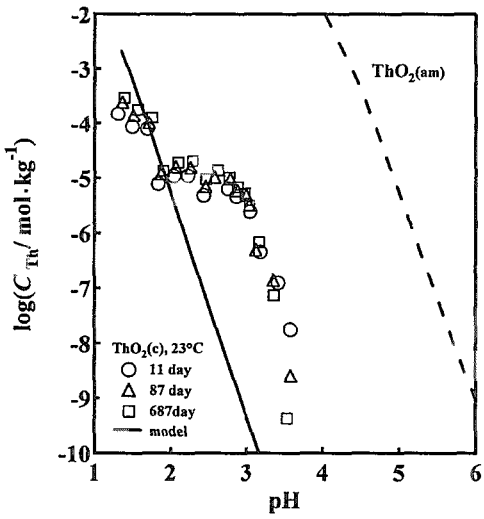

Fig. 5 Characterization of ThO_2 solids when present in trace concentrations (Rai et al.[9]).

Solid Solutions

The formation of solid solutions can decrease the solubility of a minor components by many orders of magnitude. Possibilities of solid solutions exist between trivalent rare earths and actinides, among tetravalent actinides, and possibly among other actinide oxidation states. Reliable data for solid solutions do not exist. In order to develop these data, it is imperative that the quality data for end members are available. The end member data for important trivalent and tetravalent actinides have recently become available, making it possible in the future to develop meaningful data for solid solutions of environmental importance.

Complexing/Binding Agents

In addition to inorganic reactions in geologic materials involving precipitation/dissolution and adsorption/desorption, actinide reactions with organic ligands and microbial surfaces can in some cases enhance mobility (e.g., reactions with organic ligands that may be present in low-level waste repositories) and in others immobilize actinides (e.g., binding to microbial surfaces). There also are a variety of natural (e.g., isosaccharinic acid) and synthetic (e.g., ethylenediaminetetraacetic acid, EDTA; nitriloacetic acid, NTA) organic ligands often associated with low-level waste repositories that can strongly complex actinide ions, which can mobilize actinides in geologic environments. Isosaccharinic acid (ISA) is a degradation product of cellulose[11-13] and is shown[11-14] to solubilize actinides in a wide pH range. Even though some of these organic ligands are very strongly complexing, their reactions with actinides are currently poorly understood. For example, 1) the structures, species, and constants of actinide-ISA are unknown, 2) no data are available for trivalent actinide-ISA complexes, and 3) new innovative techniques are required to identify these species. Microbial surfaces can uptake high concentrations of actinides. However, these reactions are also poorly understood. There are many technical challenges in deciphering these fundamental reactions. Technical difficulties include 1) microbial surfaces contain different functional groups which provide sites for binding actinides with different strengths, 2) chemical environments of functional groups depend on the cell structure, 3) data on the characterization of functional groups are not available, and 4) data on actinides binding to microbial surfaces are extremely limited.

Kinetic/Equilibrium Redox Reactions

Oxidation/reduction reactions can significantly affect actinide behavior in geologic environments. For example, reducing conditions can immobilize U(VI) and Np(V) by converting them to their fairly insoluble tetravalent states and can make Pu potentially more mobile by converting Pu(IV), commonly considered to be the dominant and immobile oxidation state in geologic environments, to Pu(III). Significant challenges exist in deciphering the effect of oxidation/reduction reactions on fundamental bases. These challenges include 1) overcoming difficulties in characterizing redox potentials of most geomedia because of mixed potentials, redox couples not in equilibrium, and difficulties quantifying all redox species participating in a given reaction, and 2) obtaining reliable data for actinides for environmentally important conditions such as the effect of pH and reducing agents (e.g., Fe(II), sulfides, organics) and whether the reactions are controlled by equilibrium or kinetic phenomena. Innovative techniques are required to characterize the redox potentials of geologic media. Some of our recent studies[15] have shown that the reduction of Pu(IV) to Pu(III) can occur in the presence of reducing agents commonly encountered in geologic environments (e.g., Fe(II) and hydroquinone, an analog for humic acid) and can enhance the solubility of PuO_2(am) by as much as 20 orders of magnitude. This process, common under environmental conditions, has been completely ignored in the past, yet may play a very important role in determining Pu behavior in reducing geologic environments. Obtaining reliable fundamental data on all of these aspects is required before fundamental capabilities for determining actinide behavior in geologic environments can be developed.

SUMMARY

As discussed, there are many aspects or areas that need further study and validation in order to address future thermodynamic data needs in disposing of radioactive wastes. Areas for further study include mixed systems, elevated temperatures, solubility-controlling solid phases, solid solutions, complexing/binding agents, and kinetic/equilibrium redox reactions. The challenges are not insurmountable, but careful and extensive further experimental studies are required to develop reliable long-term predictability of actinide behavior in geologic environments.

ACKNOWLEDGMENTS

This research was conducted at the Pacific Northwest National Laboratory, operated by Battelle for the U. S. Department of Energy (DOE) under contract DE-AC06-76RLO 1830, in collaboration with Japan Nuclear Cycle Development Institute (JNC) under an agreement with DOE for a project on "Development of Fundamental Thermodynamic and Adsorption Data". We thank Ms. Kathleen R. Hanson for editorial and Ms. Debra M. Hinton for text processing of this document (NUCEF paper 9F.doc).

REFERENCES

[1] I. Grenthe, J. Fuger, R. J. M. Konings, R. J. Lemire, A. B. Muller, C. Ngyen-Trung, H. Wanner., *Chemical Thermodynamics of Uranium. Vol.* 1. North-Holland, New York (1992).

[2] R. J. Silva, G. Bidoglio, M. H. Rand, P. B. Robouch, h. Wanner, I. Puigdomenech, *Chemical Thermodynamics of Americium. Vol.* 2. Nuclear Energy Agency, Organization for Economic Co-Operation and Development, New York (1995).

[3]. R. J. Lemire, J. Fuger, S. Kastriot, H. Nitsche, W. J. Ullman, P. Potter, P. Vitorge, M. H. Rand, H. Wanner, and J. Rydberg, *Chemical Thermodynamics of Neptunium and Plutonium. Chemical Thermodynamics: Vol.* 4. Elsevier Science B. V., Amsterdam (2001).

[4] D. Rai, L. Rao, H. T. Weger, A. R. Felmy, G. R. Choppin, and M. Yui, *Thermodynamic Data for Predicting Concentrations of Pu(III), Am(III), and Cm(III) in Geologic Environments*. JNC TN8400 99-010, (Japan Nuclear Cycle Development Institute, Tokai Works, Japan ,State,1999).

[5] D. Rai, L. Rao, H. T. Weger, A. R. Felmy, G. R. Choppin, and M. Yui, *Thermodynamic Data for Predicting Concentration of Th(IV), U(IV), Np(IV) and Pu(IV) in Geologic Environments*. JNC TH8400 99-009, (Japan Nuclear Cycle Development Institute, Tokai Works, Japan ,(1999).

[6] G. R. Choppin, M. Bronikowski, J. Chen, J. Byegard, D. Rai, and M. Yui, *Thermodynamic Data for Predicting Concentrations of* AnO_2^+ *and* AnO_2^{2+} *Species in Geologic Environments*. JNC TN8400 99-012, (Japan Nuclear Cycle Development Institute, Tokai Works, Japan ,State,1999).

[7] A. R. Felmy, D. Rai, S. M. Sterner, M. J. Mason, N. J. Hess, and S. D. Conradson, *J. Solution Chemistry* **26**, 233-248 (1997).

[8] A. R. Felmy and D. Rai, *J. Solution Chemistry* **28**, 537-557 (1999).

[9] D. Rai, D. A. Moore, C. S. Oakes, and M. Yui, *Radiochimica Acta* **88**, 297-306 (2000).

[10] D. Rai, A. R. Felmy, R. W. Fulton, and J. L. Ryan, *Radiochimica Acta* **58**, 9-16 (1992).

[11] B. F. Greenfield, A. D. Moreton, M. W. Spindler, S. J. Williams, and D. R. Woodwark, *Materials Research Society Symposium Proceedings* **257**, 299-306 (1992).

[12] B. F. Greenfield, M. H. Hurdus, N. J. Pilkington, M. W. Spindler, and S. J. Williams., *Materials Research Society Symposium Proceedings* **333**, 705-710 (1994).

[13] B. F. Greenfield, G. J. Holton, M. H. Hurdus, N. O'Kelley, N. J. Pilkington, A. Rosevear, M. W. Spindler, and S. J. Williams., *Materials Research Society Symposium Proceedings* **353**, 1151-1158 (1995).

[14] D. Rai, L. Rao, and D. A. Moore, *Radiochimica Acta* **83**, 09-13 (1998).

[15] D. Rai, Y. A.. Gorby, J. K. Fredrickson, D. A. Moore, M. Yui., *Journal of Solution Chemistry (submitted)* (2001).

JP0250318

IS THERMODYNAMIC OF ACTINIDES APPLICABLE TO NATURAL DYNAMIC SYSTEMS?

Jae Il Kim

Forschungszentrum Karlsruhe, Germany

A modeling of the actinide migration behavior in natural aquifer systems entails sound knowledge of thermodynamics of actinides, which is considered as relevant to describe their geochemical reactions. For obvious reasons, thermodynamic constants of actinides are appraised from closed laboratory systems of equilibrium state. On the other hand, the geochemical reactions of actinides in natural dynamic systems undergo open chain of multiple reactions that appear to be non-equilibrium or often irreversible. For the appraisal of such complexities, a challenging question indubitably arises: "Is thermodynamics of actinides applicable to natural dynamic systems?" The question inevitably triggers off another: " Is there any alternative scientific tool available then?" This paper summarizes the present state of the thermodynamic approach being applied to the assessment of various geochemical reactions of actinides and discusses the limitations involved in application to natural dynamic systems.

This is a blank page.

JP0250319

JAERI-Conf 2002-004

PRESENT STATUS OF THE STUDY ON RADIONUCLIDE DIFFUSION IN BARRIER MATERIALS

Tetsuji YAMAGUCHI and Shinichi NAKAYAMA
Fax: 81-29-282-6678, e-mail: yamaguch@sparclt.tokai.jaeri.go.jp
Japan Atomic Energy Research Institute
Tokai, Ibaraki, 319-1195 Japan

When long-lived radionuclides are transported by groundwater through fractures in the rock mass surrounding a high-level radioactive waste repository, their diffusion into pores in the rock matrix and ensuing sorption onto mineral surfaces are expected to retard their transport along the pathways. There are pressing needs to incorporate the retardation mechanism into performance assessment of geological disposal in fractured rock. In JAERI, we have characterized the pore structure of the Japanese Inada biotite granite and confirmed that Fick's diffusion law can be applied to the transport of aqueous species in granite. Effective diffusivity was determined by the through-diffusion method for cationic, anionic and actinide complex species to explore the mechanism of diffusion of the aqueous species. Contribution of surface diffusion, or diffusion in adsorbed state, was observed in addition to pore diffusion for divalent cationic species. The results of this study enable us to provide a scientifically sound basis for radionuclide diffusion in granite for performance assessment of geological disposal.
Key words: Matrix diffusion, Granite, Pore structure, Diffusion coefficient, Surface diffusion

1. INTRODUCTION

After emplacement of radioactive wastes in a deep underground repository, long-lived radionuclides may be leached from the wastes and may subsequently be transported through the surrounding rock mass. Major water bearing fractures in the rock surrounding the repository are considered to form the main transport paths. Diffusion into the pores or micro fissures in the rock matrix and ensuing sorption onto mineral surfaces are important processes leading to the retardation of radionuclide transport through the geosphere. To evaluate the migration of radionuclides in deep geological formations, it is essential to understand the mechanisms of the diffusion of radionuclides into the rock matrix and to quantify the diffusivity. Granite was used in this study because it occurs widely in Japan and is being considered as a potential host rock for the deep underground disposal of radioactive wastes.

It is well-known that Fick's diffusion law can be applied to diffusion in porous materials.

$$J = -D_e \partial c / \partial x \qquad (1)$$

where J : diffusive flux (Bq m^{-2} s^{-1}),
D_e : effective diffusion coefficient (m^2 s^{-1}),
c : concentration of radionuclides in pore water (Bq m^{-3}),
x : length coordinate in diffusion direction (m).

When this theory is applied to the diffusion of ions in a rock, the pore size is assumed to be significantly larger than the diffusing ions. This assumption should be verified. The effective diffusivity of an aqueous species through the interconnected pore space in a rock matrix is often assumed to be proportional to its diffusivity in bulk solution (D_v) and to the geometric

parameters of the rock: ε (porosity), δ (constrictivity) and τ^{-2} (τ: tortuosity).

$$D_e = D_v \varepsilon \delta \tau^{-2}. \quad (2)$$

This relationship has been proposed for diffusion in macro-porous media by Brakel and Heertjes [1], and has been applied to the diffusion in the rock matrix by Neretnieks [2]. Although it is convenient to use this relationship to describe diffusion in rock matrix, several researchers [3-5] suggested the contribution of diffusion in adsorbed state, or surface diffusion, based on the fact that effective diffusion coefficients of cationic species were much larger than the calculated values based on Eq. (2). The evidence of the surface diffusion, however, has not been provided.

For actinides, empirical data on diffusion in barrier materials are very limited in number except for U(VI) because of difficulty in experiments such as low solubility, strong adsorption onto minerals and onto container walls, complexation with ligands in water and redox reactions. In order to overcome these difficulties, experiment should be performed under well-controlled conditions for a long time.

In this study we have characterized the pore structure of the Japanese Inada biotite granite to confirm that Fick's diffusion law can be applied to the transport of aqueous species in granite. Effective diffusivity was determined by the through-diffusion method for cationic, anionic and actinide complex species to explore the mechanism of diffusion of the aqueous species.

2. EXPERIMENTAL

2.1 Analysis of pore structure

The water saturation method and the mercury intrusion porosimetry were applied to the characterization of micropores in granite from Inada, Ibaraki, eastern Japan [6]. Although these techniques have been commonly used to characterize pores in rocks, special cares should be taken for precise measurement of the porosity and the pore size of low-porosity rocks. In the water saturation method, analysis of drying curves of water-saturated weight [7] enabled precise measurements of porosity. In the mercury intrusion porosimetry, a major part of the error comes from rough surfaces of the sample, which was reduced by cutting the samples into rectangular parallelepipeds, instead of crushing. The volume of the rock sample put into the measurement cell of the mercury porosimeter was optimized. The pore structure of Inada granite was observed by SEM (Super Scan 330 FEG, Shimadzu) after polishing and depositing carbon on the surfaces.

2.2 Diffusion experiment

Diffusive transport of aqueous species in granite was studies by a through-diffusion method. A granite disk having a diameter of 4.0×10^{-2} m and a thickness of 5×10^{-3} m without visible cracks was fitted tightly in an acrylic diffusion cell [8] and any gap between the rock disk and the acrylic were filled with a silicone gasket. The granite disk was sandwiched between two reservoirs, each with a capacity of 1.18×10^{-4} m^3. The assembled diffusion cell was soaked in a working solution to be used in the diffusion experiments or in distilled and deionized water (DDW) under vacuum to evacuate all air from the interconnected pores in the granite. The diffusion cell was then kept under atmospheric pressure for 30 days to

pre-condition the granite disk with the working solution. Solutions were prepared from reagent grade chemicals (Wako Pure Chemical Industries, Ltd., Tokyo) and DDW (Milli-Q Labo System, Millipore).

After pre-conditioning the granite disk with a 10^2 mol m^{-3} KI solution, the solution in a reservoir, source reservoir, was replaced by a 10^2 mol m^{-3} KI solution containing ^{125}I and ^{134}Cs to start the diffusion of I^- and Cs^+. At 7 days intervals, $1x10^{-6}$ m^3 aliquot was taken from the other reservoir, measurement reservoir, and its activity determined by γ–spectrometry with a pure Ge detector. The $1x10^{-6}$ m^3 aliquot removed from the measurement reservoir was replaced by an equal volume of the 10^2 mol m^{-3} KI solution to maintain the water levels in the two reservoirs. This balancing avoids occurrence of pressure difference that leads to advective transport from the source to measurement reservoir. The experiment was performed at (25.0± 0.5)°C in a water bath. At the termination of the diffusion, the inner wall of the measurement reservoir was rinsed with 10^4 mol m^{-3} HNO_3 to determine the amount of the tracers adsorbed on the cell walls. Diffusion experiment for tritiated water, $^{133}Ba^{2+}$, Np(IV) and Pu(IV) carbonate complexes were performed in the same manner. The experimental conditions were summarized in Table I.

3. RESULTS AND DISCUSSION

3.1 Pore structure

The porosity of Inada granite sample was determined to be (0.49±0.07) % by water saturation, which agreed with the value determined by mercury intrusion. The pore-size distribution of the granite was logarithmic normal with the modal diameter of 160 nm as shown in Fig. 1. Figure 2 shows the SEM images of the polished surface of the granite. Pores of a few tens to a few hundreds nm wide were observed at grain boundaries. This size is so large that the Fick's diffusion law is applicable to the diffusion of ions in the granite. The fact that the pore size was fairly uniform suggests the applicability of the pore-diffusion model to the diffusion of ions in the granite.

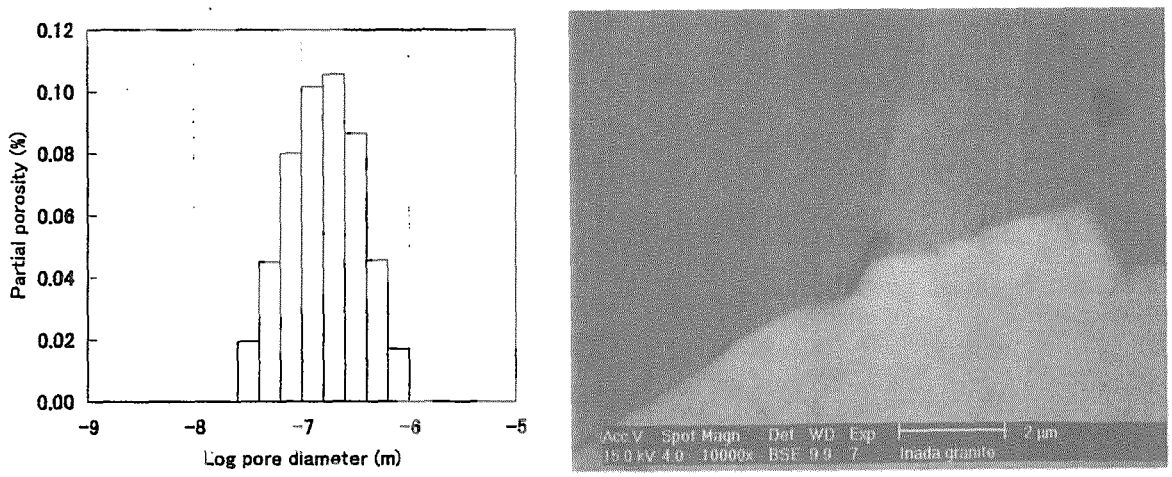

Fig. 1 Pore size distribution obtained by mercury intrusion (left) and SEM image (right) for Inada granite.

Table I Summary of diffusion experiments

Species	D_e ($m^2 s^{-1}$)	R_d ($m^3 kg^{-1}$)	Conditions
$^{125}I^-$	$(5.80\pm0.05)\times10^{-13}$	$(1.3\pm0.6)\times10^{-4}$	10^2 mol m^{-3} KI solution
$^{134}Cs^+$	$(5.04\pm0.18)\times10^{-13}$	$(7.5\pm0.8)\times10^{-4}$	pH = 6.0, 25 °C, aerobic
$^{125}I^-$	$(7.98\pm0.07)\times10^{-13}$	$< 2.3\times10^{-4}$	10^2 mol m^{-3} CsI solution*
$^{134}Cs^+$	$(6.32\pm0.09)\times10^{-13}$	$< 1.8\times10^{-4}$	25 °C, aerobic
$^{125}I^-$	$(5.06\pm0.09)\times10^{-13}$	$< 2.8\times10^{-5}$	10^2 mol m^{-3} SrI_2 solution* 25 °C, aerobic
HTO	$(8.97\pm0.07)\times10^{-13}$ $(7.78\pm0.06)\times10^{-13}$ $(6.41\pm0.07)\times10^{-13}$ avg. $(7.7\pm1.4)\times10^{-13}$	$(4.0\pm1.9)\times10^{-5}$ $(-7.4\pm5.7)\times10^{-5}$ $(3.6\pm5.3)\times10^{-5}$ avg. $< 8\times10^{-5}$	DDW pH = 5.5 25 °C aerobic
$^{133}Ba^{2+}$	$(1.66\pm0.03)\times10^{-13}$ $(2.12\pm0.03)\times10^{-13}$ $(2.08\pm0.03)\times10^{-13}$ avg. $(1.95\pm0.21)\times10^{-13}$	$(7.4\pm0.6)\times10^{-5}$ $(9.0\pm0.5)\times10^{-5}$ $(7.6\pm0.7)\times10^{-5}$ avg. $(8.0\pm0.9)\times10^{-5}$	10 mol m^{-3} $BaCl_2$ solution pH = 6.5 25 °C aerobic
$^{125}I^-$	$(5.15\pm0.10)\times10^{-13}$ $(7.22\pm0.31)\times10^{-13}$ $(6.07\pm0.13)\times10^{-13}$ avg. $(6.1\pm0.9)\times10^{-13}$	$(-1.2\pm0.31)\times10^{-5}$ $(-0.3\pm1.0)\times10^{-5}$ $(-1.28\pm0.45)\times10^{-5}$ avg. $< 1.6\times10^{-5}$	
$^{133}Ba^{2+}$	$(1.99\pm0.04)\times10^{-13}$ $(2.25\pm0.03)\times10^{-13}$ $(2.90\pm0.07)\times10^{-13}$ avg. $(2.38\pm0.38)\times10^{-13}$	$(1.94\pm0.10)\times10^{-4}$ $(2.12\pm0.09)\times10^{-4}$ $(2.72\pm0.20)\times10^{-4}$ avg. $(2.26\pm0.35)\times10^{-4}$	1 mol m^{-3} $BaCl_2$ solution pH = 6.1 25 °C aerobic
$^{125}I^-$	$(6.62\pm0.36)\times10^{-13}$ $(8.6\pm0.9)\times10^{-13}$ $(10.08\pm0.31)\times10^{-13}$ avg. $(8.4\pm1.7)\times10^{-13}$	$(0.9\pm1.0)\times10^{-5}$ $(-2.7\pm3.2)\times10^{-5}$ $(3.2\pm0.9)\times10^{-5}$ avg. $< 3.1\times10^{-5}$	
$^{133}Ba^{2+}$	$(6.57\pm0.21)\times10^{-13}$ $(7.43\pm0.09)\times10^{-13}$ $(5.71\pm0.11)\times10^{-13}$ avg. $(6.6\pm0.7)\times10^{-13}$	$(8.1\pm0.7)\times10^{-4}$ $(9.56\pm0.30)\times10^{-4}$ $(7.59\pm0.34)\times10^{-4}$ avg. $(8.4\pm0.9)\times10^{-4}$	10^{-1} mol m^{-3} $BaCl_2$ solution pH = 6.2 25 °C aerobic
$^{125}I^-$	$(10.05\pm0.48)\times10^{-13}$ $(3.90\pm0.47)\times10^{-13}$ $(6.29\pm0.39)\times10^{-13}$ avg. $(6.7\pm2.6)\times10^{-13}$	$(5.6\pm1.9)\times10^{-5}$ $(-5.3\pm1.8)\times10^{-5}$ $(-3.9\pm1.4)\times10^{-5}$ avg. $< 3.9\times10^{-5}$	
$Pu(CO_3)_2(OH)_2^{2-}$	$(1.28\pm0.29)\times10^{-13}$ $(2.00\pm0.45)\times10^{-13}$ $(2.76\pm0.61)\times10^{-13}$ avg.$(2.0\pm1.4)\times10^{-13}$	$(5.7\pm2.7)\times10^{-4}$	$[NaHCO_3^-] = 10^2$ mol m^{-3} $[S_2O_4^{2-}] = 10$ mol m^{-3} pH = 9.2, Eh = 70 mV vs. NHE 24.5±3.2°C, Ar, O_2 content~3×10^{-6}
$Np(CO_3)_4^{4-}$, $Np(CO_3)_5^{6-}$	$(5.41\pm0.10)\times10^{-13}$ $(2.85\pm0.10)\times10^{-13}$ $(3.84\pm0.14)\times10^{-13}$ avg.$(4.0\pm1.5)\times10^{-13}$	$(12.3\pm1.5)\times10^{-5}$ $(4.7\pm1.5)\times10^{-5}$ $(-0.6\pm2.3)\times10^{-5}$ avg. $< 1.4\times10^{-4}$	$[NaHCO_3^-] = 10^3$ mol m^{-3} $[S_2O_4^{2-}] = 50$ mol m^{-3} pH = 8.9, Eh = -450 mV vs. NHE 26±1°C, Ar, O_2 content~1×10^{-6}

* DDW was placed in the measurement reservoir.

3.2 Effective diffusivity

The concentration of an species in pore water in one-dimensional diffusion system is derived from Eq. (1) as:

$$(\varepsilon+\rho R_d)\partial c/\partial t = D_e \partial^2 c/\partial x^2 \qquad (3)$$

assuming that local adsorption equilibrium is attained

$$q = R_d c \qquad (4)$$

where q : amount of the species adsorbed onto the rock (mol kg^{-1}),
ρ : bulk density of the rock (2.64×10^3 kg m^{-3}),
R_d : distribution ratio (m^3 kg^{-1}).

The initial and boundary conditions are

$$c(x, 0) = 0 \quad \text{at } 0 < x \leqq L, \tag{5}$$

$$c(0, t) = c_1, \tag{6}$$

$$c(L, t) = c_2 << c_1, \tag{7}$$

where L : thickness of the rock sample (5×10^{-3} m),
c_1 : concentration of a species in the source reservoir (Bq m^{-3}),
c_2 : concentration of a species in the measurement reservoir (Bq m^{-3}).

The solution of Eq. (3) under the conditions of Eqs. (5) - (7) had been given by Crank [9]. The concentration of a species in the measurement reservoir after a long period is approximated to

$$c_2(t)/c_1 = AV_2^{-1}(D_e L^{-1} t - (\varepsilon + \rho R_d)L/6) \tag{8}$$

where A : cross section of the rock sample (1.256×10^{-3} m^2),
V_2 : volume of the measurement reservoir (1.18×10^{-4} m^3).

The values of D_e and $(\varepsilon + \rho R_d)$ were determined from the slope and the intercept on the concentration axis of the extrapolated linear region of the diffusion curve, Eq. (8).

Figure 2 shows the time dependence of the concentrations of ^{134}Cs and ^{125}I in the 10^2 mol m^{-3} KI solution in the measurement reservoir. The concentration of ^{125}I increases linearly with time. The effective diffusivity of $(5.80 \pm 0.05) \times 10^{-13}$ m^2 s^{-1} was obtained from the slope by using the least squares fitting. The intercept on the concentration axis was very small, which indicated that the adsorption of I^- on granite was negligibly small ($R_d < 1.9 \times 10^{-4}$ m^3 kg^{-1}). The concentration of ^{134}Cs increased linearly after 140 days from the start of the diffusion. An effective diffusivity of $(5.04 \pm 0.18) \times 10^{-13}$ m^2 s^{-1} and a distribution ratio of $(7.5 \pm 0.7) \times 10^{-4}$ m^3 kg^{-1} were obtained. Results of all of the diffusion experiments were summarized in Table I.

In order to check the validity of the constant proportionality between D_e and D_v assumed in Eq. (2), experimentally obtained D_e's and literature data for strontium, cobalt [10], uranium [8, 11] and uranine [12] are plotted versus D_v in Fig. 3. D_v's for the diffusing species under the experimental conditions were estimated by taking into account mode of diffusion [13] (salt diffusion or tracer diffusion), concentration of the diffusing species, ionic strength of the solution and temperature [11]. Except for the data for Ba^{2+} and Sr^{2+} the data points lie on a curve. A positive correlation with a nearly constant D_e/D_v ratio is observed between D_e values in the granite and diffusivity in water for most of the species, which validates the constant proportionality between D_e and D_v. However, unexpectedly high D_e values are obtained for Sr and Ba, which have high distribution ratio. The data for Sr had been explained by supposing that the adsorbed Sr ions are mobile in adsorbed state (surface diffusion) [10].

In case that both the surface and the pore diffusion contribute to the diffusion on ions in rocks, effective diffusivity should be expressed as [10]

$$D_e = D_v \varepsilon \delta \tau^{-2} + D_s \rho R_d \tag{9}$$

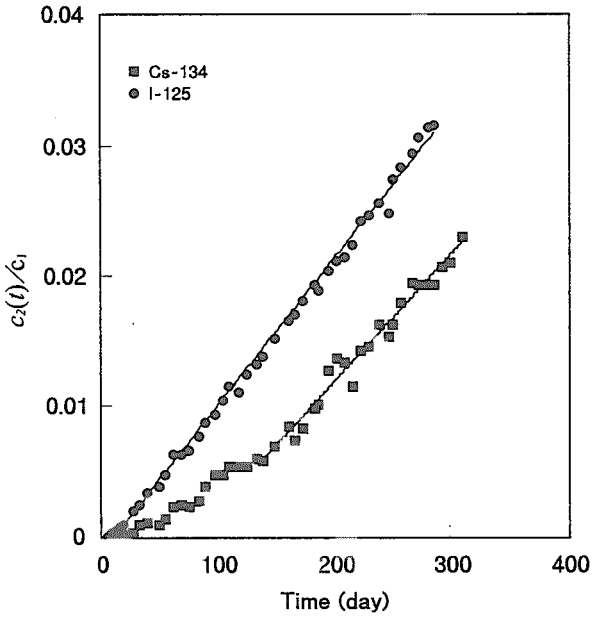

Fig. 2 Through-diffusion curve of cesium and iodine through a 5-mm thick Inada granite disk.

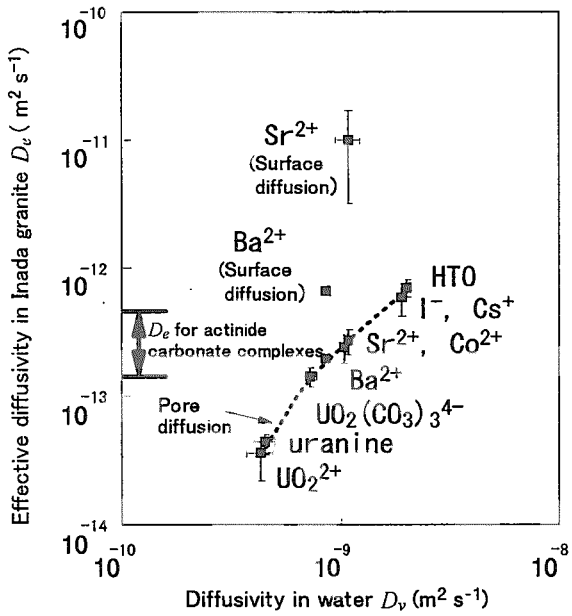

Fig. 3 Correlation between effective diffusivities of species in Inada granite and their diffusivity in aqueous solution.

The 1st term of Eq. (9), contribution of the pore diffusion, was estimated to be (2.1±0.5)x10^{-13} m^2 s^{-1} for Ba^{2+} based on a $\varepsilon\delta\tau^{-2}$ value of (2.5±0.6)x10^{-4} [10] and a D_v value of 8.48x10^{-10} m^2 s^{-1} [13]. In the diffusion experiments using the 10 mol m^{-3} $BaCl_2$ solution, the effective diffusivity, D_e, of (1.95±0.21)x10^{-13} m^2 s^{-1} and the distribution ratio, R_d, of (8.0±0.9)×10^{-5} m^3 kg^{-1} were obtained. This value is close to the estimated value of (2.1±0.5)x10^{-13}. The 1 mol m^{-3} $BaCl_2$ solution produced the larger D_e and the larger R_d of (2.38±0.38)x10^{-13} m^2 s^{-1} and (2.26±0.35)×10^{-4} m^3 kg^{-1}, respectively. We obtained the largest D_e, (6.6±0.7)x10^{-13} m^2 s^{-1}, and the largest R_d, (8.4±0.9)×10^{-4} m^3 kg^{-1}, for the 10^{-1} mol m^{-3} $BaCl_2$ solution.

The effective diffusivity of I^-, non-sorbed species, was not affected by $BaCl_2$ concentrations; (6.1±0.9) x10^{-13}, (8.4±1.7)x10^{-13} and (6.7±2.6)x10^{-13} m^2 s^{-1} for 10, 1 and 10^{-1} mol m^{-3} $BaCl_2$ solution, respectively. These values are close to an estimated value, 6.4x10^{-13} m^2 s^{-1}, obtained from an equation for the effective diffusivity of iodine in rocks [14]

$$D_e = 6.4\text{x}10^{-10}\varepsilon^{1.3} \qquad (10)$$

where ε was 0.0049.

The results for I^- show that the physical property of the pore structure was almost the same between the experiments, and accordingly the variation in D_e of Ba^{2+} was not physically caused. The variation in D_e value was also not due to the speciation of barium in the solution because complexations of Ba^{2+} by Cl^- and $S_2O_3^{2-}$ are negligible and carbonate precipitation is not favorable under the working pH range (6.1 - 6.5) [15]. The effective diffusivity of Ba^{2+} increased as the distribution ratio increased. This fact is strongly indicative of surface diffusion. The linear relationship between the effective diffusivity and the distribution ratio of Ba^{2+} gives the D_s value in Eq. (9) of (2.4±0.1)x10^{-13} m^2 s^{-1}. This D_s value is smaller than the value for Sr^{2+}, 3.5x10^{-12} m^2 s^{-1}, obtained previously [10].

Figure 4 shows schematics of the diffusion of $^{133}Ba^{2+}$ through the granite in the present experiment. Gradient of $^{133}Ba^{2+}$ concentration exists both in aqueous phase and in adsorbed phase between the source reservoir and the measurement reservoir. Diffusion of $^{133}Ba^{2+}$ is driven by both of these gradients. Diffusive flux in adsorbed phase, $-D_s\rho\partial q/\partial x$, prevails over that in aqueous phase, $-D_p\varepsilon\partial c/\partial x$, when distribution ratio is high.

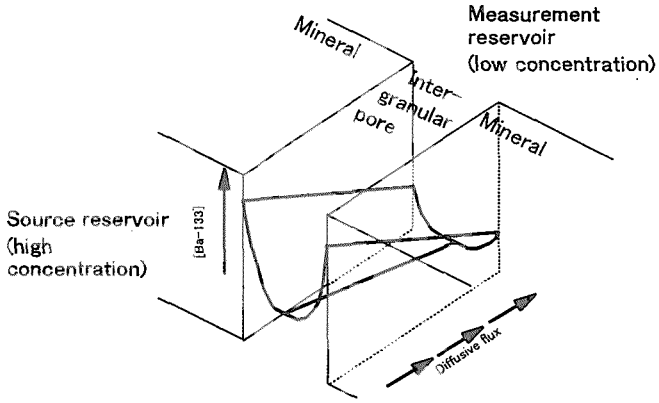

Fig. 4 Schematics of the aqueous and adsorbed phase diffusion of Ba^{2+} in the diffusion experiments through Inada granite disk.

Speciation calculation using a thermodynamic database [16] showed that Pu and Np were present predominantly as $Pu(CO_3)_2(OH)_2^{2-}$ and $Np(CO_3)_n^{4-2n}$ (n = 4, 5), respectively, under the experimental conditions. The concentration of plutonium in the measurement reservoir increased linearly with time in the period of 400 - 588 d after the start of the diffusion. An effective diffusivity value of $(2.0\pm1.4)\times10^{-13}$ m^2 s^{-1} was obtained on the average of triplicate experiments. The concentration of neptunium in the measurement reservoir increased linearly with time in the period of 50 - 329 d after the start of the diffusion. A D_e value of $(4.0\pm1.5)\times10^{-13}$ m^2 s^{-1} were obtained. These D_e values are comparable to previously obtained value for $UO_2(CO_3)_3^{4-}$, which was consistent with an empirical correlation between D_e and D_v. The range of D_e for actinide carbonate complexes were also shown in Fig. 3. The diffusivity is not high enough to be indicative of surface diffusion.

4. CONCLUDING REMARK

We have characterized the pore structure of the Japanese Inada biotite granite, which showed applicability of the Fick's diffusion law to the transport of aqueous species in granite. Effective diffusivity was determined by the through-diffusion method for cationic, anionic and actinide complex species to explore the mechanism of diffusion of the aqueous species. Contribution of surface diffusion, or diffusion in adsorbed state, was observed in addition to pore diffusion for divalent cationic species. The results of this study enable us to provide a scientifically sound basis for radionuclide diffusion in granite for performance assessment of geological disposal.

Diffusion of radionuclides in low-permeability engineered barrier materials such as compacted bentonite and cementitious materials is of great importance in the performance assessment of repositories. However, long-term assessment of the diffusive mass transport in low-permeability materials includes large uncertainties because pore structures and long-term degradation of the materials are poorly known. Future studies should emphasize understanding the diffusion mechanisms in low-permeability engineered barrier materials, data acquisition on long-term degradation of the materials and quantifying uncertainties associated with long-term mass transport analysis.

5. ACKNOWLEDGEMENT

Authors acknowledge Professors K. Higashi and H. Moriyama (Kyoto University), Dr. T. T. Vandergraaf (AECL) and Prof. S. Nakashima (Tokyo Institute of Technology) for helpful discussion. Dr. H. Isobe (present affiliation: Kumamoto University) is acknowledged for technical support. We are grateful to Mr. Y. Tamura, Mr. I. Kitagawa, Mr. H. Okamoto, Mr. A. Kijima, Mr. Y. Kawasaki (WASTEF, JAERI) for performing Pu experiments. Experimental supports from graduate students, Ms. C. Kawada (Tokai University, present affiliation: Toshiba Corporation) and Mr. K. Asahara (Kyoto University, present affiliation: Chubu Electric Power Co., Inc.) are greatly acknowledged. I hereby acknowledge that this study was performed as a part of nuclear safety research program of JAERI for many years.

6. REFERENCES

[1] J. V. Brakel and P. M. Heertjes, Int. J. Heat Mass Transfer, 17, 1093-1103 (1974).

[2] I. Neretnieks, Geophys. Res. 85, 4379-4397 (1980).

[3] M. H. Bradbury, A. Green, D. Lever and I. G. Stephen, "Diffusion and permeability based sorption measurements in sandstone, anhydrite and upper magnesian limestone samples", AERE-R 11995. (1986).

[4] K. Skagius and I. Neretnieks, Water Resour. Res., 24, 75-84 (1988).

[5] M. Tsukamoto and T. Ohe, T., Chem. Geol. 90, 31-44 (1991).

[6] T. Yamaguchi, H. Isobe and S. Nakayama, Radioactive Waste Research, 3, 99-107 (in Japanese) (1997).

[7] T. W. Melnyk and A. M. M. Skeet, Can. J. Earth Sci., 23, 1068-1074 (1986).

[8] T. Yamaguchi and S. Nakayama, J. Contam. Hydrol. 35, 55-65 (1998).

[9] J. Crank, "The mathematics of diffusion. 2nd ed.", Oxford Univ. Press, London (1975) pp. 49-53 .

[10] T. Yamaguchi, Y. Sakamoto, and M. Senoo, J. Nucl. Sci. Technol., 30, 796-803 (1993).

[11] T. Yamaguchi, Y. Sakamoto, S. Nakayama and T. T. Vandergraaf, J. Contam. Hydrol., 26, 109-117 (1997).

[12] M. Kumata, T. Iwai, T. Sagawa, T. Suzuki and K. Nishiyama, "Diffusion experiment of a radionuclide in granitic rock cores", JAERI-M 90-179 (in Japanese), JAERI, Tokai, Japan (1990).

[13] Y. H. Li and S. Gregory, Geochim. Cosmochim. Acta, 38, 703-714 (1974).

[14] K. Nishiyama, S. Nakashima, R. Tada and T. Uchida, Mining Geol. (in Japanese), 40, 323-326 (1990).

[15] A. Dean, "Lange's Handbook of Chemistry", McGraw-Hill, New York (1978) pp 5.7.

[16] T. Yamaguchi, "Consideration of thermodynamic data for predicting solubility and chemical species of elements in groundwater. Part 2: Np, Pu", JAERI-Data/Code 2000-031 [in Japanese], JAERI, Tokai, Japan (2000).

JP0250320

JAERI-Conf 2002-004

OVERVIEW OF WASTE FORM DEGRADATION PROCESS MODELS FOR PERFORMANCE ASSESSMENT

F.M.G. Wong[1], C. Stockman[2], R. Rechard[2], and P. Brady[2]

Yucca Mountain Site Characterization Office
1551 Hillshire Dr. M/S 471
Las Vegas, NV 89134
Fax: (702) 792-1323, e-mail: frank_wong@notes.ymp.gov
[1] Stone & Webster, Inc., [2] Sandia National Laboratory

The *Waste Form Degradation Process Model Report* (Waste Form Degradation PMR)[1] is one of nine PMRs that have the shared objective of describing the technical information that was used in the total system performance assessment (TSPA) conducted to evaluate the postclosure performance of a potential monitored geologic repository at Yucca Mountain. The TSPA-SR (site recommendation) will be used in the preparation of a document for a Secretarial decision on whether to recommend the Yucca Mountain site for development as a repository. The Waste Form Degradation PMR summarizes the results of investigations on the degradation of the radioactive spent nuclear fuel (SNF), high-level waste (HLW), dissolved radionuclides, and colloidal radionuclides.

The culmination of these investigations was the construction of the Waste Form Degradation Model to predict the dissolved or colloidal radionuclides available for transport in the TSPA for SR (TSPA-SR). The Waste Form Degradation Model consists of eight major modeling/analysis components: (1) Radioisotope Inventory, (2) In-Package Chemistry, (3) Commercial Spent Nuclear Fuel (CSNF) Degradation, (4) CSNF Cladding Degradation (5) U.S. Department of Energy (DOE) Spent Nuclear Fuel (DSNF) Degradation, (6) HLW Degradation, (7) Radioisotope Dissolved Concentration (solubility), and (8) Radioisotope Colloidal Concentration. These eight components are generally connected sequentially starting with the radioisotope inventory as input and ending with projected radioisotope dissolved and colloidal concentration.

Within the analysis for the TSPA-SR analysis, the function of the Waste Form Degradation Model is to determine three outputs over time: (1) dissolved concentration, (2) reversible colloidal concentration, and (3) irreversible colloidal concentration of radionuclides.

This paper will describe and summarize the eight components of the Waste Form Degradation Process Model.

Key Words: Waste Form Degradation, Performance Assessment, Process Model

1. INTRODUCTION

The overall objective of the *Waste Form Degradation Process Modeling Report* (Waste Form Degradation PMR)[1] is to summarize the technical basis of the Waste Form Degradation model. The degradation of the waste eventually leads to mobilization of radionuclides and release into other components of the engineered barrier system (EBS) which are simulated in the total system performance assessment (TSPA). The function of the Waste Form Degradation Model is to determine three outputs over time: (1) dissolved concentration, (2) reversible colloidal concentration, and (3) irreversible colloidal concentration of radionuclides (Figure 1).

2. COMPONENTS OF THE WASTE FORM DEGRADATION MODEL

The Waste Form Degradation Model consists of eight major modeling/analysis components: (1) Radioisotope Inventory, (2) In-Package Chemistry, (3) Commercial Spent Nuclear Fuel (CSNF) Degradation, (4) CSNF Cladding Degradation (5) U.S. Department of Energy (DOE) Spent Nuclear Fuel (DSNF) Degradation, (6) HLW Degradation, (7) Radioisotope Dissolved Concentration (solubility), and (8) Radioisotope Colloidal Concentration. These eight

components are generally connected sequentially starting with the radioisotope inventory as input and ending with projected radioisotope dissolved and colloidal concentration (Figure 2). The *Radioisotope Inventory Component* developed for the TSPA-SR uses updated values for the inventory. The sources of information are based on internal documents for CSNF, reports from the National Spent Nuclear Fuel Program (NSNFP) for DSNF, and the Environmental Impact Statement (EIS) for HLW. An updated screening was conducted and resulted in 27 radionuclides identified as important (24 based on human dose and 3 mandated by the Groundwater Protection Requirements of the proposed U.S. Environmental Protection Agency [EPA] standard 40 CFR 197 [64 FR 46976]).

The *In-Package Chemistry Component* developed for the TSPA-SR couples the seepage rate of water into the package and degradation of the steel, aluminum, DSNF, CSNF, and HLW inside the package to evaluate water chemistry parameters such as hydronium ion concentration, total carbonate concentration, dissolved partial pressures of carbon dioxide and oxygen, ionic strength, and fluoride and chloride ion concentrations (i.e., pH, $p[CO_3]_T$, P_{CO_2}, P_{O_2}, [I], [F], [Cl]). The analysis is performed using the EQ3/6 geochemical code. The sources of information for the EQ3/6 geochemical simulations include a chemical thermodynamics database and information on the in-package environment. These results influence degradation of the CSNF cladding and matrix, HLW degradation, radionuclide solubility, and colloid availability and stability. The degradation of the CSNF matrix and HLW, in turn, influence the In-Package Chemistry Component.

The *CSNF Matrix Degradation Component* predicts a log rate using two linear regression equations based on pH, $p[CO_3]_T$, P_{O_2}, and temperature (T) to evaluate matrix degradation over time; one equation is applicable for pH less than or equal to 7 and the other is applicable for pH greater than 7. The regression variables used, pH, $p[CO_3]_T$ and P_{O_2}, are coupled to in-package chemistry to account for uncertainty. The sources of information include flow through, static, batch reactor, and drip tests involving the dissolution of fresh and spent reactor fuels under both saturated and unsaturated conditions.

The *CSNF Cladding Degradation Component* evaluates degradation of the cladding and is coupled to the CSNF Matrix Degradation and In-Package Chemistry components developed for the TSPA-SR. The sources of information include failure data from reactor operation, pool and dry storage, and transportation. To better evaluate the performance of the cladding, two steps of degradation are included: perforation and matrix exposure. Perforation mechanisms include cladding damage during reactor use, creep failures at high temperatures during dry storage, transportation, or initial disposal, mechanical failure from earthquakes, and localized corrosion after disposal. The process of exposing the matrix and releasing radionuclides is through potential unzipping of the cladding caused by expansion of the fuel matrix as the uranium dioxide (UO_2) forms secondary minerals.

The *DSNF Degradation Component* developed for TSPA-SR uses a constant, bounding degradation rate based upon experimental data for N-Reactor SNF for all the DSNF waste types with the exception of naval SNF. However, the radioisotope inventory is the weighted mass average of DSNF waste types. Naval SNF degradation behavior is bounded by that of the CSNF.

The *HLW Degradation Component* developed for TSPA-SR uses bounds on parameters of a phenomenological model to develop a simplified (Arrhenius-type) rate equation of

degradation that is dependent only upon pH and temperature. Conservative estimates of the model parameters are based upon experimental data for the degradation of borosilicate glass.

In the *Dissolved Radioisotope Concentration Component*, the solubilities of important radionuclides (as determined by updated screening) were reevaluated. The sources of information include EQ3/6 simulations of in-package chemistry for three categories of radionuclides. Three radioisotope solubilities were abstracted as a direct function of in-package chemistry (Np, U, Am) and three radionuclides solubilities (Ac, Cm, Sm) set equal to that of Am. Four additional radioisotope solubilities were defined by probability distributions (Pu, Pb, Pa, Ni). All other radioisotope solubilities were set at bounding values. The distributions and bounding values were based on results of the process modeling of the in-package chemistry.

For the *Colloidal Radioisotope Concentration Component*, the conceptualization directly used YMP-relevant experimental results from YMP-specific work and from the published literature. The conceptualization identified the availability and the stability of three categories of colloids: (1) existing colloids in the groundwater, (2) colloids generated during degradation of the waste, and (3) colloids generated during degradation of the disposal container.

3. DISCUSSION OF THE MODEL COMPONENTS

3.1 Radionuclide Inventory Component

The function of the radioisotope inventory abstraction component is to estimate the inventory of those radionuclides most important to human dose. The inventory abstraction component is input for the waste form degradation models and is developed from a series of steps that starts with radioisotope inventories of various spent nuclear fuel assemblies and HLW then estimates the radioisotope inventory when packaged in disposal containers. Three important aspects of the radionuclide inventory are (1) selecting the most important radionuclides for human dose out of the few hundred found within the waste, (2) obtaining the radioisotope inventories of various wastes, and (3) grouping the fuels into the waste packages selected for modeling in the TSPA-SR analysis.

Three sources were used for inventory data[1]: the commercial utilities for, the DOE NSNFP for DSNF, and the Yucca Mountain Environmental Impact Statement (EIS) program for the HLW, mixed oxide fuel (MOX), and plutonium ceramic. From this radioisotope inventory, the most important radionuclides for human dose were evaluated. Arrival scenarios were developed for CSNF, and the inventory was assigned to WP configurations. Average and bounding inventories were developed for each package configuration recommended for the repository. Then, the package-specific radionuclide activities were combined using the number of WPs in each group as a weighting factor to get the radionuclide activities in each allocation category.

The relative importance of individual radionuclides for human inhalation and ingestion doses was evaluated for several waste types, time frames, and release scenarios. In this evaluation, the effects of inventory abundance, radionuclide longevity, element solubility, and element transport affinity were considered.

3.2 In-Package Chemistry Component

The function of the In-package Chemistry Model Component is to estimate the fluid chemistry inside the waste package over time after the initial breach of the waste package.

The water chemistry parameters in the model include hydronium ion concentration, dissolved partial pressures of carbon dioxide and oxygen, ionic strength, and fluoride and chloride ion concentrations. This chemistry is used by the several other model components (see Figure 2) because the rate of degradation of the matrix of waste, the resulting dissolved concentration of radionuclides, the stability of any colloids, and degradation of cladding are all dependent on the chemistry of fluids within the WP. The in-package chemistry component in the TSPA-SR couples the seepage rate of water into the package with the degradation of the steel, aluminum, SNF, and HLW inside the package to evaluate the key water chemistry parameters. These results influence degradation of the CSNF cladding and matrix, HLW degradation, radionuclide solubility, and colloid availability and stability. The degradation of the CSNF cladding and matrix, and HLW, in turn, influence the in-package chemistry component.

3.3 CSNF Degradation Component

The main function of the CSNF Degradation Model Component is to determine the rate of degradation of the CSNF matrix as a function of temperature and water chemistry (specifically, pH and partial pressures of O_2 and CO_2). This degradation rate is then directly used by the Cladding Degradation Model Component (Section 3.4) to determine the rate at which the CSNF cladding splits open and exposes more of the fuel matrix. In addition, the CSNF degradation model examines the distribution of radionuclides within the fuel and establishes a gap fraction for the more volatile radionuclides.

Under oxidizing conditions, in the presence of water or water vapor, UO_2 in CSNF is not stable and alters. Alteration of the UO_2 matrix can liberate radionuclides important to human dose. As described in Section 2, the CSNF matrix degradation component uses two linear regression equations to predict a log rate for matrix degradation over time.

The CSNF matrix degradation component is based on experimental measurement of the dissolution rate of a number of fresh and spent fuels. These materials were examined under both saturated and unsaturated conditions using flow-through reactors as well as static, batch, and drip reactors. These tests also give empirical information on secondary phase production, colloids, and effective solubility limits for the more insoluble radionuclides. The secondary phases are similar to those observed in the corrosion of natural uraninite deposits, indicating that the experimental results are indeed relevant to the long-term behavior.

3.4 CSNF Cladding Degradation Component

This component evaluates degradation of the cladding and is coupled to the CSNF Matrix Degradation and In-Package Chemistry components in the TSPA-SR. The degradation of CSNF cladding is assumed to proceed through two distinct steps: cladding failure (usually by small perforations), and progressive exposure of the fuel matrix.

Initial breach of the cladding may occur because (1) the cladding fails within the reactor or during storage or transportation, (2) an earthquake severely shakes and severs the rods, (3) the cladding fails from localized corrosion, or (4) the cladding fails from creep or stress corrosion cracking. While other mechanisms of initiating cladding perforations, such as rock fall or DHC, were explored, they were screened out based on low probability.

After the cladding has initially been breached, it is assumed to unzip because the fuel volume increases during alteration of the UO_2, (i.e., the alteration of the UO_2 to secondary phases of uranium is assumed to cause enough pressure due to volume expansion to burst the cladding

from within). This mechanism for increasing the exposed surface area of the matrix is sensitive to environmental conditions such as temperature. The anticipated temperature of the fuel matrix is not high enough, nor does it occur for a long enough period, to cause unzipping in a dry environment, so the dry unzipping is not included. Once the Zircaloy cladding has been perforated, unzipping in a wet environment does not occur in time periods of 40 years, based on observed behavior within storage pools at reactors. However, because unzipping in a wet environment could not be entirely ruled out, and because complete exposure of the matrix bounds diffusive releases of radionuclides through the perforation, it is conservatively assumed that clad unzipping in a wet environment can occur. The rate of wet unzipping was conservatively estimated by relating it to the movement of the alteration front.

3.5 DSNF Degradation Component

This component determines the rate of degradation of the DSNF waste category and of the immobilized plutonium ceramic waste. The degradation behavior of DSNF (excluding the naval SNF) will be represented by the metallic uranium SNF from N-Reactor. The naval SNF degradation behavior will be represented by that of the CSNF. TSPA-SR will use a degradation rate and a corresponding effective surface area that bounds the experimental data on N-Reactor fuel collected over a range of conditions in the last few years. In the TSPA-SR, the DSNF degradation component uses a constant, bounding degradation rate of N-Reactor SNF to bound all the DSNF waste types except naval SNF. However, the radioisotope inventory of the DSNF components is the weighted mass average of all waste types.

In addition, the immobilized ceramic plutonium waste form was also evaluated. This waste form will consist of disks of a plutonium-containing, titanium dioxide-based ceramic that will be enclosed in stainless steel cans, which in turn will be encased in a borosilicate glass matrix within the high level waste canisters.

3.6 High-Level Waste Degradation Component

This component provides a conservative model for calculating the rate of degradation of borosilicate glass for the range of conditions (immersion, humid air, and dripping water) to which it may be exposed after the waste packages fail. For TSPA-SR, this component uses bounds on parameters of a phenomenological model to develop a simplified (Arrhenius-type) rate equation of degradation that is dependent only upon pH and temperature.

The HLW model is implemented in the TSPA-SR analysis to calculate the rate of glass degradation. The rate of radionuclide release from the HLW matrix will be calculated by multiplying the glass degradation rate by the mass fraction of the radionuclide in the glass. This approach for calculating the radionuclide release rate is based on the conservative assumption that the release of radionuclides is congruent with the degradation of borosilicate glass.

The model parameters account for the pH, temperature, surface area, and the combined effects of glass composition and solution composition on the rate of glass corrosion. Conservative estimates of the values for the model parameters are provided based on experimental data. Consistent with the conceptual model for in-package chemistry, degradation of borosilicate glass is conservatively assumed to occur as if the glass were fully immersed, although it is expected that much of the glass will be exposed to humid air or dripping water conditions.

3.7 Dissolved Radioisotope Concentration Component

This component evaluates the dissolved concentration of radionuclides (or parents of radionuclides) that are important to human dose, as determined by the radioisotope screening described in the inventory section (Section 3.1). In the dissolved radioisotope concentration component, the solubilities of important radionuclides were reevaluated: three radioisotope solubilities were abstracted as a direct function of in-package chemistry (and three more radionuclides equated to one of these); four radioisotope solubilities were defined by a probability distribution; and all others were set at bounding values based on results of the process modeling of the in-package chemistry.

The dissolved concentration limits calculation builds upon three primary feeds: (1) estimates of in-package fluid major element composition (pH, Eh, ionic strength, carbonate levels), (2) measured (and estimated) thermodynamic parameters describing the stabilities of aqueous species and solid radioisotope phases, and (3) a determination of the likely solubility-controlling phases for the specific radionuclides of concern. In nature, the controlling phase may either be a pure radionuclide solid phase with the radioisotope as the dominant element, or a solid phase with trace amounts of the radionuclide as can occur with coprecipitation. For TSPA-SR, the pure phases were chosen because, in general, they yield higher dissolved concentrations. Where insufficient information can be gleaned from field observations or experimental results, it is conservatively assumed that the most amorphous and hydrated (hence, most soluble) oxide of the particular radioelement forms.

A systematic review of thermodynamic data and controlling phases has been performed for a large range of chemical conditions. When uncertainties were encountered, choices were made that would result in higher predicted solubilities. Inherent limitations within the databases can lead to an uncertainty, up to a factor of 2, when the ionic strength exceeds about 0.7 mol/L. However, this uncertainty is small relative to other uncertainties within the system.

3.8 Colloidal Radionuclide Concentration Component

The function of this component is to calculate the concentration of colloid-associated radionuclides that may be transported from the waste package. A conceptualization was developed that directly used experimental results. The conceptualization identified the availability and the stability of three categories of colloids: (1) Waste-form colloids formed during degradation of HLW glass (Note: these colloids are further classified into "reversibly attached" and "irreversibly attached" radionuclide types), (2) Corrosion-product colloids formed during corrosion of iron-containing waste packages, (3) Groundwater colloids present in the waste-form area.

Colloid transport is potentially important for radionuclide elements that have low solubility and can be entrained in, or sorbed onto, waste form, engineered barrier, or geologic barrier materials that form colloidal particle substrates. Of these radionuclides, only those that are a major part of the waste inventory and have potentially large dose conversion factors are of potential importance to the performance of the disposal system. Considering these screening criteria, plutonium is the dominant radionuclide. Americium is also considered for the TSPA-SR.

Radionuclides are attached to colloids as a result of two types of processes: irreversible and reversible attachment. For waste form colloids, radionuclides can be incorporated into the substrate material before it is suspended as colloids. All colloid types may sorb radionuclides to form pseudocolloids, depending on the affinity of the colloid mineral substrate for a

dissolved radionuclide. The contributions of each colloid type are summed to produce the mobile colloid source term for each important radionuclide.

The abstractions are based on laboratory results from waste form corrosion testing and testing of adsorption and desorption properties of Pu and Am on clay and iron-(hydr)oxide colloids. To the extent that the laboratory tests and test conditions represent anticipated repository conditions, the abstraction is valid for calculating the colloid-associated radionuclide concentrations and colloid mass concentrations.

4. SUMMARY

The performance of the potential Yucca Mountain repository will depend on the rate of radionuclide release from the waste packages after the containers are eventually breached. After breach, water, or water vapor may enter the packages and contact exposed waste forms. The waste forms will degrade slowly and release radionuclides, as solutes and colloids, into the contacting groundwater as a result of a broad range of processes and events. This Waste Form Degradation PMR [1], together with the supporting Analysis Model Reports AMRs, describes the approach and scientific basis for modeling.

5. REFERENCES

[1] DOE Office of Civilian Radioactive Waste Management (OCRWM), Waste Form Degradation Process Model Report, TDR-WIS-MD-000001, July 2000.

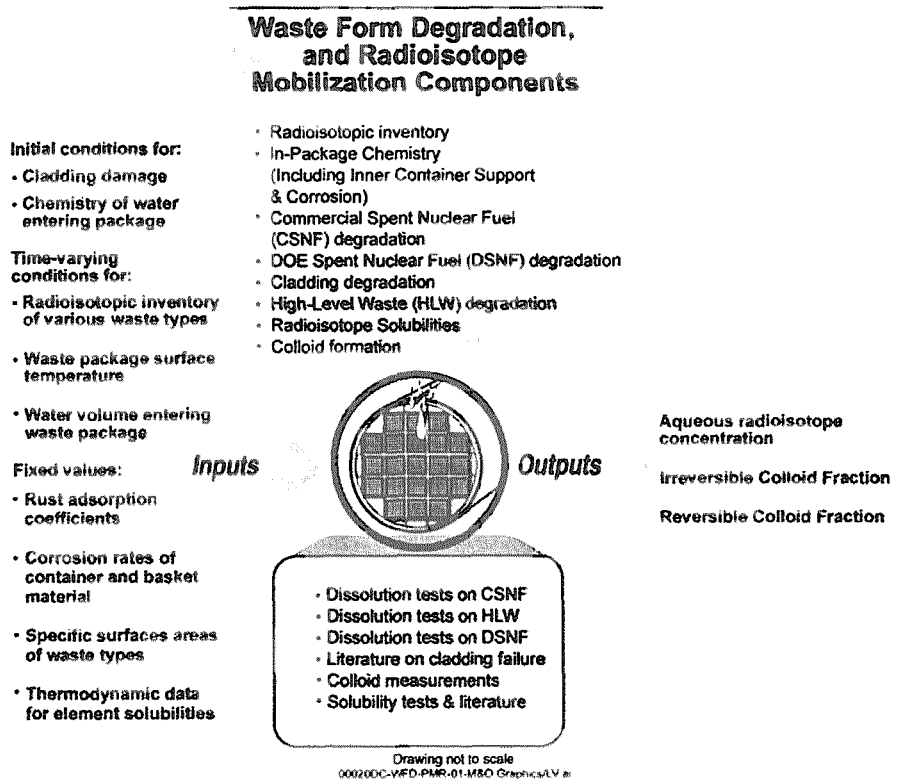

Figure 1. Summary of Inputs, Outputs, Components, and Assumptions of Waste Form Degradation Model [1]

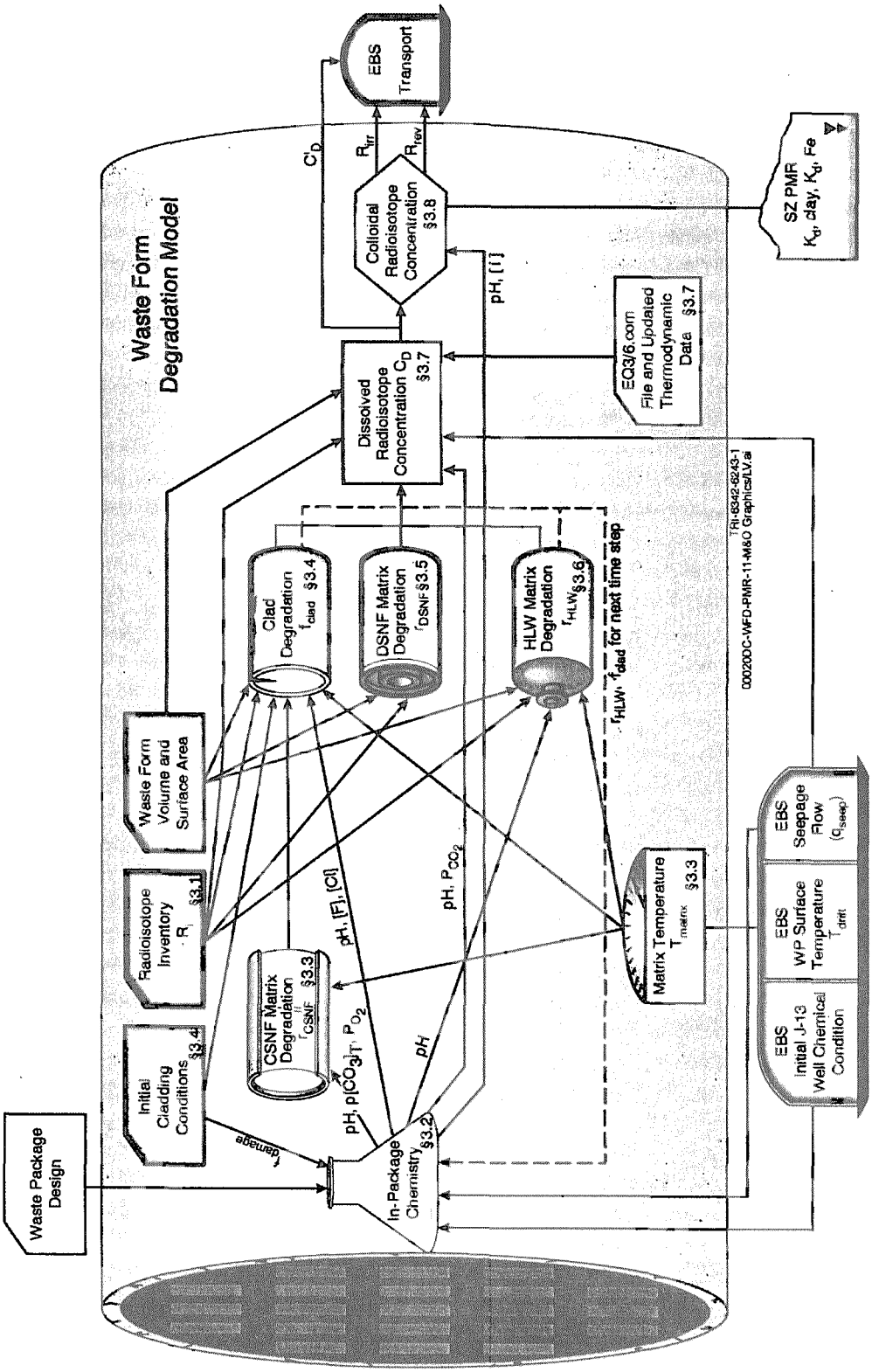

Figure 2. Linkage of Components in Waste Form Degradation Model [1]

JP0250321

JAERI-Conf 2002-004

THERMODYNAMIC MODELS AND DATA FOR ASSESSING RADIONUCLIDE MIGRATION IN THE NEAR FIELD: USES AND LIMITATIONS

M. OCHS

BMG Engineering Ltd.
Ifangstrasse 11, CH-8952 Schlieren-Zürich, Switzerland
Tel.: +41 - 1 - 732 92 83, Fax.: +41 - 1 - 730 66 22, e-mail: michael.ochs@bmgeng.ch

The focus of the present contribution is on the use of thermodynamic data and models to explain and predict the effects of solubility limits and sorption/uptake reactions on dissolved concentrations and migration of radionuclides in clay- and cement-water systems. This topic is approached by addressing the current state, limitations, and possible pitfalls of relatively common applications of speciation and sorption models:

- calculation of near field water chemistry as influenced by compacted clay or cement,
- prediction of radionuclide solubility limits in homogeneous solutions.

Subsequently, promising developments, as well as critical shortcomings and future challenges in this field are discussed, in particular with regard to:

- model-supported selection of K_d values for clays and cement,
- extrapolation to "intact" materials, such as compacted bentonite or whole concrete,
- linking to diffusive and advective transport.

Key Words: thermodynamic data, models, solubility limits, sorption, speciation

1. INTRODUCTION

In the field of environmental (geo)chemistry, thermodynamic solution and surface chemical models today represent fairly well established tools for interpreting and predicting the movement and fate of many trace elements. In comparison, the development and use of such models for the assessment of radionuclide migration through the near field of nuclear waste repositories is still largely neglected. As the only notable exception, the frequent use of thermodynamic speciation calculations to predict dissolved concentrations of radionuclides may be cited, and to a lesser degree, also the definition and assessment of general water chemistries.

As a matter of fact, it could be argued that the role of solubility calculations for setting maximum radionuclide concentrations in the near field is often overestimated. On the other hand, the capabilities of thermodynamic speciation/sorption models for addressing questions of radionuclide uptake and transport are rarely utilized to their full potential. Distribution coefficients (K_d), which are crucial input parameters for performance assessment models, are often selected from sorption databases without considering the use of thermodynamic sorption models. Further, the application of speciation and sorption models to transport phenomena is only weakly developed.

2. ASSESSMENT OF GROUNDWATER CHEMISTRY

Calculations of near field water chemistries are necessarily based on a clear definition of the composition of the surrounding groundwater(s). In most recent or on-going PA exercises, the composition of the groundwater surrounding a repository is sufficiently well known from

sampling campaigns and measurements pertaining to a specific candidate site (e. g. [1]). Alternatively, a hypothetical groundwater composition can be defined (e. g. [2]). No matter which approach is taken, thermodynamic ("speciation") calculations have shown to be a very important tool for establishing and cross-checking the composition of incoming groundwater. Of particular importance is that thermodynamic models, if used appropriately, can be used to guarantee an internally consistent composition in terms of

- mineral solubility limits and concentration of dissolved species,
- solution composition and partial pressure of relevant gases,
- pH, pe, and the concentrations of all related redox species.

Although the calculation of a groundwater composition is frequently done and is comparatively straightforward, there are several potential problems which are often underestimated:

- In order to derive an accurate and internally consistent composition, it is of course necessary to use an internally consistent thermodynamic database. Criteria for the internal consistency of a thermodynamic database are given in e. g. [3] and [4] and are not further discussed here.
- Many redox reactions that are thermodynamically favorable will not take place in the absence of microbial mediation. Similarly, many redox-sensitive species will react only with chemical reaction partners suitable for transferring electrons. Therefore, a pe value can only reflect a given system's potential, but the redox-reactions allowed to take place still have to be very carefully selected by the modeler.
- Similarly, many thermodynamic databases (correctly) contain solubility products (K_{sp}) for minerals that form under "geological" conditions (effects of temperature, pressure, reaction pathways...), but that do not precipitate from homogeneous solutions. While the dissolution of such minerals has to be accounted for, their precipitation is usually not relevant under repository conditions. The proper selection of mineral equilibria is again dependent on the modeler's expertise.

These three points are of course very general. However, it is important to keep them in mind, since they do not only apply to the calculation of groundwater composition, but to practically all thermodynamic databases and calculations, including sorption models.

3. ASSESSMENT OF NEAR FIELD WATER CHEMISTRY

In order to derive the composition of the near field aqueous phase, the interaction of groundwater with buffer materials (and with waste containers/corrosion products, etc.) has to be considered. The most common buffer materials are clay (bentonite) and cements, which possess drastically different properties. Because of their overriding importance for modeling (i) the near field water chemistry and (ii) radionuclide retention, relevant features and models are discussed in some detail below.

3.1. Bentonite

Bentonite consists largely of smectite clays as well as a number of accessory minerals. The composition of bentonite porewater is determined by two processes:

- The interaction of groundwater constituents with surface functional groups of the clay minerals. The main reactions influencing porewater chemistry are the exchange of major

cations with the exchangeable ions already present at the clay siloxane surface, and acid-base reactions at the edge surface.

- Mineral equilibria involving the accessory minerals of bentonite as well as new phases that may precipitate upon oversaturation.

Mineral equilibria can be modeled in the standard fashion (see section 2); thermodynamic models and data for reactions at clay surfaces are discussed further below.

Smectite itself is made up by 2:1 expandable layer silicates, which feature two different types of surfaces [5]:

(1) The siloxane (layer) surface hosts a permanent (structural) negative charge due to isomorphous replacements in the tetrahedral (e. g. Al for Si) or octahedral (e. g. Mg for Al) layers, and therefore acts as an ion exchanger. Exchange reactions can in principle be modeled by electric double layer (EDL) or mass-action/site-binding models. In practice, the latter are used almost exclusively.

(2) The edge surfaces of clay platelets are characterized by broken bonds, leading to silanol and aluminol surface functional groups, similar to those of Si- and Al-oxides. The acid-base equilibria of these groups, as well as their interaction with dissolved metal species and ligands can be described with established surface complexation models.

While the basic model approaches are well established, there are different methods for taking the activity of the surface species into account [6, 7]. These include the mole- or equivalent-fraction approach in case of ion exchange equilibria, and in case of surface complex formation the use or omission of electrostatic correction terms, which can also be calculated with different EDL models (double layer, triple layer, etc.).

Therefore, it is extremely important to realize that the corresponding surface chemical thermodynamic databases are model-dependent and not generally valid. In addition, the equilibrium constants for surface chemical reactions are dependent on the speciation of the respective key elements, and thus on the underlying TDB for solution species.

- The situation is relatively simple in case of the ion exchange equilibria, for several reasons: (1) the properties of the surface sites can be treated as being constant under all conditions; (2) the major cations involved exist under most conditions only in the form of a single species (Na^+...); (3) in many cases, constants derived with different models can relatively easily be converted to each without having to re-evaluate the original raw data, because of (1) and (2) above. However, in case of thermodynamic sorption models of radionuclides that simultaneously undergo ion exchange and surface complexation, the ion exchange constants are of course related to the surface complexation model and both models need to be evaluated together (see below).
- On the other hand, surface complexation constants for the interaction of metal species or ligands with the edge sites of clays are always directly connected with the respective surface hydrolysis constants, which are in turn dependent on the type of electrostatic correction model used. Therefore, surface complexation constants cannot be used directly with other models, but need to be re-fitted using the original experimental data. At the same time, the derivation of surface complexation constants implicitly contains all thermodynamic data for the relevant solution species of the respective element. This means that surface complexation models need to be re-evaluated when changes are made to relevant entries in a solution TDB.

3.2. Cementitious materials

Cementitious materials are fairly complex, but it appears that their influence on porewater composition can be described sufficiently well by relatively simple models that assume equilibrium with only a few mineral phases [8]. The critical issue is to obtain a correct description of cement evolution as a function of time; however, this is not within the scope of this contribution. The most characteristic feature of all cement-equilibrated solutions is a high pH: freshly hydrated cement leads to a pH of >13, whereas for degraded cement equilibrium with portlandite can be assumed, which gives a pH of 12.5.

3.3. Calculation of porewater composition for compacted bentonite

After re-saturation of the buffer, the interaction of groundwater with buffer materials determines the composition of the water that will come in contact with the immediate waste containments/overpack. A correct description of the interaction of groundwater with buffer materials is also the basis for all subsequent assessments of radionuclide migration.

The basic aspects of modeling groundwater-bentonite interaction have already been discussed in section 3.1. While a description of porewater chemistry seems to be fairly straightforward, one encounters difficulties when applying the respective thermodynamic models to compacted bentonite. The main water parameter, pH, is controlled by two important buffer systems: the edge sites of the clay edge surface, and the carbonate buffer system [9]. In case of the edge site buffer, the calculated pH is dependent on the surface chemical model, e. g., because different electrostatic correction terms react differently to changes in ionic strength. Since most bentonites contain calcite, gypsum, and halides as impurities, pH becomes also a function of the amount of impurities present, or of the amount of impurities that is allowed to dissolve in the model calculations. This is illustrated in Figure 1.

3.4. Assessment of radionuclide solubility limits

Based on the above discussion, two areas can be identified that are critical for a reliable assessment of radionuclide solubility limits through thermodynamic calculations:

(1) A reliable and consistent thermodynamic database is needed for the radionuclide considered [3]. If separate radionuclide and geochemical databases are used, it is not only necessary that the radionuclide database is internally consistent, but it must also be consistent with regard to the geochemical database. While an evaluation of the available thermodynamic data is clearly outside the scope of this paper, some shortcomings can be pointed out:
   - There is a clear lack of high-quality data for less-well researched elements (e. g. Zr) and some important ligands (e. g. carbonate species). This is especially true for highly alkaline cement-equilibrated near field waters [10].
   - Methods and data for activity coefficient corrections are often not adequate (but in many cases the resulting error is probably small in comparison to uncertainties associated with the TDB itself).

(2) It is necessary to obtain a good description of the near field water composition itself. As illustrated in section 3.3., this may not be a trivial task. However, pH variations of ±1 unit and the concomitant changes in carbonate speciation could have significant effects.

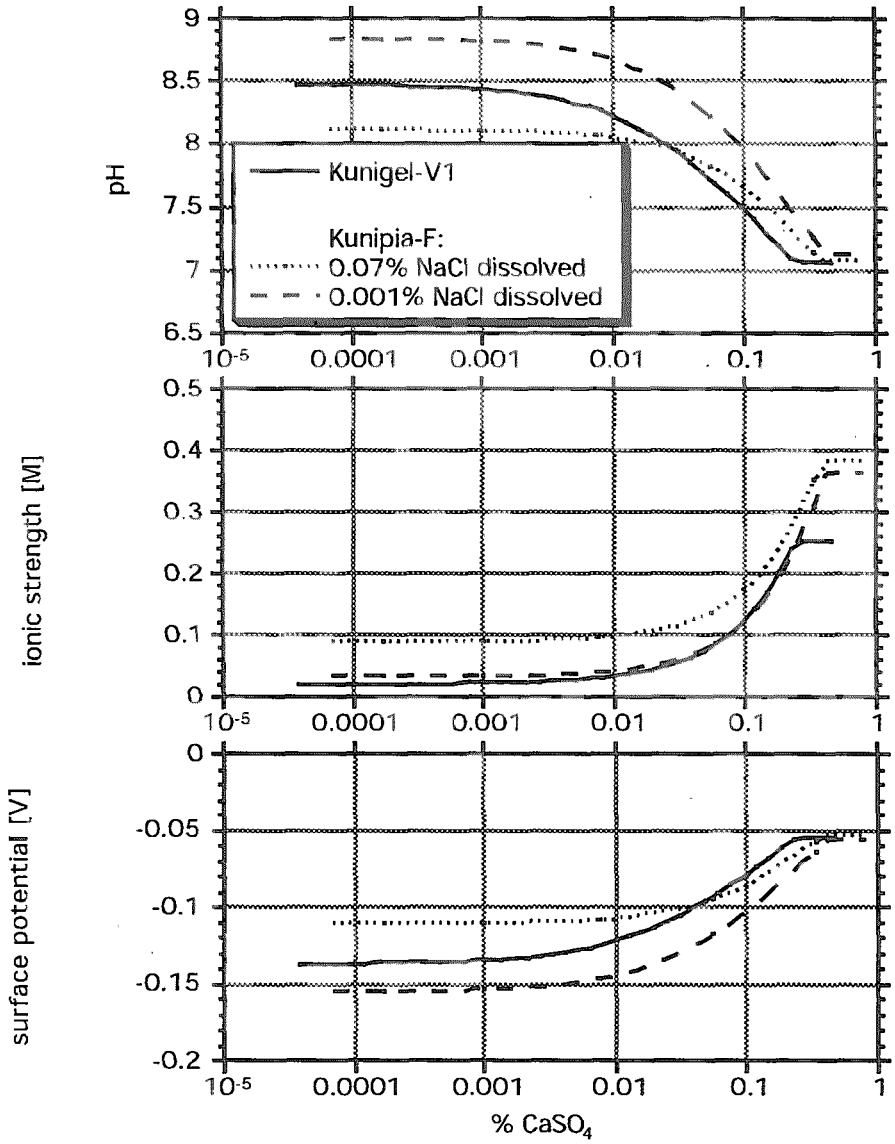

Figure 1: Illustration of the interdependencies between pH, ionic strength and edge surface potential in compacted bentonite. These parameters are plotted vs. % $CaSO_4$ impurity dissolved in the porewater of compacted Kunigel-V1 (dry density = 1800 kg/m^3) and Kunipia-F (dry density = 1800 kg/m^3) bentonite. The total content of $CaSO_4$ is 0.38% in Kunigel-V1 and 0.67% in Kunipia-F; the total content of NaCl is 0.001% in Kunigel-V1 and 0.071% in Kunipia-F; both bentonites contain enough calcite to reach saturation (from [9])

4. DEVELOPMENTS AND POTENTIAL FUTURE APPLICATIONS

4.1. Model calculation of K_d values

The use of thermodynamic sorption models, in particular surface complexation and ion exchange models, for the calculation of K_d values is receiving increased attention within the radioactive waste management community [11]. Such models allow to simultaneously calculate the speciation of a key element in solution and on the surface, and K_d may the be calculated as follows:

$$K_d\,[\mathrm{m^3/kg}] = \frac{\text{stoichiometric sum of surface species of element X [mol/kg]}}{\text{stoichiometric sum of solution species of element X [mol/m}^3\text{]}} \quad (1)$$

There are a number of examples available that illustrate the successful development and application of thermodynamic sorption models (e. g. [12, 13]), which are not reviewed in detail here. Instead, some issues that may be critical for the future development in this area are briefly discussed.

- The availability of a reliable radionuclide TDB is probably even more important for sorption modeling than for the calculation of solubilities. This is not always easily recognized, but the extent to which an element undergoes surface complexation can be extremely dependent on the stability constants for the solution reactions (formation of dissolved species with e. g. OH^-, CO_3^{2-}...).
- Similarly, an adequate description of the overall water chemistry is extremely important. While in the "traditional" areas of application (simple oxides etc) solution compositions are usually well constrained, the uncertainties in the porewater composition of bentonites make sorption modeling very challenging. Such uncertainties are probably more critical than shortcomings in the sorption models themselves.
- While surface complexation/ion exchange models promise to be very valuable tools for metal oxides, bentonite and other clays, as well as other complex sorbents (e. g. fracture infill), there is increasing evidence [10, 14] that radionuclide uptake by cementitious materials occurs through incorporation mechanisms that may be described by solid-solution models.
- Finally, it needs to be pointed out that model supported K_d values must only be derived based on sorption models as described above. It can be very misleading to calculate solution speciation alone and then make qualitative judgements about sorption, since speciation may be influenced drastically by the presence of surface functional groups.

4.2. Linking K_d values and transport parameters

In the case of both bentonite and cement-based buffer materials, the link between batch-type sorption and transport modeling involves an extrapolation of modeling approaches typically developed for dilute suspensions to "intact" or "real" materials, such as compacted bentonite or concrete. Basically, it should be possible to apply thermodynamic models to such systems, and attempts to link relatively simple sorption and diffusion models in order to calculate overall (apparent) diffusion coefficients for compacted bentonite show promising results [15-17]. However, one has to be aware that the direct experimental acquisition of transport parameters is often not possible (in contrast to batch sorption data!) and data reduction procedures based on transport models need to be used to derive meaningful constants. Therefore, a direct comparison of thermodynamic model results and experimental data is often not possible. This is also demonstrated for intact hardened cement paste, where

changes in physical parameters (porosity) due to mineral dissolution/precipitation reactions need to be understood before sorption in such systems can be interpreted [18]. It finally has to be admitted that to date, there is a clear lack of experimental data from sufficiently constrained systems to test the application of thermodynamic models to intact materials.

5. CONCLUDING REMARKS

Some of the gaps in terms of model development and contents of thermodynamic databases have already been addressed in different sections above. Further gaps are not discussed in detail here, but it is pointed out that present applications are more or less restricted to 25 °C. Instead, only some concluding remarks are made here. Thermodynamic models are usually non-unique, and this holds not only for application-oriented models, such as sorption models, but also for basic chemical models used to derive thermodynamic constants (e. g. selection of species to be considered for evaluating titration data). It has to be realized that model development depends not only on experimental data and available supporting information, but to a significant degree on choices made by the modelers. The more different decisions in model building can be constrained by an improved system understanding or definition, the more likely it will be that thermodynamic modeling can be used successfully for performance analysis. An appropriate and effective use of thermodynamic data and models is therefore critically dependent on an improved definition of repository-specific boundary conditions.

6. REFERENCES

[1] Nagra, "Geosynthesis Wellenberg 1996. Results of investigation phases I and II", NTB 96-01, Nagra, Wettingen, Switzerland (1997), in German

[2] JNC, "H12: Project to Establish the Scientific and Technical Basis for HLW Disposal in Japan", TN1410 2000-001, JNC, Tokai-mura, Japan (2000).

[3] Wanner, H., Mat. Res. Soc. Symp. Proc. Vol. 212, 815-822 (1991)

[4] Engi, M., "Thermodynamic data for minerals: A critical assessment", Ed. by G.D. Price and N.L. Ross, Chapman & Hall, London, UK (1992), pp. 267-328.

[5] Sposito, G., "The Surface Chemistry of Soils", Oxford University Press, New York (1984)

[6] Sposito, G., "The Thermodynamics of Soil Solutions", Oxford University Press, New York (1981)

[7] Stumm, W., Morgan, J.J., "Aquatic Chemistry", 3rd. ed., John Wiley & Sons, New York (1996)

[8] Berner, U., "A thermodynamic description of the evolution of pore water chemistry and uranium speciation during the degradation of cement", PSI Report 62, Paul Scherrer Institut, Villigen, Switzerland (1990).

[9] Ochs, M., Lothenbach, B., Shibata, M., Yui, M., "Bentonite Porewater Chemistry", JNC TN8400 99-075, JNC, Tokai-mura, Japan (1999).

[10] Berner, U., "Concentration limits in the cement-based Swiss repository for long-lived. intermediate-level radioactive wastes (LMA)", PSI Report 99-10, Paul Scherrer Institut, Villigen, Switzerland (1999).

[11] OECD-NEA, "Using thermodynamic sorption models for guiding radioelement distribution coefficient (K_d) investigations. A status report", OECD, Paris, France (2001).

[12] Wanner, H., Albinsson, Y., Wieland, E., Fresenius J. Anal. Chem., 354, 763-769 (1996).

[13] Bradbury, M.H., and Baeyens, B., J. Contam. Hydrol., 27, 223-248 (1997).

[14] Ziegler, F., Scheidegger, A.M., Johnson, C.A., Dähn, R. and Wieland, E., Environ. Sci. Technol., 35, 1550-1555 (2001).

[15] Ochs, M., Boonekamp, M., Wanner, H., Sato. H., Yui, M., Radiochim. Acta, 82, 437-443, (1998)
[16] Ochs, M., Lothenbach, B., Wanner, H., Sato. H., Yui, M., J. Contam. Hydrol., 47, 283-296 (2001).
[17] Tachi, Y., Shibutani, T., Sato, H., Yui, M., J. Contam. Hydrol. 47, 171-186 (2001).
[18] Berner, U., Radiochim. Acta 82, 423-428 (1998).

Acknowledgements: This paper benefited from many discussions with co-workers and colleagues, which are warmly appreciated. Many ideas and concepts were developed in the framework of projects carried out under the auspices of JNC and ANDRA, whose support is gratefully acknowledged.

JP0250322

JAERI-Conf 2002-004

THE ROLE OF TITANATE CERAMICS IN IMMOBILISATION OF WASTES ARISING FROM PARTITIONING AND WEAPONS DISPOSITION

K.P. HART, Y. ZHANG, B.D. BEGG, Z. ALY, A. BROWNSCOMBE, R. A. DAY, M.W.A. STEWART, G.R. LUMPKIN, E. R. VANCE AND A. JOSTSONS

Australian Nuclear Science and Technology Organisation
PMB1, Menai, NSW 2519, AUSTRALIA
Fax: 6129 5437179, e-mail: kph@ansto.gov.au

The development of ceramics for the immobilisation of radioactive wastes has been on-going at ANSTO since 1980 and has involved collaboration with JAERI, the USDOE, LLNL and other international laboratories. This work has examined various processing routes, radiation damage effects and long-term aqueous durability for a range of titanate ceramics. Within these studies, information on the long-term behaviour of ceramics chosen to immobilise excess Pu and actinide-rich wastes arising from partitioning strategies have been obtained. Overall, the long-term durability, limitations on criticality under processing and disposal conditions and existence of viable natural analogues endorse the use of titanate ceramics for immobilisation of actinide-rich wastes.

1. INTRODUCTION

Most of the early development of synroc focused on the synroc-C formulation for immobilising liquid HLW from the reprocessing of commercial LWR spent fuel. Subsequently, ANSTO has responded to developments in R&D on partitioning and transmutation, excess plutonium disposition and the needs of global remediation programs by developing a variety of titanate ceramic waste forms for specific applications.

The actinides in synroc-C partition primarily into zirconolite ($CaZrTi_2O_7$) with smaller amounts into perovskite ($CaTiO_3$). Perovskite is mainly designed to immobilise strontium and hollandite ($BaAl_2Ti_6O_{16}$) is used mainly to immobilise caesium. The synroc-C formulation is flexible and a single precursor composition can be used to immobilise HLW loadings in the range 0 to 30wt.% without significant effects on the chemical durability in aqueous media. A summary of the early work on Synroc-C, including process demonstration, has been published previously (1). Matrices including pyrochlore-rich and zirconolite-rich ceramics have been considered for the conditioning of the Am/Cm/rare earth stream from HLW partitioning (2).

In the aftermath of the cold war, the US and Russia agreed to large reductions in their stockpiles of nuclear weapons. The US initiated a two-track strategy for the disposition of 50 tonnes of surplus plutonium:

- using the plutonium as mixed-oxide fuel in existing commercial power reactors; and
- geologic disposal of plutonium immobilised in a pyrochlore-rich titanate ceramic

ANSTO began work on Pu immobilisation in 1994 with Lawrence Livermore National Laboratory, California, USA, the local laboratory for US DOE on Pu disposition. The initial effort was on zirconolite-rich formulations but the change in US DOE program requirements shifted the emphasis to pyrochlore-rich titanate ceramics. For these ceramics doped with high levels of Pu, the avoidance of nuclear criticality is essential during waste form processing, storage, and over the very long term in the repository environment. Avoidance of nuclear criticality is ensured in Pu-rich titanate wasteforms by having high loadings of neutron absorbers such as Gd, Sm and Hf in solid solution in the Pu host phases. Such conditions can

be met by the zirconolite-rich and pyrochlore-rich titanates. In fact, pyrochlore-rich ceramics have been selected for the immobilisation of this Pu by the US.

Results from the above studies on pyrochlore-rich ceramics will be presented in detail for the immobilisation of excess Pu and further discussion will focus on their relevance to the immobilisation of other actinide-rich waste streams.

2. STUDIES ON PYROCHLORE-RICH TITANATES

The baseline pyrochlore waste form was designed to consist of 95wt.% pyrochlore ($Ca_{0.89}Gd_{0.22}Hf_{0.23}U_{0.44}Pu_{0.22}Ti_2O_7$) and 5wt.% of a hafnium substitute rutile ($Hf_{0.1}Ti_{0.9}O_2$). The actual product, formed after sintering for 4 hours at 1350°C, contains some brannerite (UTi_2O_6) which also contains Pu, Gd and Hf. A small (<2%) amount of the Pu inventory remained unincorporated in the sintered pyrochlore made from high-fired oxides, as a reacted oxide $(Hf,REE,Pu,U)O_2$, whereas in materials made from alkoxide powders the actinides were fully dissolved in the titanate phases. The theoretical density of the baseline pyrochlore ceramic is about 6.0 gm/cm^3 and the observed density of ceramics sintered for 4 hours at 1350°C is about 5.6 gm/cm^3.

The mineralogy and partitioning of Pu, U and the neutron absorbers among the phases in the pyrochlore-rich ceramic have been studied extensively. It is influenced by impurities in the Pu feed stocks destined for immobilisation. The plutonium assay in the candidate materials varies from under 10wt.% to over 99wt.%. The uranium content varies from trace depleted uranium in plutonium to trace plutonium in fully enriched (93% ^{235}U) uranium. In general, the impurities in the existing feed stock include: aluminium, carbon, calcium, chlorine, iron, fluorine, gallium, potassium, magnesium, molybdenum, sodium, silicon, tantalum, tungsten and zinc. The observed volume abundances of pyrochlore (60-90%), brannerite (0-22%), zirconolite (0-25%) and rutile (0-16%) depend on impurities in the various sources of Pu. All primary Pu-containing phases have been found to accommodate more neutron absorbers (Gd and Hf) than plutonium on a molar basis as per the original design.

Leach testing was carried out at 90°C in deionised water, as described elsewhere (3). Analysis of inactive elements was carried out by ICP/MS but for Pu, the level of activity was determined by alpha spectrometry carried out on 0.1 mL of leachate evaporated onto a stainless steel planchette. This method allowed the contribution of ^{241}Am to be separated from that of the Pu[1], unlike in our previous studies (3).

The test results for Pu releases for a wide range of zirconolite-rich and pyrochlore-rich formulations (4) are shown in Figure 1. The variation between the Pu release rates after 7 days is about a factor of 20 with the difference reducing to about 4, for the smaller number of samples studied so far, after about 300 days. Overall, the release rates decreased by about one order of magnitude between 3.5 days (i.e. 0 to 7 day period) and 324 days.

---

1 The Pu used in this study consisted of (wt%): 93% ^{239}Pu, 5% ^{240}Pu, 0.5% ^{241}Pu and 1.5% ^{241}Am. From alpha spectrometry the contribution of ^{239}Pu could not be separated from ^{240}Pu and hence, the release rates of Pu are based on both isotopes.

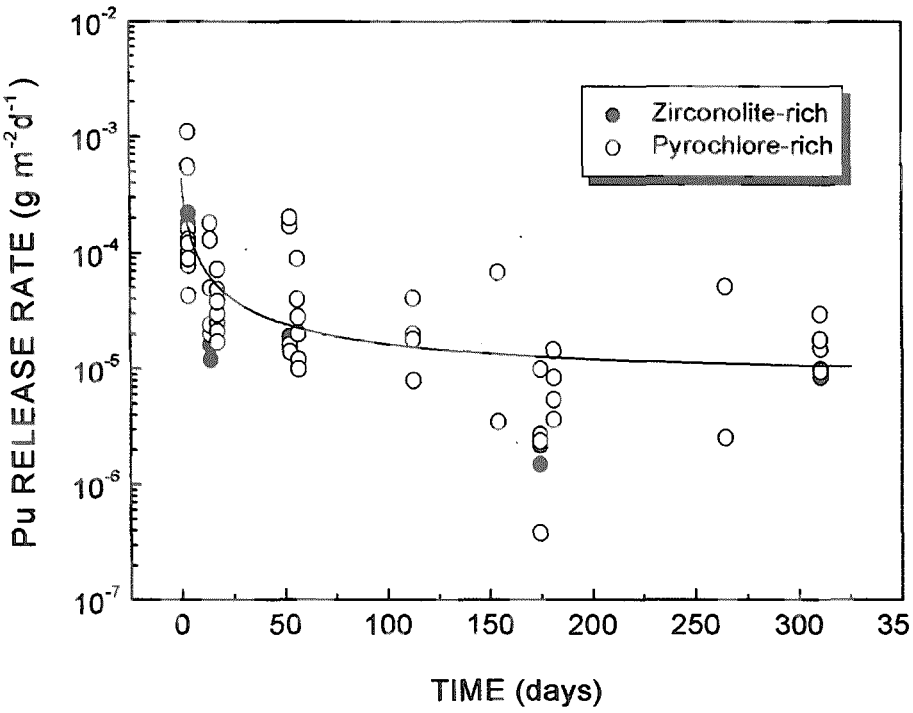

Figure 1 Total, normalised Pu release rates from zirconolite-rich (HIPed) and pyrochlore-rich (sintered) formulations measured at 90°C in deionised water. For convenience, all the different batches of sintered material have been given the same symbol and the line shown on the graph is intended to be indicative only.

The addition of impurities to the baseline ceramics improves the overall durability of the formulations. Studies of the microstructures of these formulations has shown that the addition of impurities reduces the amount of unreacted actinide oxides and improved the development of the design phase composition (5).

Overall, it appears that for multi-phase compositions, correctly milled, that all ceramic phases tend to have a similar, high aqueous durability. The releases of Gd, U and Pu approach similar longer-term release values and suggest that there should be no long-term criticality considerations for a repository environment. However, Hf (also a neutron absorber) under these test conditions has tended to have lower releases than those for the former elements.

Longer-term releases of U and the neutron absorbers bracket those of Pu, suggesting that these elements may have similar source terms from the ceramic matrices within a repository environment.

In addition to the static tests, extensive flow through testing of the ceramics was carried out to evaluate the kinetics of releases to help develop an understanding the long-term releases of Pu and U relative to the neutron absorbers (Gd and Hf).

Dissolution tests (Single-Pass-Flow-Through), tests for Pu-doped samples were carried out at 70°C with pH 5.6 buffer within the N_2 glove box (6). The powdered sample was placed between Teflon membranes, held together by two Teflon rings, and positioned near the

middle of the Teflon leaching vessel. The leachates were collected twice per week and were acidified after pH measurement with 3% by volume of analytical grade HNO_3. The level of ^{239}Pu was calculated from the β-activity of ^{241}Pu measured by liquid scintillation counting and the other elements were analysed by Inductively Coupled Plasma Mass Spectrometry (ICP-MS). The powdered specimens, after dissolution tests, were gently rinsed with deionised water and dried at the test temperature for SEM and TEM examinations.

Figure 2 shows the releases measured under flow-through conditions for pyrochlore-rich baseline ceramic (6). The long-term releases are; ~0.1-1 g m^{-2} d^{-1} for Ca, ~10^{-4} g m^{-2} d^{-1} for U, Gd and Ti, and 10^{-6}-10^{-5} g m^{-2} d^{-1} for Hf and Pu. Within experimental error these results are comparable to those obtained from static testing. Under these conditions experimental data for Hf have established that, where solubility constraints are not important, the releases of this element closely follow those of Pu. This latter results extends the data obtained for Hf under static conditions.

Further analysis of the kinetics of release obtained under flow-through conditions for Gd and U suggest that releases initially can be viewed as being associated with fast surface reaction followed by, in the longer-term, an equilibrium between reaction thermodynamics and the kinetic leaching conditions. Thermodynamic calculations suggest that longer-term releases of U, Gd, and Ti releases could be controlled by equilibrium of the corresponding hydroxide species.

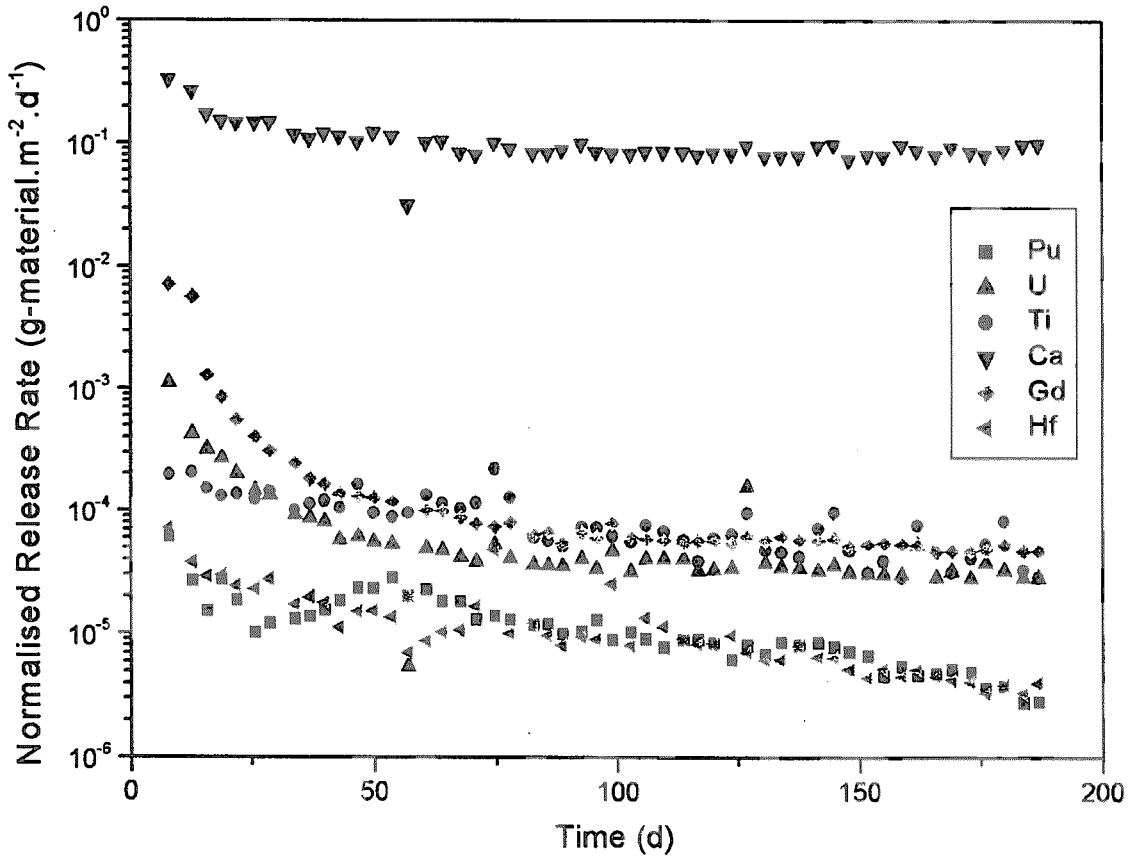

Figure 2 Normalised elemental releases from pyrochlore-rich baseline ceramic measured at 70 °C in pH 5.6 leachant at a flow rate of ~ 10 mL d^{-1}

Examination of the leached solids using SEM and TEM supported the overall findings of the leaching results for both static and flow-through conditions.

The long-term durability of actinide-containing phases in the pyrochlore-rich ceramics over geological time has also been investigated using natural samples. The results from this extensive study are reported elsewhere (7). Importantly, the results showed that the relative durability of phases in the natural samples increased in the order of perovskite << brannerite ≤ pyrochlore ≤ zirconolite which is consistent with that determined from studies on synthetic samples.

These recently obtained results for pyrochlore-rich ceramics are supported by extensive laboratory tests of polyphase synroc and single-phase materials that have been carried out over the previous 20 years at ANSTO and in laboratories overseas. Most of these experiments have been carried out at temperatures of 70-150°C in deionised water, sodium chloride, bicarbonate or silicate solutions. Extensive investigations on zirconolite, the most durable of the synroc phases, have been carried out by Malmström (8) under hydrothermal conditions 150-700°C, at pressures of 50 and 200 MPa. Overall the results show that pyrochlore is the next most durable phase to zirconolite followed by perovskite and brannerite. Other laboratory studies, involving leaching tests beyond 3000 days, continue to be supported by studies of natural minerals of the relevant synroc phases from known geological environments.

Previous work on the effect of radiation damage on releases from ceramic waste forms, carried out in conjunction with JAERI and other laboratories, have shown that the Pu leach rate may increase by about a factor of 10 from titanate ceramics in accelerated damage tests after amorphisation. The leaching behaviour of actinide doped specimens in accelerated damage tests could be influenced by alpha radiolysis effects that would not be important in Pu immobilisation given the longer half lives of ^{239}Pu and ^{235}U then those of actinides used in the short-term tests. The latter is in accordance with results from natural titanate minerals that have shown that these materials have generally remained as closed systems for migration U-Th-Pb isotopes for time periods of up to 5.5 x 10^8 years (7).

3. CONCLUSIONS

Overall, the results from current studies extend the database for titanate ceramics and confirm the suitability of these matrices for the immobilisation wastes arising from actinide-rich streams. Further, the ability to tailor the phase composition to reflect additives and impurities in the wastes streams underlines the applicability of this approach to a wide range of actinide-rich wastes including those arising from partitioning and transmutation initiatives as well as disposition of fissile materials. Of additional importance is the ability to include high loadings of neutron absorbers, like Gd and Hf, to avoid criticality during processing and also under repository conditions.

4. REFERENCES

[1] A. Jostsons, Status of synroc development, proc. of 9th Pacific Basin Nuclear Conference, Sydney, 1-6 May, 1994, N.R. McDonald, Ed., pp 865-871, (1994).

[2] J. Lefevre, G. Baudin and M. Salvatores, Partitioning of long-lived radionuclides", Proc. Safewaste '93, Avignon, France, June 14-18, 1993, Vol. 1, pp 416-429, French Nuclear Energy Soc., Paris, France, (1993).

[3] Hart, K. P., Vance, E. R., Stewart, M. W. A. Stewart, Weir, J., Carter, M. L, Hambley, M., Brownscombe, A., Day, R. A., Leung, S., Ball, C. J., Ebbinghaus, B., Gray, L. and Kan, T. (1998) Mat. Res. Soc. Symp. Proc. **506**, 161-168.

[4] K. P. Hart, Y, Zhang, E. Loi, Z. Aly, M. W. A. Stewart, A. Brownscombe, B. B. Ebbinghaus and W. Bourcier, Aqueous durability of titanate ceramics designed to immobilise excess plutonium in Scientific Basis for Nuclear Waste Management XXIII, *Mat. Res. Soc. Symp. Proc. Vol 608*, Eds. R. W. Smith and D. W. Shoesmith, Materials Research Society, Pittsburgh,PA, USA, 353-358.

[5] Vance, E.R., Jostsons, A., Moricca, S., Stewart, M.W.A., Day, R. A., Begg, B. D., Hambley, M. J., Hart, K. P. and Ebbinghaus, B. B., Ceramic Transactions, **93**, 323-329, 1999.

[6] Y. Zhang, K. P. Hart., W. Bourcier, M. G.Blackford, A. Brownscombe, P. J. McGlinn, Z. Aly, B. S. Thomas, and E. Loi, Kinetic dissolution studies on pyrochlore-rich titanate ceramics, 24th International Symposium on the Scientific Basis for Nuclear Waste Management, August 27-31, 2000, Sydney, Australia (in press).

[7] G.R. Lumpkin, "Alpha-decay damage and aqueous durability of actinide host phases in natural systems", J. Nucl. Mat. 289, pp 136-1666 (2001).

[8] J.C. Malmström, "Zirconolite: experiments on the stability in hydrothermal fluids" Ph.D. Thesis, ETH Zürich, Switzerland, published by the Swiss Geotechnical Commission, No 93 (2000).

JP0250323

JAERI-Conf 2002-004

Field Test of Nuclide Migration in Bentonite-based Materials at Aerated Zone

--- Cooperative Research Program on Field Migration Test between CIRP and JAERI ---

Fan Zhiwen*, Cui Anxi*, Gu Cunli*, Zhao Yingjie*, Sun Qinghong*

M.Mukai**, T.Maeda**, J.Matsumoto**, T.Tanaka**, H.Ogawa**

* China Institute for Radiation Protection
270 Xuefu Street, Taiyuan, Shanxi 030006 China
Fax: 86(351)7020407, E-mail: fanzw@public.ty.sx.cn

** Department of Fuel Cycle Safety Research
Tokai Establishment, Japan Atomic Energy Research Institute
Shirakata 2-4, Tokai, Naka, Ibaraki, Japan, 319-1195
Fax: 029-282-5934 E-mail: mukai@sparclt.tokai.jaeri.go.jp

ABSTRACT

A field test was jointly conducted by China Institute for Radiation Protection (CIRP) and Japan Atomic Energy Research Institute (JAERI) to explore moisture movement with Br^- and migration of radioactive tracer ^{237}Np, ^{238}Pu and ^{90}Sr in bentonite-based materials at aerated zone. The test ran under two rainfall conditions, the artificial rainfall with sprinkling density of 15 mm/d and 5 mm/hr, and the natural rainfall.

Tracing test of Br^- implies that there does have water going through the bentonite specimen. However, the curves are very complex and further work need be conducted to quantify this movement. ^{238}Pu has no observable movement during the test period under either rainfall conditions, and ^{237}Np has very short movement dominated by diffusion. Bentonite-based materials are effective to retard nuclide migration.

Key words: LILW, Disposal, Bentonite, Nuclide Migration, Aerated zone

1. INTRODUCTION

Safety of radioactive waste disposal is one of the challenges for nuclear power development and nuclear application. A seven-year project was launched by China Institute for Radiation Protection (CIRP) and Japan Atomic Energy Research Institute (JAERI) to demonstrate safety and improve safety assessment methodology of near-surface disposal of low-and-intermediate level radioactive waste. The project includes field test, laboratory test and modeling of nuclide migration in aquifer, in aerated zone soil and in engineered barrier materials at aerated zone[1].

For a multi-barriered disposal system, engineered barriers play important roles in the long-term safety. Bentonite and bentonite-based materials have been widely investigated as backfill/buffer materials in a disposal facility. The field test for bentonite was designed to explore migration of stable element tracers Br, Sr, Nd and Ce, and radioactive tracers ^{237}Np, ^{238}Pu and ^{90}Sr in bentonite based materials[2]. It is expected that the field test would obtain reasonably realistic data compared to the laboratory experiment. This paper will focus on moisture movement traced by Br and migration of radioactive tracers ^{237}Np, ^{238}Pu and ^{90}Sr.

2. EXPERIMENTAL

2.1 MATERIALS

The materials used in the test are mixture of sand and bentonites. Two kinds of bentonites were tested, Japanese bentonite (JB) named Kunigel V1, and Chinese bentonite (CB) collected from a bentonite mine in inter-Mongolia, China. Table I lists the chemical compositions of the two bentonite used in the tests. Mineral constitutes of Japanese bentonite are given in Table II. Chinese bentonite is Ca-based bentonite, while Japanese bentonite is Na-based. According to X-ray refraction analysis, the primary mineral in Chinese bentonite is montonite with content up to 80.92%. The secondary minerals are α-cristobalite, mordenite and orthoclase.

Table I. Chemical compositions of the two bentonite

Chemical Composition (%)	Chinese Bentonite	Japanese Bentonite
SiO_2	60.97	68.90
Fe_2O_3	1.26	1.69
FeO	0.09	0.71
Al_2O_3	12.69	13.70
TiO_2	0.099	0.24
MnO	0.018	0.08
CaO	1.72	2.62
MgO	2.65	2.54
K_2O	0.119	0.36
Na_2O	0.75	2.72
P_2O_5	0.030	0.05
Burnt loss	19.87	9.11
Total	100.26	99.41

Table II. Mineral constitutes of Japanese bentonite

Mineral constitute	Content (%)	Mineral constitute	Content (%)
Smectite	46 ~ 49	Calcite	2.1 ~ 2.6
Quartz	0.5 ~ 0.7	Dolomite	2.0 ~ 2.8
Chalcedony	37 ~ 38	Analcime	3.0 ~ 3.5
Plagioclase	2.7 ~ 5.5	Pyrite	0.5 ~ 0.7

2.3. PROCEDURES

2.2.1 Specimen preparation and burial

Fig. 1 shows the bentonite specimen. Each bentonite specimen includes three sections, bentonite section, tracer layer and loess section. Bentonite section is a mixture of bentonite (15%) and sand (85%), which is compacted to bulk density of 1.80 g /cm^3 with initial water content of 10% (wt). Tracer layer, quartz sand dipped with tracer solutions, is put on the surface and is trimmed as plain as possible. For radionuclide tracers, the amount of tracers in each specimen is 6.2×10^3 Bq for ^{238}Pu 5.2×10^4 Bq for ^{237}Np and 3.0×10^5 Bq for ^{90}Sr. After

placing the tracer layer, loess with size less than 2 mm is filled and compacted to field density. Then the specimen is placed in the pits[2].

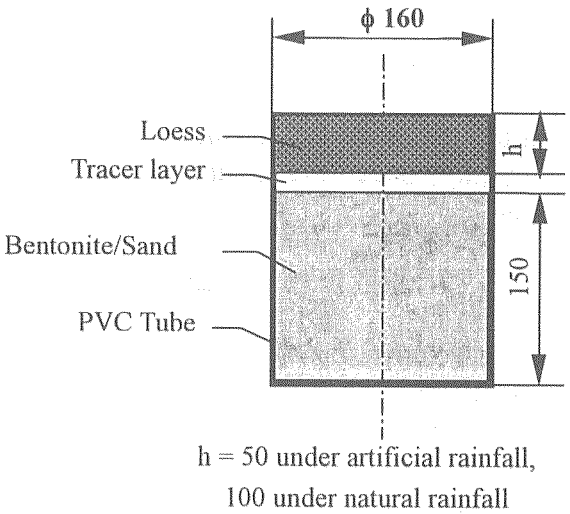

Fig. 1 Schematic of bentonite specimen

2.2.2. SAMPLING AND NUCLIDE MEASUREENT

Table III lists the sampling dates of each designed specimen. Due to very slow movement, we can not get effluents. The specimen is excavated on the designated date and taken to laboratroy. The specimen is sliced for tracer distribution analysis.

Table III Sampling dates of the field test for bentonite

Pit No.	Bentonite	Tracers	Start-Sampling date	Duration (days)
Additional	JB	Br^-	1998/08/02-1999/08-17	380
Additional	CB	Br^-	1998/08/02-1999/08-17	380
3	JB	^{238}Pu, ^{237}Np, ^{90}Sr	1997/07/01-2000/07/11	1106
	CB			
4	JB	^{238}Pu, ^{237}Np, ^{90}Sr	1997/06/25-2000/05/10	1050
	CB			
5	JB	^{238}Pu, ^{237}Np, ^{90}Sr	1997/07/01-1998/07/21	385
	CB			
	JB		1997/07/01-1999/08/02	762
	CB			

3. RESULTS AND DISCUSSIONS

3.1 WATER MOVEMENT IN THE TEST PITS UNDER NATURAL RAINFALL

Fig. 2 shows the distribution of Br^- and moisture content in the bentonite/sand specimen under natural rainfall. During this period of time, the rainfall is 307.5 mm, lower than annual

average[4]. The distribution curves of Br^- demonstrate that Br- moves through diffusion under natural rainfall conditions. The distribution is symmetric with short up-ward movement of the concentration peaks. The moisture distribution curve furhter proves the distribution. As the initial moisture in the bentonite/sand specimen is 10%, it is clear that after the experiment, the moisture in the bentonite/sand section remains at its original, while the upper and lower loess section both are at very low moisture content, 6% and 8% respectvely, which implies that there is no moisture exchange between the specimen and its surrounding media. Diffusion is the only driving force of nuclide migration under the natural rainfall condition. This is important to interprete the nuclide migration distribution.

3.2 WATER MOVEMENT IN THE TEST PITS UNDER ARTIFICIAL RAINFALL

Fig. 3 shows the distribution of Br^- and moisture content in the bentonite/sand specimen under the artificial rainfall. Since we added the same amount of Br- to specimens for the two rainfall conditions, we can see that under artificial rainfall condition, part of Br^- added have moved out of the boundary of bentonite specimen. The shape of the figures for both Chinese bentonite and Japanese bentonite demonstrate the complex water flow in the specimens. As the specimen is composed of three sections, the loess section, the quartz tracer layer and the bentonite/sand section, there exists two interfaces in the specimen. Clearly, the quartz tracer layer is conductive. The laboratory measurement shows that the hydraulic conductivity values

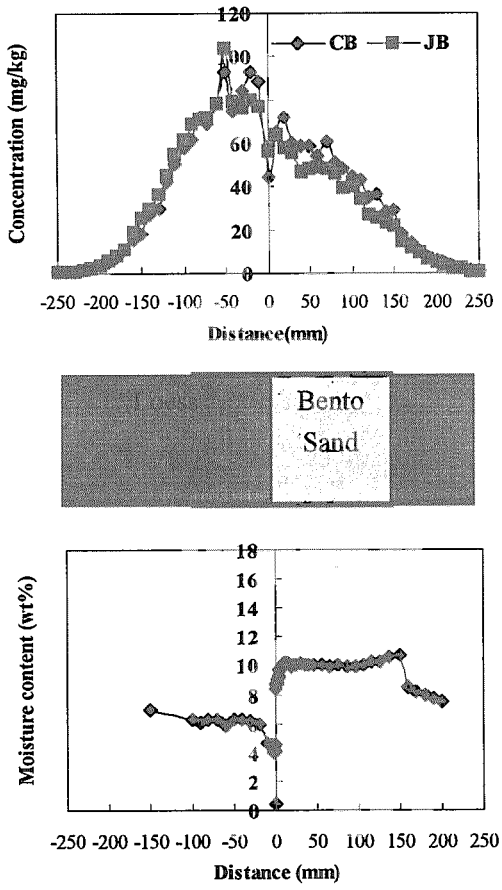

Fig.2 Distribution of Br^- and moisture in bentonite/sand specimen under natural rainfall condition

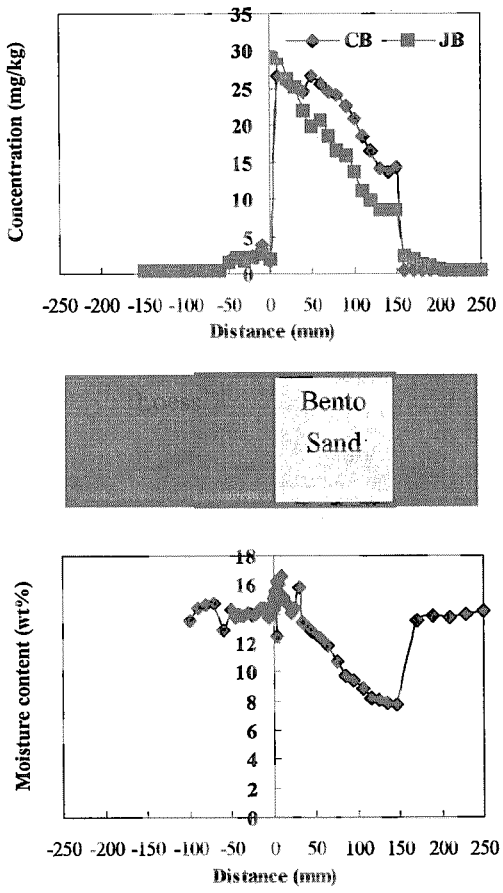

Fig.3 Distribution of Br^- and moisture in bentonite/sand specimen under artificial rainfall condition

of loess and bentonite/sand are at the order of 10^{-6} m/s and 10^{-10} m/s respectvely.[5] There is significant difference in water permeability. The moisture distribution may furhter help to interprete such distribution of Br^- along the specimen. The flux in the specimen is controlled by low permeable bentonite/sand. Since the moisture content in loess is up to 14%, there would have bigger diffusion capacity. In addition, due to bigger water flow in both upper and lower loess, there exists bigger concentration gradient. As a results, the Br^- moved to the loess was taken away by faster water flow.

3.3 RADIONUCLIDE MIGRATION IN THE SPECIMEN UNDER NATURAL RAINFALL

Fig. 4 demonstrates the distribution of radioactive tracer ^{237}Np, ^{238}Pu and ^{90}Sr in the bentonite/sand specimen under natural rainfall condition after 1050 days. ^{238}Pu has no observable movement. ^{237}Np has small down ward movement but without concentration peak movement. ^{90}Sr is widely distributed and it seems that the fraction in the upper direction is larger than that in the lower direction. As described in Section 3.1, the migration of nuclides under natural rainfall condition is driven by diffution, the diffusion capacity of the three nuclides should be in the order of $^{90}Sr > ^{237}Np > ^{238}Pu$. Laboratory measured Kd values of ^{237}Np, ^{238}Pu and ^{90}Sr in bentonite/sand also provide evidence to such distribution.[6]

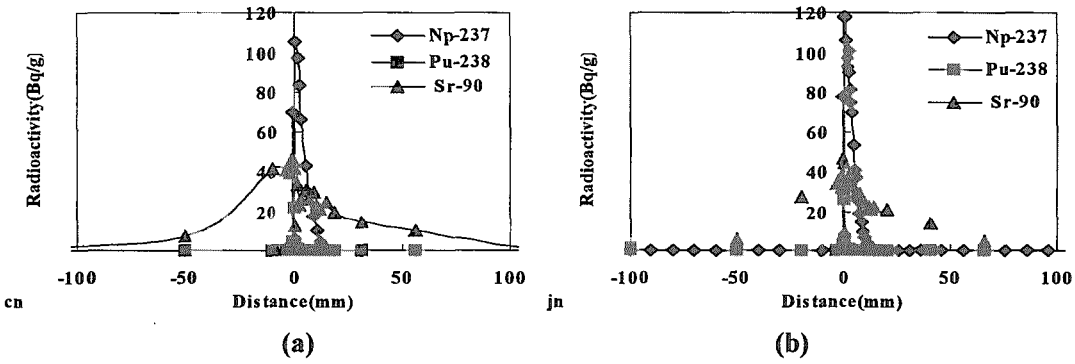

Fig. 4 Distribution of radioactive tracer ^{237}Np, ^{238}Pu and ^{90}Sr in the Chinese bentonite specimen (a) and the Japanese bentonite specimen (b) under natural rainfall condition after 1050 days

3.3 DISTRIBUTION OF ^{237}Np WITH TIME

Fig.5 shows distribution of ^{237}Np in specimen made of Chinese bentonite and sand at various times under artificial rainfall condtion (ar) and under natural rainfall condition (nr). ^{237}Np moved down with time under the artificial rainfall condition. There is no remarkable differences in distribtuion between the artificial rainfall and the natural rainfall. In the first 385 days, the movment is the fastest. Later, the migration slows down. Further calculation of the radioactivity moved below the tracer layer is listed in table IV. As mentioned in Section 3.1, nuclide migration under the natural rainfall is driven by diffusion. The calculated activity moved below the tracer

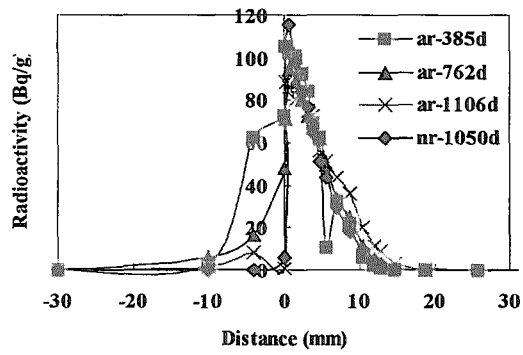

Fig.5 Distribution of ^{237}Np in bentonite/sand specimen with times under two rainfall conditions

layer is 15852 Bq for 1050 days under the natural rainfall, which is even smaller than the 385 day's migration under the artificial rainfall. Even for simple and conservative, the 1050 day's diffusion contributed 79.2% of the total migration of 1106 days under the artificial rainfall condition.

Table IV Total radioactivity below the tracer layers

Rainfall	Duration (days)	Total Radioactivity below the tracer layer (Bq)
Artificial rainfall	385	16472
Artificial rainfall	762	17710
Artificial rainfall	1106	20017
Natural rainfall	1050	15852

4. CONCLUSIONS

^{238}Pu does not have observable movement in the bentonite/sand specimen under the artificial rainfall and the natural rainfall conditions within the period of the field test.

^{237}Np has some movement bigger than ^{238}Pu and smaller than ^{90}Sr. In the test period, ^{237}Np moves down with time under artificial rainfall. Diffusion is the primary driving force for ^{237}Np movement in the bentonite/sand specimen under both natural rainfall condition and artificial rainfall condition.

Tracing test with Br^- demonstrates that the water do go down through the bentonite specimen rather than go around the specimen. However, the water flow along the specimen is very complex.

REFERENCES

[1] Li Shushen, Wang Zhiming, Safety Assessment Methodology for Shallow Land Disposal of Low Level Radioactive Waste – Overview Report (Draft). September 2001.

[2] Fan Zhiwen, Toshi Maeda, Feng Shengtao, Gu Cunli and etc. Field Test of Nuclide Migration in Engineered Barrier Materials at Aerated Zone. Sub-project Report 9. September 2001.

[3] Zhao Yinjie, Wu Qinghua etc. Field Tracer Test for Nuclide Migration in Loessial Aerated Zone, Sub-project Report 8. September 2001.

[4] Du Zhongde, Zhou Honggui, Wu Qinghua and etc. Environmental Characteristics of CIRP's Field Test Site, Sub-project report 1. August, 2001.

[5] Cui Anxi, Fan Zhiwen and etc. Barrier Performance of Bentonite Materials. December, 2000.

[6] TADAO, Tanaka. Adsorption characteristics of 85, 90Sr, 237Np, 239Pu and Stable Sr, Ce, Nd for Soil, Bentonite, Mortar and Quartz Sand. Sub-project Report 4, September 2001.

JP0250324

JAERI-Conf 2002-004

RECENT ACTIVITIES AT UNDERGROUND RESEARCH LABORATORIES IN JAPAN

K.AOKI

Japan Nuclear Cycle Development Institute

4-49 Muramatsu Tokai-mura Naka-gun Ibaraki, 〒319-1184

With a view to contributing to the HLW disposal project, JNC carries out R&D on geological disposal technologies for HLW and its basic geoscientific research in two Underground Research Laboratories (URLs) located in Mizunami and Horonobe. The URL in Mizunami is for conducting research on crystalline rock as an example of fractured media, while that in Horonobe is for sedimentary rock as porous media. The aim of the URLs is to enhance the reliability of geological disposal technologies and develop advanced safety assessment methodologies by collecting data for design studies and for input to safety assessment and by developing investigation and characterization techniques.

Investigation of the geological environment will be conducted in a stepwise manner as the investigation program moves forward. Investigation from the surface (first phase) will be followed by excavation of shafts and drifts (2nd phase) and, eventually, detailed investigations in the underground facility (3rd phase). In each phase, information on the geological environment will be collected, evaluated and verified. The investigation techniques used will also be improved and integrated as necessary. At the same time, the applicability of engineering technologies for the design and construction of an underground facility will be verified.

The URLs can provide a wide range of possibilities for underground research by universities or other research institutes, as well as serve as a tool for enhancing public understanding of R&D activities related to the geological disposal.

[1] URL in Mizunami

As part of the first phase surface-based investigation initiated in 1996, geological mapping, airborne and surface geophysical survey have been performed followed by research of four deep boreholes of a thousand meter depth. The geological environment from the surface to deep underground has been modeled and the excavation effects of the underground facility on the geological environment are to be evaluated.

Shaft sinking will start in 2002, with excavation of a major part of the research drift scheduled for completion by 2009. The Mizunami URL will examine techniques for investigation and characterization of the geological environment and application of basic engineering technologies deep underground for crystalline rock.

Subsequently, as part of the investigation phase during construction, modeling results will be verified by comparing them with actual data. The techniques used for the surface explorations and

the modeling of the geological environment will be documented in technical reports. The appropriateness of engineering strategies, including design and construction techniques for the underground facility, will also be confirmed.

[2] URL in Horonobe

The underground facility will be constructed at a depth of 500 m or more; shaft sinking will begin in 2005, with the aim of completing a major part of the drift by 2010. In the Horonobe URL Research Center, the focus will be on sedimentary rocks, with studies conducted on investigation and characterization techniques for the geological environment, long-term stability of the underground facility and the surrounding rock mass and application of basic engineering technologies deep underground. Verification of the design for the engineered barriers, the complex long-term evolution of the barriers, improvement of models, verification of the applicability of design techniques and safety assessment methods will also form part of the program.

Identifying the site for constructing the underground facility within Horonobe will be the first step of the surface-based investigation phase. At the selected location and in its neighboring region, preliminary activities will include data acquisition from the surface such as geophysical surveys and boreholes, modeling of the geological environment from the surface to deep underground and estimating the effects of constructing an underground facility on the geological environment. Based on the results of these studies, an underground facility will be designed and the project will enter the next phase of investigation.

The results obtained from these URLs will be widely published and are expected to make a timely contribution as follows to the disposal program and to the establishment of safety regulations:

i. Techniques will be developed for characterizing the geological environment from the surface to deep underground, based on investigation from the surface. This will take into account requirements relating to the design of the disposal system and safety assessment.
ii. Data obtained from investigations during the excavation phase will serve to verify the results from the surface-based investigation phase and the evolution of the geological environment during drift excavation. Models will also be refined based on the geological data.
iii. Detailed investigation in the underground facility during the third phase will contribute to ameliorate geological investigation techniques that take into account the requirements of disposal system design and safety assessment. Data will also be collected on the geological conditions to check the reliability of models.

TRU Chemistry

This is a blank page.

JP0250325

JAERI-Conf 2002-004

MOLECULAR INTERFACIAL REACTIONS BETWEEN PLUTONIUM AND MANGANESE OXIDE HYDROXIDE SURFACES

H. NITSCHE

Univ. of California at Berkeley and Lawrence Berkeley National Laboratory, The Glenn T. Seaborg Center, 1 Cyclotron Road, Ms 70A-1150, Berkeley, CA 94720, USA, HNitsche@lbl.gov

Actinides can migrate in the environment mostly via aqueous media such as groundwater and surface, river, lake and seawater. Models predicting the hydrological transport through the environment require as input an actinide concentration, the true amount that is actually available for transport. Three major processes define the actinide source term: (1) solubility, (2) organic interaction, and (3) sorption. They are dependent on each other and each individual process is the result of several sub-processes. Also, colloid formation plays a major role in the actinide source term, and it is common to each of the three main processes. The current state of knowledge of several of these processes will be discussed and emphasis will be given to the interfacial reactions of plutonium with manganese oxides and oxyhydroxides surfaces.

Manganese oxides, present as minor phases in the vadose zone and other subsurface environments, may preferentially sequester actinides and transition metals over iron oxide/hydroxide minerals present in much larger amounts. Key thermodynamic and kinetic parameters governing the sorption of aqueous plutonium species in defined oxidation states on characterized mineral surfaces as a function of pH, actinide concentration, and ionic strength were determined on manganese oxyhydroxide minerals.

The minerals were characterized using X-ray diffraction, X-ray absorption spectroscopy (XAS), and potentiometric titration, and the oxidation state of the sorbed plutonium was determined using XAS and optical absorption spectroscopy. \The results indicate that manganese oxide hydroxides, which show a variety of structure and manganese valence states, have large sorption capacities for Pu(VI) and Pu(V). Sorption increases as a function of mineral surface area and pH, especially at pH values above the pH_{PZC} where the mineral has a net negative surface charge. In addition, manganite and hausmannite (both predominantly Mn(III) minerals) reduce Pu(VI) and Pu(V) to Pu(IV), which then sorbs to the mineral. Redox reactions occur between the plutonium and the manganese, both in solution and on the minerals. XAS measurements show that plutonium is bound to these minerals in an inner sphere configuration, and that there is no evidence of PuO_2 precipitation on the surface. Based on these initial results, if plutonium contaminants in the environment contact manganese oxide hydroxide minerals, the plutonium can be sequestered through sorption at the mineral surface under specific conditions.

This is a blank page.

JP0250326

MICROBIAL TRANSFORMATIONS OF RADIONUCLIDES IN TRANSURANIC WASTES

A.J. FRANCIS
Environmental Sciences Department
Brookhaven National Laboratory, Upton, New York 11973, USA

ABSTRACT

Microorganisms have been detected in transuranic wastes and in waste-repository sites under consideration for the disposal of nuclear waste. Microorganisms can facilitate the mobilization and immobilization of radionuclides under appropriate conditions. Dissolution of radionuclides by microorganisms is brought about by changes in the Eh and pH of the medium, by their production of organic acids, such as citric acid, extracellular metabolites, and siderophores. Immobilization or precipitation of radionuclides is due to changes in the Eh of the environment, enzymatic reductive precipitation (reduction from higher to lower oxidation state), biosorption, and bioaccumulation, and bioprecipitation reactions. Free-living bacteria suspended in the groundwater fall within the colloidal size range and may have strong radionuclide sorbing capacity, giving them the potential to transport radionuclides in the subsurface. To date, we have only limited information on the interactions of microorganisms with radionuclides. Additional studies are needed to fully evaluate the role of microbes in the mobilization and immobilization radionuclides in the waste repositories and in the environment.

Key words: Uranium, technetium, biotransformation, bacteria, biocolloids

1. INTRODUCTION

Transuranic waste is radioactive waste containing more than 100 nanocuries (nCi) (3700 becquerels (Bq)) of alpha-emitting transuranic isotopes per gram of waste, with half-lives greater than 20 years. The term transuranic means those elements with an atomic number greater than that of uranium (i.e., atomic number >92). Radionuclides present in TRU waste include among others Am-241, Ba-137, Cm-244, Co-60, Cs-137, Pu-238, -239, -240, -241, Ra-226, Sr-90, Tc-99, Th-230, -234, U-233, -234, -235,-236, -238; Y-90. Of particular concern are the radionuclides U, Pu, Am, Np, and Tc because of their long half-life. The radionuclides in TRU waste may be present in various forms, such as elemental, oxide, coprecipitates, ionic, inorganic-, and organic-complexes, and naturally occurring minerals depending on the process and waste stream. In addition to the radionuclides the TRU waste consists a variety of organic materials (cellulose, plastic, rubber, chelating agents) and inorganic compounds (nitrate and sulfate). Significant microbial activity is expected in the waste because of the presence of organics and nitrate, which serve as carbon and nitrogen sources and nitrate and sulfate as electron acceptors in the absence of oxygen. This causes great concern in terms of gas generation and pressurization of containment areas in the repository.

Microbial activity could also affect the chemical nature of the radionuclides by altering the speciation, solubilities and sorption properties and thus could increase or decrease the concentrations of radionuclides in solution. Under appropriate conditions, dissolution or immobilization of radionuclides is brought about by direct enzymatic or indirect non-enzymatic actions of microorganisms. These include (i) oxidation-reduction reactions, (ii) changes in pH and Eh, (iii) chelation or production of specific sequestering agents, (iv) bioaccumulation by biomass, (v) biocolloid formation, (vi) bioprecipitation, and (vi) biotransformation of radionuclide-organic and -inorganic complexes. Key microbial processes involved in the mobilization or immobilization of selected radionuclides of interest is summarized in Table 1. Among the radionuclides, biotransformation of uranium has been

extensively studied, whereas we have only limited understanding of the microbial transformations of other radionuclides present in TRU waste [1, 2].

Table 1. Biotransformation of Selected Radionuclides in TRU Wastes.

Process	Th	U	Np	Pu	Am	Cs	Tc	Ra
Dissolution[1]	+	++	?	+	?	++	++	++
Reduction[2]	NA	++++	?	?	NA	NA	++++	NA
Biosorption	?	++++	+	++	+	++	+	ND
Biocolloid[3]	+	+	+	+	+	ND	?	ND

NA- not applicable; ND- not determined.
[1]- Dissolution due to oxidation from lower to higher valence state, changes in pH, production of organic acids and sequestering agents such as siderophores.
[2]- Reductive precipitation due to enzymatic reduction from higher to lower valence state.
[3]- Association of radionuclides with suspended bacteria, which can be potentially transported as biocolloids.

Fundamental understanding of the mechanisms of microbial transformations of radionuclides under repository relevant conditions would help to assess the microbial impact on long-term behavior of radionuclides stored in deep geological formations. In this paper, biotransformation of various chemical species of U under aerobic and anaerobic conditions, and the bioreduction of Tc by clostridia under anaerobic conditions, and the potential formation of radionuclide bearing biocolloids are examined.

2. BIOTRANSFORMATION OF URANIUM

Uranium exists in U(III), U(IV), U(V), and U(VI) oxidation states, of which U(IV) and U(VI) are the predominant ones in the environment. The direct implication of microorganisms in the biotransformation of uranium is of considerable interest because of its potential application in bioremediation of contaminated sites, in pre-treating radioactive wastes, and in processes critical to the performance of nuclear waste repositories. Both aerobic and anaerobic microorganisms are involved in the mobilization and immobilization of various chemical forms of uranium. Dissolution of uranium by autotrophic sulfur- and iron-oxidizing bacteria due to production of sulfuric acid and by heterotorphic bacteria and by fungi due to production of organic acids and chelating agents such as siderophores has been well documented in the literature.

2.1. Immobilization of Uranium

The immobilization of U is brought about by bioreduction and bioprecipitation reactions. Uranium is reduced by a wide variety of facultative and strict anaerobic bacteria under anaerobic conditions in the presence of suitable electron donor. Consequently, the

potential exists for the use of anaerobic bacteria to concentrate, contain and stabilize uranium in contaminated groundwaters and in waste with concurrent reduction in waste volume. However, the long-term stability of bacterially reduced U in the natural environment is not known.

2.1.1. Biosorption and Bioaccumulation of Uranium. Biosorption and bioaccumulation of U has been observed in a wide range of microorganism. It has been and perhaps it still is one of the intensely investigated areas of research because of the potential use of biomass to remove U from waste streams. Extracellular and intracellular association of U with bacteria was observed but the extent of its accumulation differs greatly with the species of bacteria. Uranium forms complexes with the carboxylate, phosphate, amino, and hydroxyl functional groups present on the cell surface; and intracellularly, by binding to anionic sites or precipitating as dense deposits.

Extracellular association of uranium with bacterial cell surfaces is primarily due to physical- and chemical- interactions involving adsorption, ion exchange, and complexation and does not depend on metabolism. Bacterial cell walls, exopolymers, proteins, and lipids contain functional groups, which are able to bind uranium.

Intracellular accumulation of U in *Pseudomonas fluorescens* and *P. aeruginosa* has been observed, but it existed as fine-grained, platy minerals [3, 4]. In *P. fluorescens*, Krueger et al. [4] observed that surface bound U was spread over the entire cell envelope (outer membrane-peptidoglycan-plasma membrane complex) and in about 10% of the cells, the U penetrated into the cytoplasm which appeared as platy U-crystals aligned in the periplasmic space. In contrast, intracellular accumulation of dense deposits of U in *P. aeruginosa* was extremely rapid; this did not involve metabolically mediated active transport. In *Halomonas* sp. U accumulated as electron-dense intracellular granules and was also bound to the cell surface. Intracellular accumulation involves transporting the metal across the cell membrane, which depends on the cell's metabolism. The intracellular transport of the U into the cell involves an as-yet unidentified transport system. Uranium transport across bacterial cell membranes may be mediated by the mechanism used to convey metabolically essential ions; however, additional studies are needed to clarify the exact mechanism involved.

2.1.2. Charaterization of Uranium Associated with Bacteria. Recently, nuclear magnetic resonance spectroscopy (NMR), time resolved laser fluorescence spectroscopy (TRLFS), and extended X-ray fluorescence spectroscopy (EXAFS) have been used to determine the the functional groups involved in the complexation of U with bacteria.

^{31}P-NMR studies showed that U was bound to the phosphate of the phospholipid fraction isolated from *Mycobacterium smegmatis* [5, 6].

TRLFS studies with several species of *Bacillus* showed the formation of inner-sphere complexes of U with phosphate groups on cell surface of the biomass, and suggested that the polysaccharides, techoic acids or phospholipid layers of the membranes are responsible for uranium binding. Intact cells formed more stable complexes with U(VI) than did the cell wall fraction. The bacterial phosphate binding occurs through organophosphate groups. The acidophilic bacteria *Thiobacillus ferrooxidans* and *Thiomonas cuprina* accumulated large quantities of U(VI) at pH's from 1.5 to 4. TRLFS studies showed that *T. ferroxidans* formed a strong inner-sphere complex with U(VI) whereas *T. cuprina* formed a weaker one [7].

EXAFS analysis of the association of U with halophilic and non-halophilic the bacterial cells showed that it was associated predominantly with phosphate as uranyl hydrogen phosphate and additional forms of phosphate such as hydroxophosphato or polyphosphate complexes as well as other ligands such as carboxyl species. These results demonstrate that phosphate, including the polyphosphates, bind significant amounts of U in bacteria.

Uranium associated with the bacteria is not very stable, as it was removed completely by Na_2HCO_3 from *Halomonas* sp, from an *Arthrobacter* sp by 0.1 sodium hydrogen carbonate [8], 0.1M EDTA, and Na_2CO_3, [9] and from Bacillus strains by EDTA [10]. Although bacteria possess a variety of functional groups, studies suggest that cellular phosphate is the predominant functional group complexes with U. Inorganic phosphate generated inside cells during starvation or under stress bind U and other cations.

2.2 Biotransformations of Uranium-Organic and -Inorganic Complexes

Although a wide variety of microorganisms are present in radioactive wastes and in natural radioactive mineral deposits, the extent to which they regulate the mobility of radionuclides complexed with organic ligands is not fully evaluated. Chelating agents used for decontamination and cleanup operations at the nuclear facilities constitute a significant portion of the waste. The persistence of radionuclides complexed with chelating agents in the disposal environment is a major concern because of the potential for increasing the transport of radionuclides. The types of organic complexing agents used are carboxylic acids (such as citric, hydroxy-acetic, oxalic, and tartaric acids), and amino-carboxylic acids (such as ethylenediaminetetraacetic acid (EDTA), diethylenetriaminepentaacetic acid (DTPA), nitrilotriacetic acid (NTA), and N-hydroxyethylene-diaminetriacetic acid (HEDTA)).

Many of these chelates either are poorly biodegraded under aerobic conditions, or undergo little anaerobic biodegradation. Biotransformation of radionuclide-complexes may result in precipitation of the released ion as water-insoluble hydroxides, oxides or salts. Such transformations may result in the retardation of nuclide migration. Information on microbial transformation of chelating agents is limited in particular there is a paucity of information on the biotransformation of organic ligand complexed with radionuclides as well as their fate under anaerobic conditions. This lack of knowledge often complicates studies aimed at predicting soil-retention characteristics of radionuclides and developing methods for in-situ stabilization of radionuclides. The following is a brief review of our understanding of the biotransformation of uranium-organic and -inorganic complexes under aerobic and anaerobic (denitrifying, iron-reducing, fermentative, sulfate-reducing) conditions.

2.2.1. Aerobic Conditions

2.2.1.1. Biotransformation of Binary Uranyl-citrate Complex by *Pseudomonas fluorescens*. Citric acid, a naturally occurring compound, is a multidentate ligand, which forms stable complexes with various metal ions. It forms different types of complexes with transition metals and actinides including formation of a bidentate, tridentate, binuclear, or polynuclear complex species. Biodegradation of metal citrate complexes is dependent upon the type of complex formed between the metal and citric acid; bidentate complexes are readily biodegraded whereas the tridentate complexes are recalcitrant [11]. *Pseudomonas fluorescens* metabolized the bidentate complexes of Fe(III)-, Ni-, and Zn-citrate, whereas complexes involving the hydroxyl group of citric acid, the tridentate Al-, Cd- and Cu-citrate complexes, and the binuclear U-citrate complex are not [12]. The presence of the free hydroxyl group of citric acid is the key determinant in effecting biodegradation of the metal complex. The lack of degradation was not due to their toxicity but was limited by the transport and/or metabolism of the complex by the bacteria. No relationship was observed between biodegradability and stability of the complexes. The tridentate Fe(II)-citrate complex, although recalcitrant, was readily biodegraded after oxidation and hydrolysis to the bidentate Fe(III)-citrate form, denoting a structure-function relationship in the metabolism of the complex [13].

Nunes and Gill [14] reported the formation of a cyclic 2:3 U-citrate complex involving hydroxo- and oxo-bridges above pH 6.5. Adding excess citric acid to equimolar (0.52mM) uranyl citrate resulted in the metabolism of the excess citric acid; the uranyl citrate complex

was not toxic to the bacterium. In the presence of 1-, 2-, and 3-fold excess citric acid, the citric acid remaining in each complex after biodegradation was 0.75, 0.80, and 0.83 mM, respectively. The final stoichiometry of U-citric acid in all three treatments was approximately 2:3, indicating the formation of 2:3 U-citric acid complex [15].

2.2.1.2 Ternary Iron- and Uranium-citrate Complexes. Citric acid forms ternary mixed-metal complexes with various metal ions involving the hydroxyl and carboxyl groups of citric acid. The presence of 1:1:2 Fe:U:citric acid in solution was confirmed by potentiometric titration, UV-vis spectrophotometry, gel-filtration chromatography, and extended X-ray absorption fine structure (EXAFS) analysis. Comparison of the EXAFS spectra show the 1:1:2 Fe:U:citric acid complex has structural characteristics similar to the 1:1 U:citric acid complex [15]. Biotransformation studies of Fe-U-citrate complex by *P. fluorescens* showed that the ternary 1:1:2 Fe:U:citric acid complex was recalcitrant. When a one-fold excess citric acid was added to this complex, the excess citric acid was completely degraded with no change in the stoichiometry of the complex. However, with two-fold excess citric acid, a 1:1:1 Fe:U:citric acid complex remained in solution after the excess citric acid was biodegraded. These results suggest that similar to the U-citrate complex, the Fe-U-citrate complex is recalcitrant to biodegradation. The persistence of mixed-metal-citrate complexes in wastes and contaminated environments may result in the mobilization of uranium.

2.2.2. Denitrifying Conditions

2.2.2.1. Metabolism of Uranyl-citrate Complex by *Pseudomonas fluorescens*. Citrate metabolism by *Pseudomonas fluorescens* under denitrifying conditions was facilitated by the enzyme aconitase as in aerobic metabolism. Biodegradation of the various metal-citrate complexes by *P. fluorescens* under denitrifying conditions was similar to that observed aerobically, but the rates were much lower. The bacterium completely degraded bidentate complexes of Fe(III)- and Zn-citrate, whereas the Ni-citrate complex was degraded only partially (~59%). The released ferric ion was in the colloidal form, and was not reduced to Fe(II) under denitrifying conditions. Tridentate complexes of Al-, Cd-, Cu-, and Fe(II)-citrate, and the binuclear U-citrate complex, were not metabolized by the bacterium.

2.2.2.2. Biotransformation of Uranyl-organic and -inorganic Complexes by *Halomonas sp.* Biotransformations of uranyl nitrate, uranyl-citrate, uranyl-ethylenediaminetetraacetate (EDTA), and uranyl carbonate by a denitrifying halophilic bacterium, *Halomonas* sp., isolated from the Waste Isolation Pilot Plant (WIPP) repository site was investigated [16]. Adding uranyl nitrate, uranyl-citrate, or uranyl-EDTA to the brine or bacterial growth medium resulted in the precipitation of uranium as a uranyl hydroxophosphato species [$K(UO_2)_5(PO_4)_3(OH)_2 \cdot nH_2O$]. Dissolution of the uranium precipitate was concomitant with the growth of the bacterium under anaerobic conditions. The bacterium completely metabolized the citrate released from uranyl-citrate complex, but not the EDTA released from the U-EDTA complex. The UV-vis spectra of the culture medium during growth revealed the formation of a uranyl dicarbonate complex $[UO_2(CO_3)_2]^{2-}$ due to CO_2 production from the metabolism of the carbon source. There was no change in the speciation of added uranyl carbonate. These results show that uranium phosphate can be solubilized to uranyl carbonate species as a result of bacterial action.

2.2.3. Anaerobic Conditions

2.2.3.1. Biotransformation of Uranyl-inorganic Complexes. A wide variety of facultative and strict anaerobic bacteria reduced U(VI) added as uranyl-nitrate or uranyl carbonate to

U(IV) under anaerobic conditions. These include axenic cultures of iron-reducing, fermentative, and sulfate-reducing bacteria. Mixed cultures of bacteria in uranium contaminated ground waters and in wastes also reduced uranium. Clostridia are strict anaerobic spore-forming fermentative bacteria ubiquitous in soils, sediments, and wastes.

$$U(VI)_{aq} \xrightarrow[\textit{fermenters, sulfate reducers}]{\textit{dissimilatory metal reducers}} U(IV)_s$$

They catalyze the reduction of metals from higher to lower oxidation state. Reduction of soluble U(VI) to insoluble U(IV) by the anaerobic bacterium, *Clostridium sp.* in culture medium was confirmed by X-ray absorption near edge spectroscopy (XANES) and X-ray photoelectron spectroscopy (XPS). Uranium was reduced only in the presence of growing or resting cells. Organic-acid metabolites, the extracellular components of the spent culture medium, and heat-killed cells failed to reduce uranium under anaerobic conditions [17].

2.2.3.2. Metabolism of Uranyl–organic Complexes by Fermentative, Iron- and Sulfate-reducing Bacteria. *Clostridium sphenoides* (ATCC 19403), which utilizes citric acid as the sole carbon source, metabolized equimolar Fe(III)-citrate with the degradation of citric acid and reduction of Fe(III) to Fe(II) but not the U(VI)-citrate complex. However, in the presence of excess citric acid or added glucose U(VI)-citrate was reduced to U(IV)-citrate. *Clostridium* sp. (ATCC 53464) which ferments glucose but not citrate reduced Fe(III)-citrate and U(VI)-citrate only when supplied with glucose. The metals reduced by the *Clostridium* sp. were present in solution as metal-citrate complexes. These results show that the complexed uranium is readily accessible as an electron acceptor despite the inability of the bacterium to metabolize the organic ligand complexed to the actinide. We have also shown that the metabolism of the metal-citrate complex is dependent upon the type of complex formed between the metal and citric acid. Fe(III) forms a bidentate complex with citric acid and was metabolized, whereas U forms a binuclear complex with citric acid and was recalcitrant.

The resting cells of the sulfate-reducing *Desulfovibrio desulfuricans* and the facultative iron-reducing *Shewanella halotolerans* bacteria reduced U(VI) complexed with oxalate or citrate to U(IV) under anaerobic conditions with little precipitation of uranium. The reduced U(IV) remained in solution complexed with oxalate or citrate [18, 19]. These results show that complexed uranium is readily accessible for the microorganisms as an electron acceptor, despite the inability of the bacteria to metabolize the organic ligand complexed to the actinide.

3. BIOTRANSFORMATION OF TECHNETIUM

Technetium (Tc) can exist in oxidation states 0, +3, +4, +5, +6, and +7. Tc is readily reduced and oxidized. Uncomplexed Tc(III, IV) undergoes hydrolysis and precipitates from solution. Tc(V) and Tc(VI) undergo disproportionation to Tc(IV) and Tc(VII). The safe disposal of the Tc-containing wastes and environmental contamination of Tc are major concerns.

Microorganisms affect the dissolution or precipitation of Tc by oxidation-reduction reactions and by complexation with organic by-products and macromolecules. Chemolithotrophic, aerobic, facultative, and anaerobic (fermentative and sulfate-reducing) bacteria reduced pertechnetate ion to an insoluble form. For example, *Clostridium sphenoides* capable of citrate and glucose metabolism and *Clostridium* sp. capable of fermenting glucose but not citric acid reduced Tc(VII) to Tc(IV). The reduced Tc was predominantly associated with the cell biomass. It also was present in solution complexed with bacterial metabolic

products (MW>5000). Adding diethylenetriaminepentaacetic acid (DTPA) to *Clostridium* sp. resulted in the formation of a soluble Tc(IV)-DTPA complex, whereas with *C. sphenoides* only a small amount of Tc was present in solution, indicating that insoluble Tc species were formed.

The nature and stability of the Tc-organic complexes is not known. Moreover, the ability of the bacterium to metabolize Tc-organic complexes such as Tc-citrate is also not known. Tc may be present as insoluble or soluble form or as colloids, depending on the type and extent of bacterial activity in subsurface environments and therefore, the potential exists for the transport of reduced Tc in these forms. *Clostridia* are ubiquitous and form spores, which are highly resistant to destruction. They can survive on almost any surface for long periods of time. These results suggest that these organisms may play a major role in regulating the mobility of Tc under anaerobic conditions in wastes and subsurface environments.

4. BIOCOLLOIDS

Microbes can affect the transport of actinides by forming biocolloids. Significant numbers of bacteria exist in all subterranean environments including extreme environments. They are present in the groundwaters of all the repository environments investigated, they fall within the colloidal size range of 1 nm to 1 μm, and can be transported with bulk-liquid flow. Growing bacteria are several micrometers long with volumes of several cubic microns, while non-growing bacteria, under oligotrophic conditions, at a minimum may be as small as 0.2 - 0.3 μm with a volume not less than 0.05 μm^3. In addition, biomass accumulated on surfaces (biofilms) can become detached and generate biocollids. Microorganisms are important sources of organic colloids, as are their metabolic by-products and exocellular polymers. Microbes bioaccumulate and biosorb radionuclides intracellularly or extracellularly. Francis et al., [20] evaluated the interactions of dissolved actinides ^{232}Th, ^{238}U, ^{237}Np ^{239}Pu, and ^{243}Am, with a pure and a mixed culture of halophilic bacteria isolated from the Waste Isolation Pilot Plant repository under anaerobic conditions. The sizes of the bacterial cells ranged from 0.54 x 0.48 μm to 7.7 x 0.67 μm. The association of actinides with mobile bacterial cells (10^6 to 10^9 cells ml^{-1}) suspended in a fluid medium containing NaCl or $MgCl_2$ brine, at various growth phases was determined by sequential microfiltration. The amount of actinide associated with the suspended cell fraction (calculated as mol $cell^{-1}$) was very low: Th, 10^{-12}; U, 10^{-15} - 10^{-18}; Np, 10^{-15} - 10^{-19}; Pu, 10^{-18} - 10^{-21}, and Am, 10^{-18} - 10^{-19}; it varied with the bacterial culture. The differences in association were attributed to the extent of bacterial bioaccumulation and biosorption, pH, the brine's composition, and the speciation and bioavailability of the actinides. Plutonium uptake by *Acetobacterium* sp. isolated from groundwater from Grimsel Test Site (GTS) Switzerland, varied from 30-145 pg of Pu mg^{-1} dry wight of cells [21, 22]. The chemical form of the Pu, i.e., its ionic-, organic-, and inorganic-complexes and its solubility affect its bioavailability to bacteria. These results suggest the potential for the subterranean microbes to facilitate the transport of actinides associated with them.

Fundamental knowledge of the microbial transformations of several chemical forms of radionuclides under various microbial process and environmental conditions will be useful in developing appropriate waste treatment and management strategies as well as predicting the microbial impacts on the long-term performance of the waste repositories.

Acknowledgments

This research in part was supported by the Environmental Sciences Division, Office of Biological Environmental Research, Office of Science, U.S. Department of Energy, under contract No. DE-AC02-98CH10886.

REFERENCES

1. Francis, A.J. 1998. J. Alloys and Compounds 271/273:78-84.
2. Francis, A.J. 2001. Microbial transformations of plutonium and implications for its mobility. In "Plutonium in the Environment" A. Kudo, (Ed) Elsevier Science Ltd., Co., UK. pp 201-219.
3. Strandberg, G.W., S.E. Shumate II, and J. R. Parrot Jr. 1981. Appl. Environ. Microbiol.41:237-245.
4. Krueger,S., G.J. Olsen, D. Johnsonbaugh, and T.J. Beveridge. 1993. Appl. Environ. Microbiol. 59: 4056-4064.
5. Andres, Y., J. MacCordick, and J. C. Hubert. 1993. Appl. Microbiol. Biotechnol. 39:413-417.
6. Andres, Y., J. MacCordick, and J. C. Hubert. 1994. FEMS Microbiol. Lett. 115: 27-32.
7. Panak, P., S. Selenska-Pobell, S. Kutschke, G. Geipel, G. Bernhard, and H. Nitsche. 1999. Radiochim. Acta 84: 183-190.
8. Sakaguchi, T. 1996. *Bioaccumulation of Uranium*. Kyushu University Press, Hukuoka, Japan. pp 61-95.
9. Marques, A.M., X. Roca, M.D. Simon-Pujol, M.C. Fuste, and F. Congregado. 1991. Appl. Microbiol. Biotechnol. 35: 406-410.
10. Panak, P., J. Raff, S. Selenska-Pobell,, G. Geipel, G. Bernhard, and H. Nitsche. 2000. Radiochim.Acta. 88: 71-77.
11. Francis, A.J., C.J. Dodge, and J.B. Gillow. 1992. Nature 356:140-142.
12. Joshi-Tope, G. and Francis, A. J. 1995. J. Bacteriol. 177:1989-1993.
13. Francis, A.J. and C.J. Dodge. 1993. Appl. Environ. Microbiol. 59:109-113.
14. Nunes, M.T.and V.M.S. Gill. 1987. Inorg. Chim. Acta. 129: 283-287.
15. Dodge, C.J. and Francis, A.J. 1997. Environ. Sci. Technol. 31: 3062-3067.
16. Francis A.J., C.J. Dodge, J.B. Gillow, and H.W. Papenguth. 2000. Environ. Sci. Technol. 34: 2311-2317.
17. Francis, A.J., C.J. Dodge, F. Lu, G. Halada, and C.R. Clayton. 1994. 28:636-639.
18. Ganesh R., K.G. Robinson, G.R. Reed, and G. S. Saylor. 1997. Appl. Environ. Microbiol. 63:4385-4391.
19. Ganesh R., K.G. Robinson, L. Chu, D. Kucsmas, and G.R. Reed. 1999. Wat. Res. 33: 3447-3458.
20. Francis, A.J., J. B. Gillow, C.J. Dodge, M. Dunn, K. Mantione, B.A.Strietelmeier, M.E. Pansoy-Hjelvik, H.W. Papenguth. 1998. Radochim. Acta. 82: 347-354.
21. Gillow, J.B., Dunn, M., Francis, A.J., and Papenguth, H.W. 2001. Radiochim Acta. 88:769-774.
22. Gillow, J.B., Francis, A.J., Lucero, D.A., and Papenguth, H.W. 2000. The interaction of plutonium with bacteria in the repository environment. Plutonium futures-The Science, Ed., K.K.S. Pillay and K.C. Kim, American Institute of Physics. pp 51-52.

JP0250327

JAERI-Conf 2002-004

Electrochemical investigation of actinide ions for redox flow battery

T. Yamamura, N. Watanabe, Y. Shiokawa
KINKEN, Tohoku University, Oarai, Ibaraki, 311-1313, Japan
FAX: 81-29-267-3181, email: yamamura@imr.edu

Key words: actinide, neptunium, uranium, redox flow battery

1. INTRODUCTION

The actinides produced by our domestic nuclear power plants are estimated as 7.2×10^4 tons for the depleted uranium, 9.1×10^3 tons for the recovered uranium, 6.3 tons for neptunium, 1.0×10^2 tons for plutonium, 4.0 tons for americium and 0.48 tons for curium per ten years. The minor actinides such as neptunium, plutonium, americium and curium are regarded as the high radioactive wastes to be disposed of in the deep underground repository. As for the wastes, in the 19th century just after the industrial revolution in Europe, the coal tar was the serious industrial wastes produced as the remainder of the coal after the production of the coke for steel manufacturing and the coal gas for illuminants. However, by the investigations of the coal tar chemistry the wastes have become a precious resource of the organic chemical industry. This historical episode suggests the importance of the chemical researches of the radioactive wastes.

Among all the elements in the periodic table, only four actinide elements (An: U, Np, Pu, Am) have the quite unique nature that the single element possesses two redox couples with identical structures (AnO_2^+/AnO_2^{2+}, An^{3+}/An^{4+}). The actinides satisfy the necessary condition for the redox battery, *i.e.* the two redox reactions are reversible, whereas in the existing vanadium redox flow battery one of the electrode reaction VO^{2+}/VO_2^+ is suffered from the extreme slow kinetics due to the rearrangement of the coordination structure. Therefore we have proposed the actinide redox flow batteries for the electric power storage where An(III)/An(IV) and An(V)/An(VI) couples are used for the negative and the positive electrolytes, respectively [1, 2]. Despite that all of the oxidation states of the neptunium are stable in aqueous solutions, the uranium aqueous system is suffered from the instability of U(V) due to the disproportionation reaction with the proton released by water. Thus the uranium battery requires aprotic solvents. In the present study, we are conducting the electrochemical investigation of the redox flow battery with the neptunium to choose the suitable carbon materials for the battery electrode, and with the uranium to investigate into the suitable active materials of the redox flow battery.

2. EXPERIMENTAL

Neptunium(IV) was obtained by the reaction of a neptunium stock solution with platinum black and hydrazine dihydrochloride. The neptunium(IV) was purified by an anion exchange resin and a part of the neptunium(IV) solution was oxidized to prepare the neptunium(IV) solution by the electrolysis. The uranium complexes such as $U(acac)_4$, $U(dbm)_4$, $U(ba)_4$, $U(btfa)_4$ [3], $U(fod)_4$, $U(pta)_4$, $U(dpm)_4$ [4], $UO_2(hfa)_2$, $UO_2(pta)_2$, $UO_2(fod)_2$ [5], $UO_2(dpm)_2$ [4, 6], $UO_2(ba)_2$, $UO_2(dbm)_2$, $UO_2(btfa)_2$, $UO_2(dmso)_5(ClO_4)_2$

[7] were synthesized according to the previous works and these compounds were purified mainly by the sublimation. The purified uranium complexes were transferred into an inert gas glove box, whose atmosphere was maintained to reduce the concentration of O_2 and H_2O less than 1 ppm, and dissolved in solvents at relatively high concentrations as stock solutions. This stock solutions with or without undissolved complexes were kept at 23 ±1°C in the glove box and shaken twice a day. After three days only the stock solutions with undissolved solids were measured. A small amount of sampled solutions were transferred out of the glove box, their solvents were evaporated under a reduced pressure and the remnants were dissolved in 1N HNO_3 and measured by ICP-AES (Shimadzu Corp., ICP-7500). Cyclic voltammetry measurements were conducted by using an electrochemical measurement system (Hokuto Denko Corp., HZ-3000) and an electrochemical cell installed inside of the glove box. Working electrodes such as the platinum (1.6ϕ), the plastic formed carbon (PFC, 3ϕ), the glassy carbon (GC, 5ϕ), the pyrolitic graphite with *a* surface (aPG, 5ϕ) and with *c* surface (cPG, 5ϕ) were well polished and preprocessed in 0.5 mol dm^{-3} sulfuric acid. All of the organic solvents used were purified by the distillation.

3. ELECTROCHEMICAL INVESTIGATION OF NEPTUNIUM FOR REDOX FLOW BATTERY

The anodic and cathodic peak potentials of Np(IV)/Np(III) and Np(VI)/Np(V) were reported [8, 9] for 1 mol dm^{-3} HNO_3, 0.5 mol dm^{-3} $HClO_4$, 0.5 mol dm^{-3} H_2SO_4 and 0.5 mol dm^{-3} CH_3COOH aqueous solutions. According to the works, ΔE_p for Np(IV)/Np(III) and Np(VI)/Np(V) are *ca.* 60 mV in nitric and perchloric media. The standard electrode rate constants for the carbon electrodes which are used in the practical battery have not been obtained and they are therefore evaluated in the present study.

The cyclic voltammetry of the neptunium aqueous solutions were carried out in nitric acid solutions (Fig.1) with four types of carbon working electrodes, *i.e.* GC, aPG, cPG and PFC. The emf of the battery is estimated as *ca.* 1.0V, which is independent of the types of the electrodes (Table I). The standard electrode rate constants k_0 calculated [10, 11] are significantly large for both Np(VI)/Np(V) and Np(IV)/Np(III) couples. Among the carbon

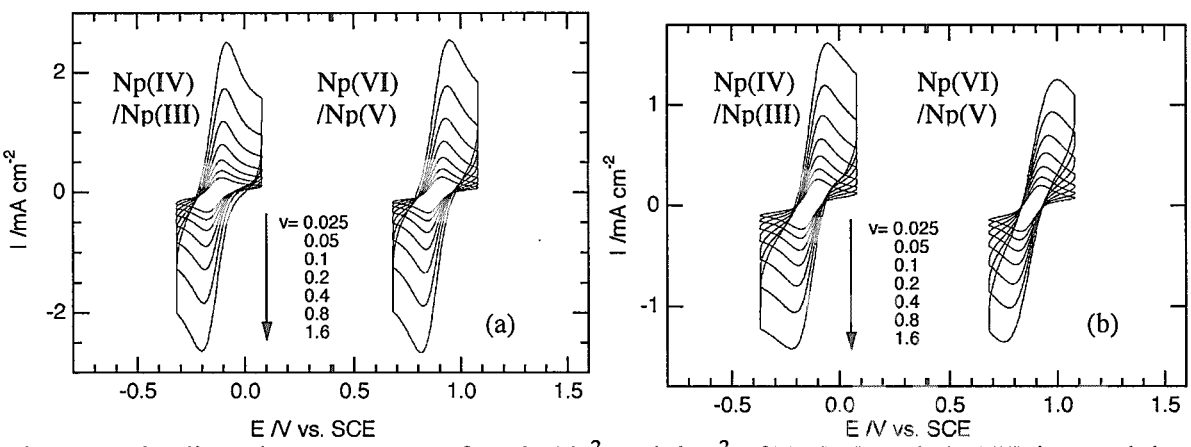

Fig.1. Cyclic voltammograms of 3.18×10^{-3} mol dm^{-3} of Np(VI) and Np(IV) in 1mol dm^{-3} HNO_3 at (a) cPG and (b) aPG electrode, respectively.

Table I. Standard rate constants k_0 for Np(IV)/Np(III) and Np(VI)/Np(V) and open circuit voltage of Np battery in 1 mol dm^{-3} HNO_3.

Electrode	k_0/cm s^{-1} for Np(IV)/Np(III)	$E_{1/2}$(IV/III) /V	k_0/cm s^{-1} for Np(VI)/Np(V)	$E_{1/2}$(VI/V) /V	ΔE /V
GC	$(9.3\pm1.0)\times10^{-3}$	0.878	$(4.8\pm0.5)\times10^{-3}$	-0.151	1.03
PFC	$(2.1\pm0.5)\times10^{-2}$	0.877	$(2.8\pm0.9)\times10^{-2}$	-0.146	1.02
aPG	$(5.6\pm0.3)\times10^{-3}$	0.874	$(2.8\pm0.2)\times10^{-3}$	-0.151	1.03
cPG	$(1.3\pm0.2)\times10^{-2}$	0.879	$(1.2\pm0.3)\times10^{-2}$	-0.142	1.02

materials, the PFC and the cPG have especially large k_0 values exceeding 10^{-2} cm s^{-1} (Table I) and these carbon materials are regarded as the candidate for the battery electrodes.

4. ELECTROCHEMICAL INVESTIGATION OF URANIUM FOR REDOX FLOW BATTERY

The emf of the uranium battery based on the aqueous solutions can be evaluated as ΔE=0.68V according to the literature data $E^0(UO_2^{2+}/UO_2^{+})$=0.16V and $E^0(U^{4+}/U^{3+})$=-0.52V [12]. This voltage is not enough for practical batteries and, moreover, this aqueous system is

Table II. Solubilities of uranium complexes in aprotic solvents.

complex	solubilities / mol dm^{-3} c)			
	AN	DMSO	DMF	PC
$UO_2(ClO_4)_2$ a)	----	>0.8	>0.8	----
$UO_2(hfa)_2$	>0.8	>0.6	>0.4	>0.6
$UO_2(fod)_2$	>0.4	1.1×10^{-3}	>0.4	>0.4
$UO_2(pta)_2$	>0.4	0.26	>0.4	>0.4
$UO_2(dpm)_2$	3.0×10^{-2}	0.16	>0.4	7.1×10^{-2}
$UO_2(acac)_2$	>0.4	>0.4	0.32	>0.4
$U(fod)_4$	2.6×10^{-4} b)	2.1×10^{-4} b)	7.4×10^{-2}	8.9×10^{-2}
$U(pta)_4$	1.8×10^{-2}	>0.4	>0.4	8.0×10^{-4}
$U(dpm)_4$	1.1×10^{-4} b)	8.9×10^{-5} b)		

a) Examined by dissolving $UO_2(dmso)_5(ClO_4)_2$ or $UO_2(dmf)_5(ClO_4)_2$ into each solvents.
b) Equilibrated for 6 months.
c) The sign of inequality indicates that the stock solution with the shown concentration was successfully prepared. The figure without the sing of inequality indicates that the solubility measurements was conducted.

suffered from the instability of U(V) due to the disproportionation with the proton released by water. Therefore the uranium battery requires the aprotic solvents.

For the uranium system with the polar aprotic solvents, the uranium β-diketones were examined because the solubility of the complex are expected to be high. The solubility of the active materials is one of the most important factors for the redox flow battery because the capacity of the battery per unit volume is determined by the solubility. Although the solubility data is poor on the uranium complexes with organic ligands into polar aprotic solvents [13], the solubilities of U(VI) β-diketone complexes are expected to be relatively high in previous works [4, 7, 14-17]. Furthermore there are important electrochemical works that the uranium β-diketones undergo electrode reactions with relatively simple mechanisms [15, 16, 18].

According to the result of the solubility experiment, the solubility of more than 0.8 mol dm^{-3} for U(VI) complexes and more than 0.4 mol dm^{-3} for a U(IV) complex were obtained (Table II). The solubility of 1 mol dm^{-3} is desired for the active materials for the battery and further investigations are required. Fig.2 shows the typical result of the cyclic voltammetry experiments for $UO_2(dpm)_2$ †. Referring to the Fig.2 and other results, the reaction scheme is deduced as following: $U^{VI}O_2(dpm)_2$ is reduced to $U^{V}O_2(dpm)_2^-$ (pc1) which is decomposed to $U^{V}O_2(dpm)$ through an intermediate. The intermediate is responsible for pa1 and the $U^{V}O_2(dpm)$ complex are stable in the solvents (pa2/pc2). Fig.3 indicates the redox potentials of the U(VI)/U(V) complexes with two β-diketones coordinated and the U(IV)/U(III) complexes with four β-diketones coordinated. In order to avoid the mutual contamination of

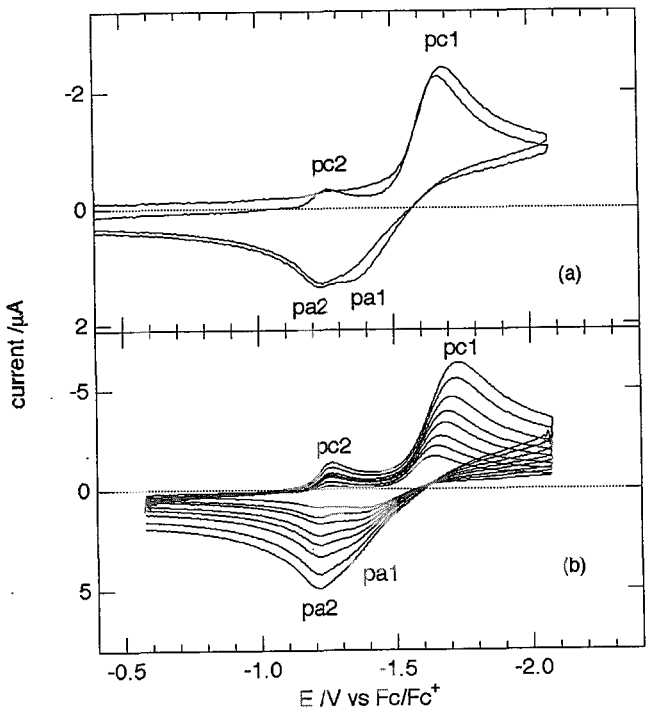

Fig. 2. Cyclic voltammograms of $UO_2(dpm)_2$ complex dissolved in DMSO solution containing 0.1 mol dm^{-3} TBAP. Concentration of $UO_2(dpm)_2$ is $1x10^{-3}$ mol dm^{-3}. Initial sweep direction is cathodic. (a) Potential is scanned repeatedly between -0.18V and -2.07V vs Fc/Fc^+. Change in shape of voltammograms between initial (thick curve) and 20th (thin curve) scan are indicated. (b) Sweep velocity ranges from 0.10 to 2.0 Vs^{-1}.

† Hereafter the further solvation of complexes in aprotic solutions is omitted.

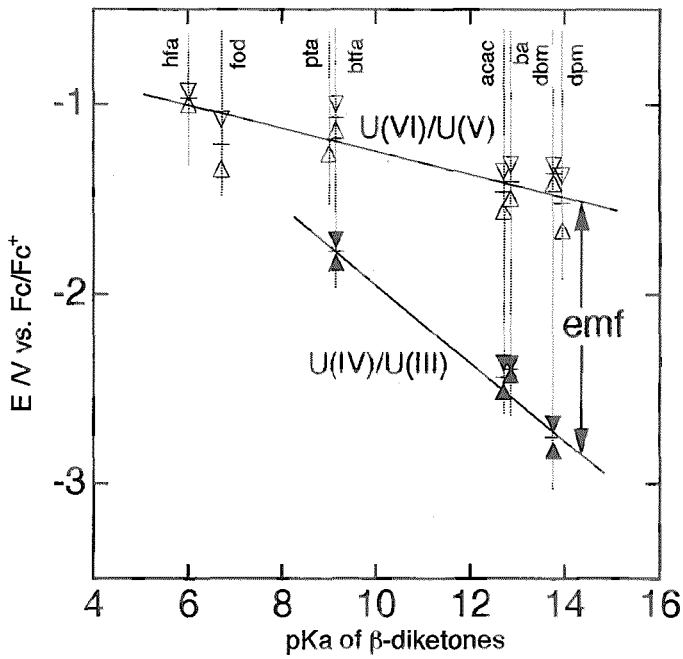

Fig. 3 Summary of redox potentials of uranium β-diketones measured by cyclic voltammetry. Open triangles and closed triangles indicate potentials of U(VI)/U(V) with two β-diketones coordinated and U(IV)/U(III) with four β-diketones coordinated, respectively. Upper triangles and lower triangles indicate potentials of reduction wave and oxidation wave, respectively. Horizontal bar indicates $E_{1/2}$

the electrolyte by the permeation of different ligands through the battery membrane, the β-diketone ligand coordinated to the uranium is required to be common in the negative electrolyte, U(IV)/U(III), and the positive electrolyte, U(VI)/U(V). Therefore the emf of the battery is evaluated as the difference along the potential axis between the U(VI)/U(V) and the U(IV)/U(III) as shown in Fig.3 by assuming that no ligand dissociation and association reaction occur. The open circuit voltage is estimated more than 1V by using the U(VI)/U(V) acetylacetone solution as the positive electrolyte and U(IV)/U(III) acetylacetone solution as the negative electrolyte. The larger electromotive force is expected when the ligands with the larger basicity is used in the battery.

5. CONCLUSIONS

The carbon material for the neptunium battery electrode is investigated and the PFC is regarded as the candidate by referring to the electrode rate constants of both Np(VI)/Np(V) and Np(IV)/Np(III) and also to the emf of the neptunium battery. The uranium β-diketones were investigated as the active materials of the uranium battery. Although the solubility of the U(VI) complexes are relatively high, it requires further studies to increase the solubility of the U(IV) complexes. The emf larger than 1V is expected by using the identical β-diketone ligand for both the positive and the negative electrolytes by assuming the ligand dissociation and the association processes followed by the redox reaction are suppressed.

REFERENCES

[1] Y. Shiokawa, H. Yamana, and H. Moriyama, J. Nucl. Sci. Tech., 37, 253-56 (2000).
[2] T. Yamamura, Y. Shiokawa, H. Yamana, and H. Moriyama, Electrochim. Acta, (submitted).
[3] T. Yoshimura, C. Miyake, and S. Imoto, Bull. Chem. Soc. Jpn., 46, 2096-101 (1973).
[4] Y. Shiokawa, R. Amano, A. Nomura, and M. Yagi, J. Radioanal. Nucl. Chem., 152, 373-80 (1991).
[5] A. Ekstrom, H. Loeh, C. H. Randall, L. Szego, and J. C. Taylor, Inorg. Nucl. Chem. Lett., 14, 301-04 (1978).
[6] K. J. Eisentraut and R. E. Sievers, J. Am. Chem. Soc., 87, 5254 (1965).
[7] T. Yamamura, S. Iwata, S. Iwamaru, and H. Tomiyasu, J. Chem. Soc., Faraday Trans., 90, 3253-59, (1994).
[8] S. Casadio and F. Orlandini, J. Electroanal. Chem., 33, 212 (1971).
[9] U. Niese and J. Vecernik, Isotopenpraxis, 18, 191 (1982).
[10] R. S. Nicholson, Anal. Chem., 37, 1351 (1965).
[11] A. J. Bard and L. R. Faulkner, Electrochemical Methods, John Wiley&Sons, New York, 1980.
[12] A. J. Bard, R. Parsons, and J. Jordan, Standard Potentials in Aqueous Solutions, IUPAC(Marcel Dekker), New York, 1985.
[13] R. Keim, ed., Chemistry in nonaqueous solutions (conductivity, molecular weight, solubility), Gmelin handbook of inorganic chemistry, Vol. System no.55 . U, uranium ; Suppl. v. D5, Springer, Berlin, 1995.
[14] A. Al-Alousy and J. Burgless, Polyhedron, 11, 531-39 (1992).
[15] K. Mizuguchi, Y.-Y. Park, H. Tomiyasu, and Y. Ikeda, J. Nucl. Sci. Technol., 30, 52 (1993).
[16] S.-H. Lee, K. Mizuguchi, H. Tomiyasu, and Y. Ikeda, J. Nucl. Sci. Technol., 33, 190-92 (1996).
[17] K. Mizuguchi, S.-H. Lee, Y. Ikeda, and H. Tomiyasu, J. Alloys Compds., 271-273, 163-67 (1998).
[18] A. Vallat, E. Laviron, and A. Dormond, J. Chem. Soc. Dalton Trans., 921-24 (1990).

JP0250328

JAERI-Conf 2002-004

SUPERCRITICAL FLUID TECHNOLOGY FOR ADVANCED NUCLEAR FUEL CYCLE

ZENKO YOSHIDA, YOSHIHIRO MEGURO, SHUICHI ISO, TAKAUMI KIMURA, OSAMU TOMIOKA*, YOUICHI ENOKIDA**, ICHIRO YAMAMOTO*, JIN OUGIYANAGI***, KOUSABURO OHASHI***

Advanced Science Research Center, Japan Atomic Energy Research Institute, Tokai, Ibaraki 319-1195, Japan
Fax;+81-29-282-5927, e-mail; zyoshida@popsvr.tokai.jaeri.go.jp
*Department of Nuclear Engineering, Nagoya University, Furo-cho, Chikusa-ku, Nagoya 464-8603, Japan
**Research Center of Nuclear Materials Recycle, Nagoya University, Furo-cho, Chikusa-ku, Nagoya 464-8603, Japan
***Department of Environmental Sciences, Faculty of Science, Ibaraki University, Mito 310-8521, Japan

Recent progress in the development of new methods for the separation of metal ions using supercritical CO_2 fluid media is reviewed. A principle, a procedure and advantages of the supercritical CO_2 fluid extraction method (SFE) or leaching method (SFL) for the separation of uranium and plutonium are summarized and feassibility of these methods to such processes as a reprocessing of the nuclear spent fuel, a partitioning of the high-level liquid-wastes, and a decontamination of the radioactive solid wastes is discussed.

Key words; supercritical CO_2, separation, uranium, plutonium, reprocessing, decontamination

1. INTRODUCTION

Recently, much attention has been paid to a supercritical CO_2 fluid as a medium for the separation of metals.[1-12] Supercritical CO_2 fluid extraction (SFE) using the supercritical CO_2 exhibits several advantages as follows over a traditional solvent extraction procedure using an organic solvent. The extraction efficiency and the extraction rate are expected to be enhanced due to rapid mass transfer in the supercritical fluid phase. The rapid and complete removal of the extraction medium is attained by gasification of CO_2 at ambient temperature and pressure after the extraction process. The extraction efficiency or selectivity can be optimized by changing the properties of the CO_2 medium optionally by tuning the pressure.[1,6,13] The use of SFE process in the field of nuclear technology exhibits a particular significance for minimizing the amount of the solvent waste.[12,14] The authors have developed the SFE of U(VI) and Pu(IV) from nitric acid solutions using the supercritical CO_2 containing tri-*n*-butylphosphate (TBP).[1,6,13]

An alternative and more attractive method is supercritical CO_2 fluid leaching (SFL) of metals from the solid samples. In this method, acid for the dissolution or pretreatment of the solid sample is not necessary. The authors have studied the leaching behavior of metals from lanthanide oxides, zirconium oxide, strontium oxide, uranium oxides, *etc*[2,7,15,16] with the supercritical CO_2 containing the HNO_3-TBP complex as a reactant, and a method has been developed for the removal of the uranium oxides from the solid[12].

In the present paper, SFE and SFL methods developed in our research group are reviewed and feasibility of the methods for the metal separation processes in the field of nuclear technology is discussed.

2. EXPERIMENTAL

2.1 Apparatus

Apparatus for SFE and SFL is shown in Fig. 1. Main part of the apparatus consisted of (1) extraction vessel made of stainless steel, (2) syringe pump, ISCO Co. Ltd., model 260D or 500D, (3) pre-warming coil, stainless steel tubing of 0.25 mm i.d. and 1 - 2 m in length, (4) restrictor, ISCO Co. Ltd., stainless steel capillary of 57 μm i.d. and 30 cm in length, (5) filter, (6) thermostat oven, and (7) liquid CO_2 cylinder. The batchwise extraction vessel (50 ml) and flow extraction vessel (40 or 10 ml) were products of JASCO. The extraction vessel for the batchwise experiment was equipped with (8) a sampling vessel of 5 ml to take a known volume of the aqueous phase after the extraction equilibrium was attained. The vessel for the flow extraction was equipped with (9) a collecting vessel where CO_2 gasified at atmospheric pressure and the solutes in the supercritical CO_2 were recovered.

2.2 Procedure for the batchwise SFE of U(VI) and Pu(IV) ions

The HNO_3 solution containing U(VI) or Pu(IV) ions was taken in the extraction vessel. A known amount of TBP was added to the solution in the extraction vessel, and the CO_2 fluid was introduced to the extraction vessel by using the syringe pump. The pressure and the temperature inside the extraction vessel were kept at P_{ex} higher than the critical pressure of CO_2, P_C (7.4 MPa) and at T_{ex} higher than the critical temperature of CO_2, T_C (31.2 °C). The extraction equilibrium was reached by stirring the aqueous solution and the supercritical CO_2 phase for 60 min. Then, 5 ml of the aqueous phase was taken quickly into the sampling vessel. The concentration of U(VI) or Pu(IV) in the aqueous phase under the extraction equilibrium was determined and the distribution ratio, D, was calculated as a ratio of the concentration of U(VI) or Pu(IV) in the supercritical CO_2 to those in the aqueous solution.

2.3 Procedure for the flow SFE of U(VI)

The HNO_3 solution containing U(VI) was taken in the extraction vessel. The CO_2 fluid is allowed to flow through the system at a given flow rate. An appropriate portion of TBP was continuously added to the CO_2 stream using a plunger-type pump. After being warmed up to T_{ex} on passing through the pre-warming coil, the supercritical CO_2-TBP mixture was

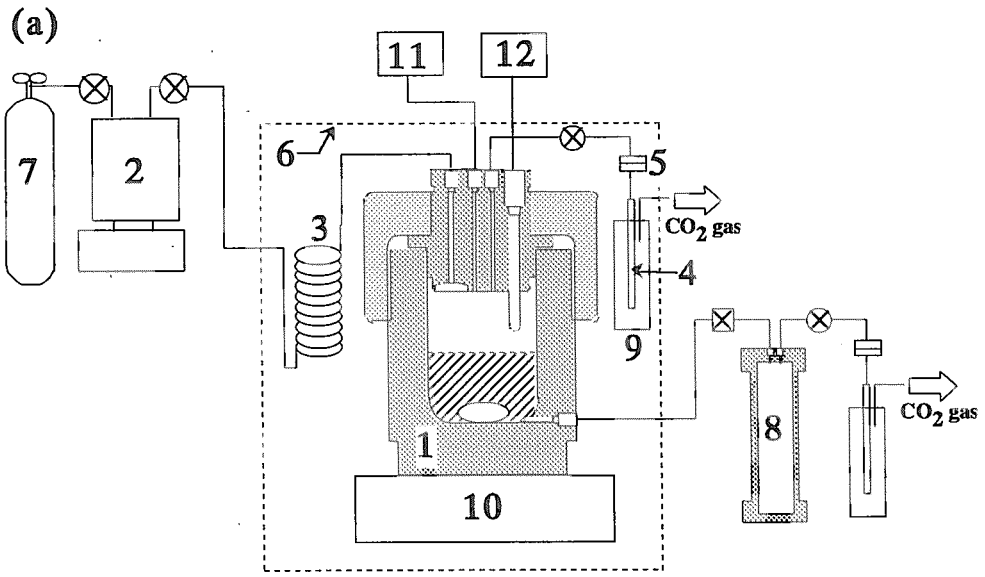

Fig. 1 Apparatus for the SFE or SFL using supercritical CO_2

introduced continuously into the extraction vessel while being bubbled through the sample solution for 30 min. Supercritical CO_2 without TBP was allowed to flow through the extraction vessel for 30 min. The effluent from the extraction vessel was depressurized down to atmospheric pressure by passing through the restrictor, and then introduced into the collecting vessel. After the extraction procedure, the concentrations of U(VI) in the sample solution and in the collecting vessel were determined. The extraction efficiency and the recovery efficiency were calculated from these results.

2.4 Procedure for SFL of uranium from solid sample

The solid sample, *e. g.*, sand containing UO_2 or U_3O_8 powders, was taken in the extraction vessel and the temperature inside the vessel was kept at 40 to 60 °C. The mixture of supercritical CO_2 and the HNO_3-TBP complex was introduced into the extraction vessel and allowed to stand at 40 to 60 °C and 12.5 to 25 MPa for a given period of time [static SFL procedure]. After the static SFL, neat CO_2 was allowed to flow through the extraction vessel at 60 °C and 20 MPa [washing procedure]. The static SFL and washing procedures were repeated twice. The effluent was introduced to the collection vessel. The solutes such as U(VI)-TBP complex and HNO_3-TBP complex in the supercritical CO_2 phase were recovered in the collection vessel.

2.5 Chemicals

The solid sample for SFL was a mixture of *ca.* 100 ~ 200 mg of UO_2 or U_3O_8 powders and 50 g of the standard sea sands (Wako, 20-30 mesh). The UO_2 powder was obtained by grinding mechanically the UO_2 nuclear fuel pellet and the U_3O_8 was prepared by heating the UO_2 powder at 480 °C in air for 2 hrs.

The HNO_3-TBP complex was prepared by mixing vigorously 100 ml of 70% HNO_3 (Wako Pure Chemicals Co.) with 100 ml of TBP (Koso Chemical Co.) in a conventional extraction tube for 30 min. The HNO_3-TBP complex liquid thus obtained was determined to contain HNO_3 and TBP at a mole ratio of 1.4 ~ 1.5 : 1 as the mixture of $(HNO_3)_2$(TBP) and HNO_3(TBP) complexes. The water content of the HNO_3-TBP complex was determined to be 1.3 M by Karl-Fischer titration method.

3. RESULTS AND DISCUSSION

3.1 The SFE of U(VI), Pu(IV) and fission product ions from HNO_3 solution with TBP[1,6,13)]

Extraction behaviors of U(VI) and the fission product ions from HNO_3 solution into a supercritical CO_2 containing TBP were studied under batchwise and flow extraction condition. Uranium(VI) was found to be extracted in the supercritical CO_2 as a form of $UO_2(NO_3)_2(TBP)_2$ with a distribution ratio, D, of, *e. g.*, 2.2 ± 0.3 for the extraction of 2 x 10^{-4} to 2 x 10^{-2} M U(VI) from 3 M HNO_3 into the supercritical CO_2 containing 0.3 M TBP at 60 °C and 15 MPa. The reaction scheme of SFE of U(VI) was confirmed as shown in Fig. 2.

The D of U(VI), $D_{U(VI)}$, increased with an increase of HNO_3 concentration (0.1 - 6 M) or TBP (0.1 - 0.3 M), along with a decrease of pressure (10 - 40 MPa) at 60 °C, and with an increase of the temperature (40 - 80 °C) at 15 MPa. A salting-out effect enhancing the distribution of U(VI) was observed by addition of a fairly high concentration of $LiNO_3$ to the aqueous phase. Results of flow extraction using a continuous flow of the supercritical CO_2 - TBP through the aqueous nitric acid solution showed that >98% of U(VI) could be extracted from 3 M HNO_3 solution into the supercritical CO_2 - 0.08 M TBP (60 °C, 15 MPa).

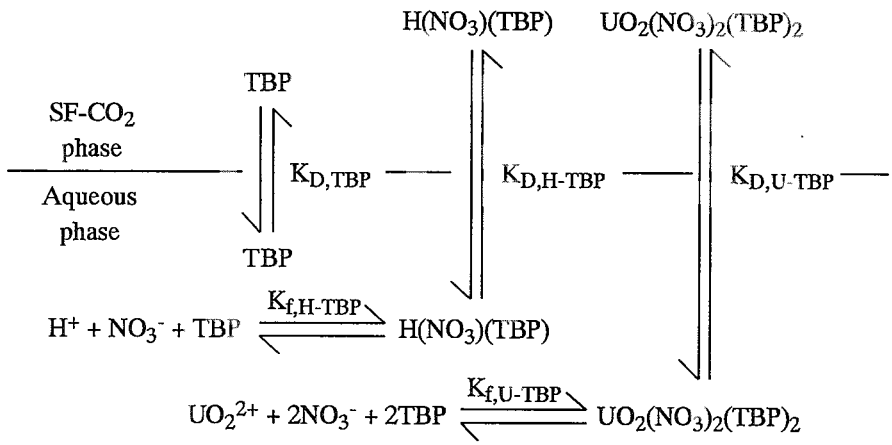

Fig. 2 Reaction scheme of extraction of U(VI) from HNO_3 solution into supercritical CO_2 contaioning TBP.

Plutonium(IV) was found to be extracted into the supercritical CO_2 containing TBP as $Pu(NO_3)_4(TBP)_2$ complex through identical reaction scheme as shown in Fig. 2. The distribution ratio, $D_{Pu(IV)}$, was determined to be $D_{Pu(IV)} = 3.1$, *e. g.*, for the extraction of 2 x 10^{-3} M Pu(IV) from 3 M HNO_3 into the supercritical CO_2 containing 0.3 M TBP at 60 °C and 15 MPa.

Main fission product elements such as lanthanides, Cs, Sr, Ba, Zr, Mo, and Pd were hardly extracted into the supercritical CO_2 phase under this condition, which suggests that SFE is feasible as a method for the separation and recovery of uranium and plutonium from the fission product elements.

Extraction equilibrium of U(VI) and Pu(IV) between HNO_3 solution and the supercritical CO_2 phase containing TBP was formulated taking into account that (i) a distribution ratio of a metal extracted is a function of a distribution constant of each component involved in the extraction reaction (see Fig. 2), (ii) the distribution constant is defined as a ratio of solubilities of the component in both phases, and (iii) the solubility in the CO_2 phase is correlated with density of CO_2. A simple linear relationship between the distribution ratio, D, of the metal ion and density, ρ , of CO_2 was derived ; $\log D = a \log \rho + A + B$, in which a is a proportional constant implying the solvation characteristic of the solute in supercritical CO_2, A is a pressure-independent constant, and B is a variable determined by the distribution equilibrium of HNO_3. The equation derived was verified experimentally by the measurement of the distribution ratio of U(VI) and Pu(IV) under various conditions of pressure and temperature. The slopes a of the log D *vs.* log ρ plots were -(2.7 ± 0.5) and -(1.6 ± 0.1) for the extraction of U(VI) and Pu(IV), respectively. The differences in D as well as the slope a between U(VI) and Pu(IV) make it possible to design the U and Pu separation method by which one can achieve an enhancement of the extraction efficiency and selectivity by tuning the operation pressure.

The SFE behavior of U(VI) of relatively high concentration was investigated in the flow SFE system using the supercritical CO_2 with TBP[17]. The aqueous phase was 30 ml of 3 M HNO_3 solution of 10^{-3} to 10^{-1} M U(VI) and the supercritical CO_2 phase contained 10^{-1} to 5 x 10^{-1} M TBP and forced to flow through the aqueous phase at a flow rate of 1 to 5 ml/min. The extraction-rate curve was measured in the SFE at 60 °C and 15 MPa, from which the

distribution ratio D_{flow} of U(VI) in the flow SFE was determined. The D_{flow} of U(VI) was compared with the $D_{U(VI)}$ determined under the equilibrium condition as described above and it was found that the extraction equilibrium of U(VI) was attained rapidly even in the flow SFE performance. The reaction process determining the extraction rate was evaluated on the basis of the modeling of the flow SFE system.

A modeling was examined[18] for the analysis of the results of extraction of U(VI) in a flow SFE system by supercritical CO_2 containing TBP from a HNO_3 solution, in which the extraction was not limited by the solubility of the U(VI)-TBP complex. The model used was that of diffusion out of a sphere into a medium in which U(VI) extracted was infinitely dilute. The extraction was shown to follow a similar mechanism to that seen in conventional solvent extraction.

3.2 The SFL of uranium form solid sample[12,16,19]

The dissolution behavior of U_3O_8 and UO_2 using the supercritical CO_2 medium containing HNO_3-TBP complex as a reactant was studied. The dissolution rate of the oxides increased with increasing the HNO_3/TBP ratio of the HNO_3-TBP complex and the concentration of the HNO_3-TBP complex in the supercritical CO_2 phase. A remarkable increase of the dissolution rate was observed in the dissolution of U_3O_8 when the HNO_3/TBP ratio of the reactant was higher than *ca.* 1, which indicates that the 2:1 complex, $(HNO_3)_2$TBP, played a role in facilitating the dissolution of the oxides. Half-dissolution time ($t_{1/2}$) as an indication of the dissolution kinetic was determined from the relationship between the amount of uranium dissolved and the dissolution time (dissolution curve). A logarithmic value of a reciprocal of the $t_{1/2}$ was proportional to the logarithmic concentration of HNO_3, C_{HNO3}, in the supercritical CO_2. The slopes of the ln $(1/t_{1/2})$ *vs* ln C_{HNO3} plots for U_3O_8 and UO_2 were different from each other, indicating that the reaction mechanisms or the rate-determining steps for the dissolution of U_3O_8 and UO_2 were different. A principle of the dissolution of uranium oxides with the supercritical CO_2 medium was found to be applicable to a method for the removal of uranium from solid matrices.

The SFL method, which is based on the efficient and selective dissolution of uranium oxides with the supercritical CO_2 containing HNO_3-TBP, has been developed for the removal of uranium from the solid waste contaminated by the uranium oxides. It was found that uranium oxides, UO_2 or U_3O_8, could be dissolved almost completely in the supercritical CO_2 phase at 60 °C and 15 to 20 MPa. Feasibility of the SFL method to the decontamination of uranium from the solid wastes was demonstrated using a synthetic waste, *i. e.*, a mixture of the standard sea sands (*ca.* 50 g) and UO_2 or U_3O_8 powders (*ca.* 100 mg of U). The sand sample after the decontamination procedure was leached completely by the concentrated HNO_3 by keeping at the boiling point for 30 min, and the concentration of uranium in HNO_3 solution was analyzed by an ICP-AES (Shimadzu, ICPS-8000E). The results are shown in Table 1

The solid sample after the SFL treatment was in a form of dried solid which contains neither acid and organic solvent nor reactant. It was found also that most of uranium (95-99%) taken was recovered in the collector. This allows the further treatment of the solid waste more easily. Uranium(VI) was quantitatively stripped as U(VI)-carbonate from the $UO_2(NO_3)_2(TBP)_2$ using $(NH_4)_2CO_3$ aqueous solution and the TBP recovered can be reused.

The most distinguished advantages with the proposed SFL method are that (i) the highly efficient removal of U(VI) is attained, (ii) a generation of the secondary wastes from the decontamination process is totally minimized, and (iii) CO_2 and even HNO_3-TBP reactant can be easily reused.

Table 1 Decontamination efficiency of synthetic uranium-containing solid wastes by the SFL method using the supercritical CO_2 + HNO_3-TBP complex

synthetic solid wastes	total amount of U remained in the solid after the SFL	decontamination factor (DF)[a)]
A; 120 mg UO_2 powders + 50 g sea sands	0.3 mg	3.5×10^2
B; 120 mg U_3O_8 powders + 50 g sea sands	0.01 mg	1.1×10^4

SFL condition; 60 °C, 20 MPa, the static SFL for 150 mins and washing for 100 mins (flow-rate of CO_2; 3.5 ml/min)

[a)]DF = {(U content before SFL) - (U after SFL)} / (U before SFL)

3.3 Other methods for the separation of metal ion from the aqueous solution by SFE using various extractants.

3.3.1 SFE of Pd(II) from the aqueous chloride solution using 2-methyl-8-quinolinol (HMQ)[11, 20, 21]; The SFE behavior of Pd(II) was investigated with 2-methyl-8-quinolinol (HMQ). The Pd(II)-HMQ complex extracted from a weakly acidic solution (pH 2 - 3) into SF-CO_2 was determined to be $Pd(MQ)_2$ on the basis of a slope analysis. The extraction constant $K_{ex,SF}$ (= $[Pd(MQ)_2]_{SF}[H^+]^2[Cl^-]^4[PdCl_4^{2-}]^{-1}[HMQ]^{-2}$) was determined to be $10^{4.3\pm0.2}$ at 45 °C , 8.5 MPa and I = 0.4 M (H, Na)Cl. The distribution behavior of HMQ between an aqueous and supercritical CO_2 phases was examined so as to discuss quantitatively the extraction equilibrium. The extraction constant ($K_{ex,Cy}$) of Pd(II) with HMQ into cyclohexane with a similar polarity to supercritical CO_2 was determined and the $K_{ex,SF}$ was compared with the $K_{ex,Cy}$. Pd(II) at the concentration range of 10^{-5} to 10^{-4} M in the aqueous solution (pH < 3) containing relatively high concentration of chloride ion was found to be extracted efficiently by SFE.

Pressure effect on the distribution of Pd(II) in SFE using HMQ was investigated. The distribution ratio D of Pd(II) was independent on the pressure in the range of 8.5 to 23 MPa, when the pH of the aqueous solution was buffered at pH = 2.7 ~ 3.5. The CO_2 pressure affected the solubility of CO_2 in the aqueous phase and therefore the pH of the non-buffered aqueous solution changed with the pressure, which resulted a change of the distribution ratio with the pressure. The SFE method using HMQ is promising for the recovery of Pd(II) in the aqueous chloride media. The HMQ forms the water-soluble protonated form, H_2MQ^+, which allows the coexistence of MQ^- of enough high concentration in the extraction system.

3.3.2 SFE of U(VI) and lanthanide(III) from aqueous solution using β-diketones[22]; The SFE behavior of U(VI), La(III) and Lu(III) was investigated comparatively with the solvent extraction behavior with the β-diketones (HA) such as 2-thenoyltrifluoroacetone (Htta),

1,1,1,2,2,3,3-heptafluoro-7,7-dimethyl-4,6-octanedione (Hfod) and 1-phenyl-3-methyl-4-benzoyl-5-pyrazolone (Hpmbp) together with TBP. An addition of TBP to the extraction medium contributed to an increase of the extractability through a so-called "synergistic effect" and an enhancement of the solubility of the solutes, *i. e.*, an extractant and a metal-extractant complex in the supercritical CO_2, (modifier effect). These effects of TBP enables the SFE procedure for the separation of U(VI) and lanthanide(III) from the aqueous solution of pH in the range of 1 to 3. The U(VI) species extracted into the supercritical CO_2 or cyclohexane was found to be UO_2A_2TBP. The extraction constant by SFE of these metal ions with β-diketones and TBP were one or two orders smaller than that by the cyclohexane extraction.

4. CONCLUSION

The SFE using supercritical CO_2 containing TBP as an extractant shows high applicability to the separation and recovery of uranium and plutonium from nitric acid solution of relatively high concentration. The SFE was concluded to be applicable to the reprocessing of the nuclear spent fuel or the partitioning of the nuclides in the high-level liquid-waste. The distribution ratio of U(VI) and Pu(IV) can be controlled by varying the operation pressure, *i. e.*, the density of CO_2 medium. This suggests a potential of a new methodological concept of "pressure-tuning" or "CO_2 density-tuning" SFE to enhance the separation efficiency and selectivity of the metal extraction.

The SFL using supercritical CO_2 containing HNO_3-TBP complex as a reactant is promising as a method for the decontamination of uranium oxides from the uranium-containing solid wastes. High decontamination factors were obtained for the removal and recovery of uranium in the solid samples present as UO_2 or U_3O_8. The most distinguished advantages with the proposed SFL method are that (i) the highly efficient removal of U(VI) is attained, (ii) a generation of the secondary wastes from the decontamination process is totally minimized, and (iii) CO_2 and even HNO_3-TBP reactant can be easily reused.

REFERENCES

1) Y. Meguro, S. Iso, Z. Yoshida, Anal. Chem., 70[7], 1262 (1998).
2) O. Tomioka, Y. Enokida, I. Yamamoto, J. Nucl. Sci. Technol., 35[7], 515 (1998).
3) M. D. Burford, M. Z. Ozel, A. A. Clifford, K. D. Bartle, Y. Lin, C. M. Wai, N. G. Smart, Analyst, 124, 609 (1999).
4) C. M. Wai, Y. M. Kulyako, B. F. Myasoedov, Mendeleev Commun., 180 (1999).
5) M. A. Khorassani, L. T. Taylor, Anal. Chim. Acta, 379, 1 (1999).
6) S. Iso, S. Uno, Y. Meguro, T. Sasaki, Z. Yoshida, Prog. Nucl. Energ., 37[1-4], 423 (2000).
7) O. Tomioka, Y. Enokida, I. Yamamoto, T. Takahashi, Prog. Nucl. Energ., 37[1-4], 417 (2000).
8) M. Shamsipur, A. R. Ghiasvand, Y. Yamini, J. Supercrit. Fluids, 20, 163 (2001).
9) Z. J. Cui, J. C. Liu, L. C. Gao, Y. Q. Wei, J. Environ. Sci., 12[4], 444 (2000).
10) C. Erkey, J. Supercrit. Fluids, 17, 259 (2000).
11) J. Ougiyanagi, S. Y. Choi, N. Ishikawa, H. Imura, T. Oriyama, K. Ohashi, Prog. Nucl. Energ., 37[1-4], 435 (2000).
12) O. Tomioka, Y. Meguro, S. Iso, Z. Yoshida, Y. Enokida, I. Yamamoto, J. Nucl. Sci.

Technol., 38[6], 461 (2001).
13) Y. Meguro, S. Iso, H. Takeishi, Z. Yoshida, Radiochim. Acta, 75, 185 (1996).
14) N. G. Smart, Z. Yoshida, Y. Meguro, S. Iso, A. A. Clifford, Y. Lin, K. Toews, C. M. Wai, Proc. Int. Conf. Future Nucl. Systems (Global '97), Oct., Yokohama, Japan, 350 (1997).
15) O. Tomioka, Y. Enokida, I. Yamamoto, Separ. Sci. Technol. in press.
16) O. Tomioka, Y. Meguro, Y. Enokida, I. Yamamoto, Z. Yoshida, J. Nucl. Sci. Technol., in press.
17) Y. Meguro, S. Iso, Z. Yoshida, Proc. ISEC 2002, in press.
18) A. A. Clifford, S. Zhu, N. G. Smart, Y. Lin, C. M. Wai, Z. Yoshida, Y. Meguro, S. Iso, J. Nucl. Sci. Tech., 433-438(2001).
19) O. Tomioka, Y. Meguro, S. Iso, Z. Yoshida, Y. Enokida, I. Yamamoto, Proc. ISEC 2002, in press.
20)J. Ougiyanagi, Y. Meguro, Z. Yoshida, K. Ohashi, Talanta, in press.
21) J. Ougiyanagi, Y. Meguro, Z. Yoshida, K. Ohashi, Proc. ICAS 2001, Anal. Sci., in press.
22) Y. Meguro, S. Iso, J. Ougiyanagi, Z. Yoshida, Proc. ICAS 2001, Anal. Sci., in press.

4. Poster Session

Criticality Safety

This is a blank page.

JP0250329

JAERI-Conf 2002-004

REACTIVITY EFFECT OF SPENT FUEL DUE TO SPATIAL DISTRIBUTIONS OF COOLANT TEMPERATURE AND BURNUP

T.HAYASHI Y.YAMANE K.SUYAMA*1 H.MOCHIZUKI*2
Department of Nuclear Engineering, Graduate School of Engineering, Nagoya University
Furo-cho, Chikusa-ku, Nagoya city, Aichi prefecture, 464-8603, Japan
*1OECD/NEA
*2The Japan Research Institute, Limited

We investigated the reactivity effect of spent fuel caused by the spatial distributions of coolant temperature and burnup by using the integrated burnup calculation code system SWAT. The reactivity effect which arises from taking account of the spatial coolant temperature distribution increases as the average burnup increases, and reaches the maximum value of 0.69%Δk/k at 50GWd/tU when the burnup distribution is concurrently considered. When the burnup distribution is ignored, the reactivity effect decreases by approximately one-third.

1 INTRODUCTION

In the near future, a storage capacity of spent nuclear fuel will not be enough in Japan. In order to storage spent fuels as reasonably as possible, an introduction of burnup credit has been planned. When the burnup credit is employed for the storage of the spent fuels, a nuclear criticality safety analysis is indispensable. Therefore, spent fuel compositions must be evaluated to calculate the effective multiplication factor, k_{eff}, for the storage of their spent fuels.

The composition depends on various parameters, such as boron concentration and its change in time, coolant-temperature and its spatial distribution, and an operation history and so on. When the composition of spent fuel is evaluated by burnup calculation, these parameters should be considered as rigorous as possible. However it is difficult that we take all the parameters into consideration completely, since huge calculation is needed when we deal with many fuel rods.

Then, to reduce the number of parameters taken into account, we assume that some parameters, which cause little reactivity effect, do not vary with each fuel rod, and that their parameter-values are fixed to give a higher value of k_{eff}. However, there is few detailed investigation on the parameters causing little reactivity effect, such as coolant-temperature and its spatial distribution, and an operation history and so on. Then the purpose of this study is to investigate the reactivity effect of spent fuel due to the consideration of the spatial distributions of the coolant-temperature and burnup.

2 Outline of Calculation

At first, we assume the distribution of coolant-temperature along the axial direction of fuel rod. Then a fuel rod is divided into imaginary subregions along its axis, and the coolant-temperature corresponding to the distribution assumed is assigned to the water region surrounding each region. Secondly, the spent fuel composition in each region is determined by the burnup calculation with SWAT code[1]. By using these compositions calculated for all subregions, the spatial distribution of composition along the axial-direction of a fuel rod is determined. Finally, the effective multiplication factor, k_{eff}, for a two-dimensional infinite array of these fuel rods is evaluated by the continuous energy Monte Carlo code MVP[2] developed by Japan Atomic Energy Research Institute. The effective multiplication factor is named as $k_{distribution}$.

On the other hand, the $k_{uniform}$ is also calculated for the same two-dimensional infinite array of spent fuel rods, which compositions have been obtained for an average coolant-temperature without the consideration of its distribution. Comparing the $k_{distribution}$ with the $k_{uniform}$, we discuss the effect of the coolant-temperature distribution. This procedure was performed for the systems having their average burnup of 10,20,30,40, and 50 GWd/t. These comparisons were also done in the cases without the burnup distribution and/or fission products(FPs).

3 Coolant-Temperature Distribution

In **Table.I**, the coolant-temperatures at inlet and outlet of reactor, and their difference are shown[3]. These are typical values of PWRs in Japan. In this study, we determined the coolant-temperature distribution based on these temperatures. We assumed that the axial specific power distribution was represented by a cosine curve, and that the ascending rate of coolant-temperature was in proportion to the specific power. Then we determined the coolant-temperature distribution as its integral from the bottom to the top of fuel rod gave the temperature-difference, 35.1K. The axial coolant-temperature distribution is shown in **Fig.1**.

Table I Typical Coolant Temperature for Japanese PWR

Inlet of reactor	560.6K
Outlet of reactor	595.7K
Difference	35.1K

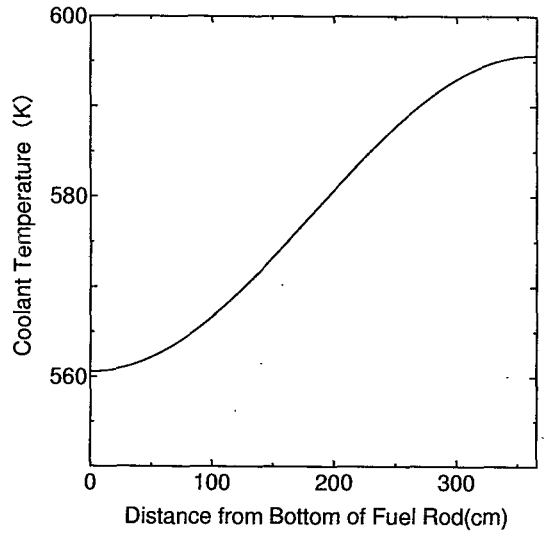

Fig. 1 Axial Coolant Temperature Distribution : PWR

4 Axial Burnup Distribution

When we take account of the axial burnup distribution, we adopted the distribution which was used in the phase II A task of the OECD/NEA Burnup Credit Criticality Benchmark [4]. The shape of its distribution, which is normalized by the average burnup, is shown in **Fig.2**.

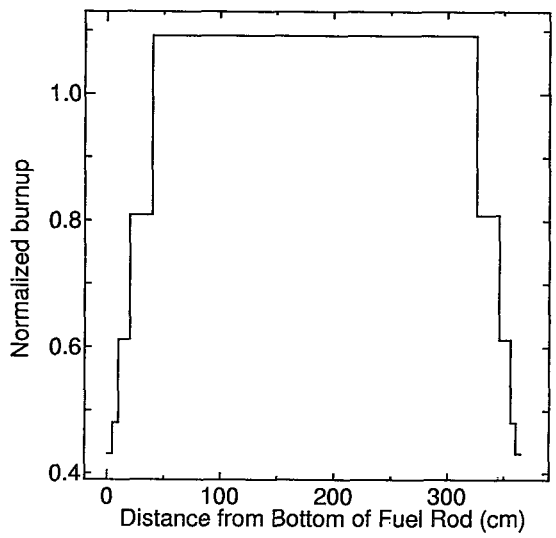

Fig. 2 Axial Burnup Distribution

5 Conditions of Burnup Calculation

Several data for burnup calculation, such as the dimension of fuel rod, temperature of each region in fuel rod, and operation history , are summarized in **Table.II**. These data were used also in the phase II A task of OECD/NEA Burnup Credit Criticality Benchmark.

Twenty-two subregions representing the axial spatial dependence are determined as follows. Each end region of a fuel rod was divided into four subregions which were identical with those for the burnup distribution as shown in Fig.2. Moreover the center region of a fuel rod which length is 285.7cm was divided into fourteen regions equally. Specific power and coolant-temperature were assigned to each subregion as mentioned in the outline of calculation. An example of both distributions are shown in **Table.III**. Then burnup calculation was performed for every subregion to obtain the fuel compositions.

Table II Data of OECD/NEA Burnup Credit Criticality Benchmark Phase II A

Lattice	17 × 17
Fuel Temperature	811K
Cladding Temperature	620K
Soluble Boron cycle av.	550ppm
Pellet Density	94.5 % T.D.
Fuel Rod Pitch	1.25984cm
Fuel Rod O.D.	0.94966cm
Fuel Rod I.D.	0.83566cm
Pellet O.D.	0.81915cm
Fuel Length	365.7cm
Fuel Enrichment	4.5wt %
Specific Power	40MW/t
No. of cycles	5
Uptime	250days × 5
Downtime	62.5days

6 Conditions of Criticality Calculation

The criticality calculations were executed by using the following 9 nuclides ^{234}U, ^{235}U, ^{238}U, ^{238}Pu, ^{239}Pu, ^{240}Pu, ^{241}Pu, ^{242}Pu, and ^{241}Am, in the case of not taking fisson products (FPs) into account. In the case of including FPs, we took account into the following 27 nuclides, ^{234}U, ^{235}U, ^{236}U, ^{238}U, ^{237}Np, ^{238}Pu, ^{239}Pu, ^{240}Pu, ^{241}Pu, ^{242}Pu, , ^{241}Am, ^{243}Am , ^{95}Mo, ^{99}Tc, ^{101}Ru, ^{103}Rh, ^{109}Ag, ^{133}Cs, ^{147}Sm, ^{149}Sm, ^{150}Sm, ^{151}Sm , ^{152}Sm, ^{143}Nd,

Table III Specific Power and Coolant Temperature of each Regions

Region No.	Length(cm)	Specific Power(MW/t)	Coolant Temperature(K)
1	5	17.252	560.56
2	5	19.218	560.59
3	10	24.464	560.70
4	20	32.339	561.15
5	20.4	43.684	562.18
6	20.4	43.684	563.70
7	20.4	43.684	565.67
8	20.4	43.684	568.01
9	20.4	43.684	570.66
10	20.4	43.684	573.55
11	20.5	43.684	576.57
12	20.4	43.684	579.65
13	20.4	43.684	582.67
14	20.4	43.684	585.55
15	20.4	43.684	588.20
16	20.4	43.684	590.54
17	20.4	43.684	592.51
18	20.4	43.684	594.03
19	20	32.339	595.05
20	10	24.464	595.50
21	5	19.218	595.61
22	5	17.252	595.64

^{145}Nd, ^{153}Eu, and ^{155}Gd. The configuration of criticality calculation is shown in **Fig.3**. Vacuum boundary conditions were applied to both the top and bottom of water reflector region, and mirror reflection condition to the side of the system. These calculations were performed for the systems having their average burnup of 10,20,30,40,and 50 GWd/tU.

7 Results

To investigate the reactivity effect due to the consideration of coolant-temperature distribution, we defined the coolant-temperature distribution effect as follows,

$$\text{Coolant-Temperature Distribution Effect} = \frac{k_{distribution} - k_{uniform}}{k_{uniform}},$$

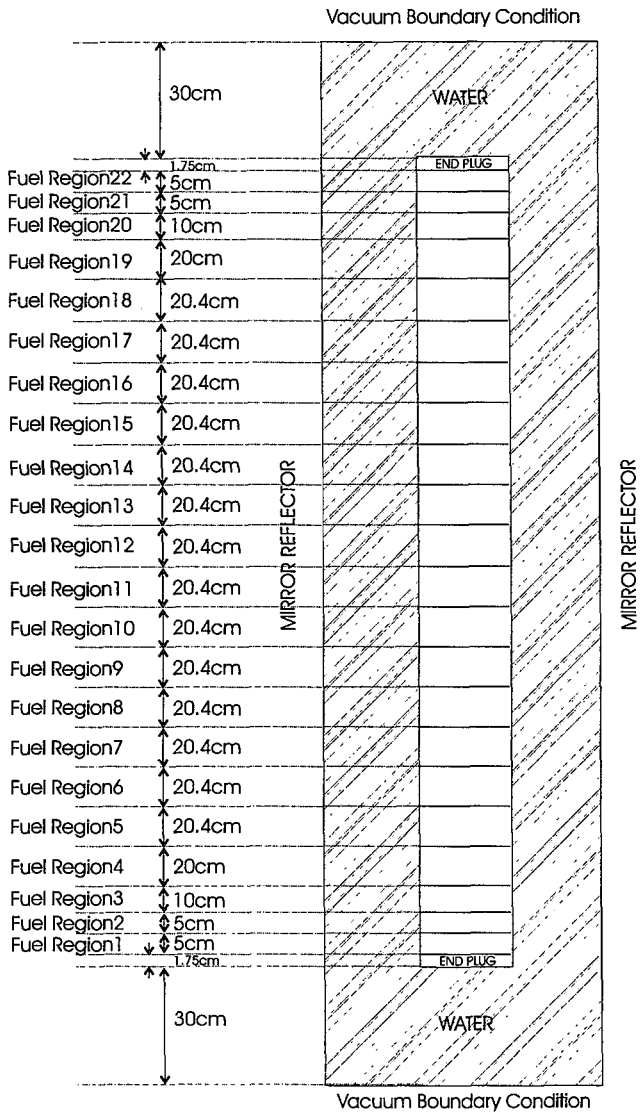

Fig. 3 X-Z Cross-Section of MVP Calculation model

where $k_{distribution}$ and $k_{uniform}$ have been defined already in the outline of calculation. The calculational results of the coolant-temperature distribution effect are shown as the function of burnup in **Fig.4**.

The following results were obtained.

1. Distribution effect increases as the burnup increases.
2. Distribution effect becomes higher in the case of axial burnup distribution is considered concurrently.
3. The effect of FPs is negligible small.

As shown in **Fig.4**, though there are a few negative values in the low-burnup region, the coolant-temperature distribution effect is positive intrinsically. Because it seems that negative values are due to the statistical error of Monte Carlo calculation. Moreover, we can explain the reason why the coolant-temperature distribution effect is positive as follows. An axial neutron flux distribution has its maximum value at slightly upper part of the fuel rod center. And, the number densities of ^{235}U, ^{239}Pu, and ^{241}Pu become large gradually toward the top of fuel rod in the case of taking the coolant-temperature distribution into account, because the neutron spectrum of the upper region becomes slightly hard so that ^{235}U does not decrease and plutonium arises. As a result, the number densities of the fissionable nuclides at the high flux region becomes large, so that the coolant-temperature distribution effect becomes positive. Then, the distribution effect reaches the maximum value of 0.69%Δk/k at 50GWd/tU when the burnup distribution is considered concurrently without FPs.

Positive effect means that the consideration of the coolant-temperature distribution gives higher k_{eff} value than the assumption of the average temperature. Hence, from the criticality safety point of view, the coolant-temperature distribution is an important parameter when the burnup credit is introduced into the storage of the spent fuel.

8 Conclusion

In the near future, the introduction of burnup credit is planned in Japan to enlarge a storage capacity of spent nuclear fuel as reasonably as possible. In this study, we intended to investigate the reactivity effect due to the introduction of burnup credit from the criticality safety point of view. Then, it is concluded that the concurrent consideration of both the coolant-temperature distribution and the burnup distribution is necessary to evaluate the storage capacity reasonably.

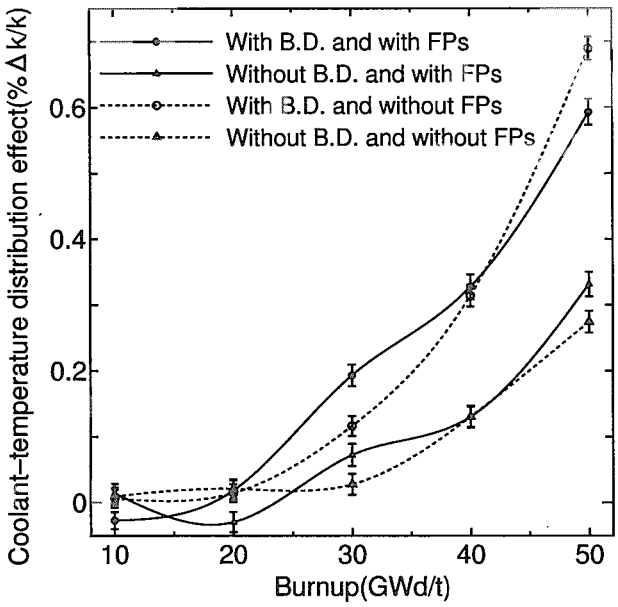

Fig. 4 Coolant-temperature distribution effect as the function of burnup

REFERENCES

1) Kenya SUYAMA, Takehide KIYOSUMI, and Hiroki MOCHIZUKI. *Revised SWAT -The Integrated Burnup Calculation Code System-*. JAERI-Data/Codes 2000-027, 2000.

2) Takamasa MORI and Masayuki NAKAGAWA. *MVP/GMVP: General Purpose Monte Carlo Codes for Neutron and Photon Transport Calculations based on Continuous Energy and Multigroup Methods.* JAERI-Data/Codes 94-007, 1994.

3) Takafumi HAYASHI, Kenya SUYAMA, Hiroki MOCHIZUKI, and Yasushi NOMURA. *Reactivity Effect of Spent Fuel Depending on Burn-up History.* JAERI-Tech 2001-041, 2001.

4) Makoto TAKANO and Hiroshi OKUNO. *OECD/NEA BURNUP CREDIT CRITICALITY BENCHMARK -RESULT OF PHASE IIA-*. JAERI-Research-96-003, 1996.

JP0250330

JAERI-Conf 2002-004

REACTIVITY EFFECT OF AXIAL BURNUP SHAPES FOR A REALISTIC PWR SPENT FUEL TRANSPORT CASK

H. A. TUAN*), H. OKUNO AND Y. NOMURA
Department of Fuel Cycle Safety Research,
Japan Atomic Energy Research Institute, Tokai-mura, Ibaraki-ken 319-1195, Japan
Fax: 81-29-282-6479, e-mail: nomura@popsvr.tokai.jaeri.go.jp
*) Permanent address: Vietnam Atomic Energy Commission,
59 Ly Thuong Kiet, Hanoi, Vietnam. Fax: 84-49-424-133, e-mail: hatuan@eudoramail.com

The reactivity effect of the asymmetry of axial burnup shape in burnup credit criticality safety is studied for a realistic PWR spent fuel transport cask based on the current OECD/NEA's Phase II-C benchmark problem. The axial burnup profiles varying from strong asymmetry to more or less no asymmetry based on in-core flux measurements are modeled in 21 zones. Continuous energy criticality calculations in 3-D model have been performed using the Monte Carlo code MCNP4B and the nuclear data library JENDL-3.2. Calculations show that k_{eff} value increases with increasing asymmetry degree of axial burnup shape. This leads to the fact that the end effect is enhanced by the possibly realistic asymmetry of burnup shape from 0 to 3.5 %Δk/k and from 3.4 to 7.7 %Δk/k respectively for average burnups of 32 MWd/kgU and 50 MWd/kgU. The end effect is more sensitive to the asymmetry of burnup shape for the higher burnup. For an axially distributed burnup, the axial fission density distribution becomes strongly asymmetric as its peak shifts toward the top end of the fuel zone where the local burnup is less than that of the bottom end. The peak of fission density distribution gets higher as either the asymmetry of burnup shape or the average burnup increases.

Key words: criticality safety, burnup credit, axial burnup shape, end effect, asymmetry

1. INTRODUCTION

In reality, the axial burnup profile of spent fuel is asymmetric due to asymmetry of reactor core configuration and operation history as well. In the late 2000, the OECD/NEA Phase II-C benchmark has been proposed by J. Ch. Neuber and Th. Lamprecht (Germany) in order to study the effect of the asymmetry of axial burnup shape on the criticality of PWR spent fuel [1]. As a study of this effect, we have performed 3-D and continuous energy Monte Carlo calculations by using the code MCNP4B [2] and the nuclear data library JENDL-3.2 at 293 K [3]. The calculated results of multiplication factor (k_{eff}), the end effect and axial fission distribution will be analyzed in this paper. In addition, the end effect in the actinide-only approach [4] is also evaluated and compared with that considering both actinides and fission products. The obtained results contribute to the currently required international comparison and help to better understand the physics of PWR spent fuel criticality safety.

2. BRIEF DESCRIPTION OF THE BENCHMARK

The benchmark is based on a sample of 850 axial burnup shapes in fuel assemblies of the Siemens Konvoi type received from the Nuclear Power Plant Neckarwestheim II, Germany. All shapes are derived from in-core 3-D power density distribution measurements based on flux measurements performed every 14 days from the cycles 5 through 12 at EOCs. At 28 fuel assembly (FA) positions the flux data are monitored at 32 equidistant axial nodes. All the 850 shapes are collapsed to a normalized shape that is represented by mean burnup ratios $\hat{\alpha}_i$ (i.e. $\hat{\alpha}_i$ is the sample mean of the ratios α_{ij} of the burnup B_{ij} at node i of the j-th axial shape to the average burnup of this axial shape, i =1 to 32 and j = 1 to 850). The sample mean and the sample variance reflect all the effects determining axial burnup shapes.

The benchmark assumes an initial enrichment of fuel assemblies of 4.0 wt.-%, average burnups of 32 MWd/kgU and 50 MWd/kgU, and a cooling time of 5 years. The transport cask

containing 21 spent fuel assemblies of 18x18 square lattice type is assumed to be fully flooded with water. The geometry and material specification of the benchmark, including atomic number densities for fuel assembly and transport cask, is given in [1].

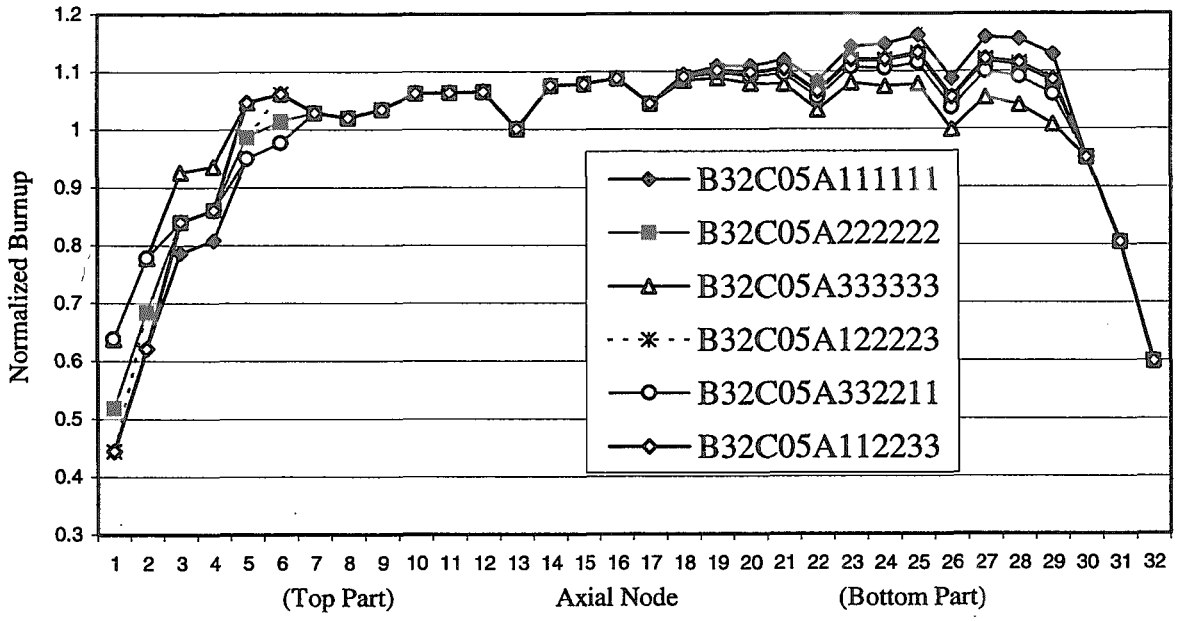

Fig.1 Typical axial burnup shapes for the average burnup of 32 MWd/kgU

The variations of the mean values $\hat{\alpha}_i$ of the top nodes of the fuel zone are bounded by the minimum and maximum values of the burnup ratios α_{ij} for each average burnup observed in the sample of axial shapes under examination. A decrease of the height of the shape at the top nodes results in higher asymmetry of the shape because of normalization. The benchmark proposes seventeen cases of axial burnup shapes for each average burnup. These cases are identified as BbbCyyAnnnnnn, of which Bbb, Cyy and Annnnnn respectively stand for the average burnup (B32 denotes the average burnup of 32 MWd/kgU), the cooling time (C05 denotes five years of cooling time) and the identification of the variation of the mean values of the top nodes 1 to 6 (n = 1, 2 or 3 denotes Min, Mean or Max, respectively). All cases are well suited to study the impact of the axial shape on the local reactivity within the fuel zone. Six typical axial burnup shapes out of seventeen for 32 MWd/kgU burnup are plotted in Fig.1 for 32 equidistant nodes numbered from the top part to the bottom part of the fuel zone. Shapes for 50 MWd/kgU burnup are less asymmetric in comparison with those for 32 MWd/kgU burnup. The proposed cases represent the variation of the axial shapes from strong asymmetry to more or less no asymmetry: the cases BbbC05A111111, BbbC05A222222 and BbbC05A333333 respectively correspond to the most asymmetric shape, the mean shape and the least asymmetric shape. In addition, the benchmark provides nuclide inventories for the cases of uniform axial burnup that are identified as B32C05Aunifo and B50C05Aunifo.

All burnup shapes are divided into 21 axial zones based on 32 equidistant nodes by means of collapsing every two or three nodes of similar burnup. Nodes in both the top and bottom parts have lower local burnups and contribute significantly to the criticality. Therefore, nodes 1 to 6 and nodes 29 to 32 respectively correspond to six zones in the top part and four zones in the bottom part, nodes 7 to 28 are collapsed into eleven zones in the middle part [1]. Such a multi-zone model is well adequate for treatment of axial burnup profile [4,5]. The benchmark provides atomic number densities of both actinides and fission products for 21 axial burnup zones and requires results of k_{eff} as well as axial fission distribution of this 21-zone model.

3. CALCULATED RESULTS

3.1 Fission source convergence

In these multi-zone Monte Carlo calculations, the initial source was specified in zones of higher fissile density. The number of neutron histories and the location of initial source, that were investigated to make convergence and applied to obtain the results presented in this paper, are given in Table I. It was found that a good convergence calculation for a uniform burnup could be obtained using NPG = 10 million histories, i.e. a half of that given in Table I.

Table I. Use of neutron histories [+)] and location of initial source

Case ID	NPG	GEN	NSG	σ	Location of initial source in the 21-axial-burnup-zone model
BbbC05Aunifo	20,000	1,200	200	0.00015	In the zones numbered 10, 11 and 12 of four central fuel rods of the central fuel assembly
BbbC05Annnnnn (Distributed burnup)	3,000	1,000	300	0.00045	In the zones numbered 3 and 19 of all fuel rods of all fuel assemblies

[+)] NPG - Number of histories per generation, GEN - Number of generations, NSG - Number of skipped generations, σ - Standard deviation of k_{eff}. Total active number of histories = NPG x (GEN – NSG).

3.2 k_{eff} vs asymmetry degree of axial burnup shape

In order to illustrate the reactivity effect of the asymmetry, we introduce an asymmetry degree of axial burnup shape for the 32-equidistant-node model as follows

$$\delta_{asym,j} = \sqrt{\frac{1}{16}\sum_{i=1}^{16}(\alpha_{33-i,j} - \alpha_{i,j})^2} \qquad (1)$$

where, α_{ij} is the burnup ratio at the node i of the j-th burnup shape. For a uniform burnup as well as for a symmetric burnup shape, δ_{asym} equals to zero.

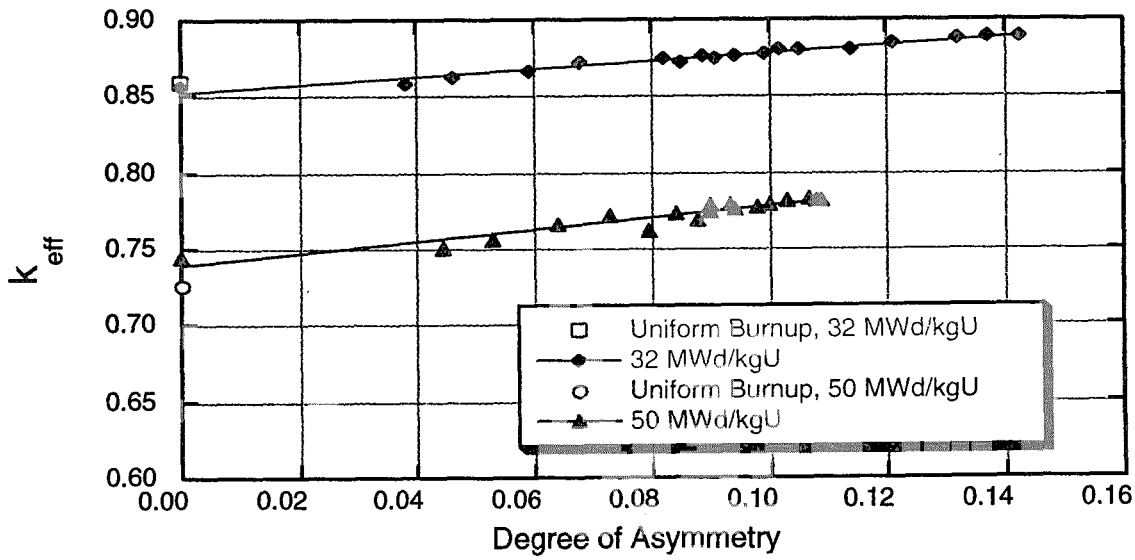

Fig.2 k_{eff} value as a function of asymmetry degree of axial burnup shape

Calculated results show a general tendency illustrated in Fig.2 that k_{eff} increases with increasing asymmetry degree of axial burnup shape. This general tendency can be represented by the following linear functions respectively for the two average burnups

$$k_{eff}[32\,\mathrm{MWd/kgU}] = 0.260\,\delta_{asym} + 0.852 \tag{2}$$

$$k_{eff}[50\mathrm{MWd/kgU}] = 0.390\,\delta_{asym} + 0.739 \tag{3}$$

where, δ_{asym} is determined by the formula (1).

Values of δ_{asym}, k_{eff} and the end effect considering both actinides and fission products are tabulated in Table II for nineteen cases of uniform burnup, symmetric burnup and asymmetric burnup. The atomic number densities of the symmetric burnup proposed by the authors, BbbC05Asym, were re-obtained by averaging those of symmetric nodes of BbbC05A333333.

Table II. Asymmetry degree of axial burnup shape, multiplication factor and end effect

Case ID	Serial No.	32 MWd/kgU			50 MWd/kgU		
		Degree of asymmetry x 100	k_{eff} +)	End effect (%Δk/k)	Degree of asymmetry x 100	k_{eff} +)	End effect (%Δk/k)
BbbC05Aunifo*)	unifo	0	0.85859	0	0	0.72593	0
BbbC05Asym*)	sym	0	0.85669	-0.2	0	0.74402	2.5
BbbC05A222222	1	9.45	0.87558	2	9.45	0.77601	6.9
BbbC05A111111	2	14.23	0.88852	3.5	10.91	0.78161	7.7
BbbC05A111112	3	13.71	0.88898	3.5	10.79	0.78068	7.5
BbbC05A111122	4	13.17	0.88785	3.4	10.66	0.78209	7.7
BbbC05A111222	5	12.12	0.88491	3.1	10.34	0.78100	7.6
BbbC05A112222	6	11.40	0.88081	2.6	10.03	0.77842	7.2
BbbC05A122222	7	10.46	0.87966	2.5	9.77	0.77717	7.1
BbbC05A222223	8	8.91	0.87621	2.1	9.02	0.77470	6.7
BbbC05A222233	9	8.21	0.87479	1.9	8.41	0.77326	6.5
BbbC05A222333	10	6.83	0.87116	1.5	7.28	0.77189	6.3
BbbC05A223333	11	5.87	0.86674	0.9	6.38	0.76513	5.4
BbbC05A233333	12	4.64	0.86184	0.4	5.29	0.75575	4.1
BbbC05A333333	13	3.83	0.85830	-0	4.44	0.75036	3.4
BbbC05A122223	14	9.93	0.87801	2.3	9.35	0.77789	7.2
BbbC05A112233	15	10.18	0.88092	2.6	9.01	0.77858	7.3
BbbC05A322221	16	9.06	0.87392	1.8	8.79	0.76857	5.9
BbbC05A332211	17	8.52	0.87200	1.6	7.94	0.76173	4.9

*) Results for uniform burnup and for symmetric burnup shape were obtained using 24 million histories. All other results for axial burnup shapes were obtained using 3 million histories (see Table I).

+) Two non-active regions of a fuel assembly located between the active region and the hardware were treated in a detail geometry assuming the non-active zone of fuel rod to be a mixture of 50%/50% Zircaloy/Air.

3.3 End effect vs axial burnup shape and assembly-averaged burnup

The end effect is defined as the relative difference between k_{eff} calculated with explicit representation of the axial burnup shape and k_{eff} calculated assuming a uniform axial burnup:

$$\text{End effect}\,(\%\,\Delta k/k) = 100\text{x}\,\frac{k_{eff}\,(\text{axial shape}) - k_{eff}\,(\text{uniform})}{k_{eff}\,(\text{uniform})} \tag{4}$$

We will investigate two burnup credit approaches: the actinide plus fission product (FP) approach and the actinide-only approach. The reactivity effect caused by the most typical burnup shapes for the two approaches is shown in Table III and Fig.3.

Table III. Reactivity effect of the axial burnup shape asymmetry with and without FPs

Type of Reactivity Effect (k_{eff} change, % Δk//k)	With FPs at burnup of [MWd/kgU]		Without FPs at burnup of [MWd/kgU]	
	32	50	32	50
The most asymmetric shape to the least asymmetric shape	3.5	4.2	2.1	3.0
End effect due to the symmetric shape	-0.2	2.5	-0.8	0.1
End effect due to the least asymmetric shape	-0.0	3.4	-0.7	0.9
End effect due to the mean asymmetric shape	2.0	6.9	0.4	3.2
End effect due to the most asymmetric shape	3.5	7.7	1.4	3.9

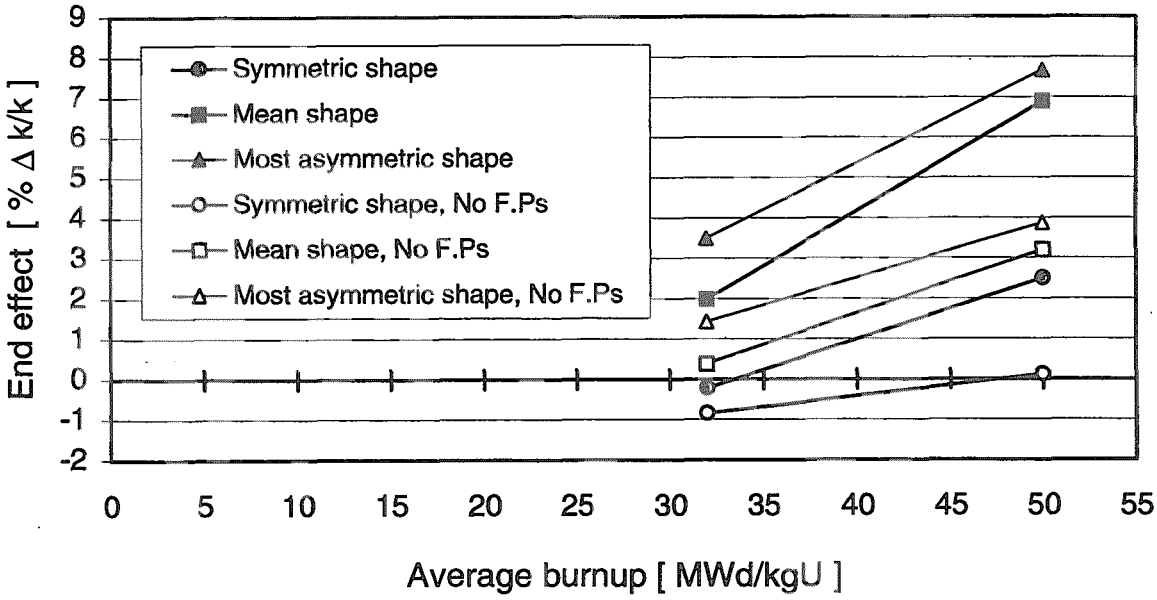

Fig.3 End effect as a function of assembly-averaged burnup for typical axial burnup shapes

It is clear from Table III that the actinide plus FP approach assuming a uniform burnup is non-conservative at most by 3.5 to 7.7 % Δk/k for the burnup of 32 to 50 MWd/kgU. In this burnup range, the most asymmetric burnup shape results in a significantly positive reactivity of 3.7 to 5.2 % Δk/k to the end effect caused by the symmetric shape. The same situation is observed for the actinide-only approach, for which the reactivity effect of burnup shape is weaker than that of the actinide plus FP approach. For both approaches, the end effect is more sensitive to the asymmetry of burnup shape for the higher burnup as it is seen clearly in Fig.3.

It is noted that the actinide plus FP approach using the most asymmetric and realistic axial burnup shapes gives maximal k_{eff} values of 0.889 and 0.782 (see Table II, cases BbbC05A111111) respectively for the two burnups, whereas the actinide-only approach

assuming a uniform burnup gives larger k_{eff} values of 0.934 and 0.824, respectively for the two burnups. So, the actinide-only approach assuming a uniform burnup is about 5 % Δk/k conservative regardless of average burnup. Obviously, this approach is more simple and free of FP data error. It may be required to investigate the effect of radial arrangement of FAs of different axial burnup shapes in the cask to make sure that the actinide plus FP approach assuming the most asymmetric and realistic axial burnup shape is always conservative.

3.4 Fission fraction and density

Fission fraction in zone i (the number of fissions in zone i) is normalized to one fission in the whole system as follows [6]

$$F_i = \frac{\int_{V_i} \Sigma_f(\vec{r},E)\Phi(\vec{r},E)d\vec{r}dE}{\sum_i \int_{V_i} \Sigma_f(\vec{r},E)\Phi(\vec{r},E)d\vec{r}dE} \tag{5}$$

Fission fractions of 21 axial fuel zones defined by Eq. (5) are given in Table IV for the typical cases of both average burnups, including the uniform burnup case and the cases numbered 1, 2, 13, 15 and 17 being identified in Table II. The heights of the upper bounds of zones are also given in the 2nd column of Table IV.

Table IV. Normalized fission fraction in 21 axial zones for 12 typical cases

Zone	Height [cm]	Fission fraction [%] at burnup of 32 MWd/kgU for serial No.						Fission fraction [%] at burnup of 50 MWd/kgU for serial No.					
		unifo	1	2	13	15	17	unifo	1	2	13	15	17
1	12.19	0.50	0	0	0.62	0	0	0.51	0	0	0	0	0
2	24.38	0.91	0	0	0.82	0	0	0.93	0	0	0	0	0
3	36.56	1.33	0	0	0.81	0	0	1.34	0	0	0	0	0
4	48.75	1.73	0	0	0.75	0	0	1.75	0	0	0	0	0
5	73.13	4.68	0	0	1.35	0	0.01	4.76	0	0	0	0	0
6	85.31	2.91	0	0	0.59	0	0.01	2.94	0	0	0	0	0
7	121.88	10.6	0.03	0	1.10	0.02	0.09	10.8	0	0	0	0	0
8	134.06	4.04	0.02	0.01	0.28	0.01	0.09	4.18	0	0	0	0	0
9	158.44	8.71	0.08	0.02	0.70	0.05	0.25	8.91	0.01	0	0.03	0	0
10	182.81	9.31	0.20	0.07	1.14	0.12	0.41	9.33	0.02	0.01	0.07	0	0.02
11	195.00	4.75	0.19	0.09	0.81	0.11	0.31	4.76	0.01	0.01	0.07	0	0.02
12	231.56	14.3	1.17	0.66	3.85	0.78	1.79	14.2	0.10	0.06	0.48	0.10	0.21
13	243.75	4.56	0.78	0.51	2.09	0.58	1.14	4.50	0.09	0.08	0.38	0.12	0.19
14	280.31	12.4	4.47	3.40	9.12	3.36	6.44	12.3	0.93	0.92	2.53	1.09	1.85
15	316.88	9.83	13.3	11.4	16.8	10.2	16.7	9.69	5.56	5.37	8.59	4.94	8.72
16	329.06	2.57	7.98	7.70	7.65	6.62	9.53	2.51	5.05	4.83	5.86	4.34	6.69
17	341.25	2.20	10.8	10.8	9.13	9.66	11.9	2.13	8.46	8.29	8.92	7.56	10.3
18	353.44	1.81	14.4	14.9	11.0	14.4	14.3	1.72	14.3	14.0	13.9	13.7	15.6
19	365.63	1.38	16.4	17.5	11.6	17.9	14.6	1.31	19.4	19.7	18.1	19.7	19.1
20	377.81	0.97	17.0	18.5	11.3	20.1	13.1	0.90	24.3	24.7	22.0	25.5	20.4
21	390.00	0.54	13.2	14.4	8.43	16.1	9.26	0.49	21.7	22.0	19.1	22.9	16.9
Sum Fi, i =16 to 21		9.47	79.8	83.9	59.1	84.7	72.8	9.05	93.3	93.5	87.8	93.7	89.0

Fission density in zone i (the number of fissions by unit volume in zone i) is normalized to one fission by unit volume in the whole system as follows [6]

$$\rho_i = \frac{\int_{V_i} \Sigma_f(\vec{r},E)\Phi(\vec{r},E)d\vec{r}dE \,/\, v_i}{\sum_i \int_{V_i} \Sigma_f(\vec{r},E)\Phi(\vec{r},E)d\vec{r}dE \,/\, v_i} \tag{6}$$

Fission densities defined by Eq. (6) can be obtained directly from the data given in Table IV. The effect of burnup shapes on the fission density distribution is illustrated in 32 equidistant axial nodes in figures 4 and 5, in which fission density distributions were deduced from the results obtained for the 21-zone model (the nodes in figures 4 and 5 are numbered from the bottom part to the top part of the fuel zone, i.e. in the reversed order to that in Fig.1).

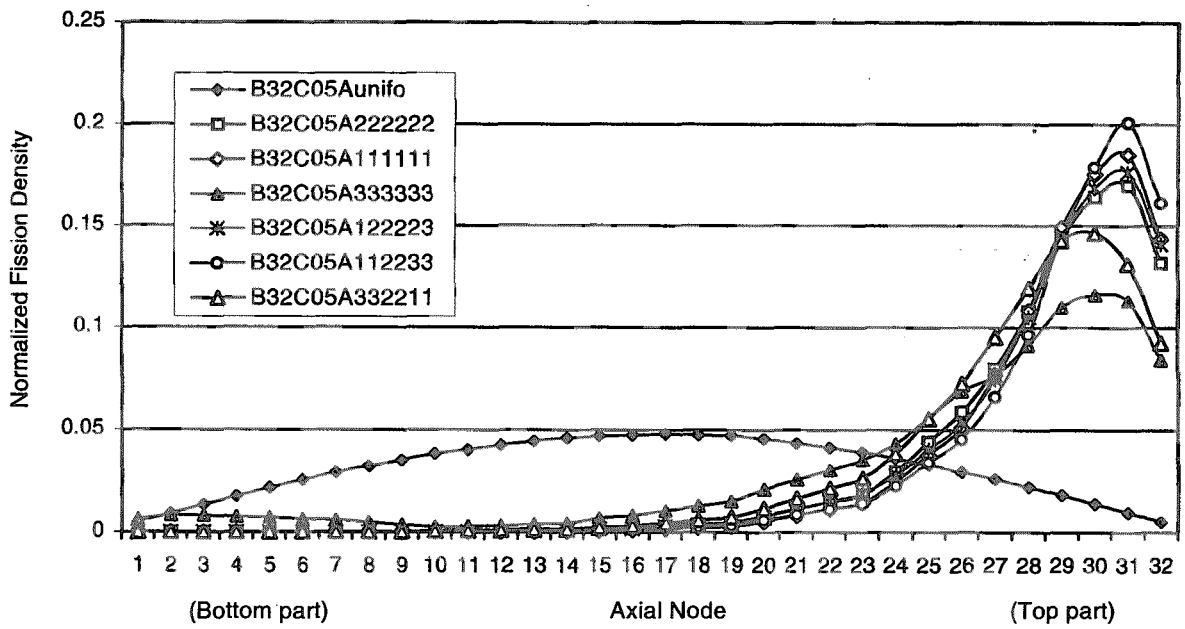

Fig. 4 Fission density distributions for typical axial burnup shapes at 32 MWd/kg burnup

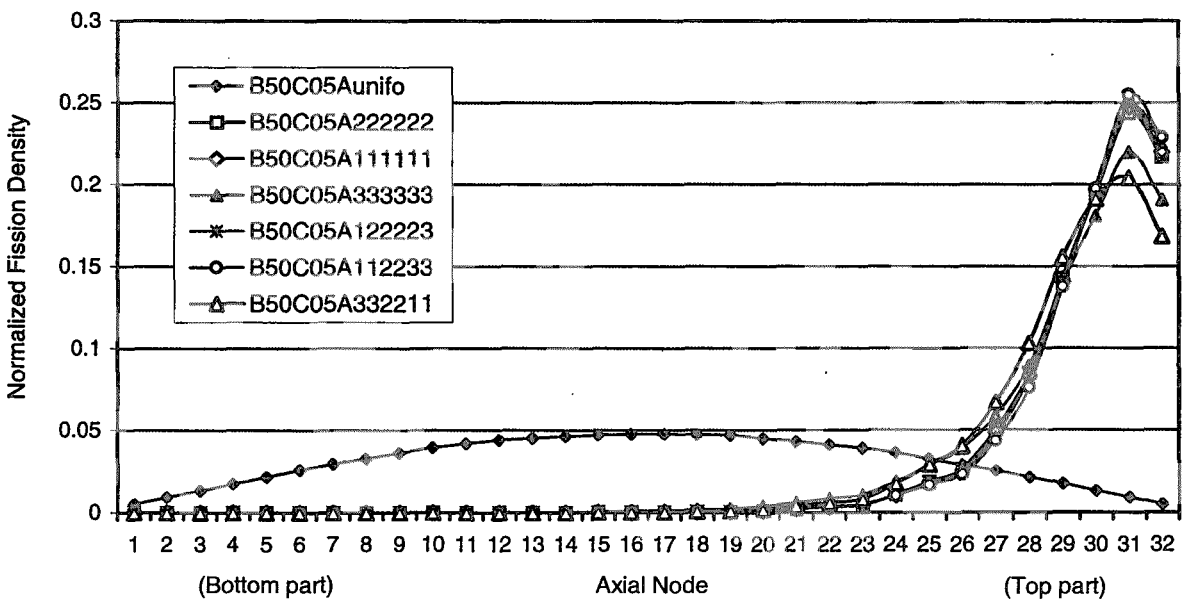

Fig. 5 Fission density distributions for typical axial burnup shapes at 50 MWd/kg burnup

The axial fission density distribution in a fuel assembly has a near-cosine shape for a uniform burnup as shown in figures 4 and 5. In case of asymmetric burnup shapes, the fission density distribution becomes strongly asymmetric as the peak shifts from the center toward the top end of the fuel zone where the local burnup is less than that of the bottom end. Most of the peaks are seen being located in the 31st node, i.e. about 20 cm from the top end of the fuel zone. Approximately, up to 80% and 90% of fission reactions respectively for the two average burnups assuming the mean burnup shape could be found in the six top nodes 27 to 32 (i.e. in the zones 16 to 21 as indicated in Table IV), while the total length of these nodes is 73 cm which accounts for less than 1/5 of the total active length.

4. CONCLUSION

Our study has been based on the current OECD/NEA's Phase II-C benchmark problem for PWR spent fuel transport cask, which consists of a realistic set of axial burnup shapes for high burnups of 32 MWd/kgU and 50 MWd/kgU. Continuous energy Monte Carlo calculations have been made for this benchmark using a 3-D model with 21 axial burnup zones. Calculations show a general tendency that the end effect increases linearly from 0 to 3.5 %Δk/k and from 3.4 to 7.7 %Δk/k respectively for the two burnups as the axial burnup shape varies from slight asymmetry to strong asymmetry. The end effect is found to be more sensitive to the asymmetry of axial burnup shape with increasing burnup.

The axial fission density distribution becomes strongly asymmetric for an axially distributed burnup as the peak shifts toward the top end of the fuel zone where the local burnup is less than that of the bottom end. The peak of fission density distribution gets higher as either the asymmetry degree of burnup shape or the assembly-averaged burnup increases.

As far as conservatism of burnup credit criticality calculation is concerned, the following conclusions can be drawn. The actinide plus fission product approach assuming a uniform burnup is non-conservative at most by 3.5 to 7.7 % Δk/k for the average burnup of 32 to 50 MWd/kgU, while the actinide-only approach assuming a uniform burnup is about 5 % Δk/k conservative. However, the trade-off between the simplicity of the latter approach and its less incentive of burnup credit should be further considered.

Whether the effect of the asymmetry of axial burnup shape on the end effect is negative or not and its magnitude for a burnup below 32 MWd/kgU should be investigated in the future.

REFERENCES

[1] OECD/NEA Burnup Credit Benchmark Phase II-C, http://www.nea.fr/html/science/wpncs/buc/specifications/phase-2c

[2] MCNP – A General Monte Carlo N-Particle Transport Code, Version 4B, LA-12625-M, March (1997).

[3] JENDL-3.2 – Japanese Evaluated Nuclear Data Library version 3.2, http://wwwndc.tokai.jaeri.go.jp/jendl/j32/j32.html

[4] J. C. Wagner, M. D. Dehart, Review of Axial Burnup Distribution Considerations for Burnup Credit Calculations, ORNL/TM-1999/246, March (2000).

[5] M.D. DeHart, Sensitivity and Parametric Evaluations of Significant Aspects of Burnup Credit for PWR Spent Fuel Packages, ORNL/TM-12973, May (1996).

[6] A. Nouri, Analysis of Phase II-B Results: Conceptual PWR Spent Fuel Transportation Cask, IPSN/98-05, NEA/NCS/DOC(98)1.

JP0250331

JAERI-Conf 2002-004

CALCULATION OF OECD/NEA SOURCE CONVERGENCE BENCHMARK PROBLEM NO.1 BY USING MCNP AND SOLVING FISSION MATRIX EQUATION

TAKESHI KUROISHI AND YASUSHI NOMURA
Fuel Cycle Safety Evaluation Laboratory,
Japan Atomic Energy Research Institute,
Tokai-mura, Naka-gun, Ibaraki-ken 319-1195, Japan
Fax: 81-29-282-6479, e-mail: kuroishi@cyclone.tokai.jaeri.go.jp

The OECD/NEA source convergence benchmark problem 1: checkerboard storage of assemblies is calculated by using the MCNP-4B continuous energy Monte Carlo code and JENDL3.2 library. Calculated results show that the fission source distributions for the thirty-six cases with various calculation conditions required in the benchmark are affected by the initial source distributions, and not converged because of the weak neutron coupling between fuel assemblies. In order to approximately estimate the converged source distribution, the fission matrix equation for the checkerboard storage is solved with the deterministic method of iterative calculations, where the multiplication factors for the isolated single assembly and the neutron interactions between two assemblies are calculated and applied to the matrix elements. Then we calculate the special case, that is, the assembly-averaged source levels are set to the fission matrix solution and the distributions inside assemblies are assumed to be cosine-like shapes as the initial fission source. Most of the source levels of the major assemblies for this case do not change at all as the generations increase. Thus the fission source distribution is obtained as almost converged.
Keywords: source convergence, Monte Carlo method, fission matrix, weak neutron coupling, criticality safety

1. INTRODUCTION

In the criticality safety analysis for a configuration comprising fissionable regions that are coupled weakly in neutron reactions each other, the slow convergence of the fission source distribution sometimes causes the non-conservative estimation of the effective multiplication factor (k_{eff}). In order to improve the robustness of criticality safety analyses, four different benchmark problems with respect to the source convergence are proposed by the OECD/NEA Expert Group on Source Convergence.

In this paper, we show the calculated results and discussion for the benchmark problem 1: checkerboard storage of assemblies. Chapter 2 describes the overview of benchmark 1. The geometric features and the calculation method are briefly described and the calculated results for the representative cases are also shown in chapter 2. It is shown that the fission source distributions for the cases required in the benchmark 1 do not achieve the convergence. The estimation of the converged fission source distribution for the checkerboard storage is discussed in chapter 3. Concluding remark is described in chapter 4.

2. OVERVIEW OF BENCHMARK 1

2.1 Problem configuration

The benchmark problem 1 comprises a notional 24x3 LWR fuel storage rack with thirty-six assemblies stored in alternate locations. This configuration is referred to the checkerboard storage. Figure 1 shows the problem geometry. The material compositions are specified in the benchmark 1. The detail information can be referred to the web site as shown below.

http://www.nea.fr/html/science/wpncs/convergence

The fuel assemblies are formed from a 15x15 square lattice of Zirconium-clad UO_2 fuel rods enriched to about 5.0%. They are centrally located within fully water-flooded steel storage racks surrounded by concrete on the three sides, water on the remaining side and water on the top and bottom. In the checkerboard storage, the water channels make the neutron interactions

between assemblies very weak. As shown in Fig. 1, the location of the fuel assembly is conventionally numbered, so that the lowest left-hand assembly is in location (1,1), middle one is in location (12,2) and the top right-hand is in location (23,3). The specifications of thirty-six assemblies are same, but the checkerboard storage configuration is not symmetric in the both horizontal (X, Y) directions. In addition, it is symmetric in the vertical direction because of no axial variation in the main part of fuel elements.

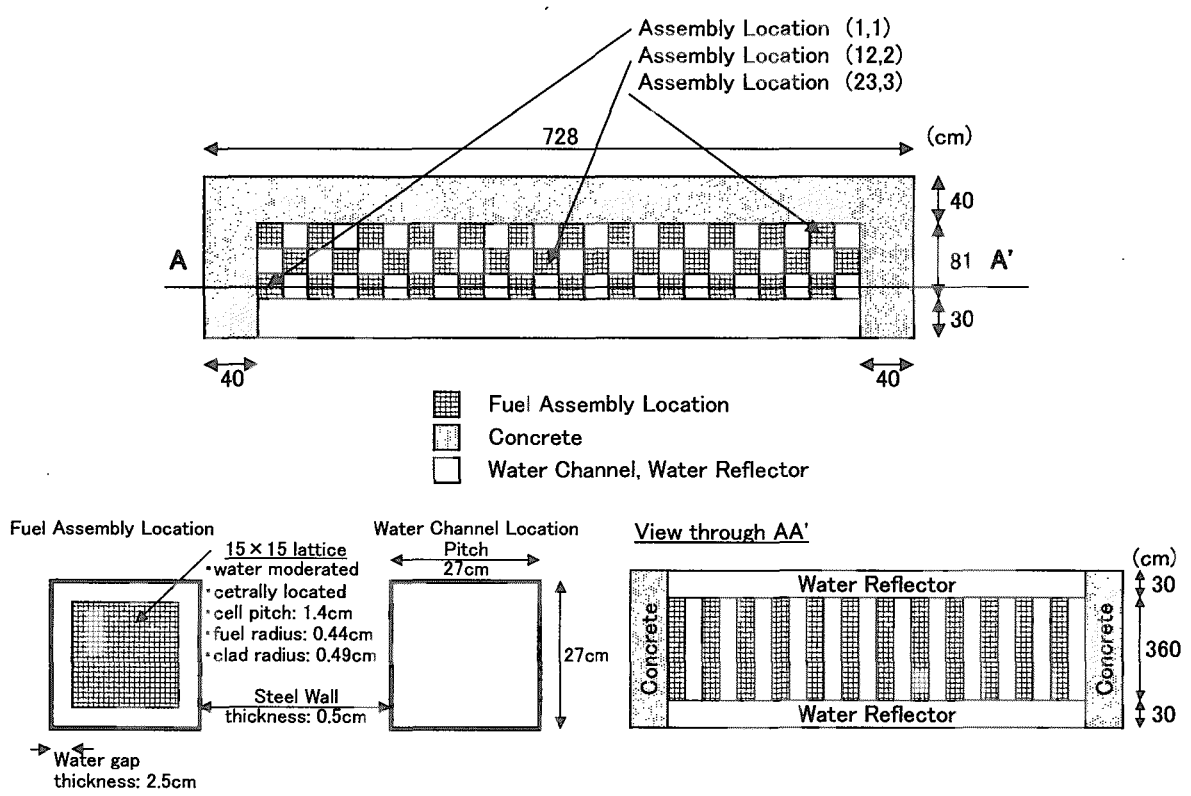

Fig. 1 Problem geometry

2.2 Required cases

In the benchmark problem 1, the calculation conditions are specified as follows: The number of scored generations should be 500. Three different numbers of skipped generations should be employed: 20, 40, and 100. Three different numbers of starting source points per iteration will be used: 1000, 2000, and 5000. Four different starting source distributions as shown below should be used.

- Uniform over the thirty-six fuel assemblies
- All starting source points in location (1,1)
- All starting source points in location (23,3)
- All starting source points in location (12,2)

Thirty-six cases in combination of the above conditions are required to be calculated.

2.3 Calculation method

The thirty-six cases as described in section 2.2 are calculated by using MCNP-4B [1] continuous energy Monte Carlo code and JENDL 3.2 [2] nuclear data library.

In order to specify the starting source points on the MCNP input deck, we can use two kinds of input card: SDEF-card and KSRC-card. In this paper, we select SDEF-card for all calculations by MCNP. All the fissile cells (regions) in the starting source location(s) for each case are specified by SDEF-card, and the source probabilities for fissile cells are specified by SIn-card to be the same, so that the initial source distribution inside an assembly is set to be uniform.

2.4 Calculated results

2.4.1 Effective multiplication factor

The calculated results of k_{eff} for the thirty-six cases and the trend of k_{eff} per generation for the case 27 (as a representative case) are shown in Fig. 2 and Fig. 3, respectively, where the fluctuation of Monte Carlo (1σ) is shown by error bar. The average value of k_{eff} for the thirty-six cases is 0.889 and the k_{eff}s are distributed in the range of +0.003, -0.002 (max: 0.892, min: 0.887). As compared with 1σ, the differences among the k_{eff}s for thirty-six cases are rather large. The change of k_{eff} closing to 500 generation is very small as shown in Fig. 3. This trend can be seen in the other cases.

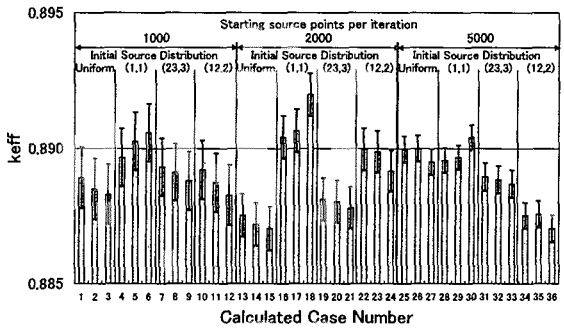

(The 1-36 cases are repeated with the skip numbers of 20, 40 and 100.)

Fig. 2 Calculated results of k_{eff}

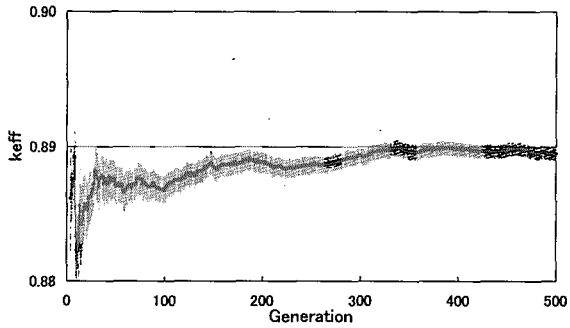

Fig. 3 Trend of k_{eff} per generation (case27)

2.4.2 Fission source distribution

The fission source distributions are calculated by tallying the cell averaged neutron flux over each assembly. The relative fission source levels are calculated by normalizing the average value of the fission source distribution to 1.0. The results of the relative fission source for case 27, 30, 33 and 36 are shown in Fig. 4(1) ~ Fig. 4(4), respectively. These four cases are associated with the largest history number among other cases: 100 skipped generations, 500 scored generations and 5000 starting source points.

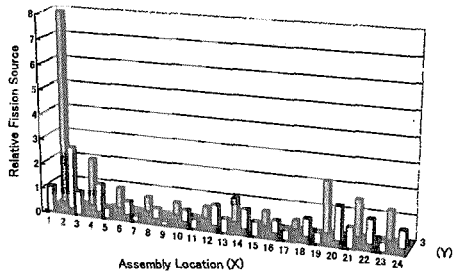

(1) Case27: uniform initial source

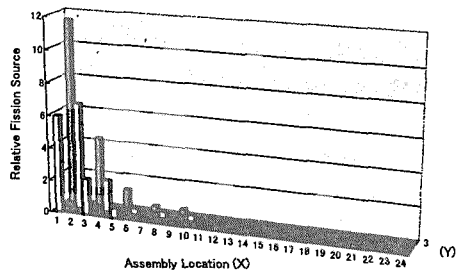

(2) Case30: initial source (1,1)

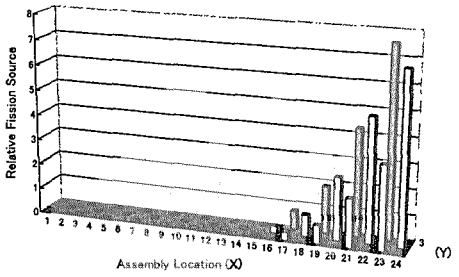

(3) Case33: initial source (23,3)

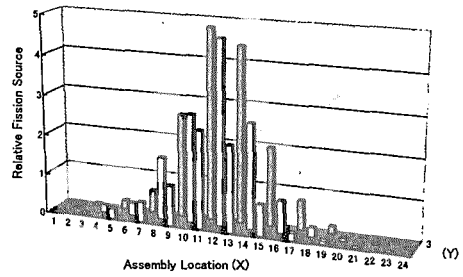

(4) Case36: initial source (12,2)

Fig. 4 Relative source distributions at 500 generation

The trends of relative fission source levels per generation for the four cases are shown in Fig. 5(1) ~ Fig. 5(4), where the relative fission source levels at several representative locations are shown every 10 generations.

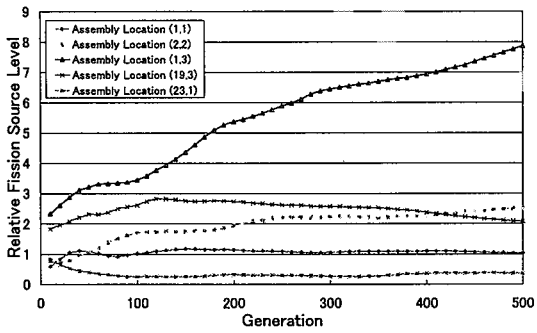

(1) Case27: uniform initial source

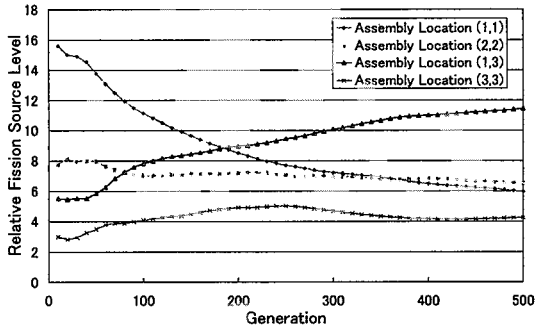

(2) Case30: initial source (1,1)

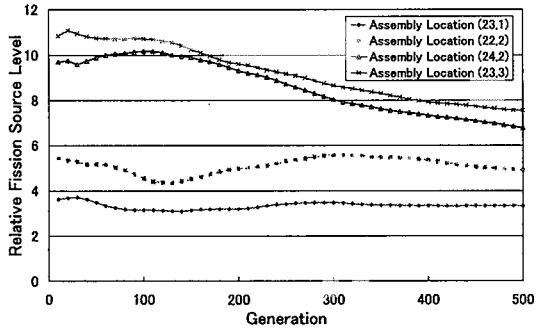

(3) Case33: initial source (23,3)

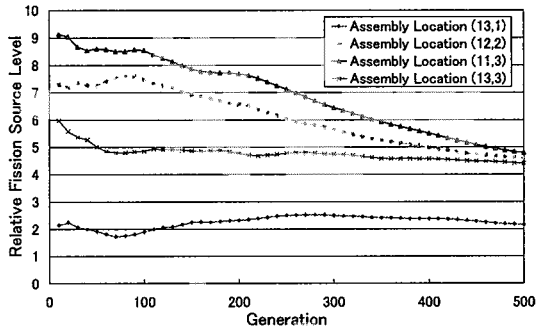

(4) Case36: initial source (12,2)

Fig. 5 Trends of relative fission source levels per generation

The calculated results of fission source distribution are summarized below.

- In case of uniform initial source, fission source distributes over all assemblies and has a local peak as shown in Fig. 4(1). The source level at the peak assembly is still increasing at 500 generation as shown in Fig. 5(1).
- In cases of initial source location (1,1), (23,3) and (12,2), the maximum peak locates near the initial source location, respectively, and there are many zero-source assemblies at locations far from the maximum point as shown in Fig. 4(2) ~ Fig. 4(4). The source levels at the peak and its neighboring assemblies are still changing monotonously (increasing or decreasing) at 500 generation as shown in Fig. 5(2) ~ Fig. 5(4).
- The dependence on the other parameter such as the number of skipped generations, the histories per generation is not observed.

It is found that the fission source distributions for the thirty-six cases cannot be converged as shown in the above results.

3. ESTIMATION OF THE CONVERGED FISSION SOURCE DISTRIBUTION

3.1 Derivation of fission matrix equation

Here we consider the weakly coupled multi cell problem as shown simply in Fig. 6.

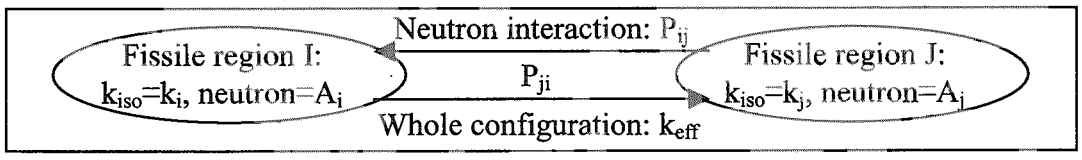

Fig. 6 Concept of weak coupling problem

For the fissile region I, the multiplication factor of isolated single region system (k_{iso}) is assumed to be k_i (i=1,m), where the region I and the other region J are coupled weakly in neutron interactions P_{ij} ($j \neq i$). The neutron balance in the n'th generation is described by equation (1).

$$A_i^{n+1} = k_{eff} A_i^n = k_i A_i^n + \sum_{j \neq i} P_{ij} A_j^n \tag{1}$$

The equation (1) in matrix expression is generalized to fission matrix equation: $(\mathbb{F} - k_{eff}\mathbb{E})\,\mathbb{A} = \mathbb{O}$, here the elements of fission matrix $\mathbb{F}$ comprise k_i and P_{ij}, $\mathbb{E}$ is the unit matrix and the elements of vector $\mathbb{A}$ are A_i. $\mathbb{O}$ is the zero-matrix. The non-trivial solution ($\mathbb{A} \neq \mathbb{O}$) induces the equation (2).

$$|\,\mathbb{F} - \lambda\,\mathbb{E}\,| = 0 \tag{2}$$

When the eigenvalue λ equals to λ_i (i=1~m), k_{eff} equals to the maximum of λ_i. In case of the two-region problem (m=2), it is very easy to solve the equation (2) for k_{eff} analytically, when the fission matrix elements are given. The result of k_{eff} and the A_1/A_2 is shown in equation (3) and (4), respectively. In case of a symmetric two-region problem, more simple relation is derived, so that, $k_{eff} = k + P$, where, $k = k_1 = k_2$, $P = P_{12} = P_{21}$ and $A_1 = A_2$.

$$k_{eff} = k - \Delta k/2 + \sqrt{(\Delta k/2)^2 + P_{12}P_{21}} \quad \text{, here } k = \max(k_1, k_2), \Delta k = |k_1 - k_2| \tag{3}$$

$$A_1/A_2 = (k_{eff} - k_2)/P_{21} = P_{12}/(k_{eff} - k_1) \tag{4}$$

3.2 Isolated single assembly and diagonally placed two assemblies

In the benchmark problem 1 as shown in Fig. 1, the checkerboard storage has thirty-six assemblies of the same specification with three different sorts of boundary conditions. Namely, one assembly is adjacent to the concrete wall of 40cm thickness on two side surfaces, thirteen assemblies are adjacent to the concrete wall on one side surface, and the others are adjacent to the water reflector or the water channels on all surfaces. The multiplication factors of isolated single assembly (k_{iso}s) for the corresponding boundary conditions are different because of the difference of the reflector effect between water and concrete. So we calculate the three different k_{iso}s of k_α, k_β and k_γ (here, the suffixes of α, β and γ indicate the three different boundaries) as shown in Fig. 7(1) ~ (3) by using MCNP. The calculation condition is 500 scored generations, 20 skipped generations, 2000 histories per generation and uniform initial source distribution.

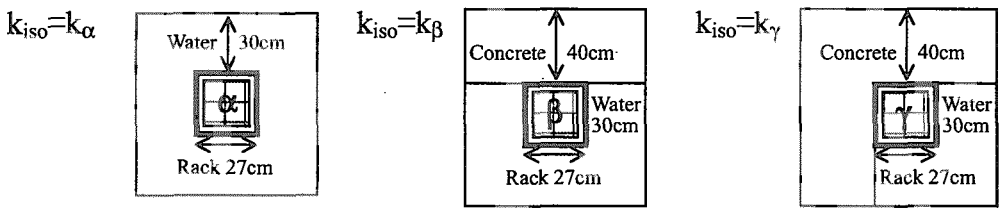

(1) All water reflected (2) concrete on 1/4 side (3) concrete on 2/4 sides

Fig. 7 Configurations of isolated single assembly surrounded by three different boundaries

In case of diagonally placed two assemblies as a part of the checkerboard storage, there are four types of assembly combination of the above three boundary conditions as shown in Fig. 8(1) ~ (4). The multiplication factors for the four configurations (k_{dia}s) of $k_{\alpha\alpha}$, $k_{\alpha\beta}$, $k_{\beta\beta}$ and $k_{\alpha\gamma}$ and the fission source rations of A_i/A_j (i,j=α, β and γ) are calculated by MCNP. Then the neutron interactions between two assemblies ($P_{\alpha\alpha}$, $P_{\alpha\beta}$, $P_{\beta\alpha}$, $P_{\beta\beta}$, $P_{\alpha\gamma}$ and $P_{\gamma\alpha}$) can be calculated by using k_{iso}s, k_{dia}s and A_i/A_j according to the equation (3) and (4).

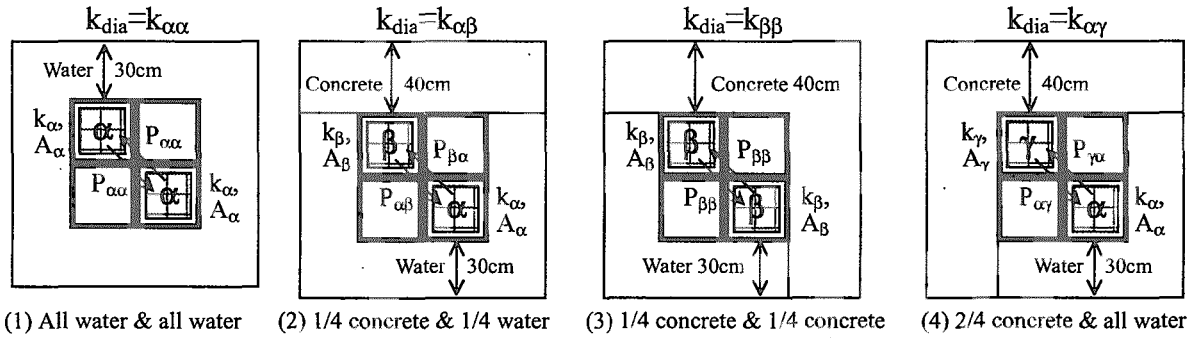

(1) All water & all water (2) 1/4 concrete & 1/4 water (3) 1/4 concrete & 1/4 concrete (4) 2/4 concrete & all water

Fig. 8 Configurations of the diagonally placed two assemblies

The calculated results of k_{iso}, k_{dia} (also 1σ) and A_i/A_j by MCNP for the cases as mentioned above are listed in table I. And the results of the neutron interactions are shown in table II.

Table I Calculated results of isolated single assembly and diagonally placed two assemblies

	k_α	k_β	k_γ	$k_{\alpha\alpha}$	$k_{\alpha\beta}$	$k_{\beta\beta}$	$k_{\alpha\gamma}$
k_{iso}, k_{dia}	0.86793	0.87783	0.88810	0.87166	0.87926	0.88354	0.88852
1σ	0.00082	0.00072	0.00078	0.00078	0.00073	0.00079	0.00077
A_i/A_j	-	-	-	1.073	2.037	0.944	3.726

Table II Neutron interactions between diagonally placed two assemblies

$P_{\alpha\alpha}$	$P_{\alpha\beta}$	$P_{\beta\alpha}$	$P_{\beta\beta}$	$P_{\alpha\gamma}$	$P_{\gamma\alpha}$
0.00373	0.00556	0.00291	0.00571	0.00553	0.00157

3.3 Solution of fission matrix equation by iterative calculation

In this section, we show the solution of fission matrix equation with some approximations for matrix elements in order to estimate the converged fission source distribution for the checkerboard storage. The approximations are described below.

- As shown in the Fig. 9, the k_{iso}s of the thirty-six assemblies in the checkerboard storage are represented by k_α, k_β and k_γ listed in table I.
- The interactions between diagonally placed two assemblies in the checkerboard storage are represented by $P_{\alpha\alpha}$, $P_{\alpha\beta}$, $P_{\beta\alpha}$, $P_{\beta\beta}$, $P_{\alpha\gamma}$ and $P_{\gamma\alpha}$ as shown in table II.
- The neutron interaction between two assemblies across a water channel is supposed to be 0.002. The effect of this value on k_{eff} of the checkerboard storage is small, but it affects the fission source distribution to some extent. This value is determined with some calculations for 3x3 configuration.
- The neutron interactions except the ones mentioned above are negligible.

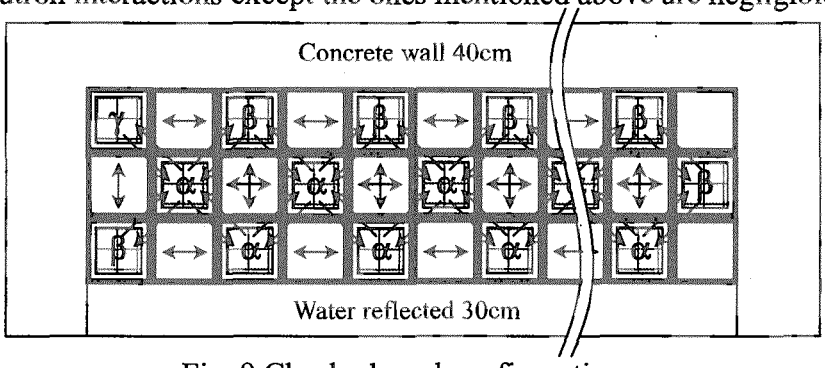

Fig. 9 Checkerboard configuration

Figure 10 shows the solution of the fission matrix equation by deterministic method of iterative calculation. The number of iteration to converge the fission source starting from the uniform initial guess is more then 4000. The convergence criterion to source change is less than 10E-05. It is found that the fission source distribution of the matrix solution has the maximum peak at the corner where the k_{iso} of an assembly becomes the maximum because of its reflector effect of the concrete wall on its two sides. The farther the distance from the assembly of the peak fission source is, the less fission source level the other assemblies indicate. The change of the fission source level is similar to the exponential curve, and it becomes very low but not zero at some assemblies located far from the assembly of the maximum peak. In comparison with the results by MCNP as shown in Fig. 4(1) ~ (4), they are found to be intermediates between the each initial source distribution and the solution of the fission matrix equation. The k_{eff} of the fission matrix equation (=0.8916) is almost the same as the maximum value for the thirty-six cases by MCNP.

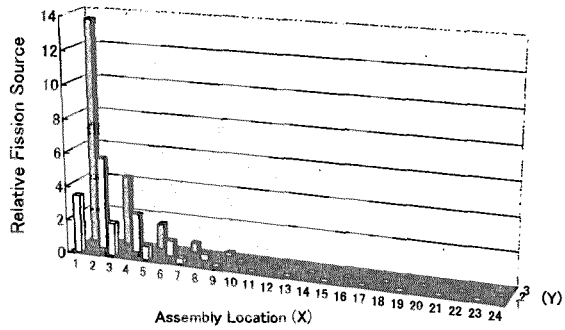

Fig. 10 Solution of fission matrix equation

3.4 Special case calculation by MCNP

The special case calculations are carried out by MCNP. As the initial source distribution, the assembly-averaged source levels are set to be the solution of the fission matrix equation as shown in Fig. 10, at the same time, the distributions inside assemblies are assumed to be cosine-like shapes to which the result of the single assembly distribution is fitted as shown in Fig. 12. The fission source distributions inside assemblies calculated by MCNP for the cases as shown in Fig. 7(1) (α type) and Fig. 8(4) (α-γ type) are shown in Fig. 11(1) and Fig. 11(2), respectively. They show that the neutron interaction between two assemblies affects the fission source distributions inside assembly just a little, and they are similar to cosine shape.

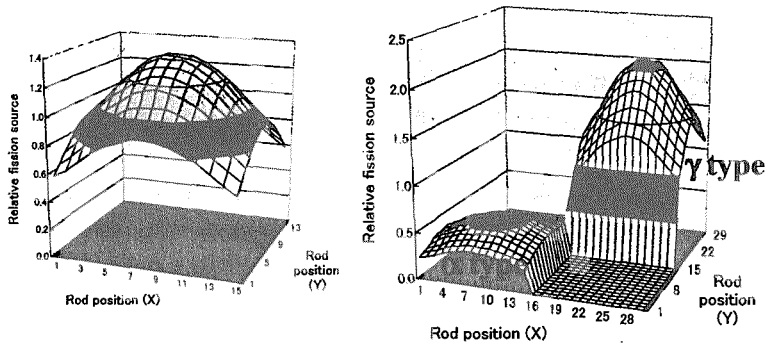

(1) Single assembly (α type) (2) Two assemblies (α-γ type)

Fig. 11 Fission source inside assembly by MCNP

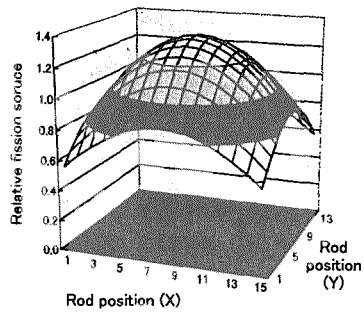

Fig. 12 Fitting cosine shape

The calculation conditions and the results for k_{eff} are shown in table III.

Table III Calculation conditions and results for the special cases

Special case	Histories per generation	Generations	Skipped generations	Total histories	k_{eff} result	1σ
1	5000	500	20	2500000	0.89029	0.00051
2	50000	50	5	2500000	0.89289	0.00050
3	100000	50	5	5000000	0.89266	0.00033

From the viewpoint of converged source estimation, there should be many assemblies of very low source level as shown in Fig. 10 obtained by fission matrix equation. So, very large number of histories per generation is necessary for Monte Carlo method to reach convergence in the source distribution. The k_{eff} of the special case 1 is about 0.2% underestimated because the number of histories per generation 5000 is not enough. The k_{eff}s of the special case 2 and 3 are almost the same in comparison with their 1σ, and they are greater than the thirty-six cases by MCNP as shown in Fig. 2. The trends of relative fission source levels per generation and the relative fission source distribution at fiftieth generation for the special case 3 are shown in Fig. 13 and Fig. 14, respectively. Even though the number of histories per generation is very large (100,000), a few assemblies have zero-source on the opposite side of the maximum peak because of their very low source level, and as shown in Fig.13, most of the fission source levels of the assemblies around the peak source level are almost constant as the generation increases. So the fission source distribution must be almost converged.

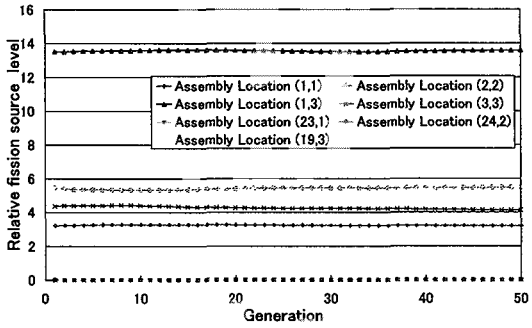

Fig. 13 Trends of relative fission source levels for the special case 3

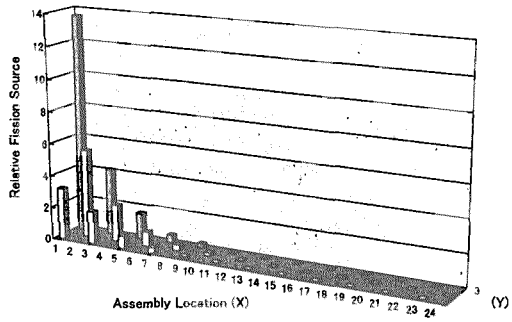

Fig. 14 Fission source distribution at the 50th generation for the special case 3

4. CONCLUDING REMARK

In the OECD/NEA benchmark problem 1: checkerboard storage of assemblies, it is very difficult to obtain the converged fission source distribution by the Monte Carlo method because each assembly is coupled in neutron reaction so weakly that the source convergence becomes very slow. This causes sometimes non-conservative estimation for the effective multiplication factor, and the results for the thirty-six cases of various calculation conditions specified in the benchmark 1 show the underestimation of k_{eff}.

As compared with the above, it is easy to obtain the multiplication factors for the isolated single assembly with its reflector effect, and also comparatively not difficult to estimate the neutron interactions between adjacent two assemblies. It is a good approximation to apply these multiplication factors and neutron interactions to the fission matrix elements for the weakly coupled configuration. The solution of the fission matrix equation shows that the fission source distribution of the checkerboard storage has the maximum peak at the corner where the isolated multiplication factor is the maximum and there are many assemblies of a very low fission source level far from there. This fact insists the necessity of the very large number of histories per generation in the Monte Carlo method to obtain the correct k_{eff} value.

In addition to using the solution of fission matrix for the initial source distribution, the assumption of the cosine-like shape inside the assemblies reduces the number of generations to reach convergence. This calculation gives almost the converged fission source distribution.

REFFERENCES

[1] "MCNP-A General Monte Carlo N-Particle Transport Code Version 4B", LA-12625-M, Ed. by J. F. Briesmeister, Los Alamos National Laboratory, Los Alamos, NM (1997)

[2] T. Nakagawa, et al., J. Nucl. Sci. Technol., 32[12] 1259-1271 (1995)

JP0250332

JAERI-Conf 2002-004

THE CALCULATION RESULTS OF OECD/NEA SOURCE CONVERGENCE BENCHMARK PROBLEM NO.2 AND NO.4 BY USING MCNP

Takehide KIYOSUMI and Yoshinori MIYOSHI

Criticality Safety Laboratory,
Japan Atomic Energy Research Institute,
Tokai-mura, Naka-gun, Ibaraki-ken 319-1195, Japan
Fax: 81-29-282-6798, e-mail: kiyosumi@melody.tokai.jaeri.go.jp

OECD / NEA source convergence benchmark problems treating the neutron weakly coupled system were evaluated using the Monte Carlo code. The neutron source distribution and the neutron flux showed the biased convergence in each case. Moreover, convergence of k_{eff} was checked when k_{eff} skipped a certain amount of generation.

Key words: Monte Carlo method, the neutron weakly coupled system, convergence, skipped generation, random numbers sequences

1. Introduction

When the distance between the fissile material units increases, an exchange of the neutron between units decreases and the neutron source distribution converges more badly for Monte Carlo calculation. In order to inquire the estimation how it applies the Monte Carlo method to such the neutron weakly coupled system, OECD/NEA prepared the four problems which set up the system concretely. In this time, we choose No.2 and No.4 among these problems and we evaluate the change for every generation of the source distribution of a neutron and the convergence over the number of skipped generations of k_{eff}, neutron source distribution and neutron flux by using the Monte Carlo code.

2. Calculation geometry

Figure 1 and Figure 2 show the geometry of OECD/NEA source convergence benchmark problem No.2, and Figure 3 show the geometry of problem No.4.

The geometry of problem No.2 is an infinite fuel pin array in water. The both ends of the fresh fuel rod or low burnup fuel rod are separated by central natural uranium or high burnup fuel region. The enrichment of fissile material in two ends of the fuel rod is axially asymmetric.

The geometry of problem No.4 is a lattice of $5\times5\times1$ separated highly enriched uranium metal spheres. The radius of sphere at the center of a lattice is 1.29cm larger than other radius of sphere. In this problem, we designate the sphere at the lowest left-hand left of a lattice cell 1, and the sphere at the uppermost right-hand cell 25.

3. Calculation methods

These benchmark problems were calculated with the continuous energy Monte Carlo neutron transport code, MCNP-4B2, and the Japanese Evaluated Nuclear Data, JENDL-3.2.

Calculation of 1000 generations was performed by 10000 histories per generation at the problem No.2. One initial neutron source distribution assumes the flat, the other initial source distribution assumes the distribution depending on the abundance of fissile material. On this problem, the change of source distribution, k_{eff}, standard deviation, neutron flux and reaction rate was derived, respectively. It is checked the results of k_{eff} and neutron flux after skipped 0, 50, 200, 400 generations. A list of each calculation is shown in Table Ⅰ.

Calculation of 1000 generations was performed by 1250 histories per generation at the problem No.4. Initial source distribution is as follows: 1010 neutrons are generated at cell 1, and 10 neutrons are generated at other 24 cells. On this problem, the change of k_{eff}, standard deviation, source distribution and neutron flux was derived, respectively. The skipped generation which is checked is the same of problem No.2.

4. Calculation results

The calculation result of benchmark problem No.2 is as follows : table II is k_{eff} in each case. The change of k_{eff} at the fresh fuel is shown in figure 4 and the change of k_{eff} at the irradiated fuel is shown in figure 5. The k_{eff} increases with skipped generations, but if 50 generations are exceeded, it is almost constant as shown in figure 4 and figure 5. The set of initial neutron source distribution dose not influence the convergence of this calculation.

About the neutron source distribution of benchmark problem No.2, if generations increase, neutron source will come to concentrate on each end containing a lot of fissile material, and if generations increase over 100th, it will come to concentrate on upper end containing more lot of fissile material and the neutron source at the lower part of fuel rod is set to 0. In spite of the consideration of the initial neutron source distribution for both fuel rods, the method of convergence is the same. In the case of irradiated fuel, the neutron source comes to concentrate on upper end of fuel rod over 50th generation.

Figure 6 shows the change of neutron flux distribution about the fresh fuel rod, and figure 7 shows about the irradiated rod. As shown in figure 6, when the skipped generation is 0, the neutron flux distribution at the central part of fuel rod becomes flat under the influence of the initial neutron source in the case of the fresh fuel. Then, the reason that the k_{eff} skipped 0 generation is small is the influence of the neutron flux at the central part of fuel rod. When the skipped generation increase, the neutron flux decrease by reduction of the neutron source intensity at the central part of fuel rod. And when the neutron source intensity at the bottom end of fuel decreases, the neutron flux of this region also decreases, and finally, only the neutron ingredient at the top end of fuel remains. It is thought that the k_{eff} skipped over 50 generations is based on the influence of the neutron at the top end of fuel. In addition, the consideration of the initial neutron source distribution hardly influences the change of neutron flux distribution. As shown in figure 7, the neutron flux in the lower half of the fuel rod decreases when the skipped generations increase in the case of the irradiated fuel. The convergence of the neutron flux in the irradiated fuel is fasten compared with the fresh fuel. In addition, the consideration of the initial neutron source distribution does not influence a neutron flux distribution.

The calculation result of benchmark problem No.4 is as follows: figure 8 shows the dependence of k_{eff} and standard deviation on random numbers sequences and skipped generations. When the skipped generation is 0, k_{eff} shows the values between 1.110 to 1.115 and when the skipped generations exceed 200, k_{eff} is stability between 1.115 to 1.118. So, skipped generations are adequate over 200 for converging k_{eff} and there is no effect on the calculation results for any random number sequence. In addition, when the skipped generation is 0, the standard deviation is 0.08 ~0.09%. When the skipped generations are over 200, the standard deviation is 0.06%.

As for behavior of the source distribution of neutron, 80% or more neutron generates at 0~50 generations from cell 1, but it comes to generate from cell 13 exceeding 50 generations, and finally, 90% or more neutron comes to generate from cell 13. To estimate that the k_{eff} of single sphere at cell 13 is 1.118 and the k_{eff} of single sphere at other cell is 1.001, it is thought that the k_{eff} of benchmark problem No.4 is influenced from cell 1 to be small when the skipped generation is 0. Conversely, when the skipped generations exceed 200, k_{eff} almost is decided by cell 13 and it is stabilized between 1.115 to 1.118.

As shown in figure 9, the neutron flux is the axis symmetrical distribution and the flux of cell 13 is 10^2 times larger than other cells. This is one of the reasons why the k_{eff} of this geometry is equal to the k_{eff} of the single sphere at cell 13. Because the neutron flux of any cell which is the shadow of cell 13, this is considered because the neutron has diffused from cell 13 as a center. In addition, the shape of neutron flux distribution is not so changed while skipped generations increase except for cell 1.

5. Conclusion

We evaluate the end effect for benchmark problem No.2 and the dispersed uranium metal spheres for benchmark problem No.4 by using Monte Carlo method.

In problem No.2, the k_{eff} converges skipped over 50 generations in the case of fresh fuel, and skipped over 200 generations in the case of irradiated fuel. Regardless of the consideration of the initial neutron source distribution, the neutron source concentrates at the region where the most numerous fissile material is. The neutron flux distribution does not change at the upper region of the fuel rod and it decrease at other region with increasing skipped generations. Although the neutron flux of the fresh fuel and the irradiated fuel converges to 0 at the lower region of the fuel rod skipped 400 generations, it is a question about whether this distribution is right. From now on, we will use the deterministic method and check that it is reappeared those results.

In problem No.4, there is the same tendency of problem No.2 that the neutron source distribution and neutron flux concentrate at the location where the most numerous fissile material is. Although the neutron flux distribution is seldom influenced when the skipped generations increase, the k_{eff} obtains convergence with better skipped 200 or more generations. Since the influence of the neutron at the cells 1～12 and the cells 14～25 decreases small if the skipped generations increase, the k_{eff} of this geometry becomes large gradually and is soon converged of the k_{eff} of the single sphere at cell 13. In addition, the k_{eff} of this geometry is not influenced to change the random numbers sequences even if the skipped generations increase.

Table I The list of each calculation at problem No.2

Initial source guess	Skipped generations	Case1_2 (Fresh fuel)	Case2_2 (Irradiated fuel)
Flat	0	Case A-1	Case C-1
	50	Case A-2	Case C-2
	200	Case A-3	Case C-3
	400	Case A-4	Case C-4
Depending on the abundance of fissile material	0	Case B-1	Case D-1
	50	Case B-2	Case D-2
	200	Case B-3	Case D-3
	400	Case B-4	Case D-4

Table II The k_{eff} and standard deviation for increasing skipped generations (No.2)

Skipped generations	Case A	Case B	Case C	Case D
0	1.34814±0.00085	1.34926±0.00043	1.06748±0.00034	1.06781±0.00031
50	1.35005±0.00028	1.35016±0.00027	1.06916±0.00021	1.06917±0.00020
200	1.35007±0.00027	1.35051±0.00027	1.06920±0.00021	1.06910±0.00020
400	1.35103±0.00020	1.35044±0.00027	1.06916±0.00020	1.06907±0.00020

Table III The k_{eff} and standard deviation of each random numbers sequences and skipped generations (No.4)

Random numbers sequence	Skipped generations			
	0	50	200	400
1	1.11172±0.00093	1.11506±0.00065	1.11639±0.00066	1.11681±0.00066
3	1.11125±0.00102	1.11558±0.00065	1.11632±0.00064	1.11651±0.00064
5	1.11231±0.00096	1.11611±0.00068	1.11618±0.00065	1.11603±0.00065
7	1.11028±0.00103	1.11450±0.00074	1.11493±0.00066	1.11472±0.00066
9	1.11056±0.00108	1.11524±0.00067	1.11689±0.00068	1.11666±0.00068
11	1.11128±0.00100	1.11549±0.00062	1.11728±0.00065	1.11740±0.00065
13	1.11223±0.00091	1.11558±0.00068	1.11623±0.00063	1.11682±0.00064
15	1.11316±0.00095	1.11622±0.00067	1.11674±0.00068	1.11639±0.00066
17	1.11422±0.00095	1.11750±0.00066	1.11735±0.00068	1.11756±0.00066
19	1.11186±0.00096	1.11574±0.00066	1.11641±0.00066	1.11713±0.00066
Default	1.11467±0.00093	1.11757±0.00066	1.11789±0.00066	1.11715±0.00066

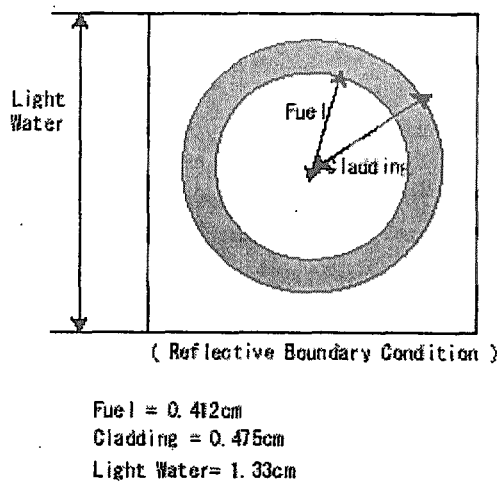

Figure.1. Radial dimension of problem No.2

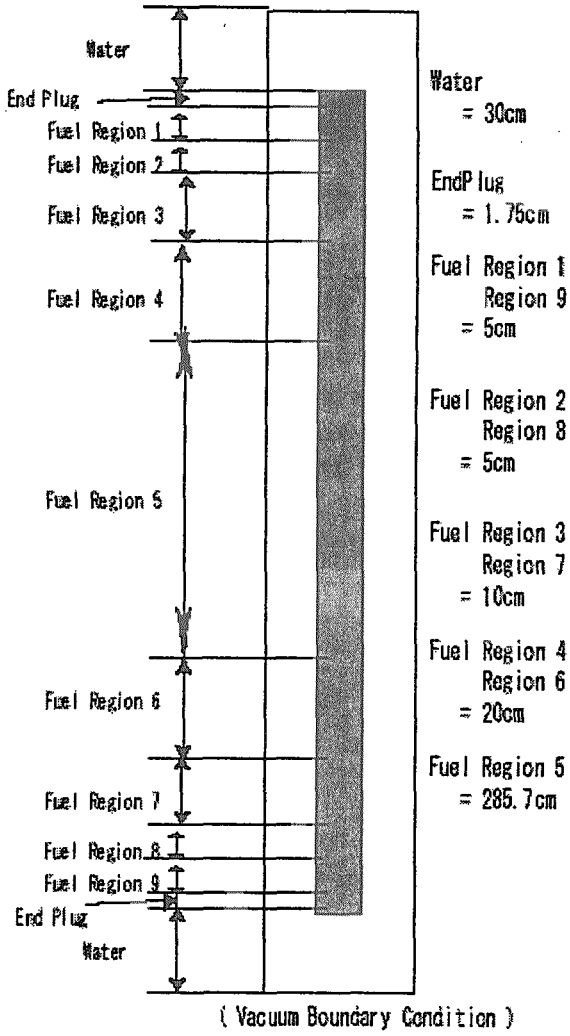

Figure.2. Axial dimension of problem No.2

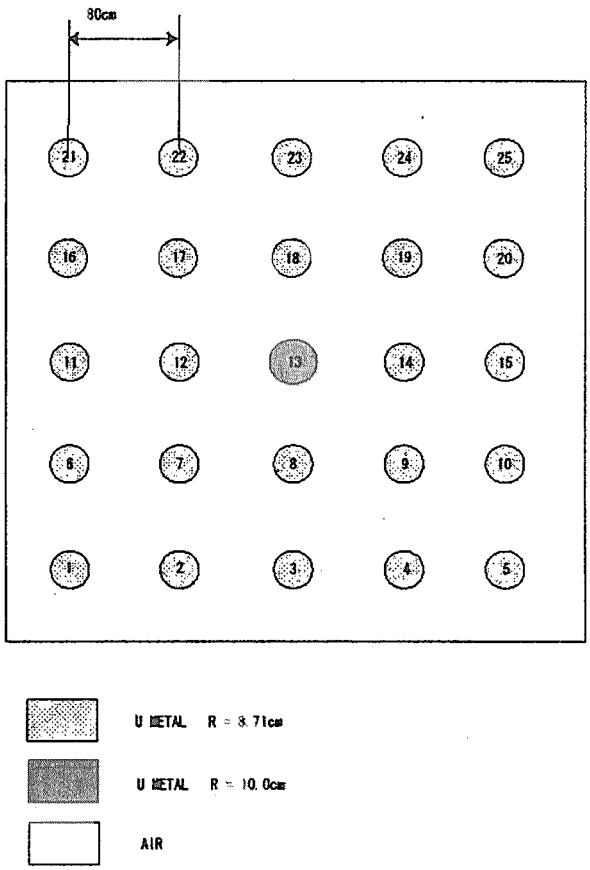

Figure 3 Geometry of problem No.4

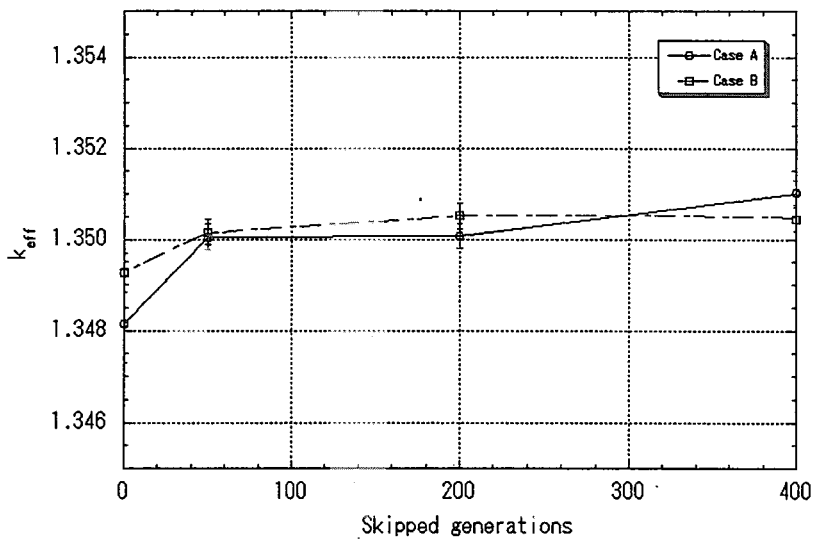

Figure 4 Change of k_{eff} for skipped generations at problem No.2 (Case A and Case B)

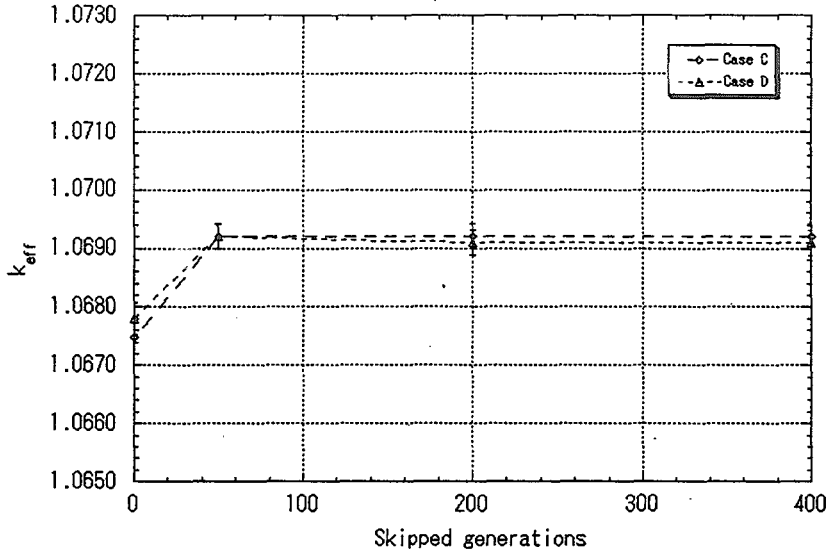

Figure 5 Change of k_{eff} for skipped generations at problem No.2(Case C and Case D)

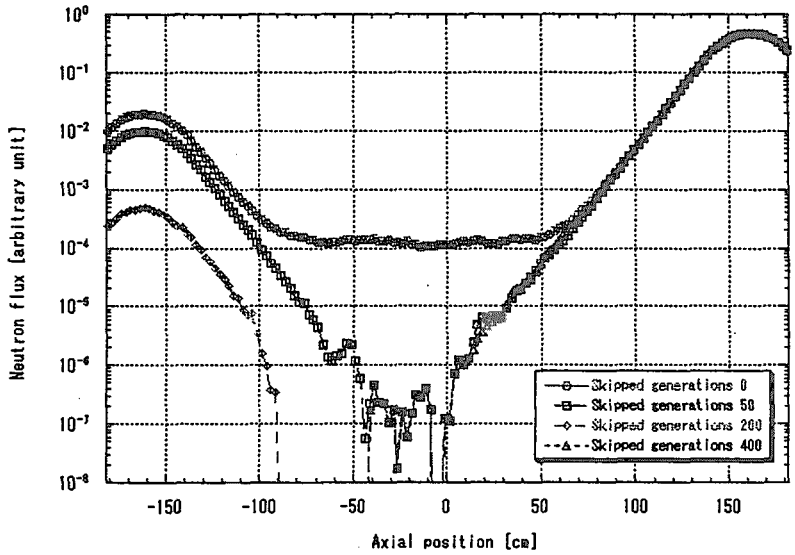

Figure 6 Neutron flux at problem No.2 (Case B)

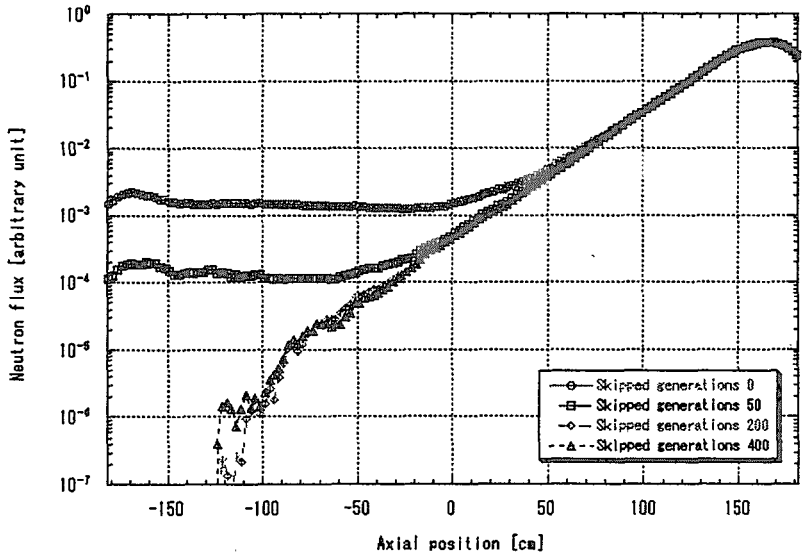

Figure 7 Neutron flux at problem No.2 (Case D)

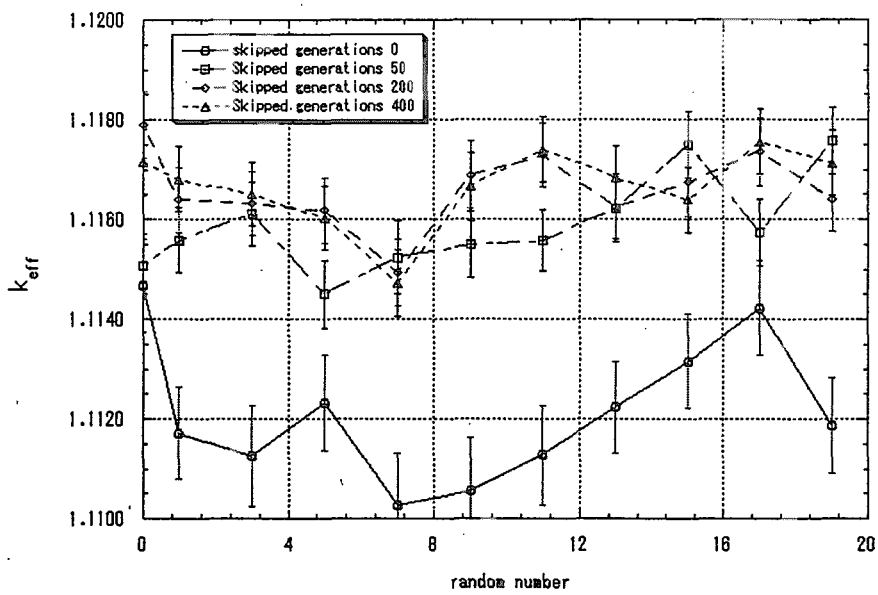

Figure 8 Change of keff for random numbers sequences at problem No.4

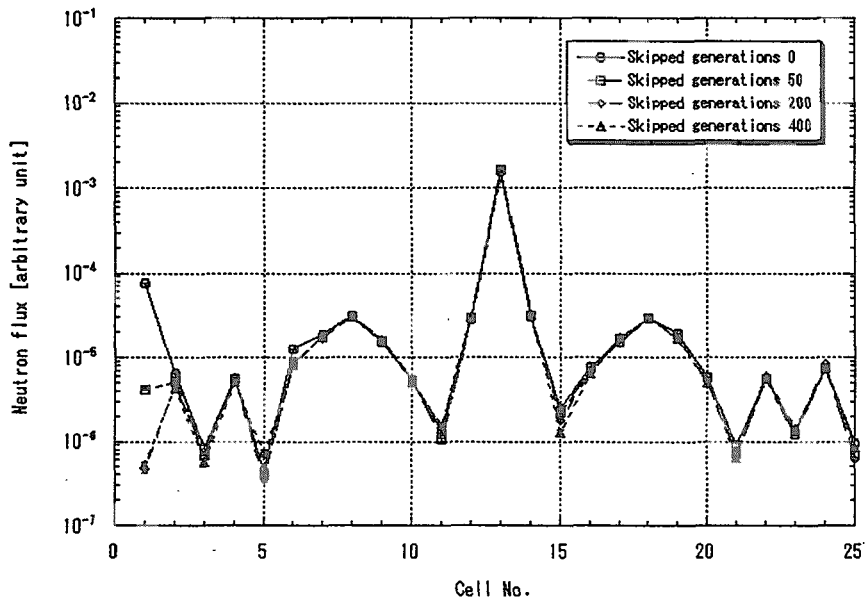

Figure 9 Neutron flux at problem No.4

JP0250333

JAERI-Conf 2002-004

CRITICAL AND SUBCRITICAL MASS CALCULATIONS OF FISSIONABLE NUCLIDES BASED ON JENDL-3.2+

H. OKUNO and H. KAWASAKI*
Japan Atomic Energy Research Institute, Tokai-mura, 319-1195, Japan
Fax: 81-29-282-6479, e-mail: okuno@cyclone.tokai.jaeri.go.jp
*CRC Solutions Institute, Inc., Mito, 1-1-8 Japan, 310-0803, Japan
Fax: 81-29-221-1169, e-mail: h-kawa@crc.co.jp

We calculated critical and subcritical masses of 10 fissionable actinides (^{233}U, ^{235}U, ^{238}Pu, ^{239}Pu, ^{241}Pu, ^{242m}Am, ^{243}Cm, ^{244}Cm, ^{249}Cf and ^{251}Cf) in metal and in metal-water mixtures (except ^{238}Pu and ^{244}Cm). The calculation was made with a combination of a continuous energy Monte Carlo neutron transport code, MCNP-4B2, and the latest released version of the Japanese Evaluated Nuclear Data Library, JENDL-3.2. Other evaluated nuclear data files, ENDF/B-VI, JEF-2.2, and JENDL-3.3 in its preliminary version were also applied to find differences in results originated from different nuclear data files. For the so-called big three fissiles (^{233}U, ^{235}U and ^{239}Pu), analyzing the criticality experiments cited in ICSBEP Handbook validated the code-library combination, and calculation errors were consequently evaluated. Estimated critical and lower limit critical masses of the big three in a sphere with/without a water or SS-304 reflector were supplied, and they were compared with the subcritical mass limits of ANS-8.1.
Key words: critical mass, subcritical mass, actinide, JENDL-3.2, MCNP-4B2

1. INTRODUCTION

As the burnup of fuel proceeds, amounts of minor actinides increase remarkably. Their influences on criticality safety of the fuel cycle facilities and transportation should not be disregarded for high burnup fuels [1]. For criticality safety control of transmutation and actinide science test facilities, criticality data on minor actinides also serve as basic data. Because it is sometimes difficult to find proper quantities we are looking for in the literature, calculations were made for the critical and subcritical masses of 10 fissionable actinides (^{233}U, ^{235}U, ^{238}Pu, ^{239}Pu, ^{241}Pu, ^{242m}Am, ^{243}Cm, ^{244}Cm, ^{249}Cf and ^{251}Cf) in metal, and in metal-water mixtures except ^{238}Pu and ^{244}Cm. These nuclides were selected that they are relatively popular and their critical masses are comparable to or smaller than that of ^{235}U. The present study is expected to become a first step to fulfil the above purposes.

2. OBJECT AND METHOD OF CALCULATION

The fissionable nuclides of which critical and subcritical masses were calculated in this study are divided into two categories:

(1) Fissile nuclides that the fission can be occurring with the thermal neutrons, such as ^{235}U, ^{239}Pu, ^{233}U, ^{241}Pu, ^{242m}Am, ^{243}Cm, ^{249}Cf and ^{251}Cf, for which both metal and a mixture of metal and water were studied.

(2) Fissionable nuclides that the fission can be occurring only with the fast neutrons, such as ^{238}Pu and ^{244}Cm, for which only metal was studied.

The density of each actinide in metal was calculated basically based on the compilation by R.G. Haire [2]. The fuel shape was a sphere and the reflector conditions assumed were three kinds: bare, surrounded with a 30cm-thick reflector of water or stainless steel specified as SS-304. The uniformity of fuel was assumed.

+ This work was carried out by the Japan Atomic Energy Research Institute (JAERI) under entrustment by the Ministry of Education, Culture, Sports, Science and Technology (MEXT) of Japan.

The criticality calculation code applied was a continuous energy Monte Carlo neutron transport code, Version 4B2, MCNP-4B2. The evaluated nuclear data file adopted was the latest released Japanese Evaluated Nuclear Data Library, JENDL-3.2 as a standard. Besides JENDL-3.2, ENDF/B-VI, JEF-2.2 and JENDL-3.3 in its preliminary version were also applied to see differences in k_{eff} caused by the differences of the evaluated nuclear data file.

In this paper, the mass of actinide, corresponding to the calculated $k_{eff} = 1$ with each specific combination of code and data library, is called "critical mass," and the masses corresponding to $k_{eff} = 0.9$ and 0.8 are called "subcritical masses." These quantities for the 10 nuclides were calculated in a precise way described as follows. The neutron multiplication factor in the infinite media, k_∞, and those for at least four sizes of the fuel sphere expected to sandwich the k_{eff} values of 1, 0.9 and 0.8 were applied to the curve $k_{eff} = k_\infty\left(1 - e^{-\alpha r}\right)^{\beta r^\gamma}$, where α, β and γ were parameters [3]. The number of neutron histories of the criticality calculations was set to one million.

3. RESULTS

3.1 Critical and subcritical masses of actinides in metal

The results for critical and subcritical masses of actinide metals are listed in Table I. It is interesting to note the following observations of the results:

Table I. Critical (k_{eff}= 1.0) and subcritical (k_{eff}= 0.9 and 0.8) masses of actinides in metal

Nuclide	Density [g/cm^3]	Reflector	Mass [kg]		
			k_{eff}= 1.0	k_{eff}= 0.9	k_{eff}= 0.8
^{233}U	18.76	None	14.81	10.02	6.58
		Water	6.94	4.58	2.97
		SS-304	6.55	4.60	3.19
^{235}U	18.92	None	46.04	31.39	21.21
		Water	21.19	13.67	8.67
		SS-304	18.66	13.06	9.04
^{239}Pu	19.85	None	10.13	7.00	4.68
		Water	5.45	3.71	2.48
		SS-304	4.94	3.53	2.47
^{238}Pu	19.77	None	8.16	5.58	3.70
		Water	6.70	4.59	3.05
		SS-304	4.43	3.12	2.16
^{241}Pu	20.02	None	11.75	8.18	5.54
		Water	5.55	3.80	2.50
		SS-304	5.40	3.85	2.72
^{242m}Am	13.72	None	12.59	8.82	6.00
		Water	4.41	3.03	2.01
		SS-304	4.73	3.45	2.49
^{243}Cm	13.45	None	10.03	7.08	4.80
		Water	3.51	2.43	1.60
		SS-304	3.91	2.84	2.05
^{244}Cm	13.51	None	29.95	20.07	13.20
		Water	24.84	16.51	10.72
		SS-304	15.36	10.62	7.11
^{249}Cf	15.11	None	6.26	4.47	3.07
		Water	2.39	1.69	1.14
		SS-304	2.81	2.10	1.52
^{251}Cf	15.23	None	2.50	1.77	1.20
		Water	1.33	0.95	0.66
		SS-304	1.29	0.95	0.68

(1) The water-reflected critical mass ranges from 35% (for ^{242m}Am and ^{243}Cm) to 83% (for ^{238}Pu and ^{244}Cm) of the bare critical mass. The stainless steel (SS) reflected critical mass ranges from 0.38% (for ^{242m}Am and ^{243}Cm) to 0.54% (for ^{238}Pu), which is narrower than the water-reflected cases.

(2) The SS-reflected critical mass is smaller than the water-reflected critical mass except for ^{242m}Am, ^{243}Cm and ^{249}Cf.

(3) There are at least nine actinides that have a smaller bare critical mass than of ^{235}U.

3.2 Critical and subcritical masses of actinides in a metal-water mixture

The critical and subcritical masses of eight actinides (^{235}U, ^{239}Pu, ^{233}U, ^{241}Pu, ^{242m}Am, ^{243}Cm, ^{249}Cf and ^{251}Cf) in a metal-water mixture were calculated. As an example, critical and subcritical masses of a sphere of ^{243}Cm-H_2O in bare, with a 30-cm-thick water, or SS are shown in Fig. 1. The minimum of the curves for the eight actinide-water mixtures is listed in Table II. It is observed from this table that the critical mass of actinide is well described as in a power of the corresponding actinide concentration. To show the relation more clearly, a graph is drawn in Fig. 2 for the bare case.

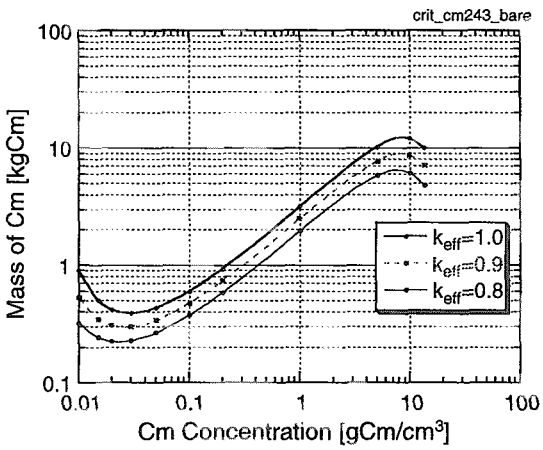

(a) bare case

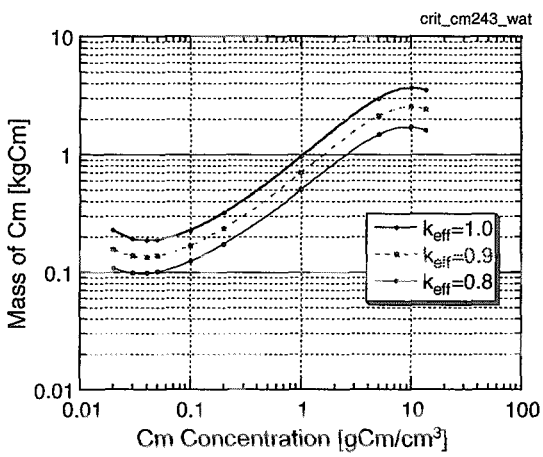

(b) water-reflected case

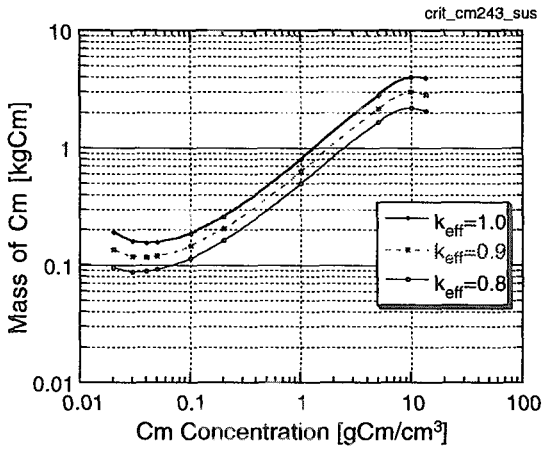

(c) SS-reflected case

Fig.1. Critical and subcritical masses of a sphere of ^{243}Cm-H_2O.

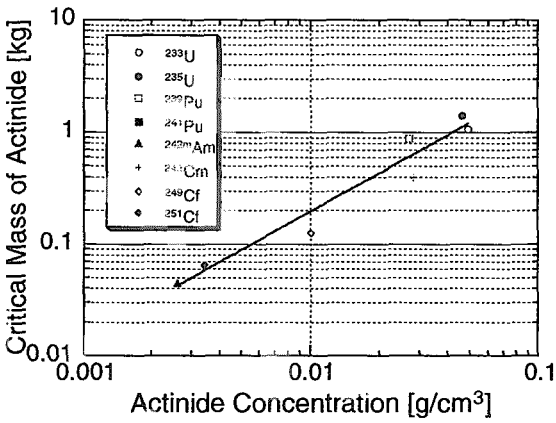

Fig.2. Relation between the minimum critical mass of eight actinides and the corresponding actinide concentration for the bare case.

Table II. The minimum critical and subcritical masses of eight actinides

Nuclide	Reflector	k_{eff}=1.0		k_{eff}=0.9		k_{eff}=0.8	
		Conc. [g/cm^3]	Mass [kg]	Conc. [g/cm^3]	Mass [kg]	Conc. [g/cm^3]	Mass [kg]
^{233}U	None	0.049	1.064	0.037	0.755	0.035	0.524
	Water	0.060	0.565	0.056	0.381	0.049	0.254
	SS	0.060	0.440	0.053	0.311	0.049	0.217
^{235}U	None	0.046	1.409	0.040	0.952	0.032	0.637
	Water	0.056	0.788	0.049	0.504	0.043	0.321
	SS	0.061	0.611	0.053	0.411	0.046	0.276
^{239}Pu	None	0.027	0.883	0.023	0.591	0.020	0.390
	Water	0.031	0.502	0.027	0.315	0.025	0.200
	SS	0.036	0.372	0.031	0.247	0.027	0.162
^{241}Pu	None	0.020	0.526	0.017	0.364	0.016	0.249
	Water	0.027	0.280	0.023	0.186	0.020	0.122
	SS	0.025	0.220	0.023	0.152	0.020	0.104
^{242m}Am	None	0.0026	0.045	0.0024	0.033	0.0020	0.024
	Water	0.0034	0.022	0.0031	0.015	0.0031	0.011
	SS	0.0034	0.019	0.0031	0.014	0.0029	0.010
^{243}Cm	None	0.028	0.391	0.028	0.298	0.022	0.224
	Water	0.041	0.186	0.039	0.135	0.036	0.098
	SS	0.041	0.155	0.036	0.117	0.034	0.088
^{249}Cf	None	0.010	0.126	0.008	0.097	0.007	0.073
	Water	0.013	0.059	0.012	0.046	0.012	0.032
	SS	0.013	0.052	0.012	0.040	0.010	0.031
^{251}Cf	None	0.0034	0.065	0.0031	0.048	0.0026	0.035
	Water	0.0041	0.033	0.0038	0.023	0.0034	0.016
	SS	0.0041	0.028	0.0038	0.020	0.0034	0.015

3.3 Comparison of NMF calculations based on various evaluated nuclear data files

To investigate the effect of the evaluated nuclear data, the neutron multiplication factor was calculated using ENDF/B-VI, JEF-2.2 and JENDL-3.3 (in the final preliminary version) instead of JENDL-3.2. The evaluated nuclear data were applied to (1) infinite media and (2) the critical sphere in (a) metal and in (b) a mixture of metal and water (only for fissiles). The results are shown in Table III. It is seen from this Table that the differences are small, maximum 2%, for the big three, however, they are sometimes larger for other nuclides.

3.4 Comparison of microscopic cross sections of ^{243}Cm

To clarify the reason of the differences in the results of the neutron multiplication factor (Table III), the microscopic capture and fission cross sections, and the number of neutrons induced per fission were compared (Fig. 3). For the well-moderated system of Cm concentration 0.03 gCm/cm^3, the neutron flux has a peak around 50 meV. The ENDF/B-VI has a smaller capture cross section and a larger fission cross section than the JENDL-3.2. Considering the differences with almost the same ν-values. The JEF-2.2 has a smaller fission cross section and a smaller ν-value with nearly equal capture cross section compares to the JENDL-3.2. These comparisons quantitatively explain that the k_{eff}'s of ENDF/B-VI are larger than those of and JENDL-3.2, and the k_{eff}'s of JEF-3.2 are smaller than those based on JENDL-3.2.

Table III. Comparison of k_{eff}'s for 10 fissionable nuclides based on different evaluated nuclear data files

Nuclide	Conc. [g/cm^3]	Radius [cm]	k_{eff}				Relative to JENDL-3.2 $\Delta k_{eff}/k_{eff}$ [%]		
			JENDL-3.2	ENDF/B-VI	JENDL-3.3 (pre.)	JEF-2.2	ENDF/B-VI	JENDL-3.3 (pre.)	JEF-2.2
U-233	18.76	6	1.037	1.016	1.028	N.A.	-2.0	-0.8	N.A.
		∞	2.550	2.563	2.560	N.A.	0.5	0.4	N.A.
	0.05	18	1.041	1.036	1.036	N.A.	-0.4	-0.5	N.A.
		∞	1.778	1.773	1.773	N.A.	-0.3	-0.3	N.A.
U-235	18.92	9	1.062	1.055	N.A.	N.A.	-0.7	N.A.	N.A.
		∞	2.287	2.279	N.A.	N.A.	-0.4	N.A.	N.A.
	0.05	20	1.045	1.033	N.A.	N.A.	-1.1	N.A.	N.A.
		∞	1.636	1.629	N.A.	N.A.	-0.4	N.A.	N.A.
Pu-239	19.85	5	1.008	1.010	1.009	1.006	0.2	0.2	-0.1
		∞	2.956	2.988	2.956	2.925	1.1	0.0	-1.1
	0.03	20	1.030	1.025	1.025	1.031	-0.5	-0.5	0.1
		∞	1.624	1.617	1.623	1.617	-0.4	-0.1	-0.4
Pu-238	19.77	5	1.066	1.019	1.039	1.040	-4.5	-2.6	-2.5
		∞	2.878	2.760	2.812	2.871	-4.1	-2.3	-0.2
Pu-241	20.02	6	1.049	1.028	1.050	1.026	-2.0	0.1	-2.2
		∞	2.910	2.919	2.912	2.738	0.3	0.1	-5.9
	0.02	20	1.065	1.075	1.065	1.070	0.9	-0.0	0.4
		∞	1.678	1.690	1.677	1.683	0.7	-0.1	0.3
Am-242m	13.72	6	1.025	N.A.	1.025	0.987	N.A.	-0.0	-3.7
		∞	3.250	N.A.	3.304	3.142	N.A.	1.6	-3.3
	0.003	16	1.049	N.A.	1.030	1.031	N.A.	-1.8	-1.7
		∞	2.027	N.A.	2.024	1.953	N.A.	-0.2	-3.7
Cm-243	13.45	6	1.058	1.107	1.190	1.158	4.7	12.5	9.5
		∞	3.553	3.577	3.488	3.653	0.7	-1.8	2.8
	0.03	15	1.029	1.163	1.001	0.895	12.9	-2.8	-13.0
		∞	2.118	2.335	2.107	1.863	10.2	-0.5	-12.0
Cm-244	13.51	9	1.084	1.113	1.107	1.064	2.7	2.1	-1.9
		∞	2.605	2.643	2.583	2.511	1.5	-0.9	-3.6
Cf-249	15.11	5	1.073	1.029	1.102	1.092	-4.1	2.7	1.8
		∞	4.040	3.678	3.979	4.185	-8.9	-1.5	3.6
	0.01	15	1.042	0.995	1.020	1.030	-4.5	-2.1	-1.2
		∞	2.190	2.103	2.187	2.183	-4.0	-0.1	-0.3
Cf-251	15.23	4	1.055	0.824	N.A.	0.825	-21.9	N.A.	-21.8
		∞	4.479	4.320	N.A.	4.319	-3.5	N.A.	-3.6
	0.003	18	1.036	1.120	N.A.	1.120	8.2	N.A.	8.1
		∞	1.824	1.975	N.A.	1.976	8.3	N.A.	8.3

N.A.: Not applied.
pre.: preliminary version

3.5 Validation of the method for ^{235}U, ^{239}Pu and ^{233}U critical systems

Validation of our criticality calculation method was made by analyzing 20 each evaluated critical experiments with various kinds of reflectors registered in the ICSBEP Handbook [4] for ^{235}U, ^{239}Pu and ^{233}U critical systems. The results showed that the bias from unity is less than 1%Δk.

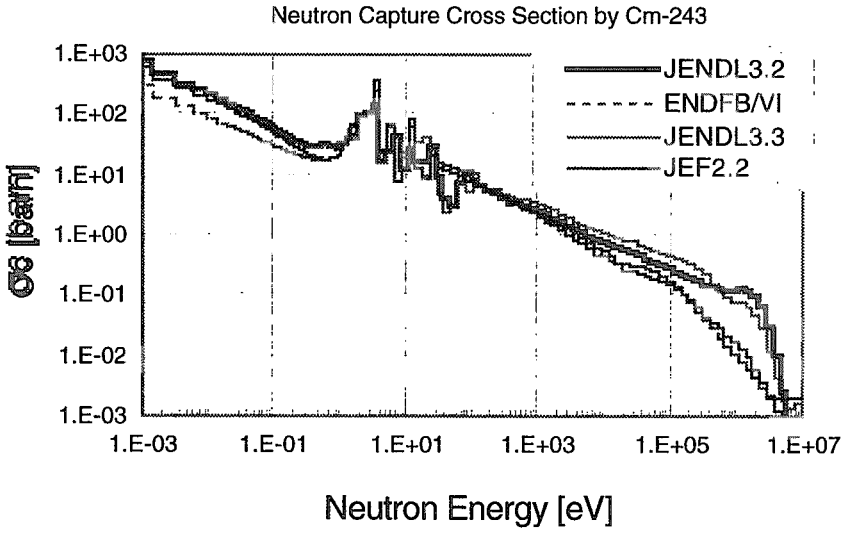

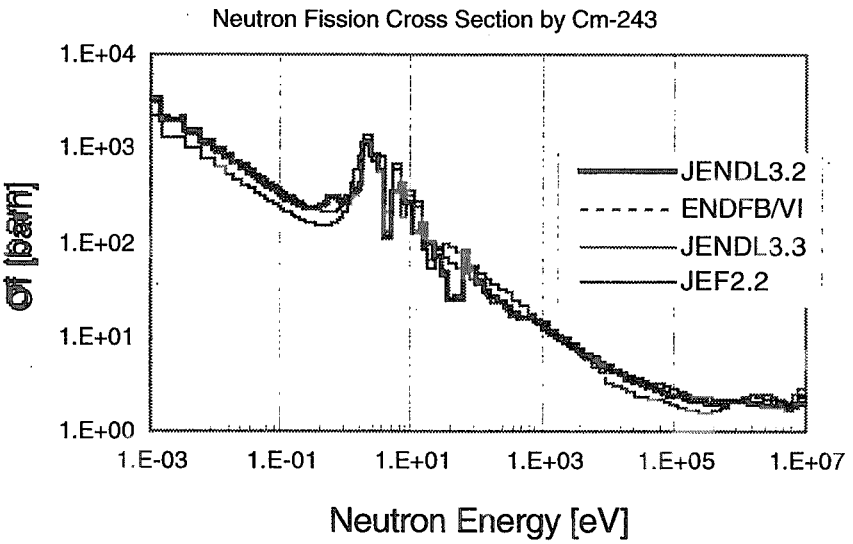

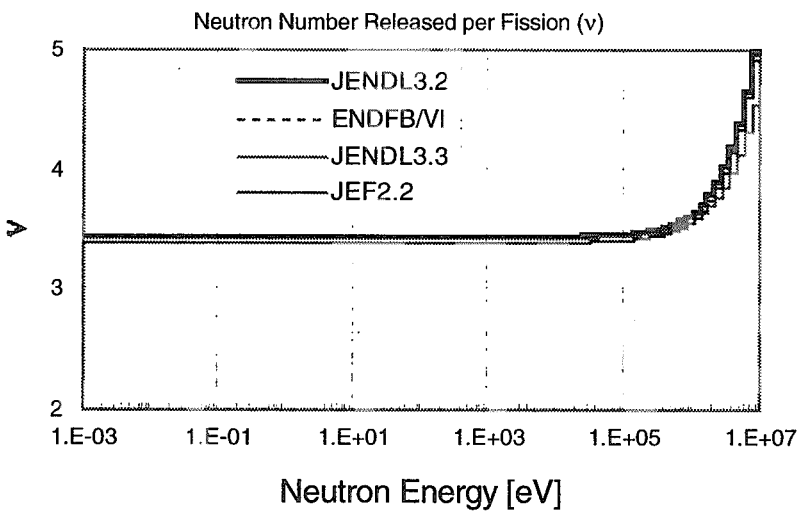

Fig. 3. Comparison of capture and fission cross sections, and number of neutrons released per fission.

3.6 Estimated critical and lower-limit critical masses of ^{235}U, ^{239}Pu and ^{233}U in a metal-water mixture

The estimated criticality multiplication factor was determined to 1.0045, 1.0019 and 1.0065 for ^{235}U, ^{239}Pu and ^{233}U, respectively, by the benchmark calculation as their corresponding average value. The estimated criticality lower limit multiplication factor was commonly set to 0.98. The estimated critical mass and estimated critical lower limit mass curves were drawn in Figs. 4 - 6 for a uniform homogeneous mixture of water and ^{235}U, ^{239}Pu and ^{233}U, respectively, in a sphere with a fully-thick water reflector. The minimum values of the curves are listed in Table IV in comparison with the subcritical mass limits of ANSI/ANS-8.1 [5] and other related values reported in [6].

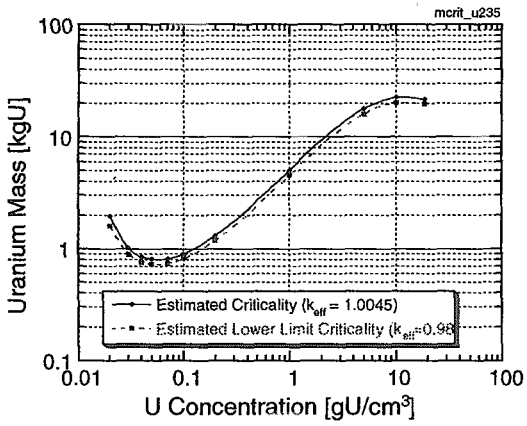

Fig. 4. The estimated critical and estimated critical lower limit masses of homogeneous ^{235}U-H_2O.

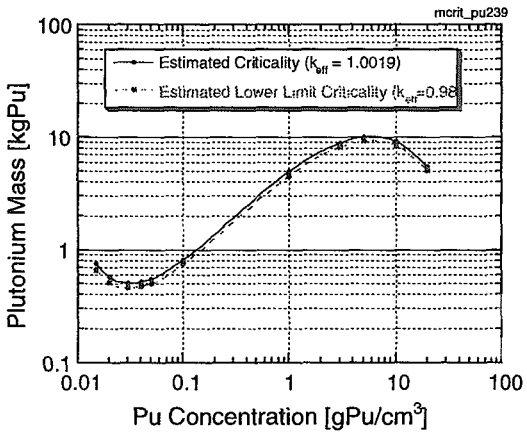

Fig. 5. The estimated critical and estimated critical lower limit masses of homogeneous ^{239}Pu-H_2O.

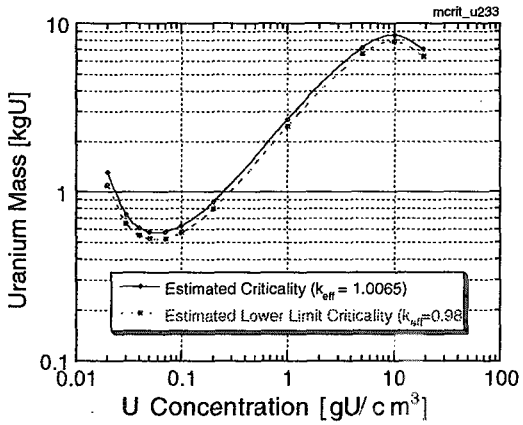

Fig. 6. The estimated critical and estimated critical lower limit masses of homogeneous ^{233}U-H_2O.

Table IV. Minimum of estimated critical mass (ECM) and estimated critical lower limit mass (ECLLM) for a homogeneous sphere of water mixture of ^{235}U, ^{239}Pu and ^{233}U with a fully-thick water-reflector, compared with subcritical mass limits [5] and related values [6]

Nuclide	Reflector			Note	Information Source
	None	Water	Iron or SS		
^{233}U	1.09	0.58	0.45	ECM	
	1.00	0.53	0.41	ECLLM	
		0.50		Subcritical mass limit	[5]
		0.55			Maubert[6]
	1.15	0.58			Trombay[6]
^{235}U	1.44	0.80	0.62	ECM	
	1.31	0.72	0.57	ECLLM	
		0.70		Subcritical mass limit	[5]
		0.81			Maubert[6]
	1.69	0.95			Trombay[6]
^{239}Pu	0.89	0.51	0.37	ECM	
	0.82	0.46	0.34	ECLLM	
		0.45		Subcritical mass limit	[5]
		0.51			Maubert[6]
		0.48			IPSN[6]
	1.00	0.56			Trombay[6]

4. CONCLUSIONS

In summary, critical and subcritical masses were calculated for 10 fissionable nuclides (^{233}U, ^{235}U, ^{239}Pu, ^{238}Pu, ^{241}Pu, ^{242m}Am, ^{243}Cm, ^{244}Cm, ^{249}Cf, and ^{251}Cf) with a combination of JENDL-3.2 and MCNP-4B2. Other nuclear data produced several % different values for the neutron multiplication factor even of metal in infinite media.

REFERENCES

[1] I.C. Gauld and J.C. Ryman, "Nuclide Importance to Criticality Safety, Decay Heating, and Source Terms related to transport and Interim Storage of High-Burnup LWR Fuel," NUREG/CR-6700, ORNL/TM-2000/284 (2001).

[2] R.M. Westfall, *private communication.*

[3] C.T. Rombough, S.H. Martonak and N.L. Pruvost, *ANS Trans.* **76**, 197 (1996).

[4] "International Handbook of Evaluated Criticality Safety Benchmark Experiments," NEA/NSC/DOC(95)03, September 2000 Edition (2000).

[5] "Nuclear Criticality Safety in Operations with Fissionable Material Outside Reactors," ANSI/ANS-8.1-1998 (1998).

[6] J. Anno and G. Sert, "French Participation at ANS/ANSI 8/15 Working Group Updating Criticality Data on ^{237}Np. Criticality & Transportation Proposals," Proc. of ICNC'99 (1999).

JP0250334

JAERI-Conf 2002-004

Current Status of Criticality Safety Benchmarks for Single Core Composed of Low Enriched Uranyl Nitrate Solution using STACY

Yoshinori MIYOSHI and Toshihiro YAMAMOTO

Japan Atomic Energy Research Institute, Department of Fuel Cycle Safety Research,
2-4 Shirakata Shirane, Tokai-mura, Naka-gun, Ibaraki-ken 319-1195 JAPAN
Fax: 81-29-282-6798, miyoshi@melody.tokai.jaeri.go.jp

Criticality experiments using 10% enriched uranly nitrate solutions have been performed at the STACY facility of NUCEF since the first criticality in 1995. The criticality data of the STACY that were published in the ICSBEP handbook contribute to diminishing the shortage of low enriched uranium solution criticality data. The temperature coefficients of reactivity of low enriched uranyl nitrate solution were measured at the STACY. The measured reactivity coefficients in the 600mm-diameter and the 800mm-diameter core tanks are -4.1 ¢ /°C and -3.0 ¢ /°C, respectively. Kinetic parameters β_{eff}/λ were measured by using the pulsed neutron method, the reactor noise analysis methods. The reactivity effects of reflector materials (concrete and polyethylene) were measured by the difference of the critical solution heights.

Key words: STACY, criticality, benchmark, temperature coefficient of reactivity, reflector, kinetic parameter

1. INTRODUCTION

From the view point of criticality safety for nuclear facilities related to the nuclear fuel cycle in Japan, experimental criticality data on low enriched uranyl nitrate solution and plutonium nitrate solution are especially needed for verification of criticality safety evaluations. Since the initial criticality in 1995, a series of experiments have been performed to procure criticality data on 10 % enriched uranyl nitrate solution for single core system at the Static Criticality Experimental Facility, STACY[1,2]. Critical solution height, neutron flux distribution and kinetic parameters were obtained with three core tanks with changing the uranium concentration between 170 gU/l and 460 gU/l. The diameters of two cylindrical tanks were 60 cm and 80cm, respectively. The thickness and width of a slab tank were 28 cm and 70 cm, respectively. Through these criticality experiments, important parameters related to criticality safety such as kinetic parameters and the effect of reflector materials have been measured. This paper describes how the experimental data of STACY contribute to benchmark in the criticality safety related issues.

2. CRITICALITY BENCHMARK DATA OF STACY

Criticality benchmark data on low-enriched uranium solutions had been insufficient since

This paper includes the result of experiment performed under the contract with the former Science and Technology Agency of Japan

most existing criticality data of uranium solutions are for high-enriched uranium. The criticality experiments at STACY started in 1995 to obtain criticality benchmark data of low-enriched uranium and plutonium solutions that are usually handled in a commercial reprocessing plant. As of yet, using a 10wt% enriched uranly nitrate solution, criticality experiments have been performed and criticality data usable for verifications of criticality safety analysis methods have been accumulated. Figure 1 shows the schematic view of the reactor room of STACY. The core tanks are installed in a water-reflector pool tank. Therefore, criticality experiments in a fully water-reflected condition is possible in addition to a bare condition.

We have participated in the International Criticality Safety Benchmark Evaluation Project

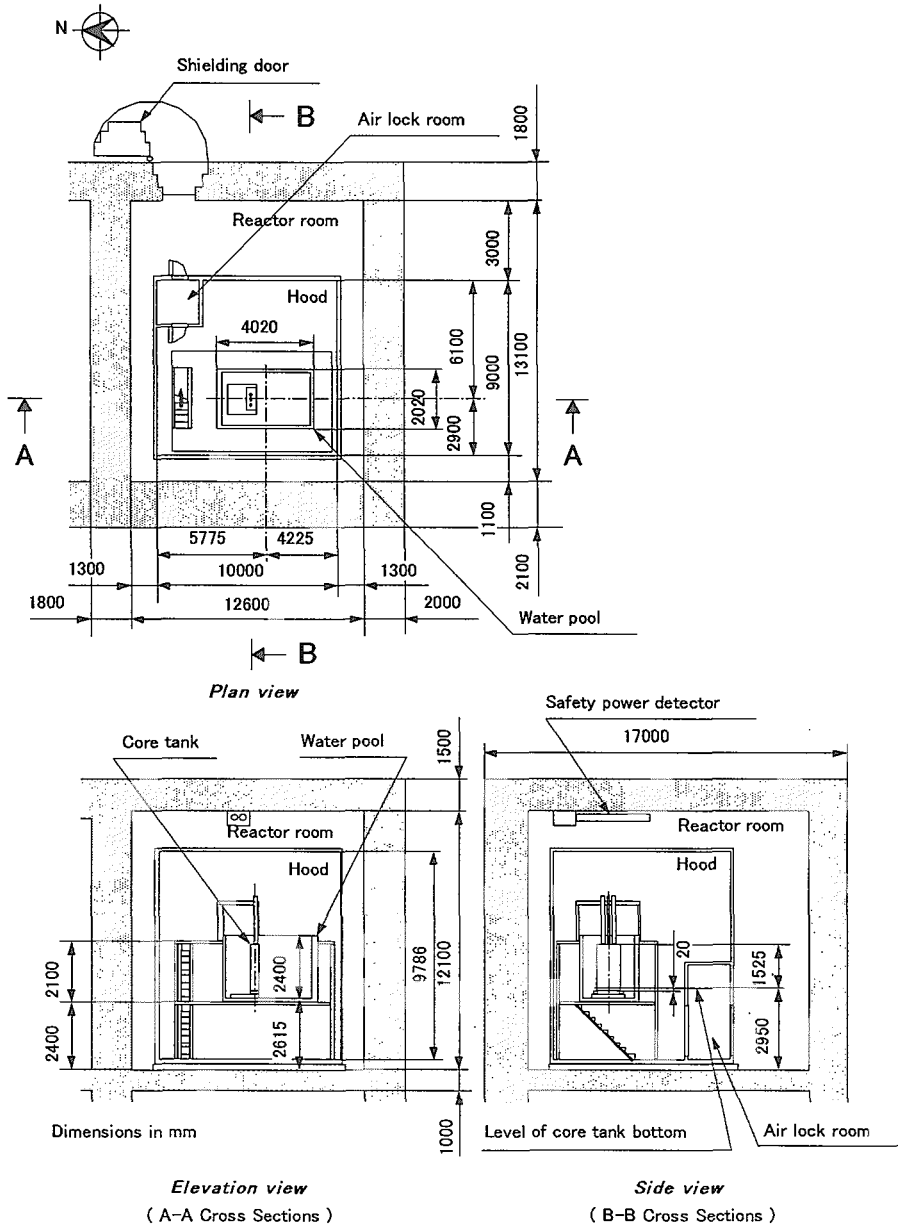

Fig.1 Schematic view inside STACY reactor room

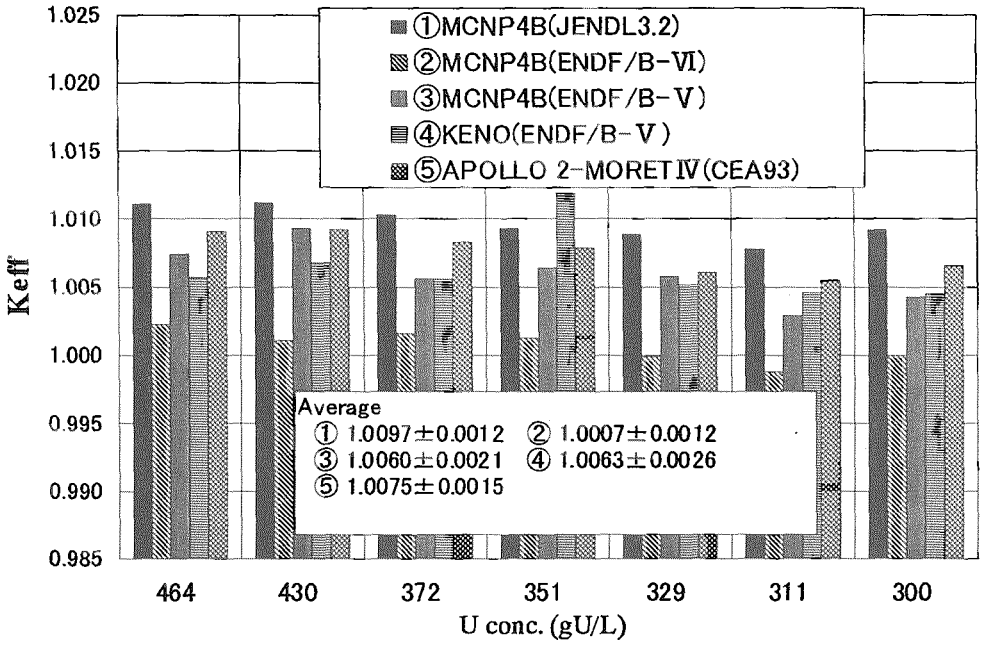

Fig.2 Calculation Results for STACY Benchmark Model

(ICSBEP) of OECD/NEA since the beginning of this project. The criticality data obtained at STACY have been carefully evaluated based on the benchmark evaluation method of the ICSBEP [3]. In the latest "International Handbook of Evaluated Criticality Safety Benchmark Experiments" published by the ICSBEP, 56 out of totally 77 evaluated criticality configurations of low-enriched uranium solutions stem from the STACY experiments. The experimental data of STACY have contributed to alleviating the world's lack of low-enriched solution criticality date. Figure 2 shows the calculated keff's by several calculation codes for the benchmark model of the STACY criticality experiments that was obtained at the water-reflected 280 cm-thickness slab core tank. This figure indicates that JENDL-3.2 gives higher keff's as much as 1%. Through the series of the STACY experiments, it is found that the overestimations of keff's by JENDL-3.2 may be mostly attributed to the evaluations of ^{235}U and ^{14}N. These two nuclides are to be revised in the release of JENDL-3.3. The comparisons of keff's calculated by JENDL-3.2 and JENDL-3.3 (preliminary evaluation) are shown in Fig. 3 [4]. These calculations were performed for the STACY experiment with the water-reflected 600-mm-diameter core tank. The reevaluation of ^{235}U and ^{14}N in JENDL-3.3 largely improved the calculated keff's.

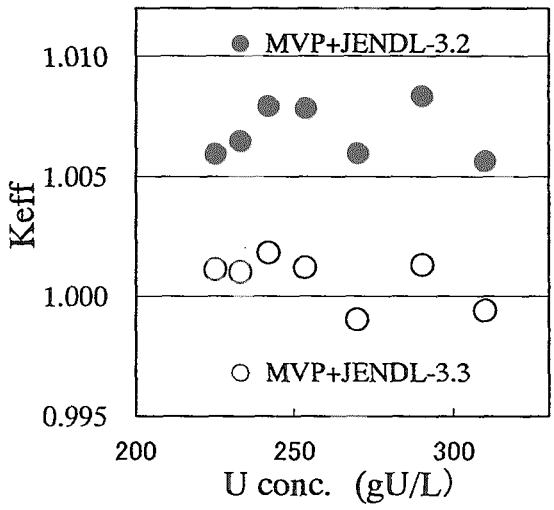

Fig.3 Comparison of JENDL-3.2 and JENDL-3.3

3. MEASUREMENTS OF KINETIC PARAMETERS

Very few measurements of kinetic parameters such as β_{eff}/λ (β_{eff} : effective delayed neutron fraction, λ : prompt neutron life time) of low-enriched uranium solutions, which are important for criticality accident analyses, have been reported in the world. At the STACY facility, β_{eff}/λ were measured with several techniques such as pulsed neutron method, reactor noise method, and the Bennet method [5]. Taking account of many aspects regarding operation conditions and S/N ratio, systematic measurements were performed mainly with the pulsed neutron method for wide range of uranium concentrations.

A pulsed neutron source (PNS), neutron counters and multichannel scalars (MCSs) were used for the measurements. The MCSs were synchronized with the PNS. The PNS fires neutrons, which are generated by D-T fusion reactions, every 50 msec. The burst width of each fire was less than 10 micro second. Neutron counters are B-10 proportional counters and located outside the core tank as well as the PNS. If water reflector was used, the PNS and the counters were submerged in the water. In the case of bare core, polyethylene moderators were attached to the PNS and the counters. After the criticality state was achieved, measurement of the PNS method was repeated at several subcritical solution levels. To evaluate the prompt neutron decay constant, an exponential decay function:

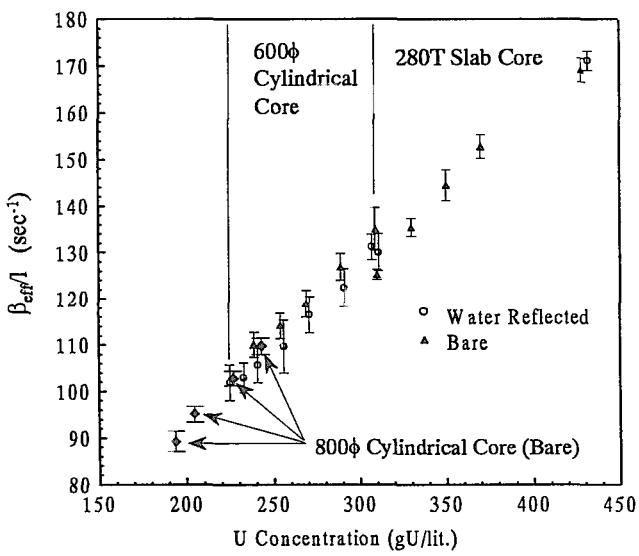

Fig. 4 Measured β_{eff}/λ vs. Uranium Concentration

$$n = C\exp(-\alpha t) + B \qquad (1)$$

was fitted on to the measured decay and the decay time constant α (sec^{-1}) was determined for each signal channel and for each subcritical condition. The α values were averaged over the signal channels. The β_{eff}/λ value of each solution condition were determined by extrapolation of the linear relation between the subcriticalities and the decay time constants to the critical condition. The values of β_{eff}/λ measured at 600-mm-diameter and 800-mm-diameter cylindrical core tanks and 280-mm-thickness slab core tank are shown in Fig. 4 as a function of uranium concentration.

Using the perturbation calculation capability of SRAC code system [6], the analyses for these measurements of β_{eff}/λ were performed. β_{eff} and λ were calculated by SRAC-CITATION code and JENDL-3.2. The calculated β_{eff}/λ agreed with the measurements within experimental uncertainties.

4. MEASUREMENTS OF TEMPERATURE COEFFICIENT

A temperature coefficient of reactivity of a solution fuel is a main parameter that affects the transient behavior in case of criticality accident. The verification of temperature coefficient that is used for a criticality accident analysis is important to assure the reliability of the accident analysis. The temperature coefficients of solution fuel, however, have never been reported throughout the world. At the STACY facility, reactivity effects due to the change in fuel temperature were measured with two cylindrical cores of 600 mm and 80 mm in diameter, which contain 10% enriched uranyl nitrate solution. Uranium concentrations in these experiments were about 254 gU/L and 201 gU/L, respectively. Fuel solution was heated in a dump tank at first, and core tank and feed line were also heated before feeding the fuel solution from the dump tank. Three divided electric heater and an annular type insulator were located on the side wall of the core tank. Temperature distribution along the axial direction was measured with a thermometer attached to the driving mechanism which was inserted in the core tank. From the change of the critical solution height with fuel temperature, the reactivity effect of temperature was evaluated from the differential worth of the solution height. Differential reactivity of fuel solution height was measured with a digital reactivity meter.

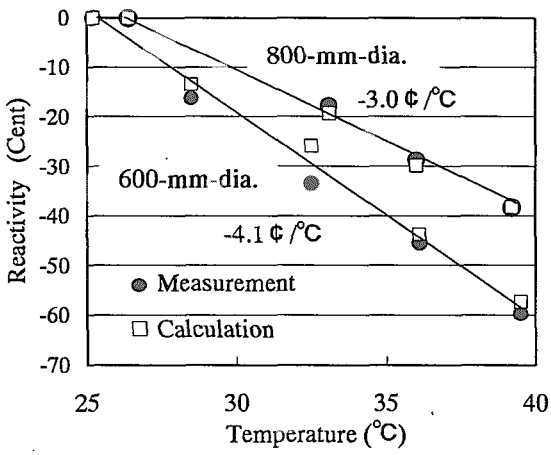

Fig.5 Calculated and Measured Reactivity Due to Temperature Change

The experimental analyses were performed using SRAC code system and JENDL-3.2. The density change due to the temperature rise was obtained by the density formula developed by Sakurai [7]. The temperature coefficients were calculated by a discrete ordinates transport code TWODANT [8] and 24-group macroscopic cross sections. The measured and calculated results of reactivity effect of fuel temperature for two cylindrical cores are shown in Fig. 5. The first-order temperature coefficients measured at the 600-mm-diamete and the 800-mm-diameter core tanks were -3.0 cent / °C and -4.1 cent / °C, respectively. The calculated coefficients agreed with measurements within 3%.

5. REFLECTOR EFFECTS OF STRUCTURL MATERIALS

Reflector effects of structural materials in a nuclear fuel facility affect the criticality. To enhance the reliability of criticality analysis method including the reflecting materials, the reflector effects of polyethylene and concrete were measured at STACY. The 600-mm-diameter core tank was surrounded by annular geometry reflectors. The 280-mm-thickness slab core tank was sandwiched on the both sides by slab geometry

reflectors. The critical solution fuel heights were measured with and without the reflectors. The reactivity effects of the reflectors were measured by the difference of the critical solution heights. The distributions of the neutron flux and the neutron spectrum index were measured for the validations of the analysis methods as well. The measurement results for the 280-mm-thickness slab core tank are shown in Fig. 6. It was found that the reactivity effects saturate beyond the thicknesses of 5 cm polyethylene and 20 cm concrete. The saturated reactivity effect of the concrete is 1.8 times as large as that of the polyethylene. The reactivity effects were calculated by SRAC-TWOTRAN and JENDL-3.2. The calculation underestimates the saturated reactivity of the concrete by 0.2%Δk/k and, on the contrary, overestimates the polyethylene slightly. Relatively good agreements between the measurements and calculations, however, might be observed.

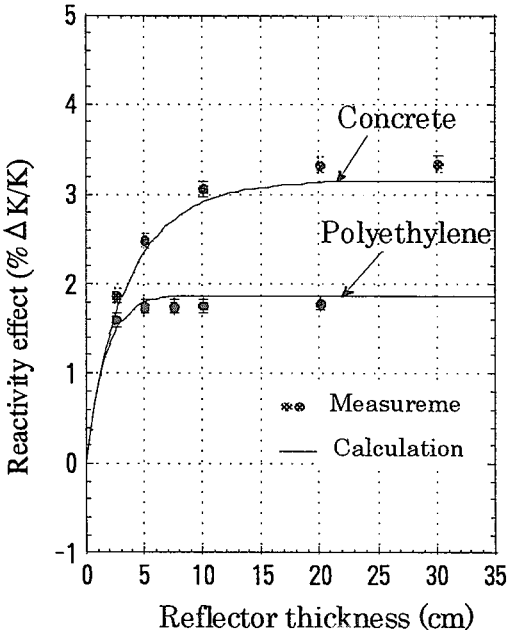

Fig.6 Reactivity Effect of Concrete and Polyethylene Reflectors

Critical configurations of the 600-mm-thickness cylindrical tank and the 280-mm-thickness slab tank with the reflectors (polyethylene, concrete, borated concrete) were evaluated as the criticality benchmark. These evaluations are published in the handbook of the ICSBEP.

6. FUTURE PROJECTS

A series of critical experiments on neutron interaction system composed of 35-cm-thickness slab core tanks started in 1999 in order to confirm the criticality safety design method for multiple unit system. Figure 7 is an anomalous example of Monte Carlo calculation for weakly interacting STACY core tanks. The ratio of fission source in symmetric core tanks, which is supposed to be unity, deviates far away from unity with 30-cm-thickness concrete. The neutron interaction effect between two tanks through various isolation materials (polyethylene and concrete) is now being studied.

Experiments on heterogeneous system simulating a dissolving process will start in 2002. Criticality benchmark data in a heterogeneous geometry simulating a dissolving process are very limited in the world [9]. It is, however, pointed out that the existing criticality data are not available for benchmark since the criticality data has devastating contradictions [10]. Therefore, the experiments of the heterogeneous system that are being planned at STACY will provide the significant benchmark data for a dissolver condition. PWR type fuel rods are arrayed in a 600-mm-diameter cylindrical tank containing 6% enriched uranyl nitrate solution.

Three grid plates having different lattice pitches are prepared for changing the volume ratio of fuel solution to fuel pellet. Reactivity effects of gadolinium as soluble poison will be measured from the change of critical solution heights. Furthermore, to investigate the neutron absorption effect of fission product elements in a criticality safety design of a dissolving process, fission product elements (Eu, Cs, Sm, Nd etc.) will be dissolved in the solution fuel and the criticality data will be measured. The criticality data will be useful for validation of criticality safety analysis methods of dissolver including the fission product elements.

Critical and subcritical experiments on plutonium solution system are scheduled after 2005. Main solution parameters are concentration of plutonium and uranium, acid molarity and concentration of soluble poison. Three cylindrical tanks will be mainly used in the benchmark experiments for single core configuration. The maximum concentration plutonium and uranium is 300 g/L. The contents of Plutoinum-240 is approximately 25%, which corresponds to the composition of typical LWR spent fuel. In the series of the experiment, a positive temperature coefficient of very dilute plutonium solution will be demonstrated experimentally.

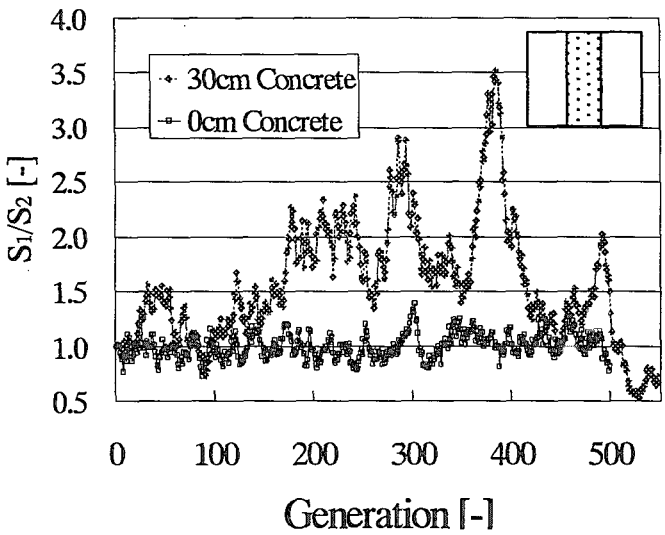

Fig. 7 Fission source ratio in each generation with and without concrete isolator

REFERENCES

[1] Y. Miyoshi, "Critical Experiments on Low Enriched Uranyl Nitrate Solution with STACY," *Proc. 1st NUCEF Int. Symposium*, JAERI-Conf 96-003,102 Japan Atomic Energy Research Institute (1996).

[2] Y. Miyoshi *et al.*, "Critical Experiments on 10% Enriched Uranyl Nitrate Solution using 60-cm Diameter Cylindrical Core," *Nucl. Technol.*, Vol. 118, No.1, 69 (1997).

[3] J.B.Briggs *et al.*, "Status of the International Criticality Safety Benchmark Evaluation Project," *Proc. 6th Int. Conf. Nucl. Criticality Safety*, Versailles, France, Sept. 20-24, 1999, 140 (1999).

[4] K.Okumura, private communications.

[5] K.Tonoike *et al.*, "Kinetic Parameter β_{eff}/λ Measurement on Low Enriched Uranyl Nitrate Solution with 600 ϕ Cylindrical Core of STACY," *Proc. 6th Int. Conf. Nucl. Criticality Safety*, Versailles, France, Sept. 20-24, 1999, 1215 (1999).

[6] K.Okumura *et al.*, "SRAC95; General Purpose Neutronics Code System," JAERI-Data/Code 96-015 (1996) [in Japanese].

[7] S.Sakurai *et al.*, "Density Equation of Aqueous Solution Containing Plutonium (IV), Uranium (VI) and Nitric Acid," *J .Nucl. Sci. Technol*, Vol.33, No.2, 187 (1996).

[8] R.E.Alcouffe *et al.*, "DANTSYS: A Diffusion Accelerated Neutral Particle Transport Code System," LA-12969-M, Los Alamos National Laboratory (1995).

[9] R.C.Lloyd *et al.*, "Criticality of 4.3wt% Uranium-235 Enriched UO_2 Rods in Uranly Nitrate Solution Containing Gadolinium," *Nucl. Sci. Eng.*, **78**, 121 (1981).

[10] H.Okuno *et al.*, "Benchmark Calculations of JACS Code System for the Criticality Experiment of Pellet-Solution Coexisting Low-enriched Uranium Fuel," JAERI-Data/Code 94-014, Japan Atomic Energy Research Institute (1994) [in Japanese].

JP0250335

JAERI-Conf 2002-004

STUDY ON RELEASE BEHAVIOR OF RADIOACTIVE NOBLE GASES AND IODINE SPECIES FROM FUEL SOLUTION UNDER SIMULATED NUCLEAR CRITICALITY ACCIDENT

Hitoshi ABE, Shinsuke TASHIRO, Tadao KOIKE, Seigo OKAGAWA and Ginzo UCHIYAMA
Japan Atomic Energy Research Institute
Tokai-mura, Naka-gun, Ibaraki-ken, 319-1195 JAPAN
Fax : +81.29.282.5745, E-mail : abe@aero.tokai.jaeri.go.jp

To estimate confinement capability into the facility for the volatile fission products, such as noble gases and iodine species, which have a possibility of affecting serious public dose, under the nuclear criticality accident in the fuel solution, release and transport behavior of the radiolysis gases and the radioactive materials under the simulated criticality accident in the fuel solution has been examined by using NUCEF–TRACY. As the results, G-value of release of the hydrogen, one of the radiolysis gases, was estimated about 0.8 molecules/100 eV by observing relationship between the energy release from fissions and released molecules of the hydrogen. At 4.5 h after the transient criticality, the release ratio of the iodine species were about 0.2% in case that the transient rod was re-inserted to the solution just after transient criticality and about 0.9 % in case that the rod was not re-inserted. The release coefficient and release ratio for Xe-141 were estimated and correlation between the values and inverse period was observed. It was proved that the release ratio of Xe-141 from the solution was over 90 % in case that the inverse period was over about 100 1/s.

Key words: Fuel solution, Criticality accident, Radioactive materials, Confinement, Fuel reprocessing plant

1. INTRODUCTION

In nuclear criticality accident in the fuel solution, it is considered that radiolysis gases and radioactive materials (fission products) are released from the solution to outside of the facility. Since radioactive noble gases and iodine species in the fission products have relatively high volatility, release ratio of the nuclides is larger than the ratio of the other non-volatile nuclides. Therefore, quantitative estimation data about release behavior of the volatile nuclides are very important for the accurate and rapid evaluation of the accident and public dose. In NRC Regulatory Guide 3.33 (NRC 1977) [1], the release ratios of the noble gases and iodine species, under the inadvertent nuclear criticality accident in a uranium fuel reprocessing plant, were assumed as 100% and 25%, respectively. However, since these values were quoted from the Regulatory Guide 1.3 [2], which referred to the loss of coolant accident for boiling water reactors, it is considered that safety margin is included in the values in the Regulatory Guide 3.33. In Japan Atomic Energy Research Institute (JAERI), to verify the confinement capability for the radioactive materials in the ventilation system in the facility and the safety margin for the values adopted in the safety evaluation of the facility, release and transport behavior of the radioactive materials and the radiolysis gases (e.g. hydrogen) under the simulated criticality accident in the fuel solution has been examined by using NUCEF (Nuclear Fuel Cycle Safety Engineering Research Facility) - TRACY (Transient Experimental Critical Facility). Furthermore, the release properties, such as release ratio (%) and release coefficient (1/s) for the radioactive

nuclides and G-value of release for hydrogen from the solution, have been evaluated quantitatively. In the present paper, perspective of the TRACY experiments including the experimental methods and evaluation results about the release properties of the compounds from the solution are reported.

2. EXPERIMENTAL

2.1 Experimental devices

The block diagram of TRACY is shown in Fig. 1. TRACY is a transient criticality experimental facility for studying the transient criticality characteristics of low-enriched uranium fuel solution (enrichment : 10 %). The characteristics are investigated under the various conditions of the excess reactivity and reactivity addition rate. The maximum total fission in TRACY is 10^{18}. TRACY has an annular type core tank with 10 cm inner diameter, 50 cm outer diameter and 200 cm height. Volumes of the gas phase and the fuel solution phase in the tank are almost 0.27 m^3 and 0.12 m^3, respectively. There is a vent-gas line connected to the tank and the vent-gas circulates through the line. The radioactive materials and radiolysis gases, released from the fuel solution to the gas phase, effuse into the line during the transient criticality. The vent-gas line is equipped with a dilution tank (11 m^3) as a large volume element. Total volume of the line is almost 11.5 m^3 including the dilution tank.

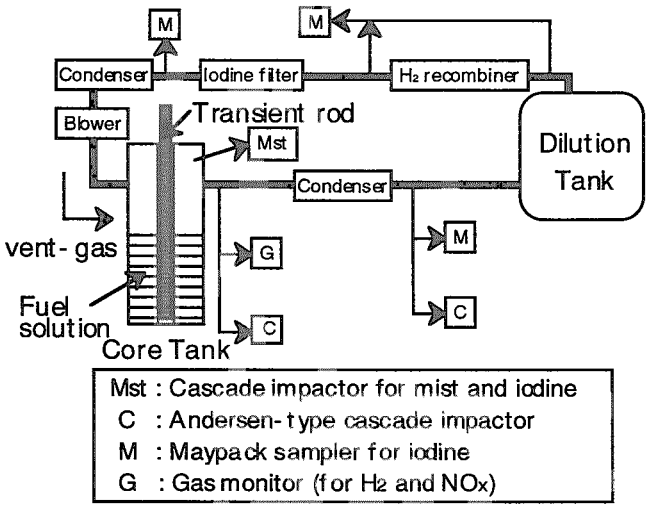

Fig. 1 Block diagram of TRACY

To observe release and transport behavior of the radioactive materials and the radiolysis gases, the core tank and the line are equipped with cascade impactors (Mst and C) and maypack samplers (M) for collecting radioactive aerosol and iodine and gas concentration measurement devices for measuring radiolysis gases. The Mst sampler consists of one membrane filter and four stage impactors for collecting the mist with liquid collector and the C sampler consists of one membrane filter and seven stage impactors without that. The M sampler consists of one membrane filter and iodine collection filter element, such as five silver plated fibrous filters (for inorganic iodine species), two silver nitrate impregnated alumina beds (for organic iodine species). The Mst and C samplers were also equipped with the iodine collection filter element. After sampling, the respective samplers were taken apart to each component and the radioactivity of the collected nuclides in the components were determined by gamma-ray spectrum analysis and corrected to those at the respective sampling times by the decay correction calculation by using JNDC nuclear data library [3]. Moreover, the quantities of the nuclides in the fuel solution before and after the each experiment were also determined by gamma-ray spectrum analysis. In the present study, release behavior of radioactive noble gases from the fuel solution to the gas phase was evaluated by using the data of the nuclides in the fuel solution.

2.2 Experimental conditions

Initial concentrations of uranium and nitric acid in the fuel solution were about 400 g/dm^3 and 0.7 mol/dm^3, respectively. The volume flow rate of the vent-gas was about 0.27 m^3/min. To collect radioactive iodine that is emerged from the fuel solution with a time lag, the fuel solution had been kept in the core tank for 5 hours after the transient criticality.

In TRACY, reactivity can be added to the fuel solution by different three reactivity addition modes, which are ramp withdrawal (RW) mode of a transient rod (variable withdrawal rate), pulse withdrawal (PW) mode of the rod and ramp solution addition mode. In the present study, the former two modes have been considered. Furthermore, to observe effect of the temperature of the solution and increase of the surface area between gas and solution phases with producing the radiolysis gas in the solution on the release behavior of the iodine species, two operations for the PW mode, in which the transient rod was re-inserted in the solution just after the transient criticality and the rod was not re-inserted for the 5 hours after withdrawal of the rod, were conducted. The fission rate oscillated with time and several fission peaks occurred for several minutes for the RW mode, whereas one sharp fission peak with a few milliseconds wide was observed for the PW mode. In case that the transient rod was not re-inserted, the fission rate decreased with time after divergence, attained minimum value at almost 2,000 s after the withdrawal of the rod and, after the minimum point, increased again and oscillated with time. In the present study, reactivity addition was varied from 0.7$ to 2.9$ as a parameter under the PW and RW modes.

3. RESULTS AND DISCUSSIONS

3.1 Release behavior of hydrogen from the fuel solution

The hydrogen concentration in the vent-gas attained to the peak just after the transient criticality and decreased exponentially with time. Fig. 2 shows the relationship between the energy caused by fission and the released volume of hydrogen from the TRACY core tank to the vent-gas line. The former was calculated by using 3.2×10^{-11} J/fissions and the latter was calculated by integrating release rate of hydrogen for 1,000 s after the transient criticality. This time width almost corresponds to the width of the first main peak of the hydrogen concentration. The plus and linear correlation were observed between the both values and the slope, in other word, G-value of release of the hydrogen could be estimated about 0.8 molecules/100 eV. In the CRAC experiments, which had been executed in France, 0.6 molecules/100 eV was reported as the value [4]. The value in the present study was approximately 30 % larger than the CRAC results.

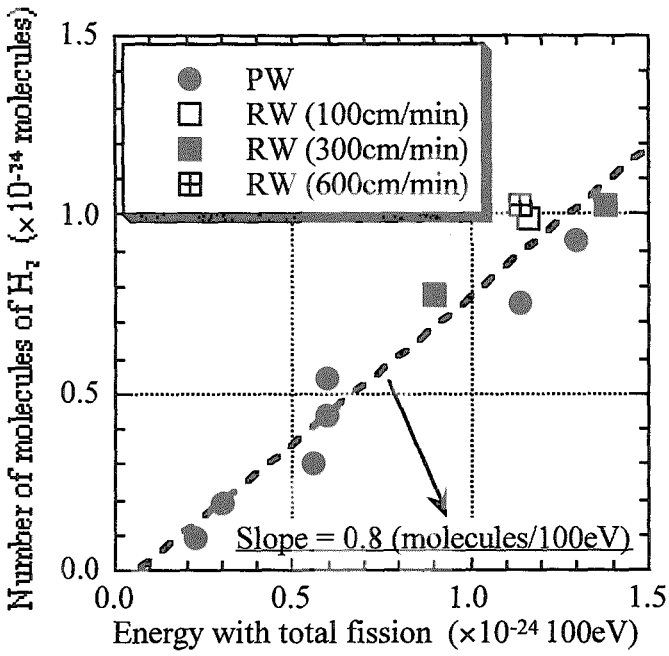

Fig. 2 Relationship between energy with total fission and number of hydrogen released from fuel solution

3.2 Release behavior of iodine species

The concentrations of I-131 and I-133 in the gas phase of the core tank began to increase with a time lag of several minutes from the transient criticality and attained approximately constant values. In the present study, release ratio of the volatile nuclides, such as iodine species and noble gas in the fission products, from the fuel solution to the gas phase in the TRACY core tank was estimated by using the following calculation model. In the model, it was assumed that the volatile nuclides are released from the fuel solution to the gas phase with release coefficient, ξ (1/s), and it is effused from the gas phase to the vent-gas line, with dilution coefficient, ψ (1/s), on the basis of the dilution effect of the vent-gas. By using these coefficients and radioactive decay constant, λ (1/s), of the each nuclide, the variation with time of the number of the each nuclide in the fuel solution and the gas phase of the core tank was calculated by solving the following differential equations simultaneously.

(in the fuel solution)

$$dP_{sol}/dt = Fs \times \eta_P + \kappa_{P'} \times \lambda_{P'} \times P'_{sol} - \lambda_P \times P_{sol} \quad (1)$$

$$dX_{sol}/dt = Fs \times \eta_X + \kappa_P \times \lambda_P \times P_{sol} - (\lambda_X + \xi_X) \times X_{sol} \quad (2)$$

$$dD_{sol}/dt = Fs \times \eta_D + \kappa_X \times \lambda_X \times X_{sol} - \lambda_D \times D_{sol} \quad (3)$$

(in the gas phase in the core tank)

$$dX_{gas}/dt = \xi_X \times X_{sol} - (\lambda_X + \psi) \times X_{gas} \quad (4)$$

$$dD_{gas}/dt = \kappa_X \times \lambda_X \times X_{gas} - (\lambda_D + \psi) \times D_{gas} \quad (5)$$

where, Fs (fissions/s) is fission rate and κ (-) is branching fraction. The subscripts P, X and D mean the values of parent nuclides (P' means parent nuclides of the P), remarkable volatile nuclide (I-131, I-133 or Xe-140, Xe-141) and daughter nuclides and sol and gas mean the values in the fuel solution and in the gas phase of the core tank, respectively. The time-integrated numbers of the X atom in the both phases were also calculated by omitting decrease of the number of the X atom or dilution effect by the vent-gas and the release ratio of the X atom, R_X (%), from the fuel solution to the gas phase was calculated by solving the following equations simultaneously.

(in the fuel solution)

$$dX^*_{sol}/dt = Fs \times \eta_X + \kappa_P \times \lambda_P \times P_{sol} \quad (6)$$

(in the gas phase in the core tank)

$$dX^*_{gas}/dt = \xi_X \times X_{sol} \quad (7)$$

(release ratio of the X atom from the fuel solution to the gas phase)

$$R_X = (X^*_{gas}/X^*_{sol}) \times 100 \quad (8)$$

where, the asterisk means the time-integrated numbers of the X atom. The R_X means the ratio of total release numbers to the total produced numbers of the X atom.

It is assumed that the time variation between the measuring points of the numbers of iodine atom in the gas phase of the core tank (I_{gas}), corresponding to the X_{gas}, can be represented as the following equations.

$$X_{gas}(=I_{gas}) = \alpha \times \exp(\beta \times t) \quad (9)$$

$$dX_{gas}/dt = \alpha \times \beta \times \exp(\beta \times t) \quad (10)$$

And the release coefficient, ξ_X, can be represented by combined the above equations as follows.

$$\xi_X = \alpha \times \beta \times \exp(\beta \times t) \times (\beta + \lambda_X + \psi)/X_{sol} \quad (11)$$

At first, α (-) and β (-) were estimated from relations between time and the relative measuring points of numbers of iodine atom, next, the release coefficients of iodine (ξ_I) in the relative measuring points was calculated by using equation (11). Moreover, the release ratio of iodine (R_I) was estimated by solving from equation (1) to (8) simultaneously by Runge-Kutta-Gill method. As the nuclear data, such as the η and λ, the respective values in JNDC nuclear data library [3] were used. The ψ was measured in an experiment using the mock-up vessel that has the same dimension and ventilation flow as the TRACY core tank and could be estimated as 0.016 1/s.

Examples of the evaluation results of the release ratio of I-133 were shown in Fig. 3. The tendency of the time dependencies of the evaluated release ratio for I-131 and I-133 was almost same. At 4.5 h after the withdrawal of the transient rod, the release ratio of the iodine species were about 0.2% in case that the transient rod was re-inserted to the solution just after transient criticality and about 0.9% in case that the rod was not re-inserted. Temperature of the solution and hydrogen concentration in the vent-gas, effused from gas phase of the core tank, for the later case were 1.7 and 4.1 times as high as the values for the former case, respectively. Therefore, it was attributed that the release ratio for the latter case was higher than the former case because the temperature of the solution in the latter case had been sustained relatively high and the surface area between gas and solution phases increased with producing the radiolysis gases in the solution.

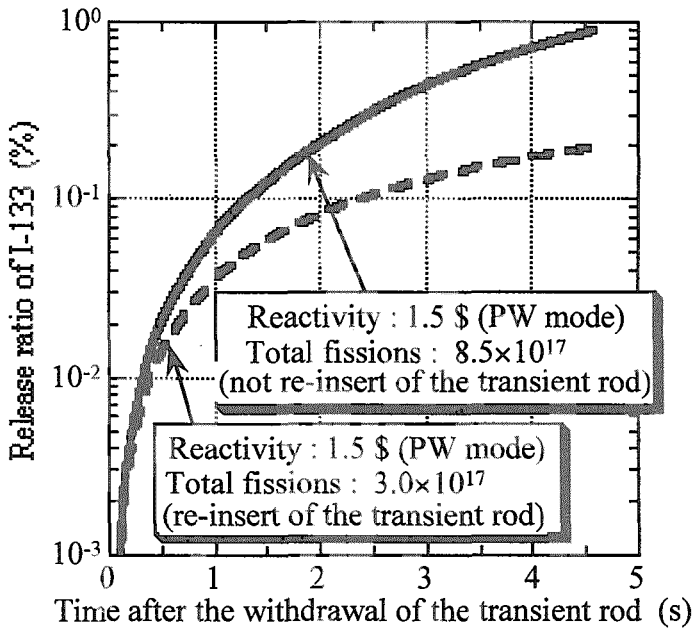

Fig. 3 Examples of evaluation results of release ratio of I-133

3.3 Release behavior of noble gases

Since the noble gases have poor chemical activity, it is regarded that the release behavior of the noble gases from the fuel solution under the transient criticality conditions is affected by the mechanical effects, such as the stirring of the solution and increasing of the surface area between gas and solution phases in the solution by the generated radiolysis gases, directly. The generation property of the radiolysis gases in the solution is represented as the function of the dynamic characteristics in the solution. Therefore, there is a possibility that the comprehensive

model for evaluating the nuclear criticality accident in the solution can be established by observing the relationship between the release behavior of the noble gases and the dynamic characteristics.

The mechanical conditions in the solution are varies with time under the transient criticality condition. Therefore, analysis of the time-course of the release behavior of the noble gases is also important. In the present study, the time-course of the release behavior was evaluated by using the isotopes, Xe-140 and Xe-141, with different lifetimes (Xe-140 : 13.6 s, Xe-141 : 1.73 s). Since Ba-140 and Ce-141, the daughter nuclides of the Xe-140 and Xe-141, have appropriate lifetimes (Ba-140 : 12.8 d, Ce-141 : 32.5 d) and specific activities for the reliable determination in the remaining nuclides in the fuel solution after the experiments, the release behaviors of the Xe-140 and Xe-141 were evaluated by using concentration of the daughter nuclides. The above differential equations were solved simultaneously by using the release coefficients of the Xe-140 and Xe-141, ξ_{Xe} ($=\xi_X$), as parameters and the radioactivity concentrations of Ba-140 and Ce-141 in the fuel solution at 5 h and 40 h after the withdrawal of the transient rod from the solution. This time periods of 5h and 40 h after the withdrawal were determined for removing the remaining amount of the parent nuclides of the Ba-140 and Ce-141 in the solution. It was assumed that the Xe-140 and Xe-141 were released from the solution to the gas phase in a very short time period just after the transient criticality and the release coefficients could be considered as a constant and average value. The release coefficients and the release ratios of the Xe-140 and Xe-141 were determined and estimated by iteration calculation with the above equations until the calculated concentrations of Ba-140 and Ce-141 were consistent with the measured concentration, respectively.

To investigate the relationship between the release behavior of the noble gases and the dynamic characteristics in the solution, correlation between the estimated release coefficients and release ratios of the Xe-140 and Xe-141 and the inverse period (1/s), which was one of the dynamic characteristics, of the each experiment. As the example, the correlation between the estimated release coefficients of the Xe-140 and Xe-141 and the inverse periods is shown in Fig. 4. In case that the inverse period was less than 1 1/s, the release coefficients and release ratios of the Xe-140 and Xe-141 increased with increasing the inverse period rapidly. The release coefficient and release ratio of Xe-141 attained to about 5 1/s and 90 % in case that the inverse period was about 100 1/s, respectively. At this point of the inverse period, the release coefficient of the Xe-141 was larger than the coefficient of the Xe-140 by almost two orders of magnitude. The mechanical effects, which affect the release behavior of the noble gases, increase with divergence with transient criticality and decrease and attenuate after convergence of the divergence by re-insertion of the

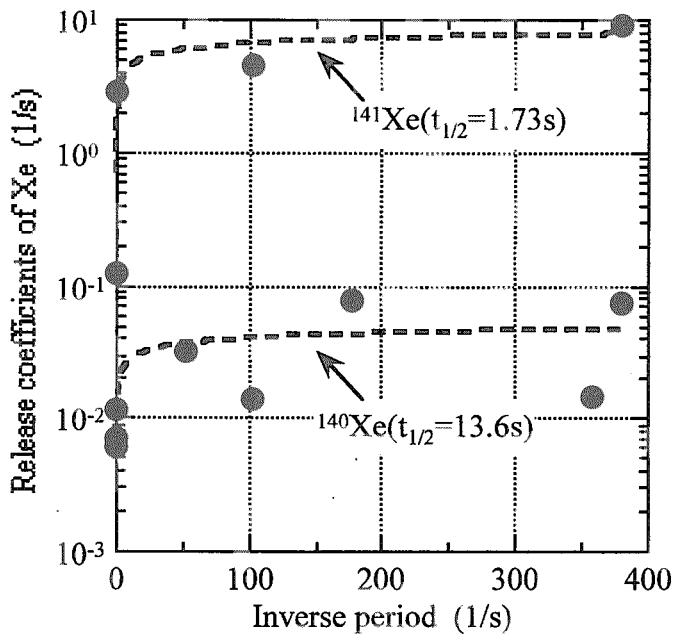

Fig. 4 Relationship between estimated release coefficient of Xe and inverse period

transient rod into the solution. Since the lifetime of the Xe-140 is relatively long, this remains in the fuel solution in considerable time width after the convergence of divergence. As noted above, in the present study, the release coefficient of the noble gas was estimated by treating as constant and average value, therefore, it was regarded that the estimated release coefficients of the Xe-140 represented not only the values in the time region of divergence but also the values in the time region after convergence of the divergence. On the other hand, the release coefficients of the Xe-141 could represented the influence of the mechanical effects on the release property of the nuclide corresponding to the time region of divergence directly because the lifetime of the Xe-141 is shorter than Xe-140. Consequently, it was considered that the release coefficients of Xe-141 were larger than the values of Xe-140.

4. CONCLUSIONS

The release properties of the radiolysis gases and volatile nuclides, such as iodine and noble gases, under the simulated transient criticality condition were observed and estimated by using TRACY. As the results, G-value of the hydrogen was estimated about 0.8 molecules/100 eV and the release ratios of iodine species were evaluated about 0.2% in case that the transient rod was re-inserted to the solution just after transient criticality and about 0.9% in case that the rod was not re-inserted, at 4.5 h after withdrawal of the transient rod from the solution. Similarly the release coefficient and release ratio for xenon isotopes with different lifetimes were evaluated and correlation between the values and inverse period, which was one of the dynamic characteristics, was observed. It was proved that the release ratio of Xe-141 from the solution was over 90 (%) in case that the inverse period was over about 100 (1/s).

In future, time dependencies of the release properties, such as the release coefficient, of the noble gases will be investigated and the comprehensive model for evaluating the nuclear criticality accident in the solution will be established by observing the relationship between the release properties of the noble gases and the dynamic characteristics, quantitatively.

5. REFERENCES

[1] Regulatory Guide 3.3, U.S. Nuclear Regulatory Commission (1977).
[2] Regulatory Guide 1.3, U.S. Nuclear Regulatory Commission (1974).
[3] K.TASAKA, et al., JAERI 1320 (1990).
[4] H.M.Forehand, Jr., NUREG/CR-2517 (1982).

This is a blank page.

JP0250336

JAERI-Conf 2002-004

Development of Solution Behavior Observation System under Criticality Accident Conditions

Akio OHNO, Hiroshi YANAGISAWA, Kazuhiko OGAWA, Eijyu AIZAWA and Kouichi SAKURABA

Japan Atomic Energy Research Institute

Fax: 81-029-282-6024, e-mail: ohno@nucef.tokai.jaeri.go.jp

A solution behavior observation system was developed for observing the behavior of fissile solution and radiolytic voids under criticality accident conditions in TRACY. The system consisted of a radiation-resistive optical fiberscope and a CCD color video camera. The system functioned properly in the mixed high radiation fields of gamma rays and neutrons under criticality accident conditions, and it succeeded in taking the images of their behavior. They provide an important information to understand phenomena of fuel solution at criticality accidents and to construct computational kinetic models. The images can also be used as teaching materials for plant workers and students in universities.

Key words: Solution behavior observation system, Radiolytic void, Criticality accident, TRACY

1. Introduction

Radiolytic gases[1] are generated with rapid increase of nuclear power in initial course of criticality accidents in fissile solution systems. The radiolytic gases are minute and grow together into voids. The voids play an important role as negative reactivity feedback for quenching nuclear power excursions in combination with increase in temperature of the fissile solution. Since the voids move up to the solution surface, nuclear power is governed dominantly by the behavior of the voids. It is necessary to observe the behavior of the voids and fissile solution for understanding phenomena of criticality accidents and constructing computational kinetic models. Moreover, requests of asking what happens at criticality accidents were brought from various fields. To meet these demands, a solution behavior observation system[2] was developed in TRACY.[3]

2. Solution behavior observation system

For the development of the solution behavior observation system, two points were taken into consideration. One is mixed high radiation fields of neutrons and gamma rays where the system is placed. The other is to assure the soundness of a penetration structure through the TRACY core tank from the safety viewpoint. To meet above conditions, a radiation-resistive optical fiberscope was adopted to lead images inside the TRACY core tank to a CCD (Charge Coupled Device) color video camera outside. A graphite-made fiber penetrator called Conax Seal, which is often used at high pressure boundaries in research reactors, was used in

TRACY.

The solution behavior observation system consisted of the radiation-resistive optical fiberscope, a CCD color video camera and a light source as shown in Fig.1. The radiation-resistive optical fiberscope and the CCD color video camera are guaranteed up to 10^4 Gy and 10^3 Gy of gamma rays, respectively. But they are not guaranteed for neutrons. The fiberscope was connected with the CCD color video camera and the light source placed at about 6m away from the TRACY core tank. The pixel number of the fiberscope and the camera are 30,000 and 410,000, respectively. The pixel number of the fiberscope , therefore, determines the resolution of the system. The detail specifications of the system are shown in Table 1. The optical fiberscope was inserted into the core tank with a stainless steel tube to avoid contamination from the fissile solution as shown in Fig.1 and the tip was adjusted to be 60cm from the bottom of the TRACY core tank to obtain optimum images.

3. Experiments and results

Experiments simulating criticality accidents were carried out with the solution behavior observation system. Reactivity was added up to 3$ at the rate of 0.2$/s by ramped withdrawal of the transient rod (Case 1) or 1.5$ at the rate of 0.14$/s by feed of fissile solution (Case 2), respectively. Reactivity addition in both experiments is close to the possible condition of the JCO criticality accident. The reactivity addition condition is shown in Table 2 in detail, together with the fissile solution used in the experiments. The fissile solution is 9.98% enriched uranyl nitrate solution and its uranium concentration is about 376gU/l.

Figure 2 shows typical still images obtained in the Case 1 experiment. The images were compared with the power around the first power peak. As shown in Fig. 2, no ripples on the solution surface were observed in course of withdrawal of the transient rod before power started to increase sharply. At the first power peak, radiation of the radiation-resistive optical fiberscope including attachments on the tip was seen due to extremely high radiation dose rate of neutrons and gamma rays. It was clearly observed in about 2s after the first power peak that the torus-shaped cluster of voids reached solution surface and then spread over. It would be understood that the torus-shaped cluster of voids reflected spatial distribution of neutron flux in the TRACY core tank, because the concentration of voids became proportional to fission density in the solution. After the voids spread over the solution surface, no cluster of voids came out until the second power peak appeared. Figure 3 shows also typical still images obtained in the Case 2 experiment. Immediately after start of solution feed, ripples were seen on the solution surface. That is due to stirring of the solution brought by solution feed. Voids of large bulk, appearing on the solution surface, were observed in about 2s after the first power peak and then spread over.

As is seen in Fig.2 and 3, the voids are observed on the solution surface in about 2s after the first power peak appeared. As the production rate of radiolytic gases is dependent to power density at each position in the core, the voids are largely generated at the central part of the core. By taking account of the solution level of about 60cm, the elevation speed of voids

in the solution was estimated to be about 15cm/s in the range of the experiments.

In order to meet the external requirements, the color motion pictures taken by the system were complied to make a video tape for education and training not only for plant workers but also for students in universities. It can also be used in activities of public acceptance and is available to distribute for demands.

4. Conclusions

The solution behavior observation system was developed in order to observe behavior of the solution and the radiolytic voids under the criticality accident conditions. The system functioned properly in the mixed high radiation fields of neutrons and gamma rays and provided clear color motion pictures necessary for understanding of critical accident phenomena and development of computational kinetic models. The elevation speed of voids in the solution was estimated from the experiments to be about 15cm/s. The images can also be used as teaching materials for plant workers and students.

-References-

(1) Spiegler, P., et al.: NAA-SR-7086, (1962).

(2) Ogawa, K., et al.: J. Nucl. Sci. Technol., 37(12), 1088(2000).

(3) Yanagisawa, H., et al.: Proc. 6th Int. Conf. Nuclear Criticality Safety (ICNC`99), Vol.II, p. 900(1999).

Table 1 Specification of solution behavior observation system

1) Optical fiberscope

Type	Fluorine containing glass core Model RCD30-A1912 by Mitsubishi Cable, Ltd
Length	12m
Radiation resistivity	10^4 Gy of γ-ray
Number of pixels	30,000

2) Light source

Type	Xenon lamp of 500W Model LS-501 by Mitsubishi Cable, Ltd.

3) Video camera

Type	1/2 inch color CCD, Model 82D2500 by Mitsubishi Heavy industries, Ltd.
Radiation resistivity	10^3 Gy of γ-ray
Number of pixels	410,000

Table 2 Experimental conditions

Conditions	Case 1	Case 2
1) Reactivity addition		
Operation mode	Ramped withdrawal	Ramped feed
Added reactivity($)	3	1.5
Average reactivity addition rate($/s)	0.2	0.14
-Withdrawal speed of transient rod(cm/s)	4.3	N/A
-Flow rate of solution feed(l/min)	N/A	57.8
Initial solution level(mm)	652.8	400.3
Final solution level(mm)	652.8	578.9
2) Solution		
^{235}U enrichment(wt%)	9.98	9.98
Uranium concentration(gU/l)	376.1	375.7
Concentration of free nitric acid(mol/l)	0.63	0.65
Delayed critical level(mm)		-
Transient rod withdrawn	526.5	525.7
-Transient rod inserted	652.8	651.1

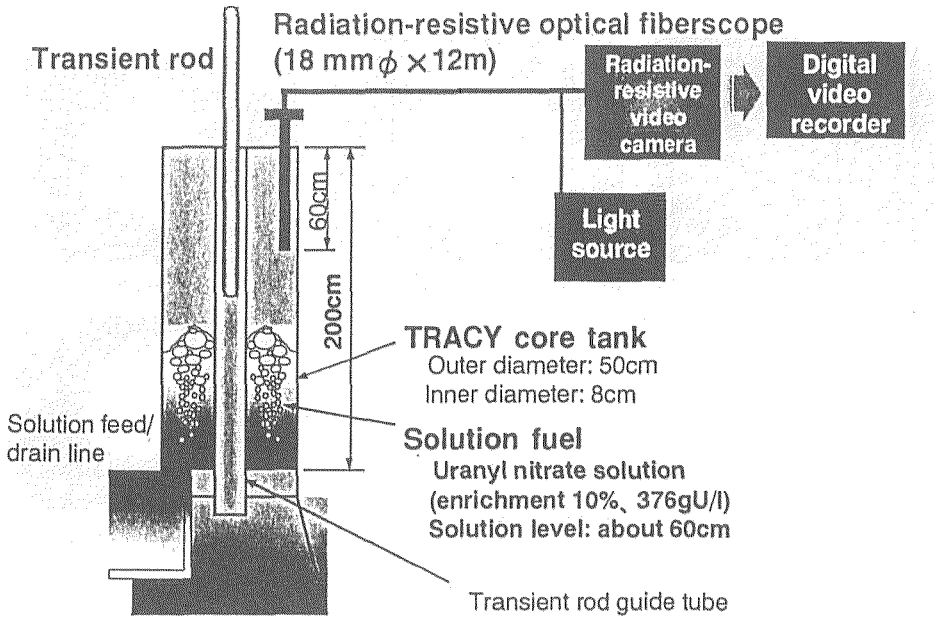

Fig. 1 Layout of solution behavior observation system

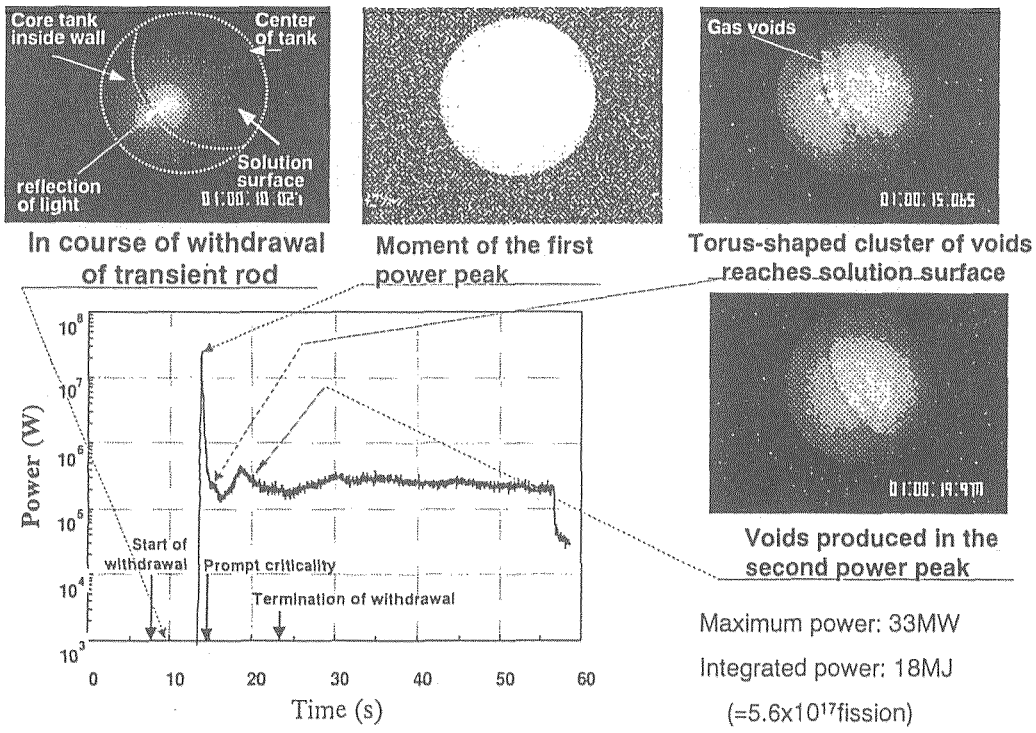

Fig. 2 Behavior of solution surface in Case 1
(3.0$, 0.20$/s:ramped withdrawal 4.3cm/s)

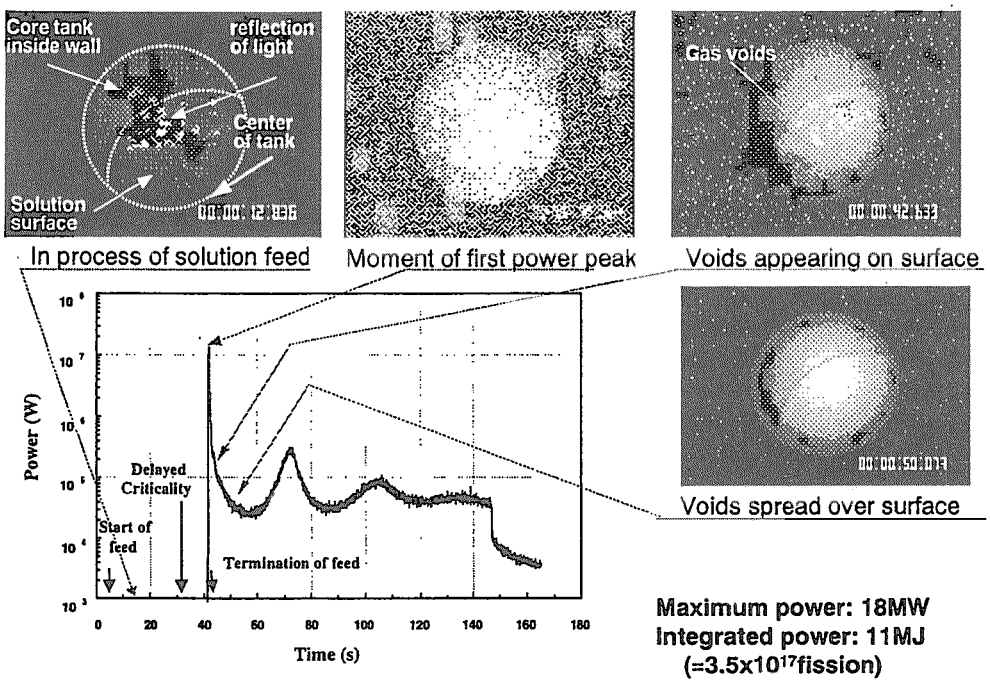

Fig. 3 Behavior of solution surface in Case 2
(1.5$, 0.14$/s:ramped feed 58 L/s)

JP0250337

JAERI-Conf 2002-004

MEASUREMENT OF POWER PROFILES FOR LONG-SUSTAINED CRITICALITY ACCIDENT USING TRACY

K.NAKAJIMA, S.WATANABE, Y.MIYOSHI, K.OGAWA, A.OHNO
Japan Atomic Energy Research Institute
Tokai-mura, Naka-gun, Ibaraki, 319-1195 JAPAN
Fax: 81-29-282-6743, e-mail: nakajima@melody.tokai.jaeri.go.jp

To study the characteristics of long-sustained criticality accidents with natural cooling conditions, a series of supercritical experiments were conducted using the Transient Critical Experiment Facility, TRACY. It was found that the power profiles in such accidents depended on the amount of inserted reactivity, not on the method of reactivity insertion. This is due to the fact that the power behavior in the long period is dominated by the temperature only. Reactivity analysis and kinetics calculation were also performed to obtain the temperature coefficient of reactivity and to investigate the effect of cooling conditions.
Key words: Long-sustained criticality accident, TRACY, Power profile, Reactivity analysis, Kinetics calculation

1. INTRODUCTION

To the present, 22 criticality accidents in fuel processing plants were reported.[1] Although about half of them were terminated in a short time (less than 20minutes), six of them, including the JCO accident occurred at Tokai-mura, Japan, in 1999, continued over than several hours (from 7hr to 37.5hr). It was reported that the accident tank at the JCO has an external cooling system, and it sustained the stable nuclear power.[2,3] On the other hand, the rest 5 accidents had no cooling system, and then it was observed that the power in those accidents oscillated very slowly under the natural cooling conditions.

To study the characteristics of such long-sustained criticality accidents with natural cooling conditions, a series of supercritical experiments have been conducted using the Transient Critical Experiment Facility, TRACY at the Japan Atomic Energy Research Institute (JAERI).

2. EXPERIMENT

2.1 Experimental conditions

TRACY is a supercritical experiment facility using 10wt% enriched uranyl nitrate aqueous solution to simulate a criticality accident in fuel processing plants.[4] The core tank of TRACY is 52cm diameter cylindrical tank made of stainless steel. The thickness of sidewall is 1cm and that of bottom plate is 8cm. It has a central guide tube where an absorber rod, which is denominated as a transient rod, positioned. Reactivity is inserted by the following three methods:

1) Pulse withdrawal
   The transient rod is withdrawn pneumatically in a very short time (about 0.1s).
2) Ramp withdrawal
   The transient rod is withdrawn mechanically in a constant speed.
3) Ramp feed
   Fuel solution is fed to the core tank from the bottom of the tank in a constant feed rate.

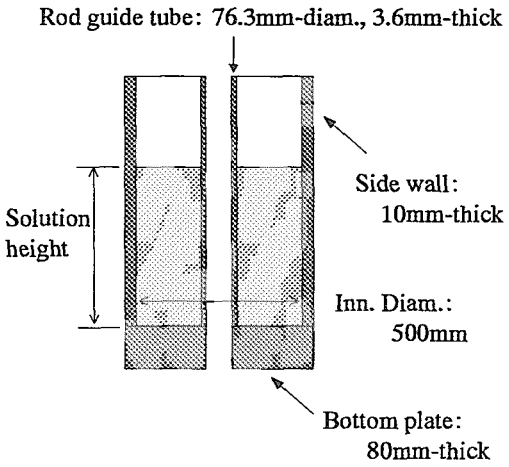

Fig. 1 TRACY Core Tank

In the present study, the ramp feed method with a feed rate of about 60liter/min was employed,

the corresponding reactivity insertion rate was about 0.15$/s. The inserted reactivity was varied from 0.5 to 1.5$. The power profile was measured for about 5 hours after the reactivity insertion. Table 1 shows the experimental conditions.

Table 1 Experimental Conditions

Run	U conc. (gU/λ)	Acidity (N)	Temp. (°C)	Hc (mm)	H0 (mm)	HF (mm)	Feed rate (λ/min)	Reactivity ($)
160	379.5	0.6	29.1	524.21	400.26	541.22	59.5	0.51
161	380.4	0.61	29.1	522.89	400.07	551.07	60	0.83
163	379.8	0.61	29.0	520.95	399.90	564.67	60	1.25
164	382.3	0.62	29.0	516.90	400.13	570.02	59.5	1.52

2.2 Results of experiments

The measured power and temperature profiles are shown in Figs. 1 to 4. As seen in Figs. 1 and 2, the power decreased exponentially due to the temperature rise after the peak followed by several small oscillations. These small oscillations are caused by the production and disappearance of radiolytic gas void. However, about 1 or 2 hours later, the solution temperature decreased slightly due to the natural cooling effect, then the power started to increase, as seen in Figs. 3 and 4. When the power reached to about 1kW, which resulted in the temperature rise, the power turned to decrease again. Such slow power oscillation continued for several hours, and finally the power and temperature became stable. It was observed in the figures that the larger inserted reactivity generated shorter oscillation period, because the larger reactivity causes larger temperature increase, i.e. the larger temperature difference from the ambient one, which is easier to decrease (cool down).

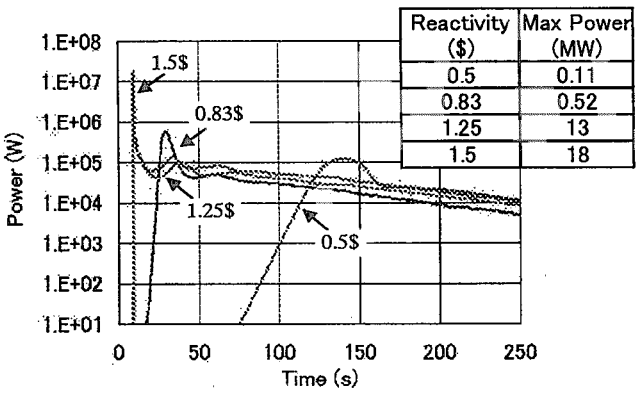

Fig. 1 Measured Power Profiles (Burst part)

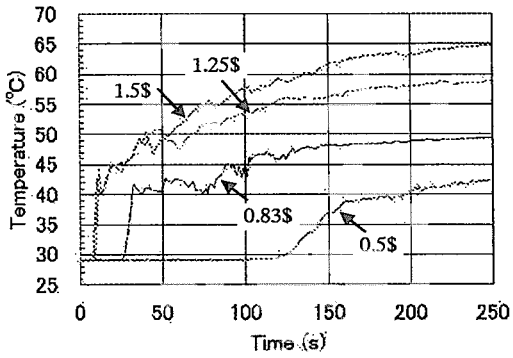

Fig. 2 Measured Temperature Profiles (Burst part)

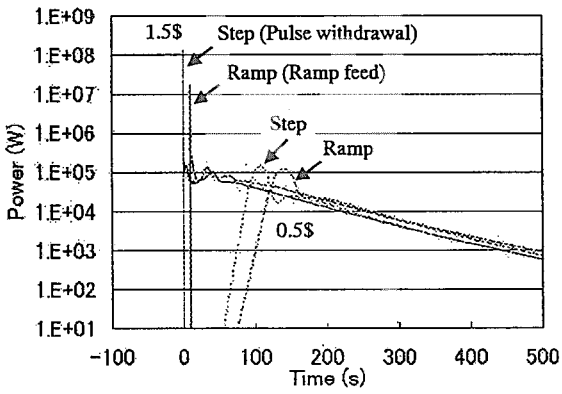

Fig. 5 Comparison of Power Profiles with Different Reactivity Insertion Method (Burst part)

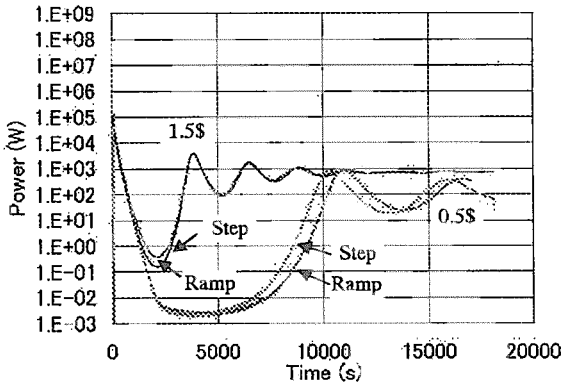

Fig. 6 Comparison of Power Profiles with Different Reactivity Insertion Method (Whole period)

2.3 Effect of reactivity insertion method

To investigate the effect of reactivity insertion method on the power behavior, the pulse withdrawal experiments with reactivity of 0.5 and 1.5$ were performed. In these cases, the reactivity was inserted in about 0.1s, we can treat it as a step reactivity insertion.

Results of the pulse withdrawal experiments are compared with the ramp feed experiments in Figs. 5 and 6. As seen in the figures, the power profiles of both methods are almost same except the very early part. Since the temperature dominated the power behavior in the long period, we can conclude that the temperature change after the first burst is almost same for the same inserted reactivities. Thus, it is important to calculate the thermal balance during the accident, when it sustained for a long time.

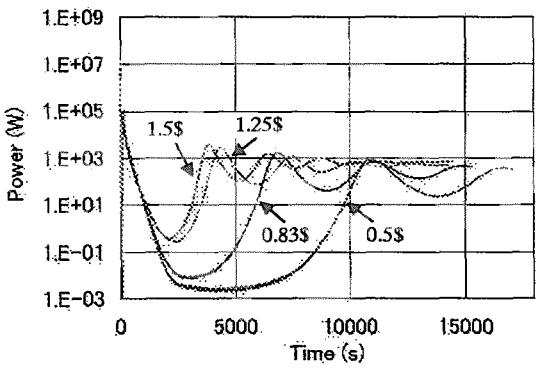

Fig. 3 Measured Power Profiles (Whole period)

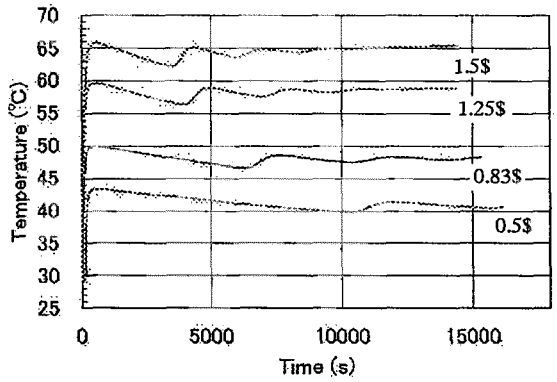

Fig. 4 Measured Temperature Profiles (Whole period)

3. REACTIVITY ANALYSIS

By using the obtained power profiles, we have calculated the reactivity change with the inverse kinetic technique.[5] In this technique, the reactivity profile $\rho_\$$ is calculated using the following equations.

$$\rho_\$ = 1 + \frac{\Lambda}{\beta_{eff}} \frac{d}{dt}[\ln P(t)] - \int_0^\infty D(\tau) \frac{P(t-\tau)}{P(t)} d\tau,$$

$$D(\tau) = \sum_i \frac{\lambda_i \beta_i}{\beta_{eff}} \exp(-\lambda_i \tau).$$

where $P(t)$: Power at time t, β_{eff} : Effective delayed neutron fraction, Λ: Prompt neutron life time, β_i, λi: Delayed neutron fraction and decay constant of i-th group delayed neutron precursor.

Figures 7 and 8 show the profiles of reactivity as a result of inverse kinetic calculation, and solution temperature for the inserted reactivity of 1.25$. As shown in Fig.8, the temperature dominates the reactivity change in such a long period. Using those data, the profile of feedback reactivity($\Delta\rho$) is obtained by subtracting the inserted reactivity(1.25$) from the calculated one, and it is shown in Fig. 9 with the solution temperature change(ΔT) from the initial one. The ratio of feedback

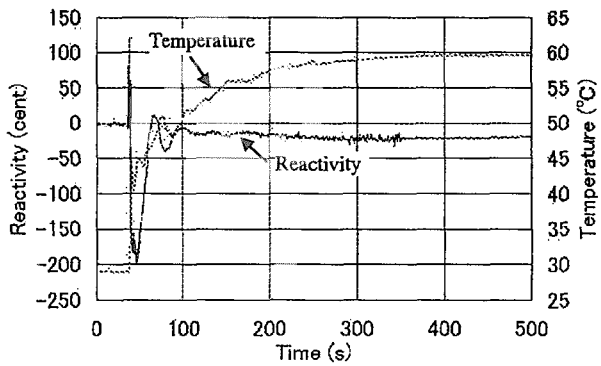

Fig. 7 Reactivity Profile for 1.25$ Insertion (Burst part)

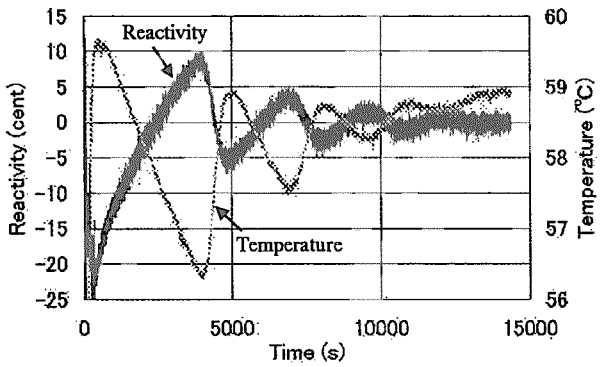

Fig. 8 Reactivity Profile for 1.25$ Insertion (Whole period)

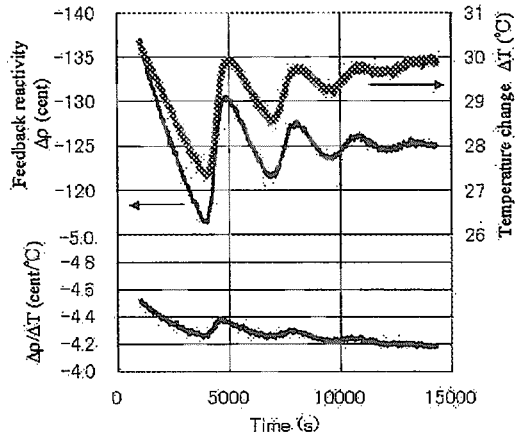

Fig. 9 Calculation of Temperature Coefficient of Reactivity (1.2$ Insertion)

reactivity and solution temperature change (Δρ/ΔT), that is the temperature coefficient of reactivity, is also shown in the lower part of the figure. This ratio varies with reactivity and temperature change; this variation would be caused by the change of temperature distribution in the fuel solution. At the end of experiment, the ratio became stable; it is about 4.2 cent/°C. This value almost agrees with the calculated temperature coefficient of reactivity.

4. KINETICS CALCULATION

The power profile for the inserted reactivity of 1.5$ was calculated using a one-point kinetics code AGNES2.[3,6] To investigate the effect of cooling conditions on the power profile, two cases of cooling conditions were used in the calculation.

Case 1: The heat is removed by the natural convection from the sidewall only. The heat capacity of the sidewall is also considered. (The cooling effect of the bottom plate is not considered.)

Case 2: The heat is removed by the natural convection from the sidewall and the bottom plate. The heat capacities of the sidewall and bottom plate are considered.

The calculated power profiles are shown in Figs. 10 and 11 with the measured one. For the burst part, the two calculated results agree well. They reproduce the peak power of experiment well, although they show lager oscillations than the experiment. This difference is caused by the lager void production in AGNES2 calculation. For longer period, two

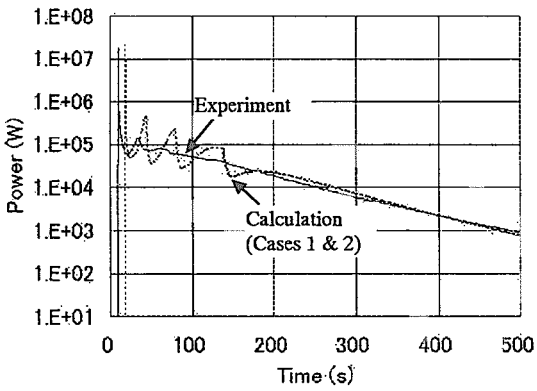

Fig.10 Calculated Power Profiles in Comparison with Experiment (1.5$ Insertion, Burst part)

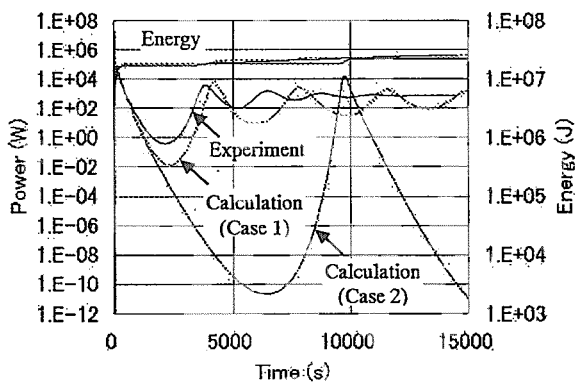

Fig.11 Calculated Power Profiles in Comparison with Experiment (1.5$ Insertion, Whole period)

calculations show quite different behavior. The case 1 shows almost the same behavior as the experiment. On the other hand, the case 2 shows a very large and long interval oscillation, it differs from the experiment greatly. However, the energy profiles are almost same for all cases, because the most of energy was released in the burst part.

5. CONCLUSION

The power profiles of long-sustained (about 5hr) criticality accident have been measured. The following conclusions are obtained.

- The power behavior depends on the total amount of inserted reactivity. Almost independent of the reactivity insertion method.
- The reactivity analysis was conducted using the measured power profiles, and the temperature coefficient of reactivity was evaluated. It varies about 10% during the power transient; this would be caused by the change of temperature distribution.
- Kinetics calculation shows the cooling effect of the bottom plate of the core tank is significant.

REFERENCES

[1] T. P. McLaughlin et al., "A review of Criticality Accidents, 2000 Revision," LA-13638, Los Alamos National Laboratory (2000).

[2] NSC Investigation Committee, " The Report of the Uranium Processing Plant Criticality Accident," Nuclear Safety Commission, Science and Technology Agency, Japan (1999) (in Japanese).

[3] JAERI Task Force for Supporting the Investigation of JCO Criticality Accident, "JAERI's Activity in JCO Accident," JAERI-Tech 2000-074, Japan Atomic Energy Research Institute (2000).

[4] H. Yanagisawa et al., "Experiments on Transient Behavior of a low-enriched Uranyl Nitrate Solution System with TRACY to Study Hypothetical Criticality Accidents in Reprocessing Plants," Proc. 6th Int. Conf. Nuclear Criticality Safety (ICNC'99), Versailles, France, Sept. 20-24, 1999, Vol. II, p.900 (1999).

[5] K. Nakajima et al., "Study on Reactivity Feedback Effects in the TRACY Transient Experiment," ibid., Vol. III, p.1286 (1999).

[6] K. Nakajima et al., "Development of a Kinetic Code in Solution Fuel Systems for the Evaluation of Criticality Accident in Solution Fuel System," Proc. Int. Seminar Criticality Safety (ISCS'87), Tokyo, Japan, p.427 (1987).

This is a blank page.

JP0250338

JAERI-Conf 2002-004

POWER PROFILE EVALUATION OF THE JCO PRECIPITATION VESSEL BASED ON RECORD OF THE GAMMA-RAY MONITOR

K. Tonoike, T. Nakamura, Y. Yamane and Y. Miyoshi

Criticality Safety Laboratory, Department of Fuel Cycle Safety Research,
Nuclear Safety Research Center, Japan Atomic Energy Research Institute
Tokai-mura, Naka-gun, Ibaraki-ken 319-1195, JAPAN
FAX: +81-29-282-6798, e-mail: tonoike@nucef.tokai.jaeri.go.jp

The γ-ray monitor installed in the Processing Facility 1 in the JCO Tokai-works had recorded the γ dose rate change over time which was proportional to the power (nuclear fission rate) in the precipitation vessel from occurrence of the criticality accident to termination of the critical condition. The shape of γ dose rate record from the point of 25 minutes after occurrence to the point of termination ("plateau" part) was normalized using the fission number 2.2×10^{18} and absolute value of the power was evaluated.

Key words: criticality accident, JCO, γ-ray monitor, power profile

1. INTRODUCTION

The first criticality accident in Japan occurred on September 30, 1999 in the JCO Tokai-works. Workers violated safety regulations and feed uranium solution of 18.8% U-235 enrichment manually into the precipitation vessel which has no criticality safe shape. The uranium solution reached critical condition and fission chain reaction initiated on 10:35 AM of the day. The critical condition had lasted for more than 19 hours and the long duration of criticality is a feature of this accident. It also lead the large number of fissions which was 2.5×10^{18}.[1]

During the accident, information source had been very limited to estimate the criticality of the precipitation vessel. Only clear evidence available which can indicate the criticality was report of the periodic neutron dose survey which had been conducted about every 1 hour around the JCO Tokai-works. From the limited information, it was difficult to describe how the chain reaction went on, how fission rate changed over time or whether power bursts existed.

In the post accident investigation where Japan Atomic Energy Research Institute (JAERI) provided intensive support[2], however, chart record of the γ-ray monitor was revealed. The record covers from the occurrence to the termination and shows the fact that quite stable chain reaction had endured for about 19 hours ("plateau" part : fission number 2.2×10^{18}) following the initial burst of about 25 minutes ("burst" part : fission number 0.3×10^{18}).

The record is fairly informative and makes it possible to estimate absolute fission rate in the precipitation vessel at any time point of the accident. It also shows how fission rate was reduced during the water purge effort from the cooling water jacket of the precipitation vessel to terminate the critical condition.

2. FACILITY LAYOUT & GAMMA RAY MONITOR

Major facilities in the JCO Tokai-works are the Processing Facilities 1 and 2 for re-conversion work of uranium for LWRs and the Conversion Test Building where the accident occurred during purification of uranium for the test fast reactor. As illustrated in Fig. 1, the Conversion Test Building is located at west corner of the JCO Tokai-works and the Processing Facility 1 is about 150 m east of the Conversion Test Building. The Processing Facility 2 is more far to north-east.

Gamma-ray monitors are installed in each of these facilities and sensed abnormal dose rate due to the accident. Dose rate in the Conversion Test Building was too high and over

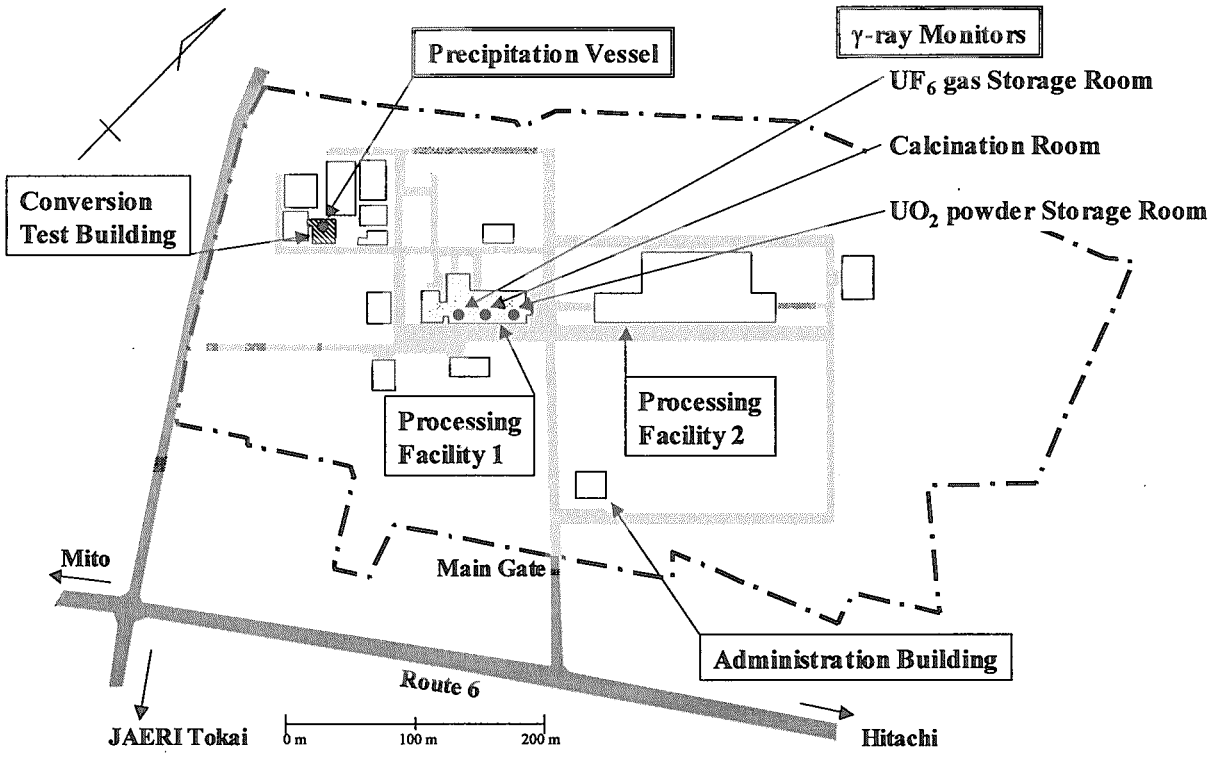

Fig. 1 Facility layout in the JCO Tokai-works

the range where the monitor can work. In the Processing Facility 2, dose rate became higher than normal but the difference was relatively small. The monitor in the Processing Facility 1 recorded γ dose rate change most clearly and the record was provided for the examination. Gamma dose rate had been measured at three locations in the Processing Facility 1 and recorded on one chart paper. Those locations are the UO_2 powder storage room, the UF_6 gas storage room and the calcination room.

3. EXAMINATION OF RECORD

Gamma dose rate of those three locations in the Processing Facility 1 was recorded periodically by a dot-impact type chart recorder as shown in Fig 2. The recorder has 6 input channels and 3 of them has been occupied. The recorder prints a dot for the first channel, waits 12 seconds, prints another dot for the second channel, waits another 12 seconds and repeats this sequence for other 4 channels. For one channel, time interval of record is 72 seconds. In fact, the first three channels are assigned for the calcination room, the UO_2 powder storage room and the UF_6 gas storage room and other three channels are not assigned. Thus, the recorder prints three dots in 24 seconds for those three locations, waits 48 seconds and resumes next series of print.

Around the time of accident occurrence, normal dose rate of the calcination room was recorded and abnormal high dose rate of the UO_2 powder storage room was printed 12 seconds later. Other 12 seconds later, high dose rate record of the UF_6 gas storage room appeared. The first abnormal record of the calcination room came out more 48 seconds later. For convenience, time of the first abnormal record of the UO_2 powder storage area is set to time zero.

Just before the occurrence, normal dose rates of those locations were 3.1×10^{-2} mR/h for the calcination room, 1.5×10^{-2} mR/h for the UO_2 powder storage room and 1.6×10^{-2} mR/h for the UF_6 gas storage room. Observed high dose rates were read out from each printed dots on chart paper and additional dose rates due to the criticality in the precipitation vessel is illustrated in Fig. 3 by subtracting those normal dose rate of each location from those

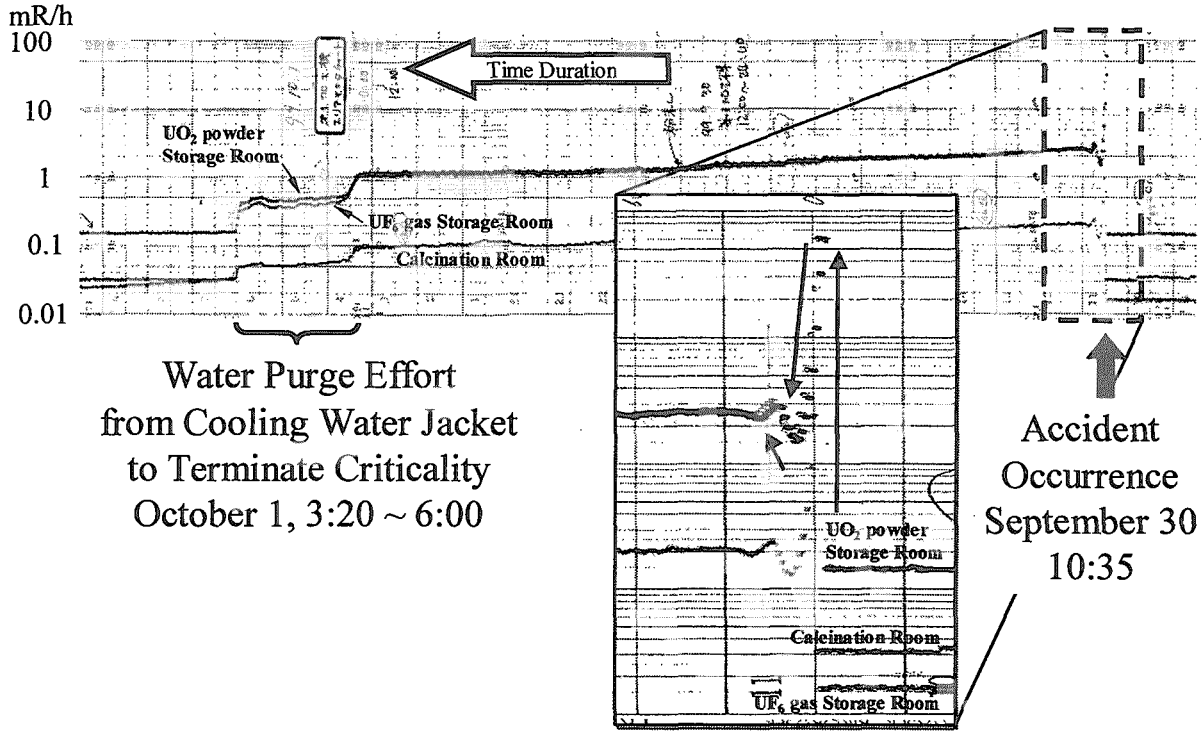

Fig. 2 Chart record of the γ-ray monitor in the Processing Facility 1

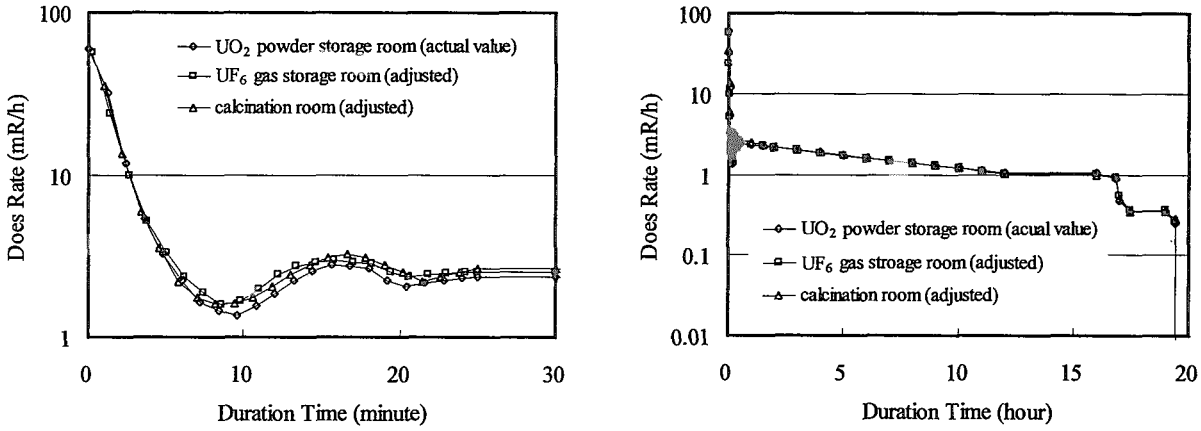

Fig. 3 Comparison of γ dose rate change of three locations in the Processing Facility 1

observed high dose rates. In the figure, curves of records of the UF_6 gas storage room and the calcination room are normalized so that their integration become equal to integration of the UO_2 powder storage room. It can be seen that those curves are almost same although their absolute values are different.

Curves of power profile appeared in Fig. 6 is an average of records of those three locations. As discussed above, the first high dose rate was recorded within 12 seconds after the criticality initiation. In other words, however, there is no information in this figure about the first maximum 12 seconds of the accident.

4. RESPONSE OF GAMMA RAY MONITOR

Records of different place where one decade divergence of dose rates existed show almost same shape. This fact suggested that all ionization chambers operated properly in their working range and correct dose rates were recorded, but there is still possibility that

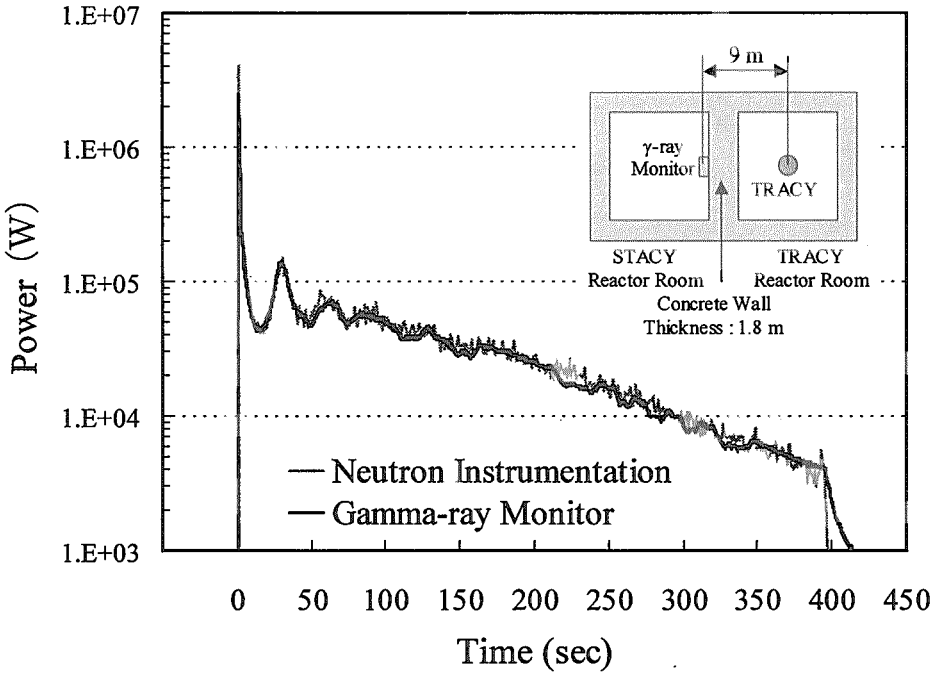

Fig. 4 Response comparison of the γ-ray monitor and neutron instrumentation at TRACY

ionization chambers exposed to too high dose rate radiation and responded improperly for several minutes following the occurrence. To confirm response of the γ-ray monitor, a monitor system including ionization chambers, amplifiers and recorders of the same type as of the Processing Facility 1 of the JCO Tokai-works was tested using the TRACY in the NUCEF, JAERI-Tokai.

The TRACY is a critical assembly using uranium nitrate solution which can realize criticality accident condition under controlled environment. Its core tank is located in the reactor room surrounded by concrete walls of 1.8 m or 2.2 m thickness and uranium solution is fed into the core tank beyond the critical condition. Composition of the uranium solution are about 390 gU/L for uranium concentration, about 10% for ^{235}U enrichment. Diameter of the core tank is about 50 cm. Fission rate change is measured by ^{235}U fission chambers (FCs) which are located in the reactor room and are sensitive to neutrons leaking from the core tank.[3]

The monitor system was set up in the next reactor room of the STACY which is the other critical assembly. The core tank and the monitor was isolated by the concrete wall of 1.8 m thickness but the monitor could detect high dose rate due to the criticality of TRACY. Figure 4 shows comparison of γ dose rate change observed by the γ-ray monitor and fission rate change observed by the FC. Those shapes are almost same, which imply the γ dose rate is proportional to the fission rate. Even in the case where initial dose rate of burst was over the range, indication of observed dose rate recovered normal within 2 or 3 minutes. From this results, it is assured that the record of JCO's γ-ray monitor indicates dose rate change correctly from just after the occurrence while the first two or three dots may be improper.

Next question is origin of the γ-ray, which may be prompt γ-ray emitted by fission reaction or secondary γ-ray produced by neutron capture reaction. Gamma-ray from fission product (FP) built up in core tank may be negligible. To clarify the question, computer analysis using the Monte-Carlo code MCNP-4B[4] was conducted with the nuclear data file JENDL-3.2[5]. For the test at TRACY, eigen value analysis was carried out about the core tank containing the uranium solution to evaluate neutron and γ-ray emission from the core tank. Then, fixed source analysis followed utilizing the result of eigen value analysis about

both of the reactor rooms of TRACY and STACY indicated in the Fig. 4. The fixed source analysis consists of two cases for γ-ray only and for both of neutron and γ-ray. Comparison of those two cases shows that prompt γ-ray contributes less than 20% of total γ dose and secondary γ-ray is dominant. In the same manner, the precipitation vessel in the Conversion Test Building of the JCO Tokai-works was analyzed by eigen value calculation first. Then, dose analysis around the Conversion Test Building and the Processing Facility 1 was conducted where the precipitation vessel was treated as a fixed source. The analysis about the JCO Tokai-works also indicates the same tendency about ratio of prompt γ-ray and secondary γ-ray as of the TRACY case.

5. FISSION NUMBER

If total fission number or integrated power output of the accident becomes known, curve of the chart record is able to normalize so that integration of the curve is equal to the integrated power to estimate fission rate change or power profile.

Small amount sample of uranium solution in the precipitation vessel had been taken and analyzed in the analytical laboratory in the NUCEF, JAERI-Tokai. Density of fission product in the solution was measured and total fission number of the accident was derived as 2.5×10^{18}. The derivation was based on volume ratio of solution in the precipitation vessel and the sample and the FP yield data. The method of fission number estimation by FP density analysis had been employed for routine analysis to characterize the TRACY experiment.[6]

Although the chart record of the γ-ray monitor indicates γ dose rate which is proportional to the fission rate in the precipitation vessel, there may be missing of record about the first spike within several seconds just after the occurrence. This means that the shape of record cannot be normalized using the total fission number because fission number of the first spike is still unknown. As long as for the first several seconds of the accident, it is possible to estimate fission number by calculation with fairly good accuracy. In the accident investigation, however, derivation from the measured data was strongly required instead of calculation. It was the record of a neutron counter in the monitoring post of JAERI-Naka that relieved the difficulty.

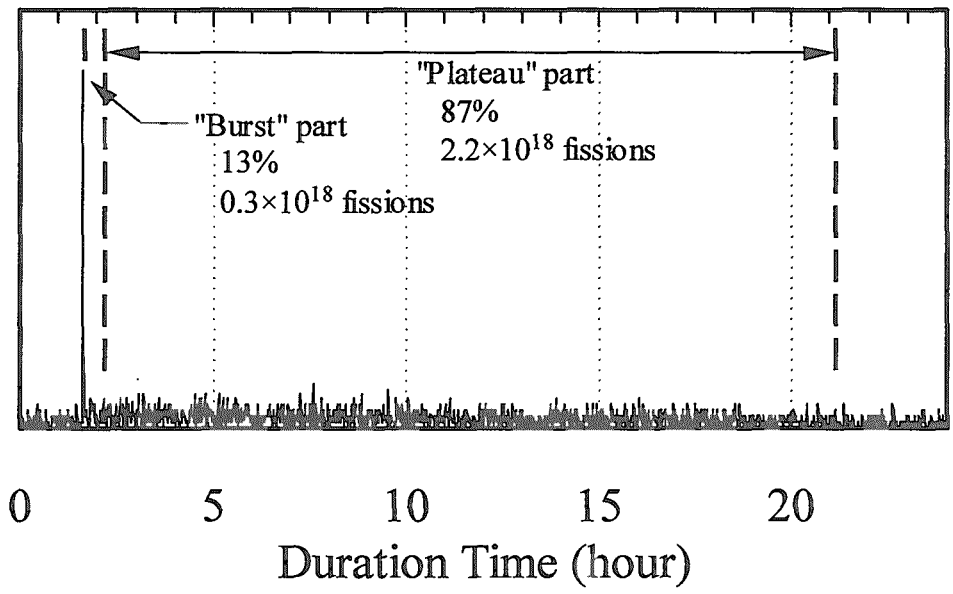

Fig. 5 Record of neutron count at the monitoring post of JAERI-Naka

The neutron counter is located about 2 km away to the west from the precipitation vessel. Neutron count had been recorded continuously as shown in Fig. 5 Although a clear spike can be seen in the "burst" part, it is difficult to discrete higher count rate of the plateau part than the background level observed before the accident occurrence. However, ratio of count number accumulated in the "burst" and the "plateau" parts was able to be determined easily as 13 : 87. This concluded that fission numbers of the "burst" and the "plateau" parts are 0.3×10^{18} and 2.2×10^{18}, respectively.

6. POWER PROFILE AND DISCUSSION

The curve of γ dose rate change illustrated in Fig. 3 was normalized from the time point of 25 minutes after the accident occurrence to the termination so that its integration be equal to 2.2×10^{18} fissions, e.g. 70 MJ. Figure 6 shows results of the normalization. Following the power transient of the first 25 minutes, the "plateau" part started with the power level of about 2 kW. The power had descended slowly fore more than 11 hours and became stable at 820 W.

Even in the power descend, the change was quite slow and the power was almost stable if every minutes was focused although there was no manned reactivity control. This stability suggests strongly that thermal reactivity feedback was effective in the precipitation vessel. Similar situation was also observed in the TRACY when the TRACY was operated in the stable mode at the power level around 1 kW or more. If heat removal capability is comparable to heat generation, chain fission reaction is inherently controlled so that heat generation be equal to heat removal.

The precipitation vessel has a cooling water jacket and was connected to a cooling tower because there might be significant heat generation from the precipitation process which is original purpose of the vessel. The cooling tower was working during the accident but it was not clear that the cooling water flowed in the jacket of the precipitation vessel because the cooling tower provided cooling water also to other process devices. Figures 6 shows that the power dropped from 820 W to 280 W around 3:30 October 1 when an outlet of a cooling water pump was disconnected from a cooling water pipe in the initial action to terminate the

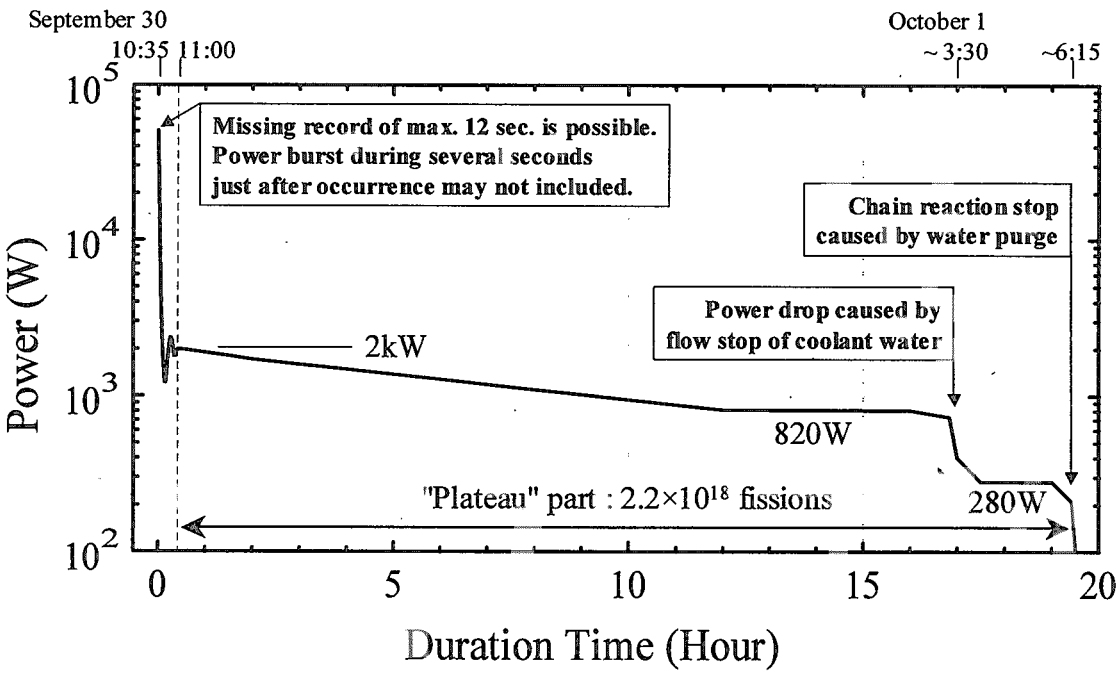

Fig. 6 Power profile and events chronology

criticality. This behavior could prove that, at this time, water flow in the jacket of the precipitation vessel stopped and heat removal capability reduced.

Water still existed in the jacket after its flow stopped and criticality had sustained for about 3 hours at the power level of 280 W. The water was purged finally from the cooling water jacket of the precipitation tank around 6:15 October 1 and criticality was terminated.

Reason of the power descend from 2 kW to 820 W is sill unknown but one possibility is reduction of excess reactivity due to water evaporation. If excess reactivity was 1.5$ or 3.0$, initial temperature of the uranium solution when the "plateau" part started was 66 °C or 87 °C, respectively. Under such temperature condition, water could evaporate at significant rate and volume of the solution could reduced. This might lead reduction of excess reactivity. Smaller excess reactivity caused lower solution temperature and lower heat generation due to the thermal reactivity feedback. Unfortunately, there is no record about the temperature and temperature estimation by calculation still has large uncertainty. Thermal mockup of the precipitation vessel was constructed and several series of experiment using water and electric heaters has been conducted to get information of thermal behavior.[7]

7. CONCLUSION

In the post accident investigation of the JCO criticality accident, chart record of γ-ray monitor installed in the accident site was revealed. It is confirmed in the TRACY test that the γ-ray monitor has enough speed of response. It could be expected that the monitor sensed and indicated γ dose rate proportional to power (fission rate) in the precipitation vessel. Absolute power (fission rate) in the precipitation vessel has been estimated for any time point of accident duration. It has been derived from the normalization so that integration of the dose rate curve of the "plateau" part is equal to the fission number 2.2×10^{18}. Quite stable behavior can be seen in the plateau part even though there was no manned reactivity or power control. It is strongly suggested that the power was so high that thermal reactivity feedback had been effective. The estimated power of several hundreds watt or more is consistent to the suggestion. In the water purge effort to terminate criticality, cooling water flow stopped, first. Due to the flow stop, heat removal from the precipitation vessel had been reduced. Power (fission rate) of the vessel dropped from 820 W to 280 W so that the power was balanced to the reduced heat removal. The power of the plateau part is initially about 2 kW but reduced to about 820 kW in the next 11 hours. The reason is still unknown but it could be reduction of excess reactivity. There is no measurement data about temperature of the uranium solution in the precipitation vessel which would relate the excess reactivity and would help to understand thermal behavior of the accident. Thermal mockup test of the criticality accident has been conducted to clarify the thermal issue.

References

[1] NSC Investigation Committee (1999), "The report of the uranium processing plant criticality accident," Nuclear Safety Commission, STA, Japan, (1999) (in Japanese).

[2] JAERI Task Force for Supporting the Investigation of JCO Criticality Accident, "JAERI's Activities in JCO Accident," JAERI-Tech 2000-074, (2000) (in Japanese).

[3] H. Yanagisawa, K. Nakajima, K. Ogawa, et al., "Experiments on Transient Behavior of a Low-enriched Uranyl Nitrate Solution System with TRACY to Study Hypothetical Criticality Accidents in Reprocessing Plants," Proc. 6th Int. Conf. Nuclear Criticality Safety (ICNC '99), Versailles, France, Sept. 20-24, 1999, Vol. II, p.900, (1999).

[4] J. F. Briesmeister ed., "MCNP™-A General Monte Carlo N-Particle Transport Code Version 4B," LA-12625-M, Los Alamos National Laboratory, (1997).

[5] T. Nakagawa, K. Shibata, S. Chiba, et al., "Japanese Evaluated Nuclear Data Library Version 3 Revision-2: JENDL-3.2," J. Nucl. Sci. Technol., **32** [12], 1259 (1995).

[6] G. Uchiyama, K. Watanabe, M. Miyauchi, et al., "Analysis of Uranium Solution for Evaluating the Total Number of Fissions in the JCO Criticality Accident in Tokai-mura," J. Radiat. Res., 42: SUPPL., S11-S16, (2001).

[7] S. Watanabe, Y. Miyoshi, et al., "Basic Test on Cooling Characteristics of JCO Precipitation Vessel using a Mock-up Device," Proc. 3rd NUCEF International Symposium (NUCEF 2001), Tokai, Japan, Oct. 31-Nov. 2, 2001, (to be published).

JP0250339

JAERI-Conf 2002-004

Basic Test on Cooling Characteristics of JCO Precipitation Vessel using a Mock-up Device

Shouichi WATANABE, Yoshinori MIYOSHI, Yuichi YAMANE, Hiroshi SHIMIZU

Japan Atomic Energy Research Institute
Department of Fuel Cycle Safety Research
2-4 Shirakata Shirane, Tokai-mura, Naka-gun, Ibaraki-ken, 319-1195 JAPAN

This test concerns thermal characteristic of the JCO precipitation vessel, and aims at confirming evaporation effect and grasping behavior of solution temperature change. A mock-up device was manufactured, and cooling characteristic tests for plateau part in the accident were performed by changing the power of electric heaters based on the observed data of the JCO gamma-ray area monitor. Relation between equilibrium temperature and cooling-water flow rate for the observed initial power was measured. Significant amount of water evaporation and temperature change in the plateau part were measured, and the experimental condition was found having a possibility of giving a condition of the accident.

Key words: JCO criticality accident, Precipitation vessel, thermal mock-up device, Static test, Power-tracking test, Water evaporation

1. Introduction

In the criticality accident of the JCO precipitation vessel, the significant power level continued from the viewpoint of thermal characteristic, and it was recorded as observed data of the JCO gamma-ray area monitor. The mock-up device for the precipitation vessel was manufactured to trace the change of power level, and a series of basic tests covering about 20-hour duration of the plateau part in the accident were performed using the device. The test concerns the cooling characteristic of the precipitation vessel, and aims at confirming the evaporation effect which can be a cause of the power reduction during the accident, and grasping the behavior of solution temperature change which can be related to the reactivity change. Static tests were performed to estimate the relation between solution temperature and cooling-water flow rate of the precipitation vessel. And power-tracking test was performed to estimate the amount of water evaporation and the solution temperature change by changing the power of electric heaters based on the observed data of the JCO gamma-ray area monitor[1].

2. Mock-up Device

2.1 Precipitation Vessel

Figure 1 shows a major part of mock-up of the JCO precipitation vessel made of stainless steel. The vessel to which a cooling-water jacket and an agitator are attached, mocks up dimensions and configurations of the major part of the JCO precipitation vessel. The solution (water) in the vessel is heated by 3 electric heaters with 15kW (5kW×3) of maximum capacity. A funnel is inserted in a hand hole. The inner diameters of the hole and the funnel are 83 mm and 46 mm, respectively. The solution volume 43 L was determined so that the heat capacity of the solution was the same as that of the JCO precipitation vessel, considering difference of specific heat between water and uranyl nitrate solution. The solution dimensions are 45 cm in diameter and 31 cm in height. As shown in the figure, thermometers locate vertically at "high", "middle" and "bottom" positions, and the three for each vertical position are arranged in radially symmetric position.

2.2 Measurement and Control System

Figure 2 shows measurement and control system of the mock-up device. The heater power was controlled by a personal computer. Both solution temperature and solution height which was reduced by water evaporation flowing out through the hand hole were measured continuously. The solution was stirred slowly using the agitator considering volume-heating of the solution in the JCO precipitation vessel. Flow rate and inlet temperature of the cooling water were fixed to be constant values.

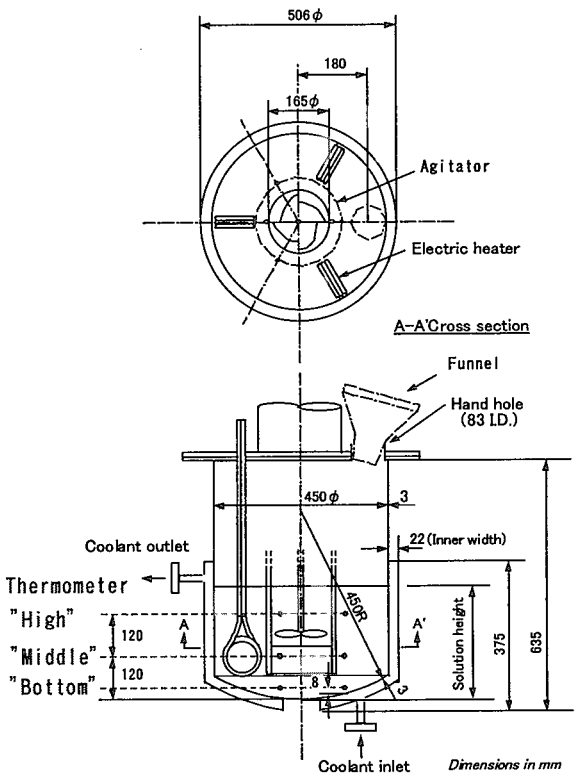

Figure 1 Mock-up of Precipitation Vessel

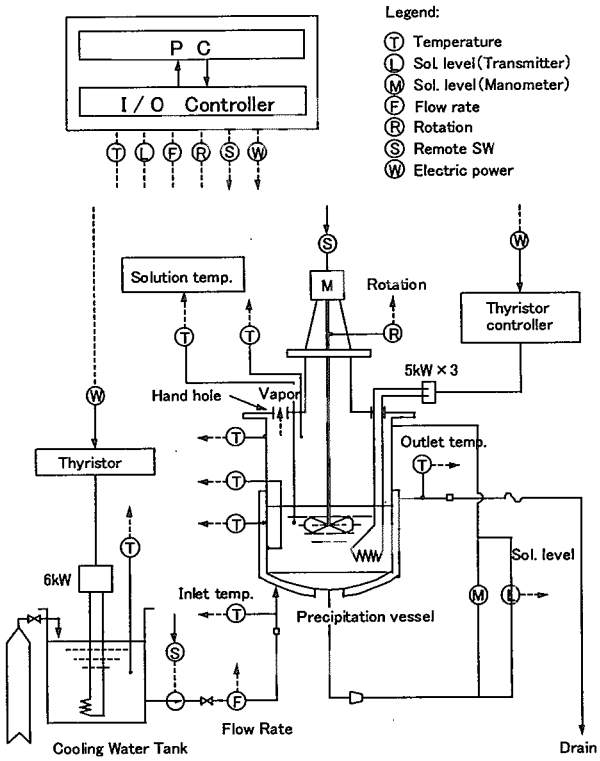

Figure 2 Measurement and Control System

3. Experimental condition

The experiment was performed based on following observed data by the JCO gamma-ray area monitor: beginning of the plateau part at 11:00 on September 30, 1999, stop of the cooling water circulation at 3:30 on the next day, and cease of the accident at 6:15 on the next day. Based on the observed power profile and other information of the accident, following experimental conditions were set up:

1. The burst of the observed power became stable at 11:00, and the power level was estimated to be about 2kW. Therefore, equilibrium solution temperature and the same power were assumed as initial condition of the experiment.
2. Although piping of the cooling water system of the JCO precipitation vessel was fractured in order to cease criticality at 3:30 on the next day, the water in the cooling-water jacket was not drained because the piping had risen on the way. Therefore, the cooling-water circulation was stopped without draining water in the experiment
3. The condition of the cooling water of the JCO precipitation vessel was unknown. Therefore, the cooling-water flow rate was determined parametrically and the inlet temperature was adjusted to 25 ℃ in the experiment.

4. Experimental Method

Prior to the experiment, the relation between the initial solution temperature and the reactivity which compensates the solution temperature was evaluated by using a neutron transport code. As an initial condition, power level was set to be 2kW and the solution temperature was assumed to be in equilibrium which corresponded to initial reactivity, and following two tests were performed:

(1) A static test was performed before the power-tracking test. The cooling-water flow rate was searched so as to satisfy both the initial power and the equilibrium temperature of the solution. One flow rate for one solution temperature was determined by following method: the solution was heated at a stretch by maximum heater power from room-temperature to the target solution temperature, then the heater power was set to be 2kW, and the steady state was attained by adjusting the flow rate in which 4-5 hours were spent. As parameters, the initial solution temperature corresponding to the initial reactivity and the cooling-water flow rate were varied.

(2) Using the result of the static test and the power profile of the JCO gamma-ray area monitor, a power-tracking test in the plateau part was performed for 17 hours in order to measure the amount of water evaporation and the solution temperature change. And the test was continued for additional 3 hours after the cooling-water circulation was stopped. The initial condition of the test was made using the above method (1).

5. Experimental Result

5.1 Static Test

Prior to the experiment, the relation between the equilibrium temperature of solution and the initial reactivity which compensates the temperature was evaluated by using a two-dimensional transport code, TWOTRAN, and a 16-energy-group cross section set collapsed from the 107-energy-group SRAC public library, JENDL-3.1. As shown in Figure 3, the equilibrium temperature was evaluated to be 66-91℃ for the initial reactivity 1.5-2.7 dollars with reference temperature 25 ℃.

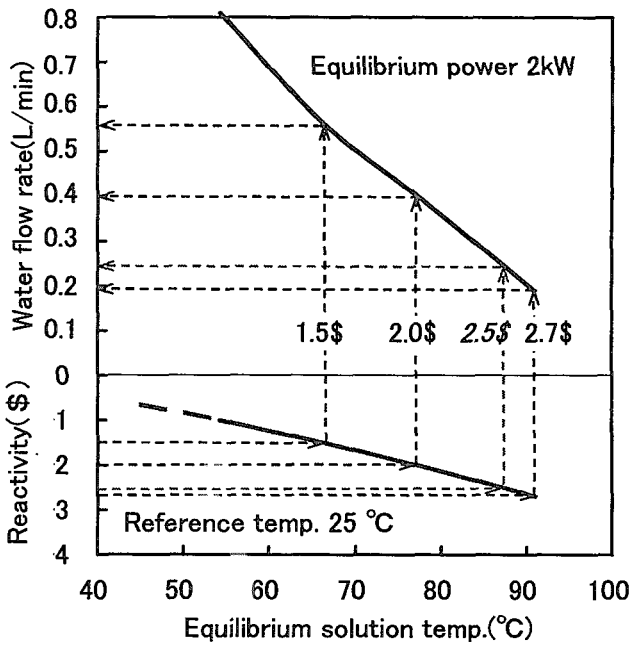

Figure 3 Relation between Water Flow Rate and Initial Solution Temperature

The relation between the equilibrium temperature and the cooling-water flow rate for the initial power was measured. As shown in the figure, the cooling-water flow rate which satisfied the initial condition of 2 kW of power was found to be 0.6-0.2 L/min for the temperature 66-91℃, while the flow rate had been supposed to be 2 L/min for the normal operation of the JCO precipitation vessel.

5.2 Power-tracking Test

The power-tracking test was performed for the case of 2.5 dollars with initial solution temperature of 87℃ and cooling-water flow rate of 0.24 L/min from the viewpoint of significant water evaporation. As shown in Figure 4, the solution temperature decreased with

the power reduction and approached constant value of about 55 ℃. The significant amount of water evaporation in the plateau part was observed and measured to be 2 L. Before and after the circulation stop of the cooling water, very small change of the solution temperature was observed, and it implies that the reactivity depending on the solution temperature was almost kept constant at this time. On the other hand, it should be noted that the reactivity in the JCO precipitation vessel was considered to be unchanged at this time, because the water-reflector condition was not changed. So, it can be mentioned that this experimental condition has a possibility of giving a condition of the accident.

5.3 Heat Balance and Thermal Constant

Heat balance for the tracking test was estimated. The total heater power is balanced with heat removals by the cooling water, the room air circulation at outer surface of the vessel and the water evaporation. The removal heat by the cooling water and the evaporation were estimated directly. As shown in Figure 5, the heat removal by room air circulation is significant,

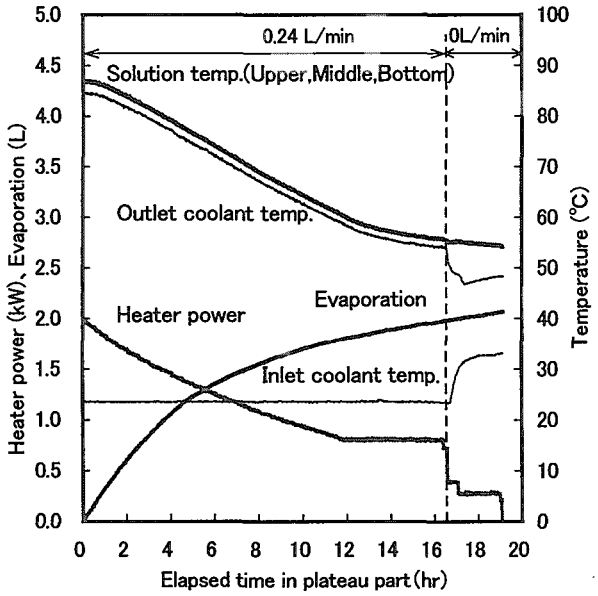

Figure 4 Temperature and Evaporation

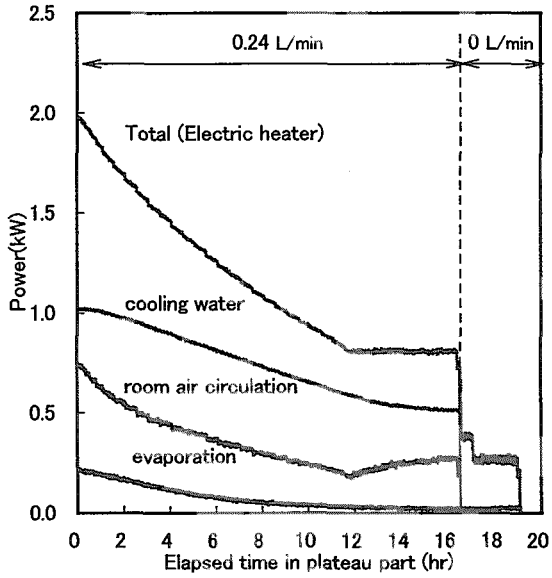

Figure 5 Heat Balance

because of the low cooling-water flow rate. In the beginning of plateau part, the percentages of the amounts of the heat removals by the cooling water, the room air circulation and the evaporation are estimated to be about 50%, 40% and 10% for total heater power, respectively.

Thermal constants were estimated based on the static test. As shown Figure 6, heat transfer coefficient of the cooling-water jacket (H1) and the coefficient at outer surface of the vessel (H2) were estimated to be 250-100 W/m^2/K and ~10 W/m^2/K for the flow rate 0.6-0.2 L/min, respectively

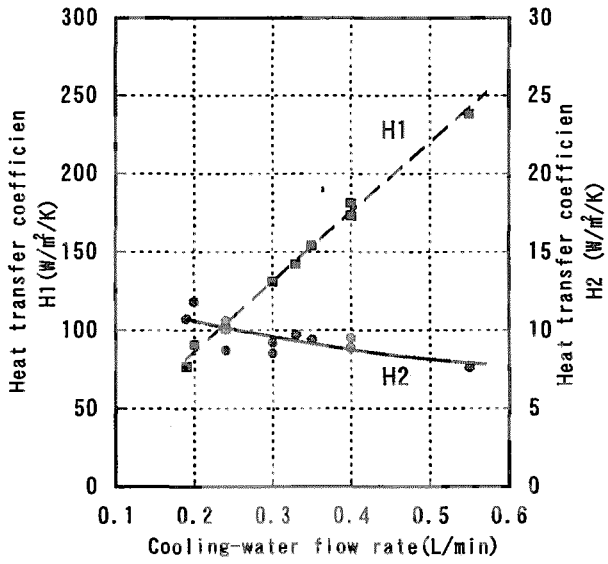

Figure 6 Heat Transfer Coefficients

6. Summary

The results of the mock-up test on the JCO precipitation vessel are summarized as follows:

- The relation between initial temperature and the cooling-water flow rate for the initial power was estimated as follows; for the initial reactivity 1.5-2.7 dollars which corresponds to initial temperature 66-91℃, the cooling-water flow rate which satisfied the initial condition of 2 kW of power was found to be 0.6-0.2 L/min,
- The cooling-water flow rate in the accident was estimated to be less than that of JCO precipitation vessel in the normal operation (2 L/min).
- Significant water evaporation (2 L) was observed in low flow rate (0.2-0.3 L/min).
- The experimental condition of ~2.5 dollars was found having a possibility of giving a condition of the accident.
- Thermal constants which are available for thermo-hydrodynamics analysis of the JCO precipitation vessel were estimated.

Reference

1) K. Tonoike, T.Nakamura, Y.Yamane, Y.Miyoshi "Power Profile Evaluation of the JCO Precipitation Vessel based on Record of the Gamma-ray Monitor" NUCEF2001 Poster Session PC-11

This is a blank page.

Separation Process

This is a blank page.

JP0250340

JAERI-Conf 2002-004

Evaluation of safety limit for handling of hydroxylamine nitrate/ nitric acid solution as a plutonium reductant

Susumu SUGIKAWA*, Miki UMEDA *, Junichi SEKINO*
Takashi MATSUDA**, Takashi KODAMA**
Japan Atomic Energy Research Institute*, Tokai-mura, Naka-gun, Ibaraki-ken, 319-1195 Japan
Japan Nuclear Fuel Limited**, Rokasho-mura, Kitakami-gun, Aomori-ken, 039-3212 Japan
Fax: 81-282-6680, e-mail: sugikawa@nucef.tokai.jaeri.go.jp

An autocatalytic reaction of hydroxylamine nitrate (HAN) in nitric acid solution was investigated to evaluate safety limit for handling of HAN/nitric acid solution as a plutonium reductant mainly by a thermal analysis. The initiation temperatures, minimum temperature for the autocatalytic reaction, were remarkably lowered with increase of nitric acid and iron concentrations. By ageing the solution, the initiation temperatures were further lowered due to an accumulation of nitric acid produced from slow decomposition of HAN. From these experimental data, safety limit for handling of HAN was evaluated.
Key words: hydroxylamine nitrate, nitric acid, safety limit, plutonium, reductant

INTRODUCTION

Hydroxylamine nitrate (HAN) has been used for many years as a plutonium reducing agent in plutonium purification processes at nuclear fuel reprocessing plants. A violent explosion of HAN/nitric acid solution in a reagent tank occurred on May 14, 1997 at the plutonium reclamation facility in the Hanford site. The accident investigation was reported by the Department of Energy (DOE) office [1-2]. The explosion was due to an autocatalytic reaction of HAN/nitric acid solution which had been concentrated due to natural evaporation through ventilation over long term storage. The autocatalytic reaction of HAN with nitric acid was reported more than 50 years ago [3-4], but there are not enough data for the evaluation of the reaction of the solution. The Hanford experiments focusing on the explosion scenario were carried out, but the conditions were limited to high concentration of HAN (3.1 to 16.7M)/nitric acid (5.5 to 8.5M) solution including iron ion [2]. The temperatures of the autocatalytic reaction were measured by a thermal analyzer using an open chamber. The temperatures were showed to be in the range from 39 to 74℃. These data were expressed in Instability Index as a function of the nitric acid to HAN ratio, nitric acid and iron concentration. These data, however, were only for high concentrations of the chemicals. The data including the lower concentrations, therefore, are desired in order to evaluate safety limit under the conditions of actual use. This paper describes the results of thermal analyses with a wide range of HAN/nitric acid concentration and evaluation of the safety limit for handling of HAN.

EXPERIMENTAL

All chemicals used for the experiments were reagent grade. HAN was obtained from Tomiyama Pure Chemical Industries, Ltd.
The thermal analyzer used in the experiments was a RADEX reaction calorimeter (SYSTAG Ltd.). A solution sample was contained in a sealed reaction vessel (7 ml). The reaction vessel was equipped with a temperature probe and a pressure transducer. The vessel was made of platinum-coated titanium for avoiding a reaction between the vessel and chemicals. The sample amount of 2 ml was selected considering maximum pressure of the reaction vessel (4.9MPa) and the real results for the sample.

The temperature and heat flow sensitivity of the reaction calorimeter were calibrated by indium metal. The two methods of thermal analyses, constant rate heating and isothermal heating, were applied for the examination of autocatalytic reaction. The constant rate heating was set at a rate of 0.5℃/min considering slow reaction kinetics. The gaseous products such as N_2O, NOx and N_2 during autocatalytic reaction were determined by gas-chromatograph and chemiluminescence analyses.

RESULTS AND DISCUSSION

1) Critical parameters for the autocatalytic reaction

The critical parameters on autocatalytic reaction of HAN/nitric acid solution were examined by thermal analysis at constant rate heating. Figure 1 shows the initiation temperatures as a function of nitric acid and HAN concentration. The initiation temperatures were remarkably lowered from 190 to 50℃ with increase in acidity from 0.2 to 4M HNO_3. At nitric acid concentration above 4M, the autocatalytic reaction was moderately occurred even at room temperature, which was visually confirmed by the formation of gaseous products. The increase with HAN concentration and nitric acid to HAN ratio did not cause the lowering of the initiation temperature. These results were inconsistent with the results of the Hanford experiment [2]. The autocatalytic reactions between HAN and nitric acid are known as follows [4]:

$$NH_3OH^+ + 2HNO_3 \rightarrow 3HNO_2 + H_2O + H_3O^+ \quad (1)$$
$$NH_3OH^+ + HNO_2 \rightarrow N_2O + H_3O^+ \quad (2)$$

Iron ion is known to act as a catalyst for the reaction of HAN with nitric acid [2]. In the presence of iron ions between 0.01 and 5gFe/l at 0.2 M HNO_3, for example, the initiation temperatures at 190℃ without iron ion were lowered to the temperature range between 180 and 75℃ as shown in Figure 2. The iron-catalyzed autocatalytic reactions are known as follows [2]:

$$2NH_3OH^+ + 4Fe^{3+} \rightarrow 4Fe^{2+} + N_2O + H_2O + 6H^+ \quad (3)$$
$$2Fe^{2+} + HNO_3 + 2H^+ \rightarrow 2Fe^{3+} + HNO_2 + H_2O \quad (4)$$

With increase of nitric acid concentration, the effect of iron ion gradually decreased. At low nitric acid concentration, the iron-catalyzed reaction may be predominant for the autocatalytic reactions shown in equation (1) and (2). At high nitric acid concentration, the autocatalytic reaction with nitric acid may be predominant. The use of stainless steel reaction vessel instead of platinum-coated titanium reaction vessel also showed the lowering of the initiation temperature. This was due to leaching of iron ion from the reaction vessel, since the iron concentration of 0.14gFe/l was determined by analysis of the sample solution after the thermal analysis.

2) Heat generation of the autocatalytic reaction

The heat of the autocatalytic reaction was determined by thermal analysis at constant rate heating. As shown in Figure 3, the heats of the reaction at 1.5M HAN increased with nitric acid concentration, while the heats of the reaction at 0.5M HAN became nearly constant at nitric acid concentrations above 2M. At the 1.5M HAN/0.2M HNO_3 solution used as a plutonium reductant, for example, the heat of the reaction is 75 joule/g of solution. The heat generation of the reaction may accelerate water evaporation. Due to concentrating HAN and nitric acid, the explosive potential of the solution will be increased.

3) Ageing effect of HAN/nitric acid solution

In order to examine self-accelerating effect of the autocatalytic reaction due to ageing of HAN/nitric acid

solution, thermal analyses at isothermal heating were carried out with reaction parameters of nitric acid, HAN and iron concentration. The typical diagram is shown in Figure 4, which an exothermic peak and abrupt pressure increase were obtained during the heating at 70℃. It was also found that the nitric acid concentration in the solution increased while HAN concentration decreased with lapsed time. This nitric acid concentration increase was due to slow decomposition of HAN and caused the lowering of the initiation temperature. In order to define stability of the autocatalytic reaction of HAN/nitric acid solution, these data were plotted in Figure 5. An occurrence of the autocatalytic reaction was defined not only by indication of exothermic peaks, but also by indication of moderate pressure increase in consequence of the evolution of gaseous product (N_2O). The reaction boundary was at temperature of 60℃ in nitric acid below 1M and at temperature of 50℃ in nitric acid between 1 and 3 M.

During the reaction, large amounts of N_2O and N_2 and small amounts of NOx, which cause abrupt pressure increase in reagent tanks, were determined by gas analysis. Figure 6 shows the formation of N_2O versus nitric acid concentration. The formation of N_2O did not depend on nitric acid concentration. One mole of HAN produced a half mole of N_2O. The stoichiometry of the reaction was consistent with shown by the equations (1) and (2) or (3) and (4), since two moles of HAN produce one mole of N_2O. Since the N_2 is not produced from the reactions, it seems to be produced from thermal decomposition of HAN as follows [5]:

$$3NH_3OH^+ NO_3^- \rightarrow N_2O + N_2 + 5H_2O + 2HNO_3 \qquad (5)$$

4) Safety limit for handling of HAN/nitric acid solution

Safe handling of HAN/nitric acid solution can be accomplished by controls of the critical parameters, nitric acid and iron concentrations and temperature of the solution. Iron ion which acts as a catalyst for the reaction might exist as a corrosion product of stainless steel construction material and impurity in nitric acid reagent. Because control of iron concentration in the process may be difficult, safety limit for prevention of the autocatalytic reaction should be evaluated with the presence of the iron ion. In particular the safety limit for preparation of chemical makeup and storage of the solution are recommended as follows considering somewhat safety margin; 3M HNO_3 and 50℃.

CONCLUSION

The critical parameters for the autocatalytic reaction were nitric acid and iron concentrations and temperature of the solution.. The initiation temperatures remarkably decreased from 190 to 50℃ with increase in acidity from 0.2 to 4M HNO_3. In the presence of iron ions between 0.01 and 5gFe/l at 0.2 M HNO_3, the initiation temperature at 190℃ without iron ion lowered to the temperature range between 180 and 75℃. By ageing the solution, the initiation temperatures were further lowered due to an accumulation of nitric acid produced from slow decomposition of HAN. During the reaction, large amounts of N_2O and N_2 and small amounts of NOx, which cause abrupt pressure increase in reagent tanks were identified as reaction products. The safety limit for preparation of chemical makeup and storage of the solution are recommended as follows considering somewhat safety margin; 3M HNO_3 and 50℃.

ACKNOWLEDGMENTS

The authors thank Dr. Y. Suzuki of JAERI for the suggestions and support to this work.

REFERENCES

1. R. Washington, DOE/RL-97-59 (1997)
2. D. G. Harlow. DOE/EH-0555 (1998)
3. A. Bothner, et. al., J. of Chem. Physics, Vol. 20 No. 3, pp459-463 (1951)
4. R. J. Gowland, et. al., J. Chem. Soc. Commun., pp1038-1039 (1983)
5. J. C. Oxley, et., al., SPIE, Vol.872, pp63-70 (1988)

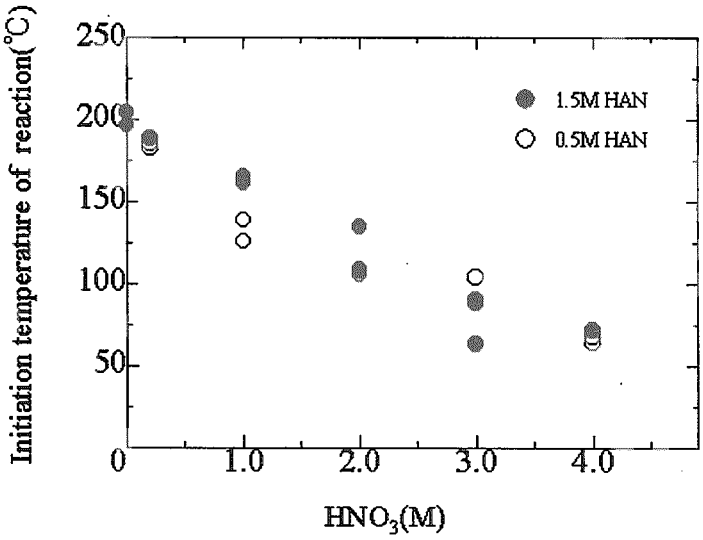

Figure 1 Effect of HAN and nitric acid concentration on initiation temperature of autocatalytic reaction

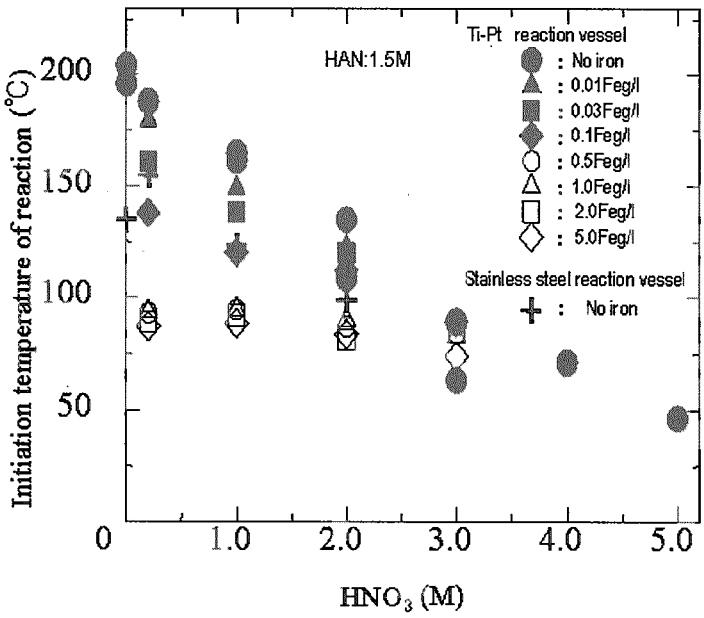

Figure 2 Effect of iron concentration on initiation temperature of autocatalytic reaction

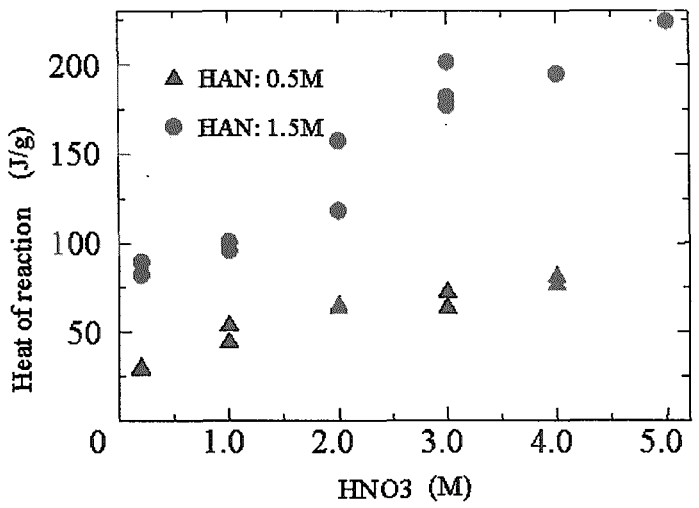

Figure 3 Effect of nitric acid and HAN concentration on heat of reaction

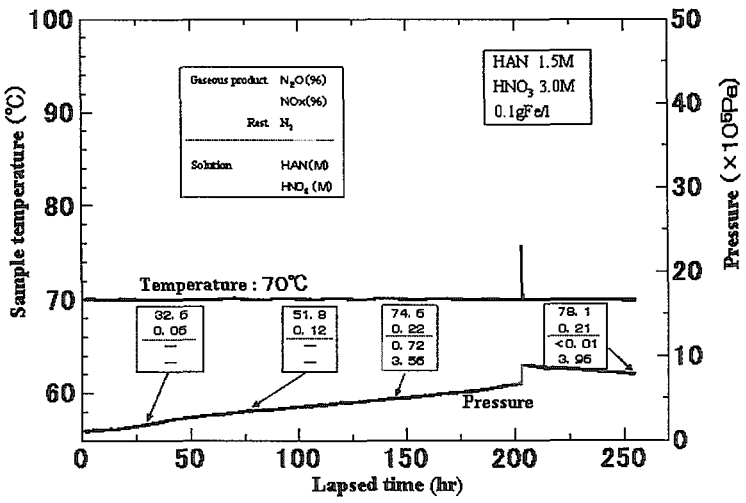

Figure 4 Typical diagram of ageing effect of HAN/nitric acid solution

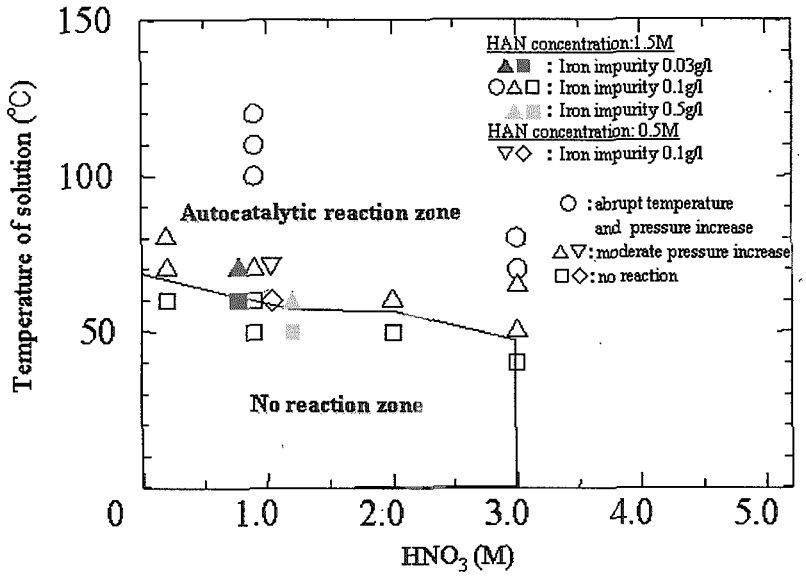

Figure 5 Boundary temperature and nitric acid concentration for autocatalytic reaction of HAN/nitric acid solution

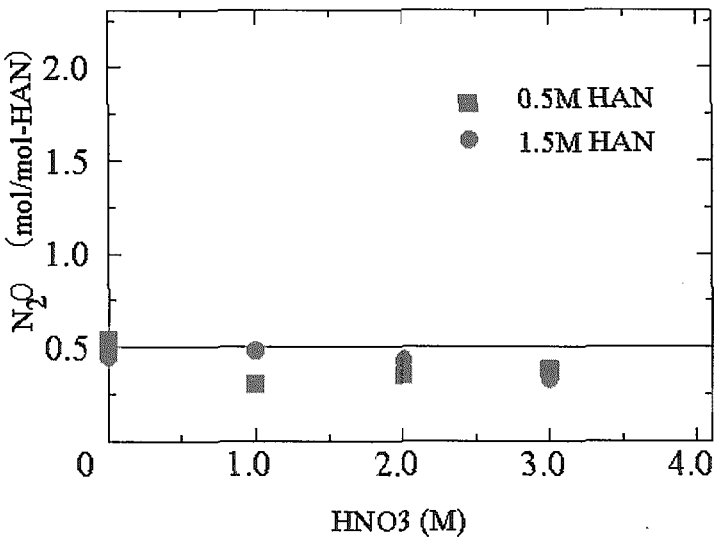

Figure 6 Formation of nitrous oxide in autocatalytic reaction of HAN/nitric acid solution

JAERI-Conf 2002-004

JP0250341

EVALUATION MODELS OF INORGANIC SOLIDS AS SEPARATION AND CONTAINMENT MEDIA

MASAMICHI TSUJI
Tokyo Institute of Technology, Research Center for Carbon Recycling and Utilization,
2-12-1, Ookayama, Meguro-ku, Tokyo 152-8552
FAX: +81-3-5734-3337, e-mail: mtsuji@chem.titech.ac.jp

Several evaluation models of inorganic solids have been reviewed for their extent of validity. They include use of the corrected selectivity coefficients (CSC), Langmuir's equation, power-exchange function, Vanselow's equation, and others. Use of the CSC plot allows calculation of the isotherm and the distribution coefficient as functions of the total charge concentration of solution phase and ratio of solid weight to solution volume. Langmuir equation is a modification of the CSC. Other models are simplified forms of the CSC plot. Activity coefficients are crucial to calculate the CSC values. Unfortunately, they are not available for actinides and hence the ion-exchange process cannot be predicted as a function of the charge fraction in solid and solution phases. Low distribution coefficients often observed on clay minerals may include electrolyte absorption or invasion into solids. Their chemical bond states of ionic species could be clearly distinguished from each other by using the MASNMR.

Key words: evaluation model, distribution, ion exchange, thermodynamics, MASNMR

1. INTRODUCTION

Ionic constituents in environmental electrolyte solutions, including ground water, seawater, and river water, replace ionic chemical species in environmental inorganic materials, e.g., various clay minerals, oxides and hydroxides of multivalent metals, and carbonates. These charge substitution phenomena could be effectively treated using the chemical thermodynamics if they form the equilibrium systems. Unfortunately, chemical thermodynamic expressions are seldom used for evaluation of the chemical processes on these solids, and instead, distribution coefficients (K_d), isotherms, Langmuir equation, and other empirical equations are often used [1-10]. But these evaluation methods of inorganic solids require lots of time-consuming work to carry out numerous distribution experiments. In addition, these are not suitable for description of highly selective solids that are suitable for effective separation of ionic constituents in highly concentrated electrolyte solutions.

Distribution of ionic constituents strongly depends on the chemical environment of the reactive site in local level in inorganic solids. Hence, inorganic solids should be well defined prior to evaluation as distribution and containment media of ionic constituents using physical proves, e.g., MASNMR, ESCA, FTIR, and XRD, for on-site, short-range, and long-range informations of atoms and crystal lattice. These probes will help us interpret the chemical reactivity of these environmental inorganic solids.

The present paper compares several evaluation models for distribution of ionic constituents on environmental inorganic solids.

2. EVALUATION MODELS

2.1 Plots of corrected selectivity coefficients

Plots of the corrected selectivity coefficient (CSC) as a function of the charge concentration in an ion exchanger phase are the reduced expression of thermodynamic generality [11-13]. They can give any distribution coefficient required for column separation or separation factors

numerically as functions of the concentration of exchange ion and ratio of solid weight to solution volume.
In the following, an exchange reaction of 1 to n valent cations is described as an example [14-18]. The same equation can be applied to other combination of cations and anion exchange. If the following Na^+-M^{n+} exchange reaction is reversible, the corresponding equilibrium constant, K, is defined uniquely.

$$n\overline{Na^+} + M^{n+} = \overline{M^{n+}} + nNa^+ \tag{1}$$

$$K = \frac{\overline{X}_M [Na^+]^n \gamma_{Na}^n f_M}{\overline{X}_{Na}^n [M^{n+}] \gamma_M f_{Na}^n} \tag{2}$$

where f_M and f_{Na} denote the activity coefficient of the ion in solid phase; $[M^{n+}]$ and $[Na^+]$ molal concentration of the ion in liquid phase; γ_M and γ_{Na} : activity coefficient of the ion in solution phase; $\overline{X}_M$ and $\overline{X}_{Na}$: the charge fraction of ions in solid phase. The following equations define the charge fraction of ions in solution and solid phases, respectively.

$$X_M = \frac{n[M^{n+}]}{n[M^{n+}]+[Na^+]}, \quad X_{Na} = \frac{[Na^+]}{n[M^{n+}]+[Na^+]}. \tag{3}$$

$$\overline{X}_M = \frac{n[\overline{M^{n+}}]}{n[\overline{M^{n+}}]+[\overline{Na^+}]}, \quad \overline{X}_{Na} = \frac{[\overline{Na^+}]}{n[\overline{M^{n+}}]+[\overline{Na^+}]}. \tag{4}$$

Obviously the sum of the charge fractions in each phase is unity:

$$X_M + X_{Na} = 1 \quad \text{and} \quad \overline{X}_M + \overline{X}_{Na} = 1 \tag{5}$$

Generally the ion-exchange experiment is carried out with the constant total ion concentration kept constant in solution phase. The ionic strength varies through the exchange of ions, but the total charge concentration is kept constant in solution phase as well as in solid phase. Hence,

$$n[M^{n+}] + [Na^+] = c_t, \quad n[\overline{M^{n+}}] + [\overline{Na^+}] = C_t. \tag{6}$$

The total charge concentration c_t of the ion in solution is given in terms of N=mequiv/cm^3, and the total concentration C_t of the ion in solid phase is expressed by the total exchange capacity (mequiv/g). If a concentration of electrolyte solution is low, molar concentration can be used instead of the molal concentration. It will be necessary to take density into consideration for concentrated electrolyte solution. The thermodynamic equilibrium constant can be determined when giving each amount in eq. (2).
The thermodynamic constant is rewritten as follows using the activity coefficients of ions in solid phase and the corrected selectivity coefficient K_{Na}^M given by the physical quantities that can be easily measured.

$$K = K_{Na}^M \frac{f_M}{f_{Na}^n} \tag{7}$$

In the constant total charge concentration in each phase, eqs. (3) - (6) can be used to give K_{Na}^M by a simple algebra as follows.

$$K_{Na}^{M} = \frac{\overline{X}_M X_{Na}^n}{\overline{X}_{Na}^n X_M} \eta\Gamma \tag{8}$$

where

$$\eta = nc_t^{n-1} \quad \text{and} \quad \Gamma = \frac{\gamma_{Na}^n}{\gamma_M}. \tag{9}$$

If the Gibbs-Duhem equation is applied to this equilibrium system, the following equation is derived by combining the CSC (eq. (8)) and the thermodynamic equilibrium constant (K). That is, the CSC is the "differential form" and the K value is the "integral form" of the thermodynamic equilibrium constant.

$$\ln K = (1 - n) + \int_0^1 (\ln K_{Na}^M) d\overline{X}_M \tag{10}$$

The thermodynamic equilibrium constant is not dependent on the total charge concentration of ions in the nature. If one considers the case of 1:1 exchange in eqs. (8) and (9) at high electrolyte concentrations, the CSC values only depend on the ratio of the activity coefficients, and the effect of the total charge concentration in liquid phase can almost be neglected in the concentration range usually used. The corrected selectivity coefficient is plotted as a function of the charge fraction of the exchange ion in solid phase, and integration is carried out in the range of $\overline{X}_M = 0 - 1$. This plot may be called a Kielland's plot or the CSC plot.
Often the maximum value of $\overline{X}_M$ differs greatly depending on the cations in case of inorganic solids. However, if distribution experiments in a binary exchange system were carried out in different total charge concentrations, experimental values will fall on the same CSC plot even if the amounts of the maximum exchange differ substantially.
The CSC plot can be expressed with the following equation using common logarithms. C_m is a generalized Kielland's coefficient.

$$\log K_{Na}^M = \log(K_{Na}^M)_{X_M, \overline{X}_M \to 0} + \sum_{m=1}^{n} (m+1) C_m \overline{X}_M^m \tag{11}$$

Initial concentration of M ion, $[M^{n+}]_o$ (mol/dm^3), the volume of solution, V (cm^3), and the total charge concentration, c_t (mequiv/cm^3), can be used for calculation of the equilibrium composition in the solution phase when w (g) of solid in the H^+ form was used. Eqs. (5), (8), (9) and (11) are combined to obtain the following relation.

$$\log \frac{\overline{X}_M (1 - X_M)^n}{(1 - \overline{X}_M)^n X_M} \eta\Gamma = \log(K_{Na}^M) \tag{12}$$

The equation of the charge balance is

$$n[M^{n+}]_o \cdot V = X_M \cdot V \cdot c_t + \overline{X}_M \cdot w \cdot C_t \tag{13}$$

The value of ($\overline{X}_M$, $\log K_{Na}^M$) on the CSC plot is substituted for eq. (12) within the limit imposed by eq. (13) to calculate X_M. Thus, a set of (X_M, $\overline{X}_M$) obtained can be used for calculating the distribution coefficient (K_d) at *any* total charge concentrations in solution phase as follows.
The K_d value is defined by the ratio of the equilibrium ion concentration in solid and solution

phases. The following equation is obtained using eqs. (4) and (6).

$$K_d = \frac{\overline{[M^{n+}]}}{[M^{n+}]} = \frac{C_t \overline{X}_M}{c_t X_M} \tag{14}$$

Hence, parameters required for distribution of chemical species can be evaluated as functions of the total charge concentration and ratio of solid weight to solution volume. Using the CSC plot, the K_d values at the infinitesimal exchange that are too large to directly determine can be estimated using the following equation derived from the above equations (11), (12) and (14).

$$(K^M_{Na})_{X_M, \overline{X}_M \to 0} = \frac{n(c_t)^n}{C_t} \cdot \frac{\gamma^n_{Na}}{\gamma_M} \cdot (K_d)_{X_M, \overline{X}_M \to 0} \tag{15}$$

A low K_d value may include electrolyte absorption or invasion into solids as well as electrostatic bonding of ionic components that occupy the ion-exchange sites. These chemical states could be distinguished from each other by MASNMR. This effect may not be neglected in clay minerals.

The integration of the CSC plot over the whole range of $\overline{X}_M = 0$–1 gives the thermodynamic constant for the specified ion-exchange reaction.

$$\ln K = (1 - n) + 2.303\{\sum_m C_m + \log(K^M_{Na})_{X_M, \overline{X}_M \to 0}\} \tag{16}$$

$$\Delta G^o = -RT \ln K$$

$$= -RT\,[(1 - n) + 2.303\{\sum_m C_m + \log(K^M_{Na})_{X_M, \overline{X}_M \to 0}\}] \tag{17}$$

A van't Hoff's equation can be used for the standard enthalpy change ΔH^o and then the standard entropy change ΔS^o.

$$\frac{\partial(\Delta G^o)}{\partial(1/T)} = -\Delta H^o \tag{18}$$

$$\Delta G^o = \Delta H^o - T\Delta S^o \tag{19}$$

When ΔG^o is a positive value, a pure M^{n+} form ion exchanger will not be formed in the experimental conditions. It should be noted that this integral value should be used for prediction of the formation of the specified ionic form, but not for evalution of the selectivity at small extent of exchange. For the latter, the differential form given by eq. (11) should be used. One may be often confused with use of eqs. (10) and (11).

2.2 Langmuir equation [19]

The following Langmuir equation is one modification of the CSC by eq. (8).

$$\frac{c_M}{Q_M} = \frac{1}{KQ_{max}} + \frac{c_M}{Q_{max}} \tag{20}$$

Q_M denotes the solid phase ion concentration, c_M the ion concentration in the solution phase,

K Langmuir constant, and Q_{max} the maximum uptake. The following equation can be obtained by rearranging eq. (8) [11].

$$\frac{c_M}{Q_M} = \frac{\Gamma c_t}{K_{Na}^M C_t} + \frac{K_{Na}^M - \Gamma}{K_{Na}^M C_t} \cdot c_M \tag{21}$$

or

$$\frac{c_M}{Q_M} = \frac{c_t}{m}\frac{1}{C_t} + \frac{m-1}{mC_t} \cdot c_M, \tag{22}$$

where $m = \frac{K_{Na}^M}{\Gamma\eta}$. Normally the m value is much larger than unity. Thus, Langmuir equation is derived when one uses the following relations.

$$Q_M = C_t \text{ and } K = m/c_t. \tag{23}$$

It should be noted that the K value depends on the experimental conditions and hence is *not* a constant.

2.3 Power-exchange function

Since this function expresses the ion selectivity using the charge fraction to solid-phase ions and the activity to liquid-phase ions in eq. (2), it takes the same form as the CSC. The activity coefficient of the solid-phase species is neglected and instead a power (n) is used as an adjustable parameter. In the Na^+/M^{2+} exchange,

$$K_{ex} = \frac{a_{Na}{}^2}{a_M}\left(\frac{\overline{X}_M}{\overline{X}_{Na}{}^2}\right)^n. \tag{24}$$

The logarithm of both sides is taken to get

$$\log\frac{a_{Na}{}^2}{a_M} = \log K_{ex} + n \log\left(\frac{\overline{X}_{Na}{}^2}{\overline{X}_M}\right). \tag{25}$$

A power (n) is determined in a region where K_{ex} keeps a constant. Thus, this relation claims that the "exchange constant" K_{ex} and an n value can describe an ion-exchange reaction. The ion-exchange data in some aluminosilicates were tabulated by Walton using this relation and have been used by Garrels et al. [20]. These data are collected mostly in low electrolyte concentrations of 10^{-6} to 10^{-4}M. Later, this equation is called the power ion-exchange function by Langmuir [19]. But a K_{ex} value is not a constant although the quantity is called an exchange constant. Since the n value is generally not an integer, the stoichiometry in an ion-exchange reaction is neglected and, hence, eq. (24) cannot be used to predict ion-exchange behavior at different concentrations. In addition, hydrolysis of aluminosilicates may interfere the uptake of ions in low electrolyte concentration. In such cases, the ternary exchange system has to be treated and will make the analysis complicated [21]. A fatal lack will be that no K_{ex} value for exchange of trivalent ions is available [22].

A Gapon equation uses the molar concentration instead of the activity in the solution phase in eq. (24), and is even now used in the soil study [23]. Unfortunately, the generality of description has been completely lost and this relation should not be used for description of distribution of ions.

2.4 Activity coefficients

It is important to correctly evaluate an activity coefficient for evaluation of the CSC values. For mixed electrolyte solutions, the average salt method is often used [24-26].

$$\frac{\gamma_{Na}^{n}}{\gamma_{M}} = \frac{\gamma_{Na}^{n}\gamma_{A}^{n}}{\gamma_{M}\gamma_{A}^{n}} = \frac{\gamma_{\pm NaA}^{2n}}{\gamma_{\pm MA}^{n+1}} \tag{26}$$

Here, the activity coefficient of mixed electrolyte solution should be used instead of the activity coefficient of a single electrolyte [27]. Several equations to evaluate the activity coefficients of each electrolyte have been used. The equation used by Kraus et al. includes the ionic strength alone and has neglected the nature of each electrolyte [28]. Hence, a large deviation cannot be avoided at concentrated electrolyte solutions. The following expressions by Glueckauf have been used for estimation of the activity coefficients of the 2:1 type electrolytes [29]. The activity coefficients of $M(NO_3)_2$ and $NaNO_3$ in their mixed solution are expressed using the activity coefficient of each electrolyte by eqs. (27) and (28), respectively.

$$\log \gamma_{(NaNO_3)}^{M(NO_3)_2} = \log \gamma^{M(NO_3)_2} + \frac{[Na^+]}{4\mu}\left(\log \gamma^{M(NO_3)_2} - \frac{8}{3}\log \gamma^{NaNO_3} - \frac{1}{3(1+\mu^{-1/2})}\right) \tag{27}$$

$$\log \gamma_{(M(NO_3)_2)}^{NaNO_3} = \log \gamma^{NaNO_3} + \frac{[M^{2+}]}{4\mu}\left(8\log \gamma^{NaNO_3} - \frac{9}{2}\log \gamma^{M(NO_3)_2} - \frac{1}{2(1+\mu^{-1/2})}\right) \tag{28}$$

Here, μ is the ionic strength given by $(1/2)\Sigma z_i^2 m_i$ where z_i and m_i denote the formal charge of ion i and the molal concentration, respectively. Change in the activity coefficient with temperature can be estimated by the method of rectifying the term of the dielectric constant.

3. CONCLUDING REMARKS

Equation (8) is the differential form of the thermodynamic constant, as shown by eq. (10). It is also the reduced expression of the ion-exchange isotherm. In other words, although the form of the ion-exchange isotherm varies with the total charge concentration of solution phase, all the experimental points fall on *one* CSC curve. It can be exemplified by several exchange systems, including ion-exchange resins and inorganic ion-exchange materials [30]. The distribution coefficient K_d can be calculated using the CSC plot as a function of the charge fraction in the range of zero to the maximum charge fraction at different total charge concentrations. But any other models described above cannot generate these quantities as a function of the charge fraction.

An ion-exchange isotherm at *any* total charge concentration can be calculated using the CSC plot determined at one total charge concentration, as long as the activity coefficients of exchange ions are given. Unfortunately, those of the actinides are not available, and hence the K_d value at a specified concentration will be determined.

The total exchangeable charge is crucial to make the CSC plot. An individual standard for determination of the total exchangeable charge needs to be used for different types of solids. The following three types of inorganic solids with adsorption/ion-exchange properties occur naturally or have been synthesized.

(a) *Variable-charge type of solids*, e.g., oxides/oxyhydroxides and acidic salts of metals (analogues of acidic and basic resins).

(b) *Substitution type of solids*, e.g., layered double hydroxides (LDHs), aluminosilicates (clays, zeolites), tobermorites, and nonstoichiometric mixed valence compounds, e.g., MnO_{2-x}s and

their salts. (c) *Intrinsically charged type of solids*, e.g., hydroxyapatites and bismutites.
It is not always easy to determine the total ion-exchange capacity giving the point of $\overline{X}_M=1$ in the CSC plot. Especially it is true for the case of clay minerals, soils and mixed solids. A reasonable and conventional basis has to be used to determine the total exchangeable charge of single-phase solids belonging to each category. Zeolites are typical cation-exchange materials with several exchange sites. Hence, often the CSC plots do not give a straight line. The total ion-exchange capacity of these aluminosilicates can be determined using the population ratio of the tetrahedral Si and Al with MASNMR and the chemical content of Si and Al. The population ratio of the tetrahedral Si and substituted Al can be determined by the intensity ratio of each signal as follows [31].

$$\frac{Si^{IV}}{Al^{IV}}=\frac{\sum_{n=1}^{n=3} I_{Si(nAl)}}{\sum_{n=1}^{n=3}\frac{n}{3} I_{Si(nAl)}} \tag{29}$$

Generally, several techniques have to be used to determine the total charge of mixed-phase or ill-defined solids such as natural clays, their deteriorated clays, or soils.
If the CSC plots could be determined using the first principle calculation based on atomic configuration of ion-exchange solids, all parameters necessary for diphasic partition of ionic constituents could be calculated including the ion-exchange isotherm. However, the informations about the relations between the atomic configuration and the ion-exchange process are not sufficiently available. But a promising case of bismutite family indicates a new avenue to use the first-principles process for smart designing of high-performance materials [32,33].

References

[1] C. E. Marshall, "The Colloid Chemistry of the Silicate Minerals", Academic Press, New York (1949).
[2] L. Wiklander, "Chemistry of the Soil", Ed. by F. E. Bear, Reinhold Publishing Co. ACS Monograph 126, New York (1955).
[3] S. Wada, Clay Science, 27, 227-236 (1987).
[4] Y. Inoue and S. Morisawa, J. Atomic Energy Soc. Jpn., 18, 524-534 (1976).
[5] N. Kato, T. Murakami, H. Tasaka and S. Ueda, J. Atomic Energy Soc. Jpn., 29, 834-839 (1987).
[6] S. Morisawa, J. Atomic Energy Soc. Jpn., 15, 503-508 (1973).
[7] T. Igarashi, J. Atomic Energy Soc. Jpn., 35, 237-244 (1993).
[8] N. Kato and h. Tasaka, J. Atomic Energy Soc. Jpn., 27, 963-967 (1985).
[9] N. Kato, K, Nakamichi, H. Tasaka and T. Asano, J. Atomic Energy Soc. Jpn., 25, 577-582 (1983).
[10] A. Dyer, "Recent Developments in Ion Exchange", Ed. by P. A. Williams and M. J. Hudson, Elsevier Applied Science, New York (1990), pp. 43-55.
[11] M. Tsuji, H. Kaneko and Y. Tamaura, J. Chem. Soc. Faraday Trans., 89, 851-856 (1993).
[12] M. Tsuji and S. Komarneni, Sep. Sci. Technol., 26, 647-659 (1991).
[13] M. Tsuji and S. Komarneni, Sep. Sci. Technol., 27, 813-821 (1992).
[14] G. L. Gains, Jr. and H. C. Thomas, J. Chem. Phys., 21, 714-718 (1953).
[15] R. Harjula, A. Dyer and S. D. Pearson, J. Chem. Soc. Faraday Trans. 88, 1591-1597 (1992).
[16] R. M. Barrer and J. D. Falconer, Proc. Royal. Soc. Lond. Ser. A 236, 227-249 (1956).

[17] R. M. Barrer, "Natural Zeolites, Occurrence, Properties and Use", Ed. by L. B. Sand and F. A. Mumpton, Pergamon Press, Oxford (1978), pp. 385-395.
[18] R. M. Barrer and J. Klinowski, J. Chem. Soc. Faraday Trans. I. 70, 2080-2091 (1974).
[19] D. Langmuir, "Aqueous Environmental Geochemistry", New Jersey, Prentice Hall (1997).
[20] R. M. Garrels and C. L. Christ, "Solution, Minerals, and Equilibria", New York, Harper & Row (1965) p.270.
[21] R. Harjula, J. Lehto, J. H. Pothuis, A. Dyer, and R. P. Townsend, J. Chem. Soc. Faraday Trans., 89, 971-976 (1993).
[22] M. Tsuji, Solvent Extr. Ion Exch., 19, 531-551 (2001).
[23] H. Tsuno, I. Somiya and H. Yanase, J. Society of Environmental Science, Japan, 13, 1-10 (2000).
[24] H. S. Harned and B. B. Owen, "The Physical Chemistry of Electrolytic Solutions", Appendix Wereinhold Publishing Co., New York (1950).
[25] D. R. Lide (Editor-in-Chief), "Handbook of Chemistry and Physics", CRC Press, 76Th Ed., Boca Raton, FL. (1995).
[26] D. Dobos, "Electrochemical Data", Elsevier Scientific Publishing Co., Amsterdam (1975).
[27] E. Glueckauf, Nature, 163, 414-415 (1949).
[28] K. A. Kraus and R. J. Paridon, J. Phys. Chem., 63, 1901-1907 (1959).
[29] L. V. C. Rees, "Properties and Applications of Zeolites", Ed. by R. P. Townsend, The Chemical Society, Burlington House, London (1980) pp. 218-243.
[30] M. Tsuji, R. Harjula and Y. Tamaura, Annual Rep. Salt Sci. Res. Found., Salt Sci. Found., Tokyo (2001) pp. 139-156.
[31] J. Sanz and J. M. Serratosa, J. Am. Chem. Soc., 106, 4790-4793 (1984).
[32] M. Tsuji, Y. Ikeda, M. Sazarashi, M. Yamaguchi, J. Matsunami and Y. Tamaura, Mater. Res. Bull., 35, 2109-2121 (2000).
[33] M. Tsuji, Solid State Ionics, (in press).

JP0250342

JAERI-Conf 2002-004

SPENT FUEL TEST ON EXTRACTION IN ADVANCED REPROCESSING PROCESS

S.HOTOKU, G.UCHIYAMA, T.ASAKURA, M.SATO, Y.ITOH and H.MINEO

Japan Atomic Energy Research Institute

Tokai-mura, Naka-gun, Ibaraki, 319-1195 Japan

Fax. 81-29-282-6677, e-mail: hotoku@procsafe.tokai.jaeri.go.jp

ABSTRACT

Extraction tests of the 44,000MWd/t spent fuel dissolver solution using bench scale reprocessing experimental equipment at BECKY(Back-end Fuel Cycle Key Elements Research Facility) were carried out using three extractors. The equipment composed diluent washing, Np oxidation, co-extraction, FP scrubbing, Np separation, Tc separation, U/Pu partitioning and U recovery steps.

Vanadium (V) oxide with nitric acid was used as an Np oxidizing agent. Butyraldehyde (decomposable and salt-free organic reducing agent) and 6M nitric acid were fed into the extractor in order to separate Np and Tc. As a result 64.8% of the Np and 98.9% of the Tc were extracted in the co-extraction step. 75.0% of the extracted Np was separated from the U and Pu stream in the Np separation step. On the other hand, 81.8% of the Tc was separated by 6M nitric acid in the Tc separation step.

In the U/Pu partitioning step, Pu was reduced from Pu (IV) to Pu (III) and stripped into aqueous phase by uranous nitrate and hydrazine in 1M nitric acid. Most of the Np remained in the U loaded solvent (organic phase). To the contrary, Tc migrated to the Pu solution (aqueous phase).

It was found that butyraldehyde and 6M nitric acid were effective in separating Np and Tc from the U and Pu stream. These technologies are expected to be applied to simplified reprocessing process.

Key words: PUREX, extraction, reprocessing, neptunium, technetium

1. INTRODUCTION

NUCEF(Nuclear Fuel Cycle Safety Engineering Research Facility) Experiment Building B is referred to as BECKY(Back-end Fuel Cycle Key Elements Research Facility). It contains bench scale reprocessing experimental equipment for dissolving, off-gas treatment, extraction and liquid waste recycling process units in the $\alpha\gamma$ cell. The extraction equipment is made up of five extractors (mixer-settler), several tanks and pumps.

Fuel reprocessing technology is required to remove the long-lived nuclides from high level liquid waste, simplify the chemical process, and also to make reprocessing process more economical in the future.

The JAERI (Japan Atomic Energy Research Institute) has been pursuing the advanced technology of fuel reprocessing "PARC"(Partitioning Conundrum Key) process[1)~5)]. It is designed to separate long-lived extractable nuclides such as ^{237}Np and ^{99}Tc during the

extraction step. This process is based on the current PUREX process and aims to enhance the separation efficiency of the extractable Np and Tc as well as U and Pu. In the separation of Np and Tc from the U and Pu stream before the U/Pu partitioning step in the PARC process, Np (VI) is selectively reduced to the Np (V) by normal-butyraldehyde (decomposable and salt-free organic reducing agent) and the 6M-nitric acid scrubbing of Tc.

The purpose of this study is to examine the behavior of the first extraction cycle (from co-extraction to U/Pu partitioning) of the PARC process used by 44,000MWd/t spent fuel dissolver solution.

2. EXPERIMENTAL

2.1 Reagents

Purchased reagents such as vanadium(V) oxide, normal-butyraldehyde, tributyl phosphate (TBP), normal-dodecane(nDD) and hydrazine nitrate were used without any special pretreatment. The spent fuel dissolver solution was adjusted to the concentration of nitric acid about 3M. In addition, the short-lived gamma-ray nuclides, ^{95m}Tc(6.1MBq), ^{95}Zr(10.4MBq) and ^{131}I(2.7MBq) were diluted with nitric acid solution in order to measure the extraction behavior of these elements. The composition of the dissolver solution is shown in Table 1.

Table 1 Composition of dissolver solution

Element / substance	Concentration
Nitric acid	3.1 M
Nitrous acid	5.8×10^{-3} M
U	216 g/l
Pu	2.4 g/l
Np	176 mg/l
Tc	366 mg/l
Ru	792 mg/l
Zr	441 mg/l
Cs	751 mg/l
Eu	18 mg/l
Am	181 mg/l

2.2 Analysis

U and nitric acid were analyzed by the potentiometric titration method. Alpha-ray and gamma-ray spectrometers were used to analyze the concentrations of Pu, ^{106}Ru, ^{239}Np and other elements (^{95m}Tc and ^{95}Zr etc.). A spectrophotometer was used to analyze the concentration of Pu and the valency of the elements in the nitric acid solution. An ICP-AES(Inductively coupled plasma atomic emission spectrometry) was used to analyze trace amounts of U, Tc, Zr and Ru in the aqueous sample.

2.3 Procedure

Extraction tests of the 44,000MWd/t spent fuel were carried out using three extractors (there were 20 stages for each extractor). The extraction flow sheet is shown in Fig.1. The extraction test was made up of these steps: diluent washing, Np oxidation, co-extraction, FP scrubbing, Np separation, Tc separation, U/Pu partitioning and U recovery.

The dissolver solution was fed into the 14th stage of extractor No.1 for 10 hours. Fig.2 shows the absorption spectrum of the dissolver solution by spectrophotometer analysis. The

valency of Pu and Np is presented as Pu(IV) or Pu(VI) and Np(V) in the solution.

Vanadium(V) oxide with 3M nitric acid was used as an Np oxidizing agent[6] and FP scrubbing solution (2M nitric acid) was fed into extractor No.1. FP scrubbing solution scrubs mainly Zr was extracted with 30%TBP/nDD.

It has been proposed that butyraldehyde used for the selective separation of Np from the U and Pu stream[1)~5)]. It was fed into the 1st stage of extractor No.2 with 30% TBP/nDD.

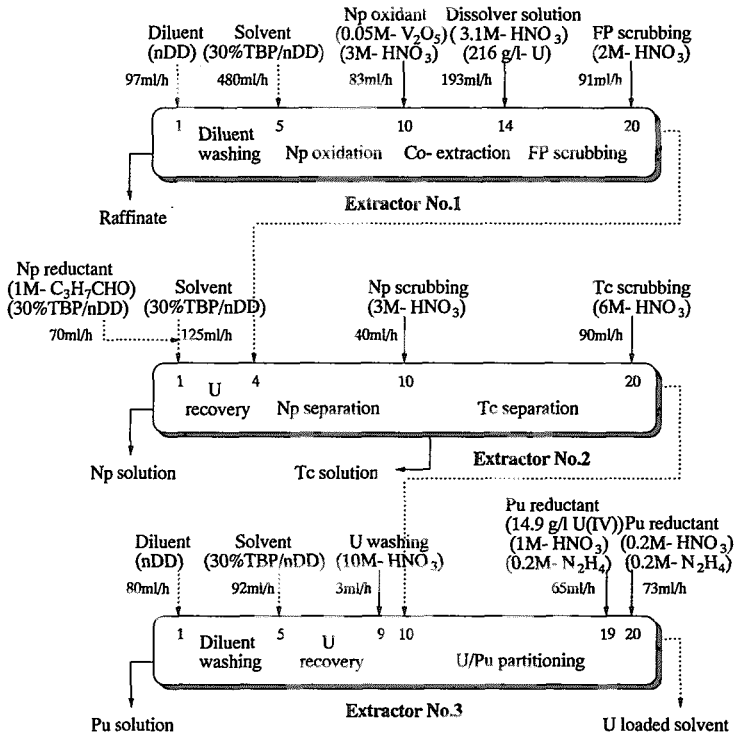

Fig.1 Extraction flow sheet of PARC process test.

Tc scrubbing solution (6M nitric acid) was fed into the 20th stage of extractor No.2. Uranous nitrate and hydrazine with nitric acid solution were used as a Pu reductant agent and fed into the 19th and 20th stages of extractor No.3.

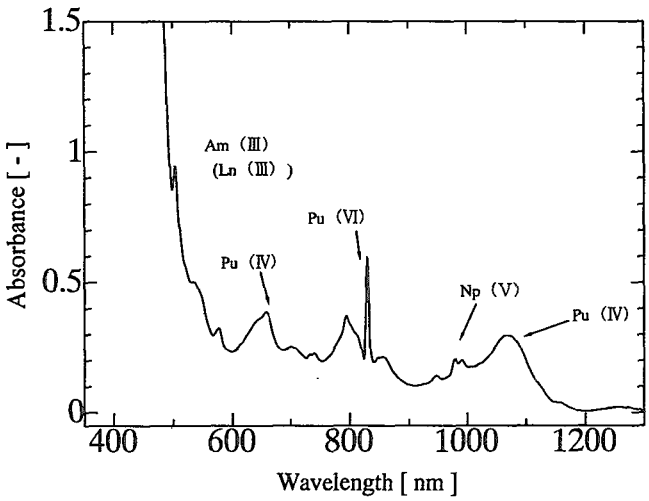

Fig. 2 Absorption spectrum of dissolver solution.

3. RESULTS AND DISCUSSION

Fig.3 shows concentration profiles of nitric acid, U and Pu in extractor No.1 and

Table 2 Distribution fraction of each element (%)

Product stream	U*	Pu	Np	Tc	Ru	Zr
Raffinate	<0.02	<0.098	35.2	<1.1	90.8	84.2
Np solution	0.001	9×10^{-4}	31.9	0.24	0.35	5.5
Tc solution	0.32	0.46	19.3	81.8	7.3	2.2
Pu solution	<0.009	70.1	0.34	8.3	0.48	2.6
U loaded solvent	102.97	29.2	13.3	<8.6	1.1	<5.6

* The value containing uranous nitrate.

Table 2 summarizes the result of distribution fraction of each element in the product stream. From the results, it was discovered that more than 99.9% of U and Pu were extracted by 30%TBP/n-dodecan in the co-extraction step.

Fig.4 shows concentration profiles of Tc and Np, as a result 64.8% of the Np and 98.9% of the Tc was extracted with 30% TBP/nDD in the co-extraction step. It was found from the result that oxidant rate of Np was insufficient in this condition. There is room for reconsidering this matter. It is necessary to improve extraction condition such as concentration of vanadium oxide or aqueous and organic flow rate(O/A ratio). However, vanadium oxide seems to be expected for oxidation of Np and extracted from raffinate solution.

Fig.5 shows concentration profiles of nitric acid, U and Pu in extractor No.2. U and Pu were almost constant in both the organic and the aqueous phases in the Np separation and the Tc separation step.

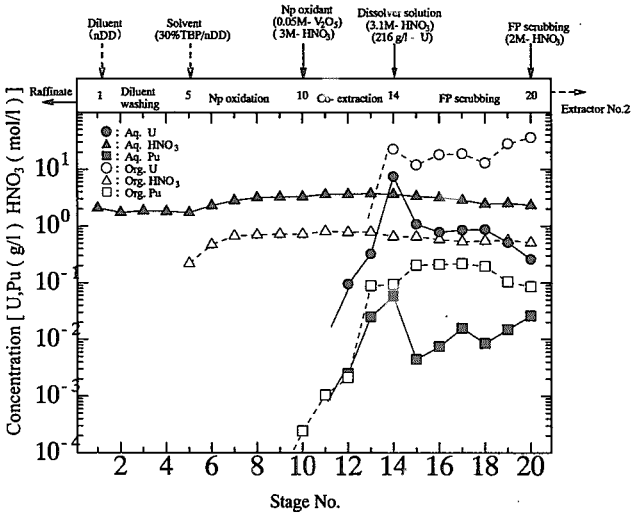

Fig.3 Concentration profiles of nitric acid uranium and plutonium in extractor No.1.

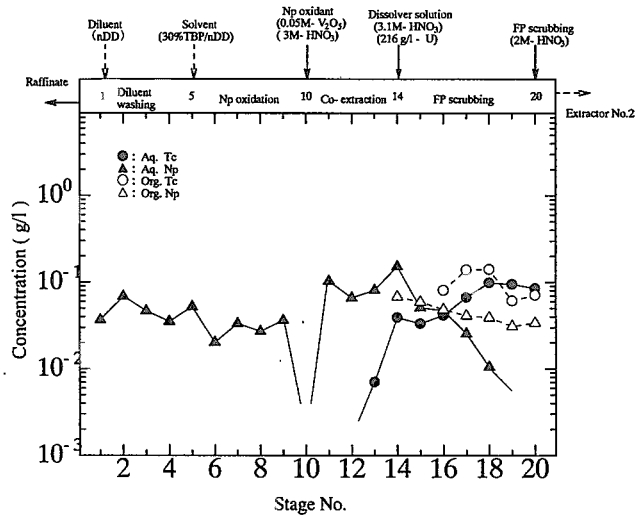

Fig.4 Concentration profiles of technetium and neptunium in extractor No.1.

Almost all of the U and Pu were recovered from aqueous phase in the U recovery step.

Fig.6 shows concentration profiles of Tc and Np. 75.0% of the extracted Np was separated from the U and Pu stream in the Np separation step. Part of Np was reoxidized from Np(V) to Np(VI) by 6M nitric acid, consequently, was extracted to 30%TBP/nDD again in the Tc separation step. On the other hand, 81.7% of the Tc was separated by 6M nitric acid. However, 16.1% of the Tc transferred to U/Pu partitioning step that was not separated from the U and Pu stream.

Fig.7 shows concentration profiles of Zr and Ru in extractor No.2. As the diagram indicates, Zr was scrubbed to some extent in the Np separation step. On the other hand, the concentration was constant in the Tc separation step.

The concentration of Ru was constant in the Np separation step, but almost all of the Ru was scrubbed by 6M nitric acid in the Tc separation step.

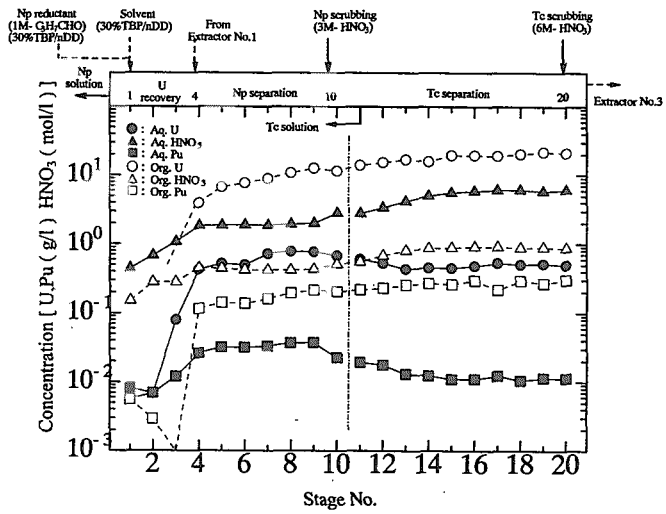

Fig.5 Concentration profiles of nitric acid uranium and plutonium in extractor No.2.

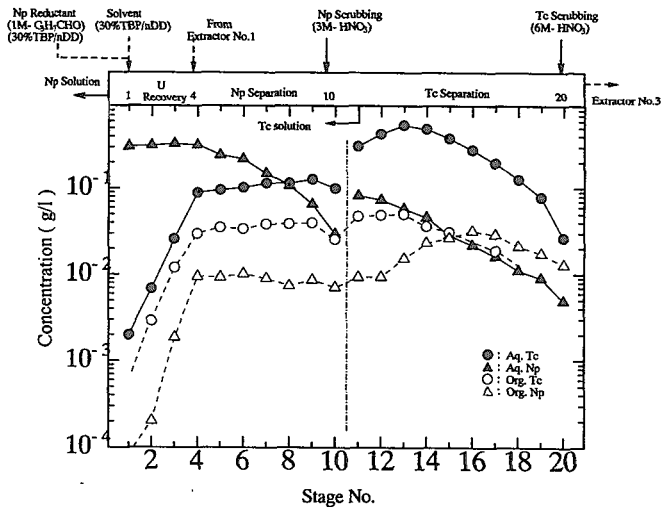

Fig.6 Concentration profiles of technetium and neptunium in extractor No.2.

In the U/Pu partitioning step (Extractor No.3) Pu was stripped into aqueous phase that was reduced from Pu(IV) to Pu(III) by U(IV) with hydrazine as shown in Fig.8. The concentration of U in organic phase was almost constant. As for Pu, the concentration in both the organic and the aqueous phases decreased in the U/Pu partitioning step.

Fig.9 shows concentration profiles of Tc and Np. Most of the Np remained in the U loaded solvent (organic phase). To the contrary, Tc migrated to the Pu solution (aqueous phase).

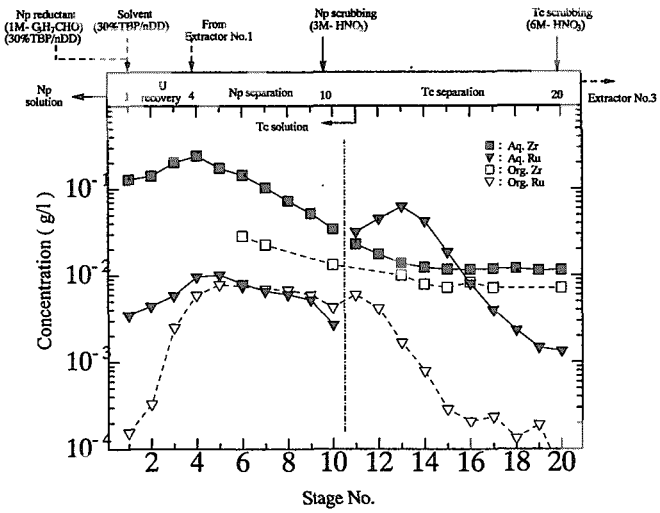

Fig.7 Concentration profiles of zirconium and ruthenium in extractor No.2.

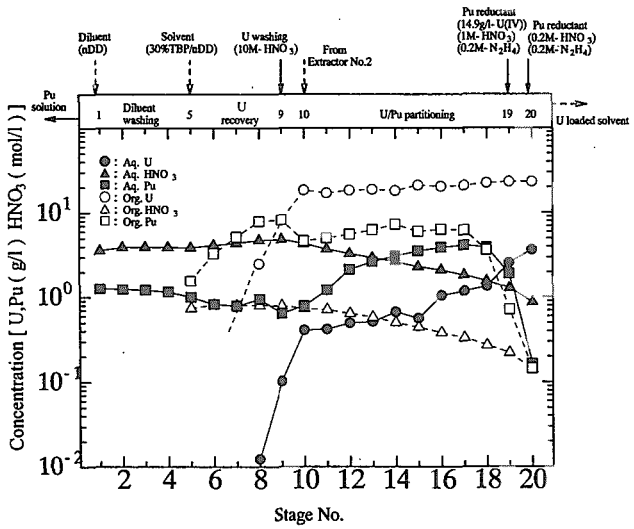

Fig.8 Concentration profiles of nitric acid uranium and plutonium in extractor No.3.

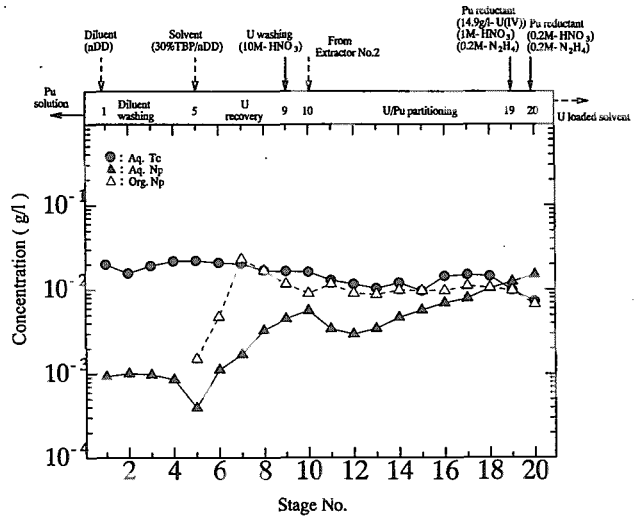

Fig.9 Concentration profiles of technetium and neptunium in extractor No.3.

4. CONCLUSIONS

These results led to the conclusion that 64.8% of the Np and 98.9% of the Tc were extracted in the co-extraction step. 75.0% of the extracted Np was separated from the U and Pu stream using by butyraldehyde as a reducing agent in the Np separation step. On the other hand, 81.8% of the Tc was separated by 6M nitric acid in the Tc separation step.

The separation efficiency of Np was not enough under this condition. It is necessary to optimize to enhance the Np oxidation and separation rate. However, it was found that butyraldehyde and 6M nitric acid were effective in separating Np and Tc from the U and Pu stream. A further direction of this study will be to clear the chemical reaction of Np. These technologies are expected to be applied to simplified reprocessing process.

REFERENCES

1) M.Maeda et al., GLOBAL95, Versailles, 11-14 Sep, 1995
2) S.Fujine et al., 10th Pacific Basin Nuclear Conference, Kobe, 20-25 Oct, 1996
3) G.Uchiyama et al., Nucl.Technol.,102,341, 1993
4) G.Uchiyama et al., ICEM97, Singapore, 12-16 Oct, 1997
5) S.Fujine et al., GLOBAL97, Yokohama, 5-10 Oct, 1997
6) N.Srinivasan et al., B.A.R.C-734 and 735, 1974

This is a blank page.

JP0250343

JAERI-Conf 2002-004

FUNDAMENTAL STUDY ON THE CONTROL OF MINOR NUCLIDES (Np, Tc) BEHAVIOR BY ELECTROLYTIC REDUCTION

T. Asakura[1], H. Hoshi[2], Y.-Z. Wei[2], M. Kumagai[2] and G. Uchiyama[1]

1. Japan Atomic Energy Research Institute, Tokai Research Establishment, Shirakata-Shirane 2-4, Tokai-mura 319-1195

2. Institute of Research and Innovation, 1201 Takada, Kashiwa-shi, 277-0861 Japan

FAX: +81-(0)29-254-4006, e-mail: asakura@procsafe.tokai.jaeri.go.jp

The reduction of technetium, neptunium, and uranium was studied using a flow type electrolytic cell containing a carbon-fiber column electrode. Qualitative reduction of Np (VI) into Np (V) was confirmed at the potential of 0.3 V vs. Ag/AgCl in 3 mol·l^{-1} HNO_3 solution. Quantitative reduction of U (VI) into U (IV) with co-existing Np and Tc was also confirmed at –0.3 V vs. Ag/AgCl in 3 mol·l^{-1} HNO_3 solution. The reductive behavior of Tc still needs to be studied further.

Keywords: Electrolysis, Reduction, flow type electrolytic cell, Neptunium, Technetium, Uranium

1. INTORDUCTION

In the field of nuclear fuel reprocessing, it is important to control the behavior of minor elements such as neptunium and technetium. In spent fuel solution, Np can exist as three valence states, Np (IV), Np (V) and Np (VI). Np (VI) and Np (IV) are well extracted by TBP, but Np (V) is less extracted [1]. In the case of Tc, it exists as its heptavalent state, TcO_4^- anion or $HTcO_4$ molecule, in spent fuel solution. Tc (VII) is fairly well extracted from spent fuel solution by TBP with uranium [2] or zirconium [3]. Tc in tetravalent state, TcO^{2+} cation typically, is less extractable. Thus, it is possible to control the behavior of Np and Tc by controlling their valence state.

Standard electrode potential of redox reaction,

$$NpO_2^{2+} + e^- = NpO_2^+,$$

is reported to be +1.15 [4] or +1.236 [5] V vs. NHE (normal hydrogen electrode). For reaction,

$$TcO_4^- + 4H^+ + 3e- = TcO_2 + 2H_2O,$$

*This work was participated under the framework of the collaboration between JAERI and IRI. A portion of this work was performed by IRI under a contract from the Ministry of Education, Culture Sports, Science and Technology.

the potential is +0.7 [4] or +0.738 [5] V vs. NHE and the potenital for reaction,

$$UO_2^{2+} + 4H^+ + 2e- = U^{4+} + 2H_2O,$$

is +0.273 to +0.330 [4-6] V vs. NHE. Thus, it is possible to reduce Np (VI) to Np (V) selectively without reducing Tc (VII) and U (VI). If Tc (VII) is reduced, Np (VI) will be also reduced,but U (VI) will not. If U (VI) is reduced, both Np (VI) and Tc (VII) will be reduced.

In this paper, electrolytic reduction of Tc, Np, or U-Np-Tc in aqueous HNO_3 solution using a flow type electrolytic cell containing a carbon-fiber column electrode is studied. First purpose of this study is to confirm electrolytic reduction of U (VI) to U (IV), to developing a reprocessing process basing on ion exchange. The Second is to utilize electrolytic reduction for selective separation in improved PUREX process [7], which is designed to separate Np and Tc selectively from U and Pu.

2. EXPERIMENTAL

Electrolytic reduction of Tc, Np, or U-Np-Tc solution

A flow-type electrolytic cell containing a carbon-fiber column electrode (Hokuto Denko Corp., HX-201, 2 m*l*) was used to reduce Tc, Np or U-Np-Tc solution. Table 1 summarizes the conditions of respective experimental runs. Conditions in Run 1 and 2 are selected to obtain knowledge about Tc behavior under U (VI) reductive conditions. Those in run 3 are for Np (VI) reduction. Run 4 was participated to confirm U (VI) reduction with coexisting Np and Tc.

Table 1 Aqueous solution for electrolytic reduction and applied potential

RUN	Concentration / mol·l^{-1}					Applied potential / V vs. Ag/AgCl
	Tc	Np	U	HNO_3	N_2H_4	
1	10^{-3}	–	–	6	–	–0.3
2	10^{-3}	–	–	6	10^{-3}	–0.3
3	–	10^{-3}	–	3	–	0.3
4	10^{-3}	10^{-3}	0.1	6	10^{-3}	–0.3

Respective solution passed through the cell at the rate of 1 m*l*·min^{-1}, and solution fraction flowing out from the cell was collected. The concentration of respective elements remaining in the solution was determined by ICP-AES for U and Tc, or gamma spectrometry (radiation at 277 eV) for Np. Photo-absorptive spectra were also measured.

Ion exchange behavior

Five milliliters of Tc solution after reduction was contacted with about 1 g of anion exchanger

(AR-01, silica-polymer composite, benzimidazole functional group) at 25 °C for 2 hours. The concentration of Tc remaining in the solution was determined by ICP-AES.

3. RESULS AND DISCUSSION

At first, Tc reduction was studied using a flow-type electrolytic cell, without N_2H_4 in feed solution (Run 1). The electrolysis, however, did not work well because of bubble formation in the solution. The solution flowing out from the cell showed a blue color, and a 380 nm peak implying the formation of nitrous acid was observed in its photo-absorptive spectrum. Then, solution with N_2H_4 was prepared as feed solution (Run 2). In this case, the formation of nitrous acid was well suppressed as expected. The concentration of Tc in the solution flowing out from the cell was almost not changed, implying that no electro-deposition occurred. Any absorption peak of Tc (IV), however, could not be observed in the spectrum of the flowing out solution. Moreover, the adsorptive distribution coefficient ratio of Tc to AR-01 increased to 13 $m\ell \cdot g^{-1}$ after reduction from 7 $m\ell \cdot g^{-1}$ before reduction. If Tc exists as TcO^{2+}, it is expected not to be adsorbed to an anion exchanger. The increase might be explained by Tc (IV)-nitrate complex formation, although there is not enough proof.

Further, Np reduction was also studied (Run 3). Figure 1 shows a photo-absorption

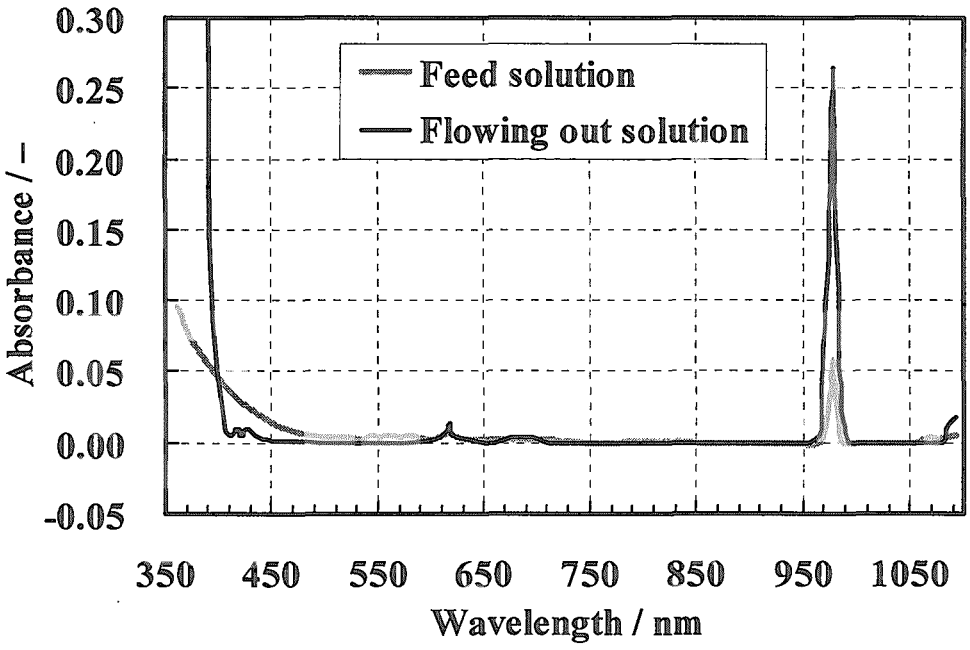

Fig. 1 Photo-absorptive spectrum of feed solution, or that of solution fraction flowing out from the electrolytic cell, collected during 0 to 5 min. Feed solution; Np: 10^{-3} mol·ℓ^{-1}, HNO_3: 3 mol·ℓ^{-1}. Flow rate: 1 $m\ell \cdot min^{-1}$. Applied potential: +0.3 V vs Ag/AgCl.

spectrum of feed solution, or that of solution flowing out from the electrolytic cell, respectively. As is apparent from Fig. 1, a photo-absorption peak at 979 nm corresponding

to Np (V) fairly was stronger in flowing out solution if compared to that observed in the spectrum of the feed solution. Respective solution fraction collected during 0 to 5 min (in Fig. 1), 5 to 10 min, 10 to 15 min or 15 to 20 min had almost the same absorbance value at the peak. Qualitatively, electrolytic reduction of Np (VI) into Np (V) by using the flow-type electrolytic cell was confirmed. It is reported that Np can be selectively stripped by batch-wise electrolytic reduction from TBP solvent loaded by U, Pu and Np [8]. Current reductive technique can be applied to selective Np separation.

Finally, the reduction for U-Np-Tc solution was examined (Run 4). The absorption spectrum of flowing out solution showed typical absorption peaks of U (IV) as Fig. 2, and

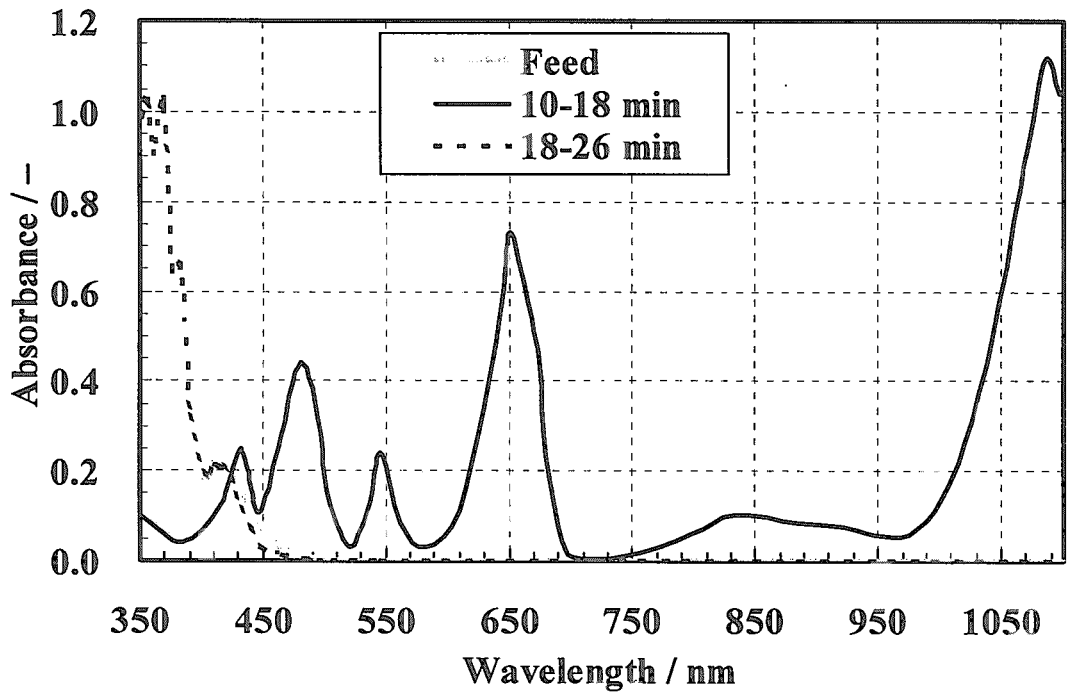

Fig. 2 Photo-absorptive spectrum of feed solution, or that of solution fraction flowing out from an electrolytic cell, collected during 10 to 18 min, or 18 to 25 min, respectively. Feed solution; U: 0.1 mol·l^{-1}, Np: 10^{-3} mol·l^{-1}, Tc: 10^{-3} mol·l^{-1}, HNO_3: 6 mol·l^{-1}, N_2H_4: 10^{-3} mol·l^{-1}. Flow rate: 1 ml·min^{-1}. Applied potential: –0.3 V vs Ag/AgCl.

quantitative U (VI) reduction into U (VI) was confirmed with co-existence of Np and Tc. In this experiment, however, nitrous acid was formed and U reduction efficiency decreased to almost zero after 18 minutes of reduction. After 18 min, the cathodic current suddenly increased as shown in Fig. 3, and the flowing out solution contained little U (IV) (Fig. 2). Thus, N_2H_4 concentration in feed solution should be increased to scavenge nitrous acid. Unfortunately, reductive behavior of Np was not known in this experiment, because large U concentration interfered photo-absorptive observation of Np valence state. The behavior of Tc was uncertain, too.

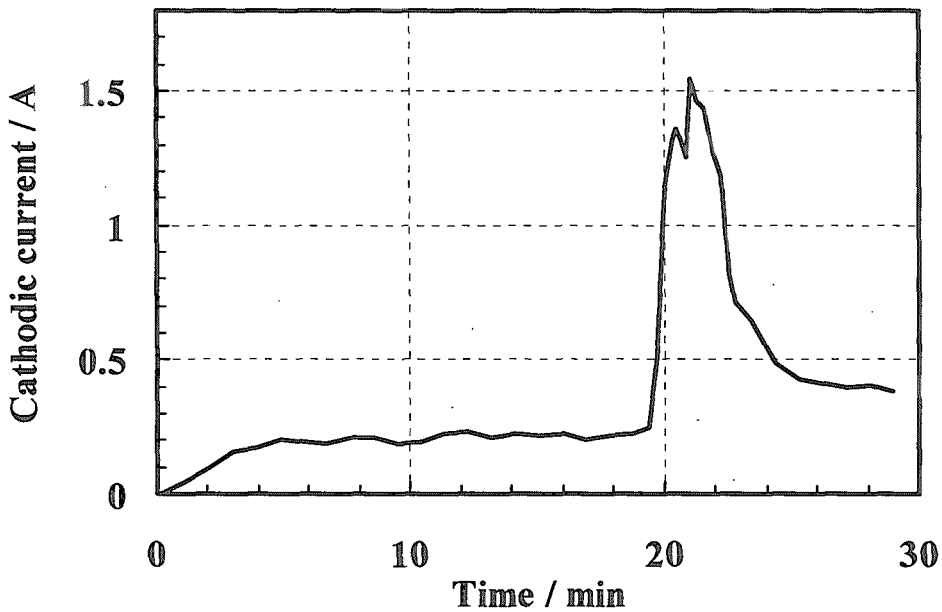

Fig. 3 Cathodic current for U-Np-Tc solution. Feed solution; U: 0.1 mol·l^{-1}, Np: 10^{-3} mol·l^{-1}, Tc: 10^{-3} mol·l^{-1}, HNO_3: 6 mol·l^{-1}, N_2H_4: 10^{-3} mol·l^{-1}. Flow rate: 1 ml·min^{-1}. Applied potential: –0.3 V vs Ag/AgCl.

4. CONCLUSION

The reduction of Tc, Np and U was studied using a flow type electrolytic cell containing a carbon-fiber column electrode. Qualitative reduction of Np (VI) into Np (V) was confirmed at the potential of 0.3 V vs Ag/AgCl in 3 mol·l^{-1} HNO_3 solution. This reductive technique can be applied to a selective Np separation. Quantitative reduction of U (VI) into U (IV) with co-existing Np and Tc was also confirmed at –0.3 V vs Ag/AgCl in 6 mol·l^{-1} HNO_3 solution. The reductive behavior Tc still needs to be studied further.

References

[1] B. Guillaume, C. Maurice, "Chemical properties of neptunium applied to neptunium management in extraction cycle of PUREX process", Extraction 84, Institute of Chemical Engineers Symposium Series No. 88, Institute of Chemical Engineers, Rugby, 31(1984).

[2] D. J. Pruett, "The solvent extraction of Heptavalent Technetium by Tributyl Phosphate", Sep. Sci. Technol., **16**, 1157(1983).

[3] J. Garraway, "The behavior of technetium in in a nuclear reprocessing plant", Extraction 84, Institute of Chemical Engineers Symposium Series No. 88, Institute of Chemical Engineers, Rugby, 47(1984).

[4] R. Tamamushi, Denki-kagaku (Electrochemistry), Tokyo Kagaku Dojin, Tokyo, 299(1967), [in Japanese].

[5] The Chemical Society of Japan, Ed., Kaitei 4-han Kagaku Binran Kiso-hen II, Maruzen, Tokyo, 464(1994), [In Japanese].

[6] M. Gourong, Z. Liufang and Z. Chengfa, "Investigation of the redox potential UO_2^{2+}/U^{4+} and the complex formation between U^{4+} and NO_3^- in nitric acid", Radiochim. Acta, **37**, 145(1985).

[7] G. Uchiyama, T. Asakura, S. Hotoku, *et al.*, "Solvent extraction behavior of minor nuclides in nuclear fuel reprocessing process", J. Radioanal. Nuc. Chem., **246**, 683(2000).

[8] G. Uchiyama, S. Hotoku, S. Fujine, *et al.*, "The method of controlling the valence state of neptunium", PAT. No. 2589886, Japan, Dec. 5, 1996.

JP0250344

JAERI-Conf 2002-004

STUDY ON THE ADSORBENT WITH AMIDOXIME FUNCTIONAL GROUP UTILIZED TO RECOVER USEFUL METALS FROM SEA-WATER

T. Asakura, D. T. Hong, A. Y. Zhang and G. Uchiyama

Japan Atomic Energy Research Institute, Tokai Research Establishment, Shirakata-Shirane 2-4, Tokai-mura 319-1195

FAX: +81-(0)29-254-4006, e-mail: asakura@procsafe.tokai.jaeri.go.jp

Japan Atomic Energy Research Institute has developed fibrous polymer containing amidoxime chelating functional group adsorbent (FPAO) for recovering U from seawater. Recovery of uranium from seawater provides an additional head-end option to nuclear fuel cycle. Fundamental experiments showed that FPAO adsorbs U(VI) the best around pH 6.0, and that adsorptive reaction is a thermo-activated process having activation energy of 28.54 $KJ \cdot mol^{-1}$. Uptake values for metals in FPAO which was immersed to actual seawater for 2 months, were determined to be 9690 for Mg, 0.026 for Ir, 0.0036 for Au, 320 for V, 290 for U, 0.97 for La, 0.83 for Ce, 8.6 for Ti, and 0.97 for Zr, as in unit of $\mu g \cdot (g\text{-dry FPAO})^{-1}$. From batch desoption experiments, it is suggested to possible to recover Mg, U or La/Ce separately by using HCl and $H_2C_2O_4$ (oxalic acid) as elutants.

Key words: Metals, Adsorbent, Sea-water, Amidoxime, Desorption

1. INTRRODUCTION

Seawater contains many kinds of useful elements such as uranium, rare-earth elements and noble metals etc. Their recovery has gained great interest in many countries. If it is possible to recover uranium from seawater, it provides an additional head-end option to nuclear fuel cycle. Since concentration of metals in seawater is very low (in parts per billion), efforts have been made over years to find an efficient method to concentrate and separate these metals from seawater. Among separation processes such as solvent extraction, ion exchange, adsorption, precipitation, etc. adsorption of metals on various inorganic and organic adsorbents shows a lot of advantages from the viewpoint of environmental protection. Requirements for the adsorbents include high physical and chemical stability, fast and selective uptake of metals, sufficient loading capacity and easy desorption.

Japan Atomic Energy Research Institute (JAERI) has developed fibrous polymer containing amidoxime chelating functional group adsorbent (FPAO) for recovering U from seawater. This adsorbent has an affinity with divalent cation, typically U(VI), and demonstration test to produce uranium from seawater has been performed. Many other valuable metals such as V, Mg, Ir, Au, La, Ce, Ti, Zr have yet to be tested on this adsorbent.

Present study deals with the kinetics of adsorption of U(VI), determining the uptake of

valuable metals in FPAO immerse in actual seawater, and identifying the proper conditions for desorption of the metals.

2. EXPERIMENTAL

2.1 Preparation of adsorbent

Using a fibrous polypropylene resin sheet as base material, acrylonitrile and methacrylic acid were graft polymerized by γ-irradiation. The grafted fibrous resin sheet was reacted with hydroxylamine at 60 °C for 1 hour and converted into fibrous polymer containing amidoxime chelating functional group adsorbent (FPAO, hereafter). The average content of the functional group in FPAO was about 3.61 mmol·(g-dry FPAO)$^{-1}$.

2.2 Kinetics of U(VI) adsorption

The adsorbent was cut into about 3×4 mm of small pieces, conditioned with 2.5 % KOH solution at 80°C for 60 min and then washed with distilled water to natural before use. U(VI) solution with a desired pH value maintained by CH_3COOH-CH_3COONa or $Na_2B_4O_7$-H_3BO_3-NaCl and with the ionic strength (μ) of 0.1 mol·l^{-1} maintained by NaCl was prepared. Other reagents used in experiments were of analytical grades and without further purification. Known weight of FPAO, pre-equilibrated by appropriate buffer solution at least for 24 h, was mixed with U(VI) solution in 100 ml triangle flask. The flask was shaken mechanically for a desired contact time in a thermostatic water bath at the desired temperature. The concentration of U(VI) in the solution was determined by ICP-AES (Shimazu ICP-1000III). The amount of U(VI) adsorbed, Q_t / mg·(g-dry FPAO)$^{-1}$ was calculated as follows:

$$Q_t = ([U(VI)]_0 - [U(VI)]_t)\cdot V/W.$$

Where $[U(VI)]_0$ or $[U(VI)]_t$ is the concentrations of U(VI) in feed solution at initial or at any time, t, respectively. V or W is the volume of U(VI) solution or the weight of dried adsorbent.

2.3 Determination of respective metals contained by FPAO immersed in seawater

FPAO was immersed in seawater, about 8 km from the seashore of Sekine-hama, Aomori-ken, in 1999 for 2 months. This loaded FPAO was decomposed to by nitric acid or calcination. A sheet of loaded FPAO (approx. 5 g), washed and dried, was cut into pieces of 5×5 mm, and then decomposed by 100 ml of concentrated nitric acid (13.8 N) at 160-180 °C for about 2 h. Then distilled water was added, the solution was filtered. The solution was adjusted to 100 ml volume, ready for analysis. This method was also used to determine the amount of metal remained in FPAO after desorption. In the second method, loaded FPAO was burned in a furnace to ash, which was then dissolved in acid solution. Concentration of respective metal was determined by ICP-AES and ICP-MS.

2.4 Desorption of metals

Loaded FPAO was washed by distilled water, dried at ambient temperature and cut into pieces of 5×5 mm. Each batch experiment was conducted with one sheet of about 5 g in a 3-liter beaker at room temperature. After finishing experiment, adsorbent was immediately separated from solution. Respective batch experiment was conducted at various concentrations of different acids (HCl, HNO_3, CH_3COOH, $H_2C_2O_4$, H_2SO_4, $HClO_4$), varying stirring speed, temperature and solid/liquid ratio. Concentration of metals in the solution was analyzed by ICP-AES and ICP-MS, allowing the amount of metals desorbed from FPAO to be calculated.

After desorption, the adsorbent was washed with distilled water and decomposed by concentrated HNO_3 as described above to determine the amount of metals remained in amidoxime adsorbent.

Desorption efficiency (η / %) for each metal was calculated as follows:

$$\eta = \frac{Md}{Md + Mr}$$

with *Md* and *Mr* being the amount of metal desorbed from adsorbent and that of metal remained in adsorbent, respectively.

3. RESULTS AND DISCUSSION

3.1 Kinetic and equilibrium study on U adsorption

Figure1 shows the influence of acidity of feed solution, pH: 1.0-9.0, on the adsorption of U(VI). It is to been seen that the amount of U(VI) adsorbed with FPAO in feed solution rapidly increases with increasing the pH values from pH 1.0 to 3.0, slowly increases from pH 3.0 to 6.0, reaches the maximum value when pH value is 6.0 and subsequently rapidly decreases from pH 6.0 to pH 9.0. So the optimum acidity is determined as pH 6.0. These facts implies that a process of releasing proton,

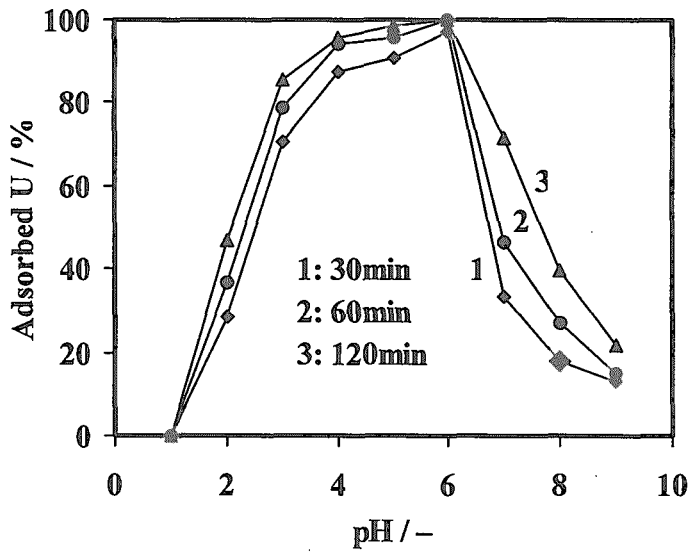

Fig.1 The influence of pH values on the adsorption.
FPAO: 0.10 g, (7.26×10^{-3} mol·l^{-1}).
[U(VI)]: 128 mg·l^{-1} (ppm).

$$R\text{-}C(NH_2)N\text{-}OH \rightarrow R\text{-}C(NH_2)N\text{-}O^- + H^+,$$

in FPAO molecule is a rate controlling-step for the adsorption of U(VI) with FPAO when the acidity of feed solution changes from pH 1.0 to 6.0. It is benefit to the adsorption of FPAO on U(VI) because decreasing the acidity of solution, that is increasing the pH value, can accelerate this process to take place. At pH value more than 6.0, especially at 9.0, the decrease is explained by the precipitation of U(VI).

As expected, the amount of FPAO and concentration of U(VI) affect on the adsorption of U(VI). Figure 2 shows the the influence of the concentration of U(VI), 50-300 ppm, on the adsorption of U(VI). In the case of 0.1 g, the adsorbed amount of U(VI) slowly and linearly increased, and the adsorption percent of U(VI) was decreased with increasing the concentration of U(VI). The adsorption percentage of U(VI) at 20 min decreased from 99.8 % to 81.3 % if the concentration of U(VI) increased from 59ppm to 300ppm. This shows the saturated adsorption capacity of U(VI) is far not reached in excess of FPAO. In the case of 0.015 g of FPAO, adsorbed U amount increases rapidly with increasing the concentration of U(VI), and subsequently slowly increases. It indicates the adsorption of the fibrous adsorbent FPAO on U(VI) gradually approach to its maximum adsorption capacity. These facts imply that FPAO possesses a large adsorption capacity on U(VI). The influence of the size of the adsorbent on the adsorption of U(VI) was also studied. Under constant amount of FPAO, the rate is faster as the size is smaller, comparing square adsorbent, 2×2mm, 3×4mm and 6×6mm.

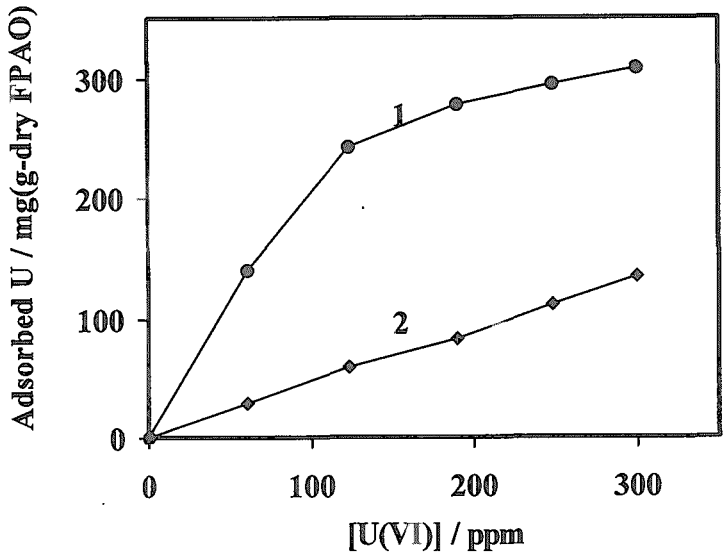

Fig.2 The relationship between the amount of adsorbed U and the concentration of U. FPAO: 1) 0.015 g, 2) 0.10 g. pH: 6.0, μ: 0.1mol·l^{-1}.

The influence of temperature (25-45°C) on the adsorption of U(VI) with FPAO was investigated for the weight of FPAO 0.1g, pH 6.0 and the concentration of U(VI) 128ppm. The results show that the adsorption process was an endothermic reaction because the amount of U(VI) adsorbed increases with increasing the temperature. According to

$$-\ln(1-F)=kt,\ F = Q_t/Q_\infty,$$

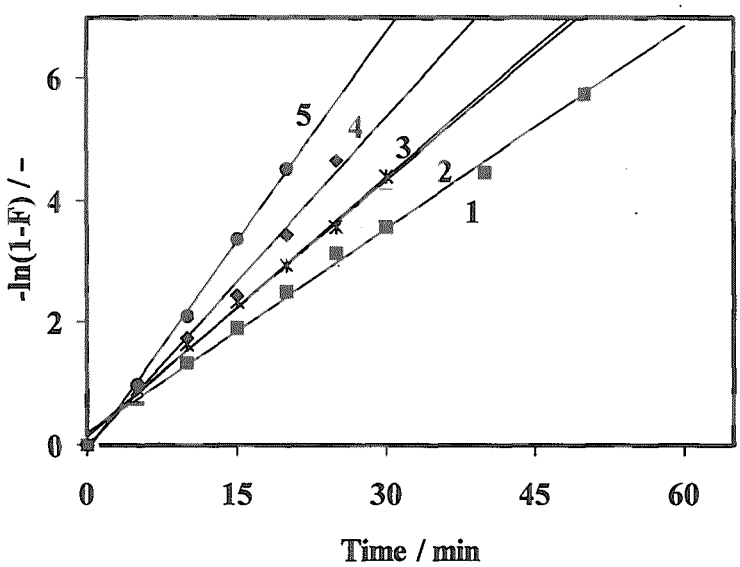

Fig.3 The relationship between -ln(1-F) and time. Dependence on the temperature.
1) 25 °C, 2) 30 °C, 3) 35 °C, 4) 40 °C, 5) 45 °C.
pH: 6.0, FPAO: 0.10 g, [U(VI)]: 120 ppm.

a graphs of –ln(1-F) versus t are shown in Figure 3. The results shows that the adsorption process of U(VI) with FPAO is a chemical adsorption because the linearity between –ln(1-F) and t. In table I, the values of the constant k at respective temperature is summarized. In Figure 4, values for k are plotted agenst $1/T$ according to Arrhenius' law. The relation between k / min and temperature T / K is expressed as,

$$k = 7.43 \times 10^3 \, e^{-\frac{28.5\times10^4}{RT}},$$

and activation energy of 28.5 KJ·mol^{-1} is obtained for this endothermic reaction.

Table I k value at respective temperature

Temperature / °C	25	30	35	40	45
k / min^{-1}	0.0771	0.0873	0.1081	0.1312	0.1558

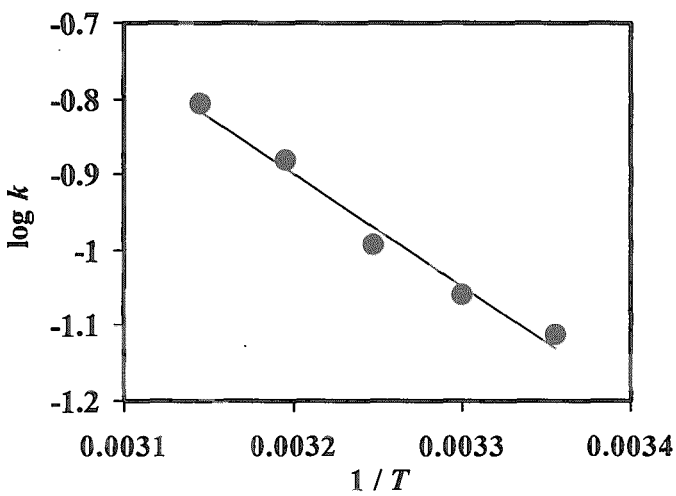

Fig.4 Arrhenius plot for k.

3.2 Adsorption of metals in FPAO contacted with seawater

The experimental results are summarized in Table II. Apparently, uptake of Mg, V, or U was significantly high, while Ti, Zr, La or Ce uptake was rather low. Uptake of Au or Ir was the lowest. Concentration factor of V, U, La, Ce, Ti was high, and that of Au was moderate. This suggested that FPAO can be used for recovering U, V and some other valuable metals such as La, Ce, Ti, Zr from seawater.

Table II. Uptake and concentration factor of metals

Element	Concentration in seawater [1] / $\mu g \cdot l^{-1}$	Principal species	Uptake / $\mu g \cdot (g\text{-}FPAO)^{-1}$	Concentration factor / $ml \cdot g^{-1}$
Mg	1.35×10^{6}	Mg^{2+}, $MgSO_4$	9690	7.18
Ir	–	–	0.026	–
Au	0.004	$AuCl_4$	0.0036	1000
V	2	$VO_2(OH)_3^{2-}$	320	160000
U	3	$UO_2(CO_3)_3^{4-}$	290	97000
La	1.2×10^{-2}	–	0.97	81000
Ce	5.2×10^{-3}	–	0.83	160000
Ti	1	–	8.6	8600
Zr	–	–	0.97	–

3.3 Desorption isotherms of loaded FPAO

Figure 5 shows the desorption isotherm of U or La with changing the kinds of elutants. As shown in the figure, 80 % or more U was eluted from loaded FPAO by HCl with concentration of 0.5 N or more, or by 1 N $H_2C_2O_4$ in 30 min. On the other hand, 0.05 N HCl or 1 N CH_3COOH was less effective to eluting U. In the case of La, 1 N $H_2C_2O_4$ did not elute it well. 0.5 N HCl eluted 90 % of La in 30 min. Ce showed the same trend as La, and about 80 % Ce was desorbed with 0.5 N HCl in 30 min. In the case of Mg, approximately 99 % of Mg was eluted by 0.05 N HCl in 30 min. In figure 6, temperature dependence of desroption of Mg, U, Ti, V is shown. It is clear from the figure that temperature hardly

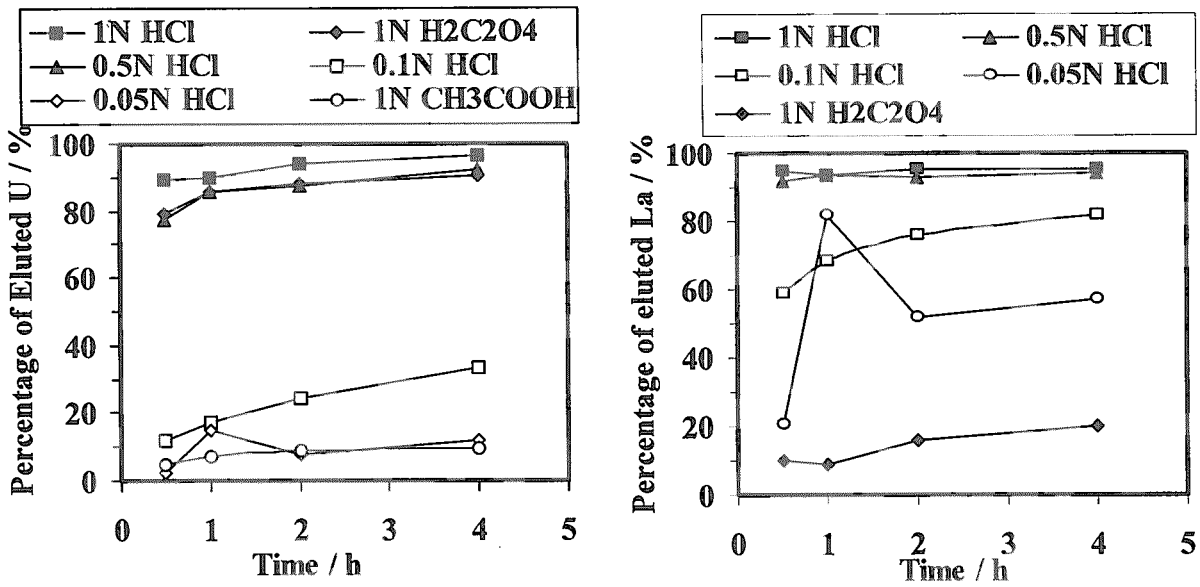

Fig.5 Desorption isotherms of U, or La . Depencence on the kinds of elutants.

affects Mg desorption. On the other hand, U is desorbed faster if the temperature is higher. Thus, it is possilbe to develop a mutual separation method for Mg, U and La/Ce. Mg can be easily desorbed from loaded FAPO with 0.05 N HCl. Lower temperature is desireble. Under this condition, majority of U, La/Ce still remains in the FPAO. Then U can be

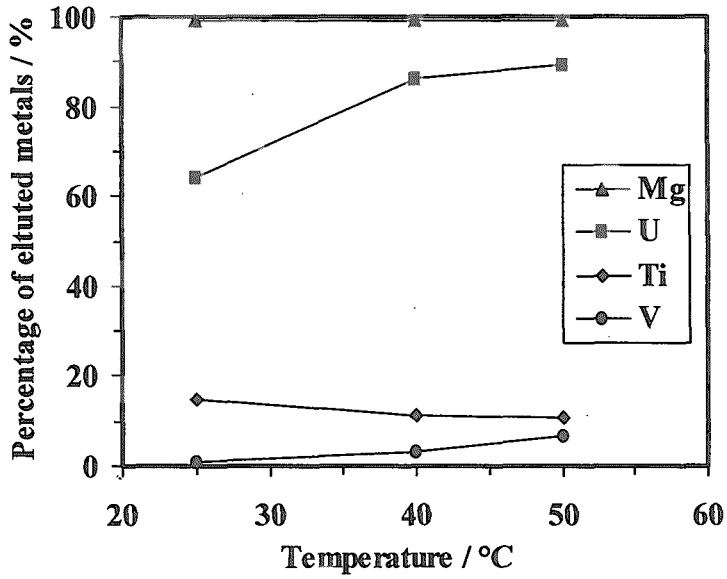

Fig. 6 Desorption of U, Mg, Ti and V. Dependence on temperature..

desorbed by H2C2O4, while La/Ce remains in FPAO, again. After those, 0.5 N HCl desorbs La/Ce.

HCl is effective elutant for Mg, U, La/Ce. It, however, seems be less effective for V, Zr and Ti: only about 20 % Ti was desorbed with 0.5 N HCl and several percentage of V was desorbed with 1 N HCl. About 25 % V was eluted by using $H_2C_2O_4$. Many another eluants such as $HClO_4$, H_2SO_4, NH_4OH, NH_4NO_3, NH_4Cl, some organic acids and mixtures of acids were examined for V, Zr and Ti but none of them showed to be suitable for V. About 60 % of Ti was eluted with 1:1 mixture of 1 N HCl and 1 N CH_3COOH 1N. About 60% of Zr was desorpted from FPAO adsorbent with 1 N NH_4OH.

Concentration factor for V is quite large and the uptake is also high. In the present work, however, no effective desorption agent for V was found.

4. CONCLUSION

Kinetics of U(VI) adsorption to FAPO is established, as endothermic process having 27.2 $KJ \cdot mol^{-1}$. The kinetic study should be expanded to other kind of metals, such as La, Ce, V, Au, Ir, Zr. The amidoxime adsorbent can be effectively employed for recovering U and some other valuable metals such as Mg, La, Ce from seawater. Value of concentration factor for V is quite high but an effective desorption agent has to be seeked.

Work in progress includes column experiments for both kinetics study and desorption study.

References

[1] R. A. Horn, "Marine Chemistry. The Structure of water and the Chemistry of the Hydro-sphere", Willey-Interscience, New York, (1966) p. 155.

This is a blank page.

JP0250345

JAERI-Conf 2002-004

SPENT FUEL DISSOLUTION TEST INCLUDING DISSOLVER OFF-GAS TREATMENT IN THE NUCEF ALPHA-GAMMA CELL: SPENT FUELS WITH BURNUPS UP TO 44 GWDT^{-1}

H. Mineo, M. Iizuka, S. Fujisaki, H. Isogai, S. Hotoku, T. Asakura, G. Uchiyama
Process Safety Laboratory, Department of Fuel Cycle Safety Research
Japan Atomic Energy Research Institute
2-4 Shirakata-shirane Tokai-mura, Naka-gun
Ibaraki, 319-1195 Japan
Fax: 81-29-282-6677, e-mail: mineo@procsafe.tokai.jaeri.go.jp

Spent fuel dissolution test was carried out to study the dissolution behavior of nuclides and the behavior of volatile nuclides, using a bench-scale reprocessing test rig in the NUCEF alpha-gamma cell. 29 and 44 GWdt^{-1} spent fuels were respectively dissolved. Study on the dissolution behavior showed that the dissolution rate of uranium and plutonium were similar. Also, other species: Cesium, Americium, Strontium and Neodymium were found to dissolve in the similar manor to uranium. The fraction of Mo dissolved was found to decrease during the dissolution. Zirconium molybdate ($Zr(Mo_2O_7)(OH)_2(H_2O)_2$) was identified from the XRD pattern of residue in the 29 GWdt^{-1} spent fuel dissolution. Those results suggested the precipitation of the hydrate during dissolution. As for the iodine-129 removal, decontamination factor of AGS (silica-gel impregnated with silver nitrate) column was more than 36,000. Measurement of iodine-129 in the dissolver solution revealed that less than 0.57% of total iodine-129 generated, which was estimated by ORIGEN II calculation, was remained in the dissolver solution. Also, measurement of iodine-129 by an iodine-stripping operation from the dissolver solution using potassium iodate suggested that another 2.72% of total iodine-129 precipitated as iodide. In addition, about 70 % of total iodine generated was measured in the AGS columns. Rest of iodine-129 was supposed to adsorb to the HEPA filter and the inner surface of dissolver off-gas lines. Those results on iodine-129 distribution were found to be almost identical to the results obtained in the study using iodine-131 as tracer. Release of carbon-14 as carbon dioxide during dissolution was found to occur when the release of Kr-85. From the measurement of carbon-14, initial nitrogen-14 concentration in the fuel was estimated to be about several ppms, which was within the range reported.

Key words: Reprocessing, Spent fuel, Dissolution, Off-gas treatment, iodine-129, carbon-14, insoluble residue

1. INTRODUCTION

It is indispensable to control and confine radioactive material safely within an area in the nuclear fuel reprocessing process. Most of radioactive material contained in spent fuel is separated from nuclear material and finally vitrified as highly radioactive waste. However, some elements like neptunium can easily be mixed into process products and waste stream, and others like radioiodine are volatile and diffusive. It is, therefore, necessary to study the behavior of such radioactive nuclides in the process and to assess the safety margin of the confinement capability.

In the dissolution process, most of volatile species in the spent fuel are released and transferred into the dissolver off-gas (DOG). Among the volatile species, iodine-129 is a long-lived (half-life: 1.57×10^7 years) and hazardous nuclide. The nuclide should strictly be controlled and confined within the process. Confinement of iodine is done by expelling as much as possible from the dissolver solution to the DOG and then by removing the iodine from the DOG using a caustic scrubber and/or adsorbent, which is called iodine-stripping operation. As a result, small portion of iodine-129 remain in the dissolver solution and insoluble residue. Such iodine distribution behavior over the dissolution process is important for the estimation of iodine release into the environment. Studies using beaker-sized equipment has been carried out, and suggested that the iodine distribution behavior was different from that obtained in a reprocessing plant and that data on iodine-129 distribution in a larger experimental rig became necessary [1]. Adsorbent such as AGS (Silica-gel impregnated with silver nitrate), will be used in the large reprocessing plant under

construction. It is important to confirm the confinement capability of the iodine removal system employing the adsorbent using actual spent fuel.

The DOG contains carbon-14, which has a half-life of 5.7×10^3 years, is generated from the neutron absorption by nitrogen and oxygen during the irradiation of nuclear fuel. The nitrogen and oxygen are an impurity and a constituent of fuel, respectively. Most of carbon-14 is released as carbon dioxide during the dissolution [2]. In the present, carbon-14 is not included in the nuclides that have to be removed in Japan. The nuclide is, however, the largest contributor to the equivalent dose rate of nearby residents [3], and it is important to study behavior of carbon-14 in the dissolution and off-gas treatment processes.

Insoluble residue has been studied extensively since it affects the operation and maintenance of a reprocessing plant [4]. The residue includes precipitates as well as metal alloy consisted of Ru, Mo, Tc, Pd and Rh. The amount of residue increases with burnup of the spent fuel [5]. Also, the amount of precipitate is affected by the acidity in the dissolution [6]. Previous work using 8 $GWdt^{-1}$ found that zirconium molybdate ($Zr(Mo_2O_7)(OH)_2(H_2O)_2$) precipitated during dissolution, which was identified by the measurement of X-ray diffraction pattern [7]. It was reported that the generation of this hydrate increased the plutonium in the residue, which may adversely affect the recovery ratio of plutonium [6]. The precipitation tends to occur under low acidity and high temperature in simulated HLLW [8].

The aim of the present study is to obtain data on the behavior of nuclides during dissolution including off-gas treatment and to confirm the confinement capability. It also includes the characteristics of insoluble residue. This paper describes the results obtained in the dissolution test using spent fuel up to 44 $GWdt^{-1}$ carried out in the $\alpha\gamma$ cell of NUCEF (Nuclear Fuel Cycle Safety Engineering Research Facility)

2. EXPERIMENTAL

2.1 Dissolution test rig

Fig. 1 shows a schematic of experimental reprocessing head-end equipment used in the study. The dissolution process comprised a dissolver, an iodine-stripping tank, a dissolver solution filter, an extraction-feed tank, a condenser, a scrubber, a HEPA filter, iodine adsorbent columns and a blower. The equipment was installed in the cell except for the adsorbent columns and blower, which have been accommodated in a glovebox above the cell.

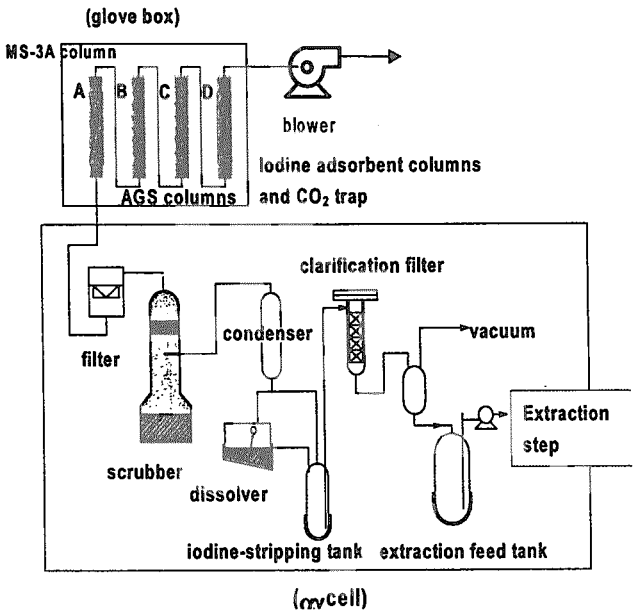

Fig. 1 Schematic diagram of dissolution test rig

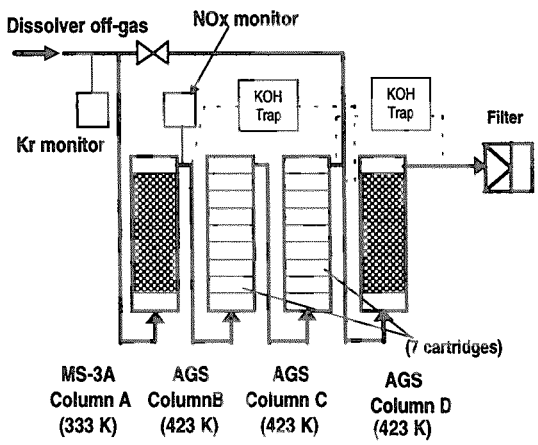

Fig. 2 Iodine adsorption columns

The blower is used to maintain the dissolution process under negative pressure for all operating condition.

Fig. 2 shows a schematic diagram of adsorbent columns used in the present study. The first column (column A) contained MS-3A to remove H_2O in the dissolver off-gas (DOG). Other three columns (Columns B, C and D) were filled with AGS (silica-gel impregnated with silver nitrate). Columns B and C had seven cartridges respectively and each cartridge is filled with 3.4 g of AGS. The AGS was supplied as AC6120 from SÜD CHEMIE AG. More than 98 % of the adsorbent were sized between 1 and 2 mm. The bulk density was 719 kg m^{-3} and its silver content was 12 % in weight. A Kr monitor and a NO_2 monitor were installed in the same glovebox. KOH aqueous solution was used to trap the carbon-14 contained in the off-gas as carbon dioxide. Two traps were connected and used for the measurement of iodine-129 as well as carbon-14 so that the decontamination factor of columns B and C with respect to iodine could be measured.

2.2 Analysis

The dissolver solution was sampled and analyzed to measure the concentration of species contained in the sample. Potentiometric titration was used for the acidity and uranium concentration measurement. ICP-AES, α and γ spectrometries were employed to measure the concentrations of uranium, plutonium, other TRU elements and FPs. The ICP-AES and an X-ray diffractometry were employed to analyze the constituent of insoluble residue collected. Kr concentration in the DOG was measured using the Kr monitor with a NaI scintillation counter. The NOx monitor measured the concentration of NO_2 in the DOG. The amount of iodine-129 on each cartridge was measured with a Ge detector for low-energy gamma ray [9]. The distribution of the nuclide over the dissolution process and DOG treatment system was measured as follows. Iodine-129 in dissolver solution was determined using a method shown by Castleman et al. [10]. Iodine remained as precipitates (AgI and PdI_2) in the residues was recovered by the iodine-stripping method developed by Sakurai et al. [11] which employs KIO_3. The precipitates can be decomposed by the below reactions and the iodine is released into DOG and trapped by the adsorbent.

$$\begin{aligned} &5AgI + KIO_3 + 6HNO_3 \rightarrow 3I_2 + KNO_3 + 5AgNO_3 + 3H_2O \\ &5PdI_2 + 2KIO_3 + 12HNO_3 \rightarrow 6I_2 + 2KNO_3 + 5Pd(NO_3)_2 + 6H_2O \end{aligned} \tag{2.1}$$

The amount of carbon-14 trapped from the DOG was determined by a liquid scintillation counter. Other iodine species such as iodine-131 generated from Cm-244, if existed, were captured by the AGS columns and were detected by the γ spectrometry.

2.3 Experimental condition

The present study used about 1.0 kg of PWR spent fuel (29 $GWdt^{-1}$, cooling time: about 17 years) and about 1.2 kg of PWR spent fuel (44 $GWdt^{-1}$, cooling time: about 12.3 years), which had respectively been cut into short pieces with a length of 40 mm before transferred into the cell. Table 1 shows the dissolution conditions employed in the present study. Nitric acid with 4 to 5 mol l^{-1} was used in the dissolution. Dissolution was carried out three times and about 300 to 400 g of the spent fuel was used in one batch of dissolution. The procedure of the dissolution was: 1) prepare HNO_3 with designated acidity and volume in the dissolver, 2) put the spent fuel into the dissolver, 3) start dissolution (time = 0) by elevating the temperature of the dissolver from ambient temperature to 373 – 374 K and 4) hold the temperature for designated dissolution period.

After the dissolution, the resultant dissolver solution was transferred to the iodine-stripping tank where remaining iodine in the solution was stripped. Table 2

summarizes the operations of iodine stripping used in the present study. In the 29 $GWdt^{-1}$ spent fuel dissolution, two-steps operation was employed. In the first-step operation, KIO_3 is added to the dissolver solution being heated up at 373 K to decompose the iodine precipitates according to the reaction (2.1), and then the solution is maintained at the same temperature for two hours. In the second-step operation, 50 % NO_2 gas is introduced and maintained at 373 K for two hours. At the 44 $GWdt^{-1}$ spent fuel dissolution, as shown in the table, iodine-stripping using NO_2 gas was firstly used, which was normal procedure employed in a reprocessing plant. In addition, the two-steps method was used as well, in order to enhance the effect of the method and to measure the amount of iodine remained as precipitates.

Table 1 Dissolution conditions

Burn-up [GWd/t]	Run No	U element [g]	HNO_3 Concentration[N] (volume [l])	Temperature [K]	Dissolution time [min]
29	SFD2-1	372.66	5.21 (1.57)	373	220
29	SFD2-2	283.95	3.98 (1.44)	373	160
29	SFD2-3	274.36	4.06 (1.29)	373	140
44	SFD3-1	325.72	5.26 (1.59)	373	220
44	SFD3-2	325.54	4.68 (1.64)	373	220
44	SFD3-3	342.74	3.93 (1.61)	373	220

Table 2 Iodine-stripping operations employed

Burn-up [GWd/t]	Iodine-stripping operations	
29	KIO_3, 373 K, 120 min + NO_2 gas, 373 K, 120 min	-
44	1) NO_2 gas, 363 K, 120 min	2) KIO_3, 373 K, 120 min + NO_2 gas, 373 K, 120 min

In all experiments the flow rate of DOG was maintained at approximately 0.4 Nm^3h^{-1}. After the iodine stripping, the dissolver solution was filtrated to remove particulate residue using sintered stainless steel filters and subsequently adjusted to 3 mol l^{-1} HNO_3 and 250 gU l^{-1} as extraction feed solution.

3. RESULTS AND DISCUSSION

3.1 Dissolution behavior

Fig. 3 shows the change in the concentrations of uranium, nitric acid, Kr-85 and temperature during the dissolution of 44,000 $MWdt^{-1}$ spent fuel using 5.26 mol l^{-1} of HNO_3. The uranium concentration increased during the first 60 minutes. After 100 minutes, the concentration did not increase, which could mean the dissolution almost completed. The Kr-85 concentration reached the maximum at 40 to 50 minutes and then leveled off. After 100 minutes the concentration

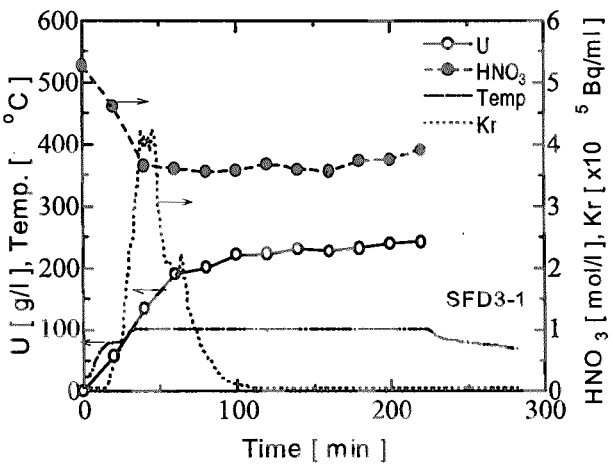

Fig.3 Change in the concentrations of uranium, nitric acid, Kr-85 and temperature

was close to background level, which could mean the end of dissolution. At lower acidity (e.g. 3.93 mol l^{-1} HNO_3), more than 200 minutes was required to complete the dissolution.

The change in the dissolved fraction of plutonium with dissolution time compared well with that of uranium, as shown in Fig. 4, which suggests that both elements dissolved similarly. The dissolved fraction of plutonium was the ratio of the mass of an element to total mass of the element estimated by ORIGEN II calculation. The extent of burnup of spent fuel was determined by the ratio of Cs-134 concentration to Cs-137 concentration [12], which were measured and adjusted taking into account of irradiation history of the fuel.

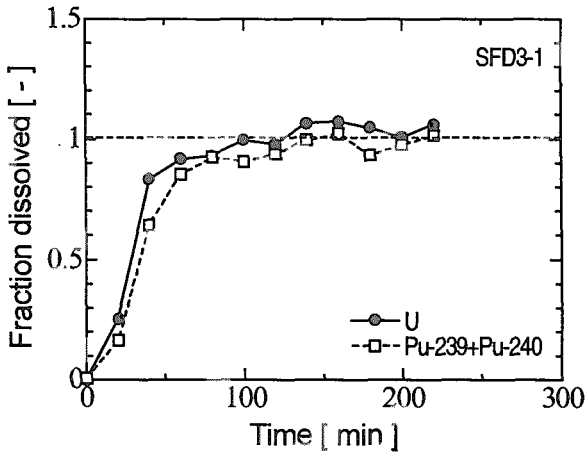

Fig. 4 Change in the fractions of uranium and plutonium dissolved

Fig. 5 illustrates the dissolution behavior of fission products contained in the 44,000 $MWdt^{-1}$ spent fuel using 3.93 mol l^{-1} of HNO_3. The ordinate of the figure is $(Z_{conc.}/U_{conc.})_{exp}$ / $(Z_{conc.}/U_{conc.})_{ORIGEN}$, where $(Z_{conc.}/U_{conc.})_{exp}$ denotes the ratio of the concentration of element Z in the dissolver solution to the uranium concentration obtained from the same sample taken. $(Z_{conc.}/U_{conc.})_{ORIGEN}$ denotes the ratio of the mass of element Z that can be estimated by ORIGEN-II calculation at a given burnup, to the mass of uranium estimated in the same calculation. When the ratio has the value 1, this could mean that the element Z dissolved in the same manner as uranium. It can be seen in the figure that the value of Nd and Sr showed about 1 and were supposed to dissolve in the same manner as uranium. Similar dissolution behavior was obtained for Am and Cs. Ru showed the value 0.5 to 0.6 during the dissolution, i.e. 40 to 50 % of total Ru generated was supposed to remain as the insoluble residue. Mo showed different behavior from other elements and the concentration decreased with time, which implies that Mo precipitated. Also, the decrease in the Zr concentration can be seen in the figure. Similar change in Mo concentration was observed in the

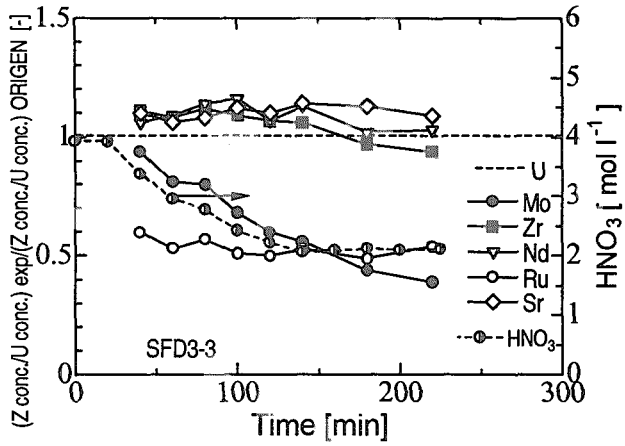

Fig. 5 Dissolution behavior of fission products

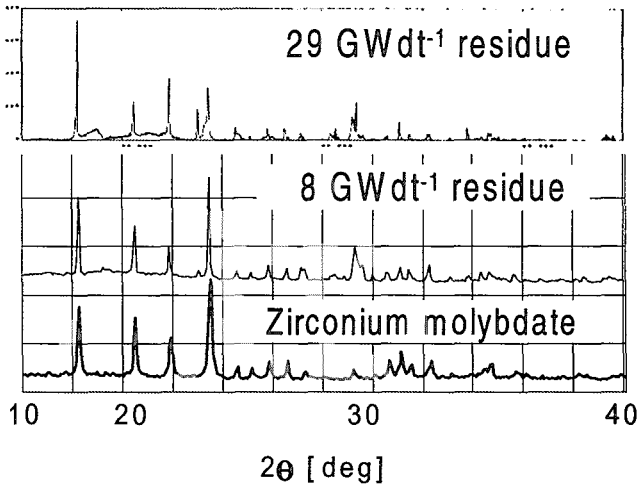

Fig.6 XRD patterns of zirconium molybdate and residues obtained after dissolution test

dissolution of 29 $GWdt^{-1}$ spent fuel, and zirconium molybdate was identified as precipitate in the residue as shown in Fig. 6. As for residue of 44 $GWdt^{-1}$, the XRD analysis was not possible because of the high radioactivity. But the molar ratio of Mo to Zr remained in the solid phase during the dissolution was estimated from the result of concentration measurement and showed the value to be close to two, which suggested the formation of zirconium molybdate. The mechanism of the precipitation during dissolution is not well understood. Further studies are required so that the increase of the residue amount can be avoided.

In Fig. 5 it was shown that a certain fraction of Ru generated remained in residue. This fraction decreased when the dissolution of spent fuel with lower burnup of 29 $GWdt^{-1}$. Fig. 7 shows those fractions as a function of burnup, together with the results obtained by other workers [13-15]. In the figure, SFD2 and SFD3 denote the dissolution of 29 and 44 $GWdt^{-1}$ spent fuels, respectively. It can be seen that the fraction increases with the burnup. At lower burnup, the degree of agglomeration of metallic-fission products such as Ru is not high, and consequently they are fine particulates easy to be dissolved [16]. As the burnup of spent fuel increases, more metallic FPs will agglomerate and become hardly dissolved [16] by HNO_3 with 4 to 7 mol l^{-1} at boiling temperature, which are typical dissolution condition of reprocessing process.

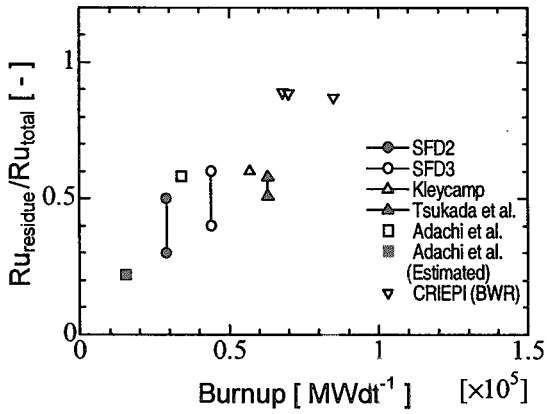

Fig. 7 Effect of burnup on the ratio of Ru in residue to total Ru generated

3.2 Radioiodine behavior

Profiles of iodine-129 captured in the AGS column were illustrated in Fig. 8, which were obtained in the dissolution of 44 $GWdt^{-1}$ spent fuel. Most of the iodine was captured in the first and second cartridges in the upstream AGS column (Column B). The decontamination factor of the AGS columns (B and C) used in the study was found to be more than 36,000. It was demonstrated that the radioiodine was effectively trapped by the adsorbent under the dissolution of actual spent fuel.

Iodine-131 and iodine-133 were detected and plotted in Fig. 8. Those nuclides are short-lived and generated from spontaneous fission of nuclide, mainly curium-244 and also from neutron-absorption fission. The gradient of the profiles should be same as the profile of iodine-129 because the AGS adsorbent captures molecular iodine.

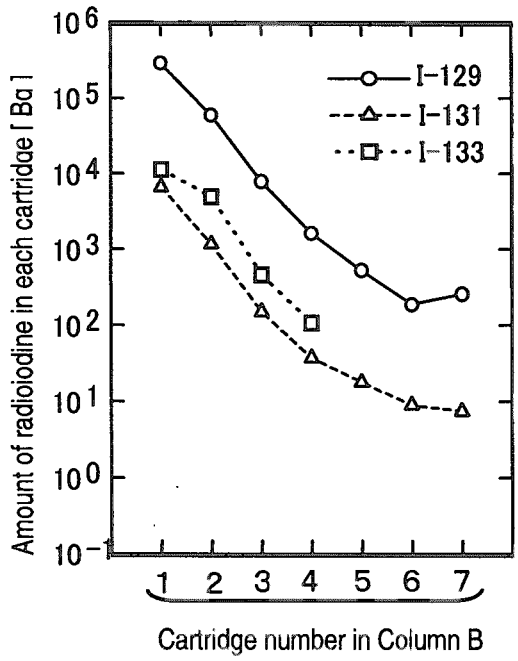

Fig. 8 Radioiodine profiles in AGS column B (SFD3-1)

Measurement of iodine-129 in the dissolver solution showed that less than 0.57% of total iodine-129 generated, which was estimated by ORIGEN II calculation, was remained

in the solution. Also, measurement of iodine-129 by an iodine-stripping operation from the dissolver solution using KIO_3 suggested that another 2.72% of total iodine-129 was trapped in the insoluble residue. Also, about 70 % of total iodine generated was measured in the AGS columns. Rest of iodine-129 was supposed to adsorb to the HEPA filter and the inner surface of dissolver off-gas lines. As shown in Table 3 the results in the present study were found to be almost identical to the results obtained in the previous study using the same test rig and iodine-131 as tracer [17]. The present study obtained comparable results to the study by Boukis and Henrich [18]. However, the fraction of iodine in the residue of the present study was somewhat higher. Also, Herrmann et al. measured higher fraction of iodine in the dissolver solution [19]. Sakurai et al. suggested that the iodine remained as precipitate would increase in a larger dissolver. Further studies are necessary to explain the difference in the distribution behavior of iodine-129, although the difference is not significantly large.

Table 3 Iodine distribution over the dissolution process and DOG treatment system

Authors		Boukis and Henrich (1991)	Herrmann et al. (1993)	This study	
Equipment size		Laboratory scale	Plant	Bench scale	
Burnups of spent fuel used		45 $GWdt^{-1}$	Spent fuel up to 40 $GWdt^{-1}$	I-131 tracer with fuel of U and FP simulating 45 $GWdt^{-1}$ spent fuel	44 $GWdt^{-1}$
Distributions	Off-gas	Balance	Balance	Balance (74 % of total I-129 on adsorption columns)	Balance (70 % of total I-129 on adsorption columns)
	Dissolver solution	0.52 %	<5 % (2 to 3 % for high burnup spent fuel)	0.37 %	< 0.57 %
	Residue	0.18 %	1 %	1.49 %	≤ 2.72 %

3.3 Carbon-14 behavior

Amount of carbon-14 released as carbon dioxide during dissolution was measured, which estimated the initial concentration of nitrogen-14 in fuels as impurity to be several ppms with the aid of ORIGEN II calculation for 29 and 44 GWd/t spent fuels. The result could compare well with the reported concentration of nitrogen in other PWR fresh fuels ranging between 5 and 20 ppm [20].

Fig. 9 shows the change in beta radioactivity of carbon-14 measured in the sample, which was obtained in the dissolution of 29 GWd/t spent fuel. Kr-monitor reading was also plotted in the same figure. It was found that release of carbon-14 as CO_2 into dissolver off-gas occurred when gaseous radionuclides such as Kr-85 were released.

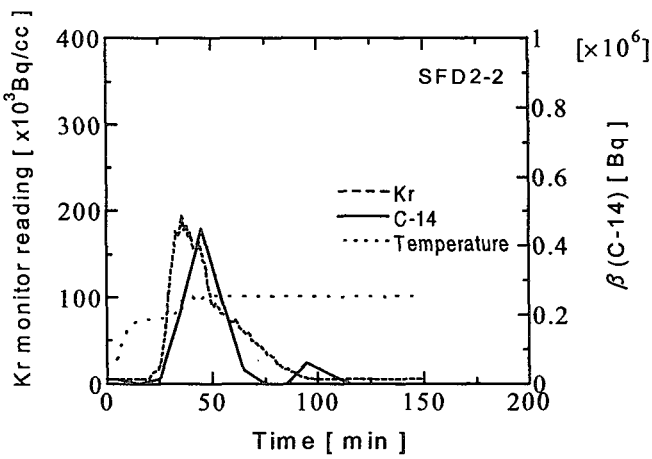

Fig. 9 Change in Kr-monitor reading and carbon-14 released during dissolution (29 $GWdt^{-1}$)

4.CONCLUING REMARKS

Spent fuel dissolution test was carried out to study the dissolution behavior of nuclides and the behavior of volatile radionuclides.

About 400 g of spent fuel can be dissolved within 150 minutes at 373 K when 5 $moll^{-1}$ HNO_3. It was found that Pu and most of MA (Am) and FPs (Nd, Sr, and Cs) dissolved in a similar manner to U. Zirconium molybdate precipitated during dissolution of spent fuel. In addition, the ratio of Ru remained in residue to the total Ru increased with burnup.

As for radioiodine treatment, the decontamination factor of the AGS columns used in the study was found to be more than 36,000. It was demonstrated that the radioiodine was effectively confined by the adsorbent under the dissolution of actual spent fuel. The fraction of I-129 remained in dissolver solution was measured to be less than 0.57 % of total generated I-129. Another 2.72 % was detected as iodine in precipitates.

It was found that release of C-14 as CO_2 into dissolver off-gas occurred when gaseous radionuclides such as Kr-85 were released. Concentration of N-14 initially contained in fuels as impurity was estimated to be several ppms for 29 and 44 $GWdt^{-1}$ spent fuels, which could compare well with the reported concentration of nitrogen in other PWR fresh fuels.

Dissolution test will be continued to obtain data on the above subjects to contribute to the enhancement of the safety of reprocessing process.

ACKNOWLEDGEMENT

Portion of this work was carried out by Japan Atomic Energy Research Institute under the auspice of Ministry of Education, Culture, Sports, Science and Technology. Authors are greatly indebted to Messrs. T. Iijima, S. Kimura, T. Yagi, H. Hagiya, M. Sawada, M. Sato, S. Yoshida and T. Shoro for their support to the dissolution tests.

REFERENCES

[1] T. Sakurai, K. Komatsu, A. Takahashi, Proc. the 24th DOR/NRC Nuclear Air Cleaning and Treatment Conference, NUREG/CP-0153, CONF-960715, 550(1996).
[2] A.Leudet, P.Miquel, P.J. Goumondy, G. Charrier, Proc. 17th DOE Nuclear Air Cleaning Confrence, Vol.1 40(1983).
[3] T. Sakurai, T.Yagi, A., Takahashi, J. Nucl. Sci., Technol., 35, 76(1998).
[4]Handbook on Process and Chemistry of Nuclear Fuel Reprocessing, JAERI-Review 2001-038, (2001).
[5] T. Tsukada, T. Kameyama, H. Yokoyama, J.-P., Glatz., J.-P., Koch, L., Garcia-Alonso, I., Proc. RECOD'94, (1994).
[6] Tsukada, T., Yokoyama, H., Sätmark, B., Glatz, J.-P., Koch, L., Pagliosa, G., Proc. RECOD'98, 274(1998).
[7] H. Mineo et al., Proc. NUCEF'98, 498(1998).
[8] T. Izumida and F. Kawamura, J. Nucl. Sci. Technol., 27(3), 267(1990).
[9] T. Sakurai, A. Takahashi, Y.E. Ming-lu, T. Kihara, S. Fujine, J. Nucl. Sci. Technol., 34, 211(1997).
[10] A.W. Castleman, Jr. Tang, I.N., and H.R. Mulkelwits, J. Inorg. Nucl. Chem., 30, 5(1968).
[11] T. Sakurai, A. Takahashi, N. Ishikawa, Y. Komaki, Nucl. Technol., 85, 206(1989).
[12] Y. Naito, private communication
[13] H. Kleycamp, Proc. RECOD'87, 583(1987).
[14] T. Adachi, M. Ohnuki, N. Yoshida, T. Sonobe, W. Kawamura, H. Takeishi, K. Gunji, T. Kimura, T. Suzuki, Y. Nakahara, T. Muromura, Y. Kobayashi, H. Okashita, T. Yamamoto, J. Nucl. Mater., 174, 60(1990).
[15] T. Kameyama, T. Tsukada, M. Kinoshita, H. Yokoyama, Denryoku-Chuo-Kenkyusho-Hokoku, T91022, March, (1992)(Japanese).
[16] K. Takahashi, D. Sugiyama, T. Fujita, T. Tsukada, M. Tsukamoto, H. Yokoyama, Denryoku Chuou Kenkyusho Hokoku, T96075, (1997), (Japanese).
[17] T. Kihara, T. Sakurai, Y. Nakano, and S. Fujine, Proc. the 5th international Conference on Nuclear Fuel Reprocessing and Waste Management (RECOD'98), (1998).
[18] N. Boukis, E. Henrich, Radiochimica Acta, 55, 37(1991).
[19] F.J. Herrmann, V. Motoi, B. Herrmann, D. Fang, L. Finsterwalder, K.D. Kuhn, A. van Schoor, Ch. Beyer, J. Furrer, W. Knoch, Proc. 22nd DOE/NRC Nuclear Air Cleaning and Treatment Conf., NUREG/CP-0130, CONF-902083-V1, 75(1993).
[20] Japan Nuclear Fuel Ltd. et al., JNFS R-91-001 (2nd ed.), (1996).

JP0250346

ON THE RATE OF REACTION BETWEEN PLUTONIUM DIOXIDE AND SILVER(II)

P.J.W. Rance[1] and G.P. Nikitina[2]
[1] British Nuclear Fuels, Sellafield, Seascale, United Kingdom
Tel: +44 19467 79263, Fax: + 44 19467 79007, e-mail: PJWR1@BNFL.com
[2] V.G. Khlopin Radium Institue, 2nd Murinsky Prospekt, St. Petersburg, Russia

The rate of dissolution of plutonium dioxide by electro-generated Ag(II) in nitric acid has been investigated under conditions in which the potential generation rate of Ag(II) far exceeds its rate of reaction with PuO_2. In such cases, the silver(II) concentration is governed by the ratio of its electrolytic generation rate and the rate of consumption by its second order reaction with water and thus remains approximately constant allowing the rate of reaction between Ag(II) and PuO_2 to be determined. The calcination temperature of the PuO_2 was found to effect not only the rate of dissolution but the form of the dissolution process. The kinetics of the dissolution of PuO_2 calcined at 550°C are best fitted by a surface area context expression $\frac{-d\{PuO_2\}}{dt} = k[Ag(II)]\{PuO_2\}_\delta^{2/3}$, whereas the dissolution of PuO_2 calcined at 1200°C is best described in a mass context i.e. $\frac{-d\{PuO_2\}}{dt} = k'[Ag(II)]\{PuO_2\}_\tau$. A value for k of 107±14 (/mol)$^{2/3}$h^{-1} was determined at 25°C and 38±0.5 $M^{-1}h^{-1}$ for k' at 40°C.

Key words: dissolution, kinetics, PuO_2, plutonium dioxide, electromediated

1. INTRODUCTION

The electromediated dissolution of PuO_2 using silver(II) in nitric acid was first described by Ryan et al[1] in 1982. The process essentially involves the generation of the highly oxidising Ag(II) ion at the anode of an electrochemical cell, this unstable species then brings about the dissolution of the otherwise insoluble PuO_2. Silver(II) is a very strong oxidising agent, the standard electrode potential of the Ag(II)/Ag(I) couple (+1.98V in 4 M nitric acid[2]) is only exceeded by species such as ozone, persulfate and fluorine. In addition to the greater simplicity of working with silver compared to fluorine or ozone, the process has the significant advantage that much less than stoichiometric quantities of silver are required as the oxidising form of the silver, Ag(II), is regenerated by electrolysis following its reduction as a result of reaction with PuO_2.

In simple terms the process can be considered to be;

$$Ag(I) \rightarrow Ag(II) + e \qquad \ldots(1)$$

$$Ag(II) + PuO_2 \rightarrow Ag(I) + PuO_2^+ \qquad \ldots(2)$$

$$2PuO_2^+ + 4H^+ \rightarrow Pu^{4+} + PuO_2^{2+} + 2H_2O \qquad \ldots(3)$$

$$Ag(II) + Pu^{4+} + 2H_2O \rightarrow Ag(I) + PuO_2^+ + 4H^+ \qquad \ldots(4)$$

However, this series of reactions will only occur in the absence of other oxidisable materials and at low temperature under conditions of low Ag(II) concentration as otherwise the second order reaction between Ag(II) and water[3] (5) can become a significant side reaction.

$$2Ag^{2+} + H_2O \rightarrow 2Ag^{+} + 0.5O_2 \qquad ...(5)$$

In practice the process is best carried out at a temperature of around 40°C which appears to be the optimum in terms of the rate of reaction between Ag(II) and PuO_2 or H_2O. One potential source of oxidisable material is the cathodic reaction product, dissolved 'NOx' in a nitric acid system. In order to limit this interference the process is conducted in an electrolytic cell which contains a divider between anolyte and catholyte chambers. Using such a system, Bourges et al[4], showed that the reaction efficiency remained high and essentially constant until the majority of the PuO_2 was dissolved. However, towards the end of the dissolution process the Faradaic efficiency was shown to decline as a result of increased build-up of silver(II) in the system and hence an increase in the significance of the parasitic reaction with water due to a reduction in the amount of PuO_2 available for reaction. The effect of the reduction in available PuO_2 was to reduce the overall Faradaic efficiency of the process from 0.75 (the value achieved up to the dissolution of 78% of the PuO_2) to 50%. Zundelevich[5] has pointed out the importance of realising that the rate of reaction between Ag(II) and PuO_2 is not instantaneous, this is particularly important when one considers the treatment of PuO_2 in combination with other oxidisable materials. In these cases it is necessary to understand the rate of reaction of Ag(II) with the various components in order to be able to predict the rate of dissolution of the plutonium component. Despite this, the only estimate for the rate of reaction with Ag(II) and PuO_2 in the literature is that deduced by Zundelvich's modelling of Bourges's results with all its implicit and explicit assumptions. Below we report some preliminary findings for the direct measurement of the rate of reaction between PuO_2 and Ag(II).

2. EXPERIMENTAL

The experiments were carried out in the equipment shown in Figure 1. The six necked vessel has a working volume of 100 ml. The anode was made from a 40x40 mm platinum foil, 0.1 mm thick. The cathode was a Pt/Ti strip (4 cm^2) housed in a 10 mm diameter glass tube the lower end of which was closed with a glass frit above which a laid a bed of silicic acid gel to prevent egress of the catholyte and cathodic reaction products.

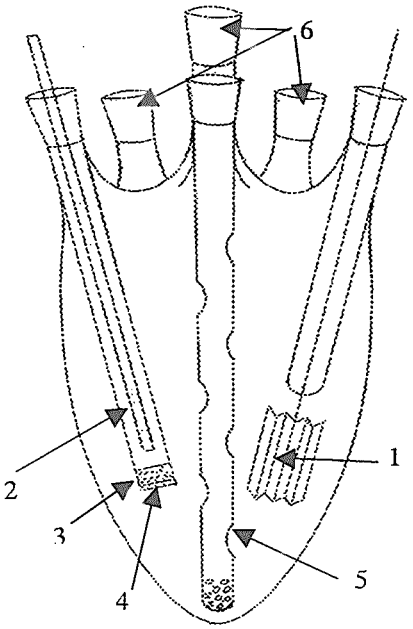

1. anode
2. cathode
3. silicic acid gel
4. sintered glass frit
5. sparger
6. sockets for reflux condenser, thermometer, sampling etc.

Figure 1. Electrolysis Vessel

The catholyte used was 4 molar nitric acid and the anolyte was 6 molar nitric acid. Agitation was brought about by sparging through another neck (~ 5 litres/hour). The remaining necks were used for a thermometer, for sampling and a reflux condenser. Electrical power was supplied by a potentiostat capable of delivering up to 5 amps current at a potential of 0-20 V.

The dissolution rate of two forms of PuO_2 was investigated in this work, one was a large surface area powder (27 m^2/g) having been calcined at 550°C whereas the other had been calcined at 1200°C and had a much smaller surface area (~0.6 m^2/g) both having particles in the 0.5-1 micron range. The different surface areas of the materials necessitated the use of different reaction conditions in order to study the dissolution kinetics. The rate of dissolution of the large surface area material was investigated at 25°C using 1 x 10^{-3} M silver and a current of 0.2 A whereas for the low surface area material it was necessary to increase the temperature to 40°C, the silver concentration to 0.05 M and the current to 0.4 A in order to achieve a convenient rate of dissolution. In each case approximately 100 mg of PuO_2 was placed in the anodic compartment of the electrolysis cell, then agitation and power to the electrodes was applied and dissolution commenced. Samples of the anolyte were taken periodically throughout the dissolution process and the plutonium concentration determined radiometrically.

3. RESULTS AND DISCUSSION

3.1 High Surface Area PuO_2

The decrease in mass of undissolved plutonium with time is shown in figure 2 for two dissolution experiments.

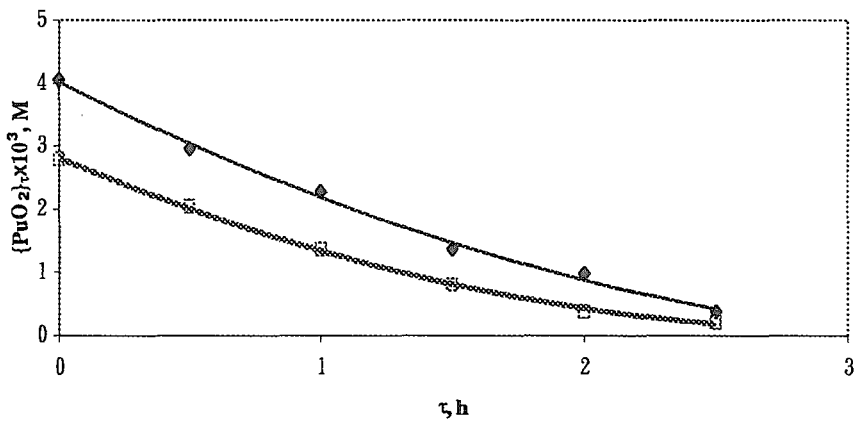

Figure 2. Dissolution rate of high surface area PuO_2

Assuming that the dissolution process is a heterogeneous surface controlled reaction between Ag(II) ions and the PuO_2 surface then the rate expression should have the form

$$\frac{-d\{PuO_2\}}{dt} = k[Ag(II)]\{PuO_2\}^{2/3} \qquad ...(6)$$

$$\text{as} \quad S_t = S_0\left(\frac{m_t}{m_0}\right)^{2/3} \qquad ...(7)$$

(S_t and m_t being the surface area and mass at time t and S_0 and m_0 being the initial surface area and mass)

Rearrangement and integration of (6) gives

$$[3\{PuO_2\}^{1/3}]_{t=t}^{t=0} = -k_{ef}\,t \qquad \ldots(8)$$

in which $k_{ef} = k[Ag(II)]$

A plot of $\{PuO_2\}^{1/3}$ against time should thus give a straight line with a gradient of one-third of $-k_{ef}$, this is the case and is shown as figure 3. Similar results were obtained with two further samples of PuO_2, the full results are shown in table I.

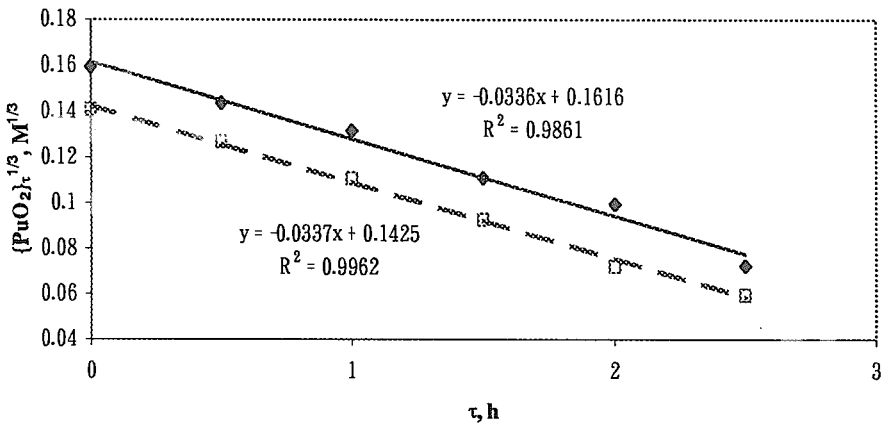

Figure 3. Surface area context, pseudo-first order plot of data in Fig. 2.

Table I. Rate of dissolution of high surface area PuO_2

1	PuO_2, mg	k_{ef}, $(M)^{1/3}/h$	R^2
1	109.9	0.101±0.006	0.986
2	90.2	0.127±0.007	0.989
3	75.7	0.101±0.003	0.996
4	130.1	0.098±0.004	0.992
mean		0.107	
standard deviation		0.014	

Such an analysis relies on the Ag(II) concentration remaining approximately constant during the reaction period. For this to be the case, the potential production rate of silver(II) by electrolysis must significantly exceed that of its reaction with PuO_2 as in such cases the Ag(II) concentration will attain its maximum value governed by the total silver concentration or the ratio of the rates of electrolytic generation and the Ag(II)-water reaction. Extrapolation of the initial dissolution rate shown in figure 2 indicates a PuO_2 dissolution rate of the order of 3×10^{-6} mol/min (100 mg over 2 hours). A current of 0.2 A is theoretically capable of oxidising 1.2×10^{-4} moles of silver per minute and the oxidation of silver at a platinum anode is known to occur with high current efficiency. Thus the potential silver(II) generation rate exceeds the rate at which it is consumed by a factor of 20 (given a Ag:Pu stoichiometry of 2) implying that the assumption of constant Ag(II) concentration throughout the experiment is valid.

Using the data of Po et al[3], it can be shown that for these conditions (25°C, 10^{-3} mol/ Ag) the maximum rate of reaction between Ag(II) and water is of the order of 1.5 x 10^{-5} mol. $^{-1}$min^{-1} i.e. 1.5 x 10^{-5} mol/min in the 100 ml used for these experiments. This is a factor of 8 lower than the potential rate of Ag(II) production in these experiments and thus, to a good approximation, essentially all the silver in the system can be assumed to be present as Ag(II).

Therefore, the mean value for k_{ef} given in table I of 0.107±0.014 $M^{1/3}$/h equates to a value of k= 107±14 (/mol)$^{2/3}$h^{-1}

3.2 Low surface area PuO_2

The rate of dissolution of PuO_2 calcined at 1200 °C is shown in figure 4 and the corresponding surface area dependent plot in figure 5.

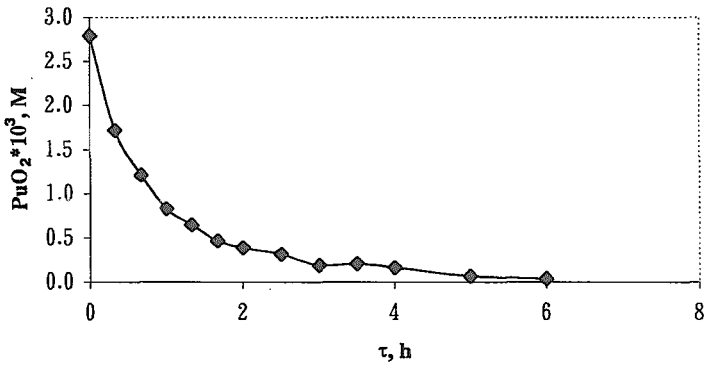

Figure 4. Dissolution rate of low surface area PuO_2

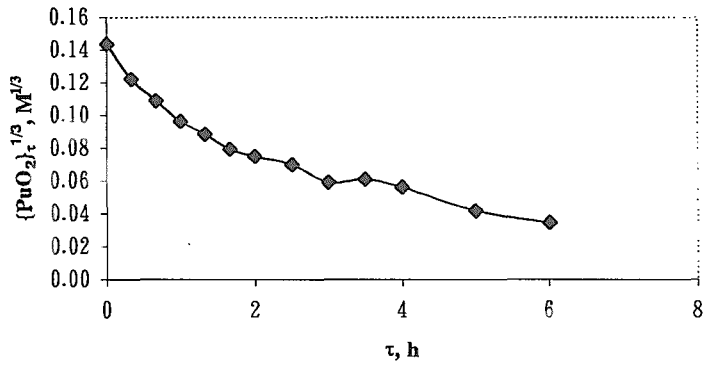

Figure 5. Surface area context, pseudo-first order plot of data in Fig. 4.

It is clear from the distinct curvature shown in figure 5 that the surface area dependency exhibited by the PuO_2 specimen calcined at 550°C is not shared by this high temperature calcined material. Instead if one plots the more usual, mass or concentration dependent form of a pseudo first order expression a good straight-line fit is obtained as shown in figure 6. This result was repeated with two further samples of high temperature calcined PuO_2, in each case the dissolution was fitted by the conventional, mass context, form of the rate expression (9).

$$\frac{-d\{PuO_2\}}{dt} = k'\{PuO_2\}[Ag(II)] \qquad ...(9)$$

The full results are given in table II.

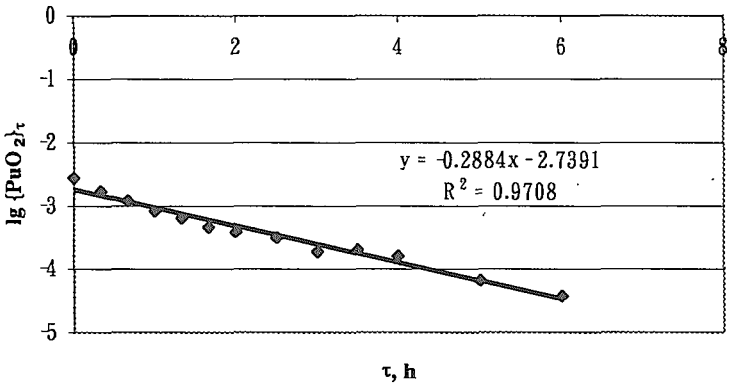

Figure 6. Mass context, pseudo-first order plot of the data in Fig. 4.

Table II. Rate of dissolution of low surface area PuO_2

1	PuO_2, mg	k'^{*}_{ef}, h^{-1}	R^2
1	117.0	0.50±0.03	0.979
2	140.0	0.57±0.05	0.943
3	75.7	0.66±0.04	0.971
mean		0.58	
standard deviation		0.08	

$^{*}k'_{ef} = k'[Ag(II)]$

Although the potential Ag(II) generation rate significantly exceeds its rate of reaction with PuO_2 (by a factor of ~50) thus allowing the assumption of constant Ag(II) concentration, it is not the case that under these conditions the Ag(II) concentration approximates to the total siver concentration as was so under the conditions used for the dissolution of the high surface area PuO_2. The higher temperature and silver concentration used in this part of the study significantly increases the significance of the silver-water reaction. Again using the data of Po[3] one can calculate that under these conditions approximately one-third of the silver will be present as Ag(II), that is the potential electrolysis generation rate of Ag(II) of 2.5×10^{-4} moles/min is matched by an equivalent rate of consumption of Ag(II) by water when the Ag(II) concentration equals 0.015 M (and the Ag(I) concentration equals 0.035 M).

Dividing the mean value of k'_{ef} given in table II by the predicted Ag(II) concentration gives a value for k' of 38±0.5 $M^{-1}h^{-1}$.

4. CONCLUSIONS

By use of conditions which result in a steady state concentration of silver(II), its rate of reaction with PuO_2 has been determined. The calcination temperature of the PuO_2 has been

shown to have an important effect in determining the reaction kinetics. As might be expected the high temperature calcined material had an appreciably slower rate of reaction with Ag(II) than did the high surface area, low calcination temperature material, to an extent that it was necessary to increase the silver concentration by an order of magnitude and the temperature by 15°C in order to achieve the same order of dissolution rate. Additionally, the two materials exhibited different forms of reaction kinetics in that the reaction of the high surface area PuO_2 followed surface area dependent pseudo first order kinetics whereas the low surface area material appeared to follow the standard mass context form of first order kinetics. This finding points to differences in the surfaces of the material affecting how the electron transfer process between silver and PuO_2 is occurring.

Values for the rate constant of reaction (10) have been determined as 107±14 $(\ /mol)^{2/3}h^{-1}$ in the case of high surface area material at 25°C and 38±0.5 $M^{-1}h^{-1}$ for low surface area material at 40°C.

$$PuO_2 + 2Ag^{2+} \rightarrow PuO_2^{2+} + 2Ag^{+} \qquad \ldots(10)$$

Work is continuing to refine the accuracy of these values, to determine the effect of temperature and to investigate the competition kinetics of Ag(II) with PuO_2 and other substrates.

5. REFERENCES

1. L.A. Bray and J.L. Ryan in Actinide Recovery from Waste and Low Grade Sources, J.D. Navratil and W.W. Schultz (eds.), Harwood, New York, 1982, p129.
2. M. Pourbaix Atlas of Electrochemical Equilibria in Aqueous Solutions, NACE 1974
3. H.N. Po, J.H. Swineheart and T.L. Allen, Inorganic Chemistry, 7, 244 (1968)
4. J. Bourges et al., Journal of the Less-Common Metals, 122, 303 (1986)
5. Y. Zundelevich, Journal of Alloys and Compounds 182, 115 (1992)

This is a blank page.

JP0250347

JAERI-Conf 2002-004

Examination of reaction conditions for oxidation of salt waste

Fuminori SATO, Munetaka MYOCHIN, Hitoshi TERUNUMA* and Osamu ARAI*
JAPAN NUCLEAR CYCLE DEVELOPMENT INSTITUTE (JNC)
Dry Process Technology Group, Tokai Works
FAX: 81-029-283-2164, e-mail: fsato@tokai.jnc.go.jp
*KAKEN CO. Engineering Development Dept.
FAX: 81-029-227-4082, e-mail: kaken@po.sphere.ne.jp

For vitrification of salt wastes from pyroprocessing, a high temperature steam oxidation method was examined for conversion of chloride salt to oxide. The solubility of oxide in typical waste glasses is much higher than that of chloride. In initial tests, the reaction of chloride to oxide by steam was only a few %. In later tests, B_2O_3 was added to salt to increase the extent of chemical reaction. After optimization of reaction temperature, highest oxide conversions of 52 and 44 mole% were attained for LiCl-KCl-B_2O_3 and NaCl-KCl-CsCl-B_2O_3 respectively.
Key words: salt waste, vitrification, pyroprocess

1. INTRODUCTION

Feasibility Studies for the commercialized fast breeder reactor (FBR) cycle system are underway at Japan Nuclear Cycle Development Institute (JNC). The purpose is to select promising concepts and identify the required R&D tasks to commercialize the FBR cycle system. In these studies, pyrochemical processing is a candidate technology for advanced nuclear fuel reprocessing of the future. Using pyroprocessing, spent nuclear fuel is often treated in molten chloride salt. Basically, molten salt is reusable but fission product (FP) material is accumulated after reprocessing large amounts of fuel. Molten salt with excessive FP must be removed from the process and treated.

Salt waste containing large amounts of highly radioactive FP may be immobilized for final disposal. But it is known that chloride as a major constituent of the salt waste has an extremely low solubility in many glasses.

For vitrification of salt waste generated by pyroprocessing, a high temperature steam oxidation method was examined to convert chloride to oxide, which has high solubility in glass [1]. This method is based on the following chemical reaction [2].

$$2MCl + H_2O\ (Gas) \rightarrow M_2O + 2HCl\ (\uparrow) \quad (M: \text{Alkali Metal})$$

By this reaction, chloride salt is converted to oxide and chlorine is separated as hydrogen chloride. In this study, [NaCl-KCl-CsCl] and [LiCl-KCl] salts were selected as representative of the RIAR and ANL pyrochemical processes.

2. EXPERIMENTAL

A schematic of the test equipment is shown in Figure 1. Chloride salt samples (~ 20g each) were placed in crucibles and fused at 1,073K-1,273K. Afterwards, steam from a moisture generator mixed with argon gas was passed through the salt. The chloride salt was partially converted to oxide. Chlorine was separated as hydrogen chloride, which was trapped by a scrubber.

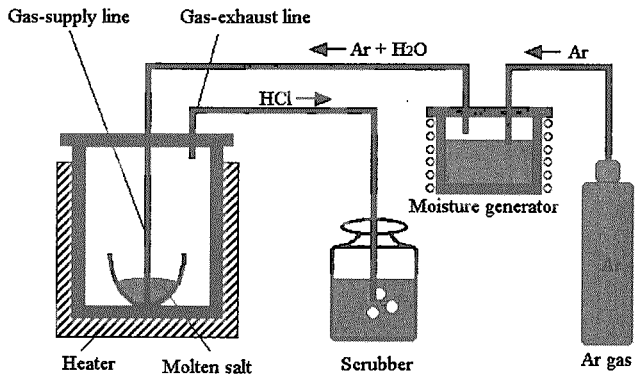

Fig. 1. Test equipment

Test parameters were salt composition (LiCl-KCl and NaCl-KCl-CsCl), reaction temperature, total weight of added water (steam ventilation time), and presence of boron oxide (B_2O_3) which assisted oxidation. After each test, the product was weighed and analyzed by XRD. The amount of hydrogen chloride in the scrubber solution was analyzed by ICP-AES and ion chromatography. From these analyses, the chemical form of the products and the extent of conversion of chloride to oxide were found.

3. RESULTS

Test results are shown in Table I

Table I. Test results

No.	Sample	Temperature (K)	Addition amount of H2O *	rate (%)
1	LiCl-KCl	1173	9.3	2.58
2	LiCl-KCl	1273	0.9**	0.94
3	NaCl-KCl-CsCl	1073	8.2	0.04
4	NaCl-KCl-CsCl	1123	8.2	0.03
5	LiCl-KCl-B2O3	1073	6.2***	35.6
6	LiCl-KCl-B2O3	1203	3.3***	51.6
7	NaCl-KCl-CsCl-B2O3	1153	10.0	38.7
8	NaCl-KCl-CsCl-B2O3	1153	21.8	43.8

*: Reaction "$NaCl+1/2H_2O = 1/2Na_2O+HCl$", stoichiometric amount of H_2O is defined as "1"

**: Volatilized salt blockades gas exhaust line and test was interrupted.

***: See discussion in section 4.

In these preliminary salt-steam reactions (test No. 1), the oxide conversions were only a few %. To improve the extent of reaction, the salt temperature was raised to 1,273K (test No. 2). In this case, molten salt volatilized and caused blockage of the gas exhaust line of the test vessel.

To improve oxide conversion without volatilizing salt, boron oxide (B_2O_3) was added to the samples. The chemical composition of samples with added B_2O_3 was fixed as

$LiCl:KCl:B_2O_3$=59:41:100 and NaCl: $KCl:CsCl:B_2O_3$=1:1:1:3 (molar basis).

In test No. 5 with $LiCl-KCl-B_2O_3$ at 1,073K, the formation of hydrogen chloride was confirmed but blockage of the gas supply line occurred. To minimize blockages, reaction temperatures were selected as 1,203K for $LiCl-KCl-B_2O_3$ and 1,153K for $NaCl-KCl-CsCl-B_2O_3$. The reason for choice of these temperatures is explained in Section 4. The highest oxide conversions reached were 51.6 and 43.8 mole% for $LiCl-KCl-B_2O_3$ and $NaCl-KCl-CsCl-B_2O_3$ respectively as seen in Table I for test No. 6 and 8.

4. DISCUSSION

From the results of tests No. 1-4 in Table I, it was confirmed that it is difficult to convert chloride to oxide by use of steam only.

In tests No. 5-8 B_2O_3 was added to salt samples to promote oxidation reaction. As a result of the addition, the conversion of the samples were improved and maximum conversion reached to about 50%. But in test No. 5 ($LiCl-KCl-B_2O_3$ at 1,073K) the blockage of the gas supply line occurred and prevented progressing the reaction any more. It is thought that a reaction product with high melting point (>1,073K) was generated in the salt as the reaction progressed and caused the blockage of the gas supply line because $LiCl-KCl-B_2O_3$ system had homogeneous liquid phase at 1,073K. (m.p. of LiCl: 883K, KCl: 1,044K, B_2O_3: 850K)

Typical result of X-ray diffraction analysis (XRD) of the reaction product is shown in Figure 2.

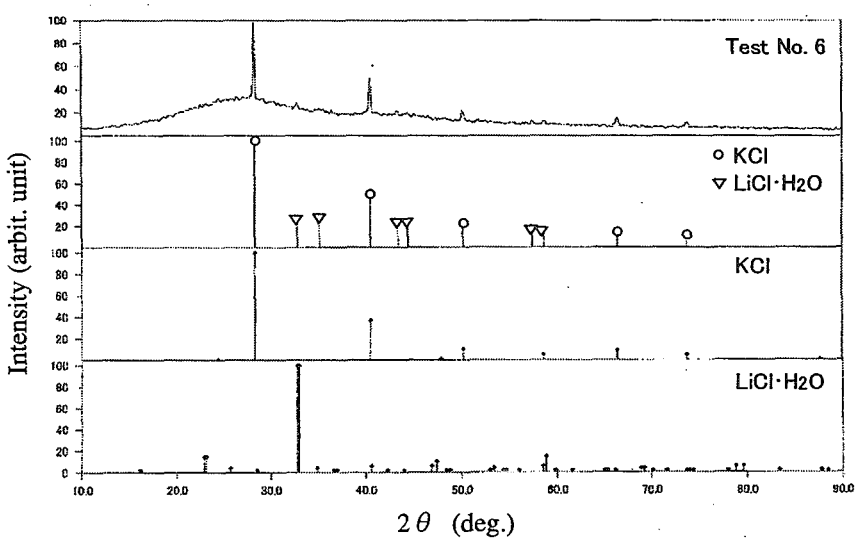

Fig. 2. XRD result of test No.6

XRD result proved that the profile had a halo pattern attributed to amorphous phase and Bragg peaks of crystalline phase. From consideration of NIST data it was confirmed that crystalline phase was a mixture of LiCl and KCl. (See Fig. 2.)

XRD result in tests No. 7 and 8 had same tendency. From these data it was confirmed that the reaction product of tests No. 6-8 was a mixture of amorphous product and unconverted chloride. Therefore it is thought that in test No. 5-8 the oxide generated did not exist as a simple substance but was mixed with B_2O_3 by the following two chemical reactions, and detected as amorphous in XRD.

$$2MCl + H_2O\ (Gas) \rightarrow M_2O + 2HCl\ (\uparrow) \quad (M{:}Alkali\ Metal) \qquad -(1)$$

$$nM_2O + B_2O_3 \rightarrow [\ nM_2O\ in\ B_2O_3\ ] \quad (detected\ as\ amorphous\ in\ XRD) \qquad -(2)$$

Especially in test No. 5, it is thought that the mixture of M_2O and B_2O_3 was deposited as a solid in the gas line. To explain this deposition the phase diagrams of Li_2O-B_2O_3, Cs_2O-B_2O_3, Na_2O-B_2O_3, and K_2O-B_2O_3 are shown in Figures 3-6 [3]. How above two reactions take place in the molten salt is explained in Figure 6.

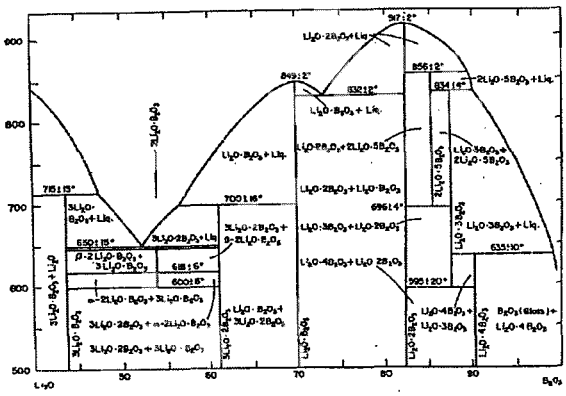

Fig. 3. Phase diagram of Li_2O-B_2O_3

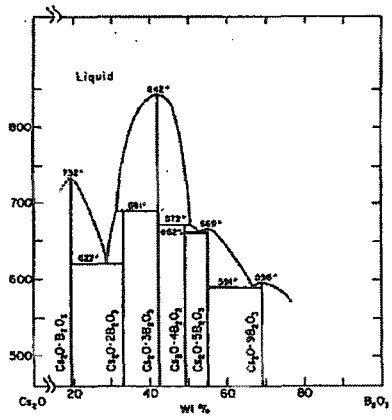

Fig. 4. Phase diagram of Cs_2O-B_2O_3

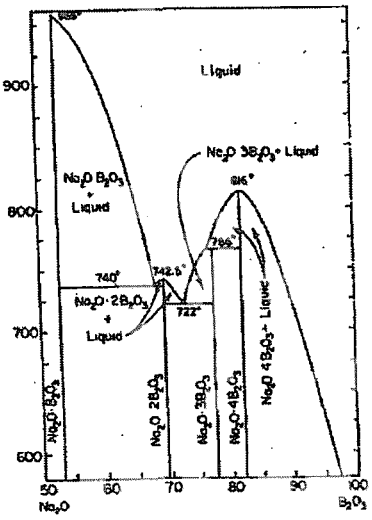

Fig. 5. Phase diagram of Na_2O-B_2O_3

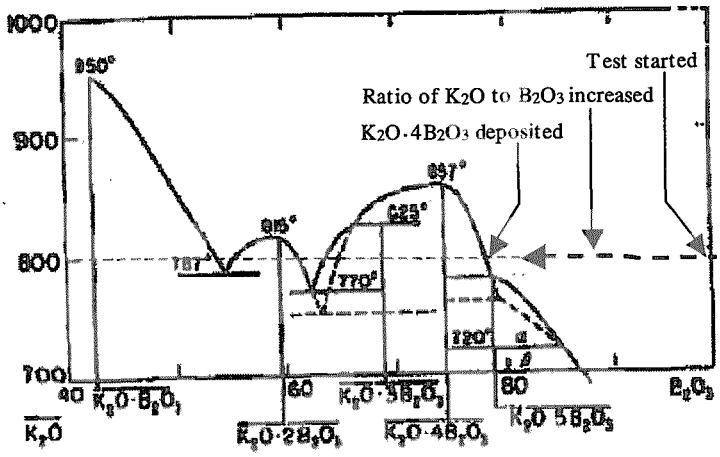

Fig. 6. Phase diagram of K_2O-B_2O_3

It is thought that the alkali metal oxide (M_2O) formed by reaction (1) immediately started to mix with B_2O_3 by reaction (2). As conversion progressed, the ratio of the oxide (M_2O) to B_2O_3 increased until finally $nM_2O \cdot mB_2O_3$ deposited as a solid as seen in Figure 6, and this blocked the gas supply line.

Therefore it was confirmed that the reaction temperature has to be more than 1,190K (melting point of $Li_2O \cdot 2B_2O_3$, see Fig. 3.) for LiCl-KCl-B_2O_3 and 1,130K (melting point of $K_2O \cdot 4B_2O_3$, see Fig. 6.) for NaCl-KCl-CsCl-B_2O_3.

5. CONCLUSIONS

For vitrification of salt waste from pyroprocessing, a high temperature steam oxidation method was examined to convert chloride salt to oxide.

In the reaction of chloride and steam only, it was confirmed that the oxidation conversion of chloride was difficult because the conversion did not progress at lower temperature ($<$ 1,173K), and chloride volatilized at higher temperature ($\geqq$1,273K).

By adding B_2O_3 to promote oxidation reaction, the highest oxide conversions were 51.6 and 43.8 mole% for LiCl-KCl-B_2O_3 and NaCl-KCl-CsCl-B_2O_3 respectively. But when the reaction temperature was lower (1,073K), the blockage of the gas supply line occurred. From consideration of the relevant phase diagrams, the cause of this blockage was thought to be $nM_2O \cdot mB_2O_3$ mixture that solidified in the gas line. It was confirmed that the reaction temperature has to be more than 1,190K for LiCl-KCl-B_2O_3 and 1,130K for NaCl-KCl-CsCl-B_2O_3.

In this examination, B_2O_3 was used at the same molar amount as chloride to assist chemical conversion and this caused an increased quantity of waste. Consequently, further optimization of reaction temperature and minimization of B_2O_3 added are the next subjects for examination.

References

[1] Osamu ARAI, Hitoshi TERUNUMA, (in Japanese with English abstract)
JNC Technical Report, JNC TJ8400 2001-004 (2001)

[2] Fumio NOGUCHI, (in Japanese with English abstract)
J. of Mining and Metallurgical Institute of Japan, 94 [1087], 605-610 (1978)

[3] Ernest M. LEVIN, Carl R. ROBBINS, and Howard F. McMURDIE,
"Phase Diagram for Ceramists Vol. 1", American Ceramic Society, inc., America (1964)

This is a blank page.

JP0250348

JAERI-Conf 2002-004

EXTRACTION OF RADIONUCLIDES FROM NITRIC ACID SOLUTIONS BY A TRUEX SOLVENT

TOSHIYUKI FUJII*, HAJIMU YAMANA* AND HIROTAKE MORIYAMA**

*Research Reactor Institute, Kyoto University, Noda, Kumatori, Sennan, Osaka 590-0494, Japan

Fax: 81-724-51-2634, e-mail: tosiyuki@HL.rri.kyoto-u.ac.jp

**Department of Nuclear Engineering, Kyoto University, Yoshida-Honmachi, Sakyo-ku, Kyoto 606-8501, Japan

The extraction behavior of short-lived fission products and neptunium under the TRUEX and PUREX conditions was studied. Fission products and neptunium were produced by neutron irradiation of natural uranium or metals of these elements. The extraction in the presence of oxalic acid was examined. The separation efficiency of radionuclides under the TRUEX condition was discussed by considering the obtained results.

Key words: TRUEX, PUREX, CMPO, Fission Products

1. INTRODUCTION

Octyl(phenyl)-*N*,*N*-diisobutylcarbamoylmethylphosphine oxide (OϕD[IB]CMPO or simply CMPO) is known to have high extractability for trivalent elements from acid solutions. Horwitz and co-workers[1] have presented the transuranic element extraction (TRUEX) process by using a TRUEX solvent, which is a mixture of CMPO and tri-*n*-butyl phosphate (TBP) in paraffin diluents. The distribution behavior of radionuclides in the process is essential information for the design of the system, and has been studied in detail for actinides and some major fission products (FP) of Sr, Cs, Ru and so on. However, there are few studies on the distribution behavior of other minor FP. Since some of these minor FP have large neutron capture cross sections, the presence of them affects the reactor activity when they are recycled with TRU. In this context, we have studied the extraction behavior of molybdenum[2], palladium[3] under the PUREX and TRUEX conditions in our recent study. For comparison, the extraction behavior of several FP (including molybdenum and palladium) and neptunium was studied in the present study. The dependence of distribution ratios on nitric acid concentration was experimentally studied, and the extraction in the presence of oxalic acid was also examined.

2. EXPERIMENTAL

Short-lived FP and ^{239}Np were produced by neutron irradiation of natural uranium. About 2 mg of UO_2 sealed in a quartz tube was irradiated for 20 minutes in a pneumatic irradiation

system with a thermal neutron flux ϕ_{th} = 2.75 x 10^{13} n/cm^2•sec in the Kyoto University Research Reactor. After the irradiation, the irradiated UO_2 was dissolved in 7 mol dm^{-3} (M) HNO_3. Insoluble residues were removed by a filter having 0.45 μm pore size. Radioactive tracers ^{99}Mo, ^{109}Pd, and ^{122}Sb were produced by neutron irradiation of metals of these elements. These pure metals were purchased from Nilaco, Inc. The irradiated metals were dissolved in HNO_3 by heating. The filtered solution or the supernatant after centrifugation was used for preparing aqueous phase. Portions of these solutions were used, and HNO_3 of various concentrations were prepared. Nitric acid solutions with 0.02 M $H_2C_2O_4$ were also prepared.

An organic solution of 1.0 M TBP diluted with *n*-dodecane was prepared as the PUREX solvent. The mixture of 0.2 M OϕD[IB]CMPO (Elf Atochem North America, Inc., 95% purity) and 1.0 M TBP diluted with *n*-dodecane was prepared as the TRUEX solvent. The TRUEX solvent was scrubbed twice with 0.5 M Na_2CO_3 solution to remove degradation products of CMPO. The PUREX and the TRUEX solvents were pre-equilibrated with fresh nitric acid solutions.

Fifteen mL each of the aqueous solution and the organic solution were contacted by magnetic stirring in a glass centrifuge tube for 20 minutes at room temperature. After separating the two phases by centrifugation, weighed portions of both phases were taken for γ-spectrometric analysis to determine the distribution ratios (*D*). In the γ-spectrometric analysis, the γ-ray measurement of ^{132}Te was interfered with the presence of ^{239}Np γ-ray, and the contribution of ^{239}Np γ-ray was corrected.

The concentrations of hydrogen ion, [H^+], in the equilibrated aqueous phases were determined by a titration using NaOH. All quantifications of aqueous and organic solutions were performed gravimetrically to avoid the large error associated with volumetric treatment. The gravimetric concentrations were converted to volumetric concentrations using the density of the solutions. The chemical reagents used were all of analytical grade.

3. RESULTS AND DISCUSSION

The distribution ratios of radionuclides under the PUREX and TRUEX conditions are shown in Figure 1 as functions of [H^+]. Under the TRUEX condition, the distribution ratios with and without oxalic acid at 3 M HNO_3 are shown in Figure 2. In Fig. 2, errors shown together are experimental ones of 1 standard deviation via γ-spectrometry. The characteristics of the TRUEX extraction behavior of each nuclide can be simply summarized

as follows.

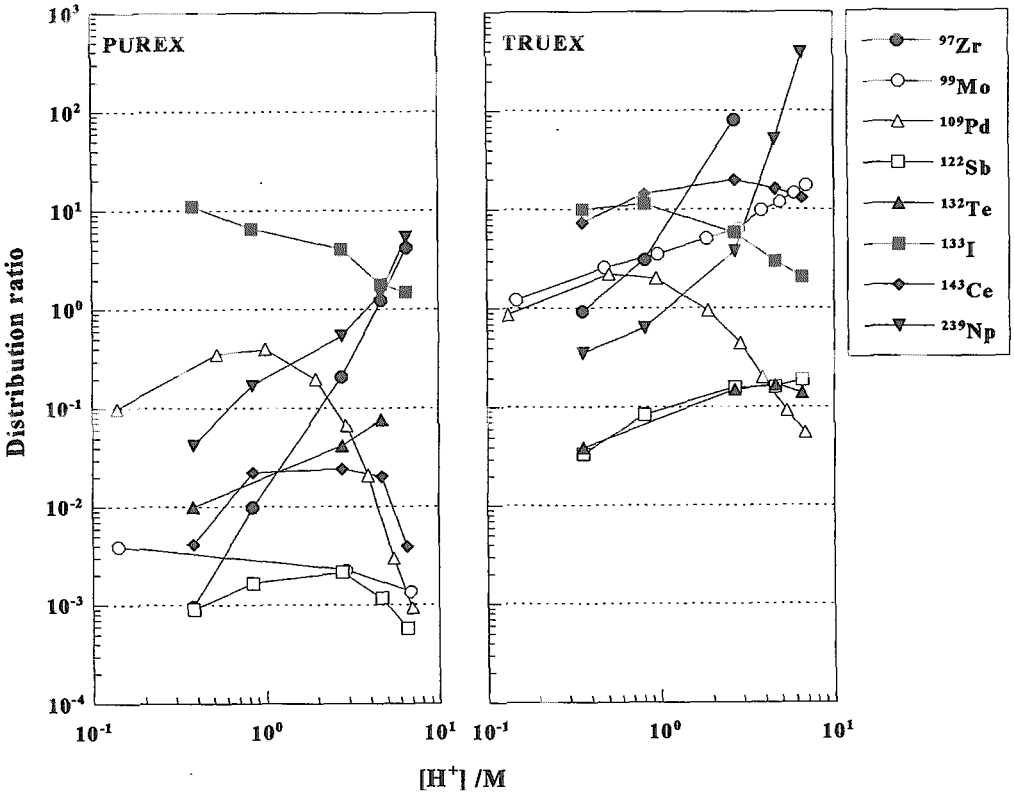

Figure 1. Distribution ratios of FP and ^{239}Np as functions of [H^+].

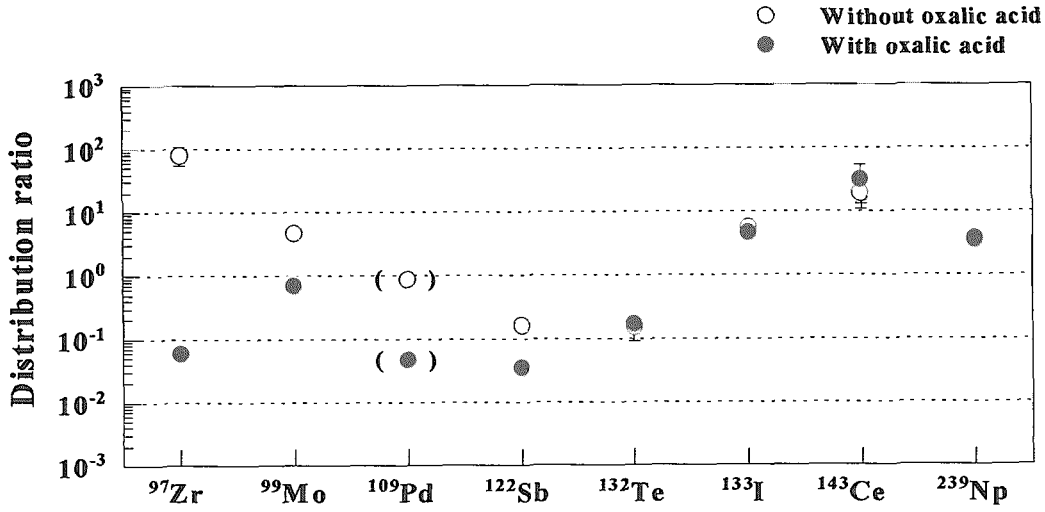

Figure 2. Distribution ratios of FP and ^{239}Np with and without oxalic acid under the TRUEX condition with 3 M HNO_3. The distribution ratios of ^{109}Pd were obtained under the condition of *ca.* 0.15 M HNO_3.

Cerium

Since the distribution ratios of cerium under the TRUEX condition have been reported to be

close to americium[4], the separations of radionuclides from cerium can be regarded as those from americium. As shown in Fig. 1, the extractability of cerium as a representative of trivalent f-elements with the TRUEX solvent is much higher than the PUREX solvent. Such a high extractability is due to the following extraction reaction of trivalent f-element by CMPO[5]:

$$R^{3+} + 3NO_3^- + 3CMPO \leftrightarrow R(NO_3)_3 \bullet 3CMPO, \quad (1)$$

where R^{3+} denotes trivalent cation. At 3 M HNO_3 under the TRUEX condition, the largest *D* value can be obtained. Under the same condition, the presence of oxalic acid does not change the *D* value.

Zirconium

The *D* values with the TRUEX solvent are about 1,000 times larger than those with the PUREX solvent. The results are consistent with the following extraction reaction which have been obtained from the PUREX[6] and TRUEX[7] studies,

$$Zr(NO_3)_2^{2+} + 2NO_3^- + CMPO \leftrightarrow Zr(NO_3)_4 \bullet CMPO, \quad (2)$$

At the high acid region under the TRUEX condition, the *D* value of Zr is larger than that of Ce. Hence, the suppression of Zr extraction is required. This can be improved by adding oxalic acid. As shown in Fig. 2, the presence of oxalic acid results in a suppression of Zr extraction, which is about 1/1,000.

Molybdenum

Under the TRUEX condition, a high acid dependence of *D* can be seen over 3 M HNO_3 in which the following extraction reaction is considered[2]:

$$MoO_2^{2+} + 2NO_3^- + 2CMPO \leftrightarrow MoO_2(NO_3)_2 \bullet 2CMPO, \quad (3)$$

The large *D* of Mo suggests that the high acid region is not preferred for the separation of Am from Mo. In the low acid region, however, the extraction mechanism of Mo is much complicated by the presence of anionic and polymeric species[8]. Although the *D* value is

reduced to about 1/10 with the addition of oxalic acid, this is not enough for the purpose of the separation of Am and Mo. Further studies of Mo decontamination are thus required.
It should be noted that the significant problem of Mo extraction is the low reproducibility of *D* possibly due to its complicated aqueous chemistry.

Palladium

The Pd extraction shows high acid dependence. The *D* values decrease with the increase of $[H^+]$ over 1 M HNO_3 suggesting that the predominant species[3] in the aqueous phase is an anionic species $Pd(NO_3)_3^-$. The high acid region is thus preferred for the separation of Am from Pd. This is an inverse tendency compared with the case of Mo.

Antimony and Tellurium

To our best knowledge, there is no data on the TRUEX extraction behavior of Sb and Te. Although no details of the extraction mechanism of these elements are obtained in the present study, it is much interesting that both Sb and Te show similar *D* values under the TRUEX condition. These *D* values are small enough to separate Sb and Te from Am. Also the *D* value of Sb is reduce to about 1/10 with the addition of oxalic acid.

Iodine

Iodine can be removed in the degassing process before the PUREX and TRUEX processes, and the decontamination of iodine is not a primary concern of this study. Although the *D* value of iodine does not show any distinct dependence with the extraction conditions; *i. e.*, kind of organic phase and presence of oxalic acid, the result is considered to be the distribution of neutral I_2. The *D* value decreases with the increase of $[H^+]$. This possibly due to the oxidation of I_2 into IO_3^-.

Neptunium

The distribution ratio steeply increases with $[H^+]$, and its acid dependence increases in high acid region. As is known, Np(V) is oxidized to Np(VI) with the increase of $[H^+]$, which is much extractable by the PUREX and TRUEX solvents[9,10]. In the case of the TRUEX extraction, the following extraction reaction of Np(VI) by CMPO has been reported[11],

$$NpO_2^{2+} + 2NO_3^- + 2CMPO \leftrightarrow NpO_2(NO_3)_2 \bullet 2CMPO. \quad (4)$$

Thus the accelerated increase of D in high acid region can be attributed to the oxidation reaction of Np. For the purpose of Np recovery with Am, the high acid region is preferable. However, at the low acid region, Np can be recovered by controlling valency; *c. f.*, heating or adding oxidizing reagent.

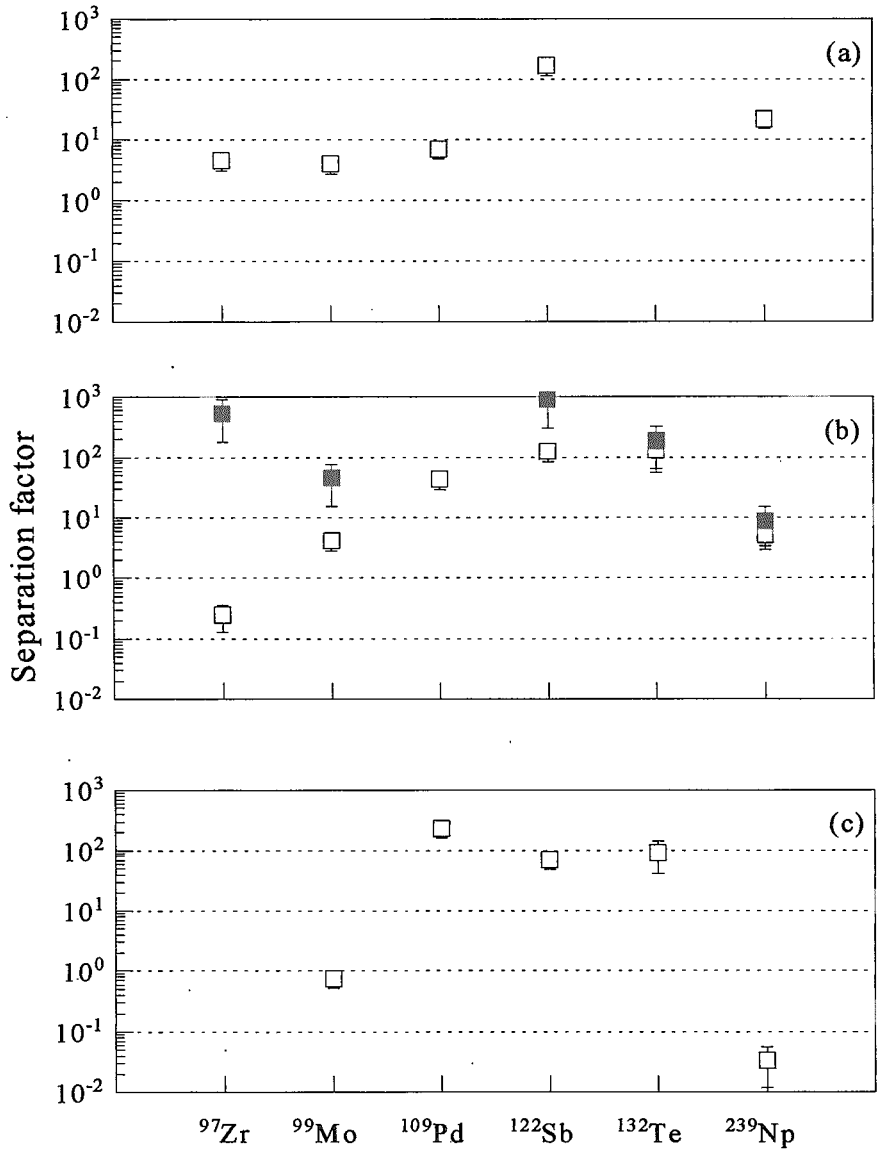

Figure 3. Separation factors between ^{143}Ce and radionuclides: (a) $[HNO_3]_{init}$ = 1 M, (b) $[HNO_3]_{init}$ = 3 M (□: without $H_2C_2O_4$, ■: with $H_2C_2O_4$), (c) $[HNO_3]_{init}$ = 7 M. Separation factor is defined as $D_{Ce}/D_{radionuclide}$.

Separation factors between ^{143}Ce and other radionuclides are shown in Figure 3. From Figs. 1, 2, and 3, it can be concluded as follows. Since the maximum distribution ratio of ^{143}Ce

was observed at 3 M HNO_3, the Am recovering would be the most effective as well. The acid dependence of Mo extraction changes at 3 M $[H^+]$ and Mo extraction is accelerated in the region $[H^+] > 3$ M. However, the region $[H^+] < 1$ M is not preferable considering hydrolysis and polymerization, and the region 1~3 M HNO_3 is preferable for the purpose of Mo decontamination. On the other hand, the high acid region is preferable for the purpose of Np recovery and Pd removal. However, Np can be recovered by oxidizing Np(V) to Np(VI) even in the low acid region, and oxalic acid would be effective for the suppression of Pd extraction. Consequently, the TRUEX extraction with oxalic acid at the region of 1~3 M HNO_3 is considered to be preferable at the present stage, though this condition is less effective for Mo decontamination.

CONCLUSIONS

The PUREX and TRUEX extractions of FP and ^{239}Np were performed. The extraction behavior of ^{97}Zr, ^{99}Mo, ^{109}Pd, ^{122}Sb, ^{132}Te, ^{133}I, ^{143}Ce, and ^{239}Np was studied. The TRUEX extraction in the presence of oxalic acid was examined. The conditions and performance of the TRUEX extraction were discussed by considering the obtained results. The TRU recovery by the TRUEX solvent is much effective at the region of 1~3 M HNO_3 with the presence of oxalic acid. For Np recovery, its valency should be controlled to be Np(VI).

ACKNOWLEDGEMENT

The authors wish to thank Mr. M. Watanabe and Mr. M. Kamiya of Japan Nuclear Cycle Development Institute for their technological comments on the present study.

REFERENCES

[1] E. P. Horwitz and D. G. Kalina, Solvent Extr. Ion Exch., 2, 179 (1984).

[2] T. Fujii, H. Yamana, M. Watanabe, and H. Moriyama, Solvent Extr. Ion Exch., 19, 127 (2001).

[3] T. Fujii, H. Yamana, M. Watanabe, and H. Moriyama, J. Radioanal. Nucl. Chem., 247, 435 (2001).

[4] M. Ozawa, S. Nemoto, A. Togashi, T. Kawata, and K. Onishi, Solvent Extr. Ion Exch., 10, 829 (1992).

[5] K. L. Nash, "Handbook on the Physics and Chemistry of Rare Earth", K. A. Gschneidner, Jr., LeRoy Eyring, G. R. Choppin, G. H. Lander, Eds., Elsevier Science, North-Holland, Amsterdam, (1994) pp. 197-238.

[6] R. L. Hickok, R. D. Cannon, "Zirconium Extraction by Tributyl Phosphate", IDO-14487, Philips Petroleum Co., Idaho, 1959.

[7] J. N. Mathur, M. S. Murali, P. R. Natarajan, L. P. Badheka, and A. Banerji, Talanta, 39, 493 (1992).

[8] K. H. Tytko and O. Glemser, Adv. Inorg. Chem. Radiochem., 19, 239 (1976).

[9] Yu. S. Fedorov, B. Ya. Zil'berman, Soviet Radiochem., 30, 546 (1988).

[10] W. W. Schulz and E. P. Horwitz, Solvent Extr. Ion Exch., 23, 1191 (1988).

[11] J. N. Mathur, P. B. Ruikar, M. V. Balarama Krishna, M. S. Murali, M. S. Nagar, and R. H. Iyer, Radiochim. Acta, 73, 199 (1996).

JP0250349

JAERI-Conf 2002-004

EVALUATION OF CONFINEMENT CAPABILITY OF RADIOACTIVE MATERIALS UNDER THE FIRE ACCIDENT IN NUCLEAR FUEL FACILITY WITH CELVA-1D

Koji WATANABE, Hitoshi ABE, Junichi TAKADA, Shinsuke TASHIRO and Gunzo UCHIYAMA
Japan Atomic Energy Research Institute
Tokai-mura, Naka-gun, Ibaraki-ken, 319-1195 JAPAN
Fax: +81.29.282.6479, E-mail: watanabe@aero.tokai.jaeri.go.jp

To reduce the clogging of smoke on the HEPA filters under the fire accident, some of ventilation systems in the plant are equipped with the pre-filters in front of the HEPA filters for collecting the relatively large smoke particles. Appropriate correspondence such as the exchange of the pre-filter is important for confinement of radioactive materials in the ventilation system under the fire accident. To study smoke generation behavior due to the burnable wastes and clogging properties of the ventilation filters by smoke loading, the verification test has been performed. The cell ventilation system analysis code, CELVA-1D was used for analysis of smoke generation and the rising of pressure drop at both the pre-filter and the HEPA filter. With the change of source term, the breakage of time of the pre-filter was also estimated.

Key words: Reprocessing plant, Fire accident, Smoke, Ventilation filter, CELVA-1D

1. INTRODUCTION

The ventilation system of nuclear fuel facility has a function with the confinement of the radioactive airborne materials in the facility. The ventilation systems generally consists of cells, ducts, confinement devices including ventilation filters and blowers. As the final confinement device, the ventilation filters are set at the end of the ventilation system. Therefore it is very important to keep the confinement capability of the ventilation filters.

In some ventilation system of nuclear fuel facilities, the pre-filters for collection of large particles are equipped in front of the HEPA filters. The pre-filters are expected to play a role of preventing smoke from loading onto the HEPA filters at the fire accident in the facility and transports into the ventilation system of the facility. But excess smoke loading onto the pre-filters can cause the clogging of pre-filters themselves. Clogging of the pre-filters will make their the differential pressure rise and then them break. Moreover, much smoke directly loading onto the HEPA filters will cause the rapid clogging and the breaking of the HEPA filters. To avoid much smoke directly loading onto the HEPA filters, the exchange of the pre-filters is needed before the breakage of the pre-filters. However, the prediction of breakage time of the pre-filters has been little studied experimentally and theoretically.

In Japan Atomic Energy Research Institute, the verification test on safety of a cell ventilation system equipped with the pre-filters and the HEPA filters under the fire accident has been performed. Behavior of Smoke generation, decontamination factor (DF) of the pre-filters and clogging properties of the pre-filters and HEPA filters due to smoke loading has been experimentally studied through the combustion test of the mock burnable materials or the mock recovery solvent. The final purpose of this test is to establish the method of

prediction of the breakage time of the pre-filters under the fire accident of nuclear fuel facility.

In this study, we propose the analytical approach to predict the breakage time of the pre-filters under the fire accident of nuclear fuel facility using a cell ventilation analysis code, CELVA-1D[1]. We estimated the smoke generation due to combustion of the mock burnable materials by the source term model related to the release rates of the mass, energy and smoke from the combustion at the cell. We made the model of time dependency of the differential pressure of the pre-filters taking account of the clogging properties and the DF of the smoke at the pre-filters. Then we combined above models into CELVA-1D and calculated the time dependency of the differential pressure of the pre-filters and HEPA filters due to smoke loading. The calculation results were compared with experimental results to verify our models in CELVA-1D.

2. EXPERIMENTAL DEVICES AND CONDITIONS

The schematic diagram of the experimental facility is shown in Fig.1. The facility consisted of the air supply duct, the 1st model cell, the 1st duct, the 2nd model cell, the 2nd duct, dilution duct, mixer, the 3rd duct, filter chamber, the exhaust duct, the blower, stuck. Air samplers and cascade impactors were set for the measurement of time dependencies of smoke concentration and smoke size distributions, respectively. The test results under burning 7.5 kg of rubber as the mock burnable material in the 1st model cell was analyzed by the CELVA-1D.

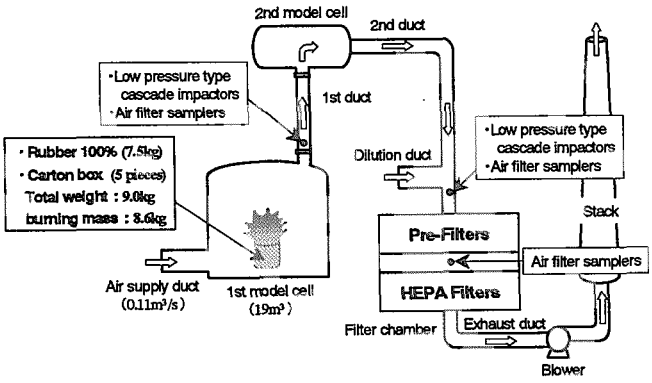

Fig.1 Block diagram of the experimental facility

3. OUTLINE OF CELVA-1D

The outline of calculation functions of CELVA-1D is shown in Fig.2. The analysis of the cell ventilation system by CELVA-1D begins from preparation for the node junction data from the information on shapes and scales of the cell ventilation. The source term data, inputs of the release rates of mass (kg/s) and energy (J/s) to CELVA-1D can calculate the time dependencies of temperature, pressure propagation and flow rates by the heat flow analysis function of CELVA-1D based on one-dimensional thermofluid analysis, which takes account of flow resistance and heat transfer of the cell ventilation system. The release rate of smoke (kg/s), smoke size distribution, the DF of the pre-filters and the clogging properties of the pre-filters and HEPA filters are inputs for calculation of the transport of the smoke and the time dependency of the differential pressure of the pre-filters and the HEPA filters.

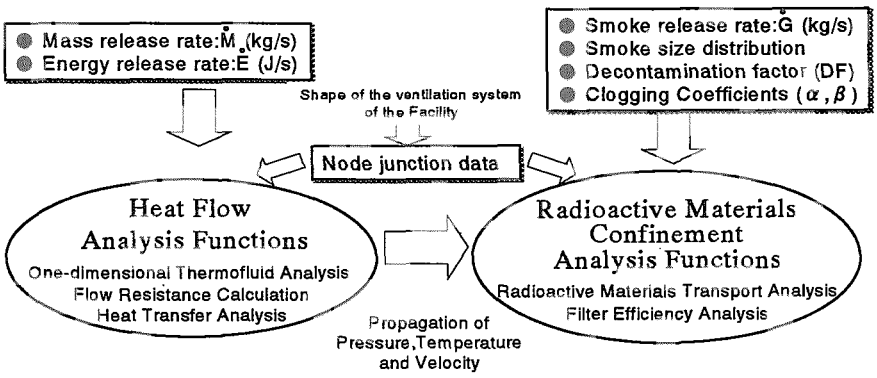

Fig.2 Outline of the Calculation Functions of CELVA-1D

4. CALCULATION MODEL

4.1 PREPARATION OF NODE JUNCTION DATA OF THE FACILITY

The node junction data of the ventilation system in the experimental facility were discretely divided into some volume elements (nodes) and connecting points between the nodes (junctions). The node junction data used for the analysis by CELVA-1D is shown in Fig. 3. The ventilation system was divided into totally 49 sections including the following; 6 sections of the air supply duct system, 10 sections of the second duct system, 9 sections of the third duct system, 10 sections of the exhaust duct, 5 sections of the dilution duct and the model cells, the filter chamber and atmosphere.

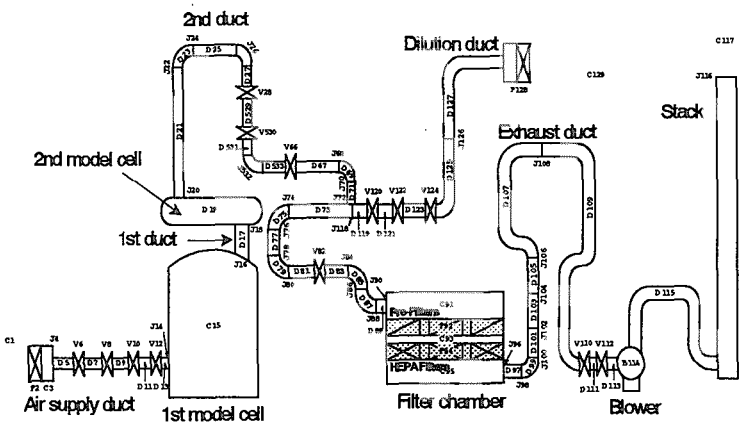

Fig.3 Node junction data for the analysis

4.2 ESTIMATION OF SOURCE TERM

The time dependencies of the release rates of mass, energy and smoke calculated by CELVA-1D are shown in Fig. 4. In the calculation, the following assumptions were considered.

Firstly, we assumed that mass release rate (kg/s) was proportional to the time dependency of the temperature of the gas phase at the first model cell (19 m^3) where the mock burnable materials were combusted. Under this assumption, we determined the mass release rate from the normalization of the time integration of the temperature with total burned mass of the mock burnable materials.

Secondly, we assumed that the release rates of smoke and energy were proportional to the mass release rate. We calculated the smoke concentration at 3rd duct and temperature of gas phase at the first model cell using CELVA-1D to compare with experimental results and inversely determined the proportional constant of the relationship of the release rates of mass

and smoke and the relationship of the release rates of mass and energy, 0.11 (-) and 2.5×10^{7} (J/kg), respectively.

Thirdly, we determined that the smoke size distribution followed the log-normal distribution with 0.5 (μm) of mass median diameter and 3.6 (-) of geometric standard deviation from comparison of experimental result.

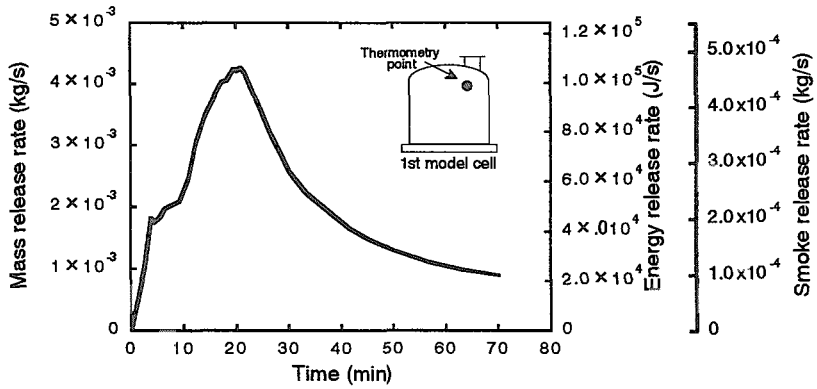

Fig.4 Estimation results of the mass, energy and smoke release rates

4.3 DECONTAMINATION FACTOR OF THE FILTERS

After the experiments of combustion, penetration experiments of di-octyl phthalate (DOP) particles through the pre-filters were performed and DOP particle size distribution were measured at upstream and downstream of the pre-filters. The DOP particle DF of the pre-filters was determined from the ratio of the concentration of each DOP particle size at upstream and downstream of the pre-filters. The relationship between the smoke loading on the pre-filters and the DF of DOP particles is shown as a function of DOP particle size in Fig. 5.

The dependency of the DF in the pre-filters to smoke loading was used for the calculation of time dependency of the differential pressure of the pre-filter by CELVA-1D. The DF of the HEPA filters was determined from the previous study[3].

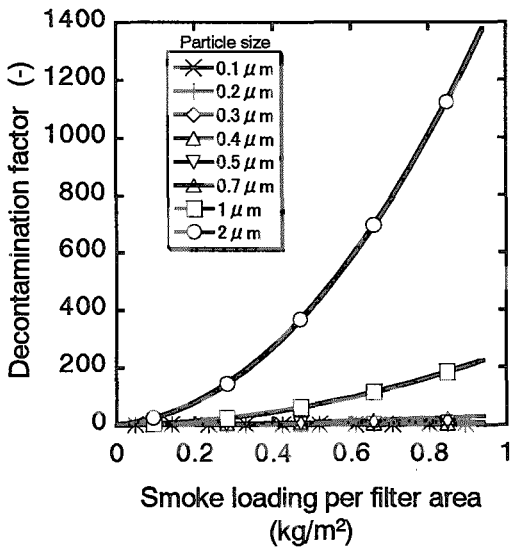

Fig.5 Relationship between the smoke loading on the pre-filter and DF of each particle size of DOP-particle

4.4 CLOGGING COEFFICIENTS OF THE FILTERS

The rising of the differential pressure between the ventilation filters was expressed by the following equation[1]-[3] in CELVA-1D,

$$\Delta P = \Delta P_0\left(1+\alpha M+\beta M^2\right) \qquad [1]$$

where ΔP_0: Differential pressure across clean the ventilation filter (Pa)

ΔP : Differential pressure across the ventilation filter (Pa)
M: Smoke loading per unit area of the ventilation filter (kg/m^2)
α: Linear clogging coefficient of the ventilation filters (m^2/kg)
β: Second order of clogging coefficient of the ventilation filter (m^4/kg^2).

The experimental results of the relationship between smoke loading and the differential pressure of the pre-filters are shown in Fig. 6. The line of this figure shows the fitting of Eq. [1]. We determined the coefficients of pre-filters from the fitting, α=72 (m^2/kg) and β=586 (m^4/kg^2), respectively. We determined the coefficients of HEPA filters, α=138 (m^2/kg) and β=3690 (m^4/kg^2), respectively from the experimental results of previous study[1].

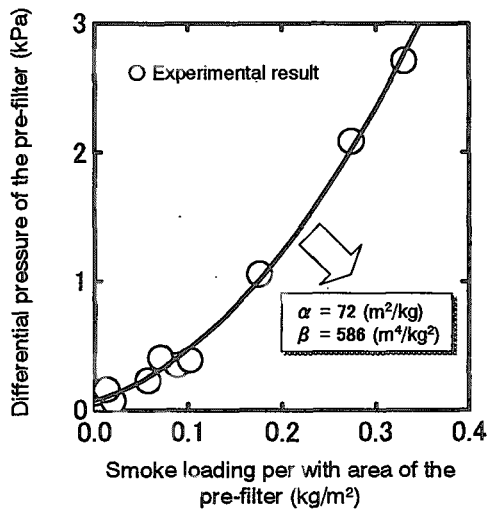

Fig. 6 Relationship between smoke loading and the differential pressure of the pre-filter

5. RESULTS AND DISCUSSION

5.1 EVALUATION OF DIFFERNTIAL PRESSURE OF THE FILTERS

The comparison between calculated and experimental results of time dependency of the differential pressure of the pre-filters and the HEPA filters is shown in Fig. 7. The calculated lines of the pre-filters and the HEPA filters show the same dependency of the experimental results. From the agreement of the calculated and experimental results, It is found that the model combined with CELVA-1D is valid for the estimation of differential pressure of the pre-filter and HEPA filter.

From experimental results among the other conditions of combustion, we found that the

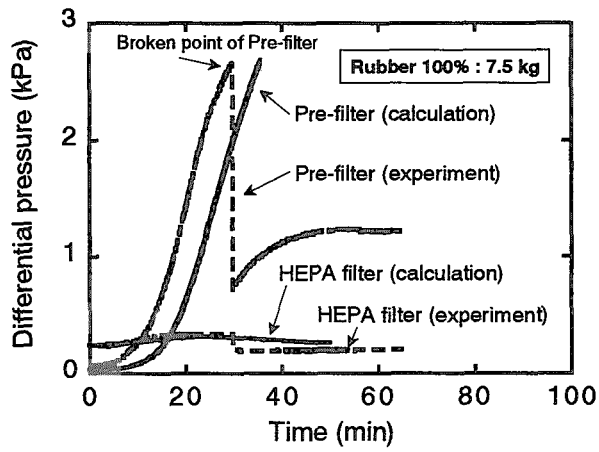

Fig.7 Comparison between calculation and experimental results of the differential pressure of the filters

differential pressure at the pre-filter broken was from 0.8 to 2.7 kPa. The scattering of this value was caused the inhomogeneous strength among the pre-filters tested. Therefore, taking into account of the scattering of the differential pressure at the pre-filter broken, we can estimate the breakage time of the pre-filters using our model when the mass release rate is known.

5.2 ESTIMATION OF BREAKAGE TIME OF THE PRE-FILTERS

To discuss the effect of the mass release rate to the breakage time of the pre-filters, the calculation of the time dependency of the differential pressure of the pre-filters was demonstrated with the change of the mass release rate.

The input conditions of mass release rate are shown in Fig. 8. The maximum of the mass release rate were changed from 0.5×10^{-3} to 7.0×10^{-3}. It was assumed that from the time at the start to maximum value of mass release rate, the slopes of mass release rates were the same with the value under 7.5 kg rubber burning and that after the time at maximum, the mass release rates were constant. We also assumed that other necessary constants and conditions for the calculation were used the same values under 7.5 kg of rubber burning. From these assumptions, the shapes of the release rates of energy and smoke were same in Fig. 8. Here, we should note that this shapes of the mass, energy and smoke were quite different from those under 7.5 kg of rubber burning.

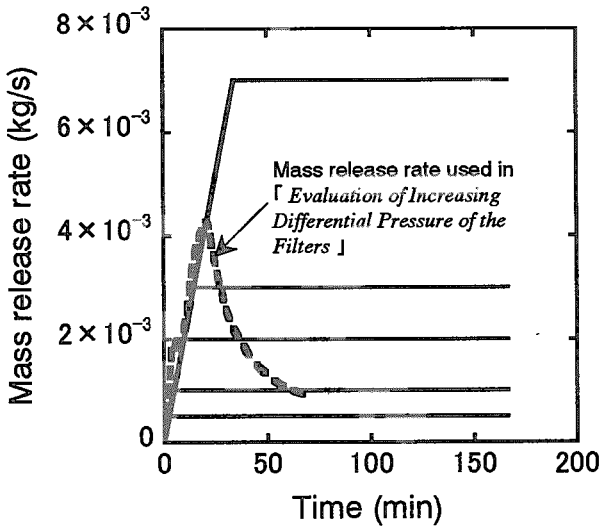

Fig.8 Time dependency of the assumed mass release rates

The time dependency of the differential pressure of the pre-filters under the conditions of the mass release rate in Fig. 8 is shown in Fig. 9. The broken lines show minimum and maximum of the differential pressure of the pre-filters broken among the experiments. From this figure, we can read the minimum and the maximum of breakage time of the pre-filter from the cross point of the curves and the broken lines. We can also see that the slope of the differential pressure of the pre-filters tends to increase rapidly with the increase of the mass release rate.

The estimated result of the breakage time of the pre-filters is shown in Fig. 10. Below 2.0×10^{-3} (kg/s) of the mass release rate, the breakage time rapidly decreases with the increase of the mass release rate. On the other hand, above 2.0×10^{-3} (kg/s) of the mass release rate, the breakage time tends to decrease gently. However the turning point of the tendency can vary under the actual condition of the mass release rate, the existence of this point is interesting in the view of consideration of the role of the pre-filters for preventing from clogging of the

HEPA filters due to smoke loading. This tendency also will help the estimation of the time for exchange of the pre-filters to keep the confinement capability to the ventilation system including the pre-filters and the HEPA filters.

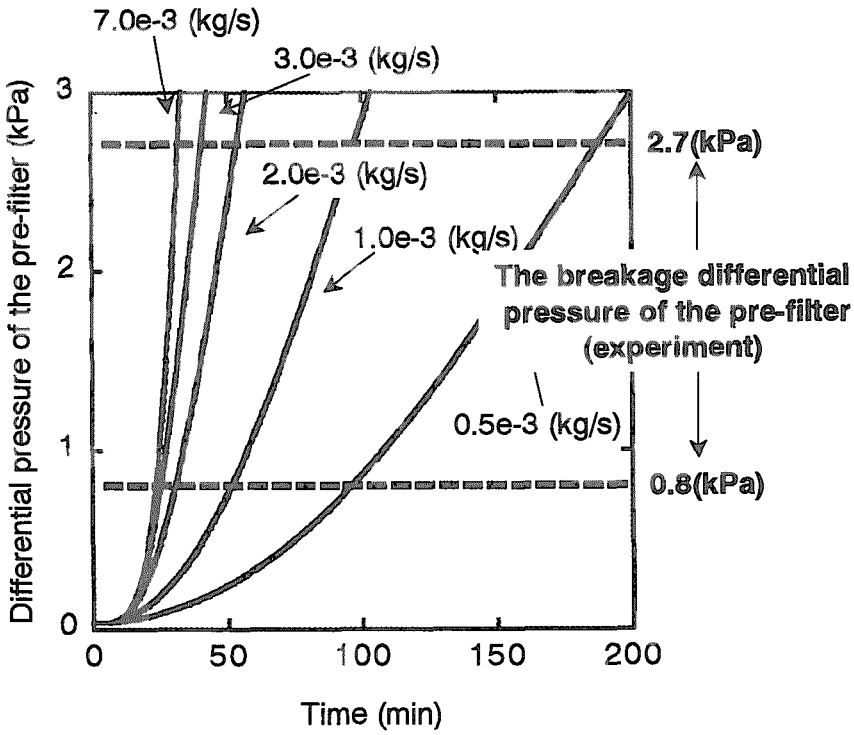

Fig.9 Time dependency of the differential pressures of the pre-filter, calculated by assuming the mass release rate as a parameter

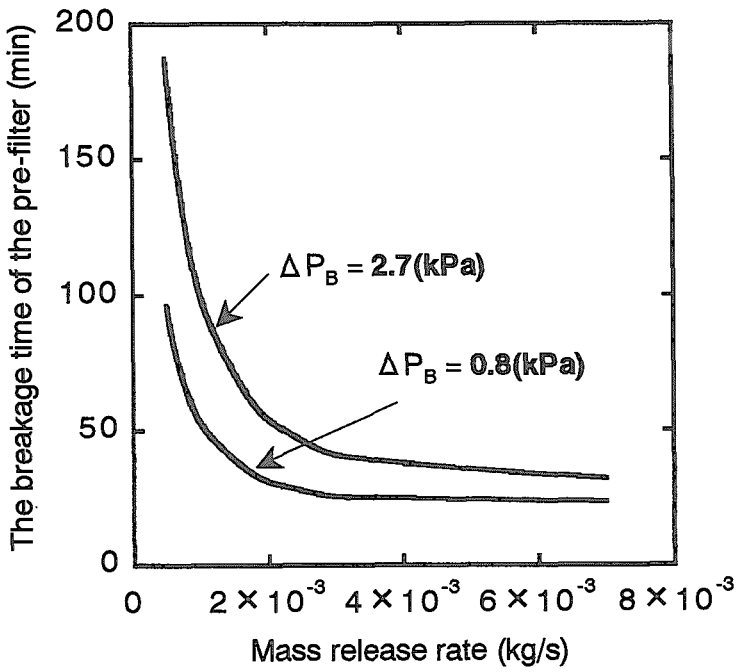

Fig.10 Evaluation results of the breakage time of the pre-filter

6. CONCLUSIONS

The confinement capability of radioactive materials was evaluated by the calculation code CELVA-1D in the ventilation system equipped with pre-filters and HEPA filters as the ventilation filters under the fire accident. In the CELVA-1D code, the source term model was the model of smoke generation due to combustion of the mock burnable materials related to the release rates of the mass, energy and smoke. The prediction model was proposed of the time dependency of the differential pressure of the pre-filters and the HEPA filters taking account of the clogging properties and the DF of the pre-filters. It was found that the calculation results of the time dependency of the differential pressure of pre-filters and HEPA filters were in fair agreement with the experimental results obtained from the test using the demonstration facility. The validity of the proposed model in the CELVA-1D was confirmed.

Moreover, the breakage time of the pre-filters was estimated as a parameter of the mass release rate with the CELVA-1D. It was found that the breakage time was drastically decreased with increasing the mass release rate in the range of below $2x10^{-3}$ kg/s of the mass release rate.

ACKNOWLEDGMENT

This work was carried out by Japan Atomic Energy Research Institute under the auspices of the Ministry of Education, Culture, Sports, Science and Technology.

REFERENCES

(1) G.Nishio, K.Watanabe, K.Kouno, N.Yamazaki, S.Mukaide and I.Yoshioka, JEARI-Data/Code 98-01 (1998) [in Japanese].
(2) G.Nishio, M.Suzuki, S.Mukaide, J.Takada, M.Tsukamoto and T.Koike, Nucl.Technol., Vol.95, 325-336 (1991).
(3) Ozaki.M., Kanagawa.A., Kuki Seijo, vol.25 No.6, 1-15 (1988) [in Japanese]

JP0250350

JAERI-Conf 2002-004

CLOGGING CHARACTERISTICS OF VENTILATION FILTER UNDER THE FIRE ACCIDENT

Shinsuke TASHIRO, Kouji WATANABE, Hitoshi ABE, Junichi TAKADA and Gunzo UCHIYAMA

Department of Fuel Cycle Safety Research, Japan Atomic Energy Research Institute

Tokai-Mura, Naka-gun, Ibaraki-Ken, 319-1195 Japan

Fax: 81-29-282-5745, e-mail: tashiro@aero.tokai.jaeri.go.jp

To evaluate the smoke behavior and its loading characteristics to the ventilation filters, the verification tests on safety of a cell ventilation system under the fire accidents burning the solid wastes (rubber, cloth) or the recovered solvent (n-dodecane, 30% tributyl phosphate (TBP)/70% n-dodecane), which are often used and wasted in the nuclear facilities, have been performed. Maximum of smoke concentration before the ventilation filter was less than 1000 mg/m^3. Mass Median diameter and geometric standard deviation of smoke before the ventilation filter were 0.2-0.4μm and 3-4 in the case of the solid wastes burning, 0.2-1 μm, 3-4 in the case of the recovered solvent, respectively. The differential pressure of a pre-filter or a HEPA filter to the mass loading per unit area were expressed by quadratic function under the different kind of the solid wastes or recovered solvents.

Key words: fire accident, smoke, filter clogging, pre-filter, ventilation system

1. INTRODUCTION

In a nuclear fuel facility, air ventilation systems consisting of cells, ducts, ventilation filters and blowers are used to confine radioactive airborne materials to the facility. Because of complexity of the air ventilation systems, the calculation code is often used to evaluate the confinement capability of radioactive airborne materials to the nuclear fuel facility. To evaluate the confinement capability of radioactive airborne materials under a fire accident in the nuclear fuel facility, it is very important to handle the information on smoke generation, mass transportation of the smoke to the air ventilation system and clogging characteristics of the ventilation filters by smoke.

The pre-filter is often set for the collection of large particles to prevent HEPA filter from clogging by large particles under usual condition in some nuclear fuel facilities. Moreover under the fire condition, the pre-filter can be expected to play the role of preventing HEPA filter from rapidly clogging. Because the concentration of smoke near the fire is so high that rapid coagulation will occur and smoke size distribution at upstream of the ventilation filter will shift larger size. But excess smoke loading onto the pre-filter will make the pre-filter clog and finally break. Then much smoke directly loading onto the HEPA filter will cause the rapid clogging and the breaking of the HEPA filter. Then the radioactive airborne materials will be released to the atmosphere. The air pollution by radioactive airborne materials is great serious problem to the public. To avoid the destruction of confinement of the radioactive airborne materials with the pre-filter broken, the exchange of the pre-filter will be necessary before the breakage of pre-filter and the rapid clogging of the

HEPA filter. Therefore it is very important for the estimation of the exchange time of the pre-filter to evaluate the clogging of the pre-filter quantitatively. Unfortunately the study on the clogging of the pre-filter under the fire accident has not been found experimentally and theoretically.

In Japan Atomic Energy Research Institute, the large-scale experiments focused on safety of a cell ventilation system of installed the cascade combination of pre-filters and HEPA filters burning the mocked materials of the radioactive wastes in the nuclear fuel facilities have been performed. The purposes of our experiments are three; the first is to study the fire behavior of radioactive wastes such as rubber, cloth and recovered solvent. The second is to verify the role of the pre-filters preventing HEPA filters from rapidly clogging and to evaluate the differential pressure rising of pre-filters with faction of mass of smoke loading onto pre-filters. The third is to establish the evaluation and simulation approaches of safety analysis of the ventilation systems in a nuclear fuel facility under such fire condition using CELVA-1D[1].

In this study, the time dependencies of smoke concentration and size distribution at the neighborhood ventilation filters and clogging characteristics of ventilation filters by smoke obtained from the experiments are mainly described.

2. EXPERIMENTAL

2. 1 EXPERIMENTAL FACILITY

The block diagram and the scale of the experimental facility are shown in Table I and Fig. 1, respectively. The mock materials were burned in the 1st model cell and the smoke generated was transported to the stack by way of the 2nd model cell, mixer and filter chamber. The filter chamber has three sets of full-size pre-filter (model CM-31-KW-R-50Z, Nihon Muki Corp.) at upstream stage and six sets half-size HEPA filter (model ATM-31H-P-E, Nihon Muki Corp.) at downstream stage, respectively. Specification of test filters is shown in Table II.

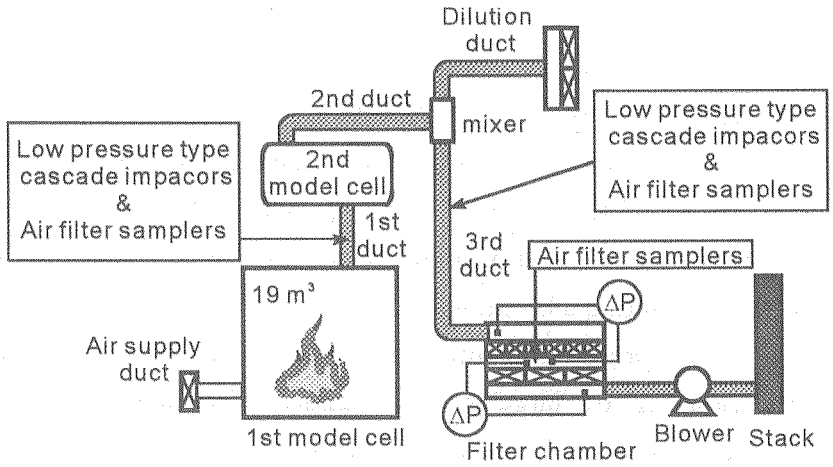

Fig. 1 The block diagram of the experimental facility.

Smoke size distributions and concentrations at 1st duct, 3rd duct and downstream of pre-filters were measured by Andersen-type low-pressure cascade impactors (model LP-20, Tokyo Dylec Corp.) and air filter samplers, respectively. The pressure in the ventilation system including at upstream and downstream of pre-filters and HEPA filters were measured

by dial-gauge type differential manometer. The temperature in the ventilation system was measured by thermo-couples. The characteristic of the burning at the 1st model cell was monitored by video system.

Table I The scale comparison of the experimental facility with a reprocessing plant.

Component	Experimental facility	Reference plant	Scale factor
1st model cell	19 m^3, cylindal	80m^3, rectangular	1/4 scale.
1st duct	5 m long, 0.4 m inner diam.	~6m long	1:1 scale of long. 2/3 scale of inner diam.
2nd model cell	6 m^3, cylindal	~30m^3	1/4 scale.
2nd duct	10 m long, 0.2 m inner diam.	~70m long	1/3 scale of inner diam.
3rd duct	10 m long, 0.6 m inner diam.	~70m long	1:1 scale of inner diam.
Filter chamber	1 chamber with 2 stages cascaded.	18 chambers	

Table II Specifications of test filters

Specification	Pre-filter	HEPA filter
Size (mm)	610×610×50	610×305×292
Thickness (mm)	50*	0.39
Area of filtration (m^2)	0.37	11.3
Diameter of fiber (μm)	30±4 (layer 1) 30±4 (layer 2)	0.72
Initial collection efficiency of particles	85 %	99.99 %

*Double layers combined. Thickness of each layer is 25 mm.

2. 2 CONDITIONS OF BURNABLE MATERIALS AND VENTILATION TIMES

The gloves made of rubber and cloth packed in 5 pieces of carton box (ϕ225 mm×350 mmH, 0.5 kg) were used as the mock burnable solid wastes. Normal-dodecane solvent and the mixture of n-dodecane 70%/ tri-n-butyl phosphate (TBP) 30% solvent filled in a stainless steel pan (ϕ422mm, area, 0.14m^2) was used as the mock burnable recovered solvent.

As the parameters, the burnable materials (rubber 100 %; 2-7.5 kg, rubber 50% and cloth 50%; 15-20 kg, cloth 100%; 7.5 kg, n-dodecane 100%; 5-12 kg, n-dodecane 70%/ TBP 30%; 12 kg) and the times of ventilation in the 1st model cell (5-20 times/hour) changed but the face velocity through the filters was adjusted 1.3 m/s in all runs to simulate normal conditions in the reference reprocessing plant.

3. RESULTS AND DISCUSSION

3.1 TIME DEPENDENCIES OF PRESSURE, FLOW RATE AND TEMPERATURE OF VENT GAS

Pressure and flow rate of vent gas except near the filters did not change during burning in all runs.

Fig. 2 shows the typical time dependencies of temperature of vent gas at the 1st model cell near 1st duct, the inlet of 1st duct, the outlet of 2nd model cell, the outlet of 2nd duct and the inlet of 3rd duct.

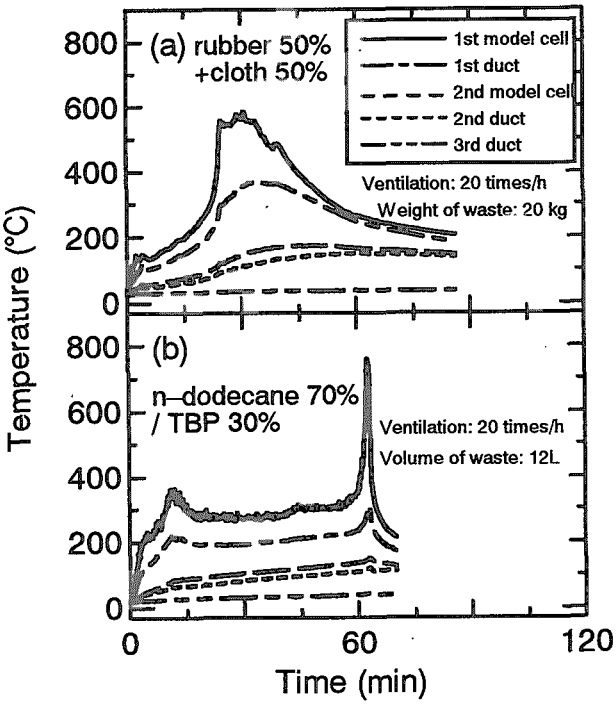

Fig. 2 Time dependency of temperature of vent gas.

In the mock solid wastes burning, the time dependency of temperature of vent gas at the 1st model cell had one peak. The peak value of temperature at this point with the time of ventilation fixed strongly depended on both the composition and weight of the burnable materials. The maximum value of temperature at this point with the change against both the composition and weight of the burnable materials under the 20 times/h of the ventilation at the 1st model cell fixed was about 600 °C in the case of the mixture of 10 kg of rubber and 10 kg of cloth burning as shown in Fig. 2(a).

In the mock recovered solvent burning, the time dependency of temperature of vent gas at the 1st model cell was stationary in the case of n-dodecane solvent burning with the change of the volume of the solvent under the 20 times/h of the ventilation. The value of temperature at this point was about 500 °C in the case of 12 litter of n-dodecane burning. But in the case of the mixture of n-dodecane/TBP burning, the time dependency of temperature of vent gas at the 1st model cell had two peaks as shown in Fig. 2(b). The temperature at 2nd peak was higher than the one at 1st peak. The maximum value of temperature at 2nd peak was about 780 °C. Just after the 2nd peak of temperature, the fire was quenched naturally. It was considered that the lack of the oxygen at 1st model cell was occurred due to the boilover burning[2],[3].

However the vent gas at the 1st model cell had different dependencies of temperature among the condition of the burnable materials or the ventilation times, the temperature of the vent gas downstream of the 3rd duct did not change as shown in Figs. 2(a) and (b). From the results of time dependencies of pressure, flow rate and temperature of vent gas, we can conclude that these properties from the fire did not have influence on the ventilation filters in our experiments.

3.2 TIME DEPENDENCY OF SMOKE CONCENTRATIONS AND SMOKE SIZE DISTRIBUTIONS

Fig. 3 shows the time dependency of smoke concentrations at the 3rd duct with the change of kind and amount of burnable materials under the ventilation times fixed.

In the mock solid wastes burning under the ventilation fixed, increasing the ratio of cloth in the same amount of solid wastes tended to refrain from smoke generation. In the mock recovered solvent burning under the ventilation fixed, smoke concentration generated from n-dodecane burning was stable but smoke concentration generated from the mixture of n-dodecane and TBP burning had two peaks. 2nd peak of smoke concentration was considered due to the boilover burning[2],[3]. In the same amount of pure rubber burning with change of ventilation at 1st model cell, decreasing of ventilation tended to refrain from smoke generation.

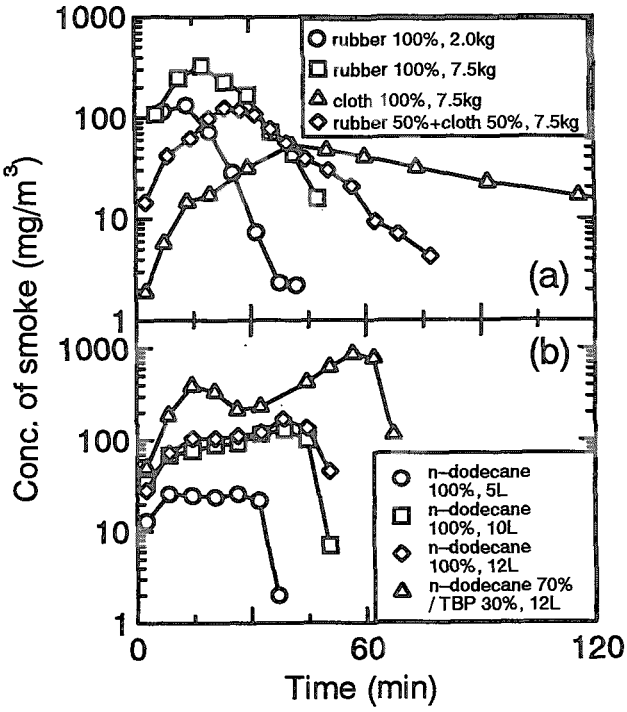

Fig. 3 Time dependency of smoke concentration at the 3rd duct.

The time dependencies of smoke size distributions did not change well under burning. Assuming the smoke size distributions were log-normal, in all runs, the range of mass median diameter and geometric standard deviation were 0.16-0.75 μm and 2.4-5.3, respectively.

Table III Time average of MMD and σg of smoke size distributions at the 3rd duct.

Wastes	Weight or volume of wastes	Ventilation times (times/h)	MMD (μm)	σ_g
Rubber	7.5 kg	5	0.46	5.3
		10	0.75	4.0
		20	0.47	3.4
Cloth	7.5 kg	20	0.54	2.4
Rubber 50%+cloth 50%	7.5 kg	20	0.25	3.0
N-dodecane	12L	20	0.16	4.2
N-dodecane 70%/TBP 30%	12L	20	0.69	2.5

3.3 THE CLOGGING CHRACTERISTICS OF THE PRE-FILTER AND THE HEPA FILTER

The typical dependency of the differential pressure at the pre-filter and the HEPA filter is shown in Figs. 4-6.

In the mock solid wastes burning under the ventilation fixed, the differential pressure at the pre-filter strongly rose but the one of HEPA filters did not rise, as shown in Fig. 4. In this figure, the sudden drop of the differential pressure at the pre-filter shows the breakage of the pre-filter. The rising of the differential pressure at the pre-filter after the breakpoint shows that all sets of the pre-filter were not broken but some sets was broken. After the experiment, it was found that only one set of the pre-filter of three in the filter chamber was broken. Similar tendency of the differential pressure at the pre-filter and the HEPA filter was shown among another solid materials condition including rubber, but the pre-filter was not always broken at the same differential pressure. The value of differential pressure at the breakpoint of the pre-filter were 0.9-2.7 kPa, 0.7 kPa under 100% rubber, 50% rubber + 50% cloth burning, respectively. After the experiment, masses loading per set of the pre-filter were 0.086-0.14 kg between the burning under materials including rubber. From these results, it was considered that the differential pressure at the pre-filter broken was not strongly dependent on the inhomogeneous strength of the pre-filter but on the smoke characteristics loading onto the pre-filter. Under 100% of cloth burning, the differential pressure at the pre-filter did not rise. It is considered because smoke concentration under 100% of cloth burning was lower than ones under another materials burning, as shown Fig. 3(a).

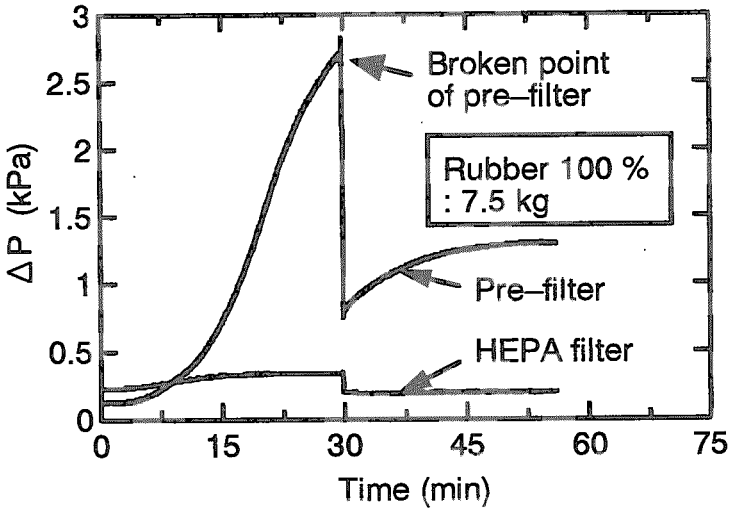

Fig. 4 Time dependency of the differential pressure of the ventilation filters due to the smoke loading under 20 times/ h of the ventilation at the 1st model cell.

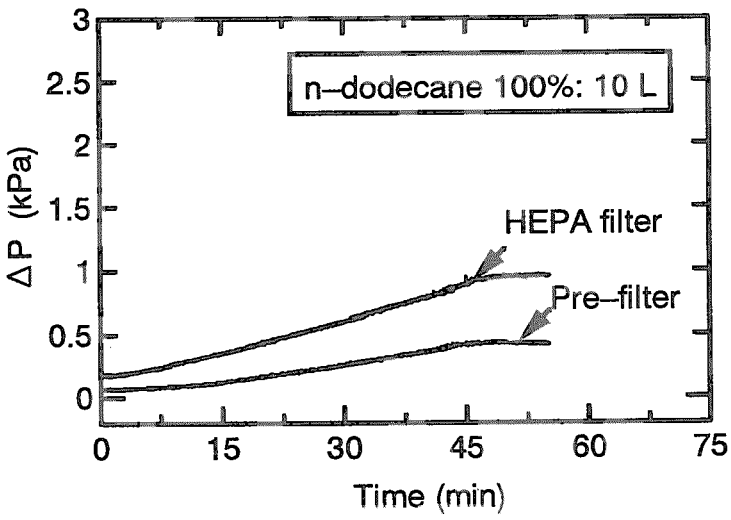

Fig. 5 Time dependency of the differential pressure of the ventilation filters due to the smoke loading under 20 times/ h of the ventilation at the 1st model cell.

In the mock recovered solvent burning under the ventilation fixed, the rising of the differential pressure at the pre-filter under 100% n-dodecane solvent burning was different from the solid materials burning. The rising of the differential pressure at the pre-filter under 100% n-dodecane solvent burning was less than the one at the HEPA filter as shown in Fig. 5. It is considered because smoke size distribution under 100% n-dodecane solvent burning as shown in Table III was so small that most of smoke was penetrated through the pre-filter and directly loading onto the HEPA filter. But the loading of smoke having small size distribution onto the HEPA filter was not generally affected to the confinement capability of the HEPA filter.

The rising of the differential pressure at the pre-filter under 30% TBP/ 70% n-dodecane solvent burning was little gentler than ones under the solid materials including rubber burning as shown in Fig. 6. The differential pressure at the HEPA filter rose with delay but was not broken. The broken characteristic of the pre-filter was similar with the case of solid materials burning from the observation of the pre-filter after the experiment. The value of differential pressure at the breakpoint of the pre-filter were 0.84-1.41 kPa under 30% TBP/ 70% n-dodecane solvent burning. After the experiment, mass loading per set of the pre-filter was 0.13-0.19 kg.

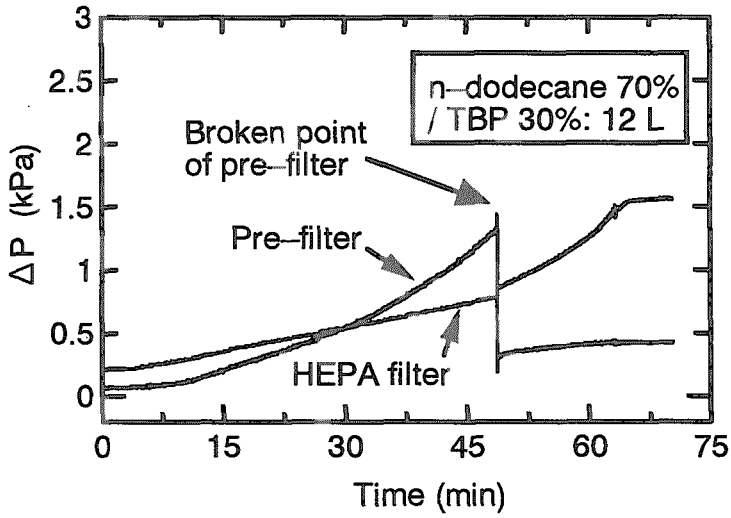

Fig. 6 Time dependency of the differential pressure of the ventilation filters due to the smoke loading under 20 times/ h of the ventilation at the 1st model cell.

From these results, it was considered that the differential pressure at the pre-filter broken was not strongly dependent on the heterogeneous strength of the pre-filter but on the smoke characteristics loading onto the pre-filter.

Under burning, the differential pressure of pre-filters strongly rose but the one of HEPA filters did not rise. It was found the pre-filter was useful for preventing the clogging of HEPA filters. The differential pressure of a pre-filter to the

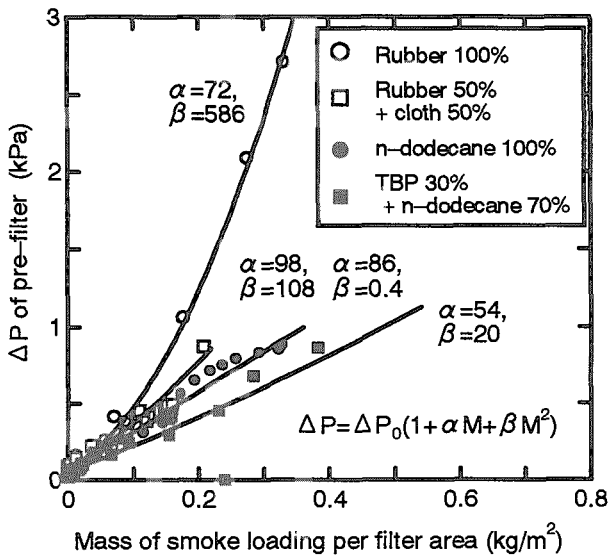

Fig. 7 The relationship of mass of the smoke loading to the differential pressure of pre-filter.

mass loading per unit the pre-filter area were fitted by the equation[1]-[4],

$$\Delta P=\Delta P_0(1+\alpha M+\beta M^2),$$

where α and β were the clogging coefficients, ($m^2\ kg^{-1}$) and ($m^4\ kg^{-2}$), respectively.

The obtained values of α and β from the experiments are shown in Fig. 7 and Table IV.

Table IV The clogging coefficients α and β

Wastes	Weight or volume of wastes	Ventilation (times/h)	α ($m^2\ kg^{-1}$)	β ($m^4\ kg^{-2}$)	M (kg)
Rubber	7.5 kg	5	125	99	$0 \le M \le 0.19$
		10	129	178	$0 \le M \le 0.18$
		20	72	586	$0 \le M \le 0.35$
Cloth	7.5 kg	20	0	0	$0 \le M \le 0.10$
Rubber 50%+cloth 50%	7.5 kg	20	98	108	$0 \le M \le 0.25$
N-dodecane	12L	20	86	0.4	$0 \le M \le 0.34$
N-dodecane 70% /TBP 30%	12L	20	54	20	$0 \le M \le 0.54$

4. CONCLUSIONS

The time dependencies of smoke concentration and size distribution near the ventilation filters and clogging characteristics of ventilation filters by smoke were obtained from large-scale experiments using a cell ventilation system installed the cascade combination of pre-filters and HEPA filters at burning the mocked materials of the radioactive wastes in the nuclear fuel facilities. The smoke concentration was considered related to temperature of gas phase near the fire. The clogging characteristics of pre-filter were experimentally considered related to smoke size distribution, concentration, and mass loading of smoke onto the pre-filter. It was concluded that the pre-filter was effective for the preventing the HEPA filter from rapid clogging. Values of the coefficient will be adapted to the safety analysis on the confinement ability of radioactive materials in a ventilation system under a fire accident.

ACKNOWLEDGEMENT

This work was carried out by Japan Atomic Energy Research Institute under the auspices of the Ministry of Education, Culture, Sports, Science and Technology.

REFERENCES

[1] G. Nishio, K. Watanabe, K. Kouno, N. Yamasaki, S. Mukaide and I. Yoshioka, JAERI-Data/Code 98-017 (1998)

[2] K. Hashimoto, G. Nishio and K. Soda, Nuclear Technol., **101**, 218-26 (1993)

[3] G. Nishio, J. Japan Air Clean. Assoc., **25**, 16-31 (1988) [in Japanese]

[4] H. Abe, J. Takada, M. Tsukamoto, K. Watanebe and M. Murata, J. Nuclear Sci. Technol., **36**, 619-25 (1999)

JP0250351

STUDY ON SUPERCRITICAL FLUID EXTRACTION OF URANIUM AND TRANSURANIUM COMPLEXES WITH β-DIKETONES AND OTHER COMPLEXONES AS APPLIED TO DECONTAMINATION

ANDREW SHADRIN, ANDREW MURZIN, VALERY ROMANOVSKY AND VADIM STARCHENKO

V.G. Khlopin Radium Institute
194021, Russia, St. Petersburg, 2nd Murinskii Ave, 28
shadrin@atom.nw.ru

INTRODUCTION

The supercritical fluid extraction (SCFE) of metals is a field of science and engineering which has been actively developed in the last ten years. SCFE is based on the fact that the substances in supercritical state (fluids), i.e. at temperature and pressure being above the critical values, have a density close to liquid density, which provides high dissolving ability and viscosity near to that of gases which provides high penetrating ability and high extraction on rate. Carbon dioxide is the most common choice in supercritical extraction, because this gas is nontoxic, easily available, inexpensive and has moderate critical parameters ($t > 37^{o}C$ and pressure > 72 atm) [1].

The routine decontamination methods of surfaces and soils involve the use of acidic and alkaline complexone solutions for removal of radionuclides. The majority of the routine decontamination techniques generates large volumes of secondary aqueous radioactive wastes. In the case of SCFE the decontaminating agents dissolve in carbon dioxide rather than in water or organic solvents; this enables to reduce the volume of secondary radwastes considerably. Under changes of pressure or temperature the supercritical carbon dioxide turns into gaseous state, and this allows to remove readily the "solvent" and to obtain the dissolved compounds in compact form. These peculiarities of SCFE motivate interest in this process as a promising technique for surface decontamination. The conducted studies and literary data make it possible to propose the key diagram for decontamination in SC-CO_2 (Fig. 1).

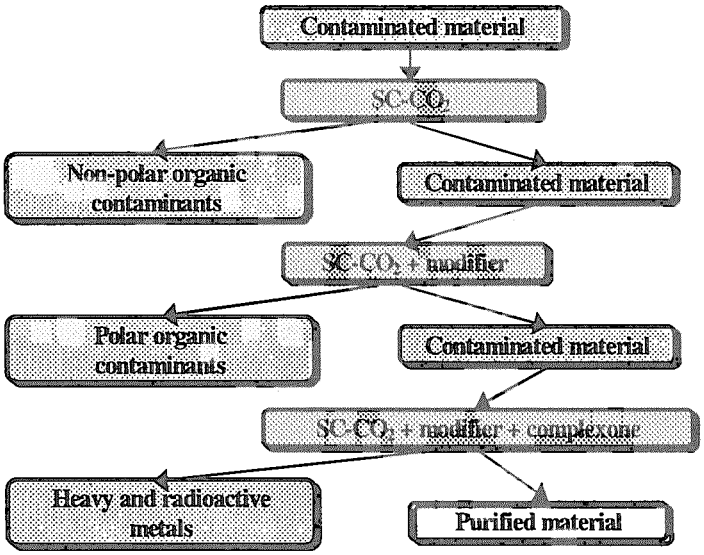

Fig. 1. Key flowsheet for supercritical fluid purification and decontamination of surfaces.

The technologies for supercritical fluid extraction of metals have been developed in the last ten years in Europe, USA and Japan. Intense studies in this field are conducted by CEA (France), BNFL (UK), DOE (USA), JAERI (Japan). The studies on SCFE of metals are aimed primarily at elaborating the methods for removal of metals from solid surfaces by SC-CO_2 to decontaminate soils, fabrics, asbestos, rubber etc., as well as to simplify sample preparation to analysis of environmental objects. The studies conducted in the framework of these projects have shown that the salts of heavy metals, uranium and rare-earth elements (REE) can be extracted from solutions and from solid surfaces (filter paper, steel andquartz sand) by SC-CO_2 containing β-diketones (hexafluoroacetylacetone (HFA, as a rule), dialkyldithiocarbamates, organophosphorus compounds or crown-ethers [2-9].

Our studies conducted in the last five years in collaboration with BNFL (Great Britain) and in the framework of ISTC Project 1160 were directed to checking the potential of SCFE of radionuclides extraction and elaborating the scientific fundamentals of SCFE decontamination technology. Experimental procedure is comprehensively described in [9-12].

IMPROVEMENT OF SCFE PROCESSES FOR EXTRACTION OF URANIUM AND TRANSURANIUM ELEMENTS BY β-DIKETONES.

It is known that the salts of uranium and rare-earth elements can be extracted by SC-CO_2 containing HFA and water [6]. It is also known that only the enol form of HFFA forms

chelate complexes with metals according to reaction of cation exchanges (equation 1), while the keto-form of HFAA cannot form complexes with metals.

$$M^{n+}(NO_3^-)_n + H^+HFFA^- \leftrightarrow M^{n+}(HFAA^-)_n + nHNO_3, \qquad (1)$$

Keto-enol tautomerism and thus the formation of β-diketone complexes with metals crucially depends on pH-medium. In [13] it is shown that the aqueous phase being in equilibrium with SC-CO_2 has pH 2.8, which is far short of optimum for formation of HFA-complexes (pK_a=4.46) [14] with metals. These facts are indicative of the necessity of changing pH-medium in the course of SCFE-process. In collaboration with BNFL we have suggested some modifiers (nitrogen-containing compounds) which permit to increase significantly the efficiency of uranium extraction (Table É) [15].

Table É Uranium extraction from air-dry uranylnitrate (SC-CO_2, 300 atm, 60°C)

HFA, μl	Pyridine, μl	Extraction of uranium, %
10	---	8 ± 3
10	30	60 ± 10
30	30	80 ± 10

Introduction of pyridine as pH-modifier enables to decrease the HFA-amounts needed for efficient extraction by a factor of 50-100. The results obtained were used in SCFD of really contaminated samples.

STUDY ON SOLUBILITY OF ACTINIDE COMPLEXES IN SC-CO_2

By solubility of complexes in SC-CO_2 it is usually meant the highest concentration of complex in CO_2. In [12] is shown that the supercritical carbon dioxide cannot be considered as an inert diluent, because CO_2 being in supercritical state interacts with soluble uranyl complexes, while forming the monosubstituted complexes and uranylcarbonate. Therefore, in what follows the "solubility" value was considered ass the amount of complex transferred into SC-CO_2 solution under given conditions. The conducted studies have shown that the solubility of $UO_2(TFA)_2 \cdot Py$ complex is rather high and exceeds 100 g/l (36 mg U/ml) (Fig. 2). This value is much higher than estimates according to literary data. It should be noted that the

detected value of complex solubility considerably exceeds the solubility needed for commercial use of processes for decontamination of solid surfaces by SC-CO_2.

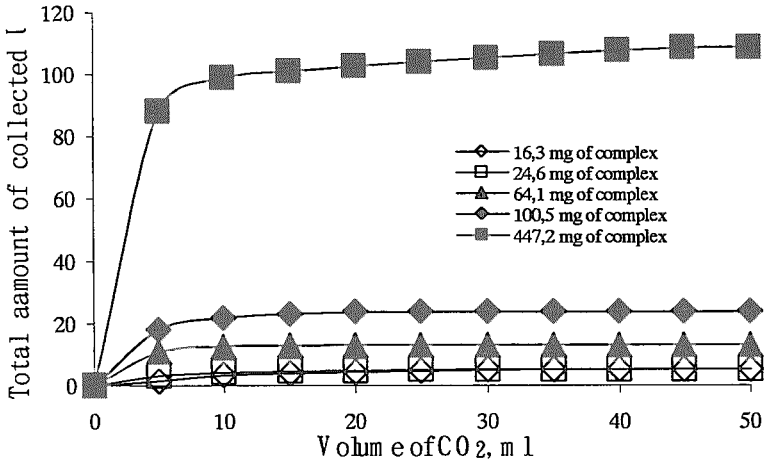

Fig. 2. Recovery of uranium from $UO_2(TFA)_2$*Py complex and collection of extract (300 atm, 60°C, 20 min, water traces).

Analysis of the data given in Table ŕÉ has revealed that the solubility of actinide complexes increases, as a rule, in the order of AA ≈ DPM ≈ TTA < TFA ≈ HFA and for additional ligands in the order of water < pyridine < TBP. There are exceptions presented by the hydrated complexes of actinides with HFA and TFA. It should be noted that the solubility of similar complexes of uranium(VI), plutonium(IV), europium(III) and americium(III) differ from one another only slightly. At the same time the solubility of corresponding complexes of neptunium(IV) is considerably lower (by a factor of 2-5).

So, the solubilities of different actinide complexes with β-diketones in SC-CO_2 were determined. It was shown that the solubilities of uranium, neptunium and plutonium complexes with non-fluorinated β-diketones (acetylacetone, dipivaloylmethane) and their adducts are not sufficient for the purposes of supercritical fluid decontamination. An exception is $UO_2(DPM)_2$·TBP adduct the solubility of which is 1.3 g/l (uranium) under standard conditions and can attain 20-30 g/l in the case of the high initial quantity of this complex. However, this fact is not of interest from the standpoint of developing the technology of supercritical fluid decontamination (SFD), because all the actinide elements should be removed by decontamination process. Hence, only fluorine-containing β-diketones, in particular TFA and HFA are promising SFD. Adducts of actinide complexes and fluorine-

containing β-diketones with water, pyridine and TBP are readily soluble in SC-CO_2 and can be used in the technology of supercritical fluid decontamination.

Table 巡 Solubility of complexes U(VI), Pu(IV), Np(IV), Eu(Am)(III) (SC-CO_2, 300 atm, 60°C, one-cell procedure, 20 mg of metal)

Neutral ligand	Solubility of actinide complexes with β-diketone, mM				
	AA	DPM	TTA	TFA	GFA
Complexes of U(VI)					
Water	-------	0.012 ±0.08	0.014 ±0.006	0.2 ±0.1	7 ±4
Pyridine	0.075±0.007	0.3 ±0.1	0.2 ±0.1	2 ±1	0.8 ±0.4
TBP	-------	5 ±1	2.0 ±0.8	4 ±1	4.2 ±0.6
Complexes of Pu(IV)					
Without ligand	0,6 ±0,4	0,4 ±0,2	unstable	unstable	unstable
Water	unstable	unstable	0,04 ±0,01	3,0 ±1,0	5,0 ±3,0
Pyridine	unstable	unstable	0,11 ±0,08	6,2 ±0,8	0,17 ±0,05
TBP	unstable	unstable	0,13 ±0,09	4,0 ±1,0	4,0 ±1,0
Complexes of (NpIV)					
Without ligand	0,18 ±0,09	0,39 ±0,06	unstable	unstable	unstable
Water	unstable	unstable	0,019 ±0,003	1,5 ±0,5	2,2 ±0,6
Pyridine	unstable	unstable	0,008 ±0,003	1,5 ±0,5	0,010 ±0,005
TBP	unstable	unstable	0,23 ±0,06	0,09 ±0,06	0,6 ±0,1
Complexes of Eu(Am)(III)					
Water	0,04 ±0,02	0,04 ±0,03	1,0 ±0,2	3 ±1	7 ±1
Pyridine	0,24 ±0,09	9 ±3	0,09 ±0,06	not detected*	0,07 ±0,01
TBP	8,9 ±0,9	7 ±3	13 ±4	6,9 ±0,5	7 ±3

SELECTION OF COMPLEXONES FOR SUPERCRITICAL FLUID EXTRACTION OF CESIUM AND STRONTIUM

It is known that the contaminated soils and other objects, as a rule, contain not only transuranium elements, but also such radionuclides as Cs-137 and Sr-90. SCFE of cesium and strontium is studied to a much lesser degree than that of uranium, heavy metals and even transuranium elements. Analysis of the available literary data on SCFE of metals shows that the metals forming complexes according to ion-exchange mechanism are extracted most efficiently [16]. In this case a neutral complex of metal cation and hydrophobic anion is transferred into SC-CO_2 phase. It was also shown that cesium and strontium can be efficiently extracted by solutions of commercial D2EHPA and dicyclohexyl-18-crown-6 (DCH18C6) in SC-CO_2 [9].

The solutions of D2EHPA and DCH18C6 in SC-CO_2 permit to remove from solid surfaces not only cesium and strontium, but also uranium and plutonium (Fig. 3), i.e. to conduct the combined decontamination of surfaces. As a result of studies, a mixture of commercial complexones was prepared; solution of this mixture in SC-CO_2 enables to remove efficiently uranium, transuranium elements, cesium and strontium from stainless-steel surfaces.

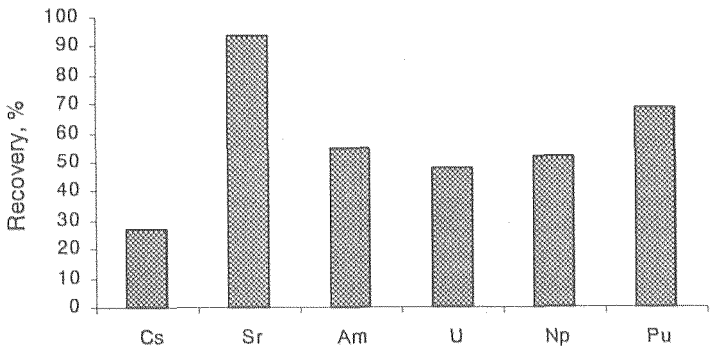

Fig. 3. SFE of radionuclides by solutions of D2EHPA and DCH18C6 in SC-CO_2

SCFE DECONTAMINATION OF REAL CONTAMINATED SPECIMENS

In collaboration with "Mayak" PA there was performed a series of tests on SCFE decontamination of porous materials (asbestos, rubber), fabrics (cotton, Dacron), metal surfaces (stainless-steel, carbon steel, brass, copper, nickel), plastics and soils. The studies have shown that the SC-CO_2 containing HFA and a modifier enables to remove 97-99% of α-emitters from surface of a material being processed in two successive operations (Fig. 4 and 5), which, as a rule, is sufficient for re-use of decontaminated materials.

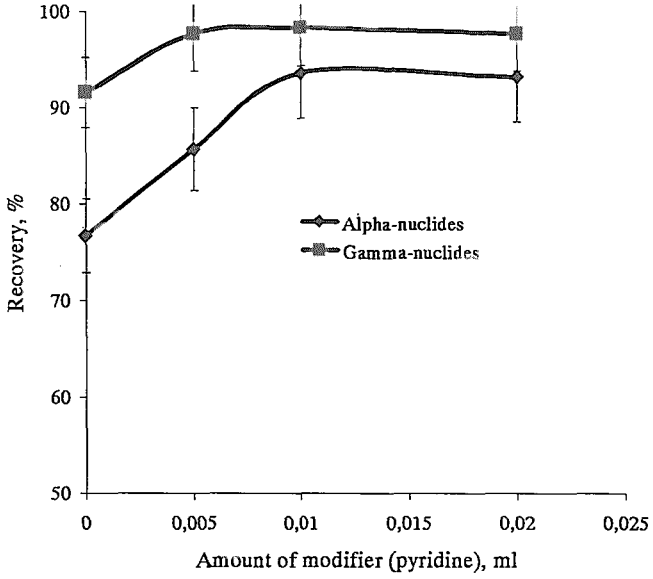

Fig. 4. Effect of modifier on radionuclide removal from stainless-steel surface by SC-CO_2 containing HFA and pyridine

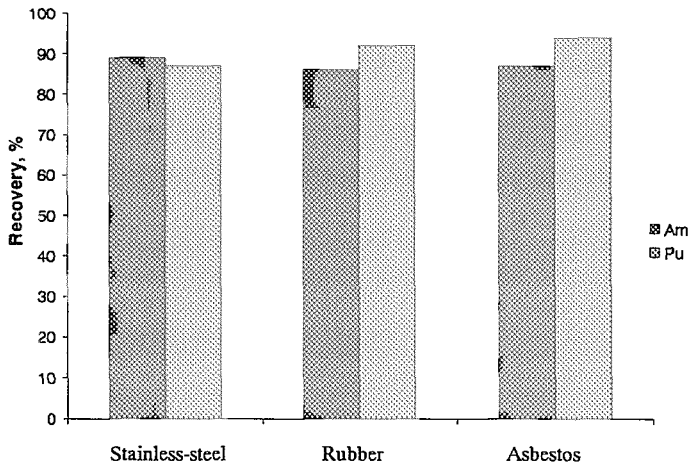

Fig. 5. Decontamination of surfaces of different materials by SC-CO_2 containing HFA and pyridine

The process of soil decontamination is a considerably more complicated task as compared with surface decontamination. The studies conducted with the use of labeled soils and quartz sand showed that the SCFE of americium decreases by a factor of 4-6 in the presence of humic acids and calcium carbonate. At the same time it is possible to extract 55-

75% of α-emitters in three successive operations of soil treatment by SC-CO_2 containing HFAA (Fig. 6).

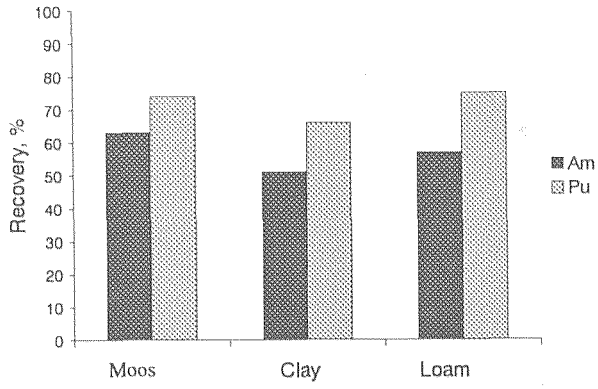

Fig. 6. Decontamination of soil by SC-CO_2 containing HFA and pyridine

The use of D2EHPA and DCH18C6 solutions in SC-CO_2 for supercritical fluid decontamination makes it possible to remove from the surface being decontaminated not only transuranium elements, but also such γ- and β-emitting long-lived nuclides as Cs-137 and Sr-90 (Fig .3). To demonstrate efficiency of this system, the real contaminated stainless-steel was decontaminated with the use of SC-CO_2 containing DCH18C6 and D2EHPA. It is shown that 92-95% of α-activity and 70-75% of Co-60 can be removed from stainless steel in one extraction by SC-CO_2 containing water, D2EHPA and crown-ether.

Hence, the conducted tests have demonstrated the possibility for decontamination of solid surfaces by SCFE. To demonstrate the potential of the subcritical CO_2 for decontamination purposes, some experiments on decontamination of really contaminated stainless-steel surface were carried out. The data obtained are given in Tables III and IV.

Table III. Removal of transuranium elements from real contaminated stainless-steel surface by subcritical (liquid) and supercritical CO_2

Amount of complexone, μL				Residue of element on surface, %	
Water	Pyridine	TFA	D2EHPA	Am	Pu
Subcritical (liquid) CO_2 (70 atm, 40 °C)					
10	10	10	0	$55_{\pm 8}$	$56_{\pm 14}$
10	10	30	0	$31_{\pm 4}$	$10_{\pm 6}$
10	0	0	10	$30_{\pm 12}$	$59_{\pm 13}$
Supercritical CO_2 (300 atm, 60 °C)					
10	10	10	0	$45_{\pm 10}$	$40_{\pm 15}$
10	10	30	0	$15_{\pm 6}$	$8_{\pm 4}$
10	0	0	10	$22_{\pm 5}$	$38_{\pm 3}$
10	0	0	30	$18_{\pm 11}$	$22_{\pm 14}$

Table IV. Decontamination of real contaminated stainless-steel surface in liquid (60 atm, 25 ¡Ñ) and supercritical (300 atm, 60 ¡Ñ) CO_2

Material	Composition of decontaminating mixture		
	10 µL Í ₂Î , 30 µL HFA, 10 µL pyridine in 35 mL ÑÎ ₂	10 µL Í ₂Î , 10 µL D2EHPA, 40 mg DCH18C6 in 35 mL ÑÎ ₂	
	Residue Am^{241}, $Eu^{154-155}$, Ce^{144}, %	Residue Am^{241}, $Eu^{154-155}$, Ce^{144}, %	Residue Cs^{137}, %
Plastic	$48_{\pm 9}$	$73_{\pm 18}$	$42_{\pm 11}$
Cotton	$60_{\pm 12}$	$28_{\pm 5}$	$46_{\pm 8}$
Steel	$15_{\pm 4}$	$17_{\pm 6}$	$47_{\pm 7}$

In the course of the experiments no significant difference was detected between decontamination under liquid and supercritical conditions. Americium and plutonium were recovered by 70-80% with the use of both liquid and supercritical CO_2 containing D2EHPA or TFA (in the presence of pyridine). The conducted experiments show that the subcritical CO_2 can be applied to surface decontamination. Recovery of transuranium elements by 99% can be achieved in two-three successive treatment operations of stainless-steel surface by the subcritical CO_2 containing D2EHPA or TFA (in the presence of pyridine).

CONCLUSION

During the experiments on supercritical fluid decontamination of really contaminated materials it was revealed the following:

- double treatment of surfaces by supercritical carbon dioxide containing hexafluoroacetylacetone and modifier enables to remove 97-99% of α-emitting actinides;
- double treatment of surfaces by supercritical carbon dioxide containing di-2-ethylhexylphosphoric acid and dicyclohexyl-18-crown-6 enables to remove more than 99% of β+γ-emitters and more than 90% of α-emitters;
- triple treatment of soils by supercritical carbon dioxide containing hexafluoroacetylacetone enables to remove 55-75% of α-emitters;
- the decontamination efficiency with the use of complexone solutions in liquid and supercritical CO_2 differs only slightly (70-80% of TRU and more than 50% of Sr and Cs were removed from really contaminated stainless-steel surface in single

treatment operation with the use of D2EHPA and DCH18C6 solution in liquid CO_2).

So, the studies conducted at the Khlopin Radium Institute in the last five years have shown that the methods of supercritical fluid extraction and extraction by liquid CO_2 can be successfully used for decontamination of surfaces and porous materials.

The work was done under financial support of RF MinAtom, BNFL (UK) and ISTC (Project 1160).

REFERENCES

[1] J.L. Hedrick, L.J. Muicahey, L.T. Taylor, "Microchimica Acta", 1992, Vol. 108, p.115.
[2] N. Saito, Y. Ikushima, T. Goto Bull. "Chem. Soc. of Japan", 1990, Vol. 63, N 5, p. 1532.
[3] C.M. Wai, Anal. Sci., 1995, Vol. 11, p. 165.
[4] K.E. Laintz, C.M. Wai, C.R. Yonker, R.D. Smith, J. "Supercritical Fluids", 1991, Vol. 4, p. 194.
[5] K.E. Laintz, C.M. Wai, C.R. Yonker, R.D. Smith, "Anal. Chem", 1992, Vol. 64, p. 2875.
[6] Y. Lin, C.M. Wai, F.M. Jean, R.D. Brauer, "Environ. Sci. Technol. ", 1994, Vol. 28, N 6, p. 1190.
[7] K.E. Laintz, E. Tachikawa, Anal. Chem, 1994, Vol. 66, N 13, p. 2190.
[8] Y. Lin, R.D. Brauer, K.E. Laintz, C.M. Wai, "Anal. Chem. ", 1993, Vol. 65, p. 2549.
[9] A. Shadrin, A. Murzin, V. Starchenko, "Spectrum'98, Denver, Colorado, USA", September 13-18, 1998, "Proceedings, American Nuclear Society Inc, USA", 1998, p. 94.
[10] A. Shadrin, A. Murzin, N. Smart, "5th Meeting on Supercritical Fluids", 23-25 March 1998, "Nice, France, Proceedings", 1998, p.155.
[11] A. Shadrin, A. Murzin, V. Babain, "5th Meeting on Supercritical Fluids", 23-25 March 1998, Nice, France, Proceedings, 1998, p.791.
[12] A. Murzin, V. Babain, A. Shadrin, I. Smirnov et al. Paper for "Radiochemistry", in press.
[13] K.L. Toews, R.M. Shroll, C.M. Wai, N.G. Smart, "Anal. Chem. ", 1995, Vol. 67, p. 4040.
[14] J. Stary, "The solvent extraction of metal chelates", 1964, Pergamon Press.
[15] Patent PCT/GB99/01629/
[16] A.A. Clifford, N.G. Smart, A.Yu. Shadrin, "Analytica Chimica Acta", 1997, Vol. 356, p. 73.

JP0250352

JAERI-Conf 2002-004

THERMODYNAMIC STUDY OF AM(III) AND EU(III) EXTRACTION BY *ISO*-BUTYL-BIS-TRIAZINYL-PYRIDINE

CLÉMENT HILL AND CÉCILE ROUBE

Commissariat à l'Energie Atomique, DEN/DRCP/SCPS/LCSE - BP 17171 – 30207 Bagnols-sur-Cèze, France

Fax : 33 - 4.66.79.65.67, e-mail : clement.hill@cea.fr

In order to better understand the extraction mechanisms of An(III) and Ln(III) by bis-triazinyl-pyridines (Btp), as well as the affinity of the latter towards An(III), the extraction of ^{152}Eu and ^{241}Am by 2,6-bis(5,6-*iso*-butyl-1,2,4-triazin-3-yl)-pyridine (*i*Bu-Btp) was deeply studied. The distribution ratios (D_M) of both radiotracers were determined by γ spectrometry. The analyses of the slopes of "log-log" plots of experimental D_M values *vs* the concentration of *i*Bu-Btp or that of nitrate anions at equilibrium, allowed the stoichiometry of the extracted complexes to be estimated. The extraction constants of Eu(III) and Am(III) were thereafter calculated at different temperatures and thermodynamic data, such as ΔH_{ex} and ΔS_{ex}, were deduced from the Van't Hoff's law.

Key words: actinides(III), lanthanides(III), bis-triazinyl-pyridines, extraction, thermodynamics

1. INTRODUCTION

The separation of trivalent minor actinides (An(III) = Am(III) and Cm(III)) from trivalent lanthanides (Ln(III), accounting for about one third of the total amount of fission products), is a key step for the partitioning of long-lived radionuclides from the highly active effluents issuing the reprocessing of nuclear spent fuels. However, this separation is very difficult because An(III) and Ln(III) exhibit similar chemical properties.

Several studies in media of low acidity have shown already that nitrogen-containing polydendate ligands were able to separate An(III) from Ln(III) when mixed with lipophilic anions [1,2]. However, a new family of extractants, namely bis-triazinyl-pyridines (Btp*s*, Fig. 1), has been developed by Z. Kolarik *et al.* [3] in the framework of the European contract NEWPART (FI41-CT-96-0010 [4]). These molecules appeared to be very efficient extracting agents. As compared to former studied nitrogen-containing polydendate ligands, Btp*s* are still selective towards An(III) in very acidic conditions ($[HNO_3] \geq 2$ mol/L).

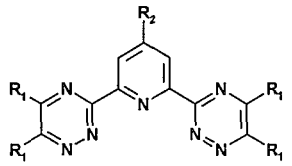

with R_1 = H, Methyl, *n*-Propyl, *i*-Propyl, *n*-Butyl, *i*-Butyl and R_2 = H, *i*-Nonyl

Fig. 1 General formula of Btp*s*

In order to better understand the extraction mechanisms of An(III) and Ln(III) by Btps, as well as the affinity of the latter towards An(III), the extraction of ^{152}Eu and ^{241}Am by 2,6-bis(5,6-*iso*-butyl-1,2,4-triazin-3-yl)-pyridine (*i*Bu-Btp) was investigated. *i*Bu-Btp was chosen for this thermodynamic study, because it was fairly stable against acidic hydrolysis and rather hydrophobic as compared to former studied Btp*s*.

Thanks to the systematic determination of the distribution ratios of ^{152}Eu and ^{241}Am, the stoichiometry of the extracted complexes was estimated through the analysis of the slopes of "log-log" plots of experimental isotherms. Moreover, thermodynamic data, such as ΔH_{ex} and ΔS_{ex}, were calculated thanks to the Van't Hoff's law.

2. EXPERIMENTAL

2,6-bis-(5,6-di-*iso*-butyl-1,2,4-triazin-3-yl)-pyridine was synthesized at CEA-Marcoule (initial purity 98.5%). Other reagents were commercially available and used as received. *i*Bu-Btp was dissolved in a mixture of hydrogenated tetrapropene (TPH) and *n*-octanol ($80/20\%_{vol}$).

Liquid-liquid experiments were performed in 2 mL Eppendorf microtubes, vigorously shaken for 90 minutes, the time required to reach the equilibrium state according to preliminary kinetic studies. Temperature, ranging from 10 to 50°C, was monitored with the help of a thermostated bath.

The experimental determination of distribution ratios (D_M) of Am(III) and Eu(III) was the following: 200 µL of organic phase were contacted with 200 µL of aqueous phase, spiked with tracer amounts of ^{241}Am and ^{152}Eu ($[\text{Activity}]_{aq,\ ini.}$ ~ 8000 kBq/L). After phase disengagement by natural gravity, temperature being kept constant, aliquots of each phase (40 µL diluted in 560 µL of original matrix: nitric acid for aqueous samples and TPH/*n*-octanol ($80/20\%_{vol}$) mixture for organic samples) were withdrawn for gamma radiometric measurement. The γ-activities at 59.54 keV and 121.78 keV, for ^{241}Am and ^{152}Eu respectively, were measured using a HPGe detector (Eurysis Mesures).

D_M values were calculated as follows: $D_M = [\text{Activity}]_{org,\ eq.}/[\text{Activity}]_{aq,\ eq.}$, where $[\text{Activity}]_{org,\ eq.}$ and $[\text{Activity}]_{aq,\ eq.}$ were the radioactivity concentrations of ^{241}Am and ^{152}Eu in the organic and aqueous phases at equilibrium, respectively. Separation factors $SF_{Am/Eu}$ were calculated from the ratio: D_{Am}/D_{Eu}.

3. LIQUID-LIQUID EXTRACTION STUDIES

3.1. Determination of the stoichiometry of the extracted complexes

The well-known "slope analysis method" was applied to the log-log plots of experimental isotherms, that is to say the variations of :

- D_M *vs* $[\overline{i\text{Bu-Btp}}]_{eq}$ (Fig. 1);
- D_M *vs* $[NO_3^-]_{eq}$ (Fig. 2);
- D_M *vs* $[HNO_3]_{eq}$ at constant or variable ionic strength.

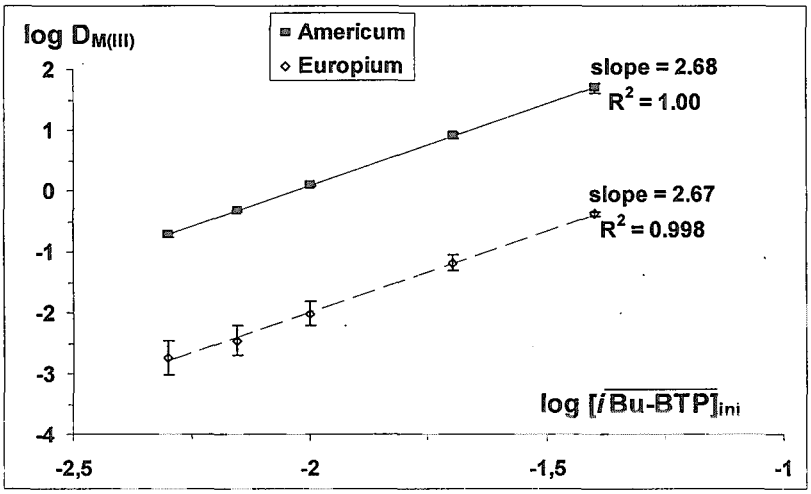

Aqueous solution: ^{241}Am & ^{152}Eu (tracers) in $[HNO_3]_{ini}$ = 1 mol/L.
Organic solutions: *i*Bu-BTP in a mixture of hydrogenated tetrapropene (TPH) and *n*-octanol (80%/20%vol).

Fig. 1 Log-log plots of the variations of D_M *vs* $[\overline{i\text{Bu-Btp}}]_{eq}$ at 30°C

In all these experiments, $[\overline{i\text{Bu-Btp}}]_{eq}$ was approximated by $[\overline{i\text{Bu-Btp}}]_{ini}$, since only tracer amounts of ^{241}Am and ^{152}Eu spiked the aqueous solutions. The possible dissolution of *i*Bu-Btp into the aqueous phases was neglected. Indeed, TOC measurements performed on acidic aqueous samples previously contacted with *i*Bu-Btp solutions did not reveal any presence of organic compounds when $[HNO_3]_{ini} < 2$ mol/L.
The possible extraction of nitrate salts, XNO_3 (with X = Li, Na or NH_4), used to set the ionic force up, was also neglected. Therefore, $[NO_3^-]_{tot,\ eq.}$ was assumed to equal $[XNO_3]_{ini}$ + $[HNO_3]_{eq}$. However, since non ideal conditions were involved when investigating the *salting-out* effect of XNO_3, experimental D_M values were corrected by stoichiometric activity coefficients, $\gamma^4(M^{3+})$, calculated by the Mikulin relation (same values of $\gamma^4(M^{3+})$ were used for ^{241}Am and ^{152}Eu). $[HNO_3]_{eq}$ was measured by titration.

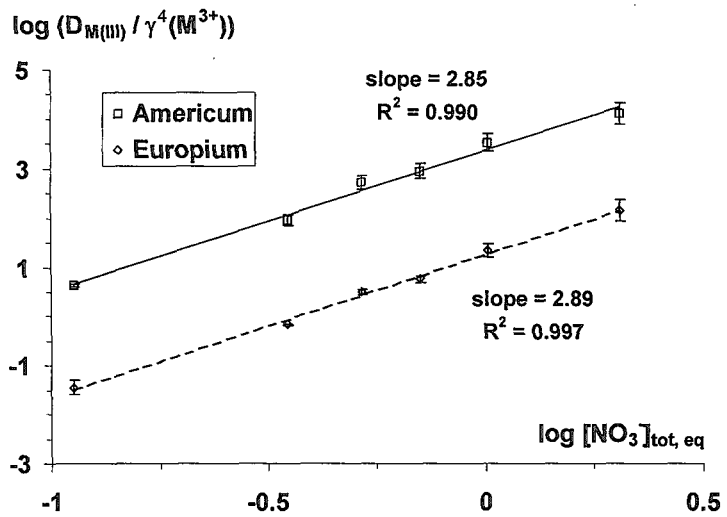

Aqueous solutions: ^{241}Am & ^{152}Eu (tracers) in mixtures of $[HNO_3]_{ini}$ = 0.1 mol/L and $0 \leq [LiNO_3]_{ini} \leq 2$ mol/L.
Organic solutions: $[i\text{Bu-BTP}]_{ini}$ = 0.01 mol/L in a mixture of TPH and *n*-octanol (80%/20%vol).

Fig. 2 Log-log plots of the variations of D_M *vs* $[NO_3^-]_{eq}$ at 10°C

These systematic studies allowed the stoichiometry of the extracted complexes to be determined:

Eq. 1 $$M^{3+} + 3\,\overline{BTP} + 3\,NO_3^- \xrightleftharpoons{K_{ex}} \overline{M(NO_3)_3(BTP)_3}$$

This result was in good agreement with the X-ray crystallographic pattern previously obtained for the Gd(III) complexes of 2,6-bis-(5,6-diethyl-1,2,4-triazin-3-yl)-pyridine [4].
Obviously, HNO_3 did not take part to the formation of the metallic complexes, since no increase of D_M *vs* $[HNO_3]_{eq}$ was observed at constant ionic strength (I = 2 mol/L for $LiNO_3$, $NaNO_3$ and NH_4NO_3, Fig. 3).
However, HNO_3 might be directly extracted by *i*Bu-Btp, since a bell shape curve was observed for D_M *vs* $[HNO_3]_{eq}$, when $[HNO_3]_{eq}$ exceeded 2 mol/L (Fig. 4). Besides, partial dissolution of *i*Bu-Btp into acidic aqueous phases was pointed out by TOC measurements, when $[HNO_3]_{eq}$ exceeded 2 mol/L.

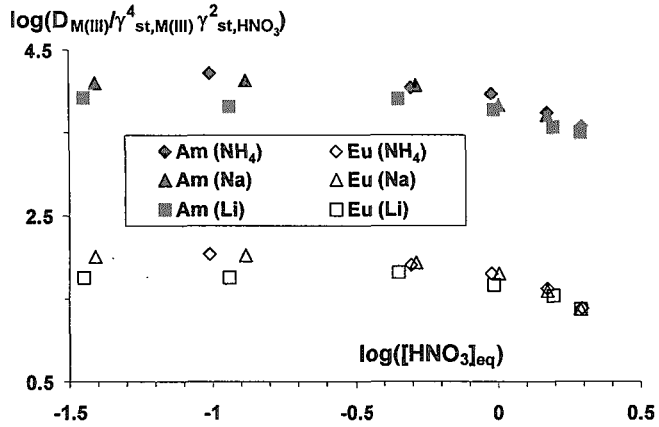

Aqueous solutions: ^{241}Am & ^{152}Eu (tracers) in mixtures of $[HNO_3]_{ini}$ + $[XNO_3]_{ini}$ = 2 mol/L. Temp. = 20°C.
Organic solutions: $[\overline{i\text{Bu-BTP}}]_{ini}$ = 0.01 mol/L in a mixture of TPH and *n*-octanol (80%/20%vol).

Fig. 3 Log-log plot of the variation of D_M *vs* $[HNO_3]_{eq}$ at constant ionic strength (I = 2)

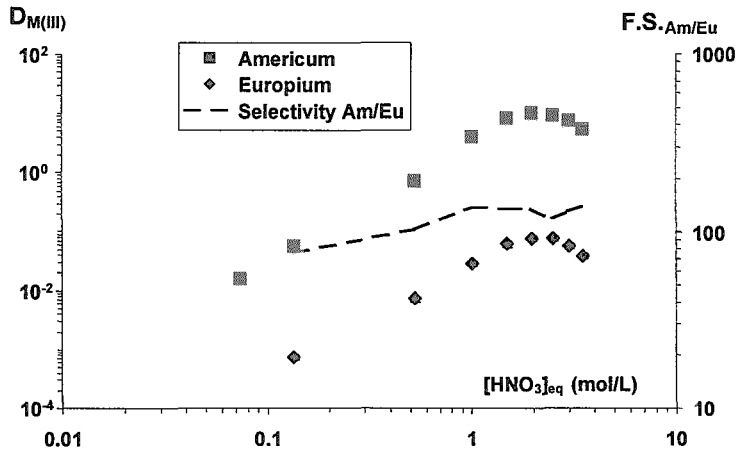

Aqueous solutions: ^{241}Am & ^{152}Eu (tracers) in $0.07 \leq [HNO_3]_{ini} \leq 3.5$ mol/L. Temp. = 20°C.
Organic solutions: $[\overline{i\text{Bu-BTP}}]_{ini}$ = 0.01 mol/L in a mixture of TPH and *n*-octanol (80%/20%vol).

Fig. 4 Log-log plots of the variations of D_M *vs* $[HNO_3]_{eq}$ at variable ionic strength

3.2. Determination of the extraction constants K_{ex}

Assuming Eq.1, apparent extraction constants of Am(III) and Eu(III) were calculated for each point of experimental isotherms. Table I gathers the average data obtained for each variation of D_M *vs* $[\overline{i\text{Bu-Btp}}]_{eq}$, for a given temperature ranging from 10 to 50 °C.

Table I Extraction constants of Am(III) and Eu(III) at different temperatures

Aqueous solutions: ^{241}Am & ^{152}Eu (tracers) in $[HNO_3]_{ini}$ = 1 mol/L.
Organic solutions: $0.003 \leq [\overline{i\text{Bu-BTP}}] \leq 0.04$ mol/L in a mixture of TPH and *n*-octanol (80%/20%vol).

t (°C)	10	20	30	40	50
log(K_{ex} Am)	9.25	8.92	8.42	8.07	7.80
log(K_{ex} Eu)	7.09	6.80	6.34	6.08	5.90

3.2. Thermodynamic data

Thermodynamic data, such as ΔH_{ex} and ΔS_{ex}, were deduced from the application of the Van't Hoff's law (Fig. 5):

$\Delta H_{ex}(Am) = -66 \pm 10$ kJ/mol $\Delta S_{ex}(Am) = -55 \pm 30$ J/mol.K

$\Delta H_{ex}(Eu) = -54 \pm 15$ kJ/mol $\Delta S_{ex}(Eu) = -56 \pm 30$ J/mol.K

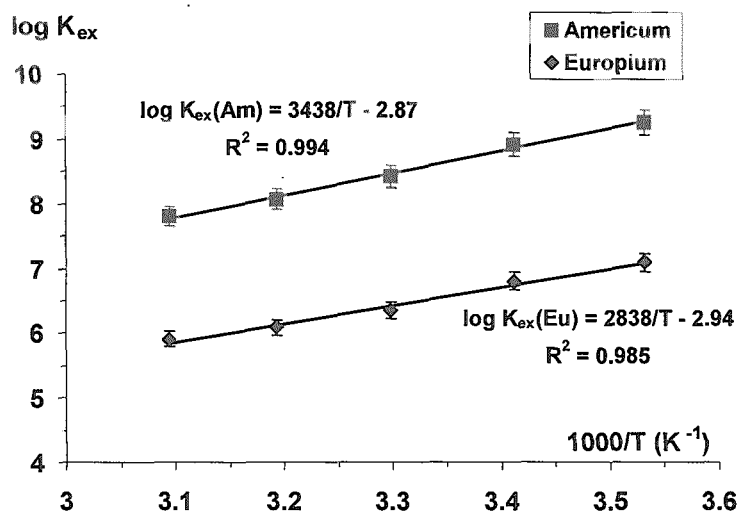

Aqueous solutions: ^{241}Am & ^{152}Eu (tracers) in $[HNO_3]_{ini}$ = 1 mol/L (10°C ≤ temperature ≤ 50°C).
Organic solutions: 0.003 ≤ [*i*Bu-BTP] ≤ 0.04 mol/L in a mixture of TPH and *n*-octanol (80%/20%vol).

Fig. 5 Van't Hoff's law: $\log K_{ex}$ *vs* 1/T

4. CONCLUSION

The extraction of trivalent americium and europium by *i*Bu-Btp was deeply investigated in the "TPH/*n*-octanol (80/20%$_{vol}$)" mixture. The stoichiometry of the extracted complexes was estimated thanks to the "slope analysis" method, by varying different parameters, such as the initial concentration of *i*Bu-Btp in the organic phase or that of nitrate anions in the aqueous phase. Thermodynamic data were calculated, based on the presumed extraction equilibrium. The extraction appeared more exothermic for Am(III) than for Eu(III). Considering the complexation of trivalent metallic cations by *i*Bu-Btp as the driving force of the free enthalpy of extraction, the fact that "$\Delta H_{ex}(Am) < \Delta H_{ex}(Eu)$" could reflect a more covalent character of the "N...Am(III)" bonds as compared to the "N...Eu(III)" bonds in the extracted complexes.

REFERENCES

[1] P.Y. Cordier, C. Hill, P. Baron, C. Madic, M.J. Hudson and J.O. Liljenzin, J. All. Comp., 271-273, 738-741 (1998).
[2] I. Hägström, L. Spjuth, A. Enarsson, J.O. Liljenzin, M. Skälberg, M.J. Hudson, P.B. Iveson, C. Madic, P.Y. Cordier, C. Hill, and N. François, Solv. Extr. Ion Exch., 17(2), 221-242 (1999).
[3] Z. Kolarik, U. Müllich and F. Gassner, Solv. Extr. Ion Exch., 17(1), 23-32 (1999).
[4] C. Madic, M.J. Hudson, J.O. Liljenzin, J.P. Glatz, R. Nannicini, A. Facchini, Z. Kolarik and R. Odoj, "New partitioning techniques for minor actinides", Project report EUR 19149 EN, Ed. by the European Commission, Luxembourg (2000).

This is a blank page.

JP0250353

JAERI-Conf 2002-004

SANEX-BTP PROCESS DEVELOPMENT STUDIES

C. HILL D. GUILLANEUX, L. BERTHON and C. MADIC

Commissariat à l'Energie Atomique, DEN/DRCP/SCPS/LCSE - BP 17171 – 30207 Bagnols-sur-Cèze, France

Fax : 33 - 4.66.79.65.67, e-mail : clement.hill@cea.fr

Bis-triazinyl-pyridines (Btp*s*) have been developed at CEA-Marcoule to separate actinides(III) from lanthanides(III). Although high separation performances were observed in the counter-current hot test carried out in 1999 on a highly active effluent, the extraction and back-extraction yields of actinides(III) were lower than expected from calculation. A strong sensitivity of the extractant towards air oxidation and acidic hydrolysis was actually pointed out. Therefore, the hydrolysis of *bis*-triazinyl-pyridines was deeply investigated (qualitative determination of the degradation products) in different experimental conditions. It appeared that the branching of the alkyl groups on the α position of the triazine rings hindered the hydrolysis of the extractant. The formulation of the solvent was thus optimized and tested again in 2001 on a genuine DIAMEX back-extraction solution in the ATALANTE facility.

Key words: actinides(III), lanthanides(III), bis-triazinyl-pyridines, separation

1. INTRODUCTION

The separation of trivalent minor actinides (An(III) = Am(III) and Cm(III)) from trivalent lanthanides (Ln(III), accounting for about one third of the total amount of fission products), is a key step for the partitioning of long-lived radionuclides from the highly active effluents issuing the reprocessing of nuclear spent fuels. However, this separation is very difficult because An(III) and Ln(III) exhibit similar chemical properties.

Several studies in media of low acidity have shown already that nitrogen-containing polydendate ligands were able to separate An(III) from Ln(III) when mixed with lipophilic anions [1,2]. However, a new family of extractants, namely bis-triazinyl-pyridines (Btp*s*, Fig. 1), has been developed by Z. Kolarik *et al.* [3] in the framework of the European contract NEWPART (FI41-CT-96-0010 [4]). These molecules appeared to be very efficient extracting agents. As compared to former studied nitrogen-containing polydendate ligands, Btp*s* are still selective towards An(III) in very acidic conditions ($[HNO_3] \geq 2$ mol/L).

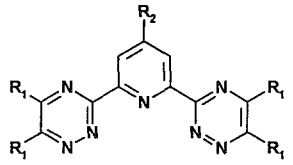

with R_1 = H, Methyl, *n*-Propyl, *i*-Propyl, *n*-Butyl, *i*-Butyl and R_2 = H, *i*-Nonyl

Fig. 1 General formula of Btp*s*

Various Btp molecules were synthesized and studied at CEA-Marcoule for "An(III)/Ln(III)" groups separation. Among them, 2,6-bis(5,6-*n*-propyl-1,2,4-triazin-3-yl)-pyridine (*n*Pr-Btp) was chosen to perform a counter-current hot test in December 1999 on a genuine radioactive effluent in ATALANTE facility. The observed decontamination performances were very satisfactory ($1{,}400 < DF_{Ln(III)} < 450{,}000$), although extraction and back-extraction yields of Am(III) and Cm(III) were lower than predicted by flowsheet modeling. Since experimental concentration profiles of An(III) and Ln(III) in organic and aqueous solutions were better modeled when the actual concentration of *n*Pr-Btp was lowered by 20%, partial degradation

of *n*Pr-Btp during the hot test was assumed to explain the unexpectedly bad results obtained. Therefore, hydrolytic degradation of *n*Pr-Btp under acidic and oxidative conditions was investigated.

2. DEGRADATION STUDIES ON *n*Pr-BTP

Two different methods were used to investigate the stability of *n*Pr-Btp under various acidic and oxidative conditions:

1. a qualitative one, consisting in the systematic evaluation of the extracting properties of the solvent after hydrolysis,
2. a more quantitative one, involving the determination of the degradation products of *n*Pr-Btp by Gas Phase Chromatography and Electro-spray Ionization Mass Spectrometry.

2.1. Evolution of the extracting properties of *n*-Pr-Btp

*n*Pr-Btp was diluted in a mixture of hydrogenated tetrapropene (TPH) and *n*-octanol (70/30%$_{vol}$) as for the 1999 hot test. The solvent was contacted with different nitric acid solutions (with or without nitrous acid) for hydrolysis. Organic samples were withdrawn from time to time to evaluate the extracting properties of the hydrolyzed solvent by measuring the distribution ratios of ^{241}Am and ^{152}Eu (used to mimic "An(III)/Ln(III)" groups separation). These studies revealed a steady decrease of the extraction properties of the solvent when the atmosphere was rich in oxygen or when $[HNO_3]$ exceeded 0.5 mol/L.

For example: D_{Am} decreased of 80% after 2 days of hydrolysis, when $[HNO_3]_{ini}$= 1 mol/L. Furthermore, the extracting properties of *n*Pr-Btp quickly decreased when $[HNO_2]_{ini}$ exceeded 0.005 mol/L.

For example: D_{Am} decreased of 50% after 2 hours, when $[HNO_3]_{ini}$ = 1 mol/L + $[HNO_2]_{ini}$ = 0.01 mol/L.

The nature of the organic diluent turned up to influence the stability of *n*Pr-Btp. On the contrary to aliphatic, alcoholic or aromatic diluents, nitrobenzene and chlorinated diluents seemed to prevent *n*Pr-Btp from degrading (Fig. 2). However, these organic diluents would not be acceptable for the further development of industrial separation processes.

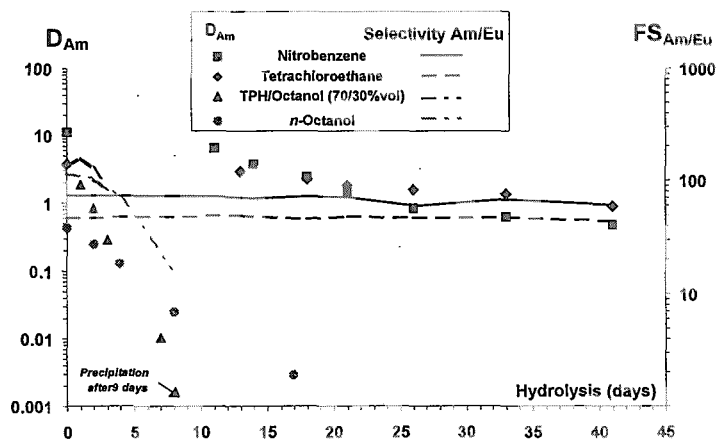

Hydrolysis cycles at 25°C: 1 hour mixing followed by 2 hours settling (24 hours/day).
Hydrolyzing aqueous solution: $[HNO_3]$ = 1 mol/L.
Hydrolyzed organic solutions: [*n*Pr-Btp] = 0.02 mol/L in various organic diluents.
Extraction tests at 25°C: $[HNO_3]$ = 1 mol/L, spiked with ^{152}Eu and ^{241}Am.

Fig. 2 Influence of the nature of the organic diluent on the stability of *n*Pr-Btp under acidic hydrolysis/oxidation.

2.2. Determination of *n*Pr-Btp degradation products

The main degradation products of *n*Pr-Btp were qualified by Gas Phase Chromatography and Electro-spray Ionization Mass Spectrometry. They appeared to be almost the same whatever the initial experimental conditions (presence or absence of an acidic aqueous phase in contact with the *n*Pr-Btp solvent), only their quantities and rates of occurrence varied.
A degradation pathway was proposed for *n*Pr-Btp, the first step of which being the attack of one $-CH_2$ group on the α position of the triazinyl rings, resulting in the formation of a nitro compound (observed by ^{15}N NMR). Thereafter, the compound would degrade into an alcohol (which was the main degradation product observed in the absence of hydrolyzing aqueous phase) or into a ketone (which was the main degradation product after the hydrolysis of *n*Pr-Btp by nitric acid). In the same way, the attack of a second CH_2 group would result in the formation of difunctional compounds (dialcohols and diketones). The alcohol compounds could also loose one propyl chain. Side and minor reactions could consist in the breaking of triazinyl rings leading to cyano compounds.

3. OPTIMIZATION OF THE BTP SOLVENT FORMULATION

Since *n*Pr-Btp proved to be unstable, other substituted Btp molecules were investigated to develop a new Btp solvent. Acidic hydrolysis being the most relevant criterion for the selection of the new candidate, the stability of several Btp*s* was compared.

3.1. Hydrolysis of substituted Btp molecules

Molecules bearing branched alkyl groups on the α position of the triazinyl rings, such as Cy-Btp-Me and *i*Pr-Btp, appeared to be much more stable than *n*Pr-Btp or *n*Bu-Btp, bearing linear alkyl groups. Cy-Btp-Me and *i*Pr-Btp had not been chosen when preparing the hot test of 1999 because of several practical reasons: tedious synthesis, low solubility in organic diluents, slow kinetics of extraction. However, they showed good stability over 30 days of hydrolysis (Fig. 3).

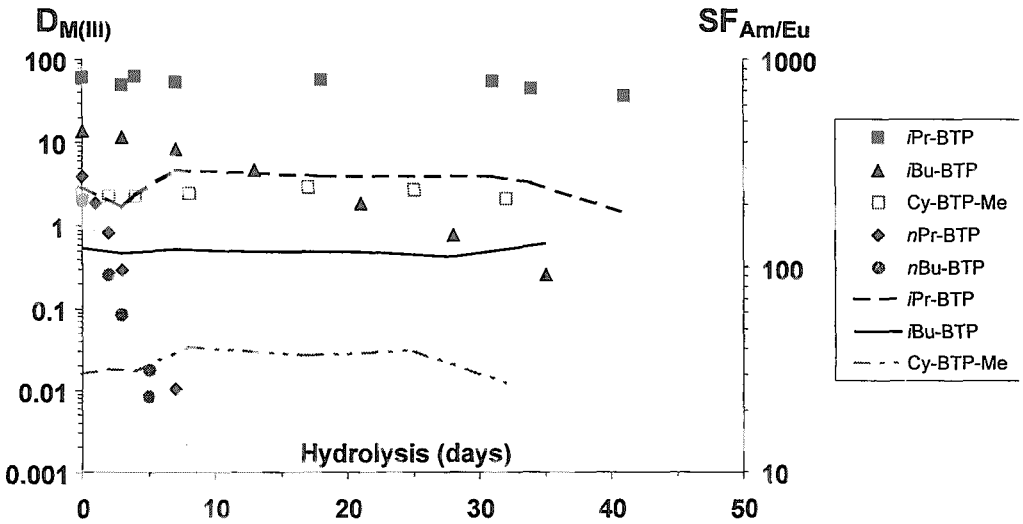

Hydrolysis cycles at 25°C: 1 hour mixing followed by 2 hours settling (24 hours/day).
Hydrolyzing aqueous solution: $[HNO_3]$ = 1 mol/L.
Hydrolyzed organic solutions: [Btp] = 0.005 or 0.01 mol/L in *n*-octanol or "n-octanol /TPH".
Extraction tests at 25°C: $[HNO_3]$ = 1 mol/L, spiked with ^{152}Eu and ^{241}Am.

Fig. 3 Comparison of the stability of different Btp*s* under acidic hydrolysis.

3.2. Kinetics of extraction of substituted Btp molecules

The major common drawback of Cy-Btp-Me and *i*Pr-Btp was their too slow kinetics of extraction for the implementation of counter current hot tests in mixer-settlers or centrifugal contactors. Several attempts were made to accelerate their kinetics by using other co-extractants, such as: TBP or diamides. In some cases, the latter modifiers fastened the kinetics of extraction of the Btp*s* and in other cases, they enhanced their extraction performances or their stability under acidic hydrolysis, but lowered their selectivity.
The case of *i*Pr-Btp was rather peculiar. When aqueous solutions were spiked with ^{241}Am and ^{152}Eu at tracers level and *i*Pr-Btp diluted in mixtures of TPH and *n*-octanol (as for *n*Pr-Btp), the observed kinetics of extraction was fast for Am(III) and very slow for Eu(III) (Fig. 4). Moreover, a precipitate occurred when aqueous solutions simulating genuine DIAMEX back-extraction effluents were used ($[Ln(III)]_{tot, ini.} \sim 18\ 10^{-3}$ mol/L).

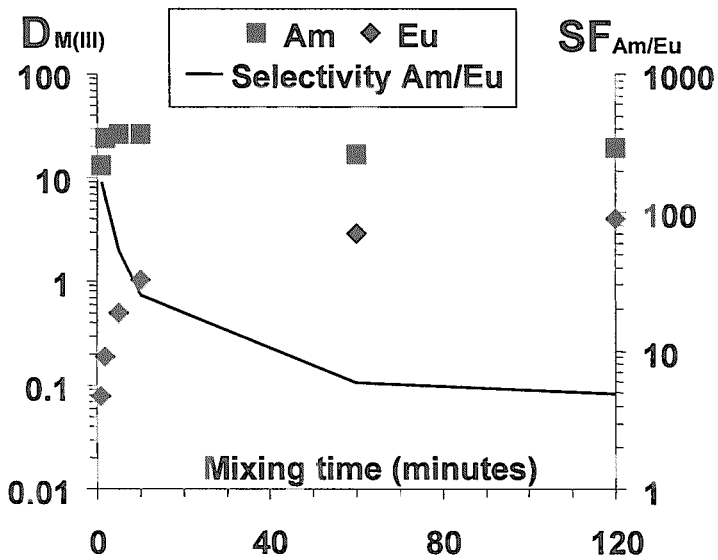

Aqueous solution: $[HNO_3]$ = 1 mol/L, spiked with ^{152}Eu and ^{241}Am.
Organic solution: [*i*Pr-Btp] = 0.01 mol/L in "TPH/*n*-octanol" mixture; θ = 25°C.

Fig. 4 Kinetics of extraction of *i*Pr-Btp in "TPH/*n*-octanol"

No precipitation occurred with these feed solutions when *i*Pr-Btp was dissolved either in pure *n*-octanol, tetrachloroethane or nitrobenzene, but the kinetics of extraction became very slow both for Am(III) and Eu(III): more than an hour required to reach the equilibrium state in micro-tubes (Fig. 5: case of *n*-octanol). Tetrachloroethane and nitrobenzene being unacceptable for further industrial process development, *n*-octanol was finally chosen.
Phase transfer catalysts, such as diamides were mixed with *i*Pr-Btp to fasten its kinetics. Figure 5 also shows the case of dimethyl-dibutyl-tetradecyl-malonamide (C_{14}) in *n*-octanol: equilibrium was reached within 15 minutes, but selectivity decreased a little bit as compared to pure *n*-octanol. Other diamides have been tested as co-extractants of *i*Pr-Btp in *n*-octanol. Good results were observed with dimethyl-dioctyl-hexylethoxy-malonamide (C_2OC_6), but their back-extraction appeared to be too slow in diluted nitric acid to develop a process flowsheet (the equilibrium was reached only after 2 hours of mixing). That is why, hydrophilic complexing agents, such as citric acid or glycolic acid, were required to favor and fasten the back-extraction of An(III) and Ln(III).

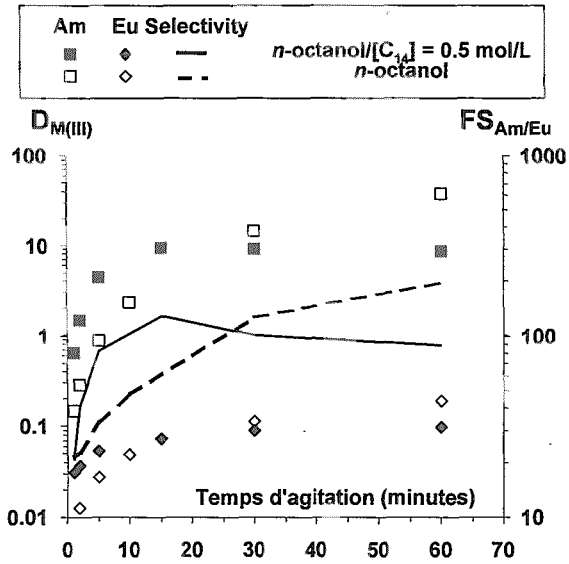

Aqueous solution: synthetic solution simulating a DIAMEX back-extraction effluent, spiked with ^{152}Eu and ^{241}Am

Organic solution: $[\overline{i\text{Pr-Btp}}]$ = 0.01 mol/L in various diluents; θ = 25°C.

Fig. 5 Kinetics of extraction of *i*Pr-Btp in *n*-octanol and "*n*-octanol/diamide" mixtures

3.3. Optimization of the formulation of SANEX-*i*Pr-Btp solvent

Preliminary to the hot test of June 2001, numerous series of experiments have been carried out in micro-tubes on synthetic aqueous solutions simulating DIAMEX back-extraction effluents. The influence of different parameters, such as the concentration of *i*Pr-Btp or C_2OC_6 in *n*-octanol and that of Ln(III), An(III) and Pd(II) in the aqueous feed to be treated, was evaluated on the extraction yields and extraction kinetics of Ln(III) and An(III). A process flowsheet was designed on the basis of the following solvent formulation:

$$[\overline{i\text{Pr-BTP}}]_{ini} = 0.01 \text{ mol/L} + [\overline{C_2OC_6}]_{ini} = 0.5 \text{ mol/L in } n\text{-octanol.}$$

The flowsheet was first tested on a battery of eight centrifugal-contactors, using a synthetic nitric acid solution containing Nd(III) and Eu(III) at 2000 and 100 mg/L, respectively. The hydrodynamic behavior of the solvent was very satisfactory and the concentration profiles of Nd(III) and Eu(III) in aqueous and organic phase appeared in good agreement with the models.

The flowsheet was then tested on genuine highly active effluents in June 2001 (no palladium in the feed), using two batteries of 16 stages (Fig. 6) in the CEA-Marcoule ATALANTE facility.

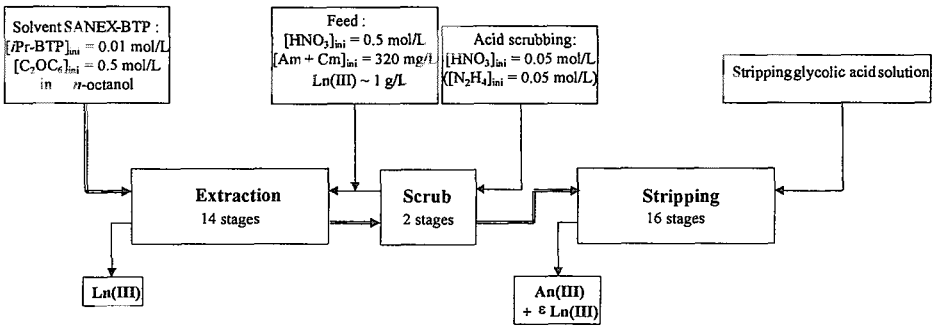

Fig. 6 Process flowsheet of the SANEX-Btp hot test of June 2001

A one through process flowsheet was firstly run and gave far better recovery yields for An(III) than the solvent based on *n*Pr-Btp tested in 1999. Analyses of aqueous and organic samples are still under progress, but online analytical measurements of Am(III) and Eu^{154} allowed satisfactory decontamination factors to be foreseen.
After this opened-cycle process flowsheet, a solvent recycling process flowsheet was run to treat 3.85L of DIAMEX back-extraction effluent and produce 6.5L of "Am(III) + Cm(III)" raffinate. This hot test pointed out partial degradation of *i*Pr-Btp, probably because of alpha-radiolysis. For instance, the extraction performances of the solvent decreased by 40% after two cycles (much less indeed than previous *n*Pr-Btp solvent, the extraction performances of which had decreased by more than 50% after just one cycle). Analyses of aqueous and organic samples are also still under progress.

4. CONCLUSION

The SANEX hot test carried out at CEA-Marcoule in 1999 with 2,6-bis(5,6-*n*-propyl-1,2,4-triazin-3-yl)-pyridine pointed out the strong sensitivity of this extractant towards air oxidation and acidic hydrolysis. Qualitative determination of the degradation compounds of *n*Pr-Btp allowed a better understanding of its degradation mechanism: *n*Pr-Btp mainly degraded into alcoholic derivatives through the oxidation of its propyl substituents. Therefore, many efforts were put forward to strengthen the stability of Btp*s* under hydrolysis and to optimize the formulation of the new Btp solvent. 2,6-bis(5,6-*iso*-propyl-1,2,4-triazin-3-yl)-pyridine (*i*Pr-Btp) mixed with dimethyl-dioctyl-hexylethoxy-malonamide (C_2OC_6) in *n*-octanol was chosen to carry out two hot tests on genuine DIAMEX back-extraction solutions in June 2001 (no palladium in the feed). During these hot tests, *i*Pr-Btp turned out to be sensitive to alpha-radiolysis and became unusable in multi cycles process flowsheets. Further researches will be devoted to the strengthening of *i*Pr-Btp towards alpha-radiolysis.

ACKNOWLEDGEMENTS

This work has been partially financially supported by the European Union Nuclear Fission Safety Program.

REFERENCES

[1] P.Y. Cordier, C. Hill, P. Baron, C. Madic, M.J. Hudson and J.O. Liljenzin, J. All. Comp., 271-273, 738-741 (1998).
[2] I. Hägström, L. Spjuth, A. Enarsson, J.O. Liljenzin, M. Skälberg, M.J. Hudson, P.B. Iveson, C. Madic, P.Y. Cordier, C. Hill, and N. François, Solv. Extr. Ion Exch., 17(2), 221-242 (1999).
[3] Z. Kolarik, U. Müllich and F. Gassner, Solv. Extr. Ion Exch., 17(1), 23-32 (1999).
[4] C. Madic, M.J. Hudson, J.O. Liljenzin, J.P. Glatz, R. Nannicini, A. Facchini, Z. Kolarik and R. Odoj, "New partitioning techniques for minor actinides", Project report EUR 19149 EN, Ed. by the European Commission, Luxembourg (2000).

JP0250354

JAERI-Conf 2002-004

DEVELOPMENT OF FRACTIONATION PROCESS OF ^{129}I IN PREPARATION FOR TRANSMUTATION OF LLFP

Kenji TAKESHITA and Yoshio NAKANO

Department of Environmental Chemistry and Engineering,
Tokyo Institute of Technology,
4259 Nagatsuta, Midori-ku, Yokohama, 226-8502, Japan

ABSTRACT

A new off-gas treatment system with a Ag^0-impregnated adsorbent process and a thermal swing adsorption (TSA) process using H^+-exchanged mordenite was proposed for the fractionation and recovery of a long-lived fission product (LLFP), ^{129}I, in dissolver off-gas (DOG). The adsorption and desorption tests of simulated off-gas on H^+-exchanged zeolite were carried out. From the experimental results, the features of the proposed system and the operating conditions required for the recovery of iodine were discussed. The conclusions obtained are summarized as follows,

(1) In the TSA process, alkyl iodide in DOG can be recovered completely as molecular iodine (I_2), when the adsorption operation is switched to the desorption one at the beginning of the breakthrough of NOx. All of iodine and alkyl iodide in DOG is immobilized as AgI on the Ag^0-impregnated adsorbents by recycling the recovered I_2 from the TSA process to the Ag^0-impregnated adsorbent process.

(2) In the TSA process, CO_2 and noble gas are partitioned from NOx, H_2O and iodine under the condition that the concentration of oxygen in DOG is maintained to more than 10vol%. ^{14}C as well as ^{129}I can be fractionated in the TSA process.

(3) The TSA process plays an important role for the fractionation and recovery of long-lived radioactive nuclides in DOG, ^{129}I and ^{14}C. The volume of zeolite required for the TSA process is evaluated as $0.38m^3$ (=0.19 m^3/column x 2 column) for an 800 ton/y reprocessing plant. The TSA process can be designed compactly.

I. INTRODUCTION

In the dissolution process of reprocessing plant, most of volatile radioactive elements contained in the spent nuclear fuel, ^{14}C ($t_{1/2}$=5370y, chemical form: CO_2), ^3H ($t_{1/2}$=10y, H_2O), ^{129}I ($t_{1/2}=1.6x10^7$y, I_2 or alkyl iodide) and ^{85}Kr ($t_{1/2}$=30y, Kr), are transferred to the DOG (dissolver off-gas) treatment system. If the long-lived nuclides such as ^{129}I and ^{14}C are released to the atmosphere, they remain in the biosphere for a long time and may be accumulated finally in human beings and animals according to the food chains. The transmutation of a long-lived fission product (LLFP), ^{129}I, which is fissioned to other short-lived nuclides in a nuclear reactor, is attractive from the viewpoint of environmental protection[(2)]. Therefore, off-gas treatment technology to fractionate and recover iodine effectively from DOG should be applied to the transmutation system of ^{129}I.

Both alkaline scrubbing process using NaOH solution and solid adsorbent process using $AgNO_3$-impregnated adsorbents were investigated previously for the recovery of iodine from reprocessing off-gas. In the commercial reprocessing plants, which are operating now in France and U.K., the alkaline scrubbing process was applied to the recovery of iodine from DOG [(1),(3)]. NOx and CO_2 are co-absorbed simultaneously with iodine and $NaNO_3$, Na_2CO_3, $NaHCO_3$, NaI and $NaIO_3$ are formed in the NaOH solution. The decontamination factor of 100 is obtained for the iodine, however, the alkaline scrubbing process has some disadvantages that a large amount of alkaline sludge containing both ^{14}C and ^{129}I is generated and alkyl iodide can not be recovered [(3)]. On the other hand, the solid adsorbent process shows the decontamination factor higher than 1000 and can fractionate iodine from other radioactive nuclides [(1), (3)]. From these futures, the solid adsorbent process was adopted in the commercial reprocessing plant constructing at Aomori Prefecture, Japan. When these conventional iodine recovery processes are applied to commercial reprocessing plants, the individual irradiated dose by the release of off-gas to the atmosphere does not exceed that recommended by ICRP[(4)]. However, the accumulation of iodine to the environment should be considered for a long-term operation of reprocessing plant. A new off-gas treatment system with high recovery efficiency of iodine is worthy to be developed. In this study, a new system with an Ag^0-impregnated adsorbent process and a thermal swing adsorption (TSA) process was proposed.

Figure 1 shows the flow sheet of proposed system. Molecular iodine (I_2) is immobilized as AgI on the Ag^0-impregnated adsorbents. Alkyl iodide is trapped as I_2 in the TSA process, as shown in the later section, "III. Results and discussion", and the recovered I_2 is recycled to the

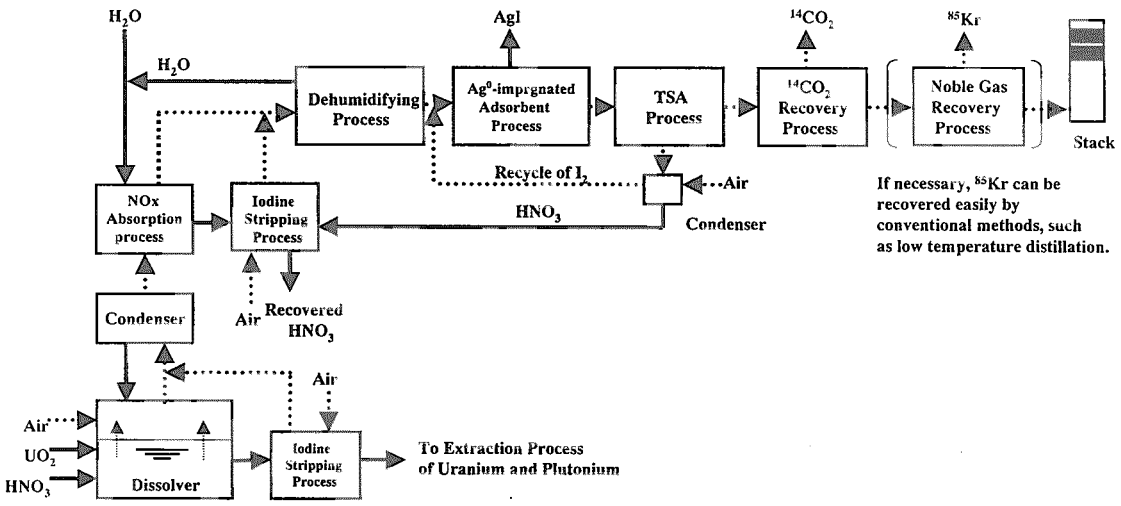

Fig.1 DOG treatment system with Ag^0-impregnated adsorbent process and thermal swing adsorption (TSA) process.

solid adsorbent process. Then, both NOx and H_2O are also co-adsorbed with iodine in the TSA process and recovered as HNO_3. The recovered HNO_3 is transferred to the iodine stripping process and is reused. AgI on the spent adsorbents is reduced by hydrogen gas and converted to NaI by reacting with NaOH[5]. NaI is used as a fuel in the transmutation system. Then, the regenerated Ag^0-impregnated adsorbents are reused for the adsorption of iodine [5]. If NOx, H_2O and iodine are partitioned from CO_2 and noble gas in the TSA process, ^{14}C and ^{85}Kr can be fractionated and recovered by the conventional separation techniques without pretreatment[9]. The secondary wastes may be depressed by introducing the proposed system based on the concept of material recycle and reuse. **Figure 2** shows the schematic diagrams of TSA process, in which polar gases, such as NOx, H_2O, I_2 and alkyl iodide, is recovered continuously by repeating thermal swing operation between two zeolite columns.

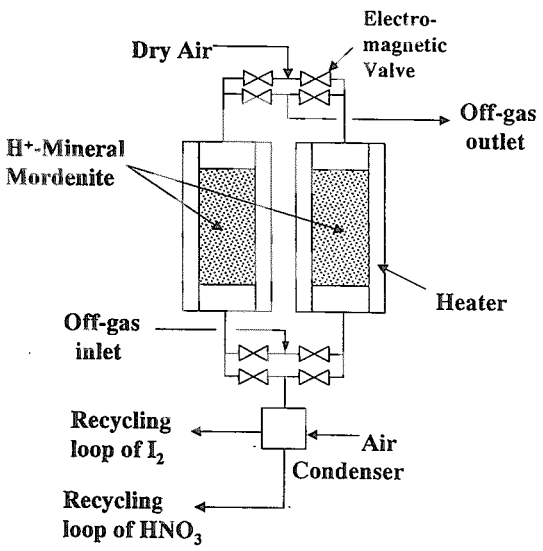

Fig.2 Thermal swing adsorption (TSA) process.

The main object of this study is to evaluate the applicability of proposed system to the fractionation and recovery of ^{129}I from DOG. The adsorption and desorption of simulated off-gas on H^+-exchanged zeolite were tested by a temperature-programmed desorption (TPD) equipment. From the experimental results, the features of proposed system and the operating conditions required for the improvement of iodine recovery were discussed. In the present stage, the adsorption of iodine on the Ag^0-impregnated adsorbents can be estimated easily by the mathematical model shown in the previous paper [6]. Thus, the mass balance of proposed system was calculated by use of both the extended ABNOX code [8] and the mathematical model [6],[7]. From these calculation results, the dimensions of TSA process were evaluated for an 800 ton/y reprocessing plant.

II. EXPERIMENTAL

2.1 Preparation of zeolite

Mineral zeolite mined in Akita Prefecture, Japan, was used as an adsorbent, which has mordenite structure and a trace amount of quartz. The zeolite was crushed and sieved in the

range of 100 to 200 μm in diameter. The exchangeable cations in the zeolite, such as Na^+, K^+, Ca^{2+} and Mg^{2+}, were ion-exchanged to H^+ in 1M HNO_3 solution at 80℃ for 24 h. **Table 1** shows the components of zeolite before and after the ion exchange. These results suggest that about 60% of exchangeable cations are exchanged to H^+.

Table 1 Chemical composition of used zeolite

	Mineral mordenite	H+-exchanged mineral mordenite
Na	0.986	0.458
Ca	0.381	0.053
Mg	0.108	0.054
K	0.322	0.05
Fe	0.285	0.289
Ti	0.025	0.023
Al	1.29	1.34
Si	7.89	8.52
Si/Al ratio	6.17	6.34

[mmol/g-zeolite]

2.2 Adsorption and desorption tests of simulated off-gas

The adsorption and desorption of simulated DOG were measured by using a temperature-programmed desorption (TPD) equipment, which consists of a generator of test gas, an adsorption column and a mass spectrometer, as shown in **Figure 3**. The simulated off-gas was the mixture of NO (0.34 vol%), CO_2 (0.05vol%), H_2O (0.23 vol%), CH_3I and O_2 balanced with He. The concentrations of CH_3I and O_2 were adjusted in the range of 0 to 0.01 vol% and 2.9 to 10 vol%, respectively. 0.5g of H^+-exchanged zeolite was packed in a quartz column (6mm in diameter) and degassed by the gas stream of He at 500°C. After that, the

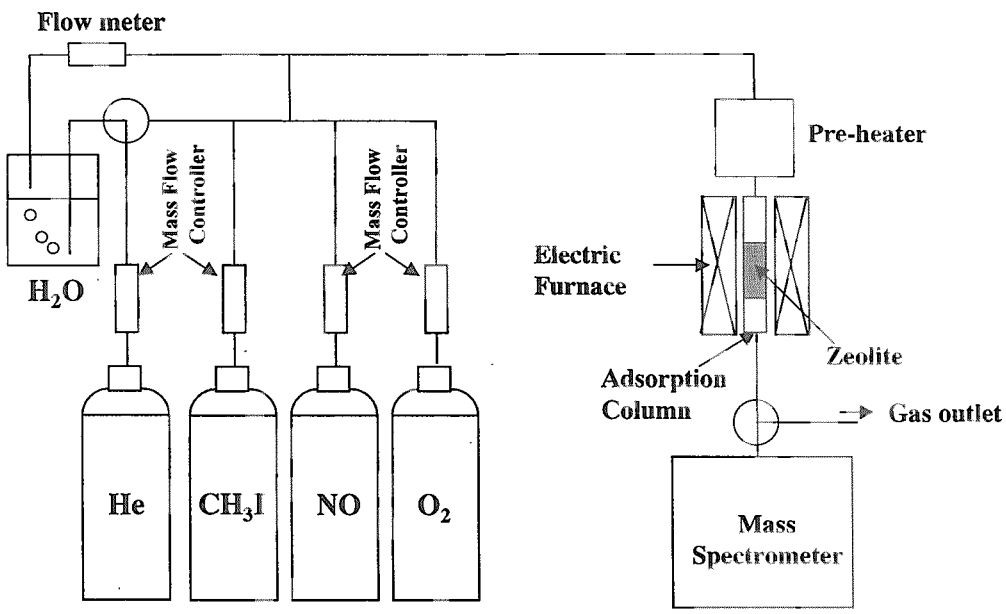

Fig.3 Experimental apparatus to measure adsorption and desorption of simulated off-gas.

column temperature was kept constant at 64°C. The breakthrough curves of NOx, CO_2, H_2O and CH_3I were measured by flowing the simulated off-gas at 100cm^3-STP/min. The desorption tests were carried out by switching the simulated off-gas to pure He gas during the course of breakthrough experiment. Then, the column temperature was increased at the rate of 10℃/min by the electric furnace and the concentrations of gas components released from the column, CO_2, NO, NO_2, H_2O and CH_3I, were measured by the mass spectrometer. The concentration of I_2 in the released gas was measured by the $KMnO_4$ absorption method[6]. It is known that a part of NO_2 forms N_2O_4. In this paper, the concentration of NO_2 was given as $[NO_2]+2[N_2O_4]$ by counting a N_2O_4 molecule as two NO_2 molecules.

III. RESULTS AND DISCUSSION

3.1 Adsorption and Desorption Behavior of Simulated off-gas in TSA Process

Figure 4 shows the breakthrough curves of CO_2, NO, NO_2, CH_3I and H_2O under the condition that the oxygen concentration in the simulated off-gas is 10vol%. The order of breakthrough was CO_2>NOx ($NO+NO_2$)>CH_3I>H_2O. CO_2 was expelled by NOx. This means that CO_2 can be separated from NOx, CH_3I and H_2O, when the adsorption operation of TSA process is switched to the desorption one at the beginning of the breakthrough of NOx. It is

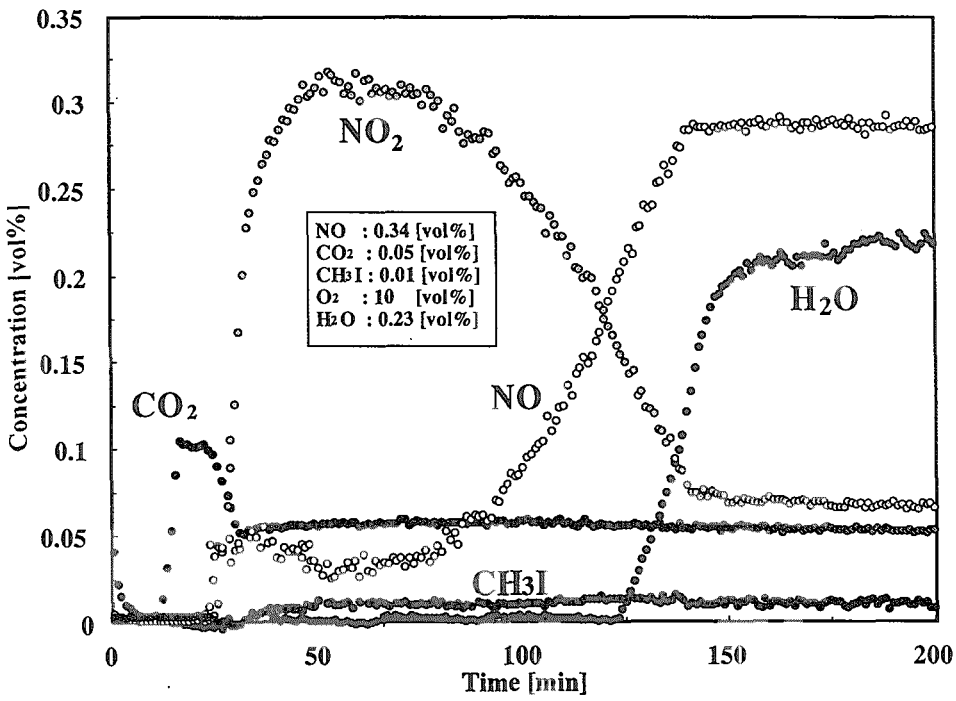

Fig.4 Breakthrough curves of simulated off-gas containing CH_3I. The oxygen content in the simulated off-gas was adjusted to 10vol%.

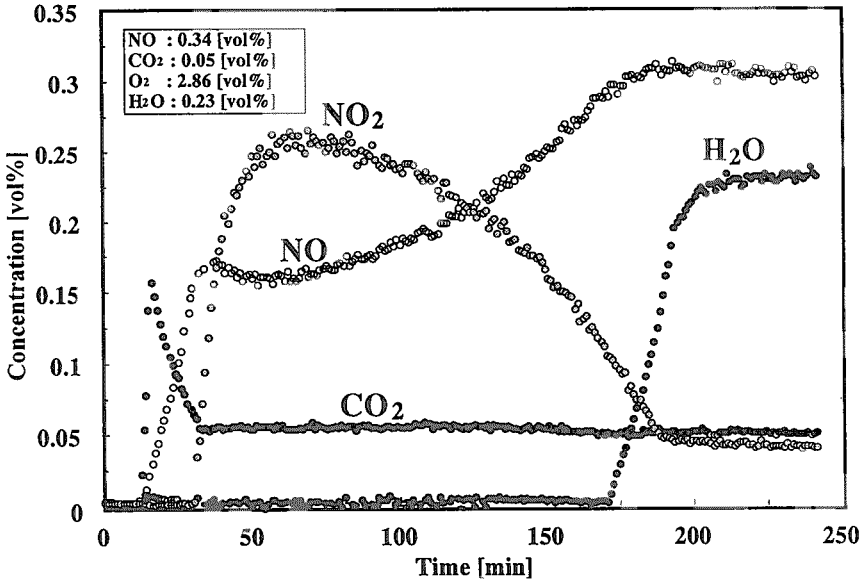

Fig.5 Breakthrough curves of simulated off-gas. The oxygen content in the simulated off-gas was adjusted to 2.9vol%.

possible to fractionate ^{129}I and ^{14}C completely in the TSA process. If setting a simple zeolite process after the TSA process, $^{14}CO_2$ can be recovered easily from DOG. This is because DOG at the outlet of TSA process does not contain polar gases, such as NOx, H_2O and CH_3I. Furthermore, it should be noted that the breakthrough curve of NO_2 was obtained, in spite that NO was added in the simulated off-gas. These results suggest the formation of the adsorption band of NO_2 on the zeolite. NO may be oxided catalytically to NO_2 on the zeolite in the presence of oxygen. **Figure 5** shows the breakthrough curves under the condition that the oxygen concentration in the simulated off-gas is 2.9vol%. NO is not oxided sufficiently to NO_2 and is co-adsorbed with CO_2. $^{14}CO_2$ can not be fractionated under the condition that the concentration of oxygen is low. For

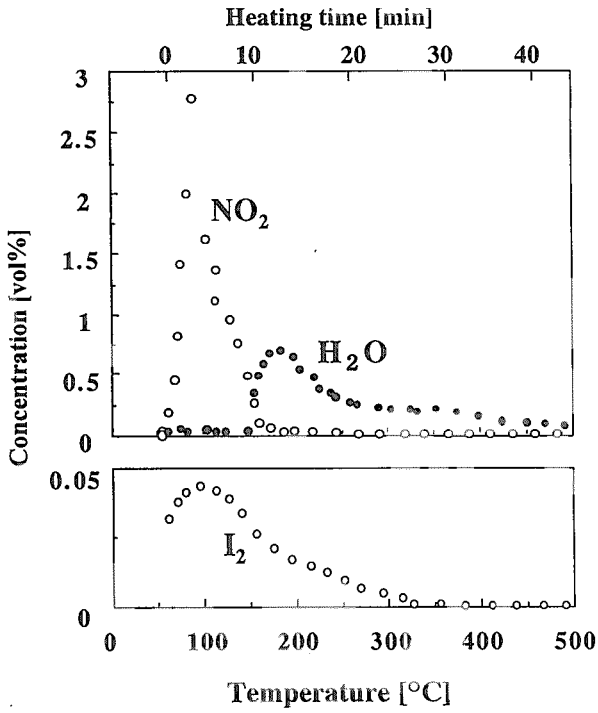

Fig.6 Desorption curves of NO_2, I_2 and H_2O. The column operation was switched from adsorption to desorption at the breakthrough point of NOx.

the fractionation of ^{14}C, it is important to promote the oxidation of NO to NO_2 by maintaining the concentration of oxygen more than 10vol% in DOG.

Figure 6 shows the results of desorption test, in which the adsorption operation was carried out under the same conditions as Fig.4 and was switched to the desorption one at the beginning of the breakthrough of NOx. Most of NO_2, I_2 and H_2O were recovered by increasing the column temperature until 300°C. The desorption of I_2 indicates that CH_3I is decomposed to I_2, according to

$$CH_3I + NO_2 + \frac{1}{2}O_2 \rightleftarrows CH_3NO_3 + \frac{1}{2}I_2 \qquad (1).$$

CH_3I can be recycled as I_2 to the Ag^0-impregnated adsorbent process at the presence of oxygen.

3.2 Evaluation of Dimensions of TSA Process

To evaluate the dimensions of TSA process required for an 800 ton/y reprocessing plant, the relation between the component of DOG and the flow rate of air blown to the dissolver was calculated by the extended ABNOX code[8]. **Table 2** shows the operating conditions of dissolver, condenser, NOx absorption process, dehumidifying process and Ag^0-impregnated adsorbent process. The evolution of radioactive elements, ^{129}I, ^{14}C and ^{85}Kr, was calculated from the data of the nuclide composition of spent PWR fuel (average fuel exposure : 33 MWd/kg) stored for 150 days after discharge[9]. **Table 3** shows the components of DOG at the inlet of TSA process. The concentration of oxygen in DOG increased with increasing the flow rate of air blown to the dissolver. The appropriate air flow rate is evaluated as about 70 m^3/h under the conditions that the oxygen concentration higher than 10 vol% is maintained and that the NOx concentration is minimized.

Table 2 Operating conditions of condenser, NOx absorber, iodine stripping process, dehumidifying process and Ag^0-impregnated adsorbent process

Process	Operation Conditions
Condenser	Temperature of inlet gas : 363 K Temperature of outlet gas : 303 K Residence time : 20 sec
NOx absorption	Reactor :Bubble-cup column (12 stages) Temperature : 303 K Off-gas containing NOx is in contact with water countercurrently.
Iodine Stripping	Reactor :Gas-bubble column Temperature : 303 K Iodate is reduced to I_2 by the reaction with NOx. Air containing NOx is used as the stripping gas.
Dehumidifying	Reactor : Silica gel column Content of water vapor in inlet gas :3.2 vol% Content of water vapor in outlet gas : 0.32 vol%
Ag^0-impregnated adsorbent	Adsorbent: Ag^0-loaded silica gel (Ag^0S) Temperature : 403 K Decontamination factor of I_2 : 100

From these calculation results, the dimensions of TSA process required for the iodine recovery was estimated roughly for an 800 ton/y reprocessing plant. The factors concerning adsorption kinetics, for example the shape of breakthrough curves, were not considered in this

Table 3 Composition of DOG at the inlet of thermal swing adsorption process. Flow rate of air blown in the dissolver was changed in the range of 30 to 200 m^3/h

Flow rate of air blown in dissolver [m^3/h]		30	50	75	100	200
Composition of off-gas at 298 K [vol%]	H_2O vapor	0.319	0.319	0.319	0.319	0.319
	N_2	94.805	90.331	86.475	84.507	81.601
	O_2	1.087	8.345	12.273	14.228	17.010
	$NO+NO_2$	3.144	0.621	0.677	0.750	0.959
	I_2+CH_3I	1.32E-03	7.53E-04	4.80E-04	3.52E-04	1.70E-04
	Kr	0.063	0.036	0.023	0.017	0.008
	Xe	0.543	0.311	0.198	0.145	0.070
	CO_2	0.038	0.036	0.034	0.034	0.032

calculation. As shown in Fig.2, the adsorption and desorption operations are repeated between two zeolite columns in TSA process. The requisite to operate the TSA process is that the time required for the regeneration of column is the same as that for the adsorption. The regeneration time of column is given as the sum of the heating time of column and the cooling one by blowing air. Therefore, the adsorption capacity of NOx required for a zeolite column is described as

$$[\text{Adsorption capacity of NOx}] = [\text{Flow rate of DOG}] \times [\text{Conc. of NOx}] \times [\text{Regeneration time}] \quad (2)$$

Thus, the volume of zeolite column is given as

$$[\text{Column volume}] = [\text{Adsorption capacity of NOx}] / ([\text{Adsorption capacity of NOx}] \times [\text{Bulk density of packed zeolite}]) \quad (3)$$

The adsorption operation is switched to the desorption one at the beginning of the breakthrough of NOx. Then, the adsorption capacity of NOx on the zeolite column is evaluated as 16 cm^3-STP/g-zeolite, which was calculated from the experimental results of Fig.4. The shell-and-tube type reactor is used as the zeolite column, because of the promotion of heat conduction of column. The tubes are packed with the zeolite particles. The dimensions of tube, which are packed with zeolite particles, were assumed as 0.1m in diameter and 2m in length. The heating and cooling experiments for the tube packed with zeolite were carried out. The regeneration time (= heating time + cooling time) was given as 4.7 hr under the conditions of the heating until 500°C at 10°C/min and the cooling by blowing air. Assuming that the bulk density of packed zeolite is 0.7 g/cm^3, the volume of zeolite column is given as 0.19 m^3 from Eqs.(2) and (3). Then, the number of tubes is evaluated as about 12. Accordingly, total volume

of zeolite required for the TSA process was evaluated as $0.38m^3$ (=0.19 m^3/column x 2 columns). These results suggest that the TSA process can be designed compactly

IV. Conclusions

(1) In the TSA process, alkyl iodide in DOG can be recovered completely as molecular iodine (I_2), when the adsorption operation is switched to the desorption one at the beginning of the breakthrough of NOx. By recycling the recovered I_2 to the Ag^0-impregnated adsorbent process, all of iodine and alkyl iodide in DOG is immobilized as AgI on the Ag^0-impregnated adsorbents.

(2) In the TSA process, CO_2 and noble gas are partitioned from NOx, H_2O and iodine under the condition that the concentration of oxygen in DOG is maintained to higher than 10vol%. ^{14}C as well as ^{129}I can be fractionated in the TSA process.

(3) The TSA process plays an important role for the fractionation and recovery of long-lived radioactive nuclides in DOG, ^{14}C and ^{129}I. Total volume of zeolite required for the TSA process is evaluated as $0.38m^3$ for an 800 ton/y reprocessing plant. The TSA process can be designed compactly.

Acknowledgement

The present research was performed under the Innovative and Viable Nuclear Energy Technology (IVNET) Development Project of the Ministry of Economy, Trade and Industry (METI) of Japan.

References

(1) D.W.Holladay, "Literature Survey: Method for the Removal of Iodine Species from Off-gases and Liquid Waste Streams of Nuclear Power and Nuclear Fuel Reprocessing Plants, with Emphasis on Solid Sorbents",ORNL/TM-6350, Oak Ridge National Laboratory (1979).

(2) L.H.Baetsle et al., "Status and Assessment Report on Actinide and Fission Product Partitioning and Transmutation", Proc. of 5th International Information Exchange Meeting, Mol Nov.25-27, p.87 1998

(3) J.C.Wilhelm et al., "Inorganic Adsorber Material from Off-gas Cleaning in Fuel Reprocessing Plants", Proc. of 12th AEC Nuclear Air Cleaning Conf., p.540 (1972).

(4) S.Matsuoka and T.Sakurai, "Radiological Significance and Management of Off-gas Arising from Reprocessing Plant", Nihon-Genshiryoku-Gakkai Shi, **28**, 701 (1986) [in Japanese]

(5) G.Modolo and R. Odoj, "Investigations on the Partitioning of ^{129}I from Silver-impregnated Silica in

Preparation for Future Transmutation", Nuclear Technology, **117**, 80 (1997)

(6) K.Takeshita and Y.Nakano, "Prediction of a Breakthrough Curve of Iodine on a Reduced Silver-loaded Adsorbent Bed", Nuclear Technology, **133**, 338 (2001)

(7) K.Takeshita et al., "Effect of Grain Size of $AgNO_3$ Loaded in Porous Material on Adsorption of CH_3I", J. Nucl. Sci. Technol., **32**, 941 (1995)

(8) R.M.Counce, "Nitrogen Oxide Absorption into Water and Dilute Nitric Acid in an Engineering-scale Sieve-plate Column. Description of a Mathematical Model and Comparison with Experimental Data", ORNL-5438, Oak Ridge National Laboratory (1978)

(9) M.Benedict et al., "Nuclear Chemical Engineering (2nd ed.)", McGraw-Hill, Chapter 8 (1981)

JP0250355

JAERI-Conf 2002-004

RESEARCH ON PYROCHEMICAL PROCESS FOR NITRIDE FUEL AT JAERI

Yasuo Arai, Takashi Iwai, Osamu Shirai, Hirokazu Hayashi and Kazuo Minato

Tokai Research Establishment
Japan Atomic Energy Research Institute
Tokai-mura, Naka-gun, Ibaraki-ken, 319-1195 Japan
FAX: 81-29-264-8420, e-mail: arai@popsvr.tokai.jaeri.go.jp

Research on pyrochemical process for nitride fuel at JAERI is summarized. Following the introduction of nitride fuel cycle for transmutation based on the double-strata concept, recent experimental results of electrolysis of actinide nitrides in chloride molten salt, redox reaction of actinides at liquid electrodes, nitrogen release behavior at dissolution of metal nitrides and nitride formation of actinides in liquid Cd are given besides the preparation of thermodynamic database relating to pyrochemical process. Although most of the present results concerned U, Np and Pu bearing materials, it was suggested that pyrochemical process is a promising technology for the treatment of spent nitride fuel for transmutation of long-lived minor actinides.
Key words: pyrochemical process, transmutation, minor actinides, nitride fuel, molten salt

1. Introduction

JAERI (Japan Atomic Energy Research Institute) has proposed the transmutation of long-lived MAs (minor actinides) such as Np, Am and Cm by use of sub-critical ADS (accelerator driven system) based on the double-strata fuel cycle concept [1]. Besides the construction of high-energy proton beam accelerator or design study of transmutation plant, the technological development of separation of MAs from HLLW (high-level liquid waste), fabrication of MAs nitride fuel for ADS and treatment of spent fuel is the important subject investigated hereafter. Pyrochemical process has several advantages over aqueous process for the treatment of spent fuel for MAs transmutation. They include compactness of the equipment, resistance to radiation damage, safety margin to criticality and high proliferation resistance, which should be essential for treating highly radiotoxic, spent fuel containing MAs as a primary component. In addition, JAERI's ADS will use MAs nitride fuel with N-15 enriched nitrogen in order to prevent the formation of hazardous C-14 from N-14. Pyrochemical process is expected to have practical feasibility of recycling expensive N-15 compared with aqueous process.

Recent R&D activities on pyrochemical process at JAERI include electrolysis of UN, NpN, PuN and (U,Pu)N in LiCl-KCl molten salt, redox reaction of U^{3+}/U, Np^{3+}/Np and Pu^{3+}/Pu at liquid (Cd, Bi) electrodes, nitrogen release behavior at dissolution of metal nitrides and nitride formation in liquid Cd besides preparation of thermodynamic database relating to pyrochemical process for nitride fuel. In this paper the typical results obtained so far are summarized [2].

2. Double-Strata Fuel Cycle [1]

In several countries, scenario study of MAs transmutation is pursued by use of power reactors or dedicated system such as ADS. From the viewpoint of fuel cycle, the latter is regarded as a "double-strata" concept that is constituted by commercial power reactor fuel cycle (the first stratum) and MAs transmutation fuel cycle (the second stratum). In the double-strata concept, each fuel cycle shall be designed and optimized independently. Commercial

power reactor fuel cycle insists on economy and reasonable utilization of Pu in LWR or FBR cycle, while MAs transmutation fuel cycle focuses on effective transmutation of hazardous long-lived MAs. According JAERI's concept, pyrochemical process is used for the treatment of the spent fuel of the second stratum, in which MAs are concentrated with large decay heat and fast neutron emission. A flowsheet of the second stratum is shown in Fig. 1.

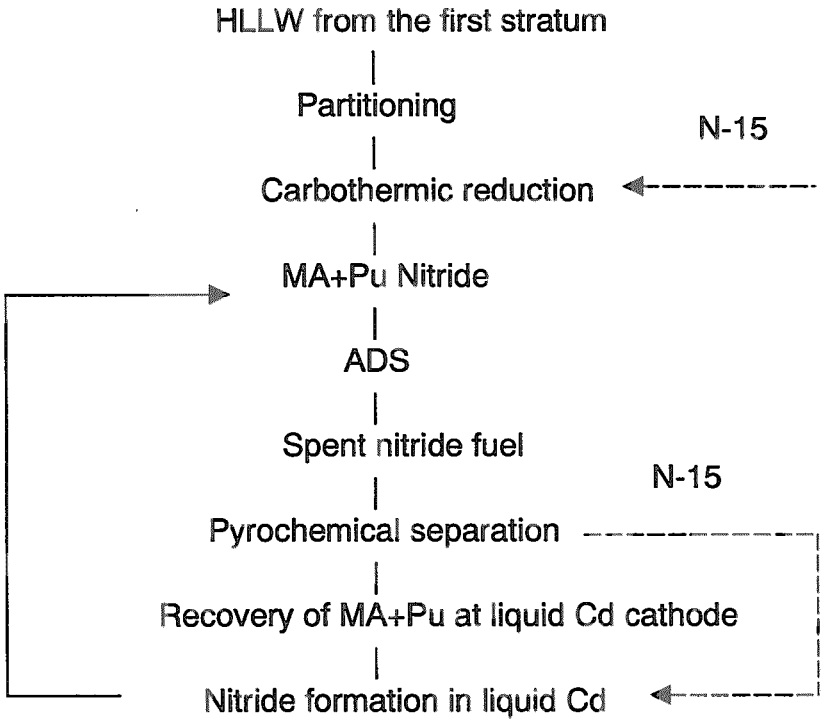

Fig. 1 Flowsheet for MAs transmutation fuel cycle proposed by JAERI

Since the second stratum handles principally MAs partitioned from HLLW of the first stratum, the heavy metal throughput of the second stratum is less than ~1/30 of that of the first stratum. This point will result in compact equipment and effective MAs transmutation in the second stratum. According to JAERI's concept, one ADS plant transmutes MAs and LLFP (long life fission products such as Tc-99 and I-129) produced by ten LWR plants of 1,000MWe per year. In this case, the MAs amount transmuted corresponds to ~250kg/y and the MAs system inventory is estimated as ~5.5ton based on some assumptions. This means that, if N-15 is recovered and recycled in the second stratum, necessary amount of N-15 is only 20~30 kg/y, which will not be a penalty from economical viewpoint. This is one of the reasons that pyrochemical process has been developed at JAERI for MAs transmutation fuel cycle [3].

3. Electrolysis of Actinide Mononitrides [4-6]

The spent nitride fuel is submitted to the electrolysis in LiCl-KCL molten salt in order to remove fission products. Metallic electrical property of nitride fuel enables us to apply the similar manner with that developed in ANL (Argonne National Laboratory) for metal fuel [7]. So far, electrolysis of UN, NpN, PuN and (U,Pu)N has been carried out in the molten salt containing a small amount of trivalent ions of actinides. The temperature of the electrolysis was chosen at 723, 773 and 823K. Cyclic voltammograms for NpN are shown in Fig. 2, in

which anodic and cathodic peaks are observed. They correspond to the following reaction:

$$NpN = Np^{3+} + 3e^- + 0.5N_2 \quad (1).$$

Equation (1) was a slow reaction and considered as a rate-determining step of the electro-dissolution, since the current did not increase in proportion to square root of the potential scanning rate, and the cathodic peak seemed to shift more negative side as increasing scanning rate. In addition, the equilibrium potentials of UN, NpN and PuN vs. Ag/AgCl reference electrode were determined from electromotive force measurements. The results at 723, 773 and 823K were summarized in Table I. The equilibrium potential could be interpreted by comparison with the theoretical redox potential of the nitrides derived from free energies of formation and nitrogen partial pressure in the molten salt.

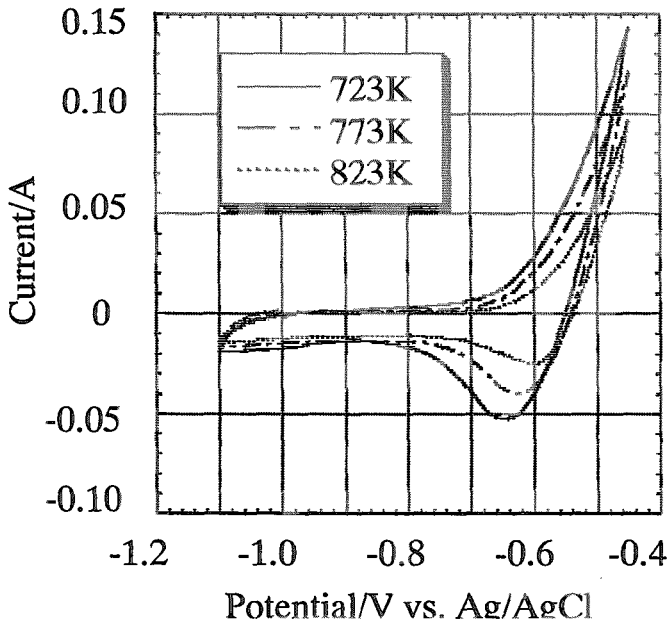

Fig. 2 Cyclic voltammograms of NpN in LiCl-KCl-$NpCl_3$ melt
($NpCl_3$ concentration; 0.53wt.%, scan rate; 0.01V/s)

Table 1 Equilibrium potential of UN, NpN and PuN vs. Ag/AgCl reference electrode determined from electromotive force measurements at 723, 773 and 823K

	UN	NpN	PuN
723K	n.d.*	-0.779V	n.d.*
773K	-0.670V	-0.773V	-0.880V
823K	n.d.*	-0.766V	n.d.*

* not determined

In case of the electrolysis of UN, however, the formation of ternary compound UNCl was identified at anode along with U^{3+}. Since UNCl is hardly soluble in the molten salt, the formation of UNCl would adversely affect the efficiency of recovery at cathode. On the other hand, the formation of such a compound was not observed in case of the electrolysis of NpN and PuN. The results were derived from greater stability of trichloride of transuranium elements and lesser stability of the tetra valence ions compared with uranium. Nitride fuel

for MAs transmutation is so-called U-free fuel, so the problem of formation of actinide nitrogen chloride could be avoided in this case.
Fig. 3 shows the appearance of Np metal recovered at solid Mo cathode from electrolysis of NpN. Since the electro-deposits contained a large amount of the salt, they were heated at 1073K in Ar gas stream to separate it from Np metal. However, some salt components such as LiCl, KCl and $NpCl_3$ were still identified in the X-ray diffraction pattern in addition to alpha-Np phase.

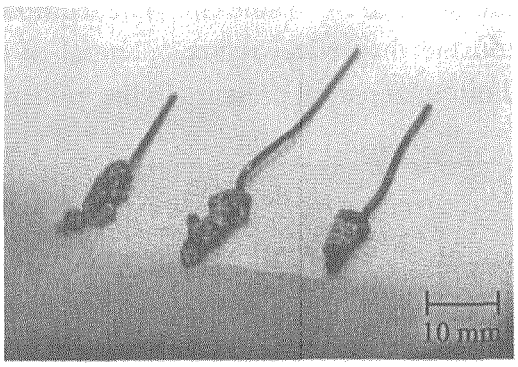

Fig. 3 Appearance of electro-deposits at solid Mo cathode obtained by current-controlled electrolysis of NpN at 773K

The electrolysis of $(U_{1-x}Pu_x)N$ with several compositions is also investigated. In addition, actinide nitride samples prepared from carbothermic reduction usually contain several hundred to a few thousand ppm of oxygen as primary impurities. The effect of oxygen impurities on the efficiency of electrolysis is being studied for technological application.

4. Redox Reaction at Liquid Electrode [8-10]

In the treatment of spent nitride fuel for transmutation, MAs and Pu are recovered at liquid cathode together. For the moment liquid Cd is the first candidate of cathode material and liquid Bi is considered as the second. So the redox reaction of U^{3+}/U, Np^{3+}/Np and Pu^{3+}/Pu couple at the interface between the molten salt and liquid metal phase (Cd, Bi) was investigated by comparison with that at solid cathode. Cyclic voltammograms of LiCl-KCl molten salt containing a small amount of actinide trichloride were obtained at 723, 773 and 823K. Typical results for LiCl-KCl-$NpCl_3$ melts were shown in Fig. 4. The voltammograms at liquid Cd and Bi electrodes were compared with that at solid Mo electrode. Peaks corresponding to electro-dissolution and -deposition were observed as shown in the figure. At 773K, the redox potentials of U^{3+}/U, Np^{3+}/Np and Pu^{3+}/Pu couple at liquid Cd electrode vs. Ag/AgCl reference electrode were observed more positively by 0.01, 0.18 and 0.28V, respectively, than those at solid Mo electrode. On the other hand, those at liquid Bi electrode were observed more positively by 0.38, 0.48 and 0.51V than those at solid Mo electrode at the same temperature. These potential shifts could be thermodynamically interpreted by a lowering of activity of actinides in the liquid phase due to the formation of intermetallic compounds with Cd or Bi. Indeed, the potential shift almost corresponded to the free energies of formation of the intermetallic compounds such as UCd_{11}, $NpCd_6$, $PuCd_6$, UBi_2, $NpBi_2$ and $PuBi_2$, which are considered as the most stable intermetallic compounds in

the respective binary systems at 773K.

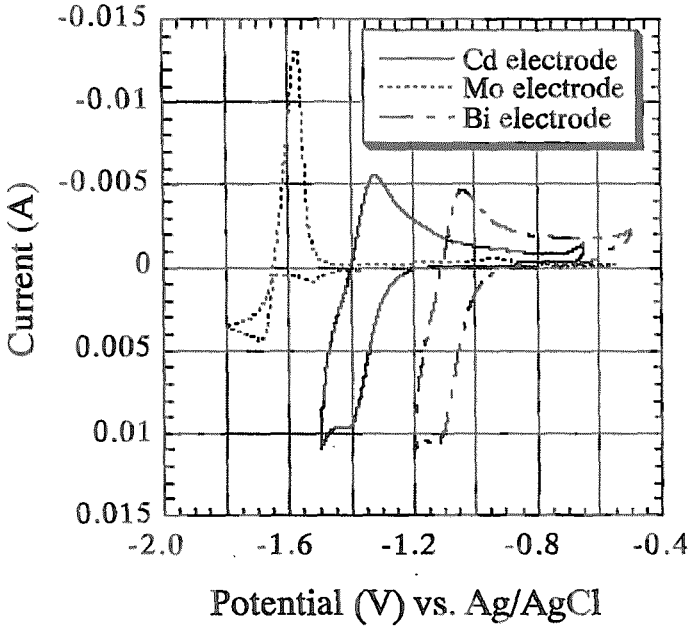

Fig. 4 Cyclic voltammograms of Np^{3+}/Np couple at Cd, Bi and Mo electrodes at 723 K. Concentration of $NpCl_3$ and scan rate are 0.465 wt.% and 0.01 V/s, respectively.

In addition, the recovery of Pu into liquid Cd cathode with high concentration was demonstrated under a joint research with CRIEPI (Central Research Institute of Electric Power Industry). Cathodic current density for effective recovery of Pu was considered to be controlled by diffusion of Pu^{3+} in the molten salt and proportional to its concentration. At Pu concentration of 2.11wt.% in the molten salt and cathodic current density of 41mA/cm^2, for example, the current efficiency was nearly 100% and the concentration of Pu in the cathode reached 7.75wt%. Recent results showed that the concentration could reach more than 10wt.% without any problems. At higher cathodic current densities, however, Li and Pu metals were precipitated at the surface of liquid Cd cathode and reacted with ceramic parts, which decreased recovering efficiency. Further, it was shown that Pu recovered beyond the solubility limit in liquid Cd formed an intermetallic compound $PuCd_6$ and accumulated at the bottom of cathode. Figs. 5 shows the appearance of liquid Cd cathode after recovery of Pu. Investigation of co-deposition behavior of Pu and U is underway.

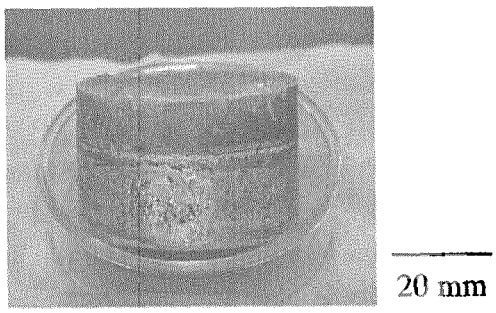

Fig. 5 Appearance of liquid Cd cathode after recovery of Pu
(Upper part is the solidified salt containing $PuCl_3$)

5. Nitrogen Release Behavior at Dissolution of Metal Nitrides [11]

The cost accompanying the use of N-15 may become prohibitive, unless one makes devices to recover and recycle it in the fuel cycle. It is the one of the key technologies of MAs treatment of spent nitride fuel for transmutation.

This point has been demonstrated by dissolving NdN and DyN, which are regarded as surrogates of TRU nitrides, by oxidizing them with $CdCl_2$ in LiCl-KCl molten salt at first. During heating, the carrier gas (He) was introduced to a gas chromatography apparatus with an automatic gas sampler. A fraction of the gas was also sampled and analyzed by mass spectrometry. It was found that nitrogen contained in DyN was readily released for 97-99% as N_2 gas, while that in NdN was slightly less than these values. The difference in behavior between DyN and NdN was considered to be related with the relative larger amount of oxygen impurity in the latter; 0.51wt.% for the former and 1.45wt.% for the latter. It is likely that some nitrogen exists in the bottom sediment along with Nd, O and Cl.

Secondly, nitrogen releasing behavior is examined during the electrolysis of UN, PuN and (U,Pu)N as mentioned in the preceding chapter. Using the similar apparatus with the above case, N_2 gas release behavior during the electrolysis has been monitored. These results suggest that recovery of more than 90% of N-15 in the spent fuel is technically feasible as N_2 gas. If it is the case, N-15 has to be added to the second stratum only at the rate of 20kg/y or less, which would not be penalty from economical viewpoint.

6. Nitride Formation Behavior in Liquid Cd [12]

The actinide metal recovered by the electrolysis is to be converted to their nitrides. This will be done by nitride formation in liquid metal such as Cd. The existing thermodynamic data indicate that the free energy of formation of actinide mononitrides is rather close to each other among actinide elements, those of trichloride are significantly more negative for the rare earths compared with actinides and activity coefficients of metals in liquid Cd alloys are smaller for the rare earths compared with actinides [13].

So nitride formation behavior in liquid Cd containing actinide and rare earth elements are investigated at first. Nitrogen gas was fed into liquid Cd-2wt.%U-1wt.%Gd-1wt.%Ce alloy in Mo container at 773-873K. It was found that U was preferentially converted to U_2N_3 while most of the rare earths remained dissolved in liquid Cd. The similar result was reported from Japan elsewhere [14]. These results follow the theoretical expectation based on the above thermodynamic characteristics. Nitride formation of Pu recovered in liquid Cd with high concentration has been also investigated. However, detailed characterization of such nitrides is the important subjects hereafter since palletized or vibro packed nitride fuel for transmutation has to be industrially fabricated.

7. Basic Study and Preparation of Thermodynamic Database [15, 16]

In order to support the development of pyrochemical process for nitride fuel, some basic research has been carried out. In addition, structural analyses of molten salts, such as $LaCl_3$, YCl_3 and UCl_3, were made by XAFS and the computer simulation method was developed using molecular dynamics. The electrochemical behavior of lanthanides was studied by high-temperature UV-visible spectrophotometry as well as electrochemical measurement in

LiCl-KCl eutectic melt. Lanthanides were used as surrogates of americium in this case. From the high-temperature UV-visible spectra of Nd^{3+} and Nd^{2+} in LiCl-KCl-$NdCl_3$ melt with Nd metal, it was found that the disproportionate reaction occurred in the presence of Nd metal. The analysis of this kind of behavior is very useful to evaluate the behavior of americium in the chloride salt. Besides the experimental approach, the thermodynamic analysis becomes a strong tool to predict the high-temperature processes. The thermodynamic datafile is being prepared for the calculation of the LiCl-KCl-MCl_x-$CdCl_2$-MN-Cd-M-N-C-O system (M; actinides).

8. Conclusion

Recent activities of JAERI on pyrochemical process for spent nitride fuel for MAs transmutation are summarized. Electrolysis of UN, NpN, PuN and (U,Pu)N, redox reaction of U^{+3}/U, Np^{3+}/Np and Pu^{3+}/Pu at liquid Cd and Bi electrodes, nitrogen release behavior at dissolution of metal nitrides and nitride formation behavior in liquid Cd have been experimentally investigated in addition to preparation of thermodynamic database in relation to pyrochemical process. Although the results obtained so far concerned mainly U, Np and Pu bearing materials, it was suggested that pyrochemical process is a promising technology for the treatment of spent nitride fuel for MAs transmutation. On the other hand, TRU-HITEC (Module for TRU High Temperature Chemistry) is under construction at NUCEF of JAERI Tokai for the experiments on Am and Cm bearing materials. The first electrolysis test of AmN is planned from fiscal year 2003. [17]

ACKNOWLEDGEMENT

The authors wish to express special thanks to Drs. A. Iwamoto and T. Ogawa of Department of Material Science and Drs. M. Ochiai and T. Osugi of Department of Nuclear Energy System of JAERI for the interest in this study.

REFERENCES

(1) T. Mukaiyama, T. Takuzuka, M. Mizumota, Y. Ikeda, T. Ogawa, A. Hasegawa, H. Takada and H. Takano, Review of research and development of accelerator-driven system in Japan for transmutation of long-lived nuclides, Progress in Nucl. Energy, 38, 107-134 (2001).

(2) Y. Arai and T. Ogawa, Research on nitride fuel and pyrochemical process for MA transmutation, Proc. 6th OECD/NEA Information Exchange Mtg. on Actinide and Fission Products P&T, December 11-13, 2000, Madrid (CD-ROM) (2001).

(3) T. Ogawa and Y. Arai, Nitride/pyroprocess for MA transmutation and fundamental database, Proc. OECD/NEA Workshop on Pyrochemical Separation, March 14-16, 2000, Avignon, 157-164 (2001).

(4) F. Kobayashi, T. Ogawa, M. Akabori and Y. Kato, Anodic dissolution of uranium mononitride in lithium chloride-potassium chloride eutectic melt, J. Am. Ceram. Soc., 78, 2279-2281 (1995).

(5) O. Shirai, M. Iizuka, T. Iwai and Y. Arai, Recovery of Np by electrolysis of NpN in LiCl-KCl eutectic melts, J. Nucl. Sci. Technol., 37, 676-681 (2000).

(6) O. Shirai, T. Iwai, K. Shiozawa, Y. Suzuki, Y. Sakamura and T. Inoue, Electrochemical

dissolution of plutonium nitride in LiCl-KCl eutectic melts, J. Nucl. Mater., 277, 226-230 (2000).

(7) Y. I. Chang, The integral fast reactor, Nucl. Technol., 88, 129-138 (1989).

(8) O. Shirai, M. Iizuka, T. Iwai, Y. Suzuki and Y. Arai, Electrode reaction of plutonium at liquid cadmium in LiCl-KCl eutectic melts, J. Electroanalytical Chem. 490, 31-36 (2000).

(9) O. Shirai, M. Iizuka, T. Iwai and Y. Arai, Electrode reaction of the Pu^{3+}/Pu couple in LiCl-KCl eutectic melts -comparison of the electrode reaction at the surface of liquid Bi with that at a solid Mo electrode-, Analytical Sciences, 17, 51-57 (2001).

(10) M. Iizuka, K. Uozumi, T. Inoue, T. Iwai, O. Shirai and Y. Arai, Behavior of plutonium and americium at liquid cadmium cathode in molten LiCl-KCl electrolyte, J. Nucl. Mater., 299, 32-42 (2001).

(11) F. Kobayashi, T. Ogawa, M. Takano, M. Akabori, A. Itoh and K. Minato, Dissolution of metal nitrides in LiCl-KCl eutectic melt, Proc. Int. Conf. on Future Nuclear Systems (GLOBAL'99), August 29-September 3, 1999, Jackson Hole, (CD-ROM) (1999).

(12) M. Akabori, A. Itoh and T. Ogawa; Nitridation of uranium and rare-earths metals in liquid Cd, J. Nucl. Mater., 248, 338-342 (1997).

(13) T. Koyama, K. Uozumi, M. Iizuka, Y. Sakamura and K. Kinoshita, Pyrometallurgical data book, CRIEPI Report T93033 (1995) (in Japanese).

(14) Y. Kasai, I. Kakehi, S. Moro, S. Yonezawa, T. Higashi and K. Tozawa, Design study on advanced nuclear fuel recycling system -Conceptual design of recycling system using dry reprocessing technology-, Proc. Int. Conf. on Future Nuclear Systems (GLOBAL'99), August 29-September 3, 1999, Jackson Hole, (CD-ROM) (1999).

(15) Y. Okamoto, M. Akabori, A. Itoh and T. Ogawa, X-ray absorption study of molten uranium chloride system, Actinides-2001 International Conference, November 4-9, 2001, Hayama, Japan.

(16) H. Hayashi, et al., unpublished data.

(17) K. Minato, M. Akabori, A. Maeda, S. Miyamoto, O. Amano and T. Arai, TRU-HITEC -a new facility for TRU high temperature chemistry-, NUCEF 2001, October 31-November 2, 2001, Tokai, Japan.

JP0250356

TRU-HITEC —A NEW FACILITY FOR TRU HIGH TEMPERATURE CHEMISTRY

Kazuo Minato[1], Mitsuo Akabori[1], Atsushi Maeda[2], Satoshi Miyamoto[3], Osamu Amano[4] and Tomoaki Arai[5]

[1] Department of Materials Science, Japan Atomic Energy Research Institute
Tokai-mura, Naka-gun, Ibaraki-ken, 319-1195 Japan
Fax: +81-29-282-5922, e-mail: minato@popsvr.tokai.jaeri.go.jp

[2] Department of Safety Research Technical Support, Japan Atomic Energy Research Institute
Tokai-mura, Naka-gun, Ibaraki-ken, 319-1195 Japan

[3] Research and Development Department, The Japan Atomic Power Company
6-1, 1-chome, Ohtemachi, Chiyoda-ku, Tokyo, 100-0004 Japan

[4] Nuclear Power R&D Center, Engineering Research & Development Division
Tokyo Electric Power Company
4-1, Egasaki-cho, Tsurumi-ku, Yokohama, 235-8510 Japan

[5] Nuclear Power Engineering Sec., Nuclear Power Department
Tohoku Electric Power Company, Inc.
7-1, Ichibancho 3-chome, Aoba-ku, Sendai, Miyagi, 980-8550 Japan

For a basis of the future nuclear fuel cycle, it is very important to understand and control the behavior of TRU in the nuclear fuel cycle. However, the properties and behavior of TRU, such as Am and Cm, are not known very well. One of the reasons why the data are lacking is that few facilities are available for the research on Am and Cm in a controlled atmosphere in the world. Within a collaborative program between the Japan Atomic Energy Research Institute and the Japan Atomic Power Company - Tokyo Electric Power Company - Tohoku Electric Power Company, a new facility, called the Module for TRU High Temperature Chemistry (TRU-HITEC), is under construction in NUCEF. It consists of three hot cells shielded by steel and polyethylene and a glove box shielded by leaded acrylic resin, where a high purity argon gas atmosphere will be maintained. At TRU-HITEC fundamental properties and behavior of TRU, especially of Am, are to be studied for a basis of the future nuclear fuel cycle including the partitioning and transmutation of long-lived nuclides. TRU-HITEC will be available in 2003.

Key words: Transuranic elements, Americium, Curium, Pyrochemical processes, Transmutation

1. INTRODUCTION

The concentration of transuranics (TRU) in the spent nuclear fuels will increase when using high burnup fuels and MOX fuels. For a basis of the future nuclear fuel cycle, which may include the pyrochemical processes for spent fuels and the partitioning and transmutation of long-lived nuclides, it is very important to understand and control the behavior of TRU in the nuclear fuel cycle. However, the properties and behavior of TRU, such as Am and Cm, are not known very well. An application of the pyrochemical processes to the reprocessing of the spent fuels is expected to reduce the costs of the reprocessing, but few data are available on the chemical and electrochemical properties of Am and Cm that are necessary to develop the processes. One of the reasons why the data are lacking is that few facilities are available for the research on Am and Cm in a controlled atmosphere in the world.

Under these circumstances, a new facility is needed to study TRU behavior in the nuclear fuel cycle. Within a collaborative program between the Japan Atomic Energy Research Institute and the Japan Atomic Power Company - Tokyo Electric Power Company - Tohoku Electric Power Company, a new facility, called the Module for TRU High Temperature Chemistry (TRU-HITEC), is under construction in NUCEF.

2. OUTLINE OF TRU-HITEC

Figure 1 shows a schematic diagram of TRU-HITEC. It consists of three hot cells shielded by steel and polyethylene and a glove box shielded by leaded acrylic resin. The hot cells and glove box are connected with each other. Each cell is equipped with a wide window made of leaded glass and acrylic resin and three master-slave manipulators. At the rear of the cells, windows and ports for gloves and suits are arranged, which enable us to access installed apparatuses by hands when the radiation dose rate is adequately low. A high purity argon gas atmosphere will be maintained in the cells and glove box, where impurities of oxygen and moisture are $O_2 < 1$ ppm and dew point < -70°C.

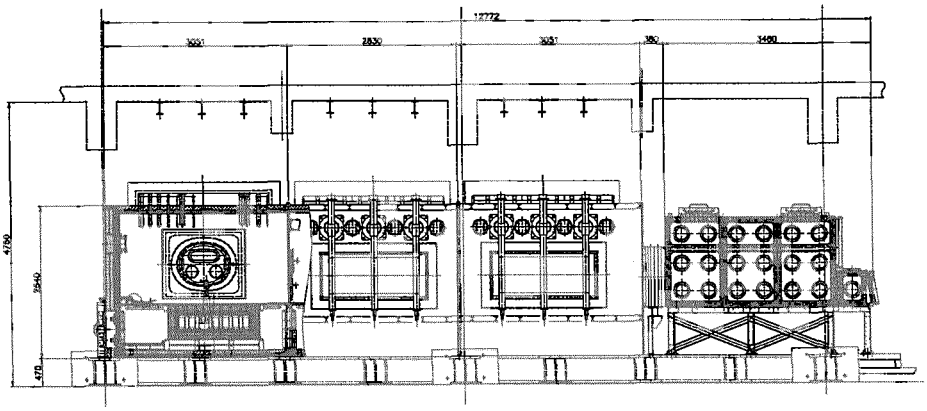

Fig. 1 Schematic diagram of TRU-HITEC.

The experimental apparatuses listed in Table I are to be installed in the cells and glove box. Electrochemical cells and a cathode processor are for pyrochemical process studies, and a differential thermal analyzer, a high-temperature X-ray diffractometer, etc., are for fundamental property measurements.

Table I Experimental apparatuses installed in TRU-HITEC

- Electrorefiners (2 sets): electrochemistry/electolysis
- Cathode processor
- Differential thermal analyzer
- Induction heating equipment: sample preparation/treatment
- Infrared image furnace: sample preparation/treatment
- High temperature X-ray diffractometer
- Oxygen potential measurement equipment

In TRU-HITEC, radioisotopes of Am-241, Am-243, Cm-244 and Np-237, and nuclear fuels of Pu, U and spent fuel can be handled. Table II shows maximum quantities of actinides that can be handled in TRU-HITEC.

Table II Maximum handling quantities of actinides in TRU-HITEC

Am-241	10 g	(1.27×10^{12} Bq)
Am-243	0.2 g	(1.48×10^{9} Bq)
Cm-244	0.02 g	(5.99×10^{10} Bq)
Np-237	10 g	(2.61×10^{8} Bq)
Pu	50 g	
U	400 g	
Spent fuel	~ 0.1 g	

3. RESEARCH PLAN AT TRU-HITEC

At TRU-HITEC fundamental properties and behavior of TRU, especially of Am, are to be studied for a basis of the future nuclear fuel cycle including the partitioning and transmutation of long-lived nuclides.

One of the main research objectives at TRU-HITEC is to study pyrochemical processes for nuclear fuels. Two sets of molten salt electrochemical cells, a cathode processor, a furnace for sample preparation, etc., are being designed that are to be installed in TRU-HITEC. Figure 2 shows a schematic diagram of experimental apparatus for pyrochemical reprocessing.

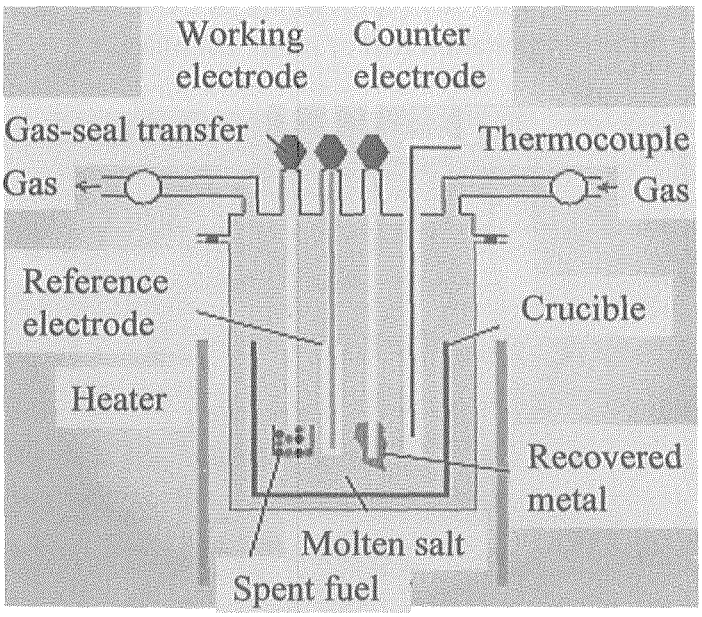

Fig. 2 Schematic diagram of experimental apparatus for pyrochemical reprocessing.

Figure 3 shows E-pO^{2-} diagram for Pu in LiCl-KCl eutectic melts, as an example of basic data that are important for evaluation of the pyrochemical reprocessing. The diagram shows the chemical forms of Pu as a function of E(V) and pO^{2-}. As shown in Fig. 3, an agreement of the experimental data with the thermodynamic estimation is not good even for Pu.

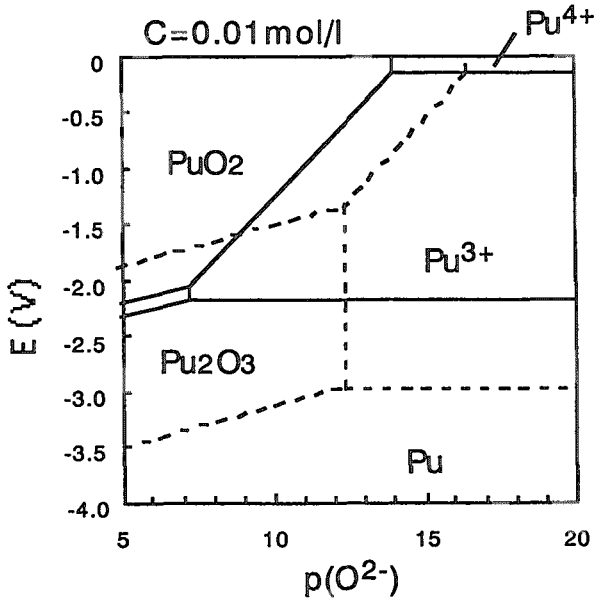

Fig. 3 E-pO^{2-} diagram for Pu in LiCl-KCl eutectic melts.
Solid lines indicate experimental data by L. Martinot and J. Fuger;
Broken lines indicate thermodynamic estimation by JAERI.

As the first experiment at TRU-HITEC, a basic study on chemical and electrochemical behavior of Am in the pyrochemical processes is planned. The data of E-pO^{2-} diagram for Am are important for evaluation of the pyrochemical reprocessing. The basic data in the Am-Cl-O-N system are to be studied for the reprocessing of oxide fuel and nitride fuel. The nitride fuel is a candidate for a transmutation fuel of minor actinides.

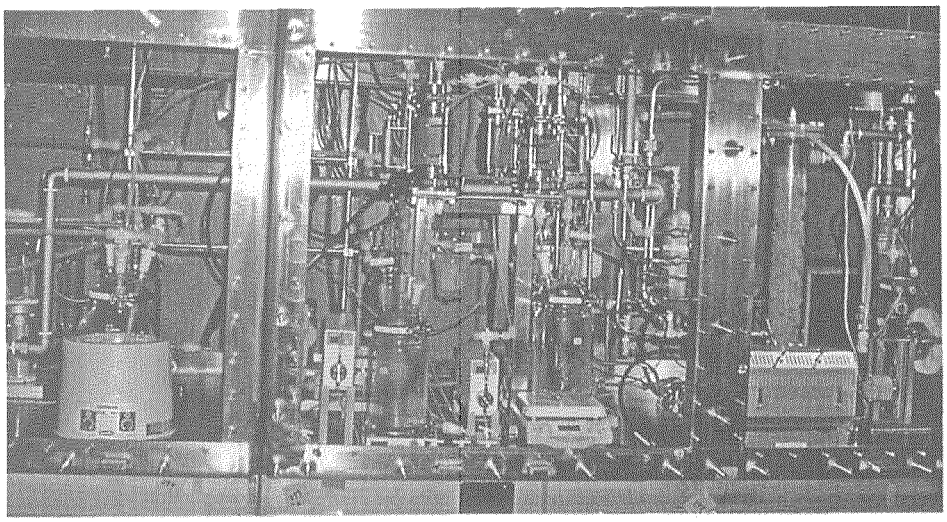

Fig. 4 Photograph of the Am recovery apparatus.

For the experiments at TRU-HITEC, Am-241 will be recovered from an americium aqueous waste in NUCEF. The process of the americium recovery is based on adsorption of Am by tannin gel. The construction of the Am recovery apparatus has been completed in NUCEF. The Am recovery apparatus consists of tannin gel columns, pumps, heaters, etc., in glove boxes. Figure 4 shows a photograph of the Am recovery apparatus, where the panel of the glove box is removed for an illustrative purpose.

4. SCHEDULE OF TRU-HITEC PROGRAM

Table III shows the schedule of the TRU-HITEC program. TRU-HITEC is now under construction and will be available in 2003. For the Am recovery, hot runs will be started in 2002 after the confirmation of the processes through cold runs. The recovered Am will be supplied to the experiments at TRU-HITEC.

Table III Schedule of the TRU-HITEC program

	2000	2002	2004	2006
● **TRU-HITEC**				
– Design				
– Construction				
– Research on Am and Cm				
● **Am recovery apparatus**				
– Design/construction			Am-241	
– Am-241 recovery				

ACKNOWLEDGEMENTS

The authors wish to express their thanks to Dr. A. Iwamoto, Director of Department of Materials Science, JAERI, Dr. T. Ogawa, Deputy Director of the Department, and Dr. Y. Suzuki, Director of Department of Safety Research Technical Support, JAERI, for their technical support and interest.

This is a blank page.

JP0250357

JAERI-Conf 2002-004

DEVELOPMENT OF SOLVENT WASHING PROCESS USING BUTYLAMINE COMPOUNDS

Y. ITOH, K. KAMEI, S. HOTOKU, T. ASAKURA, H. MINEO AND G. UCHIYAMA

Process Safety Laboratory

Japan Atomic Energy Research Institute

Tokai-mura, Naka-gun, Ibaraki-ken, Japan, 319-1195

Fax: 81-029-282-6677, e-mail: itoh@procsafe.tokai.jaeri.go.jp

An advanced PUREX process has been studied in which salt-free technologies are applied for the reduction of radioactive waste volumes. Normal butylamine compounds are developed as salt-free solvent washing reagents.

The solvent washing tests were carried out with two types of butylamine compounds for solvent washing reagents. A small size mixer-settler used in the tests was composed of two washing steps. DBP in the solvent was washed effectively under the conditions of pH of more than 1.5. Decontamination factors for DBP and for total alpha nuclides were 2.5～7.9 and 120～2,500. Those for total beta nuclides varied widely.

As for the solvent washing mechanism of DBP and radionuclides, some reaction formulae were proposed on the basis of the information of the previous papers about the pH dependence of partition and the complex formation in the washing process.

The study on electrolysis of butylamine was also conducted for waste treatment.

Key words: PUREX process, salt-free, solvent washing, butylamine compounds, electrolysis

1.INTRODUCTION

An advanced PUREX process has been studied in which salt-free technologies are applied for the reduction of radioactive waste volumes. As a part of the advanced technologies normal butylamine compounds are developed as salt-free solvent washing reagents.

Normal butylamine (n-butylamine) has some properties suitable for the solvent washing reagent. It is a basic compound (Kb=3.36, at 25℃), and is stable and easy to prepare. Furthermore TBP loss is expected to be very small during plant operation, because the TBP distribution ratio, which is defined as the ratio of TBP concentration in the 0.25M n-butylamine oxalate aqueous phase to that in the organic phase (30% TBP – 70% n-dodecane), was measured to be smaller than 2×10^{-3}. The effectiveness of n-butylamine compounds as solvent washing reagent was found with the bicarbonate and the oxalate in the previous experiment[1].

2.EXPERIMENTAL

2.1 Washing test

In this study the solvent washing tests were carried out with two types of butylamine compounds for solvent washing reagents and with degraded solvents which were generated through the uranium stripping process. The burnups of the spent fuel were 8,000, 29,000 and 44,000 MWd/tU.

The experimental flow sheet is shown in Fig.1. A small size mixer-settler of 16 stages in the glove box was used in the tests. The solvent washing process under development consists of two washing steps. In the washing tests, 4-4 stages and 7-9 stages of the mixer-settler were used for each washing step. The solvent washing behaviors were studied under many flow sheet conditions such as butylamine compounds and pH in aqueous phase. For comparison sodiume carbonate and nitric acid were also used in the case of 44,000MWd/tU.

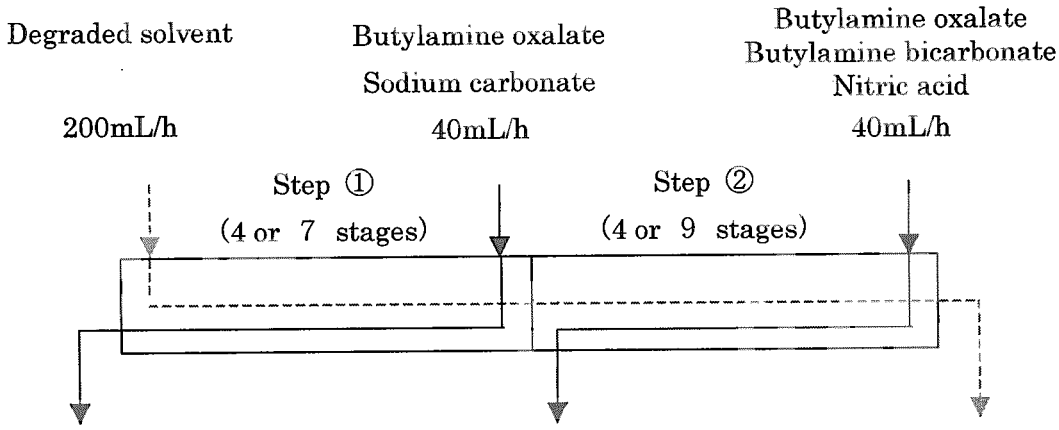

Fig.1 Solvent washing flow sheet

Analysis items of each stage are shown in Table Ⅰ. DBP samples were prepared by the separation process using sodium hydroxide and carbon tetrachloride.

Table Ⅰ Analysis items

Items	Methods
pH	Potentiometric titration
DBP	Ion exchange chromatography
Radionuclides	2π gas flow counter Ge detector Si detector

2.2 Electrolytic decomposition study

Butylamine decomposition cell is shown in Fig.2. Butylamine, nitric acid and

silver nitrate were mixed in the cell. Experimental conditions are shown in Table Ⅱ.

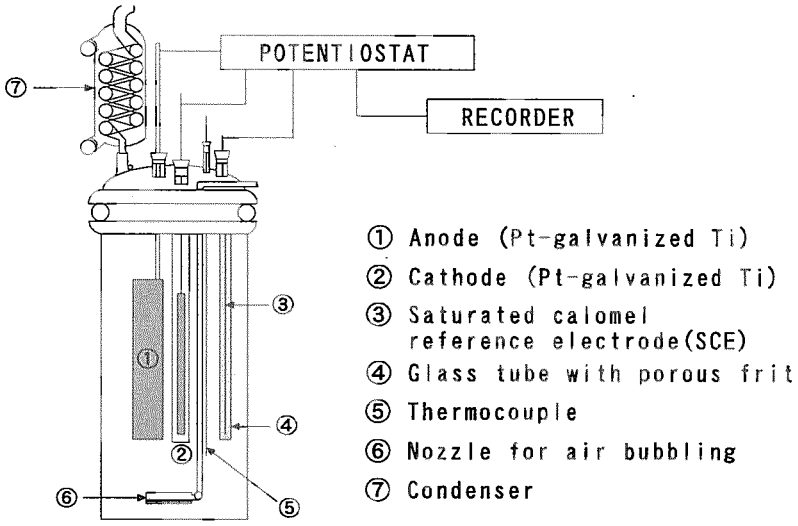

Fig.2 Decomposition cell (volume : 100mL)

Table Ⅱ Experimental conditions of electrolytic decomposition

Items	Conditions
Nitiric acid concentration (M)	0.01 , 1.0 , 2.0 , 3.0
Silver concentration (g/L)	0 , 2 , 4 , 6 , 8 , 16
Butylamine concentration (g/L)	0.18 , 0.36 , 0.72
Potential (V vs SCE)	1.5 , 1.6 , 1.7 , 1.8 , 1.9 , 2.0
Temperature (℃)	40 , 50 , 60

Underlines indicate reference values.

3.RESULTS AND DISCUSSION

3.1 Washing effect

(a) DBP

DBP concentration profiles in case of 29,000 MWd/tU is shown in Fig.3. Comparing pH of aqueous phase of each stage with that of washing reagents, the difference was explained by the influence of nitric acid in the solvent and of dissolving of hydrogencarbon.

DBP in the solvent was washed effectively under the conditions of pH of more than 1.5. The result is consistent with the fact that the wash efficiency for DBP increased as the pH of the washing reagent[2]. It can be said that DBP is washed with butylamine compounds by dissociation with the hydroxide ion in the following.

$$HDBP_{org} + OH^-_{aq} \rightarrow DBP^-_{aq} + H_2O$$
$$DBP^-_{aq} + C_4H_9NH_3^+{}_{aq} \rightarrow C_4H_9NH_3DBP_{aq}$$

Decontamination factors for DBP were 2.5~7.9 in three burnups experiment.

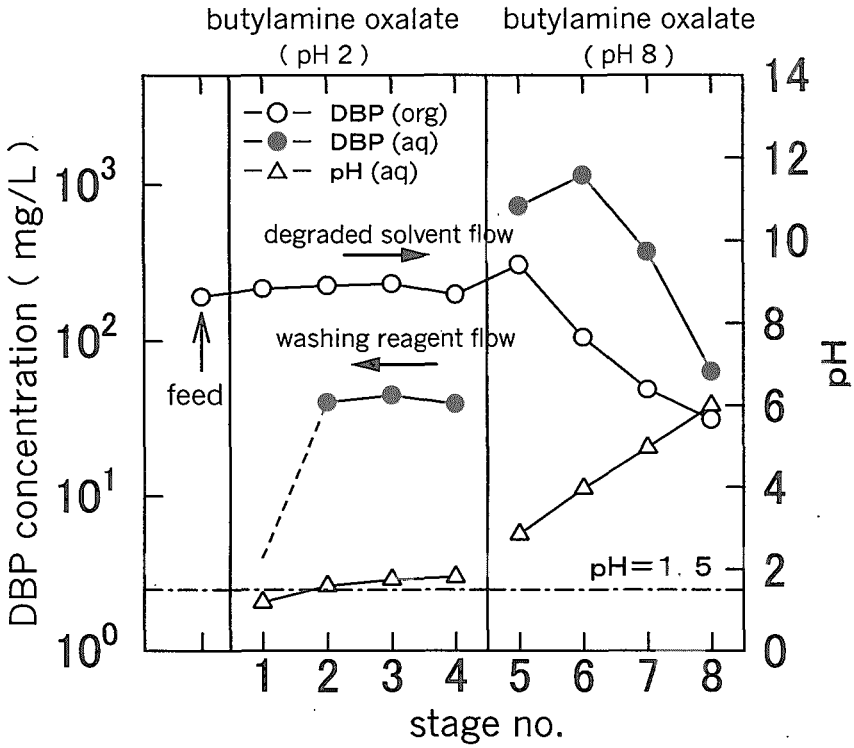

Fig.3 DBP concentration profiles (29,000 MWd/tU)

(b) Radionuclides

α- and β-nuclides concentration profiles in the organic phase are shown in Fig.4, obtained by means of 2π gas flow counter. Decontamination factors for α-nuclides were 120~2,500. Those for ^{241}Am and ^{239}Pu+^{240}Pu were of the similar orders analyzed by α and γ ray spectra. Washing process proceeded almost in the first step, which was low pH region and used butylamine oxalate reagent. This implies that α-nuclides, Am and Pu would make complexes with the oxalate ion.

Decontamination factors for β-nuclides varied widely. Those for ^{137}Cs were of the orders of several 10s and 100s, while those for ^{106}Ru, ^{95}Nb and ^{95}Zr were about or less than 10. The profiles in Fig.4(b) was similar to that of ^{137}Cs. It may be said that Cs also would make oxalate complexes. ^{106}Ru was washed not so much in both steps. Since pH did not exceed 7 in the most cases, the result can be explained by pH dependency of the washed fraction for Ru as shown in [2].

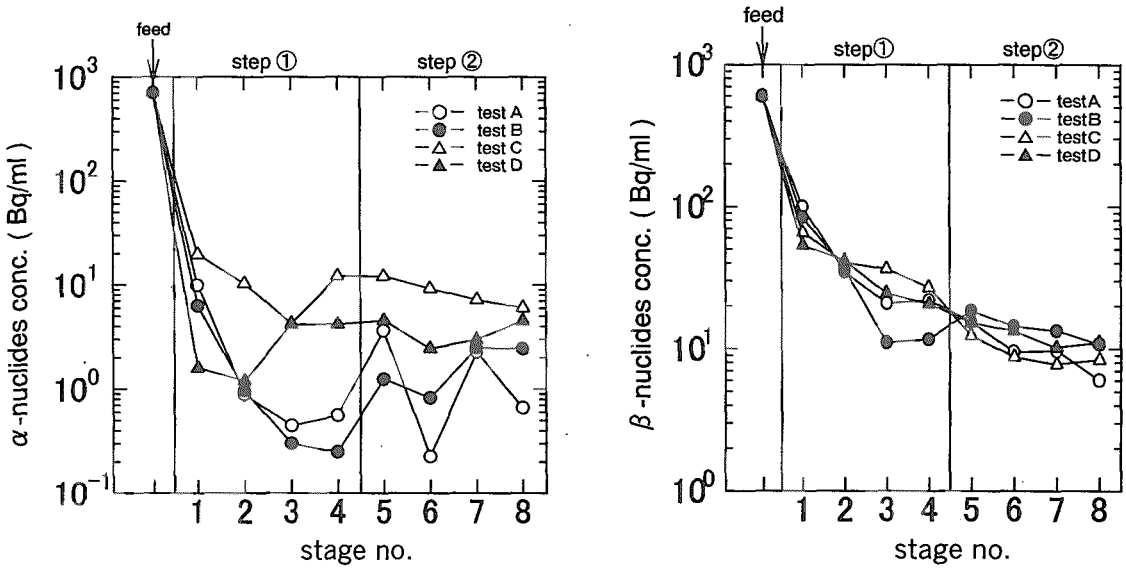

(a) α - nuclides (b) β - nuclides

Fig.4 α - and β - nuclides concentration profiles in organic phase (29,000 MWd/tU)

Washing reagent in step① + step② :

Test A butylamine oxalate (pH2) + butylamine bicarbonate (pH7)

Test B butylamine oxalate (pH2) + butylamine oxalate (pH8)

Test C butylamine oxalate (pH8) + butylamine bicarbonate (pH7)

Test D butylamine oxalate (pH8) + butylamine oxalate (pH8)

Compared with decontamination factors obtained by using sodiume carbonate and nitric acid, butylamine compounds would be more efficient as the washing reagent for α - nuclides.

3.2 Electrolytic decomposition behavior

The optimum condition for electrolytic decomposition of butylamine was the nitric acid concentration of 3M, the silver nitrate concentration of 8 g/L, the solution temperature of 60 ℃ and the decomposition electric potential of 1.7 V vs. SCE. Its decomposition curve is shown in Fig.5. Decomposition rate suddenly decreased over 100 min. The potential dependency of decomposition rate constant is shown in Fig.6. As potential loaded the rate constant increased especially at 1.7 V vs. SCE. On the other hand efficiency is going down because of the increase of over-current.

Electrolytic decomposition of butylamine oxalate was also conducted, the curve of which was the same shape as in Fig.5.

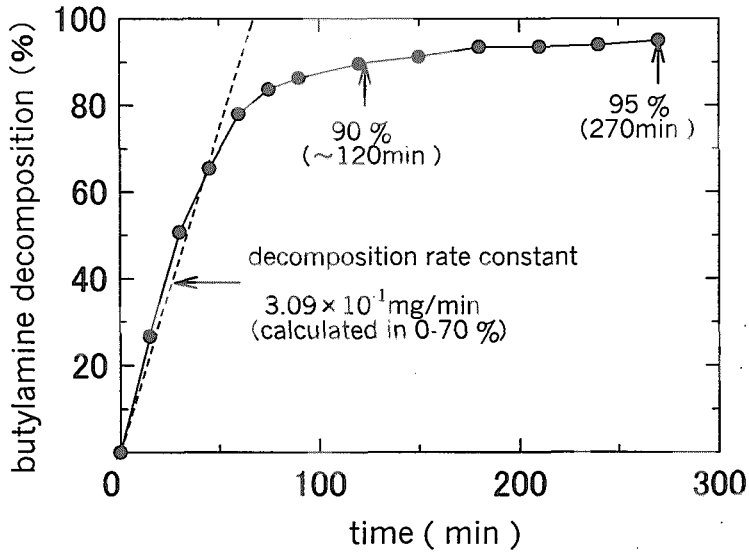

Fig.5 Decomposition curve at optimum condition

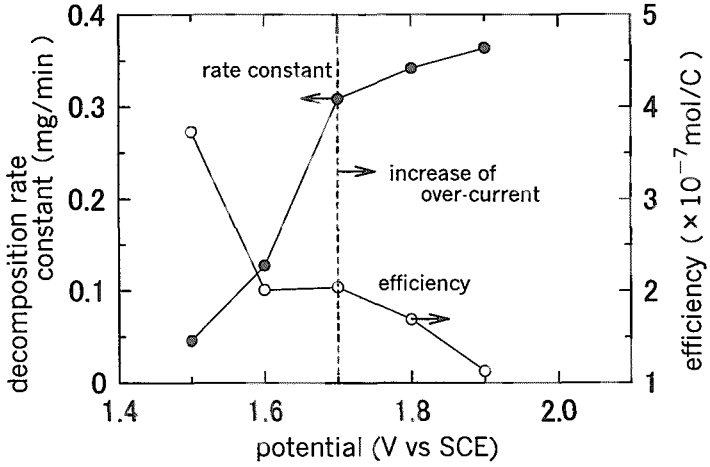

Fig.6 Potential dependency of rate constant and efficiency.

4.CONCLUSION

These results confirm the effectiveness of n-butylamine compounds as solvent washing reagent in the case of the reprocessing for the power plant's spent fuels. It is the next subject to improve the washing efficiency of n-butylamine compounds, such as the pH adjustment.

REFERENCE

[1] G. Uchiyama, S. Fujine and M. Maeda, Nucl. Technol., 120, 41-47, 1997.

[2] N. Uetake, H. Yamamoto, K. Tutumi, Y. Kondou, N. Tamura, M. Ozawa and Y. Kishimoto, J. At. Energy Soc. Jpn., 33, 96-106, 1991.

Radioactive Waste Disposal

This is a blank page.

JP0250358

JAERI-Conf 2002-004

FIELD TRACER MIGRATION TEST IN AQUIFER

-- Tracer Migration Test in Assembly

-- Cooperative Research Program on Safety Assessment Methodology Between CIRP and JAERI--

Yang Yuee*, Wang Zhiming*, Liu Chunli*, Jing Ling*, Jiang Hong*
M.Mukai**, T.Maeda**, J.Matsumoto**, T.Tanaka**, H.Ogawa**

*China Institute for Radiation Protection
270 Xuefu Street, Taiyuan, Shanxi 030006 China
Fax: 86-351-7020407

**Department of Fuel Cycle Safety Research
Tokai Establishment, Japan Atomic Energy Research Institute
Shirakata 2-4,Tokai, Naka, Ibaraki, Japan, 319-1195
Fax: 29-227-5401

ABSTRACT: A field tracer migration test in aquifer at the China Institute for Radiation Protection's field test site is briefly introduced in this paper. Tracer migration test in experimental assembly is the emphasis of the paper. Test conditions and assembly construction are introduced. Assemblies filled with undisturbed aqueous medium were inserted into the aqueous medium through Experimental Shaft wall, in order to acquire the data on tracer migration in aqueous medium. Comparison of migration velocity between ^{3}H and Br^{-} in the assembly is introduced in this paper. The results indicate that Br^{-} migrates at faster velocity than ^{3}H under same condition. Migration velocity, retardation coefficient, distribution coefficient, dispersion coefficient and dispersivity of tracers are evaluated for ^{90}Sr, ^{237}Np and ^{238}Pu from the test results. It is found from the results that the retardation coefficients of ^{90}Sr range from 195 to 251. And the retardation coefficients of ^{237}Np and ^{238}Pu are nigh. Migration distance of ^{90}Sr, ^{237}Np and ^{238}Pu in soil are less, especially, for ^{238}Pu. It is indicated that loess has stronger sorption capacity for the radionuclides. A comparison of nuclide migration pattern suggests that their migration velocity follows $^{90}Sr > ^{237}Np > ^{238}Pu$. It is found that there are the eccentric phenomena of radionuclide migration and effect of humic acid on ^{90}Sr migration.

Key words: field tracer migration test, radionuclide, migration, experimental assembly, ^{3}H, Br^{-}, ^{90}Sr, ^{237}Np, ^{238}Pu

1 FOREWORD

Field tracer migration test in aquifer is an important part of the methodology study on safety assessment of radioactive waste disposal. This test is also the cooperative research between China Institute for Radiation Protection (CIRP) and Japan Atomic Energy Research Institute (JAERI) about "Cooperative Research on Assessment Method on Radiological Safety for Shallow Land Disposal of Low-level Radioactive Waste Phase Ⅱ". The test mainly consists of 3 parts: (a) the tracer migration test in the assemblies (Type I); (b) the radioactive tracer migration test in aquifer with a frame (Type II); (c) the stable element migration test in aquifer (Type III). To understand

the migration differences of non-adsorption tracers, the mixed migration experiments for ^{3}H and Br^{-} were carried out using assembly.
Field tracer migration test was conducted in the Underground Research Facility (URF) of the CIRP's field test site. URF consists of an Inclined Shaft, a Gallery, 3 Vaults and an Experimental Shaft. A plain view drawing of Gallery, Vaults and Experimental Shaft is shown in Fig.1. The depth of URF is 28 m to the ground level. Experimental shaft with a size of 2.5 m diameter × 6 m depth is in the west of Gallery of URF. It penetrated the first phreatic aquifer. Water table is 30 m. Type II and Type III were directly conducted below undisturbed aqueous medium of Vault 1 and Vault 2, and Type I was conducted in the assemblies filled with undisturbed aqueous medium sampled from aquifer. Assemblies were inserted into the aqueous medium through Experimental Shaft wall.

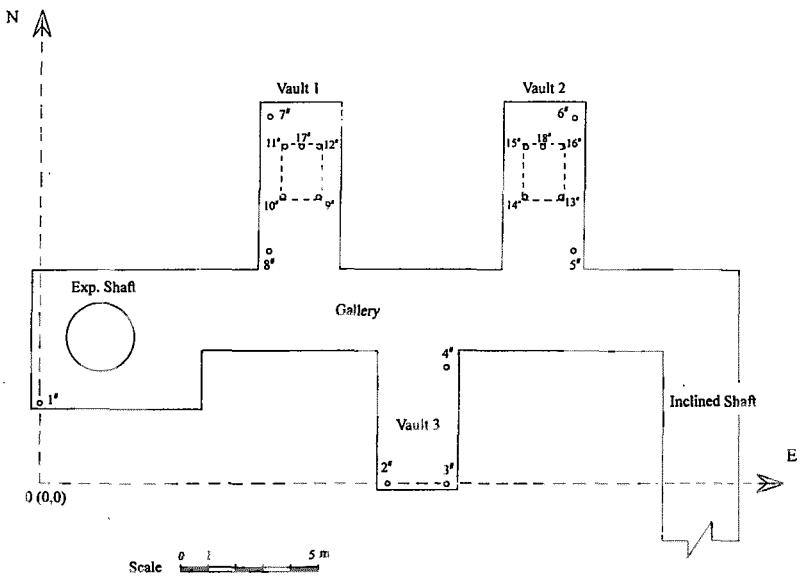

Fig.1 Plain view drawings of Gallery, Vaults and Exp. Shaft

2 EXPERIMENTAL

The purpose of migration test in assembly is to acquire the data on tracer migration in aqueous medium filled the assemblies. 2 kinds of tracers are used for the tests. One includes radionuclides, ^{3}H, ^{90}Sr, ^{237}Np and ^{238}Pu. The other is stable element, Br^{-}, Sr, Nd and Ce. The objective of migration test of ^{3}H and Br^{-} is to get exact groundwater velocity through aqueous medium.
An assembly consists of two columns filled with undisturbed aqueous medium, flange and sampling plate. Fig.2 shows the schematic diagram of the assembly.
The assemblies were inserted aquifer through wall of experimental shaft. One end of the assembly was contact closely with loess of aquifer and groundwater through the assembly flow out from the other end of assembly. The effluent through the assemblies was collected into sample bottle and measured. The tracers in the assemblies disperse and migrate due to water dynamics. The assembly test can confine tracer to a given area.

An entire assembly is designed to consist of two sections of columns, each with a length of 50 cm. The column was designed to have two kinds of inner diameters, Φ 108 and Φ 240, for use in placement of either plane source or point source separately. The column is made of plexiglass. The undisturbed aqueous medium is collected at aquifer layer 3 m vertically below the opening of the experimental shaft. Aqueous medium is loess. The columns' soil was collected at horizontal direction according to actual water flow direction. The measuring results of aqueous medium are: dry bulk density is (1.62±0.10) g/cm^3, water content (v/v) is (42.4±2.2)%.

Tracer absorbed on quartz sand acts as tracer source layer. The size of point source is ϕ 14 mm× 24 mm high. The thickness of plane source is 5 mm.

The effluent through the assemblies was periodically collected in sample bottle, and transported to laboratory for measurement of ^{3}H and Br$^-$.

Assemblies were taken out when test finished. The soil filled the assemblies is cut into one-dimensional sample for Plane Source assembly and two-dimensional sample for Point Source assembly. The number of Point Source samples for each layer is 31. Figure 3 show soil sample distribution in cross-section for the assembly with Φ 240 mm.

Soil samples were put in plastic box. After natural air-dry and weigh, samples were transported to laboratory for measurement.

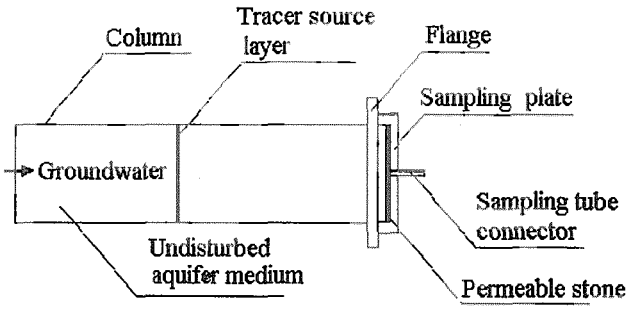

Fig.2 Schematic diagram of assembly

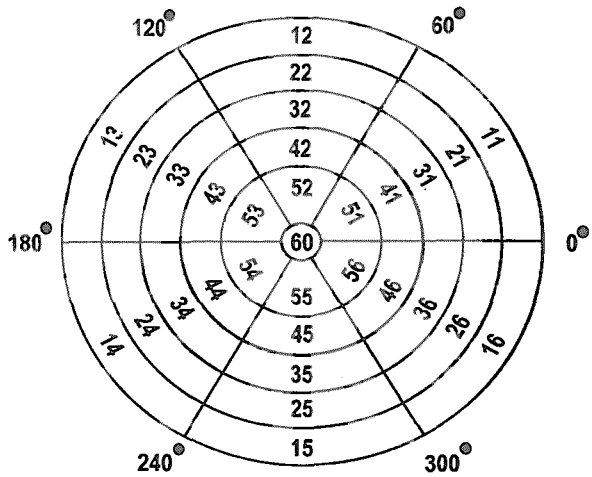

Fig.3 Soil sample distribution in cross-section for the assembly with Φ 240mm

3 EXPERIMENTAL RESULTS AND ANALYSES

3.1 Measurement method of samples

Direct measurement of ^{3}H concentration in water sample was made using Tri-comb 2250 liquid scintillation counter; Br^{-} in water samples was measured with model 721 spectrophotometer. Concentration of Sr, Nd and Ce in water sample was measured using ICP. ^{237}Np concentration in soil samples were first measured with HPGe low energy photo-spectrometry and then, after chemical separation and concentration, the concentration of ^{90}Sr and ^{238}Pu were measured using low background α, β counter and low background α spectrometer respectively.

3.2 Migration of ^{3}H and Br^{-}

(1) Water flow velocity

The pore velocity, u_w, was calculated by the following equation

$$u_w = \frac{L}{t} \tag{1}$$

where, u_w is pore velocity (cm/d), L is distance from source layer (cm), t_0 is time at which peak or mass center appear.

The water velocities during non-adsorption tracer migration test are listed in Table 1. The water velocities during the entire non-adsorption tracer migration test is needed when retardation coefficient Rd and longitudinal dispersivity α_L of radionuclides were calculated. Because the water velocities of some assemblies during the entire non-adsorption tracer migration test are not constant, the water velocities calculated need to be corrected. The correction coefficient of water velocities for assemblies 2, 3, 7 and 8 are 1.26, 1.58, 1.19 and 1.68 respectively.

The pore velocities are listed in Table Ⅰ.

Table Ⅰ Water velocity during non-sorption tracer migration test

Assembly No.	Tracer	Accumulative water volume by peak (L)	L (cm)	Pore velocity (cm/d)
2	^{3}H	1.80	47.6	0.70
3	^{3}H	1.54	45.0	1.71
7	Br^{-}	1.53	48.0	1.40
8	^{3}H	1.61	45.5	1.14

Tracer source layers are plane source in Table Ⅰ. The inner diameter is Φ 108 mm.

(2) Comparison for migration velocity of both ^{3}H and Br^{-}

In order to compare the migration velocities of both ^{3}H and Br^{-} under the same experimental condition, mixed migration experiments for ^{3}H and Br^{-} were conducted using assemblies filled with disturbed aqueous medium.

Based on the results and breakthrough curves, the migration velocities of ^{3}H and Br^{-} were calculated using moment method, as shown in Table Ⅱ. Figure 4 shows the breakthrough curves

of ^3H and Br^- in effluent of the assembly 14#. Similar phenomena also were observed in other tracers mixed migration experiment.

Table II Migration velocities of ^3H and Br^-

Assembly No.	Shape of source	Inner diameter of assembly (cm)	Tracer	Pore velocity (cm/d)
12	Point source	24	^3H	1.04
			Br^-	1.23
13	Point source	29	^3H	0.90
			Br^-	1.05
14	Plane source	29	^3H	1.11
			Br^-	1.31

It can be found from Table II that Br^- migrates at faster velocity than ^3H whatever tracer source layer is point source or plane source when the aqueous medium is loess.

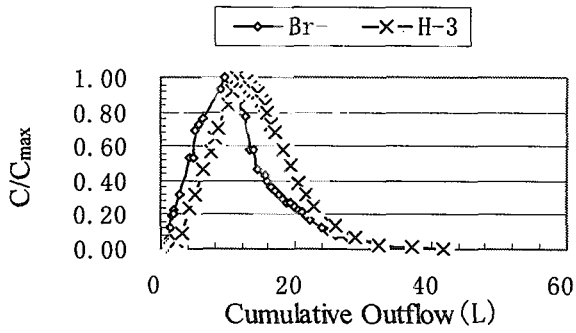

Fig.4 Breakthrough curves of ^3H and Br^- in assembly 14#

3.3 The migration of ^{90}Sr, ^{237}Np and ^{238}Pu

Figure 5 shows longitudinal distribution of the radionuclides in soil.

Migration velocity of tracers can be calculated by the following equation

$$U_N = X_{max}/t \qquad (2)$$

where, U_N is migration velocity of tracer (cm/d), X_{max} is position of peak (or mass center) of tracer (cm), t is test period (d).

The retardation coefficient, Rd, is

$$Rd = \frac{u_w}{U_N} \qquad (3)$$

also

$$Rd = 1 + \frac{\rho \cdot}{n_e} Kd \qquad (4)$$

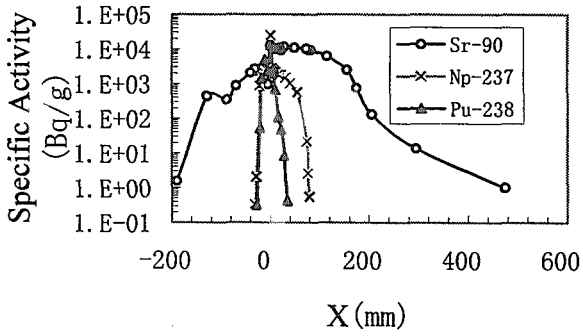

Fig.5 Specific activity distribution of radionuclides in soil of assembly 2# (t=976 d)

Where, Kd is distribution coefficient (ml/g); ρ is dry density of soil, ρ=1.62 g/cm^3; n_e is effective porosity, n_e=0.254.
The fitted results of nuclide migration parameters are listed in Table III. Form of source layer is plane source. It can be found that migration distances of other tracers are very short except ^{90}Sr.

Table III Fitted results of radionuclide migration velocity and other parameters

Assembly No.	t (d)	Radio-nuclides	X_{max} (cm)	Migration velocity U_N (cm/d)	Retardation coefficient Rd	Distribution coefficient Kd (ml/g)
2#	976.3	^{90}Sr	2.95	3.02E-3	290	45.3
		^{237}Np	0.1	1.02E-4	8.60E+3	1.35E+3
		^{238}Pu	0.1	1.02E-4	8.60E+3	1.35E+3
3#	976.0	^{90}Sr	5.25	5.38E-3	502	78.6
		^{237}Np	0.1	1.02E-4	2.64E+04	4.14E+03
		^{238}Pu	0.1	1.02E-4	2.64E+04	4.14E+03
8#	514.0	^{90}Sr	2.05	3.99E-3	481	75.3
		^{237}Np	-0.95	/	/	/
		^{238}Pu	0.55	1.07E-3	1.79E+03	280

Longitudinal dispersion coefficient, D_x, is calculated by

$$D_x = \frac{1}{2}\frac{d\sigma_x^2}{dt} \tag{5}$$

Where, D_x is longitudinal dispersion coefficient (cm^2/d); σ_x^2 is variance of longitudinal concentration distribution (cm^2).
The mass center and variance of concentration of tracers are calculated by moment method. Position of mass center is calculated by first moment

$$x_0(t) = \frac{\int_{-\infty}^{\infty} C(x,t)x\,dx}{\int_{-\infty}^{\infty} C(x,t)dx} = \frac{\sum_i C_i \cdot x_i \cdot \Delta x_i}{\sum_i C_i \cdot \Delta x_i} \tag{6}$$

Where, x_0 (t) is distance of mass center at time t (cm); c (x, t) is concentration of tracer at x and t (Bq/g), x is longitudinal coordinate(cm).
Variance is calculated by quadratic moment

$$\sigma^2 = \frac{\int C(x-x_0)^2 dx}{\int C dx} = \frac{\sum C_i (x-x_0)^2 \cdot \Delta x}{\sum C_i \cdot \Delta x} \tag{7}$$

And the relationship between longitudinal dispersivity, α_L, and longitudinal dispersion coefficient, Dx, is as follows

$$D_x = \alpha_L \cdot u_w \tag{8}$$

The fitted results of longitudinal dispersion coefficient and longitudinal dispersivity are listed in Table IV.

Table IV Fitted results of variance and dispersion coefficient

Assembly No.	t (d)	Pore velocity u_W (cm/d)	Radio-nuclides	Variance σx^2 (cm^2)	Dispersion coefficient D_x (cm^2/d)	Longitudinal dispersivity α_L(cm)
2#	976.3	0.59	^{90}Sr	33.03	1.69E-2	2.28E-2
			^{237}Np	2.90	1.49E-3	2.01E-3
			^{238}Pu	0.50	2.56E-4	3.46E-6
3#	976.0	1.25	^{90}Sr	29.76	1.52E-2	7.72E-3
			^{237}Np	1.611	8.25E-4	4.19E-4
			^{238}Pu	0.662	3.39E-4	1.72E-4
8#	514.0	1.00	^{90}Sr	15.61	1.52E-2	9.05E-3
			^{237}Np	1.911	1.86E-3	1.11E-3
			^{238}Pu	0.338	3.29E-4	1.96E-4

3.4 Effect of humic acid on nuclide migration

Humic acid is placed upstream of tracer source layer in assemblies 3# and 8#. The objective of placing humic acid is to observe effect of it on nuclide migration. Normalized migration velocity, u_g, is used as inter comparison scale. It represents nuclide migration distance at unit time and unit water flow velocity. In other words, it is the nuclide migration velocity at unit water flow velocity.

Comparison is conducted only for the radioactive, ^{90}Sr, because the peaks or mass centers of concentration distribution of the other tracers (^{237}Np and ^{238}Pu) are very short, so it is difficult to compare their migration. The normalized migration velocity of ^{90}Sr is calculated and listed in Table V.

It can be found from the table V that the normalized migration velocity of ^{90}Sr in assembly 2# without humic acid is smaller than those in the assemblies with humic acid whatever according to the peaks or mass centers. This indicates that the humic acid retards migration of ^{90}Sr in Loess. It is difficult to decide whether or not the effect exists for ^{237}Np and ^{238}Pu, because the peaks or mass centers of concentration distribution of them are minor.

Table V Normalized migration velocity of ^{90}Sr

Assembly No.	u_g [(cm/d)/cm/d]		Notes
	By peak	By mass center	
2	3.44E-3	7.42E-3	Without humic acid
3	1.99E-3	3.58E-3	With humic acid 1g
8	2.08E-3	5.52E-3	With humic acid 10g

3.5 Eccentric phenomena of concentration distribution

Assembly 5# was filled undisturbed aqueous medium. The inner diameter of it is Φ240 mm. Tracer source is point source. Figure 6 is radial distribution of ^{90}Sr in soil of assembly 5# when longitudinal distance is 16.5 mm.

It can be found from the figure 6 that the concentration of each sector at downward orientation is larger than the corresponding sector at upward orientation.

As an example, eccentric grade of ^{90}Sr at orientation 52-55 in soil is shown in Fig.7. The eccentric grade, P, is defined as

$$P=A_d/A_u \qquad (9)$$

Where, A_d is specific activity of nuclide at downward orientation, and A_u is specific activity of nuclide at upward orientation.

It is found from the figure that all of the eccentric grades are more than 1. The eccentric grade near tracer source are 1.77~2.84 and the average value is 2.3. Moreover, the eccentric grade decreases with longitudinal distance, x, and tends to 1. The eccentric grades also exist for other nuclides.

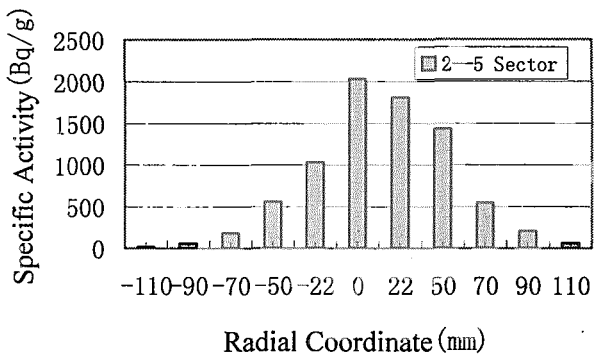

Fig.6 Radial distribution of ^{90}Sr in soil of assembly 5# (x=16.5 mm)

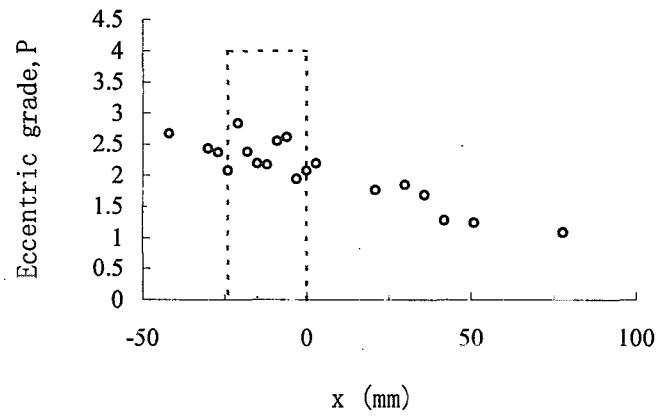

Fig.7 Eccentric grade of ^{90}Sr along orientation 52-55 in soil of assembly 5#
(square frame in Figure represent position of point source tube)

4 CONCLUSION AND DISCUSSION

According to measuring results of effluent and soil samples, some preliminary conclusions were obtained:

(1) As a whole, migration distance of peak or mass center for ^{90}Sr, ^{237}Np and ^{238}Pu in soil are minor. Especially, there is no obvious migration for ^{238}Pu. It is indicated that loess has stronger sorption capacity for the radionuclides.

(2) A comparison of nuclide migration pattern suggests that their migration velocity follows $^{90}Sr > ^{237}Np > ^{238}Pu$.

(3) ^{3}H and Br^{-} are all non-adsorption tracers, but their migration velocities are different. The study of this phenomenon is worth. Br^{-} migrates at faster velocity than ^{3}H. This may be due to that Br^{-} is negative charge. The migration of Br^{-} increases because of effect of exclusion.
(4) It is shown the humic acid retards migration of ^{90}Sr under the same condition (for example, assembly diameter, tracer source type, and tracer quantity). It is difficult to decide whether or not the effect exists for ^{237}Np and ^{238}Pu, because the peak or mass centers of concentration distribution of them are minor.
(5) It can be found from the Figure 7 that eccentric phenomena exist in course of tracer migration in assemblies. The possible reasons are that radionuclides sedimentated down or water flow field is not uniform in this area. This phenomenon should be noted.

This is a blank page.

JP0250359

DIFFUSION COEFFICIENT TEST OF ^{237}Np IN BENTONITE BACKFILL MATERIALS

Anxi Cui*, Zhiwen Fan*, Jinsheng Zhang*, Cunli Gu*
M. Mukai**, T. Maeda**, J. Matsumoto**, T. Tanaka**, H. Ogawa**

*China Institute for Radiation Protection
270 Xuefu Street, Taiyuan, Shanxi 030006 China
Fax: 86-351-7020407, e-mail: cuianxi@hotmail.com

**Department of Fuel Cycle Safety Research
Tokal Establishment, Japan Atomic Energy Research Institute
Shirakata 2-4,Tokai, Naka, Ibaraki, Ja`an,319-1195
Fax: 81-29-227-5401

ABSTRACT: This paper describes the work on diffusion coefficient test of Np in bentonite backfill materials. Due to its very low permeability, diffusion is the dominant migration mechanics in bentonite. The bentonite comes from Inner Mongolia of China. ^{237}Np was used as tracer. The special apparatus for diffusion test was setup, the diffusion coefficient of Np in pure bentonite and sand-bentonite mixture were tested. The tracer was introduced between two bentonite columns. After a specific contacting period, the bentonite columns were taken out and cut to very thin slices. The radioactivity in bentonite slices was analyzed to give the nuclide concentration versus distance curves. The diffusion coefficient could be estimated. The diffusion coefficient of pure bentonite at different density was tested. When the density of pure bentonite samples varied from 1.1, 1.3, 1.5 to 1.7g/ml, their diffusion coefficient were $1.36\times10^{-13}m^2/s$ $1.16\times10^{-13}m^2/s$, $1.07\times10^{-13}m^2/s$ and $8.26\times10^{-14}m^2/s$ respectively. The diffusion coefficient of Np in sand-bentonite mixture sample was $4.13\times10^{-13}m^2/s$. To estimate the distribution coefficient (K_d) value of Np in mixture sample by diffusion method, the diffusion coefficient of Br was measured. The concluded K_d value was 77ml/g for the sand-bentonite mixture. The K_d value obtained by batch test methods was 30ml/g. The reason is related with the error of Br diffusion coefficient and solid-liquid ratio.

Key words: Np, Diffusion coefficient, Bentonite, Backfill materials

1. INTRODUCTION

Disposal is considered as the final solution for radioactive waste. To design the disposal facility, both for I/LLW or HLW, multi-barrier concept is always the important principle to follow for isolating the radioactivity in the disposal site for a long time. Bentonite (some cases the mixture of Bentonite and sand) is usually used as backfill material in radioactive waste disposal facility due to its low permeability and strong sorption ability for radionuclides. Performance assessment study of the disposal facility shows that backfill materials plays important role for the whole system as engineered barrier. Model calculation of the radionuclide migration in the backfill material needs many parameters, of those, diffusion coefficient is the important one. This paper describes the work on diffusion coefficient test of Np in bentonite backfill materials.

The tested bentonite was collected from Inner Mongolia of China (mixture 2 uses the

bentonite from Japan). The chemical composition and properties of the bentonite are given in table I and table II. The diffusion coefficient of pure bentonite was tested for different densities, as 1.1, 1.3, 1.5 to 1.7g/cm3 respectively. The mixture of sand and bentonite was made with sand: bentonite as 85%:15% in weight, the initial water content is 6% for pure bentonite and 10% for mixture. The tracer used in test is ^{237}Np.

Table I chemical composition of bentonite

Components	W, %	Components	W, %	Components	W, %
SiO_2	60.97	TiO_2	0.099	K_2O	0.119
Fe_2O_3	1.26	MnO	0.018	Na_2O	0.75
FeO	0.09	CaO	1.72	P_2O_5	0.030
Al_2O_3	12.69	MgO	2.65	Burnt loss	19.87
Total: 100.26					

Table II Basic properties of the bentonite

Items	value	Items	value
Particle density(g/cm3)	2.61	Cation exchange capacity (mmol/100g)	83.40
Water content(%)	30.44	Exchangeable K^+(mmol/100g)	0.34
Dry bulk density(g/cm^3)	1.31	Exchangeable Na^+(mmol/100g)	1.60
Saturation ratio(%)	80.25	Exchangeable Ca^+(mmol/100g)	52.92
Liquid limit(%)	99.8	Exchangeable Mg^+(mmol/100g)	27.86
PH	7.32	Plastic index	58.8
Total surface area(m^2/g)	617.48	Plastic limit(%)	41.0
Particle distribution(mm , %)			
> 0.25	3.09		
0.25 ~ 0.10	0.92		
0.10 ~ 0.05	22.69		
0.05 ~ 0.01	8.4		
0.01 ~ 0.005	5.2		
< 0.005	59.7		

2. DIFFUSION THEORY

Molecule diffusion in aqueous phase is the dominant mechanism when considering a tracer diffusion in a porous media. The diffusion is caused by chemical potential when the concentration difference existing. Diffusion equation can be described as the Fick's law as following:

$$F = -D \cdot \frac{dC}{d\Delta} \qquad (1)$$

where: F is the solute flow rate in unit time(per second) and unit area (per m^2); D is diffusion coefficient; C is the concentration of the diffusion solute.

$\frac{dC}{d\Delta}$ is concentration difference.

The equation of diffusion in a one-dimension case can be described as Fick's second law

as follows:

$$\frac{dC}{dt} = D \cdot \frac{d^2C}{dx^2} \qquad (2)$$

The solution of equation (2) in the one-dimension case, where the diffusion coefficient is regarded as constant value, and independent of concentration, is written as:

$$C(x,t) = \frac{M}{\sqrt{4\pi Dt}} \exp(\frac{x^2}{4Dt}) \qquad (3)$$

where: t is the diffusion time; x is the diffusion distance; M is the total amount of diffusion species per unit area.
Equation 3 can be rewritten as:

$$\ln C(x,t) = \ln \frac{M}{\sqrt{4\pi Dt}} + \frac{x^2}{4Dt} \qquad (4)$$

The equation shows the relation between concentration and distance under the assumpted condition, that is the lnC has a liner relationship with x^2. If the curve of C and x^2 can be obtained through test, then the diffusion coefficient will be drawn of from the slope of the line[1,2].

3. DIFFUSION TEST AND SAMPLE CUTTING APPARATUS [1,2,3,4,5]

The apparatus for diffusion test consists with two parts: over package and diffusion cell. The specially designed diffusion cell can hold and maintain the specimen as integrated during and after testing. The diffusion cell was put into over package and first was saturated for a certain period of time, then under the saturated condition. The diffusion cell is easy for connection with a sample cutting device. The diagram sketch of the diffusion apparatus is shown in figure1 to figure 3.

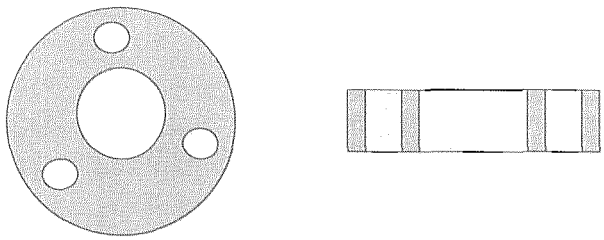

Figure 1. Diagram of diffusion cell from birds view and A-A section

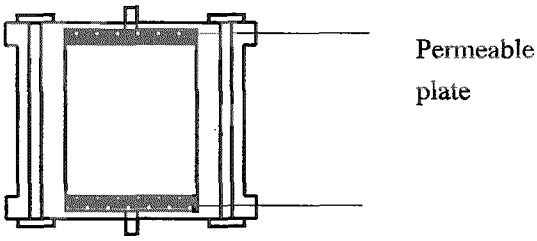

Figure 2. Diagram of diffusion apparatus over package

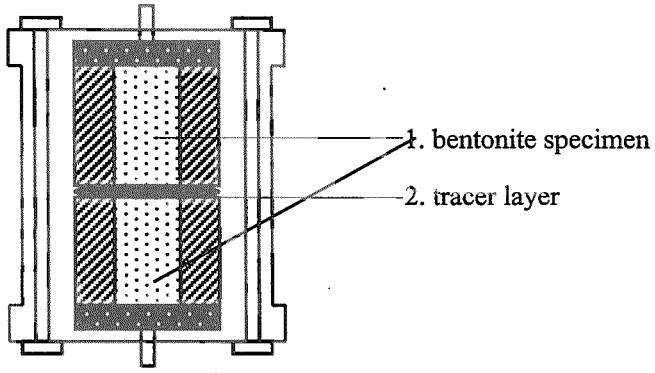

Figure 3. Diagram of inside view for diffusion apparatus

For the test specimen preparation in diffusion cell, the certain amount of bentonite estimated by the expected density was put into the cell and compacted. The same two diffusion cells with bentonite specimen were set in one over package and saturated by pressured water. After two months contacting with pressure water, the bentonite column was saturated. Then the ^{237}Np tracer was introduced between the two cells. The contacting time for ^{237}Np and diffusion column was about 50 days. And the diffusion column was taken out for cutting to thin slices.

Sample cutting apparatus was designed with screw thread for the distance counting. When the screw turning for one rotation, the screw was push forward for 1 mm. Thus according to the angle the screw turned, an expected distance of specimen can be put out of the cell for cutting. Experiments showed the pure bentonite specimen could be cut to a 0.2 mm thin slices. The diagram of the cutting device is ahown in figure 4.

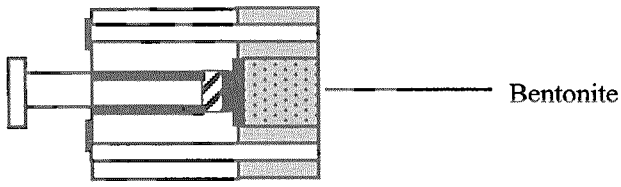

Figure 4. Sample cutting apparatus

In fact, after contacting with ^{237}Np tracer, the diffusion cells were taken out and the bentonite column was cut to a 0.5 or 1.0mm slices, air dried for two weeks for sample analysis. The measurement of the sample was done by a γ spectrometer for the Np concentration in each sample. And the calculated lnC was obtained to draw the curve of lnC versus x2, then the diffusion coefficient can be estimated according to equation 4. The density of pure bentonite samples varied from 1.1, 1.3, 1.5 to 1.7g/cm^3 in experiment, and the sand –bentonite mixture is 1.85g/cm^3.

4. RESULTS

The diffusion test results for different density of bentonite are shown in figure 5 to figure

10. The equation in the figure is the regression results of the tested data. The estimated diffusion coefficient is listed in table III.

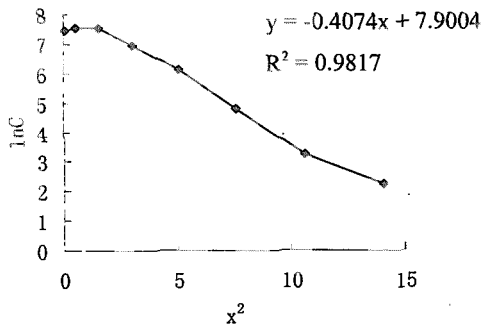

Figure 5 Diffusion curve of Np in bentonite ρ=1.1g/cm³, contacting time 50 days

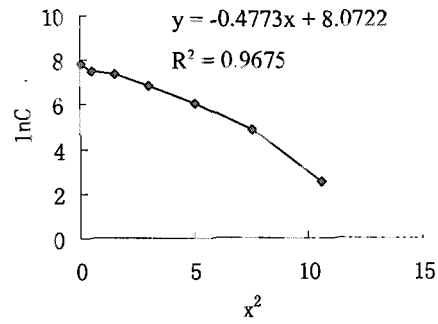

Figure 6 Diffusion curve of Np in bentonite ρ=1.3g/cm³, contacting time 50 days

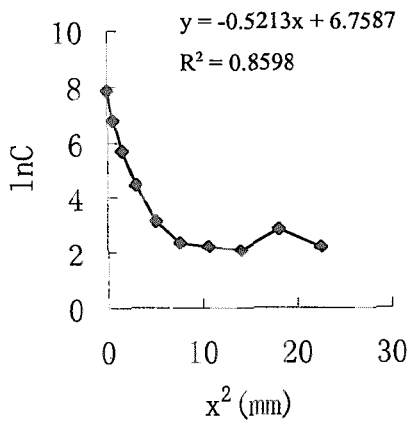

Figure 7 Diffusion curve of Np in bentonite ρ=1.5g/cm³, contacting time 50 days

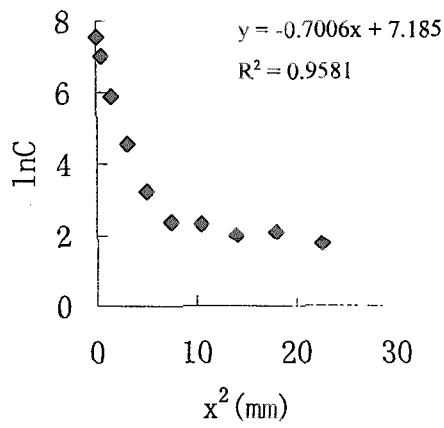

Figure 8 Diffusion curve of Np in bentonite ρ=1.7g/cm³, contacting time 50 days

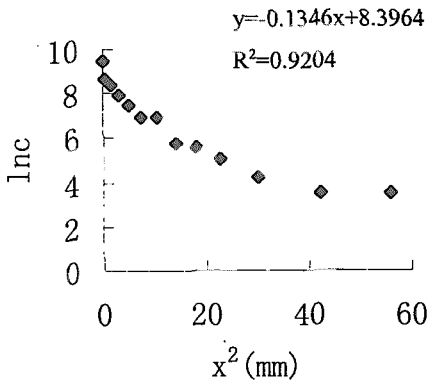

Figure 9 Diffusion curve of Np in mixture1 ρ=1.85g/cm³, contacting time 50 days

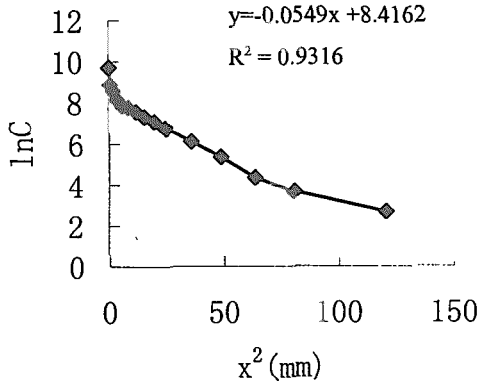

Figure 10 Diffusion curve of Np in mixture2 ρ=1.85g/cm³, contacting time 50 days

Table III. Diffusion coefficients (m^2/s) of Np in Bentonite

Sample No.	media	Density(g/cm^3)	Regressed equation	Diffusion coefficients (m^2/s)
1	Bentonite	1.1	$\ln C=-0.4074x^2+7.9004$	1.36×10^{-13}
2	Bentonite	1.3	$\ln C=-0.4773x^2+8.0722$	1.16×10^{-13}
3	Bentonite	1.5	$\ln C=-0.5213x^2+6.7587$	1.07×10^{-13}
4	Bentonite	1.7	$\ln C=-0.7006x^2+7.185$	8.26×10^{-14}
5	Mixture1	1.85	$\ln C=-0.1346x^2+8.3964$	4.13×10^{-13}
6	Mixture2*	1.85	$\ln C=-0.0549x^2+8.4162$	1.01×10^{-12}

*Mixture2 used the Japan Bentonite Kunigel-V1

4.1 The diffusion coefficient becomes lower with the density increased, this is because of the lower porosity and thus the lower water content.

4.2 The addition of sand caused the diffusion coefficient also decreased because of the lower adsorption ability of mixture.

4.3 The diffusion coefficient of pure bentonite at different density was tested. When the density of pure bentonite samples varied from 1.1, 1.3, 1.5 to 1.7g/ml, their diffusion coefficient were $1.36\times10^{-13}m^2/s$ $1.16\times10^{-13}m^2/s$, $1.07\times10^{-13}m^2/s$ and $8.26\times10^{-14}m^2/s$ respectively. The diffusion coefficient of Np in sand-bentonite mixture1 sample was $4.13\times10^{-13}m^2/s$ and mixture2 $1.01\times10^{-12}m^2/s$.

4.4 To estimate the distribution coefficient (K_d) value of Np in mixture sample by diffusion method, the diffusion of non-adsorption species Br^- (added as KBr) in mixture was conducted. The diffusion coefficients of Br in mixture1 and mixture2 were $1.55\times10^{-10}m^2/s$ and $2.80\times10^{-10}m^2/s$, the concluded K_d value were 77ml/g and 54ml/g[1]. However, the K_d value obtained by batch test methods was 30ml/g and 24ml/g respectively. The reason is related with the error of Br diffusion coefficient and solid-liquid ratio.

Reference:

1. Yngve Albinsson, Radioactive Waste Management and Nuclear Fuel Cycle, 1991,Vol.15(4), pp. 221-239.

2. Yao Jun et al., Diffusion of ^{237}Np in Bentonite, China Institue of Atomic Energy, 1998.

3. Xu Guoqiang et al., Diffusion Study of Cs-137, Pu-239, Am-241 in Bentonite, Beijing Geological Research Institute of Nuclear Industry. 1997.

4. Masaki Tsukamoto, Radiochimica Acta 66/67, 397-403(1994).

5. Zhou Kanghan, Performance Study of Backfill Materials for Geological Disposal of HLW, pp.98-106, Thesis Application for Doctor Degree of Qinghua University, 1997.

JP0250360

JAERI-Conf 2002-004

STUDY ON THE DISTRIBUTION COEFFICIENT FOR EVALUATION OF NEPTUNIUM MIGRATION IN LOESS MEDIA

--- Cooperative Research Program on Field Migration Test between CIRP and JAERI ---

Tadao TANAKA*, Toshikatsu MAEDA*, Masayuki MUKAI*,
Junko MATSUMOTO*, Hiromichi OGAWA*,
Zhentang LI**, Hongqing ZHANG**, Xudong WANG**, Anxi CUI**, Liangtian GUO**

* Department of Fuel Cycle Safety Research,
Tokai Establishment, Japan Atomic Energy Research Institute,
Shirakata 2-4, Tokai, Naka, Ibaraki, Japan, 319-1195.
Fax: 81-292-282-5934, e-mail: tanaka@sparclt.tokai.jaeri.go.jp

** China Institute for Radiation Protection,
270 XueFu Street, Taiyuan, Shanxi 030006, China.

We have performed adsorption experiments of ^{237}Np onto the loess by a batch system, migration experiments of ^{237}Np through the loess media by a column system, and migration tests of ^{237}Np through natural loess media in the field test site of CIRP, Shanxi, China. The valid distribution coefficient (K_d) value was determined on the basis of the ^{237}Np concentration in both the static batch and the dynamic column experiments. An adsorption ratio corresponding to the ^{237}Np concentration at the peak position of the ^{237}Np migration through the column was calculated from the adsorption isotherm. The apparent K_d calculated was in well agreement with the K_d value estimated from the migration behavior of ^{237}Np in the migration system. The valid K_d value of ^{237}Np, of which specific activity is very low due to a long half-life, can be determined in the batch and column systems. Applicability of the K_d determined by the batch system into the evaluation of radionuclide migration was confirmed through analyses of the result obtained from the ^{237}Np migration test in natural loess media.

Key words: Adsorption, ^{237}Np, Loess, Migration, Distribution coefficient

1. INTRODUCTION

Low-level radioactive waste disposed to geologic media can migrate into the biosphere with circulating groundwater, accompanied with retardation by adsorption onto the geologic barrier. Thus, understanding the retardation process in radionuclide migration is important in the assessment of radioactive waste disposal sites. The retardation process can be conservatively quantified by using simple thermodynamic equilibrium: distribution coefficient (K_d) that is defined by the ratio of radionuclide concentrations on geologic media and in groundwater[1],[2]. The K_d has been generally determined from adsorption equilibrium in a static batch system, despite adsorptive conditions in the batch system are different from those in the dynamic migration system. Therefore, there is a need to validate whether K_d values obtained from the batch system are adequate to estimate the migration behavior of radionuclides through the geologic media.

JAERI and China Institute for Radiation Protection (CIRP) have studied on the migration behavior of some elements including transuranic radionuclides in natural environment, under the cooperative research project[3],[4]. In the research project, we have performed adsorption experiments of ^{237}Np in a batch system to provide relevant adsorption data of ^{237}Np onto the loess, migration experiments of ^{237}Np in a column system to elucidate the migration behavior of ^{237}Np through the loess media, and we have also conducted migration tests of ^{237}Np through natural loess media in the field test site of CIRP, Shanxi, China. In the present study, we discuss on determination methodology of valid K_d value to evaluate quantitatively the migration behavior of ^{237}Np through the loess. In addition, applicability of the K_d determined by the batch system into the evaluation of radionuclide migration was discussed through analyses of the result obtained from the ^{237}Np migration test in natural loess media.

2. BATCH ADSORPTION EXPERIMENTS

2.1 Loess sample, radionuclide and solution

The loess samples collected from the aerated zone and the aquifer zone of the field test site of CIRP was used in this experiment. The loess was sieved to remove coarse particles larger than 0.5 mm. Nitrates of $^{237}NpO_2^+$ was used for the experiment. An equilibrated solution using for experiment was prepared as follows: the loess sample amounting to 5 g had been contacted with 100 cm^3 of deionized water for 7 days. The solution was filtered using Millipore filters of 450 nm pore diameter. The solution phase separated by the filtration was used as the equilibrated solution.

2.2 Experimental procedure

The loess sample amounting to 0.5 g had been contacted with 10 cm^3 of deionized water for 7 days. Then 0.1 cm^3 of ^{237}Np stock solution was added. The temperature was controlled at 25 ℃ by using an air circulation box. The solution containing the sample was gently agitated on a shaker at 60 rpm for 7 d. After the adsorption process of 7 d in the contact time, the solution was filtered using Millipore filters of 450 nm pore diameter. Concentration of ^{237}Np in the filtrate was measured using a γ -ray detector.

Distribution coefficient of ^{237}Np, K_d^{ads} (cm^3/g), was calculated by

$$K_d^{ads} = \frac{C_0 - C}{C} \frac{V}{W}, \quad (1)$$

where C_0 is the initial concentration of ^{237}Np in solution (Bq/cm^3), C the concentration of ^{237}Np solution after the adsorption process (Bq/cm^3), V the volume of solution (cm^3), W the weight of loess sample (g).

2.3 Adsorption properties of ^{237}Np

Specific activity of ^{237}Np is very low, due to a long half life. The concentration of ^{237}Np applying in the present experiments is in about 10^{-9} - 10^{-5} mol/dm^3. In higher concentration range, the adsorption isotherm of ^{237}Np may be not based on Henry's type. If so, the adsorption properties of ^{237}Np on the loess are affected by its concentration.

Figure 3 shows the adsorption isotherm of ^{237}Np on the loess. Plot of lnQ versus lnC was in a linear relation. This result indicates that the adsorption isotherm of ^{237}Np is based on Freundlich's type:

$$Q = aC^{1/n}. \quad (1<n<10) \quad (2)$$

Hence,

$$K_d^{ads} = aC^{(1-n)/n}, \quad (3)$$

where a and n are constant.

Thus relationship between ^{237}Np concentration and apparent K_d^{ads} is given by $K_d^{ads} = 4 \times 10^2 C^{-0.42}$ or $K_d^{ads} = 3 \times 10^4 Q^{-0.72}$. The relationship between ^{237}Np concentration and apparent distribution coefficient K_d^{ads} corresponding to the ^{237}Np concentration (Q) adsorbed on the loess is shown in **Fig.4**. The K_d^{ads} values decreased with increasing ^{237}Np concentration. In the migration test of ^{237}Np, such as column experiments and field test, the ^{237}Np concentration is expected to vary in wide ranges during the test period. In such cases, it is necessary to take account of the influence of ^{237}Np concentration into the evaluation of ^{237}Np migration.

In the migration test, information relating to ^{237}Np concentration through a media for K_d determination was the ^{237}Np concentration introduced into the media and the concentration peak of ^{237}Np migrated through the media. The ^{237}Np concentration introduced into the

media is defined as an initial concentration; C_0 in the case introduced as a solution or Q_0 in the case introduced as a raveled soil. The concentration peak of ^{237}Np migrated through the media is indicated by the peak dissolving in solution phase C_m, which is observed in breakthrough curves of ^{237}Np concentration in solution phase, or the peak adsorbing on solid phase Q_m, which is observed in distribution profiles of ^{237}Np in the media. Based on the C_0, Q_0, C_m or Q_m, valid K_d value for the migration evaluation may be estimated from the results obtained in the batch adsorption experiments.

3.DISTRIBUTION COEFFICIENTS FOR ANALYSES OF RADIONUCLIDE MIGRATION

In the porous loess media, ^{237}Np migration with water movement is expressed by the equation[1]:

$$\frac{\partial C}{\partial t} + \frac{\rho}{\theta}\frac{\partial Q}{\partial t} = D\frac{\partial^2 C}{\partial X^2} - V\frac{\partial C}{\partial X} \tag{4}$$

where C is ^{237}Np concentration in solution (Bq/cm^3), Q concentration of ^{237}Np adsorbed on porous loess media (Bq/g), ρ density of loess media (g/cm^3), θ water content, D dispersion coefficient (cm^2/min), V velocity of water (cm/min), t time (min), X length (cm).

Provided the reaction of ^{237}Np between solution and loess media is based on the instantaneous reversible reaction, the migration of ^{237}Np can be explained by introducing the distribution coefficient:

$$Q = K_d^{mig} C \tag{5}$$

and

$$R_f = 1 + \frac{(1-f)\rho}{\theta} K_d^{mig} \tag{6}$$

where f porosity, K_d^{mig} distribution coefficient in migration system (cm^3/g), R_f retardation factor.

Substituting Eq.(5) and (6) into Eq.(4), we obtain

$$\frac{\partial Q}{\partial t} = \left(D\frac{\partial^2 Q}{\partial X^2} - V\frac{\partial Q}{\partial X}\right)\frac{1}{R_f}. \tag{7}$$

Therefore, if the values of K_d^{mig}, V and D in the column system are known, one-dimensional concentration distribution of ^{237}Np in the loess media can be estimated by solving Eq.(7). On the other hand, if the K_d^{mig} value is unknown, it can be determined by fitting the concentration distribution calculated from the Eq.(7) to that obtained in the migration experiment, under the available initial and boundary conditions[5],[6].

4.MIGRATION TESTS OF NEPTUNIUM

Migration tests on the cooperative research program consist of tracer migration tests in aerated and aquifer zones at a CIRP's field test site, large scale simulation test, fundamental laboratory experiment. Details of these migration tests were reported elsewhere[3],[4]. Schematic illustration of each migration test is shown in **Fig.5**, together with the test results obtained as migration behavior.

(1) Fundamental experiment by small-scale column (MT-1)

The column made of Teflon was 2.5 cm in inner diameter and 5 cm in height, and it had membrane filters, 5 μm pore size, at the top and the bottom. A loess layer was prepared by charging 32.1 g of the loess into the column to make a bed thickness of 5 cm. Bulk density

and porosity of the loess layer were 1.31 g/cm^3 and 48 %. After the loess layer was contaminated by passing through 5 cm^3 of the ^{237}Np solution, a total of 500 cm^3 of the equilibrated solution was fed into the contaminated loess layer, from the bottom at a flow rate of *ca.* 0.5 cm^3/min by a micro tube pump. At the end of the experiment, loess samples were taken from the column at every 0.5 cm section in depth. The water velocity, V, and the dispersion coefficient, D, in the present experimental system had been found to be 0.19 cm/min and 0.028 cm^2/min, respectively, from breakthrough property of tritiated water as a non-reactive tracer.

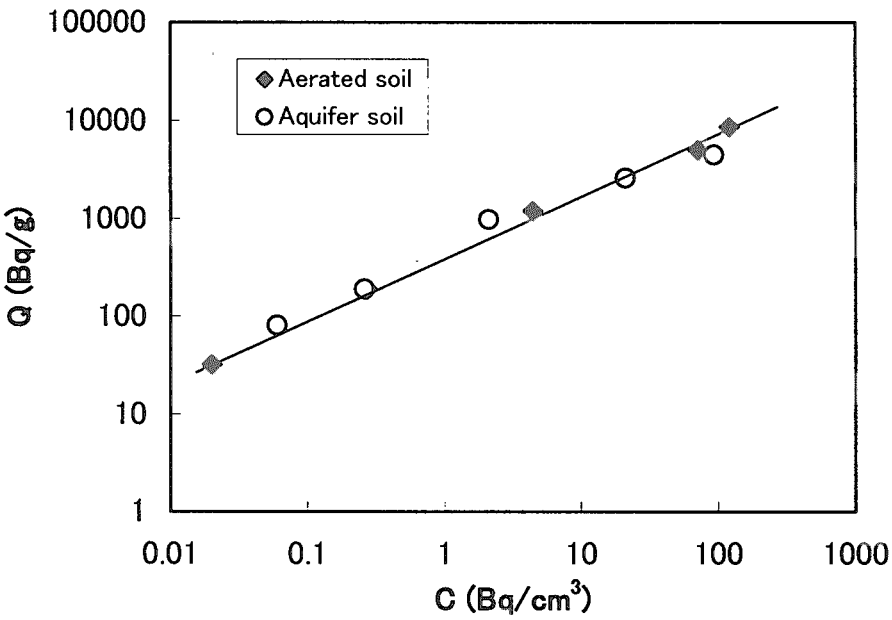

Fig.3 Adsorption isotherm of ^{237}Np on the loess.

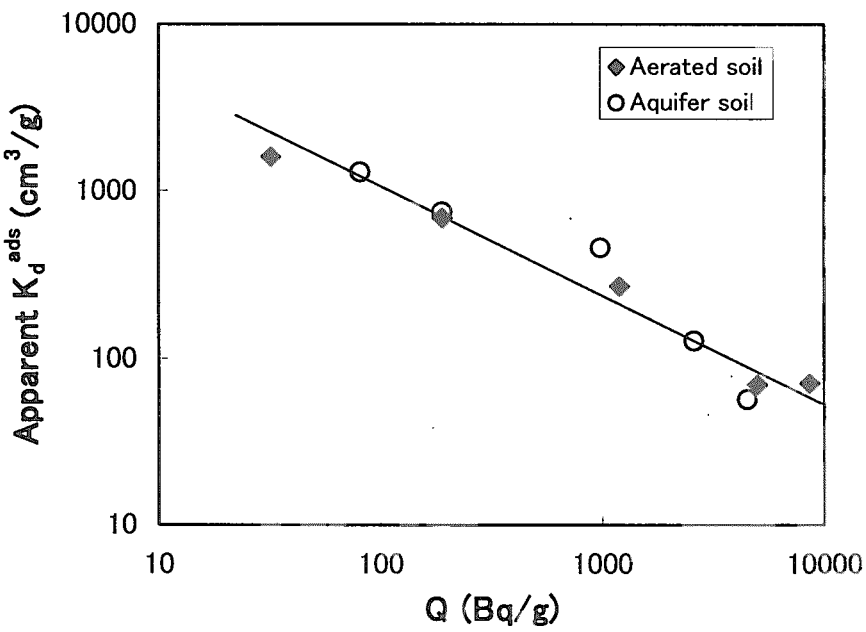

Fig.4 Influence of ^{237}Np concentration Q on K_d^{ads}

(2) Simulation tests by large-scale column (MT-2 and MT-3)

Demonstrative simulation test by large-scale column was conducted in laboratory of the CIRP, using undisturbed soil samples taken from the aerated zone and the aquifer zone in the field test site. Two sets of equipments were provided to perform each migration test; one is tested for 1.5 years and the other for 3 years. The undisturbed soil column for the aerated zone test (MT-2) had 28 cm in diameter and 120 cm in height, and it had disturbed soil layers at the top and the bottom, a wick rope that reduced water content in the column and a sprinkler. Quartz sand with 60-80 mesh mixed with tracer solution was placed on the undisturbed soil to be made a bed thickness of 5 mm. Distilled water was used as test water and the averaged sprinkling density was 5.5-5.6 mm/d for each column.

The soil tank set the undisturbed soil of 80 x 30 x 30 cm was prepared for the aquifer zone test (MT-3). A point source with 4 cm ϕ x 4 mm, which was mixture of the quartz sand and tracer, was placed on the center axis at a distance of 10 cm from the inflow section. The groundwater was directly introduced into the test tanks through a pump.

(3) *In-situ* migration tests in aquifer zone (MT-4)

The *in-situ* column tests were conducted using an undisturbed soil column referred as assembly, in the Underground Research Facility (URF). Two sizes of tracer source were applied; one is point source with 2.3 cm ϕ x 1.8 cm, and the other is plane source with a thickness of 5 mm (Assy 2 and Assy 3). Both are mixture of tracer and the quartz sand. Tracer migration in the assembly is tested by directly installing the assembly from the experimental shaft wall into the aquifer. Flow rate of the groundwater was controlled by an attached valve on the end of out flow port.

(4) Field migration tests in aerated zone (MT-5 and MT-6)

The pits for the tests were dug to 50 cm deep from the ground surface. Tracer source material placed on the bottom with 120 x 50 cm and thickness of 7 mm, and then the pit was filled with loess soil up to ground surface level. The quartz sand is used as the tracer source material for the tests under artificial rainfall condition (MT-5) while loess soil for the tests for natural rainfall condition (MT-6). The intensity of the artificial rainfall is controlled at a rate of 5mm/h and each pit is showered for 3 hours a day.

(5) Field migration test in aquifer zone (MT-7)

The test pit was provided in the URF for testing three dimensional migration behavior of tracer elements under natural groundwater flow condition. The dimension of the pit was 2 m long and 1.5 m in width. In the pit, one tracer injection pipe and twelve sampling pipes were inserted into the aquifer layer up to the depth of about 2.6 m below the floor of the URF.

5.DETERMINATION OF VALID DISTRIBUTION COEFFICIENT

Results of the adsorption experiments showed that the adsorption properties of ^{237}Np on the loess are affected by its concentration and relative K_d^{ads} of ^{237}Np between loess and solution decreased with increasing ^{237}Np concentration. In the present migration tests, information relating to ^{237}Np concentration through a media for K_d determination was the ^{237}Np concentration introduced into the media and concentration peak of ^{237}Np migrated through the media. Based on the concentration peak adsorbing on the loess, which was observed in distribution profiles of ^{237}Np in the media as shown in Fig.3, valid K_d value for the migration evaluation was estimated from the results obtained in the batch adsorption experiments. K_d^{mig} value was determined by fitting the concentration distribution calculated from the ^{237}Np migration model of Eq.(7) to that obtained in the migration tests (in Fig.5).

MT-1

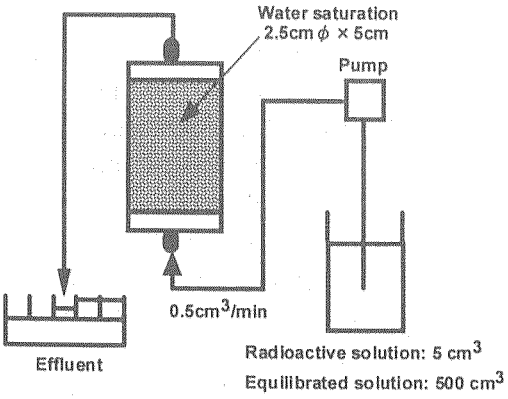

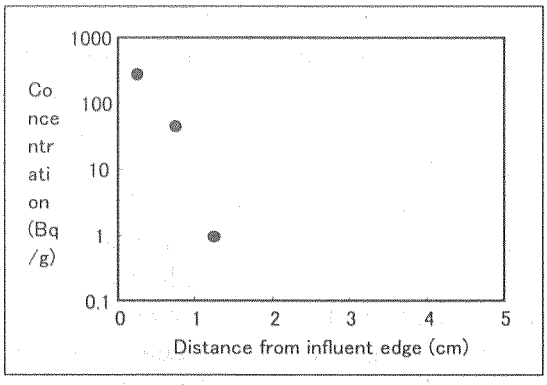

MT-2

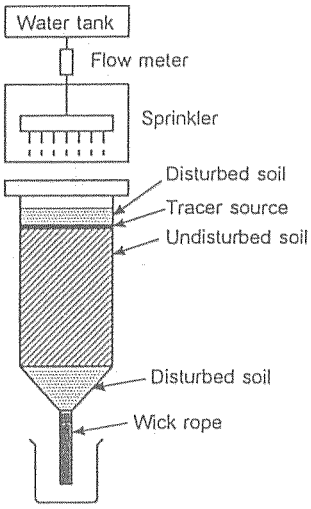

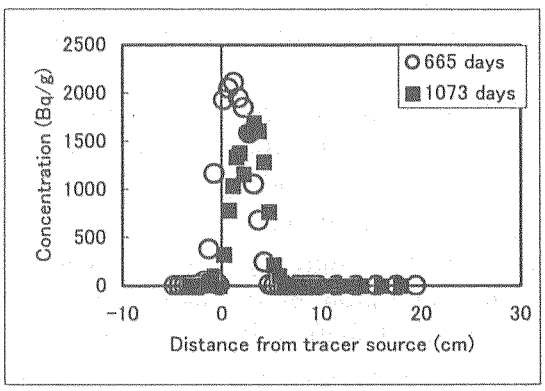

MT-3

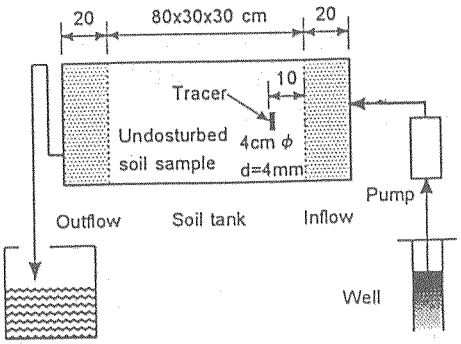

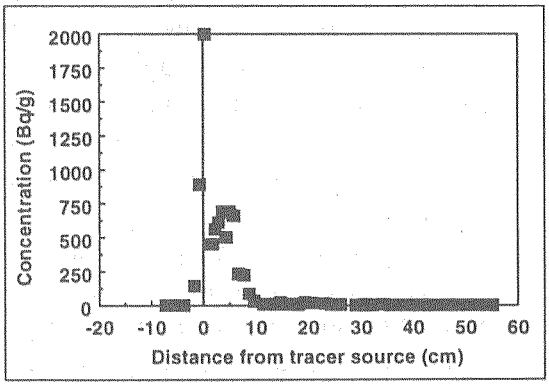

MT-4

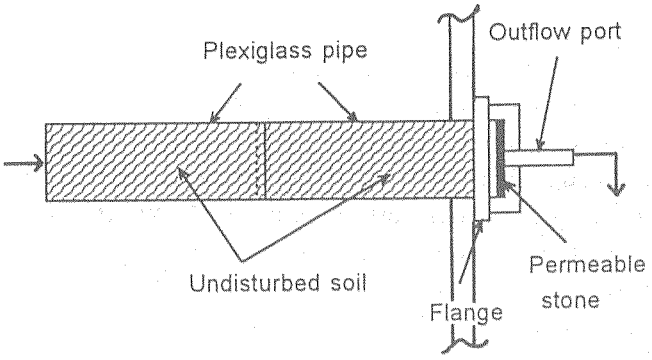

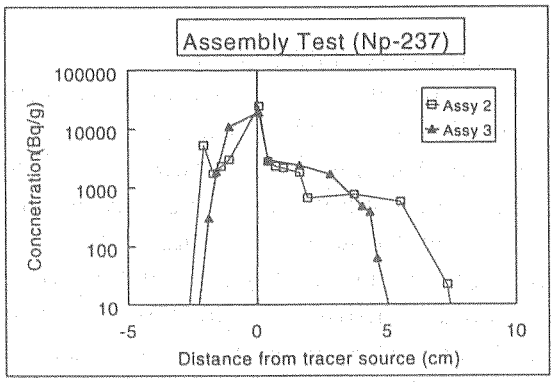

Fig.5 (a) Migration tests conducted under the cooperative research project[3],[4].

MT-5

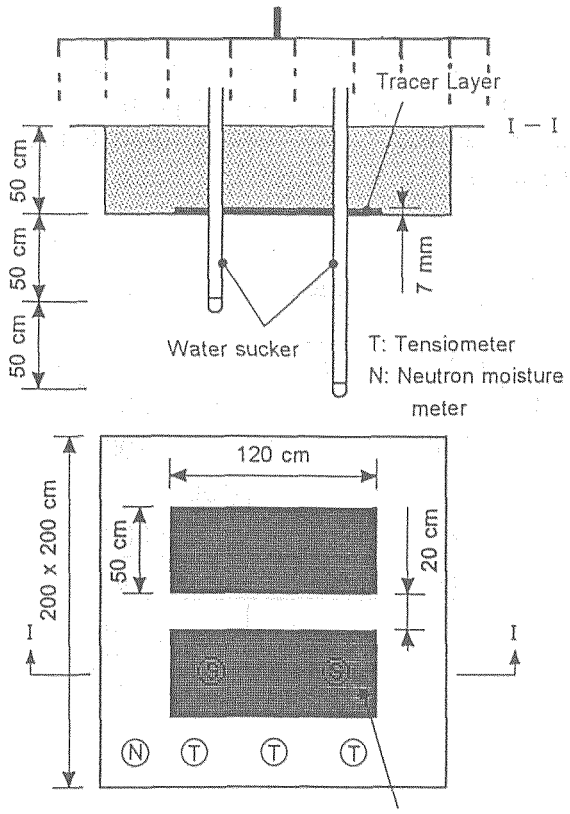

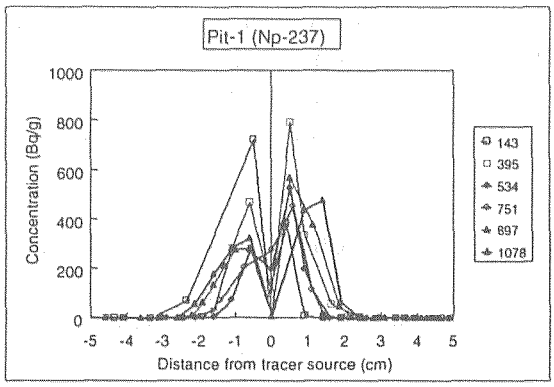

MT-6

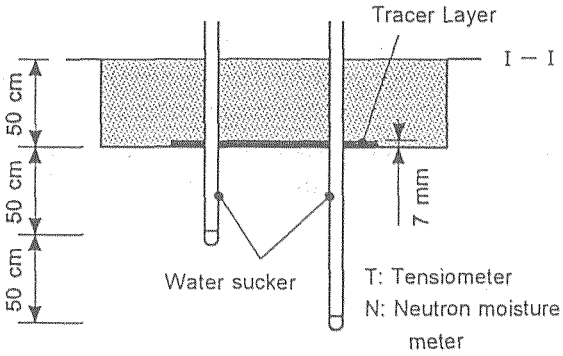

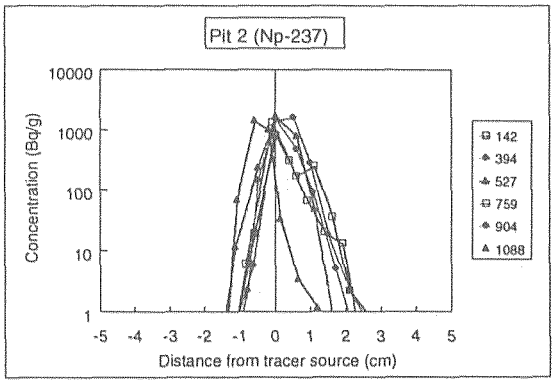

MT-7

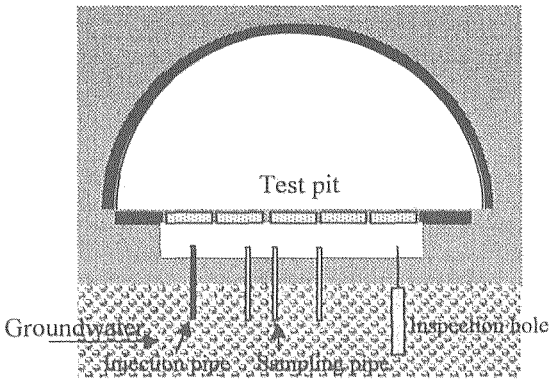

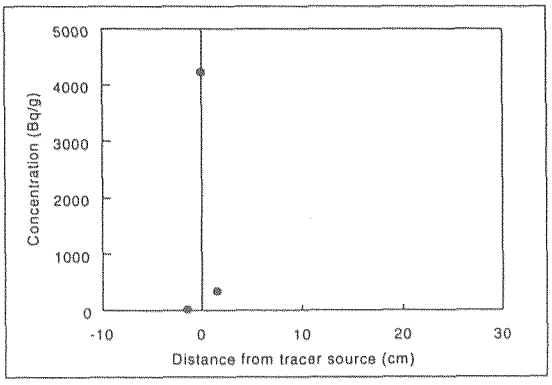

Fig.5 (b) Migration tests conducted under the cooperative research project[3],[4].

The K_d^{ads} calculated was in well agreement with the K_d^{mig} value estimated from the migration behavior of ^{237}Np in the column system. In the MD-6 and MD-7 of the field tests, their K_d^{mig} values could not calculated since the peak of ^{237}Np concentration did not move. On the other hand, we had clarified that the concentration distribution profiles of ^{237}Np in MD-6 and MD-7 could be estimated by using mean K_d^{ads} value 200 cm^3/g, calculated from K_d^{ads} values from migration test number MD-1 to MD-5[4].

Table I Comparison between K_d^{ads} and K_d^{mig} in the migration tests.

Test No.	Q (Bq/g)	K_d^{ads} (cm^3/g)	K_d^{mig} (cm^3/g)
MD-1	300	490	300 - 500
MD-2	1700 - 2100	120 - 140	110 - 200
MD-3	800 - 900	220 - 240	190
MD-4	1000 - 3000	90 - 210	110 - 390
MD-5	450 - 800	240 - 370	55 - 190
MD-6	1000	200	- (200)
MD-7	4200	70	- (200)

6.CONCLUSIONS

The adsorption properties of ^{237}Np on the loess are affected by its concentration and apparent K_d^{ads} decreased with increasing ^{237}Np concentration. Apparent K_d^{ads} corresponding to the ^{237}Np concentration at the peak position of the ^{237}Np migration through the column was calculated from the adsorption isotherm, and it was in well agreement with the K_d^{mig} value estimated from the migration tests. The valid K_d value can be determined on the basis of the ^{237}Np concentration in both the static batch and the dynamic column experiments.

REFERENCES

[1] Y.Inoue, W.J.Kaufman: *Health Phys.*, **9**, 705 (1963).
[2] H.M.Selim, J.M.Davidson, P.S.C.Rao: *Soil Sci.Soc.Am.J.*, **41**, 3 (1977).
[3] M.Mukai, *et al.*: *J.Nucl.Fuel Cycle and Environ.*, **7**, 31 (2001).
[4] CIRP and JAERI: "*Final report: Cooperative Research Program on Field Migration Test between CIRP and JAERI*", (2001), in press.
[5] H.Kamiyama, et al.: *JAERI-Research 94-009*, (in Japanese), (1994).
[6] T.Ohnuki, S.Takebe, T.Yamamoto: *J.Nucl.Sci.Technol.*, **26**, 795 (1989).

JP0250361

JAERI-Conf 2002-004

ANALYSIS OF FIELD TEST OF NUCLIDE MIGRATION IN AERATED LOESS LAYER

- Cooperative Research Program on Field Migration Test between CIRP and JAERI -

M.Mukai, T.Tanaka, T.Maeda, J.Matsumoto, H.Ogawa,
Jinsheng Wang*, Shushen Li*, Yingjie Zhao*, Qinghua Wu*, Zhiming Wang*
Japan Atomic Energy Research Institute, Tokai, Ibaraki, 319-1195 Japan
Fax: 81-292-82-5934, e-mail: mukai@sparclt.tokai.jaeri.go.jp
* China Institute for Radiation Protection,
XueFu Street 270, Taiyuan, Shanxi, 030006 China

Field test of nuclide migration has been conducted as a cooperative research program between JAERI and CIRP. In the program, nuclide migration in aerated loess layer has been tested to evaluate conventional migration model demonstratively. Using the values determined from laboratory tests, concentration distribution of field test has been estimated. The estimation showed difference with the actual distribution in view of the movement of concentration peaks. From the observation on water potential, adjustment was needed for water flow rate. Two values of water flow rate, 0 and 0.86 cm/d from supplemental tests, were used for the re-estimation of Sr-90 migration. Between these, 0 cm/d showed better agreement to the concentration distribution corrected with recovery ratio and fitting analysis showed very low water flow rate of 0.135 cm/d. Dispersivities calculated using 0.135 cm/d of water flow rate for Sr-90 and Np-237 were almost a half as small as those obtained by fitting analysis because of difference of water saturation condition between estimation and the actual test. Though some care was needed to determine water flow rate and dispersivity, the conventional migration model was able to estimate nuclide migration in natural aerated loess layer as long as obtained an appropriate set of parameter values.
Key words: Radionuclide migration, Field test, Aerated layer, Loess, Cooperative research

1. INTRODUCTION

Migration of radionuclide in geologic media is generally evaluated using a migration model on the basis of combined equation for advection and dispersion by groundwater flow together with adsorption onto geologic media. This model has been included into a part of safety assessment for low level radioactive waste in shallow land disposal, because this is a single existing model practically applicable to actual situation. Though this migration model has been applied to various scale laboratory experiments with satisfactory results, there has still been uncertainty in the applicability to migration in natural environment specially for transuranic nuclides. Thus, to demonstrate the applicability of the migration model to the nuclide migration in natural environment is one of most important issue to secure the reliability of safety assessment.

Japan Atomic Energy Research Institute (JAERI) and China Institute for Radiation Protection (CIRP) have been conducted field migration tests of radionuclides as a cooperative research program[1]. In the program, a field test of radionuclide migration in aerated loess layer has been performed at the CIRP's field test site. Tracing test in aerated layer was performed to observe tracer migration behavior in loess soil using the radioactive tracers of Sr-90, Np-237, Pu-238 and H-3 and stable element tracers of Sr, Nd, Ce and Br. Four pits were provided for tests under artificial rainfall condition by regular water showering and five pits were for natural rainfall

condition. Soil samples were taken several times to observe migration behavior of tracers. Laboratory experiments by batch and column method were also performed to provide Kd and dispersivity for migration model to analyze the results of the field test.

Primary objective of this study is to evaluate the applicability of conventional migration model to estimate TRU radionuclides migration in natural loess layer. To accomplish this objective, following procedure has been performed:

1) Obtain the values of input parameters to migration model, using the information which is available from the information sources of the site investigation, laboratory experiments, test condition of the field migration tests before the finish of field test.

2) Comparison of migration distributions between estimated by the model using the determined values of input parameters and the actual field migration tests.

3) Discussion on the comparison. If there is difference between the distributions, review the values of input parameters and migration model.

2. ANALYSIS MODEL AND NECESSARY PARAMETERS

2.1 Migration model for calculation

A migration model to be evaluated is conventionally applied to the field of study on radionuclide migration:

$$\partial C/\partial t + (1 - f)\rho/\theta \cdot \partial Q/\partial t = D(\partial^2 C/\partial x^2) - Vx(\partial C/\partial x) \quad (1)$$

$$Q = Kd \times C \quad (2)$$

where, Q represents concentration of radionuclide in soil, C that in water, D dispersion coefficient, Vx water flow rate in x direction, f porosity, ρ specific gravity, θ, water content, and Kd distribution coefficient. This model treats radionuclides migration by advection of water flow and dispersion, and simple thermodynamic equilibrium among many models proposed for adsorption behavior of radionuclide onto geologic medium.

2.1 Water flow rate

Most general method to obtain water flow rate (V: cm/s) is by using specific flux (q: cm/s) calculated with infiltration amount into the pits and effective porosity (ne) which contributes water flow path.

$$V = q / ne \quad (3)$$

This method can be used very effectively to obtain water flow rate for whole period of test under the condition like artificial rainfall where water content at the depth of several 10 cm could be assumed to be constant.

2.1.1 Amount of infiltration water

Amount of infiltration water is obtained using monthly amount of artificial sprinkling and indoor

evaporation under artificial rainfall condition. When calculating specific flux in equation (3), intermission of sprinkling should be taken into consideration because sprinkling is interrupted by some reasons such as an adjustment of the sprinkling device, soil sampling, electric interruption, and so on. Average infiltration rate at time t is calculated as follow:

$$Fav(t) = (Qacc(t) - Eacc(t)) / Nday \quad (4)$$

where, Fav(t) represents average infiltration rate (cm/d), Qacc(t) and Eacc(t) are accumulative amount of sprinkling and evaporation (cm), respectively, Nday number of days from the start of sprinkling (d). Combining equation (3) and (4), average water flow rate at time t (V(t): cm/d) is given by using effective porosity as;

$$V(t) = Fav(t) / ne \quad (5)$$

2.1.2 Effective porosity

Effective porosity was obtained from results of field migration test using H-3 and Br tracers under artificial rainfall condition by calibrating the equation (3). In Pit-1 and Pit-7, H-3 and Br were used as water tracer, and the tracers were sampled periodically at the depths of 1 m and 1.5 m in the pits with water suckers. Average infiltration rates during the period when the peak of the tracers was moving from 1.0 to 1.5 m are 9.06 mm/d for Pit-1 and 9.65 mm/d for Pit-7.

Water flow rate can be directly obtained by analysis on concentration change of the tracers at the two depths as 2.27 cm/d for Pit-1 and 2.00 cm/d for Pit-7 by simple calculation dividing the distance between two water samplers with the period of which a concentration peak needed to pass through. From these results, effective porosity of soil in Pit-1 and Pit-7 under artificial rainfall condition are calculated and summarized as 0.40 for Pit-1 and 0.48 for Pit-7.

2.2 Distribution coefficient

Two results from different tests are available to obtain distribution coefficient for aerated loess. One is laboratory experiments by batch method[2], the other is migration test using undisturbed aerated layer columns[3]. Part of the result of the tests are summarized as below:

	Sr-90	Np-239	Pu-238
Batch method	190	70 - 1600	1200
Column test	55	133-199	

2.3 Dispersivity

Among the three radionuclides used for the test, Pu-238 could not be determined the value because of insufficient information on its migration in the laboratory tests. Information on the migration for the other nuclides was able to be obtained and analyzed to determine the relationship between dispersion length (DL) and migration distance of tracer peak (Lp).

$$DL\ (cm) = 0.1 \times Lp\ (cm) \quad (6)$$

The procedure to determine dispersion length for a certain nuclide is as follows:

i) Determine movement distance of water using test period and flow rate.

ii) Calculate retardation factor using soil properties and distribution coefficient.

iii) Estimate migration distance of the peak of nuclide concentration using the movement distance of water and the retardation factor.

iv) Estimate dispersion length of the nuclide using the equation (6).

3. COMPARISON BETWEEN ESTIMATED AND ACTUAL DISTRIBUTION

The following values of the parameters were used in an estimation of migration distribution for Pit-1 after 3 years.

Water flow rate (cm/d)		3.36 (at effective porosity: 0.40)		
		Sr-90	Np-237	Pu-238
Distribution coefficient (cm^3/g)		55	200	1200
Dispersion length (cm)		2.47	1.04	0.59
Initial concentration (KBq/cm^3)		6.91	1.87	0.189
Soil properties	porosity	0.5		
	density	2.7 g/cm^3		
	degree of saturation	0.8		

Figures 1 shows estimated distribution of tracers in Pit-1 3 years after the test start and measured distribution of tracer concentration in Pit-1 at 6 soil sampling times, respectively. No movement of the concentration peak was observed in the concentration distribution of Sr-90 as well as Np-237 in the field test. Migration of Pu-238 distribution of the field test shows good agreement with that of the estimation in the sense that the both are remained at the original position.

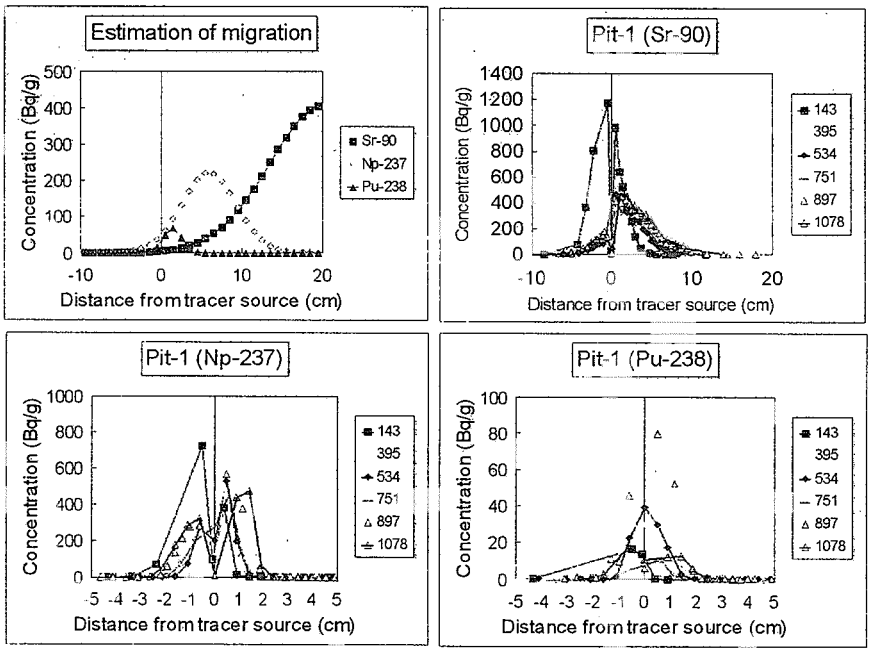

Fig. 1 Estimation and measured distribution of tracer concentration in the Pit-1.

4. DISCUSSION ON RESULT OF COMPARISON

Some degree of disagreement was found from the result of the comparison between the estimation and actual distribution. To discuss the reason for this, further analyses have been done on

hydraulic condition in test pit, recovery ratio of sampling, and migration estimation under a low rate of water flow.

4.1 Hydraulic condition in test pit

Supplemental tests were performed to study hydraulic condition in the test pit where quartz sand were used as tracer source. The test was conducted as the same sprinkling condition as Pit-1 and Pit-7. Measured data of martic potential was converted to water content and unsaturated water conductivity and summarized as their vertical distribution in Fig. 2. Both water content and conductivity show considerably change between the upper and lower layers of the plane of discontinuity which corresponds to the position of the quartz sand layer. The discontinuity of water conductivity can affect considerably on water infiltration movement through the plane and could generate horizontal water flow on the plane.

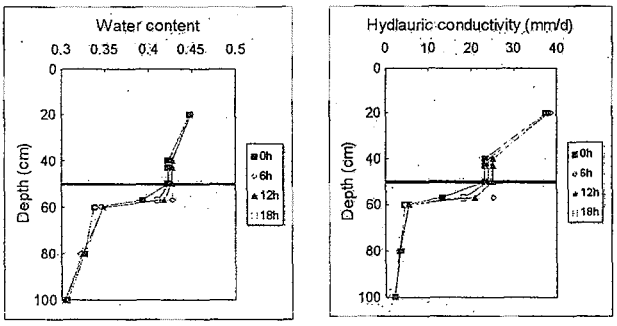

Fig. 2 Vertical distribution of water content and unsaturated hydraulic conductivity calculated

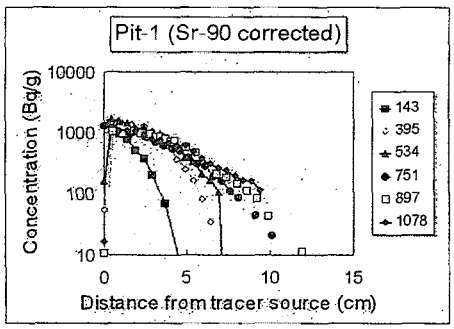

Fig. 3 Corrected distribution change of Sr-90 with recovery ratio in Pit-1.

4.2 Correction using recovery

Recovery of tracers for 6 soil samplings was obtained by integrating concentration distribution of tracers in soil sample. Recovery showed smaller difference between Sr-90 and Np-237 compared with the difference among 6 sampling times. Figure 3 shows corrected distribution of Sr-90 with the recovery ratios. Concentration decreases quickly in the upper layer above the tracer source, while in the lower layer below the source, concentration near the source deceased gradually, and concurrently, concentration between 5 and 10 cm gradually increased.

4.3 Estimation of water flow rate through quartz sand layer

To study on the effect of a quartz sand source layer on the soil water flow passed through it, a comparative test has been performed using quartz sand and loess for the tracer source layer[4]. From the test, water flow rate of 0.86 cm/day was obtained by analysis on the movement of H-3 added as a tracer in the quartz sand layer. This value indicates the water flow rate at the beginning stage of 3-year test, however, it is questionable that the test could simulate the flow condition at the middle to last stage of 3-year test where the flow condition had changed from unsteady to steady unlike at the beginning stage.

Obtaining the water flow rate by other methods is very difficult even by means of numerical

simulation together with detailed information on the water characteristics of quartz sand and loess because of the nonlinear equation of unsaturated water movement and the hysteresis of soil water. Thus, the value of 0.86 cm/day is considered to be a single practical information on the flow rate of soil water. Only exception to be worth to consider would be the value of zero (0 cm/day) when assuming that the water flow at the beginning has caused by a burst flow and the water flow at the middle to final stage has been kept at zero by the barrier effect of quartz sand layer. Hence using 0.86 and 0 cm/day, concentration distribution of Sr has been calculated as estimation and comparison to the actual distribution which was distinctly obtained from the Pit-1 test.

4.4 Comparison between re-estimated and actual distribution

The estimation result with 0.86 cm/day is shown in Fig. 4 and that with 0 cm/day is in Fig. 5. Judging from the result, distribution using 0 cm/day shows much better agreement to the actual distribution than that using 0.86 cm/day. However, this dose not directly indicate that the flow rate in Pit-1 was almost zero. In addition to that, it is uncertain that the instantaneous release condition of tracer has been satisfied under such a flow condition where water flow was blocked by quartz sand layer.

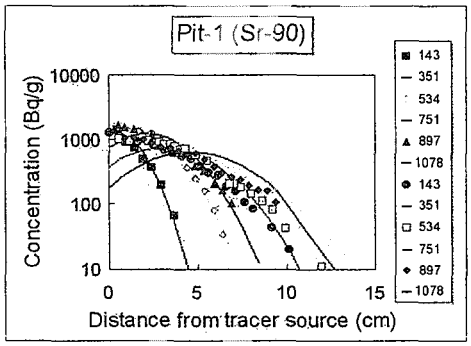

Fig. 4 Calculated distribution of Sr-90 concentration using water flow of 0.86 cm/day through the tracer layer in the Pit-1.

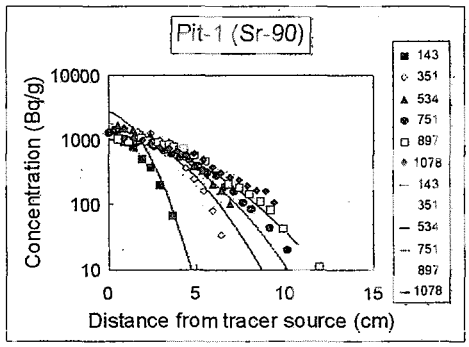

Fig. 5 Calculated distribution of Sr-90 concentration assuming no water flow through the tracer layer in the Pit-1.

Fitting the actual concentration distribution to determine parameter values would depart from the demonstrative procedure, where parameter values should be obtained from experiments and tests prior to the main test, to evaluate given models by comparing estimation with actual. While fitting can provide us for supplemental information on the value of water flow otherwise insufficient. For this reason, we have obtained the values of water flow rate, dispersivity and initial concentration in Pit-1 by fitting.

In the procedure of fitting, correction has been made on the actual concentration distribution with recovery ratio for each sampling, then value of distribution coefficient was fixed at 55 on the basis of the results from laboratory experiment, simulation tests and assembly test. The values at every sampling times of each parameter were averaged with weight of the number of elapsed days. The values for water flow rate and dispersivity are determined and summarized as 0.135 cm/day and 1.68 cm^2/day, respectively. As a matter of course, concentration distribution at each sampling

showed reasonable agreement with the actual distribution (Fig. 6).
Water flow rate by fitting, 0.135 cm/day, is found to be not close to 0.86 but 0 cm/day. Dispersivity by fitting, 1.68 cm^2/day, is found to correspond to almost twice as large as the value of 0.78 which is estimated by relationship between flow rate and dispersivity determined mainly from the result of the assembly test. The larger dispersivity could be caused by more complicated behavior of water flow under unsaturated condition compared with the flow under saturated condition of the assembly test.
As to the Np in Pit-1, result of the distribution calculation using 0.135 cm/day for water flow rate in Fig. 7 showed reasonably comparable to the actual one. As the same as the case of Sr, the value of diffusivity for Np, 0.2 cm^2/day, obtained by fitting was about twice as large as the estimated value using the result of the assembly tests (0.09 cm^2/day).

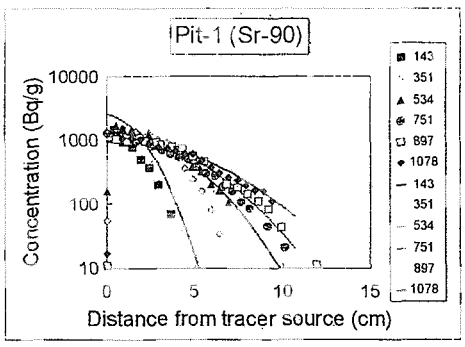

Fig. 6 Calculated distribution of Sr-90 concentration using water flow of 0.135 cm/d through the tracer layer in the Pit-1.

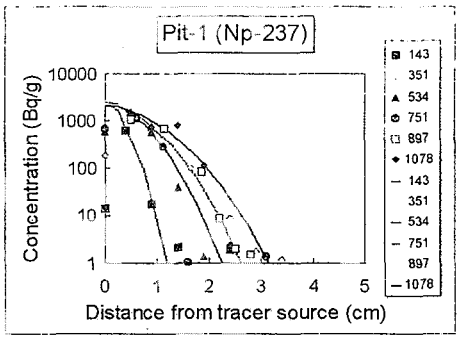

Fig. 7 Calculated distribution of Np-237 concentration using water flow of 0.135 cm/d through the tracer layer in the Pit-1.

5. MIGRATION DISTRIBUTION UNDER NATURAL RAINFALL CONDITION

In the Phase-II program, a few of the instruments necessary for measurement of evaporation could not be used because of mechanical troubles. Obtained data without these instruments is considered to have less accuracy than the Phase-I data. For this reason, instead of analyzing in the same course as artificial rainfall condition, fitting procedure has be taken for analysis on the data of natural rainfall condition. Distribution of Sr-90 concentration is shown in Fig. 8.
In the fitting procedure, distribution coefficient was fixed, while water flow rate, dispersivity and initial concentration were fitted to obtain good agreement with concentration distribution of each sampling time. Relationship between values of these parameters and elapsed time from the test start is shown in Fig. 9. In the figure, initial concentration and dispersivity show relatively steady while water flow rate shows gradual decrease with elapsed time.
This could be explained that the test was started in June of rainy season. Rainfall in rainy season moved tracers quickly first, then it slowed with decreasing rainfall amount and increasing evaporation. Long term average of water flow rate by the analysis was found to be 0.24 cm/day. Assuming 0.15 for yearly average of water content in aerated loess, the value of 0.24 cm/day corresponds to about 130 mm of infiltration amount. This value is considered to be reasonable

because the amount of infiltration at the test site observed in Phase-I was about 100 mm. As to dispersivity, analyzed value of 0.7 cm^2/day is about a half as small as that obtained from the test under artificial rainfall condition.

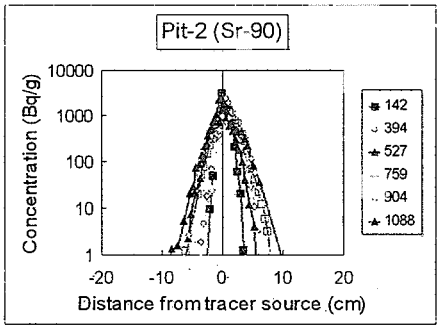

Fig. 8 Result of distribution of tracer concentration at each soil sampling in the Pit-2.

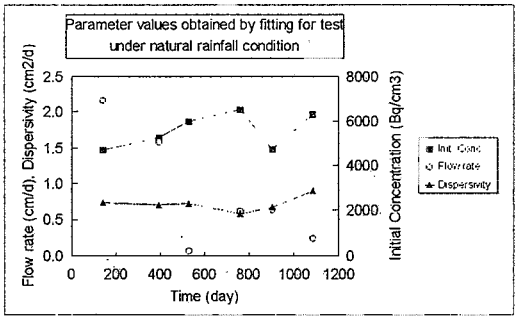

Fig. 9 Relationship between these parameters and elapsed time of sampling from the test start in Pit-1.

6. CONCLUSIONS

Determining method to obtain reliable values of parameters for migration analysis were discussed. Using the values, estimation of concentration distribution of aerated field migration test under artificial rainfall condition has been calculated. The estimation showed difference with the actual distribution in view of the movement of concentration peak of tracers. From the observation on water potential, a plane of discontinuity of water content and conductivity existed at the depth of tracer source layer and adjustment on water flow rate was needed. Two values of water flow rate, 0 and 0.86 cm/d from the comparative test on quartz sand tracer source layer, were used for the re-estimation calculation of Sr-90 migration. Between these, 0 cm/d showed better agreement to the concentration distribution corrected with recovery ratio and fitting analysis showed very low water flow rate of 0.135 cm/d. Dispersivities calculated using 0.135 cm/d of water flow rate for Sr-90 and Np-237 were almost a half as small as those obtained by fitting analysis because of difference of water saturation condition between estimation and the actual pit. Though some care was needed to determine water flow rate and dispersivity among the three parameters, the existing model for radionuclide migration was able to estimate radionuclide migration in natural aerated loess layer as long as obtained an appropriate set of parameter values.

REFERENCES

[1] M.Mukai, et al., Journal of Fuel Cycle and Environment, 7(1), 31-40 (2001).

[2] H.Ogawa, Li Shushen, et al., "Safety assessment methodology for shallow land disposal of low level radioactive waste -Overview Report-", in printing.

[3] Ni Shiwei, et al., "Laboratory simulation tests of radionuclide and stable element migration in loess aerated zone", Proc. NUCEF '98, Tokai, Japan (1998).

JP0250362

JAERI-Conf 2002-004

DEVELOPMENT OF AIRLESS CORE SAMPLING SYSTEM (ALCS) FOR SAFETY ASSESSMENT OF GEOLOGICAL DISPOSAL OF HLW

KUNIO ARAKI, AKIFUMI OUSHIKA, MASATO UEDA AND GUNJI OKANO

Enterprises Promotion Buraeu, Chuou-Kaihatsu Co.

Post 169-8612, 3-13-5, Nishiwaseda, Shinjuku-ku, Tokyo, Japan

Fax: 81- 3- 3208- 3572, e-mail: kunio_araki@ckc-unet.ocn.ne.jp

Airless Core Sampling System (ALCS) is being developed to obtain core samples maintaining the original underground conditions, especially without any penetration of water by cooling water into the core during a series of operations. ALCS consists of De-Aerated Water Supply System (DAWS) and Improved Fresh Water Core Sampling System (IFCS). DAWS is the de-aerated water preparation system reducing air pressure at an elevated temperature. IFCS is the airless water generation system by the introduction of suspended pure nitrogen bubbles with surfactant. The airless water thus prepared as lubricated fresh water is supplied to the bit of the boring machine with an additional function such as smooth cutting down function of a core with gravels, fractured rocks and/or clay in any formation, automatic slime removal function by suspended bubbles and an automatically casing function for the core sample to be isolated from the air during the transport of the sample into the testing facility filled by an inert gas.

IFCS was tested using suspended air bubbles, where core samples with fractured structure were taken up smoothly filled with fine particles in those cracks without any relaxation. The theoretical analyses have been carried out on the effect of ALCS as a total system and the final concentration of oxygen is calculated to be as low as ca.0.2ppm in the airless water to be supplied to the boring machine. The field test of ALCS must be carried out further. The application limit of ALCS has also been discussed.

Key words: Airless Core Sampling System, Radioactive Wastes, High-Level Waste, Safety Assessment, Geological Disposal

1. INTRODUCTION

For the safety assessment of the radioactive waste disposal system underground, the characteristics of natural barrier is important [1]～ [3]. Especially, the reductive-oxidative condition characteristics are important to assess the safety of the geological disposal of high-level waste and TRU wastes into the geological formation, because some nuclides such as Pu, Np, U and Tc easily change their solubility and Kd values according to their chemical form [4]～ [7].

There are 3 traditional all-core sampling methods by drilling for all core sampling, i.e., the method ① with mud such as slurry of bentonite and high-polymer, the method ② with fresh water (hereafter the abbreviation of the traditional FWCS is used, tentatively) and the method ③ with mist or jet foam. However, almost all of the three methods have some problems during the sampling procedure. For example, permeability, chemical condition and mechanical property of the core will be changed by penetration of water by the traditional FWCS (method ①), slurry of mud(method ②) with air and air directly (method ③). In

addition, the core sampling methods with mud or fresh water are difficult to give a smooth core with gravels, crushed rock and/or clay in an unconsolidated layer and/or fractured zone. In this paper, it is reported that ALCS is being developed to obtain core samples keeping the original underground conditions.

2. PURPOSE

The purpose of this paper is to report that ALCS [8] is being developed to obtain core samples keeping those original characteristics in the underground conditions, such as hydrological characteristics and geochemical characteristics without any penetration of the surface water with air into the core in the sampling processes, as well as keeping its original mechanical characteristic with smooth surface cutting and without any relaxation of cores.

3. ALCS AS A SYSTEM

ALCS mainly consists of De-Aerated Water Supply System (DAWS) and Improved Freshwater Core Sampling System (IFCS) [9]. DAWS is the de-aerated water preparation and supply system where the partial pressure is reduced at an elevated temperature and the de-aerated water is supplied to IFCS. IFCS is the airless water generation system with nitrogen suspension and with strongly electrolytic and neutral surfactant (Fig.1). The airless water is supplied to the bit of the boring machine equipped with a case to confine the core automatically.

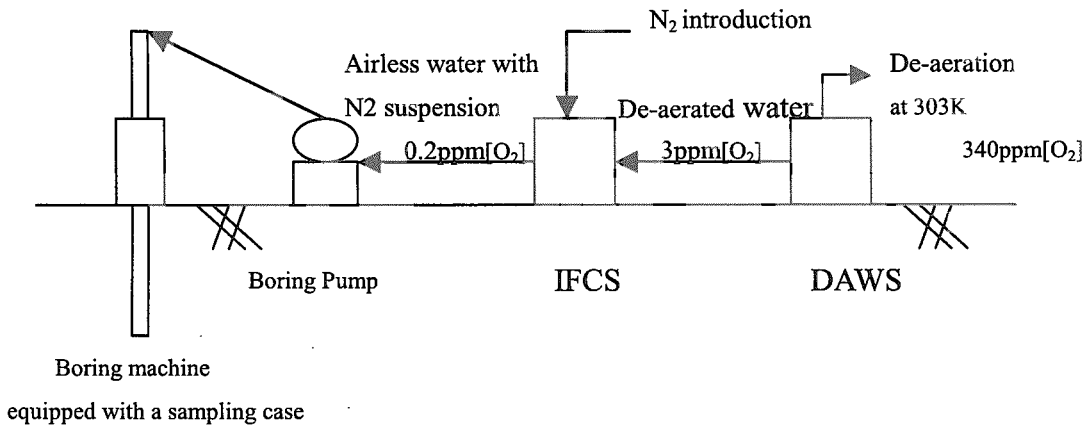

Fig.1 Block Diagram of ALCS with IFCS and DAWS

ALCS with lubricated airless water provides several functions such as the smooth core cutting function for gravels, fractured rocks and/or clay in the unconsolidated formation and/or fractured zone, the automatic slime removal function by suspended bubbles, the automatic casing function for a core sample and an excellent core supply function keeping original characteristics. These functions provide the core which retains the original underground characteristics such as hydrological, geochemical and mechanical characteristics. These functions are important for the safety assessment of the underground disposal of radioactive wastes, especially for the geological disposal of high-level waste and of

TRU-wastes.

The explanation will be started with IFCS in its mechanism to take an excellent core with the original characteristics underground and its test results. DAWS will be explained within the oxygen removal analyses in ALCS as a total system.

4. IFCS MECHANISM AND ITS TESTING RESULT

IFCS has specific functions to smooth cut down taking an excellent core from a layer without any penetration of water, to remove slime automatically after cutting down process by a bit and to extract almost entire oxygen from the de-aerated water supplied by DAWS.

4.1 Mechanism of IFCS for Smooth Cut Down to Take a Core with Little Water Penetration

IFCS generates the lubricated airless water with small amount of surfactant and suspended nitrogen to the boring machine. The surfactant gives lubrication to the de-aerated waster for the smooth water supply to the bit of boring machine, for the smooth cutting down to take a core and for the stabilization of suspended nitrogen bubbles, which is good for the automatic slime removal beyond the bit resulting upward flow decreasing the water pressure and the amount of water to be supplied (Fig. 1 and Photo. 1).

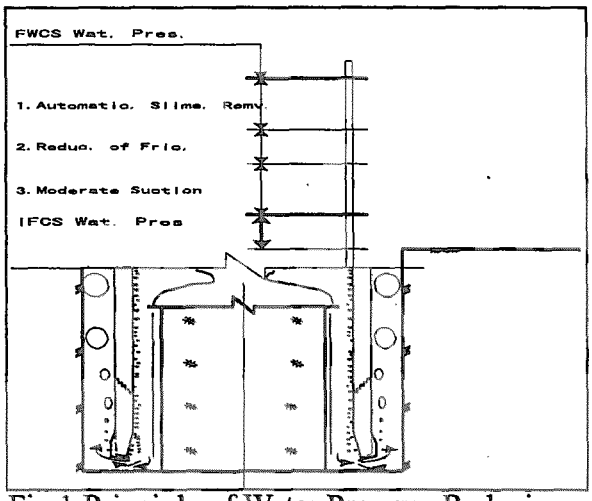

Fig.1 Principle of Water Pressure Reducing Effect for IFCS from the Traditional Fresh Water Core Sampling Method (FWCS)

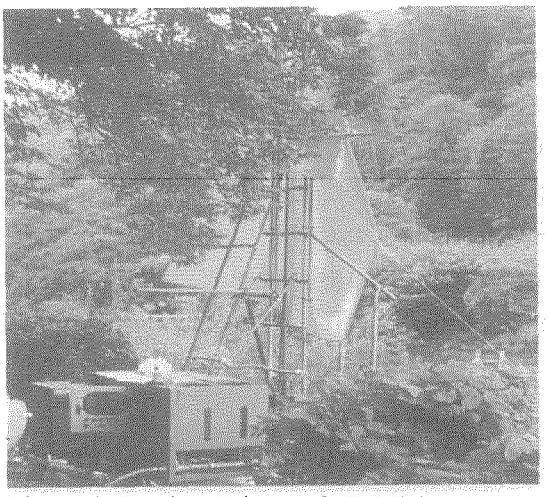

Photo.1 Testing View of IFCS in Cretaceous Granite on a River side by a ϕ 66mm Bit, The Applied Air: 8 times to the Water Volume

In the case of the traditional FWCS method and the mist core sampling method, the pressurized and high-speed water or air must be supplied to remove slime to the surface of the ground. The pressurized water or air causes the penetration of the surface water and/or the penetration of the air, where the penetration of the air by any way may result the relaxation of the core, boiling phenomenon at the bit and the flow away phenomenon of fine particles and/or clay in the layer from the core.

4.2 Typical Test Results of IFCS on Smooth Cutting and Automatic Slime Removal Functions

IFCS was tested with a machine using air, in a Cretaceous granite zone between GL-80 m ~–90 m on the river side with a ϕ 66 mm bit and the suspended air volume was 8 times to the unit volume of the lubricated water. The core samples were taken between GL-80.0~ -87.5 m by IFCS method where the recovery of core was 100 %, the drilling rate was 2.0~

2.6 m/hr, the applied pressure of lubricated water for drilling was ca. 100 kPa (ca. 1/2.5 of the traditional FWCS) and the amount of the apparent water volume with air suspension was 5.1 L/min, hence, the actual volume of the water was 0.64 L/min (ca. 1/20 of the FWCS). For comparison, the core samples were taken between GL-87.5～-90.0 m by the traditional FWCS method where the core recovery was 100 %, the drilling rate was 1.9 m/hr, the pressure and the amount of the fresh water was 250～300 kPa and 15～20 L/min) (Photo. 2).

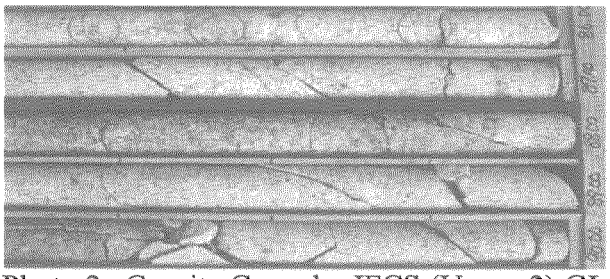

Photo.2a Granite Cores by IFCS (Upper 2) GL -85.6～-87.0 m with fine particles vs. Cores GL-87.6～-90.0 m by Fresh Water Sampling Method with relaxation and no fine particles

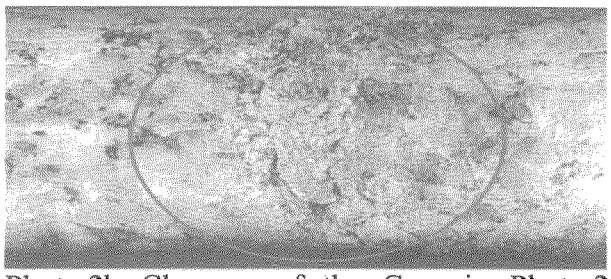

Photo.2b Close-up of the Core in Photo.2 (Circled on the top) Taken by the IFCS Method GL between -85.7～-86.0 m with naturally filled fine material in the crack

The core samples taken by IFCS were observed to be cores with little relaxation and with tight and fine particles in cracks. On the other hand, the core samples taken by the traditional FWCS method were observed that they were partly fractured with strong relaxation and partly cracked with no fine nor any small particle.

IFCS was also tested by air and a ϕ 116 mm bit, in a Jurassic siliceous mud layer on the river side in the direction 40° from vertical axis at ca.–32.0～-32.3 m in the direction of boring (Photo. 3a, 3b). Excellent core samples were obtained with the fractured structure

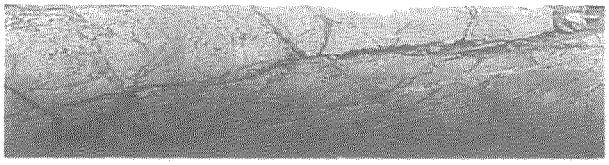

Photo.3a Siliceous Mudstone Cores Taken by IFCS Method between 32.0～32.3m, with water pressure of 40kPa with fine particles and without any relaxation

Photo.3b Cores by the Traditional Mist Boring Method between 32.3 ～ 32.6m, excess compressed air over inner water pressure resulting relaxation and no fine particles

and fine particles in detailed natural shape, where the rate of drilling was 0.6 m/hr, the 2 volume of the air was charged to the 1 volume of the lubricated water, the pressure and the amount of water supplied for automatic removal of slime was ca. 40 kPa (in the case of the traditional FWCS air pressure was ca. 7 times to that of IFCS). For comparison, Mist Boring method was tested at the position of ca.–32.3～-32.6 m next to the test position of IFCS. The cores were obtained in fractured pieces due to the compressed air penetration in jet foam at the bit removing slime from the bottom to the surface and the rate of drilling was 0.25 m/h. The applied air was 300 kPa and 10～15 L/min under the pressure to the bit of the boring machine. In the case of the traditional FWCS method, only slime was obtained instead of

core at the corresponding siliceous mudstone layer due to the water penetration by raised water pressure to remove slime from the top of the bit.

These results show that IFCS with a ϕ 116 mm bit or a ϕ 66 mm bit has the effective smooth cutting function and the automatic slime removal function without any relaxation of the core nor loosing fine particulates from the core, because of the lubricated water with surfactant and air suspension, where the water pressure and the water volume were reduced.

5. THEORETICAL ANALYSES OF AIRLESS WATER GENERATION BY ALCS

In ALCS, DAWS provides the de-aerated water under the reduced pressure at an elevated temperature and then IFCS provides airless water with nitrogen suspension. The theoretical consideration has been made by the application of Henry's Law in the analyses as follows.

5.1Reference Case for Analyses

The reference case is assumed as follows: The operation temperature is 293 K, which is almost same as the average temperature in Japan. In DAWS, the total pressure is kept at first under 101 kPa with the saturated water vapor pressure of 4.24 kPa and the dry air partial pressure of 97.1 kPa at 303 K. The total air pressure is reduced to 5.07 kPa with the saturated water vapor pressure of 4.24 kPa and the partial dry air pressure of 0.830 kPa. This total pressure is selected not to have any boiling of water under the pressure. In IFCS, the nitrogen suspension was introduced 10 times of de-aerated water in volume at 293 K with surfactant.

Finally, the airless water is supplied to the bit of the boring machine equipped with a case in order to confine a core automatically, which should be isolated from air during the transportation to the experimental facilities filled with the inert gas, such as the one in NUCEF.

5.2De-Aeration of Water in DAWS

The oxygen concentration in the de-aerated water is analyzed, where the total pressure of the lubricated water is decreased from 101 kPa into 5.07 kPa at an elevated temperature of 293 K in DAWS.

The reducing factor of the oxygen partial pressure over the water from 101 kPa to 5.07 kPa ($f_r|_{K=302K}^{Pt=101kPa\to5.07kPa}$) at 303 K is calculated to be 0.00855 taking the saturated water pressure into account (eq. 5-1).

$$f_r|_{K=303K}^{Pt=101kPa\to5.07kPa}=\frac{(P_{total}|_{K=303K}^{Pt=5.07kPa}-P_W|_{K=303K}^{Pt=5.07kPa})}{(P_{total}|_{K=303K}^{Pt=101kPa}-P_W|_{K=303K}^{Pt=101kPa})}=0.00855 \qquad \text{(eq. 5-1)}$$

Where $P_{total}|_{K=303K}^{Pt=101kPa}$ and $P_{total}|_{K=303K}^{Pt=5.07kPa}$ are of those dry air partial pressure under the total pressure at 303K, $P_W|_{K=303K}^{Pt=5.07kPa}$ and $P_W|_{K=303K}^{Pt=101kPa}$ are the same partial pressure of the water vapor at 303K [10].

The oxygen content in weight $[O_2]_{K=303K}^{Pt=5.07kPa}$ under 5.07 kPa at 303 K is calculated to be

$3.07*10^{-3}$ $gO_2/L\ H_2O$ (eq. 5-2).

$$[O_2]_W\,|_{K=303K}^{Pt=5.07kPa} = f_r\,|_{K=303K}^{Pt=101kPa\to5.07kPa} *[O_2]_w\,|_{K=303K}^{Pt=101kPa} = 3.07*10^{-3})\ \ (g\ O_2/L\ H_2O)\quad \text{(eq. 5-2)}$$

Where $[O_2]_W\,|_{K=303K}^{Pt=5.07kPa}$ and $[O_2]_W\,|_{K=303K}^{Pt=101kPa}$ (0.359 g $O_2/L\ H_2O$ under 101 kPa at 303 K[10]) are the oxygen concentration in the water under the total air pressure of 5.07 kPa and 101 kPa.

Thus, ca. 3 ppm of oxygen concentration is obtained theoretically in the water of DAWS by the reduction of total pressure from 101 kPa to 5.07 kPa at 303 K.

5.3Preparation of Airless Water in IFCS

In IFCS, the pure nitrogen is introduced and dispersed in the form of suspension into the de-aerated water supplied from DAWS. The ca. 3 ppm (for calculation, the value of 3.07 ppm must be used again) of oxygen in de-aerated water must be redistributed again between the unit volume of water and the 10 times volume of gas phase under 101 kPa at 293 K. The partitioning constant ($R_{w/g}\,|_{K=293K}^{Pt=101kPa}$) is estimated from the rate between the oxygen concentration in the airless water and that of in the gas phase, which must be corrected by the water vapor pressure.

The partial pressure of the dry oxygen under the total pressure of 101 kPa at 293 K is calculated and found to be 19.8 kPa (eq.5-3).

$$P_{O_2}\,|_{K=293K}^{Pt=101kPa} = 0.2*(P_{total}\,|_{K=293K}^{Pt=101kPa} - P_W\,|_{K=293K}^{Pt=101kPa}) = 19.75\ \ \text{(kPa)}\quad \text{(eq.5-3)}$$

The amount of the oxygen in 10 L of the air is calculated to be 2.51 $gO_2/10\ LH_2O$ (eq.5-4).

$$10*[O_2]_{Air}\,|_{K=293K}^{Pt=101kPa} = 10*\frac{M}{24.0}*\frac{P_{O_2}\,|_{K=293K}^{Pt=101kPa}}{P_{total}\,|_{K=293K}^{Pt=101kPa}} = 2.51\ \ (g\ O_2/10\ LH_2O)\quad \text{(eq.5-4).}$$

The distribution factor of oxygen concentrations between 10 L of air and 1 L of water is calculated to be 0.0578 (eq.5-5).

$$R_{10G/W}\,|_{K=293K}^{Pt=101kPa} = \frac{[O_2]_{10G}\,|_{K=293K}^{Pt=101kPa}}{[O_2]_W\,|_{K=293K}^{Pt=101kPA}} = 0.0578\ \ \text{(by weight)}\qquad \text{(eq.5-5)}$$

The concentration of the oxygen in the lubricated airless water is calculated to be 0.168 ppm (eq.5-6).

$$[O_2]_w\,|_{K=293K}^{Pt=IFCS} = 3.07*\frac{R_{10G/W}\,|_{293K}^{101kPa}}{1+R_{10G/W}\,|_{293K}^{101kPa}} = 0.168\ \ \text{(ppm)}\qquad \text{(eq.5-6)}$$

Thus, ca.0.2 ppm in the airless water is obtained theoretically by IFCS.

6.RESULTS AND DISCUSSION

6.1Results

The following results are obtained:

(1) The concept of ALCS has been established, which consists of DAWS and IFCS with several functions such the smooth core cutting function with gravels, fractured rocks

and/or clay in a formation, the automatic slime removal function by suspended bubbles, the automatic casing function to confine the core and an excellent core supply function to retain the original hydrological, geochemical and mechanical characteristics as it is underground.

(2) It has been confirmed by the tests, which has been done, that IFCS has the effective smooth cutting function and the automatic slime removal function without any relaxation of the core nor loosing fine particulates, because the lubrication of the water and suspended air works effectively.

(3) The operation condition of IFCS is compared mainly with that of the traditional FWCS:

① IFCS was tested by air, in granite between GL-80.0 m～–87.5 m with a ϕ 66 mm bit and the air/water ratio was 8/1 in volume. The cutting rate was 2.0～2.6 m/hr (FWCS method gave 1.9 m/hr) and the core recovery ratio was 100%. Little relaxation was found in the recovered core and the crack was filled by fine material. The pressure applied for IFCS boring was found to be 100 kPa (about 1/2 of the traditional FWCS method). The apparent amount of the lubricated fresh water was 5.1 L/min (this volume is about 1/3 of the traditional FWCS) and the actual water volume without air is calculated to be ca. 1/20 compared with that of the FWCS

② IFCS was also tested by air and a ϕ 116 mm bit in siliceous mud layer in the direction of 40° at ca. – 30 m in its direction. The core recovery ratio was 100% without any relaxation. Core was recovered with natural fine material in the fracture, however, the mist boring method gave cores with relaxed structure without any fine material in cracks and the traditional FWCS method gave only slimes at the corresponding position of the same layer. The cutting rate by IFCS was ca. 0.6 m/hr, where this value was 3 times to that of mist boring method. The pressure of the lubricated fresh water for IFCS was 40 kPa (at GL ca. –20 m in its depth), which is the ca. 1/8 value of the mist boring. The apparent volume of the water applied was found to be 5.1 L/min (1/2 vol. of the compressed air for the mist boring), where the actual water volume was calculated to be ca. 0.25 L/min.

(4) The analyses have been carried out on the de-aerated water preparation in DAWS and on the airless water preparation in IFCS, as a system. The de-aeration of air under 5.07 kPa is found to be effective to get de-aerated water with ca. 3 ppm oxygen dissolved at an elevated temperature as high as 303 K. The introduction of pure and suspended nitrogen into de-aerated water under 101 kPa is found to be effective to get airless water with ca. 0.2 ppm oxygen dissolved at 393 K.

(5) It is confirmed that ALSC are useful for the safety assessment of underground disposal of radioactive wastes, especially for the geological disposal of high-level and TRU wastes.

6.2Applicability of ALCS

(1) ALCS is applicable to provide cores with their original characteristics underground such as mechanical property, geohydrological property and geochemical property, especially, without any penetration of cooling water with air during the core sampling procedure.

(2) ALCS is also applicable to provide bore-holes for several field tests in a good condition such as mechanical property, geohydrological property and geochemical property,

especially, without any penetration of the cooling water with air into the wall of a bore-hole.

6.3Further Investigation to be made

(1) ALCS seems to have some limit to get nice core from coastal sand, where some characteristics may be changed from underground condition, because of the suspended nitrogen. Therefore, the further development must be continued on this point.

(2) Concerning with IFCS, it is desirable to continue all-core boring test further for the practical use on some other layers than those tested already.

(3) The result of theoretical analyses must be confirmed by field test as a whole.

ACKNOWLEGEMENT

Authors would like to express their hearty thanks for Mr. S. Takebe, Mr. S. Hagiwara, Japan Atomic Energy Research Institute, Mr. I. Seko, Mr. J. Setoyama, Mr. M. Saito, Mr. Nishie, Mr. Y. Shinohara and Mr. A. Oubo, Chuou-Kaihatsu Co. for their helpful discussions.

REFERENCE

[1] D. Isherwood, Preliminary Report on Retardation Factors and Radio-nuclide Migration, Lawrence Livermore Lab. Rep. UCID 17551 (1977)

[2] K. Araki, S. Tashiro, T. Banba, K. Abe, K. Kobayashi, K. Sato, H. Amano and T. Kashiwagi, Preliminary Research on Geological Isolation of High-Level Radioactive Waste at the Japan Atomic Energy Research Institute, Proc. Symp. Underground Disposal of Radio-active Wastes, Otaniemi, July 1979, vol. 2. pp35, IAEA (1980)

[3] K.Araki, M. Motegi, Y. Emoto, Y. Kaji, S. Ikari, T. Nada and T. Watanabe, Natural Analogue Study on Engineered Barriers for Underground Disposal of Radioactive Wastes, Joint International Wastes, Joint International Waste Management Conference, Progress Report, pp601-609, ASME, JSME, and AESJ, 1989, Oct., Kyoto, Japan

[4] D. G. Brookins, Geological Aspects of Radioactive Waste Disposal, Springer-Verlag, New York (1984)

[5] OECD/NEA, Using Thermodynamic Sorption Models for Guiding Radioelement Distribution Coefficient (Kd) Investigations, A Status Report, OECD/NEA, Paris, Republic of France (2001)

[6] T. Shibuya, M. Shibata and Y. Sueyama, Data Base on Sorption of Radioactive Nuclides to Bentonite and Rocks, JNC TN8410 99-050, JNC, Japan (1999)

[7a] S. Takebe and M. Abe, Development of Data Base on Distribution Coefficients (1) Data Correction of Distribution Coefficients, JAERI-Data/Code 2001-005, JAERI, Japan (2001), [7b] ibid (2), JAERI-Data/Code 2001-006, JAERI, Japan (2001)

[8] Y. Oubo, K. Araki and S. Nishie, Core sampling Method and Core Sampling System, Japanese Patent Application No. 2000-141163 (2000)

[9] I. Seko, G. Okano, K. Araki, Y. Oubo and T. Oukuma, Core sampling Method and Core Sampling System, Japanese Patent Application No. 2001-95066 (2001)

[10] Chemical Society, Japan, The Chemical Hand Book, Maruzen Co., Tokyo, Japan (1984)

JP0250363

JAERI-Conf 2002-004

CORRELATION BETWEEN MOLECULAR SIZE AND FUNCTIONAL GROUPS OF HUMIC ACID ON THE COMPLEXATION WITH ^{237}Np, ^{238}Pu AND ^{241}Am

Tadao TANAKA, Seiya NAGAO* and Hiromichi OGAWA

Department of Fuel Cycle Safety Research,
Tokai Establishment, Japan Atomic Energy Research Institute,
Shirakata 2-4, Tokai, Naka, Ibaraki, Japan, 319-1195.
Fax: 81-292-282-5934, e-mail: tanaka@sparclt.tokai.jaeri.go.jp

The effects of humic acid on interaction affinity with ^{237}Np, ^{238}Pu and ^{241}Am have been examined with respect to different molecular size fractions, which were isolated from the Aldrich Chemical's humic acid into 5,000-30,000 daltons, 30,000-100,000 daltons and 100,000 daltons-450 nm in molecular size range. At the pH of 5.5, little ^{237}Np interacted with the humic acid. The ^{238}Pu and ^{241}Am preferentially interacted with the humic acid of 100,000 daltons-450 nm in the humic acid concentration range below several mg/dm^3, although the interaction affinity reduced with increasing humic acid concentration. On the other hand, the ^{238}Pu and ^{241}Am preferentially interacted with the humic acid fractions of 30,000-100,000 daltons, in the humic acid concentration range over several mg/dm^3. FTIR spectral structures, CAP/MAS ^{13}C-NMR spectral structures and acid-base titration curves revealed that there are different structures and functional groups between different molecular size fractions. The molecular size selectivity of humic acid on the complexation with TRU nuclides may be caused by more than two different functional groups concerning to the complexation, steric hindrance around the functional groups.

Key words: Humic acid, Functional groups, Molecular size, Complexation, TRU nuclides

1. INTRODUCTION

Much of the dissolved organic matter in natural groundwater consists of humic substances, which are formed during microbial degradation of biomass in soil and groundwater. Humic acid is one of the resulting product and stable to further degradation. As such humic acid has substantial chelation properties for metals, it considerably affects the sorption and migration behavior of radionuclides in soil. From a geochemical point of view, it is important to know the reactivity of humic acid with radionuclides released from radioactive-waste repository[1]. Molecular size of humic acid may be particularly significant to the migration behavior of radionuclide.

The interaction affinity of humic acid with ^{237}Np, ^{238}Pu and ^{241}Am has been examined with respect to different molecular size fractions, which were isolated from the Aldrich Chemical's humic acid into 5,000-30,000 daltons, 30,000-100,000 daltons and 100,000 daltons-450 nm in molecular size range. Each molecular size fraction has been characterized with respect to their FTIR spectral structures, CAP/MAS ^{13}C-NMR spectral structures and acid-base titration curves.

2. EXPERIMENTAL

Humic acid purchased from Aldrich Chemical Co. was further purified to remove insoluble humin, fulvic acid and ash following the procedure described by Nash *et al.*[2],[3]. The purified humic acid was dissolved in a small amount of 0.1 M NaOH, and the humic acid

*Present address: Hokkaido University, Sapporo, Hokkaido 060-0810, Japan

solutions of desired concentrations were prepared by diluting with 0.01 M $NaNO_3$.

The 0.1 cm^3 of radioactive solution containing ^{237}Np, ^{238}Pu or ^{241}Am, which were prepared in ca. 10^4 Bq/cm^3 (carrier free), was added to 10 cm^3 of the humic acid solution. The ionic strength was adjusted to 0.01 M with $NaNO_3$. pH of the solution was adjusted to 5.5 with 0.1 M HCl or NaOH to minimize hydroxyl metal complex formation. Samples were gently agitated at 25 ℃ for 7 days in a water jacket. These were then ultrafiltrated with Millipore filters of 450 nm in pore size, and 5,000, 30,000 and 100,000 in molecular weight cut-off (nominal molecular weight in dalton). Concentrations of the ^{237}Np and ^{241}Am in each filtrate were determined using an Ortec γ-ray detector, and that of the ^{238}Pu was determined using a Packard liquid scintillation counter. Concentration of dissolved organic carbon in each filtrate was determined using a Shimadzu spectrophotometer[3].

The humic acid solution used was fractionated into different molecular sizes namely 100,000 daltons-450 nm, 30,000-100,000 daltons and 5,000-30,000 daltons by a sequential ultrafiltration technique. The fractionated humic acid samples were protonated with 0.1M HCl, freeze-dried for FTIR spectral analysis, CAP/MAS ^{13}C-NMR spectral analysis and acid-base titration. The FTIR spectra were obtained using a Jasco Model VAROR-Ⅲ FTIR spectrophotometer with 1 % KBr disks. The CAP/MAS ^{13}C-NMR spectral were obtained using the cross polarization with magic angle spinning. The spectra were collected using a JEOL CSH270 spectrometer at a magnetic field of 67.8 MHz with a 90° pulse width of 4 μs and a contact time of 2 ms. The external standard was hexa-methoxy benzene with the shift of the methyl carbons assigned as 17.36 ppm. The exchangeable proton capacity was determined from the acid-base titration curves. About 10 mg of the fractionated humic acid was dissolved with a sufficient amount of 0.01 M NaOH in titration cell maintained at 25 ℃. Nitrogen gas was passed over the solution to avoid the absorption of carbon dioxide from the atmosphere during the titration, and the sample was titrated from a pH of about 11 to a pH with 0.01 M HCl at a total ionic strength of 0.01 M.

3. RESULTS AND DISCUSSION

3.1 Interaction between radionuclides and humic acid

Figure 1 shows size distribution of humic acid and radionuclides, which were determined from their concentrations in each filtrate passed through the filters. From the distribution profile of humic acid concentration, the bulk of dissolved humic acid is in the molecular size range from 30,000 to 100,000 daltons. In addition, with increasing humic acid concentration the fractional percentage gradually shifts from 100,000 daltons-450 nm to 30,000-100,000 daltons. It has been reported that humic acid molecules wind up like random coils from spread molecules as flexible, linear or branched polymer with increasing humic acid concentration[4].

The distribution profile of ^{238}Pu was similar to that of humic acid, except for 0 mg/dm^3 of humic acid concentration, in which ^{238}Pu forms particulate species due to pH higher than 6. These results indicate that the dissolved humic acid contributes a forming of humic complexes of ^{238}Pu. The distribution profile of ^{241}Am reveals that ^{241}Am also interact with humic acid. However, most of ^{241}Am species was trapped by the filter of 30,000 daltons in cut-ff molecular, except for 0 mg/dm^3 of HA concentration. Thus ^{241}Am may preferentially interact with the humic acid fractions larger than 30,000 daltons.

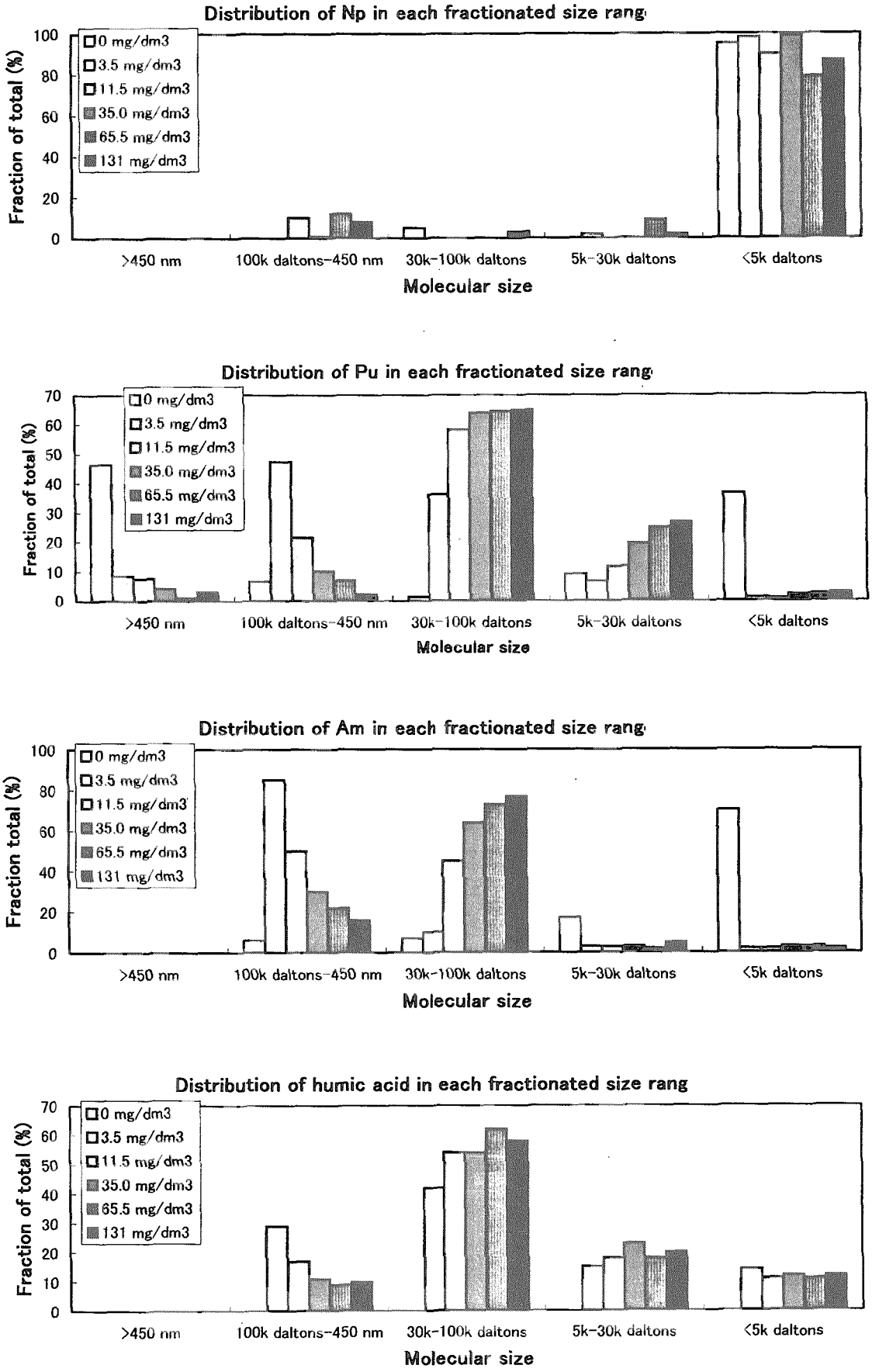

Fig.1 Size distribution of radionuclides and humic acid.

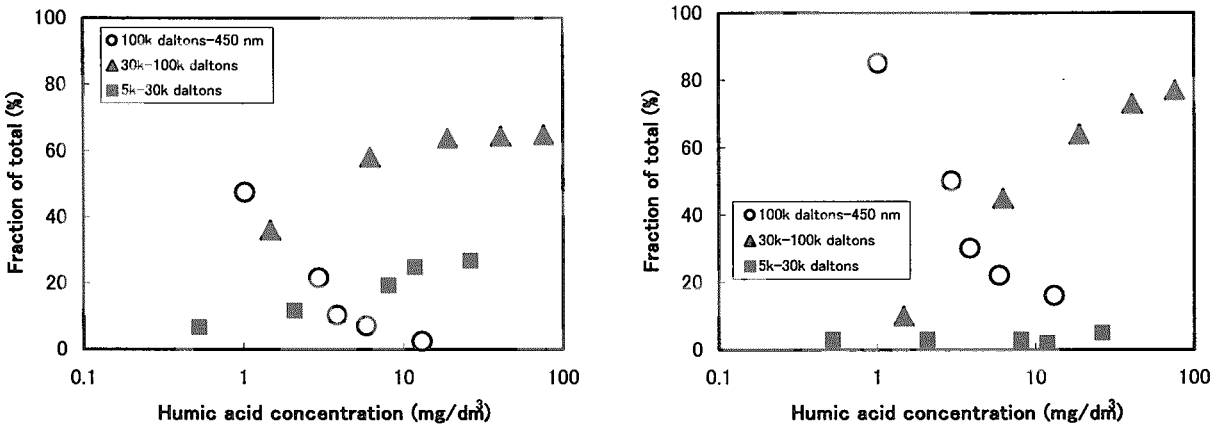

(a) ^{238}Pu (b) ^{241}Am

Fig.2 Relationship between radionuclide concentration and humic acid concentration

The distribution of ^{237}Np in the filtrates showed a different profile from those of humic acid, ^{238}Pu and ^{241}Am. Whole ^{237}Np species was not trapped by all the four kinds of filters and was in the fraction less than 5,000 daltons, in which fraction the ^{237}Np is existed as cationic species. This indicates that the ^{237}Np did not form humic complexes. It has been known that ^{237}Np(V) have little interaction with humic substances in acidic conditions[5],[6].

At the pH of 5.5, little ^{237}Np interacted with the humic acid. **Figure 2** shows the relationship between percentages of radionuclides and humic acid concentration in each size fraction, for ^{238}Pu and ^{241}Am, which were observed any interactions with humic acid in Fig.1. The ^{238}Pu and ^{241}Am preferentially interacted with the humic acid fraction of 100,000 daltons-450 nm in the humic acid concentration range below several mg/dm^3, although the interaction affinity reduced with increasing humic acid concentration. On the other hand, concentration of ^{238}Pu and ^{241}Am in the fraction of 30,000-100,000 daltons increased with increasing humic acid concentration, and the ^{238}Pu and ^{241}Am preferentially interacted with the humic acid of 30,000-100,000 daltons, in the humic acid concentration range over several mg/dm^3. These show that the binding between the radionuclides and the humic acid of 100,000 daltons-450 nm is not based on coordination bond but rather soft bond such as electrostatic attractive forces, as compared with the binding with humic acid of 30,000-100,000 daltons. The interaction of ^{238}Pu with the humic acid of 5,000-30,000 daltons was in the same manner as that with 30,000-100,000 daltons, while that of ^{241}Am was little detected. This indicates that ^{238}Pu forms a complex with humic acid of 5,000-30,000 daltons, while ^{241}Am does not. These results indicate that both ^{238}Pu and ^{241}Am preferentially form complexes with humic acid of 30,000-100,000 daltons.

3.2 Functional groups of humic acid

The FTIR spectra of humic acids fractionated by molecular size clearly indicate dominant absorbance due to aromatic, aliphatic, carboxylic and phenolic groups[7],[8], as shown in **Fig.3**. The broad band at 3,400-3,000 cm^{-1} is attributed to hydrogen bonding and O-H stretching. The strong doublet between 2,970 and 2,850 cm^{-1} and the single near 1,470

cm^{-1} represent aliphatic groups. The strong absorbance at about 1,720 cm^{-1} is a representative of the protonated carboxylic acids COOH and ketonic C=O groups. The peak at about 1,610 cm^{-1} and the weak but broad absorbance between 1,400 and 1,500 cm^{-1} can be assigned to the C=C stretching of aromatic rings. The distinct peak near 1,400 cm^{-1} may be due to the OH bending deformation and C-O stretching of phenolic OH. The OH deformation and C-O stretching of COOH is evidenced by the week absorbance in the region 1,300 to 1,200 cm^{-1}.

Most important difference between the spectra of the humic acid fraction of 100,000 daltons-450 nm daltons and those of 30,000-100,000 daltons and 5,000-30,000 daltons is the loss of the aliphatic groups at 2,970-2,850 cm^{-1} and at 1,470 cm^{-1}. Alternatively, the spectra of 30,000-100,000 daltons and 5,000-30,000 daltons indicate increased absorbance of the aromatic C=C at 1,610 cm^{-1} and at 1,500-1,400 cm^{-1} as compared to the spectra of the 100,000 daltons-450 nm fraction. The absorption band at 1,400 cm^{-1} that is attributed to phenolic OH has disappeared from the spectra of 5,000-30,000 daltons. Such distinct differences between the spectra indicate that the characteristics of reactive functional groups on humic acid are dependent on the molecular size. The present FTIR analyses show, the main reactive functional groups on the humic acid of 100,000 daltons-450 nm are aliphatic COOH (and OH), while those of 30,000-100,000 daltons and of 5,000-30,000 daltons are aromatic COOH and phenolic OH, and aromatic COOH, respectively.

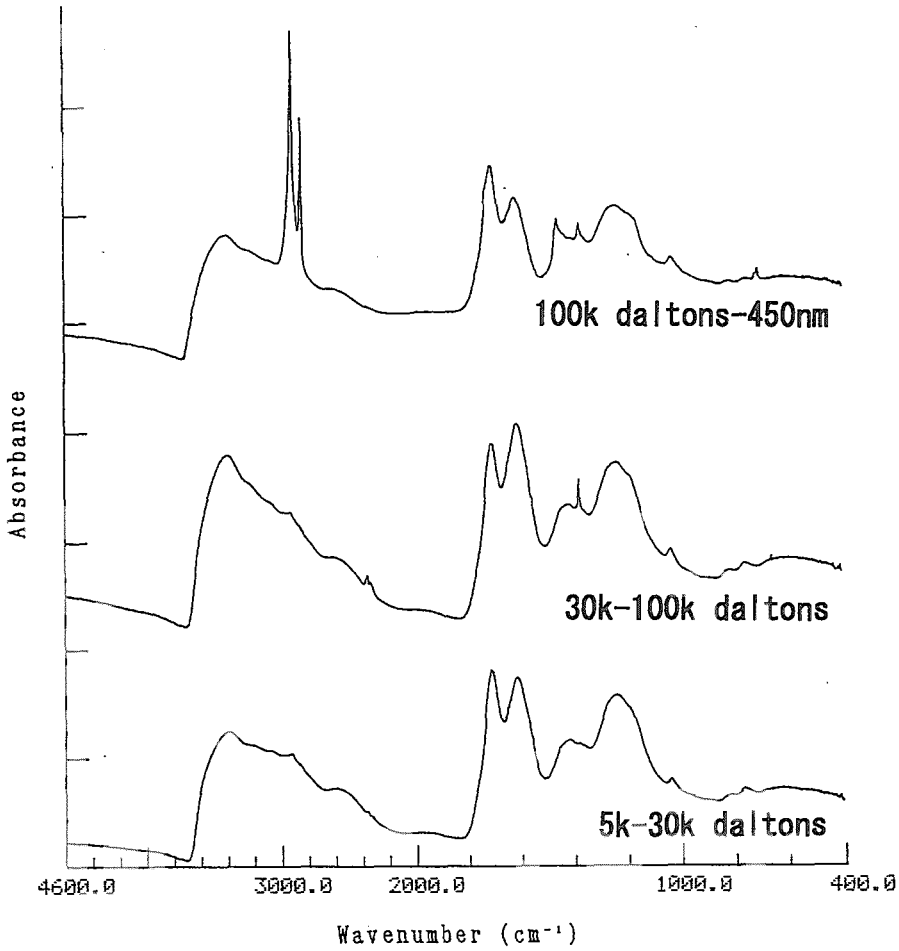

Fig.3 FTIR spectra of the fractionated humic acids.

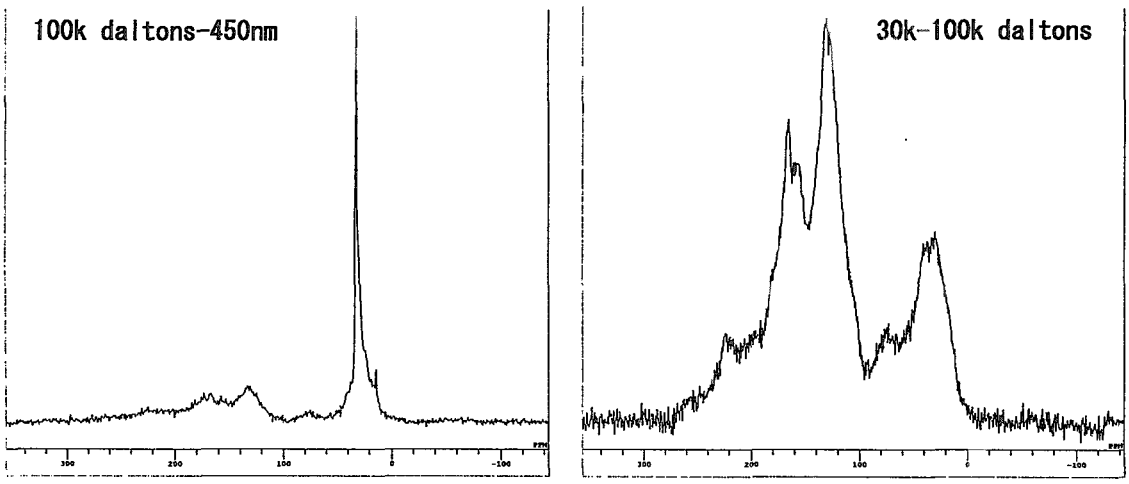

(a) Humic acid of 100,000 daltons-450 nm (b) Humic acid of 30,000-100,000 daltons

Fig.4 CAP/MAS ^{13}C-NMR spectra of the fractionated humic acids.

Table I Chracterization of humic acid by ^{13}C-NMR spectral structures.

Functional group	Chemical sift (ppm)	Spectrum area (%)		
		100k-450nm	30k-100k	5k-30k
Aliphatic C	10～ 50	49.8	17.7	15.6
o-alkyl	50～100	7.0	12.5	11.2
-CH_2OH	100～107	0.8	2.5	2.0
C=C & Aromatic C	110～160	22.2	41.8	42.9
-COOH	160～200	15.2	20.6	23.5
Carbonyl C	200～220	5.0	4.9	4.8

The solid-state ^{13}C-NMR spectra of the humic acid fractions of 100,000 daltons-450 nm and 30,000-100,000 daltons are shown in **Fig.4**. The ^{13}C-NMR spectrum of the 5,000-30,000 daltons fraction was nearly same as that of the 30,000-100,000 daltons. The spectra were assigned as shown in Table I[9]. Although the ^{13}C-NMR data are not highly quantitative, relative amounts of aliphatic vs. aromatic carbons were compared by calculating the integrated areas for the selected regions of interest with the results for each fractionated humic acid listed in **Table I**. These data show that the 100,000 daltons-450 nm fraction is mainly occupied with aliphatic carbons, but the 5,000-30,000 daltons and the 30,000-100,000 daltons fractions are dominated with aromatic carbons. Relative area of reactive COOH group increased with decreasing molecular size.

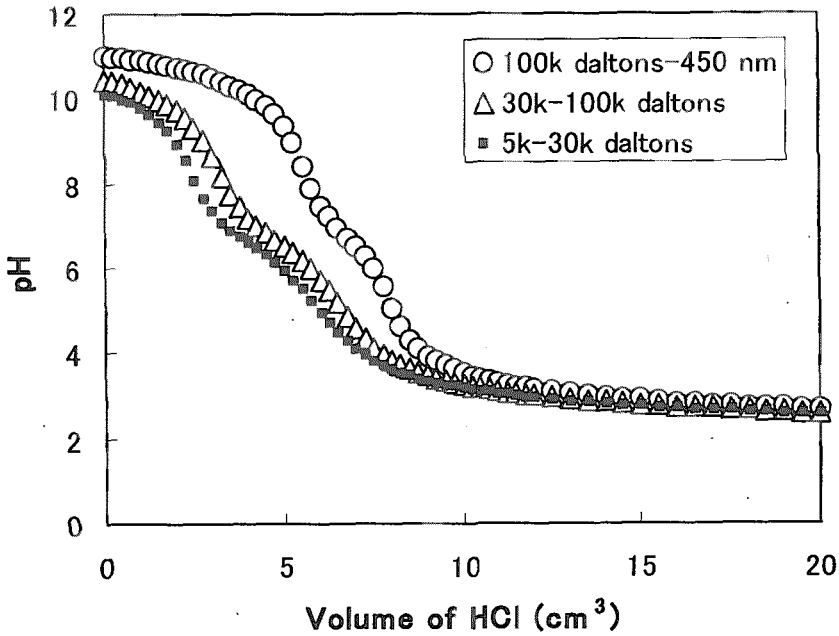

Fig.5 Titration curves for the fractionated humic acids.

Table II Characterization of proton exchangeable groups of the fractionated humic acids.

	100k-450nm	30k-100k	5k-30k
First equivalent point (-OH)			
pH	8.4	8.1	8.2
p*K*a	10.6	9.9	9.7
H^+ exchangeable capacity (meq/g)	5.5	3.3	2.5
Second equivalent point (-COOH)			
pH	5.1	5.2	5.2
p*K*a	6.7	6.6	6.3
H^+ exchangeable capacity (meq/g)	2.5	3.3	3.3

Protonation capacity and p*K*a of the functional groups were discussed from the acid-base titration curves, as shown in **Fig.5**. All three humic acid fractions had two equivalent point in the titration curves; First equivalent point seems to be corresponding to the carboxylate $-COO^-$ groups and the second seems to be corresponding to phenolic or alcoholic $-O^-$ groups. The COOH and the -OH group equivalences of the fractionated humic acid fractions were determined which, in turn, allowed calculation of p*K*a values of these groups. **Table II** gives the calculated equivalence of -COOH and -OH groups and their p*K*a values at ionization of 0.5. The data indicate that the humic acid fraction of 100,000 daltons-450 nm has higher proton exchangeable capacity and are weaker acids as compared with that smaller than 100,000 daltons. However, -COOH groups corresponding to the second equivalent point of 100,000 daltons-450 nm fraction are lower than the smaller fractions. Amount of proton exchangeable capacity corresponding to –OH group in the fraction of 5,000-30,000 daltons is smaller than the others. These reflect the results observed in the FTIR and the ^{13}C-NMR spectra.

3.3 Correlation between complexation ability and functional groups of humic acid

The FTIR spectral structures and the ^{13}C-NMR spectral structures indicated that the functional groups on the humic acid of 100,000 daltons-450 nm were dominated with COOH, CHO and OH groups of aliphatic carbon structures, while those on the humic acid of 5,000-30,000 daltons and 30,000-100,000 daltons were dominated with both aromatic COOH and phenolic OH. The acid-base titration curves showed that proton exchangeable capacity of the humic acid of 100,000 daltons-450 nm is larger than the other molecular size fractions. The results from the FTIR and the ^{13}C-NMR spectral analyses suggest that the aliphatic functional groups may not take part in the complexation of metals. For the 100,000 daltons-450 nm fraction having aliphatic branched structure, small amount of COOH group and large proton exchangeable capacity possibly seem to cause low complex ability and high ion exchangeability. In addition, steric hindrance may have has an effect on the complexation by humic acid winding up like random coils from the branched structure.

Gamble *et al.*[10] studied on interactions between Cu^{2+} and fulvic acid, and postulated that two types of reactions are involved in the interactions; the most important reaction involves both the phenolic OH and COOH groups, and another reaction of lesser importance involves the COOH groups only. The present results can be explained by the theory reported by Gamble *et al.*. The humic acid of 30,000-100,000 daltons is dominated with the aromatic COOH and phenolic OH and it preferentially interacts with ^{238}Pu and ^{241}Am. On the other hand, ^{241}Am did not interact with the humic acid of 5,000-30,000 daltons, which is mainly dominated with the aromatic COOH, despite ^{238}Pu is interacted. This contradiction may be attributed to that the interaction with ^{241}Am involves steric hindrance of the COOH groups.

4.CONCLUSIONS

The effects of humic acid on interaction affinity with ^{237}Np, ^{238}Pu and ^{241}Am have been examined with respect to different molecular size fractions. At the pH of 5.5, little ^{237}Np interacted with the humic acid. The humic complexation ability of ^{238}Pu and ^{241}Am were affected by the molecular size of humic acid. The humic acid fraction at different molecular size ranges had different structures and functional groups, each other. The molecular size selectivity on the complexation with transuranic nuclides may be caused by more than two different functional groups concerning to the complexation and/or steric hindrance around the functional groups.

REFERENCES

[1] J.F.McCarthy and J.M.Zachara: *Environ.Sci.Technol.*, **23**, 496-502 (1989).
[2] K.Nash,K, *et al.*: *Environ.Sci.Technol.*, **15**, 843-837 (1981).
[3] T.Tanaka and S.Ni: *JAERI-M 93-185*, (1993).
[4] T.Kanno: *Radioactive Waste Research*, **1**, 131-162 (1995).
[5] K.H.Lieser and U.Muhlenweg: *Radiochim.Acta*, **43**, 27-30 (1988).
[6] G.A.Burney and R.M.Harbour: *NAS-NS-3060*, (1974).
[7] J.J.Alberts, Z.Filip and N.Hertkorn: *J.Contaminant Hydrogy*, **11**, 217-330 (1992).
[8] F.J.Stevenson: "*Humus Chemistry*", pp.267-278, John Wiley & Sons, New York (1982).
[9] Nihon-kagaku-kai: "Kagaku-to-sousetsu No.4, Tsuti-no-kagaku", pp.85-86, (1998), Gakujutsu-Shuppan-Senta, Tokyo (1989).
[10] D.S.Gamble, M.Schnitzer and I.Hoffman: *Can.J.Chem.*, **48**, 3197-3204 (1970).

JP0250364

JAERI-Conf 2002-004

SORPTION BEHAVIOR OF NEPTUNIUM ONTO SMECTITE UNDER REDUCING CONDITIONS IN CARBONATE MEDIA

AKIRA KITAMURA, TSUTOMU TOMURA AND TOMOKI SHIBUTANI

Waste Isolation Research Division, Waste Management and Fuel Cycle Research Center,
Tokai Works, Japan Nuclear Cycle Development Institute (JNC)
4-33 Muramatsu, Tokai-mura, Naka-gun, Ibaraki, 319-1194, Japan
Fax: 81-29-287-3704, e-mail: ak@tokai.jnc.go.jp

Sorption behavior of neptunium onto smectite was investigated under reducing conditions in carbonate media. Distribution coefficient (K_d) of neptunium on smectite was determined by a batch method as a function of total carbonate concentration (C_T) in a weak alkaline solution. The C_T value was ranged from 0.09 M (M≡mol·dm^{-3}) to 1.0 M. The obtained K_d value decreased with increasing the total carbonate concentration. It was found that both Np(IV) and Np(V) coexisted in the solution by a TTA-extraction method. In the present experimental conditions, contribution of neptunyl ion, NpO_2^+, carbonate complexes of Np(V), $NpO_2(CO_3)_n^{(2n-1)-}$ (n=1, 2 and 3), and a carbonatohydroxo complex of Np(IV), $Np(CO_3)_2(OH)_2^{2-}$, to the sorption onto smectite was expected. The K_d values of respective species of neptunium were estimated by a least-squares fit to the experimental data. From the obtained K_d values of respective species, sorption behavior of neptunium onto smectite was discussed.
Key words: radionuclide migration, neptunium, sorption, smectite, reducing conditions, carbonate media

1. INTRODUCTION

Understanding the radionuclide migration behavior is important for safety assessment of a geological disposal of high-level radioactive wastes (HLW). Chemical compositions and pH value of a groundwater around the repository of HLW will affect the migration behavior of cationic radionuclides due to the complexation with anionic ligands when the radionuclides will dissolve to the groundwater. In the report of "H12: Project to Establish the Scientific and Technical Basis for HLW Disposal in Japan" [1], several types of hypothetical groundwater are summarized. Four types of hypothetical groundwater, which are FRHP (fresh-reducing-high pH), FRLP (fresh-reducing-low pH), SRHP (saline-reducing-high pH) and SRLP (saline-reducing-low pH), have been defined and modeled as generic groundwater compositions for the performance assessment for HLW disposal in the "H-3" first progress report [2]. In some special locations in Japan, however, middle salinity, reducing, neutral pH waters which contain high concentration of HCO_3^- have been found. Thus, a new type of hypothetical groundwater "MRNP" (mixing-reducing-neutral pH) has been defined as an additional generic groundwater compositions [3]. The MRNP groundwater contains high concentration of HCO_3^- (5×10^3 ppm) and Cl^- (1×10^4 ppm).

Thus, investigation of migration behavior of radionuclides in buffer materials and rocks in highly carbonate media is important for the performance assessment for HLW disposal. Especially, Np-237, which is an α-emitter and has the long half-life of 2.14×10^6 years, is regarded as one of the most hazardous radionuclides for HLW disposal. In a deep geological environment which is expected to be under reducing conditions, a tetravalent neptunium will be dominant, while a pentavalent neptunium is dominant in the near-neutral solutions contact with air. Expected dominant aqueous species of neptunium in a deep geological environment are $Np(OH)_4(aq)$ and $Np(CO_3)_2(OH)_2^{2-}$ in the "H-12" report [1]. Consequently, it is important to understand the migration behavior of Np(IV). Extensive studies have been performed to obtain the data to elucidate the sorption and diffusion behavior of neptunium. The previous studies on neptunium sorption onto bentonites under reducing conditions, however, are insufficient to evaluate the sorption behavior of Np(IV), especially in highly

carbonate media.

In the present study, sorption of neptunium onto smectite under reducing conditions in highly carbonate media has been investigated. Distribution coefficient (K_d) of neptunium onto smectite, which is a major component of bentonite, is determined in a weak alkaline solution as a function of total carbonate concentration (C_T). Considering the redox state speciation of neptunium, the K_d values of respective aqueous neptunium species are obtained. The sorption behavior of neptunium carbonate complexes is discussed.

2. EXPERIMENTAL

2.1 Preparation of Smectite

The bentonite sample of Kunipia-F® (Kunimine Industries Co.), which was commercially purified from Kunigel-V1® (Kunimine Industries Co.), was used as a starting material for purification of smectite. Before purification, Kunipia-F® contains 99 wt.% of Na-type smectite and some impurities, for example, quartz and calcite. A counter ion of Na^+ on the smectite may be replaced with other counter ions such as Ca^{2+}. Thus, further purification was required for the present study.

The dried Kunipia-F® of 20 g and 1 M ($M \equiv mol \cdot dm^{-3}$) NaCl of 1 dm^3 was mixed in a glass beaker and was shaken for 3 hours. After 1 hour leaving, the coagulated suspension was obtained by a decantation method. After adding an aliquot of distilled water to the suspension, the suspension was centrifuged at 3×10^3 rpm for 15 min for removal of the mineral impurities and large particles above 5×10^{-7} m. The centrifuged suspension was washed with a HNO_3 and NaCl mixed solution at a pH around 3.1, re-centrifuged and decanted for several times. For removal of NaCl, a dialysis method was performed by using a semipermeable membrane. The remained suspension was finally evaporated to dryness. The detail of the above procedure is described in the literature [4].

2.2 Sorption Procedure

Distribution coefficient (K_d) of neptunium onto smectite was determined by a batch method. A stock solution of $^{237}NpO_2Cl$ in an 1.4 M HCl solution was obtained from Amersham Co., and used without further purification. In a polypropylene tube, 0.2 g of smectite powder was added into 20 ml of an 1 M NaCl and 0.01 M $Na_2S_2O_4$ mixed solution. Reagent of $NaHCO_3$ powder was also added into the tube for ranging a total carbonate concentration (C_T) from 0.09 M to 1.0 M. The initial concentration of Np-237 was set at 1×10^{-6} M. The sample was gently contacted with shaking at 22±3 °C to attain sorption equilibrium. The pH value was measured by using a pH/ion meter, IM-55G (DKK-TOA Co.), with a glass electrode, GST-5421C (DKK-TOA Co.), and the pH of the solution was adjusted around 9. The redox potential E_h (vs. SHE) in the solution was monitored during the experimental procedure by using a glass electrode, PST-5421C (DKK-TOA Co.).

After shaking time of 16 d and 42 d, the solution of the sample was filtered by using an ultrafilter with the molecular weight cut-off (MWCO) of 10^4 (Advantec USY-1, Toyo Roshi Kaisha Ltd.), and the total neptunium concentration in the solution was determined. After shaking time of 42 d, a TTA-extraction method [5, 6] was applied to the determination of the oxidation state of neptunium. The method was performed as follows. The concentration of HNO_3 in the filtrate was adjusted around 1 M by adding 10 M HNO_3. The filtrate and 0.5 M TTA (thenoyltrifluoroacetone) in a xylene solvent was vigorously shaken for 10 min for extraction of Np(IV) to the organic phase. After removal of aqueous phase, 10 M HNO_3 was added to the organic phase and vigorously shaken again for 10 min for back-extraction of Np(IV) to the aqueous phase. The concentrations of Np(IV) and Np(V) were defined as the concentration of neptunium in the organic and aqueous phase after the TTA-extraction method, respectively. The α-ray counting of Np-237 was performed by using either the alpha

spectrometer Octête PC™ (EG&G ORTEC Co.) or the liquid scintillation counter, 2770TR/SL (Packard Instruments Co.) with the scintillator Ultima Gold™ XR (Packard Instruments Co.).

All the procedures except α-ray counting were performed in a glove box filled with N_2 gas (O_2 < 1 ppm) to avoid the contamination of O_2 and CO_2 gas in air.

2.3 Desorption Procedure

A desorption experiment was performed after the sorption procedure. After equilibration of sorption experiment, a mixed solution containing 1 M KCl and 0.01 M $Na_2S_2O_4$ was added to the suspension which was containing the neptunium-sorbed smectite. After a shaking time of 3 d, an aliquot of the solution was filtered by using the ultrafilter with the MWCO of 10^4, and the α-ray of Np-237 in the filtrate was detected by either the alpha spectrometer or the liquid scintillation counter. A HCl solution was added to the suspension adjusting the HCl concentration to 1 M after the desorption procedure with KCl. The same procedures for the filtration and α-ray counting was performed after shaking time of 3 d.

Finally, sorption of neptunium onto the vessel wall of polypropylene tube was investigated. After removal of the smectite and the solution which was not used to the above desorption experiment, the polypropylene tube was washed by distilled water. A concentrated HCl solution (around 11.4 M) was introduced to the tube, and the neptunium concentration in the concentrated HCl solution was determined.

Similar to the previous procedure (see section 2.2), all the procedures except α-ray counting were performed in a glove box filled with N_2 gas (O_2 < 1 ppm).

3. RESULTS AND DISCUSSION

3.1 Distribution Coefficient by the Batch Experiment

Experimental K_d ($m^3 \cdot kg^{-1}$) of neptunium onto smectite is calculated by the following equation:

$$K_d = \frac{(C_0 - C_f)V}{C_f W}, \qquad (1)$$

where C_0 (M) and C_f (M) denote the concentrations of the neptunium before and after equilibration, respectively, V (m^3) the volume of the solutions and W (g) the weight of the dried smectite sample.

The obtained K_d values are shown as a function of C_T in Fig. 1. The final pH value of the samples was 8.6±0.3. It is found that the K_d values decrease with increasing C_T. As shown in Fig. 1, little difference in the K_d values between the shaking time of 16 d and that of 42 d is found. Based on this, it is judged that the sorption of neptunium onto smectite approximately equilibrated. Below C_T of 0.08 M, it was presumed that the

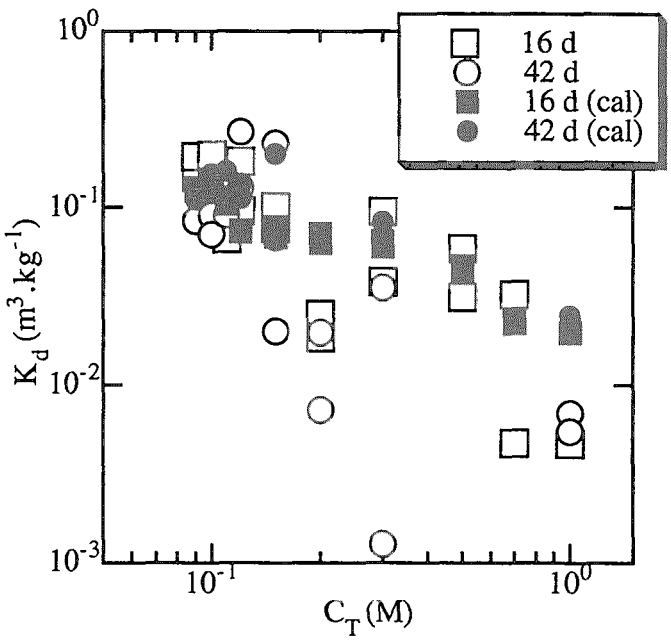

Fig. 1 Experimental and calculated K_d values of neptunium onto smectites as a function of C_T

concentration of neptunium in solution was steeply decreased with decreasing C_T due to the precipitation of Np(IV). Thus, only the K_d values above C_T of 0.09 M were adopted as reliable data in the present study. The K_d values were not determined for several samples due to a weak sorption of neptunium onto smectite, especially in high C_T solutions.

3.2 Speciation of Redox States of Neptunium in Solution

Experimental results for the ratio between the concentration of Np(IV) ([Np(IV)]) and the total neptunium concentration ($[Np]_{total}$) in the solution are shown as a function of C_T in Fig. 2. The E_h (vs. SHE) values have been held around –0.4 V. It is found, however, that a major oxidation state below C_T of 0.05 M is pentavalent. According to the thermodynamic database developed by the Nuclear Energy Agency in the Organization for Economic Co-operation and Development (OECD /NEA) [7], a major oxidation state is tetravalent in the present experimental conditions. The dominant aqueous species of Np(IV), on the other hand, only $Np(OH)_4$ (aq.), $Np(CO_3)_4^{4-}$ and $Np(CO_3)_5^{6-}$ are accepted to the thermodynamic database by OECD/NEA [7]. Considering the two aqueous species of Np(IV), however, the solubility of Np(IV) is calculated to be much lower than the concentration of Np(IV) experimentally obtained from the present study. Several researchers have determined an equilibrium constant of a carbonatohydroxo complex of tetravalent actinides, $An(CO_3)_2(OH)_2^{2-}$ (An: U [8,9], Np [9-11] or Pu [12,13]), which is considered to be a dominant species of An(IV) in a weak alkaline solution containing carbonate or hydrogencarbonate ions. The solubility of NpO_2(am), including the carbonatohydroxo complex of $Np(CO_3)_2(OH)_2^{2-}$, in an 1 M NaCl solution as a function of C_T at pH 8.6 is calculated as shown in Fig. 3. The ionic strength correction is performed by a "specific ion interaction theory (SIT)" model [14].

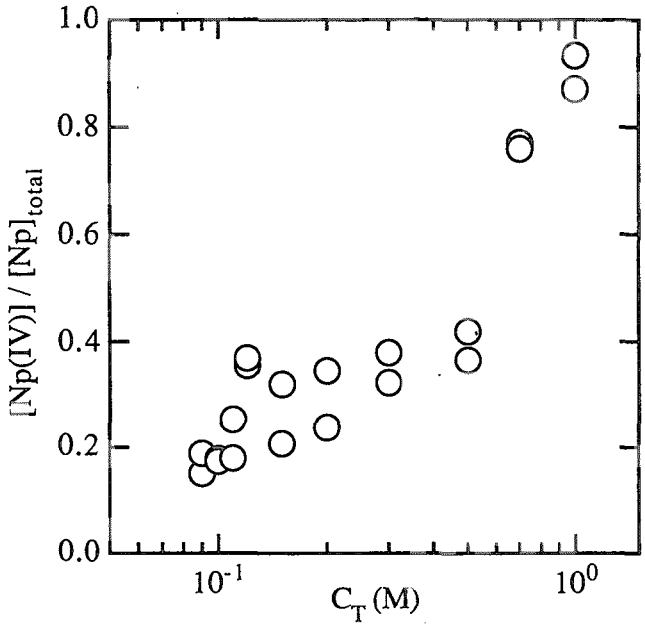

Fig. 2 Ratio between aqueous concentration of Np(IV) and that of total neptunium determined by a TTA-extraction method

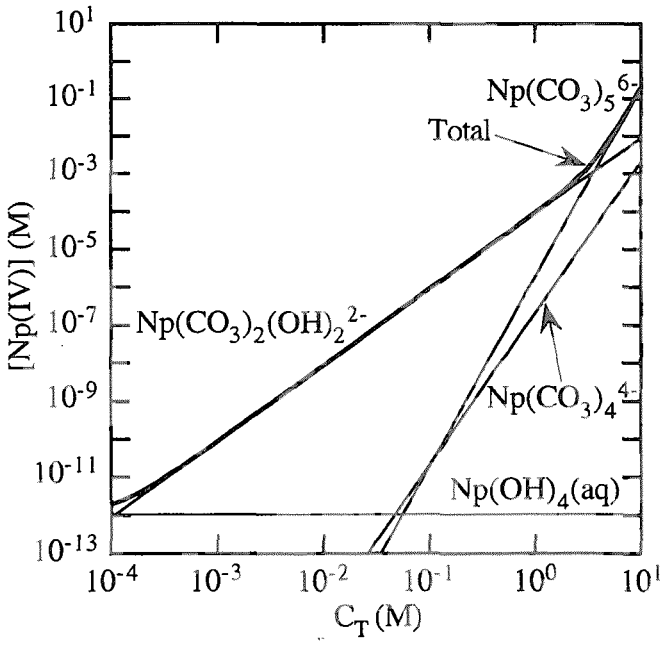

Fig. 3 Solubility of Np(IV) as a function of C_T in an 1 M NaCl solution at pH 8.6

It is also found that the ratio of $[Np(IV)]/[Np]_{total}$ increases with increasing C_T. The present result

shows that the steady-state is reached rapidly in high hydrogencarbonate solutions and that high hydrogencarbonate solutions appear to stabilize the tetravalent state, similar to the results by Rai et al. [10].

3.3 Analytical Procedure

As mentioned above, result of the TTA-extraction method shows that both Np(IV) and Np(V) coexist in the solution for the sorption experiments. Based on the result, it is considered that K_d values shown in Fig. 1 result in sorption by several species of Np(IV) and Np(V). Thus, the experimental K_d value is expressed as

$$K_d = \sum_i K_{di} X_i, \qquad (2)$$

where K_{di} and X_i denote the distribution coefficient and the molar fraction of species i of neptunium in solution, respectively.

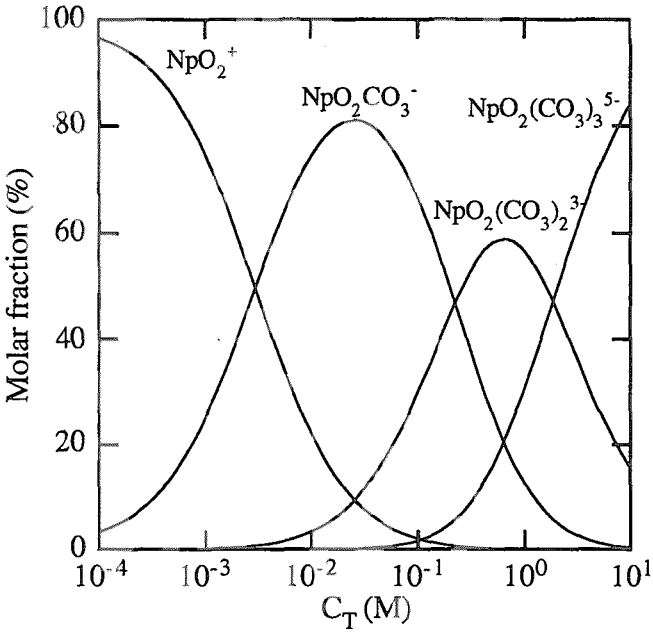

Fig. 4 Fraction of Np(V) species as a function of C_T in an 1 M NaCl solution at pH 8.6

According to the thermodynamic data by OECD/NEA [7], several hydrolysis species and carbonate complexes are considered to be formed in a weak alkaline solution containing carbonate or hydrogencarbonate ions. The fractions of the species of Np(V) at pH 8.6 in an 1 M NaCl solution are shown as a function of C_T in Fig. 4. In the present experimental conditions (C_T from 0.09 to 1.0 M), three carbonate complexes, $NpO_2(CO_3)_n^{(2n-1)-}$ (n = 1, 2 or 3), are considered to be the dominant species. Neptunyl ion (NpO_2^+) is also considered to be remained in the present conditions. On the other hand, the dominant species of Np(IV) is considered to be $Np(CO_3)_2(OH)_2^{2-}$ as shown in Fig. 3. Thus, equation (2) can be represented as

$$K_d = \frac{1}{C_f}(K_{d1}[NpO_2^+] + K_{d2}[NpO_2CO_3^-] + K_{d3}[NpO_2(CO_3)_2^{3-}] + K_{d4}[NpO_2(CO_3)_3^{5-}] + K_{d5}[Np(CO_3)_2(OH)_2^{2-}]), \qquad (3)$$

where K_{d1}, K_{d2}, K_{d3}, K_{d4} and K_{d5} denote the distribution coefficient of NpO_2^+, $NpO_2CO_3^-$, $NpO_2(CO_3)_2^{3-}$, $NpO_2(CO_3)_3^{5-}$ and $Np(CO_3)_2(OH)_2^{2-}$, respectively.

Respective concentrations of Np(V) are calculated as multiplying the molar fraction with [Np(V)] which is obtained from a TTA-extraction method. The concentration of $Np(CO_3)_2(OH)_2^{2-}$ is considered to be equal to [Np(IV)] of experimental results as shown in Fig. 3. For the K_d values after 16 d, the concentration ratio between [Np(IV)] and $[Np]_{total}$ is assumed to be same as that after 42 d. Then, a least-squares fitting analysis with equation (3) is performed to the experimental data shown in Fig. 1. In the analysis, distribution coefficients of respective species, K_{dn} (n = 1 – 5), are treated as a free parameter. The result

of numerical computation is shown as painted marks in Fig. 1, and the obtained K_{dn} values are listed in Table I. The obtained K_{d1} (for NpO_2^+) and K_{d2} (for $NpO_2CO_3^-$) values are similar to the previously reported K_d values in weak alkaline groundwaters under aerobic conditions [15-18]. It is considered to be reasonable that the obtained K_d values of respective species are decreasing with increasing the number of negative charge of the species, because the surface of the smectite is considered to be negatively charged in alkaline solutions [4,19]. The obtained K_{d5} (for $Np(CO_3)_2(OH)_2^{2-}$) value will be discussed later.

3.4 Desorption Results

The fractions of neptunium desorbed by 1 M KCl and the residual completely desorbed by 1 M HCl solution are shown as a function of C_T in Fig. 5. It is reported that neptunium desorbed by 1 M KCl solution is probably located ion-exchange site on the outer surface of the mineral, while specifically sorbed neptunium was fixed in the interlayer of smectite [20]. At low C_T values below 0.2 M, it is observed that most of neptunium is not desorbed by KCl but desorbed by only HCl. At high C_T values above 0.3 M, on the other hand, it is observed that all neptunium is desorbed by KCl. The present result is considered to be due to the contribution of different neptunium species for the different C_T values. Considering the results shown in Figs. 2 and 4, the dominant species of neptunium contributed to the sorption onto smectite is expected to be NpO_2^+ at low C_T solutions. At high C_T solutions, on the other hand, that is expected to be $Np(CO_3)_2(OH)_2^{2-}$. As mentioned previously, the surface of the smectite is considered to be negatively charged in alkaline solutions [4,19]. Thus, NpO_2^+ is expected to be sorbed onto negatively charged smectite surface as an electrostatic sorption, while $Np(CO_3)_2(OH)_2^{2-}$ is expected to be sorbed as a weaker sorption than NpO_2^+. Further investigation may be required to elucidate the desorption behavior.

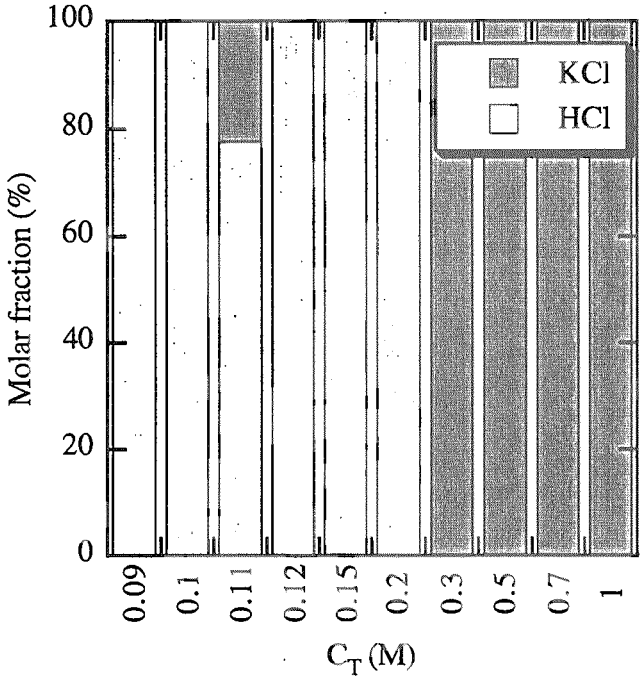

Fig. 5 Fraction of neptunium sorbed ion-exchangeably and specifically onto smectite by the desorption experiments with 1 M KCl and 1 M HCl, respectively

3.5 Discussion of Mechanism of Sorption of Neptunium onto Smectite

Despite the low E_h values around −0.4 V measured in the present study, it is found that the dominant redox states of neptunium for the sorption onto smectite is pentavalent in carbonate media below C_T of 0.5 M, as shown in Fig. 2. As mentioned above, the obtained K_d dependency on C_T has been well explained by considering the major contribution of NpO_2^+. The K_d value for Np(IV) (K_{d5}) also has been determined.

There are a few studies on the sorption of Np(IV) onto mineral surfaces considering with the aqueous neptunium species. Pratopo et al. study on Np(IV) sorption onto quartz [21] and Ca-type bentonite [22] under reducing conditions in carbonate media with pH ranged from 4.5 to 13. As shown in Table 1, Pratopo et al. have determined the K_d of

$Np(CO_3)_2(OH)_2^{2-}$ (K_{d5}) onto quartz [21] and Ca-type bentonite [22], which are much larger than that of NpO_2^+. There is a large discrepancy between the K_{d5} value by the present study and those by Pratopo et al. A reason of the discrepancy may be due to the calculation of molar fraction of aqueous neptunium species, even the distribution coefficient is dependent on pH in general. The studies of Pratopo et al. have no information for the speciation of neptunium in the experimental results. Thermodynamic calculation of the redox states and molar fractions of neptunium may provide the major contribution of Np(IV) under reducing conditions in alkaline solutions. The experimental results, however, the contribution of Np(IV) is smaller than the thermodynamic calculation, such as the present study and the solubility study on Np(IV) by Rai et al. [10]. Furthermore, it is difficult to describe the experimental K_d value which decreases with increasing C_T, without the contribution of Np(V), especially of NpO_2^+. Thus, the small K_{d5} value (for $Np(CO_3)_2(OH)_2^{2-}$) in the present study is considered to be reasonable.

As shown in Table I, it is found that the K_{dn} value of the respective species decreases with increasing the number of negative charge of the species independent of the redox state of neptunium in the present study. Considering with the desorption results as mentioned above, carbonate and carbonatohydroxo complexes of neptunium are expected to be sorbed onto smectite as a weak electrostatic interaction (it may be ion-exchangeable). The neptunyl ion (NpO_2^+), on the other hand, may be sorbed onto smectite as a formation of surface complex. Further experiments will be required to elucidate the mechanism of sorption of neptunium onto smectite under reducing conditions in carbonate media.

Table I Distribution coefficient of respective neptunium species onto smectite, quartz and Ca-type bentonite obtained from a least-squares fitting analysis

species	K_{di} ($m^3 \cdot kg^{-1}$)		
	smectite (present)	quartz* ([21])	Ca-type bentonite ([22])
NpO_2^+	$K_{d1} = 4.8\times10^{-1}$	$(1.31\sim13.1)\times10^{-3}$	$10^{-2.10\pm0.01}$
$NpO_2(OH)_2^-$			$10^{2.82\pm0.39}$
$NpO_2CO_3^-$	$K_{d2} = 1.8\times10^{-1}$	$< 3.93\times10^{-4}$	
$NpO_2(CO_3)_2^{3-}$	$K_{d3} < 5.3\times10^{-4}$	$< 3.93\times10^{-4}$	
$NpO_2(CO_3)_3^{5-}$	$K_{d4} < 7.0\times10^{-5}$		
$Np(CO_3)_2(OH)_2^{2-}$	$K_{d5} = 1.4\times10^{-2}$	6.56×10^{-1}	$10^{1.01\pm0.24}$
$Np(CO_3)_2(OH)_4^{4-}$		6.13×10^{-2}	$10^{0.93\pm0.37}$
$Np(OH)_5^-$		$> 1.04\times10^{4}$	

*Converting the surface-based distribution coefficient with the specific surface area of 1.31×10^2 $m^2 \cdot kg^{-1}$ in the literature [21].

4. CONCLUSIONS

Distribution coefficient of neptunium onto smectite was determined under reducing conditions in carbonate media by a batch method. The experimentally determined distribution coefficient decreased with increasing the total carbonate concentration. Considering with the molar fractions of Np(IV) and Np(V), distribution coefficient of respective species of neptunyl ions, carbonate complexes of Np(V) and carbonatohydroxo

complex of Np(IV) was determined by a least-squares fitting analysis. It was found that the distribution coefficient of respective species decreased with increasing the number of negative charge. Considering with the desorption results, carbonate and carbonatohydroxo complexes of neptunium are expected to be sorbed onto smectite as a weak electrostatic interaction.

ACKNOWLEDGEMENTS

The author should acknowledge Dr. H. Sato, Waste Isolation Research Division, Waste Management and Fuel Cycle Research Center, Tokai Works, Japan Nuclear Cycle Development Institute, for many suggestions and useful discussion.

REFERENCES

[1] Japan Nuclear Cycle Development Institute (JNC), JNC TN1410 2000-001(2000).
[2] Power Reactor and Nuclear Fuel Development Corporation (PNC), PNC TN1410 93-059(1993).
[3] M. Yui et al.: JNC TN8400 99-030(1999).
[4] T. Shibutani et al., JNC TN8400 99-066(1999) (in Japanese).
[5] A. M. Poskanzer, B. M. Foreman Jr., J. Inorg. Nucl. Chem., 16, 323-336(1961).
[6] S. C. Foti, E. C. Freiling, Talanta, 11, 385-392(1964).
[7] R. J. Lemire et al.: "Chemical Thermodynamics of Neptunium and Plutonium", North-Holland, Amsterdam(2001).
[8] D. Rai et al., Radiochim. Acta, 82, 17-25 (1998).
[9] M. I. Pratopo, H. Moriyama, K. Higashi, Radiochim. Acta, 51, 27-31(1990).
[10] D. Rai et al., Radiochim. Acta, 84, 159-169(1999).
[11] A. Kitamura, Y. Kohara, JNC TN8400 2001-006(2001).
[12] D. Rai et al., Radiochim. Acta, 86, 89-99(1999).
[13] T. Yamaguchi et al., Radiochim. Acta, 66/67, 9-14(1994).
[14] I. Grenthe et al.: "Modelling in Aquatic Chemistry", OECD, Paris(1997).
[15] L. L. Ames et al., RHO-BW-CR-127-P/PNL-3992(1981).
[16] B. Torstenfelt et al., Radiochim. Acta, 44/45, 111-117(1988).
[17] D. Stammose et al., Appl. Clay Sci., 7, 225-238(1992).
[18] J. F. Relyea et al., PNL-SA-7352, vol. 2(1978).
[19] W. Stumm, J. J. Morgan: "Aquatic Chemistry", 3rd ed., John Wiley & Sons Inc., New York(1996).
[20] N. Kozai et al., J. Nucl. Sci. Technol., 30, 1153-1159(1993).
[21] M. I. Pratopo et al., Radiochim. Acta, 55, 209-213(1991).
[22] M. I. Pratopo et al., J. Nucl. Sci. Technol., 30, 560-566(1993).

JP0250365

JAERI-Conf 2002-004

EFFECT OF TEMPERATURE ON THE SORPTION OF NEPTUNIUM ON MAGNETITE

K. NAKATA, S. NAGASAKI*, S. TANAKA, Y. SAKAMOTO**, T.TANAKA** AND H.OGAWA**

Departments of Quantum Engineering and System Science, University of Tokyo, Bunkyo-ku, Tokyo 113-8656, Japan

Fax: 81-3-5841-8622, e-mail:nakata@flanker.q.t.u-tokyo.ac.jp

*Graduate School of Frontier Sciences University of Tokyo Bunkyo-ku, Tokyo 113-8656, Japan

**Departments of Environmental Safety Research, Tokai Research Establishment Japan Atomic Energy Research Institute, Tokaimura, Naka-gun, Ibaraki 319-1195,Japan

Sorption and desorption experiments of Np on iron oxide were carried out at 25, 40 and 60 °C under ambient aerobic condition. Magnetite(Fe_3O_4) was used as one of representative iron oxide and sorption behavior was investigated. The sequential desorption method by using 1.0 M KCl and 0.1M $K_2C_2O_4$ solution was applied to magnetite-Np system to obtain the information on the sorption form of Np at each temperature. The results showed that the Np sorption on magnetite was strongly influenced by temperature. The amount of sorbed Np at each pH value increased with increase of temperature. Furthermore, the results of desorption experiment showed that the amount of Np sorbed exchangeably and the amount of Np sorbed on non-crystalline phase increased with increase of temperature. According to these results, the sorption of Np on magnetite is considered to include chemical sorption.

Apparent standard reaction entropy was calculated using of Vant't Hoff equation for exchangeable sorption and sorption on non-crystalline phase as 35~37 and 52~54(KJ/mol), respectively. These two different values of standard reaction entropy are considered to indicate the possibility of two or more kind of sorption site on the surface of magnetite.

Key words: Neptunium, Magnetite, Sorption, Desorption, Temperature

1. INTRODUCTION

According to the performance allocation analysis on multi-barrier system for high-level radioactive waste disposal, it was found out that Np-237 dominates the hazard at the exit of the natural barrier, namely at the inlet of the biosphere. Neptunium-237 is present in the high-level radioactive wastes, although in comparison to other radionuclides its amount is small. However, because of its long half-life and its mobile nature under aerobic conditions due to the high chemical stability of its pentavalent state, NpO_2^+, Np-237 is

considered as a possible long-term pollutant of the ecosystem[1]. The understanding of the Np sorption behavior is required in order to describe quantitatively its transport in surface and groundwater systems. Iron oxides are expected to play an important role in regulating the migration of radionuclides because of their widespread existence, and high sorption capacity[2]. Therefore, Np sorption data on iron oxides are required to describe the mobility of Np in natural waters. Neptunium sorption on iron oxides has been investigated in some cases [3,4]. However, the effect of temperature on sorption, which may yield important information about sorption mechanisms, have not been extensively studied in Np-iron oxide systems.

In this work, sorption and desorption experiments of Np on iron oxides were carried out at 25, 40 and 60 °C under ambient aerobic condition. Magnetite(Fe_3O_4) was used as one of the representaive iron oxides and sorption behavior was investigated. The sequential desorption method by using 1.0 M KCl and 0.1 M $K_2C_2O_4$ solution was applied to these system to obtain the information on the sorption form of Np at each temperature.

2. EXPERIMENTAL

2.1. Chemicals

Magnetite powder was obtained from Rare Metallic Co., Ltd. (Tokyo, Japan). Magnetite powder was sieved to a particle size of less than 250 μm before the sorption experiment.

9.2×10^{-2} M Np in 2.2 M HNO_3 was obtained from LMRI, France and diluted with deionized water to obtain a 1.8×10^{-2} M Np stock solution. The oxidation-state of Np was confirmed to be pentavalent because the evidence of presence of Np(IV) was not obtained by a solvent extraction technique using 0.5 M thenoyltrifluoroacetone (TTA) in xylene [5].

2.2. Procedures

(1) Sorption

Sorption experiments were conducted by batch method. Batch experiments were conducted as follows: 1 g of individual iron oxide were placed in 50 ml polypropylene tube with 40 ml of solution. The pH of the solution was adjusted to 4 to 8 using HNO_3 and NaOH solutions. The ionic strength was adjusted to 0.1 M by a $NaNO_3$ solution. The polypropylene tubes were placed in a shaker bath at 25, 40 or 60 °C for 7 days to allow equilibrium of the pH. Then, Np solution was added to each tube so that the concentration of Np became 6.0×10^{-6} M. The tubes were placed in a shaker bath again at each temperature for7 days. After 7 days, the pH was measured and 5 ml aqueous samples were taken from each tube after filtration with a 0.45 μm-pore size membrane filter. The Np concentration of

the aqueous samples was measured. Blank tests with 0.1 M $NaNO_3$ solutions were carried out in parallel with the sorption experiments in order to measure the Np sorption onto the wall of polypropylene tubes.

(2) Desorption

To investigate the chemical form of Np sorbed, a sequential desorption method was applied. After the end of the sorption experiments, liquid and solid phase were separated by centrifugal separator. At first, for the 1 g solid phase, 40 ml of the 1.0 M KCl solution was added and placed in a shaker bath for 7 days at each temperature that the sorption experiment was carried out. Then the liquid phase and solid phase were separated using a centrifugal separator. The liquid phase was filtrated with a 0.45 μm-pore size membrane filter, and the Np concentration in the filtrate was measured to evaluate the amount of Np desorbed by the KCl solution. After that, same procedure was carried out with 0.1 M $K_2C_2O_4$ solution.

In this work, the concentration of Np was measured using a liquid scintillation counter (Packard Institute).

3. RESULTS

3.1 Speciation

The speciation of Np(V) in 0.1 M $NaNO_3$ was calculated at the pH range between 2 to 10, at 25 and 60°C to investigate the change of speciation at 25°C and 60°C. The

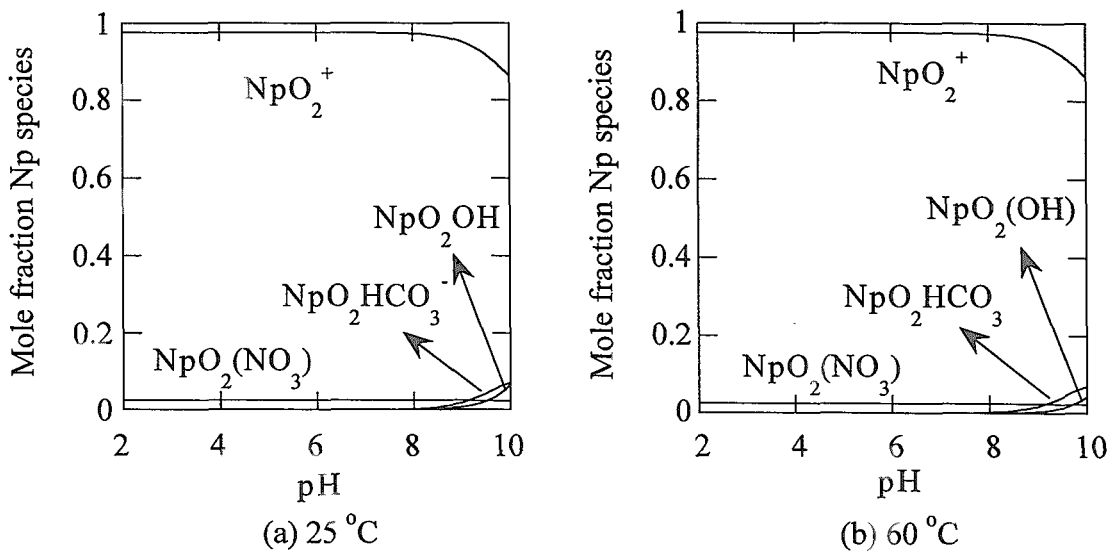

Figure 1. Calculated speciation of $6x10^{-6}$ M Np(V) in 0.1M $NaNO_3$ (a) 25 °C (b) 60 °C. Equilibrium constants used in Np(V) speciation were quoted from [6] and [7].

calculated speciation was showed in Figure.1 (a)25 °C and (b)60 °C. According to the calculated speciation, NpO_2^+ is dominant spices in solution at both 25 and 60 °C. This result indicated that the change of Np species in solution with the change of temperature do not affect the results of sorption and desorption experiments.

3.2 Sorption

The results of sorption experiments on magnetite are summarized in Figure 2. The fraction of sorbed Np, K (%), was calculated by using the following equation,

$$K = \frac{C_b - C_f}{C_b} \times 100,$$

where C_b and C_f represent the final concentrations of Np in the absence and presence of iron oxides, respectively. These results showed that the Np sorption on magnetite was strongly influenced by temperature. The amount of sorbed Np at each pH value increased with increase of temperature. According to results of sorption experiments, the sorption of Np on magnetite is considered to include the chemical sorption because the amount of Np sorbed on magnetite was strongly influenced by temperature.

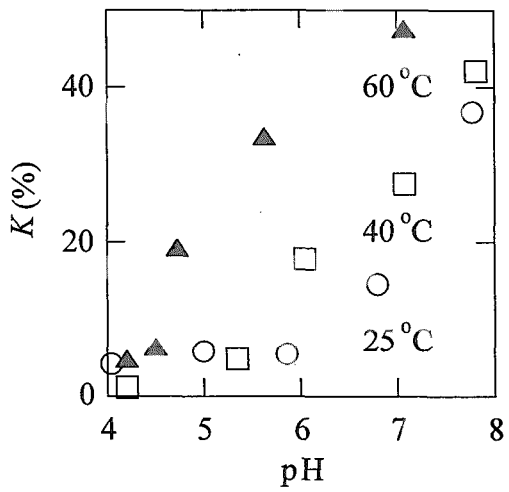

Figure 2. The fraction of sorbed Np on magnetite at 25, 40 and 60°C

3.3 Desorption

In the sequential desorption method used in this study, Np loosely or ion-exchangeably sorbed was considered to be desorbed by a KCl solution. Previous investigations[8] indicated that oxalate can desorb only non-crystalline phase of iron. Furthermore, we confirmed by using ICP and XPS that we could extract non-crystalline phase of iron oxide by a $K_2C_2O_4$ solution. According to these investigations, Np sorbed on a non-crystalline phase of iron oxides and Np sorbed on the surface of magnetite non-exchangeably is considered to be desorbed by a $K_2C_2O_4$ solution. The remaining Np which was not desorbed by KCl and $K_2C_2O_4$ solutions sorbs on the crystalline phase of iron oxides. Therefore, in this paper, we defined the Np desorbed by the KCl solution as "Np sorbed exchangeably", and that desorbed by the $K_2C_2O_4$ solution as "Np sorbed on non-crystalline phase" and the remaining Np as "Np sorbed on crystalline phase".

The results of desorption experiment from magnetite with KCl and $K_2C_2O_4$ solition

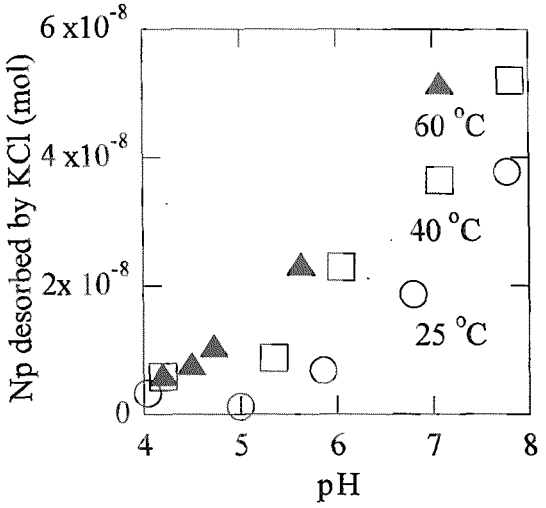

Figure 3. The amount of desorbed Np with 1.0 M KCl solution at 25, 40 and 60 °C

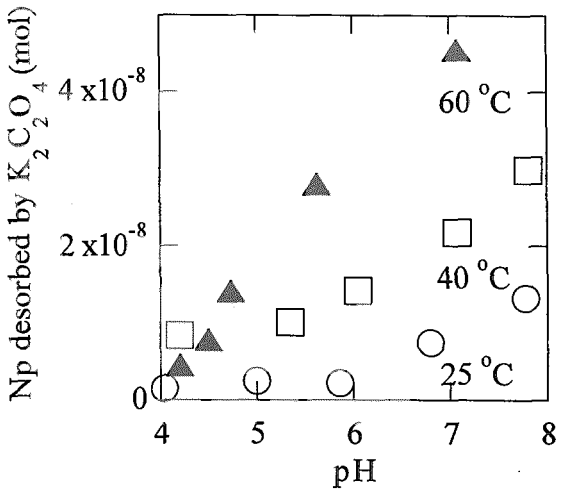

Figure 4. The amount of desorbed Np with 0.1 M $K_2C_2O_4$ solution at 25, 40 and 60 °C

are summarized in Figures 3 and 4, respectively. As shown in Figures 3 and 4, the amount of Np desorbed with KCl and $K_2C_2O_4$ increased with increase of temperature. These results were considered to indicate Np sorbed exchangeably and sorbed on non-crystalline phase also include the chemical sorption.

The relationships between the amount of Np sorbed exchangeably and that sorbed on non-crystalline phase was also investigated. It was found out that the amount of Np sorbed on non-crystalline phase was proportional to the amount of Np sorbed exchangeably for magnetite-Np system at each temperature (Figure5). Furthermore, it was also found out that the slope in Figure 5. increased with increase of temperature.

To explain these results, we considered the following possibilities. It was proposed in our previous study[9] that the surface of magnetite in both acidic and alkaline solutions would be covered with non-crystalline phase. Np would be sorbed on the surface of non-crystalline phase by 2 kinds of sorption mechanisms. One of the sorption mechanisms is conjectured to be ion-exchangeable sorption because some fraction of sorbed Np was desoebed

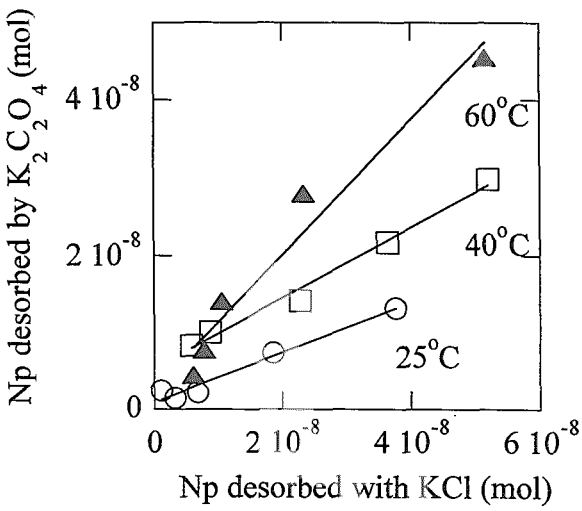

Figure 5. Relation between the amount of Np desorbed by KCl and $K_2C_2O_4$

with 1.0 M KCl solution. The other sorption mechanism is conjectured to be non-exchangeable sorption, such as surface complexation, and desorbed by $K_2C_2O_4$ solution because $K_2C_2O_4$ solution dissolved the non-crystalline phase that covered the surface of magnetite. It is also conjectured that the slope in Figure 5. increased with increase of temperature because dependence of sorption on non-crystalline phase on temperature was different from that of ion-exchangeable sorption.

To investigate the possibility of 2 kinds of sorption mechanisms, apparent standard reaction entropy was calculated using of Vant't Hoff equation for ion-exchangeable sorption and sorption on non-crystalline phase, as follows. At first, the apparent equilibrium constant K was calculated by using following equations.

$$K_1 = \frac{\text{(Amount of Np desorbed with KCl)}}{\text{(Concentration of Np in solution)}}$$

$$K_2 = \frac{\text{(Amount of Np desorbed with } K_2C_2O_4\text{)}}{\text{(Concentration of Np in solution)}}$$

Then results were plotted with 1/T as abscissa against K calculated in the manner described above in logarithm. According to the Vant't Hoff equation, the slope of this plot represents the value of -ΔH/R. Figure 6. shows the plot for calculation of apparent standard reaction entropy for ion-exchangeable sorption at pH=6.5 and 7.0.

$$\frac{dLnK}{dT} = \frac{\Delta H}{RT^2} \qquad \text{(Vant't Hoff equation)}$$

Apparent standard reaction entropy was calculated for exchangeable sorption and sorption on non-crystalline phase as 35~37 and 52~54(KJ/mol), respectively. These two different values of standard reaction entropy are also considered to indicate the possibility of two or more kind of sorption mechanism on the surface of magnetite.

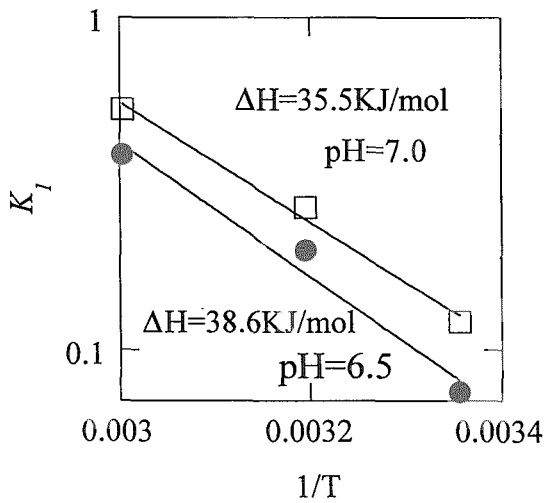

Figure 6. The plot for calculation of apparent standard reaction entropy for ion-exchangeable sorption at pH=6.5 and 7.0.

5. CONCLUSIONS

1. The amount of sorbed Np increased with increase of temperature. This is considered because the sorption of Np on magnetite includes chemical sorption
2. The amount of Np desorbed with KCl and $K_2C_2O_4$ solution increased with increase of temperature. These results are considered to indicate Np sorbed exchangeably and sorbed on non-crystalline phase also include the chemical sorption.
3. The amount of Np sorbed on non-crystalline phase was proportional to the amount of Np sorbed exchangeably for magnetite-Np system at each temperature. Furthermore, the proportion of amount of Np on non-crystalline phase to the amount of Np sorbed ion-exchangeably increased with increase of temperature. This is conjectured because Np would be sorbed on the surface of non-crystalline phase by 2 kinds of sorption mechanisms.
4. Apparent standard reaction entropy was calculated using of Vant't Hoff equation for exchangeable sorption and sorption on non-crystalline phase as 35~37 and 52~54(KJ/mol), respectively. These two different values of standard reaction entropy are also considered to indicate the possibility of two or more kind of sorption site on the surface of magnetite.

REFERENCES

[1] R. C. Thompson, Radiation Research, 90, 1 (1982).

[2] K. Idemitu, K. Obata, H. Furuta, Y. Inagaki, Mat. Res. Soc. Symp. Proc., 353, 981 (1995).

[3] S. Nakayama, Y. Sakamoto, Radiochimica Acta., 52/53, 153 (1991).

[4] O. Tochiyama, S. Endo, Y. Inoue, Radiochimica Acta., 68, 105 (1995).

[5] F. L. Moore and J. E. Hudgens Jr, Analytical Chemistry, 29, 1767 (1957).

[6] F.P.Bertetti, Mat.Res.Soc.SympProc., Vol 412, 631 (1995).

[7] J.C.Sullivan, Radiochim. Acta, 61, 57 (1993).

[8] U. Schwertmann, Can. J. Soil Sci., 53, 244 (1973).

[9] K. Nakata, S. Nagasaki, S. Tanaka, S. Tanaka, Y. Sakamoto, T. Tanaka and H. Ogawa, Radiochimica Acta., 88, 453 (2000).

This is a blank page.

JP0250366

JAERI-Conf 2002-004

THE EFFECTS OF SILICA SAND CONTENT AND TEMPERATURE ON DIFFUSION OF SELENIUM IN COMPACTED BENTONITE UNDER REDUCING CONDITIONS

HARUO SATO AND SHINYA MIYAMOTO*
Japan Nuclear Cycle Developemt Institute (JNC),
4-33 Muramatsu, Tokai-mura, Naka-gun, Ibaraki-ken, 319-1194, Japan
Fax: 81-29-287-3704, e-mail: sato@tokai.jnc.go.jp, *mshinya@tokai.jnc.go.jp

Apparent diffusivities (Da) in compacted bentonite for Se were obtained at a dry density of 1.6 Mg/m^3 as a function of silica sand content (0–50wt%) and temperature (22.5, 60°C) under reducing conditions. A Na-bentonite, Kunigel-V1® and ^{75}Se were used as a clay material and as a tracer in diffusion experiments, respectively. The obtained Da values showed a tendency to increase with increasing silica sand content and temperature. The Da values were moreover well correlative with smectite partial density, defined by the density of smectite aggregates in bentonite. This indicates that Se diffusion is predominantly controlled by the properties in part of smectite. The activation energies for Da values calculated from the temperature dependencies were in a range of 17 to 32 kJ/mol, but neither systematic tendency with respect to dry density nor smectite partial density was found.
Key words: Apparent diffusivity, Diffusion, Bentonite, Selenium, Activation energy

1. INTRODUCTION

In JNC, tests and researches regarding geochemistry and radionuclide migration in buffer materials and geosphere as problems related to a geological disposal of high-level radioactive waste (HLW) have been carried out in the Quantitative Assessment Radionuclide Migration Experimental Facility (QUALITY) as a link in the chain of a follow-up of the second progress report (H-12 report) [1], which has explained on a technical feasibility of the geological disposal of HLW in Japan. The QUALITY is a hot facility, which has 12 controlled atmosphere glove boxes and 9 air glove boxes, and the hot operation started on August 18, 1999. Much hot data regarding solubility, sorption and diffusion have been obtained and some outcomes have been reported to date [e.g. 2]. The equipments and details of the QUALITY are described in [3].

Although much data with respect to diffusion and sorption of radionuclides for bentonite have been reported so far, almost data have been obtained under air and data for redox sensitive elements obtained under reducing conditions, reflected a deep geological environmental condition, are quite limited. Selenium, important for dose evaluation in safety assessment, is one of the redox sensitive elements. Particularly ^{79}Se, its half-life $T_{1/2}$>6.5E4y, is identified as one of the important radionuclides. Although the half-life of ^{79}Se has not distinctly been determined, a value of $T_{1/2}$=1.13E6y has also been reported recently [4]. It is known from conventional studies that Se forms anions in solution and is little sorptive on bentonite [e.g. 5]. Selenium is found in oxidation states between –II and VI. In the pH range of natural waters, SeO_4^{2-} is predominant under strongly oxidising conditions [6], while HSe^- dominates under reducing conditions [6, 7]. Thus the chemical species of Se depends on the redox condition and pH of solution, being possible that Se retardation in bentonite can not be expected.

In the H-12 report, distribution coefficients (Kd) of radionuclides on bentonite were conservatively determined from measured apparent and effective diffusivities (Da and De, respectively). The Kd values for cases that no measured datum exists or those for cases that the reliability of data is controversial, were therefore determined based on chemical analogy or existing knowledges. The Kd of Se was also conservatively estimated to be Kd=0 based on Da values for Se obtained under reducing conditions [8] and De values for I (data of I^- were used as an analogue of HSe^-). The authors have proposed for Se an experimental method regarding non-steady state diffusion in bentonite under reducing conditions in previous study [8] and have reported a density dependency of Da values for Se. Quantitative data with respect to retardation

property in compacted bentonite and thermodynamic data of Se for diffusion are however lacking. Thereon, in this study, Da values for Se in bentonite under reducing conditions were obtained as a function of silica sand content and temperature as a link in the chain of database development and the reliability improvement of the H-12 report, and furthermore the effects of those parameters on diffusion in bentonite and diffusion mechanism for Se were discussed.

2. EXPERIMENTAL

2.1 Experimental conditions

The experiments were carried out by an in-diffusion method [e.g. 8]. Table I shows the experimental conditions. A sodium bentonite, Kunigel-V1® (Kunimine Industries Co. Ltd.), of which a lot of data regarding fundamental properties have been reported, was used in a series of diffusion experiments. The major constitutent minerals of the bentonite are Na-smectite and chalcedony, which makes up 46–49 and 37–38wt%, respectively [9]. Some other minor minerals such as quartz, plagioclase, calcite, dolomite, analcime and pyrite are also contained as impurities. Quantitative details of the minerals are described in [9]. The diffusion experiments were performed at a dry density of 1.6 Mg/m^3. Since Se is redox sensitive, all diffusion experiments were carried out in a controlled N_2 atmosphere glove box to reproduce a relevant disposal condition. A stock solution, $Na_2{}^{75}SeO_3$ (purchased from AEA Technology), was used as a tracer in the experiments. All experiments were carried out at room temperature (22.5°C) and 60°C in order to discuss diffusion behaviour thermodynamically.

Table I Experimental conditions for diffusion experiments

Method :	In-diffusion method (one way diffusion)
Bentonite :	Kunigel-V1® (Na-smectite, 46–49wt%)
Dry density :	1.6 Mg/m^3 (sample size: ϕ20mmx20mm)
Silica sand content :	0, 30, 50wt% (mixed with silica sand with particle sizes of 1–5mm and 0.1–1mm at a mixture ratio of 1:1)
Tracer solution : (carrier concentration)	^{75}Se (Na_2SeO_3 solution, 2.63 MBq/5ml (1.31E-8 M) 50ppm-Se (6.3E-4 M)
Introduced tracer quantity :	EC, $T_{1/2}$: 119.8d (136keV (58.3%), 265keV (58.5%), 280keV (24.8%), 121keV (17.1%), 401keV (11.4%)) 50μl/sample (21.96 kBq/sample)
Temperature :	room temperature (22.5±2.5°C), 60±0.1°C (oven)
Atmosphere :	N_2 atmosphere (O_2 concentration < 1ppm)
Saturated solution :	degassed distilled water + reductant (initial [$Na_2S_2O_4$]=5.2E-3 M)
pH of contacted solution :	7–7.5 (pH of solution contacted with bentonite)
Diffusing time :	1–14 days
Repetability :	n=2

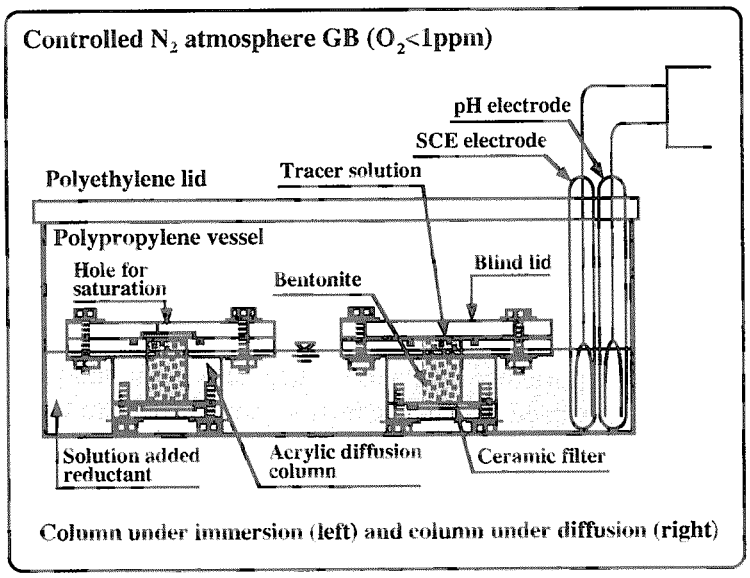

Fig.1 Set-up for diffusion experiments for Se
The left side of the figure shows the diffusion column under immersion and the right side of the figure shows the diffusion column under diffusion.

2.2 Diffusion experiments

Fig.1 shows set-up for diffusion experiments of Se. The diffusion columns to be used in a series of diffusion experiments are made of acrylic resin and have a cylindrical space of 20mm in diameter and 20mm thick, in which bentonite can be filled. The bentonite powder was dried at 110°C more than overnight and was filled into the cylindrical space of the diffusion column together with silica sand so as to obtain contents of 30 and 50wt%. The filling and compaction of the bentonite were performed by using a hydraulic press [10]. The diffusion columns filled with the bentonite were evacuated for air by exchanging with N_2 gas in a vacuum chamber and were then transferred to a controlled N_2 atmosphere glove-box. The diffusion columns with bentonite were after this immersed in degassed distilled water with sodium dithionate ($Na_2S_2O_4$)

for about 5 months to be saturated. Throughout the saturation of the bentonite, the bentonite contacted with the degassed distilled water added $Na_2S_2O_4$ in order to keep low Eh via alumina ceramic filters with a pore size of 2μm used to prevent the bentonite from the swelling as shown in Fig.1.

After the saturation of the bentonite, a small volume of $Na_2{}^{75}SeO_3$ (50μl, about 22 kBq), was pipetted on the surface of one end of each cylindrical bentonite and a blind lid was then sealed shut. The other end of the bentonite remained in contact with degassed distilled water with $Na_2S_2O_4$ via a ceramic filter. The Eh and pH of the solution contacting with the bentonite were monitored throughout the saturation and diffusion experiments. Although the reductant was added to obtain initially a concentration of $[Na_2S_2O_4]$=5.2E-3 M, it was then added to adjust the Eh of the solution if necessarily. The experiments were run for 1 to 14 days. After the diffusion periods, each cylindrical bentonite was cut with a knife into about 1mm thick slices. Each slice was immediately weighed in order to accurately calculate distance sliced from the surface of bentonite specimen and was analyzed for radioactivity with a Geiger Müller (GM) counter (Aloka Co., Ltd.). The concentration profiles of ^{75}Se in the bentonite were obtained based on the analyzed data. Since the half-life of ^{75}Se, 119.8d, is short, the concentration profiles were determined by correcting the decay of radioactivity in the analyses.

2.3 Background measurements for βγ-radioactivity including ^{75}Se from bentonite

The background of βγ-radioactivity including ^{75}Se from bentonite was quantitatively measured as a function of dry density (0.8, 1.6, 1.8 Mg/m^3) and slice thickness (0.5, 1.0, 5.0mm). The same type of diffusion columns as those used in diffusion experiments were used in the measurements. A series of measurement procedures were also carried out in the same way.

2.4 Preparation of a standard sample of ^{75}Se

A standard sample loaded ^{75}Se was prepared to determine detection efficiency for ^{75}Se of GM counter. The standard sample was prepared by pipetting a stock solution of 50μl with a radioactivity of 20.635 kBq on a paper with approximately the same size as bentonite slice. Since the half-life of ^{75}Se is short, initially loaded radioactivity of ^{75}Se was accurately corrected by considering the half-life when the standard sample was analyzed.

3. DIFFUSION THEORY

The Da values for ^{75}Se were determined based on the Fickian law [11]. The diffusion equation for one-dimensional non-steady state considered decay term is generally expressed as follows.

$$\frac{\partial C}{\partial t} = \frac{\partial}{\partial x}\left(Da\frac{\partial C}{\partial x}\right) - \lambda \cdot C \qquad (1)$$

Assuming that Da is independent of distance and is constant, Eq.(1) is arranged as follows.

$$\frac{\partial C}{\partial t} = Da\frac{\partial^2 C}{\partial x^2} - \lambda \cdot C = \left(\frac{De}{\alpha}\right)\frac{\partial^2 C}{\partial x^2} - \lambda \cdot C \qquad (2)$$

Where C is the radioactivity concentration in the bentonite (cpm/m^3), t is the diffusing time (s), x is the distance from diffusion source (m), Da is the apparent diffusivity (m^2/s), λ is the decay constant (1/s), De is the effective diffusivity (m^2/s), and α is the rock capacity factor (–).

With respect to soluble elements, the analytical solution for an instantaneous planar source can be applied for the calculations of Da values. However, with respect to elements which solubilities in the porewater of bentonite are low, there is a possibility to precipitate on the surface of bentonite. The boundary condition in this case is presumed to be controlled by the solubility of the tracer. If the bentonite sample is assumed to be a semi-infinite medium, the analytical solution for a constant concentration of boundary condition is derived as follows.

Initial condition: $C(t, x)= 0,\ t=0,\ |x|\neq 0$
Boundary condition: $C(t, x)=Co,\ t\geq 0,\ x=0;\ C(t, x)=0,\ t>0,\ |x|=\infty$

$$\frac{C}{Co}=\frac{1}{2}\left\{exp\left(|x|\sqrt{\frac{\lambda}{Da}}\right)erfc\left(\frac{|x|}{2\sqrt{Da\cdot t}}+\sqrt{\lambda\cdot t}\right)+exp\left(-|x|\sqrt{\frac{\lambda}{Da}}\right)erfc\left(\frac{|x|}{2\sqrt{Da\cdot t}}-\sqrt{\lambda\cdot t}\right)\right\} \quad (3)$$

Where Co is the boundary concentration (cpm/m^3).

Analytical method to determine Da was considered from the concentration profiles of ^{75}Se in bentonite in a series of diffusion experiments. Comparing the concentrations at the surface of bentonite (Co), neither Co change with time nor that with temperature was found. This indicates that Co is constant. Since the tracer solution used in this study includes a 50ppm of Se (equivalent to 6.3E-4 M) as a carrier, it is considered that Se precipitated at the surface of bentonite and that Co was controlled by the solubility of Se. The Da values for ^{75}Se were determined by a least squares fitting to the concentration profiles. Since Eq.(3) includes infinite arithmetrical series, it is difficult to determine Da values by fitting to Eq.(3). Thereon, Da values were numerically determined by discretizing Eq.(2) based on a difference method [11]. In the calculations of Da values, IDBENTO1, a calculation code for a least squres fitting, was used.

4. NUMERICAL ANALYSES BASED ON DIFFERENCE METHOD

4.1 Governing equations

The calculations were made by an explicit method which can forwardly be calculated among difference methods. The concentration profile of a tracer in bentonite can be calculated by Eq.(2). Initial and boundary conditions are the same as those for a constant boundary concentration.

4.2 Discretization and simulation by explicit method

Fig.2 shows a conceptual model for non-steady state diffusion simulation by the explicit method. Let consider Δx and Δt as a thickness in the direction of the depth of bentonite divided equally and a width of time, respectively. Both distance and time step are numbered as shown in Fig.2, and each node expresses concentration at a distance and a time step. The discreted equations for Eq.(2) and initial and boundary conditions based on the explicit method are given as follows.

Defining as $C(t, x)=C_{i,j}$, Eq.(2) is written as the following difference equation.

$$\left(C_{i+1,\ j}-C_{i,\ j}\right)/\Delta t = Da\left(C_{i,\ j+1}-2C_{i,\ j}+C_{i,\ j-1}\right)/\Delta x^2-\lambda\cdot C_{i,\ j} \quad (4)$$

Therefore, the following difference equation is derived, arranging Eq.(4).

$$C_{i+1,\ j}=C_{i,\ j}+Da\cdot\Delta t/\Delta x^2\left(C_{i,\ j+1}-2C_{i,\ j}+C_{i,\ j-1}\right)-\Delta t\cdot\lambda\cdot C_{i,\ j} \quad (5)$$
$$\left(i=1,\ 2,\ 3,\ \cdots,\ j=2,\ 3,\ 4,\ \cdots n_x\right)$$

Where n_x is the number of divisions in the direction of the depth of bentonite. Where input condition of $Da\cdot\Delta t/\Delta x^2$ in the numerical analysis adopted in this analysis must be constantly $\leq (1-\Delta t\cdot\lambda)/2$ not to cause numerical dispersion [12].

Distance from starting point and accumulative time, x_j and t_i, respectively are calculated as follows.

$$t_i=(i-1)\Delta t\ \ (i=1,\ 2,\ 3\cdots),\ \ x_j=(j-1)\Delta x\ \ \left(j=1,\ 2,\ 3\cdots n_x+1\right) \quad (6)$$

Initial and boundary conditions are expressed by the following difference equations.

Initial condition: $C_{i,j}=0,\ i=1,\ j\neq 1$

Boundary condition: $C_{i,j=Co}$, $i \geq 1$, $j=1$; $C_{i,j=0}$, $i \neq 1$, $j=n_x+1$

The concentration profiles were calculated as parameters for Da and Co, and Da and Co input when total sum of the residuals squared between calculated and measured concentrations was the smallest, were chosen.

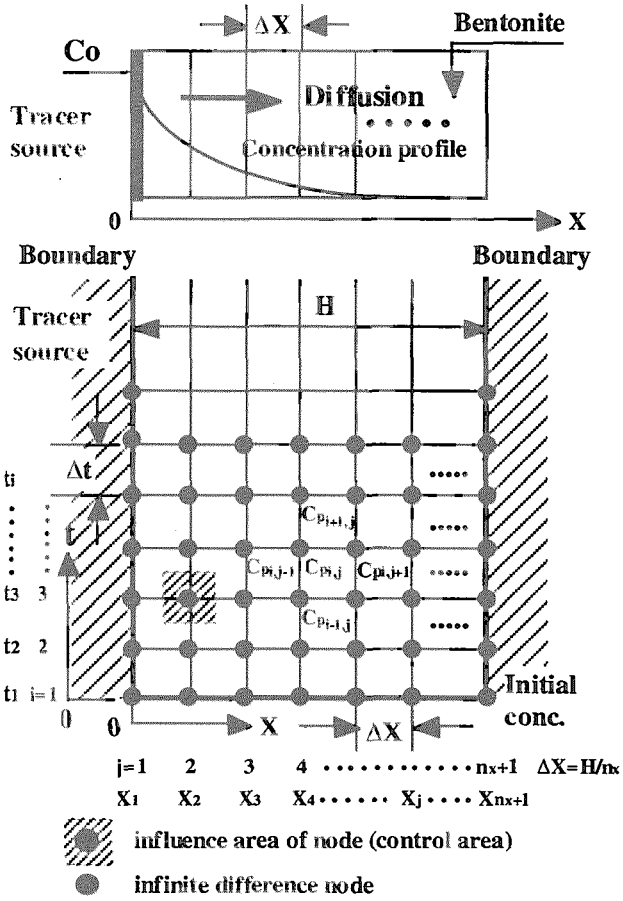

Fig.2 A conceptual model for non-steady state diffusion simulation by explicit method
H is the thickness of the sample in the figure.

5. RESULTS AND DISCUSSION

5.1 Background for βγ-radioactivity including ^{75}Se from bentonite

Fig.3 shows a correlation between counts per minute (cpm) and dry weight of bentonite. The obtained cpm values were approximately the same degree as level for natural radioactivity over the measurements, indicating that the obtained cpm values are not originated from bentonite. Average value was therefore used in the calculations of concentration profiles of ^{75}Se.

5.2 Da values of ^{75}Se and correlations with silica sand content and temperature

Although the Eh of solution contacted with bentonite rose a little with respect to diffusion experiments conducted at 60°C, that of the solution at 22.5°C was stable around −400mV throughout the saturation and diffusion experiments. The pH of the solution was also in a range of 7 to 7.5 and no significant change was found. The dominant species of Se in the porewater of bentonite in this condition is predicted to be HSe^- judging from Eh-pH diagrams [6, 7].

Fig.4 shows examples of concentration profiles for ^{75}Se as a function of the depth of bentonite from diffusion source at 22.5 and 60°C. Although diffusion experiments were carried out in duplicate for the same condition, similar concentration profiles were obtained. The diffusion of ^{75}Se at 60°C is faster than that at 22.5°C. The detection efficiency for the analysis of ^{75}Se by GM counter was 0.88% from comparison with standard sample.

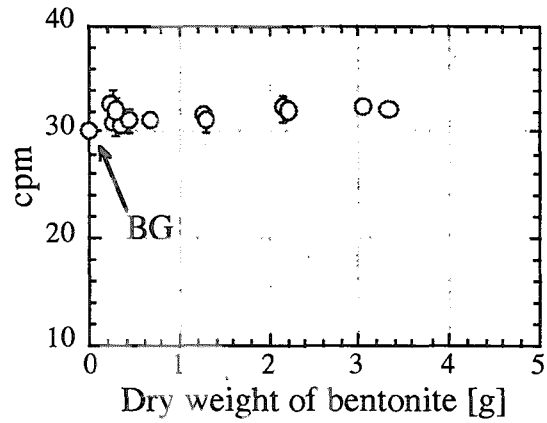

Fig.3 A correlation between cpm values and dry weight of bentonite
The plot on the vertical line shows cpm obtained without bentonite.

Fig.5 and Table II show dependencies of Da values for ^{75}Se on silica sand content and temperature and a summary of the Da values obtained in this study, respectively. The obtained Da values showed a tendency to increase with increasing silica sand content and temperature. The effects of silica sand content and temperature on Da are on the whole summarized as follows.

(1) The Da values for both temperatures show a tendency to increase with increasing silica sand content in bentonite. (2) The Da values show a tendency to increase with increasing temperature.

(3) The increasing rate of Da for temperature is approximately constant, unconcerned with silica sand content.

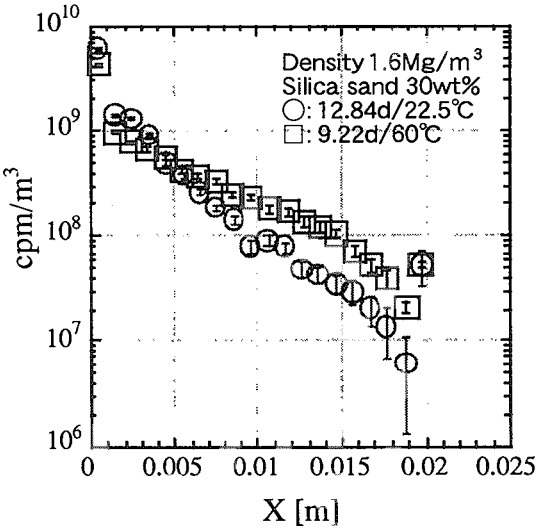

Fig.4 Examples of concentration profiles for ^{75}Se as a function of distance from diffusion source at 22.5 and 60℃

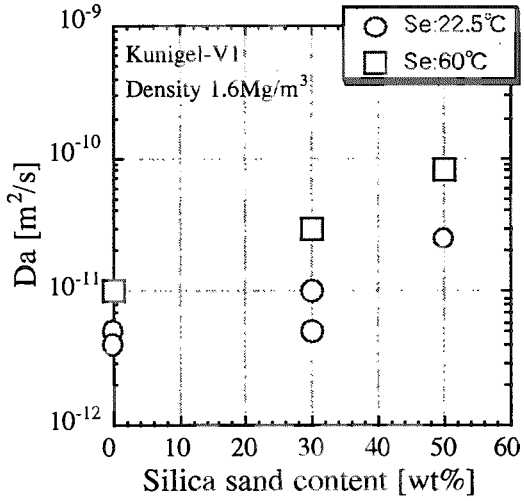

Fig.5 Dependencies of Da values for ^{75}Se on silica sand content and temperature

The Da values for ^{75}Se were compared with those for various elements previously reported [8, 13–17]. Fig.6 shows dependencies of Da values for various elements previously reported together with new data for ^{75}Se with respect to Kunigel-V1® on the dry density. The Da values for ^{75}Se are smaller than those for SeO_3^{2-} obtained under anaerobic conditions and are similar degree to those for Cs [13] and Ni [16] at the same dry density. These Da values for ^{75}Se are additionally about one order of magnitude lower than those for Tc, of which dominant species in the porewater of bentonite is TcO_4^- which is the same anion as Se. As described above, it is clear in any cases that Se is retarded under reducing conditions.

5.3 Correlations between Da values and smectite partial density

The Kunigel-V1® is composed of 46–49wt% of smectite and some impurities. Smectite, major clay mineral of the bentonite, is considered to compensate spaces between the impurities in bentonite and it is presumed that radionuclides mainly diffuse in smectite compensating the spaces between the impurities, because radionuclides can not pass through minerals composing the impurities. It is well known also from many literatures reported to date that the diffusion of radionuclides in smectite depends on the dry density. We here consider a density focused on smectite aggregates, so called the "smectite partial density". This parameter is equivalent to the "montmorillonite density" reported by Kuroda et al. [18]. The smectite partial density defined here is more generalized than that proposed by Kuroda et al. and can be applied for all kinds of bentonites. The smectite partial density for a bentonite added an arbitrary weight of silica sand is calculated by the following equation.

Table II A summary of Da values for ^{75}Se obtained as a function of silica sand content and temperature

No.	Temp. [°C]	Silica sand content[wt%]	Time[d]	Da[m²/s]	Co[cpm/m³]	ρ_{dm}[Mg/m³]*
1	22.5	0	14.03	5.0E-12	1.5E9	1.14
2	22.5	0	13.96	4.0E-12	1.5E9	1.14
3	60	0	13.03	1.0E-11	2.0E9	1.14
4	60	0	12.17	1.0E-11	2.0E9	1.14
5	22.5	30	12.84	1.0E-11	2.0E9	0.91
6	22.5	30	12.80	5.0E-12	2.0E9	0.91
7	60	30	9.22	3.0E-11	1.0E9	0.91
8	60	30	9.05	3.0E-11	1.0E9	0.91
9	22.5	50	1.964	2.5E-11	1.0E9	0.72
10	22.5	50	1.809	2.5E-11	1.0E9	0.72
11	60	50	1.881	8.0E-11	1.0E9	0.72
12	60	50	1.094	8.0E-11	1.5E9	0.72

*ρ_{dm}: smectite partial density which was defined by the density of only smectite aggregates in bentonite and can be calculated by Eq.(7)

$$\rho_{dm} = \frac{(1-fs)\cdot fm\cdot \rho_d}{1-\left\{(1-fs)(1-fm)\Big/\frac{1}{n}\sum_{k=1}^{n}\rho_{im,k} + fs/\rho_s\right\}\rho_d} \quad (7)$$

Where ρ_{dm} is the smectite partial density (Mg/m^3), ρ_d is the dry density of bentonite (Mg/m^3), fs is the silica sand content (Mg/Mg), fm is the smectite content in bentonite (Mg/Mg)(assumed as 0.5 for Kunigel-V1®), ρ_s is the pure density of silica sand (Mg/m^3)(2.7Mg/m^3), $\rho_{im,k}$ is the pure density of the k-th impurity (Mg/m^3)(assumed as 2.7 Mg/m^3 for all impurities), and n is the number of the kind of mineral composing the impurities of bentonite.

Fig.7 shows correlations between Da values for ^{75}Se and ρ_{dm}. The Da values were well correlative with ρ_{dm} for both temperatures. This indicates that Se diffusion is predominantly controlled by the properties in part of smectite. However, the tendency found in this study is different from that found in Pb diffusion [17]. Since both dominant species and sorption behaviours between both elements are different, the diffusion behaviours of both elements can not be simply compared, but this difference is one of the future studies to be paid attention.

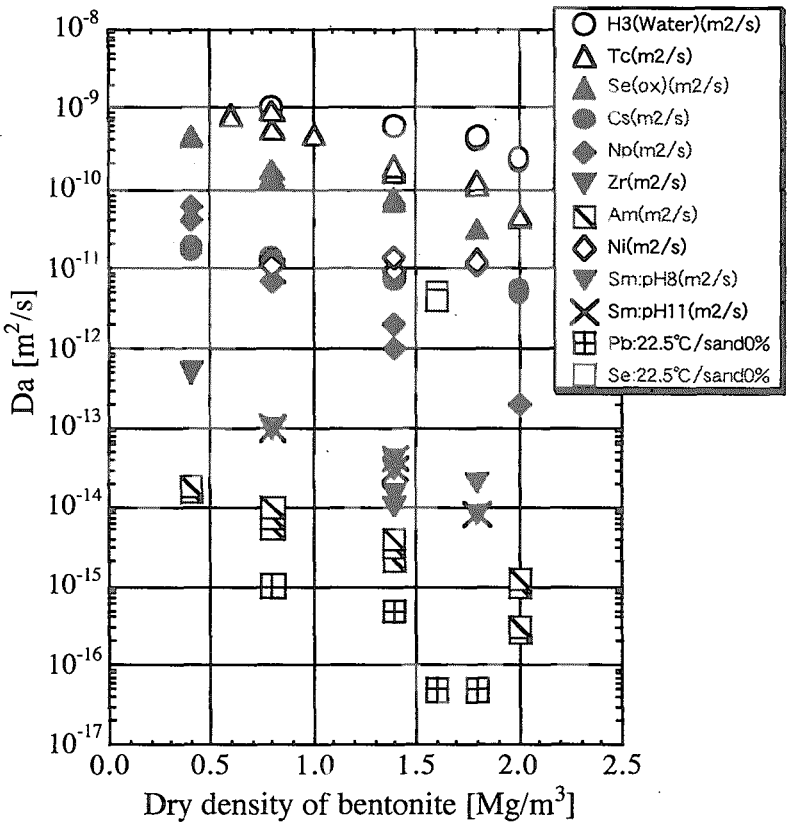

Fig.6 Dependencies of Da values for various elements reported to date together with new data for ^{75}Se (□Se: 22.5℃/sand 0%) on the dry density
Selenium marked (ox) was measured under anaerobic conditions, but not under reducing conditions.

5.4 Activation energy (ΔEa) for Da

The Da values for ^{75}Se clearly increased with increasing temperature as described above. Activation energies (ΔEa) for the Da values of ^{75}Se were calculated from the temperature dependencies based on the Arrhenius plot [19]. The calculated ΔEa values were in a range of 17 to 32 kJ/mol and neither systematic tendency with respect to dry density of bentonite nor that with respect to smectite partial density was found. Since no temperature dependency of ionic diffusivity in free water (D^o) for HSe^-, D^o_{HSe-}, has been reported, ΔEa for D^o_{HSe-} can not be

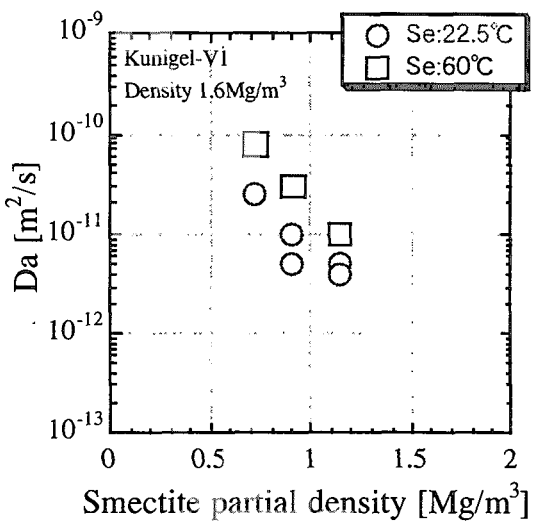

Fig.7 Correlations between Da values for ^{75}Se and smectite partial density

calculated, but ΔEa values of D^o values for popular ions are generally 15 to 25 kJ/mol. Although ΔEa values obtained in this study are a little higher than those ΔEa values, they are approximately the same degree. It is difficult to discuss quantitatively based on this study the difference between ΔEa values obtained in this study and those of D^o values for popular ions. Although the difference of porewater is considered as a possibility, we will treat as a future work with respect to quantitative discussion.

6. CONCLUSIONS

The Da values for ^{75}Se in compacted sodium bentonite were obtained at a dry density of 1.6 Mg/m^3 as a function of silica sand content and temperature under reducing conditions. The obtained conclusion is summarized as follows.

(1) The obtained Da values were smaller than those for SeO_3^{2-} obtained under anaerobic conditions and it was found that Se was retarded under reducing conditions.

(2) The Da values increased with increasing silica sand content in bentonite and temperature.

(3) The Da values were well correlative with smectite partial density. Based on this, Se diffusion in bentonite is predominantly controlled by the properties in part of smectite.

(4) The ΔEa values for Da, in a range of 17 to 32 kJ/mol, were similar degree to those of D^o values for popular ions. However, quantitative discussion for fact that ΔEa values obtained in this study were a little higher than those of D^o values for popular ions is future study.

REFERENCES

[1] Japan Nuclear Cycle Developement Institute, JNC TN1410 2000-001 (2000).
[2] T. Ashida, T. Shibutani, H. Sato, Y. Tachi, K. Kitamura, and K. Kawamura, JNC TN8400 99-083 (1999), in Japanese.
[3] H. Igarashi, K. Kawamura, K. Yamada, M. Yui, and J. Ohuchi, WM'00 Conference, February 27–March 2, 2000, Tucson, AZ, USA (2000).
[4] C. Li, J. Guo, and D. Li, J. Radioanalytical and Nucl. Chemistry, Vol.220, No.1, 69-71 (1997).
[5] T. Shibutani and M. Yui, PNC TN1410 96-071, 153-55 (1996), in Japanese.
[6] K. V. Ticknor, D. R. Harris, and T. T. Vandergraaf, Atomic Energy of Canada Limited Research Company, TR-453 (1988).
[7] D. G. Brookins, "Eh-pH Diagrams for Geochemistry", Springer-Verlag, Berlin Heidelberg (1988).
[8] H. Sato, Radiochimica Acta, 82, 173-78 (1998).
[9] M. Ito, M. Okamoto, K. Suzuki, M. Shibata, and Y. Sasaki, J. At. Energy Soc. Japan, Vol.36, No.11, 1055-58 (1994), in Japanese.
[10]H. Sato, T. Ashida, Y. Kohara, M. Yui, and N. Sasaki, J. Nucl. Sci. Technol., Vol.29, No.9, 873-82 (1992).
[11]J. Crank, "The Mathematics of Diffusion", 2nd Ed., Pergamon Press, Oxford (1975).
[12]Y. Fujiwara, "Analytical Method for Partial Differential Equation by Computer", Science Library, Tokyo (1971), in Japanese.
[13]H. Sato and T. Shibutani, PNC TN8410 94-284, 71-89 (1994), in Japanese.
[14]H. Sato and M. Yui, Scientific Basis for Nuclear Waste Management XVIII (T. Murakami and R. T. Ewing, eds.), Mat. Res. Soc., 269-76 (1995).
[15]Y. Tachi, Y. Kohara, N. Uchidate, and T. Shibutani, JNC TN8400 99-089 (1999), in Japanese.
[16]H. Sato and M. Yui, J. Nucl. Sci. Technol., Vol.34, No.3, 334-36 (1997).
[17]H. Sato and S. Miyamoto, JNC TN8400 2001-018 (2001).
[18]Y. Kuroda, K. Idemitsu, H. Furuya, Y. Inagaki, and T. Arima, Scientific Basis for Nuclear Waste Management XX (W. J. Gray and I. R. Triay, eds.), Mat. Res. Soc., 909-16 (1997).
[19]T. Keii and Y. Ono, "Activation Energy", Kyoritsu Press, Tokyo (1985), in Japanese.

JP0250367

JAERI-Conf 2002-004

COLLOIDS-ASSOCIATED CONCENTRATIONS MODEL AND EXPERIMENTAL STUDIES FOR A WASTE FORM DEGRADATION PROCESS MODEL

F.M.G. Wong[1], C. Stockman[2], C. Mertz[3], S. Alcorn[4], and R. Aguilar[2]

Yucca Mountain Site Characterization Office
1551 Hillshire Dr. M/S 471
Las Vegas, NV 89134
Fax: (702) 792-1323, e-mail: frank_wong@notes.ymp.gov
[1] Stone & Webster, Inc., [2] Sandia National Laboratory, [3] Argonne National Laboratory ,
[4] Management Solutions

A Waste Form Degradation Process Model [1] has been developed as part of the total system performance assessment (TSPA) that will be used to evaluate the postclosure performance of a potential monitored geologic repository at Yucca Mountain. For the Colloidal Radioisotope Concentration Component of this degradation model, the conceptualization directly used Yucca Mountain Project (YMP)-relevant experimental results from YMP-specific work and from the published literature. The conceptualization identified the availability and the stability of three categories of colloids: (1) existing colloids in the groundwater, (2) colloids generated during degradation of the waste, and (3) colloids generated during degradation of the disposal container. The function of the colloidal radioisotope concentration component is to calculate the concentration of colloid-associated radionuclides that may be transported from the waste package.

Attachment of radionuclides can range from instantaneously reversible to completely irreversibly bound attachment. This process was modeled using these two bounding end members. For waste form colloids, radionuclides can be incorporated into the substrate material before it is suspended as colloids. All colloid types may sorb radionuclides to form pseudocolloids, depending on the affinity of the colloid mineral substrate for a dissolved radionuclide. The contributions of each colloid type are summed to produce the mobile colloid source term for each important radionuclide.

The models are based on laboratory results from waste form corrosion testing and testing of adsorption and desorption properties of Pu and Am on clay and iron-(hydr)oxide colloids. To the extent that the laboratory tests and test conditions represent anticipated repository conditions, the model is valid for calculating the colloid-associated radionuclide concentrations and colloid mass concentrations.

This paper will describe and summarize the models and experimental studies used in the colloidal radioisotope concentration component of this waste form degradation process model.

Key Words: Colloids, Colloidal Source Term, Colloidal Concentration Limits, Waste Form Degradation

1. INTRODUCTION

The function of the colloidal radioisotope concentration component of the Waste Form Degradation Process Model [1] is to calculate the concentration of colloid-associated radionuclides that may be transported from the waste package [2]. This colloidal model component describes the observed types, formation, and stability of radionuclide-bearing colloids that result from degradation and decomposition of the waste forms contained in failed waste packages. In addition, contaminant-colloid attachment/detachment mechanisms and transport characteristics anticipated in the repository are discussed for colloids formed from degradation of the waste forms, colloids formed from man-made materials introduced into the repository, and naturally occurring colloids. The abstraction of these models is intended to capture the most important characteristics of radionuclide-colloid behavior for use in predicting the potential impact on repository performance of colloid-facilitated radionuclide transport.

Colloid transport is potentially important for radionuclide elements that have low solubility and can be entrained in, or sorbed onto, waste form, engineered barrier, or geologic barrier

materials that form colloidal particle substrates. Of these radionuclides, only those that are a major part of the waste inventory and have potentially large dose conversion factors are of potential importance to the performance of the disposal system. Considering these screening criteria, plutonium is the dominant. Americium is also considered for the TSPA analysis.

2. COLLOID TYPES

The radionuclide-bearing colloids are formed by radionuclide entrainment as discrete phases in, or by radionuclide sorption onto, colloidal substrates. They are, therefore, classified into "types" based on the source of the substrate material and can be further classified based on how the radionuclides are attached to the substrates. Three major types of colloids are recognized to be important for the colloidal radionuclide concentration component based on the source of the colloid substrate material: (1) Waste-form colloids formed during degradation of high-level waste (HLW) glass (Note: these colloids are further classified into "reversibly attached" and "irreversibly attached" radionuclide types); (2) Corrosion-product colloids formed during corrosion of iron-containing waste packages; (3) Groundwater colloids present in the waste-form area.

Based on laboratory evidence, waste-form colloids are produced from degradation of borosilicate HLW glasses. Fewer colloids have been observed in laboratory testing of commercial spent nuclear fuel (CSNF), and experimental data are not yet available for defense spent nuclear fuel (DSNF) and other waste forms, although testing is underway at National Spent Nuclear Fuel Program. The waste-form colloids that have been observed consist principally of smectite-type clay minerals. The laboratory evidence suggests that as HLW glass degrades, colloids are generated and often contain "entrained" plutonium. The engulfed solid inclusions of plutonium may be isolated from the aqueous system by the colloid itself and so may not be in equilibrium with the surrounding aqueous environment. Therefore, the engulfed plutonium in the waste-form colloids is conservatively assumed to be irreversibly associated with the waste form colloids.

Corrosion-product colloids consist of ferric iron-(hydr)oxide minerals, primarily goethite (FeOOH) and hematite (Fe_2O_3) that are assumed to form as a result of corrosion of the waste package (WP) materials [2].

Groundwater colloids potentially present in the repository include those already present in the geosphere such as microbes, organic macromolecules (humic substances, including humic and fulvic acids), and mineral colloids (primarily clay minerals, silica, and iron-[hydr]oxide minerals). Microbe-facilitated radionuclide transport is disregarded because the relatively large size of microbes makes them susceptible to filtration. Based on the very low complexation capacity of humic substances in this system, they are not considered to be important groundwater colloids. Clays, silica, hematite, and goethite colloids occur in groundwater in the vicinity of Yucca Mountain, and it is assumed that small quantities of these colloids will enter a failed WP and be available to interact with released radionuclides. Consequently, mineral colloids are considered and will, henceforth, be referred to generically as groundwater colloids. These groundwater colloids are assumed to consist of smectite clays, which are fairly strongly sorbing minerals, and have been recognized at Yucca Mountain [3]. This assumption is based on the fact that smectite colloids are the dominant colloid in groundwaters at the Nevada Test Site and the fact that it is a conservative choice because clay minerals are more sorptive than silica and are comparable to iron-(hydr)oxide minerals.

The colloid source term includes contributions from the various types of colloids, discussed above (i.e., waste-form, corrosion-product, and groundwater colloids with reversibly and irreversibly attached radionuclides). The contributions of each colloid type are summed to produce the mobile colloid source term for each important radionuclide. The concept of reversibly and irreversibly attached radionuclides on colloids is illustrated in Figure 1.

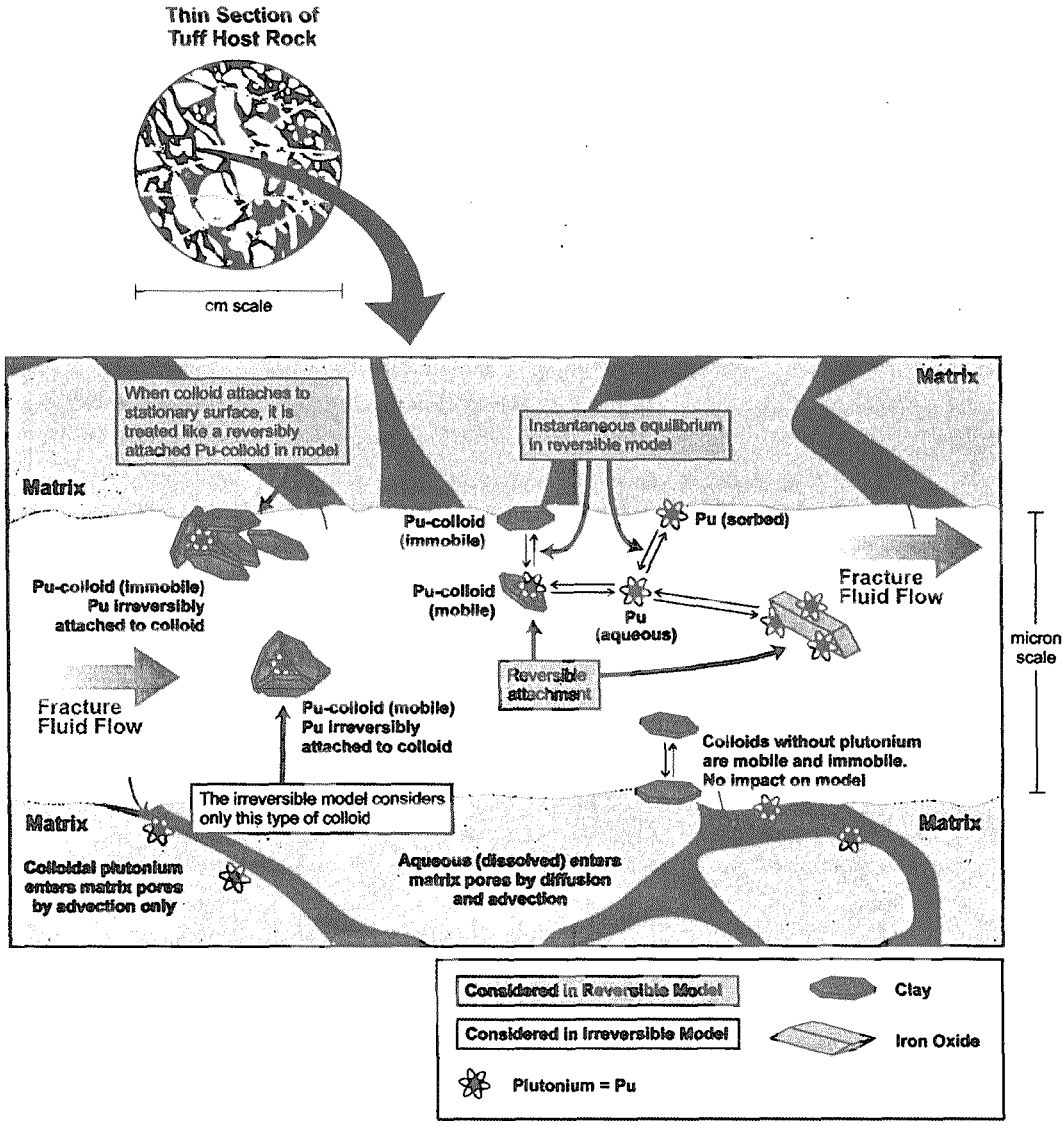

Figure 1. Conceptual Model of Formation of Reversibly and Irreversibly Attached Radionuclides on Colloids

3. MODEL DESCRIPTION

The colloid concentration component is implemented by summing the contributions of the three colloid types to the colloid radioisotope concentration for each radionuclide. A model was developed to calculate the colloid radioisotope concentration for each of the three colloid types. The model for the waste form colloids includes the contributions of the engulfed (irreversible attached) plutonium observed in waste glass tests. The models for all three colloid types include reversibly attached radionuclides. These models are based on the population of each colloid type (expressed in terms of mass of colloids per volume of fluid) and experimental data for the sorption of radionuclides onto the colloid substrate materials involved. The effects of pH and ionic strength on the stability of dispersions of each colloid

type are considered. The location of the boundaries between pH and ionic strength regimes in which each type of colloid substrate is stable or unstable are defined together with the colloid mass concentration in each regime.

3. 1 Waste-Form Colloids

Three broad categories of waste form are to be placed in the repository. The most abundant waste type is CSNF from commercially owned and operated electric power reactors. DSNF is a diverse collection of waste from reactors at DOE nuclear-complex sites. HLW is a borosilicate glass-based waste form. In the following descriptions, CSNF and DSNF are treated together.

The waste form concentration model includes contributions from colloids with reversibly and irreversibly-attached radionuclides. The model for the concentration of irreversibly attached radionuclide is based on the experimental data for HLW glasses. It was observed experimentally that, as the ionic strength increased, colloid concentration generally decreased and ultimately a threshold value was reached above which the colloids were not observed or were observed in very low quantities [4]. As this threshold was approached, it was also observed for one glass that the colloid size increased significantly due to aggregation of the colloids. The threshold at which flocculation occurred was approximately 0.05 mol/kg.

Colloids formed from HLW glasses in the ANL tests consist predominantly of a smectite clay substrate often containing discrete radionuclide-bearing phases entrained within the clay. For modeling purposes it is assumed that colloids derived from HLW are all radionuclide-bearing smectite. The radionuclides are conservatively assumed to be irreversibly attached to the smectite colloid substrate. Figure 2 represents the abstraction of the experimental results. Based on ionic strength conditions near the waste form, the concentration of irreversibly attached colloidal plutonium is calculated.

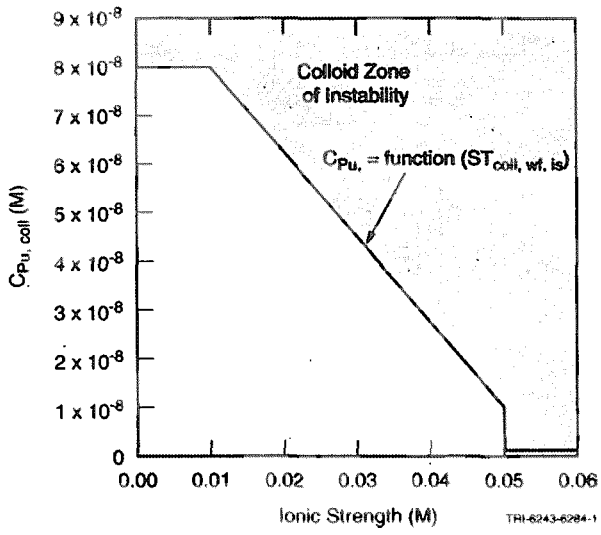

NOTE: Schematic relationship (used in abstraction) between RN-bearing colloid concentration and ionic strength. The function represents the bound of the HLW corrosion experimental data; the maximum value represented, 8×10^{-8}, is the maximum concentration of colloids observed in the HLW experiments.

Figure 2. Schematic Relationship Between Radionuclide-Bearing Colloid Concentration and Ionic Strength

3.2 Corrosion Product Colloids

Corrosion product colloids are assumed to be generated as a result of the corrosion of iron-bearing components of the WP. In this section, radionuclide uptake of mobile corrosion product colloids, assumed to be iron-(hydr)oxides such as hematite and goethite, is described.

Data are not available on the concentration of corrosion product colloids that may be generated as a result of corrosion of the WP materials. Limited data do exist, however, for concentrations of iron-colloids in natural systems. At the Morro de Ferro natural analog site (Poços de Caldas, Brazil) concentrations of iron-hydroxide [$Fe(OH)_3$] colloids were measured in deep groundwaters adjacent to an iron-rich rock body. The measured concentration, 0.25 mg/L, is similar to concentrations of other inorganic colloids found in natural waters at other deep sites [5]. Consequently, it is conservatively assumed that the concentration of these colloids is comparable to that of the groundwater colloids (all mineralogies) that are observed in natural groundwaters [2]. Colloid concentrations observed in natural waters represent concentrations developed over a wide range of hydrogeochemical conditions, which provides some assurance that the approach used is reasonable. A maximum value of 1 mg/L [1] was used in the TSPA calculations, which imparts a four-fold conservatism relative to concentrations observed at the analog site.

The abstraction of corrosion-products colloid stability is shown in Figure 3. At pH values close to the pH_{ZPC} (pH at zero-point charge), the dispersion is determined to be unstable regardless of ionic strength, and a minimum mass concentration is established. The same situation applies if an input pH value is several pH units away from the pH_{ZPC} and ionic strengths are greater than 0.05 mol/kg. At intermediate pH values the combined effect of ionic strength and pH are described by two lines; above the lines, the colloidal dispersion is unstable, and a minimum mass concentration is established.

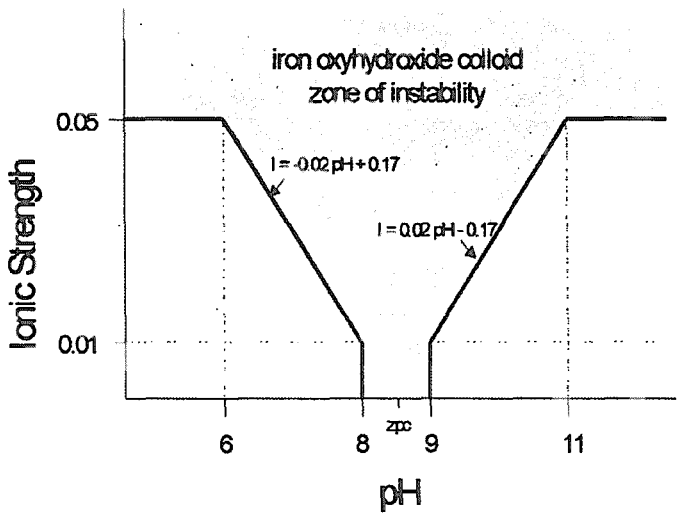

NOTE: Schematic representation (used in abstraction) of iron-(hydr)oxide colloid stability as a function of ionic strength and pH. At and near the ZPC colloids are unstable, even at low ionic strengths. At higher ionic strengths the pH range at which colloids are unstable is greater. Above ionic strength 0.05 colloids are assumed to be unstable for all pH (For details, see [2])

Figure 3. Schematic Representation of Iron-(Hydr)oxide Colloid Stability as a Function of pH and Ionic Strength

3.3 Groundwater Colloids

Smectite colloids are expected to be in the groundwater that enters the degraded WPs. The basis for modeling the mass concentration and the radioisotope concentration associated with these colloids as they exit the WP is described below.

Several workers [5,6] have studied and compiled the characteristics of colloids in groundwaters from crystalline and sedimentary rocks in saturated and unsaturated hydrologic regimes throughout the world. Data on colloid concentration and ionic strength for these groundwaters [1] show a general inverse correlation above an ionic strength of about 0.01 mol/kg and provide a predictive tool for estimating groundwater colloid mass concentration. This relationship is not precise because there are other factors, such as pH, that can significantly affect concentration.

To be useful for TSPA analysis calculations, these data were converted to mass or surface area per unit volume. For naturally occurring colloids, it has been observed that the number population and colloid size correlate using a power [2]. In general, the number of colloids increases by a factor of 1000 as colloid diameter decreases by a factor of 10 (assuming spherical colloids). Expressed mathematically, the colloid population is proportional to the inverse of the colloid diameter cubed. By taking the first derivative of the cumulative distribution, combining with masses of individual colloids assuming spherical geometry and then integrating the function between a lower and upper size limit, the total colloidal mass is obtained. Colloid masses were calculated using the number populations [1] and extrapolated to include colloid sizes between 10 nm and 1 micrometer. A colloid mineral density of 2.5 g/cm^3 was assumed. Details of this abstraction are described in [2].

Figure 4 illustrates the abstraction. The upper and lower bounding lines capture the highest and lowest concentrations of colloids. Between ionic strengths of 0.01 and 0.05 mol/kg, the number and mass concentrations decrease as groundwater colloids are destabilized. The decrease is assumed to be linear in log-log space.

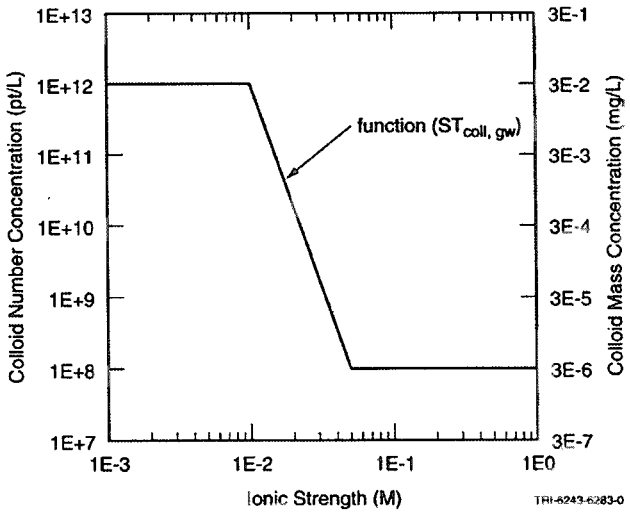

NOTE: Schematic relationship (used in abstraction) between groundwater colloid concentration and ionic strength. Colloid masses were calculated using number populations extrapolated to include colloid sizes between 10 nm and 1 micrometer. A colloid mineral density of 2.5 g/cm^3 was assumed.

Figure 4. Schematic Relationship between Groundwater Colloid Concentration and Ionic Strength

It is assumed that sorption for groundwater colloids is similar to clay minerals [2], and the same K_d values used for waste-form colloids are used for groundwater colloids. The concentration of a reversibly-sorbed radionuclide is determined using appropriate K_d values.

3.4 Mobile Colloidal Radionuclide Source Term

The mobile colloidal radionuclide source term is the sum of the radionuclide contribution from waste-form colloids (reversibly and irreversibly attached), corrosion-product colloids, and groundwater colloids. The total colloid mass concentration is also provided for recalculating reversibly attached radionuclide concentrations as dissolved concentrations change during transport.

4. Model Confidence, Limitations, and Validation

The model abstractions are based on laboratory results from waste form corrosion testing and testing of adsorption and desorption properties of Pu and Am on clay and iron-(hydr)oxide colloids. To the extent that the laboratory tests and test conditions represent anticipated repository conditions, the abstraction is valid for calculating the colloid-associated radionuclide concentrations and colloid mass concentrations. The approach for the colloidal-radionuclide source term is based on Yucca Mountain (YM)-specific field and laboratory studies and results from YM-relevant studies. The development of the conceptual model and implementation requires consideration of colloid generation, colloid-radionuclide interaction, colloid stability behavior, and to some extent, colloid transport/ retardation behavior. Information used for groundwater colloids, waste-form colloids, and corrosion-product colloids was obtained primarily from YM-specific studies. Consequently, the colloid-concentration model is expected to be representative of YM behavior.

Field evidence of small concentrations of radionuclides associated with colloids migrating considerable distances provides insight into possible colloid behavior at YM. At the Benham nuclear test site at the Nevada Test Site, rapid transport of colloid-associated Pu appears to have occurred [7]. At a point approximately 1.3 km from the blast site, 1×10^{-14} mol/L colloid-associated plutonium was detected 30 years after the detonation. It is difficult to determine what fraction of the transport was due to transport on colloids, injection through fractures by the blast, or transport as dissolved Pu. However, in the cases of other detonations, fracture injections have not been observed to extend beyond a few hundred meters, and dissolved Pu would be expected to sorb strongly to the fracture surfaces. It is plausible that the Pu was transported as Pu irreversibly attached to colloids. This example underscores the potential significance of the irreversibility of radionuclide attachment to smectite colloids observed in waste form corrosion experiments [4]. Irreversibly attached colloids are included in the abstracted model as a contribution to the colloid-associated radionuclide concentration.

Based on the considerations discussed above, this model is appropriate for its intended use.

5. REFERENCES

[1] DOE Office of Civilian Radioactive Waste Management (OCRWM), Waste Form Degradation Process Model Report, TDR-WIS-MD-000001, July 2000.

[2] DOE OCRWM, Waste Form Colloid-Associated Concentration Limits: Abstraction and Summary, ANL-WIS-MD-000012, 2000.

[3] W.L. Kingston and M. Whitbeck, Characterization of Colloids Found in Various Groundwater Environment in Central and Southern Nevada, DOE/NV/10384-36, 1991.

[4] DOE OCRWM, Colloid-Associated Radionuclide Concentration Limits: ANL, ANL-EBS-MD-000020, 2000.

[5] J.F. McCarthy and C. Degueldre, "Sampling and Characterization of Colloids and Particles in Groundwater for Studying Their Role in Contaminant Transport," Chapter 6 of Environmental Particles, Ed. by J. Buffle and H.P. van Leeuwen, Vol.2, Lewis Publishers, Boca Raton, Florida, 1993.

[6] J.F. McCarthy and J.M. Zachara, "Subsurface Transport of Contaminants," Environmental Science & Technology, 23, (5), 496-502,American Chemical Society, 1989

[7] A.B. Kersting, et al, "Migration of Plutonium in Ground Water at the Nevada Test Site, Nature, 397, 56-59, Macmillan Publishers, London, England, 1999.

JP0250368

EFFECTS OF IRON ON LEACHING BEHAVIOR OF SLAG LAYER OF MOLTEN SOLIDIFIED PRODUCTS

Toshikatsu Maeda*, Tsunetaka Banba and Hiromichi Ogawa
Department of Fuel Cycle Safety Research,
Tokai Research Establishment, Japan Atomic Energy Research Institute,
Tokai, Ibaraki JAPAN, 319-1195
*Fax: 81-29-282-5085, e-mail: toshi@koala.tokai.jaeri.go.jp

Static corrosion tests were performed for slag specimen of molten solidified products of simulated wastes doped with zero to five weight percents of iron in deionized water and in alkaline solution at 25℃ to understand and quantify the effects of iron on the leachability of slag. It was observed that iron significantly decreased the release of silicon from the slag in alkaline solutions, implying that iron-bearing precipitates inhibited the dissolution of the slag.
Key words: molten solidified products, slag, leach test, iron

1. INTRODUCTION

Melting and solidification process can be applied to treatment of various kinds of wastes, resulting solid waste forms of a wide range of chemical compositions, which is called as molten solidified products. Waste constituents are separated into two different phases during melting process. These two phases are produced by the difference in specific gravity. They are referred to as "metallic layer" and "slag layer". It is reported that long-lived radionuclides such as actinides contained in radioactive wastes are incorporated into the slag layer [1]. It is therefore important to investigate the leachability of the slag layer for evaluating the long-term barrier performance of molten solidified products. The major components of the slag layer are silica (SiO_2), calcium oxide (CaO) and alumina (Al_2O_3) that originate from non-metallic components such as ash and concrete. A typical minor component in the slag layer is iron. Most of iron in metal wastes such as carbon steel and stainless steel is incorporated into the metallic layer, but a fraction of the iron is oxidized and incorporated into the slag layer during the melting process. It is reported that a slag layer could contain iron up to about 30wt% [2]. The purpose of the present study is to understand and quantify the effects of iron on the leachability of the slag layer. The tests were conducted both in neutral and alkaline conditions simulating repository environments.

2. EXPERIMENTAL

2.1 Preparation of the sample

Slag samples were prepared by melting a mixture of SiO_2, CaO, Al_2O_3 and Fe_2O_3 in an alumina crucible at 1600℃ for 30 minutes in air. The basicity, defined as the ratio of CaO and SiO_2 in weight, of the slag was fixed to 0.33. The slag samples were ground and sieved.

2.2 Leach tests

Static corrosion tests were performed for the slag granules of the size of 0.50 mm to 1.0mm in deionized water or in a 0.10mol・dm^{-3} NaOH solutions. The slag granules and the leachant were placed in a polypropylene container with the surface-to-volume ratio, S/V, of $60m^{-1}$ and kept at 25℃ for periods of up to 30 days. The leachate pH was measured at the end of the corrosion tests. The leachate was filtered with a 450nm-pore Millipore filter to remove suspended particles. The filtered solution was diluted with a 0.10mol・dm^{-3} HNO_3 solution prior to the concentration measurement to prevent re-precipitation. The concentrations of silicon, calcium, aluminum and iron in the solution were measured by an inductively coupled plasma mass spectroscopy, ICP-MS.

2.3 Accelerated leach tests

In order to measure the saturated concentrations of constituent elements released from slag sample in the leachates, accelerated leach tests were conducted in alkaline solution using powdered slag sample, which contain zero and five weight percents of iron. The grain size of the sample was under 75μm, and static corrosion tests on the sample were performed in 0.10mol・dm^{-3} NaOH solutions with S/V of $2000m^{-1}$ and kept at 25℃ for periods of up to 90 days. After the corrosion tests, the pH of the leachate were measured immediately. The leachate was filtrated through 1.8nm-pore Millipore filters, and the solution concentrations of silicon and other constituent elements of the slag were measured by ICP-MS.

3. RESULTS

3.1 XRD profiles of slag specimens

Figure 1 shows the X-ray diffraction profiles of prepared slag specimens. No peaks were observed for both iron free slag specimen and 5.0wt% iron doped slag specimen. The specimens doped with 1.0wt% and 3.0wt% iron showed no peaks, either. All of the slag specimens used in this study have amorphous structure like glass does.

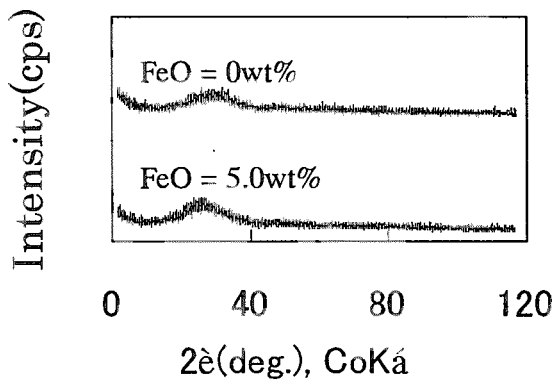

Fig.1 XRD profiles for slag specimens

3.2 Results of leach tests

Figure 2 shows the pH values of the leachates as a function of corrosion time. It can be seen from the figure that pH of the leachate appears to be stable during leaching periods in the both cases of neutral and alkaline conditions.

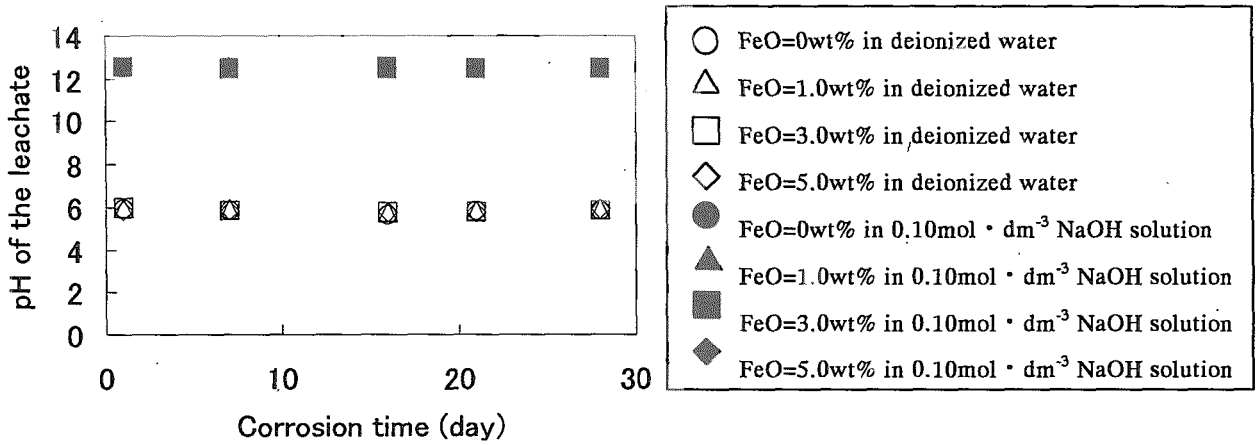

Fig.2 Leachate pH as a function of corrosion time

The normalized elemental mass loss values, NL, of silicon for each sample in deionized water and in alkaline solution are shown in Fig.3. For each slag sample, the NL of silicon in alkaline solution was about two orders of magnitude higher than those in deionized water. It can be seen that there is no differences between NL of silicon for iron free sample and iron-doped sample in deionized water. On the other hand, in alkaline solution, iron-doped sample has smaller NL of silicon compared with iron free sample.

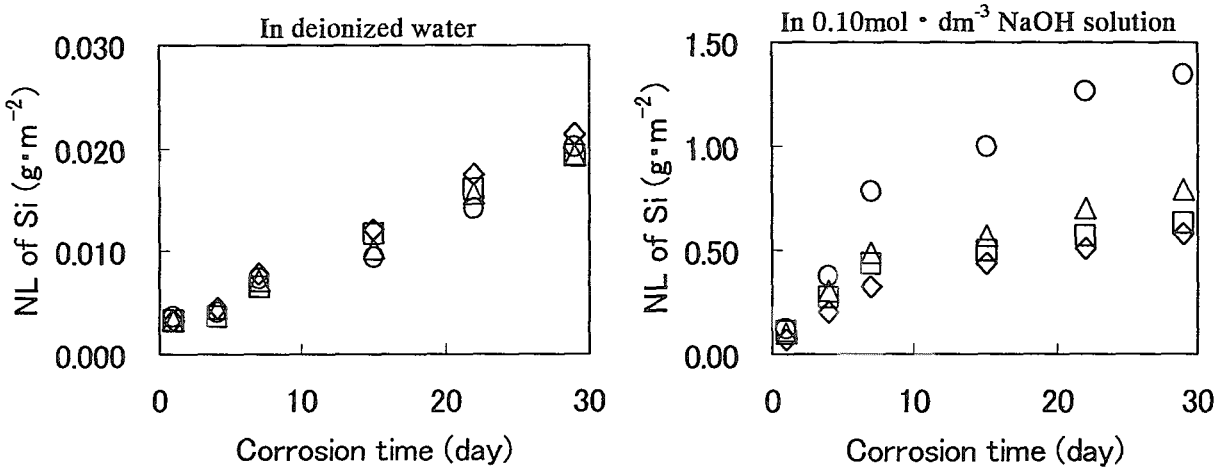

Fig.3 Normalized elemental mass loss of silicon as a function of corrosion time (In the Figure, the symbols of circles, triangles, squares and diamonds represent zero, one, three and five weight percents of iron doped slag specimens, respectively.)

3.3 Results of accelerated leach tests

As shown in Fig.3, there is a difference of the silicon NL between for iron free and iron-doped slag samples in alkaline solutions. Accelerated tests were conducted to measure the saturated Si concentrations in leachates in alkaline solution for powdered slag samples that contain zero and five weight percents of iron. Figure 4 shows the results of the accelerated tests. There is no increase in Si concentrations for each slag sample between the period of 50 days and 90 days. It suggests that Si concentrations are saturated in 90 days for both slag samples.

Figure 4 also shows that the saturated concentration of silicon for iron-doped slag samples is lower than that for iron free sample in alkaline solutions.

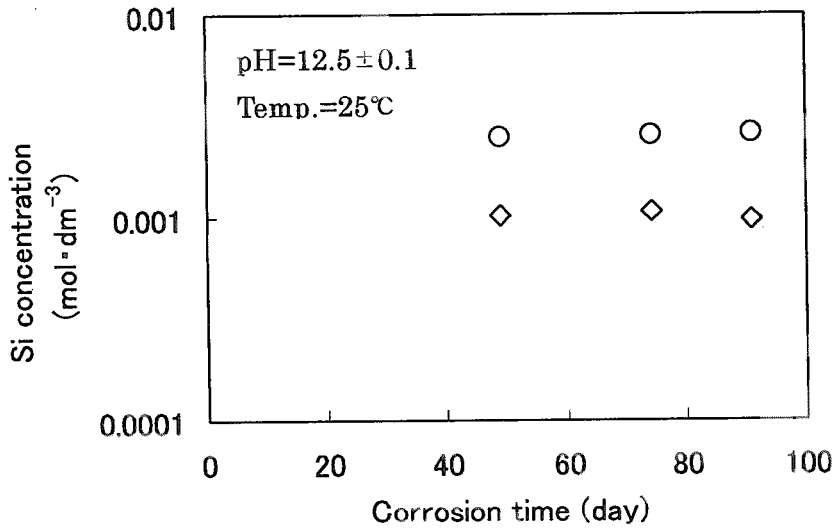

Fig.4 Silicon concentrations in the leachates as a function of corrosion time (In the figure, the symbols of circles and diamonds represent and five weight percents of iron doped slag specimens, respectively.)

4. DISCUSSIONS

As shown in Fig.1, the X-ray diffraction profiles support that each slag specimen is non-crystalline. In addition, the major chemical components and its melting conditions suggest that each sample prepared in this test can be regarded as a glass. According to these results, it is considered that we can discuss about the corrosion behavior of the slag on the basis of the dissolution mechanism for the glass waste form [3].

Similarly to glass structure, silicon is thought to be a network former of the slag. The degree of network dissolution is a reasonable measure for the release of other constituent elements and hence for the chemical durability of the slag sample. The sample dissolution is therefore discussed based on the leaching of silicon. Results of the corrosion tests shown in Fig.3 suggest that iron doped in the slag sample significantly reduced the release of silicon from the sample in alkaline solutions.

A possible reason can be supposed to explain these effects. The iron dissolved with silicon formed a precipitated layer on the surface of the slag, and the layer acted as a protective layer, which can reduce corrosion rates by inhibiting dissolution of the sample. Since a large amount of iron dissolved to form the protective layer in alkaline solutions, the inhibition of the sample dissolution by the layer must be significant compared to that in deionized water.

In addition, as shown in Fig.4, the saturated concentration of silicon for iron-doped slag samples is still lower than that for iron free sample in alkaline solutions. It suggests that the precipitated layer acts not only as a protective layer but also as a solubility control solid, which reduced the amount of dissolved species. The dominant precipitate for the iron-doped slag sample in alkaline condition is presumed to be iron-bearing mineral.

5. CONCLUSIONS

Static corrosion tests were carried out using slag specimen doped with zero to five weight percents of iron in deionized water and in alkaline solution at 25℃. It was observed that iron significantly decreased the release of silicon and aluminum from the slag sample in alkaline solutions. It was supposed that iron-bearing precipitates inhibited the dissolution of the slag in alkaline conditions.

REFERENCES

[1] T.Amakawa et al., Yokosuka Research Laboratory Rep. No.W98010, Central Research Institute of Electric Power Industry (1998)

[2] N.Nakashio et al., JAERI-Research 2001-001, Japan Atomic Energy Research Institute (2001).

[3] W.Lutze et al., Radioactive Waste Forms for the Future, North Holland (1988)

This is a blank page.

JP0250369

JAERI-Conf 2002-004

REVIEW OF IMMOBILIZATION TECHNIQUES OF RADIOACTIVE IODINE FOR GEOLOGICAL DISPOSAL

HIROYASU KATO, OSAMU KATO AND HIROMI TANABE
Radioactive Waste Management Funding and Research Center
No.15 Mori Bldg, 2-8-10, Toranomon, Minato-ku, Tokyo, 105-0001, Japan
Fax: 81-3-3504-1297, e-mail: h-kato@rwmc.or.jp

Iodine-129 is one of the key nuclides on the safety assessment for the geological disposal of radioactive waste containing transuranic elements, which will be generated from fuel cycle facilities such as reprocessing and MOX fuel fabrication. To improve safety in disposal, it is implemented to develop the advanced iodine waste form in which iodine-129 can be sustained with gradually releasing for more than hundreds of thousands years. In this paper, iodine immobilization techniques under currently development in Japan are reviewed from the points of views in the treatment techniques for immobilization, required pre-treatment techniques of the spent filters and chemical and physical properties of immobilized waste form. The techniques can be classified into three categories by the applicability of iodine release models from the waste. The possibilities of reduction of maximum dose by geological disposal of iodine-129, adopting the advanced iodine waste forms will be discussed.

Key words: iodine, immobilization, geological disposal, spent filter, radioactive waste

INTRODUCTION

Iodine-129 is one of the key nuclides on the safety assessment for the geological disposal of radioactive waste containing transuranic elements, which will be generated from fuel cycle facilities such as reprocessing and MOX fuel fabrication. Hereafter the waste containing transuranic elements is called TRU waste in this paper. The Progress Report on Disposal Concept for TRU Waste in Japan [1] (hereafter, The TRU Progress Report) reported that the major part of iodine-129 was contained in spent iodine filter generated from the operation of domestic reprocessing plants, and that the spent filter was solidified by cement, then disposed in a repository with engineered barriers composed of cementitious materials and bentonite materials. The TRU Progress Report concluded that the current cement solidification technique may offer the safe disposal with regard to the spent filters containing large quantities of iodine-129, however the result of the safety assessment depends on the conditions of the geological environment.

On the safety assessment of TRU waste disposal, the maximum dose rate caused by the overall waste is dominated by iodine-129. The rate by iodine-129 mainly depends on its chemical and radiological properties. Silver iodide (AgI) is the main chemical form of iodine in the waste and it may be decomposed to soluble ions under reduced condition of deep geological disposal. Generally, iodine ion has low sorption property on the engineered barrier materials and the natural materials such as rocks and soils. Moreover iodine-129 is extremely long-lived radionuclide (half-life:1.57×10^7 y). Therefore iodine-129 will be rapidly released from the repository, and migrate to biosphere through geological layer with relatively less

decay. Thus, a dose of iodine-129 may be significantly affected by the condition of the geological environment. At the viewpoint of the maximum dose reduction, it is necessary to develop the waste form in which iodine-129 is controlled to be released for more than hundreds of thousands years. This advanced waste form would improve the flexibility in providing acceptable performance in a wider range of geological environments in Japan.

In this study, the iodine immobilization techniques under currently development in Japan are reviewed from the points of views in treatment techniques for immobilization, required pre-treatment techniques of the spent filters (heating, crushing, conversion of chemical form of iodine compounds, etc.), and chemical and physical properties of immobilized waste form. Eight promising iodine immobilization techniques are introduced. The techniques could be classified into three categories by the applicability of iodine release models from the waste. The possibilities of reducing iodine-129 maximum dose on geological disposal by adopting the advanced iodine waste forms are discussed.

IMMOBILIZATION TECHNIQUES OF IODINE

According to The TRU Progress Report, spent iodine filter will be mainly generated from the operation of domestic commercial reprocessing plants. The fresh iodine filter is silver silica gel (AgS), which is composed of appox. 81wt.% silica-gel and appox. 19wt.% silver nitrate. Generated radioactive iodine (I^- or IO_3^-) reacts with silver nitrate in the filter, and forms AgI or $AgIO_3$. Therefore spent filter is mixture of AgI, $AgIO_3$ and silica gel except for minor impurities.

The iodine immobilization techniques under currently development in Japan require some pre-treatment processes of the spent iodine filters such as heating process for removal of impurities, crushing process for improvement of reaction efficiency, and conversion of chemical form of iodine compounds. Outline of each immobilization technique is showed as follows, and pre-treatment processes required for respective immobilization technique and chemical and physical properties of each solidificates and proposed release model from immobilized waste forms are shown in Table I and Table II, respectively.

HIP treatment of the spent filter [2,3]

HIP (Hot Isostatic Pressing) process is a method under the operating condition of high-temperature and high-pressure. Furthermore, because of its isostatic pressing, not one-dimensional pressing, products has less residual stress. Therefore it is possible to keep their high mechanical properties of products for a long time.

Structure of silica gel of spent filter is amorphous and porous. Under the simultaneous application of high-pressure and high-temperature, it is possible to transmute an amorphous silica gel into crystalline quartz, which has high mechanical properties and is thermodynamic stability. It is reported that the solubility of silica gel into solution tends to become smaller as crystallized material than amorphous one. Radioactive iodine is confined as its chemical form of AgI or $AgIO_3$ among crystalline quartz grains. Thus the leach rate is reduced to low. It is possible to produce a solidificate having a high physical ability for iodine retention, applying HIP treatment.

Table I Each immobilization technique, mechanism of the iodine confinement and required pre-treatment process of the spent iodine filter

Iodine Immobilization Techniques	Mechanism of Iodine Confinement	Required pre-treatment process of the spent iodine filter
HIP treatment of the spent filter	Confinement by SiO_2 (quartz) matrix	(1)Grinding (<40 μ m) (2)Pre-heating(480℃) (3)Packing into capsule and sealing up
Low temperature vitrification with AgI	Confinement by AgI-Ag_2O-P_2O_5 glass	(1)Separation of AgI by the vacuum distillation method
Low temperature vitrification with $BiPbO_2I$	Confinement by B_2O_3-SiO_2-PbO glass	(1)Recovery of iodine from the spent iodine filter (2)Production of $BiPbO_2I$ by ion exchange of iodine with $BiPbO_2NO_3$
Hot press of the spent filter with metallic copper powder	Confinement by metallic copper matrix	(1)Pre-heating (400℃, 20 hours)
Hot press of apatite with spent filter	Confinement by apatite matrix	(1)AgI separation from the spent iodine filter (2)Capture of AgI by zeolite (3)Coating by apatite
High performance cement solidification with IO_3^-	Sorption on the cement or its composing minerals	(1)Dissolution of iodine from the spent iodine filter into the solution by reduction reaction (2)Conversion of I^- into IO_3^- by oxidation reaction with ozone gas bubbling
Synthesis of iodine sodalite	Low solubility of iodine sodalite	(1)AgI separation from the spent iodine filter (2)Conversion of AgI into NaI
Synthesis of lead vanado-iodoapatite	Low solubility of lead vanado-iodoapatite	(1)AgI separation from the spent iodine filter (2)Conversion of AgI into PbI_2

Table II Chemical and physical properties of each solidificate and proposed release model of iodine from the waste form.

Mechanism of Iodine Confinement	Chemical and physical properties	Proposed release model of iodine from the waste form
Confinement by SiO_2 (quartz) matrix	-Density: >2.0 g/cm^3 -Compression strength: >98Mpa -Permeability of water: <10^{-10} m/s -effective diffusivity: 4×10^{-16} m^2/s	Leaching model (by Diffusion)
Confinement by AgI-Ag_2O-P_2O_5 glass	-Density: 5.5~6.0 g/m^3 -Compressive strength: 40MPa~100MPa -Leaching rate: 7×10^{-8} ~ 5×10^{-9}g/cm^2/d	Leaching model
Confinement by B_2O_3-SiO_2-PbO glass	-Density: 6.4g/cm3 -Iodine loading: 1 wt.%	Leaching model
Confinement by metallic copper matrix	-Content of the spent filter: ca. 30 vol.% -Corrosion rate: 1~4 μ m/y	Leaching model (by corrosion)
Confinement by apatite matrix	-Density: 3 g/cm^3 -Mechanical strength: 300 MPa	Leaching model
Sorption on the cement or its composing minerals	-Density: 1.74 g/cm^3 -Compression strength: 22Mpa -Distribution coefficient of iodate: ca.900ml/g	Sorption model
Low solubility of iodine sodalite	-Solubility: 10^{-4} - 10^{-5} mol/L.	Solubility limit model
Low leachability or solubility of lead apatite	-Leaching rate (MCC-5): ca. 4×10^{-5} g/cm^2/d	Leaching model or solubility limit model

Typical HIP treatment was carried out under the condition of a temperature at 750℃, a pressure at 1000kgf/cm^2(=98Mpa), after grinding, pre-heating the filter, packing into capsule and sealing up as pre-treatment processes.

As for the iodine release mechanism from the HIP solidificate, the path of iodine exudation is a quartz grain boundary layer. Iodine retention ability of the solidificate is dominated by the diffusion of a quartz grain boundary. Therefore diffusion model of a quartz grain boundary is applied to iodine release model from the solidificate..

Low temperature vitrification with AgI [2,4]

This immobilization technique makes possible to confine radioactive iodine as AgI-Ag_2O-P_2O_5 glass waste forms. Proposed vitrification process consists of two steps:

- Separation of AgI from the spent iodine filter by the vacuum distillation method as pre-treatment process.
- Vitrification with the separated AgI.

  An AgI-Ag_2O-P_2O_5 glass system can homogeneously contain up to 60mol% AgI, which leads to high volume reduction efficiency (approximately 1/25). It also can vitrify the AgI without volatilization of iodine because of its low melting temperature (below 500ºC).

The physical properties of AgI-Ag_2O-P_2O_5 glass waste forms were examined parametrically by changing the AgI content and Ag/P ratio of the silver phosphate. Homogeneous glasses could be made without crystallization

Leach tests of this glass waste form were carried out according to the MCC-1 static leach test procedure. The tests were done under the reducing condition in an anaerobically controlled glove box, which was purged by nitrogen gas with 3% hydrogen. After immersion, iodine concentration in the leachate was analyzed by ICP-MS. Leaching behavior of the glass was different between the first 10 days period and the after period. During the first 10 days, the leaching rate was $7x10^{-8}$g/cm^2/d, and duration after 10 days it decreased to $5x10^{-9}$g/cm^2/d. These leach rates indicated a fairly long life for this glass. The observation by the SEM showed that precipitation layer was very tightly attached and its thickness was about 10 μm. It was concluded that formation of the precipitation layer limited the dissolution of iodine in the glass.

Low temperature vitrification with $BiPbO_2I$ [5]

This immobilization technique consists of an iodine recover process and a vitrification process as same as the vitrification technique with AgI mentioned above. A special iodide compound, $BiPbO_2I$, was used to form a homogeneous dispersion of an iodine in B_2O_3-Si_2O-PbO glass system. In the vitrification process, a melting temperature is low (520 °C) to avoid an iodine volatilization during the virification of an iodine compound.

- Recovery of iodine from the spent iodine filter as pre-treatment

  A reductant (N_2H_4, etc) was used to release an iodine nuclide from a spent iodine filter into a solution. Then, the iodide ion was fixed into $BiPbO_2I$ by reacting with an inorganic anion exchanger, $BiPbO_2NO_3$. The ion exchange reaction can be described as follows:

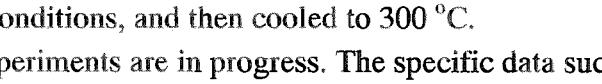

$$BiPbO_2NO_3 + I^- \rightarrow BiPbO_2I + NO_3^-$$

- Vitrification with recovered $BiPbO_2I$

The composition of the glass frit was B_2O_3:SiO_2:PbO = 30:10:60 [mol%]. The glass frit was mixed with $BiPbO_2I$. The mixture was melted at 520 °C for 30 min under aerobic conditions, and then cooled to 300 °C.

Experiments are in progress. The specific data such as volatile rate and leaching rate will be obtained in the near future.

Hot-press of the spent filter with metallic copper powder [2]

The solidified waste form of the spent iodine filter in copper matrix has been developed by hot press method with metallic copper powder. The form can be expected to perform long-term normal state and good corrosion resistance in reducing condition.

Required pre-treatment process is pre-heating the spent iodine filter at 400℃ and 20 hours. After the mixing of dried spent filter and metallic copper powder, hot-press were carried out under a temperature at 750℃, a pressure at 25Mpa and keeping time at 3 hours. Thus the spent iodine filter was confined into metallic copper matrix.

A release of iodine from the solidificate occurs with corrosion of copper matrix. Therefore the corrosion test of copper matrix was carried out. The corrosion rate of copper matrix obtained from the experiment was 1～4 μ m/y in anaerobic condition.

Hot-press of the spent filter with apatite [2]

The apatite solidification technique is a method for solidifying spent iodine filter directly or zeolites that absorbed AgI separated from the filter, with physically and chemically stable apatite matrix. The method is to solidify mixture of apatite particles and the spent iodine filter or the zeolite under relatively high temperature and pressure such as hot-press. And before the solidification, the filter or the zeolite are coated by apatite to reduce the leaching paths of iodine. Thus the iodine is encapsulated with apatite matrix that are insoluble mineral.

In the case of no direct solidification of spent iodine filter, following pre-treatment process is required.

- AgI separation from the spent iodine filter
- Capture of AgI by zeolite that have higher ability of iodine absorption, to reduce total volume of the waste.

Experiments are in progress, and the specific data such as leaching rate will be obtained in the near future.

High performance cement solidification with IO_3^- [2,6]

Hydrated cement minerals as monosulfate, ettringite and hydrotalcite have high sorption property for anions. High sorption performance cement containing large amounts of calcium-aluminate compounds has been developed by mixing alumina cement with calcium compounds such as calcium sulfate and calcium hydroxide. And the distribution coefficient of IO_3^- on monosulfate and ettringite was reported to be more than two orders of magnitude higher than those of I^-. Therefore high performance cement solidification with IO_3^- was

proposed as the high iodine retention waste form.

The pre-treatment and immobilization process consists of three steps:

- Dissolution of iodine from the spent iodine filter into the solution by reduction reaction
- Conversion of I^- into IO_3^- by oxidation reaction with ozone gas bubbling
- Mixing of the IO_3^- with high sorption performance cement which is hydrated material of a mixture of $CaSO_4 \cdot 2H_2O$ and alumina cement in a volume ratio of 15.5/100, and contains large amounts of monosulfate and ettringite.

As a result of the sorption experiment for the high performance cement under a reducing condition, it was reported that the distribution coefficient of IO_3^- on the cement reached to about 900 ml/g.

Synthesis of iodine sodalite [2,7]

Sodalite $[Na_8(AlSiO_4)_6Cl_2]$ is a mineral in nature which contains halogenous chlorine. Iodine sodalite $[Na_8(AlSiO_4)_6I_2]$ is proposed as a stable waste form to immobilize radioactive iodine. The sodalite aluminosilicate lattice consists of truncated octahedral which provide large "cages" in which allow to place ions or atoms. The incorporation of iodine into the cage structure has been studied. It has been reported that the sodalite was synthesized easily from clay minerals such as kaolin or some chemical reagents in the study of immobilization of iodine from nuclear fuel reprocessing and solidification of halide salt waste from pyrochemical reprocessing. Because solubility of sodalite in aqueous solution is comparatively low, iodine release is restricted by solubility limit of sodalite.

The iodine sodalite was synthesized of stoichiometric mixtures of SiO_2, $NaAlO_2$ and NaI by heating in argon gas flow at the temperatures of 800℃ for 2hours.

Required Pre-treatment processes for this technique are as follows:

- AgI separation from the spent iodine filter
- Conversion of AgI into NaI

Solubilities of the iodine sodalite in the several types of leachates were measured by the batch methods. The solubilities of the synthesized iodine sodalite were in the range of 10^{-4} - 10^{-5} mol/L.

Synthesis of lead vanado-iodoapatite [8,9]

As stated above, apatite materials have low solubility and leachability. A immobilization technique for the synthesis of apatite containing iodine has been developed. A lead vanado-iodoapatite, $Pb_{10}(VO_4)_6I_2$ was synthesized. Because iodine compounds used as starting materials or product were volatile, the starting materials were reacted in a sealed quartz ampoule and a waste form was made from the product by hot-pressing. The stoichiometric amounts of PbO, PbI_2 and V_2O_5 were mixed and pressed to a pellet at 35MPa at room temperature. The pellet sample was put in a evacuated quartz ampoule. The quartz ampoule was sealed and heat-treated at 700℃ for 5 hours. After some properties were measured with pulverized product, the waste form was made by hot-pressing the powder at a pressure of 9MPa and temperature of 773K.

Required Pre-treatment processes for this technique are as follows:

- AgI separation from the spent iodine filter
- Conversion of AgI into PbI_2

The X-ray diffraction pattern of the product showed apatite structure and chemical analysis suggested some evaporation of iodine in a sealed quartz tube. Thermogravimetry -differentialthermal analysis showed that the apatite was stable up to 800K under argon atmosphere. 7 days soxhlet leaching test(MCC-5) was performed with the hot-pressed sample. The leaching rate of iodine, lead and vanadium were 3.98×10^{-5}, 1.55×10^{-5} and 1.61×10^{-4} g cm^{-2} d^{-1}, respectively.

POSSIBILITY OF DOSE REDUCTION ON GEOLOGICAL DISPOSAL

According to The TRU Progress Report, the dose rate with disposal of traditional cement solidificate of the spent iodine into multi-barrier system was evaluated, and the maximum dose rate of Iodine-129 reached to 1 μ Sv/y under reference geological condition of crystalline rock which hydraulic conductivity was 10^{-9} m/s. The dose rate was remarkably affected by increase of hydraulic conductivity of the rock. It is reported that the controlled-release-term of iodine-129 by the advanced iodine waste for about 10^5 years was requested in order to reduce a maximum dose rate of one order less that the value obtained with traditional cement solidified waste.

Iodine release models from the iodine wastes made by immobilization techniques in this paper, are roughly classified into 3 types at the viewpoint of dominant release mechanism; they are leaching model, sorption model and solubility limitation model as listed in Table II. It is reported to be possible that that the controlled-release-term of iodine-129 from each waste form exceed more than 10^5 years, if applied those specific corresponding models to iodine release evaluation, assuming that the waste form would be physically stable without any change of chemical properties with regard to iodine release for long-term.[1,2]

As for the geological disposal for the iodine-129 waste form, it will be necessary that the examinations of suitable disposal systems for proposed iodine waste form, and the long-term performance assessments of overall systems including the waste forms were necessary, in order to examine the applicabilities of respective iodine waste forms to the geological disposal.

CONCLUSION

Eight immobilization techniques and their respective mechanisms of immobilizations, required pre-treatment process, physical and chemical properties of iodine immobilized forms, proposed iodine release model, were reviewed for the purpose of examination of applicabilities of respective iodine-129 immobilized form to geological disposal.

It becomes clear that some immobilization techniques require not only grinding and heating the spent iodine filter, but also more complicated process such as separation of AgI from the spent iodine filter and conversion of AgI. Examinations of suitable disposal systems for proposed iodine waste form and the long-term performance assessments of overall systems including the waste form itself may be necessary. Furthermore, evaluation of economic efficiencies for the treatment process and the disposal is future problem as well as an

improvement of reliability on long-term performance assessment of the developed iodine waste form on geological disposal.

ACKNOWLEDGEMENTS

The authors would like to express their thanks to Mr. T. Nishimura of Kobe Steel, Ltd., Mr. T. Yoshida of Hitachi Ltd., Mr. M. Kaneko of Toshiba Co., Mr. T. Nakazawa of Mitsubishi Materials Co., Mr. A. Sakashita of Mitsubishi Heavy Industries Ltd., Mr. T. AMAYA of JGC Co., Dr. M. Uno of Osaka Univ. and Mr. M Fukumoto of Japan Nuclear Cycle Development Institute for their supports.

REFERENCES

[1] TRU Coordination Office, Progress Report on Disposal Concept for TRU Waste in Japan, JNC TY1400 2000-002, TRU TR-2000-02, Japan Nuclear Cycle Development Institute, The Federation of Electric Power Companies (2000).

[2]H. Fujihara et al., Radioactive Iodine Waste, Journal of Nuclear Fuel Cycle and Environment, Vol.6, No.1, pp.51-81, (1999).

[3]H. Fujihara et al, Fixation of radioactive iodine by hot isostatic press, ICEM'99, Nagoya, Japan, Sep. (1999).

[4]H. Fujihara, T. Murase, T. Nishi, K. Noshita, T. Yoshida and M. Matsuda, Mat. Res. Soc. Symp. Proc., Vol.556, pp.375-382, (1999).

[5]T. Amaya, S. Shibuya and H. Kodama, 2001 Fall Meeting of the Atomic Energy Society of Japan, M59, (2001)

[6]M. Toyohara, M. KANEKO, H. UEDA and N. MITSUTSUKA, Journal of Nuclear Science and Technology, Vol.37, No.11, p.970, (2000)

[7]T. Nakazawa et al., Iodine immobilization by sodalite waste form, Scientific Basis for Nuclear Waste Management, 2000 (in printing).

[8]M. Uno et al, , 2001 Spring Meeting of the Atomic Energy Society of Japan, M59, (2000)

[9]M. Shinohara, M. Uno, K.Kurosaki and S. Yamanaka, Some properties of a lead vanado-iodo apatite $Pb_{10}(VO_4)_6I_2$, 16th IUPAC Conference Chemical Thermodyanamics, Canada.

TRU Chemistry

This is a blank page.

JP0250370

ACTINIDE CHEMISTRY IN CONCENTRATED ALKALI: IMPLICATIONS FOR CLEANUP OF PROCESSING PLANTS

Kenneth L. Nash, Artem V. Guelis, Mark P. Jensen, James C. Sullivan, Andrew H. Bond
Argonne National Laboratory
Alexander Yu. Garnov, Linfeng Rao
Lawrence Berkeley National Laboratory

During 50 years of plutonium production for defense purposes in the U.S., a large industrial complex with facilities scattered around the country was developed. The first, and ultimately the largest, of these facilities, at the Hanford site in Washington state, produced plutonium for more than 40 years. During this period, three main actinide partitioning processes were employed, the bismuth phosphate precipitation process, and the REDOX and PUREX solvent extraction processes. Liquid process wastes were at first disposed of directly to open trenches and later to underground waste storage tanks. Ultimately, 177 tanks were constructed and used for "temporary" storage of waste effluents at this site. During the years of plutonium production and byproduct recovery, wastes were mixed between tanks and subject to evaporation to conserve limited space. Similar underground storage tanks containing wastes of less diverse composition exist at other production facilities. All are presently scheduled for cleanup and closure as part of the decommissioning of a large portion of the U.S. defense complex.

Because the tanks are of carbon steel construction and to assist with control of the solubility of metallic fission byproducts, the effluents were made strongly alkaline upon their release to the tanks. Over the years of waste storage, these tank wastes have spontaneously separated into sludge, solution/slurry, and salt cake phases. Remediation of the millions of gallons of these waste materials is one of the most imposing tasks to be faced in the ongoing cleanup of the U.S. defense complex. Present site closure plans call for the removal of the wastes from the tanks. The wastes are to undergo minimal processing, primarily to remove non-radioactive constituents, and the remaining radioactive portions vitrified prior to permanent disposal in a geologic repository. Reduction of the Al, Cr, P, and S content of the wastes is to be accomplished using an alkaline scrub of the sludge phase. It is expected that this alkaline sludge wash will only remove the target species and leave the important actinides and fission products in the sludge phase as feedstock for vitrification. Given the extreme diversity of tank wastes and the diverse redox chemistry of the light actinides, the assumption of consistent insolubility of actinides in alkaline solutions appears to be debatable.

Working with simulants of sludges from the $BiPO_4$, Redox, and PUREX processes and with representative solutions, we are investigating the nature of the interactions of actinide cations components of tank sludge simulants and possible leachates. A variety of complementary analytical techniques have been employed in this investigation. We have observed that Pu dissolves somewhat more readily from Redox and $BiPO_4$ sludge simulants than it does from PUREX sludges, though Pu(IV) oxide/hydroxide most probably controls solubility under most conditions. On the other hand, U and Np have

been observed to dissolve from sludges much more readily under many circumstances. At base concentrations above 1 M, the solubility of oxidized actinides is moderate and is dominated by mononuclear hydroxides, even in the presence of moderate concentrations of carbonate. Continuing research focuses on the influence of chelating agents known or suspected to be in the tanks on actinide solubility and speciation. In this presentation, the results of these observations will discussed to provide insights into behaviors that might be exhibited by actinides during alkaline sludge washing procedures. The potential impact of alkaline actinide chemistry on hydrometallurgical processing of actinides will also be explored.

This work was supported by the Assistant Secretary for Environmental Management under U.S. Department of Energy Contract Numbers W-31-109-ENG-38 at Argonne National Laboratory and DE-AC03-76SF0098 at Lawrence Berkeley National Laboratory.

The submitted manuscript has been created by the University of Chicago as Operator of Argonne National Laboratory ("Argonne") under contract No. W-31-109-ENG-38 with the U.S. Department of Energy. The U. S. Government retains for itself, and others acting on its behalf, a paid-up, non-exclusive, irrevocable worldwide license in said article to reproduce, prepare derivative works, distribute copies to the public, and perform publicly and display publicly, by or on behalf of the Government.

JP0250371

JAERI-Conf 2002-004

Electrochemistry Studies of $UO_2(acac)_2L$(acac = acetylacetonate, L = dimethyl sulfoxide, *N,N*-dimethylformamide, tetrahydrofuran) Complexes in Non-aqueous Solvents

Seong-Yun Kim, Gunzo Uchiyama, Koichiro Mizuoka*, Yasuhisa Ikeda*
Department of Fuel Cycle Safety Research, Japan Atomic Energy Research Institute,
2-4 Tokai-mura, Ibaraki-ken, 319-1195, Japan
Tel.: +81-29-282-6675. Fax: +81-29-282-6677, E-mail: skim@procsafe.tokai.jaeri.go.jp
*Research Laboratory for Nuclear Reactors, Tokyo Institute of Technology
2-12-1 O-okayama, Meguro-ku, Tokyo 152-8550, Japan

Electrochemical studies on $U^{VI}O_2(acac)_2L$(acac = acetylacetonate, L = dimethyl sulfoxide (dmso), *N,N*-dimethylformamide(dmf), tetrahydrofuran(thf)) complexes in non- aqueous solvents containing tetrabutylammonium perchlorate as supporting electrolyte have been carried out by using cyclic voltammetry to compare the stability of the reduction products of U(VI) complexes with bidentate ligands. It was found that the $U^{VI}O_2(acac)_2dmso$ and $U^{VI}O_2(acac)_2dmf$ complexes are quasi-reversibly reduced to $[U^{V}O_2(acac)_2dmso]^-$ and $[U^{V}O_2(acac)_2dmf]^-$ species and that the $U^{VI}O_2(acac)_2thf$ complex is irreversibly reduced to $[U^{V}O_2(acac)_2thf]^-$ species at the Pt electrode.
Keywords: Uranyl(VI) complexes, Electrochemical reactions, Acetylacetonate, Non-aqueous solvents

1. INTRODUCTION

Although many electrochemical studies on U(VI) complexes have been carried out, little information is available concerning the coordination chemistry of U(V) in solutions. Electrochemical reactions of uranyl(VI) complexes have been extensively studied in aqueous[1] and non-aqueous solutions[2] and their mechanisms have been proposed. However, the properties of reduction products, *i.e.* U(V) complexes, have not been examined in detail[1, 3]. Previously, we have investigated the electrochemical properties of uranyl(VI) complexes by using cyclic voltammetry(CV), normal pulse voltammetry(NPV), and spectrophotometer equipped with an optical transparent thin layer electrode(OTTLE) cell[4-8]. As a result, we have clarified that these complexes are reduced to U(V) complexes quasi-reversibly or reversibly to form relatively stable U(V) species (probably yl-type, UO_2^+) and that the U(V) complexes have small molar extinction coefficients in the visible region. Furthermore, recently we have carried out the electrochemical study of U^{4+} perchlorate in DMSO to examine whether the so-called bare U(V) ions (U^{5+}) are generated by electrochemical oxidation of U^{4+} ions[9]. It was found that the U^{4+} ions in DMSO is not oxidized to U^{5+} ions. From these results, it is expected that the uranyl complexes with bidentate or multidentate ligands at their equatorial planes can form stable U(V) complexes by electrochemical reduction and that the U(V) species in non-aqueous solvents are present more stably as the yl-type (UO_2^+) than as the bare type (U^{5+}).

In the present paper, we report the results of the electrochemical studies on $UO_2(acac)_2L$[acac = acetylacetonate, L = dimethyl sulfoxide(dmso), *N,N*-dimethylformamide(dmf), tetrahydrofuran(thf)] complexes in non-aqueous solvents by using cyclic voltammetry.

2. EXPERIMENTAL

2.1 Materials. The $UO_2(acac)_2L$ complexes were prepared by dissolving $UO_2(acac)_2H_2O$ in warm DMSO, DMF and THF solvents. The $UO_2(acac)_2H_2O$ complex was prepared by the procedure of Comyns *et al.*[10]. Solution containing

uranyl complex was cooled, and the resultant orange crystals were filtered and dried under vacuum for 1 day. DMSO, DMF and THF were dried by standard procedures before use[11]. Tetrabutylammonium perchlorate(TBAP, Fulka Chemika) used as supporting electrolyte was recrystallized three times from ethanol and dried *in vacuo* at 70℃ for 72 hours.

2.2 Measurements of CV. Measurements of cyclic voltammetry were performed at 23 ±1℃ under nitrogen atmosphere with a BAS CV-50W voltammetric analyzer and a BAS CV cell as reported previously[9]. Electrochemical cells used a three electrode system: a Pt working electrode(surface area S = 0.02 cm^2), a platinum-wire counter electrode, and a reference electrode (BAS RE-1B Ag/AgCl in 3M NaCl, BAS RE-5 Ag/Ag^+ in TBAP/acetonitrile solution). A ferrocene/ferrocenium (Fc/Fc^+) couple was used as the reference redox system[12]. The potential of reference electrode was determined as –0.530(DMSO in Ag/AgCl), -0.073(DMF in Ag/Ag^+), -0.169(THF in Ag/Ag^+) V *vs.* Fc/Fc^+. All potentials reported here are *vs.* Fc/Fc^+. All sample solutions were deoxygenated by passing N_2 gas into solutions for at least 10 min before starting measurements.

3. Results and Discussion

3.1 $U^{VI}O_2(acac)_2dmso$ complex system

The CV measurements for DMSO solution containing $U^{VI}O_2(acac)_2dmso$ (1.00×10^{-3} M) and TBAP (0.10 M) were carried out in the potentials between -0.43 and -1.73 V at different scan rates (v = 0.03 - 0.10 V/s). The results are shown in Fig. 1. As seen from this figure, one strong cathodic peak(E_{pc1}) and two weak anodic peaks(E_{pa1}, E_{pa2}) are observed at around -1.49, -1.38, and -1.20 V, respectively. The values of $\Delta E_{p1} = E_{pc1} - E_{pa1}$ increase with an increase in the scan rate, *i.e.* 0.102 V at v = 0.03 V/s and 0.122 V at v = 0.10 V/s, which are much larger than the theoretical value (0.057 V) for the reversible one-electron transfer process at 23℃. The value of $(E_{pc1} + E_{pa1})/2$ is constant, -1.43 ± 0.001 V, depending on the scan rate. Furthermore, the plot of cathodic peak currents (i_{pc1}) *vs.* $v^{1/2}$ was found to give a good linear relationship (Fig. 2). From these results, it is proposed that the electrochemical reduction of $U^{VI}O_2(acac)_2dmso$ complex in DMSO proceeds through the following mechanism:

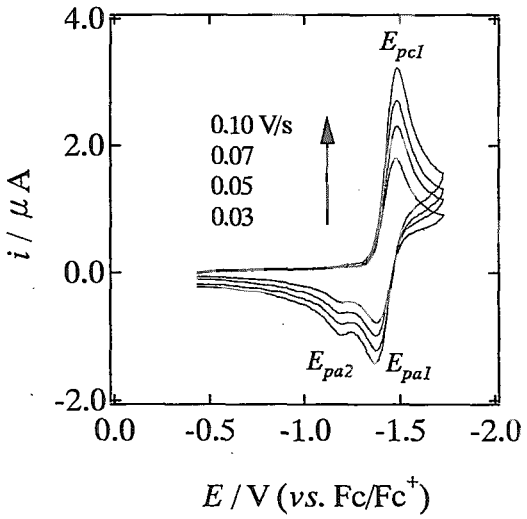

Fig. 1 Cyclic voltammograms of DMSO solution containing $U^{VI}O_2(acac)_2dmso$(1.00×10^{-3}M) and TBAP(0.10M) measured in the potential range from -0.430 and -1.730 V at different scan rates.

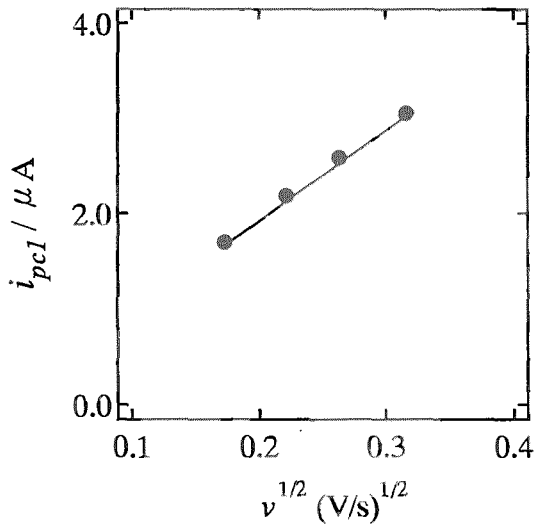

Fig. 2 A plot of i_{pc1} *vs.* $v^{1/2}$ for the cyclic voltammograms of Fig. 1.

$$U^{VI}O_2(acac)_2dmso + e^- = [U^{V}O_2(acac)_2dmso]^- \qquad E_{pc1}/E_{pa1} \qquad (1)$$

$$[U^{V}O_2(acac)_2dmso]^- + xDMSO \xrightarrow[\text{fast}]{} [U^{V}O_2(acac)(uni\text{-}acac)(dmso)_{x+1}]^- \qquad (2)$$

$$[U^{V}O_2(acac)(uni\text{-}acac)(dmso)_{x+1}]^- + DMSO \xrightarrow[\text{fast}]{} U^{V}O_2(acac)(dmso)_{x+2} + acac^- \qquad (3)$$

where uni-acac and x symbolize the acac ligand coordinated to UO_2^{2+} as unidentate and any number of coordinated dmso, respectively. Although it is difficult to assign the final species generated by the electrochemical reduction of $U^{VI}O_2(acac)_2dmso$ from the present study, it is most likely that the non-charged species $U^{V}O_2(acac)(dmso)_{x+2}$ is formed through the intermediate $[U^{V}O_2(acac)(uni\text{-}acac)\ (dmso)_{x+1}]^-$. Therefore, the peak E_{pa2} is supposed to correspond to the oxidation of $U^{V}O_2(acac)\ (dmso)_{x+2}$ (Eq. 4) followed by the coordination and chelation reactions of uni-acac (Eqs. (5) and (6)):

$$U^{V}O_2(acac)(dmso)_{x+2} \rightarrow [U^{VI}O_2(acac)(dmso)_{x+2}]^+ + e^- \qquad E_{pa2} \qquad (4)$$

$$[U^{VI}O_2(acac)(dmso)_{x+2}]^+ + acac^- \xrightarrow[\text{fast}]{} U^{VI}O_2(acac)(uni\text{-}acac)(dmso)_{x+1} + DMSO \qquad (5)$$

$$U^{VI}O_2(acac)(uni\text{-}acac)(dmso)_{x+1} \xrightarrow[\text{fast}]{} U^{VI}O_2(acac)_2dmso + xDMSO \qquad (6)$$

In the Fig. 1, the E_{pa1} peaks coupled with E_{pc1} are small. This indicates that the reaction (1) is almost reversible. In generally, if the reaction, $O + ne^- = R$, is reversible, the peak currents(i_p) are related to $v^{1/2}$ as follows:

$$i_p = 299n(\alpha n_a)^{1/2}SC_OD_O^{1/2}v^{1/2} \quad (\text{at } 23℃) \qquad (7)$$

where C_O (M) is the concentration of species O, D_O (cm^2/s) is the diffusion coefficient of species O, and S (cm^2) is the surface area of electrode. From the slope(9.46×10^{-6}) of Fig. 2, the diffusion coefficient (D_O) of $U^{VI}O_2(acac)_2dmso$ at 23℃ was estimated as 3.91×10^{-6} cm^2/s by using $\alpha n_a = 0.64$, $n = 1$, $C_O = 1.00 \times 10^{-3}$ M, and $S = 0.02$ cm^2.

3.2 $U^{VI}O_2(acac)_2dmf$ complex system

The CV measurements were carried out for DMF solution containing $U^{VI}O_2(acac)_2dmf$ (1.52×10^{-3} M) and TBAP (0.10 M). The potentials was scanned between -0.073 and -1.773 V at different scan rates (v = 0.03 - 0.11 V/s). The results are shown in Fig. 3. As seen from this figure, one strong cathodic peak(E_{pc1}) and two weak anodic peaks(E_{pa1}, E_{pa2}) are observed at around -1.54, -1.40, and -0.83 V, respectively. The values of $\Delta E_{p1} = E_{pc1} - E_{pa1}$ decrease with an increase in the scan rate, *i.e.* 0.148 V at v = 0.03 V/s and 0.144 V at v = 0.11 V/s, which are much larger than the theoretical value (0.057 V) for the reversible one-electron transfer process at 23℃. The value of $(E_{pc1} + E_{pa1})/2$ is nearly constant, -1.47 ± 0.001 V, without depending on the scan rate. Furthermore, the plot of cathodic peak currents (i_{pc1}) *vs.* $v^{1/2}$ was found to give a good linear relationship (Fig. 4). From these results, it is proposed that the electrochemical reduction of $U^{VI}O_2(acac)_2dmf$ complex in DMF proceeds through the following mechanism:

$$U^{VI}O_2(acac)_2dmf + e^- = [U^{V}O_2(acac)_2dmf]^- \qquad E_{pc1}/E_{pa1} \qquad (8)$$

$$[U^{V}O_2(acac)_2dmf]^- + xDMF \xrightarrow[\text{fast}]{} [U^{V}O_2(acac)(uni\text{-}acac)(dmf)_{x+1}]^- \qquad (9)$$

$$[U^{V}O_2(acac)(uni\text{-}acac)(dmf)_{x+1}]^- + DMF \xrightarrow[\text{fast}]{} U^{V}O_2(acac)(dmf)_{x+2} + acac^- \qquad (10)$$

where uni-acac and x symbolize the acac ligand coordinated to UO_2^{2+} as unidentate and any number of coordinated dmf, respectively. Although it is difficult to assign the final species generated by the electrochemical reduction of $U^{VI}O_2(acac)_2dmf$ from the present study, it is most likely that the non-charged species $U^{V}O_2(acac)(dmf)_{x+2}$ is formed through the intermediate $[U^{V}O_2(acac)(uni\text{-}acac)\ (dmf)_{x+1}]^-$. Therefore, the peak E_{pa2} is supposed to correspond to the oxidation of $U^{V}O_2(acac)(dmf)_{x+2}$ (Eq. 11)

followed by the coordination and chelation reactions of uni-acac (Eqs. (12) and (13)):

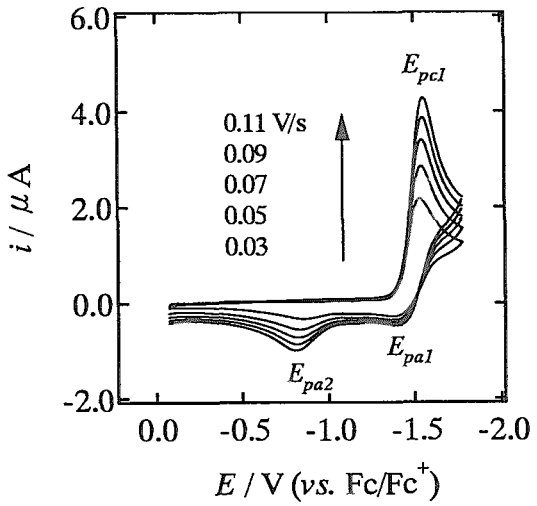

Fig. 3 Cyclic voltammograms of DMF solution containing $UO_2(acac)_2dmf(1.52 \times 10^{-3}M)$ and TBAP(0.10M) measured in the potential range from -0.073 and -1.773V at different scan rates.

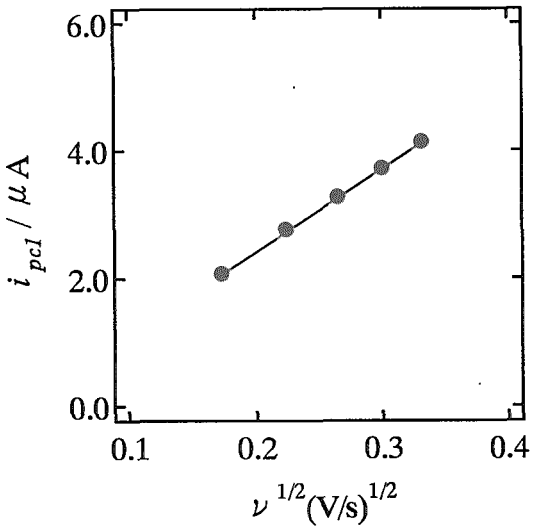

Fig. 4 A plot of i_{pc} *vs.* $\nu^{1/2}$ for the cyclic voltammograms of Fig. 3.

$$U^{V}O_2(acac)(dmf)_{x+2} \rightarrow [U^{VI}O_2(acac)(dmf)_{x+2}]^+ + e^- \qquad E_{pa2} \qquad (11)$$

$$[U^{VI}O_2(acac)(dmf)_{x+2}]^+ + acac^- \xrightarrow[\text{fast}]{} U^{VI}O_2(acac)(\text{uni-acac})(dmf)_{x+1} + DMF \qquad (12)$$

$$U^{VI}O_2(acac)(\text{uni-acac})(dmf)_{x+1} \xrightarrow[\text{fast}]{} U^{VI}O_2(acac)_2dmf + xDMF \qquad (13)$$

In the Fig. 3, the E_{pa1} peaks coupled with E_{pc1} are very small. This indicates that the reaction (8) is almost irreversible. Generally, if the reaction, $O + ne^- = R$, is irreversible, the peak currents(i_p) are related to $v^{1/2}$ as following Eq.(7). Where n_a is the number of electron transfer in the rate-determining step. The αn_a value can be estimated by the following Eq.(14)[13]:

$$E_{p/2} - E_p = 0.0472/(\alpha n_a) \qquad (\text{at } 23^\circ C) \qquad (14)$$

where E_p and $E_{p/2}$ are the potential at $i = i_p/2$, respectively. In the present system, the $E_{p/2} - E_p$ value is 0.074 V and hence the αn_a value is evaluated as 0.64. By using αn_a = 0.64, n = 1, C_O = 1.52 x 10^{-3} M, and S = 0.02 cm^2, the diffusion coefficient of $[U^{VI}O_2(acac)dmf]$ was estimated as 3.14 x 10^{-6} cm^2/s (at 23℃) from the slope(1.29 x 10^{-5}) in plot of i_p *vs.* $v^{1/2}$ shown in Fig. 4. Furthermore, the peak potential (E_p, V) is related with the standard rate constant (k_s, cm/s) as follows[13]:

$$E_p = E_{1/2} - [(RT)/(\alpha n_a F)]\{0.780 + (1/2)\ln[(\alpha n_a F v D_O)/(RT)] - \ln k_s\} \qquad (15)$$

where $E_{1/2}$ is the half-wave potential. Thus, the k_s value was calculated from Eq. (15) by using $E_{1/2}$ = -1.47 V, αn_a = 0.64, and D_O = 3.14 x 10^{-6} cm^2/s, and is 6.5 x 10^{-4} cm/s at v = 0.11 V/s.

3.3 $U^{VI}O_2(acac)_2thf$ complex system

Fig.5 shows the cyclic voltammograms of THF solution containing $U^{VI}O_2(acac)_2thf$ (1.00×10^{-3} M) and TBAP(0.10 M) measured at potentials between -0.169 and –1.869 V at different scan rates (v = 0.05 - 0.25 V/s). As can be seen from Fig. 5, a single cathodic peak(E_{pc1}) is observed at –1.62 V with a coupled anodic peak(E_{pa1}) at around -0.875 V. These suggest that the coupled peaks, E_{pc1} and E_{pa1}, correspond to the redox reaction, $U^{VI}O_2(acac)_2thf + e^- \rightarrow [U^{V}O_2(acac)_2thf]^-$. The values of $\Delta E_{p1} = E_{pc1} - E_{pa1}$

are 0.743 V at v =0.05V/s and 0.846 V at v =0.25V/s, which are close to the theoretical value (0.057 V) for the irreversible one-electron transfer process at 23℃. In addition, the plot of cathodic peak currents (i_{pcl}) *vs.* $v^{1/2}$ gives a good linear relationship as shown in Fig. 6.

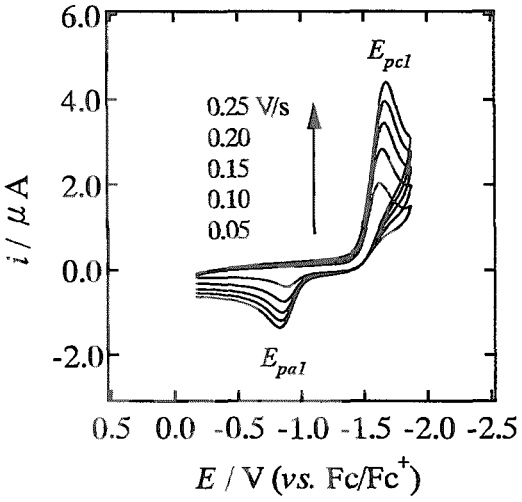

Fig. 5 Cyclic voltammograms of THF solution containing $UO_2(acac)_2thf$(1.00 × 10^{-3}M) and TBAP(0.10M) measured in the potential range from -0.169 and -1.869V at different scan rates.

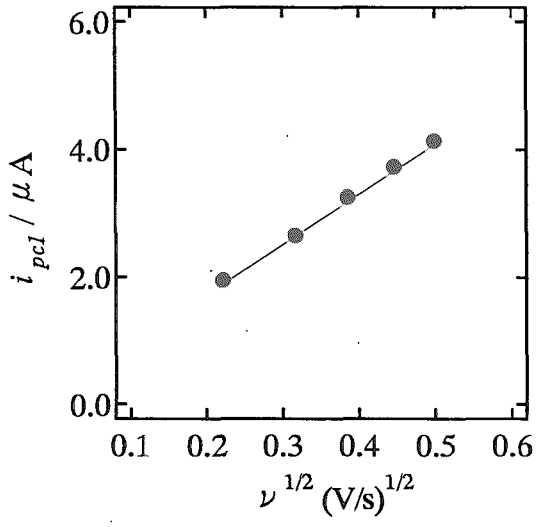

Fig. 6 A plot of i_{pc} *vs.* $\nu^{1/2}$ for the cyclic voltammograms of Fig. 5.

From these results, it is concluded that the electrochemical reactions corresponding E_{pcl} and E_{pal} peaks are irreversible and are followed by the rapid chemical reactions. Hence, the following EC mechanism may be proposed as plausible one:

$$U^{VI}O_2(acac)_2thf + e^- \rightarrow [U^{V}O_2(acac)_2thf]^- \qquad E_{pcl} \qquad (16)$$

$$[U^{V}O_2(acac)_2thf]^- \xrightarrow[\text{fast}]{} U^{V}O_2(acac)thf + acac^- \qquad (17)$$

$$U^{V}O_2(acac)thf \rightarrow [U^{VI}O_2(acac)thf]^+ + e^- \qquad E_{pal} \qquad (18)$$

$$[U^{VI}O_2(acac)thf]^+ + acac^- \xrightarrow[\text{fast}]{} U^{VI}O_2(acac)_2thf \qquad (19)$$

As the succeeding chemical reactions, the dissociation and association reactions of $acac^-$ seem to be reasonable, because such processes from the non-charged complexes and result in the stabilization of products. From the slope(7.89 x 10^{-6}) in plot of i_{pcl} *vs.* $v^{1/2}$ in Fig. 6, the diffusion coefficient of $U^{VI}O_2(acac)_2thf$ at 23℃ was estimated as 2.95 x 10^{-6} cm^2/s by using C_O = 1.00 x 10^{-3} M, and S = 0.02 cm^2 in Eq. (7).

4. CONCLUSIONS

The $U^{VI}O_2(acac)_2dmso$ and $U^{VI}O_2(acac)_2dmf$ complexes are reduced to $[U^{V}O_2(acac)_2dmso]^-$ and $[U^{V}O_2(acac)_2dmf]^-$ species quasi-reversibly and that the $U^{VI}O_2(acac)_2thf$ complex is irreversibly reduced to $[U^{V}O_2(acac)_2thf]^-$ species at the Pt electrode. The reduction potentials (i_{pcl}, *vs.* Fc/Fc^+) for the U(V) were determined to be -1.49 V for $U^{VI}O_2(acac)_2dmso$, -1.54 V for $U^{VI}O_2(acac)_2dmf$, and -1.62 V for $U^{VI}O_2(acac)_2thf$. The plot of cathodic peak currents (i_{pcl}) *vs.* *DN* (donor number) gives a good linear relationship. This means that the reduction of $U^{VI}O_2(acac)_2L$ complexes becomes difficult with an decrease in the basicity of the coordinated L(L = dimethylsulfoxide (dmso), *N,N*-dimethyl- formamide(dmf), tetrahydrofuran(thf)). The U(V) species formed in the reduction of $U^{VI}O_2(acac)_2L$ complexes existed stably in

non-aqueous solvents. As we expected, the U(VI) complexes with bidentate ligands at their equatorial planes were found to form stable U(V) complexes by electrochemical reduction, that is, those generated in the reduction of $U^{VI}O_2(acac)_2L$ were not reduced to U(IV).

5. REFERENCES

1. (a) B. McDuffie and C.N. Reilley, *Anal. Chem.*, **38**, 1881-1887 (1966). (b) S. Casadio and F. Orlandini, *J. Electroanal. Chem.*, **26**, 91-96 (1970). (c) L. Sipos, L.J. Jeftic, M. Branica and Z. Galus, *J. Electroanal. Chem.*, **32**, 35-47 (1971). (d) D.W. Wester and J.C. Sullivan, *Inorg. Chem.*, **9**, 2838-2840 (1980). (e) D. Hodko and V. Pravdic, *Electrochim. Acta*, **30**, 1341-1344 (1985).
2. (a) H. Bildstein and V. Fleischer, V. Gutmann, *Inorg. Chim. Acta*, **2**, 347–350 (1968). (b) E.A. Kanevskii, B.V. Rengevich and G.R. Pavlovskaya, *Radiokhimiya*, **17**, 534-535 (1975). (c) P. Zanello, A. Cinquantini and G.A. Mazzocchin, *Inorg. Chim. Acta*, **21**, 195-199 (1977). (d) P. Zanello, A. Cinquantini, P.D. Bernardo and L. Magon, *Inorg. Chim. Acta*, **24**, 131-137 (1977). (e) P. Zanello, A. Cinquantini, G.A. Mazzocchin and O. Traverso, *Inorg. Chim. Acta*, **27**, 157-161 (1978). (f) P. Zanello, A. Cinquantini and G.A. Mazzocchin, *J. Electroanal. Chem.*, **131**, 215-227 (1982). (g) P. Seeber and P. Zanello, *J. Chem. Soc. Dalton Trans.*, 601-603 (1985). (h) S. Marouani and A.L.M. Gross, *J. Electrochim. Acta*, **33**, 147-155 (1988). (i) L. Bahadur and J.P. Pandey, *J. Electrochem. Soc.*, **137**, 3755-3760 (1990).
3. (a) G. Gritzner and J. Selbin, *J. Inorg. Nucl. Chem.*, 30, 1799-1804 (1968). (b) D. Cohen, *J. Inorg. Nucl. Chem.*, 32, 3525-3530 (1970). (c) J.T. Bell, H.A. Friedman and M.R. Billings, *J. Inorg. Nucl. Chem.*, 36, 2563-2567 (1974). (d) C. Miyake and S. Yamana, H.O. Nishiguchi, *Inorg. Chim. Acta*, 95, 17-21 (1984). (e) C. Miyake, T. Kondo, S. Imoto and H.O. Nishiguchi, *J. Less Common Met.*, 122, 313-317 (1986). (f) S.P. Best, R.J.H. Clark and R.P. Cooney, *Inorg. Chim. Acta*, **145**, 141-147 (1988).
4. K. Mizuguchi, Y.Y. Park, H. Tomiyasu and Y. Ikeda, *J. Nucl. Sci. Technol.*, **30**, 542-548 (1993).
5. S.H. Lee, K. Mizuguchi, H. Tomiyasu and Y. Ikeda, *J. Nucl. Sci. Technol.*, **33**, 190-192 (1996).
6. K. Mizuguchi, S.H. Lee, Y. Ikeda and H. Tomiyasu, *J. Alloys Comp.*, **271-273**,163-167 (1998).
7. S.Y. Kim, K. Hatakeyama, H. Tomiyasu and Y. Ikeda, *J. Nucl. Sci. Technol.*, **35**, 437-442 (1998).
8. S.Y. Kim, H. Tomiyasu and Y. Ikeda, submitted to *J. Nucl. Sci. Technol.*, (2001).
9. S.Y. Kim, M. Harada, H. Tomiyasu, Y. Shiokawa and Y. Ikeda, *J. Nucl. Sci. Technol.*, **37**, 99-1002 (2000).
10. A.E. Comyns, B.M. Gatehouse and E. Wait, *J. Chem. Soc.*, 4655-4665 (1958).
11. D.D. Perrin and W.L.F. Armarego, *"Purification of Laboratory Chemicals"*; Pergamon Press: Oxford, U.K., (1988).
12. G. Gritzner and J. Kuta, *Pure Appl. Chem.*, **56**, 461-466 (1984).
13. (a) R.S. Nicholson, *Anal. Chem.*, **37**, 1351-1355 (1965). (b) R.S. Nicholson and I. Shain, *Anal. Chem.*, **36**, 706-723 (1964). (c) H. Matsuda and Y. Ayabe, *Z. Elektrochem.*, **59**, 494-503 (1955).